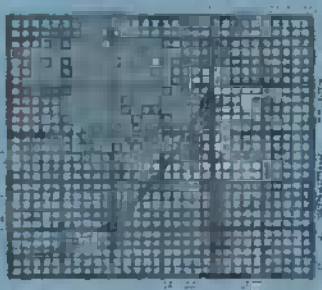
FATIGUE AT ELEVATED TEMPERATURES



STP 520

Carden | McEvily | Wells

AMERICAN SOCIETY FOR TESTING AND MATERIALS

FATIGUE AT ELEVATED TEMPERATURES

A symposium
presented at
The University of Connecticut
Storrs, Conn. 18–23 June 1972

ASTM SPECIAL TECHNICAL PUBLICATION 520
A. E. Carden, A. J. McEvily, and C. H. Wells, editors

List price $45.50
04-520000-30



AMERICAN SOCIETY FOR TESTING AND MATERIALS
1916 Race Street, Philadelphia, Pa. 19103

© BY AMERICAN SOCIETY FOR TESTING AND MATERIALS 1973
Library of Congress Catalog Card Number: 73-76958

NOTE

The Society is not responsible, as a body,
for the statements and opinions
advanced in this publication.

Printed in Baltimore, Md.
August 1973

Foreword

The symposium on Fatigue at Elevated Temperatures held at the University of Connecticut, Storrs, Connecticut, 18-23 June 1972 was organized because of the growing importance of this topic. Committee E-9 on Fatigue of the American Society for Testing and Materials sponsored the symposium in cooperation with the American Society of Mechanical Engineers (Materials Division) and the American Society for Metals (Materials Systems and Design Division). The Steering Committee for this symposium consisted of L. F. Coffin, Jr., E. G. Ellison, M. Gell, J. C. Grosskreutz, H. F. Hardrath, G. Jacoby, S. S. Manson, A. J. McEvily, E. M. Smith, S. Taira, and C. H. Wells.

The purpose of the symposium was to provide a broad coverage of the topic in its various aspects, as well as to provide an opportunity for the presentation of the latest research findings. The symposium was organized on this basis, and this resultant publication is, therefore, of a tutorial as well as a research nature.

The contributions of the session chairmen for their capable performance gratefully acknowledged. These session chairmen were, J. C. Grosskreutz, D. Hoeppner, R. Pelloux, C. Laird, H. F. Hardrath, R. Wetzel, R. W. Stentz, W. H. Sharp, E. Steigerwald, J. W. Pridgeon, F. VerSnyder, R. P. Wei, R. Goldhoff, E. Krempl, A. E. Carden, W. H. Tuppeny, Jr., W. L. Greenstreet, A. O. Schaefer, and B. Wei.

The contributions of the authors and discussors are also gratefully acknowledged. The contribution of S. R. Crosby, graduate assistant, Metallurgy Department, University of Connecticut, who prepared the index, is likewise gratefully acknowledged.

Related ASTM Publications

Probabilistic Aspects of Fatigue, STP 511 (1972), $19.95 (04-511000-30)

Metal Fatigue Damage—Mechanism, Detection, Avoidance, and Repair, STP 495 (1971), $21.00 (04-495000-30)

Effect of Notches on Low-Cycle Fatigue, STP 490 (1972), $3.00 (04-490000-30)

Contents

PAGE

Introduction 1

Introductory Statement

Fatigue at High Temperature—L. F. COFFIN, JR. 5

Mechanisms of Fatigue

Mechanisms of High Temperature Fatigue—M. GELL AND G. R. LEVERANT 37
Discussion 67

Correlation of Substructure with the Elevated Temperature Low-Cycle Fatigue of AISI 304 and 315 Stainless Steels—K. D. CHALLENGER AND J. MOTEFF 69
Discussion 78

Relationship Between Thermal Fatigue and Low-Cycle Fatigue at Elevated Temperature—SHUJI TAIRA 80
Discussion 100

Fatigue of Protective Metal Oxides in Combustion Chamber Exhaust Gases—R. R. DILS 102

Effects of Frequency and Environment on Fatigue Crack Growth in A286 at 1100 F—H. D. SOLOMON AND L. F. COFFIN, JR. 112
Discussion 121

Extent to Which Material Properties Control Fatigue Failure at Elevated Temperatures—J. WAREING, B. TOMKINS, AND G. SUMNER 123
Discussion 137

Temperature Dependence of Fatigue Crack Propagation in an Al-2.6Mg Alloy—F. JEGLIC, P. NIESSEN, AND D. J. BURNS 139
Discussion 148

Derivation of a Failure Law for Creep Under a Cyclic Stress—J. A. WILLIAMS 149

Creep-Fatigue Interaction During Crack Growth—P. N. ATANMO AND A. J. MCEVILY, JR. 157
Discussion 165

Thermal-Mechanical Fatigue Crack Propagation in Nickel- and Cobalt-Base Superalloys Under Various Strain-Temperature Cycles—C. A. RAU, JR., A. E. GEMMA, AND G. R. LEVERANT 166

PAGE

Threshold for Fatigue Crack Growth in Ferritic Steels at 300 C—L. P. POOK AND A. A. BEVERIDGE 179

General Discussion on Mechanisms of Fatigue 191

Test Methods

Fatigue at Elevated Temperatures: A Review of Test Methods—A. E. CARDEN 195

Discussion of the Test Method and Equipment for the Evaluation of Low-Cycle Creep-Fatigue Failure Criteria—R. M. SCHNEIDEROVITCH AND A. P. GUSENKOV 224

High-Temperature Fatigue Testing of Automotive Valve Steels—E. T. VITCHA 231

Discussion 241

Evaluation of Thermal Fatigue Resistance of Metals Using the Fluidized Bed Technique—M. A. H. HOWES 242

Discussion 253

Thermoacoustic Fatigue Testing Facility for Space Shuttle Thermal Protection System—C. E. RUCKER AND R. E. GRANDLE 255

Fatigue of Supersonic Transport Materials Using Simulated Flight-by-Flight Loading—L. A. IMIG 264

Ultrasonic Fatigue in Steam with Small Amounts of Sodium Chloride—A. F. CONN AND N. A. NIELSEN 273

General Discussion on Test Methods 282

Materials

Fatigue in the Design of High-Temperature Alloys—H. F. MERRICK, D. H. MAXWELL, AND R. C. GIBSON 285

Discussion 298

Effects of Grain Size and Temperature on the Cyclic Strength and Fracture of Iron—H. ABDEL-RAOUF, T. H. TOPPER, AND A. PLUMTREE 300

Discussion 310

Creep Testing of Alpha Iron During Thermal Cycling—D. EYLON, D. G. BRANDON, AND A. ROSEN 311

Discussion 319

PAGE

High-Strain Fatigue Properties of Cast ½Cr-Mo-V Steels—W. J. ELDER, J. B. MARRIOTT, AND M. C. MURPHY 320
Discussion 331

Effect of Carbon Content on High-Temperature Properties of 2¼Cr-1Mo Steels—R. R. SEELEY AND R. H. ZEISLOFT 332
Discussion 342

Fatigue Crack Propagation in Steel Alloys at Elevated Temperatures—H. I. MCHENRY AND A. W. PENSE 345

Low-Cycle Fatigue Behavior of Types 304 and 316 Stainless Steel at LMFBR Operating Temperature—C. F. CHENG, C. Y. CHENG, D. R. DIERCKS, AND R. W. WEEKS 355
Discussion 364

Combined Low-Cycle Fatigue and Stress Relaxation of Alloy 800 and Type 304 Stainless Steel at Elevated Temperatures—C. E. JASKE, H. MINDLIN, AND J. S. PERRIN 365
Discussion 376

Effects of Combined Creep and Fatigue Loading on an Austenitic Stainless Steel at High Temperature—W. E. WHITE, R. I. COOTE, AND I. LE MAY 377
Discussion 386

Fatigue Crack Growth Characteristics of Several Austenitic Stainless Steels at High Temperature—R. SHAHINIAN, H. H. SMITH, AND H. E. WATSON 387
Discussion 399

Effect of Several Metallurgical Variables on the Thermal Fatigue Behavior of Superalloys—D. H. BOONE AND C. P. SULLIVAN 401
Discussion 415

Thermal Fatigue Characterization of Cast Cobalt and Nickel-Base Superalloys—D. F. MOWBRAY, D. A. WOODFORD, AND D. E. BRANDT 416
Discussion 425

High-Cycle Fatigue Properties of a Dispersion Strengthened Nickel-Base Superalloy—J. H. WEBER AND M. J. BOMFORD 427
Discussion 436

Effect of Mean Stress on the High-Cycle Fatigue Behavior of Udimet 710 at 1000 F—D. M. MOON AND G. P. SABOL 438

PAGE

Bend Fatigue of Two Iron-Nickel-Base Superalloys at Elevated Temperature—A. J. OPINSKY 451

Combined Creep-Fatigue Behavior of Inconel Alloy X-750—P. K. VENKITESWARAN, D. C. FERGUSON, AND D. M. R. TAPLIN 462
Discussion 472

Low-Cycle Fatigue with Combined Thermal and Strain Cycling—U. S. LINDHOLM AND D. L. DAVIDSON 473

Low-Cycle Fatigue Behavior of Zircaloy at 573 K—R. R. HOSBONS 482
Discussion 489

Thermal Fatigue Behavior of T-111 and ASTAR 811C in Ultrahigh Vacuum—K. D. SHEFFLER AND G. S. DOBLE 491

Effect of Interrupting Fatigue by Periods of Heat for Aluminum Alloy Structural Elements—J. R. HEATH-SMITH AND F. E. KIDDLE 500
Discussion 511

Test Results of Fatigue at Elevated Temperatures on Aeronautical Materials—G. P. VIDAL AND P. L. GALMARD 512

Effect of Surface Integrity on Fatigue of Structural Alloys at Elevated Temperatures—P.S. PREVEY AND W. P. KOSTER 522

Thermal Ratchetting

Review of Thermal Ratchetting—DAVID BURGREEN 535
Discussion 550

Ratchetting Under Cyclic Axial Strain with Torsional Stress—H. YAMANOUCHI, Y. ASADA, AND Y. WAKAMATSU 552
Discussion 562

Analytical and Experimental Study of Thermal Ratchetting—A. V. A. SWAROOP AND A. J. MCEVILY, JR. 563
Discussion 572

Lifetime Predictions and Design

Predicting Service Life in a Fatigue-Creep Environment—E. G. ELLISON AND E. M. SMITH 575
Discussion 611

A Realistic Model for the Deformation Behavior of High-Temperature Materials—A. K. MILLER 613
Discussion 624

PAGE

Ductility Exhaustion Model for Prediction of Thermal Fatigue and Creep Interaction—J. F. POLHEMUS, C. E. SPAETH, AND W. H. VOGEL 625
Discussion 636

Strain Rate and Holdtime Saturation in Low-Cycle Fatigue: Design-Parameter Plots—J. B. CONWAY, J. T. BERLING, AND R. H. STENTZ 637
Discussion 647

Comparison of Experimental and Theoretical Thermal Fatigue Lives for Five Nickel-Base Alloys—D. A. SPERA 648
Discussion 657

Temperature Effects on the Strainrange Partitioning Approach for Creep Fatigue Analysis—G. R. HALFORD, M. H. HIRSCHBERG, AND S. S. MANSON 658
Discussion 668

Kinetic Deformation Criteria of Cyclic Fracture at High Temperature—S. V. SERENSEN, R. M. SCHNEIDEROVITCH, AND AND A. P. GUSENKOV 670

Method for Low-Cycle Fatigue Design Including Biaxial Stress and Notch Effects—D. C. GONYEA 678

Some Considerations of the Application of Cyclic Data to the Design of Welded Structures—B. J. L. DARLASTON AND D. J. WALTERS 688

Elevated Temperature Test of Welded Furnace Wall Sections—C. W. LAWTON AND J. E. BYNUM 699

Parametric Study to Establish Design Curves and to Evaluate Design Rules for Ratchetting—T. R. BRANCA AND J. L. MCLEAN 709

Nondestructive Testing in Fatigue: A 1972 Update—R. B. SOCKY 722

Codes: Asset or Liability—W. E. COOPER 733

The Challenge to Unify Treatment of High Temperature Fatigue—A Partisan Proposal Based on Strainrange Partitioning—S. S. MANSON 744
Discussion 775

Closure Statement

Summary 785

Index 787

Introduction

An increase in the efficiency of a power generating unit, in the rate of an industrial chemical process, or in the speed of supersonic aircraft, have in common an association with an increase in temperature. The technological advances, required to obtain such performance increases, are largely dependent upon the development of new materials and design methods for structures capable of withstanding the rigors of elevated temperature service. However, before these developments can be put into practice, it is necessary that the materials be thoroughly characterized with respect to resistance to stress, temperature, and environment, and that the reliability of associated design procedures be established. These are both formidable tasks of the utmost importance, especially where long-time service experience is lacking. Consider, for example, the problems associated with the design of a nuclear reactor component of a relatively new alloy which is expected to be in service at elevated temperatures for forty years or more. Such a design can be made reliable only after the response of the alloy for the service conditions has been quantified.

In addition to this trend toward higher operating temperatures there is also a trend toward more efficient and economical design. This latter goal can only be achieved through an understanding of the load-structure-stress-strain-temperature-environment-material interactions. Whereas in the past creep behavior at elevated temperatures may have been the principal consideration, experience has shown that, in fact, fatigue may often be the controlling factor. All aspects of the fatigue process are modified in the creep range. Mechanisms of crack initiation and growth, test methods, lifetime predictions, and design methods all are changed. In addition new factors are introduced such as thermal fatigue, thermal ratchetting, and stress relaxation. Each of these serves to make fatigue at elevated temperatures a very complex subject, but it is this very complexity which offers a challenge to researchers and design engineers concerned with creep-fatigue interaction.

The present volume is intended to provide a comprehensive overview of this subject, as well as to provide current research findings in four major subareas:

1. Mechanisms: The processes of crack initiation and growth leading to creep-fatigue failure.
2. Test Methods: The techniques for carrying out elevated temperature fatigue tests and for analyzing the resultant data.

Copyright© 1973 by ASTM International www.astm.org

3. Materials: A review of the alloys used in elevated temperature creep-fatigue design, together with the latest data on their properties.

4. Prediction Methods and Thermal Ratchetting: A review of current approaches to creep-fatigue lifetime predictions, including thermal ratchetting, and a consideration of code design procedures and emerging design philosophies.

It is expected that the information contained in this volume will be of use to metallurgists, materials test engineers, and designers who are concerned with this important problem. It is hoped that interaction between the various disciplines involved will be promoted, and that this volume will serve as an impetus for rapid advance in the field of fatigue at elevated temperatures.

Introductory Statement

L. F. Coffin, Jr.[1]

Fatigue at High Temperature

REFERENCE: Coffin, L. F., Jr., **"Fatigue at High Temperature,"** *Fatigue at Elevated Temperatures, ASTM STP 520,* American Society for Testing and Materials, 1973, pp. 5–34.

ABSTRACT: This report was prepared as the keynote address given at the 1972 Symposium on Fatigue at Elevated Temperatures at the University of Connecticut, 18–23 June, 1972. It describes the high-temperature fatigue problem as a failure process in a notch in some structure involving nucleation and early growth at the notch root, high-strain crack propagation through the plastic zone of the notch, and elastic crack growth to ultimate failure. Several of the important disciplines bearing on these three steps in the failure process are discussed. Particular attention is given to a description of the high-temperature phenomenology, distinctions between high- and low-cycle fatigue effects at high temperature, failure criteria including frequency and holdtime effects, the importance of the environment vis-a-vis creep in considering time effects on fatigue behavior, high-strain crack propagation, elastic crack growth, ratchetting effects, and methods for treating notches.

KEY WORDS: fatigue (materials), thermal fatigue, fatigue failure, crack initiation, crack propagation, transgranular corrosion, intergranular corrosion, plastic deformation, elastic deformation, stress analysis

Fatigue at elevated temperatures may have different meanings to each person who encounters the problem, depending on their previous training, current interests, and professional responsibilities. His work may involve him in a narrow part of the problem for which he seeks highly specific answers, whether it be the understanding of fatigue crack initiation, or the determination of the design life of a pressure vessel. By publishing this symposium on fatigue at elevated temperatures, the many viewpoints will be presented so that the reader may broaden his perspective and tackle his work with a broader vision.

To encourage a broader appreciation of the problem and to attempt to lower the communication barriers, it is appropriate to consider the several physical aspects of the problem, and to examine the many disciplines that are brought to bear either to understand the problem, to prevent it from occurring, to design around its complexities, or to live with it. Referring to Fig. 1, we imagine an engineering structure containing a notch. The struc-

[1] Metallurgy and Ceramics Laboratory, General Electric Co., Research and Development Center, Schenectady, N. Y. 12301.

Copyright© 1973 by ASTM International www.astm.org

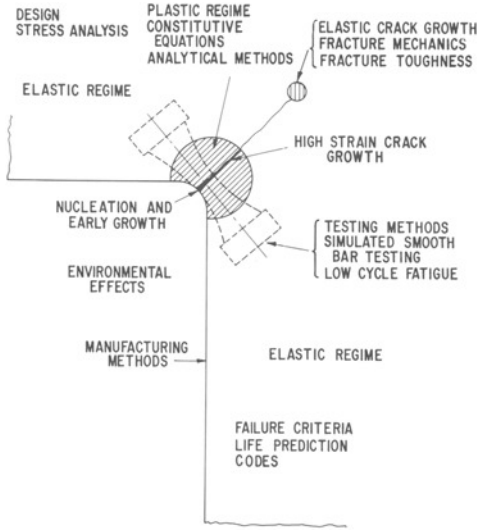


FIG. 1—*Schematic view of high-temperature fatigue problem showing physical stages in failure process and relevant disciplines.*

ture might be a turbine rotor, or a pressure vessel, loaded centrifugally, or by internal pressure, and it presumably has some temperature gradient acting in the notch region. The centrifugal, pressure, or thermal stresses are cycled, most commonly from zero to tension by start-stop or load-unload operation of the equipment. We then envisage the fatigue process to occur in three stages: first, nucleation and early growth of cracks within the plastic zone developed at the notch root; second, crack propagation of a stable crack through the plastic zone; third, propagation of the crack through the elastic zone, the crack generating its own plastic zone, until fracture of the structure results, either by sudden fracture, leakage, or by excess vibration or deformation. These stages are shown in Fig. 1.

Also in Fig. 1 we identify some of the many disciplines which must be brought to bear on the problem. Consider first the plastic zone. Identification of the appropriate stresses and strains are required through analytical tools, such as finite element analyses. This requires the selection of appropriate material information and constitutive equations, heat transfer analysis, etc. With the aid of appropriate failure criteria, the conditions for the occurrence of microcracks or for nucleation and early growth can be specified. Elastoplastic analysis further aids in the specification of conditions for crack growth through the plastic zone, again coupled with an appropriate fracture criterion. Finally, elastic stress analysis and fracture mechanics concepts allow the determination of crack growth in the elastic regime.

Along the way we can identify several additional disciplines. Included are environmental effects on nucleation and growth, manufacturing techniques

for surface preparation in the critical area, choice of material, testing methods for developing failure criteria, low-cycle fatigue studies, development of high- and low-strain crack growth rules, time dependency, fractography, etc. Groups of these and other disciplines are lumped together into such activities as life prediction, design, code development, etc. There is also a whole structure of disciplines directed towards other aspects of the problem such as metal physics, corrosion and electrochemistry, physical and process metallurgy, statistics, and others.

To obtain some semblance of order among this confusion of disciplines, it is necessary to keep the physical picture of the problem in mind. Too often, in the interest of obtaining answers, we forget that fatigue failure is progressive, starting from a single grain or microscopic flaw, gradually growing to a size where it compromises the integrity of the structure. Our models or criteria should be continually examined to be sure that, indeed, the physical aspects of the phenomenon have not been lost sight of, or better yet, are the building blocks for the model or criterion. The present paper is presented with this thought in mind.

Plastic Zone and Its Relationship to Low-Cycle Fatigue

The various stages of the fatigue process just described are represented in Fig. 1. Important in this model is (*a*) an analytical knowledge of the deformation state within the plastic zone and (*b*) the establishing of a failure criterion for crack initiation and early growth in terms of the strains so produced in this zone. To be as quantitative as possible it is desirable to have a complete elastoplastic solution for stresses and strains in the vicinity of the notch. Although rigorous constitutive equations are lacking for such calculations a recent approach by Mowbray and McConnelee [*1,2*][2] appears attractive in attacking this problem. They utilize a finite element analysis where constitutive equations are derived from families of "isocycle" stress-strain curves converted to effective stress-strain curves to construct a complete stress-strain representation within the plastic zone. Figure 2 shows a typical solution for a notch of $K_t = 3.46$, and indicates the plastic zones for various average net section stress amplitudes. It would appear that the analytical tools for treating complex geometries are developing more rapidly than concomitant material laws [*3*].

The fatigue literature contains numerous references in which the stabilized or steady-state stress-strain curve is similarly utilized to establish the local strain distribution at the notch root [*4-6*]. Notch root strains are commonly and simply determined by the Stowell [*7*] or Neuber [*8*] formulation. The applicability of these methods to high-temperature problems will be discussed later.

As a result of repeated cyclic plastic strain in the plastic zone microcracks nucleate and grow to some observable size at the free surface. One way to

[2] The italic numbers in brackets refer to the list of references appended to this paper.

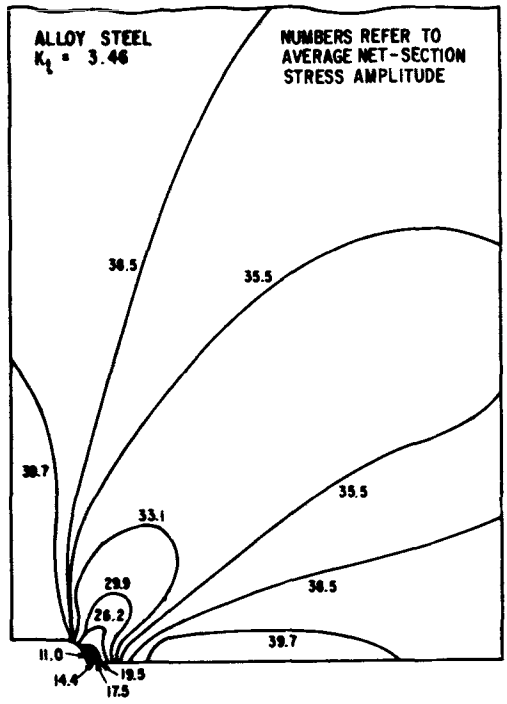


FIG. 2—*Progesssion of plastic flow in grooved cylinder test specimen of 2¼Cr-1Mo steel by finite element stress analysis* [1].

simulate this situation is to imagine a low-cycle fatigue specimen located as in Fig. 1 such that its minimum cross section is some fraction of the plastic zone. Provided suitable corrections are introduced to account for the different stress states, fatigue failure of this specimen can be made to approximate the nucleation and early growth of cracks in the component of Fig. 1. There is, however, a size and strain gradient problem since, in the test specimen, the crack is initiated and grows in a uniform strain field to some fraction of the cross-sectional area, while in the plastic zone this same process occurs in a strain gradient. Hence the concept of "smooth specimen simulation"—as Morrow et al [*9*] have named it—is sound provided the plastic zone is sufficiently large relative to the minimum diameter of the standard low-cycle fatigue test (~0.25 in.) and the strain gradient is acceptably small. For smaller plastic zones, either proportionally smaller fatigue specimens, or earlier indications of failure in standard size specimens are required. By these arguments, and with the assumption that the plastic zone of our structure (Fig. 1) is large relative to the test specimen, we can insert the massive volume of low-cycle fatigue information as a critical link in the chain of events leading to structural fatigue failure.

The foregoing logic may be further generalized with respect to sorting out specific aspects of the fatigue problem. Assuming that the physical picture is as shown in Fig. 1, the usefulness of low-cycle specimen fatigue is clearly that of determining the nucleation and early growth characteristics of a metal, a process otherwise difficult to represent quantitatively in our present state of understanding. On the contrary, high-cycle fatigue specimen testing is, in reality, the combination of all the processes described in Fig. 1—nucleation and early growth, propagation in the plastic zone of the stress concentration, and stable crack growth—a confusion of phenomena. The separation of the study of stable crack growth into a separate discipline, such as has occurred in recent years, seems fully justified from physical considerations. It is important that this phenomenon be closely related to the specifics of engineering structures by such methods as linear elastic fracture mechanics, crack opening displacements, etc. Despite the confusion of phenomena, interpretations and failure criteria derived from total failure information in high-cycle fatigue specimen tests are probably most useful for the definition of crack nucleation.

High-Temperature Low-Cycle Fatigue Testing Methods

From the above rationale we can justify the uniaxial fatigue test as an appropriate basis for providing both the deformation and fracture information needed to establish criteria for crack initiation in real structures. Tests performed under fixed strain limits most closely approximate the deformation behavior within the plastic zone, although the use of "Neuber control" has been introduced [*10*] recently as an alternative approach in notch geometries. Experimental methods for controlled strain testing have been extensively covered in the recent *Manual on Low Cycle Fatigue Testing* [*11*], and this book is recommended for the libraries of those concerned with fatigue testing.

There are certain techniques which are more significant to high-temperature fatigue testing than to room temperature. Most important of these is the consideration of time dependency. This affects both the deformation and fracture aspects of the testing program, because it is an important ingredient of the deformation and fracture aspects of the structure (Fig. 1). Time, through creep or relaxation phenomena, redistributes the stress-strain profiles in notches, or at crack tips, and consequently changes the stress or strain inputs or both to our crack nucleation and early growth fracture criterion. Similarly time effects will strongly influence the failure process as we shall discuss later in more depth. Consequently, time is an important factor in high-temperature fatigue testing and can be introduced through consideration of strain rate, frequency, holdtimes, strain-range partitioning, etc. The role that it plays in the deformation and fracture process is controversial, and some airing of this important topic will undoubtedly come forth in this conference.

This same matter of time dependency raises important questions of interpretation from low initial cost testing methods such as bending or torsion. Introduction of holdtimes in these geometries leads to relaxation processes that do not necessarily occur at constant total strain. Nor, in fact is it easy to ascertain just what the stress-strain-time relationships are in such geometries. Although more costly initially, experiments performed with statistically determinate specimens under closed loop control gives more interpretable and meaningful results which, in the long run, justifies the initial equipment investment.

It is instructive to discuss one particular problem that arises in diametral strain control of hourglass shaped push-pull test specimens. It has been found in certain high-strength, low-ductility cast structures, such as the nickel-base superalloys, that a pronounced and random transverse strain is produced under both elastic and plastic axial loads. The effect is due to the inherent anisotropy of the individual crystals in the structure and the comparatively coarse grain size commonly used. The behavior is seen in Fig. 3, where a circumferential traverse of the diametral strain is shown for an as-cast test specimen at a fixed stress range. To eliminate scatter in strain measurements in testing materials of this type, after obtaining such a profile, we locate two diametral extensometers 90 deg apart in such a position as to give a response typical of the average transverse strain for the material in question.

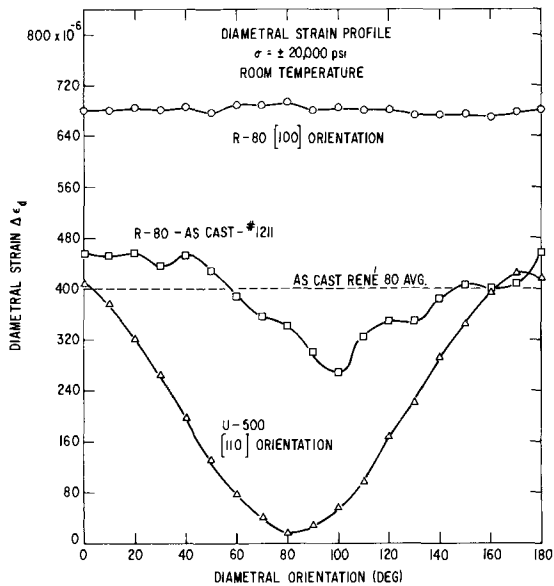


FIG. 3—*Diametral strain anisotropy in cast and single crystal nickel-base superalloys under axial loading.*

It is also interesting to observe in this figure the highly isotropic response in transverse strain for a single crystal test specimen when the [100] growth orientation is directed axially, and the highly anisotropic orientation for the [110] orientation. The transverse anisotropy phenomenon is obviously not confined to cast or single crystal materials [*12*] nor to high temperature, but it is particularly applicable to the widely used cast nickel-base superalloys.

In our own testing work at high temperature, we evaluate the fatigue behavior of materials not only at several strain ranges (usually with plastic strain limits) but also at several frequencies. For any one temperature a minimum of nine tests are required—three strains and three frequencies for each strain. These test results are then fitted to appropriate fatigue equations, using a regression analysis procedure, from which six independent coefficients are found to characterize the stress range, strain range, and frequency response of the material at the specific temperature selected. A more extensive development of this approach follows.

Phenomenological Representation of High-Temperature Fatigue

Before discussing some of the significant aspects of high-temperature fatigue, it is instructive to characterize the behavior from a phenomenological viewpoint. One such method employs observations made from controlled strain range experiments on test specimens of the type shown in the plastic zone of Fig. 1. The work of Berling and Slot [*13*] on three stainless steels at three temperatures and at different strains has been widely referenced and is of value to display the phenomenological viewpoint by combining their test results with high-temperature fatigue equations developed in recent years [*14–16*]. These fatigue equations are extensions of equations used for low-temperature fatigue developed from a strain viewpoint [*17,18*], where the important effects of time are introduced by the frequency of cycling.

The first of these equations relates the stress range, the plastic strain range and frequency as

$$\Delta\sigma = A\Delta\epsilon_p{}^{n'}\nu^{k}{}_{1} \tag{1}$$

where

$\Delta\sigma$ = stress range,
$\Delta\epsilon_p$ = plastic strain range,
ν = frequency, and
A,n',k_1 = coefficients determined from test data by regression analysis.

The quantity n' is the cyclic strain hardening exponent. Using Berling and Slot's data and some unpublished data obtained by our laboratory, the cyclic stress-strain behavior of AISI 304 stainless steel, a commonly used material in nuclear application, is shown in Fig. 4. Here the frequency effect is accounted for by rewriting Eq 1, through the combination of the stress

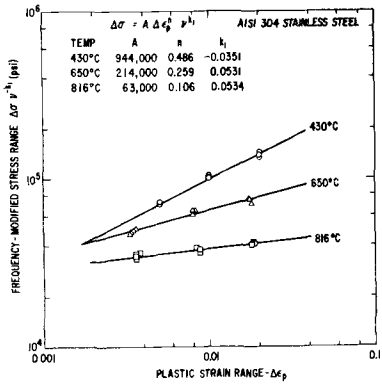


FIG. 4—*Representation of data of Berling and Slot* [13] *for AISI 304 stainless steel by Eq 1, showing interaction of frequency and stress range on plastic strain range for several temperatures.*

range and frequency, where the term $\Delta\sigma\nu^{-k_1}$ is called the frequency modified stress range. Referring to Table 1, the coefficients of A, n', and k_1 are given. It is seen that the cyclic strain hardening exponent decreases rapidly with increasing temperature, as does A, while k_1 increases. The negative value of k_1 at 450 C implies some cyclic strain aging [*15*].

The use of frequency rather than strain rate for the high-temperature cyclic stress-strain behavior is consistent with other fatigue equations introduced in what follows. It is, however, more common to use strain rate in preference to frequency for quantifying high-temperature deformation behavior, and this is easily done for a triangular waveform if the plastic strain rate is defined as $\dot{\epsilon}_p = 2\Delta\epsilon_p\nu$. Equation 1 then becomes

$$\Delta\sigma = B\Delta\epsilon_p^{n_1'}\dot{\epsilon}_p^{m} \quad \ldots\ldots (2)$$

where $B = A/2k_1$, $n_1' = n' - k_1$ and $m = k_1$. Equation 1 or 2 may be useful in analytical procedures for elastoplastic cyclic stress-strain solutions [*1,2*].

Further characterization of the high-temperature fatigue behavior can be accomplished with the aid of two additional equations. The first of these is a high-temperature modification [*14–16*] of the low-temperature Coffin-Manson equation, relating the plastic strain range, fatigue life, and frequency of cycling,

$$\Delta\epsilon_p = C_2(N_f\nu^{k-1})^{-\beta} \quad \ldots\ldots (3)$$

One form of this equation is shown in Fig. 5, for AISI 304 stainless steel at the three temperatures of interest. Here the frequency and life are combined into a term called the frequency-modified fatigue life, a useful parameter for relating frequency of cycling and cycles to failure. Figure 5 shows the deleterious effect of temperature on fatigue life as expressed in terms of the plastic strain range. Note the increasingly negative slope with increasing

TABLE 1—*Coefficients for high-temperature fatigue equations for several materials.*

Coefficient	A286–595 C		AISI 409, deg F	AISI 304, deg F		AISI 316, deg F		AISI 348, deg F		Udimet 500, deg F
	Air	Vacuum	427	650	816	650	816	650	816	816
A'	446 000	690 000	125 000	226 000	68 000	216 500	99 000	152 100	88 400	160 740
β'	0.12	0.16	0.052	0.187	0.094	0.143	0.117	0.102	0.131	0.132
k_1'	0.045	0.12	0.007	0.089	0.071	0.074	0.091	0.038	0.127	0.075
A	427 000	916 000	118 000	214 100	63 260	266 000	94 250	181 900	106 860	520 000
n'	0.122	0.35	0.064	0.258	0.105	0.24	0.151	0.191	0.224	0.185
k_1	0.0026	0.116	0.0013	0.053	0.053	0.052	0.079	0.015	0.115	0.057
C_2	1.32	0.37	2.65	1.108	1.72	0.354	1.081	0.382	0.365	0.0736
k	0.65	0.99	0.889	0.81	0.81	0.86	0.90	0.77	0.92	0.864
β	0.97	0.44	0.831	0.707	0.87	0.57	0.74	0.527	0.56	0.712
R_1	2.36	5.78	1.36	2.0	5.72	3.29	6.0	2.36	9.3	3.71
R_2	2.24	1.03	1.29	1.55	1.54	1.38	1.26	1.70	1.21	1.37
$E \times 10^{-6}$	25.0	25.0	27.1	21.6	18.8	21.95	18.4	21.8	19.05	25.1

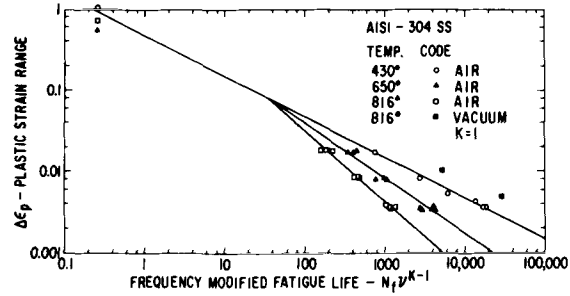


FIG. 5—*Representation of data of Berling and Slot* [13] *for AISI 304 stainless steel by Eq 5, showing plastic strain range versus frequency-modified fatigue life at several temperatures in air. Vacuum data at 816 C.*

temperature and the convergence at low life. Similar behavior has been found for several materials [*19*].

By eliminating the plastic strain range between Eqs 1 and 3, a high-temperature form of the low-temperature Basquin equation [*17,18*] results, or

$$\Delta\epsilon_e = \frac{\Delta\sigma}{E} = \frac{A'}{E} N_f^{-\beta'} \nu^{k_1'} \quad \ldots\ldots\ldots\ldots\ldots\ldots (4)$$

where $A' = AC_2^{n'}$, $\beta' = \beta n'$, $k_1' = \beta n'(k - 1) + k_1$. A complete list of coefficients for several materials found by regression analysis of test data is given as Table 1. Equations 3 and 4 provide a handy way of representing high-temperature fatigue, particularly when they are rewritten by combining the strain range and frequency, such that $\Delta\epsilon_p \nu^{\beta(k-1)}$ is called the frequency modified plastic strain range, and $\Delta\epsilon_e \nu^{-k_1'}$ is the frequency modified elastic strain range. Using a representation for elastic and plastic strain ranges suggested by Manson at low temperatures [*20*], we have Fig. 6, the frequency modified elastic and plastic strain ranges versus cycles

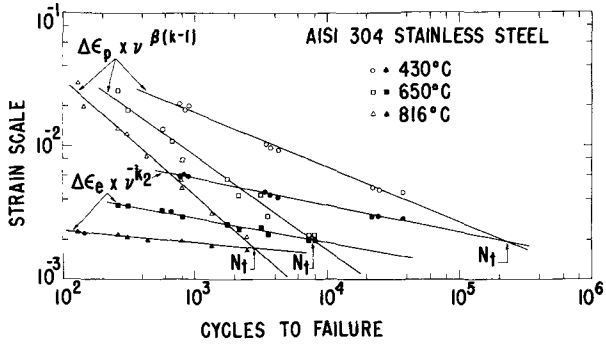


FIG. 6—*Representation of data of Berling and Slot* [13] *for AISI 304 stainless steel by Eqs 3 and 4, showing frequency-modified elastic and plastic strain range at several temperatures in air.* N_t *is transition fatigue life.*

to failure, for the three temperatures, 430, 650, and 816 C, for AISI 304 stainless steel.

Several features arising from the increasing temperature on fatigue phenomenology are observed in this figure. We see the increasingly negative slope and decreasing life of the plastic strain cycles to failure representation, also observed in Fig. 5. Increasing temperature and concomitant softening causes a progressive decrease in the elastic strain (or stress range/elastic modulus). With increasing temperature the transition fatigue life N_t (the life where the elastic and plastic strain ranges are equal) shifts to lower values of life. More will be said of this term at a later point. Increasing temperature is seen to have a small effect on the exponent β'.

From an engineering design viewpoint the total strain range $\Delta\epsilon$ is a more commonly used quantity since from it the pseudostress range $E\Delta\epsilon$ can be derived. The total strain range can be found analytically by combining Eqs 3 and 4 or

$$\Delta\epsilon = C_2(N_f\nu^{k-1})^{-\beta} + \frac{A}{E} C_2{}^{n'} N_f{}^{-\beta n'} \nu^{-\beta n'(k-1)+k_1} \quad \ldots\ldots\ldots (5)$$

The similarity of this equation with Manson's "universal slopes" low-temperature equation [*20*] or

$$\Delta\epsilon = D^{0.6} N_f{}^{-0.6} + \frac{3.5\sigma_u}{E} N_f{}^{-0.12} \quad \ldots\ldots\ldots\ldots\ldots (6)$$

can be shown. Letting $k = 1$, and $k_1 = 0$, the frequency terms are eliminated and if $C_2 = D^{0.6}$, $\beta = 0.6$, $n' = 0.2$, and $A = 3.5\sigma_u/D^{0.12}$ Eq 5 transforms to Eq 6. Since D is the true fracture strain and σ_u is the ultimate strength, some feeling for the several coefficients of Eq 5 can be established.

Equation 5 can be used to show the effect of temperature and frequency on the total strain fatigue behavior of metals at high temperature. Using AISI 304 stainless steel as an example, with the help of the coefficients of Table 1, Fig. 7 results. Two frequencies are considered, 10 and 0.001 cpm, and the three temperatures. Note the increasingly strong frequency effects as the temperature is raised. Further, note the large difference in life at intermediate strains. For example at a strain of 0.003, the life at 10 cpm decreases from 5×10^5 cycles to 7×10^3, a 70 fold decrease, for a change in temperature from 450 to 816 C. At 0.001 cpm on the other hand the lives are 5×10^5 and 260, a 1900fold decrease. It should be pointed out that this latter comparison is based on an extrapolation of test data to lower frequencies on the assumption that the frequency exponents of Eq 5 are independent of frequency. More will be said about the validity of this assumption later.

Close examination of Fig. 7 shows a knee developing in the fatigue curve as the temperature is increased. This knee is a result of a shift or transition in the dominant strain component of Eq 5 from plastic to elastic

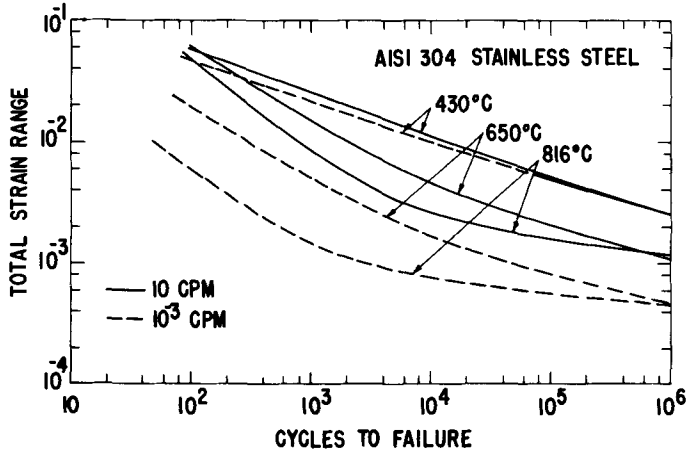


FIG. 7—*Representation of data of Berling and Slot* [13] *for AISI 304 stainless steel by Eq 5, showing total strain range versus cycles to failure for two frequencies at several temperatures in air.*

strain at higher lives (say 10^5 cycles) as the temperature is raised. This effect is also apparent in Fig. 6. The transition fatigue life characterizes this behavior.

Transition Fatigue Life

Failure by low-cycle fatigue is commonly considered to occur for lives less than 10^4 or 10^5 cycles. This definition arose from early concern in the low-cycle fatigue phenomenon for metals which were sufficiently ductile that cyclic effects developed at lives in the order of 10^4 or 10^5 cycles. Here significant plastic strains occurred, and this led to a field of interest apart from the more classical high-cycle phenomenology. It is now apparent that this definition of low-cycle fatigue is unsatisfactory, particularly when lower ductility metals are considered from the low-cycle fatigue view and as a more unified view of the entire fatigue spectrum develops. A more rational definition for separating the high- and low-cycle regimes should be based on whether plastic effects are important, independent of the strength, or ductility of the material. For this reason the transition fatigue life is a useful concept. The transition fatigue life need not be defined as occurring when the ratio of the plastic to elastic strains are equal; in fact, a ratio of less than unity might be preferred for reasons to be discussed at a later point.

Landgraf [*18*] has shown how the transition fatigue of steels is changed by the hardness of the material. It is seen by an examination of Fig. 5 that temperature also changes the transition fatigue life. A quantitative expression for N_t can be derived by equating Eqs 3 and 4. Thus

$$N_t = \left(\frac{A'}{C_2 E}\right)^{1/(\beta'-\beta)} \nu^{(k_1-\beta(1-k))/(\beta'-\beta)} \quad \ldots\ldots\ldots\ldots\ldots\ldots (7)$$

Since A' is a measure of strength, C_2 a measure of ductility, and $1/(\beta' - \beta)$ is negative, increasing strength and decreasing ductility lower the transition fatigue life. Using the constants of Table 1, at a frequency $\nu = 1$ cpm, or reading directly from Fig. 4, $N_t = 231\,000$, 7800, or 2800 cycles for temperatures of 430, 650, and 815 C, respectively. Substantially lower transition fatigue has been found to occur for the cast nickel-base superalloys because they combine high strength and low ductility. For cast Udimet 500 at 816 C, it was found that $N_t = 20$ [*16*].

The importance of the knowledge of the transition fatigue life cannot be overemphasized. When compared to a specific life of interest it distinguishes:

1. Method of testing the material.
2. Analytical procedures for attacking the problem.
3. Operating initiation and crack growth law.
4. Degree to which mean stress and rachetting can be factored into the problem.

Referring to Fig. 1, assume that N_d is the design life for initiating a crack in a structure of a size equivalent to that in the specimen test. Then if $N_d \leq N_t$, low-cycle fatigue test procedures are required for material evaluation while if $N_d \gg N_t$, high-cycle fatigue information is more meaningful. When $N_d \leq N_t$, elastoplastic solutions are required for design, but if $N_d \gg N_t$, linear elastic stress analysis approaches are preferable. Again, if $N_d \leq N_t$, mean stresses will relax, and rachetting processes are possible [*21–23*], while when $N_d \gg N_t$, mean stresses and residual stresses play an important part in the life of the structure.

If N_d represents a design life associated with crack propagation, and $N_d \leq N_t$, a crack growth law based on gross plastic strains is required, [*24*] while if $N_d \gg N_t$, elastically controlled crack growth laws are applicable [*25,26*].

Failure Criteria at High Temperature

The principal objective in formulating a criterion for fatigue failure at high temperature is to properly account for the damaging effect of time and temperature. A typical problem facing the designer is how to deal with extended hold periods with occasional stress reversals. Referring again to Fig. 1, pressure or centrifugal elastic stresses in a structure induce in a notch a constant strain, while removal and reapplication of these stresses leads to a plastic strain reversal in the notch, and a subsequent stress relaxation. The events are shown in Fig. 8. Degradation in fatigue life under such circumstances can be quite severe as many investigators have shown. Figure 9, from the work of Berling and Conway [*27*], shows the effect of tensile strain hold periods on the fatigue life of AISI 304 stainless steel at 650 C.

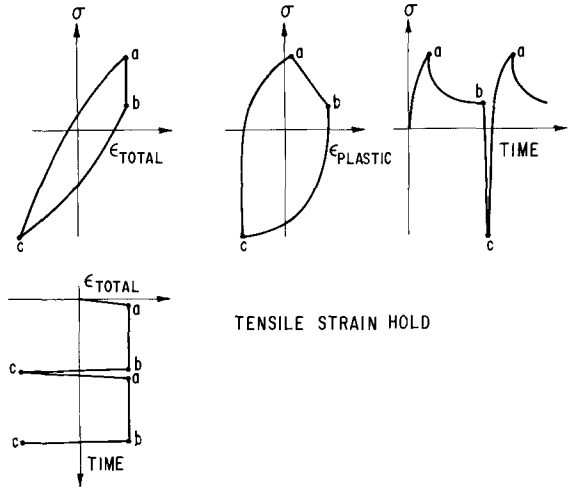


FIG. 8—*Effect of constant tensile strain hold periods of stress-strain-time records-schematic.*

Criteria for predicting failure under such conditions can be broken down into two categories. They are: (*a*) consideration of cyclic and time dependent effects as separate phenomena, determining the damage fraction of each and combining, usually by assuming a linear damage accumulation rule, and (*b*) consideration of the cyclic and time effects as a single process expressible in terms of several variables including the strain rate or frequency of the cycle.

Krempl and Wundt [*28*], Esztergar and Ellis [*29*], and Coffin and Goldhoff [*30*] have reviewed some of these approaches in more detail than is possible here. Briefly, the linear creep-fatigue damage criterion stems from the early work by Lazan on elevated temperature experiments involving cyclic stresses with superimposed mean stress [*31*]. The linear

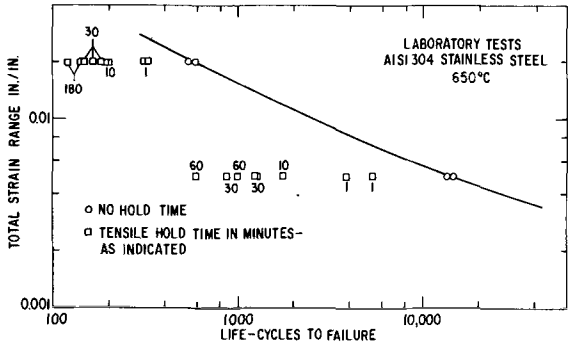


FIG. 9—*Effect of holdtime on life of AISI 304 stainless steel at 650* C [27].

damage rule originally proposed by Robinson [*32*], for varying stress-rupture life prediction, assumes that the damage fractions φ, for fatigue and creep, total to unity, or

$$\varphi_{\text{fatigue}} + \varphi_{\text{creep}} = 1 \text{ (at failure)} \quad \ldots\ldots\ldots\ldots\ldots\ldots (8)$$

Various experimenters, including Taira and Ohnami [*33*], Swindeman [*34*], and Manson et al [*35*], have followed this approach. Recently, Lagneborg and Attermo [*36*] showed that a linear creep-damage rule did not apply in experiments on a 20Cr–35Ni stainless steel subjected to cyclic strains and hold periods and a steady stress at 700 C. Rather, an interaction term was additionally needed, which was the product of the life fraction and time fraction. An explanation for the inadequacy of Eq 8 in representing the time-dependent fatigue behavior will be discussed in another paper in this conference [*37*].

The second category of failure criteria, (*b*) considers the complex straining as a time-dependent fatigue process. Manson and Halford [*38*] extended Manson's method of universal slopes [*20*] to elevated temperature by introducing a lower bound fatigue life as 10 percent of the life predicted by Eq 6. A still lower life is predicted, based on creep considerations, given by Eq 8. More recently, Manson et al [*39*] have developed a different approach to account for the time dependent portions of the cycle by separating the nonelastic cyclic strains into plastic and creep and summing the separate life fractions to unity. They then compare this "strain-range partitioning" method to their 10 percent rule [*38*]. Timo [*40*] developed fatigue curves for constant hold periods by combining low-cycle fatigue tests having different hold periods with creep-rupture information to obtain high-cycle fatigue data points on these curves. Here the assumption is made that the fatigue life corresponding to a particular rupture strength is the time to rupture in the rupture test divided by the hold period of the fatigue test. Conway et al [*41*] propose that holdtime lives can be predicted from tests for no hold-times, based on the linearity on a log-log plot of the time to fracture and the length of this hold period in tension-hold-only tests (such as Fig. 9) from which the time to fracture for any holding time can be calculated. Figure 10 shows such a representation.

The concept of Conway et al fits quite naturally into the fatigue Eq 5. It has been suggested [*15*], that holdtime behavior could be predicted from Eq 5 by assuming that

$$\nu = \frac{1}{t_c' + t_h} \quad \ldots\ldots\ldots\ldots\ldots\ldots\ldots\ldots (9)$$

where t_c' is the time for strain reversal and t_h is the hold period for each cycle. Using the appropriate coefficients of Table 1, obtained from the data of Berling and Slot [*13*], good agreement with the Conway et al representation is shown in Fig. 10. The dashed lines can be found by cross plotting

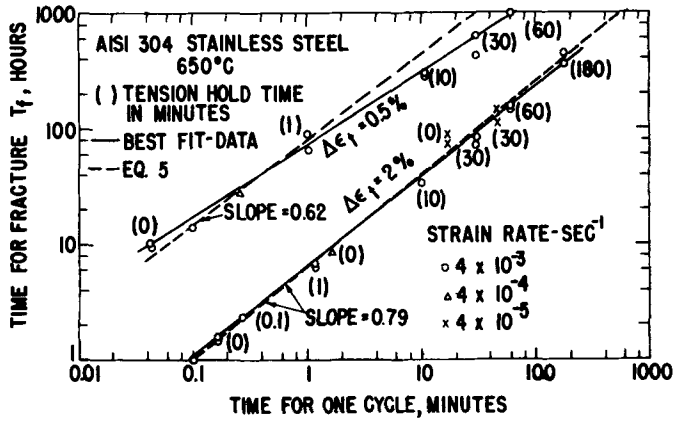


FIG. 10—*Comparison of period of cycle versus time to failure for holdtime tests with analytical results derived from Eq 5.*

Fig. 7 at the appropriate total strain range and determining from the corresponding frequency and life the period and total failure time. Conway et al indicate different slopes for log period versus log time to failure for different strain ranges. These can be found quantitatively by examining Eqs 3 and 4. Since $\tau = 1/\nu$ and $t_f = N_f/\nu$, and assuming the strains are large ($\Delta\epsilon_t \approx \Delta\epsilon_p$), Eq 3 becomes

$$t_f = \left(\frac{C_2}{\Delta\epsilon_p}\right)^{1/\beta} \tau^k \quad \ldots\ldots\ldots\ldots\ldots\ldots\ldots\ldots (10)$$

Now assuming the strains are small ($\Delta\epsilon_t \approx \Delta\epsilon_e$), Eq 4 becomes

$$t_f = \left(\frac{A'}{E\Delta\epsilon}\right)^{1/\beta'} \tau^{1-(k_1'/\beta')} \quad \ldots\ldots\ldots\ldots\ldots\ldots\ldots\ldots (11)$$

Using Table 1, for AISI 304 stainless steel at 650 C, the slope ranges from 0.81 at high strains to 0.522 for low strains. At intermediate strains the log t_f versus log τ relationship is not linear.

Kanazawa and Yoshida [*42*] have investigated the frequency and holdtime behavior of a 17Cr-10Ni-2Mo austenitic stainless steel. They suggest that strain rate rather than frequency correlates better with holdtime results.

Although attention has been drawn to the effect of frequency and holdtimes on the austenitic stainless steels, it is also an important factor in cast and directionally solidified nickel-base superalloys at high temperature. As indicated earlier, because of their generally low ductility and high strength, the transition fatigue life for this class of materials is low, such that in their design life range the behavior is one of high-cycle fatigue. Translated in terms of a phenomenological description of their behavior, Eq 4 is applicable, while from physical considerations, the failure mecha-

nism is a result of crack growth in an elastic regime. As the temperature is raised, two effects occur simultaneously: (*a*) creep deformation becomes an increasingly important mode of deformation and (*b*) the fracture mode becomes increasingly intergranular. Since creep deformation leads to greater strain localization in the plastic zone at the crack tip, and intergranular fracture produces a more extended crack for a given plastic strain, a decreasing frequency can greatly accentuate fatigue failure. This behavior can be expressed analytically from Eq 4 or

$$\frac{N_{f_{\nu=\nu_1}}}{N_{f_{\nu=\nu_2}}} = \left(\frac{\nu_1}{\nu_2}\right)^{k_1'/\beta'} \quad \ldots\ldots\ldots\ldots\ldots\ldots\ldots\ldots (12)$$

Table 2 shows the trend with temperature for two nickel-base superalloys. Here the life ratio N_{f_1}/N_{f_2} is found when $\nu_1/\nu_2 = 10$.

TABLE 2—*Coefficients for Eqs 4 and 12.*

Material	Temperature, deg C	A'	β'	k'	k'/β'	$\frac{N_{f_1}}{N_{f_2}}$ for $\frac{\nu_1}{\nu_2} = 10$
Cast U-500	815	160 740	0.132	0.075	0.569	3.74
Directionally Solidified	760	116 250	0.0932	0.0238	0.255	1.80
Mar M-200	926	61 440	0.117	0.1043	0.891	7.75

Environmental Effects

From physical considerations, the central question in high-temperature fatigue is what causes the degradation of fatigue properties at these temperatures with increasing time. Emphasis on creep-fatigue criteria for failure prediction would suggest that creep and rupture mechanisms play an important role. In fact, fatigue fractographic evidence, generally shows a tendency towards intergranular fracture with increasing temperatures and times to failure, and this is consistent with stress-rupture fractography. On the other hand, evidence can be cited to support the position that the time-dependence of high-temperature fatigue is the result of the environment, and more specifically, oxygen. Not only is there the findings of several investigators, including White [*43*], Achter et al [*44*], and Nachtigall et al [*45*], showing the increase in fatigue life in vacuum, but also there is the tangible evidence that most fatigue cracks produced by slow cycling at elevated temperature are nearly always filled with oxide products. Additionally, in an investigation of the damage and fracture mechanisms of cast Udimet 500 in high-temperature fatigue, surface ridging at grain boundaries was found to be the source of crack nucleation [*46*]. In A286, a highly localized surface oxidation was identified as the nucleation site for fatigue cracks under high-temperature low-cycle fatigue [*47,48*]. In Fig. 11 surface

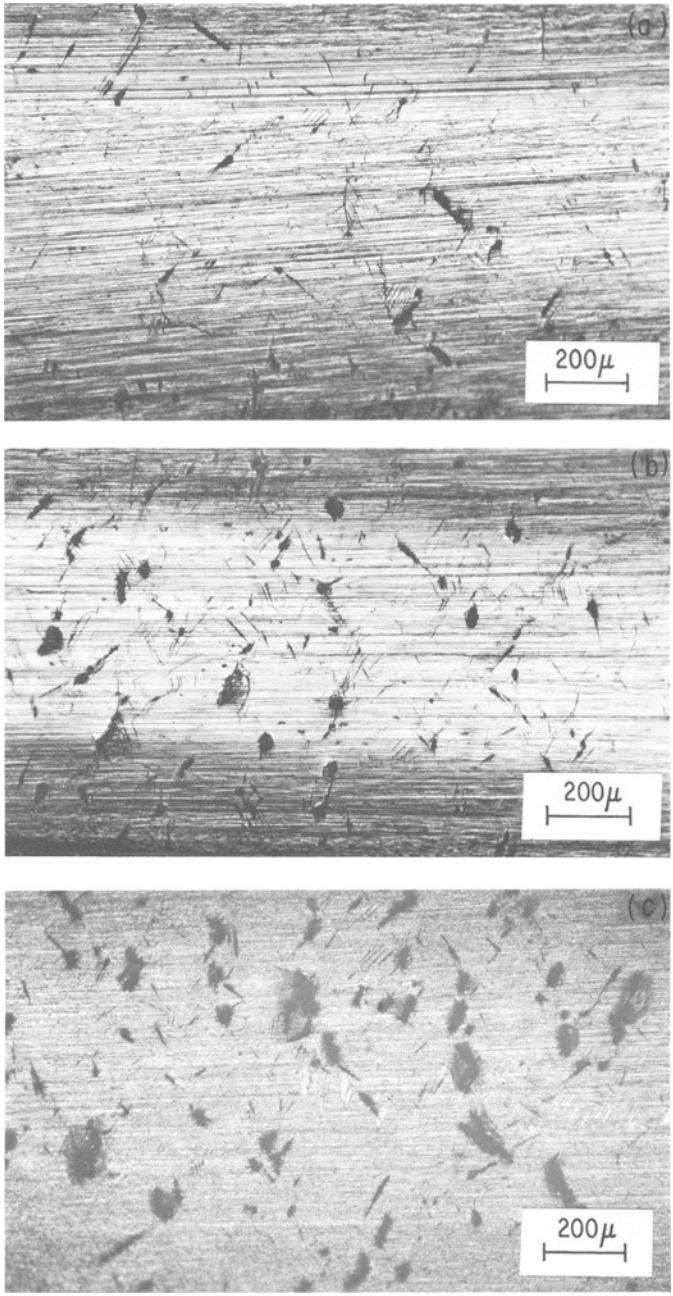


FIG. 11—*Surface markings on A286 test specimens at 593 C in air.* $\Delta\epsilon_p = 800 \times 10^{-6}$: (a) $\nu = 5.6$ *cpm*, (b) $\nu = 1$, *and* (c) $\nu = 0.22$ *cpm* [48].

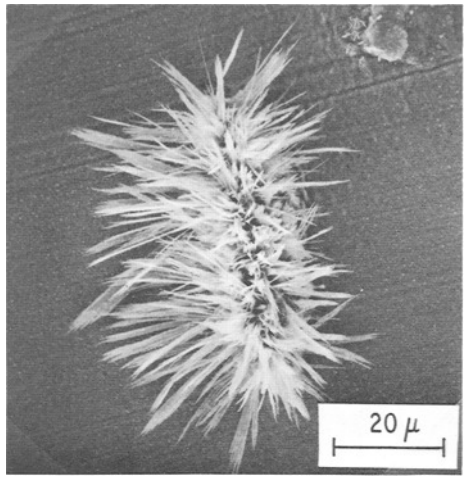


FIG. 12—*Oxide growth on fatigue crack nucleus. A286 at 593 C in air.* ν = *0.2 cpm plus 290 second tension hold period* [48].

markings found on A286 hourglass shaped test specimens at 1100 F are shown to become increasingly heavy as the frequency is lowered. Examination of the localized oxide formed at low frequency reveals the fascinating structure shown in Fig. 12.

Recently some controlled strain experiments were conducted on A286 at 1100 F in high vacuum and on cast Udimet 500 at 1500 F, in push-pull loading. In both of these materials the strong frequency effect found in air was seen to disappear when the experiments were conducted in a vacuum of 10^{-8} torr. These results are shown in Figs. 13 and 14. It was also observed

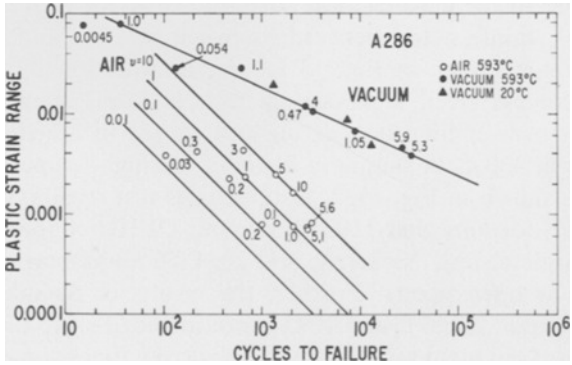


FIG. 13—*Plastic strain range versus fatigue life for A286 in air and vacuum at 593 C. Numbers adjacent to test points indicate frequency in cpm. Solid lines are regression analysis of Eq 5* [48].

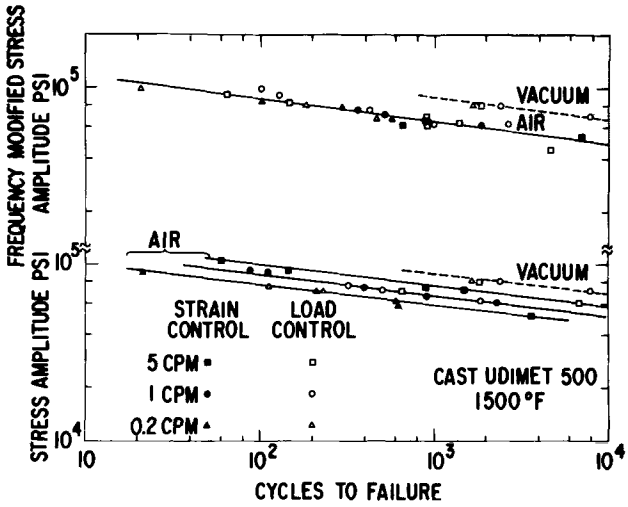


FIG. 14—*Test results of stress amplitude versus fatigue life for cast Udimet 500 in air vacuum at 816 C (lower curve). Air tests both stress and strain control; vacuum tests stress control only. Frequency-modified stress amplitude versus fatigue life for same test results, after Eq 4* [48].

that the mode of fracture in this medium for each of these materials was transgranular in contrast to the intergranular fractures found in air. Based on these and other observations, it was concluded that, for the frequencies employed, the degradation in fatigue life found in air at elevated temperature with decreasing frequency is a result of the environment.

A subsequent study [*49*] has revealed additional information on the effect of high vacuum on the low-cycle fatigue behavior of A286, Nickel A, C1010 steel, and AISI 304 stainless steel. For example, there appears to be little difference in the plastic strain range-life behavior of A286, Nickel A, and AISI 304 stainless steel between room temperature and elevated temperature. This is shown in Fig. 13 for A286. Additionally in Fig. 5 for AISI 304 stainless steel, high-vacuum tests at 816 C show a substantial improvement over similar tests in air and exceed in life those tests conducted in air at 430 C. A summary figure of the high-temperature vacuum test results is shown in Fig. 15. It also includes test results obtained many years ago [*50*] for annealed 1100 aluminum, OFHC copper, C1018 steel, AISI 347 stainless steel, Nickel A, and 2024 T6 aluminum in air at room temperature as open points. Further, the results of Swindeman [*51*] on D43 columbium at 20, 871, and 1093 C are included since these tests were also performed in high vacuum. Also, data on the fatigue behavior of tantalum [*52*] at 315, 593, and 732 C in high-purity argon have been added, on the basis that the environment of these experiments was sufficiently inert to be considered applicable in the present comparison. A single test point for In 718, a nickel-base superalloy, tested at 648 C, is also included.

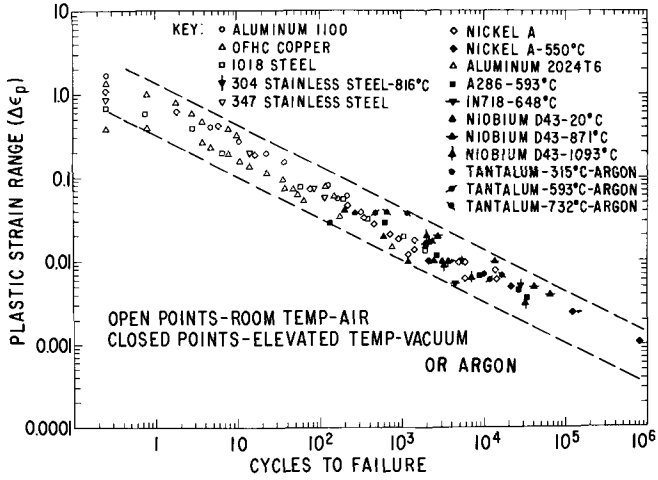


FIG. 15—*Summary plot of plastic strain range versus cycles to failure for several metals in room-temperature air or high-temperature vacuum or argon* [49].

The dashed lines of Fig. 15 define the broad scatterband of the data (excluding the tensile ductility of 2024T6) and are drawn with a slope of $-\frac{1}{2}$. It is readily seen that the high-temperature, high-vacuum results are a continuation of the room-temperature results. This compilation of data strongly suggests that in the absence of environmental influences, the two-slope plastic strain range-life relationship, typically shown in Fig. 5, disappears and is replaced by a single slope, narrow scatterband, straight line of slope $\beta = 0.5$ for all the materials considered.

It is important to note that in all the tests used in the plotting of Fig. 15, failure was produced by fatigue cracks which propagated transgranularly. This observation is consistent with a model proposed earlier [*19*] suggesting that the two-slope behavior of Fig. 5 is the result of a progressive transition in fracture mode from transgranular to intergranular with elevated temperature in air. Decreasing frequency and plastic strain aid in this transition. Assuming a reaction zone at the tip of a propagating crack due to oxidation increasing temperature and decreasing frequency enhance this zone, while decreasing plastic strain confines the crack advance to the more damaged portion of this zone. It is further argued that the reaction zone is selective to grain boundaries because of the greater activity due to stress, concentration gradients, precipitates, etc. Finally, for a given plastic strain, intergranular cracks advance further than transgranular cracks all else being equal. Thus, in Fig. 5, higher temperatures, lower plastic strains, and lower frequencies lead to decreased lives. Now, if the crack propagation is at all times transgranular, as is observed in all the high-vacuum experiments, this is the result of the elimination of a reaction zone, and its deleterious influence on crack propagation.

One interesting consequence of Fig. 15 is its relation to models predicting the exponent β of Eq 3. Morrow [*53*] has proposed that $\beta = 1/(5n' + 1)$ where n' is the cyclic strain hardening coefficient; while Tompkins [*54*] has developed a theory for crack propagation from which $\beta = 1/(2n' + 1)$. Knowing n' to be a function of temperature and material, and assuming it to be independent of environment, it is difficult to reconcile the predicted values of β with the constant value shown in Fig. 15. The implication here is that it is the mode of cracking rather than the cyclic strain hardening exponent that governs fatigue life.

High-Strain Crack Propagation

Referring again to Fig. 1, following initiation and early growth, the crack grows by propagation through the plastic zone. Methods for considering this aspect of the problem are not well developed; however, the work of Boettner et al [*55*], Weiss [*56*], and Tompkins [*54*] have proposed models for crack growth. A common fracture of these models is that the crack growth rate dc/dN is proportional to crack length c or log c is proportional to N. Solomon [*24*] has studied the growth of cracks from single side notch plane stress specimens subjected to a constant plastic strain range as a function of temperature and frequency. Based on results from 1018 steel at temperatures from 25 to 350 C and A286 at 1100 F he has developed a crack growth law

$$\frac{dc}{dN} = \frac{\varphi c(\Delta\epsilon_p)^{\alpha}}{\epsilon_f{}^{\alpha'}} \nu^{k-1} \quad \ldots\ldots\ldots\ldots\ldots\ldots\ldots\ldots (13)$$

where φ and α' are constants, $\alpha = 1/\beta$ from Eq 5, ϵ_f is the fracture ductility. The format of this relationship follows closely the frequency-modified fatigue law, Eq 5. This work will be discussed in more detail in another paper presented at this conference [*37*].

High-strain crack propagation experiments are particularly useful in evaluating the effect of a broad frequency range on fatigue behavior. It will be shown [*37*] that, at least for A286 at 1100 F, three failure regimes appear to exist, depending on the frequency. At very low frequencies, the behavior is time dependent, but not cycle dependent. Here $k = 0$ in Eq 13. The physical processes involved may be associated with stress–rupture or environmental damage. At low to intermediate frequencies the failure process is the result of an environmental interaction, as determined by comparative crack growth measurements in air and vacuum. Here $k = 0.49$. Finally, at very high frequencies, a time-independent, cycle-dependent failure process dominates. This is based on studies by Organ and Gell [*57*] on wrought Udimet 700 at 1400 F and Tien and Gamble [*58*] who found that single crystals of Mar-M200 at room temperature behave in air at 20 000 cpm in a manner comparable to specimens cycled at 10 Hz in vacuum.

Crack Growth in the Elastic Regime

The literature abounds with papers dealing with fatigue crack growth through an elastic stress field and numerous crack growth laws relating dc/dN to ΔK or K_{max}, the stress intensity range or the maximum stress intensity to some power have been proposed. At temperatures sufficiently high for time dependent effects to be important, it has been shown that crack growth rates can be similarly represented provided time effects have been properly taken into account. James [*59*], for example, has found that, for AISI 304 stainless steel at 1000 F, at low values of ΔK a crack growth law in the form of

$$\frac{dc}{dN} = B(\Delta K)^m \quad \ldots\ldots\ldots\ldots\ldots\ldots\ldots\ldots (14)$$

exists where B is a function of frequency. Popp and Coles [*25*] have studied the effect of holdtimes on crack growth of In 718 at 1000 F and find that the coefficient B in Eq 14 can be represented by a Larson-Miller type parameter relating temperature and holdtime per cycle.

Greater emphasis needs to be placed on the development of crack growth laws in the elastic regime at high temperature. As was pointed up earlier, when applications are such that $N_d \gg N_t$, such approaches constitute the only rational way to treat the fatigue problem. It might further be pointed up that many aircraft engine materials exhibit transition fatigue lives in the order of 100 cycles at temperature such that at design lives of 10 000 cycles elastic crack growth concepts apply.

Deformation and Fracture Aspects of Ratchetting

Since the subject of ratchetting will be dealt with at some length in this symposium, it would be well to discuss this briefly here. It has been observed frequently that, in the presence of cyclic plastic strain, simultaneously applied mean stresses cause progressive monotonic deformation, or ratchetting [*21–23*]. Other manifestations of this same phenomenon are plastic instabilities or shape changes in ductile metals subjected to large cyclic plastic strains, [*21*] or, for mixed cyclic and monotonic strains, a resulting flow stress for monotonic strain which, in the limit, is determined by the stress range of the stabilized hysteresis loop [*60*]. Although little work has been done to describe the flow rules for such processes, it has been suggested [*23*] that the ratchetting rate, $\dot{\epsilon}_p$ (strain advance per cycle) can be expressed as

$$\dot{\epsilon}_p = A\sigma_m \times \frac{\Delta\epsilon_p}{\Delta\sigma} \quad \ldots\ldots\ldots\ldots\ldots\ldots\ldots\ldots (15)$$

where σ_m is the mean stress, $\Delta\epsilon_p$ the plastic strain range, and $\Delta\sigma$ the cyclic stress range. Equation 15 is similar to a plasticity solution derived by

Swift [*61*] for the progressive growth of a cyclically bent beam subjected simultaneously to an axial stress. Equation 15 can be also expressed as

$$\dot{\epsilon}_p = B\sigma_m \times \frac{\Delta\epsilon_p}{\Delta\epsilon_e} \quad \ldots\ldots\ldots\ldots\ldots\ldots\ldots\ldots\ldots\ldots (16)$$

Thus the process is a low-cycle fatigue phenomenon, and the transition fatigue life (where $\Delta\epsilon_e = \Delta\epsilon_p$) characterizes the regime where a particular material will be sensitive to the phenomenon. For a given plastic strain and mean stress, as the temperature is raised, $\Delta\sigma$ and $\Delta\epsilon_e$ decrease, and the ratchetting rate becomes more significant. Further, at high vacuum, the life is extended, as is the total ratchetting strain $\epsilon_r = \dot{\epsilon}_p N_f$. Hence large ratchetting strains can be expected, and this is confirmed as seen in Fig. 16 where a pronounced specimen shortening and minimum diameter fattening (except at the diameter measuring probes) is observed.

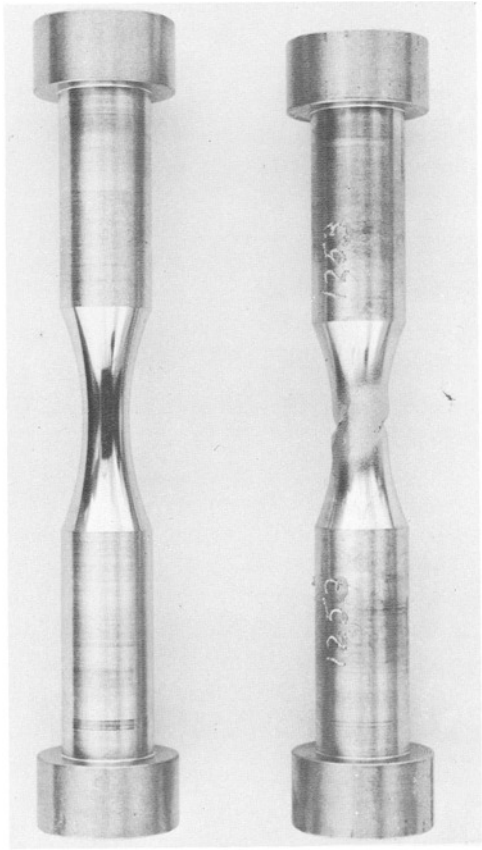


FIG. 16—*Appearance of specimen of AISI 304 stainless steel following vacuum test at 816* C. ν = *1 cpm*, $\Delta\epsilon_p$ = *0.01*, N_f = *6200* [49].

Similar arguments can be used to consider mean stress or residual stress relaxation. It is apparent from Eq 16 that the ratio of plastic to elastic strain must be very low to prevent mean stress relaxation.

Many situations occur in practice where cyclic strains and mean stresses are superimposed and where ratchetting processes or mean stress relaxation can occur. There is little experimental work or predictive approaches developed to account for these situations, particularly from strain considerations. The work of Yamanouchi [*62*] is of interest here. He reports fatigue studies on thin tubes involving steady torsion, an axial cyclic strain, and a cyclic temperature for three materials—ASTM 302-B, AISI 304, and SCM 3, a 1Cr-0.2Mo steel. He finds that, despite torsional strain ratchetting, there is no effect of these strains on the low-cycle fatigue resistance of the material. Further, the ratchet strain increases with the repetition of axial strain, the magnitude of the steady torsional stress, and axial strain amplitude.

A related study [*60*] on Nickel A at room temperature was conducted with a mixed cyclic and monotonic strain program. Specific ratios were maintained of total cyclic strain range to the longitudinal strain advance per cycle until failure, and from these tests a failure criterion was found, where

$$\left(\frac{N_f}{N_{f_0}}\right)^{\beta} = 1 - \frac{\epsilon_f}{\epsilon_{f_0}} \quad \ldots\ldots\ldots\ldots\ldots\ldots\ldots\ldots\ldots\ldots (17)$$

where

N_f = fatigue life for a total mean strain ϵ_f,
N_{f_0} = pure fatigue life, and
ϵ_{f_0} = fracture ductility in simple tension.

Also

β = 0.563 for Nickel A at room temperature.

According to Eq 17, for strain ratios less than 0.05, the effect on fatigue life would be small, in accord with Yamanouchi.

Another way to consider the effect of cyclic and monotonic strain is to compare the ratio of the mean or creep strain to the accumulated cyclic plastic strain after many cycles. When this ratio is small, the corresponding mean stress will likewise be small and the effect on fracture negligible. Unfortunately, this question has not been studied systematically at elevated temperature.

Notches

Although the literature abounds with various treatments of the notch problem at room temperature, relatively little work has been done on the elevated temperature low-cycle fatigue resistance of notched bars where

time-dependent effects are important. Although not directly related to the question of time, of interest are the experiments of Krempl [*63*] on notched bars of three low-strength structural steels, a 2.25Cr-1Mo steel and AISI 304 stainless steel subjected to fully reversed loads at room temperature and 550 F. Since the notch root undergoes cyclic plastic strain, comparisons of the strain in this region with smooth bar data are suggested. Notch root strain measurements were compared with smooth bar fatigue results for equivalent lives. It was found that neither the axial strain range nor estimates of the effective strain range based on the octahedral shear strain or the maximum shear strain correlated well. On the other hand Mowbray and McConnelee [*1,2*] have applied finite element analysis techniques to these geometries, using cyclic stress-strain curves and find good agreement with smooth bar results.

An approach which follows that of Topper et al [*9*] is currently being studied at our laboratory. From Neuber's rule it can be shown that

$$K_f \Delta S = (\Delta\sigma \Delta\epsilon E)^{1/2} \quad \ldots\ldots\ldots\ldots\ldots\ldots\ldots\ldots (18)$$

where ΔS is the nominal stress range applied to a notched member whose fatigue concentration factor is K_f and $\Delta\sigma$ and $\Delta\epsilon$ are the local stress and strain ranges in the notch root. By assuming conditions at the notch root to be equivalent to those in a smooth bar, the quantity $(\Delta\sigma\Delta\epsilon E)^{1)2}$ can be evaluated from smooth bar data for a particular life, and ΔS determined. For high temperature where time dependency must be considered, it is attractive to combine the high-temperature fatigue Eqs 4 and 5 with Eq 18, after rewriting or

$$K_f \Delta S = E[\Delta\epsilon_e{}^2 + \Delta\epsilon_e \Delta\epsilon_p]^{1/2} \quad \ldots\ldots\ldots\ldots\ldots\ldots\ldots\ldots (19)$$

Since time effects are introduced through the frequency in Eqs 4 and 5, Eq 18 or 19 provide means for evaluating frequency and holdtime effects in notches.

Figure 17 shows some preliminary results from the utilization of this technique. Here specimens of three different cylindrical notch geometries, K_t = 1.5, 2.0, and 3.0, were prepared and subjected to fully reversed uniaxial loads at several stress levels and frequencies. The material was A286 at 1100 F. This figure compares the notch bar fatigue results (the individual test points) with smooth bar data expressed in the form of Eq 18 or 19, using Eqs 4 and 5 and the appropriate coefficients of Table 1. From each test for a specific notch geometry a value of K_f is found from Eq 18 by equating the actual and predicted life, from which a mean value of K_f was determined for each notch. Hence Fig. 17 really shows the applicability of this mean K_f for various stress ranges and frequencies of cycling.

An important consideration that arises in translating from the nominal stresses applied to the actual structure to those in the local notch is the role of the nominal mean stress. Nominal stresses in the structure are often

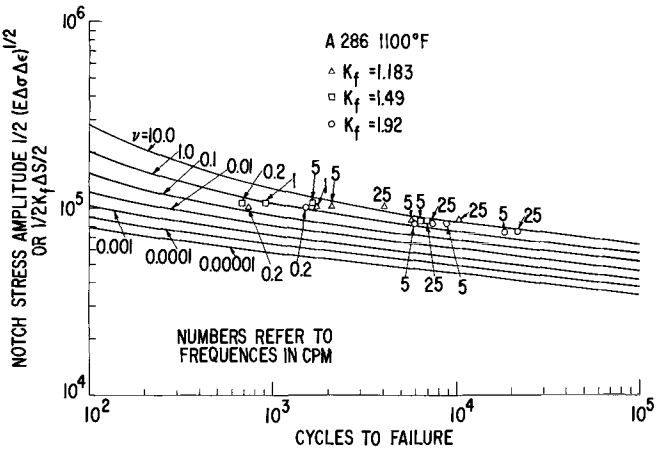


FIG. 17—*Comparison of test results on notched bars of A286 at 593 C at several stress amplitudes and frequencies with calculated notch stress amplitude (unpublished data).*

cycled between zero to tension, while uniaxial data are most often strain limited and fully reversed. The applicability of uniaxial data of this type will depend on the degree to which mean stress relaxation can occur in the notch root. Here again the transition fatigue life serves as the guide. Thus when $N_i \approx N_t$, that is, where the cycles for initiation is of the order of the transition fatigue life, mean stress relaxation of the applied stresses occurs in the notch, and fully reversed uniaxial data are applicable. When $N_i \gg N_t$, mean stresses as determined by stress analysis must be taken into account in predicting initiation life.

Summary Remarks

Many important aspects of the high-temperature fatigue problem such as mechanisms for fatigue nucleation and growth, metallurgical aspects, material selection, and thermal fatigue have been omitted from this paper because of space. Despite this, it has been my intent to treat the high-temperature fatigue problem as a failure process in a notch in some structure in terms of nucleation and early growth at the notch-root, high-strain crack propagation through the plastic zone of the notch, and elastic crack growth to ultimate failure and to discuss the role that some of the important disciplines play in treating the problem. A number of points have been made throughout the paper and are summarized here:

1. In developing models employing constitutive equations and failure criteria for structural design more attention needs to be paid to fatigue as a process of failure by nucleation and growth.

2. Greater attention should be given to the transition fatigue life in determining the approach taken to the problem both in testing and design.

3. More effort is needed in the development of improved constitutive equations for elevated temperature stress analysis commensurate with the advances that have occurred in computational methods.

4. Fatigue nucleation at elevated temperature is very complex. Greater attention to the categorization of the multiplicity of fatigue nucleation mechanisms is required, together with recognition of the specific aspects of the environment.

5. More work in the development of crack growth relationships to the regime of initiation and early growth would be helpful in extending design crack growth procedures to cover a greater proportion of the total fatigue process.

6. Although progress has been made in studying high-strain crack growth, much more effort is needed, particularly to the effect of very low frequencies and of various atmospheres on specific materials.

7. It has been shown here that the environment may be more important than creep in fatigue failure. Greater attention should be paid to the effects of specific atmosphere in future work in material evaluation and failure criteria.

8. Studies on mechanisms for ratchetting and investigations of failure criteria for cyclic-monotonic strain interaction at elevated temperature should receive more attention.

References

[1] Mowbray, D. F. and McConnelee, J. E., 1st International Conference on Structural Mechanics in Reactor Technology, Berlin, 1971.

[2] Mowbray, D. F. and McConnelee, J. E. in *Cyclic Stress-Strain Behavior Analysis, Experimentation, and Failure Prediction, ASTM STP 519*, American Society for Testing and Materials, 1973.

[3] Krempl, E., *Extension Seminar*, International Conference on the Mechanical Behavior of Materials, Kyoto, 1971.

[4] Peterson, R. E., *Materials Research and Standards*, Vol. 3, 1963, p. 122.

[5] Manson, S. S. and Hirschberg, M. H. in *Proceedings*, 1st International Conference on Fracture, Japan Society for Strength and Fracture of Materials, 1965, p. 479.

[6] Crews, J. E. and Hardrath, H. F., *Experimental Mechanics*, Vol. 6, 1966, p. 313.

[7] Hardrath, H. F. and Ohman, L., NACA 1117, National Advisory Committee for Aeronautics 1953.

[8] Neuber, H., WADD TR 60-906, Wright Air Development Division, 1961.

[9] Topper, T. H., Wetzel, R. M., and Morrow, J., *Journal of Materials*, Vol. 4, 1969, p. 200.

[10] Morrow, J., Wetzel, R. M., and Topper, T. H. in *Effects of Environment and Complex Load History on Fatigue Life, ASTM STP 462*, American Society for Testing and Materials, 1969, p. 74.

[11] *Manual on Low Cycle Fatigue Testing, ASTM STP 465*, American Society for Testing and Materials, 1969.

[12] Lee, D., *Metallurgical Transactions*, Vol. 3, 1972, p. 315.

[13] Berling, J. T. and Slot, T. in *Fatigue at High Temperature, ASTM STP 459*, American Society for Testing and Materials, 1969, p. 3.

[14] Coffin, L. F. in *Fracture 1969*, Chapman and Hall, London, 1969, p. 643.

[15] Coffin, L. F. in *Proceedings*, Air Force Conference on Fracture and Fatigue of Aircraft Structures, AFDL TR 70-144, Air Force Development Laboratory, 1970, p. 301.

[16] Coffin, L. F., *Metallurgical Transactions*, Vol. 2, 1971, p. 3105.
[17] Raske, D. T. and Morrow, J. in *Manual on Low Cycle Fatigue Testing, ASTM STP 465*, American Society for Testing and Materials, 1969, p. 1.
[18] Landgraf, R. W. in *Achievement of High Fatigue Resistance in Metals and Alloys, ASTM STP 467*, American Society for Testing and Materials, 1971, p. 388.
[19] Coffin, L. F., *Journal of Materials*, Vol. 6, 1971, p. 388.
[20] Smith, R. W., Hirschberg, M. H., and Manson, S. S., NASA Technical Note D-1574, National Aeronautics and Space Administration, 1963.
[21] Coffin, L. F., *Transactions*, American Society of Mechanical Engineers, Vol. 82D, 1960, p. 671.
[22] Yamanouchi, H., Asada, Y., and Imamura, N., *Mitsubishi Heavy Industries Technical Review*, Vol. 7, 1970, p. 51.
[23] Coffin, L. F., *Transactions*, American Society of Mechanical Engineers, Vol. 87D, 1965, p. 351.
[24] Solomon, H. D. TIS Report 71-C-327, General Electric Co., Nov. 1971.
[25] Popp, H. G. and Coles, A., *Proceedings*, Air Force Conference on Fracture and Fatigue in Aircraft Structures, AFDL TR 70-144, Air Force Development Laboratory, 1970, p. 71.
[26] Pelloux, R. M., *Proceedings*, Air Force Conference on Fracture and Fatigue in Aircraft Structures, AFDL TR 70-144, Air Force Development Laboratory, 1970, p. 409.
[27] Berling, J. T. and Conway, J. B., 1st International Conference on Pressure Vessel Technology, Delft, 1969.
[28] Krempl, E. and Wundt, B. in *Hold Time Effects in High-Temperature, Low Cycle Fatigue, ASTM STP 489*, American Society for Testing and Materials, 1971.
[29] Eztergar, E. P. and Ellis, J. R., International Conference on Thermal Stresses and Thermal Fatigue, Berkeley, England, 1969.
[30] Coffin, L. F. and Goldhoff, R. M., General Electric Report 71C-114, 1971.
[31] Lazan, B. in *Proceedings*, American Society for Testing and Materials, Vol. 49, 1949, p. 757.
[32] Robinson, E. L., *Transactions*, American Society of Mechanical Engineers, Vol. 74, 1952, p. 777.
[33] Taira, S. and Ohnami, M. in *Joint International Conference on Creep and Fatigue*, London, Institute of Mechanical Engineers, 1963, p. 357.
[34] Swindeman, R. in *Joint International Conference on Creep and Fatigue*, London, Institute of Mechanical Engineers, 1963, p. 371.
[35] Manson, S. S., Halford, G., and Spera, D. A., *A. E. Johnson Memorial Volume*, National Engineering Laboratory, Glasgow, 1971.
[36] Lagneborg, R. and Attermo, R., *Metallurgical Transactions*, Vol. 2, 1971, p. 1821.
[37] Solomon, H. D. and Coffin, L. F., Jr. in *Fatigue at Elevated Temperatures, ASTM STP 520*, American Society for Testing and Materials, this publication.
[38] Manson, S. S. and Halford, G. in *International Conference on Thermal and High Strain Fatigue*, M/R 32, London, Metals and Metallurgical Trust, 1967, p. 154.
[39] Manson, S. S. Halford, G. R., and Hirschberg, M. H., NASA TMX-67838, National Aeronautics and Space Administration, 1971.
[40] Timo, D. P., International Conference on Thermal Stresses and Thermal Fatigue, Berkeley Nuclear Laboratories, England, 1969.
[41] Conway, J. B., Berling, J. T., and Stentz, R., International Conference on Thermal Stresses and Thermal Fatigue, Berkeley, England, 1969.
[42] Kanazawa, K. and Yoshida, S., Extension Seminar, International Conference on Mechanical Behavior of Materials, Kyoto, 1971.
[43] White, D. J., *Proceedings*, Institute of Mechanical Engineering, Applied Mechanics Group, Vol. 184, 1969–1970, p. 223.
[44] Achter, M. R. in *Fatigue Crack Propagation, ASTM STP 415*, American Society for Testing and Materials, 1967, p. 181.
[45] Nachtigall, A. J., Klima, S. J., Freche, J. C., and Hoffman, C. A., NASA TN-D2898, National Aeronautics and Space Administration, June 1965.
[46] McMahon, C. J. and Coffin, L. F., *Metallurgical Transactions*, Vol. 1, 1970, p. 3443.

[47] Coffin, L. F., Jr., *Transactions*, American Society for Metals, Vol. 56, 1963, pp. 339–344.
[48] Coffin, L. F., International Conference on Corrosion Fatigue, 1971, Storrs, Conn.
[49] Coffin, L. F., *Metallurgical Transactions*, Vol. 3, 1972, p. 1777.
[50] Coffin, L. F. and Tavernelli, J. R., *Transactions*, American Institutes of Mining, Metallurgical and Petroleum Engineers, Vol. 215, 1959, p. 794.
[51] Swindeman, R. W. in *Fatigue at High Temperature*, *ASTM STP 459*, American Society for Testing and Materials, 1969, p. 31.
[52] Hill, P. T., LaForce, R. P., Berning, R. F., and Coffin, L. F., Jr., Report GESP-595, General Electric Co., 1971.
[53] Morrow, J. in *Internal Friction, Damping and Cyclic Plasticity*, *ASTM STP 378*, American Society for Testing and Materials, 1964, p. 72.
[54] Tompkins, B., *Philosophical Magazine*, Vol. 18, 1968, p. 1041.
[55] Boettner, R. C., Laird, C., and McEvily, A. J., *Transactions*, Metallurgical Society, American Institute of Mining, Metallurgical, and Petroleum Engineers, Vol. 233, 1965, p. 379.
[56] Weiss, V., *Fatigue, An Interdisciplinary Approach*, Syracuse University Press, Syracuse, N.Y., 1965, p. 179.
[57] Organ, F. E. and Gell, M., *Metallurgical Transactions*, Vol. 2, 1971, p. 943.
[58] Tien, J. K. and Gamble, R. P., *Metallurgical Transactions*, Vol. 2, 1971, p. 1933.
[59] James, L. A., *5th National Symposium on Fracture Mechanics*, Urban, Ill., 1971.
[60] Coffin, L. F. in *Achievement of High Fatigue Resistance in Metals and Alloys*, *ASTM STP 467*, American Society for Testing and Materals, 1970, p. 53.
[61] Swift, H. W., *Engineering*, Vol. 166, 1948, pp. 333 and 357.
[62] Yamanouchi, H., Extension Seminar, International Conference on Mechanical Behavior of Materials, Kyoto, 1971.
[63] Krempl, E., 1st International Conference on Pressure Vessel Technology, Delft, 1969.

Mechanisms of Fatigue

M. Gell[1] *and G. R. Leverant*[1]

Mechanisms of High-Temperature Fatigue

REFERENCE: Gell M. and Leverant, G. R., "**Mechanisms of High-Temperature Fatigue,**" *Fatigue at Elevated Temperatures, ASTM STP 520*, American Society for Testing and Materials, 1973, pp. 37–67.

ABSTRACT: A review is presented of high-temperature fatigue mechanisms, with emphasis on nickel-base superalloys. It is shown that the slip character of a material (wavy versus planar), the extent of creep in the fatigue cycle, and the degree of oxidation all influence the mode and rate of fatigue crack initiation and propagation. These concepts are then used to explain the generally observed effects of temperature, mean stress, holdtime, and frequency on high-temperature fatigue life.

KEY WORDS: fatigue (materials), high temperature fatigue, crack initiation, crack propagation, intergranular fracture, transgranular fracture, fatigue fracture, environmental effects, coatings, nickel-base superalloys, stainless steels

Fatigue at elevated temperatures is a complex subject. In general, we are dealing with a creep-fatigue interaction that depends sensitively on temperature, frequency, holdtime, mean stress, and environment. At present, lifetime prediction systems are governed by a number of empirical and phenomenological relationships, and order-of-magnitude agreement with service experience is considered good. One of the main objectives of mechanisms research should be to demonstrate that there are a limited number of quantifiable phenomena operative during high temperature fatigue. Once these phenomena are established, more accurate lifetime prediction systems can be established.

Our knowledge of high-temperature fatigue mechanisms is at an early stage of development. Only a few materials systems have been investigated and most of these only over a limited range of variables. In this paper, we will be relying heavily on the results of a major research effort conducted on nickel-base superalloys at Pratt & Whitney Aircraft over the last decade. This understanding, combined with that obtained on ferrous materials and some pure, single phase materials, should be applicable to other high-temperature materials systems.

[1] Group leader and senior research associate, respectively, Materials Engineering and Research Laboratory, Pratt & Whitney Aircraft, East Hartford, Conn. 06457.

Copyright© 1973 by ASTM International www.astm.org

Deformation Behavior

Slip Character

A concept which is particularly useful in rationalizing the various fatigue cracking modes and their dependence on variables such as strain rate and temperature is that of slip character [*1–3*].[2] Qualitatively, slip character is a measure of the degree to which dislocations tend to disperse during plastic deformation. Materials deforming by planar slip are those in which dislocations remain in planar arrays, and planar shear offsets are produced on polished surfaces, Fig. 1. This type of deformation is favored by a low stacking fault energy, ordering, the presence of coherent precipitates, low temperatures, and small strains. Austenitic stainless steels, high zinc alpha brasses, and nickel-base superalloys are examples of alloys exhibiting a planar slip character at ambient temperatures. The initial stage of fatigue cracking in planar slip materials is along slip planes and is referred to as Stage I cracking. For planar slip materials, the degree of slip homogeneity is important in determining the rate of slip band crack initiation and propagation.

Wavy slip or homogeneously deforming metals exhibit uniformly distributed, nonplanar dislocation arrangements and a general surface rumpling, Fig. 2. This type of deformation is favored by a high stacking fault energy, incoherent precipitates or particles, and large strains, but, most importantly, by temperatures greater than $\sim 0.4T_M$ [*1–6*]. Most metals, regardless of their slip character at low temperatures, exhibit wavy slip at temperatures $\gtrsim 0.4T_M$ because thermal activation allows dislocations to cross slip and climb out of their original slip planes. Fatigue cracking under wavy slip conditions can occur in two modes: transgranular cracking perpendicular to the principal stress axis which is called Stage II fracture, or intergranular cracking.

An additional parameter of importance at temperatures $\gtrsim 0.4T_M$ is frequency of cycling, that is, strain rate. The reason for this is that dislocation climb and cross slip are time-dependent processes so the amount of slip dispersal occurring at a crack tip in a given cycle will depend upon the frequency of cycling. A consequence of this is that high cyclic frequencies at high temperatures can produce planar slip, that is, a slip character equivalent to that obtained at normal frequencies at low temperatures. In a similar fashion, holdtimes under stress during part of a cycle are equivalent to a reduction in frequency and, therefore, are conducive to slip dispersal. An example of the effect of strain rate on slip character during monotonic tensile deformation is shown in Fig. 3 for ⟨100⟩ single crystals of a nickel-base superalloy, MAR-M200 [*7*]. At a strain rate of 3 percent/min at 1550 F, the slip character is wavy as evidenced by the homogeneous

[2] The italic numbers in brackets refer to the list of references appended to this paper.

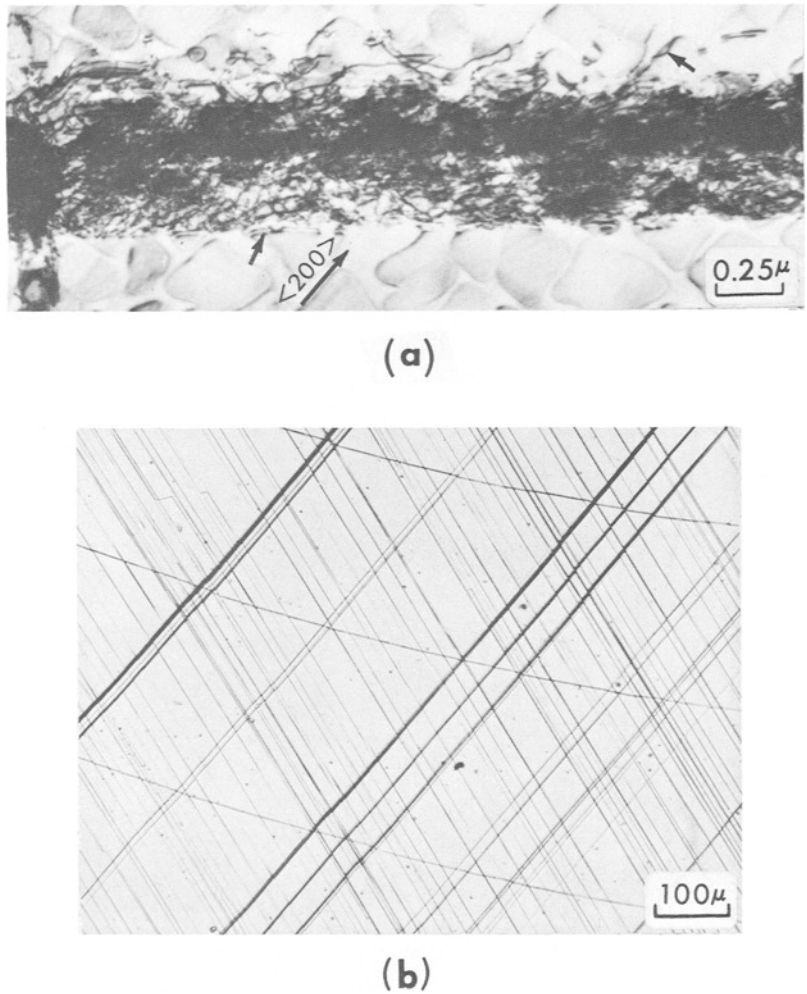


FIG. 1—*Planar low-cycle fatigue deformation produced in single crystal Mar-M200 at room temperature*: (a) *transmission electron micrograph showing dislocations in a slip band and* (b) *corresponding shear offsets produced on electropolished specimen surface* [14].

dislocation structure, but, at 500 percent/min, planar bands of dislocations are present.

The concept of slip character will be used extensively in the next section to explain phenomena related to crack initiation and propagation.

Fatigue Crack Initiation and Propagation

Fatigue fracture consists of an initiation and propagation stage. It is important to distinguish between these two stages because frequently one of

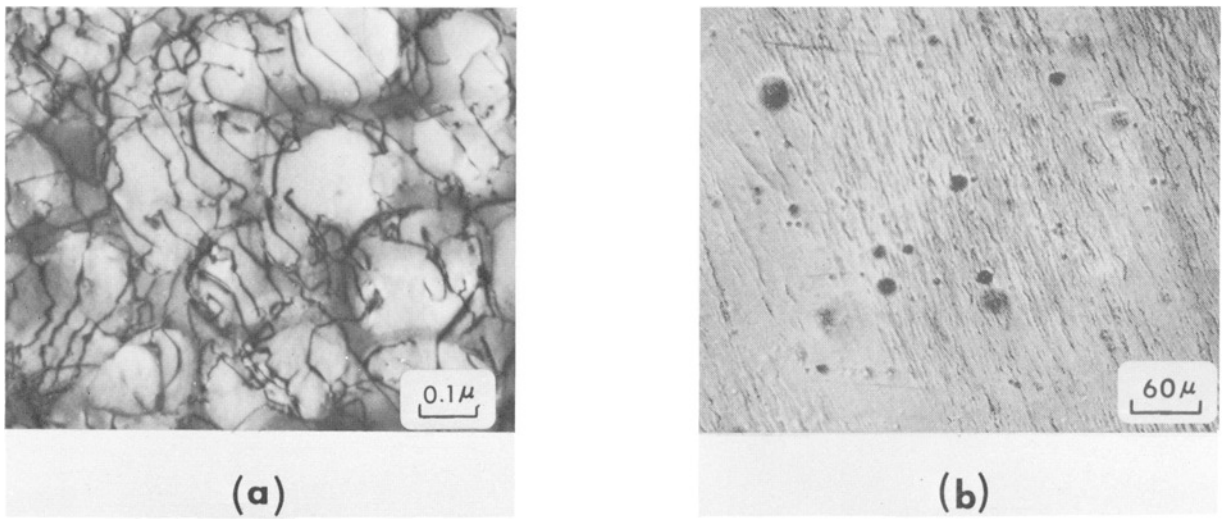
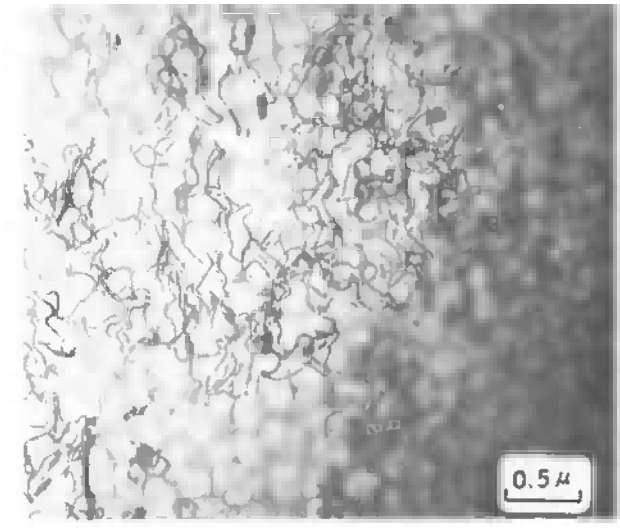
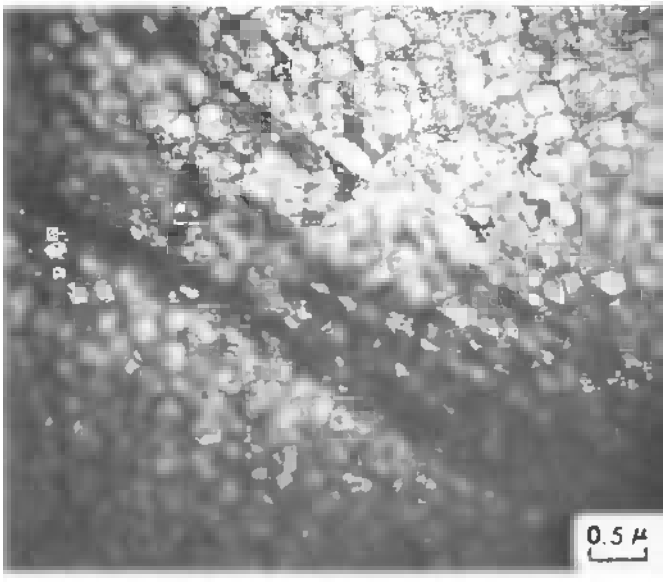


FIG. 2—*Wavy homogeneous deformation demonstrated in* (a) *transmission electron micrograph showing dislocations in single crystal Mar-M200 fatigued at 1700 F* [14] *and* (b) *surface shear offsets in α-iron deformed at room temperature* [53].



(a)



(b)

FIG. 3—*The effects of strain rate on plastic deformation at 1550 F in single crystal Mar-M200*: (a) *homogeneous dislocation distribution produced at a strain rate of 3 percent/min and* (b) *planar dislocation arrays produced at a strain rate of 500 percent/min* [7].

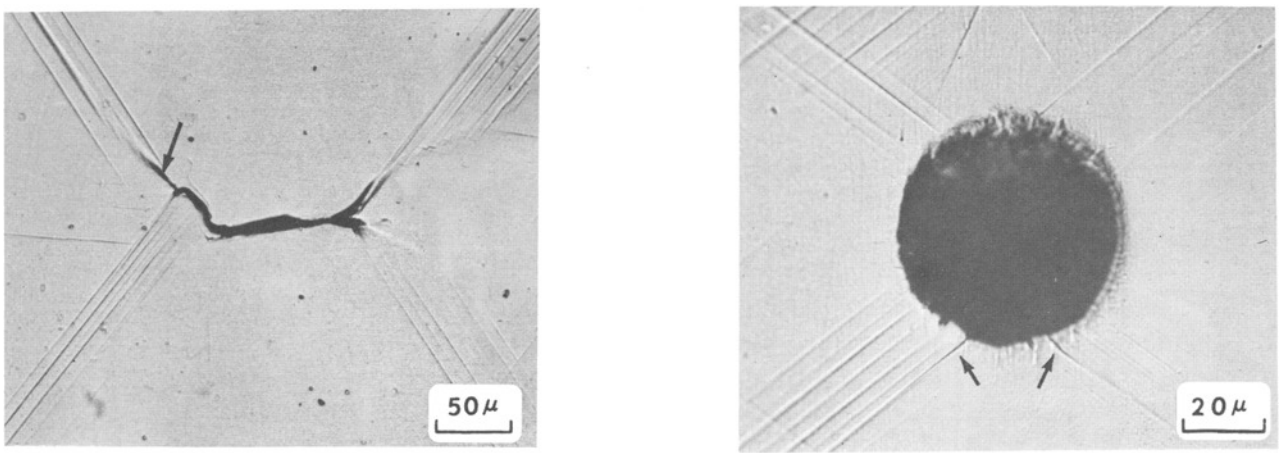


FIG. 4—*Planar slip and Stage I crack initiation at microstructural defects* (arrows) *in single crystal Mar-M200* (a) *pre-cracked MC carbide and* (b) *surface casting pore* [14].

the two will represent the major part of component life. The mechanism of cracking and, therefore, the influence of service variables on each stage may differ. The distinction between initiation and propagation has not always been clear because the same mechanism may control both phases, or the crack length at the end of the initiation stage may be less than the resolving power of the technique used to investigate cracking.

Crack Initiation Sites

Crack initiation in engineering materials usually occurs at microstructural defects. These defects can be hard nonmetallic inclusions such as borides, carbides (Fig. 4*a*), nitrides, and sulfides. Crack initiation in cast materials may also occur at porosity (Fig. 4*b*). These defects may be found at inter- and intragranular locations, with the site for crack initiation depending on the creep component in the cycle, as will be seen. The size of the defect controls the rate of crack initiation, the initial rate of crack propagation, and, therefore, the fatigue life. Figure 5 shows the strong sensitivity of fatigue life on defect size in the room temperature testing of single crystals of the nickel-base superalloy MAR-M200. The yield strength of the alloy was the same for all conditions of defect type and size. The MC carbides in these materials are in platelet form and contain pre-existing cracks in the plane of the plate (Fig. 4*a*). Material containing large carbides (0.30 mm) fails upon loading above the proportional limit, whereas the alloy with smaller carbides (0.15 mm) exhibits much improved fatigue lives. Cracking in material with no MC carbides shows a further improvement in fatigue life and fracture originates at 0.20 mm size casting pores. When the pore size was reduced by a factor of five to 0.04 mm, a commensurate increase

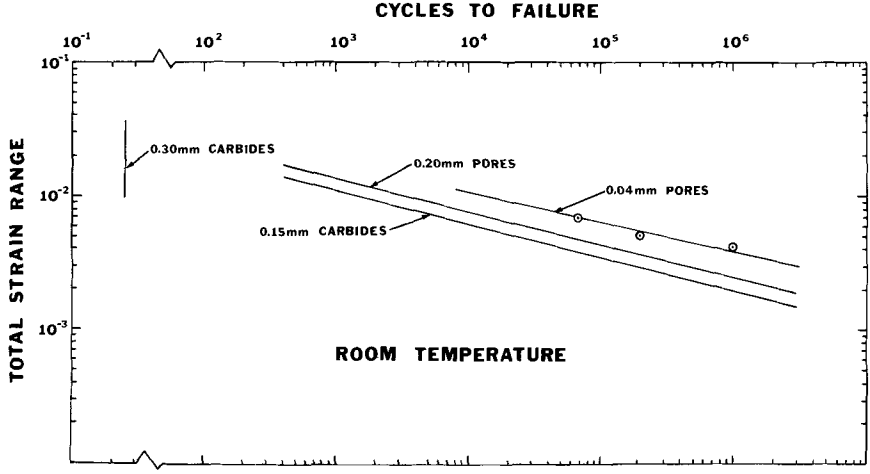


FIG. 5—*The effect of carbide and pore size on the fatigue life of directionally solidified Mar-M200 at room temperature.*

in fatigue life was obtained. The magnitude of the improvements in fatigue life can be explained using fracture mechanics. These results also illustrate that fatigue usually originates at the defect in the microstructure having the highest stress concentration. If that defect is eliminated, fatigue failure will occur at the next weakest link in the structure.

In wrought, recrystallized materials with low stacking fault energy, cracks may initiate along coherent annealing twin boundaries [*8–10*]. In nickel-base superalloys, these may be considered planar defects because the strengthening γ' precipitate does not form across the boundary. These boundaries thus have a lower critical resolved shear stress than other planes in the alloy, and dislocations are concentrated along these boundaries [*11*].

Transgranular Crack Initiation and Propagation

The most comprehensive series of studies on elevated temperature transgranular cracking modes and their relationship to microstructural defects and deformation modes have been those performed on wrought [*6,10,12*] and cast [*2,13,14*] nickel-base superalloys. Both Stage I and Stage II crack initiation are found depending on the temperature and the frequency of cycling. Stage I crack initiation is favored by low temperatures and high frequencies, conditions which are conducive to planar slip [*2,14*]. In contrast, low frequencies and high temperatures, which promote slip dispersal, generally lead to Stage II crack initiation [*2,14*]. An example of the effect of frequency on mode of crack initiation and propagation is shown in Fig. 6 for ⟨100⟩ oriented single crystals of MAR-M200. At the lower frequency, the crack initiates at a subsurface micropore and propagates radially in the Stage II mode. At some critical crack length, where the crack tip strain rate has increased sufficiently, a transition to Stage I cracking is found. At the higher frequency, a Stage I crack is initiated immediately adjacent to a subsurface micropore, and the entire fracture occurs in the Stage I mode. These results may be interpreted as follows: it is likely that planar bands of dislocations are generated around the micropore at both frequencies. In the case of the lower frequency, however, these bands disperse before a Stage I crack can be initiated, and eventually a Stage II crack is initiated in the homogeneous dislocation array adjacent to the micropore. At the higher frequency, many cycles are accumulated before the planar deformation can disperse, and these cycles are sufficient to initiate Stage I cracking within the band. For these particular results, the gaseous environment does not affect the initial mode of cracking, because of its subsurface location. More generally, since environment can influence the slip distribution of these materials, the transgranular mode of cracking should also be affected (Section on Environmental and Coatings Effects).

Low-temperature fracture in most materials is initiated in the Stage I mode and when a crack gets long enough, usually when it encounters a

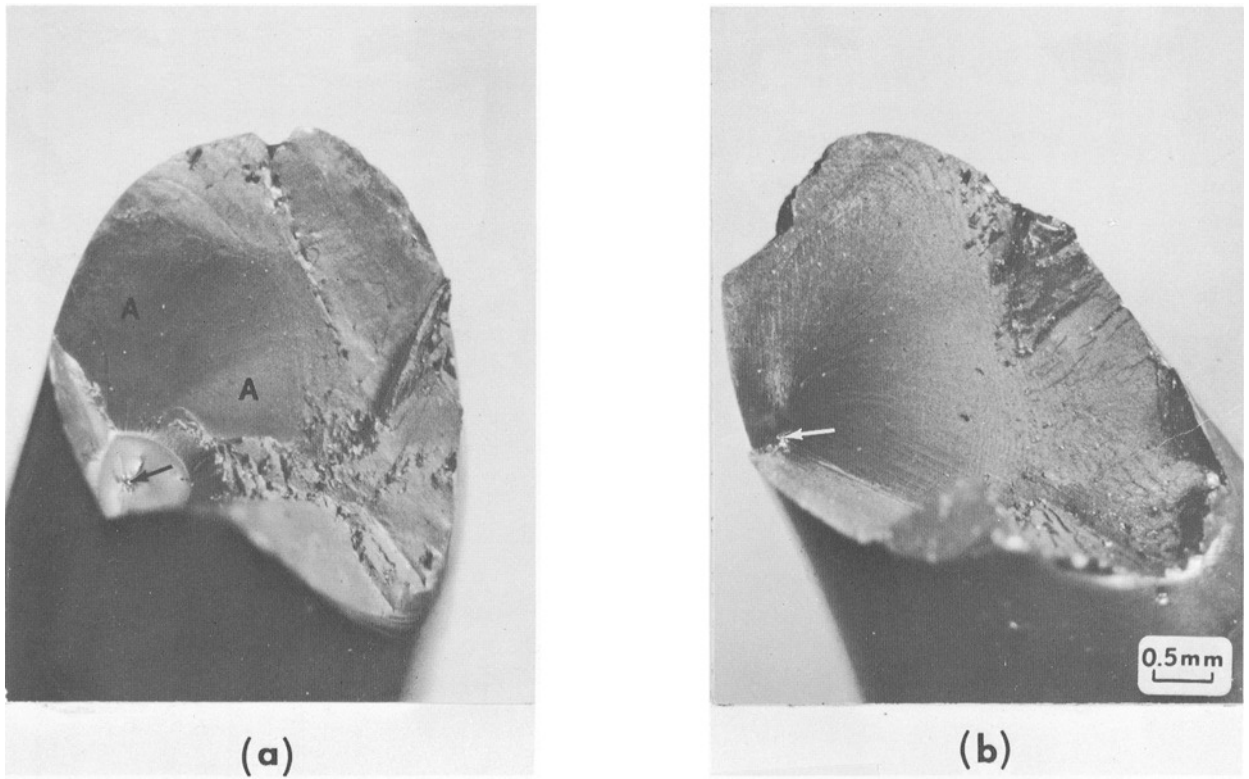


FIG. 6—*The effect of frequency on the mode of cracking in single crystal Mar-M200 at 1550 F*: (a) *20 Hz*: *Stage II crack initiation and propagation from subsurface pore* (arrow) *followed by Stage I propagation* (areas A) *and* (b) *1030 Hz*: *Stage I crack initiation and propagation from subsurface pore* (arrow), *no Stage II.*

grain boundary, there is a transition to Stage II fracture. At elevated temperatures, because of the strain rate dependence of the deformation mode, a crack may start out in Stage II and then change to Stage I (Fig. 6). In nickel-base superalloys, the temperature and strain rate conditions necessary to give planar slip have been determined quantitatively [*7*]. Since the nature of deformation at the crack tip governs whether Stage I or Stage II cracking will occur, the concept of a crack tip strain rate intensity factor can be used to specify the conditions for transgranular cracking.[3]

Cleavage-type markings are often observed on Stage I fracture surfaces in nickel- and aluminum-base alloys [*15–18*]. These markings and the general absence of striations on Stage I fracture surfaces have often been mistaken as indications of very rapid crack propagation. This need not be the case. Fracture occurs on crystallographic slip planes because of the concentration of plastic deformation in these planes. When the local strain at the crack tip exceeds a critical value, cyclic cleavage occurs [*16,19*]. Crack growth rates may vary from 10^{-8} cm to 10^{-3} cm per cycle, depending on the strain range and the heterogeneity of slip. In fact, the maximum life obtained in wrought Udimet 700 at 1400 F as a function of frequency was for conditions of homogeneous planar slip [*11*] (see Fig. 19).

Intergranular Crack Initiation and Propagation

Intergranular crack initiation in fatigue is analogous in many respects to crack initiation in creep. For example, high fatigue stresses, relatively low temperatures, and short tests favor the formation of triple point or wedge cracks (Fig. 7*a*), whereas low stresses, relatively high temperatures, and long tests are conducive to cavitation, Fig. 7*b*. Intergranular cracking in fatigue can initiate both at the surface and at subsurface locations and is, therefore, sometimes difficult to distinguish from pure creep cracking.

Most thorough studies of intergranular crack initiation in fatigue have been performed on wrought pure metals [*20–23*] and solid solution alloys [*22,24–26*], although additional studies have been performed on more complex systems [*6,10,12,27–32*]. These studies have generally shown that in systems where grain boundary migration is easy, that is, systems with virtually no second phases at grain boundaries, the boundaries align themselves at 45 deg to the stress axis during cycling. In addition, it has been found that the cavity distribution as a function of grain boundary orientation peaks for grain boundaries oriented at 45 deg to the stress axis even in systems where grain boundary migration is limited [*25*], and statistical analysis have shown that the cavitation on 45-deg boundaries exceeds the percentage of 45-deg boundaries in the total boundary population [*21*]. These results, together with the observation [*27*] of grain boundary sliding during fatigue of a low-carbon austenitic stainless steel, strongly suggest

[3] Leverant, G. R. and Gell, M., unpublished research.

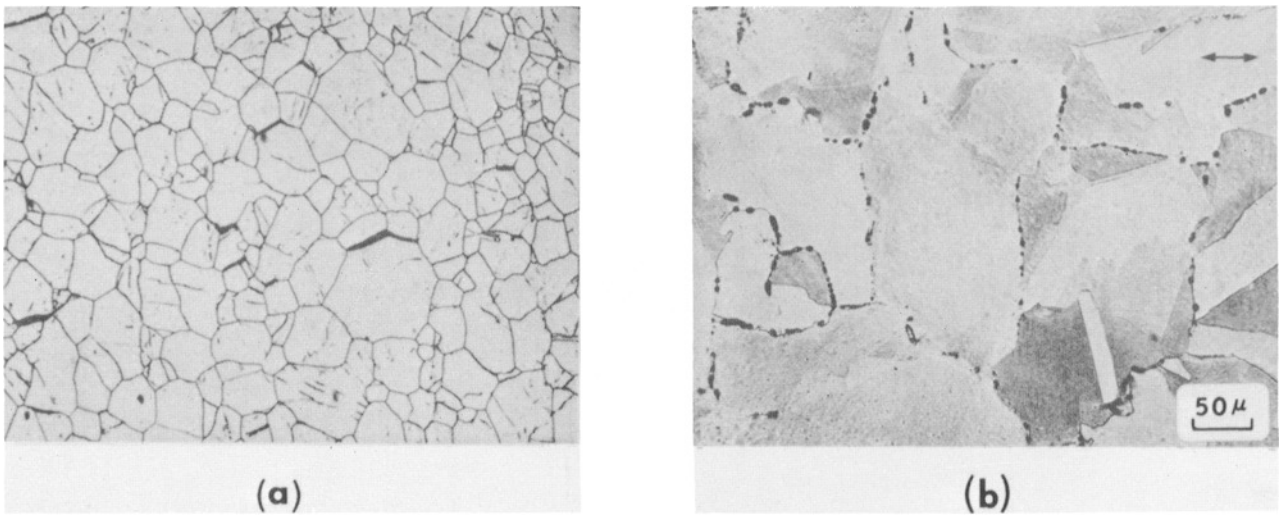


FIG. 7—*Intergranular crack initiation in fatigue* (a) *Type 316 stainless steel fatigued at 1112 F (600 C) with a hold in the cycle; after Dawson et al* [31]. (b) *Cavitation in copper fatigued at 752 F, (400 C), stress axis horizontal* [21].

that cavity nucleation is a shear-controlled process in systems in which grain boundary shear is not hindered by second phase particles in the grain boundaries. A critical experiment has been performed that reinforces the evidence for shear-controlled cavity nucleation [*21*]. It has been found that in pure copper the cavity distribution peaks on boundaries oriented 45 deg to the stress axis in push/pull cycling but on boundaries oriented 0 and 90 deg to the specimen axis in torsional cycling. In addition, however, it was noted that the number of cycles to failure in torsional fatigue was much larger than in push/pull fatigue for equivalent shear stress amplitudes. This suggests that the normal stress across the boundary is important in cavity linkup and crack growth.

It is generally recognized that cavities are stable only after attaining a critical size which is a function of the surface energy of the material in question. The question arises as to whether this critical size is attained by mechanical means, that is, grain boundary sliding or by condensation of vacancies at the shear-initiated cavity nucleus. It has been shown that all compressive cycling produces cavities, whereas compressive creep for equivalent times or to equivalent strains did not produce cavitation [*21*]. In addition, even tensile creep was not as effective as push/pull cycling in nucleating cavities in pure copper [*23*]. These experiments, as well as others [*24,26*], prove that vacancies produced by cyclic plastic deformation can stabilize cavities. It also indicates that an earlier model [*33*] for creep cavitation that requires a tensile component of stress across a grain boundary for cavity formation cannot be directly applied to fatigue.

Several authors have pointed up that easy grain boundary migration and easy cavitation go hand in hand. This would be expected since both grain boundary sliding and grain boundary migration are facilitated by the same metallurgical factors, for example, the absence of particles in the grain boundaries. It has even been suggested [*21*] that an additional vacancy supersaturation due to complex slip during migration contributes to accelerated cavity growth. In any case, it is known that copious cavitation can be found even when grain boundary migration is severely restricted [*25*].

The sites of cavity nucleation have not been identified in single phase systems. Although these systems must contain second phase particles along some grain boundaries, the density of cavities suggests that nucleation may occur at ledges in grain boundaries rather than exclusively at particle-matrix interfaces.

Recent testing of an austenitic steel [*27*] with and without $M_{23}C_6$ carbide particles in the grain boundaries has provided additional evidence for grain boundary shear as the mechanism of cavity nucleation. The alloy without carbides in the boundaries failed intergranularly and had a low endurance limit at 1292 F (700 C). In contrast, the alloy with $M_{23}C_6$ carbides at 1 μm intervals in the boundaries failed transgranularly and had a considerably higher endurance limit under identical conditions of testing. Grain bound-

ary sliding was observed in the carbide-free alloy but not in the carbide-containing alloy.

Intergranular cracks are often initiated at the interface between second phase particles residing in the grain boundaries and the adjacent grains [*11*,*28*] (Fig. 8). In stainless steels, the interface between $M_{23}C_6$ and columbium carbide precipitates and the matrix has been identified as a fatigue crack initiation site [*28*]. Because $M_{23}C_6$ carbides are coherent with one adjacent grain and incoherent with the other [*34*], it is likely that the crack initiates at the incoherent carbide-matrix interface [*35*]. The interface between incoherent thoria particles and the nickel matrix has been observed as a crack initiation site in TD nickel as well [*36*].

Two indirect pieces of evidence exist which suggest that healing or sintering of grain boundary cracks may occur during the compressive half-cycle or a compressive creep hold in high-strain fatigue. Type 304 stainless steel tested under various hold conditions at 1200 F exhibited intergranular cracking only if the hold was in tension [*37*]. If tensile and compressive holds were both present, transgranular cracking and longer lives resulted. In addition, during the cyclic creep-rupture testing of Type 316 stainless steel at 1300 F (707 C) it was found that the tensile creep rate following the compressive half-cycle decreased with increasing compressive stress, whereas the compressive creep rate was independent of the tensile stress in the cycle [*38*]. In systems where this healing is found, fatigue lives should be enhanced by decreasing mean stress.

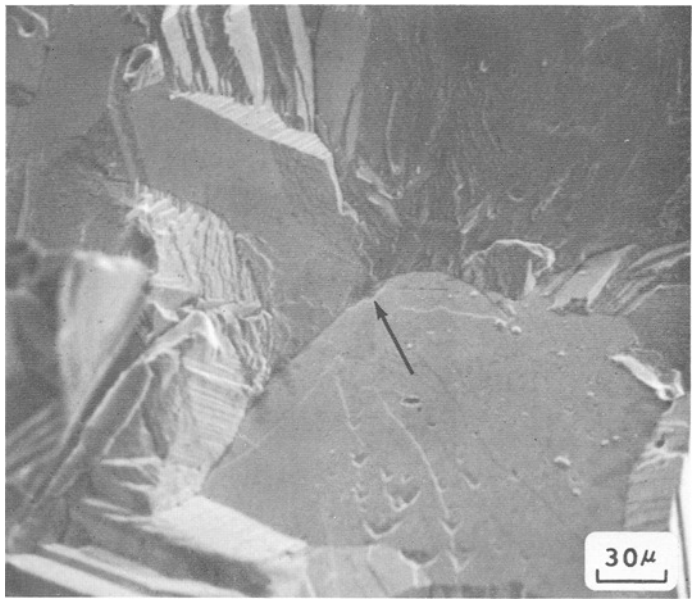


FIG. 8—*Grain boundary crack initiation at particle* (arrow) *in wrought Udimet 700 tested at 1400 F (760 C) and 600 cpm. Crack propagation is transgranular* [11].

Triple point or wedge cracking is found, as in creep, at lower temperatures and at higher stresses than cavitation. Examples of this type of cracking have been found in austenitic stainless steels [*27,31*], magnesium, and some dilute magnesium alloys [*22*]. This type of cracking requires large shear offsets at the triple points and should be enhanced by large strain ranges and cycles containing a creep hold [*31*].

An additional shear-controlled type of intergranular crack initiation is that related to the presence of precipitate-free zones (PFZ) adjacent to grain boundaries. Concentration of plastic deformation in these zones has been shown to lead to crack initiation in a wrought, nickel-base superalloy [*6*], a columbium-stabilized austenitic stainless steel [*20*], and a magnesium-zirconium alloy [*29*]. In the case of nickel-base superalloys, the PFZ is on the side of the grain boundary where the $M_{23}C_6$ carbide is incoherent with the matrix [*35*]. There is some indication that an optimum PFZ width for minimization of fatigue resistance exists [*28*].

In the case of wedge cracking, where coordinated shear over an entire grain facet is possible, the following relationship [*39*] is applicable for estimating the conditions which will favor this fracture mode.

$$\sigma \geq \left[\frac{2G\gamma}{\pi(1-\nu)\,d}\right]^{1/2}$$

It can be seen that a large grain size, d, and a low effective fracture surface energy, γ, are conducive to this cracking mode.

It is important to be able to predict whether cracking will be intergranular or transgranular because, in general, intergranular crack initiation and propagation occur at a faster rate than transgranular cracking [*13,14*]. The absence of intergranular fatigue cracking partly accounts for the superior fatigue properties of directionally-solidified and single-crystal nickel-base superalloys compared to polycrystalline alloys of the same composition [*13,14,40,41*]. An ability to determine whether cracking is trans- or intergranular and to determine the relationship between the mode of cracking and the crack growth rate would be valuable.

A qualitative understanding of the modes of cracking to be expected can be had by using the concept of the "creep component" in a fatigue cycle. In a constant stress test, this component can be determined by measuring the specimen elongation in each cycle. For a given alloy, the creep component during fatigue increases with increased temperature, mean stress, holdtime, and with reduced frequency. As the creep component in the cycle is increased, the mode of crack initiation and propagation will undergo the changes outlined in Table 1. Where there is no creep component or it is small, the normal low temperature behavior is observed. Crack initiation and propagation are transgranular, with the propagation mode showing the normal Stage I to Stage II transition (line 1). Exceptions to this may

TABLE 1—*Changes in the mode of fatigue crack initiation and propagation as creep component becomes more important.*

1.	Transgranular initiation—transgranular propagation
2.	Intergranular initiation—Stage I propagation
3.	Intergranular initiation—Stage II propagation
4.	Intergranular initiation—intergranular propagation

arise if grain boundaries contain brittle phases that are sources of intergranular initiation. The first observed effect of an increased creep component is usually a transition from transgranular to intergranular initiation; the propagation stage may be left unchanged (line 2). With a further increase in the creep component, thermally activated cross slip and climb produces a change in the intragranular deformation mode from planar to wavy, and, as a result, Stage II cracking occurs (line 3). Finally, when sufficient creep occurs in each cycle, both initiation and propagation stages become intergranular (line 4). Figure 9 shows an example of the effect of temperature on the mode of surface cracking of polycrystalline Udimet 700. Slip band cracking is evident at 70 F and grain boundary cracking at 1700 F.

Environmental and Coating Effects

Just as temperature and frequency are important in determining the mode and rate of cracking, so too is the gaseous environment. It will be seen that oxygen, like an increased creep component, acts to promote intergranular cracking and that oxygen can have a variety of influences on the mode and rate of transgranular cracking [*42*].

Transgranular Fracture

Figure 10 shows the effect of temperature on fatigue life of ⟨100⟩ oriented single crystals of MAR-M200. At room temperature, the life in vacuum is greater than that in air, at 1400 F the lives are the same, and at 1700 F the life in vacuum is less than that in air.

At room temperature, oxygen adsorption has little effect on crack initiation but lowers the surface energy at the tips of Stage I cracks [*16*]. As a result, cyclic cleavage and a faster rate of propagation are promoted. In vacuum, crack growth also occurs on slip planes, but the fracture propagates by a ductile rupture mode.

At temperatures around 1400 F, crack initiation occurs below the specimen surface in air and at the specimen surface in vacuum, Fig. 11 [*42,43*]. Experiments have shown that surface slip is more uniformly distributed and surface shear displacements are smaller in tests conducted in air than in vacuum (Fig. 12), and it has been suggested that thin oxide film formation on surface slip offsets leads to greater surface work hardening [*42,43*]. As a result of the more homogeneous surface slip, surface crack initiation is

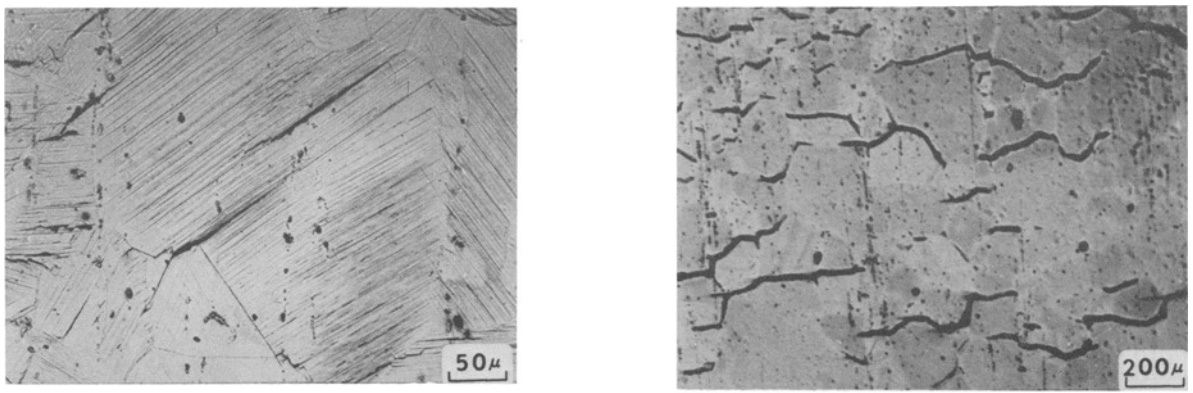


FIG. 9—*The effect of temperature on surface crack initiation in wrought Udimet 700* (a) *planar slip and Stage I cracking at room temperature and* (b) *intergranular cracking at 1700 F* [6, 9].

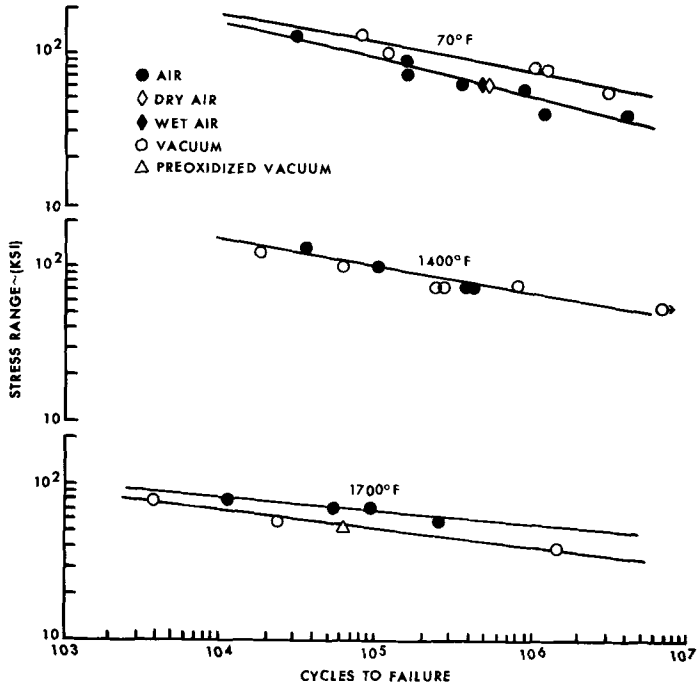


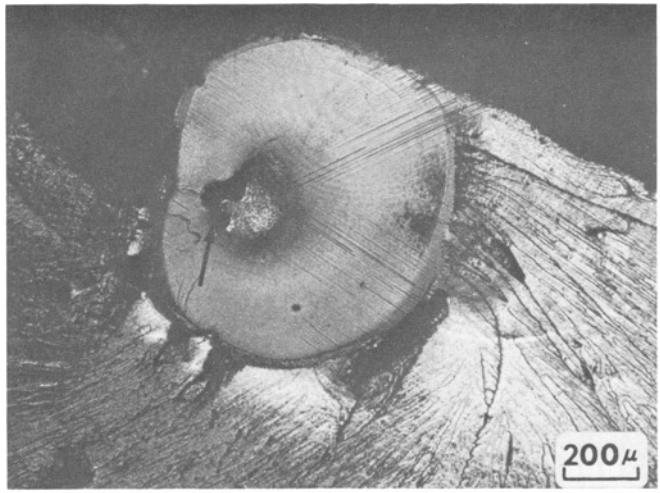
FIG. *10—The effect of vacuum, air, and temperature on fatigue life of single crystal Mar-M200* [43].

retarded, and subsurface cracks are generated. The initiation and propagation of the subsurface cracks are in vacuum, so that lives in air and vacuum are about the same.

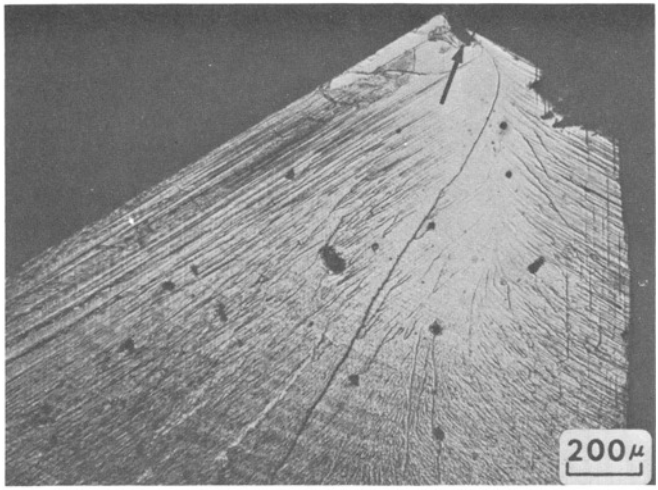
At temperatures around 1700 F, surface oxide formation is more rapid, and the thicker oxide is easily cracked [*42,43*]. At these temperatures, oxide forms on surface-connected crack surfaces and reduces the degree of crack resharpening occurring during the compressive half-cycle of Stage II crack growth, Fig. 13*a*. Cracks formed in vacuum tests or from subsurface origins in air tests are sharper, Fig. 13*b*. As a result, the rate of crack growth in vacuum is greater than that in air. Figure 14 shows schematically Stage II crack growth in vacuum and air.

Intergranular Fractures

In a single crystal, surface oxidation occurs at a reasonably uniform rate over the entire surface, except where phases or nonmetallic inclusions that are less oxidation resistant than the matrix intersect the surface. The rate of penetration of the oxide in these phases can be many times greater than that in the surrounding matrix. In polycrystals of most structural alloys, grain boundaries are surfaces along which these precipitates, or nonmetallic



[a]



[b]

FIG. 11—*The effect of environment of crack initiation in single crystal Mar-M200 at 1400 F*: (a) *subsurface Stage I crack at casting pore* (arrow) *in air test and* (b) *surface Stage I crack at casting pore* (arrow) *in vacuum test* [43].

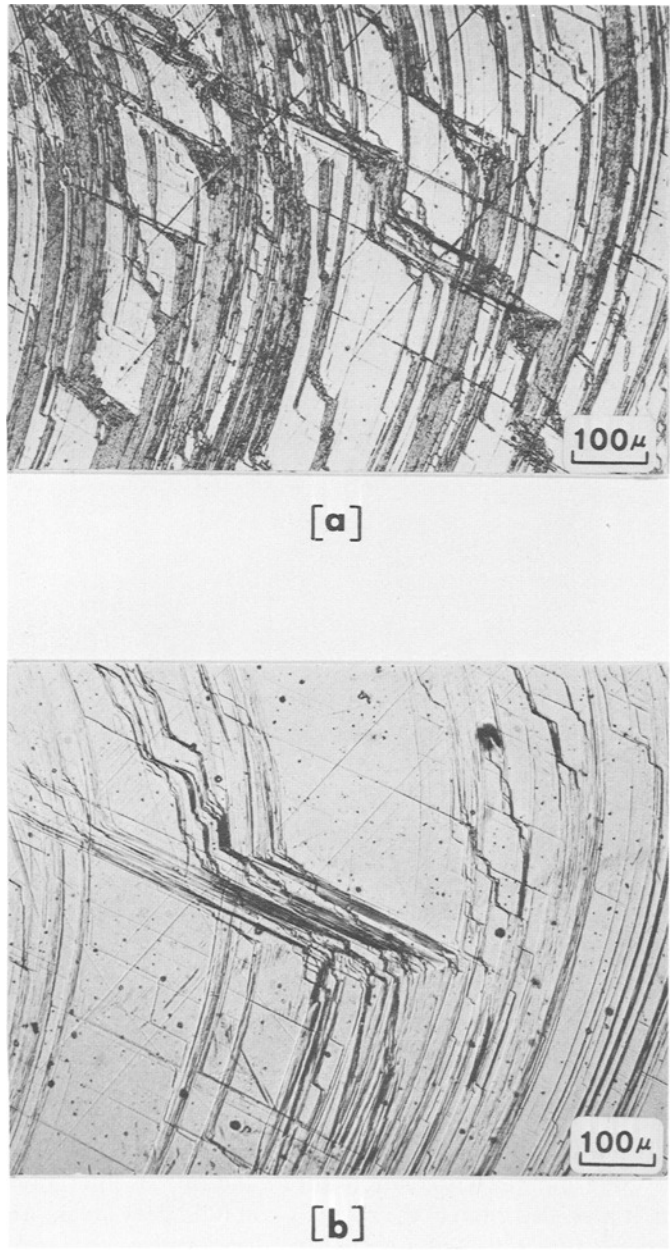


FIG. 12—*Slip distribution produced in Mar-M200 single crystal specimens fatigued in* (a) *air and* (b) *vacuum at 1400 F* [43].

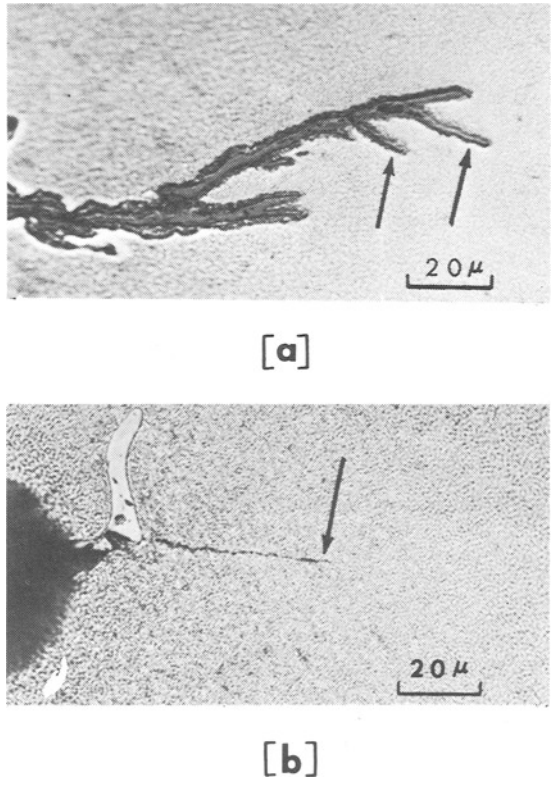


FIG. 13—*Fatigue cracks produced in single crystal Mar-M200 at 1700 F* (a) *surface-initiated crack* (b) *subsurface initiated crack* [2].

inclusions are preferentially concentrated. As a result, oxide penetration along a grain boundary intersecting the surface is deeper than in the matrix (Fig. 15*a*). Since the oxide is brittle and often poorly bonded to the surrounding metal, a fatigue crack can easily form in the oxide or at the oxide-metal interface (Fig. 15*b*). The pre-oxidation of a Udimet 700 specimen at 1800 F followed by fatigue testing at 1400 F produces many surface intergranular cracks, whereas testing of specimens without prior oxidation produces a single intergranular crack [*44*]. Thus, pre-oxidized or preferentially-oxidized phases or grain boundaries serve as incipient cracks.

Just as grain boundary oxidation affects the rate of intergranular crack initiation, it may also control the rate of grain boundary crack propagation. The microstructure ahead of a grain boundary crack is changed by oxidation [*13,40,41,45*]. Not only is oxide formed near the crack tip, but also, for a distance ahead of the crack, the region is depleted of oxide-forming elements (Fig. 15*b*). As a result of oxidation, the crack in the next period will propagate into a region having changed chemical and mechanical

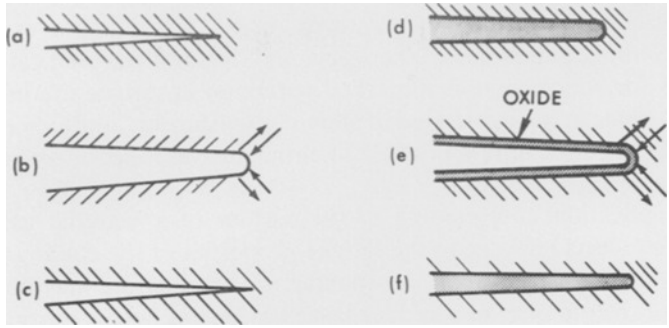


FIG. 14—*Schematic drawings of State II crack growth in vacuum* [a, b, c] *and air* (d, e, f) [42].

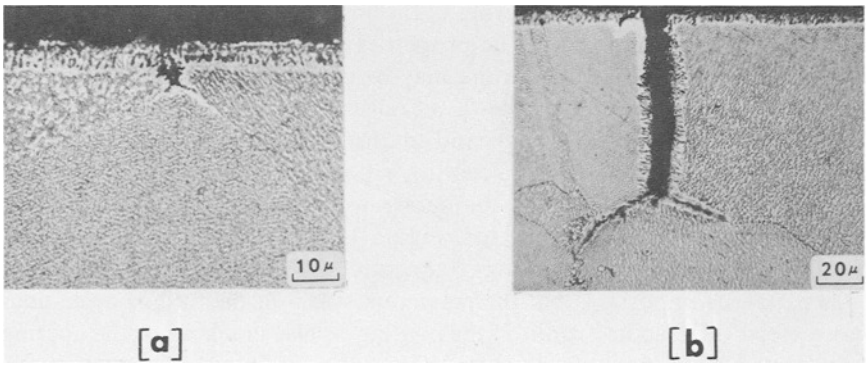


FIG. 15—*The influence of oxygen on crack initiation and propagation in Udimet 700 at 1400 F*: (a) *preferential grain boundary oxidation and* (b) *surface-connected intergranular crack* [42].

properties. Thus, there are a number of possible influences of oxygen on the rate of intergranular crack growth. If the rate of crack growth in the absence of oxygen (that is, in a vacuum test) is greater than the size of the zone affected by oxidation, then the crack propagation rate will be relatively unchanged by oxidation. This case would be found at relatively high strain ranges and frequencies and at low temperatures. On the other hand, at low strain ranges, low frequencies, and high temperatures, the increment of crack growth in each cycle may be controlled by the size of the oxygen-affected zone at the crack tip. This may be viewed as a stress corrosion phenomenon [*45*].

Effect of Surface Coatings

It often is necessary to use oxidation-resistant coatings in high temperature materials applications in order to extend the service lives of components. The use of nickel-aluminide coatings on gas turbine engine blades

and vanes that operate at temperatures above 1500 F is one example. In addition, the discussion in the previous sections has indicated many instances for which there is a marked reduction in fatigue life in air compared to that in vacuum. Under such circumstances, and where fatigue properties are critical, it is possible to eliminate the effect of oxygen by use of a suitable surface coating.

The application of a coating to the surface of a material can have a number of effects relevant to the fatigue properties of the coating-substrate composite: (1) the deformation behavior of the substrate may be changed because of the presence of a surface layer having a different elastic modulus and yield strength from that of the substrate; (2) as long as the coating is sound, oxygen is kept away from the substrate and the effects of oxygen absorption and gross oxidation are eliminated; and (3) since the coating is at the surface, the fatigue properties of the coating in a gaseous environment become important. If the fatigue properties of the coating are better than that of the substrate, increased life may be expected. Figure 16*a* shows an intergranular crack initiated in a nickel-base superalloy below the uncracked coating. On the other hand, if the fatigue properties are poorer than the substrate, cracks in the coating will serve as surface notches and as paths for the oxygen to reach the substrate. Reduced fatigue life of the composite would then be expected. Figure 16*b* shows cracking initiated at the surface of a coating. Coatings frequently are more brittle than the substrate, so it is important that the maximum strain in the fatigue cycle does not exceed the fracture strain in the coating or else cracking of the coating will occur in the first tensile cycle. The strain for tensile fracture of the coating may be a sensitive function of temperature, as some coatings will undergo a ductile-to-brittle transition [*46*]. The effect that a coating has on composite fatigue properties depends on the strain range, the maximum tensile strain, temperature, frequency, and the nature of the coating itself. Some of these effects are discussed in more detail elsewhere in this publication.[4]

Phenomenological Effects

There are certain trends exhibited by most materials subject to high-temperature fatigue [*47–49*]. In this section, these trends will be discussed and explanations for them attempted based on the mechanisms described in the previous sections.

Temperature

Most materials exhibit reduced cycles to crack initiation and failure with increased temperature, Fig. 17. The yield strength of a material usually declines with increased temperature, and thus, in a given fatigue cycle, there

[4] See p. 401.

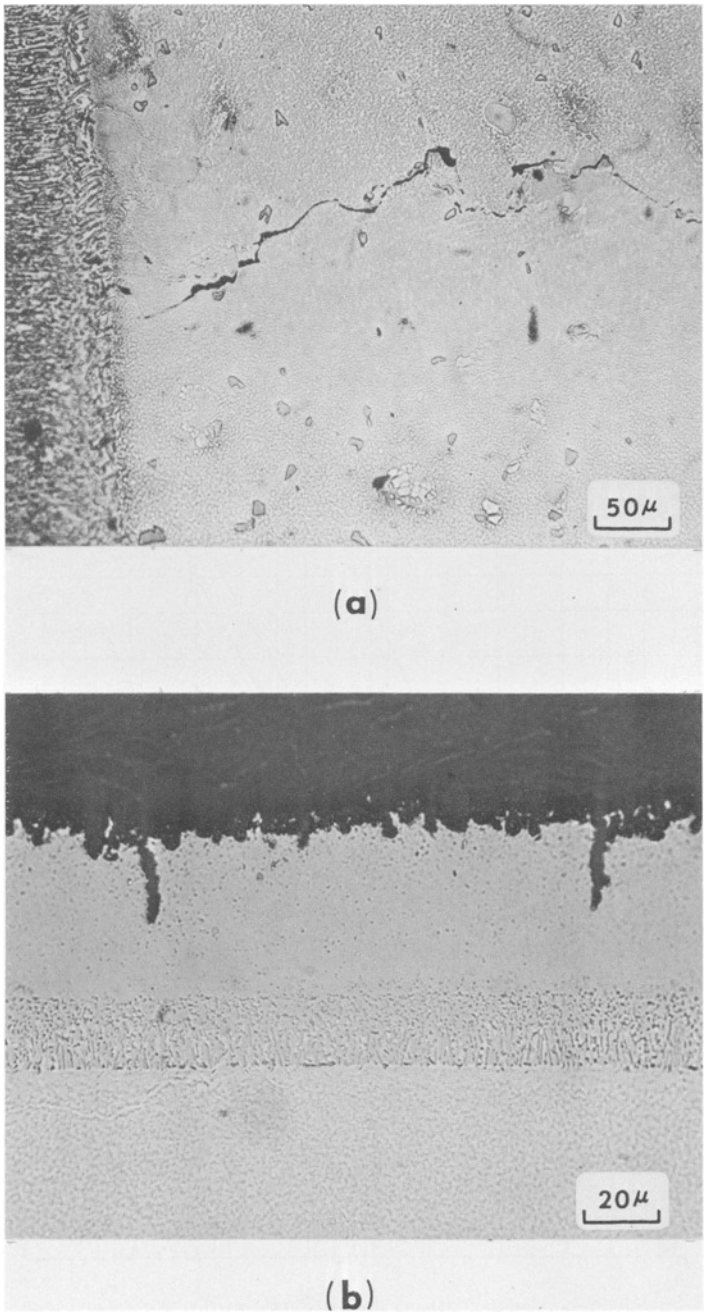


FIG. 16—*The influence of coatings on cracking in nickel-base superalloys*: (a) *intergranular cracking below coating in a thermomechanical fatigue test of B-1900 + hafnium alloy* (b) *coating fatigue cracks in single crystal Mar-M200 fatigued at 1700 F.*

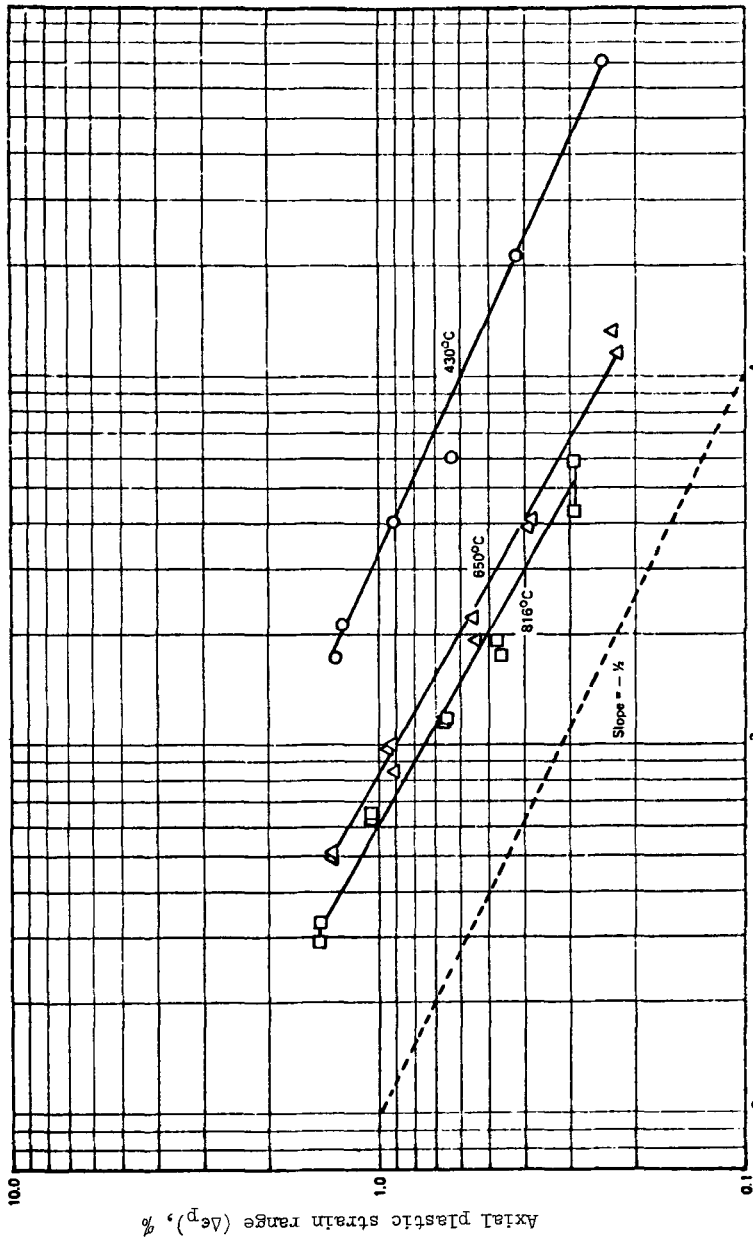


FIG. 17—*The fatigue life of Type 316 stainless steel as a function of temperature* [52].

is greater cyclic plasticity as the proportion of the plastic strain to total strain range increases. Even at a constant plastic strain range, fatigue properties are reduced with increasing temperature because of the transition from transgranular to intergranular cracking, Fig. 9.

Fatigue properties may improve with increased temperature under certain circumstances. Most ferrous materials and some nickel-base superalloys experience strain aging at temperatures above room temperature [*10,50*]. During strain aging, the pinning of dislocations by interstitial atoms such as carbon or the precipitation of phases on dislocations can lead to both a dispersal of planar slip and an increased yield strength. The former can lead to improved fatigue properties, while the latter can produce higher stress ranges for a given total strain range and reduced fatigue life.

As discussed in the section on Deformation Behavior, increased temperature promotes dispersal of planar slip. Slip dispersal can promote improved fatigue properties with increased temperature when fracture is entirely transgranular. This has been demonstrated for the case of single crystal nickel-base superalloys over a wide range of temperatures [*42,43*].

Frequency

At low temperatures, large changes in frequency have little or no effect on fatigue properties except for frequencies approaching the ultrasonic range [*51*]. At elevated temperatures where time dependent processes become significant, reductions in frequency generally produce major reductions in the cycles for crack initiation and propagation, Fig. 18. One of the common explanations for the frequency effect is that elastic strain is converted into plastic strain as a result of creep deformation or stress relaxation. However, it has been shown that there is a frequency effect even when tests are compared on a constant plastic strain range basis [*52*]. As with increased temperature, the effect of thermally activated deformation processes and oxidation on the promotion of intergranular cracking significantly accounts for lowered fatigue properties as frequency is reduced.

In materials that have a planar slip character at low temperatures, the effect of frequency on elevated temperature fatigue will be similar to that shown in Fig. 19 [*11*]. The fatigue life of wrought Udimet 700 at 1400 F increases by a factor of about 100 as the frequency is increased from 2 to 600 cpm. With a further increase in frequency to 60 000 cpm, the fatigue life is reduced by a factor of about seven. At the low frequencies, crack initiation occurs at surface-connected grain boundaries, and the initial mode of crack propagation is intergranular. With increased frequency, intergranular cracking produced by oxidation and creep deformation becomes less important, and fatigue life increases. At 180 cpm, crack initiation occurs at subsurface grain boundaries, but crack propagation is almost entirely transgranular, the initial mode being Stage I, Fig. 8. With an increase of frequency from 600 to 60 000 cpm, fatigue life is reduced by a factor of

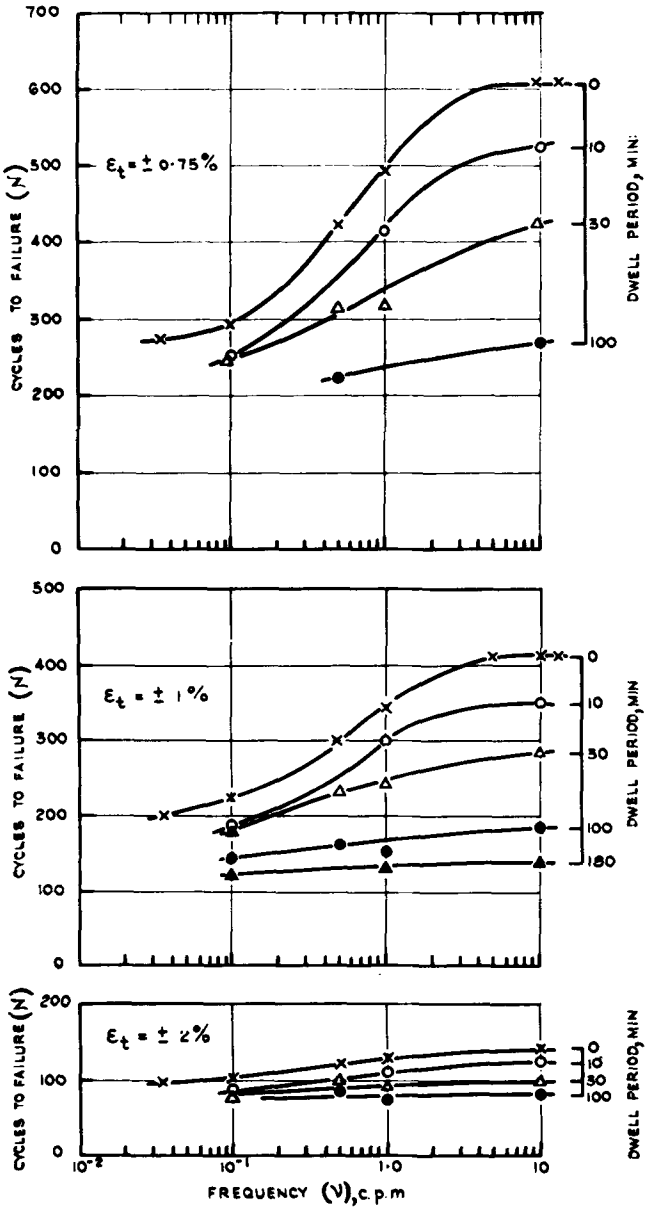


FIG. 18—*The fatigue life of a Cr-Mo-V steel as a function of frequency and dwell period* [54].

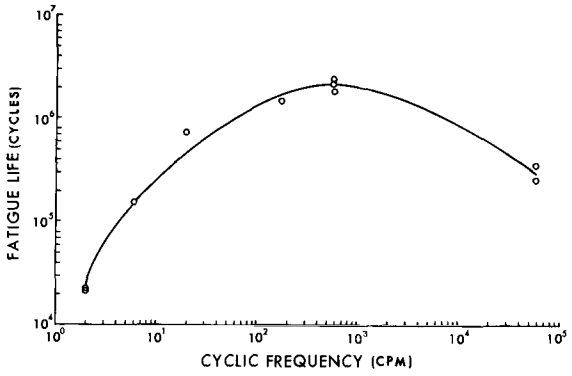


FIG. 19—*The effect of frequency on the fatigue life of wrought Udimet 700 at 1400 F* [11].

seven by the concentration of deformation in fewer slip bands; this accelerates Stage I crack initiation and propagation.

Combined Effects of Temperature and Frequency

Figure 20 shows schematically the effect of frequency at different temperatures on the fatigue life of a wavy and a planar slip material. At low temperatures, T_0, for both materials there is no frequency effect. For the wavy slip material, there is a reduction in life with increased temperature and reduced frequency. For the planar slip material at temperature T_2, the life first increases then falls with frequency. Raising the temperature to T_3 is equivalent to moving the T_2 curve downward and to the right, so that for the frequency range indicated, there is only an increased fatigue life with

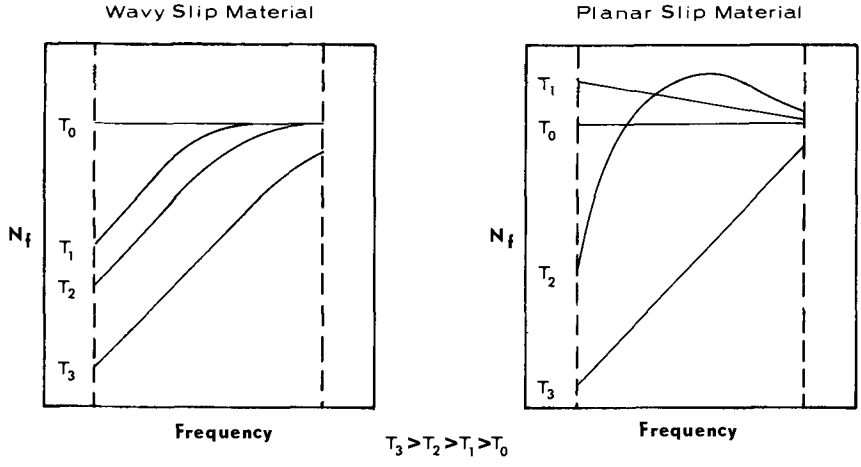


FIG. 20—*The effect of frequency and temperature on the fatigue life of wavy and planar slip materials.*

increased frequency. Lowering the temperature to T_1 is equivalent to moving the T_2 curve upward and to the left so that there is a reduced fatigue life with increased frequency. These trends with frequency have been demonstrated in single crystal MAR-M200 tested at 1400, 1550, and 1700 F.[3]

Dwell and Mean Stress Effects

Increased tensile dwells (Fig. 18) and mean stress enhance thermally activated deformation, cavitation, and intergranular cracking, and, as a result, generally reduce fatigue life [*47–49*]. The increased time per cycle upon introduction of a dwell period also promotes intergranular oxidation.

One of the more interesting effects is that of a compressive dwell. There is evidence (section on Fatigue Crack Initiation and Propagation) that compressive dwells retard or eliminate cavitation. On the other hand, once cavities are formed, the shape and, therefore, the rate of cavity growth may be dependent on whether a dwell is in tension or compression. A sharper, flattened cavity can be produced with a compressive hold and a rounder one with a tensile hold [*32*].

Summary

Elevated temperature fatigue fracture can be intergranular (along grain boundaries) or transgranular (across grains). The rate of crack initiation and propagation is much faster when it occurs intergranularly than when it occurs transgranularly. It is, therefore, important to be able to predict the mode of failure for given service conditions. If failure is transgranular, then it can occur in one of two modes: the Stage I mode is along slip planes and is in directions of high shear stress and the Stage II mode is noncrystallographic and normal to the principal stress direction. It is presently possible to predict under certain circumstances whether transgranular cracking will occur in the Stage I or Stage II modes, but the more significant transition from transgranular to intergranular cracking requires additional work.

The transition from transgranular to intergranular fracture and the rate of intergranular cracking can be related to the creep component and the amount of oxidation occurring in a fatigue cycle. Increasing the creep component and the degree of oxidation promotes intergranular cracking. The creep component is dependent on the temperature, frequency, holdtime, and mean stress. Cracking often starts in the form of cavities or microvoids at the surface of nonmetallic precipitates in grain boundaries. It has been demonstrated that such cavity formation occurs more easily in the presence of a fatigue stress than for the case of simple creep. Oxidation attack also promotes intergranular cracking because grain boundaries and their environs are zones of chemical segregation and precipitation that have poor

oxidation resistance. The preferential oxide penetration along a grain boundary is equivalent to a grain boundary notch of the same depth.

Perhaps the most success to date has been in relating the slip character and transgranular fracture mode of a material to conditions of temperature and frequency. Planar slip is favored by low temperatures, small strains, and high frequencies in materials of low stacking fault energy. It has been demonstrated in nickel-base superalloys that Stage I fracture occurs when planar slip is generated at a stress concentration or at a crack tip and that Stage II fracture occurs when wavy or homogeneous slip is generated. The conditions of temperature and strain rate for generation of each type of deformation have been determined.

These concepts of slip character, creep component, oxidation, and fracture mode have been used in a qualitative manner to explain the common phenomenological observations made in investigations of high-temperature fatigue.

References

[1] Wells, C. H., *Acta Metallurgica*, Vol. 17, 1969, pp. 443–449.

[2] Gell, M. and Leverant, G. R., *Fracture 1969*, Chapman and Hall, London, 1969, p. 565.

[3] Wells, C. H., Sullivan, C. P., and Gell, M. in *Metal Fatigue Damage: Mechanisms, Detection, Avoidance, and Repair, ASTM STP 495*, American Society for Testing and Materials, 1971, pp. 61–122.

[4] Nine, H. D. and Wood, W. A., *Journal Institute of Metals*, Vol. 95, 1967, pp. 252–254.

[5] Ronay, M., Reimann, W. H., and Wood, W. A., *Transactions*, American Institute of Mining, Metallurgical, and Petroleum Engineers, Vol. 223, 1965, pp. 298–304.

[6] Wells, C. H. and Sullivan, C. P., *Transactions Quarterly*, American Society for Metals, Vol. 61, 1968, pp. 149–155.

[7] Leverant, G. R., Gell, M., and Hopkins, S. W., *Materials Science and Engineering*, Vol. 8, 1971, pp. 125–133.

[8] Boettner, R. C., McEvily, A. J., and Liu, Y. C., *Philosophical Magazine*, Vol. 11, 1965, pp. 95–106.

[9] Wells, C. H. and Sullivan, C. P., *Transactions Quarterly*, American Society for Metals, Vol. 57, 1964, pp. 841–855.

[10] Wells, C. H. and Sullivan, C. P., *Transactions Quarterly*, American Society for Metals, Vol. 60, 1967, pp. 217–222.

[11] Organ, F. E. and Gell, M., *Metallurgical Transactions*, Vol. 2, 1971, pp. 943–952.

[12] Wells, C. H. and Sullivan, C. P., *Transactions Quarterly*, American Society for Metals, Vol. 58, 1965, pp. 391–402.

[13] Leverant, G. R. and Gell, M., *Transactions*, American Institute of Mining, Metallurgical, and Petroleum Engineers, Vol. 245, 1969, pp. 1167–1173.

[14] Gell, M., Leverant, G. R., and Wells, C. H., *Achievement of High Fatigue Resistance in Metals and Alloys, ASTM STP 467*, American Society for Testing and Materials, 1970, pp. 113–153.

[15] Gell, M. and Leverant, G. R., *Acta Metallurgica*, 1968, Vol. 16, pp. 553–361.

[16] Duquette, D. J. and Gell, M., *Metallurgical Transactions*, Vol. 2, 1971, pp. 1325–1331.

[17] Stubbington, C. A. and Forsyth, P. J. E., *Metallurgica*, Vol. 74, 1966, p. 15.

[18] Thompson, K. R. L. and Craig, J. V., *Metallurgical Transactions*, Vol. 1, 1970, pp. 1047–1048.

[19] Gell, M. and Leverant, G. R., *Transactions*, Metallurgical Society, American Institute of Mining, Metallurgical, and Petroleum Engineers, Vol. 242, 1968, pp. 1869–1879.

[20] Wigmore, G. and Smith, G. C., *Metal Science Journal*, Vol. 5, 1971, pp. 58–64.

[21] Williams, H. D. and Corti, C. W., *Metal Science Journal*, Vol. 2, 1968, pp. 28–31.
[22] May, M. J. and Honeycombe, R. W. K., *Journal*, Institute of Metals, Vol. 92, 1963–1964, pp. 41–49.
[23] Gittins, A., *Metal Science Journal*, Vol. 2, 1968, pp. 51–58.
[24] Skelton, R. P., *Philosophical Magazine*, Vol. 14, 1966, pp. 563–572.
[25] Gittins, A., *Metal Science Journal*, Vol. 2, 1968, pp. 114–117.
[26] Brookes, P. E., Kirby, N., and W. T. Burke, *Journal*, Institute of Metals, Vol. 88, 1959–1960, pp. 500–508.
[27] Driver, J. H., *Metal Science Journal*, Vol. 5, 1971, pp. 47–50.
[28] Driver, J. H. and Honeycombe, R. W. K., *Journal*, Iron and Steel Institute, Vol. 209, 1971, pp. 729–738.
[29] Skelton, R. P., *Metal Science Journal*, Vol. 2, 1968, pp. 144–148.
[30] Hill, G. J. in *Thermal and High Strains Fatigue*, Institute of Metals, M & R Series, No. 32, 1967, pp. 312–327.
[31] Dawson, R. A. T., Elder, W. J., Hill, G. J., and Price, A. T. in *Thermal and High Strain Fatigue*, Institute of Metals, M & R Series, No. 32, 1967, pp. 239–269.
[32] Wells, C. H. and Sullivan, C. P. in *Fatigue at High Temperature*, *ASTM STP 459*, American Society for Testing and Materials, 1969, pp. 59–74.
[33] Hull, D. and Rimmer, D. E., *Philosophical Magazine*, Vol. 4, 1959, pp. 673–687.
[34] Singhal, L. K. and Martin, J. W., *Transactions*, American Institute of Mining, Metallurgical, and Petroleum Engineers, Vol. 242, 1968, pp. 814–819.
[35] Wilson, D. J. and Freeman, J. W., "The Dependence of Mechanical Characteristics of Waspaloy at 1000–1400°F on the Gamma Prime Phase," NASA CR-72572, National Aeronautics and Space Administration, 1 Oct. 1969.
[36] Leverant, G. R. and Sullivan, C. P., *Transactions*, American Institute of Mining, Metallurgical, and Petroleum Engineers, Vol. 245, 1969, pp. 2035–2039.
[37] Berling, J. T. and Conway, J. B., referenced in *Hold-Time Effects in High Temperature Low-Cycle Fatigue, ASTM STP 489*, American Society for Testing and Materials, 1971, p. 12.
[38] Halford, G. R., "Cyclic Creep-Rupture Behavior of Three High-Temperature Alloys," NASA TN D-6309, National Aeronautcs Space Administration, May 1971.
[39] Smith, E. and Barnby, J. T., *Metal Science Journal*, Vol. 1, 1967, pp. 56–64.
[40] Johnston, J. R. and Ashbrook, R. L., "Oxidation and Thermal Fatigue Cracking of Nickel- and Cobalt-Base Alloys in a High Velocity Gas Stream," NASA TN D-5376, National Aeronautics and Space Administration, Aug. 1969.
[41] Howes, M. A. H., "Thermal Fatigue Data on 15 Nickel- and Cobalt-Base Alloys," NASA CR-72738, National Aeronautics and Space Administration, May 1970.
[42] Gell, M. and Duquette, D. J., *Corrosion Fatigue*, National Association of Corrosion Engineers, 1973, in press.
[43] Duquette, D. J. and Gell, M., *Metallurgical Transactions*, Vol. 3, 1972, pp. 1899–1905.
[44] Paskiet, G. F., Boone, D. H., and Sullivan, C. P., *Journal*, Institute of Metals, Vol. 100, 1972, pp. 58–62.
[45] McMahon, C. J. and Coffin, L. F., *Metallurgical Transactions*, Vol. 1, 1970, p. 3443.
[46] Boone, D. H. and Goward, G. W., *Ordered Alloys*, Claitor's Publication Division, Baton Rouge, La., 1970.
[47] Meleka, A. H., *Metallurgical Reviews*, Vol. 7, 1962, p. 43.
[48] *Thermal and High-Strain Fatigue*, The Metals and Metallurgy Trust, London, 1967.
[49] Ellison, E. G., *Journal of Mechanical Engineering Science*, Vol. 11, 1969, pp. 318–339.
[50] Coles, A. and Chitty, A., *Thermal and High-Strain Fatigue*, Metals and Metallurgy Trust, London, 1967, p. 328.
[51] Stephenson, N., Memorandum No. M. 320, National Gas Turbine Est, Pyestock, Hants, England, June 1958.
[52] Conway, J. B., Report No. GEMP-1004, General Electric Nuclear Material and Propulsion Operation, Cincinnati, Ohio, March 1968.
[53] Dieter, G. E., *Mechanical Metallurgy*, McGraw-Hill, New York, 1961, p. 94.
[54] Coles, A., Hill, G. J., Dawson, R. A. T., and Watson, S. J., *Thermal and High-Strain Fatigue*, Metals and Metallurgy Trust, London, 1967, p. 270.

DISCUSSION

Alfred Fox[1] *(written discussion)*—Your slide plotting the fatigue life versus frequency for Udimet 700 at 1400 F, showing fatigue life to increase from a frequency of 1 cpm to a frequency of 600 cpm and then showing a drop in fatigue life with a further increase in frequency. My question is whether this further drop could be associated with localized internal heating and creep effects.

M. Gell and G. R. Leverant (authors' closure)—The tests at 60 000 cpm were monitored continuously using an optical pyrometer with an accuracy of ±3 F, and no increase in temperature was observed. In addition, an increase in temperature would lead to enhanced slip dispersal and a higher, rather than a lower, fatigue life.

E. G. Ellison[2] *(written discussion)*—Dr. Gell has stated that an oxide filled crack propagated more slowly than one which initiated in vacuum. Does this mean that when the high strain cyclic results were plotted on the usual graph, total strain range versus cycles, that the air results were "above" the vacuum data? This would be unusual, unless, of course, the definition of failure explains it (initiation versus final fracture).

Messrs. Gell and Leverant—The crack growth rates in a single crystal nickel-base superalloy were slower in air than in vacuum, and the life in air was greater than that in vacuum [*2,42,43*].[3] However, in the air tests, the crack that led to failure was initiated at a subsurface location, so the life was not determined by crack growth in air [*43*].[3] It should be noted that the results just described are for transgranular crack propagation at very high temperatures, for example 1700 F. It is not known whether intergranular propagation in air would be faster or slower than intergranular propagation in vacuum under similar circumstances.

[1] Bell Telephone Laboratories, Murray Hill, N. J.
[2] University of Bristol, Bristol, England.
[3] See references in paper.

K. D. Challenger[1] *and John Moteff*[2]

Correlation of Substructure with the Elevated Temperature Low-Cycle Fatigue of AISI 304 and 316 Stainless Steels*

REFERENCE: Challenger, K. D. and Moteff, John, "**Correlation of Substructure with the Elevated Temperature Low-Cycle Fatigue of AISI 304 and 316 Stainless Steels,**" *Fatigue at Elevated Temperatures, ASTM STP 520*, American Society for Testing and Materials, 1973, pp. 68–79.

ABSTRACT: The dislocation substructure of AISI 304 and 316 stainless steels resulting from high strain fatigue for various strain rates at temperatures ranging from 430 to 816 C has been evaluated by transmission electron microscopy. The substructure is characterized quantitatively and correlated with the observed mechanical behavior. Dislocation cells or subgrains were observed for all test conditions with exception of one test where failure occurred in the high-cycle range. These results suggest that a change in deformation mechanisms appear to occur between 650 and 816 C. The Hollomon strain hardening equation is written in terms of the dislocation cell size for both monotonic and cyclic loading predicting higher strengths and strain hardening capabilities could be effected through cell size refinement.

KEY WORDS: thermal fatigue, stainless steels, dislocations (materials), strains, intergranular corrosion, substructures, breeder reactors

The objective of this study is to supply the much needed substructure data for AISI 304 and 316 stainless steels subsequent to high-temperature, low-cycle fatigue (LCF). This information is necessary for a more fundamental understanding of the mechanical behavior of these alloys at temperatures where their strength becomes time dependent. The interest in these materials stems from their expected use in the liquid metal fast breeder reactors (LMFBR) as fuel cladding and structural materials. In a LMFBR, not only will they be subjected to an extremely high neutron flux and fluence at temperatures near one half their absolute melting point (0.5 *Tm*) [*1*],[3] but

*This work was performed under the sponsorship of the United States Atomic Energy Commission through Contract No. AT(11–1)-2107.

[1] Materials development engineer, Breeder Reactor Department, General Electric Co., San Jose, Calif. 95114.

[2] Associate professor of Materials Science, Department of Materials Science and Metallurgical Engineering, University of Cincinnati, Cincinnati, Ohio 45221.

[3] The italic numbers in brackets refer to the list of references appended to this paper.

Copyright© 1973 by ASTM International www.astm.org

also stresses, both static and cyclic, approaching or possibly exceeding their yield strength.

Many studies have been performed that examined the dislocation substructures resulting from fatigue. The various dislocation arrangements reported for a variety of metals can be summarized as either cellular [*2*], two-dimensional (bands or planar arrays [*2,3*]), or clusters of loops [*4*]. Excellent reviews of this subject have been performed [*5,6*]. The parameters that are believed to determine the character of the substructure are: (1) slip character of the material (stacking fault energy, crystal structure, etc.), (2) temperature, and (3) cyclic strain amplitude (LCF life). Increased temperature, strain range or stacking fault energy all increase the propensity for dislocation cell formation.

A quantitative correlation between substructure and fatigue behavior should help explain some of the problems in LCF predictions.

Only very recently Coffin [*7*] has presented an empirical relation to predict LCF at elevated temperatures that appears to overcome the severe temperature limitations of the familiar LCF prediction equations based on the materials behavior under monotonic loading [*8–10*]. However, it is not the purpose of this study to propose any empirical prediction equation but to use the substructure data presented in this report in conjunction with that previously reported for fatigue [*11,12*] and creep [*13,14*] to provide the needed link between dislocation substructure and the observed LCF behavior. This connection should provide the necessary information for optimization of the dislocation substructure.

Experimental Procedure

Commercial grade AISI 304 and 316 stainless steels received in the form of 15-mm-diameter fully annealed rod were used for this study. The chemical composition of these Pacific Northwest reference heats is given in Ref *11*.

The specimen blanks were reannealed at 1066 C for $\frac{1}{2}$ h, water quenched to room temperature, machined, and subsequently stress relieved at 760 C in argon for 1 h. This treatment resulted in an equiaxed grain size of approximately ASTM 5 (70 μm) with some intergranular carbide precipitation. The test procedures for the fatigue and tension tests have been previously reported by Slot et al [*15*]. Basically, the procedure involves subjecting an inductively heated hourglass shaped specimen to electrohydraulic actuated, servo-controlled, push-pull fatigue. The controlled parameter for these tests was the total diametral strain.

Specimens were tested at strain ranges varying from 0.5 to 2.0 percent at true axial strain rates of 4×10^{-3}, 4×10^{-4}, and $4 \times 10^{-5} s^{-1}$. The reported tension tests were conducted on the same equipment at similar true strain rates.

Transverse disks suitable for electropolishing were cut adjacent to the fracture with a water-cooled precision cutoff machine. These disks were then trimmed in this same apparatus to size and thinned by standard twin-jet electropolishing techniques. A more detailed description of the procedure for thin foil preparation is reported elsewhere [*16*].

The characteristics of the substructure that were measured are: (1) dislocation cell or subgrain size, (2) mobile dislocation density, and (3) lattice misorientation between adjacent subgrains.

Discussion and Results

The tensile and fatigue data with their corresponding substructure characteristics are presented elsewhere [*12*].

Unfortunately, the dislocation cell size was the only characteristic of the substructure that allowed a meaningful correlation with mechanical properties as excessive scatter was found in the data on mobile dislocation density and subgrain misorientation. Trends do exist, however, where the stress (saturation stress of cyclically loaded specimens) was proportional to the square root of the mobile dislocation density and the lattice misorientation increased with increasing temperature.

The dislocation substructure typical of each test temperature for AISI 316 and 304 stainless steels are presented in Figs. 1 and 2, respectively. Either a cellular dislocation distribution or subgrains were observed in all specimens except AISI 316 stainless steel tested at 430 C – $\Delta\epsilon_t = 0.51$ percent where a planar dislocation array of a very high dislocation density had resulted, Fig. 1*a*. The fatigue life of this test was approximately 80 000 cycles and thus approaches the high-cycle range where this planar array of dislocations has been previously observed [*17*]. The substructure evolves from a very ragged dislocation cell arrangement at 430 C (Fig. 1*b*) to more distinctly defined cells at 650 C (Fig. 1*c* and *d*) to subgrains with regular low-angle boundaries at 816 C (Fig. 3*e* and *f*). Profuse $M_{23}C_6$ precipitation on cell boundaries has occurred at 650 C; the amount of precipitate present after each test was found to be directly related to the total time of the test, namely N_f/frequency. The precipitation evident in Fig. 1*c* and *d* represents close to the maximum amount observed. The cell walls at 430 and 650 C consist of a mass of dislocation tangles, multipoles, and loops, whereas at 816 C the subboundaries were identified as {111} twist boundaries, Figs. 1*f* and 2*d*.

The cells formed in AISI 304 stainless steel were generally slightly smaller and exhibited less recovery than those formed in AISI 316 stainless steel after fatigue at 650 C. A decrease in strain rate or range or an increase in temperature all promote a greater degree of recovery in the substructure. It is interesting to note that similar changes in the test parameters also promote intergranular fracture.

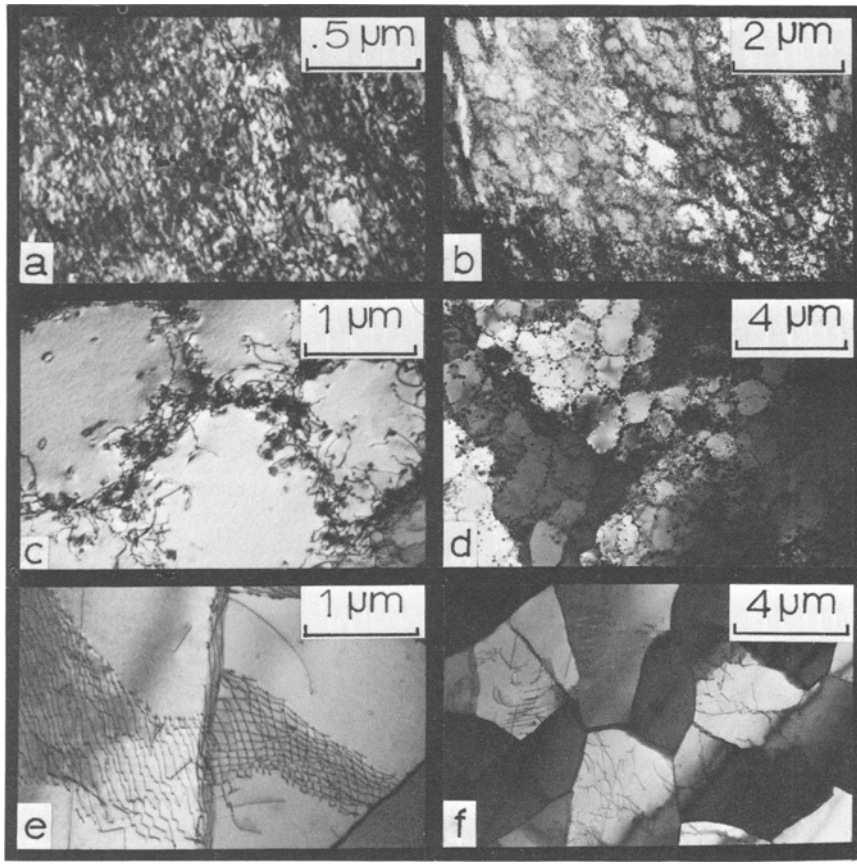


FIG. 1—*Typical dislocation substructure in AISI 316 stainless steel resulting from fatigue at* (a) *430 C*; $\Delta\epsilon = 0.5$ *percent*, (b) *430 C*; $\Delta\epsilon = 1.75$ *percent*, (c) *and* (d) *650 C, and* (e) *and* (f) *816 C.*

The substructure resulting from monotonic tensile loading is presented in Fig. 3. A substructure similar to that resulting from fatigue is observed; however, significantly less recovery is present in the substructure after monotonic loading. Although not evident in Fig. 3, the dislocation loop density appears to be considerably greater after fatigue consistent with the results of Feltner [*18*].

The effect of saturation stress, σ_s, on the subgrain size, d, of AISI 316 stainless steel is illustrated in Fig. 4. Two distinctly different behaviors are observed where at 816 C and low strain rates (4×10^{-4} and 4×10^{-5} s^{-1}) $d^{-1} \propto \sigma_s$, whereas at all strain rates at 650 C and the fastest strain rate at 816 C, $d^{-1/2} \propto \sigma_s$. The first relationship has been observed for subgrains resulting from creep of these alloys [*13,14*] and many other alloys [*19*]. The second relation was observed by Warrington for pure copper [*20*]. Here the sub-

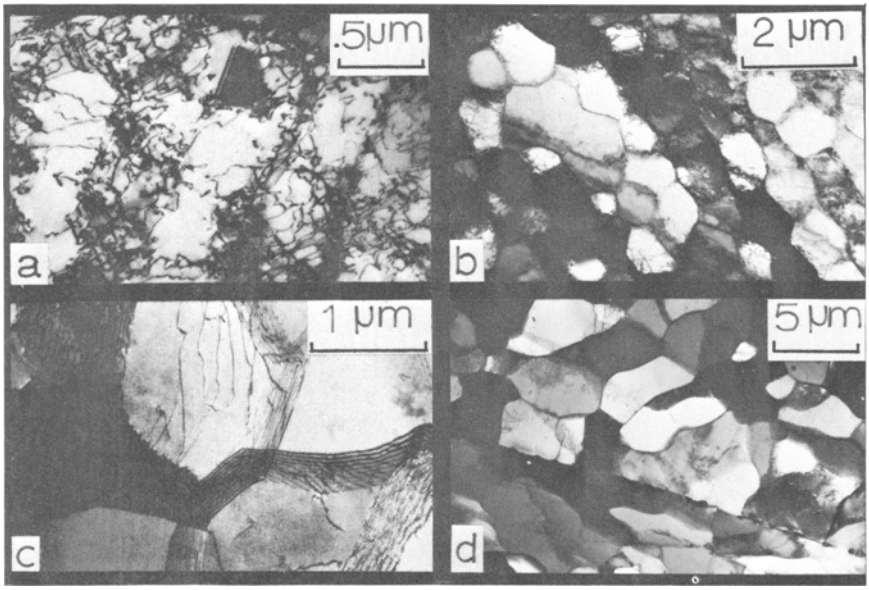


FIG. 2—*Typical dislocation substructure in AISI 304 stainless steel resulting from fatigue at* (a) *and* (b) *650 C and* (c) *and* (d) *816 C.*

grains were produced at elevated temperatures and subsequently tested at 0 C where the $d^{-1/2} \alpha \sigma$ was observed.

It was previously observed [*11*] that at a constant temperature and strain rate an increase in the total strain range had seemingly no effect on the subgrain size even though the saturation stress is increased through strain

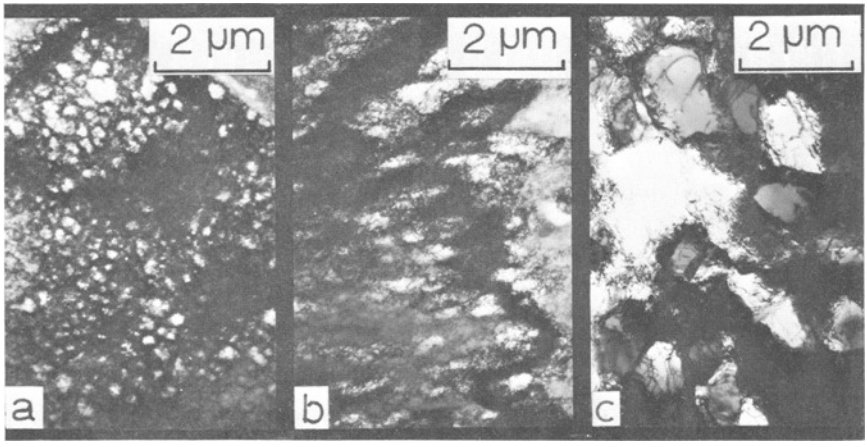


FIG. 3—*Typical dislocation substructure in AISI 316 stainless steel resulting from monotonic tensile loading at* (a) *430 C,* (b) *650 C, and* (c) *816 C.*

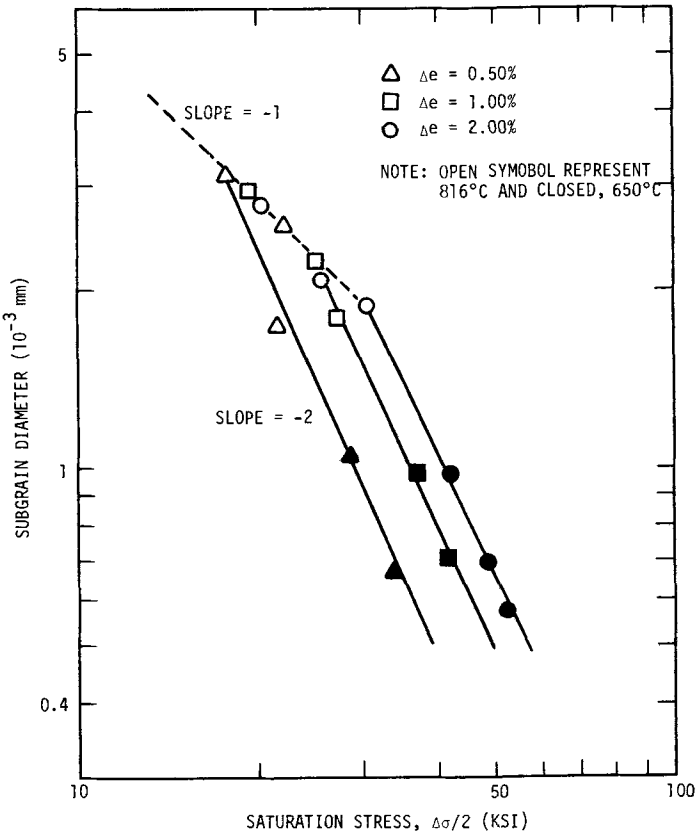


FIG. 4.—*Subgrain size dependence on saturation stress for the fatigue of AISI 316 stainless steel* [11].

hardening. We also have recently reported [*12*] that this tensile and fatigue data could be represented by the Hollomon equation.

A connection between the strain hardening exponent and the subgrain size is suggested since they both remain essentially constant at a fixed temperature and strain rate. This correlation was presented in a recent publication [*12*]. The influence of the cell or subgrain size on the strain hardening exponents n_f and n_t (cyclic and monotonic, respectively) is depicted in Fig. 5*a*. Although a straight line of slope -1 is drawn through the double log plot, extension to either high or lower values of d should result in the sigmoidal shaped curve denoted in the figure by the dashed line. This behavior is expected since, for these materials, the strain hardening exponent ranges from 0.5 to 0.6 low temperatures and approaches zero at high temperatures. A similar power relation is found to exist between the strength coefficients, k_f and k_t, and cell size, d, as illustrated in Fig. 5*b*. Although k_t and k_f appear to have the same power relation to $(1/d)$, a

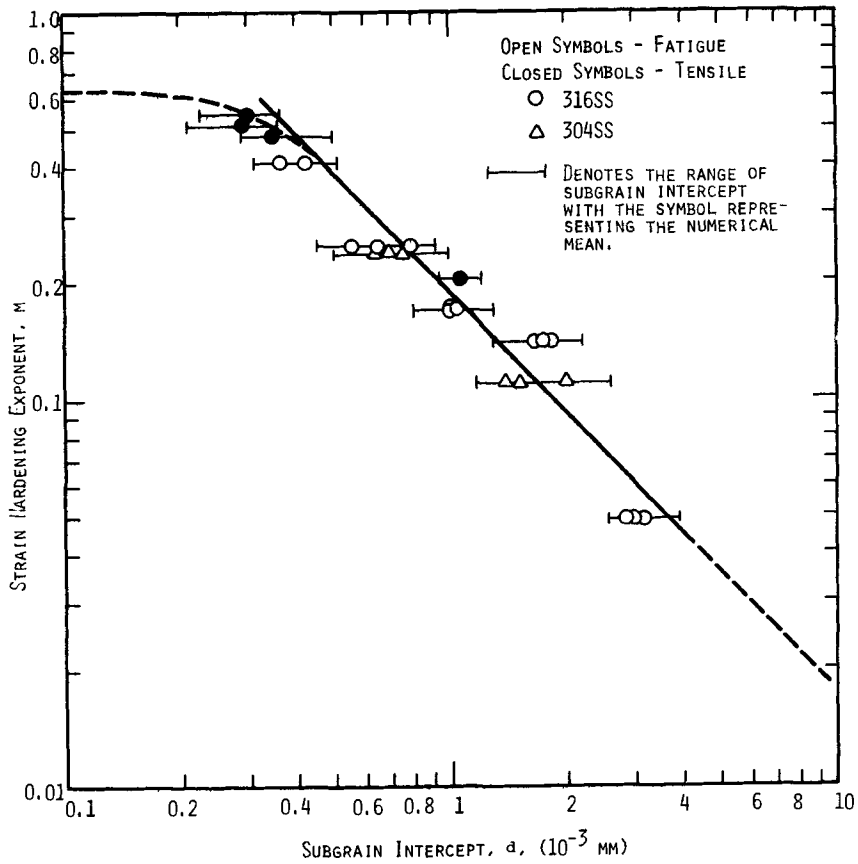


FIG. 5—*The dependence of* (a) *the strain hardening exponent and* (b) *the strength coefficient on the dislocation cell or subgrain size for AISI 304 and 316 stainless steels after both cyclic and monotonic loading* [12].

different coefficient in the relation exists. Hollomon equations can be devised from these results where the strength is a function of dislocation cell size, namely, [*12*],

$$\sigma_t = 60d^{-4/3}(\epsilon_t)^{0.0002/d} \qquad \text{(tensile)}$$

$$\frac{\Delta\sigma_s}{2} = 310d^{-4/3}\left(\frac{\Delta\epsilon_p}{2}\right)^{0.0002/d} \qquad \text{(fatigue)}$$

Thus, the Hollomon equation is interpreted where both the strength coefficient, k, and the strain hardening exponent, n, are a function of the dislocation cell size. However, it is believed that the strengths are only related indirectly to the cell size, but directly to the perfection of the cell boundary, that is, the strength of the boundary. Both Li [*21*] and Abson and Jonas [*22*] have proposed that the yield strength of the boundary increases as the perfection of the boundary decreases (due to an increase in

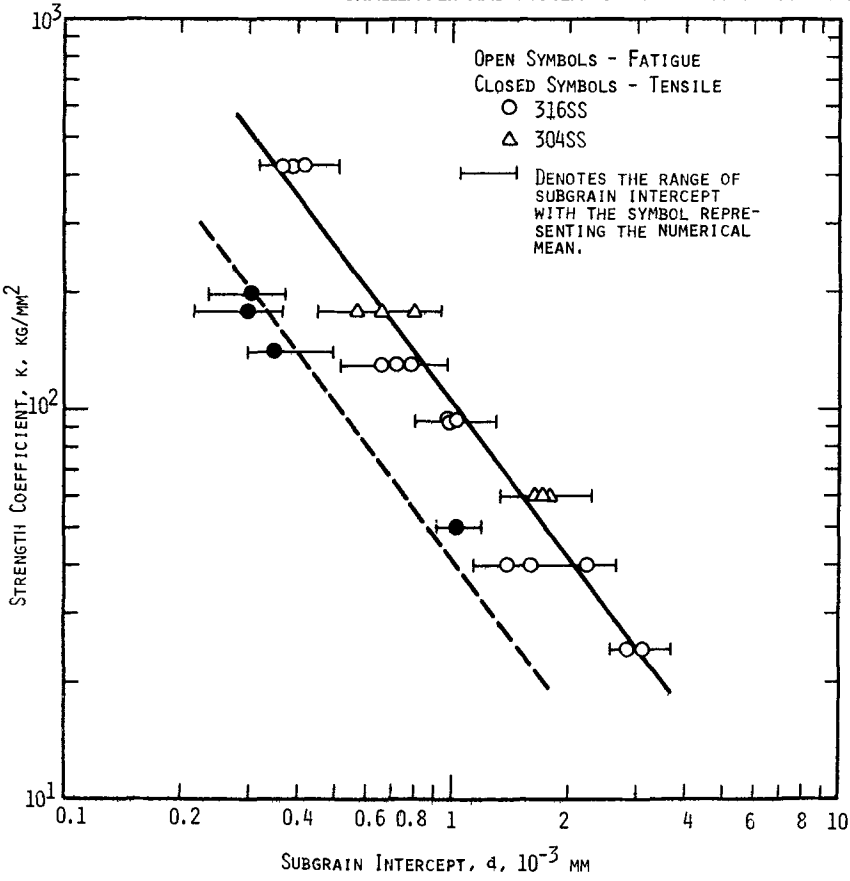


FIG. 5—(*Continued.*)

the density of redundant dislocations) and the misorientation increases. In the present study, the perfection of the boundary is a function of d, but the degree of misorientation across the boundaries seems to be directly related solely to the degree of polygonization present in a boundary. The misorientation is very low, <0.1 deg, for the cells produced at 650 C and averages about 0.5 deg for the subgrains produced at 816 C; however, the cells at 650 C appear to be more effective in increasing the strength of the material. The cell size and subgrain size has been used for the correlations in this study as it is believed that greater accuracy is possible in this measurement than in the measurement of dislocation densities.

The subgrain sizes reported in Refs *13* and *14* for creep are compared to those resulting from fatigue in Fig. 6. At 816 C, the slope of the double log plot of d versus σ is -1 for both the creep and fatigue results with the actual subgrain size being slightly smaller after creep. A possible explanation for the difference in subgrain sizes is that the creep texts were conducted under

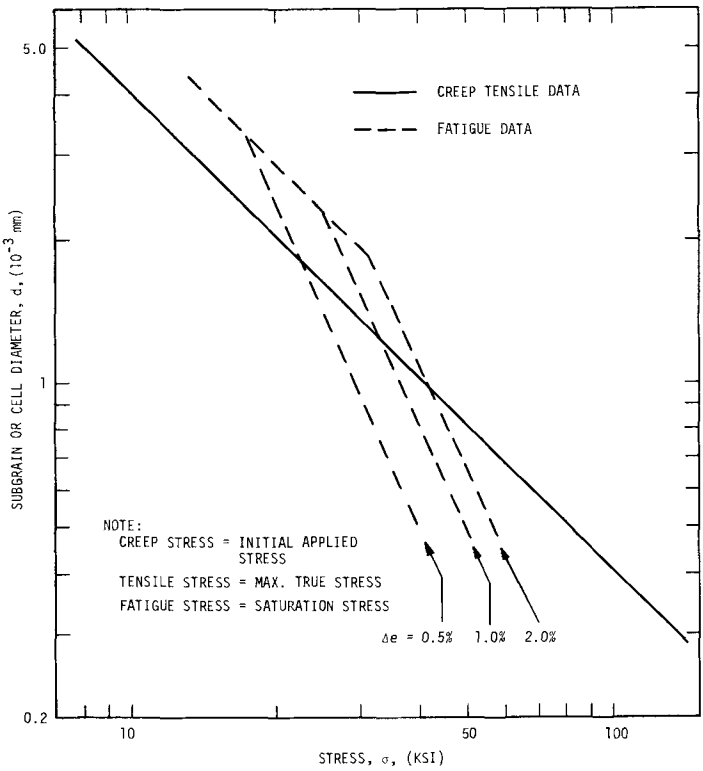


FIG. 6—*Comparison of dislocation cell sizes produced by creep and fatigue deformation in AISI 316 stainless steel for the temperature range of 650 to 816 C.*

constant load so that the final stress is slightly higher than that plotted in Fig. 6. At 650 C, the higher strain hardening capacity in fatigue testing versus creep testing is believed to have caused the change in slope from -1 to -2 in this plot resulting in smaller cells for the fatigue tests. In fact, in Ref *13*, it is noted that subgrain formation was very difficult in AISI 316 stainless steel creep tested at 650 C. This was believed due to the $M_{23}C_6$ precipitation occurring before a cell structure had evolved and thus preventing the rearrangement necessary for cell formation. In fatigue testing, the test is begun only shortly after reaching temperature and cell formation is believed to occur during the first few cycles so that any carbide precipitation should occur after cell formation and on the cell boundaries further strengthening the boundary.

The important conclusion to be drawn from this discussion is that at elevated temperatures ($T > 0.6\ Tm$), where $n \rightarrow 0$, similar deformation mechanisms appear to be operating whether the loading is static or cyclic. But at intermediate temperatures (0.4 to 0.6 *Tm*) the deformation mechanisms are much more strain rate sensitive so that different mechanisms

occur at high strain rates (possibly dislocation cross slip) and more time dependent mechanisms (possibly dislocation climb) begin to operate at low strain rates.

Conclusions

1. The substructure of AISI 304 and 316 stainless steels after high-strain fatigue in the temperature range of 430 to 816 C is characterized by the formation of dislocation cells or subgrains provided failure occurs in the low-cycle range ($N_f \lesssim 10^4$ cycles).

2. The cell size is related to the saturation stress through a power function, $d \propto \sigma^{-b}$, where $b = 1$ for deformation at 816 C and 2 for 650 C.

3. The cell size has a pronounced effect on both the strength coefficient and strain hardening exponent of the Hollomon equation for both monotonic and cyclic loading:

$$\sigma_t = 60d^{-4/3}(\epsilon_t)^{0.0002/d} \qquad \text{(tensile)}$$

$$\frac{\Delta\sigma_s}{2} = 310d^{-4/3}\left(\frac{\Delta\epsilon_p}{2}\right)^{0.0002/d} \qquad \text{(fatigue)}$$

4. Decreased strain rate promotes increased polygonization in the substructure and intergranular fracture.

5. At temperatures above 0.5 *Tm*, the creep and fatigue behavior of these alloys is very similar; $d \propto \sigma^{-1}$ for both modes of deformations. However, at lower temperatures this correlation does not exist and thus different deformation mechanisms are believed to be controlling.

References

[1] Brager, H. R., Straalsund, J. L., Holmes, J. J., and Bates, S. F., *Metallurgical Transactions*, Vol. 2, 1971, p. 1893.

[2] Feltner, C. E. and Laird, C., *Acta Metallurgica*, Vol. 15, 1967, p. 1633.

[3] McGrath, J. T. and Bratina, W. J., *Philosophical Magazine*, Vol. 12, 1965, p. 1293.

[4] Feltner, C. E., *Philosophical Magazine*, Vol. 8, 1963, p. 2121.

[5] Swann, P. R., *Electron Microscopy and Strength of Crystals*, Interscience, New York, 1963, p. 131.

[6] Plumbridge, W. J. and Ryder, D. A., *Metals and Materials Metallurgical Review*, Vol. 3, 1969, p. 321.

[7] Coffin, L. F., Jr., *Metallurgical Transactions*, Vol. 2, 1971, p. 3105.

[8] Coffin, L. F., Jr., *Transactions*, American Institute of Mining, Metallurgical, and Petroleum Engineers, Vol. 76, 1954, p. 931,

[9] Manson, S. S., NACA TN-2933, National Advisory Committee for Aeronautics.

[10] Berlin, J. T. and Conway, J. B., *Metallurgical Transactions*, Vol. 1, 1970, p. 805.

[11] Challenger, K. D. and Moteff, John, *Metallurgical Transactions*, Vol. 3, 1972, p. 1675.

[12] Challenger, K. D. and Moteff, John, *Scripta Metallurgica*, Vol. 6, 1972, p. 155.

[13] Challenger, K. D. and Moteff, John, submitted for publication.

[14] Cuddy, L. J., *Metallurgical Transactions*, Vol. 1, 1970, p. 395.

[15] Slot, T., Stentz, R. H., and Berling, J. T. in *Manual on Low Cycle Fatigue Testing, ASTM STP 465*, American Society for Testing and Materials, 1969, p. 100.

[16] Challenger, K. D., M.S. thesis, University of Cincinnati, Cincinnati, Ohio, June 1971.

[17] Hirsch, P. B., Patridge, P. G., and Segall, R. L., *Philosophical Magazine*, Vol. 4, 1959, p. 721.

[18] Feltner, C. E., *Acta Metallurgica*, Vol. 11, 1963, p. 817.
[19] Sherby, O. D. and Burke, P. M., *Progress in Materials Science*, Vol. 13, 1967, p. 325.
[20] Warrington, D. H. in *Proceedings*, European Regional Conference of Electron Microscopy, Delft, 1960, p. 354.
[21] Li, J. C. M., *Transactions*, American Institute of Mining, Metallurgical, and Petroleum Engineers, Vol. 227, p. 239.
[22] Abson, D. J. and Jonas, J. J., *Metals Science Journal*, Vol. 4, 1970, p. 24.

DISCUSSION

J. C. Grosskreutz[1] (*written discussion*)—What mechanism do you have to account for your proposal that the degree of strengthening is due to the configuration of the cell boundaries? Do you think the dislocations withn the boundaries are part of the mobile population?

K. D. Challenger and John Moteff (*authors' closure*)—To answer your first question, the mechanism we are thinking of was first proposed by D. Kuhlmann-Wilsdorf, where the bowing out of free mesh lengths of dislocations from the cell wall control the saturation stress. The average mesh length will decrease with increasing subboundary dislocation density, which in the case of this study, is the same as decreasing cell size. The smaller the free mesh length, the higher the saturation stress.

The answer to your second question is no. To qualify this one might say that the mobile dislocations must come from the subboundary. In fact, we have observed recently that for creep deformation in these alloys, the mobile dislocation density is proportional to the subboundary area.

Campbell Laird[2] (*written discussion*)—The relationship you have observed between the cyclic hardening parameters and the more or less constant cell size shown by Types 304 and 316 steels is interesting. However, it is in conflict with the earlier work of the Pratt & Whitney Aircraft laboratory on nickel and TD nickel. In that study, the two materials showed virtually identical cyclic stress strain response, but the cell sizes were different. For the TD nickel, the thoria particles effectively controlled the cell size, but the structure of the dislocations within the walls was interpreted to control the cyclic response. How do you reconcile the differences between the Pratt & Whitney Aircraft results and your own?

[1] National Bureau of Standards, Washington, D. C. 20234.
[2] Department of Metallurgy, University of Pennsylvania, Philadelphia, Pa. 19104.

Messrs. Challenger and Moteff—We believe that the answer to this question is partially contained in our answer to Dr. Grosskreutz's question. Although the strain hardening parameters are found related to the dislocation cell size, we believe the strengthening mechanism is related to the free dislocation mesh lengths. This mesh length is related to the subboundary dislocation density or the perfection of the subboundary. We found that for these alloys the subboundary perfection decreased with decreasing cell size, thus relating cell size and subboundary perfection. However, this was not the case for the Pratt & Whitney Aircraft work.[3] Although the thoria particles controlled the dislocation cell size, the dislocation free mesh length remained a function of only test conditions. Thus, the cell size was not related to the subboundary perfection for their experiment.

H. Abdel-Raouf[4] (*written discussion*)—What is the effect of deformation mode (cyclic or monotonic) on the misorientation across the cell walls?

Messrs. Challenger and Moteff—As we mentioned, there is extreme scatter in the data obtained on lattice misorientation across cell or subgrain boundaries that prevented any significant conclusions in this regard. However, a trend does exist where the misorientation increases with increasing test temperature. Now, if we relate this observation to the degree of recovery present in the substructure, then one would say that the monotonically loaded specimens had less misorientation, but this is only speculation.

E. Krempl[5] (*written discussion*)—Subgrain size appears to be affected by the total strain the material was subjected to. Did you observe any influence by comparing monotonic tests (total strain about 30 percent and higher) with low-cycle fatigue tests (total strain less than 2 percent)?

Messrs. Challenger and Moteff—As a general rule, we find that the subgrain or dislocation cell size is smaller for monotonic loading than cyclic when compared under similar test conditions and at the same stress (saturation stress versus maximum true stress). However, as we indicated, we believe that this is due to the difference in the strain hardening behavior of the material under the different loading conditions. Even though a different subgrain size is obtained for the different loading conditions, a plot of log stress versus log (strain hardening exponent) is a straight line passing through all of the data.

[3] Leverant, G. and Sullivan, C., *Transactions*, American Institute of Mining, Metallurgical, and Petroleum Engineers, Vol. 242, 1968, p. 2347.

[4] Department of Mechanical Engineering, University of Waterloo, Waterloo, Ont., Canada.

[5] Division of Mechanics, Rensselaer Polytechnic Institute, Troy, N. Y. 12181.

Shuji Taira[1]

Relationship Between Thermal Fatigue and Low-Cycle Fatigue at Elevated Temperature

REFERENCE: Taira, Shuji, **"Relationship Between Thermal Fatigue and Low-Cycle Fatigue at Elevated Temperature,"** *Fatigue at Elevated Temperatures, ASTM STP 520*, American Society for Testing and Materials, 1973, pp. 80–101.

ABSTRACT: This paper discusses the correlation between thermal fatigue and low-cycle fatigue at elevated temperature in terms of the change in microstructure of materials during the fatigue process. It substantiates the formula for life prediction in fatigue at elevated temperature which has been proposed by the author and co-workers with experimental proof. It is found that the characteristic feature of the low-cycle fatigue of a low-carbon steel at the test temperature above 500 C is taken as a diffusion controlled process characterized by the formation of subgrains in the change of microstructure, proved by observations with an optical microscope as well as X-ray diffraction techniques. The same feature is observed in the case of thermal fatigue where the upper bound of temperature in temperature cycling is close to or above 500 C. The temperature level of low-cycle fatigue giving the same fatigue life as a thermal fatigue testing, that is, the equivalent temperature of thermal fatigue is close to the upper bound of temperature of thermal fatigue. In contrast, for the test of thermal fatigue or low-cycle fatigue where such a high temperature is not included in either the range or the level of test temperature, the fatigue damage is taken as controlled by the slip mechanism. The equivalent test temperature is close to the mean of the upper and the lower bound of thermal fatigue.

KEY WORDS: X-ray diffraction, fatigue (materials), thermal fatigue, equivalent temperature, damage, carbon steels, subgrain, grain boundaries, crack initiation

In the last several years there has been a marked increase in research efforts aimed at a better understanding of the cyclic dependent mechanical behavior of metals at elevated temperatures, especially of thermal fatigue and high-temperature low-cycle fatigue of structural materials [*1–3*].[2] However, it should be noted that most of the recent investigations in this field are concerned with high-temperature low-cycle fatigue, and papers related to thermal fatigue are limited. This may be attributed to the trend that thermal fatigue is regarded simply as a special case of high-temperature low-cycle fatigue, while there is still room to study the effect of temperature cycling superimposed on strain cycling in the fatigue process. The aim of

[1] Professor, Department of Mechanical Engineering, Kyoto University, Kyoto, Japan.

[2] The italic numbers in brackets refer to the list of references appended to this paper.

Copyright© 1973 by ASTM International www.astm.org

the present study is to discuss the correlation between thermal fatigue and low-cycle fatigue on the basis of the observation of the change in microstructure of materials during fatigue process using a low-carbon steel as the specimens, so as to establish the method of life prediction in thermal fatigue of a material from the test results on high-temperature low-cycle fatigue of the same material.

Several years ago I proposed a formula for life prediction of fatigue of metals at elevated temperature based on the cumulative damage hypothesis, for the purpose of introducing the effect of temperature cycling in the formula of fatigue at elevated temperature [*4*]. The formula facilitates replacing the complex test of thermal fatigue by the simple test of low-cycle fatigue at a temperature which gives the same fatigue life in both cases. I believe that the formula is promising for the primary aim of this line of work; the quality of the formula may be improved by referring to the information on the change in structure of materials during fatigue at elevated temperature of strain cycling with or without superimposed temperature cycling.

For observation of the microstructure of material, an optical microscope and X-ray diffraction techniques were employed. The change in microstructure, which has occurred in the fatigued material, was carefully observed mainly by optical microscope. Since, at an early stage of this work, it was found that the characteristic feature of the change in microstructure during fatigue at elevated temperature was the formation of subgrain, X-ray diffraction profile analysis and X-ray microbeam techniques have been employed to substantiate this phenomenon as experimental tools that are sensitive for detecting the formation of substructures.

Material Tested and Testing Procedure

Material Tested and Specimens

The test material is a 0.16 percent carbon steel. Relevant details on the chemical composition is listed in Table 1.

TABLE 1—*Chemical composition of the material tested, weight percent.*

C	Si	Mn	P	S	Cu	Ni	Cr
0.16	0.19	0.43	0.013	0.029	0.08	0.02	0.04

In Fig. 1, the sketch of the specimen geometry is shown. Round specimens for thermal and low-cycle fatigue tests have a gage section in the shape of an hourglass. After machining, both types of specimens were annealed at 950 C for 30 min in a vacuum. Table 2 shows the mechanical properties of the annealed material at room temperature.

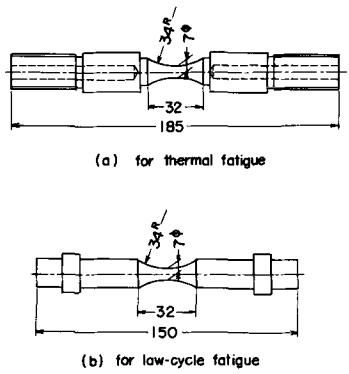


FIG. 1—*Test specimens.*

TABLE 2—*Mechanical properties at room temperature.*

Yield Point, kg/mm²	Tensile Strength, kg/mm²	Elongation, %	Reduction in Area, %
26.0	41.0	38.8	44.0

Testing Equipment

Figure 2 is a schematic drawing of the testing equipment for thermal fatigue and low-cycle fatigue at elevated temperatures. In thermal-fatigue testing, the specimen was clamped in the fixtures of the so-called Coffin type, such that it was in compression at high-temperature range and tension at low-temperature range during thermal cycling. For cyclic heating of the specimen, an induction coil surrounding the gage section was em-

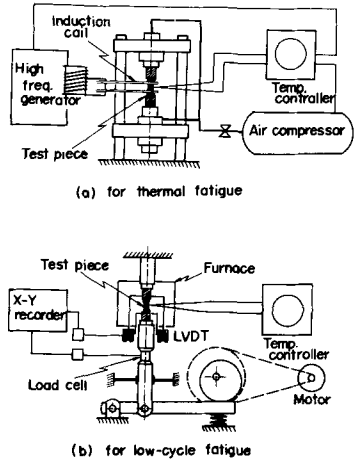


FIG. 2—*Schematic drawing of testing apparatus.*

ployed. In order to cool the specimen, compressed air was blown into it through central holes drilled from both ends of the gage section. Attention was paid to the geometry of the coil to give a flat axial temperature profile in the gage section. Figure 3 shows axial temperature distribution during a thermal cycle for three kinds of temperature range.

Push-and-pull low-cycle fatigue tests were carried out at several temperature levels. The test specimen was heated by means of an electric furnace. The strain range was controlled by employing a linear variable differential transducer (LVDT) fixed to two sets of extension rods clamped to the ridges close to the ends of the gage length [5].

The rate of cycling in thermal as well as low-cycle fatigue tests is about 2 cpm without holdtime in the cycle.

Observation of Microstructures

In order to observe the change in microstructures of the material during fatigue process, the fatigued specimens before fracture and the failed specimens containing cracks of about 1 mm depth were cut along the axis and electropolished. The surface revealed by polishing was observed carefully by optical microscope and also by X-ray diffraction technique [6–8].

Test Results

Microstructure Change During Thermal Fatigue

Figure 4 shows the change in microstructures of the specimens during thermal fatigue in the conditions of temperature cycling as are shown in Fig. 3. Looking at the case of test condition of (*a*) 200 to 600 C, for instance, etched veins that have appeared by preferential corrosion are found in ferrite grains as early as the cycle number corresponding to 10 percent of the fatigue life ($n = 40$). These etched veins turn to the boundaries of subgrains during further cycling of temperature; thus, the subgrains develop

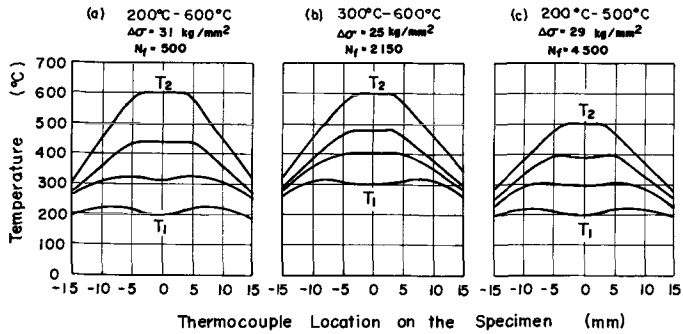


FIG. 3—*Temperature distributions along the axis of specimen during a thermal cycle.*

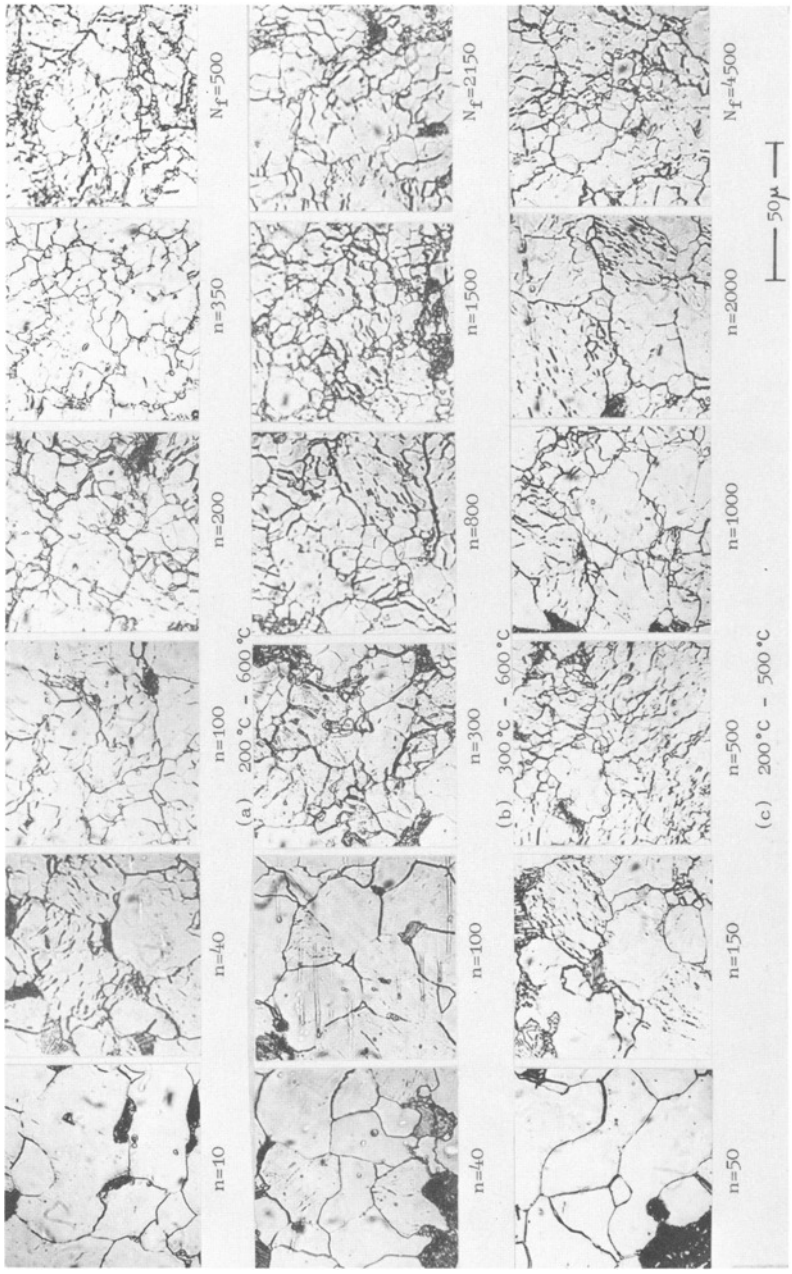


FIG. 4—*Micrographs of thermal-fatigued specimens.*

rapidly at the beginning of fatigue process resulting in the microscopically visible network of subgrain boundaries at $n = 100$. At a later stage of fatigue ($n = 200$ and 350), an equilibrium size of subgrains develop, and original grain boundaries and sub-boundaries become indistinguishable.

Similar changes in the microstructure were observed in other test conditions of (*b*) 300 to 600 C and (*c*) 200 to 500 C. From the micrographs of failed specimens for three different test conditions, it is understood that the size of subgrains tends to approach the equilibrium size of about 2 μm in all cases (note original grain size: 25 μm). The presence of such subgrains is substantiated also by the microbeam X-ray patterns as shown in Fig. 5, where it is found that the diffraction ring is composed of fine discrete spots indicating the proof of independent subgrains [*7*].

Therefore, the major change of microstructure during thermal fatigue in the range as described previously consists of the formation and development of subgrains, as is characteristic of the change in microstructure of various metals deformed at elevated temperature [*9*]. The schematic representation of the change in subgrain size and the clearness of the subgrain appearance during thermal fatigue is illustrated in Fig. 6, being derived from the micrographs shown in Fig. 4.

An additional distinguishing feature of the change in microstructures during the thermal fatigue is the evidence of outstanding mobility of structure in the vicinity of grain boundaries. As is seen in Fig. 4, the migration begins to occur at some grain boundaries simultaneously with the formation of subgrains.

Microstructure Change During Low-Cycle Fatigue at Elevated Temperatures

Figure 7 indicates the change in microstructure in the case of low-cycle fatigue at test temperatures of 200 and 500 C. The microstructure of material fatigued at 200 C (Fig. 7*a*) exhibits no clear evidence of subgrains, which is typical of the high temperature fatigue at 500 C but has the appearance of grain-boundary serration, suggesting a high dislocation density within the grains. On the other hand, in the case of fatigue at 500 C (Figs. 7*b* and *c*), the surface of every grain has a rumpled or folded appearance from the early stage of fatigue. And the subgrain boundaries outlined by the folds develop gradually with the increase in the number of cycles. Thus, we find an outstanding difference in the change in microstructure, observed on micrographs, between the material fatigued at 200 and 500 C. In this connection, micrographs that are taken on failed material by strain cycling tested at various temperature levels are demonstrated in Fig. 8, in order to visualize the difference of microstructure of failed material in different temperatures of low-cycle fatigue. These were chosen from other series of studies. It is found that the formation of substructures below 400 C is relatively inactive, while a remarkable trace of subgrains at 500 C is found.

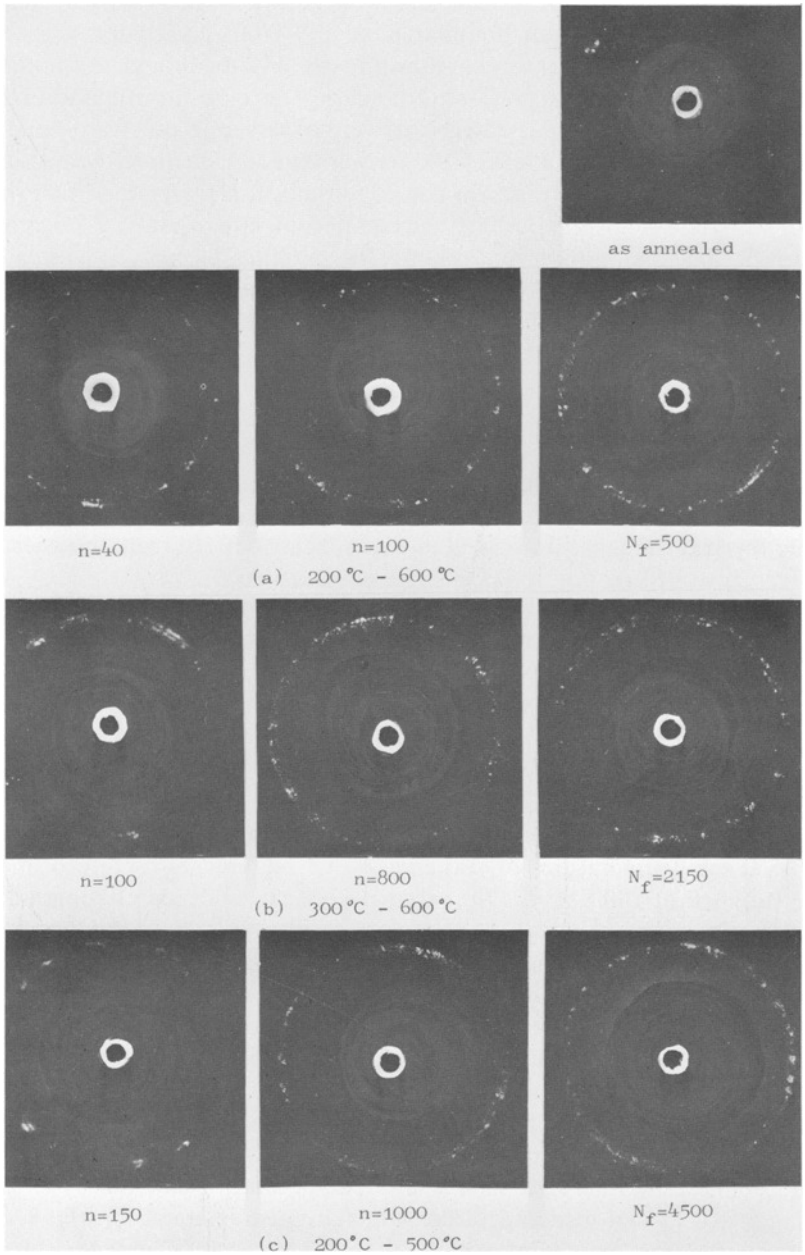


FIG. 5—*Microbeam X-ray diffraction patterns obtained from thermal-fatigued specimens.*

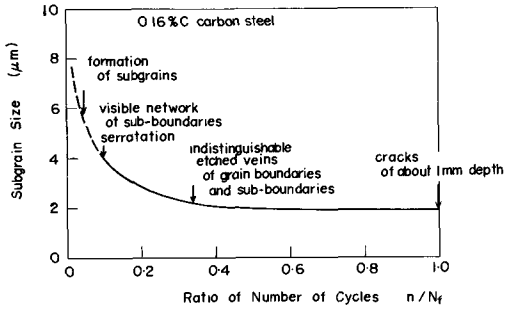


FIG. 6—*Change in subgrain size during thermal fatigue.*

The feature of microstructure of failed material by strain cycling is also studied by employing the X-ray microbeam technique. The X-ray patterns are exhibited on Fig. 9 for the case of tests at 23, 200, and 500 C. The pattern of the 500 C test shows fine discrete spots similar to those shown in Fig. 6. It corresponds to the observation by microscope. However, the pattern of 200 C is quite different from the case of 500 C, but close to the pattern of the room-temperature test, showing a little vague spotty ring of diffraction pattern.

Change in Integral Breadth of X-ray Diffraction Profile During Thermal Fatigue and Low-Cycle Fatigue

The integral breadth B of X-ray diffraction profile supplied by use of the precise X-ray diffractometer is another measure to evaluate the change in microstructure of materials. In order to confirm the result of the qualitative observation described above, the measurement of the integral breadth was carried out, employing (220) diffraction, for the specimens before and during the test of low-cycle fatigue at 200 and 500 C, and also of thermal fatigue of temperature cycling between 200 and 500 C. The result is shown in Fig. 10 as a diagram of the integral breadth ratio B/B_0 (B_0 is initial value) versus the ratio of number of cycles n/N_f (N_f is cycle number at failure). The breadth increases markedly at a very early stage of fatigue and thereafter holds almost the same value till failure in all cases. It is interesting to note that the mode of change in the breadth during thermal fatigue of temperature cycling between 200 and 500 C is close to that of low-cycle fatigue at 500 C rather than that at 200 C.

It is known that the integral breadth of the X-ray diffraction profile itself is a measure of the compound effect of microlattice strain of matrix and subgrain size. Also its change offers information on the average change in microstructure of irradiated area by X-ray (80 mm^2). We find a significant difference between the level of integral breadth during fatigue at higher (500 C) and intermediate temperature range (200 C).

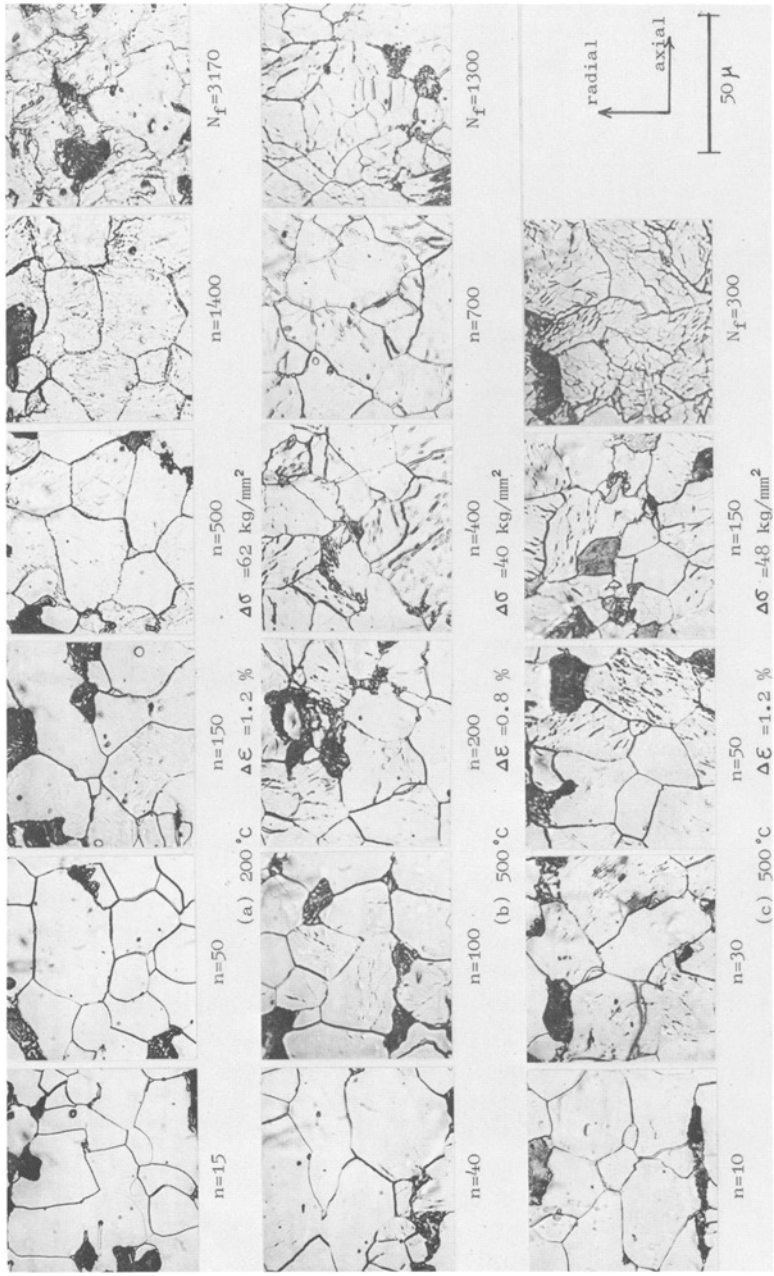


FIG. 7—*Micrographs of low-cycle fatigue specimens.*

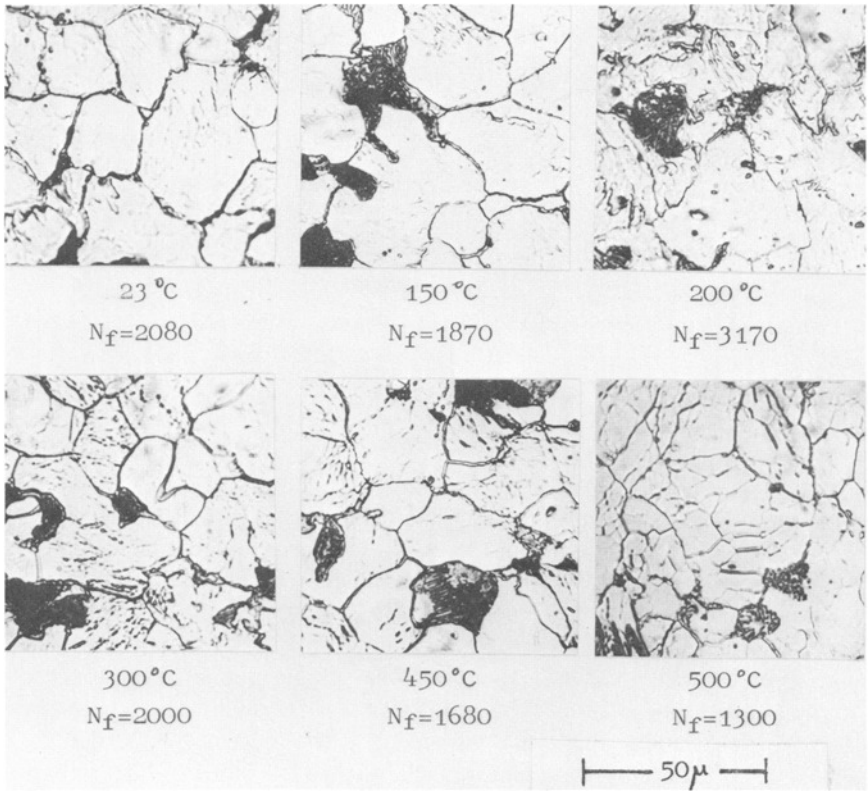


FIG. 8—*Micrographs of failed specimens in low-cycle fatigue tested at various temperature levels.*

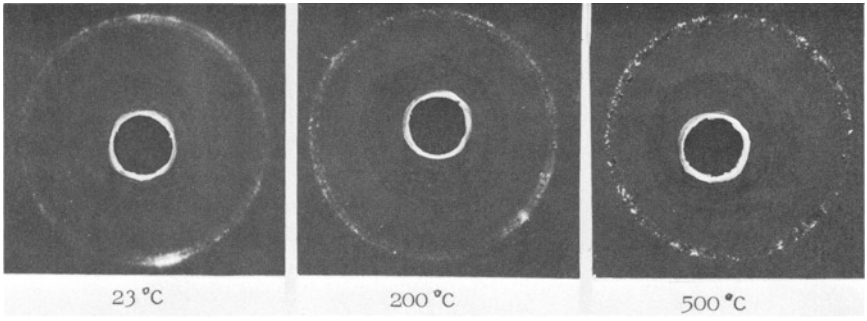


FIG. 9—*Microbeam X-ray diffraction patterns obtained from low-cycle fatigued specimens.*

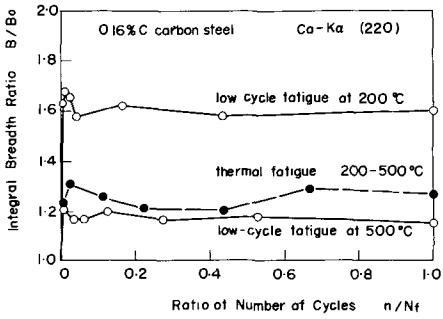


FIG. 10—*Change in integral breadth ratio during thermal fatigue and low-cycle fatigue.*

Discussion

Change in Microstructure During Thermal Fatigue and Low-Cycle Fatigue at Elevated Temperature

Although the observation of change in microstructure during fatigue is limited to a few test conditions on a low-carbon steel, the result leads us to the following brief discussion on the mechanism of fatigue at elevated temperature.

When we compare the micrographs shown in Fig. 4 for thermal fatigue with those shown in Fig. 7 for low-cycle fatigue and also compare the X-ray microbeam patterns shown in Fig. 5 for thermal fatigue with those shown in Fig. 8 for low-cycle fatigue, it is found that the fundamental character of the change in structure is parallel to the mode of fatigue by the strain cycling both with and without superimposed temperature cycling. However, it is understood that the remarkable increase of integral breadth at early stage of fatigue, as seen in Fig. 10, is a proof of notable work hardening due to the increase of dislocation density in matrix of initially clean crystal structure by cycling of plastic strain. On the other hand, the effect of elevated temperature may be softening due to recovery of structure. Thus the change in microstructure during fatigue at elevated temperature is taken as a proof of the equilibrium process of cyclic work hardening and cyclic softening. Thus, the rate and the extent of increase in integral breadth at early stage (Fig. 10) are more pronounced for fatigue at lower temperature ranges. The equilibrium value of breadth ratio for individual test conditions is kept during subsequent cycle numbers till failure. This observation complies with the existence of the steady state of plastic strain range $\Delta\epsilon_p$ as well as that of stress range $\Delta\sigma$ in testing [*8,10,11*].

It should be noted that initiation and propagation of microscopic crack are extremely local phenomena [*12,13*], probably relevant to local sliding along subgrain boundary [*14–16*]. Formation of substructure is the evidence of recovery of matrix, resulting from movement of dislocations towards sub-boundaries. Thus, high density of dislocation exists along the

sub-boundary in well developed subgrain structures. This sort of mechanism would be accelerated by elevating temperature during strain cycling, as the diffusion controlled mechanism. From the features of microstructure change, the fatigue by strain cycling at higher temperature range could be considered to belong to this category.

In contrast to the above, evident appearance of subgrains has not been observed in the microstructure for the fatigue at lower temperature range except in the final stage of fatigue life, where formation of substructure is observed on the X-ray microbeam pattern. Instead, trace of slip appearing in matrix is rather pronounced in this case, similar to the case of low-cycle fatigue at room temperature. Thus, this would be called a slip controlled mechanism.

Relation Between Thermal Fatigue Strength and Low-Cycle Fatigue Strength

The quantitative relation between plastic strain per cycle $\Delta\epsilon_p$ and number of cycles to failure N_f has hitherto been determined by the well-known relation in the form

$$\Delta\epsilon_p \cdot N_f^{\alpha} = C \quad \ldots\ldots (1)$$

by Manson [*17*] and Coffin [*18*] for a wide number of materials in both thermal and low-cycle fatigue. In many cases the value of the exponent α in Eq 1 is said to be $1/2$ for a better correlation of data. It also appears from Coffin's investigation [*18*] that the value of C in Eq 1 can be determined approximately by taking the tension test as a part of low-cycle fatigue or a thermal fatigue by taking $1/4$ cycle. Thus, $C = \epsilon_f/2$, where ϵ_f is the fracture strain in tension. However, the influence of temperature is not included in this type of formula. Therefore, the author and co-workers [*4*] have proposed several years ago a formula for fatigue at elevated temperature that included the terms of temperature variation together with plastic strain amplitude, based on the fundamental idea of the above formula.

According to our concept that the fatigue damage per half cycle is proportional to the nth power of plastic strain range $(\Delta\epsilon_p)^n$ and damage factor $\lambda(T)$, the relationship between $\Delta\epsilon_p$ and N_f is expressed by such a cumulative damage equation as

$$\lambda(T) \cdot (\Delta\epsilon_p)^n \cdot N_f = C_1 \quad \ldots\ldots (2)$$

where C_1 is a material constant independent of the temperature, and the effect of temperature is included in the damage factor $\lambda(T)$ [*4*]. Then, the constant C in the Manson-Coffin Eq 1 corresponds to $\sqrt{C_1/\lambda(T)}$ in the case of $\alpha = 1/2$ and $n = 2$. Based on the hypothesis of cumulative damage, the Miner's rule, $\sum_i (n_i/N_{fi}) = 1$, can be established from Eq 2 for low-cycle fatigue under varying temperature with a constant plastic strain range. In order to check the validity of this formula, two kinds of low-cycle fatigue tests were carried out under the stepwise changing temperatures from 200

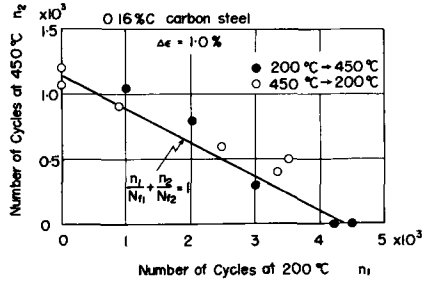


FIG. 11—*Experimental results of low-cycle fatigue under two stepwise changing temperatures.*

to 450 C and from 450 to 200 C, respectively, keeping the total strain range constant ($\Delta\epsilon$ = 1 percent). The results are given in Fig. 11, which shows that all points lie close to a straight line of the Miner's rule.

The damage factor $\lambda(T)$ in Eq 2 can be determined in the form of $\lambda(T)/\lambda(T_0)$(T_0: a reference temperature) from the test results on low-cycle fatigue at several temperature levels. Figure 12 represents the ratio $\lambda(T)/\lambda(T_0)$ as a function of temperature for a 0.16 percent carbon steel (T_0 = 500 C) as well as an 18Cr-12Ni-Cb austenitic stainless steel (T_0 = 650 C) in low-cycle fatigue at various temperatures. Looking at the case of 0.16 percent carbon steel, it is found that $\lambda(T)$ is almost independent of the temperature up to 300 C, while it increases notably in the temperature range between 300 and 500 C.

The threshold temperature for the latter material is around 400 C. The exponent n in Eq 2 has been considered as a constant independent of temperature. Figure 13 shows the result of an experiment [*19*] to elucidate the influence of temperature level in low-cycle fatigue on the value of n, using

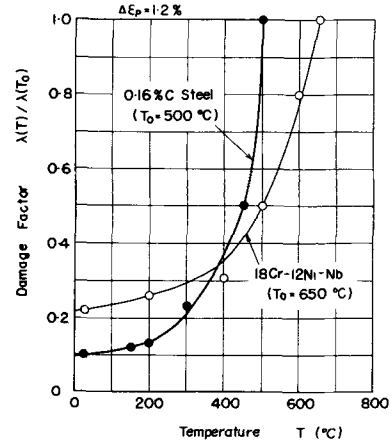


FIG. 12—*Temperature dependence of the damage factor* λ(T).

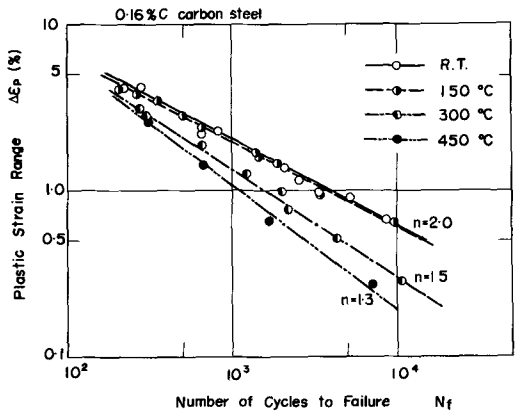


FIG. 13—*Experimental results of low-cycle fatigue at various temperatures represented in the diagram of plastic strain range versus numbers of cycles to failure.*

0.16 percent carbon steel as the test material. It is found from Fig. 13 that the value of n decreases from 2 towards 1 as the temperature increases [*20,21*] up to 500 C. Thus, strictly speaking, referring to Eq 2, the value of $\lambda(T)/\lambda(T_0)$ should depend on the magnitude of plastic strain range applied [*4*], while the $\lambda(T)/\lambda(T_0)$ versus T relationship in Fig. 12 has been obtained for the tests of constant plastic strain amplitude of $\Delta\epsilon_p = 1.2$ percent.

In spite of the proposition of Eq 2, the author considers that there might exist a unique relationship between the effective plastic strain range $\Delta\epsilon_p^*$ and the number of cycles to crack initiation or critical damage for failure N_f in the form of $(\Delta\epsilon_p^*)^n \cdot N_f = C_2$, in which n and C_2 are constants independent of temperature. The effective plastic strain $\Delta\epsilon_p^*$ is the strain having a real contribution to the crack initiation or the critical fatigue damage, and it is a function of the temperature, the macroscopic plastic strain $\Delta\epsilon_p$, the rate of strain and frequency, etc.

Equivalent Temperature of Fatigue at Elevated Temperatures

If we were able to know the correlation between thermal fatigue and low-cycle fatigue, we might find a temperature level for the test of low-cycle fatigue yielding the same number of cycles to failure under the same amount of plastic strain range in thermal fatigue of the temperature range between T_1 and $T_2(T_2 > T_1)$, and we could replace a complex testing of thermal fatigue by the rather simpler tests of low-cycle fatigue at the constant temperature. The temperature is called the equivalent temperature T_e [*4*] and is derived from Eq 2. In order to simplify the discussion, two extreme cases of temperature cycling in thermal fatigue are noted here, in view of the characteristic change of microstructure.

1. When the cyclic temperature ($\Delta T = T_2 - T_1$) in thermal fatigue is within the lower temperature range, it is found that the value of exponent n

in Eq 2 is nearly equal to 2 and the relation in the form that

$$\Delta\epsilon_p \cdot N_f^{1/2} = C \quad \ldots\ldots (3)$$

shows a better representation of data in low cycle fatigue as is seen in Fig. 12. In this case the following equation can be obtained from Eq 2 (see Appendix).

$$\lambda(T_e) = \frac{1}{T_2 - T_1}\int_{T_1}^{T_2}\lambda(T)dT \quad \ldots\ldots (4)$$

Using a $\lambda(T)/\lambda(T_0)$ versus T diagram such as Fig. 12, the value of $\lambda(T_e)/\lambda(T_0)$ can be derived from Eq 4, and we obtain the value of T_e again from Fig. 12. Thus, it is found that the equivalent temperature T_e is close to the mean temperature T_m, that is,

$$T_e \cong T_m = \frac{T_1 + T_2}{2} \quad \ldots\ldots (5)$$

For the 0.16 percent carbon steel used in the present investigation it can be said from Fig. 13 that Eq 5 is valid at temperatures below 400 C. In this temperature range, the formation of subgrains by the aid of diffusion mechanism is relatively inactive, and the appearance of grain-boundary serration suggests that the rather high dislocation density, existing within the grains and the slip mechanism, is more pronounced before failure. It is supposed that the mode of fatigue damage in either low-cycle fatigue or thermal fatigue within this temperature range would be similar. Some typical materials and test temperatures of thermal fatigue corresponding to this category are listed in Table 3.

2. In the case of low-cycle fatigue in which the test temperature is close to or within the high-temperature level where the value of $\lambda(T)$ is large enough, the exponent n in Eq 2 has a value of about unity, resulting in the relation

$$\Delta\epsilon_p \cdot N_f = C \quad \ldots\ldots (6)$$

TABLE 3—*Examples of materials and test temperatures for thermal fatigue and their equivalent temperatures.*

Case	Material	T_1, deg C	T_2, deg C	T_m, deg C	Ref No.
(1.) $T_e = T_m$	AISI 347	100 to 225	475 to 600	350	[22]
	18Cr–12Ni–Cb (AISI 347 type)	150, 200	600, 650	400	[4, 23]
	Inconel	538, 760	871	705, 816	[24]
(2.) $T_e = T_2$	2¼Cr–1Mo	10 to 50	550 to 610	300 to 310	[4, 23]
	1Cr–1Mo–¼V cast	30 to 105	570	300 to 340	[25]
	18Cr–9Ni (AISI 304 type)	200	700	450	[26]
	18Cr–11Ni–Cb (AISI 347 type)	100	600	350	[27]

For thermal fatigue in which the upper bound of temperature T_2 is close to the high temperature or is higher than the threshold temperature T_2' where Eq 6 is available, the relation

$$\lambda(T_e) \cong \frac{1}{T_2' - T_1}\int_{T_1}^{T_2'} \lambda(T)dT + \frac{\lambda(T_2)}{2} \quad \ldots\ldots\ldots\ldots (7)$$

can be obtained from Eq 2 (see Appendix) instead of Eq 4 for Case 1. It is understood that Eq 7 gives a larger value of $\lambda(T_e)$ than Eq 4, leading to the equivalent temperature close to the upper bound of temperature in thermal fatigue, that is,

$$T_e \cong T_2 \quad \ldots\ldots\ldots\ldots\ldots\ldots\ldots\ldots (8)$$

Two such kinds of equivalent temperature are shown in Fig. 14 as a schematical representation on the relation between $\lambda(T)$ and T.

As was mentioned already, the equivalent temperature for thermal fatigue of the 0.16 percent carbon steel where the upper bound of temperature cycling is over 500 C is nearly equal to the upper bound. At such a high temperature the diffusion process is a controlling mechanism of fatigue, yielding formation and development of visible network of sub-boundaries in the course of thermal and low-cycle fatigue. The majority of damage of thermal fatigue is likely to cumulate in the material at the upper side of each cyclic temperature.

The examples of experimental results on thermal fatigue belonging to this category are also shown in Table 3.

Such a critical temperature relevant to the category (2) leads materials to an abrupt drop of fatigue life, and it may be inherent to materials and correspond to a temperature at which notable decrease in work hardening

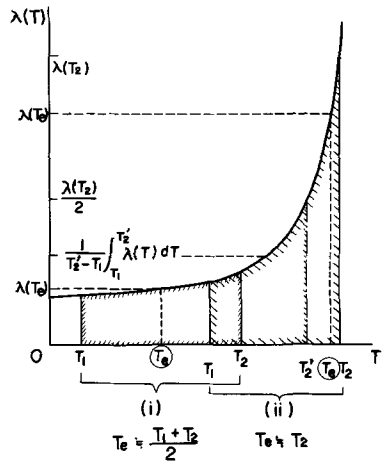


FIG. 14—*Schematic representation of the relation between damage factor and equivalent temperature.*

and creep resistance begins to occur. As is supposed from Fig. 12, the critical temperature for an 18Cr-8Ni-Cb austenitic stainless steel is above 700 C, where growth of precipitations, grain boundary sliding, grain boundary crack, void formation, etc. become notable, resulting in the decrease in the high-temperature fatigue strength.

Summary

The change of microstructure in materials during thermal fatigue and low-cycle fatigue at elevated temperature was studied by optical microscope and X-ray diffraction techniques. The experimental fact leads us to a conclusion that thermal fatigue is a particular case of low-cycle fatigue and can be determined as a low-cycle fatigue under cyclic varying temperature. From this standpoint it is natural to make an attempt to estimate the thermal fatigue life on the basis of the test results on low-cycle fatigue at various temperature levels. One of the most appropriate and easiest hypotheses is to take the equivalent constant temperature, already proposed by the authors, which has the same effect on thermal-fatigue behavior as the cyclic varying temperature. The equivalent temperature can be divided into two main classes as follows:

1. The value of the equivalent temperature is close to the mean value of the upper and lower bound of temperature in thermal fatigue. In this temperature range between upper and lower bound, the formula in the form of $\Delta\epsilon_p \cdot N_f^{1/2} = C$ is available. In this type of fatigue process, change of slip mechanism is controlling the fatigue life.

2. At the higher temperature range where diffusion process is a controlling mechanism, the change in microstructures during fatigue differs from that of Case 1. A distinguishing feature of the microstructure in material is the clear evidence of subgrain formation at the temperatures above 500 C. The fatigue law of $\Delta\epsilon_p \cdot N_f = C$ is more suitable for the representation of fatigue data. When the upper bound of temperature in thermal fatigue is close to or within this high-temperature range, the equivalent temperature is close to the upper bound of the temperature cycling.

APPENDIX

As was proposed already by the author [4], it is assumed that the stress-strain relationship in accordance with a cycle of temperature cycling in the range between T_1 and T_2 is represented schematically as Fig. 15 and in the process of fatigue an increment of damage $\Delta\phi$ to be cumulated in the material during one-half cycle of

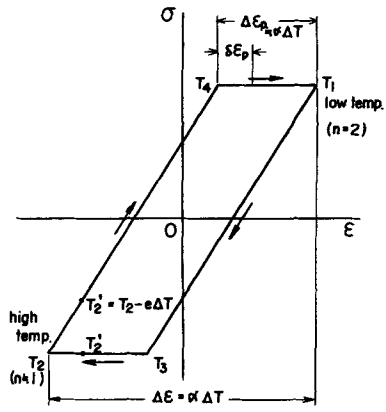


FIG. 15—*Schematic diagram of the stress-strain relationship in thermal stress cycling.*

the plastic strain $\Delta\epsilon_p$ is proportional to the nth power of the plastic strain and it is represented by formula as follows taking $\lambda(T)$ as a function of the temperature:

$$\Delta\phi = \lambda(T)\cdot(\Delta\epsilon_p)^n \quad \ldots\ldots (9)$$

Applying Eq 9 to the case of thermal cycling, the fatigue damage per cycle is given by the sum of the damage $\Delta\phi_1$ during the heating path ($T_1 \rightarrow T_2$) and that $\Delta\phi_2$ during the cooling path ($T_2 \rightarrow T_1$) (see Fig. 15).

$$\begin{aligned} 2\Delta\phi &= \Delta\phi_1 + \Delta\phi_2 \\ &= \int_{T_1}^{T_2} n\lambda(T)\cdot(\delta\epsilon_{p1})^{n-1}\, d(\delta\epsilon_{p1}) + \int_{T_2}^{T_1} n\lambda(T)\cdot(\delta\epsilon_{p2})^{n-1}\, d(\delta\epsilon_{p2}) \\ &= \int_{T_3}^{T_2} n\alpha^n\cdot\lambda(T)\cdot(T - T_3)^{n-1}dT + \int_{T_4}^{T_1} n\alpha^n\cdot\lambda(T)\cdot(T - T_4)^{n-1}dT \\ &= \int_{T_1}^{T_2} n\alpha^n\cdot\lambda(T)[(T - T_1)^{n-1} - (T - T_2)^{n-1}]\, dT \quad \ldots\ldots (10) \end{aligned}$$

where α is coefficient of thermal expansion.

1. When the temperature level in thermal fatigue is relatively low and the exponent n in Eq 2 or Eq 9 has a value of 2 in the temperature range between T_1 and T_2, the thermal fatigue damage given in Eq 10 results in

$$2\Delta\phi = 2\alpha^2\cdot\Delta T\int_{T_1}^{T_2}\lambda(T)dT \quad \ldots\ldots (11)$$

While the damage during one cycle of mechanical fatigue equivalent to that in thermal fatigue is derived from Eq 9 by substituting $n = 2$ and $\Delta\epsilon_p = \alpha(T_2 - T_1) = \alpha\Delta T$, or

$$2\Delta\phi = 2\alpha^2\,(\Delta T)^2\cdot\lambda(T_e) \quad \ldots\ldots (12)$$

Hence

$$\lambda(T_e) = \frac{1}{T_2 - T_1}\int_{T_1}^{T_2}\lambda(T)dT \quad \ldots\ldots (13)$$

This means that the value of $\lambda(T_e)$ is equal to the mean of $\lambda(T)$ in the temperature range from T_1 to T_2. If the $\lambda(T)$ versus T curve can be assumed as a straight line, the equivalent temperature T_e becomes the mean temperature T_m, that is,

$$T_e = T_m = \frac{T_1 + T_2}{2} \quad \ldots\ldots (14)$$

2. In the case that the upper bound of temperature T_2 in thermal fatigue is high enough to reduce the value of the exponent n in Eq 2 close to unity at the temperature above the threshold temperature $T_2' = T_2 - e\Delta T$ ($e \ll 1$) (see Fig. 15), the fatigue damage per cycle is given from Eq 10 as

$$\begin{aligned} 2\Delta\phi &= \Delta\phi_{\text{low}} + \Delta\phi_{\text{high}} \\ &= \int_{T_1}^{T_2'} 2\alpha^2 \cdot \lambda(T)[(T - T_1) - (T - T_2)]dT + \int_{T_2'}^{T_2} n\alpha^n \cdot \lambda(T)[(T - T_1)^{n-1} \\ &\qquad - (T - T_2)^{n-1}]dT \\ &\cong 2\alpha^2 \cdot \Delta T \int_{T_1}^{T_2'} \lambda(T)dT + n\alpha^n \cdot \lambda(T_2)\left[\frac{1}{n}(T - T_1)^n - \frac{1}{n}(T - T_2)^n\right]_{T_2 - e\Delta T}^{T_2} \\ &= 2\alpha^2 \cdot \Delta T \int_{T_1}^{T_2'} \lambda(T)dT + \alpha \cdot e\Delta T \cdot \lambda(T_2) \quad \ldots\ldots (15) \end{aligned}$$

where $\lambda(T)$ in the second term of the right-hand side of the previous equation is taken as a constant, assuming that T_2' is close to T_2 and $e\Delta T$ is small. Also $n = 1$ is applied to the second term of the last equation.

The equivalent low-cycle fatigue damage is the sum of the damage $\Delta\phi_{\text{I}}$ and $\Delta\phi_{\text{II}}$, where

$$\Delta\phi_{\text{I}} = 2\lambda(T_e)(\delta\epsilon_{p1})^2, \quad \Delta\phi_{\text{II}} = 2\lambda(T_e)(\delta\epsilon_{p2})$$

and

$$\delta\epsilon_{p1} = \alpha(T_2' - T_1) = \alpha(1 - e)\Delta T, \quad \delta\epsilon_{p2} = \alpha(T_2 - T_2') = \alpha\, e\Delta T$$

therefore,

$$\begin{aligned} 2\Delta\phi &= \Delta\phi_{\text{I}} + \Delta\phi_{\text{II}} \\ &= 2\lambda(T_e) \cdot \alpha\Delta T[(1 - e)^2\alpha\Delta T + e] \quad \ldots\ldots (16) \end{aligned}$$

Similarly, $\lambda(T_e)$ can be obtained from Eqs 15 and 16 as

$$\begin{aligned} \lambda(T_e) &= \frac{\alpha}{(1 - 2e)\alpha\Delta T + e}\int_{T_1}^{T_2'} \lambda(T)dT + \frac{e}{(1 - 2e)\alpha\Delta T + e} \cdot \frac{\lambda(T_2)}{2} \\ &= \frac{1}{T_2' - T_1}\int_{T_1}^{T_2'} \lambda(T)dT + \frac{\lambda(T_2)}{2} \quad \ldots\ldots (17) \end{aligned}$$

Equation 17 means that $\lambda(T_e)$ is composed of $\lambda(T)$ for the low-temperature range between T_1 and T_2' and that for the upper bound of temperature. Therefore, we have

$$T_e \cong T_2 \quad \ldots\ldots (18)$$

Since, as is understood from Fig. 14, the tangent of the $\lambda(T)$ versus T curve in the temperature range above T_2' is very steep and the contribution of $\lambda(T_2)/2$ of the second term of Eq 17 to $\lambda(T_e)$ becomes significant.

References

[1] *ASTM STP 449, Low-Cycle Fatigue Bibliographic Survey*, American Society for Testing and Materials, 1968.

[2] *ASTM STP 459, Fatigue at High Temperature*, American Society for Testing and Materials, 1969.

[3] *Proceedings*, International Conference on Thermal Stress and Thermal Fatigue, Sept. 1969, CEGB, England, to be published.

[4] Taira, S. in *Proceedings*, 3rd Symposium on Naval Structural Mechanics, Pergamon Press, New York, 1963, p. 187.

[5] Taira, S., Inoue, T., and Yoshida, T. in *Proceedings*, 11th Japan Congress of Materials Research, Society of Materials Science, Japan, 1968, p. 60.

[6] Taira, S. in *Proceedings*, International Conference on Mechanical Behavior of Materials, Special Volume, 1972, p. 109.

[7] Taira, S., Hayashi, K., and Tanaka, K. in *Proceedings*, 11th Japan Congress on Materials Research, Society of Materials Science, Japan, 1968, p. 18.

[8] Taira, S., Goto, T., and Nakano, Y. in *Proceedings*, 11th Japan Congress on Materials Research, Society of Materials Science, Japan, 1968, p. 25.

[9] Dorn, J., ed., *Mechanical Behavior of Materials at Elevated Temperatures*, McGraw-Hill, New York, 1961, p. 158.

[10] Taira, S. and Honda, K., *Transactions*, Japan Institute of Metals, Vol. 1, 1960, p. 43.

[11] Taira, S., Honda, K., and Hayashi, K., *Journal*, Society of Testing Materials, Japan, Vol. 11, 1960, p. 707.

[12] Liebowitz, H., ed., *Fracture*, Vol. 1, & III Academic Press, New York, 1971.

[13] Taira, S. and Tanaka, K. in *Proceedings*, 12th Japan Congress on Material Research, Society of Materials Science, Japan, 1969, p. 15.

[14] McLean, D., *Journal*, Institute of Metals, Vol. 81, 1951–1952, p. 287.

[15] Kelley, J. W. and Figkins, R. C., *Journal*, Institute of Metals, Vol. 82, 1953–1954, p. 475.

[16] Lawrence, F. W. and Jones, R. C., *Metallurgical Transactions*, Vol. 1, 1970, p. 367.

[17] Manson, S. S., NASA TN 2933, University of Michigan Press, Ann Arbor, 27–28 June 1952, 1953.

[18] Coffin, L. F., Jr., *Transactions*, American Society of Mechanical Engineers, Vol. 76, 1954, p. 931; see also Vol. 78, 1956, p. 527.

[19] Inoue, T., and Yoshida, T., *Journal*, Society of Materials Science, Japan, Vol. 20, 1971, p. 402.

[20] Coffin, L. F., Jr., in *Proceedings*, 2nd International Conference on Fracture, Brighton, 1969, p. 643.

[21] Berling, J. T. and Slot, T. in *Fatigue at High Temperature, ASTM STP*, 459 American Society for Testing and Materials, 1969, p. 3.

[22] Coffin, L. F., Jr., *Transactions*, American Society of Mechanical Engineers, Vol. 28, 1962, p. 792.

[23] Taira, S., Ohnami, M., et al, *Transactions*, Japan Society of Mechanical Engineers, Vol. 28, 1962, p. 792.

[24] Swindeman, R. W. and Douglass, D. A., *Transactions*, American Society for Mechanical Engineers, Series D. Vol. 81, 1959, p. 203.

[25] Kusumoto, S. and Takeuchi, M., *Journal*, Society of Materials Science, Japan, Vol. 13, 1964, p. 602.

[26] Kawamoto, M., Tanaka, T., and Nakajima, H. in *Proceedings*, 6th Japan Congress on Testing Materials, 1963, p. 30.

[27] Kato, N., *Journal*, Society of Materials Science, Japan, Vol. 13, 1964, p. 589.

DISCUSSION

Paul Niessen[1] *(written discussion)*—You show very few spots in your microbeam patterns, suggesting that you have collimated the X-ray beam down to a size of one or two grains. If there is a change in subgrain size and misorientation from grain to grain, the reflection splitting from the very small areas under the beam may not be the best basis for the definition of a damage parameter.

Shuji Taira (author's closure)—In response to your comments, I should say that at least two different types of X-ray diffraction techniques have to be used to confirm the damage factor, and actually I did this to correlate the fatigue damage. In this study, both the optical microscope observation and the X-ray diffraction techniques are used.

Concerning the X-ray diffraction techniques, both the X-ray powder diffraction method and the X-ray microbeam method were used. The former is associated with the irradiated area of 2×5 mm^2 on the surface, and the latter is of around 100 μm diameter. In addition, several parts of the cross-section by the X-ray microbeam technique were observed, and so the observation supplies the effective information of the specimen as a whole.

As I mentioned in the paper, the damage of the high temperature fatigue or thermal fatigue or both might not be evaluated by only a simple factor such as the subgrain size. However, I think that the subgrain size should be a function of several microscopic parameters such as misorientation between subgrains, distortion of the crystal, rotation of crystal, etc., which are functions of materials, temperature, and environment.

M. Manjoine[2] *(written discussion)*—Is increase in damage associated with greater subgrain formation? At temperatures where the strain occurs primarily as grain boundary slip, you would think that subgrain formation would distribute the local strain, and, therefore, there would be less damage if more subgrains are formed.

Mr. Taira—What I mean in the terms of "the development of substructure" is the following: the subgrain size becomes small and the

[1] University of Waterloo, Waterloo, Ont., Canada.
[2] Westinghouse Research Laboratories, Pittsburgh, Pa. 15235.

dislocation density at the subgrain wall is extremely high as compared with matrix area, and the misorientation between subgrains become large enough so that the X-ray diffraction pattern shows discrete spots corresponding to individual subgrains.

I suggested that the observation on the substructure development would supply the important information associated with the damage factor. In my previous work on fatigue and creep under varying load, I found the difference between the dislocation movement (slip controlled), cummulative damage mechanism at lower temperature, and the diffusion controlled cummulative damage mechanism in the observations. In the case of the slip controlled mechanism, the appearance of diffraction spots is dull, while clear spots are observed in the case of the diffusion controlled mechanism. Of course, the rotation of crystal is also an important factor of high-temperature fatigue damage. The observation of the X-ray microbeam pattern of a material fatigued at high temperature suggest that the dislocations in the matrix caused by stress or strain cycling tend to move towards subboundaries, yielding a high density of dislocations at subboundaries. Formation of high dislocation subboundaries, thus, is associated with subboundary slip. By this means a higher development of substructure corresponds to more fatigue damage in the temperature range of grain boundary slip.

R. R. Dils[1]

Fatigue of Protective Metal Oxides in Combustion Chamber Exhaust Gases

REFERENCE: Dils, R. R., **"Fatigue of Protective Metal Oxides in Combustion Chamber Exhaust Gases,"** *Fatigue at Elevated Temperatures, ASTM STP 520*, American Society for Testing and Materials, 1973, pp. 102–111.

ABSTRACT: An analysis of the oxidation of an aluminized nickel-base alloy in the exhaust gases of a gas turbine main burner has been developed. Characterizations of combustion chamber exhaust gases and the temperature fluctuations induced at fireside surfaces by the exhaust gases are reviewed, and the analyses are applied to the description and simulation of the exhaust gases of a gas turbine main burner. The results of wide bandwidth gas temperature measurements at the entrance to the turbine section of a large gas turbine are used to obtain metal-metal oxide interface temperature waves at the surface of the turbine components. Simulations of the interface temperature wave in exhaust gases of laboratory combustion chambers and oxidation experiments in the laboratory combustor exhaust gases are presented. It is shown that the small fluctuations induced at the surface of the turbine components by the main burner exhaust gases can be of sufficient amplitude to affect the rate of oxidation of the turbine components. The example temperature fluctuations measured in the gas turbine cause the growth of a porous nonprotective oxide on the surface of the aluminized nickel-base alloy. A continual loss of the oxide results in a significant increase in the rate of oxidation of the material.

KEY WORDS: fatigue (materials), thermal stresses, nickel alloys, oxidation, turbine components, shear properties, interfaces

Recent investigations [*1*][2] of the oxidation of aluminized nickel-base superalloys in moderate velocity, high-temperature gas streams indicate that the measured rate of oxidation is a function of the amplitude and frequency of fluctuations in the heat flow from the gas stream to the material. In gas streams with a wide range of gas temperatures, mass flows, and Reynolds' numbers, it has been observed that small temperature fluctuations induced in the metal oxide and metal near the oxidized surface generate oscillatory shear stress intensities at the metal-metal oxide interface. The stress intensities are of sufficient amplitude to fatigue and fail the weak interfaces. The repeated failure of the interface results in the

[1] Senior research associate, Materials Engineering and Research Laboratory, Pratt & Whitney Aircraft, Middletown, Conn. 06457.

[2] The italic numbers in brackets refer to the list of references appended to this paper.

Copyright© 1973 by ASTM International www.astm.org

growth of a weak, porous oxide structure composed of chains of aluminum oxide grains extending from the interface; the continual loss of the oxide results in a significant increase in the measured rate of oxidation. This paper describes the importance of the erosive process in a large gas turbine.

Characterization of the Interface Temperature

Temperature fluctuations at the metal-metal oxide interfaces near fireside surfaces are induced frequently by the combustion and mixing processes in combustion chambers. In the bandwidth of interest to the oxidation processes, the interface temperature waves are induced by exhaust gas temperature fluctuations. Combustion and heat release in the combustor are controlled by the gas dynamics and exhaust gas temperature variations which are either linear or nonlinear functions of the combustion processes exhibit wide bandwidth distributions of fourier components [*1*,*2*]. The exhaust gas temperature fluctuations are neither gaussian nor harmonic in character, but wide bandwidth waveforms with widely varying power spectral density (PSD) functions. Since the transfer function of the metal-metal oxide interface near the fireside surfaces is only a weak function of frequency, the gas temperature fluctuations induce similarly nondeterministic waves at the interface. The random nature of the forcing function and the broadband response of the material has led to the use of the random wave descriptions available in the electrical noise [*3*] and random load fatigue literature [*4*] to characterize the features of the interface temperature waves. The analyses have been developed in connection with the referenced oxidation experiments [*1*] and are not widely available. Therefore, the information will be summarized here.

There are special system constraints which simplify the method of characterization. The initial studies show that the measured rate of oxidation increases as the frequency of a temperature excursion increases until the oxidation rate is controlled by the growth rate of the oxide. To further increase the measured rate of oxidation, it is necessary to increase the amplitude of the oscillations. Eventually, the rate of oxidation becomes insensitive to increases in either the amplitude or frequency of the temperature oscillations. Before the latter state is reached, the dependence of the oxidation rate on the oxide growth rate increases the importance of large, infrequent temperature excursions in determining the oxidation rate. In addition, the interface signals are always broadband signals. The nonlinear combustion and gas dynamics in a combustion chamber distribute the power in the exhaust gas temperature waves over a wide bandwidth, and there are no features of the interface transfer function which provide a narrow band response to the gas dynamics. For example, the absolute magnitude of the transfer function of an interface on a semiinfinite solid is inversely proportional to the square root of the frequency. The variety of

narrow band mechanical responses of a body to random loads [*4*] will not be encountered in the oxidation studies.

It has been found useful to employ the range pair counting method [*5–7*] to characterize the large interface temperature excursions. In this counting method, a pair of alternate positive and negative excursions or ranges is counted by a logic circuit which selects the lowest minimum in the wave prior to the prescribed positive range and then selects the succeeding highest maximum in the wave prior to an equivalent negative range. It has been shown [*1*] that the distribution function of the level crossings in one direction, the distribution function of pairs of alternate positive and negative level crossings, and the range pair distribution function, $n(RP)$, of a gaussian wave are quite similar for level crossings above 1σ and pair amplitudes greater than 2σ, where σ is the root mean square value of the wave. The similarity of the distribution functions arises from the lack of correlation between the information carried in the separate parts of the wave containing a large excursion. The pairs are composed of relatively independent positive and negative excursions, and the probability of a pair approaches the probability of a single excursion [*3*]. The lack of information transmitted between each part of the wave containing a large excursion suggests that the large excursions are determined primarily by the signal power and bandwidth and should be relatively insensitive to the details of the PSD function of the wave. It has been experimentally observed that the $n(RP)$ function is insensitive to the details of widely varying PSD functions of a large range of nonrandom linear and nonlinear signals and that nondeterministic waves of equal bandwidth and amplitude display equal $n(RP)$ functions for range pair amplitudes greater than 2σ. Two examples are presented in the next sections. The insensitivity of the large excursions to the details of the waves allows two simplifications in the investigation and analysis of the oxidation phenomenon. First, the $n(RP)$ function of the industrial environment can be simulated in the laboratory by a wave with a different PSD function. Second, the $n(RP)$ function induced by an industrial environment can be estimated from the gaussian wave data by setting the integrals of the PSD functions of the model interface wave and the nondeterministic experimental interface wave equal and assigning a bandwidth to the gaussian model wave equal to an effective bandwidth estimated from the PSD function of the experimental wave.

The features of a single set of large range pairs have been obtained also [*1*], and it is shown that a harmonic wave with a peak-to-peak value approximately 15 percent larger than a given range pair amplitude and with a frequency equal to the frequency of the range pairs represents an adequate simulation of the range pairs. Therefore, by varying the amplitude and frequency of harmonic perturbations of the interface temperature and measuring the rate of oxidation, it is possible to evaluate the relative importance of the growth rate of the oxide and each set of range pairs in

establishing the rate of oxidation in an industrial environment. The information is required to determine a practical solution to each oxidation problem. For example, in an environment in which the rate of oxidation is determined primarily by the amplitude and frequency of the interface temperature fluctuations, acceptable design changes that will reduce the amplitude or frequency of the oscillations can be considered as solutions. In this case, no change in the material may be necessary. Conversely, if the industrial device induces large interface temperature fluctuations which are of such magnitude and frequency that the rate of oxidation is controlled entirely by the growth rate of the oxide and acceptable design changes cannot significantly reduce the rate of oxidation, then a metallurgical solution may be the only practical solution to the oxidation problem. A metallurgical effort will usually focus on improving the adherence of the metal oxide to the metal substrate.

Description and Simulation of the Exhaust Gases of a Gas Turbine Main Burner

Dynamic Gas Temperature Measurements in the Transition Duct Exit

Wide bandwidth gas temperature measurements were conducted in the transition duct exit of a 15 000-lb thrust engine [*8*]. The engine was operated from idle to takeoff and large gas temperature fluctuations were observed throughout the transition duct exit over the entire thrust range. The fluctuations increased monotonically with engine thrust level; at takeoff, the rms value of the gas temperature fluctuations within a 0–300 Hz bandwidth, σ_{TG}, exceeded 200 F, and excursions of ± 600 F occurred approximately once every second. A typical gas temperature record is presented in Fig. 1*a*.

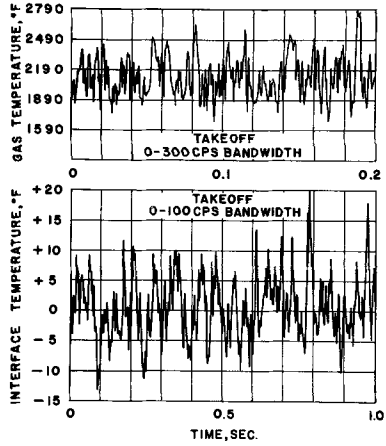


FIG. 1—*Typical gas and metal-metal oxide interface temperatures in a gas turbine transition duct exit.*

Correlation experiments [*8*] between several tens of sensors distributed throughout the transition duct exit showed that long, thin gas stream tubes persisted in the transition duct exit. The axial dimensions of the gas stream tubes exceeded several feet, and the gas stream tubes were of the order of 2 in. in diameter. The average gas temperatures of the stream tubes were quite dissimilar, and nonaxial motion of the stream tubes caused the gas temperature fluctuations at a given point in the transition duct exit. The dimensions of the gas bodies and the lack of mixing between the individual stream tubes indicates that the stream tubes are constructed from the secondary air jet gases introduced just forward of the transition duct exit. The large secondary air jet holes are located less than two duct diameters forward of the transition duct exit, and jet gases entering the combustor through these holes will only be partially mixed with the combustion products from the forward sections of the combustor when they arrive at the entrance to the turbine section.

Spectral analyses [*8*] of the gas temperature waves indicated the jet zones were driven by combustion processes in the forward sections of the combustor which regeneratively and nonlinearly amplified the longitudinal resonant acoustic pressure modes of the diffuser duct and main burner. The gas temperature fluctuations measured in the transition duct exit were constructed primarily from the ultraharmonics of the resonant acoustic modes; each ultraharmonic appears as a discrete, high Q, peak in the PSD function (Fig. 2).

The metal-metal oxide interface temperature flucuations induced at the surface of the leading edge of a first stage vane were obtained with a suitable electrical analog of the heat transfer to the leading edge of the vane [*8*]. The amplitudes of the interface temperature waves increased with thrust, reaching an rms level, σ_{Ti}, of approximately 5 F at takeoff. At this thrust level, excursions of ± 15 F occurred approximately once every second. A typical interface temperature record is presented in Fig. 1*b*. The power in the wave was contained primarily in a few discrete harmonic components (Fig. 3) and generated the $n(RP)$ function shown in Fig. 4.

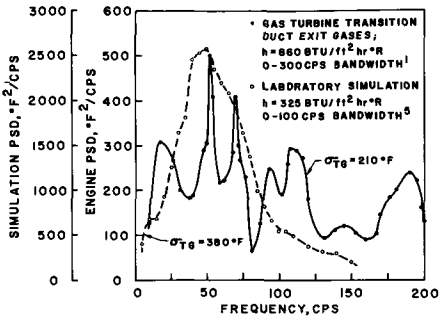


FIG. 2—*Gas temperature PSD functions.*

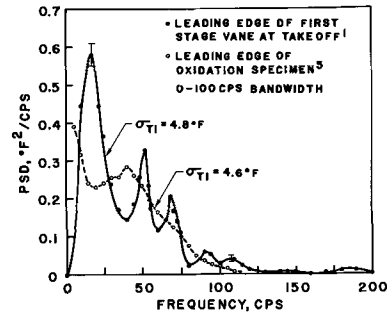


FIG. 3—*Metal-metal oxide interface temperature PSD functions.*

Simulation of the Main Burner Exhaust Gases

The main burner exhaust gases were simulated in the exhaust gases of a laboratory combustion chamber. The exhaust gases were constructed from partially mixed gas bodies with axial and nonaxial dimensions sufficient to induce a fluctuating heat flow normal to the surface of a test specimen; the combustion and mixing processes in the combustion chamber were adjusted to induce an interface temperature wave with an amplitude and bandwidth characteristic of the wave generated in the engine (Fig. 3). The main burner exhaust gases entered the turbine section of the engine at approximately 13 atm, while the exhaust gases of the laboratory combustors were maintained at 1 atm. In order to generate sufficient power in the simulated interface wave, it was necessary to compensate for the lower heat transfer coefficient of the test specimen in the laboratory gas streams by increasing the amplitude of the gas temperature fluctuations (Fig. 2). The $n(RP)$ function of the simulated interface temperature wave is shown in Fig. 4.

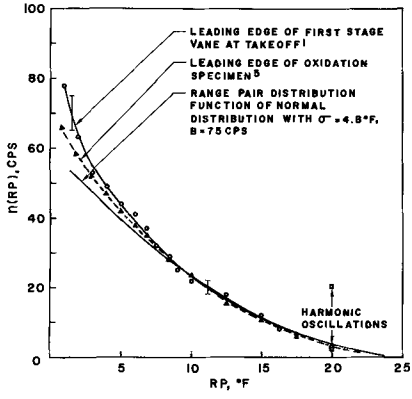


FIG. 4—*Interface temperature* n(RP) *functions.*

The engine and laboratory simulation data display two features of the range pairs in interface signals. First, it is observed that the $n(RP)$ functions of the interface temperature waves generated by the main burner and the laboratory combustor exhaust gases are insensitive to the details of the PSD functions of the waves. The combustion processes in the engine generated a highly nonlinear gas temperature wave constructed primarily from a series of discrete frequencies; the combustion processes in the laboratory combustor generated a larger, linear gas temperature wave constructed from more uniformly distributed fourier components. Both waves induced identical $n(RP)$ functions at the interface. Second, both interface $n(RP)$ functions are equal to the $n(RP)$ function of a gaussian wave of similar amplitude and bandwidth, where the bandwidth is estimated from the experimental PSD functions of Fig. 3.

Oxidation of an Aluminized Nickel-Base Alloy in the Simulated Exhaust Gases

The importance of the interface temperature fluctuations to the oxidation processes in the turbine environment was evaluated by oxidizing a typical turbine component material in the simulated exhaust gases. Aluminized SM-200 specimens were oxidized at an average specimen temperature of 2100 F, and the weight of the specimens was measured periodically. Specimens were also oxidized in a stationary gas and a uniform gas stream. The mass flow of the gas stream was set equal to the mass flow of the simulated exhaust gases, but the combustion and mixing in the combustion chamber were adjusted to induce only small temperature fluctuations at the metal-metal oxide interface. The details of the experimental procedures used to study oxidation in moderate velocity gas streams are described elsewhere [*1*]; it is sufficient for the present purposes to point up that the rate of oxidation of a specimen in a given environment is described by the rate of weight loss of the specimen.

Typical weight loss curves of specimens subjected to the simulated exhaust gases, the stationary gas, and the uniform gas stream are shown in Fig. 5. For extended isothermal tests, the rate of weight loss in the simulated exhaust gases exceeds 35 times the rate of weight loss in the stationary gas. The dependence of the weight loss in each environment on periodic temperature cycles to room temperature was obtained. The superposition of large temperature cycles had no effect on the rate of weight loss of specimens oxidized in the simulated exhaust gases. In the stationary gas and the uniform gas stream, the rate of weight loss increased as the frequency of the large temperature cycles increased from once every 72 h to once every 24 h; above this frequency, no noticeable change in the rate of weight loss occurred as the frequency of the cycles increased to once every 2 h. The maximum rate of weight loss due to this type of temperature cycling was

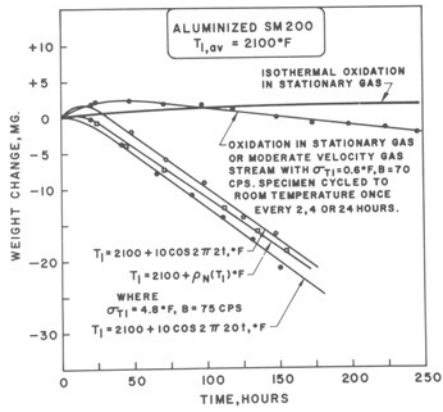


FIG. 5—*Oxidation of an aluminized nickel-base superalloy in several environments.*

approximately one sixth of the rate of weight loss caused by the simulated exhaust gases.

There is also a qualitative difference in the morphology of the oxides grown in the simulated exhaust gases and the oxides grown in either the stationary gas or the uniform gas stream. Scanning electron microscope examinations [*9*] of the oxides on the metal surfaces show that large, dense, monolithic blocks of aluminum oxide grow in the stationary gas and the uniform gas stream (Fig. 6*a*); in the simulated exhaust gases, the repeated failure of the interface results in the growth of a weak, porous oxide structure composed of chains of aluminum oxide grains extending from the interface (Fig. 6*b*). This oxide is nonprotective and is responsible for the high rate of oxidation in the simulated exhaust gases.

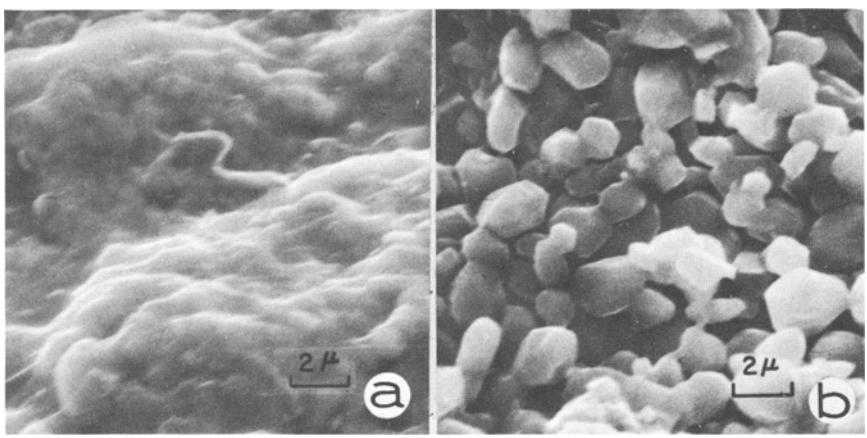


FIG. 6—*Oxides grown in stationary and moderate velocity gas streams.* (a) *stationary gas or moderate velocity gas stream where* $\sigma_{Ti} = 0.6 \pm 0.15$ *F and* $B_{Ti} = 70$ *Hz and* (b) *simulated main burner exhaust gases,* $\sigma_{Ti} = 4.9 \pm 0.8$ *F and* $B_{Ti} = 75$ *Hz.*

Additional experiments [*1*] were conducted to determine the relative importance of the growth rate of the oxide and each set of range pairs in establishing the rate of oxidation in combustion chamber exhaust gases. Specimens were oscillated between well-defined hot and cold gas streams to induce harmonic oscillations at the metal-metal oxide interface about an average temperature of 2100 F. The dependence of the rate of weight loss on the amplitude and frequency of the interface temperature oscillations was obtained, and it was determined that the rate of oxidation in the simulated main burner exhaust gases was controlled primarily by the growth rate of the oxide. At lower average specimen temperatures, the growth rate of the oxide decreases and extends the bandwidth of the growth rate controlled region. An example of the lack of dependence of the oxidation rate on the frequency of the 10 F amplitude oscillations in the simulated exhaust gases is presented in Fig. 5. Reducing the frequency of the oscillations to one half of the frequency of the oscillations in the simulated exhaust gases or increasing the frequency of the oscillations by a factor of 5 has no effect on the rate of weight loss of the specimens. The growth rate controlled region at this amplitude begins at approximately 1 Hz and increases in the frequency of the temperature oscillations above this boundary result in negligible increases in the rate of oxidation.

Since the oxidation rate is controlled primarily by the growth rate of the oxide, a large reduction in the amplitude of the interface temperature wave is required to affect significantly the oxidation rate. In addition, the secondary air jets are far into the vortex zone of mixing [*10*] when they arrive at the entrance to the turbine section, and large changes in the mixing length or the momentum flux ratio between the jets and the gas stream are necessary to increase the amount of mixing of the jets. For example, to reduce the amplitude of the interface temperature waves of the order of 40 percent requires a factor of two increase in the mixing length or a factor of four increase in the injection pressure of the jets. A 40 percent reduction in the amplitude of the interface temperature wave causes less than a 20 percent reduction in the oxidation rate [*1*]. The indicated increases in the engine shaft length or the pressure loss across the main burner are both unacceptable and inefficient. Therefore, it appears that the main burner exhaust gas temperature fluctuations are common to present gas turbine designs and that improvement of the adherence of the protective metal oxide to the substrate represents the practical solution to the oxidation problem in the turbine environment.

Conclusions

An analysis of the oxidation of an aluminized nickel-base alloy in the exhaust gases of a gas turbine main burner has been presented. It is concluded that (*a*) small temperature fluctuations induced at the surface of the

turbine components by the main burner exhaust gases can be of sufficient amplitude to affect the rate of oxidation of the turbine components, (*b*) example temperature fluctuations measured in the main burner exhaust gases of a large gas turbine cause the growth of a porous nonprotective metal oxide on the surface of the aluminized nickel-base alloy, and (*c*) continual loss of the oxide results in a significant increase in the rate of oxidation of the material.

References

[*1*] Dils, R. R., "Oxidation of Aluminized Nickel-Base Superalloys in Moderate Velocity Gas Streams," "Gas-Solid System Dynamics of Oxidation in Moderate Velocity Gas Streams," "Measurement and Simulation of Oxidation in Moderate Velocity Gas Streams," and "Oxidation of Aluminized Nickel-Base Superalloys in Combustion Chamber Exhaust Gases," presented at the 4th Annual Spring Meeting, American Institute of Mining, Metallurgical, and Petroleum Engineers, Boston, 8–11 May 1972.

[*2*] Karlowitz, B. in *Fourth Symposium (International) on Combustion*, Williams and Wilkins, Baltimore, 1953, p. 60.

[*3*] Rice, S. O., *Bell Systems Technical Journal*, Vol. 23, 1944, pp. 282–332; Vol. 24, 1945, pp. 46–156.

[*4*] Swanson, S. R., *Materials Research and Standards*, Vol. 8, 1968, pp. 10–44.

[*5*] Teichmann, A., "The Strain Range Counter," Technical Office VTO/M/416, Vickers-Armstrongs (Aircraft) Ltd.

[*6*] Schijve, J. in *Fatigue of Aircraft Structures*, W. Barrows and E. L. Ripley, eds., Pergamon Press, London, 1963, pp. 115–149.

[*7*] Burns, A., "Fatigue Loadings in Flight; Loads in the Tail Plane and Fin of a Varsity," ARC Technical Report CP 256, London, 1956.

[*8*] Dils, R. R., "Dynamic Gas Temperature Measurements in a Gas Turbine Transition Duct Exit," presented at the 18th Annual ASME Gas Turbine Conference, Washington, D.C., American Society for Mechanical Engineers, 8-12 April 1973, Paper No. 73-GT-7.

[*9*] Dils, R. R., "A Comparison of Oxides Grown in Stationary and Moderate Velocity Gas Streams," presented at 13th Annual Meeting, Electron Microscopy Society of America, Los Angeles, 14–18 Aug. 1972.

[*10*] Pratt, B. D. and Barnes, W. D., *Journal of the Hydraulics Division, Proceedings*, American Society of Civil Engineers, 1967, pp. 53–64.

H. D. Solomon[1] *and L. F. Coffin, Jr.*[1]

Effects of Frequency and Environment on Fatigue Crack Growth in A286 at 1100 F

REFERENCE: Solomon, H. D. and Coffin, L. F., Jr., "**Effects of Frequency and Environment on Fatigue Crack Growth in A286 at 1100 F,**" *Fatigue at Elevated Temperatures, ASTM STP 520*, American Society for Testing and Materials, 1973, pp. 112–122.

ABSTRACT: Previous low-cycle fatigue tests on A286, which covered a frequency range of 5 to 0.1 cpm, have shown a pronounced frequency dependence when the tests were run in air. In contrast, tests run in a vacuum did not show such a frequency effect. This led to the conclusion that, in this frequency range, environmental effects were responsible for the frequency dependence.

Air crack propagation tests have also shown a strong frequency dependence. At frequencies below 0.02 cpm the air crack propagation tests showed a stronger frequency dependence than was observed at higher frequencies and resulted in pure time dependent, cycle independent failure. In order to explain this behavior and to see if it could be observed in low frequency vacuum tests, measurements of the crack propagation rate at 1100 F were made in a 10^{-8} torr vacuum.

These vacuum crack propagation results substantiated the assertion that at 1100 F, air produces a strong influence on the fatigue life or crack propagation rate. Additionally, these tests have shown that below 0.02 cpm the pure time dependent failure noted in air persisted in a vacuum. The vacuum results could be interpreted on the basis of a linear superposition model, where at low frequencies the behavior was that of a purely time dependent failure; at high frequencies, purely cycle dependent; and at intermediate frequencies, that of a linear superposition of these phenomena. In air this linear superposition model was not applicable because of the additional environmental interaction.

KEY WORDS: fatigue (materials), crack propagation, fatigue tests, vacuum, cyclic loads, frequencies, strains, metals

In two recent investigations, the effect of high vacuum and high temperature on the low-cycle fatigue behavior of several metals has been studied [*1,2*].[2] One material, namely A286, was explored extensively, and for this material it was found that for frequencies greater than 0.1 cpm there was no effect of the frequency of cycling on the plastic strain-life relationship in high vacuum at 1100 F. Further, the fracture mode was transcrystalline in all cases. For this material and others tested under high

[1] Members of technical staff, Metallurgical and Ceramics Laboratory, Research and Development Center, General Electric Co., Schenectady, N. Y. 12301.

[2] The italic numbers in brackets refer to the list of references appended to this paper.

Copyright© 1973 by ASTM International www.astm.org

vacuum conditions, it was shown that for frequencies greater than 0.1 cpm, the plastic strain-fatigue life test results fit into a relatively narrow scatter-band such that the exponent of the Coffin-Manson relationship was 0.5 despite the temperature. The results for A286 are summarized in Fig. 13 of the keynote paper by L. F. Coffin that appears in this volume.[3] In air the Coffin-Manson exponent approaches unity, and a strong frequency effect exists. The solid lines in Coffin's Fig. 13 are the correlations obtained by the frequency modified low-cycle fatigue relationship [*3,4*]

$$(N_f \nu^{k-1})^{\beta} \Delta\epsilon_p = c_2 \quad \ldots\ldots\ldots\ldots\ldots\ldots\ldots\ldots (1)$$

as fitted to the test data by a regression analysis [*1*]. Here N_f is the life, ν the frequency in cycles per minute, $\Delta\epsilon_p$ the plastic strain range, and k, β, and c_2 are constants.

In recent studies, Solomon [*5,6*] has investigated the plastic strain controlled fatigue crack propagation of mild steel and A286 at several temperatures and frequencies. This approach offers certain advantages over the more conventional low-cycle fatigue tests in that only crack growth is measured, in contrast to the more complex processes of nucleation, early growth, and propagation included in the low-cycle fatigue test. Further, this mode of testing permits the exploration of lower frequencies, since the testing time need only involve a comparatively few cycles to obtain the crack growth information. As a portion of this investigation, A286 was studied at 1100 F in air at several frequencies. From this work it was shown that the crack growth rate could be described in terms of a frequency-modified crack growth law, namely,

$$\frac{dC}{dN} = \phi C(\Delta\epsilon_p)^{\alpha} \nu^{k-1} \quad \ldots\ldots\ldots\ldots\ldots\ldots\ldots\ldots (2)$$

where C is the measured crack length, dC/dN the crack growth rate, and ϕ, α, and k are constants. By integration of Eq 2 and specification of failure as a particular crack size, Eq 1 can be derived from Eq 2 provided $\alpha = 1/\beta$ and k is identical in both relations. Further, by dividing by C, Eq 2 can be expressed in the form

$$\frac{d \ln C}{dN} = \phi(\Delta\epsilon_p)^{\alpha} \nu^{k-1} \quad \ldots\ldots\ldots\ldots\ldots\ldots\ldots\ldots (3)$$

It was found that Eq 2 was strictly valid over specific frequency ranges and that the effect of changing the frequency could be treated in terms of three frequency regimes, each with a specific value of k. At the lowest frequencies a region with $k = 0$ was observed. Under these conditions the time to failure is constant, and the factor determining failure is the time

[3] See p. 5.

under load rather than the number of cycles. This behavior can be described as a pure time-dependent process.

The other extreme in behavior is pure cyclic-dependent fatigue. Here $k = 1$ and the crack growth rate is independent of the frequency. Such behavior was not actually observed in the air tests but was assumed to exist following, for example, the evidence of Tien [7] who showed that if the frequency is sufficiently high, the effect of oxygen on the elevated temperature fatigue behavior could be suppressed, resulting in temperature independent behavior.

In the third regime $k = 0.55$ and the fatigue crack propagation is a mixture of time and cycle dependent crack growth. The behavior in this regime is identified with the interaction of the air environment with crack propagation.

Phenomena of the above type have been described in terms of linear superposition, as proposed by Gallagher and Wei [8] for corrosion fatigue, or in terms of linear damage accumulation as proposed by Taira [9] and further extended by Manson et al [10]. Solomon has shown [6], however, that the crack growth results could not be so simply expressed. The test data obtained suggested that some additional time-dependent effect was influencing crack growth. This finding is similar to that of Lagneborg and Altermo, [11], who investigated the creep-fatigue interaction of austenitic stainless steel and concluded that an additional interaction term was required to properly represent the test findings by such a model.

It was felt that experiments carried out at pressures of 10^{-8} torr or lower would eliminate the environmental part of the high-temperature crack propagation process. With this goal in mind, a study of the crack growth rate, in A286 at 1100 F, in high vacuum, was undertaken and is herein reported.

Experimental Procedure

The A286 was obtained in a solution treated condition (1800 F for 1 h followed by a water quench) and was aged at 1325 F for 16 h prior to testing. It was from the same lot of material as was used in the air tests.

The test specimens employed were the same type as were used in previous crack propagation studies [5,6]. These specimens had a gage section 0.050 in. thick and 0.50 in. wide. They were notched through the thickness at one edge with 0.015-in.-deep notches. With repeated cycling, cracks emanated from these notches and grew in the width direction.

As with the previous studies, the through thickness strains were measured. Plastic strains were determined by means of an analog computer and used as the limits for crosshead reversal of the Instron machine employed in the investigation. All tests were performed with equal tensile and compressive plastic strains, and a single plastic strain range of $\Delta\epsilon_p =$

0.01 was employed, as calculated through the specimen thickness. From geometrical considerations, this was found to be equivalent to a longitudinal plastic strain of 0.0113 [5]. Frequency changes were achieved by varying the crosshead rate. Induction heating was used to achieve the 1100 F test temperature.

The aforementioned experimental procedure was the same as was followed in the air tests on A286 [6] and on other materials [5]. The important departure was that these tests were run in a vacuum chamber with the specimen coupled to the load train via a bellows system [1]. While heating the specimen, the heating rate was kept slow enough so that the off-gas pressure did not rise above 8×10^{-8} torr. Cycling was not begun until the pressure had stabilized below 5×10^{-8} torr but more commonly was in the range of 2 to 4×10^{-8} torr. The crack lengths were observed optically through a glass port in the vacuum chamber.

Experimental Results

Ideally it would have been best to perform these vacuum tests with the same plastic strain ranges as those used in the air crack propagation tests, namely, 0.002 and 0.005. Prior experiments, however, led to the conclusion that the use of such small plastic strain ranges would lead to correspondingly small crack growth rates and hence preclude doing tests at very low frequencies. For this reason it was decided that a plastic strain range of 0.01 should be used for the vacuum tests, and it was thus possible to perform tests with frequencies as low as 0.0013 cpm (approximately one cycle every 12 h). The highest frequency attainable was 5 cpm.

The crack lengths as a function of the cycle number are shown in Fig. 1. As in the air tests, the crack length C has been defined as the sum of the crack plus the notch depth so that at $N = 0$, C should equal 0.015 in. When semilog coordinates were used, that is, ln C versus N, the air tests showed a

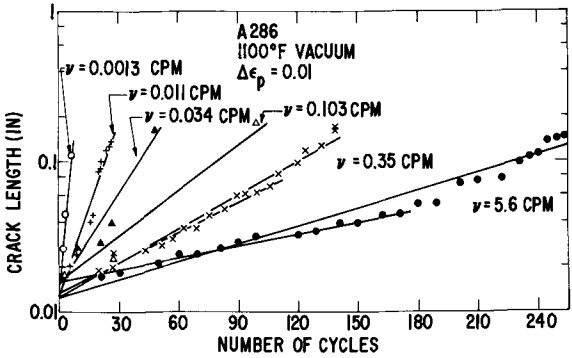


FIG. 1—*Crack length versus number of cycles for tests run at frequencies of 0.0013 to 5.6 cpm. All tests were run in a vacuum at 1100 F and* $\Delta\epsilon_p = 0.01$.

linear crack growth to the largest crack size. Here, however, a systematic deviation for the ln $C \approx N$ behavior was observed. Beyond $C = 0.045$, crack growth becomes faster than that predicted by the extrapolation from the behavior exhibited at the shorter crack lengths. It is believed that this behavior is not a result of the vacuum environment but rather results from the large plastic strain range employed. After the number of cycles required to grow the main crack to a length of 0.045 in., cracks have also nucleated throughout the minimum section of the specimen ahead of the main crack. Subsequent crack growth then entails the linkup of these cracks with the main crack and is thus greater than that when a single crack was present and growing. Evidence of such cracks not nucleated from the notch was found in the air specimens cycled at $\Delta\epsilon_p = 0.005$, but because of the fewer cycles to achieve a given crack length in air, such a process did not appear to be significant unless $C > 0.100$ in. The growth rate, d ln C/dN was computed for the vacuum tests using only the crack length data up to $C = 0.045$ in. and is shown for the 5.6 and 0.35-cpm data. Such an approach would have been satisfactory except for the fact that in some of these tests, few intermediate crack length measurements were made and thus the degree of accuracy in determining d ln C/dN was reduced. To utilize as much of the data obtained as possible, a straight line fit through all the crack length data was made in addition to the fit with $C \leq 0.045$ and such a correlation is shown in Fig. 1. The values for d ln C/dN are shown as a function of ν in Fig. 2. The lower points of the band are the results using $C \leq 0.045$ in. and the upper points the values obtained with crack lengths as long as $C = 0.180$ in.

For the air tests, a linear superposition of the pure time dependent crack growth that was observed at low frequencies and of pure cycle dependent

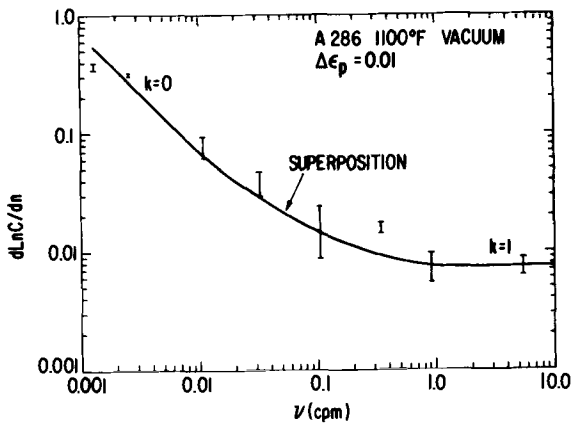


FIG. 2—*Crack growth rates in A286 versus frequency. All tests were run in a vacuum at 1100 F and* $\Delta\epsilon_p = 0.01$. *The lower bracket limits were calculated using only crack lengths less than 0.045 in., whereas the upper limits were computed using crack lengths at large as 0.180 in. The curve represents the result of using a superposition model.*

fatigue, which was postulated to exist at frequencies in excess of the testing capability, was found *not* to agree with the test results. It was felt that this discrepancy was due to an environmental influence which introduced a frequency dependency over and above that predicted by superposition. Figure 2 shows that when the air environment is removed, the results can be described in terms of the superposition of a cycle dependent growth term and a time dependent term, thus validating the proposed explanation of the air results.

The cracks obtained at the high frequencies ($\nu > 1$ cpm) are predominantly transgranular, and those obtained at the lowest frequencies ($\nu < 0.01$ cpm) almost completely intergranular in nature. At intermediate frequencies the behavior is best characterized as being mixed intergranular-transgranular. An example of such behavior is shown in Fig. 3.

Discussion

In the vacuum tests, pure cycle dependent fatigue (that is, where $k = 1$) is found at frequencies where it was not found in the air tests. Very high frequencies are required to suppress an environmental interaction in air but not in a vacuum.

If the time required for the crack to grow a lattice distance is less than the time required to form a monolayer of oxygen on the newly created surface, then the crack will in effect outrun the environment. Actually this is an upper bound type of calculation since it could be assumed that in order to produce the necessary effect the oxygen must additionally diffuse from the freshly created surface into the region ahead of the crack. The time required for saturation of gas on a surface is the inverse of the product of the impingement rate per site times the probability that an impinging molecule will stick on the surface. This time t_A can be easily calculated from the kinetic theory of gases [*12,13*].

The cycling frequency above which no environmental influence will be noted can be determined by equating t_A with the time required to grow the fatigue crack one lattice spacing [*13*]. For the vacuum tests where the oxygen partial pressure is approximately 10^{-8} torr this cycling frequency is of the order of 10^{-6} cpm [*14*]. Thus for all of the vacuum tests the fatigue cracks were growing faster than oxygen was being adsorbed on the newly created surfaces, and therefore the environment can be ruled out as being an influence on the crack propagation.

In air, however, with a pressure of about 150 torr, such interactions will occur at all but ultrahigh frequencies. The pure cycle dependent growth rate for $\Delta\epsilon_p = 0.002$ can be calculated from the $\Delta\epsilon_p = 0.01$ vacuum results using Eq 2 with $\alpha = 1/\beta = 2$. For $C = 0.015$, dC/dN can be shown to be equal to 4.4×10^{-6} in./cycle. With this value for dC/dN, the frequency above which there will be no environmental interaction can be shown [*14*]

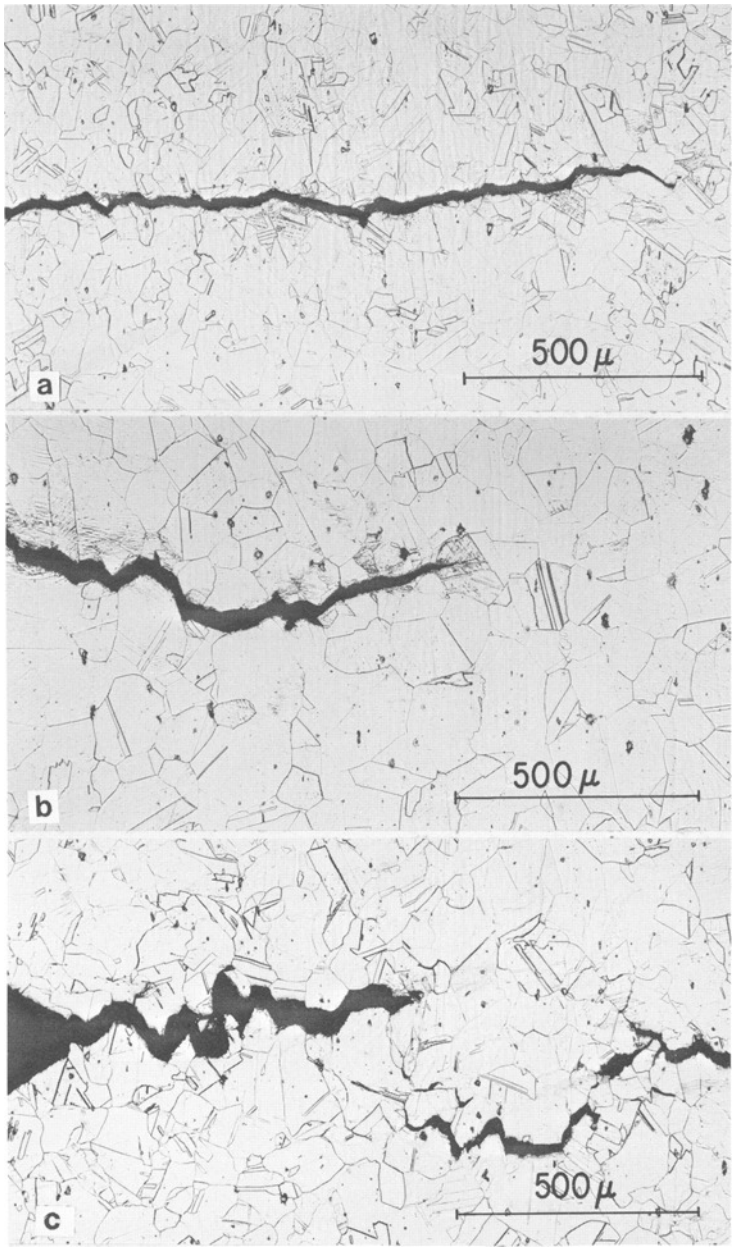


FIG. 3—*Fatigue cracks produced from cycling with* $\Delta\epsilon_p = 0.01$ *in a* 10^{-8} *torr vacuum at 1100 F.* (a) *transgranular crack grown with* $\nu = 1.0$ *cpm.* (b) *mixed transgranular-intergranular crack grown with* $\nu = 0.1$ *cpm.* (c) *intergranular crack grown with* $\nu = 0.0013$ *cpm. Here pronounced secondary cracking is visible.*

to be approximately 3×10^3 cpm. It is clear, therefore, that the rate of oxygen adsorption in the air tests is great enough to allow environmental interactions at all the frequencies studied.

A schematic representation of the vacuum crack growth rate with $\Delta\epsilon_p = 0.002$ as contrasted to the air results is shown in Fig. 4. Using the previous calculation, the vacuum curve was drawn by translating the curve obtained with $\Delta\epsilon_p = 0.01$ to one corresponding to $\Delta\epsilon_p = 0.002$. In air at extremely high frequencies the crack propagation is due to frequency independent fatigue. As the frequency is lowered, the environment interacts with the fatigue process, increasing the crack growth rate. At still lower frequencies the influence of a purely time-dependent process begins to be felt and at the lowest frequencies becomes dominant.

In a vacuum the environmental influence on the fatigue process is removed, but the pure time dependent process is still important and becomes dominant at the very low frequencies. The superposition region is one in which there is a mixture of the high frequency transgranular and low frequency intergranular fractures. The fact that this transition occurs in the vacuum test illustrates that it is related to the basic material response at varying frequencies and is not due to the environment. The intergranular failures observed at low frequencies can be due to a number of phenomena. Space limitations prevent a full discussion of this subject, but several of the more likely mechanisms operative in vacuum tests can be listed as follows:

Creep—Grain boundary fracture resulting from triple point separation, voids produced at boundaries, and the tendency for grain boundary sliding will give rise to intergranular failure [*15*]. These processes are favored at high temperatures and low strain rates.

Metallurgical Changes—The formation of brittle grain boundary phases as the result of long-time, high-temperature exposure can influence the rate

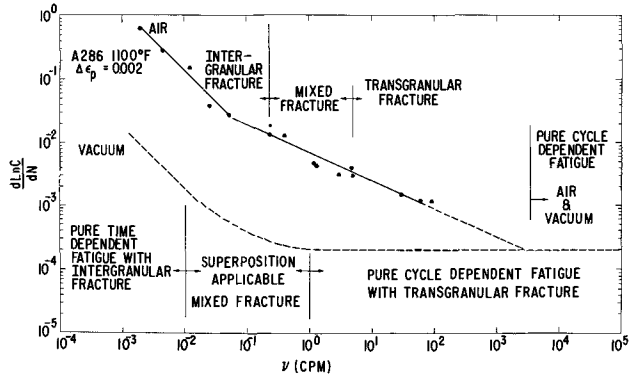


FIG. 4—*Schematic comparison of the air and vacuum crack growth behavior.*

of intergranular failure. The formation of G-phase and γ' coarsening have been noted in A286 [*16*] but for exposure times in excess of those being considered here.

Strain-Induced Metallurgical Changes—The introduction of strain can result in an interaction with metallurgical structure to cause preferential strengthening (strain-aging) of the grains and an enhancement of grain boundary cracking over a range of temperatures and strain rates.

In air the environment acts in addition to the aforementioned phenomenon. Figure 4 shows that the time-dependent crack growth rate is much higher in air than the equivalent rate in vacuum.

Conclusions

Based on controlled plastic strain crack propagation experiments conducted on A286 at 1100 F the following conclusions can be drawn:

1. Above frequencies of 1 cpm the vacuum crack propagation behavior exhibits no dependence on the cycling frequency.
2. Below about 0.01 cpm the vacuum crack propagation behavior is highly time dependent.
3. In a vacuum, the behavior at intermediate frequencies can be explained on the basis of a simple linear superposition of time and cycle dependent phenomena.
4. These vacuum tests show that the enhanced crack growth behavior with decreasing frequencies observed in previous air tests was largely due to the influence of the air environment.

Acknowledgment

We wish to acknowledge the careful and thorough work of D. C. Lord in the operation of the test equipment and his assistance in performing these experiments.

References

[*1*] Coffin, L. F., Jr., "The Effect of Vacuum on the High Temperature, Low Cycle Fatigue Behavior of Structural Metals," presented at the International Conference on Corrosion Fatigue, June 1971; also General Electric Report 71-C-108, 1971.

[*2*] Coffin, L. F., Jr., "The Effect of High Vacuum on the Low Cycle Fatigue Law," submitted to *Metallurgical Transactions* Dec. 1971; also General Electric Report 72CRD005, 1972.

[*3*] Coffin, L. F., Jr., in *Fracture, 1969, Proceedings,* Second International Conference on Fracture, Brighton, April 1969, p. 643.

[*4*] Coffin, L. F., Jr., "The Effect of Frequency on High Temperature, Low Cycle Fatigue," *Proceedings*, Air Force Conference on Fatigue and Fracture of Aircraft Structure and Materials, AFFDL TR 70–144, 1970; also "A Generalized Equation for Predicting High Temperature, Low Cycle Fatigue Including Hold Times," General Electric Report TIS 69–C–401, Dec. 1969.

[*5*] Solomon, H. D., *Journal of Materials*, Vol. 7, 1972, p. 299.

[6] Solomon, H. D., "Frequency Modified Low Cycle Fatigue Crack Propagation," submitted to *Metallurgical Transactions*, Feb. 1972.
[7] Tien, J. K., "The Influence of Ultrasonic Frequency and Temperature on the Fatigue Behavior of a Nickel-Base Superalloy," presented at the 1971 American Institute of Mining, Metallurgical, and Petroleum Engineers' meeting, 18 Oct. 1971, Detroit, Mich., Paper No. 12.
[8] Gallagher, J. P. and Wei, R. P., "Crack Propagation Behavior in Steels," presented at the International Conference on Corrosion Fatigue, June 1971.
[9] Taira, S. in *Creep in Structures*, Hoff, N. J. ed., Academic Press, New York, 1962.
[10] Manson, S. S., Halford, G., and Spera, D. A., in *A. E. Johnson Memorial Volume*, Glasgow, National Engineering Laboratory 1971.
[11] Lagneborg, R. and Altermo, R., *Metallurgical Transactions*, Vol. 2, 1971, p. 1821.
[12] Dushman S., *Scientific Foundations of Vacuum Technique*, Wiley, New York, 1962, p. 14.
[13] Acter, M. R., *Scripta Metallurgica*, Vol. 2, 1968, p. 525.
[14] Solomon, H. D. and Coffin, L. F., Jr., "The Effects of Frequency and Environment on Fatigue Crack Growth in A286 at 1100°F," General Electric Report 72CDR101, 1972.
[15] Coffin, L. F., Jr., and Goldhoff, R. M., "Predictive Testing in Elevated Temperature Fatigue and Creep: Status and Problems," presented at the 1971 International Conference on the Mechanical Behavior of Materials, Kyoto, Japan, Aug. 1971; also General Electric Report 71-C-114.
[16] Goldhoff, R. M. and Beattie, H. J., "The Properties and Structures of a Heat Resisted 1A-Mo-V Steel and Alloy A286 After Long Time Exposure at Elevated Temperatures," presented at the Extension Seminar on High Temperature Strength of Metals of the International Conference on Mechanical Behavior of Materials.

DISCUSSION

J. C. Grosskreutz[1] (*written discussion*)—You observe that a transition occurred from transgranular to intergranular cracking as frequency decreases for both the air and vacuum cases. Do you conclude generally that the cracking mode in elevated temperature fatigue is independent of the environment?

H. D. Solomon and L. F. Coffin, Jr. (*authors' closure*)—As discussed in the written version of the paper there are several mechanisms which will result in a transition from transgranular to intergranular fracture as the frequency is reduced. These mechanisms include those which are independent of the environment and hence will influence tests run in a high vacuum, as well as those such as localized grain boundary attack which are influenced strongly by the environment. The exact frequency at which such a transition occurs,

[1] National Bureau of Standards, Washington, D. C. 20234.

therefore, will be dependent upon the nature of the environment and the relative magnitudes of the environmentally sensitive and insensitive phenomena involved in a specific material.

D. R. Diercks[2] (*written discussion*)—We have been conducting low-cycle fatigue tests at Argonne on Type 304 stainless steel in air at 1100 F. We find that for a 1 percent total strain range test with a 1 min tension holdtime, the fracture mode is predominantly intergranular. However, for a similar test but with a 1 min tension plus a 1 min compression holdtime, the fracture mode is transgranular. This is further evidence that the transition between the two modes as the strain rate is varied is not a purely environmental effect, but is also influenced by the loading conditions.

Messrs. Solomon and Coffin—This is a very interesting result. It points up the need for much more work on a wide variety of materials, particularly a systematic study of the influence of the loading conditions. This study should include such variables as holdtimes, waveform, and random loading.

[2] Materials Science Div., Argonne National Laboratory, Argonne, Ill. 60439.

J. Wareing,[1] *B. Tomkins*,[1] *and G. Sumner*[1]

Extent to Which Material Properties Control Fatigue Failure at Elevated Temperatures

REFERENCE: Wareing, J., Tomkins, B., and Sumner, G., "**Extent to Which Material Properties Control Fatigue Failure at Elevated Temperatures,**" *Fatigue at Elevated Temperatures, ASTM STP 520*, American Society for Testing and Materials, 1973, pp. 123–138.

ABSTRACT: Fatigue failure at room temperature in most structural metals and alloys occurs by the rapid initiation and subsequent controlled propagation of a surface crack. Propagation is transgranular and is controlled to a large extent by continuum plasticity effects ahead of the crack. With increasing temperature, other factors affect this simple fatigue process; namely, the weakening of grain boundaries leading to intergranular propagation, the initiation and growth of other cracks in the bulk of the material by creep processes, and the more rapid oxidation effects which can occur at elevated temperatures. This paper shows the extent to which continuum material properties still control fatigue failure in elevated temperature situations, by reference to recently developed theories and the observed fatigue behavior of a stainless steel and a magnesium alloy over a range of temperatures (up to 0.73 T_m) and strain rates. The influence of secondary creep fracture is examined in the light of results of holdtime tests.

KEY WORDS: fatigue (materials), fracturing, stainless steels, magnesium alloys, crack propagation, temperature, strain rate, crack initiation, transgranular corrosion, intergranular corrosion, creep properties

The basic process of fatigue failure in metals at ambient temperature is the relatively rapid nucleation of small surface cracks followed by the steady slow growth of one or more of these cracks until material separation occurs, or the crack achieves a critical size for fast fracture. At elevated temperatures, although this process persists as the dominant one, secondary effects are observed which can particularly influence the rate of crack growth. Such effects include the weakening of grain boundaries, the development of internal grain boundary cracks or cavities, and an enhanced rate of oxidation of freshly exposed fracture surfaces. The relative weakness of grain boundaries induces a change of crack path from predominantly transgranular to intergranular at high temperatures and low rates of straining. The development of internal grain boundary cracks or cavities, usually

[1] Senior scientific officer, senior scientific officer, and principal scientific officer, respectively, United Kingdom Atomic Energy Authority, The Reactor Fuel Element Laboratories, Springfields, Salwick Near Preston, Lancs, United Kingdom.

Copyright© 1973 by ASTM International www.astm.org

under conditions where a period of stress relaxation or creep is introduced into the fatigue cycle, increases the rate of growth of the surface crack [*1–3*].[2] In some cases internal damage can produce complete structural disintegration [*4*]. The increased tendency for oxidation on freshly exposed fracture surfaces at elevated temperatures can lead to oxide formation within growing cracks, which can affect mechanically the growth rate by wedging action [*5*]. Alternatively, it has been proposed that some form of oxide attack ahead of the crack tip can occur leading to enhanced growth [*6*].

Now the ambient temperature fatigue crack growth process is a closely controlled process. A new crack surface is produced by shear decohesion at the crack tip, and the extent of such decohesion is dependent only on the extent of intense plastic deformation ahead of the crack and the applied stress-strain field [*7*]. Thus the parameters which determine the amount of crack growth per cycle are: the magnitude and direction of the applied stress-strain field, the current crack length, and a material strength parameter. To what extent do these parameters still control behavior at elevated temperature when the secondary effects mentioned previously come into operation? While the basic surface crack growth mechanism operates, it would be expected that they still strongly influence behavior.

In this paper, the elevated temperature fatigue behavior of a stainless steel (20Cr-25Ni/Cb stabilized) and a magnesium alloy (Mg-0.8Al) will be presented and examined in terms of the crack growth process in order to assess the extent that the materials parameters which affect growth at ambient temperatures still dominate behavior. The theory successfully developed to quantify the ambient temperature growth process will be used to provide baselines; deviations from the theory can be clearly seen, and the reasons for any deviations will be considered in the light of metallographic and fractographic evidence.

The elevated temperature behavior will be studied under three situations: (1) effect of temperature at a given strain rate, (2) effect of varying strain rate at a given temperature, and (3) effect of tensile hold periods during a cycle at a given strain rate and temperature. Data for both materials are used in examining the first situation, while stainless steel data only are used for the remaining two situations.

Materials and Testing Procedures

The two materials, a stainless steel and a magnesium aluminium alloy, which were fatigue tested, had widely differing characteristics. The steel, a 20 percent chromium, 25 percent nickel austenitic stainless steel, is face centered cubic in structure and is ductile at all of the test temperatures. It has a melting point of about 1420 C. Having a low stacking fault energy, it deforms primarily by planar slip at room temperature resulting in a banded

[2] The italic numbers in brackets refer to the list of references appended to this paper.

dislocation structure, whereas at elevated temperatures a capacity for cross-slip leads to the formation of a dislocation cell structure. The magnesium alloy, a magnesium 0.8 percent aluminium alloy, has a close packed hexagonal structure, melts at 650 C, and exhibits brittle characteristics at room temperature although its ductility increases considerably with increasing temperature. At room-temperature deformation occurs predominantly by (0001) $\langle 11\bar{2}0 \rangle$ slip and $\{10\bar{1}2\}$ twinning. At elevated temperatures non basal slip can occur and cross-slip takes place.

A standard thermal treatment was carried out on the specimens. The steel was heat treated by annealing at 1000 C for 1 h, which resulted in a grain size of 25 μm. The magnesium alloy was annealed at 400 C for 1 h giving an initial grain size of about 450 μm.

All tests were carried out in air on specimens with a 6.35-mm-diameter parallel gage length in a modified Instron testing machine under strain cycling push-pull conditions [*8*]. Strain control was effected by means of diametral extensometers. Heating of the specimens was achieved by conduction from heated grips, and it was possible to maintain a constant temperature along the gage length within ± 2.5 C. The majority of the tests were conducted at a constant crosshead speed. This leads to a spread in plastic strain rate levels. In the case of the holdtime tests the Instron was converted to give servo controlled operation enabling constant strain, stress relaxation to be imposed at a strain limit.

Theory

The mechanics of the fatigue crack propagation process under plane strain conditions have been analyzed theoretically in a series of recent publications [*3,7,9,10*]. The theory has been used to predict successfully ambient temperature and some elevated temperature endurance laws for a wide range of metals. It predicts the amount of crack growth derived solely from the mechanics of the process and in its simplest form does not take account of secondary fracture processes or environmental effects. In the present paper it is used to provide baseline predictions for elevated temperature endurance behavior on a plastic strain basis so that the secondary effects of elevated temperature behavior can be assessed.

Following Tomkins [*7*], the theory assumes the amount of crack growth per cycle in a ductile metal under simple push-pull conditions to be the amount of irreversible shear decohesion which occurs at the crack tip. This is approximately given by

$$dl/dN = \Delta\epsilon_p D/\sqrt{2} \quad \ldots\ldots\ldots\ldots\ldots\ldots\ldots\ldots (1)$$

where $\Delta\epsilon_p$ is the applied plastic strain range and D is the extent of intense plastic deformation at the crack tip. D can be expressed in terms of the maximum tensile stress in a cycle (σ_t), a material strength parameter $\bar{T}$

($\simeq$ ultimate tensile strength of previously cycled material), and a current crack length (l) so that

$$dl/dN = \Delta\epsilon_p[\sec(\pi\sigma_t/2\bar{T}) - 1]l \quad \ldots\ldots\ldots\ldots\ldots\ldots (2)$$

On integration, assuming that all the endurance (N_f) of a specimen is taken in crack growth, the endurance law is given by

$$\Delta\epsilon_p\left[\sec\left(\frac{\pi\sigma_t}{2T}\right) - 1\right]N_f = \ln\left(\frac{l_f}{l_o}\right) \quad \ldots\ldots\ldots\ldots\ldots\ldots (3)$$

where l_f (taken as $\frac{2}{3} \times$ specimen diameter) and l_o are the final and initial crack sizes (an initial crack size of 10 μm is consistent with metallurgical observation). Now σ_t and $\Delta\epsilon_p$ are linked in the cyclic stress-strain relationship which for many materials is a power law of the form $\sigma_t = k\Delta\epsilon_p{}^{\beta}$. Then for $(\sigma_t/T) < 0.7$, Eq 3, reduces to the Coffin-Manson law

$$\Delta\epsilon_p N_f{}^{\alpha} = \left[\frac{8}{\pi^2}\left(\frac{\bar{T}}{k}\right)^2 \ln\left(\frac{l_f}{l_o}\right)\right]^{\alpha} \simeq \text{constant} \quad \ldots\ldots\ldots\ldots (4)$$

where $\alpha = 1/(2\beta + 1)$. Some interesting points can be made from Eqs 2 through 4. Equation 4 shows that the slope of the fatigue life curve is related only to the slope of the cyclic stress-strain curve. The shape of the fatigue life curve, therefore, will reflect the shape of the cyclic stress-strain curve. The position of the fatigue life curve is dependent on the ratios of $(\bar{T}/k)$ and (l_f/l_o). As k and $\bar{T}$ are both cyclic strength parameters, variations in strength levels alone will not affect significantly the endurance for cycling at a given strain range. Regarding the ratio (l_f/l_o), which is in logarithmic form in Eq 4, this ratio must change significantly for a significant positional change to occur.

It can be clearly seen that the shape of the cyclic stress-strain curve is the most significant factor affecting endurance. It is interesting to note what happens if $\beta \leq 0$. If $\beta = 0$ perfectly plastic conditions apply, and Eq 2 indicates that D is infinite. In fact, D is limited by specimen size, so that for a specimen of width W, Eq 2 becomes

$$dl/dN = \Delta\epsilon_p(W - l) \quad \ldots\ldots\ldots\ldots\ldots\ldots (5)$$

This gives the endurance relationship

$$\Delta\epsilon_p N_f = \ln\left(\frac{W - l_o}{W - l_f}\right) \quad \ldots\ldots\ldots\ldots\ldots\ldots (6)$$

$$\simeq \ln\left(\frac{1}{1 - l_f/W}\right) \text{ for } l_o \ll l_f < W$$

This curve gives a lower bound for endurance curves if the present mechanism operates. It must be noted that β can be negative in which case, $\alpha > 1$. If $\beta < -0.5$, α is negative.

In the following sections, Eqs 2 and 6 will be used in assessing the endurance behavior of the materials under consideration.

Effect of Temperature on the Endurance of 20/25 Cb Stainless and Mg-Al 80 Magnesium Alloy

20/25/Cb Stainless Steel

Tests were carried out at temperatures of 25 C (0.18 melting point (T_m)), 750 C (0.60 T_m) and 835 C (0.65 T_m) at a constant crosshead speed of 1.27 mm/min. This gives a spread in plastic strain rate on the data of $2 \times 10^{-4}\ s^{-1} < \dot{\epsilon}_p < 2 \times 10^{-3}\ s^{-1}$. In all cases failure occurred by the steady growth of a surface initiated crack across the specimen section in a general direction at right angles to the axis of stressing. The crack path was in all cases a mixture of trans- and intergranular portions, an increasing amount of intergranular fracture occurring at the two high temperatures. The cyclic stress-strain curves based on half-life stress level are shown in Fig. 1.

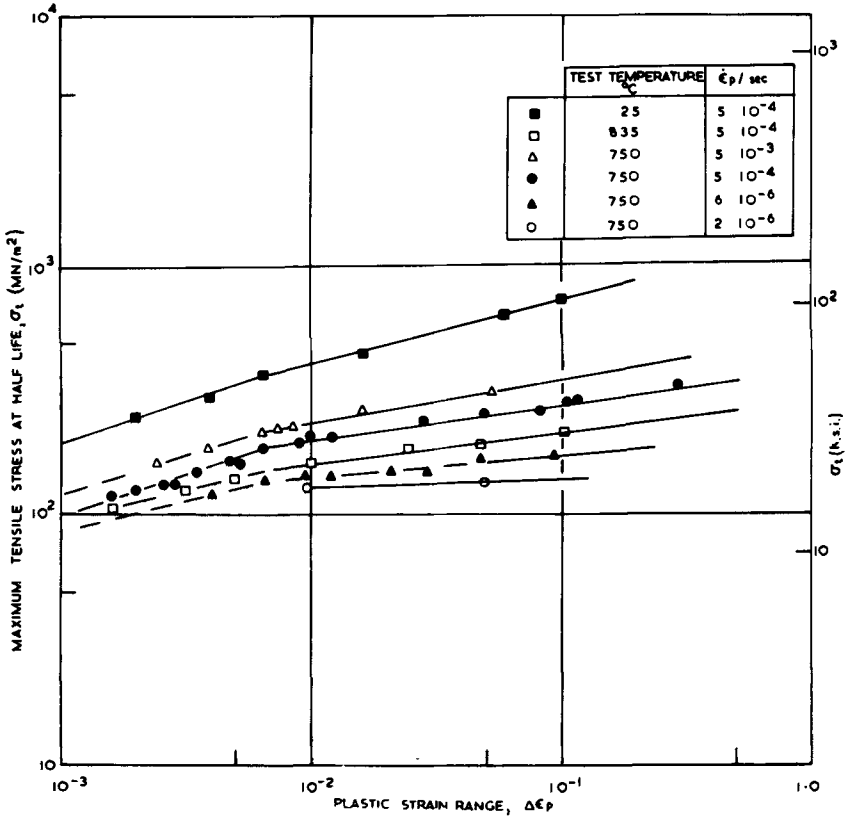


FIG. 1—*Cyclic stress-strain curves for 20/25/Cb stainless steel at various temperatures and strain rates.*

The corresponding fatigue life results are given in Fig. 2 (endurance N_f is defined as the number of cycles to complete separation), along with the predictions derived from Eq 3. (In all predictions Eq 3 is used while $D < \sqrt{2}(W - l)$. For $D \geq \sqrt{2}(W - l)$, Eq 6 is used. The resulting predictions, therefore, use both Eqs 3 and 6). The results follow the predicted trend, a reduction in the hardening exponent β with increasing temperature, resulting in an increase in the slope α of the fatigue life curve. The cyclic stress-strain curves at all three temperatures have a break at a plastic strain range of about 0.007. A break occurs in the endurance data at the corresponding place. The general positional fit of the predictions to the data is good. This is in line with Eq 4 which predicts little effect of $\overline{T}$ and l_f/l_o) for steady propagation from a small starter crack across the whole section. It is worth noting the large spread in $\overline{T}$ which exists in the data presented, from a value of 18.63 MN/m^2 (128.5 ksi) at 25 C to 4.71 MN/m^2 (32.5 ksi) at 835 C. The corresponding spread in (T/k) is only from 0.68 to 0.79.

The theory takes no account of crack path, and the results indicate that changes in the crack path do not affect the endurance seriously. As the parameter $\overline{T}$ is in effect the flow stress ahead of the crack, whereas k is a bulk material parameter, one would expect an effect of crack path only when the grain boundaries are significantly weaker than the grains. The temperatures in these tests are probably not high enough for this to be the case.

Mg-Al 80 Magnesium Alloy

Tests were carried out at temperatures of 25 C (0.32 T_m), 170 C (0.48 T_m) and 400 C (0.73 T_m) at a constant crosshead speed of 2.54 mm/min. Although the crack path varied from wholly transgranular at 25 C to wholly intergranular at 400 C, the failure crack was in all cases surface initiated and propagated across the specimen section.

The cyclic stress-strain data are given in Fig. 3. The curves for all three temperatures show distinct slope changes. The reason for these changes is quite different at ambient and elevated temperatures. At ambient temperature, the changes are a result of the deformation mode of the alloy, which is predominantly mechanical twinning. Azam et al [*11*] have described the shape of a single high-strain hysteresis loop solely in terms of tensile and compressive twinning and untwinning. A similar argument would describe the peculiar shape of the cyclic stress-strain curve. The slope change in the 170 and 400 C curves has a different origin. At these temperatures slip dominates deformation, and no slope change would normally be expected. However, metallographic examination of fractured specimens showed that, for $0.01 > \Delta\epsilon_p > 0.001$, grain growth had taken place during straining. Such grain growth did not occur for strains above 0.01.

The corresponding fatigue life predictions from Eq 3 are shown in Fig. 4. These show slope discontinuities which are in good agreement with experi-

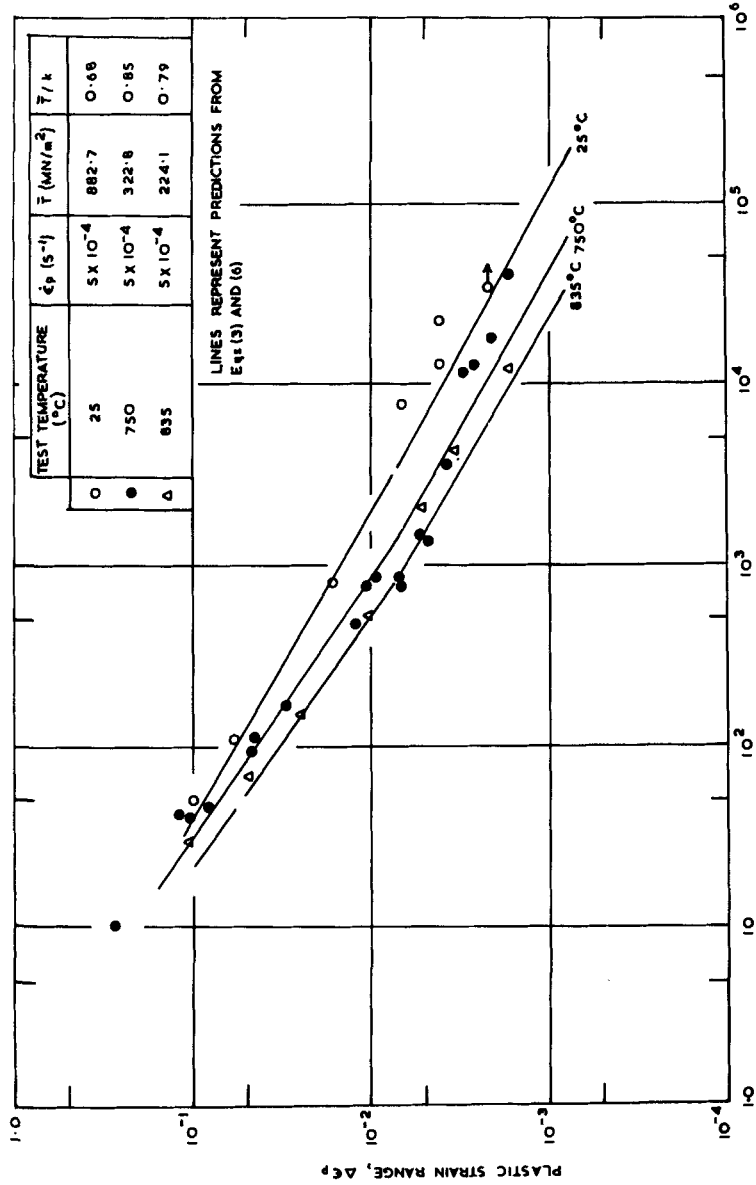


FIG. 2—*Effect of test temperature on the endurance of 20/25/Cb stainless steel.*

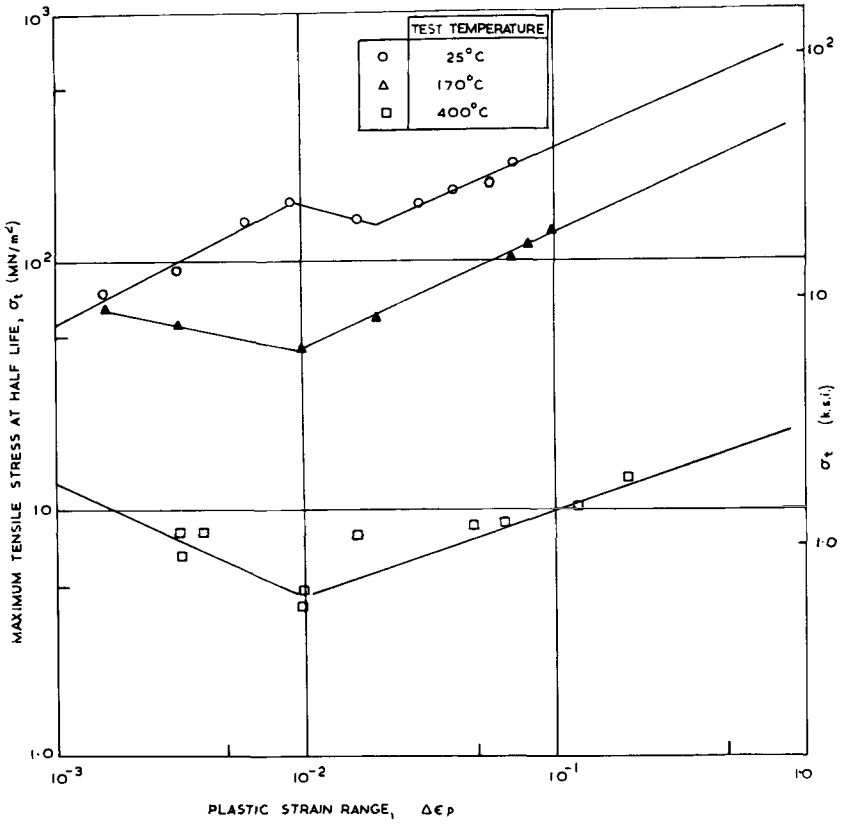


FIG. 3—*Cyclic stress-strain curves for Mg-Al 80 magnesium alloy at various temperatures.*

mental data. When the position of the predictions relative to the data is considered, some interesting deviations are observed. The 25 C prediction seems to be displaced simply along the endurance axis giving endurances a factor four up on those observed. A possible explanation for the anomaly is associated with the susceptibility of the alloy grains to cleavage at this temperature. Areas of cleavage were noted on the fracture surface, and it is possible that the final crack nucleated as a cleavage crack across a grain. This would increase l_o considerably and with a small reduction in l_f due to fast fracture, decreases $ln\ (l_f/l_o)$ by a factor of 4 to 5. With this correction, the prediction is replotted as the dashed line in Fig. 4. The other significant deviation is that of the 400 C data at plastic strains below 0.02. This is the region in which grain growth occurred, and multiple grain boundary cracking was observed from the surface at almost every boundary. The effect of multiple cracking is to cause premature failure by reducing the effective l_f to something like one half the grain size. Following Eq 3, the endurance would be decreased by a factor of 2 which is in agreement with the data.

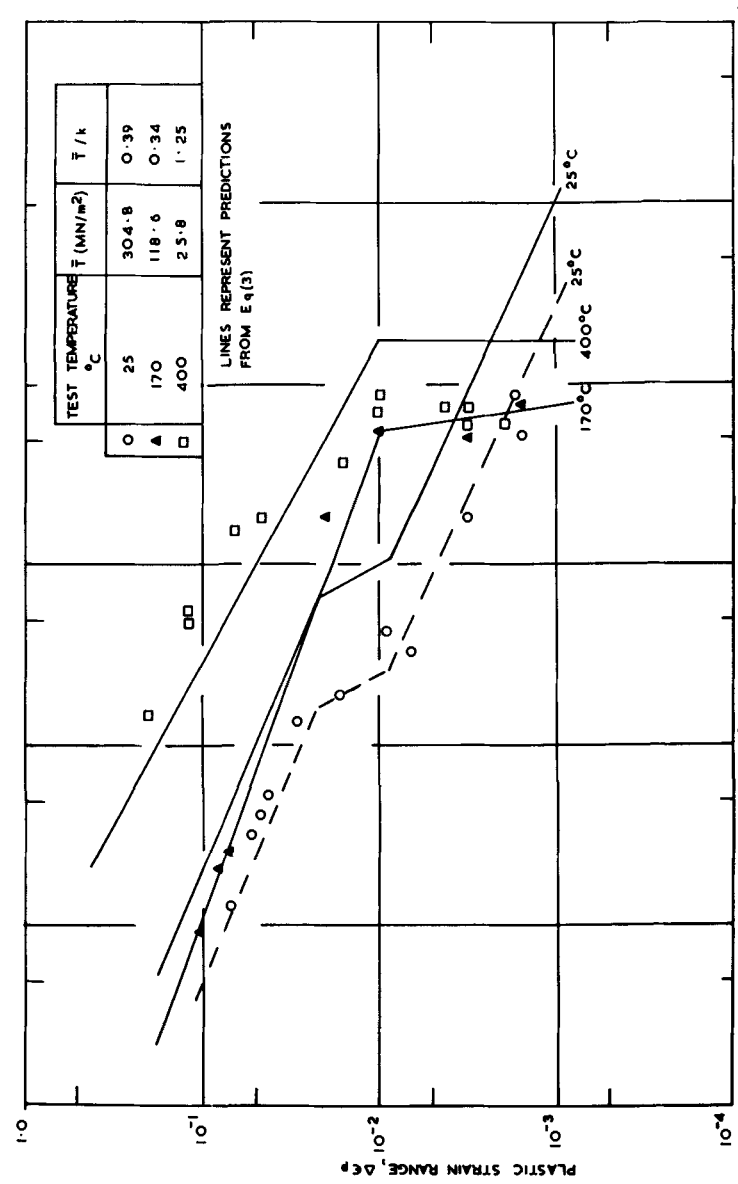


FIG. 4—*Effect of test temperature on the endurance of Mg-Al 80 magnesium alloy.*

The fatigue behavior of Mg-Al 80 shows the opposite trend to that of the stainless steel in that endurance increases with increasing temperature. This increase is particularly marked when the 400 and 170 C data are compared at the higher strain ranges. As noted earlier, this trend would not be expected if β were the major factor in determining the position of the curve. The main reason for the relative position of the 400 C data is the dramatic cyclic softening which occurred in all tests at this temperature. (Slight hardening followed by gradual softening was observed at 25 and 170 C.) The half-life stress level was approximately one fifth of that on the first cycle. The value of $(\overline{T}/k)$ for the 400 C data was thus some four times that at 170 and 25 C (see Fig. 4). It is thus the increase of the ratio (T/k) which is responsible for the increase in endurance at 400 C.

The ability of the theory to cover the wide variations of fatigue deformation and fracture behavior in this alloy indicates that even up to 0.73 T_m, the behavior is controlled primarily by the parameters controlling the mechanism of surface crack growth.

Effect of Varying Strain Rate on the Endurance of 20/25/Cb Stainless Steel at 750 C

At a constant temperature of 750 C (0.60 T_m) tests were carried out at four crosshead speeds: 12.7, 1.27, 0.0127, and 0.0051 mm/min. For a plastic strain range of 0.01, these correspond to mean plastic strain rates of 5×10^{-3}, 5×10^{-4}, 6×10^{-6}, and 2×10^{-6} s^{-1}. At all strain rates, the crack path was a mixture of inter- and transgranular, and failure was by the growth of a single major surface crack. The proportion of intergranular failure increased with decreasing strain rate.

The cyclic stress strain curves for all crosshead speeds are given in Fig. 1. As with the various temperature curves, a slope change occurs at about 0.007 plastic strain range. As expected, this slope change is reflected in the fatigue life curves of Fig. 5, with a tendency to a slope of unity as β tends to zero. As before, predictions using Eqs 3 and 6 are shown along with the lower bound prediction given by Eq 6 alone. The predictions are in good agreement with the data, particularly at the higher strain levels, and the relative changes in fatigue life curve position are well represented. The close approach to the lower bound at the lowest strain rate is worth noting. The data for the lower strain levels ($0.001 < \Delta\epsilon_p < 0.01$) at the highest crosshead speed shows a significant increase in endurance over that predicted. An obvious reason for this was not found, but it is known that in this steel significant oxide formation has been observed at the crack tip, particularly in the early stages of growth.[3] The wedging action of oxide at low-strain levels could well increase endurance. The early stages of growth,

[3] R. P. Skelton, private communication, 1971.

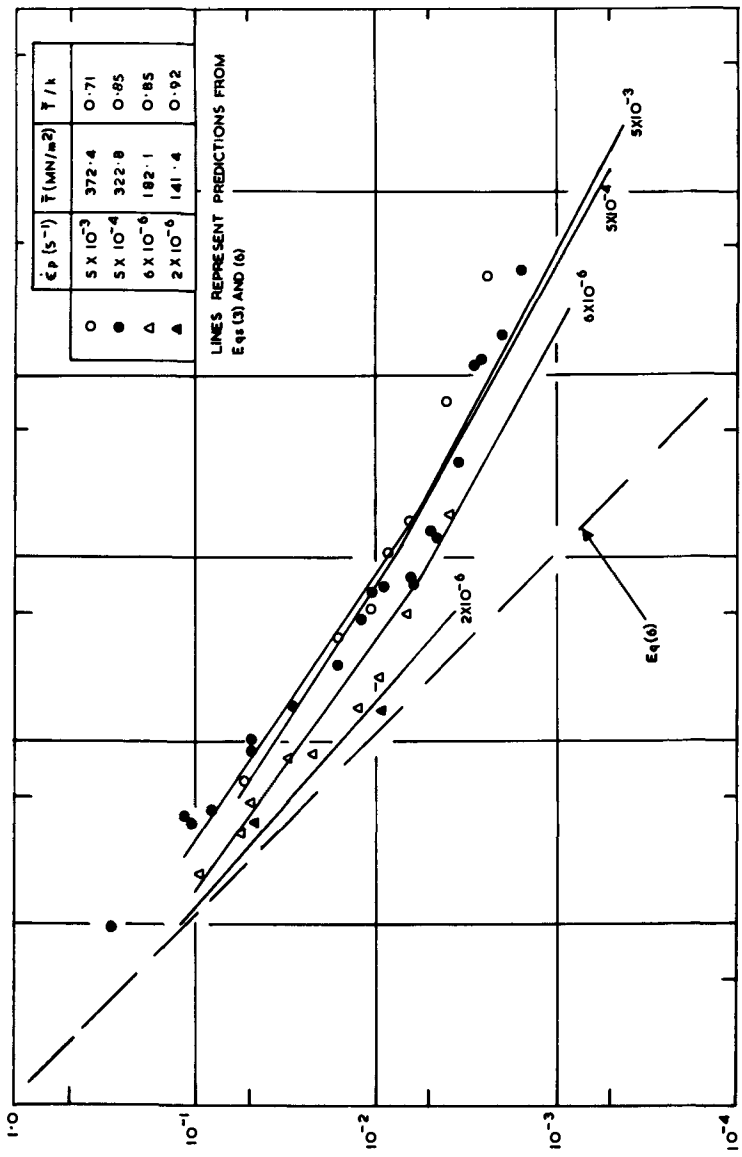


FIG. 5—*Effect of strain rate on the endurance of 20/25/Cb stainless steel at 750 C.*

where the crack growth per cycle is very small, would be most susceptible to this.

The formation of internal grain boundary fracture damage might be expected at the two lowest strain rates. Little evidence of this was found from metallography or fractography, and the order of endurance reduction with strain rate noted in Fig. 5 can be explained solely by variations in cyclic stress strain behavior and material strength level. This is in contrast to the results of Coffin [*6*] on A286 steel, who found significant endurance reductions with reductions in cycling frequency together with little effect of frequency on the cyclic stress-strain curve. He invoked crack tip oxide attack to explain the observed endurance reductions.

Effect of Tensile Hold Periods on the Endurance of 20/25/Cb Stainless Steel at 750 C

A few tests have been carried out at a crosshead speed of 12.7 mm/min incorporating hold periods at the maximum tensile strain limit. Such hold periods induce stress relaxation, producing internal grain boundary cracking with a consequent reduction in endurance [*1–3*]. Results from the present tests involving 5-min hold periods are given in Fig. 6 along with results for tests at the same crosshead speed without hold periods. A considerable reduction in endurance is observed particularly at the lower strain levels, although all failures were due to the steady growth of a surface nucleated crack. Now the cyclic maximum tensile stress-strain points for the hold period tests lie on the same curve obtained for continuous cycling at 12.7 mm/min crosshead speed. Hence, the endurance reductions cannot be explained on the basis of the theory as it stands.

The effect of internal fracture damage on the growth of a surface crack has been examined by Tomkins and Wareing [*3*]. They showed that significant internal fracture damage increases the zone size (D) so that it rapidly becomes equal to the remaining specimen section. If this were so throughout the test, the endurance for holdtime tests would be given by the lower bound prediction. In order to check this point, step tests were carried out in which hold period cycles were applied for a proportion of life followed by continuous cycling. It was found that if less than 10 percent of the life was hold period cycles, the final endurance was as for continuous cycling throughout. If over 30 percent of the life was hold period cycles, then the final endurance was as if hold period cycles had occupied the whole life. This indicates that significant internal damage occurs only after an accumulation of a few percent relaxation strain. Once damage has occurred, however, it can propagate under the faster strain rate part of the cycle.

It becomes possible to make predictions for holdtime results using Eqs 3 and 6. If after 20 to 30 percent of the continuous cycling life (given by

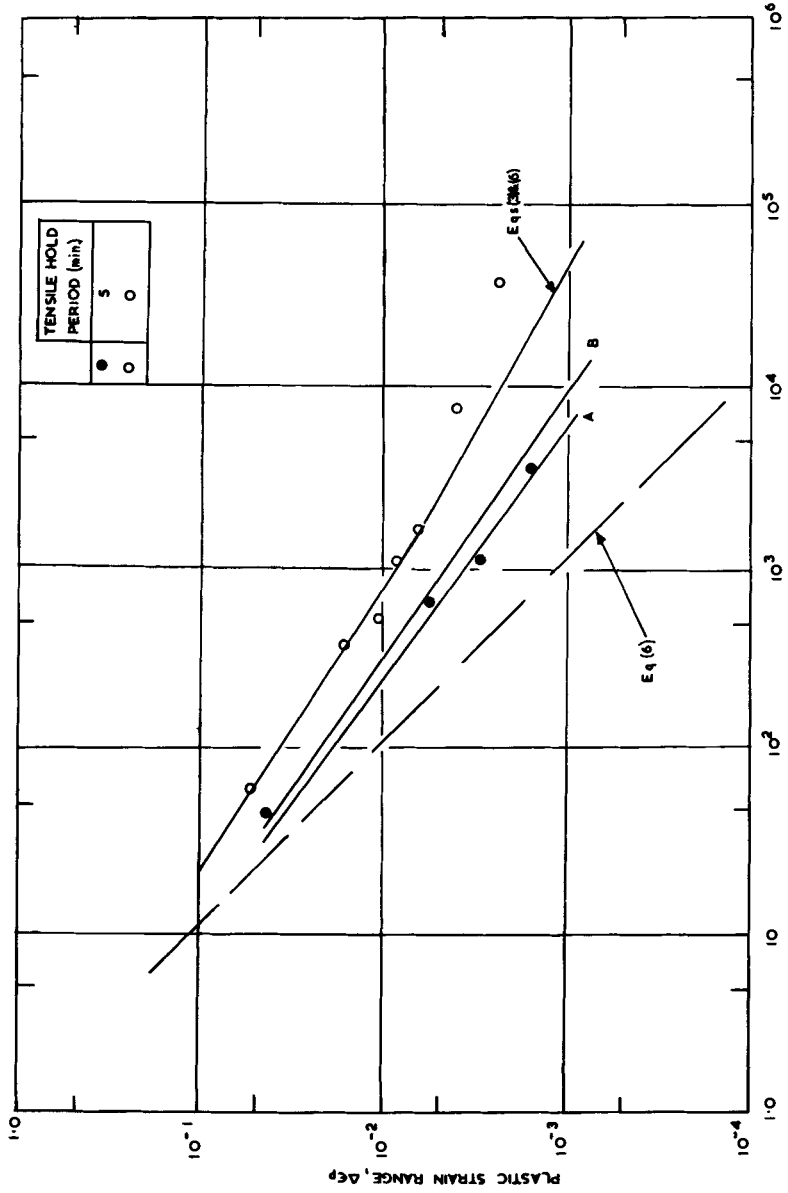


FIG. 6—*Effect of tensile hold periods on the endurance of 20/25/Cb stainless steel at 750 C.*

Eq 3), the internal damage rapidly increases the effective zone size (D) to $\sqrt{2}(W - l)$, Eq 6 gives an assessment of the additional endurance. Predictions using this method are shown as lines A and B in Fig. 6. Line A assumes 20 percent and line B 30 percent of the continuous cycling life before significant internal damage occurs. If the holdtime were increased, it would be expected to reduce the initial proportion, and eventually the lower bound prediction would provide a saturation value for endurance at very long holdtimes. The data of Berling and Conway [2] on Type 304 stainless steel at 650 supports this contention.

Discussion

The use of the theory, which describes quantitatively the mechanics of the crack growth process, has enabled comparisons to be made of the elevated temperature fatigue behavior of the metals concerned over a number of temperatures and strain rates. The theory does not predict necessarily the exact position of a particular fatigue life curve, but it does provide a ground for assessing relative behavior. The results indicate that for simple temperature and strain rate variations, the parameters controlling the mechanics of surface crack growth dominate behavior.

The possible secondary effects of grain boundary weakening and internal fracture damage are insignificant in seriously altering the crack growth rate for continuous cycling. Variations in crack path do not seem to significantly affect growth rate, but they could do so at higher values of the ratio (T/T_m). The holdtime results show that internal damage can affect crack growth rate seriously and hence endurance under some conditions. The main effect of internal damage, once developed, seems to be increasing the effective intense plastic zone size (D), that is, effectively reducing $\overline{T}$. It may be that internal damage is present in the lower strain rate, continuous cycling tests, but its effect is masked by the natural reduction in β and $\overline{T}$.

The present results throw little, if any, light on the effect of environment. In all the present tests the environment was air at ambient pressure. However, the predictions from simple mechanics are fairly accurate and predict good relative positions of endurance curves over a wide range of temperature, particularly at the higher strain levels. Over this temperature range, oxidation rates must vary considerably. The increased endurance over that predicted is some tests at the lowest strain levels may indicate a beneficial effect of oxidation. It is known, however, that at similar strain rates, material, and temperature, the endurance in a vacuum of 10^{-5} torr is considerably greater than that in air.[3]

General Conclusion

For the two metals considered over a wide range of temperature (0.18 to 0.73 T_m) and strain rate ($2 \times 10^{-6} - 5 \times 10^{-3}$ s^{-1}) variations in fatigue

endurance are dependent primarily on the parameters controlling the basic surface nucleated crack growth mechanism. The important factors are the cyclic stress-strain relationship and the strength of cycled material. Secondary fracture effects associated with elevated temperature behavior were found to be important in tests involving hold periods where their effect on the basic mechanism could be quantified.

Acknowledgments

We wish to acknowledge the help of S. A. Kidson in carrying out some of the experimental program. This paper is published by permission of R. V. Moore, managing director of the Reactor Group of the United Kingdom Atomic Energy Authority.

References

[1] Dawson, R. A. T., Elder, W. J., Hill, G. J., and Price, A. T., *Proceedings*, International Conference on Thermal and High Strain Fatigue, Metals and Iron and Steel Institute, 1967.
[2] Berling, J. T. and Conway, J. B., *Proceedings*, International Conference on Pressure Vessel Technology, Delft, 1969.
[3] Tomkins, B., *Proceedings*, International Conference on Corrosion Fatigue, Connecticut, 1971.
[4] Skelton, R. P., *Philosophical Magazine*, Vol. 14, 1966, p. 563.
[5] Gell, M., Leverant, G. R., and Wells, C. H. in *Achievement of High Fatigue Resistance in Metals and Alloys, ASTM STP 467*, American Society for Testing and Materials, 1971, pp. 113–153.
[6] Coffin, L. F., Jr., *Proceedings*, International Conference on Corrosion Fatigue, Connecticut, 1971.
[7] Tomkins, B., *Philosophical Magazine*, Vol. 18, 1968, p. 1041.
[8] Sumner, G., *Journal of Scientists Instruments*, Vol. 43, 1966, p. 238.
[9] Tomkins, B., Sumner, G., and Wareing, J. in *Fracture 1969, Proceedings*, 2nd International Conference on Fracture, Brighton, 1969.
[10] Tomkins, B., *Philosophical Magazine*, Vol. 23, 1971, p. 687.
[11] Azam, N., Didout, G., Leveque, J. P., Sanchez, P., and Weiss, M., *7th Colloque de Metallurgie*, 1963, p. 79.

DISCUSSION

L. F. Coffin[1] *(written discussion)*—In your definition of β, you use the half-life stress range. This means that there is a builtin influence of fatigue life on the strain hardening. My question is, to what degree this dependence detracts from the significance of the concept, particularly when such

[1] Corporate research and development, General Electric Co., Schenectady, N. Y. 12301.

dramatic effect in fatigue life occurs, as for Fig. 4 of the paper? Also, what would happen if a life independent cyclic strain hardening definition were employed, relative to the applicability of $\alpha = 1/(2\beta + 1)$?

J. Wareing, B. Tomkins, and G. Sumner (authors' closure)—The growth rate of a fatigue crack is defined as the product of the plastic zone size, D, and the applied plastic strain range, as indicated by Eq 2. The plastic zone size, D, is related to the cyclic stress, σ, associated with an applied strain range, ϵ_p. On integrating the growth rate equation to calculate fatigue life it is strictly necessary to use a relationship between stress and the number of cycles up to failure. However, using the half-life stress, σ_T, an average value of the stress throughout life is, in general, adequate for calculating fatigue life. Using the more rigorous approach would not significantly alter the $\alpha = 1/(2\beta + 1)$ relationship obtained from an averaging approach.

F. Jeglic,[1] *P. Niessen,*[1] *and D. J. Burns*[1]

Temperature Dependence of Fatigue Crack Propagation in an Al-2.6Mg Alloy

REFERENCE: Jeglic, F., Niessen, P., and Burns, D. J., "**Temperature Dependence of Fatigue Crack Propagation in an Al-2.6Mg Alloy,**" *Fatigue at Elevated Temperatures, ASTM STP 520*, American Society for Testing and Minerals, 1973, pp. 139-148.

ABSTRACT: Fatigue crack propagation has been studied in an Al-2.6Mg alloy between room temperature and 300 C. It is shown that the fatigue crack propagation rate is controlled by volume diffusion. The activation barrier for volume diffusion (Q_0) is lowered by the applied stress intensity range ΔK so that $Q(\Delta K) = Q_0 - C_1 \log \Delta K$. The driving force for the process is inversely proportional to the square of the stress intensity range: $A(\Delta K) = C_2 \Delta K^{-2}$. Fatigue crack propagation rate as a function of temperature and stress intensity range is given by

$$\frac{da}{dN} = C_2 \Delta K^{-2} \exp - \left[\frac{Q_0 - C_1 \log \Delta K}{RT}\right]$$

A special case of this equation is the well-known Paris equation.

KEY WORDS: fatigue (materials), crack propagation, aluminum alloys, stresses, thermal fatigue, cyclic strain, activation energy

The present paper describes, in part, a study of elevated temperature fatigue crack growth in a solid solution aluminum alloy to obtain design data and hopefully identify any thermally activated process which may underly fatigue crack propagation. Rather than specifying *a priori* an atomistic model of separation at the crack tip as done, for example, by Yokobori [*1*],[2] a large body of experimental data was assembled over a wide temperature region to provide the means for the derivation of an empirical equation describing the crack propagation process. Considering the terms and functional form of this equation, an atomistic model can then be proposed.

Experimental Design

Isothermal, constant load range, constant frequency, fatigue crack propagation tests were performed in the temperature range from 26 to

[1] Graduate student, and professors, respectively, Department of Mechanical Engineering, University of Waterloo, Waterloo, Ont., Canada.

[2] The italic numbers in brackets refer to the list of references appended to this paper.

Copyright© 1973 by ASTM International www.astm.org

300 C. Standard fracture toughness wedge opening loading (WOL) specimens, of the shape and dimensions shown in Fig. 1, were used for this investigation.

Fatigue crack growth was monitored ultrasonically. A novel high-temperature ultrasonic probe was designed to work up to 300 C. This measuring device was sensitive to fatigue crack advances of 0.0007 in. The sound wave energies reflected from the leading edge of the fatigue crack and from the bottom surface of the specimen were electronically compared and used to control the crack measurement system. A detailed presentation of the high-temperature fatigue crack monitor, its functioning and accuracy were provided previously [*2*].

All tests were performed under cyclic tensile conditions. Constant load limits of 100 lb (0.444 kN) to 2360 lb (10.497 kN) were chosen. The constant cyclic frequency was 1 Hz. Isothermal tests were repeated at least once at the following temperatures: 26, 60, 80, 100, 130, 140, 150, 160, 170, 200, 250, and 300 C. It was found that the room-temperature propagation rates were influenced by the relative humidity of the laboratory atmosphere. Therefore, fatigue tests at this temperature were carried out in a dry nitrogen atmosphere. All other tests were done in air.

Results

The basic variables of these isothermal tests were number of cycles, N, and crack length, a. An example of the basic a versus N plots for the extreme temperature of 300 C is shown in Fig. 1. Ideally, the a-N curves would have a monotonically increasing slope. The experimental output shown in Fig. 1 is not completely smooth; this may be due to alternative regions of high and low fracture resistance in the path of the propagating crack. These measurements were used directly for the computation of the derived variables, namely, fatigue crack propagation rate da/dN and the stress in-

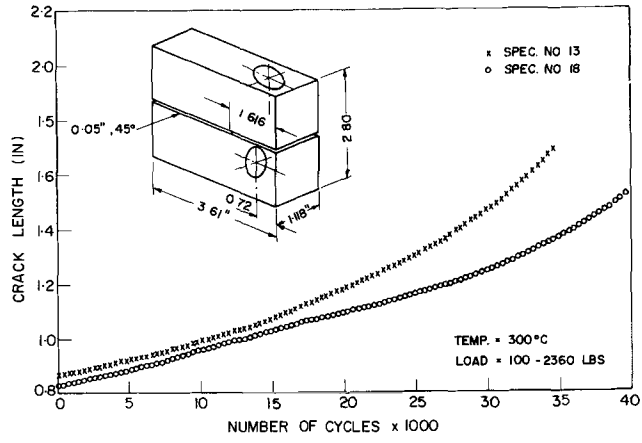


FIG. 1—*Typical fatigue crack growth date at 300 C and WOL specimen dimensions.*

tensity range ΔK. The fatigue crack propagation rate was determined as the instantaneous slope of the tangent to the a-N curve and not, as is often done, by differentiation of a polynomial fitted to the a-N data [3]. The stress intensity range was determined as a function of load range, crack length, and specimen geometry. The isothermal plot log da/dN versus log ΔK for 300 C is shown in Fig. 2 together with the regression line of log da/dN on log ΔK. Regression lines were determined for all test temperatures. In all cases, the Paris equation fits the data, namely,

$$\frac{da}{dN} = B\Delta K^n \quad \ldots\ldots\ldots\ldots\ldots\ldots\ldots\ldots\ldots\ldots (1)$$

Since the raw data was not smoothed initially by fitting it to a polynomial, the experimental scatter appears in Fig. 2. This processing of data was used because of the previously stated objective to obtain not only design data but also information of a fundamental nature. For both, a systematic analysis of experimental scatter may be important [4]. One measure of this scatter is given by the correlation coefficients in Table 1. Table 1 also shows the values of n and B for all sets of isothermal tests. The results indicate that fatigue crack growth rate increases, but the rate of increase of da/dN decreases with increasing temperature. This becomes evident, if the slope of the room-temperature test ($n = 4.35$) is compared to the slope of the test at 300 C ($n = 2.07$).

In Fig. 3 the combined test data are plotted in an Arrhenius type diagram of log da/dN versus $1/T$, the inverse absolute temperature. Regression lines of log da/dN on $1/T$ were drawn through the data points of constant stress intensity range. Each of these lines represents an Arrhenius equation of the form

$$\frac{da}{dN} = A \exp - \frac{Q}{RT} \quad \ldots\ldots\ldots\ldots\ldots\ldots\ldots\ldots\ldots\ldots (2)$$

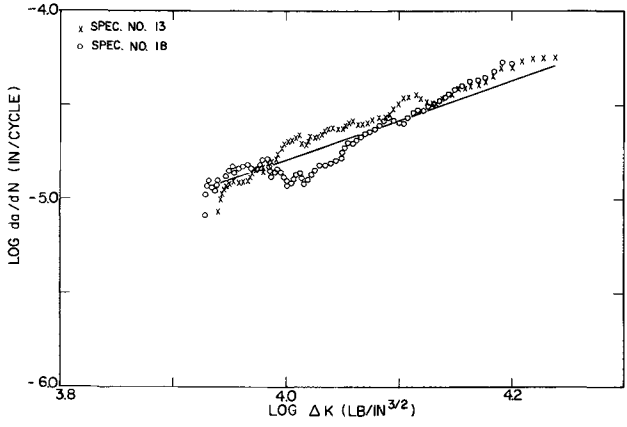


FIG. 2—*Typical data for the rate of fatigue crack growth as a function of* ΔK.

TABLE 1—*Values for* n *and* B *derived from Eqs 1 and 7.*

Test Temperature, deg C	Number of Tests Performed	Equation 1			Equation 7	
		n	Log B	Correlation Coefficient	n	Log B
26	7	4.35	−22.70	0.792	4.62	−24.30
60	2	4.05	−21.71	0.926	4.06	−21.56
80	2	3.71	−20.28	0.887	3.67	−20.06
100	2	3.57	−19.71	0.868	3.36	−18.76
130	2	3.28	−18.34	0.800	2.96	−17.06
140	3	2.78	−16.37	0.880	2.83	−16.56
150	2	2.38	−14.63	0.864	2.72	−16.06
160	2	2.52	−15.15	0.892	2.62	−15.56
170	2	2.64	−15.57	0.877	2.51	−15.16
200	2	2.50	−15.00	0.774	2.23	−14.26
250	2	2.46	−14.86	0.901	1.92	−12.26
300	2	2.07	−13.08	0.849	1.50	−10.86

This equation implies that fatigue crack propagation is a thermally activated process. A is a coefficient including a constant driving force; Q is the activation energy of the process and R the gas constant. Activation energies were calculated from each constant ΔK line. Their values range from 0.5 Kcal/g atom for a ΔK of 17800 psi $\sqrt{\text{in}}$ (19500 kNm$^{-3/2}$) to 3.7 Kcal/g atom for 8000 psi $\sqrt{\text{in}}$ (8750 kNm$^{-3/2}$). Thus, the measured activation energy is obviously a function of the stress intensity range. The rate equation for this process, therefore, would be of the form

$$\frac{da}{dN} = A \exp - [Q(\Delta K)/RT] \quad \ldots\ldots\ldots\ldots\ldots\ldots (3)$$

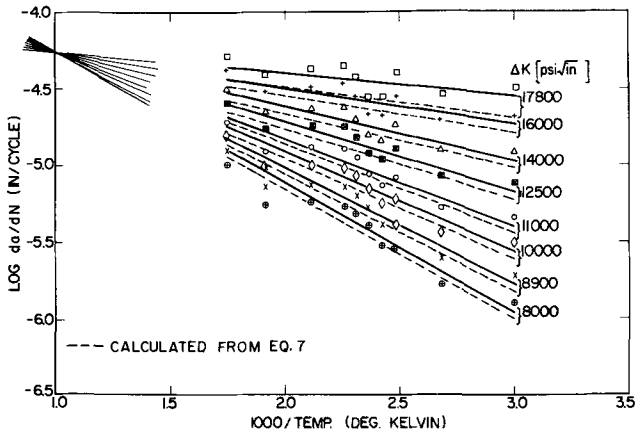


FIG. 3—*The temperature dependence of fatigue crack growth rate for various constant* ΔK *values.*

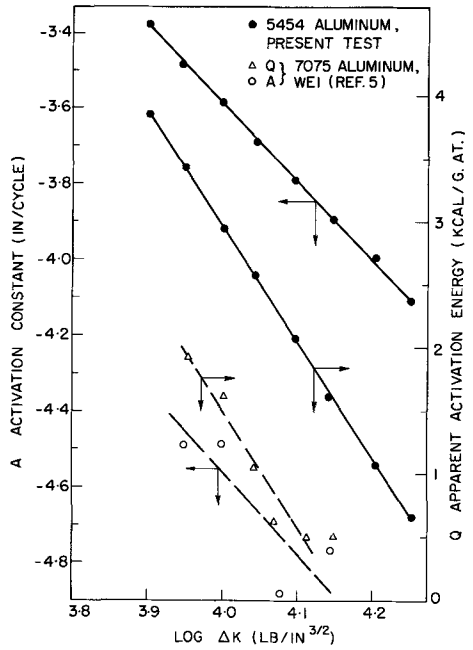


FIG. 4—*The* ΔK *dependence of the apparent activation energy and the activation constant.*

where $Q(\Delta K)$ is the apparent activation energy. A logarithmic relationship between apparent activation energy and stress intensity range was found. A plot of this relationship is given in Fig. 4. Its analytical form is

$$Q(\Delta K) = 39700 - 9185 \log \Delta K \quad \ldots\ldots\ldots\ldots\ldots\ldots (4)$$

This can be interpreted as a basic activation energy, $Q_0 = 39.7$ Kcal/g atom which is lowered by an applied stress. The significance of this value will be discussed later.

Examining the coefficient A in Eq 2, it was realized that these also are a function of ΔK, so that Eq 3 must be written as

$$\frac{da}{dN} = A(\Delta K) \exp - [Q(\Delta K)/RT] \quad \ldots\ldots\ldots\ldots\ldots\ldots (5)$$

The function $A(\Delta K)$ is plotted in Fig. 4 and can be expressed analytically as

$$A(\Delta K) = 21870\ \Delta K^{-2} \quad \ldots\ldots\ldots\ldots\ldots\ldots\ldots\ldots (6)$$

Introducing the functions $Q(\Delta K$ and $A(\Delta K)$ into Eq 5 we obtain

$$\frac{da}{dN} = 21870\ \Delta K^{-2} \exp - \left[\frac{39700 - 9185 \log \Delta K}{RT}\right] \quad \ldots\ldots\ldots (7)$$

More generally, this equation can be written as

$$\frac{da}{dN} = C_1 \Delta K^{-2} \exp - \left[\frac{Q_0 - C_2 \log \Delta K}{RT}\right] \quad \ldots\ldots (8)$$

At the beginning of this investigation, it was shown that Paris' equation predicts the rate of crack growth in isothermal, constant load cycle tests. In order to compare the Paris equation to Eq 8, the latter is rewritten as

$$\frac{da}{dN} = C_1 \Delta K^{(C_3/RT-2)} \exp - \left[\frac{Q_0}{RT}\right] \quad \ldots\ldots (9)$$

so that the Paris coefficient B is

$$B = C_1 \exp - \left[\frac{Q_0}{RT}\right] \quad \ldots\ldots (10)$$

and the Paris exponent n is

$$n = \frac{C_3}{RT} - 2 \quad \ldots\ldots (11)$$

In order to check if Eqs 10 and 11 are consistent with the results, B and n were calculated from these equations and compared to the values of B and n obtained directly from the experimental log da/dN versus log ΔK lines such as Fig. 2. It is seen in Table 1 that the experimental and calculated values are in fair agreement. Another measure of this agreement was obtained by using Eq 7 to calculate log da/dN versus $1/T$ curves for comparison with those shown in Fig. 3. This comparison is very good considering that Eq 7 was derived by a series of least squares analyses.

Discussions and Conclusions

In the foregoing, it was shown that Eq 8 correlates all experimental data. For isothermal conditions, this equation reduces to the Paris equation. Under constant stress intensity range conditions, Eq 8 reduces to an Arrhenius type equation.

Any rate equation can be written as

$$\text{rate} = M \cdot Z \quad \ldots\ldots (12)$$

where M is a mobility term and Z the driving force for the process. Since M has an exponential temperature dependence, we obtain

$$\text{rate} = Z \cdot M_0 \exp - \left[\frac{Q}{RT}\right] \quad \ldots\ldots (13)$$

M_0 is a mobility constant containing the entropy of activation. Comparing this equation with Eq 8, it is seen that the driving force for crack propagation is

$$Z\alpha \frac{1}{\Delta K^2} \quad \ldots\ldots\ldots\ldots\ldots\ldots\ldots\ldots\ldots\ldots (14)$$

This equation predicts a decrease in the driving force with an increase in the stress intensity range. This prediction is at a first glance hard to reconcile to the fact that the crack growth rate invariably increases with ΔK. This apparent dilemma is resolved when one considers that the activation energy in the mobility term is also stress dependent. The constant activation barrier Q_0 is lowered by the applied stress so that an apparent activation energy is measured

$$Q(\Delta K) = Q_0 - C_2 \log \Delta K \quad \ldots\ldots\ldots\ldots\ldots\ldots (15)$$

The numerical value of Q_0 is 39.7 Kcal/g atom. This value is comparable to the values of activation energy for volume diffusion in aluminum alloys containing 5 to 8 percent magnesium (38 Kcal/g atom) [5]. It has also been shown that secondary creep [6] and the ultimate tensile strength [6,7] for aluminum-magnesium alloys have a temperature dependence corresponding to an activation energy of 36 Kcal/g atom. These latter values were obtained from measurements in the temperature region of 150 to 280 C. Therefore, it would appear that at least in this temperature region deformation processes in these alloys are controlled by a diffusive process which may also control the fatigue crack propagation rate.

It will be noticed that all lines of constant ΔK in Fig. 3 intercept at $1000/T = 0.986$ and $\log da/dN = -4.243$. At this temperature, $T = 1012$ K, A is independent of ΔK. This temperature is close to the melting point of this alloy, 933 K. If lines of constant ΔK are considered as lines of separation at certain constant mechanical energy input, then it is not unreasonable to expect that material will separate at the melting point by thermal energy only. The value of the propagation rate at this point of thermal separation has no recognizable physical significance.

It would be desirable to test the derived thermal crack propagation equation using other data. As far as we know, the only data which can be used for such a test is that obtained by Wei [7] for a 7075-A1 alloy. This alloy contains 5.6 percent zinc, 1.6 percent copper and 0.3 percent chromium in addition to 2.5 percent magnesium. Some of his tests were performed on 0.25-in.-thick plate specimen at 143 Hz in a controlled dry gaseous atmosphere. As in the present work, Wei found that the log da/dN versus $1/T$ plots yielded very low activation energies which were functions of ΔK. Wei's data have been included in Fig. 4. For his data, $Q(\Delta K)$ and $A(\Delta K)$

were calculated from least square lines fitted to the data points. His apparent activation energies can be written as

$$Q(\Delta K) = 34100 - 8162 \log \Delta K \quad \ldots\ldots\ldots\ldots\ldots (16)$$

In this equation, the constant activation energy of 34 Kcal/g atom is again indicative of volume diffusion and the lowering of this energy by the applied stress explains his low apparent activation energies. $A(\Delta K)$ was calculated to be

$$A(\Delta K) = 1762\ \Delta K^{-1.95} \quad \ldots\ldots\ldots\ldots\ldots\ldots (17)$$

It should be noted that this equation is derived from the least square analysis of four rather widely scattered points (Fig. 4). Therefore, the agreement between this stress dependence of the driving force and our ΔK^{-2} dependence may be fortuitous. But when Eqs 16 and 17 are inserted into Eq 5, we obtain

$$\frac{da}{dN} = 1762\ \Delta K^{-2} \exp - \left[\frac{34100 - 8162 \log \Delta K}{RT}\right] \quad \ldots\ldots\ldots (18)$$

Comparing this equation with Eq 7, it is seen that this independent set of experimental data fits very well into our formulation of the crack propagation rate. This is particularly gratifying considering that Wei's data were obtained under very different experimental conditions.

Since the 5454 and 7075 aluminum alloys are metallurgically very different, it is likely that Eq 8 can be used to interpret elevated temperature fatigue crack propagation in other aluminum alloys.

In our equation, the driving force has a ΔK^{-2} dependence. This dependence can be explained in the following way: The plastic zone ahead of the crack tip is bounded by an envelope where the yield conditions prevail. During crack growth, fracture conditions must be reached at the crack tip. Inside the plastic zone, a deformation gradient is set up having as its boundaries these yielding and fracture conditions. Associated with this deformation gradient is an elastic strain energy gradient. The slope of the elastic energy gradient is inversely proportional to the distance between these two boundary conditions, that is, to the size of plastic zone, r_{pl}. The driving force for the transitional jump of the diffusing species is this elastic energy gradient.

The local elastic energy gradient can be expressed as dE_e/dx and over the entire plastic zone as $\Delta E_e/\Delta r_{pl}$. Since the boundary conditions remain constant, the gradient is a function of the plastic zone as

$$\frac{\Delta E_e}{\Delta r_{pl}} = \text{constant}\ \frac{1}{\Delta r_{pl}} \quad \ldots\ldots\ldots\ldots\ldots\ldots (19)$$

The driving force is proportional to the elastic energy difference over the range of the diffusion zone and therefore proportional to $1/r_{pl}$. If we consider that

$$\Delta r_{pl} = C_0 \cdot \Delta K^2 \quad (20)$$

it follows that the driving force

$$Z\alpha \frac{1}{\Delta r_{pl}} \alpha \frac{1}{\Delta K^2} \quad (21)$$

Thus, the consideration of the conditions at the crack tip, where the rate controlling volume diffusion takes place, explains the experimentally found reverse relationship between driving force and the square of the stress intensity range.

While it has been shown on the basis of activation energy and driving force considerations that the crack propagation is controlled by diffusion, the present experiments do not furnish the information to stipulate how diffusion ultimately enters the process of material separation. A number of atomistic models could be considered, however in the absence of microscopic experiments such considerations would be speculative.

Acknowledgments

This research was performed under Grant 9535-43 from the Defense Research Board of Canada.

References

[1] Yokobori, T. in *Physics of Strength and Plasticity*, MIT Press, Cambridge, Mass., 1969, pp. 327–338.
[2] Jeglic, F., Niessen, P., and Burns, D. J., *Experimental Mechanics*, Vol. 11, No. 2, Feb. 1971, pp. 82–85.
[3] Federowica, A. J., Powell, B. A., "A Computer Program to Obtain a Min-Max Regression Model by Linear Programming," Research Report 68-1C3-COMPR2, Westinghouse Research Laboratories, July 1968.
[4] Mukherjee, B. and Burns, D. J. in *Probabilistic Aspects of Fatigue, ASTM STP 511*, American Society for Testing and Materials, 1972, pp. 43–60.
[5] Jost, W., *Diffusion in Solids, Liquids and Gases*, Academic Press, New York, 1952.
[6] Robinson, A. T., Tietz, T. E., and Dorn, J. E., *Transactions*, American Society for Metals, Vol. 44, 1952, pp. 896–928.
[7] Sherby, O. D. and Dorn, J. E., *Journal of Metals*, Sept. 1952, pp. 959–964.
[8] Wei, R. P., *The International Journal of Fracture Mechanics*, Vol. 4, No. 2, June 1968, pp. 159–170.

DISCUSSION

Campbell Laird[1] (written discussion)—You have not specifically identified the physical basis for the diffusion result which you claim. Can you describe a mechanism consistent with your result?

F. Jeglic, P. Niessen, and D. J. Burns (authors' closure)—We pointed up that the values of Q_0 and the ΔK dependence from our and Wei's work indicate that volume diffusion process is fatigue crack propagation rate controlling. Because the free energy gradient for diffusion is due to the applied stress, the diffusing atomic defect must have its own stress field in the aluminum lattice to experience the free energy gradient. Both vacancies and magnesium atoms will have their own stress field. In microscopic work on areas immediately ahead of the crack tip, we found that cavities were present in the material ahead of the crack tip at all temperatures. Therefore, it is likely that a vacancy diffusion and condensation process is rate controlling.

[1] Department of Metallurgy, University of Pennsylvania, Philadelphia, Pa. 19104.

J. A. Williams[1]

Derivation of a Failure Law for Creep Under a Cyclic Stress

REFERENCE: Williams, J. A., "**Derivation of a Failure Law for Creep Under a Cyclic Stress,**" *Fatigue at Elevated Temperatures, ASTM STP 520,* American Society for Testing and Materials, 1973, pp. 149–156.

ABSTRACT: The problem of creep fracture under an imposed cyclic stress is considered solely in terms of wedge crack growth. The derivation of a relationship similar to that suggested by Coffin for fatigue is illustrated, and this simple model is extended qualitatively to outline one form of a creep:fatigue interaction.

KEY WORDS: fatigue (materials), crack propagation, creep tests, fracturing, stress cycle

The problem of cyclic creep or of combined creep:fatigue is one which is of commercial importance in the design and continued operation of high-temperature steam generating plant. At present, there is no universally accepted design standard to incorporate both phenomena. It is apparent that relative importance of the creep:fatigue components will be emphasized by the cycle time which can vary over many orders of magnitude in operating plant and in principle could range from "pure" creep to "pure" fatigue.

The approach, used in this paper, is to consider the simple case of creep of a material subjected to a symmetrical cycle of tensile stress and is considered as one aspect of the more general case of variable stress creep. The failure model is then examined qualitatively to illustrate how changes in the loading sequences could affect any creep:fatigue interaction which is obtained.

Creep Fracture Model

The material is considered to fail by triple point or wedge cracking, and the strain to cause crack nucleation is low. These conditions are reasonable since, under normal creep conditions, crack nucleation in many materials is relatively easy [*1*],[2] and crack models can be used which enable the final

[1] Formerly project leader, Materials Division, Central Electricity Research Laboratories, Leatherhead, Surrey, England, now at Marchwood Engineering Laboratories, Welding Section, Southampton, England.

[2] The italic numbers in brackets refer to the list of references appended to this paper.

Copyright© 1973 by ASTM International www.astm.org

failure process of a previously cavitated material to occur by the growth of wedge cracks [*2*].

Consider a small wedge crack of length, C, and wedge height (na), (Fig. 1) under the variable loading system illustrated in Fig. 2. The loading half-cycle (positive) stress is given by:

$$\sigma = \sigma_1 + m_1 t \quad \ldots\ldots (1)$$

where

σ = stress applied at time, t,
m_1 = loading rate, and
σ_1 = minimum stress applied (Fig. 2).

The stress and creep rate are assumed to be related by an equation of the form:

$$\dot{\epsilon} = A\sigma^n \quad \ldots\ldots (2)$$

where

$\dot{\epsilon}$ = creep rate,
A = a constant, and
n = a constant ranging from 2 to 8.

Growth of wedge cracks under these conditions will be controlled by grain boundary sliding, and the wedge height can be written in terms of the sliding rate or creep rate at any time, t, using the approach of Williams [*3*], Heald and Williams [*4*], and Langdon [*5*]. Using this approach, the change in wedge height, $d(na)$, caused by a creep rate, $\dot{\epsilon}$, acting for time, dt, is given by:

$$\sigma d(na) = \kappa \dot{\epsilon}^p dt \quad \ldots\ldots (3)$$

p is defined as $(n_{gbs} + 1)/n$ [*4*] where n_{gbs} is the stress index for grain boundary sliding as in the relationship, $\dot{\epsilon}_{gbs} = A_{gbs}\sigma^{n_{gbs}}$, and κ is a constant as defined in Appendix. The final failure criterion is taken as the point when the wedge height attains a critical value, (na_{CRIT}), at which stage fast,

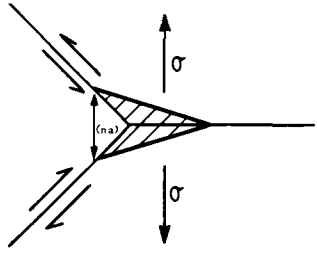


FIG. 1—*Wedge crack model.*

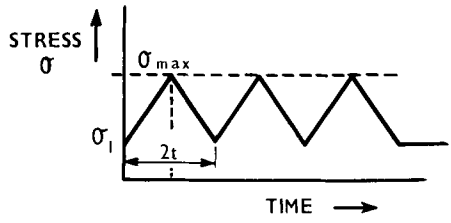


FIG. 2—*Cyclic stress system (symmetrical).*

unstable crack growth occurs [*5*], that is, for final failure, $\Sigma\sigma(na) = \sigma(na_{CRIT}) = 2\gamma$ where γ is the effective fracture surface energy.

It is accepted that such an approach is valid for elastic-brittle materials but is also a reasonable approximation in cases where the plastic deformation associated with the crack is small. One viewpoint in the analogy to a creeping material is that, basically, there will be two different deformation modes associated with a growing crack, namely, a time independent deformation on loading and a time dependent creep deformation. Under these conditions, the creep crack will grow through the time independent structure. It has been shown also that crack instability can occur under creep conditions [*7,8*]. Finally, this type of analysis can be used to derive some original basic creep data correlation parameters.

Macroscopic ductilities under creep conditions, in addition, can be very low and a good example found in practice will be the heat affected zone structure associated with certain ferritic welds. It is in such positions, for example, welded pipe junctions, where marked thermal stress variation during operation could occur leading to a slow cycle creep:fatigue interaction.

Application of Model to Cyclic Creep

In the appendix, the "damage" at failure is derived for these specific conditions to be:

$$D_f = \frac{2\gamma}{\kappa} = \int_0^{t_f} \dot{\epsilon}^p dt$$

where D_f represents a measure of the wedge height of the crack at instability. At any stage in the process, then the damage parameter D_t should be given:

$$D_t = \int_{t_1}^{t_2} \dot{\epsilon}^p dt \quad \ldots\ldots\ldots\ldots\ldots\ldots\ldots\ldots\ldots\ldots (4)$$

Obviously, further modification could be incorporated to account for a strain:time dependent further crack nucleation rate but due to the inadequacy of data on nucleation kinetics in these materials, this is not incorporated at present.

For a cyclic process of N positive symmetrical stress cycles, the damage parameter, D_t, is derived as:

$$D_t = 2N \int_0^t \dot{\epsilon}^p dt \quad \ldots\ldots\ldots\ldots\ldots\ldots\ldots\ldots (5)$$

where $2t$ is the cycle time.

At failure, $\Sigma\sigma d(na) = \sigma(na_{\mathrm{CRIT}}) = 2\gamma$, and thus Eq 4 at failure can be written as:

$$D_f = 2N_f \int_0^t \dot{\epsilon}^p dt \quad \ldots\ldots\ldots\ldots\ldots\ldots\ldots\ldots (6)$$

Transposing creep rate and stress in Eq 6 and integrating gives:

$$D_f = 2N_f A^p \left[\frac{1}{m_1(np+1)} \left\{ {\sigma_{\max}}^{np+1} - {\sigma_1}^{np+1} \right\} \right] \quad \ldots\ldots\ldots\ldots (7)$$

Now, by definition and examination of Fig. 2,

$$m_1 = 2(\sigma_{\max} - \sigma_1)\nu \quad \ldots\ldots\ldots\ldots\ldots\ldots\ldots\ldots (8)$$

where ν is the frequency and is given by $1/2t$.

$$D_f = \frac{N_f A^p}{(np+1)\nu} \left[\frac{{\sigma_{\max}}^{np+1} - {\sigma_1}^{np+1}}{\sigma_{\max} - \sigma_1} \right] \quad \ldots\ldots\ldots\ldots\ldots\ldots (9)$$

Also, due to the large stress dependence of the creep rate, for cases where $\sigma_{\max} \gg \sigma_1$:

$$D_f = \frac{N_f A^p}{(np+1)\nu} \left\{ {\sigma_{\max}}^{np} \right\} \quad \ldots\ldots\ldots\ldots\ldots\ldots\ldots\ldots (10)$$

Transposing creep rate and stress, then:

$$D_f = \frac{N_f}{(np+1)\nu} \left\{ {\dot{\epsilon}^p}_{\max} \right\} \quad \ldots\ldots\ldots\ldots\ldots\ldots\ldots\ldots (11)$$

Thus, due to the high value of n, almost all the strain will be accumulated at the maximum stress, and, to a good approximation, the strain per cycle, ϵ, will be given by the solution of the normal creep rate equation between the fixed stress limits. In the case of a stress ranging between zero, $\sigma_{\max}$ and zero, then:

$$\int_0^{\epsilon} d\epsilon = \int_0^t 2A^n dt = \int_0^t 2Am_1{}^n t^n dt \quad \ldots\ldots\ldots\ldots\ldots (12)$$

or

$$\epsilon = \frac{\dot{\epsilon}_{\max}}{(n+1)\nu} \text{ since } \nu = \frac{1}{2t} \quad \ldots\ldots\ldots\ldots\ldots\ldots (13)$$

Substitution of Eq 13 into 11 and rearranging gives:

$$N_f^{1/p} \nu^{\frac{p-1}{p}} \epsilon = \left[\frac{D_f(np + 1)}{(n + 1)^p}\right]^{1/p} \quad \ldots\ldots\ldots\ldots (14)$$

Typical values for p, namely, $0.7 < p < 1$, can be substituted in Eq 14 to give the general form:

$$N_f^x \nu^y \epsilon = \text{constant} \quad \ldots\ldots\ldots\ldots\ldots\ldots (15)$$

where values of x are approximately 1.0 to 1.4 and values of y are 0 to -0.4.

Discussion

This note has approached the problem of cyclic creep loading solely from the viewpoint of wedge crack growth and as such, ignores any fatigue component in the calculation. Thus, under conditions which can be described as "pure creep," a crack growth analysis of this type will yield a relationship between number of cycles to failure, frequency and nonrecoverable creep strain per cycle of the form:

$$N_f^x \nu^y \epsilon = \text{constant} \quad \ldots\ldots\ldots\ldots\ldots\ldots (16)$$

where x and y can take values of 1.0 to 1.4 and 0 to -0.4, respectively.

At this stage, it is of use to compare relationships which are used for room-temperature fatigue data correlation, for example, the Coffin relationship [*9*] which states:

$$N_f^\alpha \epsilon_p = \text{constant} \quad \ldots\ldots\ldots\ldots\ldots\ldots (17)$$

where ϵ_p is the plastic strain per cycle, and α is a constant of the order of 0.3 to 0.5. A similar relationship [*10*] has been applied to high-temperature fatigue in the creep range, and here the value of α was found to be 0.6 to 1.0. The data thus suggest that a general relationship of the form:

$$N_f^\alpha \epsilon = \text{constant}$$

might apply to high-temperature fatigue, and that as the creep component is increased, for example, at higher temperatures and lower cycle rates, the value of the constant, α, increases. Thus, it might be expected that an analysis based on failure mechanisms controlled by creep and grain boundary sliding processes will give an upper bound value for these constants.

Equation 16 gives a frequency dependence of the number of cycles to failure of the form, $N_f^\alpha \nu^{-y/x}$ where $-y/x$ is approximately equal to $(p - 1/p)$. For most materials for which values of p are reported $p \sim 1$ and thus the frequency effect, if present in the truly creep case is very small. The minimum reported values of p are approximately 0.7, thus yielding a $N_f^\alpha \nu^{0.4}$ relationship.

Some recent work by Coffin [*11*] on the effect of vacuum on the high-temperature fatigue properties has used a relationship of the form:

$$\Delta\epsilon_p \cdot N_f{}^{\alpha}\nu^{\beta} = c_2$$

where α, β, and c_2 were constants. In air, these data suggest that for A286 alloy at 1100 F, $\alpha = 0.97$ and $\beta = -0.33$ which is in agreement with the present analysis. The values taken for p, the index in the creep relationship, $\dot{\epsilon}^p t_f$ = constant are those for materials in air environments, and it is not clear what effect the test environment may have on the basic creep properties. However, due to the interest in various environments for reactor operation, it is likely that such data will be available.

This approach is not strictly applicable only to the cyclic stress case but can be applied to the cases of more complex sequences. Prestrain followed by creep, and stress relaxation followed by creep can be considered by combining various stress:time or strain:time functions [*12,13*].

So far, in this simplified analysis, no creep fatigue interaction has been considered, but it is of value, at this stage, to consider one such form of interaction. If a single stress cycle is considered (Fig. 3) with a nonsymmetric load/unload cycle, then the sequence can be thought of as prestrain followed by a period in which creep damage accumulates under a falling stress. Now the effect of prestrain on creep can have two opposing effects [*14,15*] depending on prestrain rate, temperature, and structure. The usual effect is that of hardening which reduces the subsequent creep rate and increases creep life, and this effect is very dependent on prestrain rate. Under these circumstances, the damage accumulation rate should be reduced, and the number of cycles to failure increased. Such a loading sequence would be of obvious relevance to the case of cyclic creep incorporating a dwell period. This approach suggests that the life would be dependent to some extent on the initial loading rate. However, when the prestressing conditions are such that grain boundary damage is introduced during the rising load period, then the opposite effect could be obtained.

This form of creep-fatigue interaction will be material dependent, and the effect could be specified if more information was available on the effect of prestrain on the damage accumulation rate of a material.

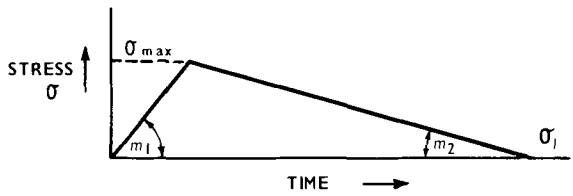


FIG. 3—*Cyclic stress system (nonsymmetrical).*

Conclusion

This paper describes the analysis of a cyclic creep process solely in terms of grain boundary sliding controlled creep crack growth. The crack growth model used has been applied previously to creep fracture processes and has been shown to generate relationships such as the Larson-Miller relationship for creep data correlation. Using this analysis, a relationship similar to that suggested by Coffin is derived for a cyclic stressing sequence, and calculated values of constants are compared with those previously reported. The model is finally generalized in qualitative terms to show how a creep fatigue interaction term could be envisaged.

Acknowledgments

The author wishes to thank R. P. Skelton and J. Barford for many helpful discussions. This work has been carried out at the Central Electricity Research Laboratories, and the paper is published by permission of the Central Electricity Generating Board.

APPENDIX

Derivation of Total Damage at Failure

For total failure caused by growth of a wedge crack, the Cottrell model [6] is used which derives the condition for critical crack growth, that is,

$$\sigma\, na = 2\gamma \quad \text{.....(18)}$$

where (na) is the wedge height and γ is the effective fracture surface energy. For wedge cracks driven by grain boundary sliding, it has been suggested [*3,4*] that

$$(na) = G\, \dot{\epsilon}_{gbs}\, t \quad \text{.....(19)}$$

where G is the grain size, t the time, and $\dot{\epsilon}_{gbs}$ the sliding rate. The total failure criterion is thus:

$$\sum \sigma na = 2\gamma \text{ ...(following Cottrell)..... (20)}$$

Combining Eq 19 and 20 gives:

$$\int_0^{t_f} \sigma\, G\, \dot{\epsilon}_{gbs}\, dt = 2\gamma \quad \text{.....(21)}$$

and in terms of the creep rate,

$$\int_0^{t_f} \dot{\epsilon}^p dt = \frac{2\gamma}{\kappa} = D_f \quad \text{.....(22)}$$

where $1/\kappa$ is a constant equal to $[A^p/A_{gbs}]\, 1/G$, p is the Monkman: Grant index, $[= (n_{gbs} + 1)/n]$ [*4*] and A, A_{gbs}, n, and n_{gbs} are the constants defined by the relevant rate equations $\dot{\epsilon} = A\sigma^n$.

References

[1] Ratcliffe, R. T. and Greenwood, G. W., *Philosophical Magazine*, Vol. 12, 1965, p. 59.
[2] Steigler, J. O., Farrell, K., McCoy, B. T. M., and Loh, H. E., *Quarterly Transactions*, American Society for Metals, Vol. 60, 1967, p. 494.
[3] Williams, J. A., *Philosophical Magazine*, Vol. 15, 1967, p. 1289.
[4] Heald, P. T. and Williams, J. A., *Philosophical Magazine*, Vol. 22, 1970, p. 1095.
[5] Langdon, T. J., *Philosophical Magazine*, Vol. 22, 1970, p. 1021.
[6] Cottrell, A. H., *Transactions*, American Institute of Mining, Metallurgical, and Petroleum Engineers, Vol. 212, 1961, p. 192.
[7] Williams, J. A., *Acta Metallurgical*, Vol. 15, 1967, p. 1559.
[8] Solderberg, R. in *Proceedings*, 2nd International Conference on Fracture, Chapman and Hall, London, 1969, p. 450.
[9] Coffin, L. F. and Tavernelli, J. F., *Transactions*, American Institute of Mining, Metallurgical, and Petroleum Engineers, Vol. 215, 1959, p. 794.
[10] Berling, J. T. and Slot, T., *Fatigue at High Temperature*, *ASTM STP 459*, American Society for Testing and Materials, 1969.
[11] Coffin, L. R., Jr., "The Effect of Vacuum on the High Temperature Fatigue Behaviour of Structural Materials," Report No. 71-C-108, General Electric Co., April 1971.
[12] Williams, J. A., *Proceedings*, 2nd IUTAM Conference on Creep in Structures, Göteborg, Sweden, Springer Verlag, Berlin, 1971.
[13] Soo, J. N., Conference on Holes in Metals, Institute of Metals, Sheffield, 1971.
[14] Williams, J. A. and Lindley, T. C., *Zeitschrift Metallkunde*, Vol. 60, 1969, p. 957.
[15] Schmidt, W., *DEW-Technische Berichte*, Vol. 9, 1969, p. 264.

P. N. Atanmo[1] *and A. J. McEvily, Jr.*[2]

Creep-Fatigue Interaction During Crack Growth

REFERENCE: Atanmo, P. N. and McEvily, A. J., Jr., "**Creep-Fatigue Interaction During Crack Growth,**" *Fatigue at Elevated Temperatures, ASTM STP 520*, American Society for Testing and Materials, 1973, pp. 157–165.

ABSTRACT: The interaction between creep and fatigue processes has been investigated during crack growth in sheet specimens of the aluminum alloy 5052 at 400 F. Fractographic studies indicate that at high frequencies (1/30 Hz) the fatigue process of crack advance is dominant, whereas at low frequencies (for example, 60 Hz) the creep process prevails. It was found that at low frequencies and at a low peak stress level (10 ksi) the cyclic process could lead to an increase in the total time to failure as compared to the creep process alone.

KEY WORDS: fatigue (materials), aluminum alloys, crack propagation, cycle ratio, creep tests, fatigue tests, fractography

Although there is much information concerning the characteristics of fatigue crack growth, relatively little deals with the crack growth in the creep range. The purpose of this study was to investigate the nature of creep-fatigue interaction, the results serve to clarify the nature of the creep-fatigue process under the particular test conditions chosen. Because of the large number of factors which can influence this interaction, it is clear that much additional work will be needed to understand more fully, in both qualitative and quantitative aspects, the full range of creep-fatigue effects.

Materials, Specimens, and Tests

To facilitate the observation of cracks, sheet specimens, 0.021 in. thick, were chosen for testing. The material was the aluminum alloy 5052-34, an alloy of relatively simple metallurgical structure, and which does not require excessively high temperatures to reach the creep range. This alloy is a non-age-hardenable type which contains $2\frac{1}{2}$ percent magnesium for solid-solution strengthening. The yield strength of this material at the test temperature of 400 F for exposure times in excess of $\frac{1}{2}$ h is approximately

[1] Formerly graduate assistant, Department of Metallurgy, University of Connecticut, Storrs, Conn. 06260; now with TRW, Cleveland, Ohio.

[2] Head, Department of Metallurgy, University of Connecticut, Storrs, Conn. 06260.

Copyright© 1973 by ASTM International www.astm.org

12 ksi [*1*].[3] To obtain an indication of the effect of stress level on the failure process in reasonably short test times, two peak stress levels were chosen, 10 and 15 ksi.

The specimens were 2 in. wide and 10 in. in length and contained a central slit to act as a stress raiser and crack localizer. To facilitate the initiation of crack growth at elevated temperatures, fatigue cracks (FC) were started at room temperature in one group of specimens. In testing these specimens, it appeared that the lifetime was quite sensitive to the initial crack length. In order to control the initial length more closely, electro-discharge machining (EDM) of the tips of the initial stress raisers was used with a second group of specimens. The tip radius of these notches was approximately 0.005 in.

Tests of three types were carried out. These were:

(*a*) Cyclic tests at 1800 cpm at $R = 0$ loading in an electro-hydraulic fatigue testing machine which automatically maintained the pre-set loading conditions. (R is defined as the ratio of minimum to maximum stress in a cycle.)

(*b*) Creep tests under constant load.

(*c*) Cyclic-creep tests between zero load and the maximum load of the cycle. Holdtimes in a given test were of constant duration, and were equal in the on-load and off-load conditions. Duration of the holdtimes ranged from 30 to 65 s. These tests were carried out in the same test machine as was used for the creep tests, with the load applied and removed automatically by a mechanism controlled by a timing device. At 10 ksi 6 s were required to load or unload; at 15 ksi 9 s were needed. The cyclic period was either 72 or 144 s.

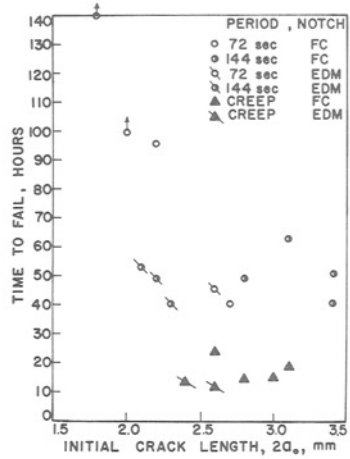
All testing was done in laboratory air with the specimens surrounded by a resistance furnace equipped with a window to permit observation of the cracks. Crack length measurements were made with the aid of a low power telescope. In addition crack opening displacement measurements were made by noting the distance between reference points on either side of the initial slit or cracks.

Results and Discussion

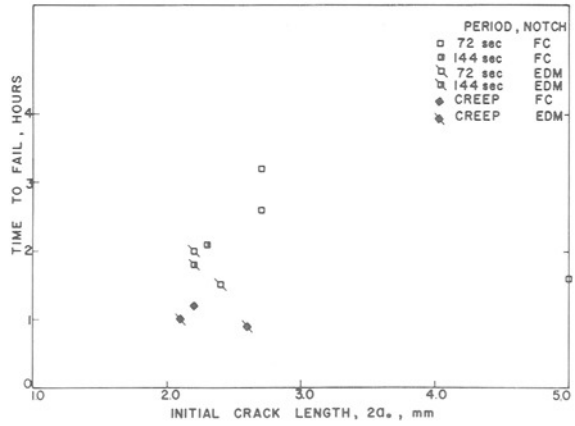
Figure 1 presents a summary of the results of the creep and cyclic-creep tests. From this figure an indication of the influence of a number of variables on the time to fail can be obtained. These variables include the stress-level, the type of starter notch, the initial crack length, and the cyclic period.

Figure 2 compares the crack growth characteristics at 10 ksi for the three types of tests. It is noted: (1) in the case of the creep and cyclic-creep tests, a major portion of the lifetime is spent in the initial advance of the crack

[3] The italic numbers in brackets refer to the list of references appended to this paper.



(*a*) 10 ksi peak gross stress.



(*b*) 15 ksi peak gross stress.

FIG. 1—*Time to failure as a function of initial crack length,* $2a_0$, *for creep and cyclic-creep tests at 400 F. FC's or EDM notches were used as stress raisers.*

through a distance of the order of the sheet thickness, and (2) in the case of the fatigue test no such delay was observed.

Since the specimens were all tested under positive mean load conditions, the specimens elongated during the 400 F tests. The extent of this elongation varied with stress level, Fig. 3, and also with type of test. The V-shape of the crack tip, Fig. 3, is typical of both the creep and cyclic-creep tests. Figure 4 summarizes the results of the crack-opening displacement (COD) measurements at a common crack-length $2a$ of 4 mm. The COD decreases with increase in intial crack length since less time for creep is available before the 4 mm length is reached. At 15 ksi the COD measurements did

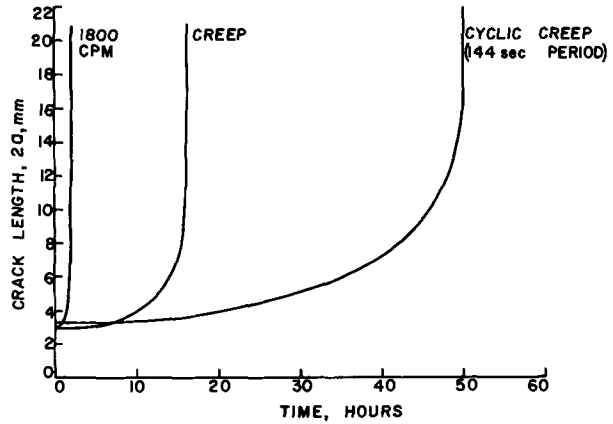


FIG. 2—*Crack length as a function of time at 400 F and a peak gross stress of 10 ksi. FC's were used as stress raisers.*

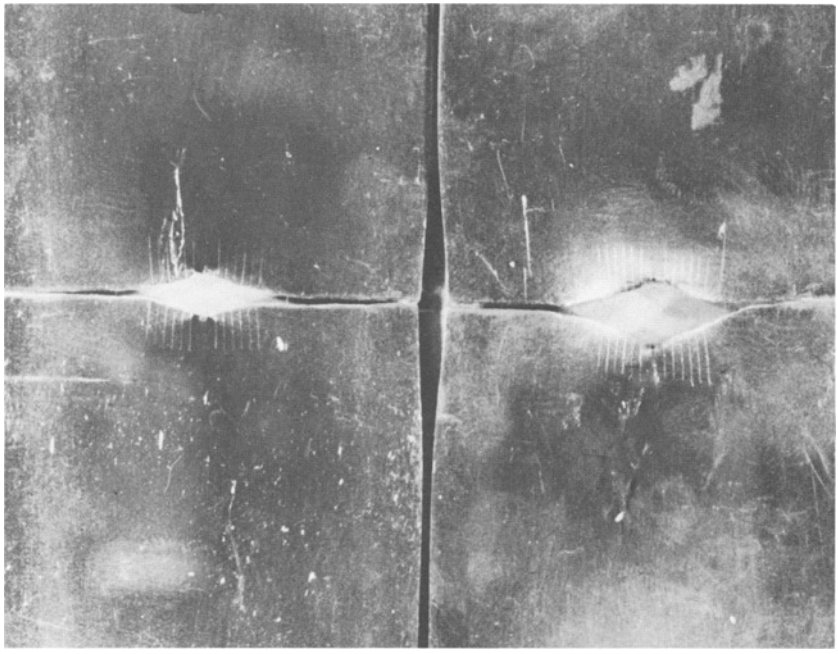
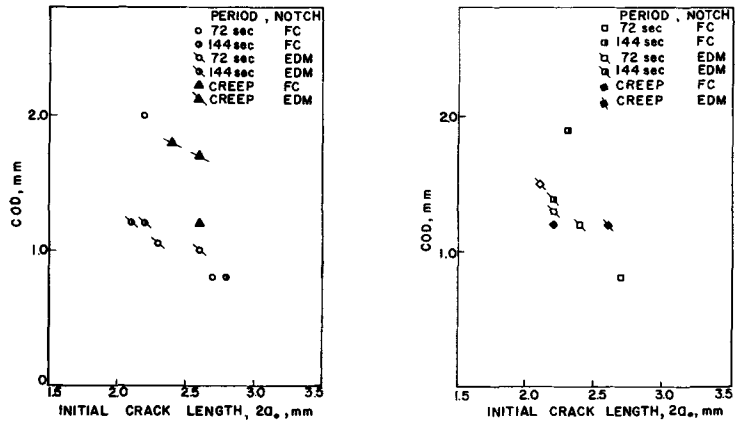


FIG. 3—*Appearance of specimens after creep testing at 400 F. Specimen on left tested at 15 ksi; specimen on right tested at 10 ksi.*



(*a*) 10 ksi. (*b*) 15 ksi.

FIG. 4—*COD measurements at 400 F and at a crack length,* 2a, *of 4mm. FC's or EDM notches were used as stress raisers.*

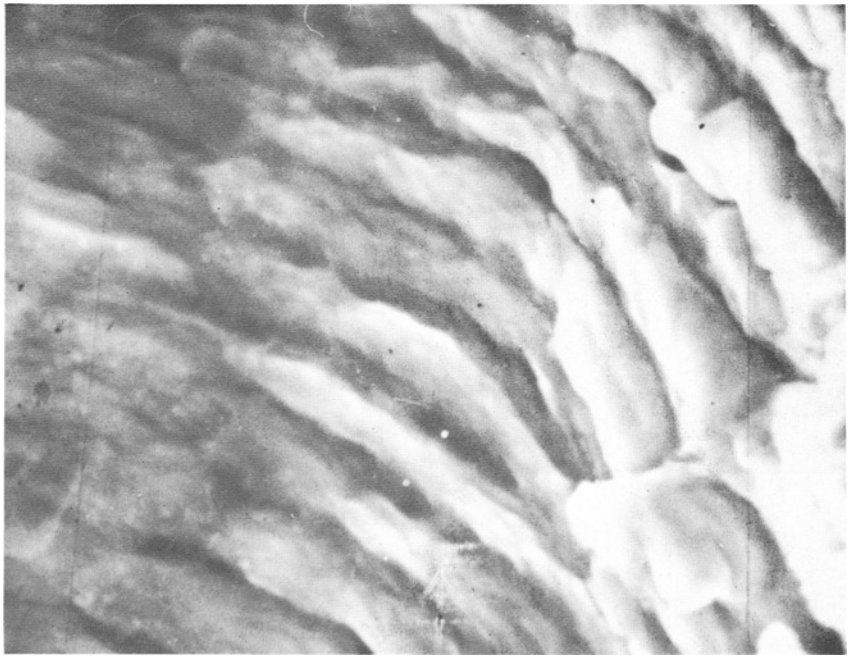


FIG. 5—*Scanning-electron-micrograph of striations on flat fracture surface. Specimen tested at 400 F at 1800 cpm. Peak gross stress 10 ksi,* R = 0 (×6000.)

not differ in comparing the creep and cyclic-creep tests. However at 10 ksi there appears to be a reduction in the COD tests in the cyclic tests. Such a reduction indicates that the creep-extensional process has been suppressed by load-unload cycling, which may account for the increased lifetime observed in the cyclic-creep tests. As the creep process is suppressed, the fatigue process of crack advance by plastic blunting [2] during the loading portion of the cycle must take on greater importance.

The appearance of the fracture surface of a specimen fatigue-cycled at 400 F is shown in Fig. 5. The striations are typical of fatigue, but in addition other parts of the fracture surface contained dimples, evidence of a rupture process of separation. During the 400 F tests the crack shifted from the flat to the slant mode of growth, as is usual with sheet specimens. However, whereas in general it is difficult to observe fatigue striations on the slant portion of the fracture surface, in the present tests they were quite evident, Fig. 6. The interval between markings corresponds to the macroscopic



FIG. 6—*SEM of striations and dimples on slant fracture surface. Specimen tested at 400 F at 1800 cpm. Peak gross stress 10 ksi,* R = 0 (×400.)

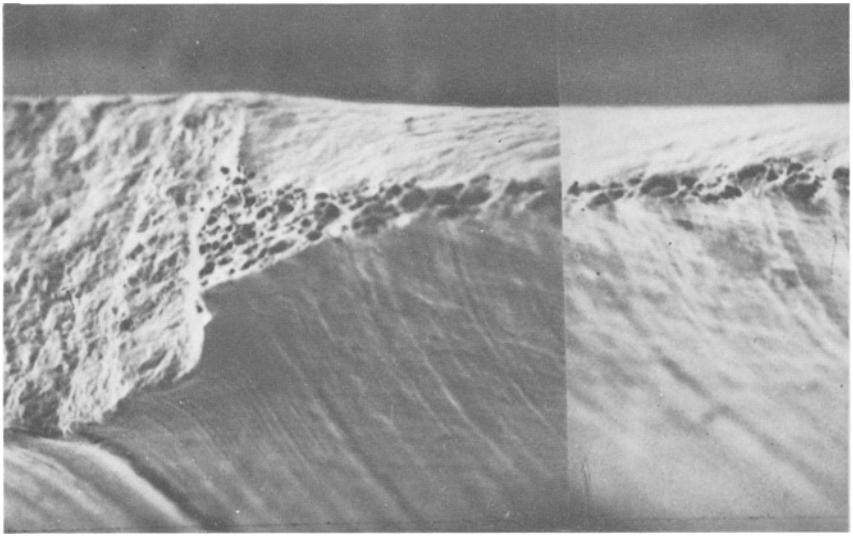


FIG. 7—*SEM of fracture appearance after creep failure at 400 F, 10 ksi gross stress* (×100).

crack growth rate. It is also seen that one portion of the crack growth lagged well behind the other.

The fracture appearance after creep failure, Fig. 7, differs considerably from the appearance after fatigue separation occurred by a process of void coalescence with the overall failure taking place in three stages. The first of these was a localized thinning and crack-tip opening process, a precursor to crack advance; a major portion of the lifetime was spent in this stage. The extent of the thinning at the initiating stress raiser was greater for the EDM notches, an indication that constraints to thinning were present even in this thin sheet material. A further indication is given in Fig. 8. The second stage of the failure process occurred as the crack advanced through the uniformly thinned region whose thickness was only 1/10 of the original value. Cracks advanced until the final stage of separation took place as a result of loss of cross-sectional area. It is noted that the fracture appearance differs from that previously observed in the case of the aluminum alloy 7075-T6 tested under similar conditions [*3*].

Fractographic features of the cyclic-creep specimens were similar to those of the creep specimens. No markings associated with load-unload effects were noted.

Conclusions

1. For the materials tested, at low frequencies in the creep range because of extreme thinning of the section ahead of a crack under a positive mean stress, straightforward application of fracture mechanics concepts to the

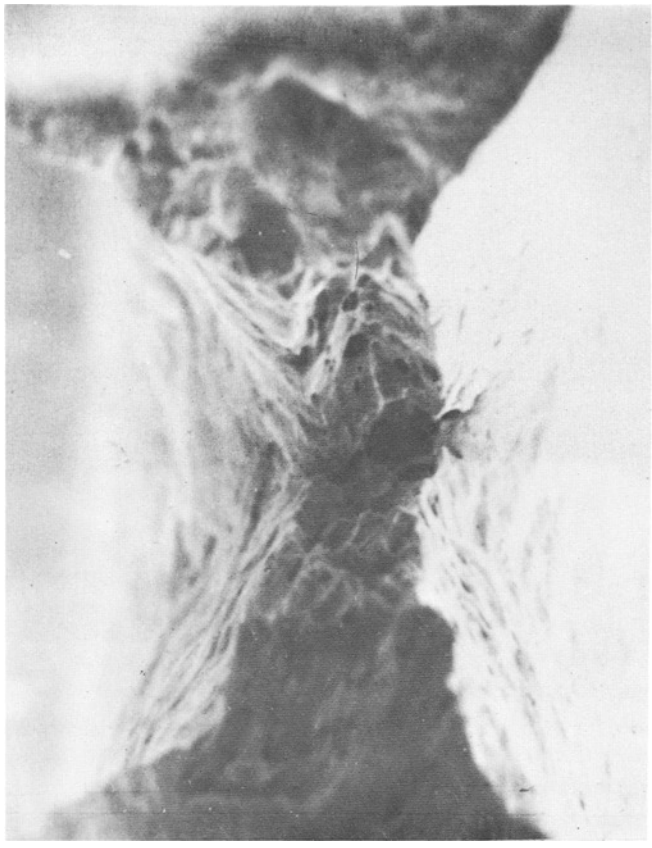


FIG. 8—*SEM view into tip of crack showing localized thinning at crack tip and open tunnel penetrating ahead of crack front* (×200).

study of crack growth behavior does not seem to be feasible. On the other hand, for materials which exhibit much less plastic deformation prior to failure, and for which the geometry does not change significantly, a correlation in terms of stress-intensity factors may be possible, as indicated by results of James[4] in tests of austenitic stainless steels.

2. Fatigue crack growth (1800 cpm) at elevated temperatures involves growth by the plastic blunting process, but may also involve additional separation processes.

3. The cyclic-creep rupture process occurs by void coalescence accelerated by the loss of section due to localized thinning.

4. Cyclic-creep lifetimes can exceed creep lifetimes, perhaps as a result of the reversal of the creep process at the crack tip during the off-load period of the test.

[4] James, L. A., Westinghouse Hanford Co., Richland, Wash., private communication.

References

[1] *Metallic Materials and Elements for Flight Vehicle Structures*, MIL-HDBK5, Department of Defense, Aug. 1962.
[2] Laird, C. in *Fatigue Crack Propogation, ASTM STP 415*, American Society for Testing and Materials, 1967, p. 131.
[3] McEvily, A. J. in *Fundamental Aspects of Stress Corrosion Cracking*, National Association of Corrosion Engineers, 1969, p. 72.

DISCUSSION

Carl Jaske[1] *(written discussion)*—Do you feel that the longer time for crack propagation under cyclic creep than under creep could be related to compressive residual stresses produced near the crack tip by the periodic unloading?

P. N. Atanmo and A. J. McEvily (authors' closure)—Yes.

[1] Batelle Memorial Institute, Columbus, Ohio 34201.

C. A. Rau, Jr.,[1] *A. E. Gemma*,[2] *and G. R. Leverant*[1]

Thermal-Mechanical Fatigue Crack Propagation in Nickel- and Cobalt-Base Superalloys Under Various Strain-Temperature Cycles

REFERENCE: Rau, C. A., Jr., Gemma, A. E., and Leverant, G. R., "**Thermal-Mechanical Fatigue Crack Propagation in Nickel- and Cobalt-Base Superalloys Under Various Strain-Temperature Cycles,**" *Fatigue at Elevated Temperatures, ASTM STP 520*, American Society for Testing and Materials, 1973, pp. 166-178.

ABSTRACT: Crack propagation rates under isothermal and thermal fatigue cycling have been determined for a conventionally-cast cobalt-base superalloy, and conventionally-cast and directionally-solidified nickel-base superalloys. Linear elastic fracture mechanics, where the crack growth rates under different strain ranges or for various crack lengths depend only on the strain intensity factor range, was found to be applicable over the range of crack growth rates of most practical importance. A comparison of crack growth rates is made for thermal fatigue under various strain-temperature cycles and isothermal low-cycle fatigue, and the influence of coatings and superimposed creep is discussed.

KEY WORDS: fatigue (materials), thermal fatigue, stresses, strains, coatings, crack propagation, cobalt containing alloys, nickel containing alloys, fracture properties, cycles

Linear elastic fracture mechanics has been used successfully to predict fatigue lifetime of various components based on laboratory measurements of fatigue crack propagation rate under appropriate conditions (temperature, strain rate, mean stress). These fracture mechanics analyses have been applied most often to low temperature, isothermal fatigue conditions, where the nominal strains are well within the elastic range. More recently, linear elastic fracture mechanics has been successfully extended to higher temperatures and strains where significant amounts of localized nonlinear deformation occur [*1–4*].[3] However, very little [*5*][4] crack propagation data

[1] Group leader, and senior research associate, respectively, Materials Engineering and Research Laboratory, Pratt & Whitney Aircraft, Middletown, Conn. 06457.

[2] Senior turbine structural engineer, Pratt & Whitney Aircraft, East Hartford, Conn. 06108.

[3] The italic numbers in brackets refer to the list of references appended to this paper.

[4] See p. 416.

Copyright© 1973 by ASTM International www.astm.org

have been obtained under thermal fatigue loading, and no systematic study of cycle parameters has been made.

Advanced airfoil designs employing complex cooling schemes and thin-walled sections have increased thermal-mechanical fatigue strains. Consequently, some locations are becoming thermal fatigue limited. These critical airfoil locations, such as the leading and trailing edges, may have widely different thermal fatigue cycles wherein the maximum tensile strains may occur at low, intermediate, or high temperatures. Because strain at one temperature is followed by reversed strain at another temperature, the mechanisms and rate of cumulative damage may vary with shape of the thermal fatigue cycle.

The purpose of the present work was to define the effects of the thermal fatigue cycle parameters on crack growth rate. This was accomplished by a series of tests where the minimum and maximum temperature, the strain range, the mean strain, the cycle shape, and the amount of creep-thermal fatigue interaction were varied systematically and the corresponding crack growth rate measured.

Experimental Procedure

The three materials investigated are each representative of a class of turbine materials. PWA 647 (MAR-M 509) is a conventionally cast, cobalt-base superalloy consisting of a solid solution (γ) matrix strengthened at higher temperatures by large MC-type carbides. PWA 1455 (B-1900 with Hafnium) is an advanced, conventionally cast, nickel-base superalloy composed of γ solid solution precipitation hardened by ordered γ' particles and containing both bulk and grain boundary carbides. PWA 1422 (MAR-M 200 with hafnium) is a directionally solidified nickel-base alloy which was tested in the $\langle 100 \rangle$ growth direction. Its microstructure is very similar to PWA 1455 except for the grain orientation and the absence of transverse grain boundaries. Table 1 summarizes some basic properties of the alloys.

Isothermal and thermal-mechanical fatigue testing was performed on $\frac{1}{2}$-in.-diameter tubular specimens with a uniform 1 in. gage length and wall thickness between 0.020 and 0.100 in. As discussed elsewhere [6], axial strain was measured and controlled with a linear variable differential transformer (LVDT) connected through quartz rods and alumina clamps to the specimen ridges. Two specimen designs were tested, one of which had external extensometry ridges and the other internal ridges. The temperature was measured and controlled either with an infrared temperature sensor or with two thermocouples welded directly on the gage length. Strain and temperature were controlled independently using a servohydraulic test machine and induction heating to produce the desired strain-temperature cycles. Typical cycling rates were 0.5 cpm, and compressed air was passed through the tube to achieve the required cooling rates.

TABLE 1—*Mechanical properties of the tested superalloys.*

	PWA 1455	PWA 1422	PWA 647
	Ni-Base B-1900 with Hf	Ni-Base Directionally-Solidified MAR-M 200 with Hf	Co-Base MAR-M 509
Grain size, (in.):			
Average	...	0.060	0.030
Maximum	0.250	...	0.050
Minimum	0.050	...	0.015
Elastic modulus, psi $\times$ *10*$^{-6}$			
Room temperature	31.0	18.5	32.5
800 F	28.0	16.7	28.5
1400 F	25.0	14.5	24.0
1800 F	22.5	11.5	21.0
0.2% offset yield stress, ksi:			
Room temperature	115.0	130.0	65.0
800 F	115.0	128.0	41.0
1400 F	114.0	126.0	33.0
1800 F	45.0	62.0	20.0
Yield strain, %:			
Room temperature	0.57	0.90	0.40
800 F	0.61	0.97	0.34
1400 F	0.66	1.07	0.34
1800 F	0.40	0.74	0.30

Cracks were started from either electrical discharge machined slots 0.050 by 0.005 in. or from 0.010 to 0.020-in.-diameter holes. Crack propagation was monitored continuously through a micrometer mounted telescope ($\times$30 to 100). On occasion, plastic surface replicas were taken during periodic cooling to room temperature and examined at magnifications up to $\times$1000. Any delay in crack growth due to cool down was small, and the data fell within the normal scatterband. Uncoated specimens were metallographically polished through 6-μm diamond paste. Some specimens were surface coated inside and out with a 0.003-in.-thick pack aluminide coating.

Results and Discussion

Various cycle parameters including: (1) maximum temperature, (2) minimum temperature, (3) nominal strain range, (4) mean strain, (5) cycle shape, and (6) superimposed creep have been varied to evaluate their effects on the rate of crack propagation in thermal fatigue. In each case, the measured total crack length ($2a$) was plotted as a function of number of cycles (N).

A fifth degree polynomial which is twice continuously differentiable [7] is computer fit through the data and used to obtain the crack growth rate (da/dn) as a function of the linear elastic strain intensity factor

$$\Delta K_\epsilon \equiv \Delta\epsilon\sqrt{\pi a}\, f\left(\frac{a^2}{Rt}\right) g\left(\frac{a}{D}\right) h\left(\frac{a}{R}\right) \quad \ldots\ldots\ldots\ldots (1)$$

where $\Delta\epsilon$ is the nominal strain range, a the half crack length,

$$f\left(\frac{a^2}{Rt}\right) \equiv 0.0574\,\frac{a}{\sqrt{Rt}} + 0.0455\,\frac{a^2}{Rt} - 0.00308\,\frac{a^3}{(Rt)^{3/2}} + 1$$

the curvature correction factor [8] for a crack in a cylinder of radius R and wall thickness t, $g(a/D)$ is the Bowie solution [9] for a hole of diameter D with two equal cracks and $h(a/R)$ is a geometric correction to convert projected length to arc length. Other authors [10,11] have reported slightly different analytical curvature corrections. The one used here is the theoretical solution which agrees best with the experimental measurements [12].

A total of 57 tests on PWA 1455, 12 tests on PWA 647, and 15 tests on PWA 1422 were performed. Extensive crack propagation data were obtained on about 50 specimens. For the range of strains investigated, the nominal inelastic strains were small compared to the elastic strain, and the linear elastic fracture mechanics equations provided a unique crack growth law independent of $\Delta\epsilon$. More specifically, Fig. 1 shows that crack growth rates between 10^{-6} and 10^{-4} in./cycle in PWA 1455 were identical at comparable ΔK_ϵ even though the nominal strain range varied between 0.0025 and 0.0040 in./in. For crack growth rates near and above 10^{-3} in./cycle, there are deviations from linear elastic fracture mechanics as indicated by more rapid growth for higher $\Delta\epsilon$ (see Fig. 1). Qualitatively, similar results were also obtained with PWA 647 and 1422 despite marked differences in metallurgical structure and constitutive behavior. For design purposes, one can use these data directly because most of the crack propagation lifetime is spent at low ΔK_ϵ. On the other hand, in the less important range of da/dn ($>10^{-3}$ in./cycle), the crack growth rate is a function of both $\Delta\epsilon$ and ΔK_ϵ because of the general cyclic plasticity.

Figure 2 compares the scatterbands obtained for crack propagation in the three alloys under similar thermal fatigue cycles. There are significant differences between the alloys. The most striking difference is the order of magnitude slower crack growth rate in the directionally solidified nickel-base superalloy (1422) at comparable ΔK_ϵ. The lower elastic modulus, Table 1, of 1422 compared to 1455 at roughly equivalent yield stresses is believed responsible. Specifically, the plastic zone at the crack tip is proportional to the Irwin-type plasticity correction, $\Delta K_\epsilon/\epsilon_y$, where ϵ_y, the yield strain, is approximately twice as large for 1422. The polycrystalline nickel (1455) and cobalt (647) base superalloys had similar crack growth rates at

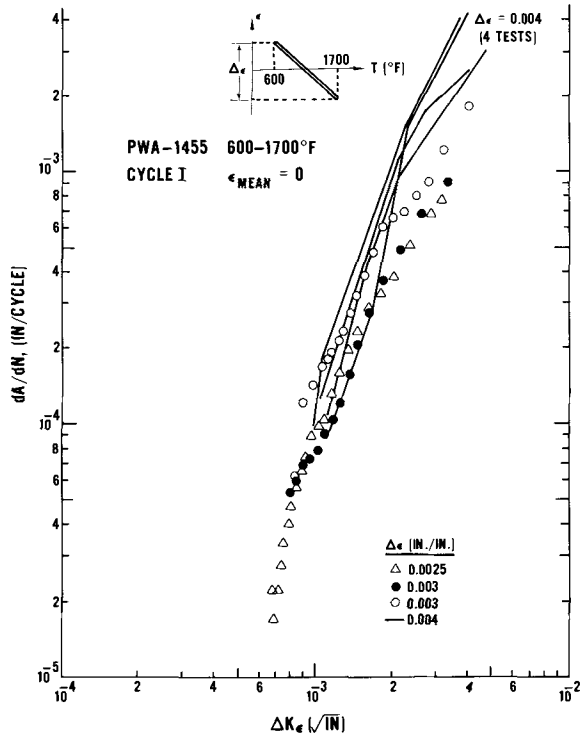


FIG. 1—*Cycle 1 thermal fatigue crack propagation rate as a function or range of strain intensity factor* (ΔK_ϵ) *for PWA 1455 cycled through a 600 to 1700 F temperature range and various nominal strain ranges* ($\Delta\epsilon$).

low ΔK_ϵ, but 647 showed a steeper slope and, therefore, more rapid propagation at higher ΔK_ϵ. The strong dependence of da/dn on ΔK_ϵ for 647 may be a result of the mode of crack propagation in this alloy. Cracking at all ΔK_ϵ occurs along a network of interconnected MC-carbides in the interdendritic zones. The two nickel-base alloys exhibit a smooth, transgranular fracture surface normal to the stress axis at low ΔK_ϵ and mixed shear and interdendritic fracture at high ΔK_ϵ. The interdendritic fracture in these alloys, however, does not occur along an almost continuous brittle path as in 647.

The shape of the thermal fatigue cycle can vary between the extremes illustrated in the insert of Fig. 3. The maximum tensile strain may be introduced at any temperature within the cycle. In the majority of testing, the maximum tensile strain was produced at the minimum temperature (called Cycle I). Figure 3 shows that Cycle I produced more rapid crack growth rates than an otherwise identical cycle where the tensile strain peaked at the maximum temperature (Cycle II). A similar but a smaller effect was observed in PWA 1422. Several tests were also performed with cycles where

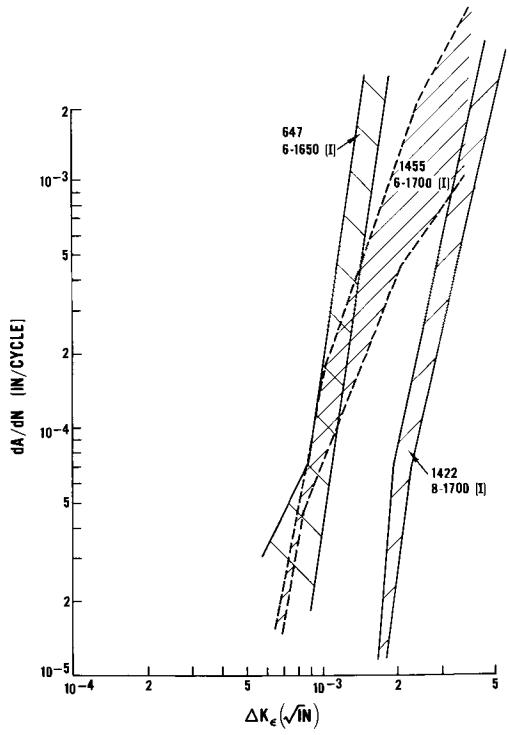


FIG. 2—*Comparison of the Cycle I thermal fatigue crack propagation rates in PWA 647, 1455, and 1422 as a function of strain intensity factor range.*

both the tensile and compressive strain peaked near the midrange of the temperature extremes. These preliminary results indicate intermediate crack growth rates for this cycle.

The minimum cycle temperature was varied from 600 to 800 F, but no significant difference in da/dn was noted. The maximum temperature was varied between 1650 and 1900 F, and the average crack growth rates in Cycle I increased slightly with increasing maximum temperature. However, the scatterbands for the various maximum temperatures still overlapped. The trend toward increasing crack growth rate with maximum temperature may result from two factors. First, for a given strain range, the plasticity at the crack tip increases with increasing temperature as ϵ_y decreases. Secondly, resharpening of the crack tip can be more effective at higher temperature.

The mean nominal strain was varied from compressive to tensile. Figure 4 shows the results for 647 under three identical cycles with the exception of the mean strain. No difference between crack growth rates at comparable ΔK_ϵ was observed, Fig. 4*a*, despite small differences in the stabilized mean stress. Crack growth rate was also insensitive to mean strain in 1455 where all results fell randomly within the scatterband indicated in Fig. 2. The 1455

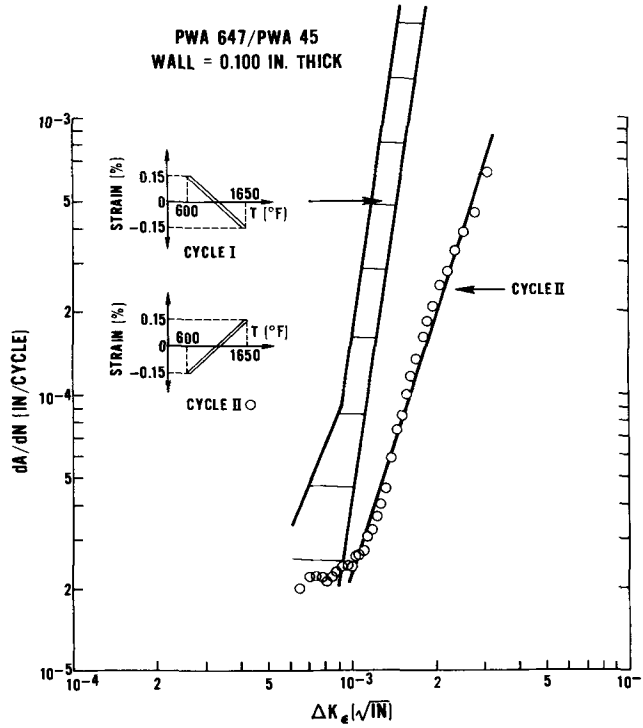


FIG. 3—*Comparison of the thermal fatigue crack propagation rates in Cycle I and Cycle II for PWA 647 cycled between 600 and 1650 F and +0.15 and −0.15 percent strain.*

results are even more significant because the stabilized maximum (σ_{max}) and minimum (σ_{min}) stress varied markedly with mean strain as shown in Fig. 4*b*. This indicates that the critical parameter for correlating crack growth data is the strain intensity factor range, ΔK_ϵ, as suggested previously [*13–15*]. The reason that the mean stress was virtually independent of mean strain for 647 is that relatively low yield strain at both the minimum and maximum temperatures allowed the stress to "shake down" to a symmetrical cycle in each case. In contrast, 1455 has a much higher yield strain at the minimum temperature which prevents yielding at the minimum temperature and precludes a "shakedown" in stress.

In order to evaluate differences between isothermal and thermal fatigue, isothermal low-cycle fatigue (LCF) crack propagation tests were performed at various temperatures within the thermal fatigue temperature extremes. Figure 5 summarizes the isothermal results for PWA 1455. The crack growth rates are insensitive to temperature between 800 and 1400 F. At higher temperatures, more rapid crack propagation is observed. The thermal fatigue crack growth rates in Cycle I (Fig. 1) are more rapid than under isothermal LCF at the lower temperatures where the fracture mode

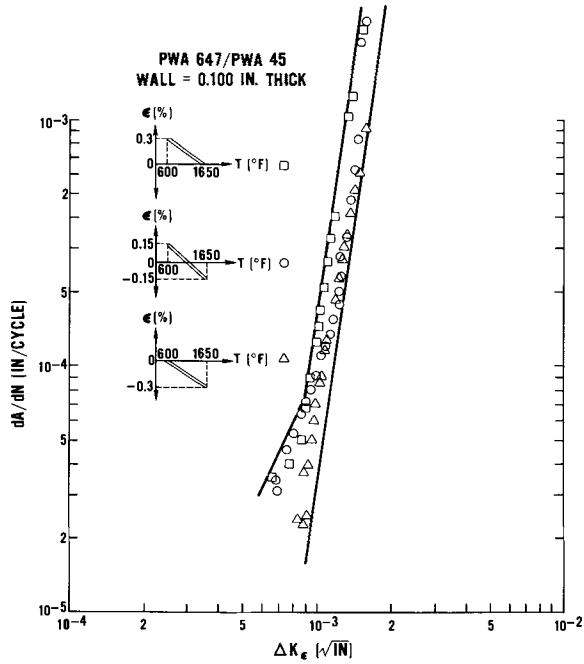


FIG. 4a—*The effect of mean strain on the Cycle I thermal fatigue crack propagation rate in PWA 647.*

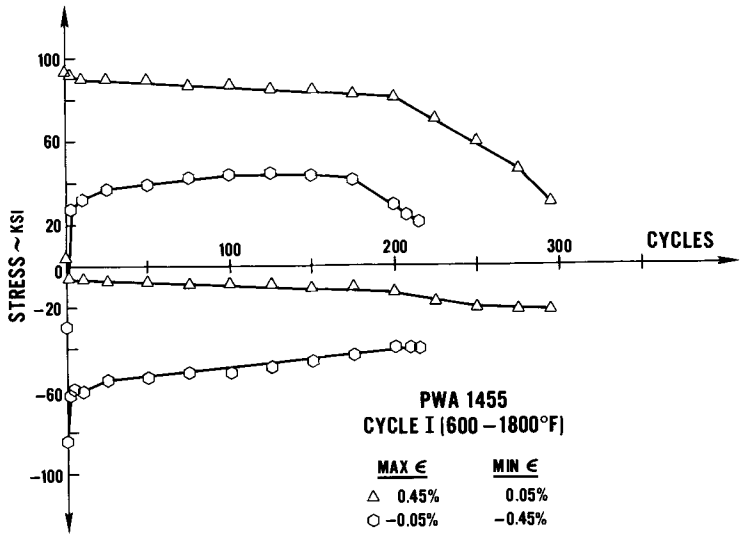


FIG. 4b—*The effect of mean strain on the maximum and minimum stress in PWA 1455 cycled between 600 and 1800 F in Cycle 1 thermal fatigue.*

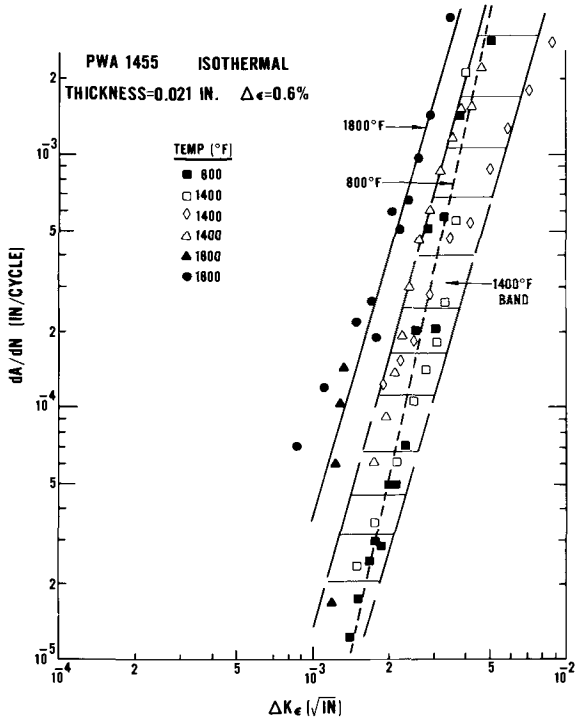


FIG. 5—*Comparison of crack propagation rates in isothermal, low-cycle fatigue at 800, 1400, and 1800 F in PWA 1455.*

is the same. The greater crack growth rate in Cycle I compared to low temperature LCF may be caused by more cyclic plasticity and more effective crack resharpening in the high temperature compressive half cycle. Because the mode of fracture is mixed intergranular and transgranular under the high temperature, isothermal LCF, but completely transgranular in Cycle I thermal fatigue, no general significance is attributed to the similarity in *da/dn*.

PWA 1455 tubes of various wall thicknesses between 0.021 in. $\leq t \leq$ 0.100 in. were investigated. In each case, material was cast to the same shape and size, and the different thicknesses were produced by machining from both the outside and inside diameter. In the uncoated condition, average crack propagation rate was unaffected by thickness, although the amount of scatter increased with decreasing thickness. The absence of a thickness effect suggests similar fracture modes at all thicknesses and mixed normal, and shear modes were confirmed by fractographic examination in each thickness. In most cases, either one or two grains were present across the wall in a given location, so the absence of the constraint of surrounding grains promoted plane stress conditions in every case.

The effect of 0.003-in.-thick aluminide surface coating on the outside wall and inside wall was also investigated. As shown in Fig. 6, no effect on crack propagation was noted for thicknesses greater than 0.024 in. In $t \approx 0.024$-in.-thick material tested isothermally or in thermal fatigue where the tensile strain peaks at low temperature ($T \leq 1400$ F), da/dn is accelerated (factor of 5 to 10) because the crack front in the relatively brittle coating leads the substrate crack and increases ΔK_ϵ. For thick-walled tubes, the coating area is so small compared to the substrate area that ΔK_ϵ and da/dn in the substrate is unaffected. When the tensile strain peaks at high temperature, for example, 1600 to 1800 F, crack initiation in the coating is so difficult that coating cracks seldom, if ever, lead the substrate crack, and no effect of the coating on da/dn is observed in any thickness. The difficulty of initiating coating cracks at these temperatures has also been dramatically demonstrated in smooth section testing of coated specimens where crack initiation occurs at subsurface locations in the substrate.

The effects of combined creep and thermal fatigue on the rate of crack propagation was investigated by periodically (every 5 to 10 cycles) incre-

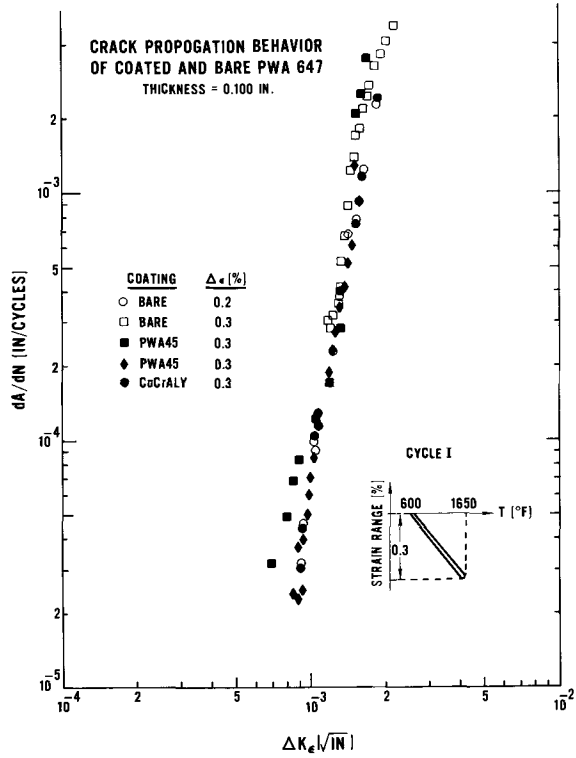


FIG. 6—*Comparison of the thermal fatigue crack propagation rates for 0.100-in.-thick coated tubes with uncoated tubes.*

menting the mean strain at maximum temperature. In this way the specimen simulates cumulative damage in airfoil leading (or trailing) edges where the creep deformation is controlled by creep of the bulk of the airfoil and is not directly related to the temperature and stress at the leading edge. In general, the rate of creep was chosen so that the total creep over the life of the specimen would be 1 to 2 percent, which is the maximum allowable in most airfoil designs. In PWA 647, creep extension of 0.0035 percent per cycle, superimposed on Cycle I thermal fatigue (600 to 1650 F), significantly increased the crack growth rate, Fig. 7. Furthermore, the superimposed creep modified the mode of cracking from a single crack to numerous parallel cracks which interacted with the primary crack. As shown in Fig. 7, a smaller creep rate of 0.00175 percent per cycle had little effect on da/dn even though numerous secondary coating cracks were produced, Fig. 8. The influence of superimposed creep is likely to be larger than shown in Fig. 7 because ΔK_ϵ was calculated assuming no shielding of the primary crack by secondary cracks. If shielding were incorporated in ΔK_ϵ, the curves for $\bar{\epsilon}_m = 0.00175$ and 0.0035 percent per cycle would be shifted to the left in Fig. 7.

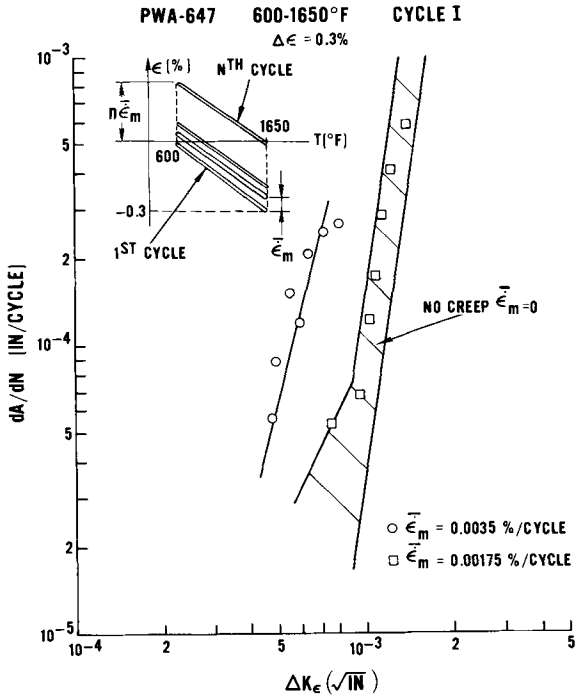


FIG. 7—*The effect of creep extension rate ($\bar{\epsilon}_m$) on the thermal fatigue crack growth rate of PWA 647 in Cycle I between 600 and 1650 F.*

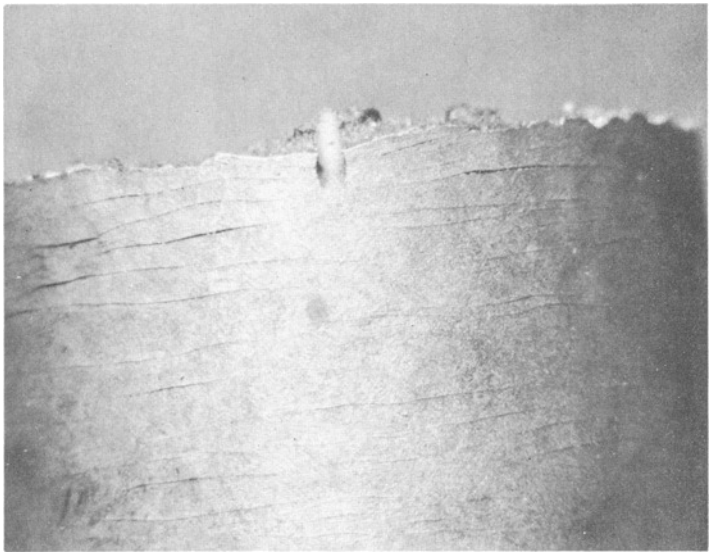


FIG. 8—*Multiple coating cracking in PWA 647 specimen in which the mean strain was increased 0.00175 percent per cycle.*

Conclusions

1. Linear elastic fracture mechanics can be applied to thermal fatigue crack propagation of nickel- and cobalt-base superalloys under conditions of small plastic strains.

2. For crack growth rates less than 10^{-4} in./cycle, the growth rate depends only on ΔK_ϵ and is independent of strain range, mean strain, and mean stress (for the range of mean strains and strain ranges investigated).

3. In PWA 647, superimposing an increasing mean strain (blade creep) on thermal fatigue cycling can markedly accelerate the crack growth rate and lead to multiple secondary cracking.

4. Cycle I thermal fatigue crack propagation rates are more rapid than low temperature isothermal LCF crack growth rates where the fracture mode is the same and slightly more rapid than Cycle II thermal fatigue.

5. Cycle I crack growth rates increased slightly with increasing maximum temperature.

6. Directionally solidified nickel-base superalloy (PWA 1422) has a markedly slower crack growth rate than a conventionally cast nickel-base superalloy (PWA 1455) of similar microstructure.

7. Coatings have no effect on growth rates of through-the-thickness cracks with one exception. Thin-walled specimens tested with the peak tensile strain in the temperature range where the coating is relatively brittle show an accelerated crack growth rate.

References

[1] James, L. A. and Schwenk, E. B., Jr., *Metallurgical Transactions*, Vol. 2, 1971, pp. 491–496.

[2] Hudson, C. M., "Fatigue Crack Propagation in Several Titanium Alloys and Stainless Steel Alloys and One Superalloy," NASA Report TN D-2331, National Aeronautics and Space Administration, 1961.

[3] Popp, H. G. and Coles, A. in *Proceedings*, Air Force Conference on Fatigue and Fracture of Aircraft Structures and Materials, AFFDL 70-144, H. A. Wood, R. M. Bader, W. J. Trapp, R. F. Hoener, and R. C. Donat, eds., Air Force Flight Dynamics Laboratory, Sept. 1970, pp. 71–86.

[4] James, L. A., "The Effect of Frequency Upon the Fatigue-Crack Growth of Type 304 Stainless Steel at 1000 F," presented at the Fifth Materials Symposium on Fracture Mechanics, Urbana, Ill., Aug. 1971.

[5] Howes, M. A. H., "Thermal Fatigue Data on 15 Nickel- and Cobalt-Base Alloys," IITRI Report B6078–38, 1970.

[6] Wells, C. H. in *Manual on Low-Cycle Fatigue Testing*, *ASTM STP 465*, American Society for Testing and Materials, 1969, pp. 87-99.

[7] Ahlberg, J. H., Nilson, E. N., and Walsh, J. L., *The Theory of Splines and Their Applications*, Academic Press, New York, 1967.

[8] Erodgan, F. and Ratwani, M., *International Journal of Fracture Mechanics*, Vol. 6, 1970, pp. 379–392.

[9] Paris, P. C. and Sih, G. in *Fracture Toughness Testing and Its Applications*, *ASTM STP 381*, American Society for Testing and Materials, 1964, pp. 30–83.

[10] Folias, E. S., *International Journal of Fracture Mechanics*, Vol. 3, No. 1, March 1967.

[11] Murthy, M. V. V. and Bapu Rao, Mon, ASME E, American Society of Mechanical Engineers, June 1970, p. 539.

[12] Adams, N. J. I., Ph.D thesis, University of Southampton, England, 1969, presented at 1970 Annual Meeting of ASTM, Toronto, Canada.

[13] Pearson, S., *Nature*, Vol. 211, 1966, p. 1077.

[14] Paris, P. C., Fifth National Symposium on Fracture Mechanics, Urbana, Ill., Aug. 1971.

[15] McEvily, A. J. in *Proceedings*, Air Force Conference on Fatigue and Fracture of Aircraft Structures and Materials, AFFDL 70-144, H. A. Wood, R. M. Bader, W. J. Trapp, R. F. Hoener, and R. C. Donat, eds., Air Force Flight Dynamics Laboratory, Sept. 1970, pp. 451–459.

L. P. Pook[1] *and A. A. Beveridge*[1]

Threshold for Fatigue Crack Growth in Ferritic Steels at 300 C

REFERENCE: Pook, L. P. and Beveridge, A. A., **"Threshold for Fatigue Crack Growth in Ferritic Steels at 300 C,"** *Fatigue at Elevated Temperatures, ASTM STP 520*, American Society for Testing and Materials, 1973, pp. 179–191.

ABSTRACT: Edge-cracked test specimens of two ferritic steels were subjected to the loading cycle $\sigma_m \pm \sigma_a$ at 300 C. The results showed that whether a crack grows or remains dormant can be predicted from the value of ΔK, the range of stress intensity factor during the fatigue cycle. The threshold value ΔK_c necessary for crack growth was slightly greater than that of similar steels at room temperature and depended on the ratio σ_m/σ_a. Crack growth data at low rates of crack growth were deduced from an integrated version of the crack growth equation $da/dN = B(\Delta K)^m$, where B and m are material constants. Crack growth rates at 300 C were similar to those at room temperature. The minimum possible rate of fatigue crack growth appeared to be somewhat greater than one lattice spacing/cycle. The methods used have the advantage that no crack growth monitoring instrumentation is required.

KEY WORDS: fatigue (materials), heat, stress cycling, fatigue tests, structural steels, crack propagation, crack initiation

Nomenclature

a	Crack length
a_f	Final crack length
a_0	Initial crack length
B	A constant
K_I	Opening mode stress intensity factor
ΔK	Range of K_I during fatigue cycle
ΔK_c	Critical value of ΔK necessary for fatigue crack growth
N	Number of cycles
m	A constant
r_p	Plastic zone radius
S	Stress

[1] Principal scientific officer and higher scientific officer, respectively, Strength of Components and Fatigue Division, Department of Trade and Industry, National Engineering Laboratory, East Kilbride, Glasgow, Scotland.

Copyright© 1973 by ASTM International www.astm.org

σ Gross stress
σ_a Alternating stress
σ_m Mean stress
σ_Y Yield stress (taken as the 0.2 percent proof stress)

Developments in fracture mechanics over the past few years have provided particularly convenient means for the analysis of fatigue crack growth data. The stress intensity factor K_I defines the elastic stress field around a crack tip. Numerous fatigue crack growth tests have been carried out on wide, thin metallic panels containing a small transverse central slit to initiate crack growth, and subjected to the general tensile stress cycle $\sigma_m \pm \sigma_a$, where $\sigma_m > \sigma_a$. Such data can be fitted [*1,2*][2] by an expression of the form

$$da/dN = B(\Delta K)^m \quad \ldots\ldots (1)$$

where

B = material constant,
ΔK = range of stress intensity factor during a fatigue cycle, and
m = exponent having a value which usually lies between 2 and 5.

Equation 1 implies that any value of ΔK, no matter how low, will result in a positive value of da/dN. However, it has been found experimentally [*2–4*] that a threshold value of ΔK, ΔK_c must be exceeded before a crack will grow. In general, the value of ΔK_c depends upon σ_m/σ_a.

Data obtained for a wide range of metallic materials [*5–11*] have been recently reanalyzed [*2*] in terms of stress intensity factors and extended [*12*]; these data were obtained from tests on 53-mm (2.1-in.)-wide plates about 6 mm (0.25 in.) thick containing edge cracks between 0.3 and 7.5 mm (0.01 and 0.3 in.) long, for both zero mean load and the general tensile stress loading cycle $\sigma_m \pm \sigma_a$, where $\sigma_m > \sigma_a$. In these tests, small cracks were grown at edge notches in plate testpieces and the material containing the edge notches then machined off. After stress relief at an appropriate temperature, the cracked plates were tested at various stress levels. Because cracks were small compared to the plate width, the value of ΔK in the reanalysis was calculated using the expression [*13*] for an edge crack in a semi-infinite plate, namely,

$$K_I = 1.1\sigma(\pi a)^{1/2} \quad \ldots\ldots (2)$$

The net section stresses involved were always well below general yield, and the plastic zones were very small compared to the crack length, so no corrections were made. Values of ΔK were plotted against endurance; for a given material and σ_m/σ_a value the resulting curve was of similar shape to a

[2] The italic number in brackets refer to the list of references appended to this paper.

conventional S/N curve, ΔK_c being the value of ΔK at which the curve becomes asymptotic to the abscissa. Therefore, ΔK_c is analogous to the conventional fatigue limit.

The results obtained are summarized in Fig. 1. For the case of zero mean load, ΔK was calculated using the tensile half of the load cycle, and the uncertainty in the determination of ΔK_c was up to ± 20 percent, but for the case of $\sigma_m/\sigma_a \geq 1$ this dropped to about ± 10 percent.

At zero mean load, a crack may be effectively propped open by the plastic zone at its tip, so that part of the compressive half of the loading cycle is required to close the crack, thus increasing ΔK above that given by taking the tensile part of the load cycle. This effect is marked particularly when determining ΔK_c, both for short crack lengths and with soft materials [2]. On the other hand, a propagating crack may close before zero load is reached [*14*], thus reducing ΔK. The consequent uncertainty in the calculation of ΔK tends to increase the scatter of experimental data at zero mean load, making interpretation of results uncertain.

The values of ΔK_c given in Fig. 1 were all obtained at room temperature; however, ferritic steels are often used at moderately elevated temperatures. Therefore, specimens of mild steel and a low-alloy Ni-Cr-Mo-V steel (Ducol W30) were tested at 300 C to determine the ΔK_c values.

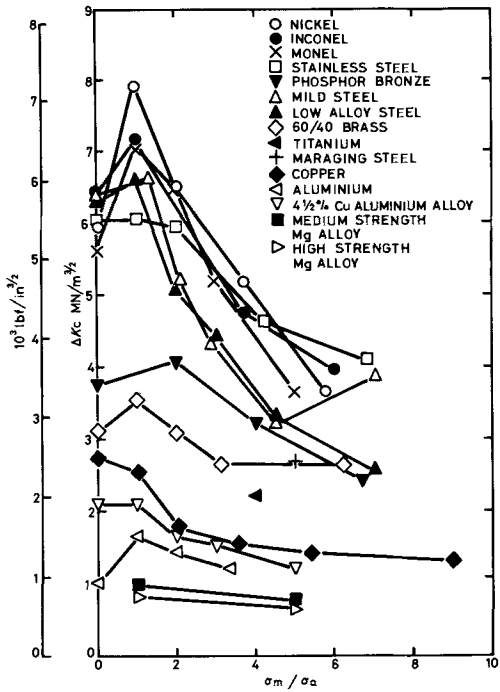


FIG. 1—ΔK_c *values for various materials.*

Test Method and Results

The steels tested have been used previously for collaborative fracture toughness tests [*15*]: their composition and mechanical properties are shown in Table 1; all specimens were cut in the longitudinal direction (Fig. 2).

TABLE 1—*Mechanical properties at 300 C.*

Material and Condition	Tensile Strength, MN/m^2	0.2% Proof Stress, MN/m^2	Elongation on $5.65\sqrt{A}$, %	Reduction in Area, %
Mild steel:				
C–0.17%, Mn–0.83% As rolled	480	160	21	55
Low- alloy steel:				
C–0.16%, Mn–1.35% Ni–0.22%, Cr–0.67% Mo–0.26%, V–0.09% Normalized 900 C Tempered 620 C	560	360	32	66

The edge-cracked specimen used to determine ΔK_c is a smaller version of that used previously [*5–12*]. It was designed to suit the furnace and the 15 kN direct stress electromagnetic fatigue machine used for these tests. The overall length of the specimen was kept short to avoid buckling in compression.

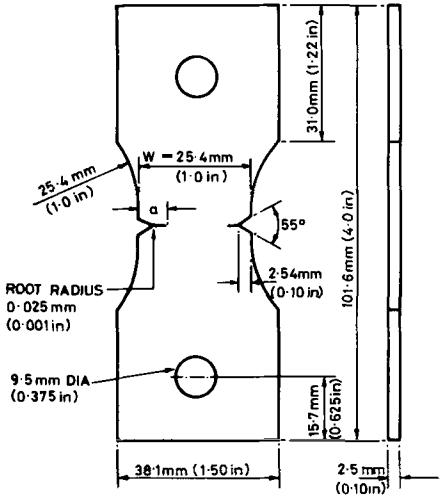


FIG. 2—*Specimen dimensions.*

The stress intensity factor is given by [*16*]

$$K_I = \sigma(\pi a)^{1/2}\alpha \quad \ldots\ldots\ldots\ldots\ldots\ldots\ldots\ldots (3)$$

where

$$\pi a = 1.98 + 0.36\left(\frac{2a}{W}\right) - 2.12\left(\frac{2a}{W}\right)^2 + 3.42\left(\frac{2a}{W}\right)^3$$

a is crack length, W is specimen width, and $2a/W \leq 0.7$. Provided that $2a/W \leq 0.4$, this does not differ greatly from Eq 2, which indicates that up to this limit there is little interaction between the two cracks.

The test technique was similar to that used previously except that the specimens were not reprofiled after initial cracking. The specimens were fitted, by means of clamps, into the fatigue machine, which operated at 33 Hz, and were subjected at room temperature to a stress cycle of 0 ± 108 MN/m^2 (0 ± 7 ton/in.^{2}), sufficient to initiate and grow cracks from the notch roots. The surface lengths of cracks were measured periodically, a test being stopped when these reached the required length. On some of the tests the machine was stopped automatically by means of foil-type continuity gages mounted adjacent to the notches. The circuit was arranged to stop the machine when a strand of foil at the required distance from the root of a notch was broken by the advancing fatigue crack. This procedure considerably simplified the precracking.

In general, the two overall crack lengths (notch plus crack) were seldom the same; crack growth took place from the longer initial crack; consequently, this was used in calculations. To avoid interaction effects the overall length of the longer crack was restricted to a maximum length of 5.1 mm (0.2 in.), corresponding to $2a/W = 0.4$, and to avoid interference from the initial notch to a minimum length of 2.6 mm (0.14 in.). The specimens were then stress relieved *in vacuo* for 1 h before fatigue testing in order to minimize any residual stresses induced in the material around the crack tip during the initial cracking. The temperatures used were 650 C for the mild steel and 570 C for the low-alloy steel.

These cracked specimens were enclosed in a furnace for testing at 300 C in air and maintained at this temperature for 16 h before a test was started. Temperature control was within ± 3 C. Tests were carried out at various stress levels with σ_m/σ_a of 0, 2, or 4.5 for mild steel, and 0 or 2 for the low-alloy steel, and were continued until a specimen failed. Testing was continued to at least 10^7 cycles before a specimen was regarded as unbroken (indicated by arrows on the figures).

Despite oxidation which had taken place the initial crack length could be determined by examination of the fracture faces of the specimens. Values of ΔK were calculated using Eq 3. The results obtained are shown in Figs. 3–5. For a given σ_m/σ_a ratio there is no significant difference between the two steels, the results fall around a curve, similar to an ordinary S/N curve,

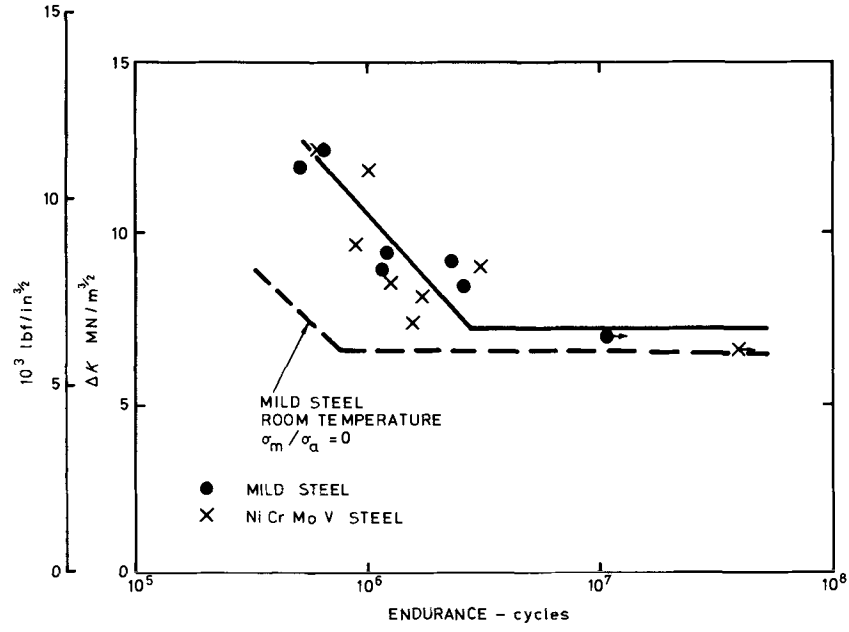


FIG. 3—ΔK *against endurance* $\sigma_m/\sigma_a = 0$.

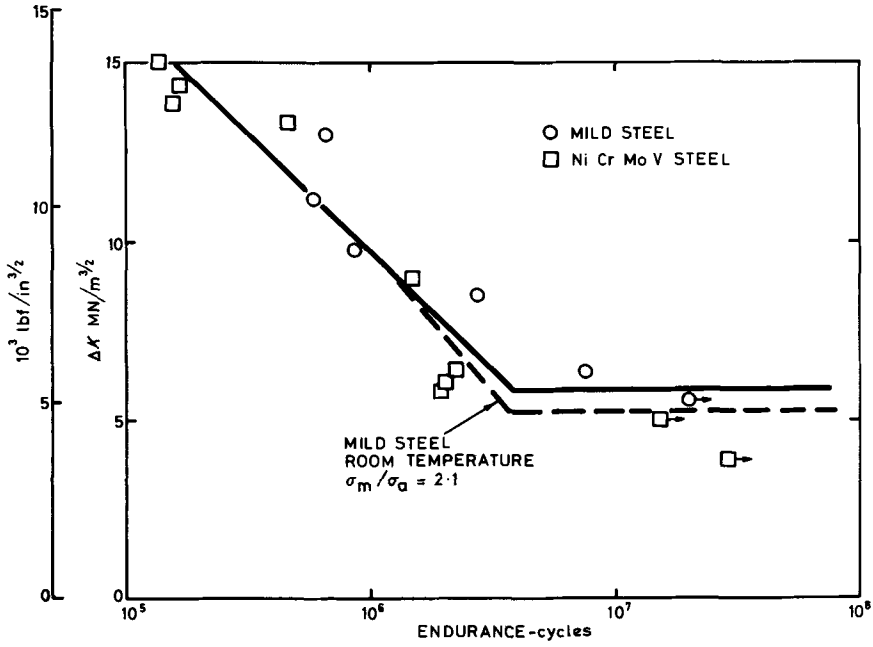


FIG. 4—ΔK *against endurance* $\sigma_m/\sigma_a = 2$.

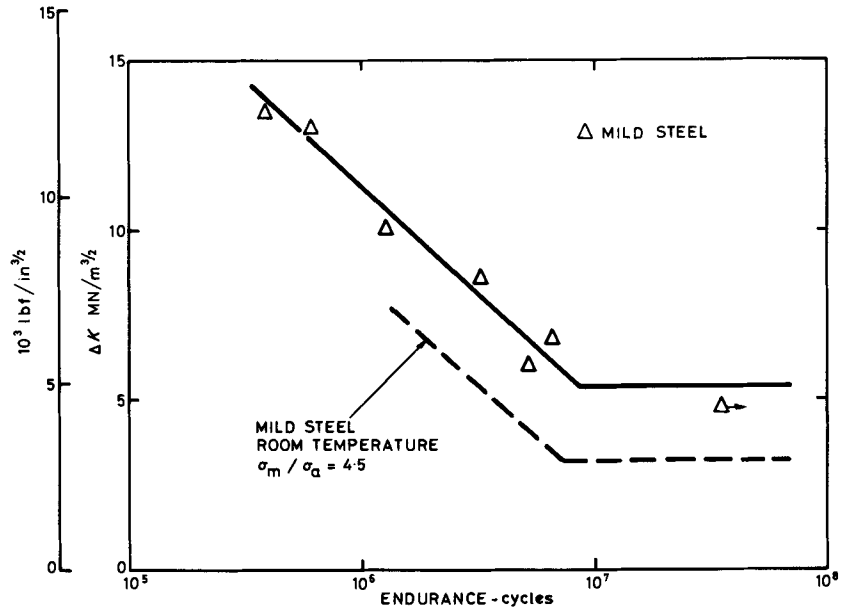


FIG. 5—ΔK *against endurance* σ_m/σ_a = 4.5.

and show a clearly defined fatigue limit. The S/N curves for mild steel at room temperature [*2,5,10*] are included for comparison. The finite life portions are not strictly comparable as different specimens were used. Values of ΔK_c were estimated from this limit and are 7.1 MN/m$^{3/2}$ (6.5 × 10^3 lb/in.$^{3/2}$) for σ_m/σ_a = 0, 5.8 MN/m$^{3/2}$ (5.3 × 10^3 lb/in.$^{3/2}$) for σ_m/σ_a = 2 and 5.4 MN/m$^{3/2}$ (4.9 × 10^3 lb/in.$^{3/2}$) for σ_m/σ_a = 4.5 (mild steel only). They are compared in Fig. 6 with room-temperature data [*2*] for mild steel and a low-alloy steel (tensile strength 680 MN/m^2 (44 ton/in.^{2})). Also shown are room-temperature (RT) data for various steels obtained by a somewhat similar technique using center-crack specimens [*3*].

A plastic zone develops at the tip of a crack in a ductile metal, its approximate radius r_p being given by the expression [*17*]

$$r_p = \frac{1}{2\pi}\left(\frac{K_I}{\sigma_Y}\right)^2 \quad \ldots\ldots\ldots\ldots\ldots\ldots\ldots\ldots (4)$$

for plane stress and one third of this amount for plane strain, where σ_Y is the yield stress (taken as the 0.2 percent proof stress). Provided that r_p is small compared with a, and that the maximum net section stress does not exceed $0.8\sigma_Y$, the plastic zone has little effect on the overall elastic stress field, and the stress intensity factor provides a reasonable description of the crack-tip stress field. If required, a correction for the effect of the plastic zone can be made by adding r_p to a when calculating K_I. A similar correc-

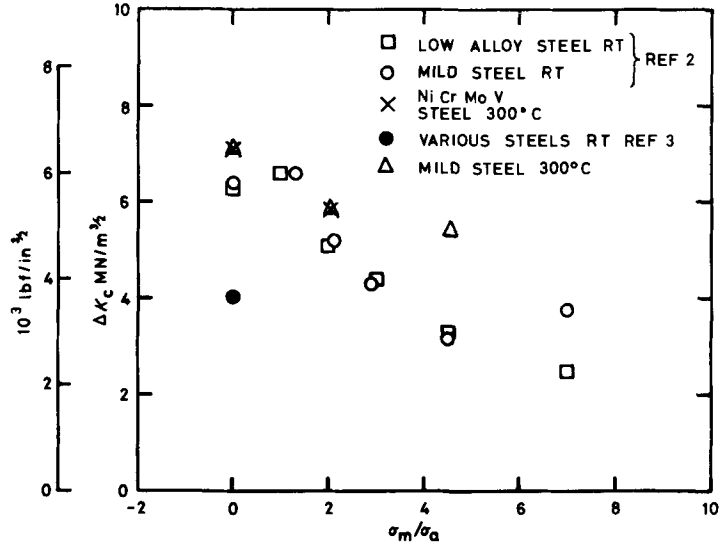


FIG. 6—ΔK_c *against* σ_m/σ_a.

tion can be made [*18*] to ΔK using Eq 4, but with K_1 replaced by ΔK and σ_Y by $2\sigma_Y$. Assuming a state of plane strain exists at the relatively low ΔK values employed, this correction would not exceed 1½ percent for the present tests.

The net section stress is less than $0.8\sigma_Y$ for all the tests except the three highest stress levels for mild steel with $\sigma_m/\sigma_a = 2$, and the mild steel results for $\sigma_m/\sigma_a = 4.5$, for which the net section stress corresponding to the fatigue limit on Fig. 5 is approximately $1.1\,\sigma_Y$. However, even when there is general yielding on the net section, unloading deformation will be essentially elastic provided that σ_a is small [*18*], so that the use of ΔK in the analysis of these results is justified.

It has been shown [*19*] that, if the life of a broken edge-cracked plate specimen is assumed to have been occupied entirely by crack growth, the initial rate of crack growth can be obtained by combining Eq 2 and the integrated form of Eq 1, giving

$$\frac{da}{dN} = \frac{a_0 - a_f(a_0/a_f)^{m/2}}{N[(m/2) - 1]} \quad \ldots\ldots\ldots\ldots\ldots\ldots\ldots\ldots (5)$$

[when $m = 2$, $da/dN = (a_0/N) \ln (a_f/a_0)$],

where

a_0 = initial crack length,
a_f = final crack length at end of test, and
N = number of stress cycles the crack takes in growing from a_0 to a_f.

Because a crack would be growing rapidly at lengths approaching that at which catastrophic failure occurs, the precise value assigned to a_f is not critical and the use of a finite width correction not necessary. Values of da/dN are not particularly sensitive to either a_f (provided it is reasonably large compared with a_0) or m. Fatigue crack growth data in the vicinity of the threshold obtained using Eq 5 are in general agreement with data obtained from conventional tests. The derivation of Eq 5 is given in Ref *19*. Initial values of da/dN were calculated for all the broken specimens using $m = 3$ and $a_f = 10$ mm (0.4 in.); the results obtained are shown in Fig. 5. Room-temperature fatigue crack growth data for mild steel [*2*], the value of ΔK_c obtained, and a crack growth rate of one lattice spacing/cycle are indicated for comparison. For the room-temperature data $m = 3.3$, and at the midpoint of the band ΔK for a crack growth rate of 10^{-6} mm/c (10^{-6} in./c) is 6.2 MN/m$^{3/2}$ (15.1 $\times$ 10^3 lb/in.$^{3/2}$).

Discussion

Fatigue crack growth is a strain-controlled process, so that both ΔK_c and ΔK for a given rate of crack growth can be expected to be proportional to Young's modulus [*20*]. Young's modulus at 300 C for the steels tested is only slightly different from the room-temperature value, and it is therefore not surprising that the fatigue crack growth properties are generally similar. None of the results obtained are inferior to those for room temperature, so it is clear that for ferritic steels the extensive room-temperature data available on the behavior of fatigue cracks can be safely used for design purposes in normal environments at temperatures up to at least 300 C. A temperature of 300 C is near the strain aging temperature for mild steel, so that strain aging caused by net section yielding may account for the high value of ΔK_c (approximately 70 percent above the room-temperature value) obtained at $\sigma_m/\sigma_a = 4.5$. A low-alloy steel is being tested with $\sigma_m/\sigma_a = 4.5$. As this material has a higher yield stress and is not susceptible to strain aging, it is anticipated that ΔK_c will be near the room-temperature value for mild steel.

The use of Eq 5 in the calculation of initial crack growth rates implies that Eq 1 is valid down to ΔK_c. The existence of ΔK_c is associated [*2*] with a crack growth rate of about one lattice spacing/cycle which is the minimum possible on physical grounds. Lower average crack growth rates may be observed, particularly when the material is attacked by its environment [*20*] (examples are: copper in air and mild steel in brine). In such cases crack growth only takes place on part of the crack front during each cycle, although Eq 5 may still hold. Carefully controlled fatigue crack growth tests in the vicinity of ΔK_c carried out by Paris and co-workers [*4,21*] show that for some materials there is an inflection in the curve of da/dN against ΔK at ΔK values of just above ΔK_c and da/dN of around one lattice spacing/cycle. Below the

inflection, m is much greater than above. Similar inflections have been observed [*19*] in some data obtained using Eq 5. Mild steel at room temperature has a threshold for fatigue crack growth at about one lattice spacing/cycle with no sign of an inflection [*2,19*]. Figure 7 suggests that at 300 C there is a threshold at rather greater than one lattice spacing/cycle. Actual crack growth rates are about the same as at room temperature or possibly slightly slower and, as is the case for fatigue crack growth rates at room temperature [*2*], yielding on the net section at high mean stress appears to have little effect on crack growth rates for mild steel. It is worth noting that these data were obtained without any crack growth monitoring instrumentation.

Values of ΔK_c obtained by Paris, with the notable exception of copper, usually agree with those obtained at National Engineering Laboratory (NEL) for similar materials and values of σ_m/σ_a. For example, room-temperature ΔK_c values for rotor steels [*4*] for a range of σ_m/σ_a agree reasonably well with the results in Fig. 5 for mild steel and a low-alloy steel; however, at 288 C (550 F), and σ_m/σ_a between 1 and 3, ΔK_c is about 30 percent lower than at room temperature, and at higher σ_m/σ_a ΔK_c is roughly the same as at room temperature. NEL elevated temperature results are therefore consistently higher. The difference can perhaps be attributed to the shorter crack lengths, and therefore higher net section stresses, used in the NEL tests. At elevated temperatures there may be therefore a need to ensure that ΔK_c data used for design purposes are based on crack length of the same order of size as in the structure concerned.

Klesnil and Lukáš [*3*] obtained ΔK_c from various steels at room temperature and $\sigma_m/\sigma_a = 0$. The specimens used were 60 mm (2.36 in.) wide by 3.4 mm (0.134 in.) thick and contained a center crack either 2.5 mm

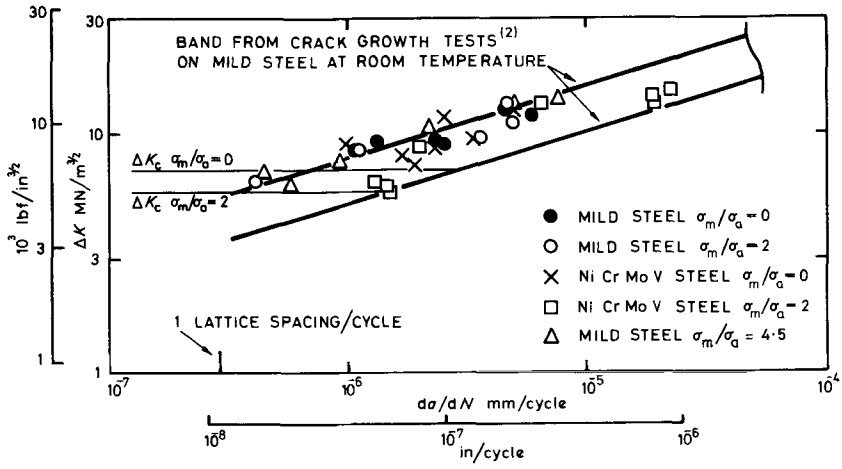


FIG. 7—ΔK *against* da/dN.

(0.10 in.) or 5.5 mm (0.22 in.) overall length. The specimens were stress relieved after precracking and ΔK_c was calculated from the stress necesssry to cause an increment in overall length of at least 0.3 mm (0.012 in.) after 5×10^6 cycles. The values of ΔK_c obtained were about 35 percent lower than those obtained at NEL. However, the observed increment of crack growth per crack tip of 0.15 mm (0.006 in.) is very much less than the specimen thickness. It is therefore possible that the results represented changes in crack front shape rather than a genuine threshold.

Conclusions

1. Whether or not an edge crack grows in ferritic steel at 300 C subjected to the loading cycle $\sigma_m \pm \sigma_a$ depends on the value of the range of stress intensity factor ΔK and the ratio σ_m/σ_a. At a given σ_m/σ_a ratio, if $\Delta K > \Delta K_c$, the crack will grow, if $\Delta K < \Delta K_c$, the crack will remain dormant. Values of ΔK_c obtained for $\sigma_m/\sigma_a = 0$ or 2 were slightly greater than those for similar steels at room temperature but, for mild steel with $\sigma_m/\sigma_a = 4.5$, ΔK_c was higher than at room temperature; this appears to be associated with yielding on the net section. The results indicate that room temperature data on the behavior of fatigue cracks can be safely used for design purposes for normal environments at temperatures up to about 300 C.

2. Crack growth data at low rates of crack growth were deduced from the results of the tests using an integrated version of the crack growth equation $da/dN = B(\Delta K)^m$. These data showed that crack growth rates at 300 C were similar to those at room temperature and suggested that the minimum possible rate of fatigue crack growth is somewhat greater than one lattice spacing/cycle.

3. The methods used have the advantage that no crack growth monitoring instrumentation is required.

Acknowledgments

This paper is published by permission of the Director, National Engineering Laboratory, Department of Trade and Industry. It is British Crown copyright and is reproduced with the permission of the Controller of Her Britannic Majesty's Stationery Office.

References

[1] Paris, P. C. and Erdogan, F., *Journal of Basic Engineering*, Vol. 85, No. 4, 1963, pp. 528–534.

[2] Frost, N. E., Pook, L. P., and Denton, K., *Engineering Fracture Mechanics*, Vol. 3, No. 2, 1971, pp. 109–126.

[3] Klesnil, M. and Lukáš, P., *Engineering Fracture Mechanics*, Vol. 4, No. 1, 1972, pp. 77–92.

[4] Paris, P. C., Weiss, V., and Wessel, E. T., "On the Threshold for Fatigue Crack Growth," presented at the 5th National Symposium on Fracture Mechanics, University of Illinois, Urbana, Ill., 1971.

[5] Frost, N. E., *Proceedings*, Institution of Mechanical Engineers, Vol. 173, No. 35, 1959, pp. 811–836.
[6] Frost, N. E., *Journal of Mechanical Engineering Science*, Vol. 2, No. 1960, pp. 109–119.
[7] Frost, N. E., *Journal of Mechanical Engineering*, Vol. 5, No. 1, 1963, pp. 15–22.
[8] Frost, N. E. and Greenan, A. F., *Journal of Mechanical Engineering Science*, Vol. 6, No. 3, 1964, pp. 203–210.
[9] Frost, N. E., *Journal*, Iron and Steel Institute, Vol. 205, No. 2, 1967, p. 206.
[10] Frost, N. E. and Greenan, A. F., *Journal of Mechanical Engineering Science*, Vol. 9, No. 3, 1967, pp. 234–237.
[11] Frost, N. E. and Greenan, A. F., *Journal of Mechanical Engineering Science*, Vol. 12, No. 3, 1970, pp. 159–168.
[12] Greenan, A. F., "Fatigue Tests on Edge-Cracked Magnesium Alloy Plate Specimens," NEL Report No. 492, National Engineering Laboratory, East Kilbride, Glasgow, 1971.
[13] Paris, P. C. and Sih, G. C. in *Fracture Toughness Testing and Its Applications, ASTM STP 381*, American Society for Testing and Materials, 1965, pp. 30–83.
[14] Elber, W., *Engineering Fracture Mechanics*, Vol. 2, No. 1, 1970, pp. 37–45.
[15] Nichols, R. W., Burdekin, F. M., Cowan, A., Elliot, D., and Ingham, T. in *Practical Fracture Mechanics for Structural Steel*, Chapman and Hall, London, 1969, pp. F1–F113.
[16] Brown, W. F. and Srawley, J. E. in *Plane Strain Crack Toughness Testing of High-Strength Metallic Materials, ASTM STP 410*, American Society for Testing and Materials, 1967.
[17] Srawley, J. E. and Brown, W. F. in *Fracture Toughness Testing and Its Applications, ASTM STP 381*, American Society for Testing and Materials, 1965, pp. 133–198.
[18] Rice, J. R. in *Fatigue Crack Propagation, ASTM STP 415*, American Society for Testing and Materials, 1967, pp. 247–311.
[19] Pook, L. P. in *Stress Analysis and Growth of Cracks, Proceedings of the 1971 National Symposium on Fracture Mechanics, Part 1, ASTM STP 513*, American Society for Testing and Materials, 1972, pp. 106–124.
[20] Pook, L. P. and Frost, N. E., "A Fatigue Crack Growth Theory," *International Journal of Fracture Mechanics*, Vol. 9, No. 1, 1973, pp. 53-61.
[21] Paris, P. C., *Closed Loop*, Vol. 2, No. 5, 1970, pp. 11–14.

GENERAL DISCUSSION ON MECHANISMS OF FATIGUE

(*written discussion*)—From the standpoint of the mechanisms researcher, Dr. Coffin's keynote address presents a real challenge. In retrospect, the synergistic interaction of elevated temperature and environment in high temperature fatigue is quite plausible and even obvious. Yet, this interaction and its characterization has been almost completely neglected in fatigue mechanisms research. In the standard reviews, the effects of temperature and environment are relegated usually to a couple of paragraphs, not because they are unimportant but because there is so little prior work on which to draw. In any event, these two important parameters have been subjected to an artificial separation in the analysis of experimental data so that their interaction has gone unappreciated.

In this same vein, elevated temperature fatigue research has emphasized the important role of strain rate or frequency. These variables have also been largely neglected in mechanisms research. Gell and Leverant's paper cites evidence that strain rate effects at the crack tip can *invert* the normal Stage I—Stage II crack growth sequence at elevated temperatures!

The relative importance of environmental effects and creep effects in the time-dependent part of elevated temperature fatigue has been discussed, but the answers are not clear at this moment. Here is another challenge to the mechanisms researcher to help lay this controversy to rest.

The fact that there are very few contributed papers at this symposium on the mechanisms of fatigue at elevated temperature is not accidental. The fact is that such experimentation is difficult, requiring control of both temperature and environment. Moreover, the interpretation of such experiments requires that thermally activated processes be considered which may affect the stability of the normal metallurgical structures and deformation modes. Nevertheless, it is important that the mechanisms of elevated temperature fatigue be investigated far more thoroughly than they have in the past. We hope that the papers given in this first session will provide that stimulus.

Copyright© 1973 by ASTM International www.astm.org

Test Methods

A. E. Carden[1]

Fatigue at Elevated Temperatures: A Review of Test Methods

REFERENCE: Carden, A. E., "**Fatigue at Elevated Temperatures: A Review of Test Methods,**" *Fatigue at Elevated Temperatures, ASTM STP 520*, American Society for Testing and Materials, 1973, pp. 195–223.

ABSTRACT: The study of fatigue at elevated temperature requires the evaluation of material response to several load-time profiles in specified thermal-chemical-nuclear-electric fields. This review of test methods emphasizes the relationships between "pure low-cycle fatigue" and tensile, fracture toughness, creep, cyclic-creep, creep fatigue (interspersion), fatigue-cycle-with-hold, dynamic creep, fatigue crack growth, and high-cycle fatigue testing. The thermal and environmental control is discussed. Special attention is given to isothermal-uniaxial, bending, torsion, and combined stress tests. Cyclic thermal testing is reviewed. Strain measurement, signal conditioning, computer utilization, fatigue crack growth, vacuum and environmental control, nondestructive testing, acoustic emission, and fractography are reviewed as they pertain to fatigue at elevated temperature. Specimen design, gripping, and testing machine characteristics are also discussed.

KEY WORDS: fatigue (materials), tests, test equipment, heating methods, fatigue, thermal fatigue, cracking (fracturing), creep-fatigue, cyclic loads, dynamic creep, strain measurement, specimen design

Prior to 1952 many, if not most, of the elevated temperature fatigue experiments were conducted in R. R. Moore-type (rotating beam) or Krouse-type (axial) fatigue machines, modified to allow a resistance furnace to surround the specimen. These machines were fixed frequency, usually 167 or 30 Hz, and constant applied moment, load, or deflection amplitude. No longer is it sufficient to evaluate the fatigue properties in air at fixed frequencies, but now chronological and environmental factors are equally significant in their respective roles in the relationships describing cycle dependent fracture. For this reason it is proper to include in the review those discussions of test methods which specifically deal with cycle time or creep or both, and corrosion (or environmental reaction) under cyclic loading at high temperature. This paper is a review of the test methods and techniques used to study the response of a material to cyclic load or strain at elevated temperature.

[1] Professor of mechanical engineering, The University of Alabama, University, Ala. 35486.

Copyright© 1973 by ASTM International www.astm.org

The principal review articles or proceedings of symposia that document the historical development of test methods at elevated temperature are listed [*1–17*].[2]

Our understanding of elevated temperature fatigue phenomena is based on the analysis and interpretation of test results. These data are obtained from controlled experiments. Test methods have a vital role in the development of elevated temperature materials technology.

Historical

It is of interest to note the interaction between the experimentalist, the experimental technique, availability of equipment, sponsorship, and the time required for new developments. Without minimizing the efforts and contributions of other men and organizations, one example is used for illustration of the point. The activity in strain controlled fatigue at elevated temperature was entered, in a sense, by way of Coffin's experimental work sponsored, in part, by the U.S. Atomic Energy Commission (AEC) at the Knolls Atomic Power Laboratory (KAPL). He was not the first, but his work was certainly a catalyst to the test techniques.

During the early fifties no commercial equipment in the United States was either available or, with modifications, widely used for strain controlled fatigue studies at elevated temperature. While Liu et al [*18*] and Manson [*19*] had performed strain controlled tests, the complexity of the experiment or the lack of commercial equipment hindered its adoption. Much of the early thermal fatigue equipment was built by the user and copied the basic design given by Coffin and Wesley [*20*]. Chronologically the low-cycle thermal-fatigue testing preceded the isothermal elevated temperature strain-cycle testing activity. The thermal cycle (the controlled variable was temperature range) induced a strain cycle. A detailed analysis of the mechanics of the experiment lagged by almost a decade [*21*]. That analysis and other thermal-fatigue work was also funded by the AEC [*22–23*].

The initial thermal-fatigue specimen design, a tubular specimen with massive, integral ends for gripping, ensured a stiff grip, failure in the desired location, reproducibility, and relatively simple measurement and control. The high cost of specimen manufacture and unstable geometry for the high-strain range tests were deficiencies. The instability problem led to the design of a zero-gage-length (ZGL) design with an hourglass shape. Isothermal extension controlled cycling of the tubular specimens was possible with a modified thermal-fatigue rig [*24*] or a scotch-yoke mechanism.

With the advent of the Instron extension cycling apparatus, isothermal fatigue was performed in commercial test equipment [*25*]. Diametral measurements were made with dial gages at first on the ZGL specimens.

[2] The italic numbers in brackets refer to the list of references appended to this paper.

These studies yielded interesting results on the general problem of cyclic plastic instability and ratchetting [*26*]. From this work, however, developed a specimen design and gripping arrangement that has been widely used in the test method. The analysis of the mechanics of the thermal-fatigue test suggested that the diametral strain measurement was adequate for a stress strain hysteresis loop and possibly control [*27*]. The time was ripe for the concept. Slot et al at the General Electric Nuclear Space Programs (NSP) Laboratory under AEC sponsorship not only used the diametral measurement for control but, with the operational amplifier technology, designed and built signal conditioning equipment that converted the diametral strain signal to an equivalent longitudinal strain measurement (Slot [*17*]). Adequate technology, availability, reliability, reasonable cost of electronic signal conditioning, control equipment, and the ingenuity of the experimentalist established a new direction for the test method. The signal conditioning used by Slot presupposes isotropic elastic properties (elastic moduli and Poisson's ratio).

As with all presuppositions the researcher is forced to look more carefully at the material under test to determine if isotropy does in fact exist. With the normal strain cycling equipment (that is, electrohydraulic under load control) the anisotropy can be determined without special equipment. The benefit from such exercise is a greater awareness of the material and processes under study. Moreover, the desire to perform constant strain rate tension tests led to the development of special signal conditioning from diametral strain signals which allow a constant true strain rate beyond the condition of necking [*28*]. A ZGL specimen was necessary to ensure measurement at the neck. Considerable analysis of experiment and innovation of test method and equipment were produced in the NSP facility under AEC sponsorship (Slot [*17*]).

During the midsixties a thermal cycling arrangement was synchronized with the extension cycle controls of an Instron, so that the thermal and mechanical parameters could be separately yet synchronously controlled (Carden [*17*]). Moreover the thermal strain component could be removed from the strain signal, and the hysteresis loop could be recorded that represented the parameters of interest. During the fifties and sixties the electrohydraulic test equipment was used more widely in fatigue studies. The capability for control and response and for combination with auxiliary thermal cycling recommend its continued use. Lindholm [*29*], and Sheffler and Doble [*30*] have utilized combined thermal and mechanical cycling.

The role played by the AEC has been mentioned. Seven papers of this conference stem directly from AEC sponsorship. With the current interest in the liquid metal fast breeder reactor (LMFBR) concept, it is likely that their involvement in fatigue at elevated temperature will continue. The time period for perfection of ideas and for production of beneficial results was generally three years or more. Thus, in the past two decades, the ex-

perimental test method for fatigue at high temperature has been developed by the participation and interaction of the experimentalist, analyst, equipment manufacturer, and sponsor. Many concepts on strain control, specimen design, specimen stability, gripping, strain measurement, and conditioning have been fostered in an environment where each participant played a particular role and allowed a healthy interaction with the other members. There are other factors, of course, but these are apparently significant ones. If testing methods are to continue to develop, it seems to this writer, at least, that the contributions of each must be cultivated.

Elevated Temperature Test Methods

A survey of the papers of this conference will show the breadth of the scope of the test methods. The test methods can be categorized by the kind of test (for example, low-cycle fatigue, high-cycle fatigue, cyclic creep, dynamic creep, fatigue crack growth, etc.) or by a reference to the kind of loading equipment used (for example, axial, bending, torsional; electrohydraulic, ultrasonic electromagnetic resonant type, etc.). Table 1 lists several of those categories and pertinent references [*4,11,17–224*].

TABLE 1—*Summary of pertinent references to test methods as related to fatigue at elevated temperature.*

I. General (fatigue at elevated temperature)	
Bibliographies and surveys	*1,9*
Symposia and books	*4,10,11,13,15,16,32–35,37,107–108*
Interaction of creep and fatigue	*1–3,8,9,11,31,94,108,115*
II. Elevated temperature testing (other)	
Physical and mechanical testing	*4,15,16,33,36,45,52,102,107,109,188,208*
Tensile	*4,15,28,52,102,103*
Creep and relaxation	*12,13,15,16,36,104,197*
Dynamic creep	*2,13,105*
Cyclic creep	*13,68,206*
Corrosion fatigue	*14*
III. Equipment and test techniques	
System requirements	*4,38–41,49,52,82,188,203*
Electrohydraulic	*17,39–41*
Screw driven	*11,17,205*
Electromagnetic and piezoelectric	53–57,*73,95,98–101,205*
Bending fatigue	*11,13,17,32,66–68,70–76,78*
Biaxial fatigue	*13,78,80–84,89–90,110–114,116,207*
Thermal fatigue	*11,13,20–27,96–97,117,119–152,195,201*
Combined thermal-mechanical	*17,29,30,77,118,128,129,137*
Ratchetting	*153–155,157–158,198*
IV. Fatigue crack growth	*14,160,186*
Axial loading	*162–167*
Bending loading	*67,159*
Cylindrical loading	*67,161*
Techniques for crack growth measurement	*168–176,178–180,182–184*
V. Vacuum	*32,58,60–65,88,213,216,217*

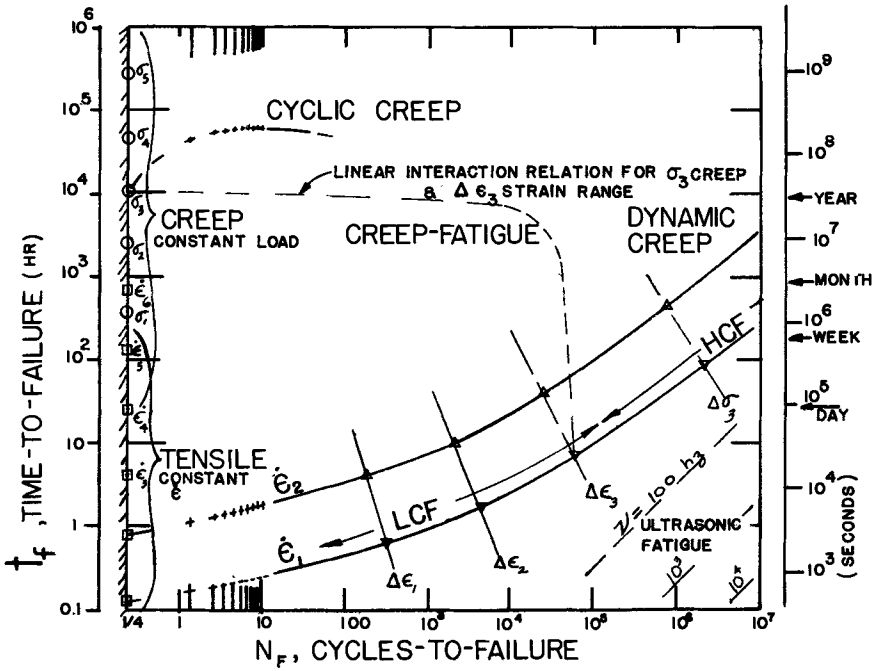


FIG. 1—*Log* t–*Log* N_f *coordinate plane* [31]. *Lines of constant frequency have a slope of* +*1. Low-cycle fatigue* (*LCF*) *and cyclic creep* (*CC*) *are discontinuous in the* N_f *variable as shown in the* 1/4 *to 10 cycle range. High-cycle fatigue* (*HCF*), *dynamic creep* (*DC*), *creep fatigue interaction* (*CF*), *and ultrasonic fatigue failures* (*USF*) *will be plotted in the regions shown.*

The log-time-to-failure and log-cycles-to-failure coordinate plane advocated by Esztergar and Ellis [*31*] is one way of categorizing the results of fatigue tests. Such a diagram is shown in Fig. 1. The results of tensile, creep, low-cycle fatigue, high-cycle fatigue, and other kinds of tests can be shown in this diagram. The thermal and chemical fields are constant for all data shown. Lines of constant load or strain amplitude (or other controlled variable) show the effect of *frequency* or *strain rate* on elevated temperature fatigue much more vividly than, say, a log-strain range versus log-cycles-to-failure plot.

Thermal Fatigue

The selection of a fatigue test method for cyclic temperature conditions depends upon the need of the consumer. King and Smith [*11*] list three categories of test techniques. Perhaps four kinds of test methods are more apt: positional, prototypic, phenomenological, and physical. In the first, generally used for development or selection, materials are placed in order of merit, or ranked. In the second, a prototype or model of a nozzel, blade, disk, tube, or other structural element is tested to predict or verify the

behavior in service. In the third, bulk measurements infer or describe a phenomena, and these are used to specify material behavior. Finally, in the study of highly local phenomena the mechanisms of deformation, crack growth, and fracture are the primary consideration in the design of the experiment.

One paper in the *Manual on Low Cycle Fatigue Testing* [*17*] is on thermal-fatigue evaluation. In addition to the discussion of test methods there and also in King and Smith's review [*11*], other works of interest show some novel development.

Phenomenological and Physical—Pirogov [*118*] describes a thermal plus mechanical cycling apparatus. Nippes and Uy [*119*] describe a modified Coffin thermal cycling rig, as do Krempl [*120*] and Neuber and Riege [*97,121*]. Kawamoto et al [*122*] describe thermal and mechanical deformation cycling with synchronization, but the machine was of the constant-grip-displacement-type rather than constant strain range. Dul'nev [*123*] describes circuitry for holding temperature. Sobolev and Pirogov [*124*] discuss methods for variable amplitude thermal cycling. In another place [*125*] they show measuring and recording techniques for obtaining the stress strain hysteresis loop. Egorov et al [*126*] discuss a test facility for high vacuum and temperature to 1500 C. Strizhalo [*127,128*] and Strizhalo and Sinyavski [*129*] describe a test method for programmed variation of load and temperature. Filatov [*130*] and Horton [*201*] describe high-temperature extensometers for thermal-fatigue testing.

Prototypic and Positional—There are several centers of activity for testing gas turbine blades and vanes in simulated thermal and mechanical cycling [*131–136*]. Special techniques for related thermal and mechanical cycling are described in Refs *137–140*. Prototypic tests of turbine disks are described by Mattavi [*116*] and Molchanov and Truchechkin [*141*].

The Glenny-type fluidized bed testing of small circular disks that are shocked thermally between two temperatures has been utilized in a number of places. Rostoker [*142*], Howes [*143–144*], and Mobray et al [*145*] describe some of the test method and results of this technique. Crack propagation rates can be inferred from replicas taken at several intervals of the life of the part or if striations are present by post-test measurement of striation spacing [*145*].

Stetson [*146–147*] did extensive work on a paddle-wheel and hole-in-plate thermal-fatigue unit for ASTM Committee C-22. Steverding [*148*] discusses laser pulses as a thermal source for thermal fatigue studies. Heinz [*149*] describes simple thermal buckling criteria for tubular members. Neudecker and King [*193*], Harman [*150*], and Richard [*151*] give examples of low-cycle thermal-fatigue test techniques for regeneratively cooled panels. Luft and Maiden [*152*] show results for thermal cycling of soldered silicon cell assemblies.

Thermal and Mechanical Ratchetting

Bree [*153*], Anderson [*154*], and Stentz [*155*] discuss the test methods for ratchetting studies. Tilly [*92*] discusses unidirectional strain accumulation in ordinary low-cycle fatigue tests. Burgreen [*156*] has analyzed the two-bar ratchetting model but without experimental accompaniment. Martin [*157*] describes a ratchetting experiment that modeled the growth of fuel element tubes. Yamanouchi and Wakamatsu [*158*] present a discussion of ratchetting under combined stress fatigue testing. Thermal ratchetting has been observed in steel storage tanks for alumina. The powder settles when the solar heat causes the vessel to expand but impedes the thermal contraction at night, causing the vessel wall to accumulate a one-directional plastic strain. Swaroop [*198*] describes the details of obtaining stress strain loops in three-bar assemblies.

Fatigue Crack Growth

The applications of fracture mechanics to elevated temperature crack growth have begun to multiply. Shahinian et al [*159*] have been active in this work for several years. However, in the symposium on *Fatigue Crack Propagation* [*160*] no paper was given describing crack growth at elevated temperature. The details of specimen design, evaluation of the stress intensity function, and optical techniques for room-temperature crack growth may be found in this reference as well as elsewhere. Brothers [*161*] has applied fatigue crack growth to elevated fatigue design problems. Coles and Popp [*37*] showed that elevated temperature fatigue crack growth, creep crack growth, and fracture toughness measurements were necessary to characterize the material for high-temperature application. James has studied fatigue crack growth as a function of temperature [*162*], frequency [*163*], stress ratio [*164*], and material [*35*]. McHenry and Pense [*165*] and McHenry [*166*] evaluated fatigue crack growth rates on several materials and designed a plastic strip specimen for low-yield strength materials. Harrison [*167*] related crack propagation under high-temperature low-cycle fatigue to a model of creep-fatigue interaction as has Carden [*106*].

Test Techniques for Crack Length Measurement—When the specimen is enclosed in a chamber, encumbered with paraphernalia, or too hot to gain visual access, the measurement of crack length is more difficult. Ways of making the surface crack tip more visible are to use plasma flame spray (brittle) coatings on the surface, polish the surface and use polarized light [*168*], use Moiré fringe techniques [*169,170*], or use a potential drop method. Markochev et al [*171*] show a good arrangement of potential pickups for center notched specimens. Loginov and Shkanov [*172*] describe equipment and procedure for observation of the initial phases of the macrocrack formation and propagation at the bottom of notches. Papirno and Parker [*173*]

used an autoflash photomicrographic technique for crack initiation study. Surface replicas [*174*] can be taken during the test for determination of surface topography and cracking. Thermal mapping [*175*] can be used, as can optical correlation, for discrimination of the surface crack regions [*176*]. A recent issue of *Materials Research and Standards* was devoted to holography [*177*] which can be used for fatigue crack length measurements. Dunegan et al [*178*] described fatigue crack measurements by acoustic emission techniques. Clark and Ceschini [*179*] have described an ultrasonic crack growth monitor, as has Jeglic et al [*180*]. Manjoine [*181*] used high-temperature strain gages for fatigue crack growth measurements. McHenry [*182*] developed an ex-furnace compliance gage for crack length measurement.

The plastic zone measurements can be inferred from interference microscopy, post-test linear variable differential transformer (LVDT), diamond stylii, or other surface contour measurements [*183–184*]. Hahn et al [*185*] used post-test etching techniques; Pelloux et al [*186–187*] used post-test scanning electron microscopy (SEM) examination of the fracture surface.

Special Considerations

This section is devoted to special considerations of heating methods; specimen design; grip design; strain measurement, control, and extensometer design; calibration, recording, and computer utilization; and finally, environmental control.

Heating Methods

It is regrettable that Van Leeuwen and Mucuoğlu [*4*] and Van Leeuwen [*188*], with such a valued survey of heating methods and equipment, gained so limited a distribution. The reports are highly recommended for a detailed consideration of many thermal and mechanical details. Three categories of the heating facilities as listed by Van Leeuwen with citations to the references of this review are:

A. Combustion furnace heating
   1. Specimen inside, [*131–136*]
   2. Specimen outside, [*147*]

B. Electric resistance heating
   1. Direct resistance (self heating), Dawson et al, Coles et al [*11*], Carden [*17*] and [*18*], [*45*], [*67*], [*118–122*]
   2. Electrical resistance furnace
      (*a*) Gas atmosphere, Hall [*11*], Krempl [*18*], Wells [*17,32*], Ritter [*11*], and [*27*], [*67*], [*157*], [*162–165*]
      (*b*) Vacuum atmosphere, Swindeman [*32*], Stegman [*32*]
      (*c*) Liquid atmosphere, [*98*]
      (*d*) Fluidized solids atmosphere, Glenny [*11*], and [*142–145*]

3. Incandescent lamps, [*49–50*]
4. Contact heaters
   (*a*) Electric blankets, [*191*]
   (*b*) Sprayed elements

C. Electric induction heating
1. Direct induction, Berling [*32*], Slot [*17*], and [*42–47*], [*203*]
2. Indirect induction (susceptor)

There is a relationship of the heating method to the design of the specimen and of the temperature measurement and control. The radio frequency (RF) induction requires close coil-to-specimen spacing and small grip ends, hinders the mounting of additional measurement devices, obscures access to and visibility of the surface for replication, etc., and the coil has a high voltage RF potential requiring insulation and safety precaution. A temperature disturbance occurs at the thermocouple mass in the field, as well as at specimen locations unequally spaced to the coil. RF noise is induced in the instrumentation cabling.

The longitudinal temperature distribution in resistance heating can be minimized by the design of internal radiant heat sinks and longer lengths of uniform cross sections [*189*]. Specimen cracks normal to the current flow are accompanied by nonuniform temperature distributions. No heating can occur after the specimen fractures as can occur with induction heating, but local melting as a result of arcing can occur during Stage III final fracture. Neither direct RF induction or resistance heating are good for very high electrical conductivity materials. The specimen impedance must be matched to the output circuit in both methods. The thermal mass is limited to the specimen and grips for both cases. Graphite and tungsten mesh heaters have been also used for vacuum atmospheres at very high temperature (Swindeman [*32*]).

Quartz lamp facilities are used for fatigue crack growth of sheet specimens and heating of tubes and panels [*190*]. Liquid baths [98], hot gas facilities [*131*], resistance heated grip ends [*191*], and internal globar heaters [*17*] have been used.

Temperature measurement is accomplished usually by thermocouples or radiation detectors. Few reports give calibration methods or internal analysis of the uncertainty of the readings. Few investigators use multiple (redundant) techniques for increased accuracy.

Specimen Design

The specimen response to low-cycle fatigue (LCF) loading can be stable, mixed, or unstable. In the former case, only the local phenomena of crack initiation and growth can be observed; in the latter, buckling and gross compounding of the local strain prevent the failure from being pure fatigue. In the mixed case there is some instability initiated before the

fatigue crack propagation is complete. Avery et al [*192*] and Neudecker and King [*193*] observed the mixed and unstable case for the thermal cycling of restrained tubes. The criterion used by Avery et al was independent of the frequency of loading, maximum temperature, or material properties. Mulcahy and Shoemaker [*194*] contributed to the analysis. The critical quantities for a condition of mixed or unstable mode of failure of a tube are the mean radius, thickness, strain range, and strain hardening exponent. Such a relationship is shown in Fig. 2. While these considerations were developed for tubular specimens, the r/t of 0.5 is a lower bound, that of a solid rod. This diagram, then, can be used to predict cycle dependent instability. The mixed region is a situation of local ratchetting, compounding strains of opposite sign at different locations, and changing geometry. Egorov et al [*195*] shows that the fracture frequently occurs in the transition region between the bulging and thinning regions. Even the solid hourglass specimen is susceptible to this kind of instability, as shown in Fig. 7, page 170, of Ref *17*. In Fig. 20*b*, page 191 of Ref *11* the specimen profile shows that the persistent slip occurs on oblique cones to produce the dual bulged regions. Such a specimen with nonhomogeneous deformation benefits from the strengthening effect of the shape of the specimen. It is not possible to test uniformly any specimen in tension to a strain range greater than the strain hardening exponent, since the instability called "necking" initiates there. Thus, the lower anchor point of the curve describing the initiation

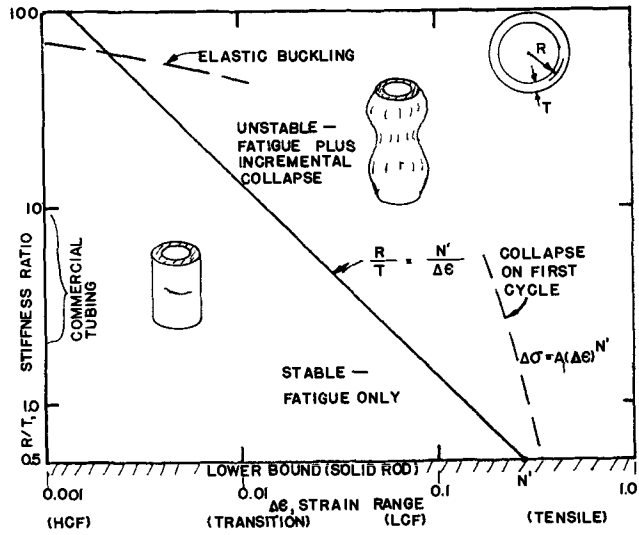


FIG. 2—*Criterion for cyclic instability for tubular fatigue specimens. At low* r/t *and strain range values the geometry is stable. At large strain range values cyclic instability is combined with fatigue unless collapse occurs on the first cycle. The lower* r/t *bound is 0.5—a solid rod. The upper practical bound is set by elastic buckling. The upper limit for tensile strain is set by the strain hardening exponent; the lower limit by the endurance limit.*

of instability on the first cycle passes through the r/t strain range point of (0.5,n). Avery suggested the form of the function to be log-linear.

The r/t of the specimen is related to the area of the specimen via the internal diameter and thickness, as shown in Fig. 3. The family of curves in Fig. 3 can be used to select tubular dimensions of maximum allowable strain range for stable geometries in LCF. Moreover, for tests in machines with load limitations and anticipated stress ranges, the maximum specimen area is determined. LCF tests are performed on specimens with certain material and geometric characteristics. Sometimes the geometric characteristic is more significant in the life of the specimen than the material.

Grip Design

A number of specimen designs and grip arrangements have been described. The grips used by Slot et al [*17*] are shown in Fig. 4, Swindeman [*191*] in Fig. 6, and Havas [*91*] in Fig. 5. Swindeman has used another grip design [*32*], and Coffin's [*17*] is similar to that shown in Fig. 4. Steele [*196*] designed a similar liquid metal grip to include X and Y motion (and X and Y rotation) for precision alignment of the grip. After alignment the grip is locked in position. Both designs use threaded end specimens. The modifications of the conical wedge are used widely for gripping. The hydraulic

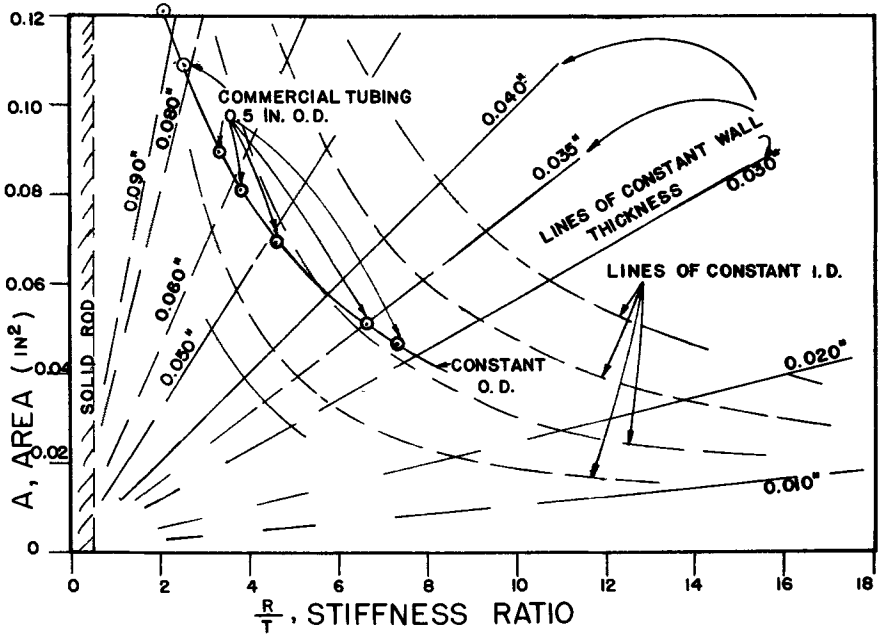


FIG. 3—*Area-stiffness ratio relationship for thin-walled tubes. Lines of constant wall thickness and internal diameter are shown. This graph with Fig. 2 can be used to select specimen dimensions to avoid (or ensure) cyclic instability and to interpret the fatigue results of tubular elements.*

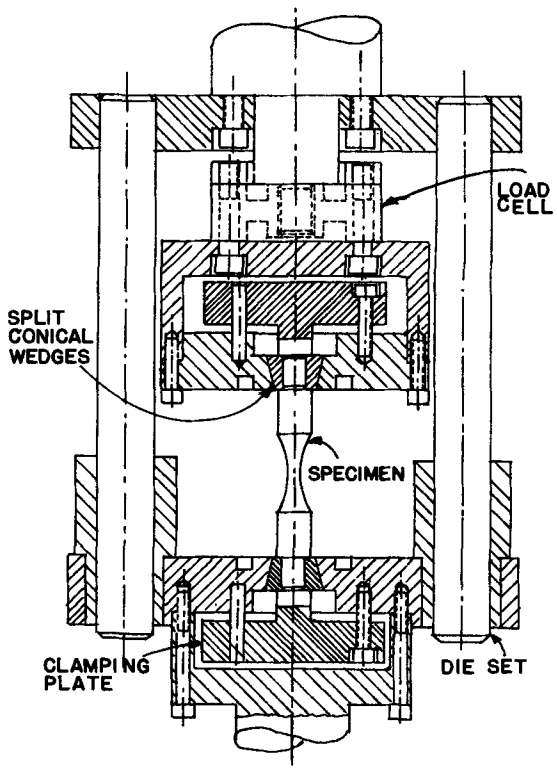


FIG. 4—*Fatigue grip design by Slot [17]. Low specimen machining costs, good alignment and rigidity, cumbersome to insert and remove specimen, no unseating problem. Compatible with induction heating.*

5-C collet chuck,[3] Fig. 7, is rigid, has quick release capability, and is good for loads up to about 2000 lb tension and compression with smooth collets gripping smooth rods of medium to high hardness (RHN C20 to C40). With knurled or grooved collet faces the load capacity is more than doubled. The desire for low-cost specimen design and high-quality dimensional control suggests the use of tubing or rod. The heated center section would be weaker than the grip end, and a minimum of machining is required. What is required is grip that will hold the specimen with high rigidity and good alignment, and failure must never occur in the grip. Tubing must be supported by a solid internal plug, preferably anchored to the base of the grip for additional load carrying capacity through friction at the innerface. Paxton [*197*] has used Swagelock[4] grips for tension and creep testing of tubing; they can be also used for LCF of soft materials when the central

[3] Enerpac Hydraulic Grip, Butler, Wis.
[4] Trademark of Crawford Fittings Inc., Solon, Ohio.

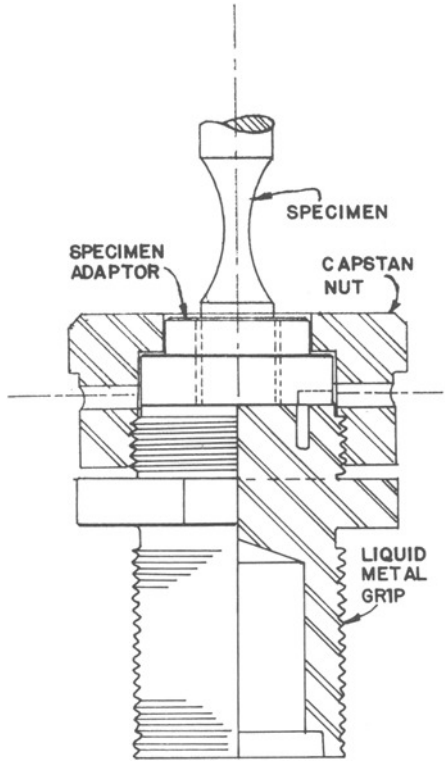


FIG. 5—*Fatigue grip design by Havas* [91] *and Steele* [196]. *Requires threaded specimen ends, alignment depends upon specimen end-face and threaded collar. No unseating problem. Medium end rigidity and removal difficulty.*

section is reduced by 2:1 or more. Swaroop [*198*] has used Superlok[5] fittings for gripping tubes in ratchetting studies. A reduced gage section is required, and the grips have low bending rigidity. Sno-Trik[4] grips are stiffer but more expensive. A number of tube fittings have been described in recent issues of *Zavavodskaia Laboratoriia* (Vol. 37, No. 3, pp. 377–378; No. 5, p. 619). Jacob's chucks can be also used for low-strength solid rods (for example, 1/4-in.-diameter copper) with a reduced central section.

Steele [*196*] also observed that the liquid metal grip generates a lateral force when the solidification is uneven circumferentially. Moreover he observed front-to-back rocking of the Instron crosshead during vertical displacement cycling. The die set arrangement, shown in Fig. 4, greatly reduces the effect of crosshead rocking and low transverse grip rigidity. Pavlovskii et al [*199*] discuss measurement of bending forces caused by gripping in axial fatigue machines. They indicate some of the criteria for the design of grips.

[5] Trademark of Parker Hannifin Co., Cleveland, Ohio.

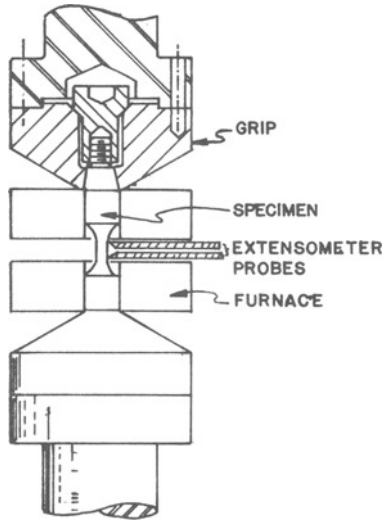


FIG. 6—Fatigue grip design by Swindeman [191, *see also* 32]. *Good end rigidity, medium specimen cost, and insertion-removal difficulty. Preload must exceed maximum test tensile load or specimen will unseat. Specimen grip heaters shown. Also compatible with induction heating.*

Strain Measurement Control and Extensometer Design

The cycle control for the Instron can be adapted to strain cycling by the use of an extensometer and voltage sensing relays. The Atcotran[6] 6401 Classifier-Controller has been used. Feltner [*17*] used Daytronic[7] equipment, and Coffin [*17,200*] used other equipment. Signal conditioning similar to that described by Slot [*17*] can convert the diametral strain signal to an analog of the longitudinal strain. Moreover a thermocouple signal can be amplified and subtracted from the diametral so that the output signal is independent of the thermal strain component. For large strain ranges the self heating can often disturb the temperature control by as much as 50 F, producing an extraneous thermal strain.

For extension cycling based on crosshead displacement the *strain* range will not be constant if the material hardens or softens. Factors of 2:1 have been observed for the initial strain range to the final. Moreover, if the diametral strain range is preserved constant the axial strain range will change during cycling such that

$$\Delta\epsilon_{lm} = \frac{(\Delta D)}{D_o}[\mu + (1/2 - \mu)R]$$

[6] King of Prussia, Pa.
[7] Cleveland, Ohio.

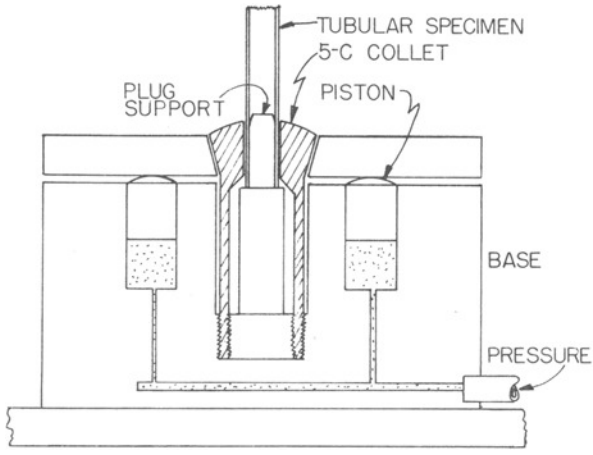


FIG. 7—*Hydraulic collet fatigue grip for tubing or rod. Tubing is gripped by friction force on inner and outer surface. Fail-safe grip release by depressurization. Low specimen cost (only cut and deburr), low insertion and removal difficulty, 5-C collet readily available for tubing to 1⅛ diameter.*

where

μ = Poisson's ratio for the elastic component,
R = ratio of plastic to (elastic plus plastic) (longitudinal strain range), and
$\Delta\epsilon_{lm}$ = longitudinal, mechanical strain range.

If ΔD is kept constant, $\mu = 1/3$ and R changes from 1 to 0 (fully hardens), the longitudinal strain range will increase by 50 percent. When μ is anisotropic, two transducers at 90-deg-circumferential orientations can be used to average the diametral strain, or an orientation of a known value of μ must be used. Sometimes, it is simpler to resort to longitudinal strain measurement on a specimen with a uniform gage section.

Horton [*201*] developed some lightweight, small LVDT longitudinal extensometers. Swindeman [*191*] has used a clip strain gage that is mounted on a diametral strain transfer device. Coffin [*17*] also utilizes a commercial longitudinal clip gage with the diametral strain transfer device. The selection of LVDT versus strain gage for the transducer depends in part on noise [*202*], clamping pressure, sensitivity, range, natural frequency, damping, seismic noise, accessibility of the specimen to the device, etc.

The strain at the outer surface of the beam shown in Fig. 8*a* and used as a clip gage is

$$\Delta\epsilon_{\text{beam}} = \frac{t(\Delta D)}{2\,Lb}$$

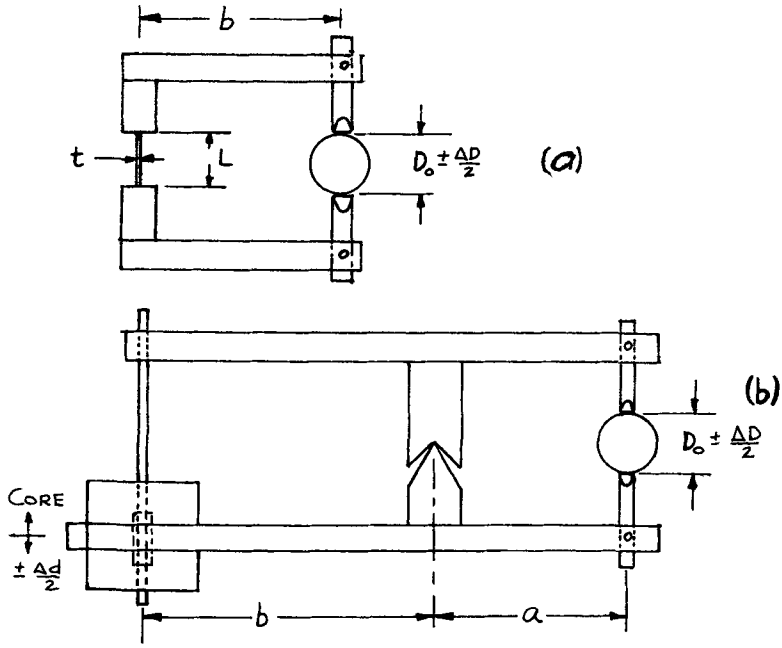


FIG. 8—*Schematic and legend for diametral clip gage* (a) *and for LVDT scissors gage* (b).

Since $\Delta Dt < Lb$, and $b < 1$, the system always demagnifies the strain in the specimen. The strain range in the beam should be kept less than 0.002 for long life. Therefore, the surface strain in the beam will always be reduced from the longitudinal strain in the specimen by a factor of four or more. A full bridge will give an output four times that of a single gage on the beam surface, and provided there is good linearity and low noise, the signal can be amplified electronically.

In the design of scissor-type LVDT diametral transducers, as shown in Fig. 8*b*, the relationships are

$$\Delta d_{\max} = b/a(\Delta D)$$

where

$$\Delta \epsilon_\theta = \Delta D / D_o$$

or

$$\Delta d_{\max} = b/a(\Delta \epsilon_l)\ D_o \mu$$

The maximum displacement range (Δd) of the LVDT core must be limited to about 80 percent of twice the double amplitude of the unit.

The optical strain measuring devices are not used widely but offer some promise in noncontact strain measuring systems. They are sensitive to power supply (light source) variations, smoke and optical filtration by the medium and seismic noise. Winslow [*203*] describes one such high tem-

perature LCF optical system. Swanson and Winslow [*204*] describe a laser unit used for diametral strain control.

Failure detection devices consist of potential drop techniques across the specimen, pressure leakage (for tubular specimens), load drop for strain controlled tests by the use of sample-and-hold comparator circuits, called underpeak detectors [*39–40*].

Testing machine stiffness also influences the terminal failure condition [*52*], the relaxation characteristic under fixed grip condition [*102*], and, in part, sets the natural frequency and dynamic response of the system [*53*].

Calibration, Recording, and Computer Utilization

Calibration of load readout is done frequently with resistance and voltage networks. There should be deadweight, proving ring, or secondary calibration under static and dynamic conditions periodically. Robinson [*205*] describes a good technique. Similarly, strain, temperature, environment, and other control and recorded parameters should be referenced against comparison calibrations periodically.

Winslow [*203*] developed a technique for recording six hysteresis loops on one sheet in an X-Y recorder. With counter circuits, pen-lift, and zero-indexing circuits, the device would record a stress strain loop at predetermined cycles set into the counter. Strizhalo and Shestopal [*206*] and Troschenko et al [*207*] describe techniques for strain, stress-strain, and plastic strain energy measurement and recording. Lozinskii et al [*208*] describe the measurement of electrical resistance and its variation during each cycle in LCF testing in vacuum and at elevated temperature.

The computer technology is being brought into the materials testing field with economic justification. While the capital investment is large, the savings in manpower for obtaining and reporting data, in active control of the test facility, predict greater use of the computer. Skoe and Swanson [*209*], Naumann and Bryant [*210*], Richards and Wetzel [*211*], Wetzel [*35*], and Il'iushin [*212*] serve as examples of the utility of computers in fatigue testing.

There has been very little published on the cost analysis of high-temperature fatigue programs. Appendix I is a brief outline of one method of cost analysis.

Environmental Control

The literature on corrosion fatigue contains numerous reference on effects of and techniques for control of environment. Frequently, there is the desire to immerse the specimen in an electrolyte and to impress a potential to polarize the specimen with regard to the bath. Fatigue testing at elevated temperature with this kind of environmental control is not common, but it is of interest and is being investigated. Chow [*98*] at Brookhaven National Laboratory has a facility for testing in liquid sodium,

the gas-cooled reactor people are interested in helium environments, and the molten salt reactor researchers have conducted a number of thermal fatigue experiments in molten fluoride salts. Perhaps the most active interest is to minimize or eliminate the effects of oxidation on fatigue. This is accomplished commonly by the use of good vacuum, for example, Sheffeler and Doble [*30*] Swindeman [*32*], La Force et al [*215*], Stegman and Achter [*63*], and Smith and Shahinian [*213*]. Pisarenko [*214*] describes equipment and techniques for studying the fatigue of heat resistant materials at high temperatures in aggressive media and in vacuum. Wilkov [*224*] studied the effect of the surface environment on the mode of microcrack formation at 78 and 300 K and in high vacuum. La Force et al [*215*] used argon environments with special provisions for reducing the contamination of residual O_2. Aubry and Bernadict [*216*] developed a special vacuum apparatus for fatigue studies with various gaseous environment and at various pressures. Swoboda [*217*] shows techniques for loading ten specimens into the vacuum chamber with simple methods for removal and insertion of individual fatigue specimens. Hockenhull and Monks developed a variable frequency (96 Hz to 20 kHz) high vacuum facility. Hardrath [*218*] shows data for the effects of temperature, aqueous environment, and outdoor exposure on fatigue strength of titanium. Peterson [*219*] describes a hot salt test technique for thermal-fatigue and fatigue tests of materials at elevated temperature.

Specimen surface preparation and residual chemical films are important, as indicated by Prevey and Koster [*220*], Bellows and Niemi [*221*], and Korenevskii and Yatsenko [*222*]. The use of oxidation resistant coatings for superalloys is used widely, for example, see Gedwill and Grisaffe [*223*].

Design of Experiments

The formulation and verification of design codes, criteria of failure, and the development of mechanistic models describing behavior rests on correct understanding of the phenomena and experience in applying previously developed analyses. This understanding and application, in turn, rests on physical (mechanistic) and phenomenological interpretations of test results. These test results are the product of experiments structured by a "test method." Test methods, as such, rarely are researched or scrutinized. Test methods, too often, become a description of how an apparatus is used rather than how a phenomenon is studied. Consideration of the controlled variables and the measurements are basic to a test method.

A definition of the dependent and independent variables for fatigue testing is necessary for proper planning. A suggested list of these is shown in Appendix II.

Because of the abnormally long time for some fatigue experiments the statistical sampling of data under these conditions is very low. For a small increase in cost, the output of data could be increased greatly. For example,

under load control, test specimens could be arranged in series or, in strain control, could be placed in parallel, one for control and the others following. Statistical techniques should be designed into a program rather than appended.

The loop of information exchange from *test method* -to- *test result* -to- *application* -to- *test method* -to- . . . , should be a closed loop. Feedback should have a correcting influence on the test method.

Concluding Remarks

There is no one test that will characterize a material response to displacement or load cycling when time and environment are left undefined. The principal variables of fatigue are the load-displacement cycle, the thermal-chemical-nuclear-electric fields, the specimen's geometrical response to load (buckling, ratchetting, crack growth, and terminal fracture), and the chronological arrangement of the stress or strain at the point that will lead eventually to failure. Test methods and understanding of the processes of fracture by fatigue are dependent mutually on the other for further development. The $\log(t)$ versus $\log(N_f)$ plane is recommended as a good coordinate reference for categorization of the effects of time (or frequency) and of the creep-fatigue interaction relationship. The results of different test methods lie in different regions on this coordinate map, yet bear a relationship to neighboring data. An appeal is made for improved methods, more economical ways of obtaining data, better utilization of facilities, utilization of the computer and electronic technologies in the performance of tests and reduction of data, of statistical analyses of data, and of some additional contribution on the design of experiments. Prototypic and full-scale testing seems to be an area of continuing development.

APPENDIX I

Estimate of Costs of Testing at Elevated Temperature

I. *Organization and Program Planning—Management*

(*a*) Familiarization with program objectives; search of the pertinent literature; definition of the problem; object and scope of the program.

(*b*) Design of experiments, explicit statement of what is to be measured and controlled, how, when, and what will be done with the data, write test procedure, describe a review and revision procedure for the test matrix, describe uncertainty allowed, describe frequency and method of calibration of measurement system, list procurement procedure for supplies, estimate costs, write PERT program and time schedule.

II. *Specimen Preparation—Project Personnel*

(*a*) Material costs, machining operations and costs; pre-test chemical metallurgical analysis, mechanical property tests; heat treatment, special surface preparation, handling, inspection and measurement, storage and marking.

III. *Testing—Project Personnel*

(*a*) Preliminary measurement, mounting of thermocouples strain transducer, etc., mounting in testing machine.

(*b*) Test monitoring, observation, data collection, maintenance of test boundary conditions.

(*c*) Post-test disassembly, sectioning, marking, measurement, storage, filing of data.

(*d*) Post-test chemical, metallographic, SEM, or EM examination.

IV. *Use-Factor Costs of Primary Test Facility*

Replacement cost of testing machine, thermal control, measurement and readout devices with the following factors: expected life, interest rate for capital investments, use factor, reliability factor, calibration and repair factor, modification (updating) factor.

V. *Data Reduction and Report Preparation—Project Personnel and Management*

(*a*) Translation of primitive data (analog to digital or . . .).

(*b*) Operation on data; change primitive data to desired values.

(*c*) Tabulation, plotting, collation of data in file, storage.

(*d*) Rental of computer, cost of writing, and debugging of program.

(*e*) Review and revision of program. Periodic review of current data; analysis, smoothing, estimate of scatter and confidence, review of test matrix and adjustment of test boundary conditions if estimated results are not within reasonable limits of predicted values.

(*f*) Reporting analysis of data, writing of draft, preparation of drawings, photographs; review, critique, revision, and final editing. Proofreading and final publication. Distribution of report.

To each of the foregoing items a cost number of manhours can be estimated for the program. The overhead rate of the organization can be assigned to the number of manhours of time required. A final cost is determined and compared to the estimate made in item (1*b*). Also, it is possible to identify the most likely places for economizing.

APPENDIX II

Variables of Elevated Temperature Fatigue Testing

A. Independent Variables. Specified, Controlled (active or passive)

1. Material
   (*a*) Alloy, composite.
   (*b*) Initial structure: grain size, ppt, prior treatment . . .
   (*c*) Coatings, quality of surface, . . .

2. Test method and specimen geometry
   (*a*) Test machine/test method.
   (*b*) Specimen geometry: characteristic length, slenderness ratio, surface to volume ratio, characteristic dimension, . . .
   (*c*) Gripping: alignment, rigidity, . . .
   (*d*) Definition of failure.
3. Programmed mechanical variables
   (*a*) Load: axial, bending, . . . as $F(t)$ includes mean, maximum, wave shape, or random function description . . . or
   (*b*) Displacement: axial, bending, . . . as $G(t)$.
4. Programmed field variables
   (*a*) Thermal.
   (*b*) Chemical: species, partial pressure, ph, . . .
   (*c*) Nuclear.
   (*d*) Electrostatic: polarity, potential, current density, . . .
   (*e*) Magnetic: field orientation, strength, . . .

B. Dependent Variables. Response of System–Measurements/Properties.

1. Material response
   (*a*) . . .
   (*b*) Resulting structure; EM, SEM, X-ray, microscopy, resistivity, damping, heat capacity, . . .
   (*c*) Changes in coating, flaking, formation of oxide films, . . .
2. Geometrical response
   (*a*) Influence of machine stiffness, natural frequency on response.
   (*b*) Specimen compliance, cyclic stress strain: specimen instability; buckling, ratchetting, fracture; specimen cracking; crack size, orientation, density, growth rate.
   (*c*) Failure in grip?; specimen end displacement during loading.
   (*d*) Time and cycles to failure.
3. Mechanical response of specimen
   (*a*) Displacements as $f(t)$, or
   (*b*) Load as $g(t)$.
4. Specimen response to field variables
   (*a*) Thermal distribution, heat flow . . .
   (*b*) Chemical reaction, products, diffusion, film growth, . . .
   (*c*) Accumulation of nuclear dose, induced radioactivity, decay products . . .
   (*d*) Currents for oxidation, corrosion, . . .
   (*e*) Induced currents, alignment of dipole constituents, . . .

References

[*1*] Meleka, A. H., *Metallurgical Reviews*, Vol. 7, No. 25, 1962, pp. 43–93.
[*2*] Lazan, B. J., "Creep-Fatigue Interacting Under Cyclic Loading Conditions," AFML Report ASD-TDR-63-644, AD 425551, Air Force Materials Laboratory, May 1963.
[*3*] Ellison, E. G., *Journal of Mechanical Engineering Science*, Vol. 11, No. 3, 1969, pp. 318–339.
[*4*] Van Leeuwen, H. P. and Mucuoğlu, M. C., "Requirements for an Axial Fatigue Machine Capable of Fast Cyclic Heating and Loading," NATO AGARDOgraph No. 66, AD 407088, North Atlantic Treaty Organization, Sept. 1961.

[5] Sklyarova, N. M., "Termostoykost' Zharoprochnykh Splavov," *Oborongiz*, Moskva, 1962; available as Thermal Stability of Heat-Resistant Alloys, Translation FTD-TT 63-147, OTS 64-13106, VOL. 11, No. 6, R 1236.

[6] Carden, A. E., "Bibliography of the Literature on Thermal Fatigue," Aug. 1967, NASA-CR-94605, National Aeronautics and Space Administration, N68-23652 on microfiche from National Technical Information Service.

[7] Wundt, B. M., *Bibliography on Low-Cycle Fatigue, ASTM STP 449*, American Society for Testing and Materials, 1968, (microfiche).

[8] Krempl, E. and Wundt, B. M., *Hold-Time Effects in High Temperature Low-Cycle Fatigue, ASTM STP 489*, American Society for Testing and Materials, 1971.

[9] Wells, C. H., Sullivan, C. P., and Gell, M. in *Metal Fatigue Damage—Mechanism, Detection and Repair, ASTM STP 495*, American Society for Testing and Materials, 1971, pp. 61–122.

[10] *Proceedings*, International Conference on Fatigue of Metals, Institution of Mechanical Engineers, London, 1956.

[11] *Thermal and High-Strain Fatigue*, Monograph Report No. 32, The Metals and Metallurgy Trust, London, 1967.

[12] "Creep and Fracture of Metals at High Temperatures," National Physical Laboratory, London, Her Majesty's Stationery Office, 1956.

[13] *Proceedings*, Joint International Conference on Creep, Institute of Mechanical Engineers, London, 1963.

[14] *Proceedings*, International Conference on Corrosion Fatigue, National Association of Corrosion Engineers, Storrs, Conn., June 1971.

[15] Borzdyka, A. M., "Metody Goryachikh Mekhanicheskikh Ispytanii Metallov," *Metallurgizdat*, Moskva, 1962; translation "Elevated Temperature Testing of Metals" available from Daniel Davey & Sons, Inc., New York, 1965.

[16] Pisarenko, G. S. et al, "Prochnost' Materialov Pri Vysokikh Temperaturakh," *Izdatel'stvo Naukova Dumka*, Kiev, 1966; available as "High Temperature Strength of Materials" from NTIS as NASA TT F-508 (TT 68–50308).

[17] *Manual on Low Cycle Fatigue Testing, ASTM STP 465*, American Society for Testing and Materials, 1969.

[18] Liu, S. I., Lynch, J. J., Ripling, E. J., and Sachs, G., *Transactions*, American Institute of Mining, Metallurgical, and Petroleum Engineers, Vol. 175, 1948, p. 469.

[19] Manson, S. S., *Heat Transfer Symposium*, University of Michigan Engineering Research Institute, 1953, pp. 9–75.

[20] Coffin, L. F. and Wesley, R. P., *Transactions*, American Society of Mechanical Engineers, Vol. 76, 1954, p. 923.

[21] Carden, A. E., *Proceedings*, American Society for Testing and Materials, Vol. 63, 1963, pp. 735–758.

[22] Carden, A. E., *Transactions*, American Society of Mechanical Engineers, Series D, *Journal of Basic Engineering*, Vol. 87D, March 1965, pp. 237–244.

[23] Horton, K. E., Foley, D. D., and Hallander, J. M., "Thermal Stress and Low Cycle Fatigue Data on Typical Materials," Preprint 65-GTP-13, American Society of Mechanical Engineers, 1965.

[24] *Effects of Cyclic Heating and Stressing on Metals at Elevated Temperatures, ASTM STP 165*, American Society for Testing and Materials, 1954, pp. 31–52.

[25] Coffin, L. F., *Transactions*, American Nuclear Society, Vol. 7, No. 1, 1964, p. 113.

[26] Coffin, L. F., *Transactions*, American Society of Mechanical Engineers, Series D, Sept. 1960, pp. 671–677.

[27] Carden, A. E., "Thermal Fatigue—An Analysis of the Experimental Method," ORNL TM 405, Oak Ridge National Laboratory, 1963.

[28] Stentz, R. H., Berling, J. T., and Conway, J. B., "A New Approach to Measuring Short-Term Tensile Behavior," GEMP 705, July 1969, General Electric Co., Cincinnati, Ohio.

[29] Lindholm, U. S., "Low Cycle Fatigue with Combined Thermal and Strain Cycling," this conference.

[30] Sheffler, K. D. and Doble, G. S., "Thermal Fatigue Behavior of T-111 and ASTAR 811-C in Ultrahigh Vacuum," this conference.

[31] Esztergar, E. P. and Ellis, J. R., "Cumulative Damage Concepts in Creep-Fatigue Life Prediction," *Proceedings*, International Conference on Thermal Stress and Thermal Fatigue, Berkeley, England, 1969.
[32] *Fatigue at High Temperature, ASTM STP 459*, American Society for Testing and Materials, 1969.
[33] *Proceedings*, First International Conference on Fracture, Vols. I-III, Japanese Society for Strength and Fracture of Materials, Sendai, Japan, 1965.
[34] *Fracture 1969*, Proceedings of the Second International Conference on Fracture, Brighton, 1969, Chapman and Hall, London.
[35] *Mechanical Behavior of Materials*, Proceedings of the 1971 Kyoto ICM, Six Vols., The Society of Materials Science, Japan, 1972.
[36] *Advanced Testing Techniques, ASTM STP 476*, American Society for Testing and Materials, 1970.
[37] *Proceedings*, Air Force Conference on Fatigue and Fracture of Aircraft Structures and Materials, AFFDL TR-70-144, Air Force Flight Dynamics Laboratory, 1970.
[38] Graf, M. E., *Zavodskaia Laboratoriia*, Vol. 33, No. 11, 1967, pp. 1441–1445.
[39] Johnson, H. C., Application of Electro-Hydraulic Servo Control to Physical Testing," *Proceedings*, National Conference on Fluid Power, Vol. 18, Oct. 1964.
[40] Butzow, G. N. and Churchill, R. W., "Electro Hydraulic Fatigue-Test-Systems Capabilities," SESA Paper, Annual Meeting, Society for Experimental Stress Analysis, Oct. 1964, Cleveland, Ohio.
[41] White, D. J., Horwood, G. P., and Czajkowski, Z., *Journal of Strain Analysis*, Vol. 5, Oct. 1970, pp. 284–291.
[42] Jaske, C. E., Mindlin, H., and Perrin, J. S., *Transactions*, American Society of Mechanical Engineers, Series B, Vol. 94B, Aug. 1972, pp. 930–934.
[43] Berling, J. T. and Conway, J. B., "Effect of Hold Time on the Low Cycle Fatigue Resistance of 304 Stainless Steel at 1200°F," *Proceedings*, First International Conference on Pressure Vessel Technology, University of Delft, Holland, Oct. 1969.
[44] Conway, J. B., Berling, J. T., Stentz, R. H., and Salyards, D. G., "Stress-Strain Behavior of Several Stainless Steels to Elevated Temperatures," GEMP 686, May 1969, General Electric Co., Cincinnati, Ohio.
[45] Taylor, R. E., Davis, F. E., Powell, R. W., and Kimbrough, W. D., "Determination of Thermal and Electrical Conductivity, Emittance and Thompson Coefficient at High Temperature by Direct Heating Methods," AFML-TR-69-277, AD 697 761, Air Force Materials Laboratory, Oct. 1969.
[46] Conway, J. B., Berling, J. T., and Stentz, R. H., *Nuclear Applications and Technology*, Vol. 9, July 1970, pp. 31–39.
[47] Cheng, C. F., Cheng, C. Y., Diercks, D. R., and Weeks, R. W., "Low-Cycle Fatigue Behavior of Types 304 and 316 Stainless Steel at LMFBR Temperature," this conference.
[48] Topper, T. H., Sandor, B. I., and Morrow, J., *Journal of Materials*, Vol. 4, No. 1, March 1969, pp. 189–199.
[49] Erismann, T. H., "European Trends in Fatigue Testing and New Developments in the Field of Fatigue Testing Systems," *Symposium on High Speed Fatigue Testing*, Nov. 1968.
[50] Dubuc, J. and Biron, A., "Effect of Creep in Low-Cycle Fatigue of Pressure Vessel Steel," ASME Paper 69-PVP-2, American Society of Mechanical Engineers, 1969.
[51] Dubuc, J., Vanasse, J. R., Biron, A., and Bazergui, A., "Effect of Mean Stress and of Mean Strain in Low-Cycle Fatigue of A-517 and A-201 Steels," ASME Paper 69-PVP-1, American Society of Mechanical Engineers, 1969.
[52] Jacoby, G., "Testing Machines for Metallic Materials," English translation, Boeing Co., Seattle, available from National Technical Information Service, N69-31087, April 1969.
[53] Litvak, V. I., *Problemy Prochnosti*, Vol. 3, Sept. 1971, pp. 26–30.
[54] Mason, W. P. and MacDonald, D. E., *The Use of High Power Ultrasonics (Macrosonics) in Studying Fatigue in Metals*, George Washington University, March 1971.
[55] Tien, J. K. and Gamble, R. P., *Metallurgical Transactions*, Vol. 2, July 1971, pp. 1933–1938.

[56] Hockenhull, B. S. and Hacking, R. G., *Proceedings*, Ultrasonics for Industry, 1969 Conference, London, Oct. 1969, Life Science and Technology Publication, Guildford, England.
[57] Sulima, A. M., Evstigneev, M. I., and Serebrennikov, G. Z., *Problemy Prochnosti*, Vol. 3, May 1971, pp. 107–110 (see also *Zavodskaia Laboratoriia*, Vol. 37, Jan. 1971, pp. 118–122).
[58] Sheffler, K. D., *Metallurgical Transactions*, Vol. 3, Jan. 1972, pp. 167–177.
[59] Kettunen, P. O. and Kocks, U. F., *Acta Metallurgica*, Vol. 20, Jan. 1972, pp. 95–103.
[60] Danek, C. J., Jr., and Achter, M. R., *ASTM Bulletin*, No. 234, Dec. 1958, pp. 48–52 (see also July 1959, p. 80).
[61] Martin, D. E., *Transactions*, American Society of Mechanical Engineers, Series D, Vol. 87, 1965, pp. 850–856.
[62] Felgar, R. P. *Experimental Mechanics*, Vol. 3, Nov. 1963, pp. 269–274.
[63] Stegman, R. L. and Achter, M. R., *Transactions*, Metallurgical Society, American Institute of Mining, Metallurgical, and Petroleum Engineers, Vol. 239. 1967, p. 742.
[64] Danek, G. T., Jr., Smith, H. H., and Achter, M. R., *Proceedings*, American Society for Testing and Materials, Vol. 61, 1961, pp. 775–788.
[65] Honeycutt, C. R. et al, *Transactions*, American Society for Metals, Vol. 60, No. 450, Sept. 1967.
[66] Jhansale, H. R. and Topper, T. H., "Equipment for Cyclic Deformation and Fatigue Studies in Pure Bending," Paper No. 1726, SESA Fall Meeting, Society for Experimental Stress Analysis, 1970, Boston.
[67] Lagneborg, R. and Attermo, R., *Metallurgical Transactions*, Vol. 2, July 1971, pp. 1821–1827.
[68] Hirschberg, M. H., Spera, D. A., and Klima, S. J., "Cyclic Creep and Fatigue of TD-NiCr (Thoria-Dispersion-Strengthened Nickel-Chromium), TD-Ni, and NiCr Sheet at 1200°C," NASA TN-D-6649, National Aeronautics and Space Administration, Feb. 1972.
[69] Edmunds, H. G. and White, D. J., *Journal of Mechanical Engineering Science*, Vol. 8, No. 3, 1966, pp. 310–321.
[70] White, D. J. and Radomski, M., *Journal of Strain Analysis*, Vol. 3, No. 4, 1968, pp. 313–324.
[71] Radomski, M. and White, D. J., *Journal of Strain Analysis*, Vol. 3, No. 4, 1968, pp. 304–312.
[72] Kawamoto, M., Shibata, T., Ishikawa, H., and Ibuki, Y., *Bulletin*, Japan Society of Mechanical Engineers, Vol. 14, Oct. 1971, pp. 1013–1020.
[73] Battenburg, J. R., "Multiple Specimen Fatigue Testing of Moulded Thermoplastics in Bending Utilizing High Frequency Pneumatic Excitation," Ph.D. thesis, University of Wisconsin, Madison, 1967.
[74] Getsov, L. B., Fedosov, A. I., Belolipetskii, Yu. P., and Kuptsova, N. I., *Zavodskaia Laboratoriia*, Vol. 37, Jan. 1971, pp. 98–102.
[75] Samgin, V. A., *Problemy Prochnosti*, Vol. 3, April 1971, pp. 105–108.
[76] Tinchurin, F. Z., Ivanov, V. S., and Shkanov, I. N., *Trudy*, Aviatsiia Institut, USSR, No. 105, 1969, pp. 68–77; English translation, AD 727916, FTD HC 23-864-70.
[77] Kogaev, V. P. et al, *Termoprochnost Materialov I Konstruktivnykh* Elementov, Akadademii Nauk Ukrainskoi, SSR, Institut Problemy Materialoved, Kiev, No. 5, 1969, pp. 148–152; English translation, AD 727842, FTD HT 23-98-71.
[78] Kagan, V. A. and Yu. Yu. Slavenas, *Zavodskaia Laboratoriia*, Vol. 34, Oct. 1968, pp. 1255–1256.
[79] Schramm, R. E., Durcholz, R. L., and Reed, R. P., *Journal of Research (C), Engineering and Instrumentation*, Vol. 75C, April-June 1971, pp. 95–98.
[80] James, L. A., *Closed Loop*, (MTS Systems Corp), Vol. 3, No. 1, 1971, pp. 7–10.
[81] Brown, B. B., "High Temperature Fatigue Test System," Watervliet Arsenal, WVT 6914, AD 698463, Oct. 1969.
[82] Kiss, E., Heald, J. D., and Hale, D. A., "Low Cycle Fatigue of Notched Prototype Piping," ASME Paper 71-WA/PVP-4, American Society of Mechanical Engineers, 1971.

[*83*] Brazewicz, W. and Jancolewicz, B., *Politechnika Warazawska*, Zeszyty Naukowe, Mechanika, No. 25, 1968, pp. 109–129.
[*84*] Topper, T. H., Gowda, C. V. B., Havard, D. G., and Jhansale, H. R., *Journal of Materials*, Vol. 6, Dec. 1971, pp. 842–861.
[*85*] Gindin, I. A., Starodubov, Ya D., and Starolat, M. P., *Zavodskaia Laboratoriia*, Vol. 37, April 1971, pp. 488–489.
[*86*] Lalli, V. R., Kececioglu, D., and McConnell, J. B., "Design Features and Results from Fatigue Reliability Research Machines," SESA Paper, Fall Meeting, Society for Experimental Stress Analysis, Oct. 1971, Milwaukee.
[*87*] Griaznov, B. A., Kaplinskii, L. A., and Troian, I. A., *Problemy Prochnosti*, Vol. 3, Sept. 1971, pp. 113–115.
[*88*] Boichuk, V. M., *Problemy Prochnosti*, Vol. 3, April 1971, pp. 53–55.
[*89*] Taira, S., Inoue, T., and Yoshida, T., "Low Cycle Fatigue Under Multiaxial Stresses (In the Case of Combined Cyclic Tension-Compression and Cyclic Torsion Out-of-Phase at Elevated Temperature)," *Proceedings*, 11th Japan Congress on Materials Research, Kyoto, 1968, pp. 60–65.
[*90*] Carden, A. E., *Papers*, JSME SemiInternational Symposium, Japan Society of Mechanical Engineers, Sept. 1967, Vol. I, 1967, pp. 65–73.
[*91*] Havas, Istvan, *Materialprufung*, Vol. 10, No. 5, 1968, pp. 151–154.
[*92*] Tilly, G. P., *Journal of Strain Analysis*, Vol. 2, No. 3, 1967, pp. 220–225.
[*93*] Tilly, G. P., *Proceedings*, Institute of Mechanical Engineers, 1965–1966, Vol. 180, Part 3I, p. 403.
[*94*] Wundt, B. M. and Curran, R. M., "Metals Properties Council Program to Study Low-Cycle Fatigue and Creep Interaction in Steels at Elevated Temperatures," paper presented at ASME Petroleum Division and PVP Conference, New Orleans, Sept. 1972.
[*95*] Kikukawa, M., Ohji, K., and Ogura, K., *Transactions*, American Society of Mechanical Engineers, Series D, Vol. 87D, 1965, pp. 857–864.
[*96*] Forrest, P. G. and Penfold, A. B., *Engineering*, 1961, Vol. 192, pp. 522–523.
[*97*] Neuber, H. and Riege, H., "Thermal Fatigue," TR-68-301, Part I, Air Force Materials Laboratory, Feb. 1970, from National Technical Information Service, AD 706376.
[*98*] Chow, J. G. Y., "High Cycle Fatigue Properties of LMFBR Materials," this conference.
[*99*] Thiruvengadam, A. and Conn, A. F., *Experimental Mechanics*, Vol. 11, July 1971, pp. 315–320.
[*100*] Organ, F. E. and Gell, M., *Metallurgical Transactions*, Vol. 2, 1971, pp. 943–952.
[*101*] MacDonald, D. E. and Wood, W. A., *Journal of Applied Physics*, Vol. 42, Dec. 1971, pp. 5531–5533.
[*102*] Hockett, J. E. and Gillis, P. P., *International Journal of Mechanical Sciences*, Vol. 13, 1971, pp. 265–275.
[*103*] Voorhees, H. R., *A Survey of Effects of Lower-than-Usual Rates of Strain on the Yield and Tensile Strengths of Metals, ASTM DS 44*, American Society for Testing and Materials, 1969.
[*104*] Keil, E. et al, *Materialprufung*, Vol. 10, No. 4, April 1968, pp. 116–121.
[*105*] Ellison, E. G. and Sullivan, C. P., *Transactions Quarterly*, American Society for Metals, Vol. 60, 1967, pp. 88–98.
[*106*] Carden, A. E., "Time and Cycle Dependent Fracture of Materials at Elevated Temperature," III Interamerican Conference on Materials, Rio de Janerio, Aug. 1972.
[*107*] Dorn, J. E., ed., *Mechanical Behavior of Materials at Elevated Temperature*, McGraw-Hill, New York, 1961.
[*108*] Kennedy, A. J., *Processes of Creep and Fatigue in Metals*, Wiley, New York, 1963.
[*109*] Pugh, J. W. in *High Temperature Materials and Technology*, Wiley, New York, 1961.
[*110*] Havard, D. G. and Topper, T. H., "New Equipment for Cyclic Biaxial Testing," paper No. 1519, SESA Fall Meeting, Society for Experimental Stress Analysis, Oct. 1969.
[*111*] Zamrik, S. Y. and Goto, T., "The Use of Octahedral Shear Strain Theory in Biaxial Low Cycle Fatigue," Interamerican Conference on Materials Technology, San Antonio, American Society of Mechanical Engineers, 1968.

[112] Kennedy, C. R., *Fatigue of Aircraft Structures, ASTM STP 338*, American Society for Testing and Materials, 1962, pp. 92–104, (see also ORNL 3398, 1963).
[113] Miller, W. R., "A Review of Torsional Fatigue Literature: Recommendations in Design and Testing," DM-70, Pratt & Whitney Aircraft Report, Aug. 1967.
[114] Carden, A. E., "Bibliography of the Literature on Multiaxial Stress Fatigue," Report MH-67-AEC-2, University of Alabama Bureau of Engineering Research, Aug. 1967.
[115] Esztergar, E. P., "Creep-Fatigue Interaction and Cumulative Damage Evaluations for Type 304 Stainless Steel," ORNL 4757, Oak Ridge National Laboratory, 1972.
[116] Mattavi, J. L., *Transactions*, ASME, American Society of Mechanical Engineers, *Journal of Basic Engineering*, Vol. 91D, 1969, pp. 23–31.
[117] Carden, A. E., "Thermal-Fatigue Resistance: Material Geometric, and Temperature Field Considerations," ASME paper, 65-GTP-5, American Society of Mechanical Engineers, 1965.
[118] Pirogov, E. N., *Atomizdat*, 1969, pp. 22ff.
[119] Nippes, E. F. and Uy, J. C., *Welding Journal Research Supplement*, Vol. 46, No. 8, Aug. 1967, pp. 371s–379s.
[120] Krempl, E., *Materialprufung*, Vol. 5, No. 7, July 1963, pp. 274–283.
[121] Neuber, H. and Riege, H., "Thermal Fatigue," AMFL TR-68-301, AD 706375, Part II, Air Force Materials Laboratory, March 1970.
[122] Kawamoto, M., Tanaka, T., and Nakajima, H., *Journal of Materials*, Vol. 1, No. 4, Dec. 1966, pp. 719–758.
[123] Dul'nev, R. A., *Zavodskaia Laboratoriia*, Vol. 32, No. 8, pp. 988–991, Aug. 1966; *Industrial Laboratories*, pp. 1217–1220.
[124] Sobolev, N. D. and Pirogov, E. N., *Zavodskaia Laboratoriia*, Vol. 32, No. 8, 1966, pp. 984–987.
[125] Sobolev, N. D. and Pirogov, E. N., *Zavodskaia Laboratoriia*, Vol. 33, No. 5, 1967, pp. 617–620.
[126] Egorov, V. I., Pirogov, E. N., and Sobolev, N. D., *Zavodskaia Laboratoriia*, Vol. 33, No. 7, 1967, pp. 878–881.
[127] Strizhalo, V. A., *Zavodskaia Laboratoriia*, Vol. 33, No. 5, 1967, pp. 620–622.
[128] Strizhalo, V. A., *Zavodskaia Laboratoriia*, Vol. 33, No. 3, 1967, pp. 367–369.
[129] Strizhalo, V. A. and Sinyavski, D. P., *Zavodskaia Laboratoriia*, Vol. 34, No. 5, 1968, pp. 589–590.
[130] Filatov, V. M., *Zavadskaia Laboratoriia*, Vol. 33, No. 9, 1967, pp. 1161–1162.
[131] Sinaiskit, B. N., *Problemy Prochnosti*, Vol. 3, July 1971, pp. 62–68.
[132] Grigor'ev, F. and Meshcheriakov, M. P., *Prochnost' i Dinamika Aviatsionnykh Dvigatelei*, No. 6. 1971, pp. 182–185.
[133] Petrenko, I. and Tret'iachenko, G. N., *Problemy Prochnosti*, Vol. 2, Oct. 1970, pp. 78–83.
[134] Voloschchenko, A. P., Tret'iachenko, G. N., and Makovetskii, I. V., *Problemy Prochnosti*, Vol. 2, June 1970, pp. 3–9.
[135] Spera, D. A., Calfo, F. D., and Bizon, P. T., "Thermal Fatigue Testing of Simulated Turbine Blades," Paper No. 710459, National Air Transportation Meeting, Society of Automotive Engineers, Atlanta, May 1971.
[136] Johnson, J. R. and Ashbrook, R. L., "Oxidation and Thermal Fatigue Cracking of Nickel- and Cobalt-Base Alloys in a High Velocity Gas Stream," NASA-TN-D 5376, National Aeronautics and Space Administration, Aug. 1969.
[137] Krishtall, M. A., Renne, I. P., and Ksurin, A. A., *Zavodskaia Laboratoriia*, Vol. 37, May 1971, pp. 596–598.
[138] Kiselevskii, V. N. in *Strength and Plasticity*, Izdatel'stvo, Nauka, 1971, pp. 350–354.
[139] Naumann, E. C. and Corbin, P. L., "Automatic Fatigue Test Temperature Programmer," U.S. Patent Application SN 576182, 1966.
[140] Nealy, D. A., Anderson, R. D., and Hufford, A. A., "Experimental Evaluation of Low Cycle Thermal Fatigue in a Turbine Vane Fabricated from Laminated Porous Material," NASA Report CR 72954, DDAD-EDR-7034, National Aeronautics and Space Administration, 1971.
[141] Molchanov, E. I. and Truchechkin, V. P., *Zavodskaia Laboratoriia*, Vol. 34, No. 10, Oct. 1968, pp. 1257–1258.

[*142*] Rostoker, W., *Journal of Materials*, Vol. 4, No. 1, March 1969, pp. 117–144.
[*143*] Howes, M. A. H., "Evaluation of Thermal Fatigue Resistance of Metals Using the Fluidized Bed Technique," this conference.
[*144*] Howes, M. A. H., "Thermal Fatigue Data on 15 Nickel and Cobalt Base Alloys," NASA CR-72738, IITRI B6078-38, National Aeronautics and Space Administration, May 1970.
[*145*] Mobray, D. F., Woodford, D. A., and Brandt, D. E., "Thermal Fatigue Crack Propagation in Cast Cobalt- and Nickel-Base Superalloys," this conference.
[*146*] Stetson, A. R., "Thermal Fatigue Tests of Diffusion Coated Alloys," RDR 1399, Jan. 166, report to ASTM C22 Ad Hoc Subcommittee.
[*147*] Stetson, A. R., private communication, with Solar Research, Memo R 66-863, 22 Sept. 1966 and R66F-927, 16 Nov. 1966, "Table Model Thermal Fatigue Unit" and "Hole-in-Plate Thermal Fatigue Unit."
[*148*] Steverding, B., *Journal of Physics*, Series D, *Applied Physics*, Vol. 4, June 1971, pp. 787–792.
[*149*] Heinz, T. A., "Thermal Tube Buckling Consideration for Nuclear Rocket Nozzles," AIAA Paper 66–583, 2nd Joint Propulsion Specialist Conference, Colorado Springs, 1966.
[*150*] Harman, D. G., "Thermal Fatigue of Rocket Nozzle Cooling Tubes," Report TM 2089, Oak Ridge National Laboratory, Feb. 1969.
[*151*] Richard, C. E. et al "Low Cycle Fatigue Evaluation for Regeneratively Cooled Panels," Airesearch Manufacturing Co., NASA CR 1884, National Aeronautics and Space Administration, Oct. 1971.
[*152*] Luft, W. and Maiden, E., *Proceedings*, American Institute of Chemical Engineers, Intersociety Energy Conversion Engineering Conference Washington, D. C., Sept. 1969, pp. 582–589.
[*153*] Bree, J., *Journal of Strain Analysis*, Vol. 3, No. 2, 1968, pp. 226–238.
[*154*] Anderson, W. F., "Creep Ratcheting Deformation and Rupture Damage Induced by a Thermal Transient Stress Cycle," paper presented at ASME meeting, American Society of Mechanical Engineers.
[*155*] Stentz, R. H., "A New Thermal Ratcheting Test Technique," paper presented at ASTM meeting, American Society for Testing and Materials, Bal Harbor, Fla., 1971.
[*156*] Burgreen, D., *Transactions*, American Society of Mechanical Engineers, Series D, Vol. 90, 1968, pp. 319–324, 469–475.
[*157*] Martin, W. R., "Mechanical Cladding-Fuel Interactions During Thermal Cycling of Metal Clad Fuel Elements," ORNL 3514, Oak Ridge National Laboratory, March 1965.
[*158*] Yamanouchi, H. and Wakamatsu, Y., "Ratchetting Under Cyclic Axial Strain With Torsional Stress," this conference.
[*159*] Shahinian, P., Smith, H. H., and Watson, H. E., To be published in *Transactions*, American Society of Mechanical Engineers, (ASME Paper 71-PVP-25).
[*160*] *Fatigue Crack Propagation, ASTM STP 415*, American Society for Testing and Materials, 1967.
[*161*] Brothers, A. J., "Fatigue Crack Growth in Nuclear Reactor Piping Steels," Report GEAP-5607, General Electric Co., March 1966 (Paper 66MET2) American Society of Mechanical Engineers.
[*162*] James, L. A. and Schwenk, E. B., *Metallurgical Transactions*, Fol. 2, Feb. 1971, pp. 491–496.
[*163*] James, L. A., "The Effect of Frequency upon the Fatigue-Crack Growth of Type 304 Stainless Steel at 1000°F," Fifth National Symposium on Fracture Mechanics, *ASTM STP 513*, American Society for Testing and Materials, 1972, pp. 218–229.
[*164*] James, L. A., "The Effect of Stress Ratio on the Elevated Temperature Fatigue Crack Propagation of Type 304 Stainless Steel," *Nuclear Technology*, Vol. 14, May 1972, pp. 163–170.
[*165*] McHenry, H. I. and Pense, A. W., "The Influence of Temperature of Fatigue Crack Propagation in A517F Steel," *Metallurgical Transactions*, 1973.
[*166*] McHenry, H. I., "Fatigue Crack Propagation in Steel Alloys at Elevated Temperature," Convair Report ERR-FW-1029, General Dynamics, Sept. 1970.

[167] Harrison, C. B., "Crack Propagation High Temperature Low Cycle Fatigue," Ph.D. thesis, Rensselaer Polytechnic Institute, Troy, N. Y., 1969.
[168] Hoeppner, D., Danforth, V., and Pettit, D. E., *Experimental Mechanics*, Vol. 11, June 1971, pp. 280–283.
[169] Neudecker, J. W., Lawton, R. G., and Stoddard, S. D., "Moire-Fringe Techniques at Extremely High Temperatures," SESA Paper 1574, Fall Meeting, Society for Experimental Stress Analysis, Houston, Oct. 1969.
[170] Luxmoore, A. and Wyatt, P. J., *Journal of Strain Analysis*, Vol. 5, Oct. 1970, pp. 302–308.
[171] Markochev, V. M., Gol'shev, V. Yu., and Bobrinski, "On the Measurements of Crack Length in Material by the Method of Electrical Potential," *Zavodskaia Laboratoriia*, Vol. 37, No. 5, 1971, pp. 598–600.
[172] Loginov, N. Z. and Shkanov, I. N., *Trudy*, Seriia Prikladnaia Mekhanika, Kazanskii Aviatsionnyi Institut, No. 95, 1968, pp. 111–116.
[173] Papirno, R. and Parker, B. S., "An Automatic Flash Photomicrographic System for Fatigue Crack Initiation Studies," paper presented at ASTM meeting, American Society for Testing and Materials, Bal Harbor, Fla., Dec. 1971.
[174] *Applications of Electron Microfractography to Materials Research, ASTM STP 493*, American Society for Testing and Materials, 1970.
[175] Kubiak, E. J., *Metal Progress*, Vol. 94, Dec. 1968, pp. 131–133.
[176] Marom, E. and Mueller, R. K., *International Journal of Nondestructive Testing*, Vol. 3, Sept. 1971, pp. 171–187.
[177] *Materials Research and Standards*, Vol. 11, No. 9, 1971, pp. 1–72.
[178] Dunegan, H. L., Harris, D. O., and Tetelman, A. S., *Materials Evaluation*, Vol. 28, No. 10, Oct. 1970, pp. 221–227.
[179] Clark, W. G. and Ceschini, L. J., *Materials Evaluation*, Vol. 27, Aug. 1969, pp. 180–184.
[180] Jeglic, F., Niessen, P., and Burns, D. J., *Experimental Mechanics*, Vol. 11, Feb. 1971, pp. 82–85.
[181] Manjoine, M., private communication.
[182] McHenry, H. I., *Journal of Materials*, Vol. 6, Dec. 1971, pp. 862–863.
[183] Sallade, P. L. and Clark, H. McI., "Fatigue Crack Propagation in Ti-6Al-4V Sheet at 80,550,830 and 1150°F," submitted for publication, *Metallurgical Transactions*.
[184] Lewis, R. P., M. S. thesis, University of Connecticut, Storrs, 1972.
[185] Hahn, G. T., Rosenfield, A. R., and Sarrate, M., in Ref. *37*, pp. 425–559.
[186] Pelloux, R. N. M., Erhardt, K., Wilson, A., and Grant, N. J., "Mechanisms of Fatigue Crack Propagation in Aluminum Alloys," AD 728659, AFML-TR-71-109, Air Force Materials Laboratory, May 1971.
[187] Pelloux, R. N. M., *Applications of Modern Metallographic Techniques, ASTM STP 480*, American Society for Testing and Materials, 1970, pp. 127–130.
[188] Van Leeuwen, H. O., "Heating Methods in Materials Testing at Elevated Temperatures," Nationaal Lucht—en Ruimtevaartlaboratorium, The Netherlands, TM-M 2087, April 1961.
[189] Kiselevskii, V. N. and Chuprina, A. F., *Zavodskaia Laboratoriia*, Vol. 31, No. 6, 1965, pp. 740–741.
[190] "High Density Radiant Heater," Data Bulletin D518.1, Research, Inc., Minneapolis, Minn.
[191] Swindeman, R. W., Oak Ridge National Laboratory, private communication, April 1971 (CF 71-4-58, pp. 41, 48).
[192] Avery, L. R., Carayanis, G. S., and Michky, G. L., *Experimental Mechanics*, Vol. 7, No. 6, June 1967, pp. 256–264.
[193] Neudecker, J. W. and King, C. R., "Thermal-Fatigue Tests of Rocket Nozzle Coolant Tubes," SESA Paper, Fall Meeting, Society for Experimental Stress Analysis, 1969, Houston.
[194] Mulcahy, T. M. and Shoemaker, E. M., *International Journal of Solids and Structures*, Vol. 6, No. 7, July 1970, pp. 1011–1019.
[195] Egorov, V. I., Kostin, V. M., and Sobolev, N. D., *Zavodskaia Laboratoriia*, Vol. 37, No. 8, Aug. 1971, pp. 964-967.

[196] Steele, Roger, Ph.D. dissertation, University of Connecticut, Storrs, Conn., in preparation.
[197] Paxton, M. M., *Elevated Temperature Testing Problem Areas, ASTM STP 488*, American Society for Testing and Materials, 1971, pp. 95–99.
[198] Swaroop, A., Ph.D. dissertation, University of Connecticut, Storrs, Conn., in preparation.
[199] Pavlovskii, V. E. Ishchenko, I. I., and Belokurov, V. N., *Prikladnaia*, Mekhanika, Vol. 7, March 1971, pp. 126–129.
[200] Coffin, L. F., *Transactions*, American Institute of Mining, Metallurgical, and Petroleum Engineers, Vol. 230, 1964, pp. 1690–1699.
[201] Horton, K. E., "Investigation of Thermal-Stress-Fatigue Behavior of Stainless Steels, Summary of Test Results on Types 304 and 304-L Stainless Steels," ATL-A-141, EURAEC 1034, Advanced Technology Laboratory, April 1964.
[202] Kaufman, E., *Measurements and Data*, July-Aug. 1970, p. 83.
[203] Winslow, H. J., *MTS Closed Loop*, Vol. II, No. 4, 1969, pp. 14–18.
[204] Swanson, S. R. and Winslow, H. J., "Extensometry for Elevated Temperature Fatigue Testing," submitted for publication.
[205] Robinson, D. C., "Determination of Dynamic Loads in a High Frequency Direct Stress Fatigue Machine," NBS-TN-578, National Bureau of Standards, July 1971.
[206] Strizhalo, V. A. and Shestopal, L. F., *Problemy Prochnosti*, Vol. 3, Sept. 1971, pp. 109–112.
[207] Troshchenko, V. T., Khamaza, L. A., and Shestopal, L. F. in *Fatigue of Metals and Alloys*, Izdatel'stvo Nauka, Moskva, 1971, pp. 31–41.
[208] Lozinskii, M. G., Marichev, V. A., Afonskaia, V. V., and Klimov, A. V., *Zavodskaia Laboratoriia*, Vol. 35, No. 3, Mar. 1969, pp. 341–343.
[209] Skoe, R. E. and Swanson, S. R. in *Advanced Testing Techniques, ASTM STP 476*, American Society for Testing Materials, 1970, pp. 59–78.
[210] Naumann, E. C. and Bryant, E. L., "Fatigue Testing Device," patent, NASA Case XLA-02131, Feb. 1967, U.S. Patent 3,304,768.
[211] Richards, F. D. and Wetzel, R. M., *Materials Research and Standards*, Feb. 1971, pp. 19–22, 51.
[212] Il'iushin, A. A. *Elasticity and Inelasticity*, No. 1, Izdatel'stvo Moskovokogo Universiteta, Moscow, 1971, pp. 52–58.
[213] Smith, H. H. and Shahinian, P. in *Effects of Environment and Complex Load History on Fatigue Life, ASTM STP 462*, American Society for Testing and Materials, 1969, pp. 217–233.
[214] Pisarenko, G. S. in *Strength and Plasticity*, Izdatel'stvo, Nauka, Moscow, 1971, pp. 372–380.
[215] La Force, R., Berning, R. F., and Coffin, L. F., "High Temperature Low Cycle Fatigue Behavior of Tantalum," NASA-CR-1930 (GESP 595), National Aeronautics and Space Administration, Sept. 1971.
[216] Aubry, B. and Bernadict, H. in *Proceedings*, International Vacuum Congress, 4th, University of Manchester, Manchester, England, April 1968, Part 2, pp. 787–790.
[217] Swoboda, H., *DFL Mittielungen*, Dec. 1968, pp. 415–417.
[218] Hardrath, H. F. in *Advanced Testing Techniques, ASTM STP 476*, American Society for Testing and Materials, 1970, pp. 79–95.
[219] Petersen, V. C., *Journal of Metals*, Vol. 23, April 1971, pp. 40–47.
[220] Prevey, P. S. and Koster, W. P., "Effect of Surface Integrity on Fatigue of Structural Alloys at Elevated Temperature," this conference.
[221] Bellows, G. and Niemi, R. M., "Surface Integrity of Machined Inconel 718 Alloy," Paper No. 71–239, Society of Manufacturing Engineers, International Engineering Conference and Tool Exposition, April 1971.
[222] Korenevskii, E. Ya. and Yatsenko, V. K., *Problemy Prochnosti*, Vol. 3, March 1971, pp. 15–20.
[223] Gedwill, M. A. and Grisaffe, S. J., "Oxidation Resistant Claddings for Superalloys," NASA-TM-X-67925, National Aeronautics and Space Administration, Oct. 1971.
[224] Wilkov, M. A. in *Mechanics of the Solid State*, University of Toronto Press, Toronto, 1968, pp. 259–270.

R. M. Schneiderovitch[1] *and A. P. Gusenkov*[1]

Discussion of the Test Method and Equipment for the Evaluation of Low-Cycle Creep-Fatigue Failure Criteria

REFERENCE: Schneiderovitch, R. M. and Gusenkov, A. P., "**Discussion of the Test Method and Equipment for the Evaluation of Low-Cycle Creep-Fatigue Failure Criteria,**" *Fatigue at Elevated Temperatures, ASTM STP 520,* American Society for Testing and Materials, 1973, pp. 224–230.

ABSTRACT: The formulation of failure criteria for cyclic loading at elevated temperature must be based on a large quantity of experimental data. The design of the experiments and the particular test method used for such formulation is the subject of this paper. Several schemes for controlling the independent variables are described, and the requirements for isothermal and cyclic thermal creep and fatigue tests with load or strain control provision are illustrated by equipment developed at the author's laboratory.

KEY WORDS: fatigue (materials), fatigue tests, cyclic loads, isothermal treatment, creep tests, stress-strain diagrams, thermal cycling tests

The study of isothermal and cyclic thermal low-cycle fatigue failure involving low cyclic frequencies and significant creep deformations is the subject of this paper. The design of laboratory experiments requires consideration of the failure of materials by creep, low-cycle fatigue, and of the interaction of creep and fatigue when deformation and "damage" from both sources accrue in a single element. Such study is of greater practical interest. A discussion of how such empirical information is used in the synthesis of a failure criterion is the subject of a companion paper at the present symposium.[2] It is necessary for the experimenter to decide which parameters must be controlled and recorded so that the essential characteristics of a material may be defined. The results of the cyclic stress strain behavior is also useful in describing the constitutive equations. The analysis of the elevated temperature behavior of real materials subjected to cyclic deformation requires much more empirical information than for low temperature.

The repetition of creep or relaxation or both in a periodic cycle leads to the accumulation of creep damage and eventual failure. When such creep

[1] Mechanical Engineering Research Institute, Moscow-Centre, USSR.

[2] See p. 670.

Copyright© 1973 by ASTM International www.astm.org

deformation is interspersed with rapid changes in load and low-cycle fatigue damage (that is, high strain rate plastic deformation), the results of an interaction of the creep and fatigue damage are such that the time to failure is not governed by a single cause but by the combination and interaction of two processes. The study of creep-fatigue damage accumulation and failure requires information from three basic kinds of mechanical property tests: (1) creep (stress rupture with a record of the strain to failure), (2) low-cycle fatigue behavior, and (3) creep-fatigue interaction behavior.

There are several experimental difficulties connected with the design and conduct of such experiments. First, the low-cycle fatigue tests must be conducted at a high frequency so that creep will be excluded from the deformation. Second, the low-cycle fatigue properties are known to be temperature dependent. In order to surmount the experimental difficulty of time dependent behavior the highest frequency low-cycle fatigue data will be assumed to be time independent. It is further assumed that these data fit the Coffin-Manson description of low-cycle fatigue failure. This supposition must be experimentally verified.

It is of great importance to include in the creep-fatigue experiments the provision for varying the ratio of creep strain in the high strain rate plastic deformation over a wide range of values. Moreover, the temperature range must span the region from low temperature where no appreciable creep occurs to the regime where creep deformation is the primary constituent of the inelastic strain. Even though such wide ranges of variation of the parameters may not have direct use in design, nevertheless they aid in formulating a parametric approach to fracture, similar to the parameter methods for stress rupture.

Requirements for the Test Method

The foregoing requirements are best satisfied by: (1) load controlled and (2) strain controlled cyclic testing. In such tests, the extremes of the cycle are fixed as an independent variable. The rate of load or deformation between extremes is constant. The argument here is that both kinds of tests are needed.

The typical variation of stress and strain with time are shown in Fig. 1 for two types of creep-fatigue experiments. In Fig. 1*a* the load controlled test is maintained at a high cyclic frequency. In Fig. 1*b* a hold period at constant load amplitude is included at each extreme of the cycle. Figure 1*c* is a strain controlled test with dwells at each extreme of the strain cycle. In the test condition represented by Fig. 1*b* the ratio of creep to plastic strain can be varied over a wide range. In Fig. 1*c* the maximum amount of time dependent deformation is limited. The hysteresis loops from each of these tests are of great value in describing the cyclic characteristics of the material. These data, in addition to the fracture information, can be utilized

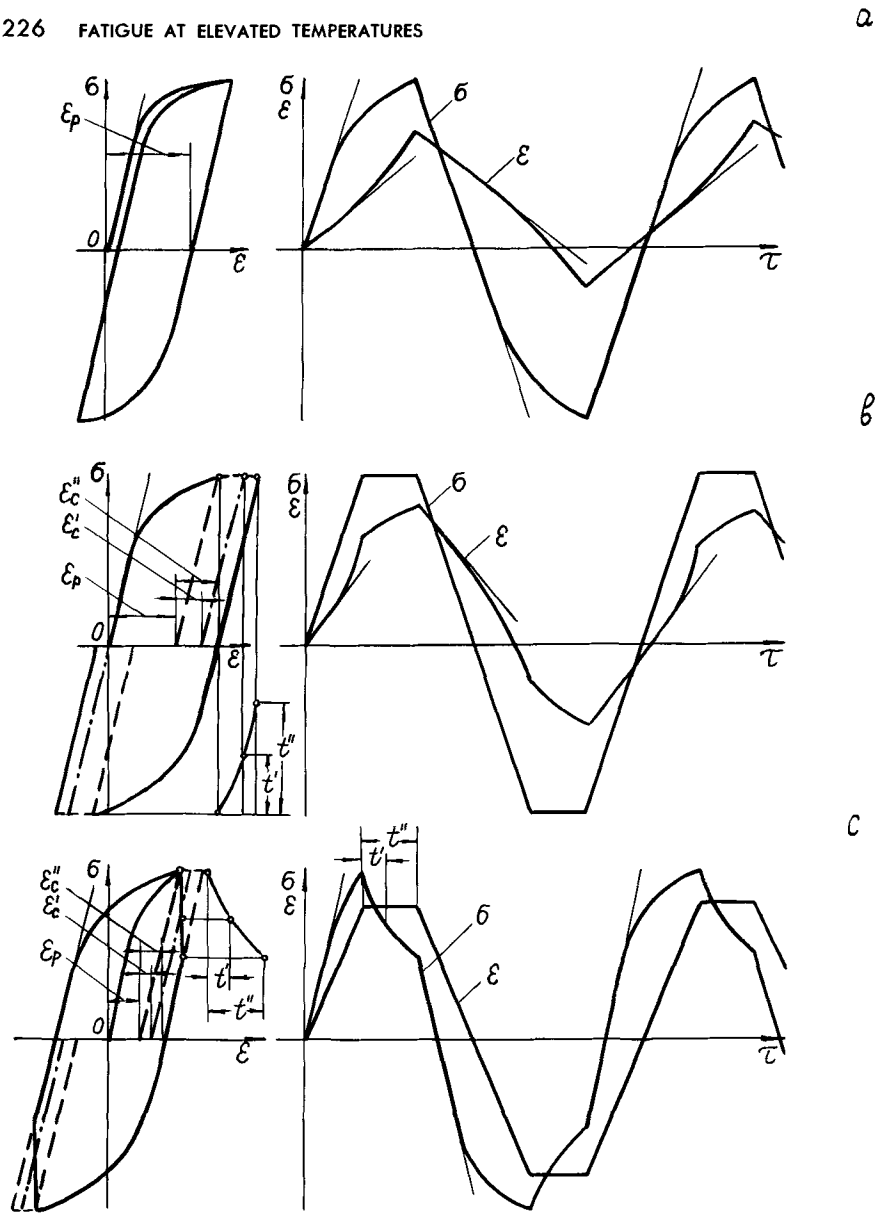


FIG. 1—*Schematic of hysteresis loops and stress strain-time relationships for creep-fatigue experiments.*

in design, that is, the cyclic stress strain data can be used to formulate a general constitutive equation of the material.

It is also desirable to formulate failure criteria for both isothermal and cyclic thermal creep-fatigue conditions. In the cyclic thermal situation care must be taken to seek out the possible arrangements between the thermal and mechanical deformation cycles that will bound the extremes in real

behavior. Idealized schematic diagrams of the possible variations in the two programs are shown in Fig. 2. These schemes are shown without dwells.

The first case of thermal-mechanical loading includes a thermal cycle frequency twice as great as the mechanical cycle. Two such schemes are shown in Figs. 2*a* and *b*. In Fig. 2*a* the minimum and maximum stress occurs at the time of maximum temperature. The time where the stress passes through zero occurs at the minimum temperature. The reverse of such a scheme is shown in Fig. 2*b*. In this case the time of zero stress always occurs at the maximum temperature, the extremes of load occur at the minimum temperature. In Fig. 2*c* the frequencies of the two programmed cycles are equal, and the thermal and mechanical cycles can be in-phase or out-of-phase. The in-phase cycle is shown in Fig. 2*c*. The out-of-phase condition

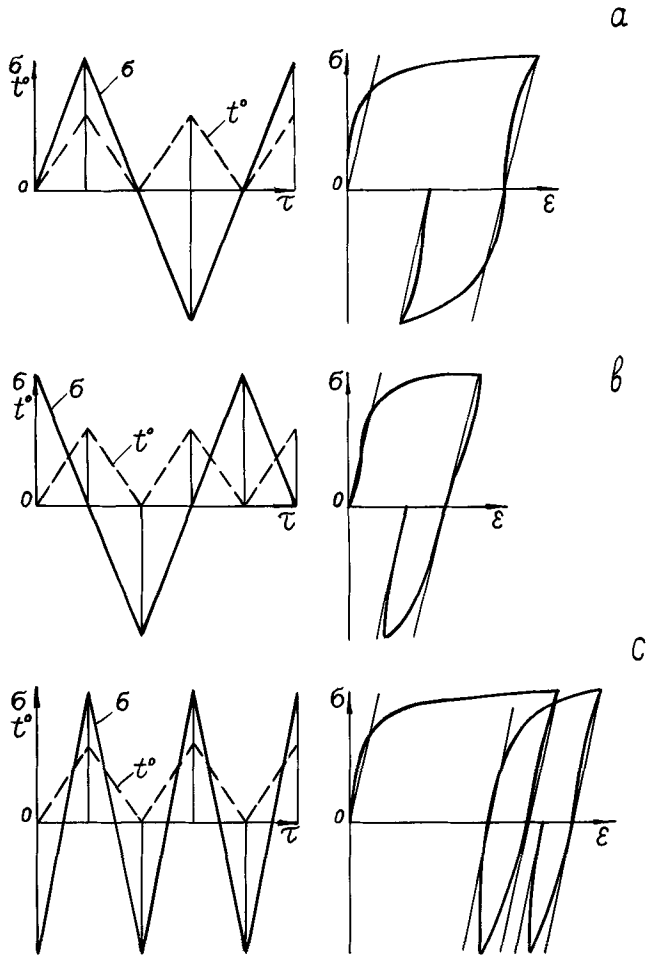


FIG. 2—*Stress and temperature program with accompanying hysteresis loops for thermal-mechanical test facility.*

is very similar to the case of thermal fatigue where a member is loaded during heating because of some deformation constraint.

Based on the above discussion the principal requirements for the design of low cycle creep fatigue experiments can now be stated:

1. The test facility must include:

(*a*) Short time monotonic tensile capacity with controlled loading or straining rates, (sufficient information must be recorded so that the proportional limit, yield and ultimate strength, and strain to failure values can be obtained).

(*b*) Constant load creep tests with strain-time curves and explicit determination of the strain to failure values.

(*c*) Low-cycle fatigue tests with provisions for both load and strain limiting control.

(*d*) Low-cycle creep-fatigue tests with stress or strain controlled loading.

The variation of the strain and load with time must be obtained for all tests as well as stress-strain relationships (hysteresis loops) for all but the constant load creep tests.

2. The time variation of stress, strain, and temperature must be recorded throughout the test.

3. The thermal control must be independently programable, but there should be means for synchronization of the thermal and mechanical cycles.

4. Test frequency, length of dwells, range of temperature, and load levels must include a wide range of programability.

5. Metallographic examination of the specimens must accompany the mechanical results of these experiments.

Description of the Present Facility

At the Mechanical Engineering Research Institute several devices for conducting the above types of tests were developed. Three types of machines are in use for generating the necessary data for the evaluation of low-cycle creep-fatigue failure criteria. The first kind is used to generate monotonic tensile and low-cycle fatigue test data with a large variation of the load or strain rate. The time to failure for medium strength steel has been obtained over the range of 15 s to 15 h of test time. The second type of test is used for low-cycle fatigue and low-cycle creep tests. These first two types of machines have a ± 10 ton load capacity and frequency ranges of from 0.002 to 2 cpm.

The third type of machine has the capacity for independent programing of temperature and strain (or load) including dwells. All of the machines are driven mechanically. Control of the load (or deformation) is derived through the control of the motor of the crosshead drive system. Some of these machines cannot be used for programed loading rate, since only the

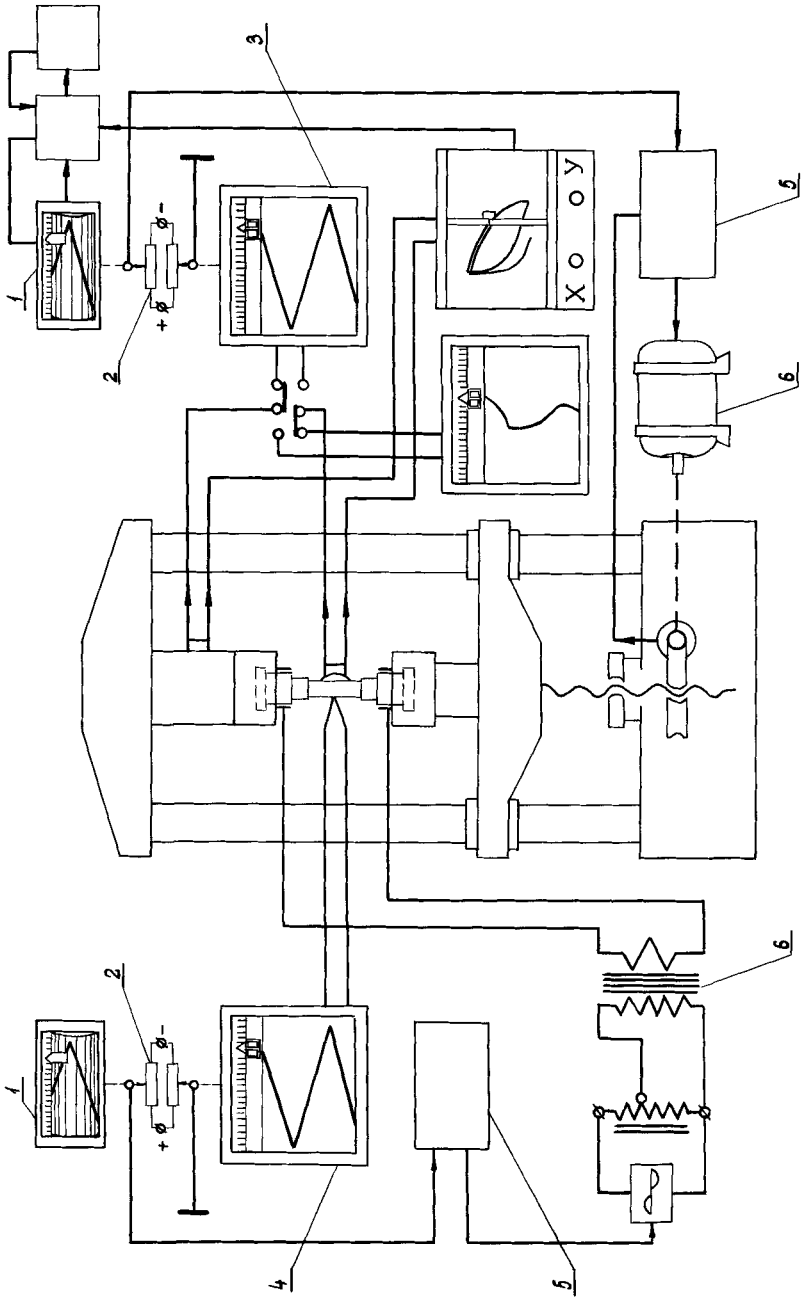


FIG. 3—*Schematic of two-program creep-fatigue test facility.*

extremes of the cycle are controlled. The characteristic stress-strain relationship is shown in Fig. 1*a*.

Static creep tests are performed in lever type constant-load machines with a maximum force of five tons. Specimens for tension-compression tests are used for creep tests also. The heating method for all tests is conduction, that is, resistance heating of the specimen. A continuous record of diametral strain is obtained for all tests.

For the third type of machine a closed-loop system is used, since the thermal and mechanical programs must be separately and synchronously controlled. A number of references can be found in the literature describing servocontrolled test equipment [*1–4*].[3] A schematic diagram for such a testing machine is shown in Fig. 3.

The programs (command signals) for the thermal and mechanical variables are introduced at (1), the indicating and recording of the variables is at (3,4); the feedback and error sensing amplifiers (5) operate in conjunction with the control element (6). The programers and feedback signals are introduced into a bridge network (2). When the bridge is unbalanced the output signal is directed to the error amplifier that provides a signal to the control element. The controller functions to eliminate the unbalance. The parameters can be controlled within ± 1 percent and the period for zero to maximum load is about 1 min. The frequency for cycling is limited to 0.05 to 1 cpm. The period of temperature dwells is from 1 min to 18 h. Accuracy of the program during dwell is ± 2.5 percent; without dwell ± 0.5 percent.

Summary

The test equipment described in this report allows great flexibility in programing uniaxial loading creep-fatigue experiments. Tests with the following controlled variables can be performed in the facility described: (1) separate, arbitrary, synchronous programs of temperature and load; (2) constant load or deformation velocity; (3) isothermal and cyclic-thermal low-cycle fatigue with three kinds of arrangements between the thermal and mechanical cycles, and (4) isothermal and cyclic thermal creep and relaxation. The primary utility of the data obtained from the facility is in the formulation of criteria for creep-fatigue failure.

References

[1] Hirschberg, M. in *Manual on Low Cycle Fatigue Testing*, *ASTM STP 465*, American Society for Testing and Materials, 1969, pp. 67–86.

[*2*] Skoe, R. E. and Swanson, S. R. in *Advanced Testing Techniques*, *ASTM STP 476*, American Society for Testing and Materials, 1970, pp. 59–78.

[*3*] Berling, L. T. and Conway, J. B., *Metallurgical Transactions*, Vol. 1, No. 4, 1970, pp. 805–809.

[*4*] White, D. I., Horwood, G. P., and Czajkowski, Z., *Journal of Strain Analysis*, Vol. 5, No. 4, 1970, pp. 284–291.

[3] The italic numbers in brackets refer to the list of references appended to this paper.

E. T. Vitcha[1]

High-Temperature Fatigue Testing of Automotive Valve Steels

REFERENCE: Vitcha, E. T., "**High-Temperature Fatigue Testing of Automotive Valve Steels,**" *Fatigue at Elevated Temperatutures, ASTM STP 520*, American Society for Testing and Materials, 1973, pp. 231–241.

ABSTRACT: The elevated temperature bending fatigue strength of seven automotive exhaust valve alloys has been determined. Inconel 751 shows the highest fatigue strength of 45 ksi at 10^8 cycles 760 C (1400 F). Coatings in air atmosphere at elevated temperature generally reduced the fatigue strength. In corrosive atmospheres consisting of a simulated lead oxide environment or a carbon monoxide/carbon dioxide atmosphere, no protection was afforded by coatings of aluminum or aluminum chromium. Within the varying surface roughness tested only the as-forged surface representing a high surface roughness and decarburization showed a drop of 24 percent in fatigue strength. Compressively stressed Stellite 6 faced valves showed ten times improvement in thermal fatigue life.

KEY WORDS: fatigue (materials), fatigue tests, high temperature tests, failure, valves, coatings, corrosion fatigue, surface properties, stress

Failure mechanisms for internal combustion engine exhaust valves are primarily of two types: (1) burning failures and (2) fatigue failures [*1–10*].[2] A brief explanation of each of these is as follows. Burning failures are generated where exhaust gases erode, corrode, or melt the valve seat face because of a loss of sealing capacity of valve face to seat face in the head of the engine. It is the primary mode of failure. Fatigue failures are the next most common mode of failure. These occur in the stem of the valves generally in the underhead area at the point of the exhaust gas impingement. While the theoretical gas temperature is 1649 + C (3000 F), bulk temperatures of the valve in this area are 704 to 760 C (1300 to 1400 F). Bending loads due to misalignment of the seat axis in the engine head to valve stem axis markedly increases the stress state of the valve underhead radius. A 0.007-in. displacement on a standard size valve can double the stress to values of 36 000 psi. A second form of fatigue failure occurs where the

[1] Manager, Materials Engineering Laboratory, TRW Valve Division, TRW Inc., Cleveland, Ohio 44110.

[2] The italic numbers in brackets refer to the list of references appended to this paper.

Copyright© 1973 by ASTM International www.astm.org

thermal gradient across the top of the head places the circumference in tension. Parts fail radially because of the hoop stresses imposed.

Very few data are available relative to the fatigue test methods to simulate these types of problems, the fatigue life of common valve materials, effects of corrosion, coatings, and surface finish on these materials. It is the purpose of this paper to present these data.

Equipment

For fatigue testing, R. R. Moore fatigue machines are modified to permit mounting a ribbon element furnace between the specimen mounting collets. The specimen size is increased to 12 in. in length to dissipate the heat conducted through the specimen and to preserve the bearings. Rotation speed is 5000 rpm. The temperature is controlled with a saturable reactor and monitored with extraneous thermocouple and a multipoint recorder. Similar modifications have been made by other people [*11*].

The thermal-fatigue apparatus is shown in Fig. 1. There are three parts to the apparatus; a burner, a pneumatic cyclinder, and a water-cooled copper quench block. The operation consists of attaching the valve to the end of the pneumatic cylinder and oscillating it between the flame of the torch and the copper quench block. The oscillating cycle is controlled by a

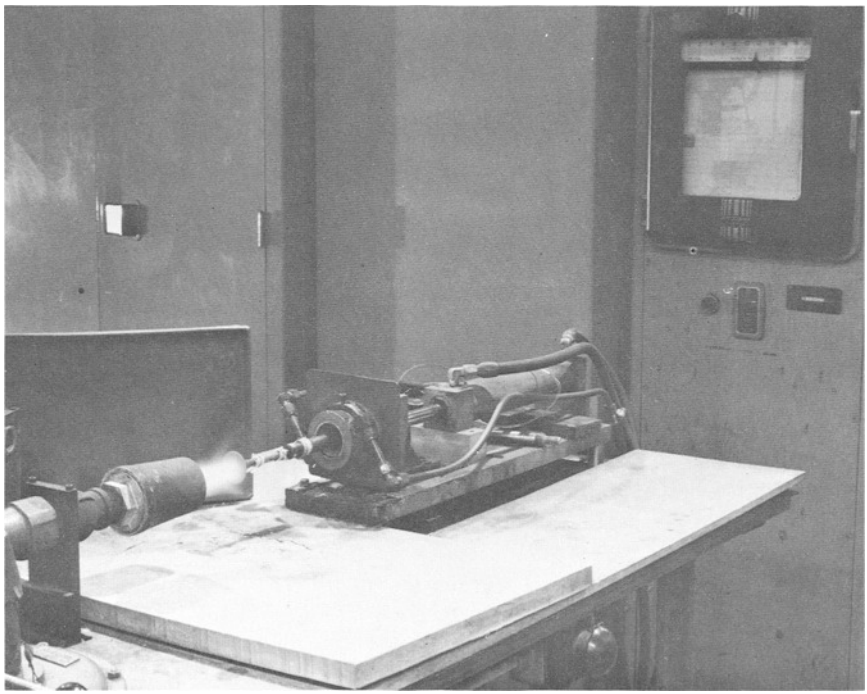


FIG. 1—*Thermal fatigue apparatus.*

timer; total cycle time is 1 min of which 40 s are spent in heating and 20 s in cooling. Temperatures oscillate from 704 C (1300 F) to 149 C (300 F) and are monitored by a thermocouple welded to the valve underhead close to the seat face. Failure is judged by the first visual appearance of a crack.

Chemistry of some of the current and new valve steels are listed in Table 1. These are primarily iron-based alloys, carbide, and carbon nitride strengthened.

TABLE 1—*Chemistry of current and new valve materials.*

Steel	Composition, weight %						
	C	N	Mn	Ni	Cr	Si	Other
21-2N	0.55	0.3	8.0	2.0	21.0	0.25[a]	0.065 S, Fe balance
21-4N	0.5	0.45	9.0	4.0	21.0	0.25[a]	0.065 S, Fe balance
21-12 N	0.2	0.18	1.25	11.5	21.0	1.00	Fe balance
Gaman H	0.5	0.48	12.0	...	21.5	2.5	Fe balance
DV-2	0.5	0.5	11.0	...	20.3	0.27[a]	0.4 V, 2.0 W, 1.0 Cb, Fe balance
VMS-513	0.08[a]	...	8.0	28.0	27.0	0.11[a]	2.0 Ti, 1 Al, Fe balance
Inconel 751	0.10[a]	...	1.0[a]	70.0[b]	15.5	0.5[b]	2.3 Ti, 1.25 Al, 1.0 Cb + Ta, 7.0 Fe

[a] Maximum.
[b] Minimum.

Bending Fatigue Data

The standard valve steel for the industry, 21-4N, has a fatigue strength at 10^8 cycles of 27 ksi, see Fig. 2. A few of the newer alloys such as 21-2N, DV-2, and VMS-513 sustain a stress of 10^8 of 30 and 34 ksi, respectively.

To answer the need for fatigue data where higher valve operating temperatures are encountered, data have been developed at 815 C (1500 F). These are shown in Fig. 3. All materials are in the solution and aged or double-aged condition. The material possessing the highest fatigue strength is Inconel 751, followed by VMS-513, DV-2, and 21-4N. Alloy 513, for example, showing a significant improvement over 21-4N. Alloys of this type should be capable of meeting the future anticipated stresses and operating temperatures.

Corrosion Fatigue Testing

To see the effects of corrosive atmospheres on fatigue life, a series of tests were run. The specimens were doped with a mixture of four moles of lead oxide (PbO) and one mole each of lead bromide ($PbBr_2$) and lead sulfate ($PbSO_4$) dispersed in glycerol. This mixture of lead salts approxi-

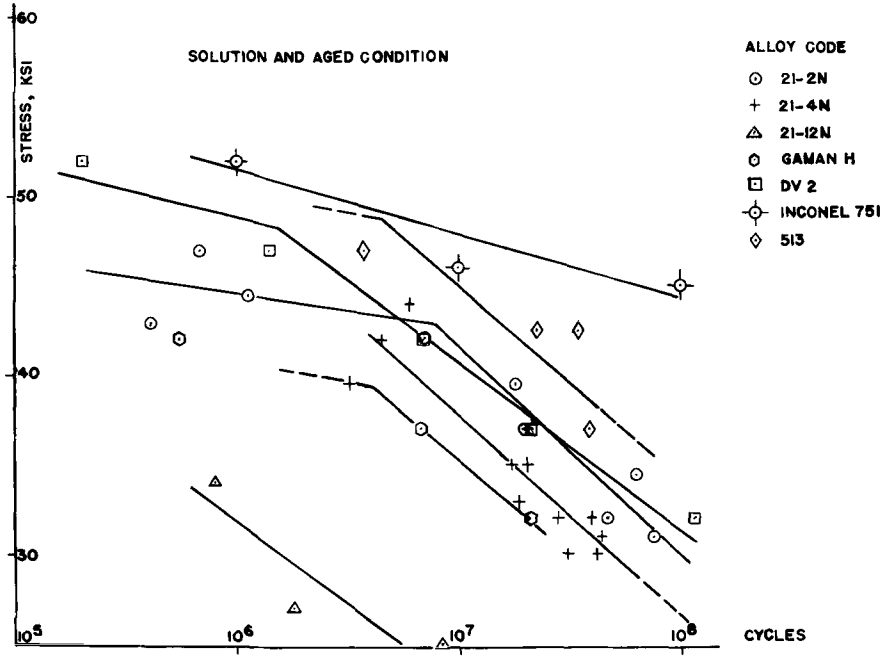


FIG. 2—*Fatigue life of valve materials at 760 C (1400 F), 5000 rpm, in reverse bending.*

mates the deposits found on the top of heads of exhaust valves and also around spark plug electrodes. To retain an atmosphere of corrosive vapor, the specimens were further wound with asbestos tape secured by nichrome wires. Numerous test procedures for simulation of valve corrosion mechanisms and products have been evolved [*12–14*]. The corrosive atmosphere reduced the fatigue life at 760 C (1400 F) on forged and aged specimens of 21-4N and 21-2N by a factor of between 15 to 90 times:

Stress, psi	Mean Life Cycles Air	Mean Life Cycles Corrosive Atmosphere
40 000	8.0×10^6	0.09×10^6
32 000	32.0	2.0
	Range Life Cycles Air	Range Life Cycles Corrosive Atmosphere
40 000	3.0 to 21.0 $\times 10^6$	0.016 to 0.6 $\times 10^6$
32 000	20.0 to 75.0	0.4 to 10.0

The corrosion mechanism is probably one of formation of liquid phases between the corrodents and the elements in the alloys [*15*].

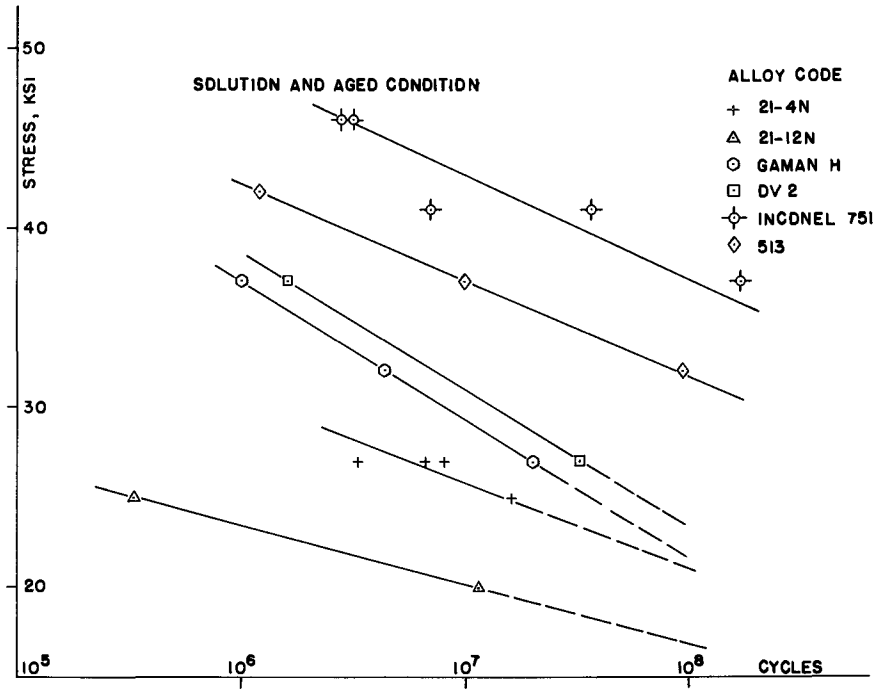


FIG. 3—*Fatigue life of valve materials at 815 C (1500 F), 5000 rpm, in reverse bending.*

Additional tests were run using carbon monoxide/carbon dioxide (CO/CO_2) atmosphere containing 2 percent CO and 12 percent CO_2. The remainder was nitrogen. This produced no change in the fatigue life over specimens run in air.

Effects of Coatings on Fatigue Life

An investigation was conducted to improve the corrosion fatigue resistance of 21-4N by the use of diffusion bonded coatings. Two coatings were tried: (1) aluminum and (2) aluminum and chromium. The latter at two thickness of 0.5 to 3.9 mils and 6 mil thickness. These tests were conducted in air and a corrosive environment of PbO, $PbBr_2$, and $PbSO_4$.

At lower stresses, the coatings did not reduce the fatigue life on the ambient air tests other than for the 6 mil coating thickness of aluminum and chromium. At higher stresses, the cycles to failure were reduced for almost all coatings over the uncoated specimens. The results of the tests are tabulated in Table 2.

Examining the coatings after testing showed the 6 mil aluminum-chromium to have extensive cracks and voids. The 3 mil coating showed less damage. This probably is due to the high-thermal surface stresses and lack of ability of the coatings to conform to surface strains were the coatings

TABLE 2—*Summary of fatigue life on uncoated, coated, specimens tested in air and corrosive atmosphere, 21-4N 760 C (1400 F) and 5000 rpm.*

Condition	Stress 32 000 psi	Stress 40 000 psi
	LIFE, CYCLES, AIR ATMOSPHERE	
Uncoated	33.0×10^6	6.5×10^6
Al coated	36.0	0.08
Al-Cr, 0.5 to 3.9 mils thick	29.0	0.10
Al-Cr, 6 mils	0.38	0.05
	LIFE, CYCLES, CORROSIVE ATMOSPHERE[a]	
Uncoated	6.0	2.1
Al coated	5.6	0.6
Al-Cr, 0.5 to 3.9 mils	2.3	0.09
Al-Cr, 6 mils	0.09	0.03

[a] Synthetic atmosphere consisting of 4 moles, PbO, 1 mole each of $PbBr_2$, $PbSO_4$.

are thicker. Cracks initiated at corrosion pits and propagated initially in intergranular manner and then switched to a transgranular mode.

Diffusion treatment of $\frac{1}{2}$ to 4 h at temperatures of 815 C (1500 F) to 967 C (1775 F) offered no improvement in fatigue life for either the aluminized or aluminum-chromium coatings when tested at 40 000 psi. This was true for both atmospheric conditions studied.

Surface Effects on Fatigue Life

To determine the effects of various types of finishes or conditions on fatigue, specimens were made where:

1. Cold working was induced by forging at 871 C (1600 F).
2. A microfinish of 20 to 40 μm was generated transverse to the axis of the specimen.
3. As-forged surface specimens were fatigue tested.
4. Smooth versus notched bar properties were developed.

In comparing the specimens made with the lower forging temperature of 871 C (1600 F) with the standard fatigue data, no improvement in fatigue life resulted. This effect is shown in Fig. 4. This was consistent with some hardness relaxation studies that were also made on this alloy 21-4N. We found after solution, peening to induce cold working, and aging that relaxation of hardness values started at as low a temperature as 538 C (1000 F). Relaxation was completed in a time as short as 15 min at temperatures above 648 C (1200 F). Figure 4 shows standard specimen, cold working, surface finish, and as-forged surface data. Please note that these data are in the aged only, rather than solution and aged condition as shown on previous charts.

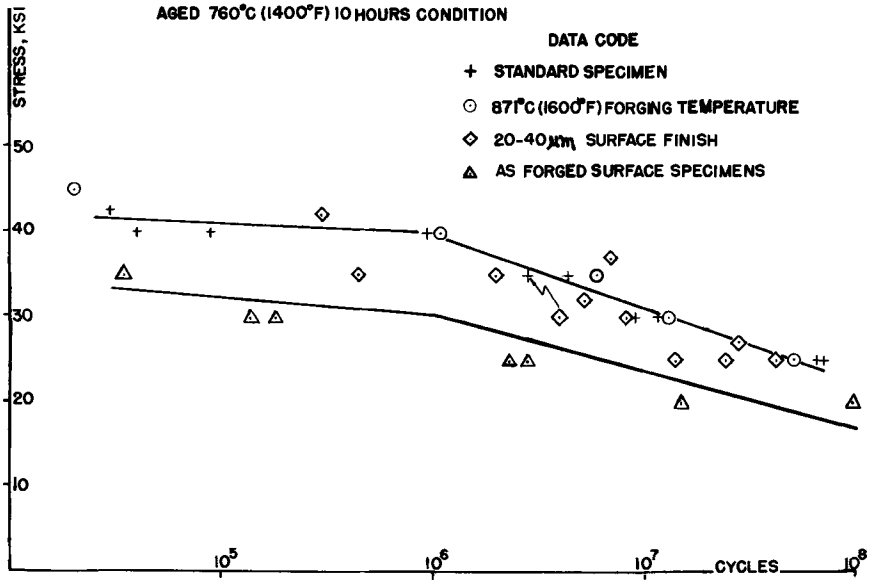


FIG. 4—*Surface finish effects on fatigue life, 21-4N steel, at 760 C (1400 F), reverse bending.*

Inconel 751 was also studied as a typical nickel-based alloy. The hardness relaxation data showed the cold-work effects persisted as high as 926 C (1700 F) for parts that were cold worked by peening. Similarly, the fatigue data for cold-worked specimens showed an improvement for shorter cycles over standard specimens. A crossover point occurred at about 10^7 cycles, and the beneficial effect of the cold working disappeared.

Again, referring to Fig. 4, surface roughness effects up to 40 μm did not grossly deviate from the standard fatigue curve. Tests of specimens with roughness up to 100 μm were also run but for heat treat conditions different than Fig. 4, and again no loss in fatigue life was observed. The only effect was one of increasing the amount of scatter in relation to the standard specimens.

The specimens identified "as-forged surfaces" in Fig. 4 represent a non-standard specimen which was manufactured by extruding to 0.310 in. diameter and friction welding this to the shanks that are used both to support and drive the specimens. This as-forged surface then represents some intentional decarburization plus the degree of surface roughness associated with the forging operation. The initial slugs for extrusion were decarburized at 1204 C (2200 F) for 2.5 h. This reduced the carbon in the first 0.005 in. of the surface from a value of 0.53 to 0.26 percent. The reduction in carbon resulted in a substantial reduction in fatigue strength at 10^7 cycles.

In considering notch versus smooth bar properties, there is a reduction in the notched fatigue life for this alloy in comparison with standard

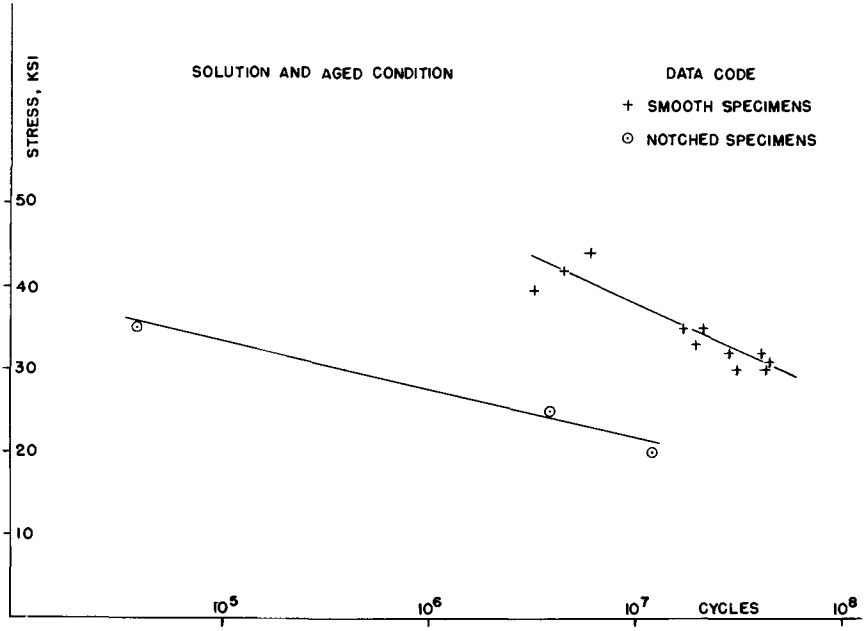


FIG. 5.—*Smooth versus notched fatigue life, 21-4N steel, at 760 C (1400 F), reverse bending.*

specimens. Figure 5 shows these effects. Our notch specimen has a stress concentration factor of 2.3 (K_t).

Thermal Fatigue Testing

The general arrangement of the thermal fatigue apparatus is shown in Fig. 1. Standard automotive valves are tested. The chemistries of the valve steels are shown in Table 3.

In running the test, valves made from the steel designated TXCR are used as a standard. These fail in approximately 2 h of testing on the schedule of heating to 704 C (1300 F) and quenching to 149 C (300 F).

TABLE 3—*Valve steels tested in thermal fatigue composition, weight percent.*

Steel	C	N	Mn	Ni	Cr	Si	Other
21–4N.....	0.5	4.5	9.0	4.0	21.0	0.25[a]	0.065 S, Fe balance
21–2N.....	0.55	0.3	8.0	2.0	21.0	0.25[a]	0.065 S, Fe balance
TXCR	0.37	...	4.25	3.75	24.0	0.8	1.3 Mo, Fe balance
Stellite 6...	1.25	...	0.5[a]	3.0[a]	28.0	1.0	4.5 W, Co balance

[a] Maximum.

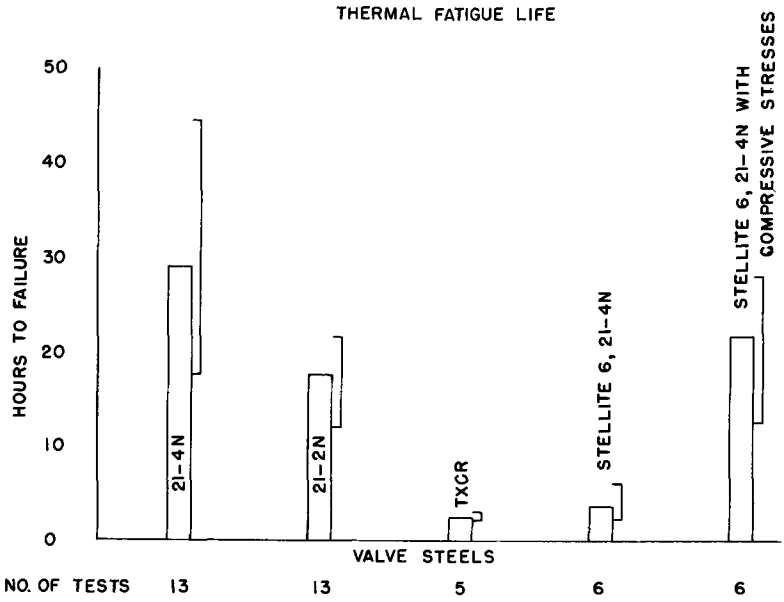


FIG. 6—*Thermal fatigue life, various valve steels, oscillated between temperatures 704 C (1300 F) to 149 C (300 F).*

Valves from this steel serve to standardize both the machine and part geometry. Figure 6 shows the test results for the four materials under consideration. The alloys 21-2N and 21-4N show, essentially, equivalent thermal fatigue life of 20 to 30 h.

For heavy-duty wear application, valves are constructed using a composite structure of a Stellite 6 alloy welded to the valve face of 21-4N. Thermal fatigue life under these circumstances drops from values of 30 to 3 h. If the Stellite 6 after it has been puddled is stressed compressively, the fatigue life is improved from a standard 3-h value to one of 21 h [*16*]. Compressive stresses are obtained by controlling a quench from the facing operation.

Conclusions

Inconel 751 possesses the highest fatigue strength of the valve steels tested. This is followed by VMS-513. This is using the stress at 10^8 cycles for 760 and 815 C as the judgment criterion.

In corrosion fatigue, the life of the standard valve steel 21-4N was reduced by 15 to 90 times in the stress range of 37 000 to 40 000 psi. Using protective coating of aluminum, or thin coatings of aluminum and chromium, reduced the life at high stresses. No loss of life occurred at lower

stresses and 10^6 cycles. None of the coating served to increase life in corrosive atmosphere fatigue tests.

Of the surface effects studied, including cold forging at 871 C (1600 F) or cold-working ground finish of 20 to 40 μm, and as-forged surfaces, only the as-forged surface resulted in a 24 percent reduction in fatigue life. Notch fatigue properties are reduced by 24 percent at 10^7 cycles where the stress concentration factor was 2.3.

Both 21-4N and 21-2N have essentially equivalent thermal-fatigue life. Composite structures consisting of Stellite 6 and 21-4N, which are compressively stressed, improve the fatigue life by a factor of ten and makes it comparable to 21-4N.

References

[1] Tauschek, M. J., *Thompson Products Engineering Bulletin*, Vol. 1, No. 1, Jan. 1956, pp. 1, 9.

[2] Tauschek, M. J., "Basic Factors Affecting Engine Valves," SAE Technical Meeting, West Coast Section, Society of Automotive Engineers, Oct. 1965, pp. 1, 4–6.

[3] Newton, J. A., "Engineering of the Poppet Valve," SAE Technical Meeting, West Coast Section, Society of Automotive Engineers, Nov. 1952, pp. 2–4.

[4] Tauschek, M. J. and Newton, J. A., "Valve Seat Distortion," SAE National Passenger Car, Body and Materials Meeting, Detroit, Mich., Society of Automotive Engineers, March 1953, pp. 1–3, 4–5.

[5] Newton, J. A., "Some Aspects of Valve Burning and Stelliting," SAE Preprint 86, National Fuels and Labor Costs Meeting, Tulsa, Okla., Society of Automotive Engineers, Nov. 1947, pp. 1–4.

[6] Young, V. C., *Diesel Power*, Oct. 1955, pp. 46–49.

[7] Moyford, R. D. and Ball, F. A. in *Proceedings*, Automotive Division, Institute of Mechanical Engineers, No. 5, 1955–1956, pp. 150–151.

[8] Young, V. C., "Fatigue Failures," Eaton Engineering Forum, Vol. XVIII, No. 4, Eaton Manufacturing Co., Dec. 1957.

[9] Giles, W. S., "Fundamentals of Valve Design and Material Selection," *Know How In Engine Design*, SAE Engineering, Part 14, SP 283, Society of Automotive Engineers, Aug. 1966.

[10] Vitcha, E. T. and Cherrie, J. C., *Metals Progress*, Vol. 100, No. 3, Sept. 1971, pp. 54–56.

[11] Drake, J. R., "Rotating Beam Strength of Cast Nickel Base Alloys at Elevated Temperatures," ASME 63WA214, Society of Mechanical Engineers, Nov. 1963, p. 1.

[12] Lamb, F. W., "Postulated Mechanism of Spark Plug Fouling," Aircraft Spark Plug and Ignition Conference, Ethyl Corp., Detroit, Mich,. Oct. 1954.

[13] Johnson, V. A. and Wilde, R. A. in *Journal of Materials*, Vol. 4, No. 3, Sept. 1969, pp. 556–565.

[14] Sawyer, J. C., *Transactions*, The Metallurgical Society of American Institute of Mining, Metallurgical, and Petroleum Engineers, Vol. 221, Feb. 1961, pp. 63–67.

[15] Rathenau, G. W. and Meyering, J. L., *Metallurgia*, Vol. 42, No. 251, 1950, pp. 167–172.

[16] Tauschek, M. J., Allowed patent application entitled "Method of Manufacturing Hard-Faced Exhaust Valves," Patent Application Serial No. 824343.

DISCUSSION

D. R. Diercks[1] (*written discussion*)—My question is of a somewhat nontechnical nature. It is my understanding that the catalytic converters to be used in internal combustion engines in the near future require the use of nonleaded gasolines. What implication does this have insofar as automotive valve life is concerned?

E. T. Vitcha (*author's closure*)—Valve life will improve. Corrosion due to lead additives in the fuel will be replaced by the milder corrosion atmosphere of air. Removal of lead will shift valve problems from a corrosion, corrosion-fatigue dominated condition to one of wear and fatigue.

[1] Materials Science Division, Argonne National Laboratory, Argonne, Ill, 60439.

M. A. H. Howes[1]

Evaluation of Thermal Fatigue Resistance of Metals Using the Fluidized Bed Technique

REFERENCE: Howes, M. A. H., "**Evaluation of Thermal Fatigue Resistance of Metals Using the Fluidized Bed Technique,**" *Fatigue at Elevated Temperatures, ASTM STP 520*, American Society for Testing and Materials, 1973, pp. 242–254.

ABSTRACT: This paper presents details from the experience gained over the last twelve years with the fluidized bed method of thermal fatigue testing. The use of the fluidized bed is discussed, and comparisons are made with other methods of testing as to advantages and disadvantages. The design and construction of a fluidized bed test facility is described and performance characteristics noted. Configurations that have been used are disks, wedges, and "window" specimens. All of these specimens may be notched. Temperature gradients in the specimens may be controlled by bed temperatures, time of exposure, and fluidization conditions. The window specimen has been used to examine thermal fatigue resistance of welds between the same and dissimilar materials. The changes that occur during thermal cycling and the effects of thermal stresses on tempering and aging mechanisms are discussed. Finally, selection and treatment of materials to minimize thermal fatigue are considered.

KEY WORDS: fluidized bed processors, fatigue (materials), failure, cracking (fracturing), crack propagation, crack initiation, plastic deformation, coatings, stress concentration, thermal fatigue

Thermal fatigue is a possible failure mechanism in any situation that involves fluctuating temperatures. If certain materials are heated or cooled rapidly, cracking sometimes occurs. The phenomenon, which is often called thermal shock, is caused by thermal gradients present during rapid temperature changes. As a result, strain is produced which is related to the coefficient of expansion of the material. Failure occurs when thermally induced stresses exceed the strength of the material after starting as a crack in the most sensitive area. In metals, the thermal-fatigue mechanism often results in the gradual formation of a network of cracks and is referred to commonly as craze cracking, heat checking, or fire cracking.

Failures due to thermal fatigue can be found in brake drums, turbine blades, internal combustion engine pistons and cylinder heads, rolls for forming hot steel, forging dies, railway wheels, furnace components, and molds used for glass and metal molding. Thermal fatigue can become the

[1] Manager, Physical and Ferrous Metallurgy, IIT Research Institute, Chicago, Ill. 60616.

Copyright© 1973 by ASTM International www.astm.org

dominant failure mode in components as the operating temperature and thermal gradients become more severe and the expected service life becomes longer.

Many methods of heating and cooling have been used to simulate the thermal cycles experienced in actual applications. Some of the earliest work used direct flame impingement on a surface. However, unless carefully controlled, the combustion products and variation in temperature conditions can introduce an arbitrary environment which can influence the cracking mechanism.

High-frequency heating and electrical resistance heating systems can be used to establish simulated thermal cycling conditions; however, they are generally expensive to construct for the multistation test facilities which are needed to amass data quickly. In considering thermal fatigue, the crack propagation rate is as important as the start of cracking. For instance, a material that cracks early might be satisfactory if the crack propagation rate is very slow. With high-frequency and resistance heating, the formation of a crack alters the flux or current density in such a way that the tip of the crack is overheated and measurement of propagation rate becomes meaningless.

The fluidized bed heating system for thermal-fatigue testing has many advantages and no significant disadvantages. The rate of heat transfer to a specimen or group of specimens is high. The heat content of a particulate solid fluidized media is also high so that a large number of specimens or a large specimen can be rapidly and repeatedly heated without lowering the bed temperature significantly. The first reported use of fluidized beds for thermal-fatigue testing was in 1958 by Glenny and co-workers.[2] Since that time there have been many applications of this technique reported to evaluate thermal fatigue resistance. A bibliography of the literature on thermal fatigue up to 1967 was compiled by Carden.[3]

Fluidized Bed Facilities

Fluidized beds have been used at IIT Research Institute for thermal fatigue testing for about twelve years. The original beds were gas fired using a silicon carbide retort to contain the fluidized media. However, gas fired beds were large because of the combustion space around the retort and inefficient so that the maximum temperature and loads that could be used in testing specimens were restricted. In addition, it was difficult to control gas fired beds in the startup period to avoid thermal shocks cracking the silicon carbide retort.

About six years ago all the thermal-fatigue equipment was rebuilt with electrically heated retorts. A schematic of a typical facility is shown in

[2] Glenny, E. et al, *Journal of the Institute of Metals*, Vol. 84, 1958–1959, p. 294.
[3] Carden, A. E., Report MH67-AEC-3 under NASA Grant NsG-381.

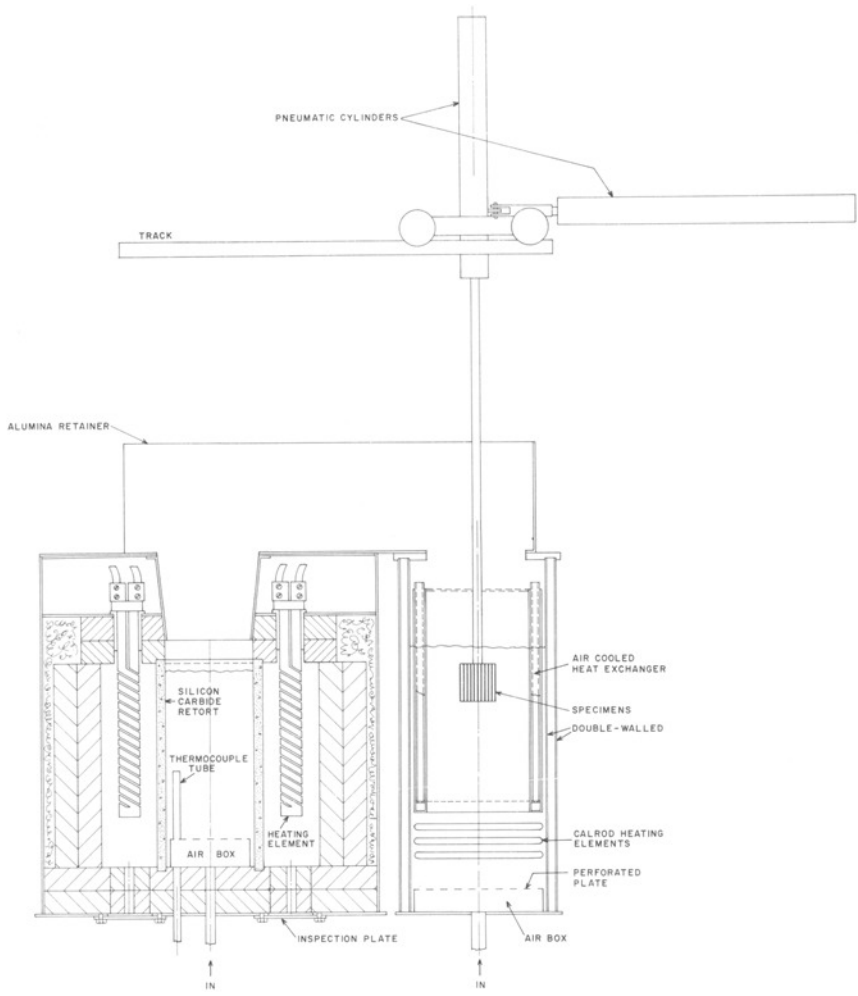


FIG. 1—*Schematic view of thermal fatigue facility.*

Fig. 1. It will be noted that the high-temperature bed is heated externally with silicon carbide elements. Internally heated beds were tried but found to be restricted in maximum temperature and power input. The bed illustrated has a power input of 55 kW which is adequate for most purposes and will give a maximum operating temperature of 2300 F (1260 C). The low-temperature bed is provided with an internal heat source of low power (14 kW) to enable the bed to be controlled at temperatures up to 800 F to achieve any desired heating cycle. Cooling is provided by an air-cooled heat exchanger situated in the bed. If the low-temperature bed is not heated, a water-cooled heat exchanger may be used.

The specimens are cycled between the high- and low-temperature beds by means of automatically controlled pneumatic cyclinders which are sequenced by timers and limit switches. The facility will cycle automatically for the number of cycles selected.

The air supply for fluidization is controlled through flowmeters. The maximum fluidization air volume requirement is about 3500 $ft^3/ft^2/h$ (1100 $m^3/m^2/h$) for the low-temperature bed at 100 F (38 C) and 900 $ft^3/ft^2/h$ (275 $m^3/m^2/h$) for the high-temperature bed at 2000 F (1093 C). Tests show that the fluidization range is narrow between sufficient air to fluidize the bed and excess air which will cause too violent movement with loss of media from the facility. The media currently used is alumina in the 28 to 48 mesh size range.

Thermal Fatigue Specimens

Three distinct types of specimens have been used for thermal fatigue evaluations (Fig. 2). However, on numerous occasions actual components and scaled-down models of components have been cycled. The left-most specimen (Fig. 2*a*) is most often used and consists of a disk with a thin fin. When the specimen is heated rapidly, the outer edge of the fin goes into compression, and on cooling the fin is in tension. It is usual to test these specimens in stacks of five to twelve plus a dummy sample on the top and bottom to avoid end effects (Fig. 2*b*). Experience has shown that the position in the stack does not affect the cracking behavior. These test specimens may be either notched or unnotched. The notch used is a V-notch of the same dimensions as that in a Charpy impact bar. In the unnotched condition cracking begins at the weakest place in the structure, and later metallographic examination helps to identify potentially harmful constituents. In the notched specimen the variable incubation period is avoided, and the initiation of cracking occurs after a consistent number of cycles in speci-

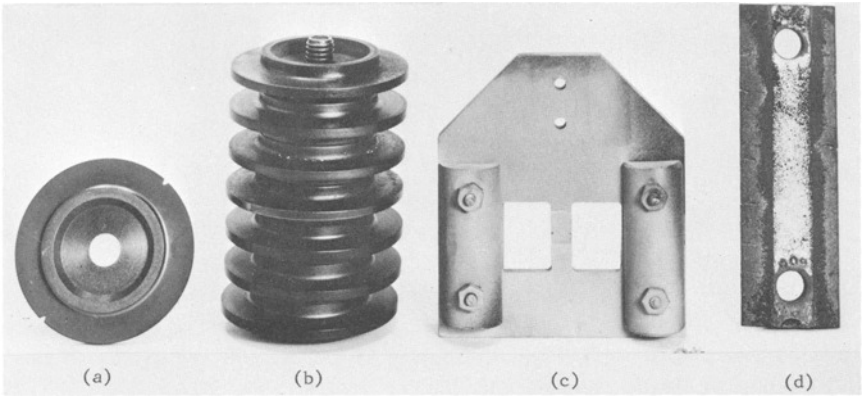


FIG. 2—*Test specimens used for thermal fatigue tests.*

mens of the same type. The notched specimen is preferable for comparing crack propagation rates and also provides valuable crack initiation data for a constant stress concentration point.

The specimen shown in Fig. 2*c* is referred to as a "window" specimen, and it is designed specifically to test welds between the same or dissimilar materials. This specimen is produced from plate, and two window openings are machined to form the central test section. Two stainless steel semicircular heat sinks clamp asbestos insulation to each edge of the specimen. When this type of specimen undergoes thermal cycling, the center test section heats and cools more rapidly than the insulated outer mass of the outside framework. This causes the test section to go into compression during heating and into tension during cooling. The specimen shown in Fig. 2*c* has a steel top half; the bottom is copper with a horizontal weld joining the two sections. A notch can be used to initiate cracks in the base metal, heat-affected zone, or weld metal. This specimen has been also used with a vertical weld running the length of the test section. The window may be removed in one piece to test the weld dilution and the metallurgical characteristics of the weld before thermal cycling.

The specimen shown in Fig. 2*d* is a tapered airfoil section with a different edge radius on each side. A smaller edge radius results in a smaller number of cycles to initiate a crack. This specimen has been used to test nickel- and cobalt-base superalloys and is adapted easily to test coatings and modifications to solidification techniques such as directional solidification.[4] These specimens are tested in sets of up to 18 arranged with the tapered edges vertical and a dummy specimen on each end to eliminate end effects.

Thermal Cycles

The thermal cycle used is usually an attempt to simulate an actual temperature or stress cycle. There are four important interrelated elements in the cycle: maximum temperature, minimum temperature, heating rate, and cooling rate. For this simulation, the actual temperature cycle at the surfaces of the part must be known and preferably also at one or more points below the surface. If materials or treatments are being compared, it may be sufficient to cycle the surface of the specimens between two temperatures; but, if a practical application is being simulated, temperature and stress gradients must be also approximated. It is found in practice that if similar stresses are produced in the specimen as in the actual part, then failure occurs in approximately the same number of thermal cycles.

Figure 3 illustrates the heating and cooling of a disk specimen instrumented with ten thermocouples. A surface temperature rise of 400 F (240 C) to 1100 F (593 C) has been achieved using a heating time of 4.0 s in a

[4] Howes, M. A. H., NASA Report CR-72738, National Aeronautics and Space Administration, 15 May 1970.

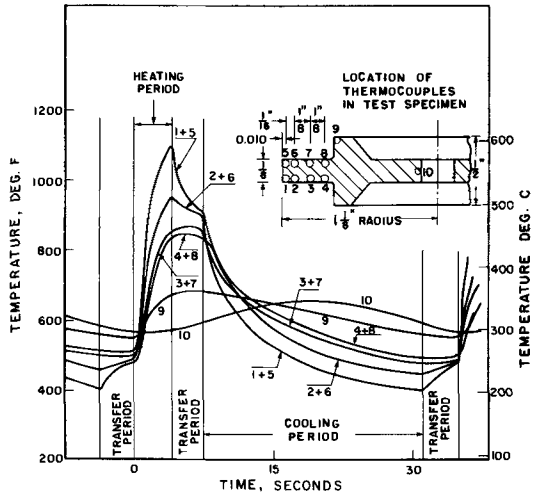


FIG. 3—*Heating and cooling of H13 thermal fatigue specimen.*

fluidized bed at 1900 F (1038 C). The specimens are then transferred to a cold fluidized bed at 110 F (43 C), and the surface temperature is reduced from 1100 to 400 F in 24.0 s. A high heating rate is achieved by using a heating bed considerably hotter than the desired surface temperature and removing the specimens when the required surface temperature is reached.

The surface temperature control from cycle to cycle depends upon the temperature difference between the bed and the required specimen surface temperature. The larger the temperature difference, the greater the possible fluctuation in specimen surface temperature between cycles. For a 400 F (204 C) temperature difference the control of a specimen surface temperature is normally within ±10 F (±6 C). For a 800 F (426 C) temperature difference surface temperatures might vary as much as ±20 F (±11 C). Calibration is carried out on specimens which have been preoxidized since it is probable that the oxide film affects the heat transfer characteristics. It is desirable that the thermocouples used be small in order to obtain rapid temperature response and to avoid disturbance of the specimen surface. The thermocouple wire used for the calibration curves shown in Fig. 3 was approximately 0.001 in. diameter (0.025 mm) to ensure an almost instantaneous response to temperature change.

Cycles in which the specimens are equalized at the bed temperatures can be used, but the cycle times may be very long (of the order of 10 min) and also place more emphasis on tensile stressing than compressive stressing. This is because the temperature gradients decrease to zero as the maximum temperature is approached, and compressive stresses at the surface are negligible at the point where the material strength properties are at a minimum. However, on cooling a through-heated specimen, the surface

tensile stresses are higher than they would be in a specimen whose central bulk had not reached the surface temperature. It is preferable to use a temperature cycle in which the specimens are equalized at the bed temperature when this condition simulates an actual application and also when surface oxidation is thought to accelerate the thermal fatigue process. The extent of surface oxidation is greater in the longer temperature cycle since the exposure time is greater. The thermal fatigue test may be also regarded as a cyclic oxidation when the bed is fluidized with an oxidizing gas.

Thus, the controls for specimen heating are bed temperature, exposure time, and, to some extent, bed fluidization level since heat transfer coefficient increases with increasing fluidization. Cooling rate is controlled by the same factors, but the minimum bed temperature is restricted normally to that which can be achieved using water-cooled heat exchangers. In order to achieve different minimum temperatures and cooling rates liquid nitrogen, water, water sprays, and air blasts have been used in place of the lower temperature fluidized bed.

Strain gages may be applied to the outer surface of the test specimens to measure the stress cycle while thermal cycling is in progress. Methods of attaching gages are satisfactory up to about 900 F (482 C). Gages with incorporated thermocouples may be used to indicate the temperature at the same location as the strain gages. In calculating the stresses indicated by the gage, allowance must be made for the change in temperature. Measurements made in this way are in close agreement with the stress values obtained by calculation. However, since most practical thermal cycles involve temperatures in excess of 900 F, the use of strain gages is not often feasible.

Test Results

Groups of up to 20 specimens, depending on the design, are cycled and examined at regular intervals. For example, inspections might be made at 10, 25, 50, 100, 200, 300, 500, 700, 1000, etc., cycles; testing usually is not continued beyond 20 000 cycles. If cracks are propagating rapidly, more inspection points may be needed for accurate determination of the crack propagation curve. Specimens are replicated using 4 to 6 specimens for significant results. Each crack is measured on both sides of the specimen, and the lengths are averaged.

It is found experimentally that once a crack has initiated in a constant thickness fin test specimen, the crack propagation rate is usually linear in form as opposed to the curved propagation curve for wedge type specimens. The reason for the linear curve has been a subject of some discussion, but it is probably due to the interaction of several compensating effects. The magnitude of the hoop stresses developed over a given length in the fin will be constant regardless of depth of the cracks. The tip of the crack will be subjected to a higher stress as the crack progresses inwards due to the

reduced cross section of the remaining fin. This is compensated for by the reduced temperature at the tip of the crack and consequently a higher minimum yield strength during the thermal cycle. In practice these compensating effects produce an approximately linear crack propagation curve for the constant thickness fin specimen. The linear curve may be extrapolated back to zero crack length to estimate the incubation cycles. Also, crack propagation may be calculated in length per cycle. Notched specimens are extremely consistent in cracking behavior, and it is customary to use a smaller number of notched specimens and to average the results of all cracks.

Some actual results using notched and unnotched disk specimens are shown in Fig. 4. This was part of an investigation to compare an 18Ni maraging alloy with a specially melted batch of H13 tool steel for a die casting application. A thermal cycle at the edge of the disk achieved a maximum temperature of 1100 F (593 C) and a minimum temperature of 400 F (204 C). This simulated the actual die temperature measured during a production run. Heating occurred in a fluidized bed at 1900 F (1038 C) for a period of 4.0 s for H13 and 3.25 s for the maraging alloy. Cooling in a fluidized bed at 110 F (43 C) occurred in 24.0 and 22.0 s, respectively. The H13 temperature cycle is shown in Fig. 3.

The crack growth of three chronologically successive cracks in one unnotched specimen of H13 is shown on the left-hand side of Fig. 4. The rates of crack growth are equal, and the lines are parallel. The curves for the notched specimens in Fig. 4 are the averages for four cracks. It will be noted that the H13 cracks initiate much faster from notched than from unnotched specimens but that the crack propagation rates are identical. Cracks initiate at a higher number of cycles in the maraging material, but, once initiated, the propagation rate is higher than in the H13 specimens. The maraging material has a lower thermal conductivity, so that the surface heats more rapidly than the H13 surface, and thus has a steeper temperature gradient from the surface inwards. H13 has a higher coefficient of expansion than

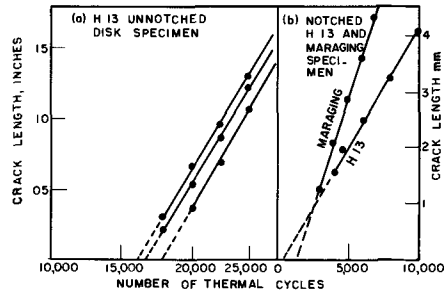


FIG. 4—(a) *Crack growth of successive cracks in one H13 specimen,* (b) *average crack growth of four cracks in H13 and maraging disk specimen. Specimens cycled between 1100 and 400 F.*

the maraging steel, but, if there is sufficient difference in the temperature gradient, the stress gradient will be higher and the crack propagation rate of the maraging alloy will be higher despite the higher hot strength.

In selecting thermal cycles for thermal fatigue tests it should be recognized that similar heating conditions may produce different thermal cycles in different materials due to differences in thermal conductivity, specific heat, etc. Since these differences will occur in a practical situation, results based on an identical surface temperature cycle will not be comparable if the thermal properties of the materials tested vary appreciably.

The difference in cycles to initiate cracks (Fig. 4) between notched and unnotched specimens is an indication of the stress concentration points present in the structure. These may be due to metallurgical structure features or inclusions from processing practices.

Examination of a large number of thermal fatigue cracks has shown that the majority are intercrystalline and follow paths of structural weakness such as dendrites, porosity, carbides, and graphite flakes. Cracks initiate from defects on the surface and often show evidence of plastic deformation before the crack propagates. Many cracks originate at points where grain boundaries intersect the surface. Directional solidification techniques have been used, particularly for superalloy turbine blades, to force crystal growth in one direction so that the uniaxial pattern of grain boundaries is not followed and fewer possible crack initiation sites are formed. It is believed that localized stress fields play a large part in causing metallurgical changes that lead to crack propagation.

In many investigations loss of hardness due to tempering or overaging has occurred more rapidly in thermal fatigue specimens that might be expected from unstressed heating data. To simulate this effect a study was made using a variable section specimen in a creep machine at temperatures in the 1000 to 1200 F (538 to 649 C) range. Specimens were made from H13 tool steel to represent steels that were hardened and tempered and also for an 18Ni maraging alloy to represent solution treated and aged alloys. The results for H13 are given in Fig. 5, which clearly shows that stress does accelerate tempering. Similarly, aging is also accelerated. An analysis of the results suggests that the Larson-Miller time parameter (P) might be modified to include the effect of stress in order to predict these effects as follows:

$$P = (T + 460)(\log t + C_1 \log \sigma + C_2)$$

where

T = temperature, deg F,
t = time, h,
σ = stress, ksi, and
C_1 and C_2 = constants.

This is a preliminary result based on a comparatively small amount of data, but the results do show that mechanical properties in areas of high

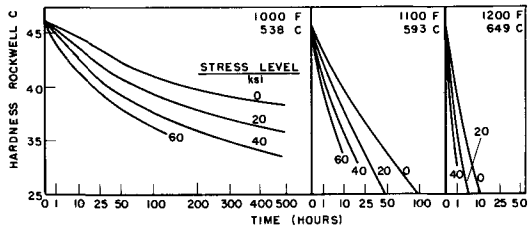


FIG. 5—*The effect of stress on the tempering of H13.*

stress can decrease at a higher rate than might be predicted normally. Figure 6 shows small areas on a thermal-fatigue specimen where plastic deformation during compression has caused material to be pushed up from the surface. Due to the stress accelerated changes discussed previously, the material in these yielded areas will have substantially lower mechanical properties than the surrounding areas and is less resistant to cracking. As thermal cycling progresses, a system of cracks will form within these yielded areas. Plastic deformation and striations are frequently observed on metals subjected to thermal fatigue, and, due to the previously-discussed mechanism, crack will probably initiate in these areas. A small weakness in the structure is quickly magnified into a potential crack site.

Oxidation has been found to affect thermal fatigue cracking. In high-temperature alloys surface oxidation at localized points can deplete the alloy of elements, and the strength of the material can be reduced locally forming a site for a possible crack to initiate. If the alloy readily oxidizes and a crack is propagating, oxide can form within the crack. Figure 7 shows oxidation occurring within an intergranular thermal crack in copper.

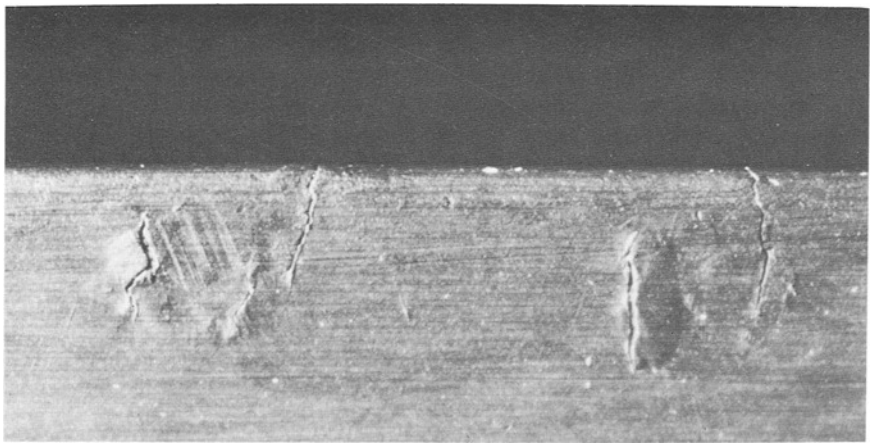


FIG. 6—*Plastic deformation occurring on the surface of a thermal fatigue specimen* (×20).



FIG. 7—*Thermal fatigue cracks in copper after thermal cycling between 800 F (427 C) and 130 F (54 C) for 3100 times* (×20).

If the crack opens up under tension stresses and a small amount of oxide forms, the crack cannot close to its original position and the crack widens. Additional stresses are imposed on the crack tip and crack propagation is accelerated probably by this mechanism. It is noticed that materials which oxidize readily form wide, easily discernible cracks, whereas materials which

resist oxidation form tight cracks apparently because stresses do not act to open up cracks unless appreciable oxide forms within the crack. Certain types of coatings have been found to increase thermal fatigue resistance[4] and are probably also effective, because they increase surface oxidation resistance.

Selection of Materials and Treatments to Resist Thermal Fatigue

Some guidelines can be laid to help selection of materials to resist thermal fatigue:

1. The material should have sufficient hot strength and ductility over the service temperature range to resist plastic deformation, and it should not undergo phase changes involving volume differences in this range.
2. Crack initiation sites should be avoided, if possible, and surface and subsurface defects should be at a minimum. This requires the use of low-inclusion material and, in some instances, directional solidification to ensure that no adverse grain boundaries break through to the surface.
3. The material should have a high oxidation resistance, or a protective coating should be used or perhaps both.

As in all types of structures involving fatigue, the design should avoid changes and discontinuities in sections which might cause stress concentration effects to occur.

DISCUSSION

W. J. Elder[1] (*written discussion*)—A linear relationship is shown between crack length and cycle number. At first sight this is surprising, since it implies an exact balance between two opposing effects; the increase in driving force with increasing crack length and the decay of the thermal driving forces as the crack propagates. In fact, if the relationship is not truly linear throughout, then the linear extrapolation used to deduce the crack initiation period is also in question.

Kenneth Hopper[2] (*written discussion*)—I wish to register my viewpoint regarding the applicability of fluidized bed-type thermal-fatigue testing to

[1] Herts, England.

[2] Pratt & Whitney Aircraft, Division of United Aircraft Corp., East Hartford, Conn. 06108.

understanding thermal fatigue and screening candidate materials for use in cyclic high temperature environments. Our experience in the laboratory with the "standard" NGTE disk (B-1900 material) has confirmed Glenny's data on the effect of edge radius, and further testing of a typical Pratt & Whitney Aircraft solid turbine blade in the fluidized bed apparatus has verified these data on component hardware. All this, I feel, indicates that fluidized bed thermal fatigue can be a valid tool for simulating severe gas turbine operating conditions and screening material.

C. E. Rucker[1] *and R. E. Grandle*[1]

Thermoacoustic Fatigue Testing Facility for Space Shuttle Thermal Protection System

REFERENCE: Rucker, C. E. and Grandle, R. E., "**Thermoacoustic Fatigue Testing Facility for Space Shuttle Thermal Protection System,** *Fatigue at Elevated Temperatures, ASTM STP 520*, American Society for Testing and Materials, 1973, pp. 255–263.

ABSTRACT: The development of a reusable space shuttle by NASA in the next decade depends in part on the design of a satisfactory thermal protection system (TPS). The booster and orbiter parts of the shuttle require TPS panels which will withstand thermoacoustic fatigue. The Langley Research Center has begun tests on early panel designs in a new acoustic fatigue facility which is capable of simulating the combined elevated temperature and acoustic environments which these panels are expected to experience. The capabilities of the facility and computer system are outlined, and problems encountered in establishing the test methods are discussed. The digital computer system which controls the acoustic and thermal test sequence and which records data from more than 20 transducers is described. Tests of a Haynes 25 TPS panel are described, and representative data from tests of the panel at 650 C are included.

KEY WORDS: fatigue (materials), acoustic environments, computerized simulation, fatigue tests, control equipment, structural analysis, temperature measurement, test facilities, environmental tests, high temperature tests, thermal environments, thermal cycling tests, automatic control, digital computers, digital techniques

One of the proposed programs of the National Aeronautics and Space Administration (NASA) in this decade is the development and flight of a reusable space vehicle known as the space shuttle. The space shuttle is to be designed for a 100 flight lifetime in order to reduce per mission cost.

Low cost and low weight have great significance in shuttle structural design. Reentry temperatures of 1000 C will be experienced which means new materials and fabrication concepts must be evaluated. Both the booster and the orbiter components of the shuttle have been envisioned to be reusable with temperature/load requirements most stringent for the orbiter. One of the technology areas to which the Langley Research Center (LRC) has committed its resources is support of the thermal protection system (TPS) development.

[1] Aero space technologist and aerospace technologist, respectively, National Aeronautics and Space Administration, Langely Research Center, Hampton, Va. 23365.

Copyright© 1973 by ASTM International www.astm.org

The facilities, equipment, and test panels discussed in this paper are being used presently to establish sonic response and fatigue testing guidelines, and to furnish thermoacoustic design information for development of a functional thermal protection system. This paper discusses the development of the LRC grazing incidence (soundwaves traveling past a test panel as on an airplane) acoustic fatigue test facility in which a computer is used for data acquisition and control. Preliminary tests which were conducted on an orbiter TPS panel are described, and data are presented for 650 C outboard side heating of the panel.

Thermal Protection System Problem

Design of the TPS panels represents a formidable development problem because of the 1000 C thermal environment and stringent weight requirements. The estimated acoustic environment ranges from 151 to 163 dB overall, depending on vehicle location and flight stage (that is, boost, maximum q, reentry). Fortunately, maximum noise levels and maximum temperatures do not occur simultaneously. Evaluation of TPS designs is complicated by a lack of fatigue data for many proposed materials and by the complex structural designs required for alleviation of thermal stresses. There are two basic types of TPS panels: the metallic system and the external insulation system. Acoustics tests at LRC are scheduled for metallic panels fabricated from Rene 41, Haynes 25, L605, and Hastelloy X. Tests of an external insulation system are also planned for a graphite/epoxy sandwich panel with a bonded mullite/ceramic external insulation. Test data in this paper are from a Haynes 25 metallic design.

Acoustic Fatigue Test Facility

Testing of the TPS structures described in the previous section required the development of new capabilities for testing. Figure 1 shows the facility developed to meet high-temperature test requirements with 0.5 by 0.5-m panel in position for testing. A summary of acoustic test facility capabilities is given in Table 1.

Environment Simulation—The air modulator noise generators (Fig. 1) create the sound field which propagates to the left, through the horn and the test section and into a termination section and acoustic treated building exhaust (muffler system) which are used to suppress external noise radiation and reduce reflections into the test section. The inset of Fig. 1 shows the orientation of the 32 quartz lamp heating array used in the initial test with the Haynes 25 TPS panel. The test section is constructed of concrete with a steel lining and is not affected adversely by radiant heating. The modulators use a 0.24-MN/m^2 air pressure source and transmit approximately 3.6-kg/s mass flow. The wall opposite the test panel was modified by recessing a 1.52-m by 1.8-m-high quartz heater array composed of 0.36-m-long

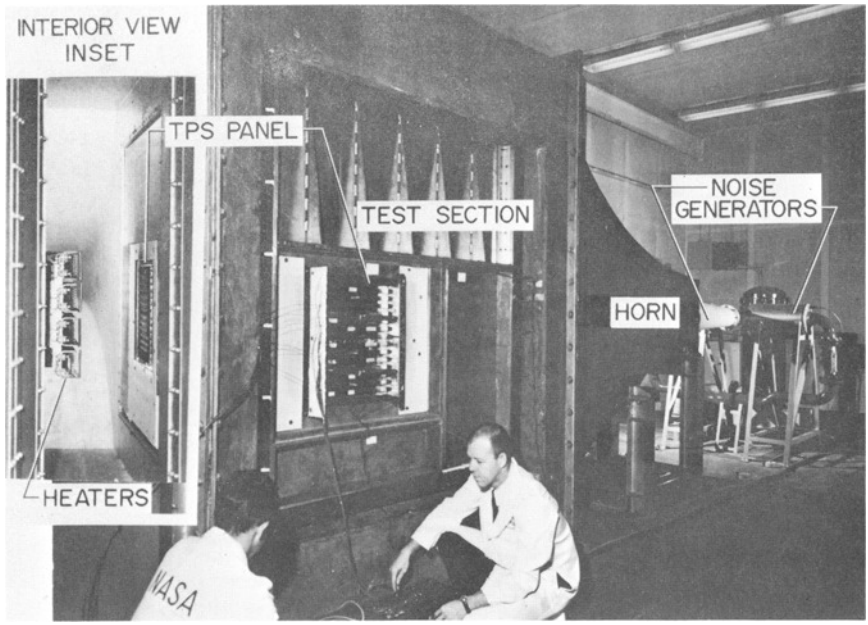


FIG. 1—*Langley Research Center grazing incidence acoustic test facility.* (inset) *View inside test section looking toward generators.*

TABLE 1—*Grazing incidence acoustic fatigue test facility capability.*

Facility	
Sound level	90 to 163 dB rms overall
Frequency	40 to 500 Hz (sine) and 40 to 1000 Hz (random)
Temperature	ambient to 650 C in 63 increments
Specimen size	1.83 by 1.83 m
Heated area	1.52 m long by 1.8 m high
Quartz heaters	72 parbolic reflectors rated at 2.5 kW each

Transducers

Type (temperature limit)	Number Available	Rating	Frequency Limitation	Comments
Strain gages (650 C)	20	gage factor to 4	dynamic only	ADC readout
Accelerometers (760 C)	3	2.5 pC/g	1000 Hz	ADC readout
Microphones (150 C)	10	174 dB	40 Hz to 10 kHz	ADC readout
Thermocouples (1300 C)	32	chromel alumel	60 ms readout time	readout from thermometer or storage register
Air modulator	2	30 kW each	40 Hz to 1 kHz	amplitude/frequency
Thermal controller	5	50 kW each	80 ms response	digital control

standard water-cooled parabolic reflectors following the tests described in this paper. This heater array was installed to obtain a large uniformly heated area. The major considerations in its selection were section stiffness to prevent wall motion, ease of maintenance, and a relatively short conception to installation time. Modifications to the termination section to reduce reflections consisted of lengthening the termination section to 10 m and applying the acoustic absorption treatment.

Experiment Control—Both the test sequence and data acquisition are under computer control. The real-time executive software system controls the acoustic loading, heating, data collection, data comparison, and test status cross checks. The software system is also responsible for: (1) selection of feedback parameters from limited preprogramed alternatives, (2) implementation of emergency or regular experiment termination by preprogramed criteria, and (3) schedule of all operations in accordance with their programed priorities.

Figure 2 shows major elements of the acquisition/control system used for TPS tests. The sine wave excitation may be controlled in frequency and amplitude, and the random spectrum's upper and lower limits constrained for amplitude/frequency control. One-third octave band filter spectrum shaping is also used by manual setting of the filters. The 72 quartz lamp heater array can be divided into as many as five sections with a separate digitally controlled SCR power controller driving from 1 to 20 lamps. The a-c power can be set in 63 increments and may be programed to simulate complex temperature distributions and sequences such as the reentry thermal TPS environment. The experiment control sequence of events utilizes the following elements: (1) a computer program is written which takes into account the design parameters of the TPS panel to be tested, (2) the computer initiates the test by applying acoustic and thermal profiles in accordance with programed instructions, (3) the computer performs the required data acquisition and stores the data, (4) the computer compares

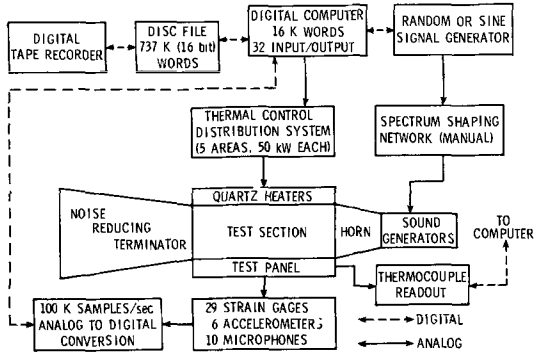


FIG. 2—*Computer control and data acquisition system used for acoustic response and fatigue tests of TPS panels.*

strain, temperature, sound level, or acceleration measurements with preprogramed values and makes necessary adjustments, and (5) the computer terminates the test when programed limits are exceeded or when the test is complete.

Data Acquisition—Two separate collection subsystems are employed: an analog to digital converter (ADC) and a thermocouple readout system (TCRO). The ADC multiplexes up to 48 channels at 100 K readings per second with a 15-bit binary output over a ± 10-V range. The ADC, which is used to collect data from strain gages, accelerometers, and microphones, is read by the computer which stores the data on the disk file and digital tape recorder for subsequent data reduction. The TCRO reads and digitizes 32 chromel-alumel thermocouples in 3.0 s and transmits the data to the digital computer. Channels of the TCRO which are of particular interest can be read more frequently than those given lower priority. During mission simulation cycles of the TPS panels for dynamic environment control, the measurement time is 60 ms, and the important channel is selected by the program. The temperature data are stored on the disk file, formated in the computer, used for closed-loop control of the simulation, and output to a typewriter (not shown) which is monitored by the test conductor.

TPS Tests

The panel illustrated in Fig. 3 and shown in test position in Fig. 1 is the first TPS panel tested in the acoustic fatigue facility. It was instrumented as shown in Fig. 3 and tested at ambient temperature and at 650 C with 141-dB random noise excitation.

TPS Instrumentation—The TPS panel was instrumented on the back surface (inboard side, not exposed to noise or radiant heat) with three types of elevated temperature strain gages. A 2.8-cm gage length temperature compensated welded gage, a 0.95-cm gage length welded gage, and a 0.79-cm

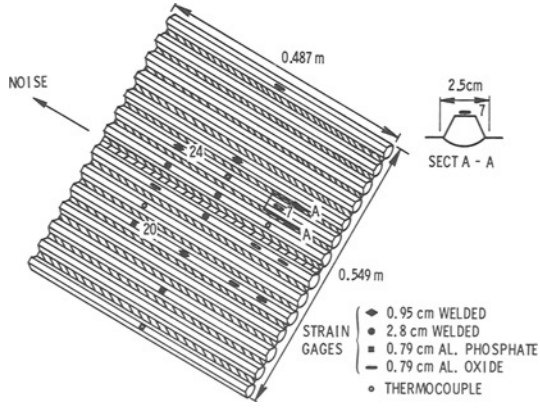


FIG. 3—*Strain gage and thermocouple locations for a Haynes 25 TPS panel test.*

gage length platinum alloy free filament gage were used. The free filament gage was attached to the panel with either an aluminum oxide refractory coating or an aluminum phosphate adhesive. Figure 3 shows the arrangement of the strain gages used in these tests and also the location of six chromel-alumel thermocouples. The selection of strain gages for this panel was made in order to gain experience with high-temperature instrumentation to be used in subsequent tests on larger panels.

Test Plan—Each TPS is designed for a different vehicle location and is excited by a slightly different environment. Figure 4 shows a typical test profile for mission simulation of a booster panel environment. A response test program is written to apply acoustic loads of not more than 155-dB overall sound pressure level as given by the reentry block (rectangle in Fig. 4 marked "reentry"), and ambient temperature data runs are made followed by data runs at 40 and 177 C (204 and 650 C for metallic radiative type panels). Sound pressure is applied in narrow band random from (50-Hz bandwidth) with a center frequency of 180 Hz corresponding to the first mode response of the panel. Root mean square (rms) transducer response for narrow band loading is ratioed directly to rms predicted strains and accelerations for each thermal condition. Strain and accelerations are also measured for a 40 to 1000-Hz broad-band acoustic loading for each thermal condition. When the data have been collected and reviewed, 100 cycles of the block loading sequence shown in Fig. 4 are applied. Control loops are established for controlled strain response during the response tests with checks on temperature and sound pressure limits. During the mission cycling reentry simulation, temperature is the primary parameter, and limit checks will be made on sound pressure. Data from transducers are collected for each cycle.

Test Results—When this paper was prepared, the first TPS test was incomplete. The Haynes 25 panel had experienced two heat cycles to 650 C. Test measurements indicated a severe temperature gradient. The outboard (heated) side near strain gage No. 7 (Fig. 3) was 555 C, while the inboard

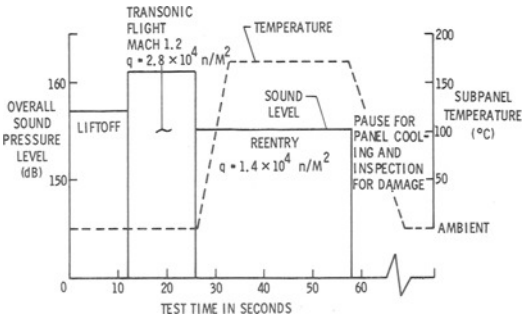


FIG. 4—*Example of mission cycle simulation on acoustic loads and thermal loads for a booster TPS panel.*

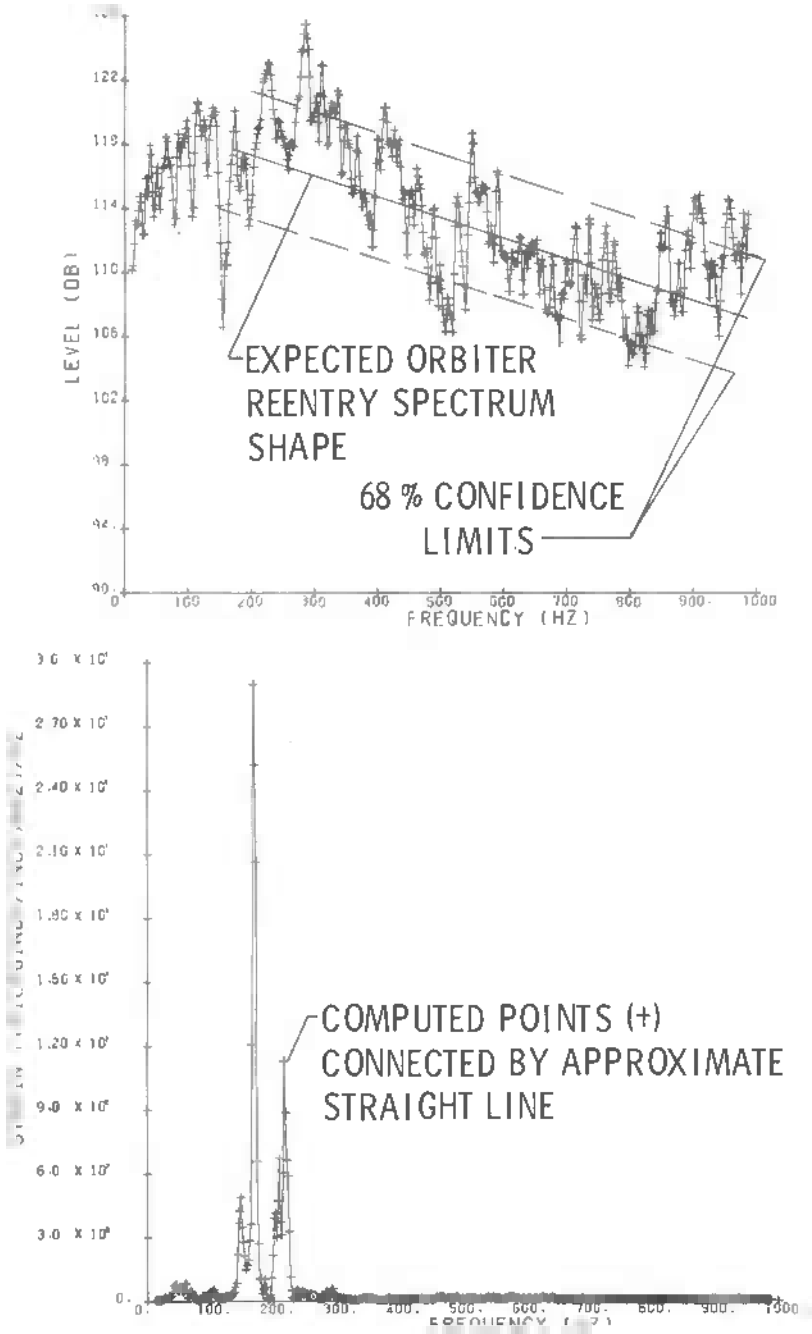


FIG. 5—*Typical data output of acoustic facility computer system*; (left) *applied sound pressure and* (right) *power spectral density of TPS panel strain response.*

side was 267 C. The outboard side near strain gage No. 20 was 513 C, while the inboard side was 257 C. During heating the panel bends considerably, but installation of a microquartz insulation blanket which is a part of the "system" does much to reduce the temperature gradient which causes the bending by reducing the heat losses through the back side. In order to reach 650 C it was necessary to blacken the panel surface by depositing a carbon residue, created by a welding torch, on the panel surface.

Test data are shown in Fig. 5 as calculated in the acoustic facility computer and plotted on the system's digital plotter. The top part of Fig. 5 shows the spectrum level of the network-shaped, board-band sound level input recorded from a microphone directly upstream of the test panel and an expected orbiter spectrum profile. The lower part of Fig. 5 shows the mean square spectral density of the output of strain gage No. 24, while the exterior surface was heated to 650 C (nominal). No thermocouple was located at the strain gage, but the temperature is estimated, by assuming the same ratio (exterior to interior) as other locations, to be about 260 C. The primary amplitude peak shown in the Fig. 5 strain plot corresponds to the predicted panel first mode frequency response. Plots such as shown in Fig. 5 can be produced on site in about 10 min and can be determined during programed pauses to be used in monitoring test progress and output evaluation.

Concluding Remarks

Initial tests conducted in the new LRC acoustic fatigue facility demonstrate capability to generate on a 0.5 by 0.5-m panel, combined environments of 650 C radiant heating and 141-dB sound pressure level, and recording data from more than 20 transducers, under computer control. Closed-loop control of experiment parameters and data acquisition have been demonstrated by tests conducted on a realistic TPS panel of Haynes 25 high-temperature material. The data acquisition system provides on-site digital plots of sound pressure, acceleration, and strain response spectra which can be determined promptly for use in monitoring test progress and evaluating test conditions and panel response.

Bibliography

Materials

Brown, W. F., Jr., and Espey, G. B., "Considerations in Selection of Wing and Fuselage Sheet Materials for Trisonic Transports," presented at International Air Transport Association 14th Technical Conference, *Symposium on Supersonic Air Transport*, Montreal, April 1961.

Figge, I. E., "Residual Strength of Alloys Potentially Useful in Supersonic Aircraft," NASA TN D-2613, National Aeronautics and Space Administration, Feb. 1965.

Figge, I. E., "Residual Static Strength of Several Titanium and Stainless-Steel Alloys and and One Superalloy at −109° F, 70° F, and 550° F," NASA TN D-2045, National Aeronautics and Space Administration, Dec. 1963.

Phillips, E. P., "Fatigue of Rene 41 Under Constant and Random-Amplitude Loading at Room and Elevated Temperatures," NASA TN D-3075, National Aeronautics and Space Administration, Nov. 1965.

Webster, D., "Strengthening Mechanisms in Dispersion Hardened Nichrome," Report No. D6-19773, Boeing Co., Defense Documentation Center.

TPS Concepts

Bauer, P. E. and Kumer, D. L., "A Survey of Reusable Metallic and Non-Metallic Thermal Protection Materials for Space Shuttle Applications," presented at AIAA Advanced Space Transportation Meeting, American Institute of Aeronautics and Astronautics, Cocoa Beach, Fla., 4–6 Feb. 1970.

NASA Space Shuttle Technology Conference, *Proceedings*, Conference held at LRC, 2–4 March 1971, NASA TM X-2274, National Aeronautics and Space Administration, April 1971.

Plank, P. P., Sakata, I. F., Davis, G. W., and Richie, C. C., "Hypersonic Cruise Vehicle Wing Structure Evaluation," NASA CR-1568, National Aeronautics and Space Administration, 1970.

Computer Control and Data Acquisition

Bosco, G. H., "A Large Vehicle Acoustic Test Facility," presented at IES National Meeting, Illuminating Engineering Society, Boston, Mass., April 1970.

Rucker, C. E. and Grandle, R. E., "Reversed Bending Fatigue Tests of Fan Jet Nacelle Treatment Acoustic Materials Using Closed Loop Computer Control," presented at 42nd Shock and Vibration Symposium, Key West, Fla., 2–4 Nov. 1971.

L. A. Imig[1]

Fatigue of Supersonic Transport Materials Using Simulated Flight-by-Flight Loading

REFERENCE: Imig, L. A., "**Fatigue of Supersonic Transport Materials Using Simulated Flight-by-Flight Loading,**" *Fatigue at Elevated Temperatures, ASTM STP 520*, American Society for Testing and Materials, 1973, pp. 264–272.

ABSTRACT: Methods to reduce the fatigue test time for structural materials which are candidates for supersonic transport airplanes were investigated by conducting real-time and accelerated fatigue tests. The tests employed sequences of stresses and temperatures to simulate the flights of a Mach 3 transport airplane. Some of the simulated flights were altered to determine the effect of the design mean stress and the number of stress cycles per flight on fatigue life. Salt solution was also applied in other tests. Notched Ti-8Al-1Mo-1V and Ti-6Al-4V were used in the investigation.

KEY WORDS: fatigue (materials), stress cycle, elevated temperature, supersonic transports, titanium alloys, environment simulation, flight simulation, salt water, axial stress, accelerated tests

The structural integrity of a supersonic transport (SST) will depend to a great extent on its ability to withstand the effects of its loading and flight environment. To simulate, in real time, the effects of the expected operating conditions of an SST on structural materials would require an impractically long time. Therefore, experiments were conducted to explore methods to reduce the test time. The two approaches taken were to increase the testing speed from that of real-time operation and to identify parameters which could be omitted from the test.

Stresses expected at a critical location in a lower wing skin were programed to simulate individual flights. The stress sequences thus formulated were applied to test specimens in "real-time" and "accelerated" tests. The test specimens were made from titanium-alloy sheet and had notches to represent moderate structural discontinuities.

The present report extends the research reported previously [*1,2*][2] for Ti-8Al-1Mo-1V. This paper also presents new test results for Ti-6Al-4V in two heat-treatment conditions.

[1] Aerospace technologist, Fatigue Section, Structural Integrity Branch, Materials Division, National Aeronautics and Space Administration, Langley Research Center, Hampton, Va. 23365.

[2] The italic numbers in brackets refer to the list of references appended to this paper.

Copyright© 1973 by ASTM International www.astm.org

Experimental Procedures

Materials and Specimens

The sheet materials for this investigation were duplex annealed Ti-8Al-1Mo-1V (1.27 mm thick), single annealed Ti-6Al-4V (1.02 mm thick), and solution treated and aged Ti-6Al-4V (1.27 mm thick). Their tensile properties, determined from tests of standard tension specimens, agree closely with the tensile properties given in Ref *3* for similar materials.

Fatigue specimens from all three materials were shaped as shown in Fig. 1. The stress concentration factor for the notch, based on net section axial stresses, was determined experimentally to be 4.1; the stress concentration factor was determined from a 300-mm-wide specimen geometrically similar to that shown in Fig. 1. The longitudinal dimension of each specimen was aligned with the rolling direction of the sheet material.

As shown in Fig. 1, specimens for accelerated tests had one notch, but specimens for real-time tests had six notches. Six notches were included in real-time specimens so that several notched sections could be tested simultaneously in each test stand. After each failure, the specimen was spliced and the test was continued until all notches had failed.

Stresses

Sequences of stresses expected on the lower surface of an SST wing were derived by Imig and Illg [*1*] for individual flights and were used in the present study. Typical stress sequences are shown in Fig. 2. Both "operational" and "check" flight maneuvers of an SST and atmospheric turbulence were considered as sources of wing loading.

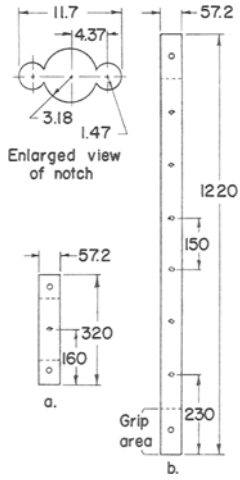


FIG. 1—*Specimen configurations (dimensions are in millimeters):* (a) *specimen for accelerated tests and* (b) *specimen for real-time tests.*

Operational flights represent routine commercial operation. Stress amplitudes, from maneuvers and turbulence, that were expected to occur at least once per flight were grouped together to form a basic operational flight (see Fig. 2*a*). Larger stress amplitudes, which were expected to occur less frequently than once per flight, were added during each 5th, 100th, 1000th and 10 000th operational flight. Thus, the flights were of differing severities; the 10 000th flight was the most severe (see Fig 2*b*). The important aspects of operational flights are that more stress cycles occurred in climb than in cruise and descent, the mean stress decreased during the flight to simulate a loss of mass due to fuel consumption, and each flight ended with a compressive stress excursion equal to one half of the design mean stress. The excursion between the ground stress and in-flight stresses is called the ground-air-ground cycle (GAG). The mean stresses for the climb, cruise, and descent segments of flight, expressed as fractions of the design mean stress (S_{lgd}), were: 1.0, 0.75, and 0.60, respectively (see Fig. 2).

Check flights, for crew training, were applied after each group of 24 operational flights. Each check flight (see Fig. 2*c*) included seven GAG cycles to represent the touch-and-go landings that occur frequently during check flying. Infrequent severe stresses were added during the 10th and 100th check flights in the manner described for operational flights. The mean stress for check flights was 0.70 of S_{lgd}.

Fatigue Tests

All specimens were tested in hydraulically actuated, closed-loop, servo-controlled testing machines. They were loaded axially. The stresses were based on the initial net area at the test section of each specimen.

To determine the effect of testing speed, the investigation employed two methods of conducting the fatigue tests which are differentiated by the labels "real-time" and "accelerated." Both testing methods used identical sequences of stresses as described in the preceding section. In real-time tests,

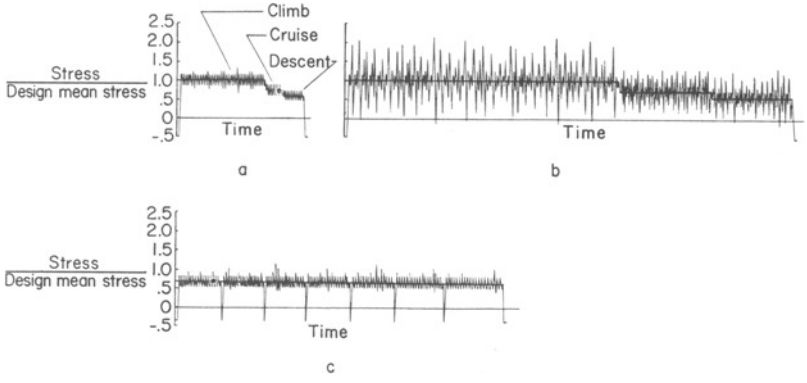


FIG. 2—*Stress sequences for operational and check flights:* (a) *basic operational flight,* (b) *10 000th flight, and* (c) *basic check flight.*

each operational flight required about 100 min to complete and included a 90-min-long period of radiant heating during the cruise segment, as shown in Fig. 3. At the end of the cruise segment, the heating was interrupted and the specimens were cooled by a stream of compressed air during the descent segment of flight. Thus, the stress cycles during descent were applied during a period of decreasing temperature. Typically, the temperature of the specimen dropped to 315 K at the end of descent; the forced cooling continued into the climb segment of the next flight until a minimum temperature of about 300 K was reached (see Fig. 3). In contrast, accelerated tests were conducted at a rate of about 2 s per basic operational flight (Fig. 2*a*) and at constant temperature.

The objectives of this investigation were to determine the relative effects of real-time and accelerated tests on fatigue life and to determine the effects of the design mean stress, the test temperature, the number of stress cycles in each simulated flight, and light salt accumulations. The values of design mean stress used were 172, 207, and 241 MN/m^2. Real-time tests were conducted with maximum cyclic temperatures of 561 and 616 K. Accelerated tests were conducted at room temperature and 561 K. The stress sequences and their variations are described next.

Type A Stress Sequence—Type A stress sequences contained all the stresses for a simulated flight as described previously and shown in Figs. 2 and 3. The results of real-time tests with Type A stress sequences were considered as standards to which the results of other tests were compared. Type A stress sequences were used in both real-time and accelerated tests of all three materials.

Type F and Type G Stress Sequences—The effect of the number of stress cycles in each flight on fatigue life was determined from tests with Type F and Type G stress sequences. Type F stress sequences were developed by omitting all cycles of the smallest amplitude from the Type A stress sequence (see Fig. 4). Basic operational flights, then, retained only a climb segment because the cruise and descent segments of the Type A stress sequences consisted entirely of the small amplitude cycles. The more severe flights (5th, 100th, 1000th, and 10 000th flights) which contained cycles of larger amplitude in cruise and descent retained the normal climb-cruise-descent arrangement.

The Type G stress sequence was composed of a single cycle ranging between the maximum stress in each Type A sequence and $-1/2\ S_{tgd}$.

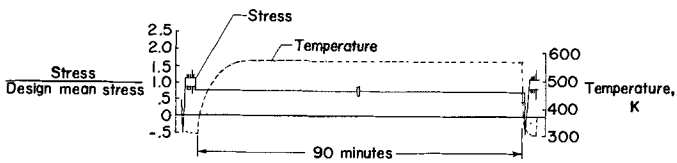


FIG. 3—*Stress and temperature for basic operational flights in real-time tests.*

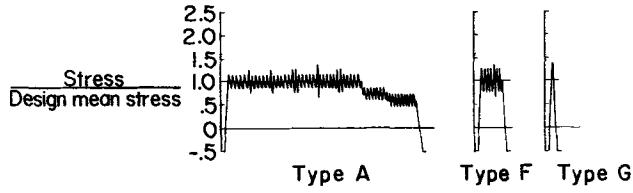


FIG. 4—*Stress sequences for study of simplified flights.*

Tests were Type F and Type G sequences were all accelerated and were conducted only on Ti-8Al-1Mo-1V.

Tests with Salt—In one series of real-time tests on specimens of Ti-8Al-1Mo-1V, a $3\frac{1}{2}$ percent solution of sodium chloride was applied each workday to determine the combined effects of light salt accumulation and long exposure to elevated temperature. The tests were conducted with a maximum cyclic temperature of 616 K and utilized the Type A stress sequence.

Results and Discussion

Median fatigue lives are presented in Tables 1–3 and are plotted in Figs. 5–7. The lives are the total number of operational flights plus check flights survived by each specimen.

TABLE 1—*Fatigue lives from real-time tests at 561 K [specimens were notched (K_T = 4.1)].*

Stress Sequence	Design Mean Stress, MN/m^2	Number of Tests	Median Fatigue Life, flights
	DUPLEX ANNEALED Ti-8Al-1Mo-1V, 1.27 MM THICK		
A	172	1	14 800
	207	6	10 050
	241	6	5 093
A[a]	207	6	6 933
	241	6	4 642
A[b]	172	2	10 760
	207	6	5 254
	241	6	4 462
	ANNEALED Ti-6Al-4V, 1.02 MM THICK		
A	207	4	16 000
	241	6	5 697
	SOLUTION TREATED AND AGED Ti-6Al-4V, 1.27 MM THICK		
A	207	6	8 433
	241	6	5 100

[a] Maximum temperature in each flight was 616 K.

[b] Maximum temperature in each flight was 616 K, and salt solution was applied to specimens once each workday.

TABLE 2—*Fatigue lives from accelerated tests at room temperature [specimens were notched* (K_T = *4.1)*].

Stress Sequence	Design Mean Stress, MN/m^2	Number of Tests	Median Fatigue Life, flights
	DUPLEX-ANNEALED Ti-8Al-1Mo-1V, 1.27 MM THICK		
	172	10	63 540
A	207	7	14 800
	241	9	7 270
	172	3	106 200
F[a]	207	3	22 150
	241	3	9 650
	172	3	111 380
G	207	3	44 930
	241	3	18 860
	ANNEALED Ti-6Al-4V, 1.02 MM THICK		
	172	6	61 722
A	207	6	13 220
	241	6	6 280
	SOLUTION TREATED AND AGED Ti-6Al-4V, 1.27 MM THICK		
	172	6	90 988
A	207	6	11 870
	241	6	6 160

[a] Cycle of largest amplitude was inadvertently omitted from 5th flights.

Results of Tests with Type A Stress Sequences

The result of both real-time and accelerated tests with Type A stress sequences are shown in Fig. 5. These results indicate the large effect of design mean stress on fatigue life. For example, Fig. 5*a* indicates that fatigue lives from accelerated tests of Ti-8Al-1Mo-1V at 241 MN/m^2 were only about one tenth of the lives at 172 MN/m^2. That result was generally true for all three materials and for accelerated tests at both room temperature and 561 K. (Note that real-time tests at 172 MN/m^2 are incomplete and should not be included in the statement.) For all three materials, the fatigue lives at 561 K were about one half the lives at room temperature.

Figure 5 indicates that the lives from real-time tests were between the lives from accelerated tests at room temperature and those at elevated temperature. Thus, in general, the results suggest that accelerated tests can adequately approximate the real-time fatigue lives of these materials, but this tentative conclusion should be verified with more complex specimens before extending it to aircraft structures.

TABLE 3—*Fatigue lives from accelerated tests at 561 K [specimens were notched (K_T = 4.1)].*

Stress Sequence	Design Mean Stress, MN/m^2	Number of Tests	Median Fatigue Life, flights
	DUPLEX-ANNEALED Ti-8Al-1Mo-1V, 1.27 MM THICK		
	172	6	33 270
A	207	6	7 105
	241	6	3 715
	172	3	21 561
F	207	4	10 571
	241	4	6 457
	172	3	54 350
G	207	3	21 530
	241	3	10 416
	ANNEALED Ti-6Al-4V, 1.02 MM THICK		
	172	6	19 186
A	207	6	16 555
	241	6	13 340
	SOLUTION TREATED AND AGED Ti-6Al-4V, 1.27 MM THICK		
	172	6	18 922
A	207	6	5 375
	241	6	3 315

Results of Accelerated Tests with Simplified Stress Sequences

The results of accelerated tests with simplified (Type F and Type G) stress sequences are compared to the results of tests with Type A stress sequences in Fig. 6. In general, progressive simplification of the stress sequences produced progressively longer fatigue lives. Arbitrary simplification of structural tests should be considered carefully because, besides producing longer fatigue lives, a simplified test may result in failure locations different from those in a more realistic test [*4*].

Results of Tests with Salt

The results of real-time tests with and without the salt solution are shown in Fig. 7. The maximum cyclic temperature in this series of tests was 616 K, and the total exposure to elevated temperature exceeded 5000 h in all tests. The results indicate a relatively small effect of the salt on fatigue life. In contrast, Royster [*5*] indicated that hot-salt stress-corrosion cracking occurred in Ti-8Al-1Mo-1V, duplex annealed, after only 800 to 1200 h of exposure to 590 K with heavy salt coatings and constant stresses of the same value as the cruise levels in the present tests. Because the two types of tests resulted in different amounts of salt corrosion, assessment of salt corrosion for a specific situation should include quantitative simulation of the features of the environment being considered.

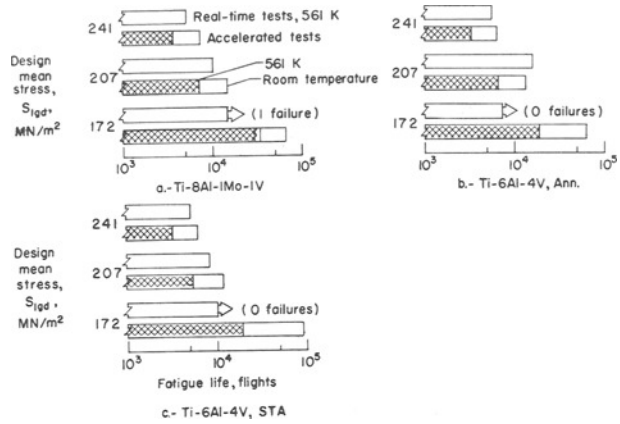


FIG. 5—*Results of real-time and accelerated tests with Type A stress sequences.*

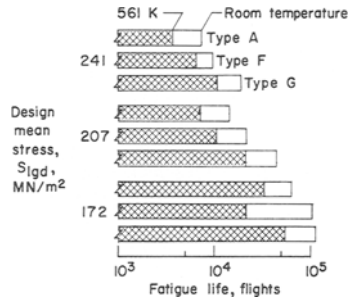


FIG. 6—*Effect of the number of stress cycles per flight on fatigue life of Ti-8Al-1Mo-1V in accelerated tests.*

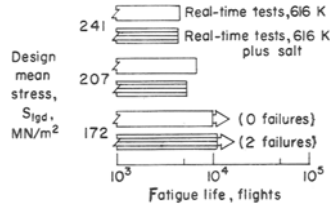


FIG. 7—*Effect of salt in real-time fatigue tests of Ti-8Al-1Mo-1V with Type A stress sequences.*

Concluding Remarks

Methods for reducing the fatigue test time for structural materials for supersonic transport airplanes were investigated by conducting real-time and accelerated tests on notched specimens of titanium alloys. The tests employed sequences of stresses and temperatures to simulate the flight of a Mach 3 transport airplane. Some of the simulated flights were altered to

determine the effect of the design mean stress and the number of stress cycles per flight on fatigue life. Salt solution also was applied in some tests.

The test results led to the following observations:

1. The fatigue lives from real-time tests were between the lives from accelerated tests at room temperature and 561 K. Both kinds of tests employed the same stress sequences.

2. Fatigue lives from accelerated tests at 561 K were approximately one half as long as the lives from accelerated tests at room temperature.

3. Progressive simplification of the stress sequences used to simulate flights produced progressively longer fatigue lives in accelerated tests at room temperature and at 561 K.

4. Exposure to a $3\frac{1}{2}$ percent salt solution had only a small detrimental effect on the fatigue life of Ti-8Al-1Mo-1V test specimens in real-time tests in which the maximum temperature was 616 K.

References

[1] Imig, L. A. and Illg, Walter, "Fatigue of Notched Ti-8Al-1Mo-1V Titanium Alloy at Room Temperature and 550° F (560° K) with Flight-by-Flight Loading Representative of a Supersonic Transport," NASA TN D-5294, National Aeronautics and Space Administration, 1969.

[2] Imig, L. A., "An Investigation of Fatigue in a Supersonic Transport Operating Environment," SAE Paper No. 700033, Society of Automotive Engineers, 1970.

[3] "Metallic Materials and Elements for Aerospace Vehicle Structures," MIL-HDBK-5A, Department of Defense, 1966.

[4] Ward, J. F. and Huston, W. B., "Evaluation of Fatigue Sensitive Areas and Cumulative Damage in Full-Scale Fatigue Testing," U.S. Air Force Symposium on Fatigue of Aircraft Structures, Dayton, Ohio, Aug. 1959.

[5] Royster, D. M., "Hot-Salt-Stress-Corrosion Cracking and Its Effect on Tensile Properties of Ti-8Al-1Mo-1V Titanium Alloy Sheet," NASA TN D-4674, National Aeronautics and Space Administration, Aug. 1968.

A. F. Conn[1] *and N. A. Nielsen*[2]

Ultrasonic Fatigue in Steam with Small Amounts of Sodium Chloride

REFERENCE: Conn, A. F. and Nielsen, N. A., **"Ultrasonic Fatigue in Steam with Small Amounts of Sodium Chloride,"** *Fatigue at Elevated Temperatures, ASTM STP 520*, American Society for Testing and Materials, 1973, pp. 273–281.

ABSTRACT: Premature failure of steam turbines is a problem in both manufacturing operations and power generation plants. Information on the influence of contaminant sodium chloride in steam on the corrosion fatigue life of Type 403 stainless steel, the most common steam-turbine blade material, is needed. High-frequency fatigue tests were conducted on bare specimens of Type 403 steel, both in a pure-steam environment at 250 F, and in steam contaminated with small quantities of sodium chloride. Tests were also conducted on shot-peened specimens diffusion-coated for corrosion protection. With 2000 ppm of salt in the steam, considerable reduction in fatigue life was observed for bare steel in relatively brief tests at high ultrasonic frequencies. Considerable increase in fatigue life was observed for the shot-peened and coated specimens. The results show that even trace quantities of a corrodent at elevated temperatures can greatly reduce fatigue lifetimes of steam-turbine blade material. The effectiveness of the coating system was demonstrated clearly in these tests, suggesting important increases in the operational lifetimes of steam-turbine equipment.

KEY WORDS: fatigue (materials), corrosion fatigue, stainless steels, ultrasonic frequencies, corrosion, corrosion prevention, diffusion coating, shot peening, fractures (materials), fractography

Failure of steam-turbine blades and shrouds after relatively brief operating periods motivated an investigation into the causes of fracture and possible methods for extending the operational lifetime of such equipment. The apparent reason for the failures was corrosion fatigue caused by low levels of sodium chloride (NaCl) in "wet" steam containing a small percentage of condensate. However, local accumulations of corrodent (NaCl) were observed on the fractured blades, indicating that salt concentration had taken place. Also, a relatively high resonant frequency of vibration in these blades may have contributed to the premature failures.

[1] Principal research scientist, Head Materials Science Division, Hydronautics, Inc., Laurel, Md. 20810.

[2] Research fellow, Engineering Department, E. I. duPont de Nemours and Co., Inc. Wilmington, Del. 19898.

Copyright© 1973 by ASTM International www.astm.org

Possible solutions, pending identification of the cause, would include: (1) improving the removal of sodium chloride from the makeup water, (2) modifying the turbine design to minimize accumulation of salt deposits, (3) selecting a more highly corrosion-fatigue-resistant alloy for the blades, and (4) surface treating existing blade materials with protective coatings or shot peening to improve their fatigue life and corrosion resistance.

The experimental program described in this paper was initiated to confirm corrosion fatigue as the cause of turbine-blade failure and to determine whether or not 2000 ppm of salt (arbitrary level) could actually accelerate fatigue failures at high frequencies. High-frequency fatigue tests, experimental results, and conclusions drawn from the work are discussed next.

High-Frequency Fatigue Testing

The early developers of high-frequency fatigue testing include Gaines [*1*],[3] Mason [*2*], and Neppiras [*3,4*]. The technique requires the magnetostriction apparatus shown in Fig. 1. In this test, longitudinal oscillations are created in a fatigue specimen at its resonant frequency, producing uniaxial, alternating strains. The maximum strains are produced at the node of the resonant specimen and are amplified by a carefully designed dumbbell-shaped configuration at the node. Details of the fatigue specimen design, which are based on Neppiras' theory [*3*], have been described by Thiruvengadam and Preiser [*5,6*]. The specimen dimensions used for these tests are shown in Fig. 2. The output from the displacement measuring coil is calibrated by direct observations of the maximum amplitudes with a microscope. The strain amplitude calculations were verified by use of strain gages mounted on the radius of test specimens.

The time to failure is determined when a crack forms in the specimen and is characterized by the increased power level required to maintain a constant displacement amplitude. This amplitude is monitored continuously on an oscilloscope. The number of cycles to failure is computed by multiplying the time to failure and the frequency. This determination differs from conventional fatigue testing where the specimen breaks into two pieces. In these high-frequency fatigue tests, the crack has typically grown to nearly half of the cross section when the increase in power is observed.

The test apparatus can be modified for operation under hostile environments such as seawater, steam, or liquid metals, and at elevated temperatures. With only the specimen exposed to the (generalized) test environment, as shown in Fig. 1, virtually any required condition may be simulated. Details of the techniques used to create the salt-steam environment required for this investigation are given next. Operational procedures have been described by Thiruvengadam et al [*5,7*].

[3] The italic numbers in brackets refer to the list of references appended to this paper.

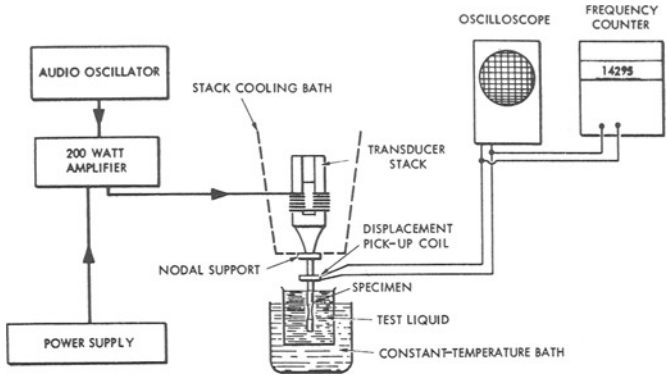
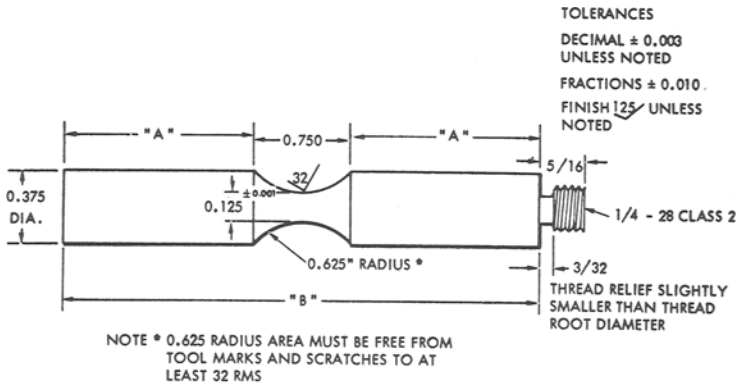


FIG. 1—*Block diagram of the magnetostriction apparatus used for high-frequency fatigue tests.*

Creation of Test Environments

The following conditions were used in this study: (1) "clean" steam saturated at 250 F and containing approximately 20 ppm total dissolved ionizable material, to generate a set of baseline data for the bare material and (2) contaminated steam saturated at 250 F, and containing about 2000 ppm of NaCl, to provide the corrosive environment for the remainder of the tests.

The steam for these tests was generated by a commercial, electric heated, aluminum sterilizer with the following modifications. A sight glass was in-



MATERIAL	A, in.	B, in.	RESONANT FREQUENCY kHz
403 STAINLESS STEEL (250°F)	2.045	4.840	14.0

FIG. 2—*Dumbbell-shaped high-frequency fatigue specimen.*

stalled on the side to allow observation of the water level. A high-temperature epoxy coating was applied to the internal aluminum surface to prevent corrosive attack by the boiling solution. All other components in contact with the boiling solution were either stainless steel or Inconel.

A flotation device was developed and used inside the steam generator for the contaminated steam tests. This device picked up steam at specific distances above the liquid surface, thus controlling the amount of impurities carried in the steam fed to the specimens. Flexible copper tubing wrapped with heating cable transferred this steam to a test chamber. To preserve steam quality, heat input to the tubing was maintained carefully at 250 F.

The specimen was positioned inside a sealed cylindrical test chamber. Steam entered the chamber through four nozzles, oriented around the small gage section of the specimen, so that steam jets would impinge continuously on this area. Throttling occurred as steam exited the test chamber through a valve after impinging on the specimen; thus, a nearly saturated condition was maintained in the chamber at all times.

A steam flow rate of 1 lb/h allowed about 20 h of continuous operation with the existing steam generator water capacity, thus eliminating a makeup feed system. Heat input to the steam generator was balanced carefully to the 1 lb/h produced, so that constant temperature and pressure were maintained.

Steam temperature was monitored by thermocouples at three locations in the system: (*a*) steam generator exit, (*b*) transfer tubing midway to the test chamber, and (*c*) inside the chamber directly where steam impinged on the specimen. In this manner the steam temperature was controlled to within 2 F.

Demineralized water was used for the clean-steam tests. After passing through the test loop, this steam yielded condensate containing approximately 20 ppm of impurities, which included about 1 ppm of copper. The copper was apparently from the feed tubing and was judged to be an acceptable impurity level for the baseline tests. Dissolved salt concentration in the condensate was measured with a Beckman conductivity bridge. The contaminated steam environment was produced by the flotation device set at a predetermined point, with a 1 weight percent NaCl solution in demineralized water in the steam generator. Condensate from steam passed through the test loop with this arrangement contained about 2000-ppm dissolved salt. The contaminated steam environment also included about 5 ppm of copper, but this amount was judged to be negligible when compared with the primary contaminant of 2000-ppm NaCl.

Materials Tested

The base material for all high-frequency fatigue tests was Type 403 stainless steel meeting specifications within the limits of ASTM Specification for Stainless and Heat-Resisting Steel Bars and Shapes (A 276-72).

Specimens were fabricated from ⅜-in.-diameter round stock having these mechanical properties:

Tensile strength, psi	113 000
Yield strength at 0.2 percent offset, psi	95 700
Elongation in 2 in., percent	25.5
Hardness, Rockwell B	96

From these specimens, 14 were selected at random for surface treatments. Of these, 12 were shot peened and then coated with a Chromalloy A12 protection system. This coating, made by the Turbine Support Division of Chromalloy American Corp., consists of a sacrificial intermetallic compound formed by pack cementation and an outer nonmetallic conversion coating. Two specimens received shot peening only.

Results of Fatigue Tests

The data for all of the specimens tested are listed in Table 1. For each test the quantity of NaCl in the condensed steam that had contacted the specimen was measured.

Faired curves through the average of the cycles to failure at each stress level (data from Table 1) for all exposure conditions of the Type 403 steel specimens are shown in Fig. 3. For uncoated specimens in contaminated steam, fatigue life was about one decade shorter than that achieved in a pure steam environment. Although these tests ranged from about 12 min at 10^7 cycles, to almost 20 h at 10^9 cycles, the corrosive effects were exhibited uniformity. Indeed, this entire range of test duration is considerably shorter than the standard corrosion fatigue tests, which typically require weeks,

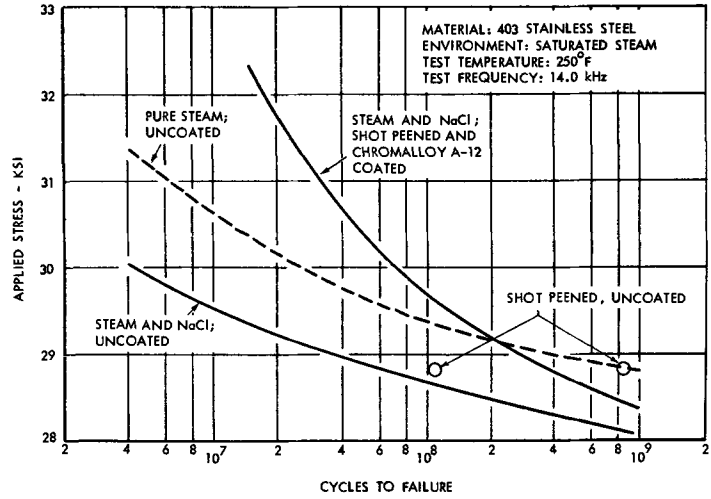


FIG. 3—*Comparison of the high-frequency fatigue tests on Type 403 stainless steel.*

TABLE 1—*High-frequency fatigue data for Type 403 stainless steel at 14.0. kHz in clean and contaminated steam at 250 F.*

Bare Material in Clean Steam			Bare Material in Contaminated Steam			Shot-Peened Bare Material in Contaminated Steam		
Applied Stress, ksi	Cycles to Failure	Salt Concentration, ppm	Applied Stress, ksi	Cycles to Failure	Salt Concentration, ppm	Applied Stress, ksi	Cycles to Failure	Salt Concentration, ppm
28.8	6.71×10^8	20	27.8	$>10^{9a}$	1800	28.8	1.06×10^8	2500
28.8	8.56×10^8	20	28.2	7.20×10^8	2300	28.8	8.96×10^8	2200
28.8	9.04×10^8	18	28.2	2.70×10^8	2500			
29.5	4.60×10^7	29	28.2	6.18×10^8	3000	Shot-Peened and Chromalloy A-12 Coated		
29.5	5.90×10^7	20	28.8	3.22×10^7	2200	Material in Contaminated Steam		
29.5	1.09×10^8	25	28.8	5.72×10^7	2300			
30.7	6.75×10^6	30	28.8	2.0×10^8	1900	28.8	3.84×10^8	2500
30.7	1.09×10^7	30	29.5	1.57×10^7	2300	28.8	2.39×10^8	3000
30.7	9.53×10^6	20	29.5	4.45×10^6	2200	28.8	5.41×10^8	2500
			29.5	1.22×10^7	2800	29.5	8.99×10^7	1100
						29.5	2.49×10^8	2000
						29.5	4.05×10^7	2500
						30.7	9.15×10^7	2700
						30.7	4.62×10^7	2700
						30.7	1.43×10^7	2500
						30.7	3.36×10^6	2700

[a] Run out—did not fail.

months, or years to complete. Thus, the results of high-frequency fatigue tests not only demonstrate the feasibility of utilizing this technique to study corrosion fatigue, but also show that even small amounts of a corroding agent (of the order of 2000 ppm of NaCl) can greatly reduce fatigue life.

Figure 3 also indicates the effectiveness of shot peening combined with Chromalloy A12 coating. Comparing the top and bottom curves, we see the effectiveness of the surface treatment in increasing the fatigue life of Type 403 steel. Despite the typical life scatter in these data, the treated specimens showed significantly larger lifetimes, and there is virtually no overlap with the data from the untreated material. The mean lifetimes of the two test series in the contaminated environment are separated of the order of one decade over most of the stress range studied.

The fatigue curve for the protected metal is seen to be considerably steeper than either of the curves for the bare metal. At the higher cycles, the data for the shot-peened and coated specimens in the salt-steam fall below the response of the uncoated stainless steel in the pure steam environment. The relative steepness of the data for the protected specimens may be due to a gradual deterioration of the coating system, allowing more of the corrosive environment to reach the metal in the higher cycle tests.

One might question the relative contributions of the shot peening and coating on the improved lifetimes shown on this figure. There is considerable scatter for the two tests run on the specimens that received only shot peening. Nevertheless, these two tests did bracket the data for the shot-peening and coated specimens tested at the same stress level. Although it is tempting from these results to attribute most of the increased life to the shot peening alone, we cannot draw firm conclusions from two fatigue tests, particularly with the rather large scatter exhibited. Indeed, if an important part of the experimentally observed increase in fatigue life is attributable to the shielding from corrosion that the coating provides, additional tests of shot-peened specimens might show a considerably shorter mean lifetime than is implied by the two test results in Fig. 3. However, the combined treatment of peening plus the Chromalloy A12 has clearly improved the fatigue life of Type 403 stainless steel under the corrosive conditions used in these tests. (Three month long fatigue tests at 30 Hz also confirm the superiority of shot peening and Chromalloy A12 coating over the no treatment condition, no failure versus failure.)

Fractography of Ultrasonic Fatigue

Fatigue fractures produced in this study have beach- or clam-shell markings characteristic of normal fatigue failures. The site of crack initiation is defined by these markings and additionally tends to show heavier oxidation than the rest of the fracture surface. Appreciable frictional heat is generated in this zone of initial fracture, and the fractography indicates that the crack

surfaces here are also smoothed by the relative motion of the surfaces as the crack is driven deeper.

Figure 4 shows typical electron fractographs of a Type 403 stainless steel specimen failed by ultrasonic fatigue. It is interesting that striations not unlike those usually developed in fatigue at much low stress cycling frequencies, for example, 30 Hz and lower, are evident in the fracture surfaces. It is not certain if there is any significant difference in the average spacing of the striations from point of initiation to the zone of termination of crack propagation. Taking 6.7×10^{-5} mm as a typical striation spacing in fractographs from replicas and assuming that each striation corresponds to a single tensile stress excursion, the ultrasonically driven crack advances at about 1 mm/s. This figure is much greater, by perhaps a couple orders of magnitude, than speeds of crack propagation measured for fatigue cracks growing at usual stress cycling frequencies.

Other metallographic studies appear to confirm the observations of Mason and Wood [*8*] that ultrasonic fatigue cracks develop from isolated slip bands and that slip-band spreading is less at ultrasonic frequencies of stressing.

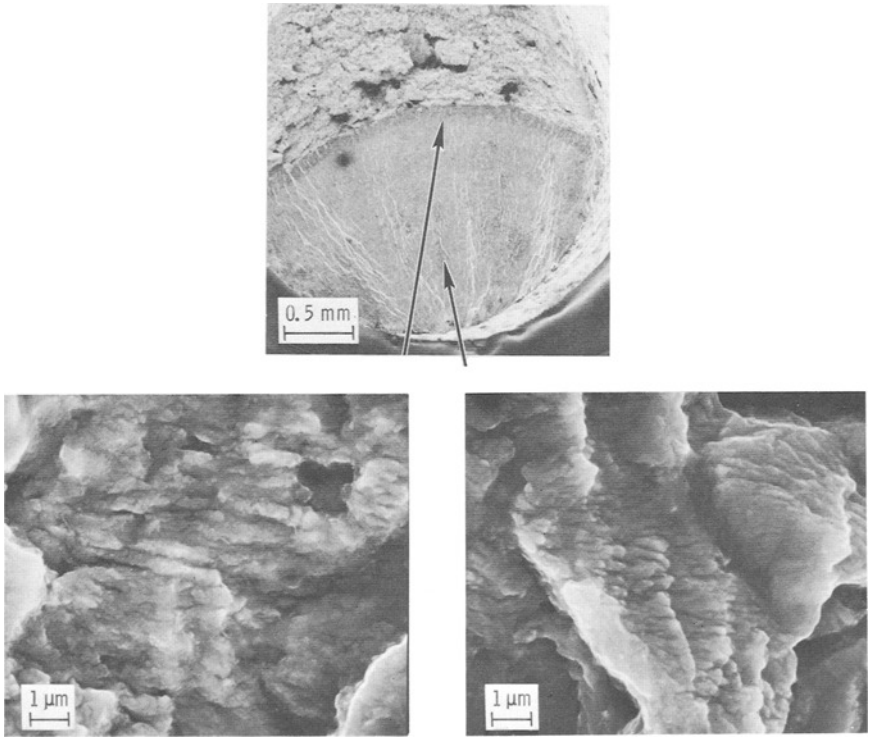


FIG. 4—*Scanning electron micrographs of fracture in shot-peened Type 403 stainless steel (×5000).*

Conclusions and Discussion

From the results of this investigation the following conclusions can be drawn:

1. The high-frequency fatigue technique can be used to determine decrease in fatigue life caused by small quantities of NaCl in a steam environment.
2. Electron fractography revealed fatigue striations similar to those characterizing fatigue failures occurring in the much lower and usual frequency ranges. It appears that active crack propagation at a cyclic frequency of 14 kHz is of the order of 1 mm/s.
3. The decrease in fatigue life of bare Type 403 stainless steel exposed to only 2000 ppm of NaCl, in steam at 250 F, was of the order of one decade over the entire range studied from 4×10^6 to 10^9 cycles to failure.
4. Surface treatment of Type 403 stainless steel by shot peening and application of Chromalloy A12 coating considerably increased fatigue life over the entire range.

Acknowledgments

We express our appreciation to S. Lee Rudy for his work in conducting the ultrasonic frequency corrosion-fatigue experiments and to E. D. Nicholson for the electron fractography of failed specimens.

H. B. Gayley of De Laval Turbine, Inc., Trenton, N. J., kindly supplied the Type 403 stainless steel stock from which the test specimens were machined.

The Chromalloy American Corp. (Turbine Support Division) provided their Chromalloy A12 coating system for evaluation in this study.

References

[1] Gaines, N., *Physics*, Vol. 3, 1932, pp. 209–229.
[2] Mason, W. P., *Journal of the Acoustical Society of America*, Vol. 28, 1956, pp. 1207–1218.
[3] Neppiras, E. A., *Proceedings*, American Society for Testing and Materials, Vol. 59, 1959, pp. 691–709.
[4] Neppiras, E. A., *Proceedings*, Physics Society (London), Series B, Vol. 70, 1957, pp. 393–401.
[5] Thiruvengadam, A., *Hydronautics*, Incorporated Technical Report 233-6, Dec. 1964 (see also *Transactions of the American Society for Metals, Journal of Engineering for Industry*, Aug. 1966).
[6] Thiruvengadam, A. and Preiser, H. S., *Hydronautics*, Incorporated Technical Report 467-Final, NASA CR-72035, Nov. 1965.
[7] Thiruvengadam, A. and Conn, A. F., *Experimental Mechanics*, Vol. 11, 1971, pp. 315–320.
[8] Mason, W. P. and Wood, W. A., *Journal of Applied Physics*, Vol. 19, No. 12, Nov. 1968, pp. 5581–5584.

GENERAL DISCUSSION ON TEST METHODS

(*written discussion*)—It is interesting to note that elevated temperature fatigue crack growth test data have been available for less than ten years. This symposium is somewhat unique in that a separate session is devoted to fatigue crack growth at elevated temperature. This probably sets a precedent for the next several decades. One of the urgent needs is to investigate the effect of temperature, frequency, wave shape, environment, and stress intensity in such fashion that the behavior of cracked structures operating at elevated temperature can be confidently predicted.

Copyright© 1973 by ASTM International www.astm.org

Materials

H. F. Merrick,[1] *D. H. Maxwell,*[2] *and R. C. Gibson*[1]

Fatigue in the Design of High-Temperature Alloys

REFERENCE: Merrick, H. F., Maxwell, D. H., and Gibson, R. C., "**Fatigue in the Design of High-Temperature Alloys,**" *Fatigue at Elevated Temperatures, ASTM STP 520,* American Society for Testing and Materials, 1973, pp. 285–299.

ABSTRACT: Nickel-base superalloys are used extensively in modern gas turbine engines and are subjected to a broad range of environmental conditions. At ambient and moderately elevated temperatures improved fatigue resistance can be obtained through refinement of grain size. Thermomechanical working, for example, microduplex processing, offers a means to achieve very fine grain sizes and exceptional fatigue strengths. At high temperatures grain boundaries are a source of weakness. Significant improvements in fatigue resistance can be achieved by the elimination of transverse grain boundaries. High-strain fatigue studies show that deformation occurs by coarse planar slip. Recent developments have enabled a combination of γ' and oxide dispersion strengthening to be achieved. This opens possibilities for improved fatigue resistance by promoting slip dispersal. Fatigue resistance is influenced also by environmental factors. The present trend in alloy development is to provide materials having high inherent oxidation and sulfidation resistance.

KEY WORDS: fatigue (materials), nickel containing alloys, design, fatigue tests, fatigue strength at N cycles, microstructure, grain size, temperature, environments

Over the past few years there has been growing sophistication in the approaches taken towards the development of more capable alloys intended for service in high-temperature machinery. These approaches have included directionally solidified alloys and eutectics, superalloy powder metallurgy, and dispersion strengthening. The advanced aircraft gas turbine engine, in particular, has forced this trend as a result of increased demand for improved alloy temperature capability and durability at a point in time when conventional alloy development practice was yielding a continually decreasing payoff (Fig. 1). Most gas turbine materials' problems are related to the rapid rise in turbine inlet temperature since the early sixties,

[1] Research metallurgist and section supervisor, Nickel Alloys Research Section, respectively, Paul D. Merica Research Laboratory, The International Nickel Company, Inc., Sterling Forest, Suffern, N. Y. 10901.

[2] Formerly with The International Nickel Company is now with The James French Baldwin Co., North Palm Beach, Fla. 33403.

Copyright© 1973 by ASTM International www.astm.org

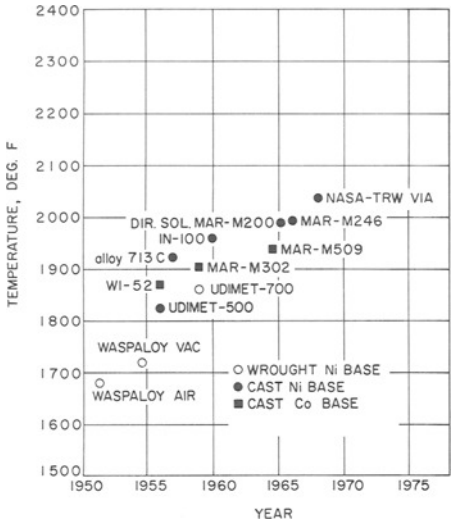


FIG. 1—*Trend in superalloy creep-rupture strength capability. Temperature to produce rupture in 100 h at a stress of 10 000 psi (68.9 MN/m²).*

and projections call for further increases in the future (Fig. 2). The impact of the disparity between alloy capability and the rise in turbine inlet temperature has been offset largely by the remarkable advancement of component cooling concepts, but the need for improved materials remains very real.

The complexity and severity of the service conditions imposed upon aircraft gas turbine components necessitates care in alloy selection in order to obtain an optimum balance of properties. As such it is an excellent context in which to discuss the role of fatigue resistance in high-temperature

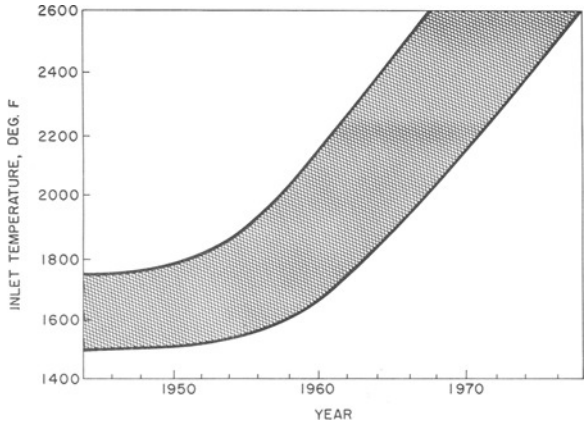


FIG. 2—*Trends in aircraft engine turbine inlet temperature.*

materials' design. The purpose of this paper is to present the results of recent research at International Nickel Company in the area of superalloy improvement, with particular emphasis on the relationship between fatigue characteristics and controlling microstructural variables in cast and wrought nickel-base alloys.

Service Considerations

Every component in a gas turbine is subjected to mechanically and thermally induced cyclic strain. The problem is compounded by the fact that fatigue strength may be only one and not necessarily the most important property required for the component in question. For example, considerable attention is being focused on the low-cycle fatigue behavior of disk alloys, but the material is still "defined" for the application by its rupture and tensile capability. Similarly, turbine blades are subjected to mechanical and thermal fatigue, but design is related to airfoil creep and root section creep and yield strengths. Creep resistance, for long service life, demands that the alloy be capable of extensive plastic deformation to prevent catastrophic, unpredictable component failure. Compositionally, blade materials are limited to those with acceptable levels of hot corrosion, sulfidation, or oxidation resistance and a degree of microstructural stability that will minimize property deterioration during service.

Recent research has shown the dependency of fatigue resistance upon frequency, temperature, microstructure, dwell time under load, rate of load application, defects, surface deterioration, notch factor, and maximum to minimum stress ratios. The turbine blade in today's advanced aircraft engine is subjected to a broad range of frequencies ranging from the variable root loading associated with rotations speed to the high excitational frequencies in airfoil twist and bending. Temperature gradients along a blade span in normal engine operation can vary by 500 F, and the unfortunate combination of fatigue and creep is unavoidable. Defects, deleterious microstructural phases, and deterioration on component surfaces can be alleviated through reliance on protective metallic diffusion coatings. However, control of overall microstructure for maximum fatigue resistance results in some sacrifice in creep resistance.

Influence of Grain Structure

Of the factors influencing fatigue, particularly high-cycle fatigue, grain size is perhaps one of the most important. In practice, improved fatigue properties by grain refinement are restricted usually to ambient and moderately elevated temperatures. A fine grain structure is also beneficial in thermal fatigue [*1,2,9*][3] although creep strength requirements may miti-

[3] The italic numbers in brackets refer to the list of references appended to this paper.

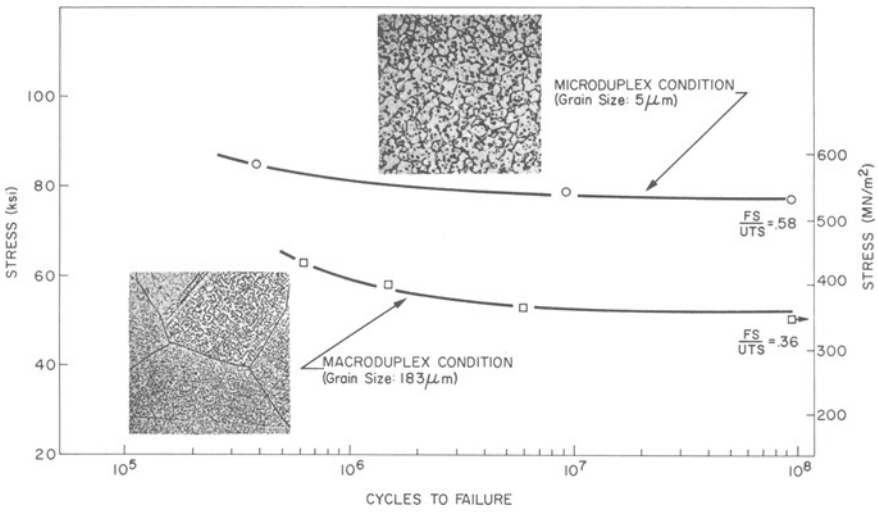


FIG. 3—*Effect of microstructure on the room temperature rotating beam fatigue properties of a 37Cr-18Fe-balance Ni alloy.*

gate against the use of fine grains at very high temperatures, for example, in turbine blades. In applications where maximum creep resistance is required in wrought alloys high annealing temperatures have been employed to develop a coarse grain structure. In this condition, the fatigue resistance is relatively low. However, processing schedules, for example, microduplex processing, and lower annealing temperatures can be often used to refine the grain size and improve fatigue resistance. The effect of grain size refinement on fatigue strength is shown in Fig. 3. Work on experimental alloys [*3*] has indicated that room-temperature rotating beam fatigue strengths at 10^8 cycles in excess of 100 ksi are attainable in face-centered-cubic (fcc) systems through the application of microduplex processing. Typical data are illustrated in Fig. 4.

A reduction in grain size will probably place an upper limit in terms of temperature of application in view of the superplastic nature of fine grained materials [*4*]. However, for ambient to moderately elevated temperature (1200 F) applications, for example, turbine shafts and compressor disks, processing of this type to attain fine grain structures offers great benefits. Of particular significance for disk applications is the fact that a reduction in grain size is also beneficial for improved low-cycle fatigue resistance. Table 1 illustrates this point with data for Alloy 901 and a Udimet[4] 700. For turbine blade and vane applications higher temperatures are encountered, and a balance between good thermal fatigue resistance, on the one hand, and good creep resistance, on the other, is desired. The demand for

[4] Registered trademark of Special Metals, Inc.

TABLE 1—*Effect of grain size on low-cycle fatigue life.*

Alloy	Grain Size Avg Linear Intercept, μm	Cycles to Failure, $E_t = 0.016$
Alloy 901	37	1850
	75	1000
Udimet 700[a]	43	2470
	95	970

[a] From Ref 7.

NOTE—Strain cycling tests for alloy 901 were performed on hourglass shaped specimens. The total longitudinal strain E_t was computed from the total diametral strain at half-life.

improved creep resistance in turbine airfoil alloys has resulted in the evaluation of cast nickel-base alloys; however, this improvement has been realized only at some sacrifice in overall fatigue resistance.

With increasing temperature there is a transition in fracture mode from transcrystalline to intercrystalline nucleation and propagation [*1,2,5,6*]. Figure 5 illustrates this transition in the case of IN-100 tested at 1350 and 1500 F. Intercrystalline crack nucleation and progagation rates are higher than transcrystalline modes [*7*], and, thus, grain boundaries constitute a source of weakness. Significant improvements in airfoil thermal fatigue resistance have been achieved through unidirectional solidification techniques, resulting in complete elimination of transverse grain boundaries.

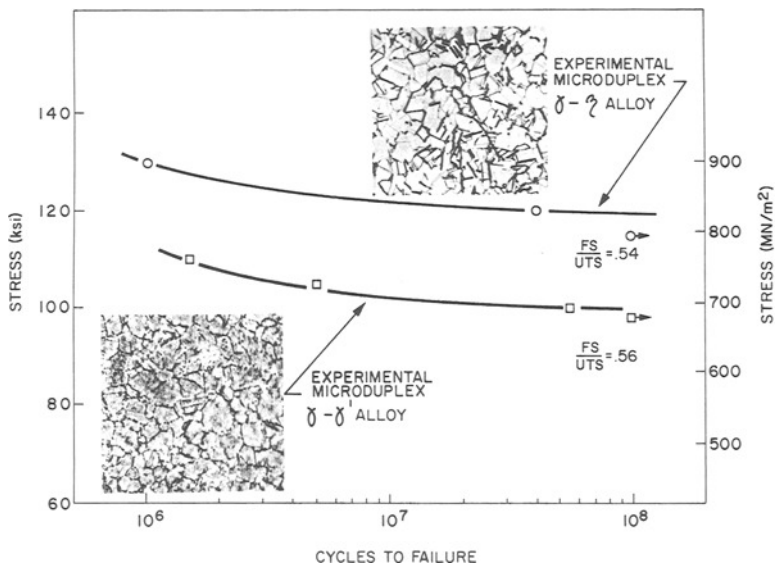


FIG. 4—*Effect of microduplex processing on the room temperature rotating beam fatigue properties of experimental* $\gamma - \gamma'$ *and* $\gamma - \eta$ (Ni_3Ti) *alloys.*

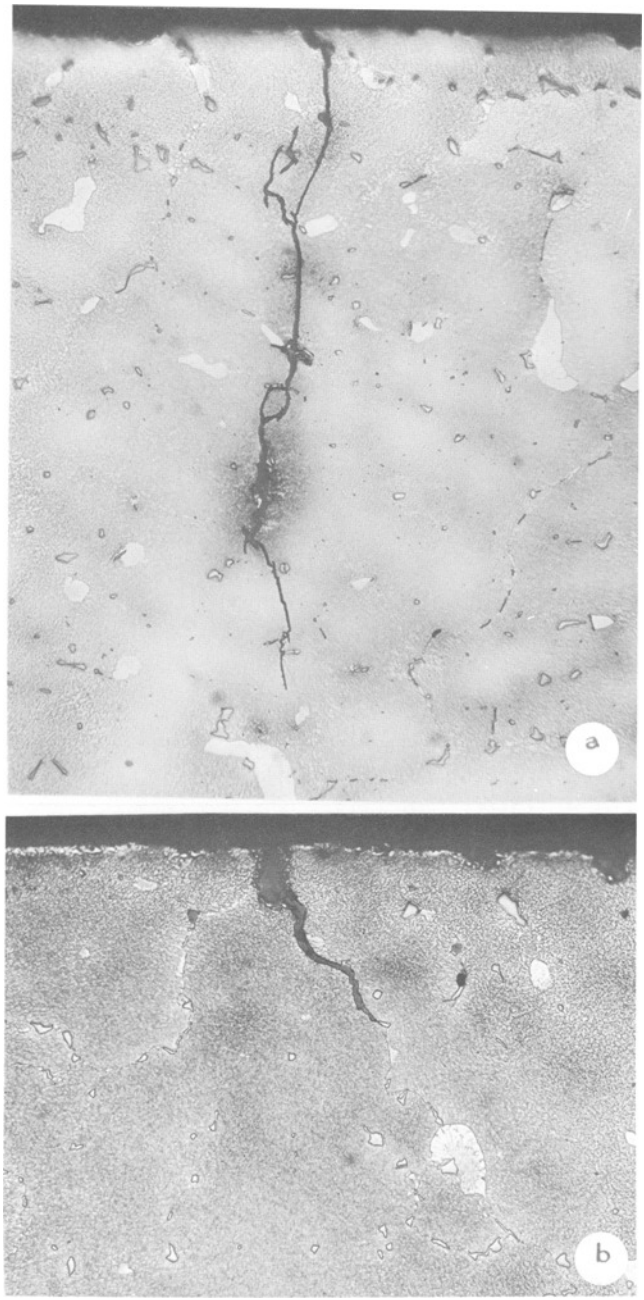


Fig. 5—Transgranular and intergranular cracking in IN-100 tested in cyclic load fatigue (zero to maximum load). (a) *1350 F (1009 K) and 110 ksi (758 MN/m²) stress range and* (b) *1500 F (1089 K) and 90 ksi (620 MN/m²) stress range* (×250).

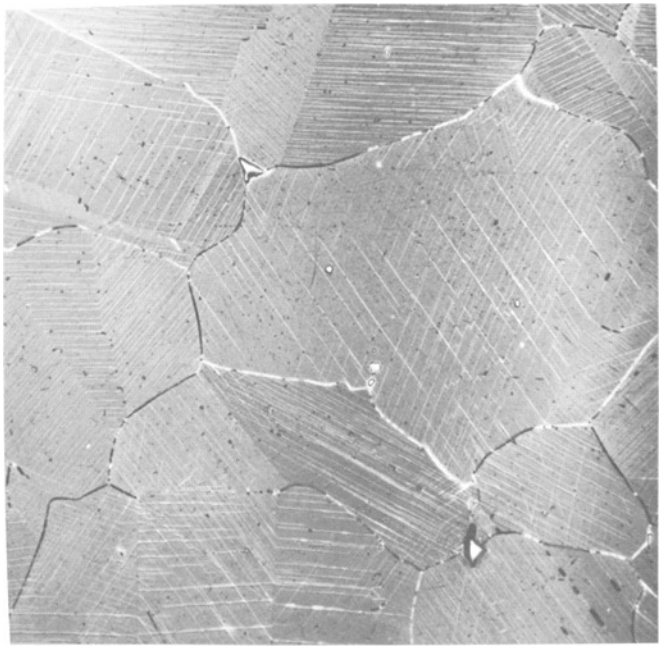


Fig. 6—Optical micrograph illustrating slip lines in Alloy 901 fatigue tested at room temperature (×500).

This has been demonstrated in tests on single crystals and polycrystalline directionally solidified MAR-M200[5] and single crystal Udimet 700 [*7*].

Influence of γ' on Fatigue

Ambient and moderately elevated temperature studies of the monotonic and fatigue deformation behavior of two phase γ-γ' nickel-base alloys have established that coarse (heterogeneous) planar slip occurs and the fact that this deformation characteristic is related usually to shear of γ' precipitates. Figure 6 shows an example of planar slip in Alloy 901. On the other hand, deformation of either the matrix γ phase or γ' phase, while still planar, is homogeneous and much finer [*8*]. Coarse planar deformation is undesirable, since it leads to large slip offsets and possible early crack initiation. Heat treatments to modify the γ' size, and distribution around γ' particles can be applied. Work by Klein [*9,10*] on simple nickel-chromium-aluminum (Ni-Cr-Al) alloys has shown that refinement of slip occurs in this case with a concomitant improvement in high-cycle fatigue resistance (10^5 to 10^6 cycles).

Our work on the high-strain low-cycle fatigue of several nickel-base alloys, however, has shown that, although bowing mechanisms may

[5] Registered trademark of Martin Marietta Corp.

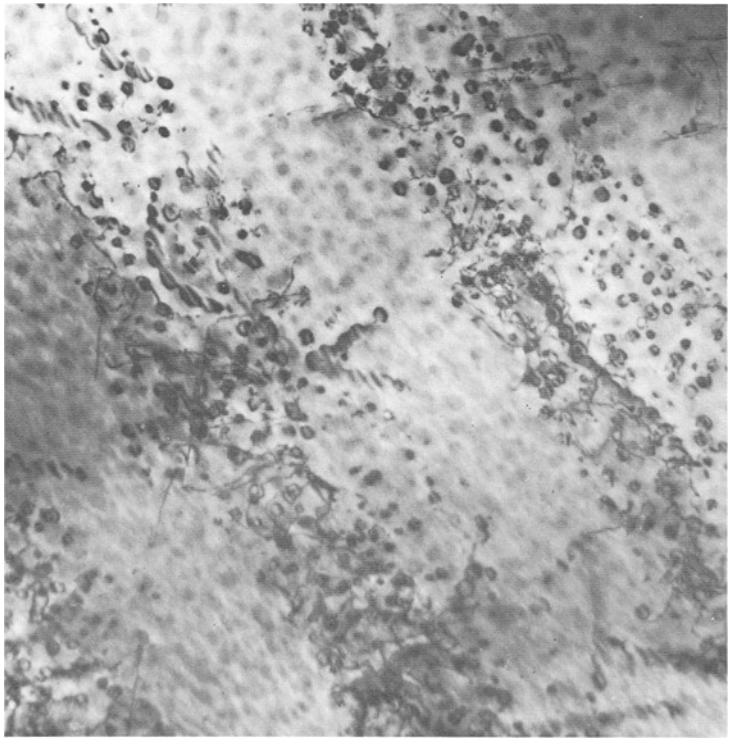


FIG. 7—*Thin foil electron micrograph showing dislocation loops and stacking fault contrast associated with* γ' *in Alloy 901 fatigue tested at room temperature* (×40 000).

operate initially, the deformation remains coarse and planar (Fig. 7) and eventually shear of γ' occurs as shown, for example, in Waspaloy[6] (Fig. 8). The concentration of slip in relatively few grains can also lead to dissolution of γ', and this probably facilitates crack initiation. Figure 9 shows typical Stage I type cracks initiated at the surface of a specimen of Alloy 901. Nevertheless, γ' particle sizes and distributions, which promote dislocation bowing mechanisms, at least initially coupled with refinement of grain structure, perhaps provide opportunity for optimization of fatigue resistance at ambient and moderately elevated temperatures.

The incorporation of nondeforming particles, that is, dispersed oxides, may also be beneficial, since these will most effectively promote dispersal and refinement of slip [*11*]. This has been observed in the fatigue of TD nickel [*12*]. Recent developments have shown that it is possible to combine γ' strengthening with oxide dispersion strengthening through the mechanical alloying process [*13*]. Although the creep behavior of a dispersion strengthened nickel-base alloy, IN-853, so produced, has been documented,

[6] Registered trademark of United Aircraft Corp.

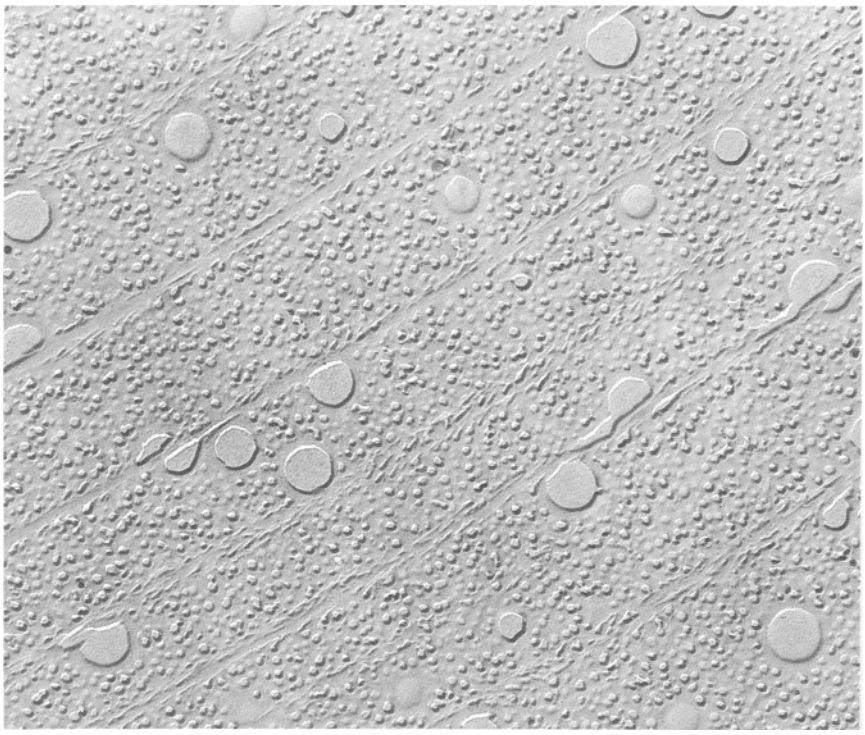


FIG. 8—*Replica electron micrograph illustrating shear of γ' during fatigue of Waspaloy at room temperature* ($\times 30\,000$).

its fatigue behavior is less well known at this time. Preliminary high-cycle fatigue results [*14*][7] have shown that the fatigue resistance of this alloy is superior to that of a nondispersion strengthened alloy of similar composition at all temperatures, as shown in Fig. 10.

At temperatures in excess of 1400 F, it becomes increasingly necessary to consider both creep and fatigue characteristics. Improved creep resistance in conventional nondispersion strengthened nickel-base superalloys has been achieved through the increases in size and volume fraction of γ' and the use of investment casting to produce the desired component configuration. Most modern alloys contain about 60 percent γ', and this is considered optimum for most applications. However, early work of Guard [*14*] showed that for ternary Ni-Cr-Al alloys, the creep properties were roughly proportional to the γ' volume fraction if the γ' particle size is kept constant. Since recovery is in large part controlled by γ', the γ' size and spacing may assume greater importance under conditions of cyclic stress, particularly at low frequencies or where holdtimes are involved. Single

[7] See p. 427.

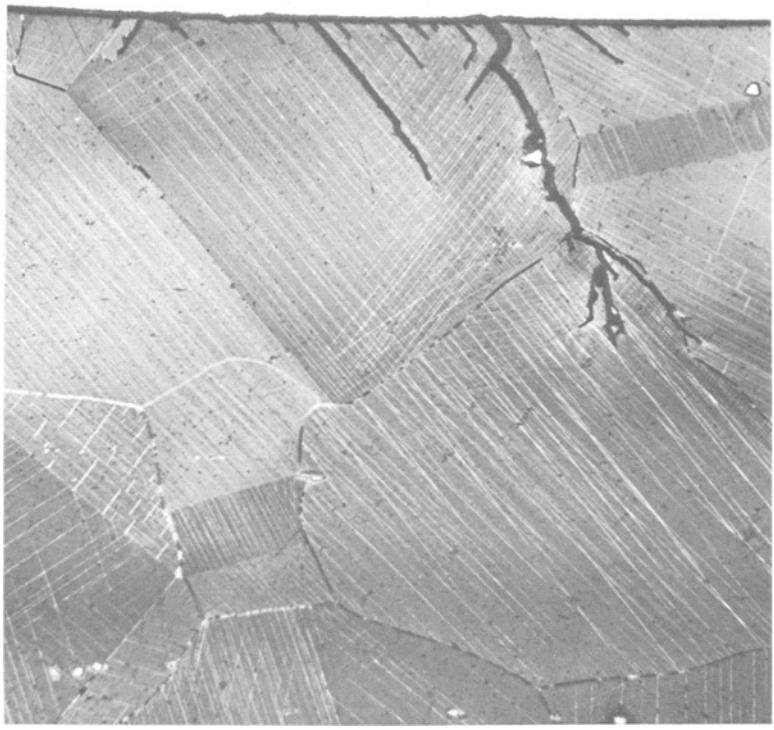


FIG. 9—*Surface generated cracks developed in Alloy 901 during high-strain fatigue at room temperature* (×500).

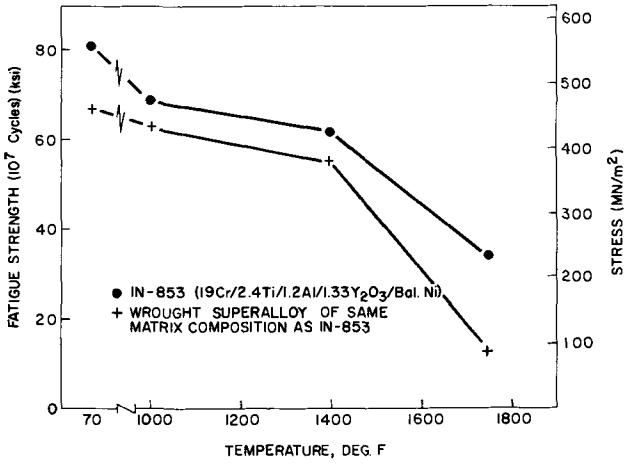


FIG. 10—*Comparison of the rotating beam fatigue strength of the dispersion strengthened nickel-base alloy, IN-853, with a wrought superalloy of the same matrix composition.*

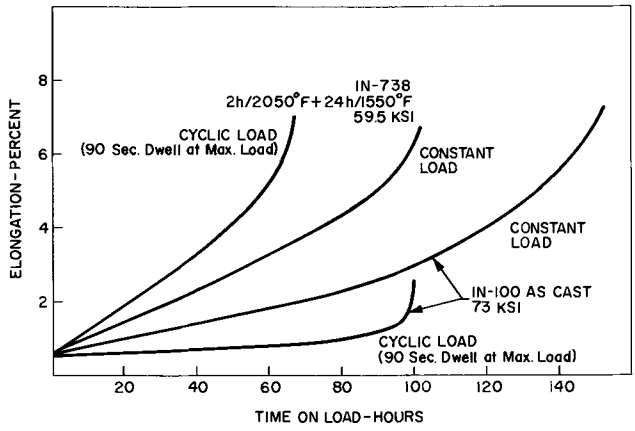


FIG. 11—*Effect of cyclic loading (zero to maximum load) on the creep resistance of IN-100 and IN-738 at 1500 F (1089 K).*

phase materials, for example, Haynes[8] Alloy 25 [*15*], undergo an acceleration of creep in cyclic creep-fatigue tests compared with constant load conditions. In two phase γ-γ' alloys it has been observed that an acceleration or retardation of creep can occur depending on the volume fraction of γ'—higher γ' contents leading to retardation of creep. An example of this is shown in Fig. 11, in which a comparison is made between the behavior IN-100 (60 percent γ') and IN-738 (40 percent γ').

Influence of Grain Boundary Structure

Since the incidence of grain boundary fracture increases with test temperature, the nature of grain boundary structure is important. However, definitive documentation of the influence of grain boundary structure is still lacking. For creep resistance it is now generally felt, particularly for the newer nickel-base alloys, that a structure consisting of isolated carbides enveloped in γ' is desirable.

Minor additions of boron and zirconium are known to affect creep rupture behavior [*16*] and also thermal fatigue [*1*]. Recently, it has been observed that improved creep rupture life and ductility is obtained with additions of hafnium. Hafnium (and also zirconium) is a potent hardener of γ', and it has been postulated [*17*] that the role of hafnium is to increase grain boundary strength. Life and ductility at high temperature are improved both because γ' lining the grain boundaries increases resistance to crack propagation (γ' deforms by fine slip) and also because gross plastic deformation is inhibited by virtue of the higher grain boundary strength than the surrounding γ-γ' matrix. It has also been suggested [*18*] that

[8] Registered trademark of Cabot Corp.

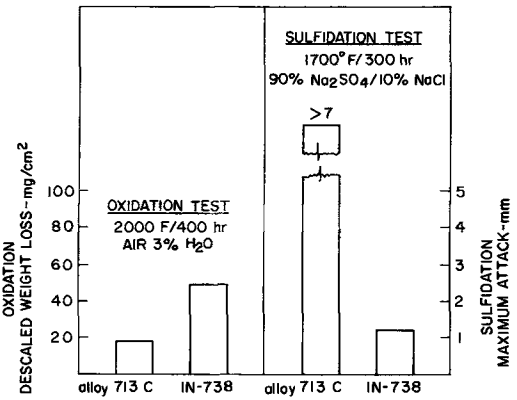
hafnium additions result in a more irregular grain boundary. This would make deformation mechanisms involving grain boundary sliding more difficult and thus confer added creep and fatigue strength.

Effect of Environment

Fatigue crack nucleation most often occurs at the surface. It is important to recognize, therefore, that environmental factors may exert a marked influence on fatigue behavior. Glenny and Taylor [*19*], for example, have noted that the thermal fatigue resistance of several nickel-base alloys is greater in argon than in air. The elevated temperature fatigue lives of nickel-base and other alloys are also generally greater in vacuum than in air. Surface oxidation, therefore, is a critical factor in fatigue. In polycrystalline Udimet 500 tested at 1500 F, McMahon and Coffin [*20*] have suggested that fatigue crack initiation is preceded by oxidation along grain boundaries. The presence of chromium carbides, which are oxidized readily, facilitates this process. Fleetwood et al [*21*] have also noted that local oxidation at grain boundaries significantly affects crack nucleation in the thermal fatigue of cast nickel-base alloys. On the other hand, Gell et al [*7*] cite examples where oxidation can retard a crack propagation. It is reasoned that oxidation can effectively cause blunting of a crack. Few data have been reported for tests in other corrosive environments. High-cycle fatigue tests on several Nimonic[9] alloys have indicated that the presence of sulfur dioxide (SO_2) and vanadium pentoxide-sodium sulfate (V_2O_5-Na_2SO_4) mixtures do not cause an appreciable reduction in fatigue life compared with air tests [*22*].

The fact that there is alloy-to-alloy variability with regard to the effect of environment on fatigue may be related to alloy composition. Many of the early nickel-base superalloys have a high chromium content (15 to 20 percent) and possess good oxidation and sulfidation resistance. The development of high-strength cast blade alloys has resulted in the gradual reduction of chromium content and an increased susceptibility to sulfidation. Although the use of protective coatings for blade and vane alloys is commonplace today, the present trend in alloy development for turbine applications is to provide materials of high inherent oxidation and sulfidation resistance. As an example of this trend we may cite a comparison between the cast nickel-base superalloys, Alloy 713C and IN-738. These alloys, which exhibit approximately equivalent creep-rupture strength, differ significantly in sulfidation resistance (Fig. 12). In this case the improved sulfidation resistance of IN-738 has been achieved by maintaining a high-chromium content and by titanium and refractory element additions. While the oxidation resistance of IN-738 is not quite as good as alloy 713C, IN-738 possesses better overall resistance to environmental attack

[9] Registered trademark of International Nickel Co., Inc.



ALLOY COMPOSITION (Nominal Weight Percent)

	C	Cr	Co	Mo	W	Al	Ti	Cb	Ta	B	Zr	Ni
alloy 713C	.12	12.5	—	4.2	—	6.1	0.8	2.0	—	.012	.10	Bal.
IN-738	.17	16.0	9.0	1.8	2.8	3.3	3.3	0.9	1.8	.02	.10	Bal.

FIG. 12—*Comparison of the oxidation and sulfidation resistance of Alloy 713C and IN-738.*

such as would be experienced in gas turbine operating conditions. From this point of view, such compositional modifications of this type should also be beneficial for improved fatigue resistance at elevated temperatures.

Summary

Nickel-base alloys used in gas turbine engines are subject to a broad range of environmental conditions. The development of improved fatigue capability lies in the ability of the metallurgist to define the macro- and microstructural variables influencing crack initiation and propagation under conditions closely simulating service. Research to date has revealed the importance of such factors as grain size, deformation mode, material cleanliness, and environment. Thus, improvements in fatigue resistance can be approached through compositional modifications, which will help mitigate environment effects, and structural manipulation by utilizing microduplex processing, unidirectional solidification, and, perhaps, dispersion strengthening.

References

[*1*] Franklin, A. W., Heslop, J., and Smith, R. A., *Journal of the Institute of Metals*, Vol. 92, 1963–1964, pp. 313–322.

[*2*] Glenny, E. and Northwood, J. E., *Foundry Trade Journal*, Vol. 119, 1965, pp. 607–620.

[*3*] Merrick, H. F., unpublished work.

[4] Hayden, H. W., Gibson, R. C., Merrick, H. F., and Brophy, J. H., *Transactions Quarterly*, American Society for Metals, Vol. 60, 1967, pp. 3–14.
[5] Wells, C. H. and Sullivan, C. P., *Transactions Quarterly*, American Society for Metals, Vol. 60, 1967, pp. 217–222.
[6] Leverant, G. R. and Gell, M., *Transactions*, Metallurgical Society, American Institute of Mining, Metallurgical, and Petroleum Engineers, Vol. 245, 1969, pp. 1167–1173.
[7] Gell, M., Leverant, G. R., and Wells, G. H. in *Achievements of High Fatigue Resistance in Metals and Alloys, ASTM STP 467*, American Society for Testing and Materials, 1970, p. 113.
[8] Gell, M. and Leverant, G. R. in *Third Bolton Landing Conference on Ordered Alloys*, Claitor's Publishing Division, Baton Rouge, La., 1969, p. 505.
[9] Klein, H. P., *Zeitschrift für Metallkunde*, Vol. 61, 1970, pp. 564–572.
[10] Klein, H. P., *Zeitschrift für Metallkunde*, Vol. 61, 1970, pp. 573–574.
[11] Ashby, M. G., *Oxide Dispersion Strengthening*, Gordon and Breach, New York, 1968, pp. 143–212.
[12] Leverant, G. R. and Sullivan, C. P., *Transactions*, Metallurgical Society, American Institute of Mining, Metallurgical, and Petroleum Engineers, Vol. 242, 1968, pp. 2347–2353.
[13] Benjamin, J. S., *Metallurgical Transactions*, Vol. 1, 1970, pp. 2943–2951.
[14] Guard, R. W., *Mechanical Behavior of Metals at Elevated Temperatures*, McGraw-Hill, New York, 1961, p. 270.
[15] Walter, W. A., AIME Spring Meeting, American Institute of Mining, Metallurgical, and Petroleum Engineers, Atlanta, Ga., 1971.
[16] Decker, R. F., Rowe, J. W., and Freeman, NACA Technical Note 4049, National Advisory Committee for Aeronautics, 1957.
[17] Doherty, J. E., Kear, B. H., and Giamei, A. G., *Journal of Metals*, Vol. 23, 1971, pp. 59–62.
[18] Kotval, P. S., Venables, J. D., and Calder, R. W., *Metallurgical Transactions*, Vol. 3, 1972, pp. 453–458.
[19] Glenny, E. and Taylor, T. A., *Journal*, Institute of Metals, Vol. 88, 1959–1960, pp. 449–461.
[20] McMahon, C. G. and Coffin, L. F., Jr., *Metallurgical Transactions*, Vol. 1, 1970, pp. 3443–3450.
[21] Fleetwood, M. J., Penrice, P. J., and Whittle, J. E., *Foundry Trade Journal*, Vol. 126, 1969, pp. 193–198.
[22] Betteridge, W., *The Nimonic Alloys*, Edward Arnold Ltd., London, 1959, p. 219.

DISCUSSION

R. M. Goldhoff[1] (*written discussion*)—The speaker showed microduplex structures attained by process techniques leading to very fine grain size with alpha particles on grain boundaries. These were in structural alloys IN 718 and Inco 901. Mention was made of possible superplastic behavior with the structures attained. Normally fine grain size compatible with superplasticity in such alloys demands powder forming techniques. The question

[1] General Electric Co., Schenectady, N. Y. 12301.

is whether or not super plasticity in these duplex structures has been actually demonstrated?

H. F. Merrick, D. H. Maxwell, and R. C. Gibson (author's closure)—The microduplex structures referred to by Dr. Goldhoff were not developed in Alloys 718 or 901. The microduplex γ-α' structures are related to a 37Cr-18Fe-0.6Ti-balance nickel alloy which does exhibit superplasticity at elevated temperatures. We have not run any high-temperature tests to determine the same is true of the experimental γ-γ' and γ-η alloys.

M. C. Murphy[2] *(written discussion)*—I refer to Dr. Merrick's diagram on oxidation and sulfidation in which he assesses these factors in terms of general weight change. Environmental factors appear to affect the fatigue behavior at high temperatures via grain boundary attack. My question, therefore, is: "Are the rates of grain boundary attack fairly represented by general surface oxidation or sulfidation rates?"

Messrs. Merrick, Maxwell, and Gibson—No.

K. D. Challenger[3] *(written discussion)*—Does twin frequency influence the low-cycle fatigue behavior? (All other conditions equal.)

Messrs. Merrick, Maxwell, and Gibson—In the alloys we examined, we did not find that twin boundaries were a preferred site for crack initiation, but we have not run rigorous experiments to determine if there is an effect of twin frequency on low-cycle fatigue behavior.

G. R. Leverant[4] *(written discussion)*—In response to K. Challenger's inquiry about cracking at annealing twin boundaries, I have found that at intermediate temperatures the twin boundaries in U-700 are preferred sites for Stage I crack initiation. This is caused by concentrated slip along these boundaries, as observed by transmission electron microscopy, and is due to the absence of the strengthening γ' precipitate across the boundary.

[2] Heaton Works, Newcastle upon Tyne, England.
[3] Materials development engineer, General Electric Co., San Jose, Calif. 95114.
[4] Pratt & Whitney Aircraft, Division of United Aircraft Corp., Middletown, Conn. 06457.

H. Abdel-Raouf,[1] *T. H. Topper,*[1] *and A. Plumtree*[1]

Effects of Grain Size and Temperature on the Cyclic Strength and Fracture of Iron

REFERENCE: Abdel-Raouf, H., Topper, T. H., and Plumtree, A., "**Effects of Grain Size and Temperature on the Cyclic Strength and Fracture of Iron,**" *Fatigue at Elevated Temperatures, ASTM STP 520*, American Society for Testing and Materials, 1973, pp. 300–310.

ABSTRACT: The influence of grain size on the cyclic deformation behavior and fracture of Ferrovac E iron under low-cycle fatigue conditions are studied at temperatures ranging from 23 to 540C and strain range of 0.010. The steady-state stress response and the related cell size are independent of the grain size. The cell size and the total dislocation density was found to depend markedly on the dynamic strain aging level. The inhomogenity of plastic deformation in the material was enhanced by dynamic strain aging. This inhomogeneity was observed by both surface damage studies and substructural investigations. The grain size has no effect on the redistribution of plastic strains. The fracture mechanism and fatigue life was dependent on the dynamic strain aging level through the degree of redistribution of plastic strains. The dependency of fatigue life on grain size is controlled by the fracture mechanism available at this temperature. At high dynamic strain aging levels, the material reveals brittle striations on the fracture surfaces. In this case, the fracture process is independent on the grain boundary resistance and life is independent of the grain size.

KEY WORDS: grain size, cracking (fracturing), fatigue (materials), plastic deformation, crack initiation, stress cycle, iron

Nomenclature

σ_{FL}	Fatigue limit stress
K_{FL}, σ_{0FL}	Constants
D	Grain size
σ	Stress
σ_0	Friction stress
G	Shear modulus
b	Burger's vector
ρ	Dislocation density

[1] Research assistant professor, professor-chairman, and associate professor, respectively, Department of Mechanical Engineering, Department of Civil Engineering, and Department of Mechanical Engineering, respectively, University of Waterloo, Waterloo, Ont., Canada.

Copyright© 1973 by ASTM International www.astm.org

l Cell size
d Dislocation spacing in cell walls
N_f Cycles to failure
a, b Constants

Fatigue properties of iron and steel are affected by the polycrystal grain size [*1*,*2*],[2] the segregation of interstitial alloying elements to grain boundaries and individual dislocations and the intrinsic character of the body-centered-cubic (bcc) structure. Klensil et al [*2*] presented metallographic evidence showing that the slip bands which were produced in the fatigue process were blocked by grain boundaries and that the fatigue limit dependency of steel on grain size can be described by Eq 1.

$$\sigma_{FL} = \sigma_{0FL} + k_{FL}D^{-1/2} \quad \ldots\ldots\ldots\ldots\ldots\ldots\ldots\ldots (1)$$

The role of cross slip in changing dependence of fatigue life on grain size was examined by Thompson and Backofen [*3*] who concluded that in α-brass which has a planar slip mode, decreasing grain size acts to increase fatigue life, while in copper and aluminum, which deform in a wavy slip mode, life is insensitive to grain size. A decrease in low-cycle fatigue life with an increase in grain size was observed in copper by Feltner and Beardmore [*4*] and in aluminum by Boettner et al [*5*].

Studies of the cyclic deformation behavior of iron [*6*,*7*] have shown that substructure cell size is a function of strain amplitude. Our recent work [*8*] which examined the effects of temperature and cyclic deformation rate on the cyclic strength and fracture of low-carbon steel, demonstrated the importance of dynamic strain aging as a fatigue strengthening mechanism.

The present paper deals with the influence of the polycrystal grain size on the cyclic strength of iron-carbon alloys in the dynamic strain aging region. Fracture mechanisms and the fatigue life dependence on grain size are investigated at different dynamic strain aging levels in low-cycle fatigue.

Experimental Procedure

The material used in this investigation is a fully annealed Ferrovac E iron of the same chemical composition as that reported in Ref *8*. Various grain sizes ranging from 75 to 970 μm were obtained by suitable heat treatment with special care to avoid the embrittlement of grain boundaries [*9*]. After this treatment the dislocation substructure was the same in all specimens since all are in a fully annealed condition. The specimens were cycled at a fully reversed strain amplitude of 0.005 (a typical low-endurance value) using an axial mode closed loop servocontrolled electrohydraulic testing system. Details of the high-temperature testing techniques employed are

[2] The italic numbers in brackets refer to the list of references appended to this paper.

given in Ref *8*. Surface damage and fracture surfaces were observed using scanning electron microscopy, while thin foil transmission electron microscopy techniques were employed to examine the related substructures.

Results

The stress at a tensile strain of 0.005 for various grain sizes and temperatures is shown in Fig. 1 plotted against $D^{-1/2}$. A set of straight lines satisfies the results for each temperature indicating applicability of the Hall-Petch equation [*10*]. Within the scatter of the individual data points the slopes appear to be independent of temperature up to 370 C, but at higher temperature (540 C) the slope decreases markedly.

During cyclic deformation at a strain amplitude of 0.005, the material exhibited cyclic hardening followed by steady-state stress response. Steady-state stress response is plotted against $D^{-1/2}$ in Fig. 2. The results give a Hall-Petch slope close to zero at all test temperatures indicating that the saturation stress is independent of the average grain diameter.

Dislocations in the cyclically deformed material were arranged in the cellular form shown in Fig. 3 at all temperatures used in this investigation. The size of dislocation cells is dependent on test temperature, decreasing as

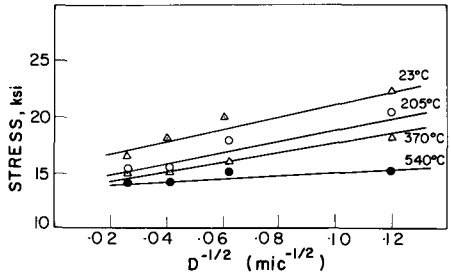


FIG. 1—*Relationship between the stress at a tensile strain of 0.005 and* $D^{-1/2}$.

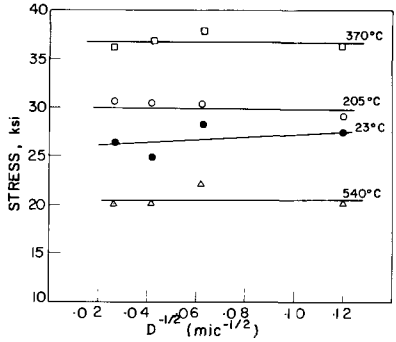


FIG. 2—*Relationship between the steady-state stress response and* $D^{-1/2}$.

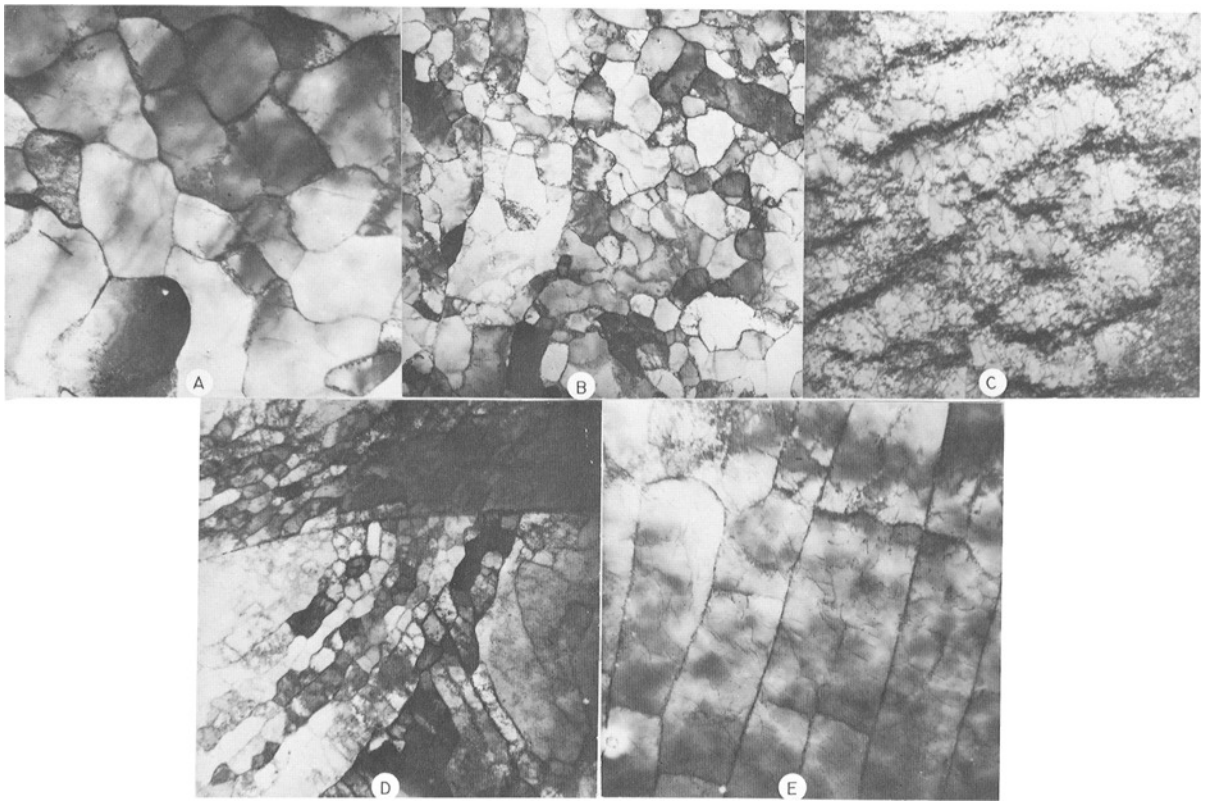


FIG. 3—(*a*) *Dislocation cells formed during cyclic deformation at room temperature* (×*14 600*); (b) *dislocation cells formed during cylic deformation at 205 C* (×*11 200*); (c) *dislocation cells formed during cyclic deformation at 370 C* (×*30 000*); (d) *substructural inhomogenity developed at 370 C* (×*11 200*); *and* (e) *dislocation cells formed during cyclic deformation at 540 C* (×*11 200*).

temperature increases up to 370 C then rapidly increasing. Measured cell sizes varied with the orientation of the grain under investigation, but mean cell size and the standard deviation which were calculated for various grain sizes indicated that the cell size was independent of the mean grain diameter. At 370 C, the cell size within individual grains was highly nonuniform. Figure 3*d* shows a band of small cells surrounded by large cells; such an inhomogeneity of substructure occurred only at the blue brittleness temperature (370 C).

Figure 4 indicates that fatigue life is dependent on grain size at test temperatures of 23, 205, and 540 C with an increase in the grain size resulting in a decrease in fatigue life in each case. At 370 C, however, fatigue life is independent of grain size.

Surface damage studies reveal a slight plastic strain concentration at room temperature, homogeneous deformation at 205 C (Fig. 5*a*), a high concentration of plastic strains at 370 C (Fig. 5*b*) and homogeneous deformation at 540 C. The degree of homogeneity of plastic strains is equated here to the uniformity of the distribution of slip traces on the surface of fatigued material. More complete details of the effects of temperature and deformation rate on the redistribution of plastic strains during fatigue were reported in Ref *8*. In addition, creep damage on the grain boundaries was observed at the highest temperature.

Discussion

Deformation

The Hall-Petch slope (k) is constant over a temperature range from 23 to 370 C during monotonic deformation as shown in Fig. 1. Armstrong et al [*11*] concluded that the grain size dependence of the lower yield stress in mild steel arises as a consequence of dislocation locking. The results presented in this paper reinforce this view since up to the blue brittleness temperature (370 C), stress must be controlled by creation of dislocation sources in strain aged grains. This creation of defects at grain boundaries

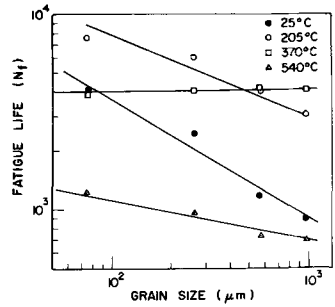


FIG. 4—*Relationship between fatigue life and grain size at different temperatures.*

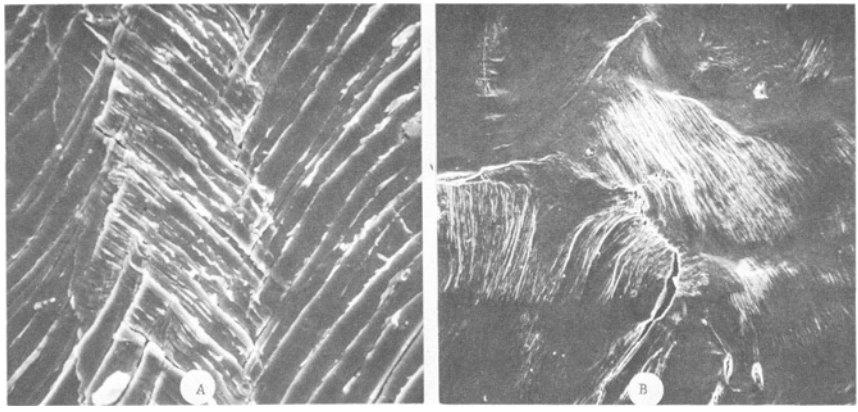


FIG. 5.—*Surface damage* (a) *at 205 C* (×*1276*) *and* (b) *at 370 C* (×*928*).

is independent of temperature [*12*]. Li et al [*13*] stated that the Hall-Petch slope will change with temperature when there is a change in ledge density in the grain boundaries or dislocation arrangements. The decrease in k at 540 C can be explained based on this argument due to the reduced aging at this temperature.

During cyclic deformation, the steady-state stress response increases with temperature to a maximum at 370 C and then decreases markedly. Figure 2 indicates that the dependency of stress response on grain size was negligible, and the Hall-Petch slope approaches zero for all temperatures used in this investigation.

Substructural investigations for specimens tested at room temperature show that dislocations are arranged in a cellular form. As the temperature increases, a rapid decrease in cell size is observed, associated with a considerable increase in the steady-state stress response. This decrease in cell size indicates an increase in total dislocation density.

Minimum cell size was observed at 370 C. Where rapid dislocation multiplication results from the available aging reactions and consequent, there is a rapid locking of mobile dislocations. Two important substructural features were observed at 370 C. The first is the presence of considerable number of dislocations around precipitates in the cell core as illustrated in Fig. 3*c*. This increase in dislocation density markedly affects the athermal stress component and thus the stress response. The second is the inhomogeneity of cell size within a grain and the consequent wide variations in dislocation density (Fig. 3*d*). By inference the deformation must be highly nonuniform within each grain with amplitudes of dislocation motion that differ markedly from one point to another. This localization of plastic strains was also observed in surface damage studies (Fig. 5*b*) of material tested at this temperature. Nonhomogeneous deformation was associated

with serrated stress-strain loops. No influence of grain size on this plastic strain inhomogeneity was observed. Our recent work [*8*] shows this inhomogeneity depends on testing temperature and cyclic deformation rate but is independent of the imposed strain amplitude suggesting that it is primarily caused by enhanced strain aging.

At 205 C both surface studies and thin foil examinations showed plastic strain to be homogeneous. This homogeneity of plastic deformation is mainly due to accelerated cross slip and will be discussed later in the paper in connection with its pronounced effect on the fracture mechanism and fatigue life.

Because of the lack of strain aging at 540 C, the stress is considerably lower and the cell size considerably larger than at 370 C. This increased cell size is due to the decrease of total dislocation density accompanying a reduction in the athermal component of the stress.

Cell size measurements show that the grain size has no effect on the size of dislocation cells for all grain sizes and temperatures used in this investigation. In monotonic deformation, Abson and Jonas [*14*] found that the Hall-Petch slope decreases with increasing plastic deformation due to the formation of a cellular structure. Brindley et al [*12*], however, indicated that this slope is constant and is not dependent on the amount of plastic strain. The present results are similar to those of Abson and Jonas in that they indicate that neither the cell size nor the steady-state stress response is dependent on grain size in cyclic deformation. Our observations are also in agreement with Johnston and Feltner [*15*] who pointed up that the cell size controls the flow stress at large strains eliminating the effect of grain size in high stacking fault energy materials. Furthermore, Dingley et al [*16*] show that in post-yield deformation the significant grain boundary hardening at yield gradually disappears and dislocation strengthening becomes inversely proportional to dislocation spacing. They demonstrate also that the hardening efficiency α in Eq 2

$$\sigma = \sigma_0 + \alpha G b \sqrt{\rho} \quad \ldots\ldots (2)$$

is constant over the dynamic strain aging region, and, as temperature increases beyond this region, α decreases due to the effect of thermal recovery. Strengthening by strain aging during cyclic deformation is caused by an increase in the dislocation density and a resulting decrease in cell size which increases the stress response. Dislocation density can be written as [*17*]

$$\rho = 2/ld \quad \ldots\ldots (3)$$

then from Eqs 2 and 3

$$\sigma = \sigma_0 + \alpha G b \sqrt{(2/d)} l^{-1/2} \quad \ldots\ldots (4)$$

assuming d is constant. Figure 6 shows the relationship between the stress response and $l^{-1/2}$ to be a straight line confirming the dependency of stress

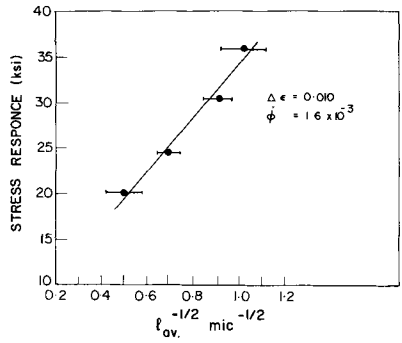


FIG. 6—*Relationship between the cyclic stress response and* $l^{-1/2}$.

response on the subgrain size given by Eq 4. The friction stress (σ_0) does not vary with grain size or the dynamic strain aging level.

Fatigue Fracture

Fatigue life changes with grain size and temperature as shown in Fig. 4. Life decreases with increasing grain size at 23, 205, and 540 C but is insensitive to grain size at 370 C. As temperature increases from 23 C, fatigue life first increases reaching a maximum at 205 C, and then decreases for a given grain size.

Fatigue life can be expressed in terms of grain size at constant temperature by the relation

$$N_f = aD^b \quad \ldots\ldots\ldots\ldots\ldots\ldots\ldots\ldots (5)$$

where a and b are constants. The coefficient a increases between 23 and 205 C and then decreases. The negative value of the grain size exponent b is lower at 205 C than at 23 C and approaches zero at 370 C where fatigue life is independent of grain size. At 540 C, b has a small negative value.

The parameters a and b which determine the dependency of fatigue life on grain size and temperature may be considered also as parameters describing the dependency of crack propagation rate on these variables. Consequently, further discussion of the temperature dependence of a and b will be presented later in this paper.

Fracture Mechanism

At room temperature, the fracture surface reveals ductile striations which are discontinuous at the grain boundaries (Fig. 7*a*). They are formed by ductile rupture at the tip of a propagating crack. As grain size increases, the average span of a ductile striation and hence the crack front advance per cycle increases which explains the negative dependency of fatigue life on grain size.

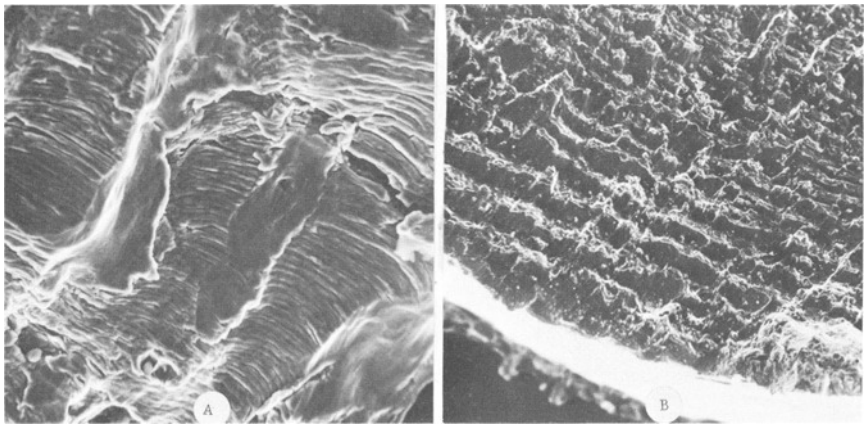


FIG. 7—*Fracture surface* (a) *at 23 C* (×*4130*) *and* (b) *at 370 C* (×*35*).

As the temperature increases to 205 C, the deformation homogeneity, due to enhanced cross slip shown in Fig. 5*a*, causes blunting of initiated cracks. The fracture process consists of the linking of minor cracks by a ductile rupture. Consistent with this argument, fracture surfaces reveal an equiaxed dimpled form. Homogeneity of plastic deformation coupled with a large number of surface cracks leads to a considerable reduction in localized mechanical energy at the crack tip, resulting in a lower crack growth rate. Grain boundaries act as obstacles to this fracture process. Consequently, an increase in grain size decreases resistance to the fracture process, resulting in a higher crack growth rate and decreased life.

When dynamic strain aging is accelerated at (370 C), deformation exhibits maximum stress response. Brittle striations which are observed to occupy about 30 percent of the total fracture surface appear continuous and are unaffected by grain boundaries. Surface damage investigations revealed heavily concentrated plastic deformation in small zones indicating plasticity was restricted by dynamic aging. This restricted plasticity also increases the stress concentration factors on the crack tip and inhibits its blunting, accounting for the brittle nature of the fracture mode. No effect of grain size on either fatigue life or the spacing of brittle striations was observed, as shown in Fig. 7*b*.

At 540 C, fractography revealed transgranular and intergranular fracture modes. Ductile striations dominate the transcrystalline part, while creep damage is evident on the grain boundaries and life decreases slightly as grain size increases. The reduction in fatigue life at this temperature can be attributed both to environmental effects on crack growth rate and to the acceleration of grain boundary damage causing intergranular failure.

Fatigue fracture parameters a and b appear to be highly dependent on the fracture mechanism and its interaction with grain boundaries. Dynamic

strain aging induces changes in cyclic deformation characteristics and the fracture mechanism. The interaction of the fracture process with grain boundaries determines the degree of fatigue life dependency on grain size. Thus, the fatigue life dependency on grain size and temperature can be explained in terms of the dynamic strain aging potential.

Conclusions

1. Steady-state stress response and related cell size are independent of the grain size for strain cycled iron under low-cycle fatigue conditions.
2. At constant strain amplitude and deformation rate, the substructure cell size appears to be temperature dependent. Dynamic strain aging enhances dislocation multiplication resulting in a decrease in the cell size.
3. Dynamic strain aging enhances the inhomogeneity of dislocation substructure and plastic deformation. The grain size, however, has no effect on the redistribution of plastic strains.
4. In the temperature region where enhanced dynamic strain aging occurs, the resulting inhomogeneous deformation controls both the fracture mechanism and fatigue life.
5. The dependency of fatigue life on grain size is controlled by the fracture mechanism At high dynamic strain aging levels, the material reveals brittle striations on the fracture surfaces and life is independent of grain size.

Acknowledgment

This work was supported by USAF, Grant Number AFOSR 71-2120 and by the National Research Council of Canada.

References

[1] Oates, G. and Wilson, D. V., *Acta Metallurgica*, Vol. 12, 1964, p. 21.
[2] Klensil, M., Holzmann, M., Lukas, P., and Rys, R., *Journal of the Iron and Steel Institute*, Vol. 203, 1965, p. 47.
[3] Thompson, A. W. and Backofen, W. A., *Acta Metallurgica*, Vol. 19, 1967, p. 597.
[4] Feltner, C. E. and Beardmore, P. in *Achievement of High Fatigue Resistance in Metals and Alloys, ASTM STP 467*, American Society for Testing and Materials, 1971, p. 77.
[5] Boettner, R. C., Laird, C., and McEvily, A. J., *Transactions*, Metallurgical Society, American Institute of Mining, Metallurgical, and Petroleum Engineers, Vol. 233, 1965, p. 379.
[6] Abdel-Raouf, H., Benham, P. P., and Plumtree, A., *Canadian Metallurgical Quarterly*, Vol. 10, 1971, p. 87.
[7] Abdel-Raouf, H. and Plumtree, A., *Metallurgical Transactions*, Vol. 2, 1971, p. 1863.
[8] Abdel-Raouf, H., Plumtree, A., and Topper, T. H. in *Cyclic Stress-Strain Behavior Analysis, Experimentation, and Failure Prediction, ASTM STP 519*, American Society for Testing and Materials, 1972.
[9] Niessen, P., Abdel-Raouf, H., and Plumtree, A., *Journal of Materials Science*, 1970, p. 919.
[10] Petch, N. J., *Journal of the Iron and Steel Institute*, Vol. 174, 1953, p. 25.

[*11*] Armstrong, R., Codd, I., Douthwaite, R. M., and Petch, N. J., *Philosophical Magazine*, Vol. 7, 1962, p. 45.
[*12*] Brindley, B. J. and Barnby, J. T., *Acta Metallurgica*, Vol. 14, 1966, p. 1765.
[*13*] Li, J. C. M. and Chou, Y. T., *Metallurgical Transactions*, Vol. 1, 1970, p. 1145.
[*14*] Abson, D. J. and Jonas, J. J., *Metal Science Journal*, Vol. 4, 1970, p. 24.
[*15*] Johnston, T. L. and Feltner, C. E., *Metallurgical Transactions*, Vol. 1, 1970, p. 1161.
[*16*] Dingley, D. J. and McLean, D., *Acta Metallurgica*, Vol. 15, 1966, p. 885.
[*17*] Abdel-Raouf, H., Ph. D. thesis, Department of Mechanical Engineering, University of Waterloo, 1972.

DISCUSSION

K. D. Challenger[1] (*written discussion*)—At the temperature where maximum strain aging was observed (370 C), the microscopic strain distribution was very inhomogeneous. I assume that the corresponding dislocation substructures was also inhomogeneous. This being the case, how did you arrive at the values you report for dislocation density and cell size?

H. Abdel-Raouf, T. H. Topper, and A. Plumtree (*author's closure*)—Our results show that the cell size was not homogeneous under maximum dynamic strain aging conditions. The reported cell size is the average size of all the observed cells.

[1] Materials development engineer, General Electric Co., San Jose, Calif. 95125.

D. Eylon,[1] *D. G. Brandon,*[1] *and A. Rosen*[1]

Creep Testing of Alpha Iron During Thermal Cycling

REFERENCE: Eylon, D., Brandon, D. G., and Rosen, A., "**Creep Testing of Alpha Iron During Thermal Cycling,**" *Fatigue at Elevated Temperatures, ASTM STP 520,* American Society for Testing and Materials, 1973, pp. 311–319.

ABSTRACT: The creep properties of alpha iron under thermal cycling conditions were investigated. A special creep testing equipment and creep testing method for nonuniform temperature conditions are described. It was found that creep rates under thermal cycling conditions are lower than the creep rates calculated from results of isothermal creep experiments. The increased creep resistance of alpha iron under thermal cycling conditions was found to be independent of the cycle time but dependent on the dwell time at the high temperature part of the cycle.

KEY WORDS: fatigue (materials), creep properties, thermal cycling tests, alpha iron, creep tests, temperature, strains

The investigation of the creep properties of metals under nonstable thermal conditions is of some importance. In normal operation the temperature is very seldom constant, for example some parts in gas turbines or internal combustion engines always operate under conditions of rapid thermal cycles of low amplitude. However, most creep investigations have been carried out under isothermal conditions, and most of the existing creep testing equipment and the conventional testing methods are unsuitable for creep experiments under thermal cycling conditions. Some creep experiments at varying temperatures were made by Webster et al,[2/3] but the thermal cycles were too slow, being on the order of hours, and conventional equipment was used. The basic feature of the newly developed rapid thermal-cycling creep testing system is its ability to give high rates of heating and cooling in the order of 50 C/s. These rates could be achieved simply by electric resistance heating of foil specimens. Thin but relatively wide specimens give a high surface-to-volume ratio, and hence rapid cooling rate.

[1] Research associate, professor, and associate professor, respectively, Department of Materials Engineering, Technion-Israel Institute of Technology, Haifa, Israel.

[2] Webster, G. A. and Piercey, B. J., *Transactions,* American Society of Metals, Vol. 59, 1966, p. 847.

[3] Webster, G. A. and Sullivan, C. P., *Journal,* Institute of Metals, Vol. 95, 1967, p. 138.

Copyright© 1973 by ASTM International www.astm.org

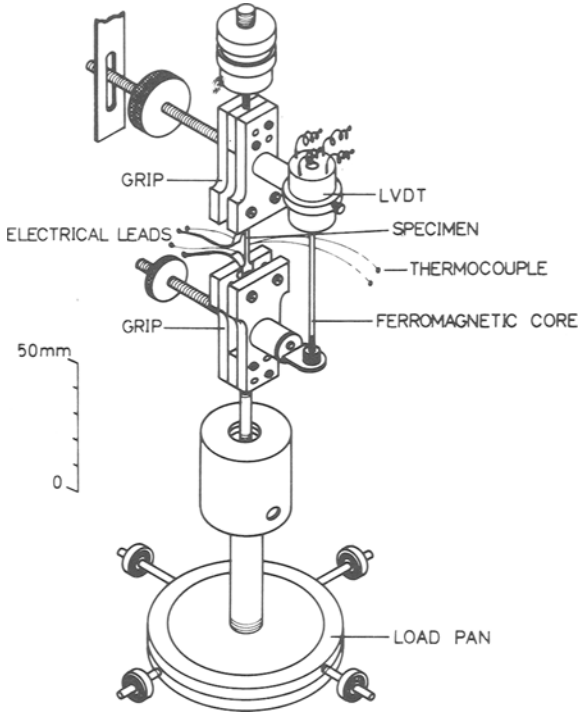


FIG. 1—*Creep specimen assembly.*

The aim of this investigation was to study the effect of thermal cycling on the creep properties of α-iron. A special testing unit was built for this work, and a method for evaluating the creep results was developed.

Experimental Procedure

Apparatus

A creep testing apparatus for measuring creep under thermal cycling conditions in alloys with low-thermal conductivity[4] was modified in order to shorten the thermal response of the strain-measuring system and to lower the thermal gradients along the specimen. The basic units of the apparatus are: creep stage, vacuum system, regulated pulse heater with repeated cycling device, and multichannel recording equipment.

The creep stage and the strain-measuring unit are shown in detail in Fig. 1. The strain is measured by a linear variable differential transducer (LVDT) attached with a ceramic holder to the upper specimen grip. The ferromagnetic core is placed loosely on a smooth Teflon surface attached

[4] Eylon, D., Kushnir, N., and Rosen, A., *Journal of Physics E: Scientific Instruments*, Vol. 3, 1970, p. 527.

by a second ceramic holder to the lower grip. The specimen is held in the grips between ceramic jaws. The upper and the lower grips are counterbalanced, and antitorque devices are built into the weight pan and the upper grip.

The power to heat the specimen is supplied to the specimen through phosphor-bronze shims gripped together with the specimen between the ceramic jaws. The temperature is measured by chromel-alumel thermocouple wires, 0.1 mm in diameter, spot welded to the point of maximum temperature on the specimen.

With the above modifications it is possible to measure creep rates 2 min after a sudden temperature drop of 50 C, without any thermal expansion effects attributable to the apparatus. The accuracy both of the temperature control and the temperature measurements is ± 1 C. The creep strains in the present experiments never exceeded 4 percent so that the test can be considered as a constant stress experiment. To avoid oxidation and contamination the experiments are carried out in a vacuum of 10^{-6} torr.

Specimen Preparation

Creep specimens were prepared from high-purity (HP) iron of the following composition: (weight percent) 0.0023C, 0.0080O, 0.003N, 0.003Si, and 0.001P and from Swedish-pure (SP) iron of the following composition: 0.02C, 0.005Si, 0.01P, 0.005Mn, and 0.005S. The iron was rolled down to 0.13-mm strips, and specimens were punched out with dimensions as shown in Fig. 2. The specimens were heated in vacuum for 9 h at 530 C. The mean grain intercept diameter for the HP iron specimens was 7 μm and for the SP iron 5 μm. Accordingly, there were in the average 20 grains across the thickness of the specimen.

Strain Rate Calibration

To determine the effective gage length, it was necessary to find the temperature gradient along the specimen and the temperature dependence of

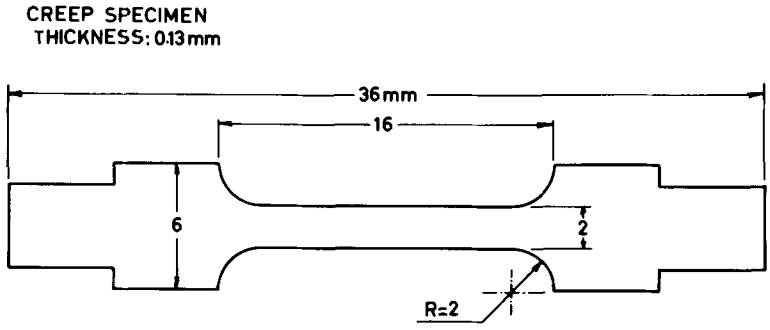


FIG. 2—*Specimen dimensions.*

the creep rate. Five thermocouples were spot welded in different locations along the center line of two specimens to provide a total of 10 measuring sites as shown in Fig. 3. The temperature gradients at different maximum temperatures, T_m, were determined by combining the data from both specimens. The thermal center of the specimen was found not to coincide with the geometrical center. Temperature measurements across the center line of the specimen showed a uniform temperature. Creep tests at different constant maximum temperatures at two stress levels of 2.8 kg mm^{-2} and 4.3 kg mm^{-2} were carried out. An arbitrary gage length of 4 mm was used to calculate the *approximate steady-state creep rate* $\dot{\epsilon}_a$, defined as the creep rate after 48 h under test (after which no further changes in creep rate were detected). The approximate strain rates as a function of temperature are shown in Fig. 4. From the temperature distribution along the specimen, Fig. 3, and the approximate strain rate versus temperature curve, Fig. 4, it is possible to determine the strain rate distribution along the specimen as shown in Fig. 5. The *effective gage length* L_e is defined as the gage length for which the maximum creep rate $\dot{\epsilon}_{am}$ gives the same total rate of elongation as that obtained from the specimen. This can be expressed as:

$$\int_0^l \dot{\epsilon}_a dl = \dot{\epsilon}_{am} L_e \quad \ldots\ldots\ldots\ldots\ldots\ldots\ldots\ldots (1)$$

The value of L_e is determined graphically, as shown in Fig. 5, for a maximum temperature of 480 C and a stress of 4.3 kg mm^{-2}. The determination

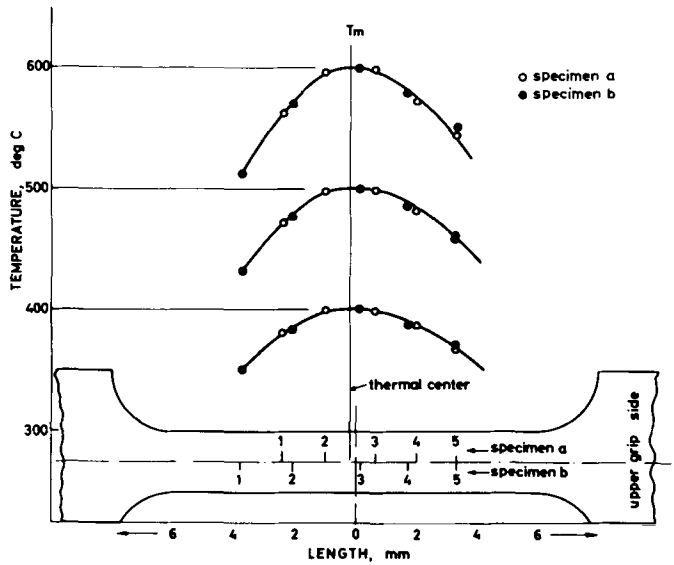


FIG. 3—*Temperature distribution along the specimen.*

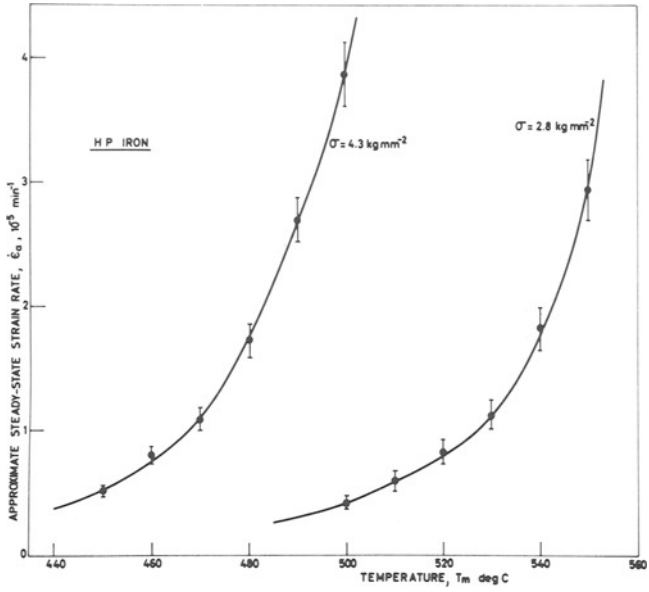


FIG. 4—*Dependence of the approximate steady-state creep rate* $\dot{\epsilon}_a$ *on temperature at two stress levels.*

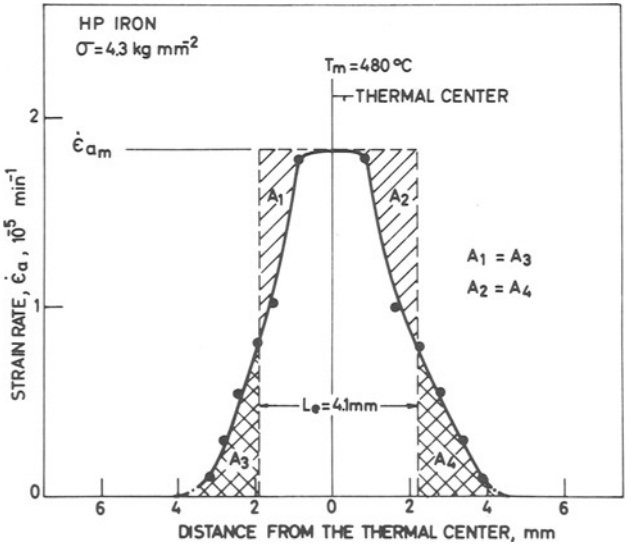


FIG. 5—*Determination of the effective gage length* L_e.

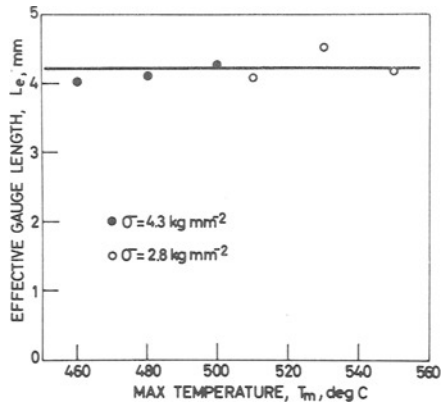


FIG. 6—*Effective gage length* L_e *at different temperatures and stress levels.*

was done for different T_m values and for different stresses. The results are shown in Fig. 6. It can be seen that within the range of the temperatures and stresses used, the effective gage length is almost constant and has a value of 4.2 mm. The error in the approximate strain rate value $\dot{\epsilon}_a$, based on the 4 mm gage length, is thus of the order of 5 percent, amply justifying the use of $\dot{\epsilon}_a$ in Eq 1.

Thermal Cycling

Thermal cycling experiments were carried out between T_1 and T_2, high and low temperatures, respectively. The amplitude of the cycle was 50 C in all cases. The regulated pulse heater maintained a constant temperature T_1 for each t_1 seconds of the total cycle time τ, as shown in Fig. 7. All experiments started by measuring the steady-state creep rates of the specimens after 48 h under test at temperatures T_1 and T_2, followed by thermal cycling at constant τ for different values of t_1. A typical result is shown in Fig. 8.

Results and Discussion

The results of the thermal cycling experiments were evaluated as follows:

1. A steady-state strain rate versus temperature curve (for example, Fig. 4) was plotted for each specimen. In order to compensate for the scatter due to specimen variation the curve of Fig. 4 was fitted to the strain rates measured for the individual specimens at temperatures T_1 and T_2.

2. The *average cycle temperature* T_{av} was determined as:

$$T_{av} = \int_0^{\tau} [T(t)/\tau]dt \quad \ldots\ldots\ldots\ldots\ldots\ldots\ldots\ldots (2)$$

Where $T(t)$ is the temperature at time t from the start of a cycle. The integration was done graphically as shown in Fig. 7*a*.

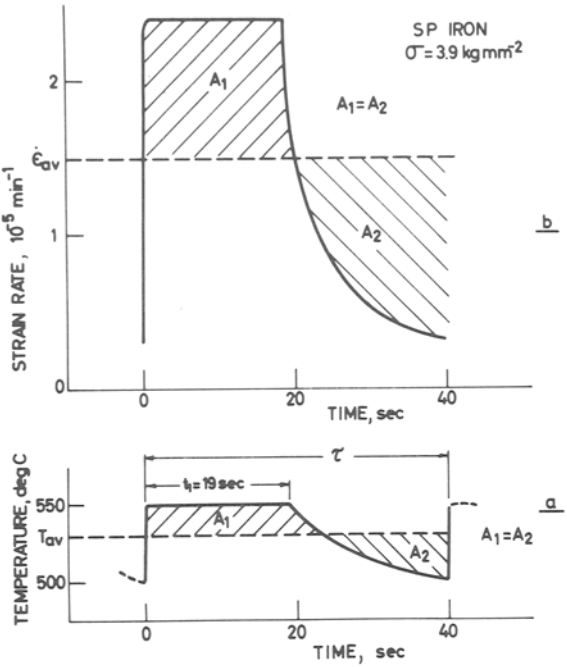


FIG. 7—*Change of temperature* (a) *and strain rate* (b) *under given thermal cycling conditions.*

It is also possible to calculate the creep rate for a given cycle (Fig. 7*b*) by combining the data obtained from the steady-state creep rate versus temperature curve (Fig. 4) and the temperature versus cycle time curve (Fig. 7*a*).

3. The *average creep rate* during thermal cycling $\dot{\epsilon}_{av}$ was obtained by measuring the slope of the envelope on the creep curve as shown in Fig. 8 and assuming an effective gage length of 4.2 mm.

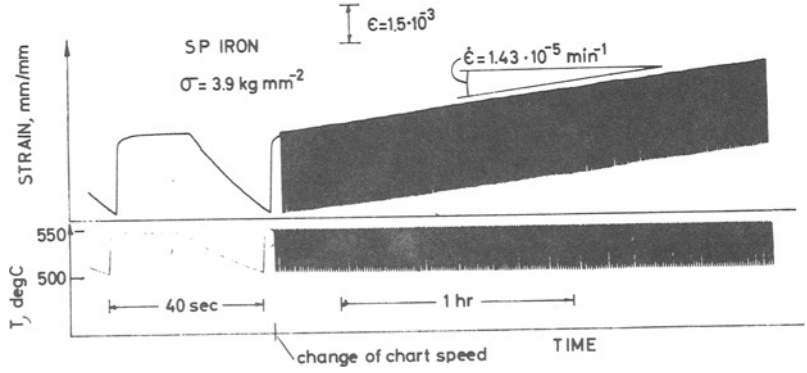


FIG. 8—*Chart record of thermal cycling creep experiment.*

4. A *calculated mean creep rate* during cycling was defined as:

$$\dot{\epsilon}_m = \int_0^\tau [\dot{\epsilon}(t)/\tau]dt \quad \ldots\ldots\ldots\ldots\ldots\ldots\ldots\ldots (3)$$

Where $\dot{\epsilon}(t)$ is the steady-state strain rate at temperature $T(t)$, assumed equal to that determined from constant temperature tests at the same temperature. This integration was also done graphically as shown in Fig. 7*b*.

Figure 9*a* and *b* are examples of plotting the results, for HP iron and for SP iron, respectively, for a given stress and constant cycle time. Here the experimental and calculated results are superimposed on the steady-state strain rate versus temperature curve. Figure 10*a* and *b* show the ratio between the calculated and experimental strain rates due to cycling $\dot{\epsilon}_{av}/\dot{\epsilon}_m$ as a function of average temperature T_{av} for the HP iron and the SP iron, respectively.

Both Figs. 9 and 10 show that thermal cycling has a small strengthening effect on the creep resistance of iron, especially when the time t_1 is long. As t_1 decreases the experimental curve approaches the calculated one. The identical effect was found for cycle times as short as 10 s and as long as 200 s, with no detectable difference between HP or SP iron.

Conclusions

Short-term temperature cycling during creep of iron in the temperature range 450 to 550 C slightly enhances the creep resistance. This conclusion is essentially unambiguous thanks to the construction and calibration of a special high-vacuum creep apparatus in which abrupt temperature changes

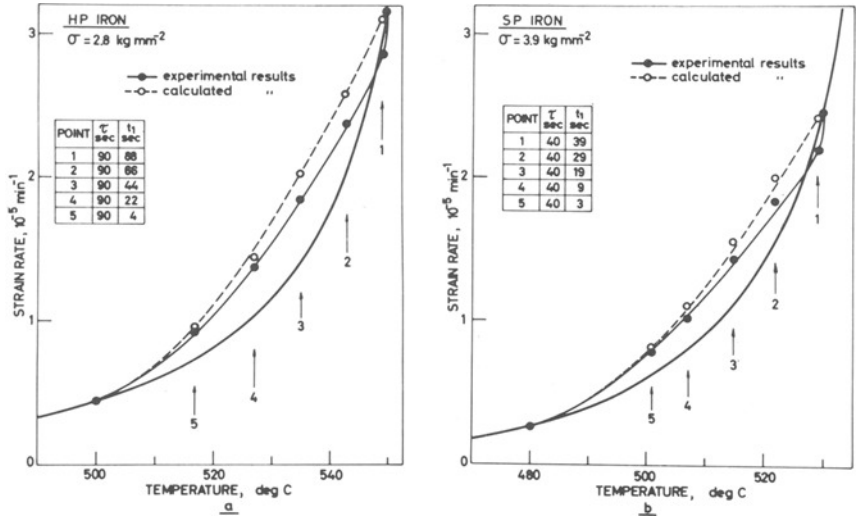


FIG. 9—*Experimental and calculated average creep rate as a function of the thermal cycling conditions*, (a) *in HP iron*, (b) *in SP iron*.

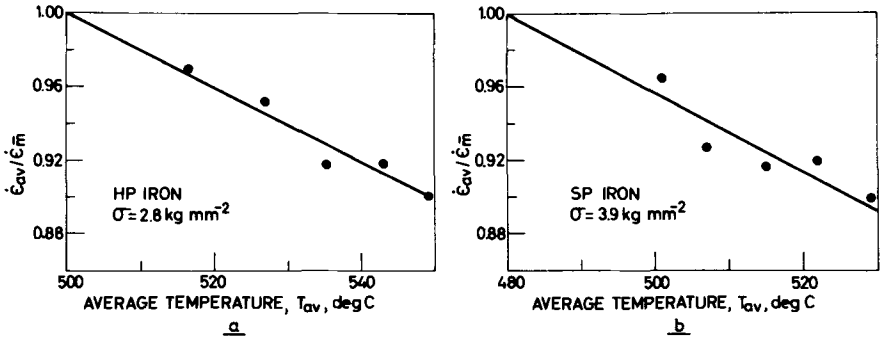


FIG. 10—*The ratio of experimental to calculated creep rate* $\dot{\epsilon}_{av}/\dot{\epsilon}_m$ *as a function of the average temperature* T_{av}, (a) *in HP iron*, (b) *in SP iron.*

can be made during creep. The present results give some confidence in the calculation of creep rates under variable temperature conditions based on data determined at constant temperature.

Acknowledgments

We would like to thank BISRA, the Inter-Group Laboratories of the British Steel Corporation, for supplying the high-purity iron. The help of N. Nir (Kushnir) during the various stages of the research is appreciated.

DISCUSSION

K. D. Challenger[1] *(written discussion)*—In your concluding remarks you mentioned that thermal cycling can enhance the creep resistance, yet your Fig. 9 indicates that the isothermal creep rate is lower than the cyclic creep rate. Is not this a contradiction?

D. Eylon, D. G. Brandon, and A. Rosen (authors' closure)—The average measured creep rate under thermal cycling conditions should not be compared to the isothermal creep rate at the same average temperature, but to the calculated mean creep rate based on isothermal creep experiments, as can be seen in Fig. 9, *a* and *b*. Because of the exponential dependence of the creep rate in temperature (Fig. 9), the contribution of the upper part of the cycle to the average creep rate is much bigger than that of the lower part of the cycle. For this reason the calculated mean creep rate is higher than the isothermal creep rate.

[1] Materials development engineer, General Electric Co., San Jose, Calif. 95114.

W. J. Elder,[1] *J. B. Marriott,*[2] *and M. C. Murphy*[3]

High-Strain Fatigue Properties of Cast ½Cr-Mo-V Steels

REFERENCE: Elder, W. J., Marriott, J. B., and Murphy, M. C., "**High-Strain Fatigue Properties of Cast ½Cr-Mo-V Steels,**" *Fatigue at Elevated Temperatures, ASTM STP 520*, American Society for Testing and Materials, 1973, p. 320–331.

ABSTRACT: Reverse-bend and push-pull tests at 550 C on small specimens of ½Cr-Mo-V cast blocks have been used to obtain data relevant to crack formation in steam turbine components. A dwell period at peak tensile strain reduced the endurance, but increases in the length of the dwell did not reduce the endurance proportionately because the peak stress relaxed rapidly.

Neither forging, aging, nor differences in the normalizing cooling rates significantly affected the endurance of the ½Cr-Mo-V steels tested, but oil quenching to produce fully bainitic structures altered the slope of the strain/endurance relationship. The data obtained from tests in air appeared to give conservative life predictions for components in service in steam.

KEY WORDS: fatigue (materials), strains, castings, cyclic loads, heat treatment, microstructure, steam, vacuum, air, crack initiation, crack propagation

Prevention of high-strain fatigue in cast cylinders and cast or forged valve bodies was an important consideration in the design of steam turbines which are successfully operating under two shift and load following regimes. Other considerations of weldability, creep ductility, and adequate creep strength led the British turbinemakers and the Central Electricity Generating Board (CEGB) to prefer ½Cr-Mo-V steel to the previously used 1Cr-Mo-V steels. This necessitated a comprehensive investigation of the high-strain fatigue properties of the ½Cr-Mo-V steel, part of which is reported here.

In practice there are two separate aspects of the high-strain fatigue problem, crack formation, and crack propagation. Crack formation can be considered a function of local surface strains and hence to be essentially

[1] Research officer, Scientific Services Department, Central Electricity Generating Board, Barnet, Herts, England.

[2] Materials group head, Quality and Metallurgy Department, English Electric-AEI Turbine Generators Ltd., Leicester, England.

[3] Senior group leader, Metallurgy Department, Research and Development Laboratories, C. A. Parsons & Co., Ltd., Newcastle upon Tyne, England.

Copyright© 1973 by ASTM International www.astm.org

independent of specimen or component size [*1*].[4] Consequently, relatively simple reverse-bend tests on small specimens can be used to obtain relevant data.

A significant amount of the damage resulting from thermal stresses in high-temperature components, in fact, occurs by creep during dwell periods at the operating temperature in addition to that resulting from the strain cycles associated with starting and stopping [*2,3*]. Since no practical test program can encompass all the stress-strain regimes likely to be encountered in service, some sort of cumulative damage law must be invoked [*4*] if designs and operating procedures are to be evaluated realistically. Reverse-bend tests cannot yield the quantitative stress data required to substantiate such a law, and so a parallel program of push-pull tests was carried out in which stress and strain were monitored continuously.

Materials Tested

For the basic program, 1/2Cr-Mo-V cast blocks, 4 by 4 by 10 in., were normalized to simulate a large turbine casing flange (Material A). Blocks from the same cast were also normalized at a faster rate to simulate the pressure wall of such a casing (Material B). Both these heat treatments produced ferrite microstructures containing about 5 percent pearlite. A radically different, fully bainitic microstructure was obtained by oil quenching blocks from the same cast (Material C). To assess the effect of overaging, a further block of cast 1/2Cr-Mo-V steel was aged for 8000 h at 600 C (Material D). A 1/2Cr-Mo-V closed die forging which had been oil quenched (Material E) and had a ferrite microstructure containing about 10 percent bainite was tested to give a comparison with the cast material. Details of composition, heat treatment, and mechanical properties of all the test materials are summarized in Table 1.

Testing Techniques

In both reverse-bend and push-pull, the specimens were subjected to fully reversed strain cycles, either continuously or with a dwell at maximum tensile strain, referenced to the top surface for the reverse-bend specimen. The dwell was varied from 1/2 to 16 h. The basic cycle speeds were standardized at 1 cpm for reverse bending and 1/2 cpm for push-pull testing. Such a small difference in cycling rate has negligible effect on fatigue endurance [*5*], particularly for tests with dwell periods. All the tests were at 550 C.

Reverse-Bend Tests

The reverse-bend test machine [*6*] used rectangular section specimens either 0.5 in. wide by 0.2 in. thick by 1 in. gage length, or 0.75 in. wide

[4] The italic numbers in brackets refer to the list of references appended to this paper.

TABLE 1—*Composition, heat treatment, and mechanical properties.*

Material	Ref	Composition, %							Heat Treatment	Mechanical Properties				
		C	Si	Mn	Ni	Cr	Mo	V		Temperature, deg C	0.2% Proof Stress, MN/m² (ton/in.²)	Tensile Strength, MN/m² (ton/in.²)	Elongation, %	Reduction of Area, %
Casing flange	A	0.14	0.45	0.46	0.10	0.38	0.40	0.25	annealed 12 h at 960 to 980 C, furnace cooled; austenitized 8 h at 950 to 980 C, normalized to simulate the cooling rate of a turbine casing flange; tempered 13 h at 690 to 710 C, air cooled	room temperature	270 (17.5)	509 (33.0)	28	66
										550	197 12.8)	330 (21.4)	26	65
Casing wall	B	0.14	0.45	0.46	0.10	0.38	0.40	0.25	annealed 12 h at 960 to 980 C, furnace cooled, austenitized 8 h at 950 to 980 C, normalized to simulate the cooling rate of a turbine casing wall, tempered 13 h at 690 to 710 C, air cooled	room temperature	347 (22.5)	571 (37.0)	22	66
										550	219 (14.2)	324 (21.0)	30	81

Fully bainitic	C	0.14	0.45	0.46	0.10	0.38	0.40	0.25	annealed 12 h at 960 to 980 C, furnace cooled; austenitized 8 h at 975 C, oil quenched; tempered 12 h at 690 to 700 C, furnace cooled	550	431 (28.0)	476 (30.9)	17	72
Cast block	D	0.14	0.34	0.55	...	0.47	0.60	0.29	austenitized at 980 C, normalized to simulate the cooling of a turbine casing flange; tempered 12 h at 690 to 700 C, furnace cooled	room temperature	319 (20.7)	517 (33.5)	32	...
Valve body forging	E	0.14	0.24	0.49	0.24	0.46	0.57	0.28	austenitized 8 h at 950 C, oil quenched; tempered 6 h at 690 C and 12 h at 720 C, furnace cooled	room temperature	382 (24.8)	556 (36.0)	26	73
										550	252 (16.3)	358 (23.2)	26	82

by 0.1875 in. thick by 2 in. gage length. For tests in air and steam (which was at atmospheric pressure and dry) the total plastic plus elastic strain at the specimen surface was derived from radius measurements over the prescribed gage length. This was not possible for tests in vacuum (<0.1 torr), for which approximate values had to be derived by calibration of the angle of the straining bars.

Since the machines employ a constant angular displacement control, the strain amplitude in the specimen increased throughout a test. The strain to define the test was taken arbitrarily as that at 40 percent of the cyclic life to failure. Two failure criteria were chosen for assessing the results—the number of cycles to form a surface crack 0.030 in. long and the number to complete fracture. The former criterion proved unsatisfactory, oxidation in particular leading to uncertainty of visual detection, especially in long-duration tests including a dwell period. There was, however, some indication of a correlation of crack formation with the number of cycles at which the strain range began to increase, and this may provide a positive indication of its occurrence in future. This paper is concerned only with complete fracture (N_f).

Push-Pull Tests

In the push-pull machines the cylindrical specimens [7] were of 1.0 in. gage length and 0.5 in. diameter. Load was measured by a series mounted load cell. For dwell tests strain was held constant (within $\pm 3.5 \times 10^{-5}$) at each peak tension for the duration of the dwell. All tests were in air.

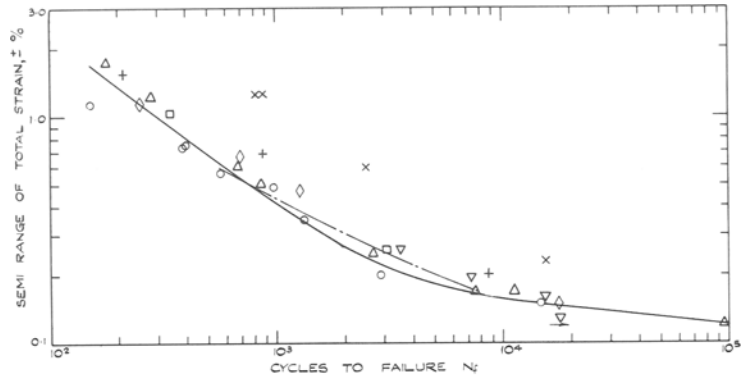
Longitudinal extensometers were mounted on ridges at the ends of the gage length to maximize strain control and prevent elastic follow-up effects within the gage length during dwell. Diametral extensometers were found to be less discriminating and subject to unacceptable errors in the presence of surface cracks and oxidation. The small stress concentration at the ridges did not affect the endurance of the ½Cr-Mo-V steel significantly and had no apparent effect on the stress-strain cycles.

Results

Basic Continuous Cycling Data

Casing flange material (A) showed similar fracture endurance in reverse-bend and push-pull (Fig. 1) over a semirange of total strain of ± 0.1 to ± 2.0 percent, representing cyclic lives of 10^5 to 10^2, respectively.

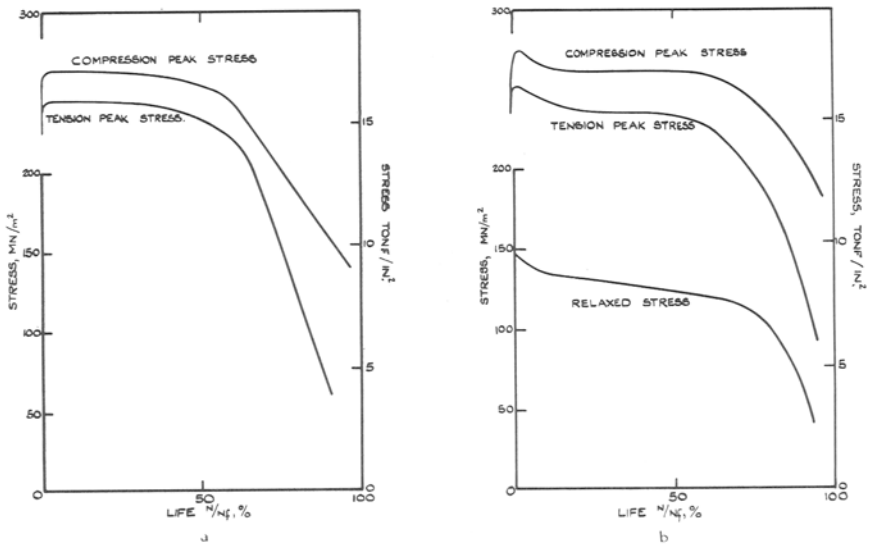
Peak compressive and tensile stresses during a typical push-pull test (Fig. 2*a*) showed that a little cyclic hardening had occurred initially, followed by plateau levels of stress. The stress then dropped rapidly as fracture approached. The test specimen failed at the ridges, but there was extensive transverse cracking over the parallel gage length.



Reverse-bend tests:
—△—Casing flange material (A) in air.
\+ Casing flange material (A) in steam.
× Casing flange material (A) in vacuum.
□ Casing wall material (B) in air.
▽ Forging material (E) in air.
— — —Cast block unaged in air [5].
◇ Cast block aged (D) in air.

Push-pull tests:
—○—Casing flange material (A) in air.

FIG. 1—*Endurance of ½Cr-Mo-V material in continuous-cycling tests at 550 C.*



(*a*) Continuous cycle test, ±0.49 percent strain N_f = 982 cycles.
(*b*) ½-h dwell test, ±0.50 percent strain N_f = 537 cycles.

FIG. 2—*Stress history during push-pull tests on ½Cr-Mo-V casing flange material (A) at 550 C.*

The plateau stresses have been compiled from a series of push-pull tests at total strain semiranges from ±0.15 to ±0.75 percent and are given as a dynamic stress/strain curve (Fig. 3) using the elastic modulus of the material derived from a conventional tension test at 550 C. The plateau stresses increased at increased cyclic strain range.

Effect of Dwell

The effect of a ½-h dwell period at maximum strain in tension over total strains from ±0.15 to ±2.0 percent for material (A) at 550 C (Fig. 4) was similar in both reverse-bend and push-pull testing. The endurance was some 20 percent less than that in the continuous-cycle tests, although the differences appeared to be increasing at the lowest strain ranges tested.

The effect of extended dwell periods of up to 16 h was investigated at semiranges of total strain of ±0.5 and ±1.5 percent (Fig. 5). The tests were in reverse bending, and a small degree of interpolation, therefore, was needed to rationalize the results to common strain ranges. Although the

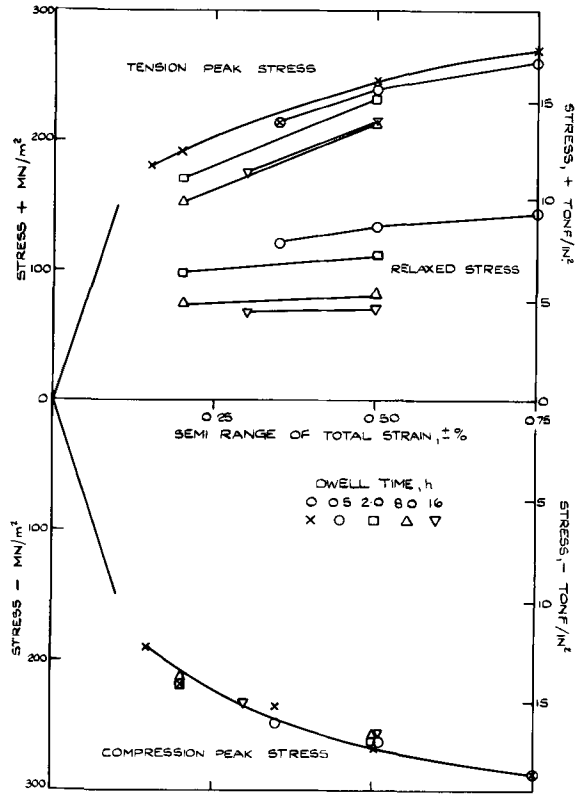


FIG. 3—*Dynamic stress-strain curve for ½Cr-Mo-V casing-flange material derived from plateau values of stress at 550 C.*

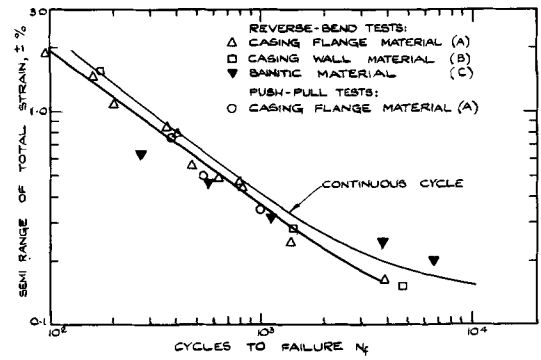


FIG. 4—*Endurance of ½Cr-Mo-V materials reverse-bend tested with ½-h dwell at 550 C.*

introduction of a ½-h dwell reduced the endurance by some 20 percent, extending the dwell period had progressively less effect.

A typical stress history (Fig. 2*b*) obtained by push-pull testing showed more pronounced hardening at an early stage in the test with dwell than in the corresponding continuous-cycling test (Fig. 2*a*). Thereafter, the cyclic peak stresses dropped to lower plateau values than in continuous cycling before the onset of fracture. Relaxed stresses followed a similar pattern.

A series of push-pull tests was used to establish the plateau values of peak cyclic stress and relaxed stress at various strain ranges with different dwell periods. The results are plotted on the dynamic stress/strain curve (Fig. 3). Compared with a continuous cycling test, repetitive tensile dwell periods reduced the peak stresses, although the reduction was negligible in compression. Increasing the dwell period increased the amount of peak-stress reduction, but the time dependence was not linear. More relaxation occurred at larger strain ranges, but relatively little further relaxation occurred as the dwell was extended beyond ½ h.

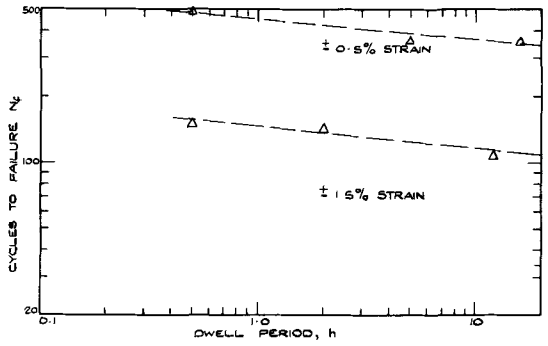


FIG. 5—*Effect of extended dwell period of endurance of ½Cr-Mo-V casing-flange material in reverse-bend tests at 550 C.*

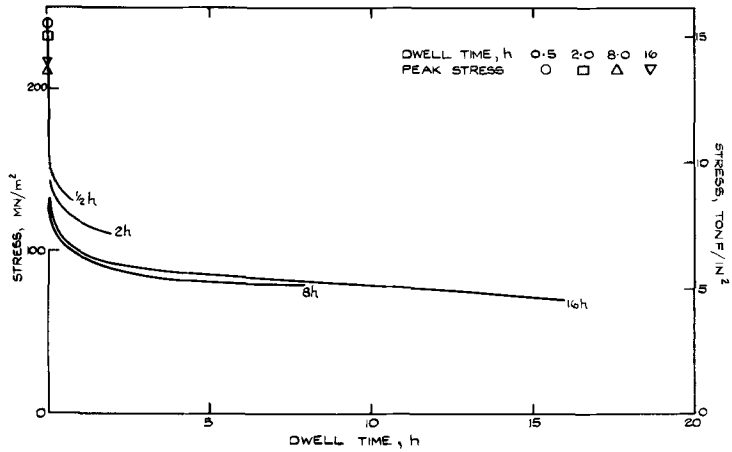


FIG. 6—*Stress relaxation from plateau tensile stresses during push-pull tests with dwell period on ½Cr-Mo-V casing-flange material at 550 C (±0.50 percent strain).*

The relaxation curves between the peak tensile and relaxed stress points in Fig. 3 for the tests at ±0.5 percent total strain semirange showed (Fig. 6) a rapid initial rate of relaxation in all cases. The stress relaxed with time appeared nearly the same for all tests, but the absolute level of stress appeared higher during the shorter dwell periods. However, the relaxation paths for the 8 and 16-h dwell tests appeared almost identical.

Metallurgical Factors

In continuous cycling and ½-h dwell reverse-bend tests (Figs. 1 and 4), no significant differences could be found between casing-flange (A) and casing-wall (B) material, the microstructures of which were similar.

The fully bainitic material (C) however, exhibited significant differences from Materials A and B (Fig. 4). Although in terms of ½-h dwell its endurance was only about half the mean endurance of Material A at ±0.6 percent strain, Material C had three times the endurance of Material A at ±0.2 percent strain. Therefore, although the differences in the cooling rates of the casing-flange and the casing-wall material did not produce significant differences in the high-strain fatigue response, differences could be expected if cooling rate and composition combined to produce a principally bainitic structure.

High-strain fatigue usually is studied on material which has not been exposed to the overaging which occurs in service. Tests on a ½Cr-Mo-V cast block aged for 8000 h at 600 C (Material D) were intended to assess such effects. Fracture endurance in continuous-cycling (Fig. 1) was not less than that of unaged material from the same batch [5].

The final metallurgical parameter considered was the effect of forging. Tests on the forged material (E) showed its fracture endurance to be similar

to that of Material A for both continuous cycling (Fig. 1) and ½-h dwell. Therefore, neither forging nor heat treatment to produce small proportions of bainite appear to offer a major inherent advantage in high-strain fatigue endurance.

Effect of Environment

The fracture endurance of Material A in continuous-cycling reverse-bend tests was better in both steam and vacuum than in air (Fig. 1). While the improvement in endurance due to the presence of steam was small, that resulting from testing in vacuum was marked and demonstrated the importance of oxidation in high-temperature high-strain fatigue tests.

Discussion

Steel of the ½Cr-Mo-V type is relatively insensitive to differences in normalizing cooling rate, and uniform high-strain fatigue crack formation properties are, therefore, to be expected in very large steam turbine castings. From the results obtained, forging appears unlikely to affect the behavior significantly compared with defect-free castings, and the data derived therefore appear equally applicable to normalized ½Cr-Mo-V value-body forgings.

Excessive cooling rates could be induced in thin-sectioned valve bodies by oil quenching, which would result in a fully bainitic microstructure and somewhat lower crack initiation resistance at high-strain ranges but better resistance at the low-strain ranges which are more common in service. Nevertheless, in the 4-in. thick section of the oil quenched valve-body tested, only about 10 percent bainite was formed, and the endurance was similar to that of the materials containing about 5 percent pearlite.

Extended aging at 600 C did not affect the properties of a ½Cr-Mo-V cast block. This illustrates the general high-temperature stability of these steels and strengthens the confidence which can be placed in extrapolations of data necessary in evaluating designs for long-service lives. While the effect of testing in steam rather than air was not marked, it did improve the endurance. Hence, data determined in air can be expected to give a somewhat conservative prediction of the behavior of a component in steam.

The data established show that at 550 C relaxation occurs very rapidly during a dwell period, high stresses being maintained for only short periods irrespective of the total length of the dwell. The tensile peak values fell about 50 percent within minutes. Such a reduction represents one to two orders of magnitude in the creep-rupture life of ½Cr-Mo-V steels [*8*], thus illustrating that accumulation of creep damage is a highly stress-dependent process. Therefore, very long periods at the lower relaxed stresses are required before the damage accumulated in the early part of the cycle is increased significantly.

Work now in progress suggests that the peak and relaxed stress levels are characteristic for a given strain range and dwell period, in that specimens previously cycled under different regimes revert to the characteristic levels. Further work is in progress to obtain long-term, high-strain fatigue endurance and creep-rupture data for ½Cr-Mo-V steel to test the available cumulative damage hypotheses [*9–13*]. Basic data will be obtained at other temperatures, and under different stress/strain regimes, to enable comprehensive design calculations to be made.

Conclusions

1. Reverse-bend testing techniques have enabled continuous-cycle, high-temperature, high-strain fatigue data to be obtained up to 10^5 cycles endurance at 550 C for cast ½Cr-Mo-V steel. Use of small specimens ensured that the data were relevant to crack formation in large components such as steam turbine cylinders.

2. A dwell period of ½ h duration at 550 C reduced the endurance by about 20 percent, although the difference appeared to be increasing at the lowest strain ranges tested. Successive increases in dwell period had progressively less effect.

3. Measurements of stress during complementary push-pull tests established that a plateau existed in both the peak and relaxed stresses for much of the test. These plateau values were used to construct a dynamic stress/strain curve for 550 C.

4. At 550 C relaxation of the peak tensile stress was always rapid, high stresses being maintained for less than 30 min. Since the rate of accumulation of creep damage is highly stress dependent, the disproportionate effect of prolonging the dwell period is predictable. The range of stress relaxed in a given time in each cycle appeared to be independent of the final length of the dwell.

5. The high-strain fatigue properties of the ½Cr-Mo-V materials tested were not very sensitive to heat treatment within the practical range, although fast cooling to produce a fully bainitic structure altered the slope of the strain/endurance relationship. Neither thermal aging nor forging appeared to affect the results.

6. Testing in steam suggested that data derived from tests in air should give a conservative prediction of the life of a component working in steam.

Acknowledgments

We wish to acknowledge the active cooperation of our colleagues in the collaborative test program. We are grateful to the CEGB, to English Electric-AEI Turbine Generators Limited, and to C. A. Parsons & Co., Ltd., for permission to present the paper.

References

[1] Dawson, R. A. T., Elder, W. J., Hill, G. J., and Price, A. T., "High Strain Fatigue of Austenitic Steels," The Metals and Metallurgy Trust, Monograph and Report Series No. 32, 1967, pp. 239–269.
[2] Dawson, R. A. T., "Factors to be Considered in the Design and Operation of Turbines to Prevent Failure by Thermal Fatigue," The Metals and Metallurgy Trust, Monograph and Report Series No. 32, 1967, pp. 40–54.
[3] Timo, D. P., International Conference on Thermal Stresses and Thermal Fatigue, Butterworths, London, 1971, pp. 453–469.
[4] Stringer, M. B., "Concepts of Cumulative Damage and Endurance Predictions in High Strain Fatigue," CEBG Report SSD/SE/RM 36/71, Central Electricity Generating Board, 1971.
[5] Coles, A., Hill, G. J., Dawson, R. A. T., and Watson, S. J., "The High Strain Fatigue Resistance of Low Alloy Creep Resisting Steels," The Metals and Metallurgy Trust, Monograph and Report Series No. 32, 1967, pp. 270–294.
[6] Forrest, P. G. and Penfold, A. B., *Engineering*, Vol. 192, 1961, pp. 522–523.
[7] Elder, W. J. and Stringer, M. B., "The Influence of Test Method and Specimen Design on the High Strain Fatigue Behaviour of Three High Temperature Steels," CEGB Report SSD/SE/RR 11/71, Central Electricity Generating Board, 1971.
[8] International Standards Organisation, "Elevated Temperature Tensile and Stress Rupture Properties of ½% Chromium ½% Molybdenum and ¼% Vanadium Steel," Report prepared by BISRA, Sheffield for ISO, Ref ISO/TC17/WG10/ETP-S99.
[9] Wood, D. S., Welding Research Supplement 90-S, 1966.
[10] Timo, D. P. and Sarney, G. W., "The Operation of Large Steam Turbines to Limit Cyclic Thermal Cracking," ASME Publication 67-WA/PWR-4, American Society of Mechanical Engineers, 1967.
[11] Esztergar, E. P. and Ellis, J. R. in *International Conference of Thermal Stresses amd Thermal Fatigue*, Butterworths, London, 1971, pp. 128–155.
[12] Marshall, P. and Cook, T. R., in *International Conference on Thermal Stresses and Thermal Fatigue*, Butterworths, London, 1971, pp. 81–88.
[13] Lagneborg, R. and Altermo, R., *Metallurgical Transactions*, Vol. 2, 1971, pp. 1821–1827.

DISCUSSION

Alfred Fox[1] (*written discussion*)—Have you subjected your bending fatigue specimen to holdtime, and, if so, have you considered the time dependent redistribution of stress as a consequence of stress relaxation?

W. J. Elder, J. B. Marriott, and M. C. Murphy (*authors' closure*)—Most of the holdtime test results reported were obtained in reverse bend. We consider that this test mode is relevant to the surface phenomena with which we are concerned in large steam turbines. We know that there is a time dependent redistribution of stress through the thickness of these specimens and the stress measurements in the paper quantify the effect.

[1] Bell Telephone Laboratories, Murray Hill, N. J.

R. R. Seeley[1] *and R. H. Zeisloft*[1]

Effect of Carbon Content on High-Temperature Properties of 2¼Cr-1Mo Steels

REFERENCE: Seeley, R. R. and Zeisloft, R. H., "**Effect of Carbon Content on High-Temperature Properties of 2¼Cr-1Mo Steels,**" *Fatigue at Elevated Temperatures, ASTM STP 520*, American Society for Testing and Materials, 1973, pp. 332–344.

ABSTRACT: The 2¼Cr-1Mo steel is an attractive material for liquid metal handling systems such as a liquid sodium loop of a liquid metal fast breeder reactor (LMFBR) steam generator. However, mass transfer of carbon from the chromium-molybdenum steel can occur in such applications and hence can alter the mechanical properties of the material. The object of this work was to determine the effect of low-carbon contents on the tensile, stress rupture, and low-cycle fatigue properties of 2¼Cr-1Mo steels at elevated temperatures.

Commercial and laboratory heats of material with carbon contents of about 0.02 to 0.19 percent were tested in the annealed condition. These carbon contents were obtained by casting to the desired level and by decarburization. The results of our tests indicate that lower carbon contents decrease strength levels, stress rupture properties, and low-cycle fatigue resistance at elevated temperatures. The decarburized material may suffer greater strength losses than the cast-to-low carbon material.

KEY WORDS: fatigue (materials), heat, carbon steels, breeder reactors, decarburizing, stress cycling, creep rupture strength

The 2¼Cr-1Mo steel is being considered for use in liquid metal fast breeder reactor (LMFBR) steam generators. It is the strongest, low-alloy steel for high-temperature service. It has good formability, weldability, and good water corrosion resistance. In addition, it has been used in boilers for 40 years. At present, design criteria for LMFBR steam generator materials require a service life of approximately 210 000 h (24 years). Operating temperatures have not been firmly established, but the peak temperatures will be approximately 1050 F.

During this long time service, the ferritic 2¼Cr-1Mo steel will be in a system with liquid sodium and an austenitic stainless steel. It is known that sodium will cause carbon depletion in the ferritic steel, and the carbon

[1] Research metallurgists, Babcock and Wilcox Co., Alliance, Ohio, 44601.

Copyright© 1973 by ASTM International www.astm.org

will be transported to the austenitic steel, causing it to be carburized. This is the only significant mass transfer effect since the transfer of substitutional alloying elements will be negligible.

This transfer of carbon and the resultant decarburization of 2¼Cr-1Mo steel brings up an important design question: how will the loss of carbon affect the mechanical properties of 2¼Cr-1Mo steels? We have conducted a test program to determine the effects of low-carbon contents on the tensile, stress rupture, and low-cycle fatigue properties of these steels at elevated temperatures.

Procedure

Material

The material for this work was obtained from two commercial heats and five laboratory heats of 2¼Cr-1Mo steels. These heats had carbon contents ranging from 0.02 to 0.19 percent. Table 1 shows the chemical composition of the materials.

TABLE 1—*Chemical composition of heats used.*

	Laboratory Heats					Commercial Heats	
Element	4158	3089	3090	3091	3092	1893	47963[a]
C	0.02	0.027	0.061	0.13	0.19	0.020	0.021
Si	0.28	0.21	0.20	0.19	0.24	0.35	0.31
Mn	0.37	0.37	0.50	0.40	0.50	0.62	0.63
Ni	0.16	0.15	0.15	0.15	0.15	0.07	...
Cr	2.34	1.85	2.35	2.00	2.10	2.28	2.41
Mo	0.96	0.95	1.04	1.08	1.02	1.05	1.05
Cu	0.14	0.10	0.10	0.10	0.10	0.28	...
P	...	...	...	...	...	0.011	...
S	...	...	...	...	...	0.018	...
N	...	0.0031	...	...	...	0.0047	0.0081

[a] After decarburization. Original heat contained 0.12 percent carbon. Original nitrogen content was approximately 0.010 percent.

Specimen blanks were produced by forging and hot rolling followed by heat treatment. The as-rolled material was heat treated 1 h at 1575 to 1650 F, cooled at 50 F/h to 1200 F or lower and then furnace cooled. Blanks of one commercial heat were decarburized from 0.12 to 0.021 percent carbon at 1500 F in a flowing atmosphere of water-saturated hydrogen for about 550 h. This method of decarburization was chosen based on two assumptions: (1) only the diffusion of carbon is important (the transfer of major elements such as chromium and molybdenum is negligible); and (2) the method of decarburization is not important since the rate is controlled by

diffusion within the metal. The decarburized material was heat treated ½ h at 1800 F in a vacuum and furnace cooled.

In order to determine if the decarburizing thermal cycle of about 500 h at 1500 F would result in differences in the tensile properties of decarburized and cast to low-carbon specimens, material cast to 0.02 percent carbon (Heat No. 4158) was homogenized for 10 min at 2000 F then given the standard heat treatment of 1650 F for 1 h and the thermal treatment of the decarburizing cycle 1500 F for 500 h.

Tension Tests

Tension tests were conducted on specimens from the commercial heats and the cast-to-low carbon heat (No. 4158) at room and elevated temperatures. The specimens had a gage diameter of 0.320 in. with a 2 in. gage length. The crosshead speed during testing was 0.05 in./min.

Stress-Rupture Tests

Stress-rupture tests were conducted on specimens from six heats. These specimens also had a gage diameter of 0.320 in. but a 3 in. gage length. These tests were conducted in accordance with ASTM Recommended Practice for Conducting Creep and Time-for-Rupture Tension Tests of Materials (E139-70).

Low-Cycle Fatigue Tests

The material for low-cycle fatigue (LCF) testing was taken from one of the commercial heats. LCF specimen blanks with the nominal carbon content of 0.12 percent were heat treated as before. Similar blanks were decarburized to a carbon content of about 0.02 percent and then heated like the previous decarburized specimens. Figure 1 illustrates the type of specimen used for the fatigue tests.

The specimens were fatigue tested on a closed loop, hydraulic test system by strain cycling between equal tensile and compressive strain limits of 0.0025 in./in. The test frequency was 0.25 Hz which resulted in an average strain rate of 0.0025 in./in./s.

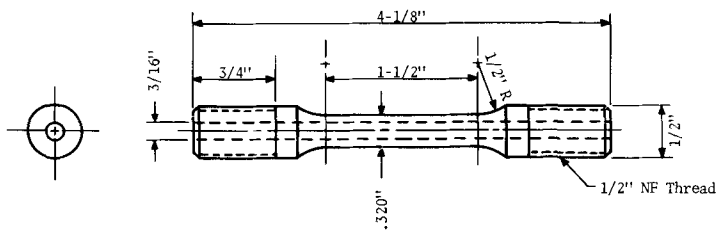


FIG. 1—*Low-cycle fatigue specimen geometry.*

The total strain range in these tests was limited to 0.005 in./in. due to the tendency of the specimen to buckle. The ratio of gage length (1.5 in.) to gage diameter (0.320 in.) was 4.7 where a more desirable ratio is 2.5 or less to avoid buckling. Axial alignment of the grips is critical and was checked periodically.

The specimen was heated using a 3-zone radiant furnace with automatic temperature control which maintained the temperature over the specimen gage length within ±5 F. Four specimens of each material were tested at 900 and 1100 F.

The strain range was controlled by a linear variable differential transducer (LVDT) type extensometer with pointed quartz rods which extended through ports in the furnace to the specimen.

The total cyclic load range on the specimen was recorded continuously by a time-base strip chart recorder. Mechanical hysteresis loops (load versus strain) were recorded on an X-Y recorder at chosen intervals.

Failure in these tests was defined as the point at which the load range decreased by 10 percent of the stabilized load range. This criterion was necessary since several specimens developed cracks on opposite sides of the gage section in a spiral fashion. The material between the cracks then acted as a plastic hinge, and the cracks stopped moving resulting in no failure or an unrealistic life.

Results and Discussion

Tensile Properties

The yield and tensile strengths of the two low-carbon commercial heats are compared to results for standard material in Fig. 2. The yield strengths of the cast-to-low carbon material fall entirely within the band for standard 2¼Cr-1Mo. However, the yield strengths of the decarburized material fall significantly below the standard material band. This loss in strength is even more pronounced when comparing tensile strengths. This difference in strengths may be due to a difference in grain size resulting from decarburization and high-temperature thermal treatments. The grain sizes ranged from ASTM No. 9 for standard material to ASTM No. 5 for decarburized material. There is also an absence of strain aging peaks with the decarburized material, whereas the cast-to-low carbon heat does show a definite peak.

Figure 3 shows tensile strengths for 0.02 percent carbon material given the standard and decarburizing thermal treatments. Very little difference in tensile strength results from the two thermal cycles. This indicates that something besides removal of carbon is occurring during decarburization.

Stress-Rupture Properties

Stress-rupture test results on 2¼Cr-1Mo material show a definite decrease in rupture strength with decreasing carbon content. Figure 4 shows

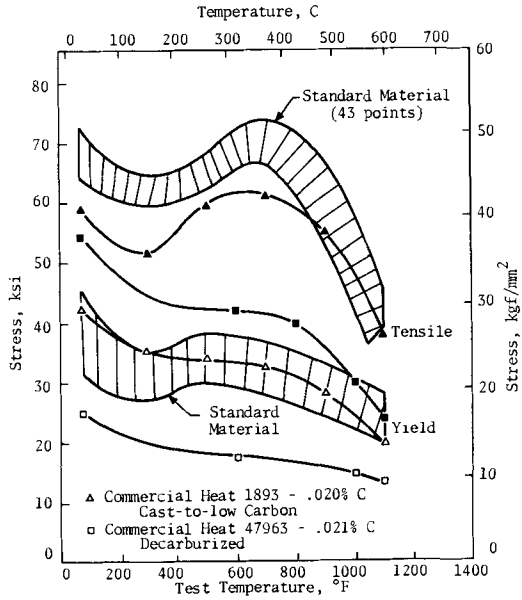


FIG. 2—*Yield and tensile strengths of low-carbon 2¼Cr-1Mo steels.*

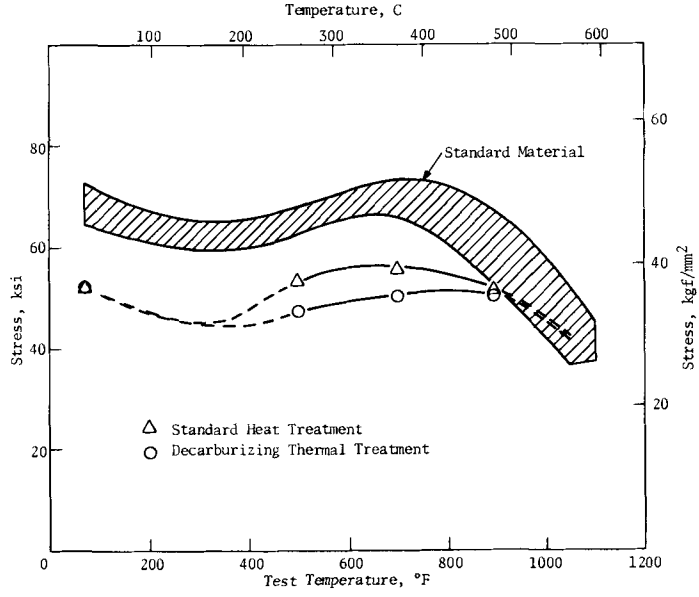


FIG. 3—*Tensile strengths of 2¼Cr-1Mo steel (Heat No. 4158, cast-to-low carbon) after various thermal treatments.*

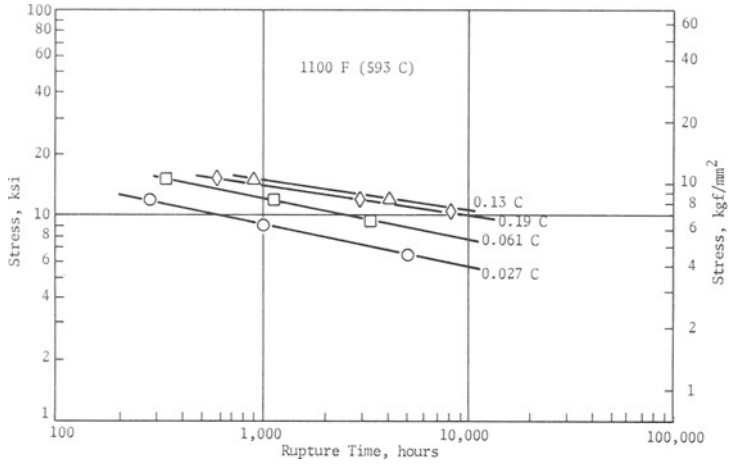


FIG. 4—*Stress-rupture curves for laboratory heats of 2¼Cr-1Mo steels with different carbon contents.*

the results obtained at 1100 F for the four laboratory heats. The stress-rupture properties for the low-carbon heats (0.061 and 0.027 percent carbon) are definitely lower than those for the higher-carbon heats. At higher-carbon contents the results are probably insensitive to the actual amount of carbon. The reversal in results between the heats with 0.13 and 0.19 percent carbon may be due to experimental error.

Larson-Miller curves, shown in Fig. 5, are used to compare properties of the three low-carbon heats with the standard material. A curve for plain-

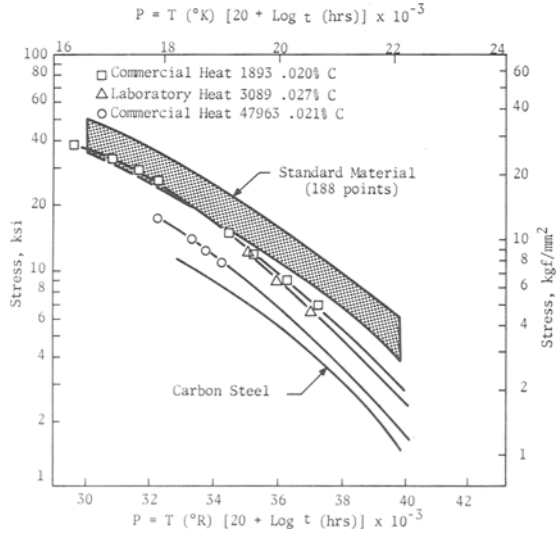


FIG. 5—*Larson-Miller master curves for 2¼Cr-1Mo steels.*

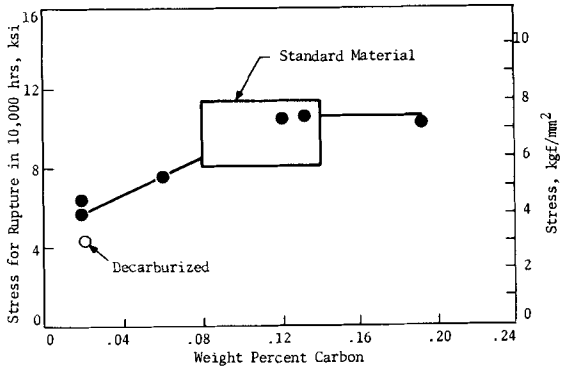


FIG. 6—*Effect of carbon content on the rupture strength of 2¼Cr-1Mo steel at 1100 F (593 C).*

carbon steel has been included for comparison. It appears that the decarburized heat has significantly lower stress-rupture resistance than either of the cast-to-low carbon heats.

Figure 6 shows the relationship between 10,000-h rupture strength and carbon content. Rupture strength definitely is influenced by carbon contents

TABLE 2—*Low cycle fatigue data for 2¼Cr-1Mo steel.*

Material	Test Temperature, deg F	Specimen Number	Cycles to Failure[a]	Indication of Cracking[b]
Standard.....	900	1	3484	3460
		3	2736	
		4	2960	3090
		5	3226	3216
			Avg 3102	
	1100	6	3150	3136
		7	4648	4568
		8	4295	
		9	3115	3078
			Avg 3802	
Decarburized...	900	D-2-4	1680	1650
		D-2-5	2160	2175
		D-2-6	1869	1905
		D-2-7	2137	
			Avg 1964	
	1100	D-3-1	1961	
		D-3-4	1340	1362
		D-3-5	2221	2211
		D-3-6	2061	2073
			Avg 1897	

[a] Failure taken as 10 percent decrease in maximum load range.
[b] By examination of hysteresis loops.

less than 0.08 percent. Statistical analysis of the variation in rupture strength with chemical composition of the experimental heats indicated a high correlation with carbon content only.

Low-Cycle Fatigue Properties

The results of the fatigue tests are shown in Table 2. The standard 2¼Cr-1Mo material exhibited a significantly longer fatigue life than the low-carbon material at both 900 and 1100 F. The low-carbon material exhibited little difference in life for the two test temperatures. The standard material showed a slight increase in life at 1100 F.

Both the standard and low-carbon material cyclic harden at 900 and 1100 F, as shown by Figs. 7 and 8 where the total cyclic load range is shown for the first 15 cycles of testing. Figure 9 illustrates this effect on the hysteresis loops for a typical test.

We have defined failure of the specimen as the point at which the load range decreases by 10 percent. This point is easily detectable on the load-time record, and the decrease in load range can be generally regarded as evidence of specimen cracking. The effect of cracking on the hysteresis loop is to produce an inflection point in the compression end of the loop as

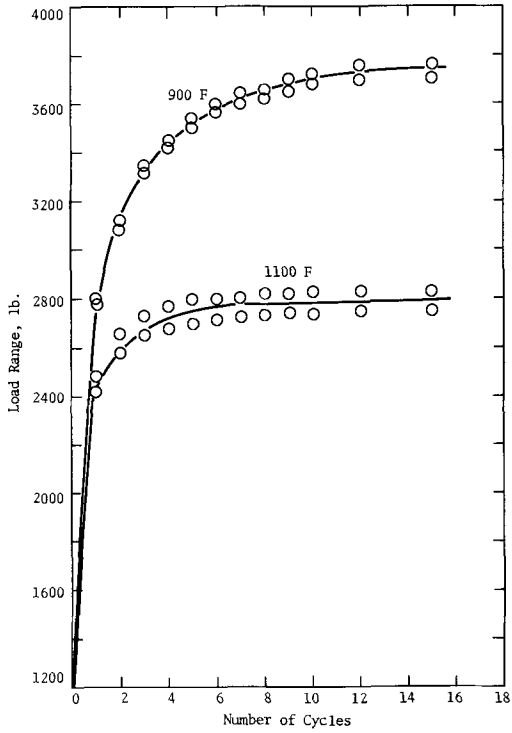


FIG. 7—*Load-range curves for standard 2¼Cr-1Mo steel.*

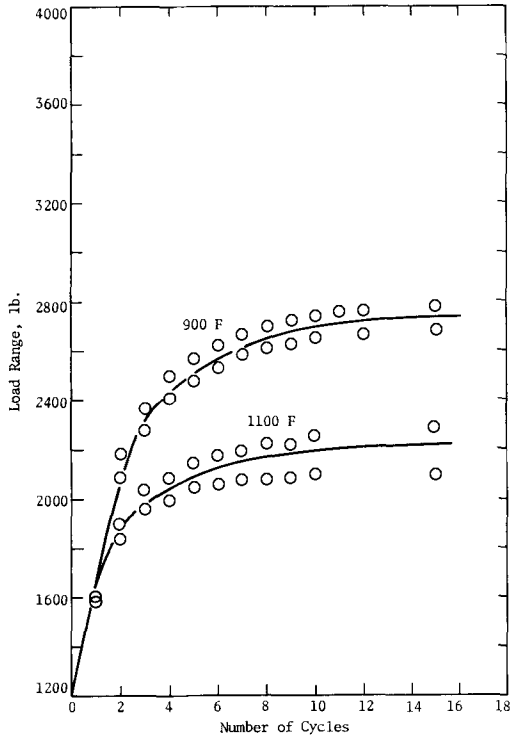


FIG. 8—*Load-range curves for low-carbon 2¼Cr-1Mo steel.*

shown in Fig. 10. Table 2 shows the number of cycles at which the shape change of the hysteresis loop was first detectable. This number agrees very well with the number of cycles to failure (as defined previously).

Figure 11 illustrates the microstructure of standard and low-carbon fatigue specimens after testing. The grain size of the standard material is about ASTM 8 and that of the low-carbon material is about ASTM 5.

Conclusions

Several conclusions can be drawn from this work:

1. The tensile strength of 2¼Cr-1Mo steel between 75 and 1100 F decreases as the carbon content is reduced, either by casting to low carbon or by decarburizing.

2. The tensile strength of 2¼Cr-1Mo steel appears to be lower for decarburized material than cast-to-low carbon material.

3. The lower strength of decarburized chromium-molybdenum material compared to material cast to the same carbon level is not due to the

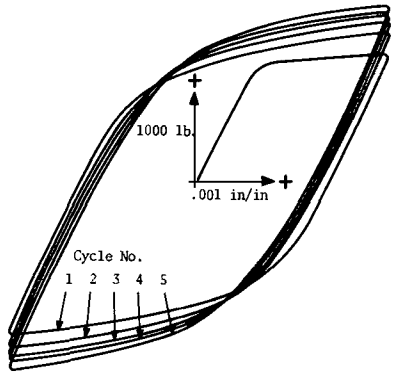


FIG. 9—*Typical hysteresis loops for standard 2¼Cr-1Mo steel (900 F, $\Delta\epsilon_t$ = 0.005 in./in.) showing cyclic hardening.*

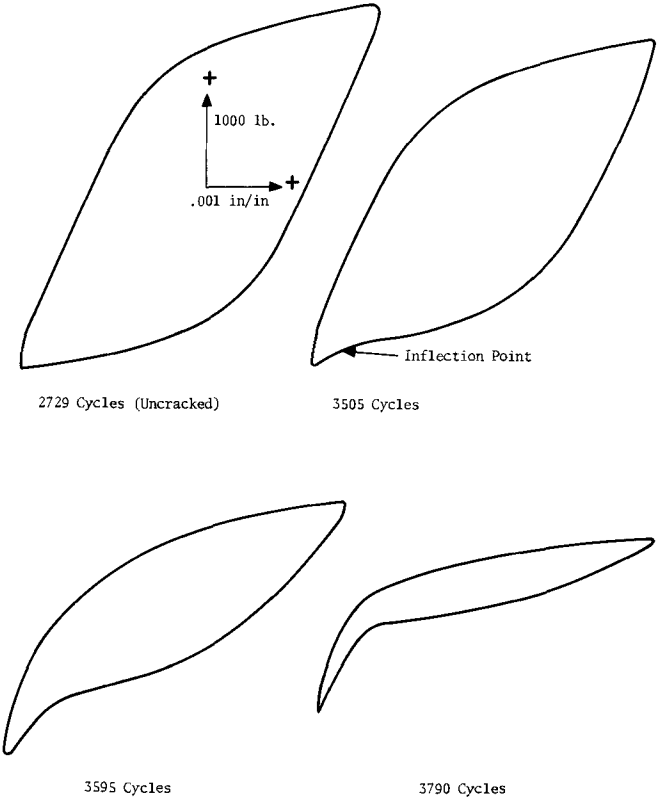
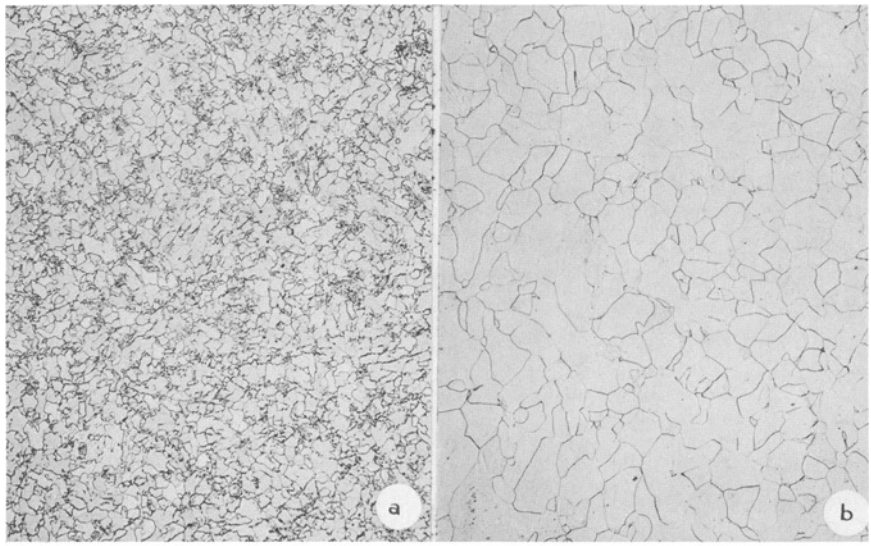


FIG. 10—*Typical hysteresis loops for standard 2¼Cr-1Mo steel (900 F, $\Delta\epsilon_t$ = 0.005 in./in.) showing crack indications.*



(*a*) Standard material (ASTM 8). (*b*) Low carbon material (ASTM 5).

FIG. 11—*Microstructures* (×*100*) *of standard amd low-carbon* $2^1/_4$*Cr-1Mo steel fatigue specimens.*

different thermal cycles. Something other than removal of carbon seems to be occurring during decarburization in water-saturated hydrogen.

4. Low-carbon contents significantly reduce resistance of $2^1/_4$Cr-1Mo steel to high-temperature strain cycling fatigue.

5. Both standard and low-carbon $2^1/_4$Cr-1Mo steels exhibit cyclic hardening at 900 and 1100 F.

DISCUSSION

M. C. Murphy[1] (*written discussion*)—From the results presented, showing laboratory decarburization to eliminate the tensile strain aging peak as well as to reduce high temperature strength, it seems possible that differences in nitrogen content could be a cause. I, therefore, have two questions:

1. Have the authors any details of the nitrogen contents of their specimens?

[1] C. A. Parsons and Company, Heaton Works, Newcastle upon Tyne, England.

2. Does decarburization in the laboratory wet hydrogen system truly represent decarburization in the practical liquid sodium system it is intended to simulate, particularly with regard to nitrogen content?

R. R. Seeley and R. H. Zeisloft (author's closure)—From the full paper:

Cast-to-low carbon	Ht—3089	C	0.027%
		N	0.0031%
	Ht—1893	C	0.020%
		N	0.0047%
Decarburized Ht—47963	Original	C	0.12%
	Decarbed	C	0.021%
	Original	N	0.010%
	Decarbed	N	0.0081%

Decarburization intended to remove carbon and the loss of the strain aging peak came as a surprise since the cast-to-low carbon exhibited such a peak.

Since nitrogen content in decarbed steel was higher, for equivalent nitrogen contents the strength of decarbed steel may even be lower than cast-to-low carbon steel.

(2) The decarburization treatment was not, as we understand, intended to simulate decarburization in liquid sodium. As we stated in the paper, "the method of decarburization is not important since the rate is controlled by diffusion within the metal." Of course the effect of decarburization atmosphere wet hydrogen versus liquid sodium may result in different conditions of the metal surface, but that was not within the scope of our work.

D. B. Scott[2] *(written discussion)*—The authors are to be complimented on their extensive work on the effect of carbon content on high-temperature properties of 2¼Cr-1Mo steels. One point, however, on heat treatment is of concern. The decarburized steel was subjected to an 1800 F normalizing treatment after decarburization; the standard steel was not subjected to a normalizing treatment after a simulated decarburization. Although it is conceded that low carbon is responsible for the serious degradation of the mechanical properties of the steel, would the difference be as great if both had the same heat treatment, hence same grain size?

Messrs. Seeley and Zeisloft—The decarburized steel was given the 1800 F treatment to get the material above the upper critical temperatures which is higher at lower carbon contents. The 1650 F treatment got the standard

[2] Windsor, Conn. 06095.

material (0.12 percent carbon) above the upper critical but unfortunately may not have gotten the cast-to-low carbon (0.02 percent carbon) into the austenite range above the upper critical. Hence, a possible source of grain size difference. Grain size was not taken into account in this work, and, therefore, the true effect of low-carbon contents may have been masked. The problem of the effects of low-carbon levels on the mechanical properties of chromium-molybdenum steel should be probably studied at a uniform grain size. However, in the practical sense, some grain growth may occur at 1050 F over long periods of time, especially if carbon content is reduced.

R. W. Weeks[3] (*written discussion*)—(*a*) You have simulated the mass-transfer effects of the environment, but, in the case of fatigue, the dynamic effects may also be important. Do you plan any tests in flowing sodium? (*b*) To what depth do you expect decarburization over 210 000 at 1050 F?

Messrs. Seeley and Zeisloft—(*a*) Not in the foreseeable future. (*b*) We do not know at the moment.

[3] Argonne National Laboratory, Argonne, Ill. 60439.

H. I. McHenry[1] *and A. W. Pense*[2]

Fatigue Crack Propagation in Steel Alloys at Elevated Temperatures

REFERENCE: McHenry, H. I. and Pense, A. W., "**Fatigue Crack Propagation in Steel Alloys at Elevated Temperatures,**" *Fatigue at Elevated Temperatures, ASTM ATP 520*, American Society for Testing and Materials, 1973, pp. 345–354.

ABSTRACT: The fatigue crack propagation characteristics of three steel alloys were evaluated at room and elevated temperatures in an air environment. The alloys and temperature ranges were: A212-B (σ_{YS} = 40 ksi) 75 to 800 F, A517-F (σ_{YS} = 104 ksi) 75 to 950 F, and 9Ni-4Co-0.30C (σ_{YS} = 185 ksi) 75 to 650 F. The compact tension specimen was used for the 9Ni-4Co-0.30C and A517-F tests. A modified compact tension specimen having deep face notches in the crack plane was used for the A212-B tests. Fracture mechanics parameters were used to evaluate the crack propagation data. When plotted as a function of the stress intensity range, ΔK, the crack growth rates increased with temperature in A517-F and A212-B; temperature did not influence the 9Ni-4Co-0.30C data. Tests at reduced cyclic frequencies were conducted on A517-F and 9Ni-4Co-0.30C steel. The crack growth rates increased as the frequency was reduced in A517-F at 500 and 950 F. In 9Ni-4Co-0.30C the growth rates at 500 and 650 F were essentially the same for cyclic frequencies of 10 and 0.002 Hz over the range of growth rates investigated.

KEY WORDS: fatigue (materials), crack propagation, alloy steels, yield strength, creep properties, plastic deformation

In recent years there have been several studies of fatigue crack growth at elevated temperatures. Growth rates generally increase with test temperatures. Clark and Trout [*1*],[3] who tested A569-4 steel at reduced temperatures (−100 F to 75 F) attributed the changes in growth rates observed to the effect of test temperature on the yield strength. Decreasing the yield strength by raising the temperature increases cyclic plasticity and consequently increases the fatigue crack growth rate. A similar conclusion was reached in subsequent work by Clark [*2*] on A533-B steel at temperatures to 550 F. Growth rate increases at elevated temperatures have also been reported by Popp and Coles [*3*] (nickel-base alloy 718), James [*4*] (304 stainless steel), Brothers [*5*] (A212-B and A387-D steels), Harrison and Sandor [*6*] (Cr-Mo-V rotor steel), and Wei [*7*] (7075-T651 aluminum alloy).

[1] Project structures engineer, Convair Aerospace Division, General Dynamics, Fort Fort Worth, Tex. 76101.

[2] Professor of metallurgy and materials science, Lehigh University, Bethlehem, Pa. 18015.

[3] The italic numbers in brackets refer to the list of references appended to this paper.

Copyright© 1973 by ASTM International www.astm.org

In the present paper, the results of an investigation of fatigue crack propagation in steel alloys at elevated temperatures are reported.

Materials

Three steel alloys having a wide range of compositions and yield strengths were evaluated:

Designation	Description	Heat Treatment	Nominal Yield Strength, ksi
A212-B[a]	plain carbon	mill N/T[c]	40
A517-F[a]	low alloy	mill Q/T[d]	100
9Ni-4Co-0.30C[b] ..	high alloy	lab Q/T[d]	190

[a] ASTM designation.
[b] Republic Steel proprietary grade.
[c] N/T = normalized and stress relieved.
[d] Q/T = quenched and tempered.

These grades are representative of steels used in a broad range of industrial applications.

The primary material for this investigation was A517-F. The other grades were tested to help distinguish the behavior common to many steels from that of a particular grade. One-inch-thick hot-rolled plates of each material were evaluated in the WR orientation. (NOTE—WR means that crack extension is in the rolling direction and the crack plane is perpendicular to the width dimension of the plate.)

9Ni-4Co-0.30C steel was received in the mill-annealed condition, machined into test specimens, and subsequently heat treated in a protective atmosphere. The heating treating sequence was as follows:

1. Normalize	1650 F ± 25 F	1 h, air cool
2. Austenitize	1550 F ± 25 F	1 h, oil quench
3. Double temper	1025 F ± 10 F	2 h/cycle, air cool

A517-F and A212-B were heat treated by the producer in accordance with the ASTM specifications. The microstructures resulting from these treatments are tempered martensite for 9Ni-4Co-0.30C and A517-F and a ferrite-pearlite aggregate for A212-B.

Test Procedures

A compact tension specimen, Fig. 1, similar to the 1-in.-thick version described by Wessel [*8*], was used for the A517-F and 9Ni-4Co-0.30C tests. Two concentric holes for attachment of a displacement gage extension were located beyond the load line.

TABLE 1—*Chemical compositions of the test materials.*

Steel	C	Mn	P	S	Si	Ni	Cr	Mo	V	Co	Cu
9Ni-4Co-0.30C											
Nominal											
(Min)	0.29	0.15				7.25	0.90	0.90	0.08	4.25	
(Max)	0.34	0.35	0.010	0.010	0.10	7.75	1.10	1.10	0.14	4.75	
Actual	0.29	0.20	0.007	0.008	0.01	7.70	0.96	1.00	0.07	4.55	
A517-F											
Nominal											
(Min)	0.08	0.55			0.13	0.67	0.36	0.36	0.02		0.12
(Max)	0.22	1.05	0.035	0.040	0.37	1.03	0.79	0.64	0.09		0.53
Actual	0.16	0.84	0.013	0.015	0.20	0.92	0.61	0.42	0.037		0.27
A212-B											
Nominal											
(Min)		0.85			0.13						
(Max)	0.31	1.20	0.035	0.040	0.33						
Actual	0.25	0.73	0.015	0.032	0.22						

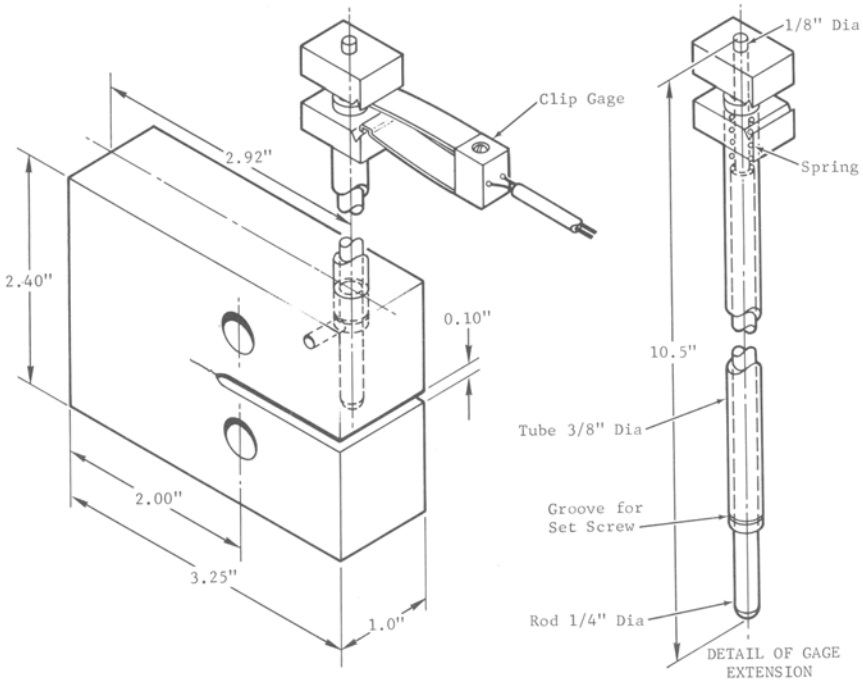


FIG. 1—*Compact tension specimen and displacement gage.*

In A212-B steel, fatigue crack growth rates of practical interest occur under conditions of general yielding. Consequently, the compact tension specimen used for the higher strength steels is not directly applicable. A plastic strip specimen was used for the A212-B tests. The specimen, Fig. 2, is basically a lengthened and side-grooved version of the compact tension specimen. The design and calibration of the plastic strip specimen is discussed in Ref 9.

Fatigue testing was conducted in a 20 000-lb capacity electrohydraulic fatigue machine using a sinusoidal loading cycle at cyclic frequency of 10, 0.1, and 0.01 Hz. Rectangular wave tests at 0.002 Hz were conducted in a 20 000 lb capacity, screw-drive test machine equipped with atuomatic timing controls. Load was maintained at the maximum level for 400 s and at the minimum level for 30 s. Loading and unloading took 25 s each. All tests were conducted in an air environment at a load ratio of $R = 0.1$ ($R = P_{min}/P_{max}$).

The specimens were precracked at room temperature using a maximum load that was less than or equal to the maximum load used in the fatigue tests. The precracked specimens were installed in the test machine (and furnace), the displacement gage extension was attached to the specimen, and the specimen was heated to the test temperature and soaked for 30 min.

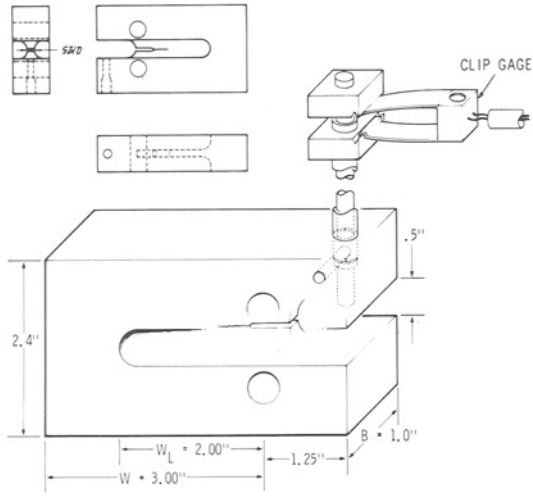


FIG. 2—*Plastic strip specimen.*

During fatigue testing, crack lengths were measured at estimated growth intervals of 0.03 in. using the compliance calibration techniques discussed in Ref *10*. The recorded data were the number of cycles N and the compliance. Crack lengths were determined from the compliance calibration. Stress intensity ranges, ΔK, were determined from the K calibration. Crack growth rates, da/dN, were calculated by the central difference method. The results were presented in log-log plots of da/dN versus ΔK.

Results and Discussion

A517-F Tests

The fatigue crack propagation characteristics of A517-F were determined at room temperature, 500, 800, and 950 F. The test results are presented in Fig. 3. For each condition, the line drawn through the data points has the form:

$$da/dN = \alpha \times 1.9 \times 10^{-21} (\Delta K)^{3.4} \quad \ldots\ldots\ldots\ldots\ldots (1)$$

where α is the temperature compensation factor and the units are in pounds and inches. The α values obtained are 1.0 at room temperature, 1.6 at 500 F, 2.9 at 800 F, and 3.3 at 950 F; that is, da/dN at a given ΔK is 3.3 times faster at 950 F than at room temperature.

The fatigue behavior at 950 F was of special interest because substantial creep occurs in A517-F at this temperature. Three specimens were tested at 950 F. Growth rates were measured over three orders of magnitude. As shown in Fig. 3, data for growth rates between 2×10^{-6} and 4×10^{-4} in./cycle fell on the line defined by Eq 1. Beyond these limits, accelerated growth

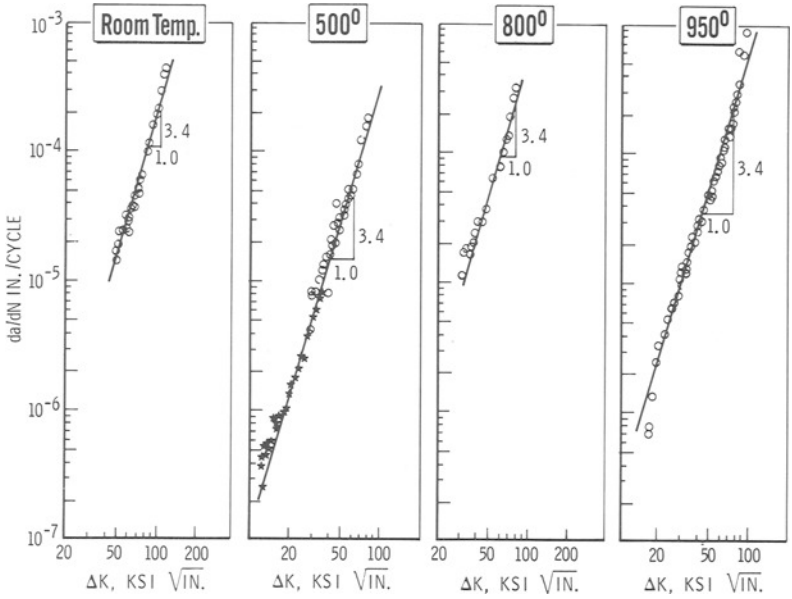


FIG. 3—*Fatigue crack growth behavior of A517-F steel.*

rates occurred at high ΔK levels, and reduced growth rates occurred at low ΔK levels. Similar nonlinear behavior at low- and high-growth rates has been observed by other investigators [*11*,*12*]. The excellent fit of the three sets of data suggests that the fracture mechanics approach to fatigue crack growth studies is valid at temperatures in the creep range.

Tests at 950 F were conducted at 0.002, 0.01, and 0.1 Hz in addition to the 10-Hz tests discussed perviously. As shown in Fig. 4, the fatigue crack propagation rate was substantially increased as the cycle rate was decreased in the 950 F tests. An increase in plasticity was apparent in the load deflection curves used for crack length measurements. This observation suggested that creep was causing additional plastic damage during each fatigue cycle; consequently, the growth rate was increased. Further justification for this explanation is given in Ref *13*.

A low-cycle rate test was conducted in A517-F at 500 F using the rectangular wave at 0.002 Hz. The results are presented in Fig. 4. A substantial increase in growth rates was observed. A possible cause of the increased growth rates is strain age embrittlement as observed by Hartbower and Gerberich [*14*].

9Ni-4Co-0.30C

The fatigue crack propagation characteristics of 9Ni-4Co-0.30C were determined at room temperature, 500 F, and 650 F. The results are presented in Fig. 5.

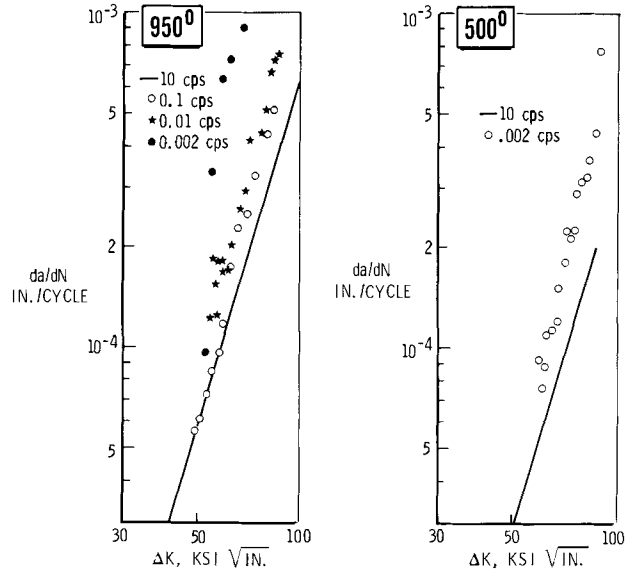


FIG. 4—*Low cycle rate fatigue crack growth behavior of A517-F steel.*

Two specimens were tested at each temperature. In one specimen growth rates were less than 1×10^{-5} in./cycle, and in the other growth rates were greater than 1×10^{-5} in./cycle. According to the Paris equation [*15*] both sets of data should have fallen on a single line having a slope n. In fact, a slope transition occurred at a growth rate of approximately 1×10^{-5} in./cycle. At the specified growth rates, the line drawn through the data points at each temperature has the form:

$$da/dN = 1.2 \times 10^{-15} (\Delta K)^{2.2}, \; da/dN < 10^{-5} \text{ in./cycle} \quad (2)$$

$$da/dN = 4.5 \times 10^{-20} (\Delta K)^{3.2}, \; da/dN > 10^{-5} \text{ in./cycle} \quad (3)$$

All of the data fall within the scatterband defined by Barsom [*11*] for high-strength steels.

The influence of cyclic frequency on growth rates was investigated by conducting 0.002-Hz-rectangular wave fatigue tests at 500 and 615 F. The data are presented with the corresponding 10 Hz data in Fig. 5. In both cases, no change in growth rate was observed.

A212-B Tests

The fatigue crack propagation characteristics of A212-B were determined at room temperature, 500, 650, and 800 F using a 10-Hz sine wave load profile. In each test a maximum load of 4000 lb was applied at a load ratio of $R = 0.1$. The results are presented in Fig. 6. Unlike the A517-F

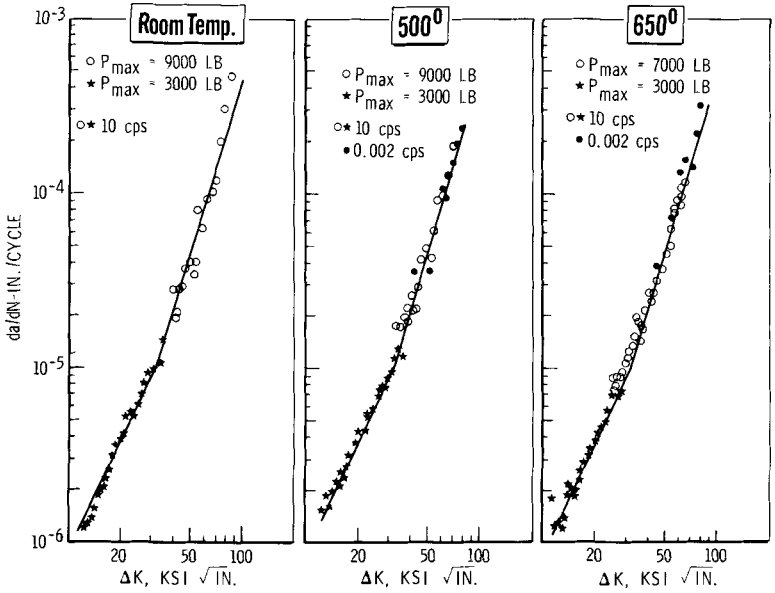


FIG. 5—*Fatigue crack growth behavior of 9Ni-4Co-0.30C steel.*

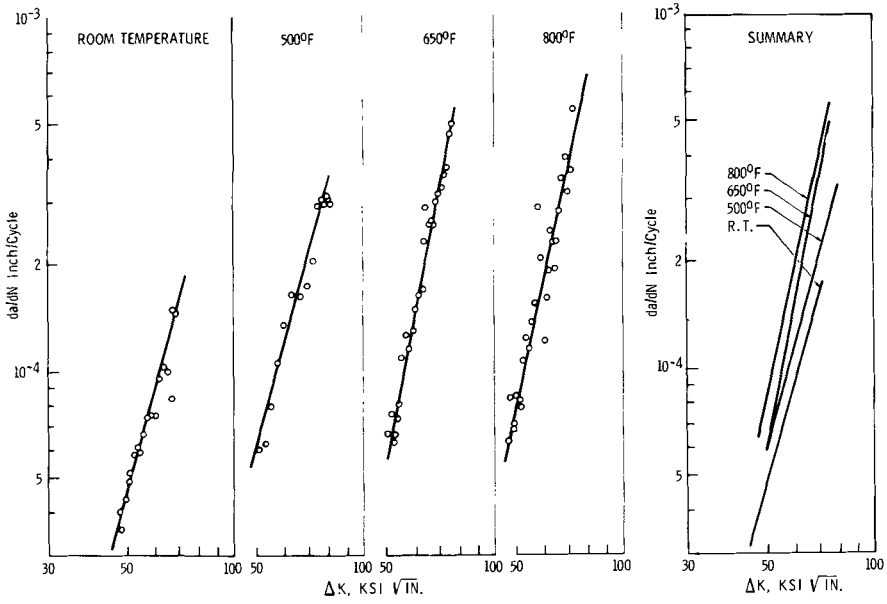


FIG. 6—*Fatigue crack growth behavior of A212-B steel.*

and 9Ni-4Co-0.30C results, the data for each temperature must be described by a different equation:

$$\text{room temperature: } da/dN = 5.7 \times 10^{-22} (\Delta K)^{3.6} \quad (4)$$

$$\text{500 F: } da/dN = 7.4 \times 10^{-22} (\Delta K)^{3.6} \quad (5)$$

$$\text{650 F: } da/dN = 9.1 \times 10^{-28} (\Delta K)^{5.0} \quad (6)$$

$$\text{800 F: } da/dN = 5.9 \times 10^{-26} (\Delta K)^{4.5} \quad (7)$$

Brothers [5] evaluated A212-B steel at room temperature, 485, 600, and 650 F. Tests were conducted at several cyclic frequencies at 600 and 650 F; the slowest cycle rate was a rectangular load profile with a 12-min holdtime at maximum load. Cyclic frequency did not influence the crack growth rates. A tenfold increase in growth rates at $\Delta K = 60$ ksi $\sqrt{\text{in.}}$ was caused by increasing the temperature from ambient to 650 F. In this investigation, the corresponding growth rates increased by less than a factor of two over the same temperature range. The reasons for the differing results are not understood completely. The principal difference in the test methods was specimen design. Brothers used a center-notch tension specimen. Stress levels were sufficient to cause general yielding. Thus, the fracture mechanics approach may not have been appropriate; that is, the stress conditions used in the comparison of growth rate data may not have been similar.

Conclusions

1. For 9Ni-4Co-0.30C steel, the temperature (room temperature, 500, and 650 F) and cycle rates (0.002 and 10 Hz) investigated had a relatively small influence on the fatigue crack growth characteristics.
2. The A517-F and A212-B steels both exhibited increased crack growth rates at elevated temperatures.
3. The fatigue crack growth rates for A517-F at 500 and 950 F increased when the cyclic frequency was decreased.

References

[1] Clark, W. G., Jr., and Trout, H. E., Jr., *Engineering Fracture Mechanics*, Vol. 2, No. 2, 1970, pp. 107–124.
[2] Clark, W. G., Jr., *Journal of Materials*, Vol. 6, 1971, pp. 134–149.
[3] Popp, H. G. and Coles, A., *Proceedings*, Air Force Conference on Fatigue and Fracture of Aircraft Structures and Materials, AFFDL TR 70–144, 1970, pp. 71–86.
[4] James, L. A. and Schwenk, E. B., Jr., *Metallurgical Transactions*, Vol. 2, 1971, pp. 491–496.
[5] Brothers, A. J., "Fatigue Crack Growth in Nuclear Reactor Piping Steels," Report GEAP-5607, General Electric Co., San Jose, Calif., 1968.
[6] Harrison, C. B. and Sandor, G. N., *Engineering Fracture Mechanics*, Vol. 3, 1971, pp. 403–420.
[7] Wei, R. P., *International Journal of Fracture Mechanics*, Vol. 4, 1968, pp. 156–168.

[8] Wessel, E. T., *Engineering Fracture Mechanics*, Vol. 1, No. 1, 1968, pp. 77–103.
[9] McHenry, H. I. and Irwin, G. R., *Journal of Materials*, Vol. 7, No. 4, 1972.
[10] McHenry, H. I., *Journal of Materials*, Vol. 6, No. 4, 1971, pp. 862–873.
[11] Barson, J. M., Imhof, E. J., Jr., and Rolfe, S. T., *Engineering Fracture Mechanics*, Vol. 2, No. 4, 1971, pp. 301–318.
[12] Clark, W. G., Westinghouse Electric Co., Pittsburgh, Pa., private communication to P. C. Paris, 1969.
[13] McHenry, H. I. and Pense, A. W., "The Influence of Temperature on Fatigue Crack Propagation in A517-F Steel," *Metallurgical Transactions*, submitted for publication.
[14] Gerberich, W. W., Hartbower, C. E., and Crimmins, P. P., *Welding Journal*, Vol. 47, No. 10, Research Supplement, 1968, p. 433S.
[15] Paris, P. C., *Fatigue—An Interdisciplinary Approach*, Syracuse University Press, Syracuse, N. Y., 1964, pp. 107–127.

C. F. Cheng,[1] *C. Y. Cheng,*[1] *D. R. Diercks,*[1] *and R. W. Weeks*[1]

Low-Cycle Fatigue Behavior of Types 304 and 316 Stainless Steel at LMFBR Operating Temperature*

REFERENCE: Cheng, C. F., Cheng, C. Y., Diercks, D. R., and Weeks, R. W., **"Low-Cycle Fatigue Behavior of Types 304 and 316 Stainless Steel at LMFBR Operating Temperature,"** *Fatigue at Elevated Temperatures, ASTM STP 520,* American Society for Testing and Materials, 1973, pp. 355–364.

ABSTRACT: Fully reversed, axial strain-controlled low-cycle fatigue tests with and without tension holdtime have been conducted in air in the temperature range of 806 to 1202 F and at a strain rate of 4×10^{-3} s^{-1} on Types 304 and 316 stainless steel after various initial heat treatments. The test results have been supplemented by metallographic and scanning electron microscopy investigations. Prior heat treatment has a greater effect on specimens tested at 1050 F than on those tested at 1202 F and a greater effect on Type 304 than on Type 316. The introduction of tension holdtimes decreases the cyclic life of both materials and causes the mode of failure to change from transgranular to intergranular. Much of the above fatigue behavior can be qualitatively understood on the basis of the supplemental metallographic results.

KEY WORDS: fatigue (materials) stainless steels, fatigue tests, tests, scanning electron microscopy, metallography

A low-cycle, high-temperature, creep-fatigue testing program on Types 304 and 316 austenitic stainless steel is being conducted at Argonne National Laboratory (ANL). The objectives of the program are: (1) to generate the necessary creep-fatigue data so that component design criteria can be formulated for liquid metal fast breeder reactor (LMFBR) components, and (2) to obtain a more basic understanding of elevated-temperature creep-fatigue damage accumulation in these steels.

In view of the complex precipitation processes that occur in these materials at high temperatures [*1*],[2] a metallurgically stable microstructure is desirable if the real effect of the external variables, such as stress and

*This work was performed under the auspices of the U. S. Atomic Energy Commission.

[1] Associate metallurgical engineer, assistant metallurgist, assistant metallurgist, and associate mechanical engineer, respectively, Materials Science Division, Argonne National Laboratory, Argonne, Ill. 60439.

[2] The italic numbers in brackets refer to the list of references appended to this paper.

Copyright© 1973 by ASTM International www.astm.org

temperature, on mechanical behavior are to be accurately defined. The effects of heat treatment and test temperature on the low-cycle fatigue properties of Types 304 and 316 stainless steel tested at 806 to 1202 F in air are evaluated in the present paper.

Materials and Test Procedure

To date, the hourglass specimens used at ANL were prepared originally for low-cycle fatigue studies at General Electric Nuclear System Programs (GE-NSP) [*2*]. The chemical composition of Types 304 (Heat 55697) and 316 (Heat 65808) stainless steel are given in Ref *3*.

The specimens were prepared from solution-annealed blanks that had been machined from rod stock. The blanks were annealed for 30 min in an argon atmosphere at 1994 F for Type 304 stainless steel, and at 1958 F for Type 316. The blanks were then air cooled at a rate of about 200 F/min. The test specimens were machined to the final configuration from these solution-annealed blanks. The grain structure was equiaxed, had an ASTM grain size of 3-4, and had an average Vicker's hardness number of 150.

Specimens were tested either in the solution annealed condition or after one of the following subsequent heat treatments:

(*a*) *Stress-relieved* (*SR*)—The as-fabricated and finished specimen was held at 1400 F for either 15 min (Type 304) or 30 min (Type 316) in an argon atmosphere.

(*b*) *Stress relieved* (*SR*) *and aged*—The stress-relieved specimen was aged for 160 h at 1200 F in an argon atmosphere.

(*c*) *Solution-annealed* (*ANN*) *and aged*—The as-fabricated and finished specimen was aged for 1000 h at 1050 F in an argon atmosphere.

The stress-relieved heat treatment was originally intended by GE-NSP investigators to remove any residual stresses present on the surface of the as-fabricated specimen. The two aging heat treatments are being used by the present authors in an attempt to attain a thermally stable microstructure prior to testing.

All tests were conducted in three closed-loop hydraulic machines made by MTS Systems Corporation and reinstalled at ANL from previous location at GE-NSP. Each machine uses a 90-deg oriented diametral extensometer, load cell, and an analog strain computer to monitor continuously the diameter change, axial load, and axial strain at the gage section of the specimen [*4*]. All tests were conducted in air in the axially controlled strain mode, fully reversed, and at a fixed strain rate of 4×10^{-3} s^{-1} with or without tension holdtimes. The majority of the tests were performed in the total strain range of 0.5 to 2.0 percent at a temperature of 1050 or 1202 F. A number of fatigued specimens were examined in the optical and scanning electron microscopes.

Results and Discussion

Experimental results plotted in Fig. 1 illustrate the effects of temperature, heat treatment, and tension holdtime on the fatigue life. Pertinent data generated at GE-NSP [2] and Battelle Memorial Institute (BMI) [5] are also included.

Effect of Temperature

The results of stress-relieved Type 304 stainless steel are plotted for three temperatures in Fig. 1*a*. Both the total ($\Delta\epsilon_t$) and plastic ($\Delta\epsilon_p$) strain ranges are plotted versus the number of cycles to failure (N_f). The curves show the expected decrease of fatigue life as the temperature increases and indicate good agreement between ANL and GE-NSP results. The usual linear relationship between ln $\Delta\epsilon_p$ and ln N_f is also observed, although at 1202 F there seems to be some deviation for small strain ranges. On the other hand, little difference exists between the fatigue data at 1050 and 1202 F for Type 316 (Fig. 1*b*). For comparison, the corresponding curves for Type 304 are also included.

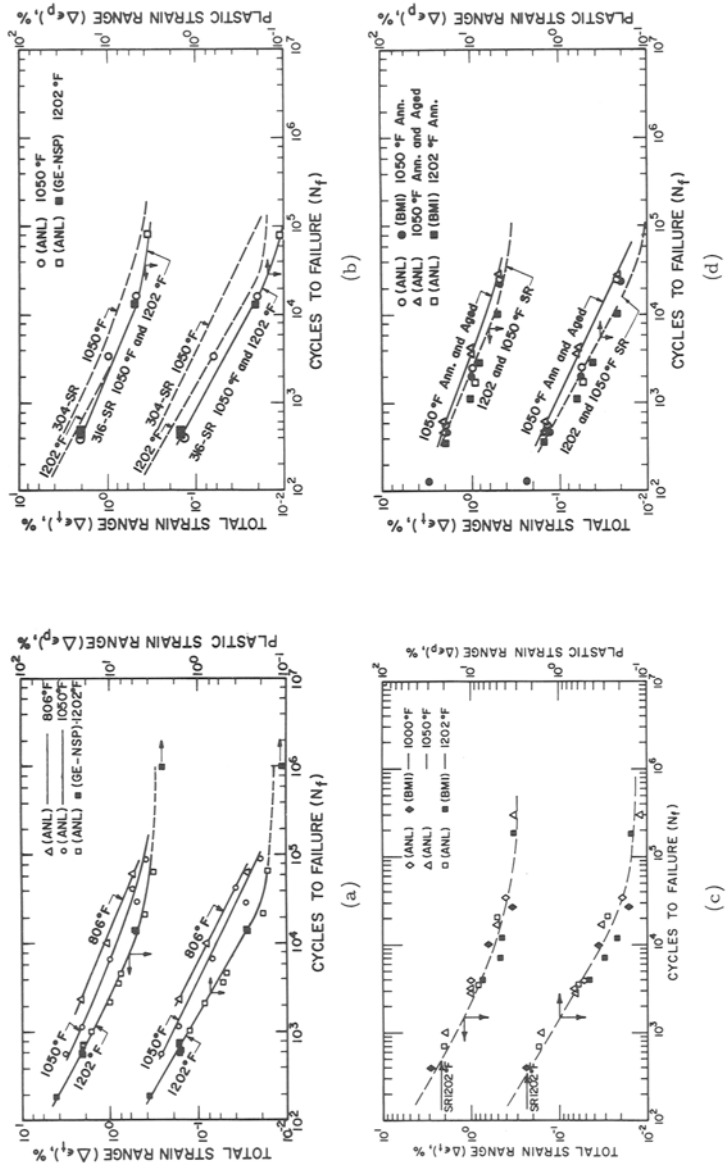
In the solution-annealed condition, the temperature effect is insignificant for both stainless steels. Figure 1*c* shows that the data for solution-annealed Type 304 at 1000, 1050, and 1202 F fall on the dashed curves for the stress-relieved material tested at 1202 F. A similar behavior is indicated for solution-annealed Type 316 tested at 1050 and 1202 F (Fig. 1*d*).

Effect of Heat Treatment

The results for Type 304 stainless steel after various heat treatments and tests at 1202 F are plotted in Fig. 1*e*. Little difference in fatigue life is noted for specimens initially in the solution-annealed (squares), stress-relieved (dashed curves), and stress-relieved and aged (circles) conditions. The same trend is observed at 1050 F (Fig. 1*f*) for both solution-annealed and aged (triangles) and stress-relieved (dashed curves) conditions. On the other hand, the data at 1000 and 1050 F (solid curves) for solution-annealed specimens appear to indicate a poorer fatigue resistance than the solution-annealed and aged or stress-relieved specimens. In the case of Type 316, the solution-annealed and aged specimens tested at 1050 F (solid curves in Fig. 1*d*) show slightly better fatigue lives than the specimens in the solution-annealed (circles) and stress-relieved (dashed curves) conditions.

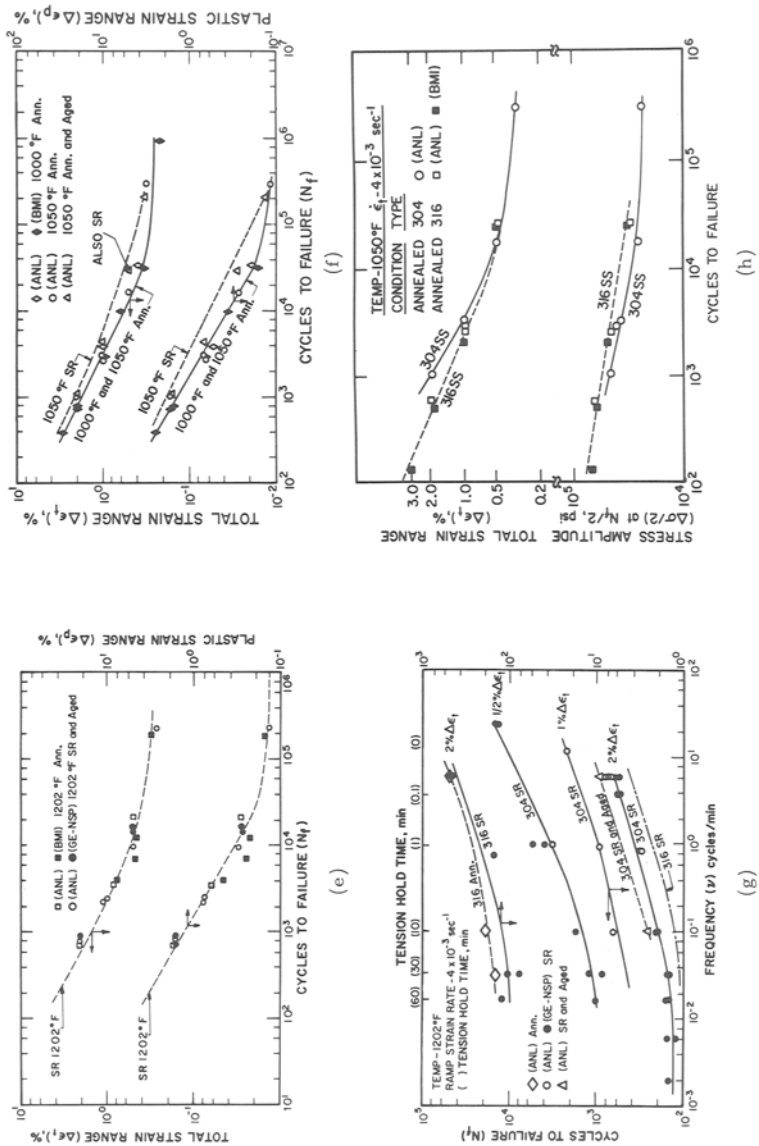
Effect of Tension Holdtime

The introduction of holdtime at peak tension strain into otherwise fully reversed cyclic tests leads to the reduction of the number of cycles to failure, as shown in Fig. 1*g*). The frequency (ν) in these figures is defined as $\nu \equiv [t_H + (1/\nu')]^{-1}$ where t_H is the tension holdtime and ν' is the ramp frequency ($\dot{\epsilon}_r = 2\nu'\Delta\epsilon_t$). In general, the cycles to failure decrease as the holdtime in-



(*a*) Effect of temperature on stress-relieved Type 304 stainless steel.
(*b*) Effect of temperature on stress-relieved Type 316 stainless steel. Type 304 curves (*dashed*) shown for comparison.
(*c*) Effect of temperature on solution-annealed Type 304 stainless steel.
(*d*) Effect of temperature and heat treatment on Type 316 stainless steel at 1050 and 1202 F.

FIG. 1—*Experimental results.*



(*e*) Effect of heat treatment on Type 304 stainless steel at 1202 F.
(*f*) Effect of heat treatment on Type 304 stainless steel at 1050 F.
(*g*) Effect of tension holdtime on Types 304 and 316 stainless steel at 1202 F.
(*h*) Fatigue life of stress-relieved Types 304 and 316 stainless steel at 1202 F.

FIG. 1—*Continued.*

creases, and a saturation effect is indicated (at least for holdtimes greater than about 60 min) in tests at 1202 F for Types 304 and 316 stainless steel in the stress-relieved condition. The data at 1050 F (not shown) are rather sparse and show no indication of a saturation effect even for holdtimes up to 600 min.

As discussed in the preceding section, the effect of heat treatment on fatigue life in the fully reversed tests without holdtime tends to be obscured by the experimental scatter, as shown in Figs. 1*d* to *f*. However, this effect is more evident in tests that involve tension holdtime (Fig. 1*g*). Again, data are sparse, but they seem to indicate that stress-relieved Type 316 is inferior to the solution-annealed steel, and stress-relieved and aged Type 304 is superior to stress-relieved Type 304 at 1202 F and 2 percent $\Delta\epsilon_t$ (Fig. 1*g*). Similarly the solution-annealed and aged Type 316 was found superior to the solution-annealed or stress-relieved condition at 1050 F and 1 percent $\Delta\epsilon_t$ (not shown).

Comparison Between Types 304 and 316 Stainless Steel

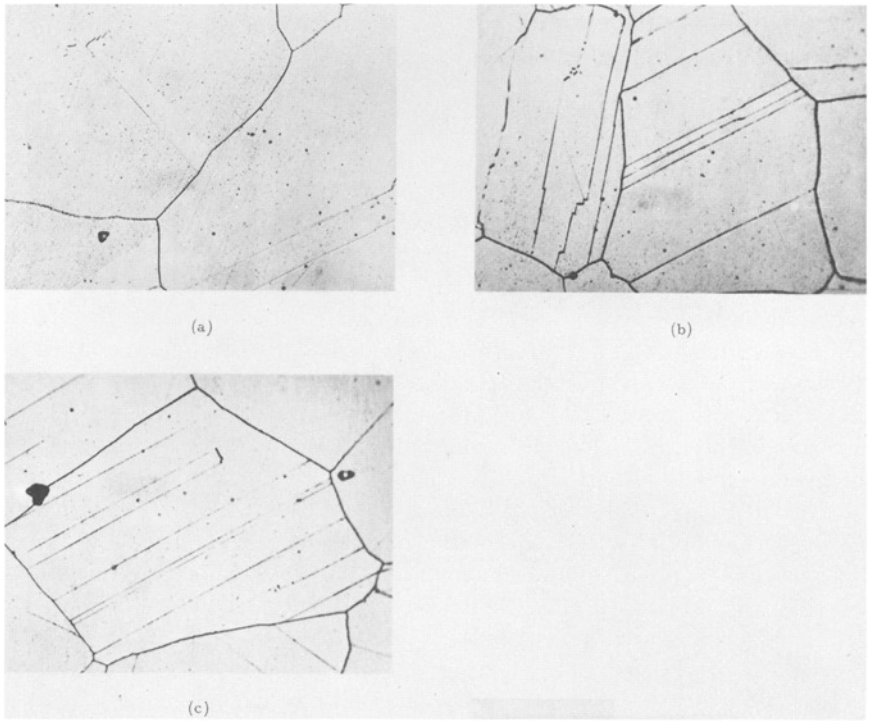
The above results indicate that for the same heat-treatment condition and test temperature, Type 316 stainless steel has a shorter fatigue life than Type 304 at the same total strain range ($\Delta\epsilon_t$) (Figs. 1*b* and *g*). This effect decreases as the total strain range decreases (Fig. 1*h*). Inasmuch as the difference in the modulus of elasticity (E) between the two stainless steels in the temperature range of 1050 to 1202 F is approximately 1 percent, the above observation of fatigue life should also hold in terms of pseudostress ($\sigma_a = E\Delta\epsilon_t/2$), which is frequently used by designers to allow simple elastic analysis at high temperatures. However, if the comparison is based on the *actual* stress, such as the saturation stress at $N_f/2$ shown in Fig. 1*h*, Type 316 is then superior to Type 304. The reason for this reversal is that, for the same actual stress, the corresponding strain range will be smaller for Type 316 than for Type 304. This is due to the higher yield strength of Type 316. Thus in a given design situation, the relative fatigue life of Type 304 versus Type 316 will depend on whether the expected loading is stress or strain controlled.

Microstructural Observations

As noted, Types 304 and 316 stainless steel aged in the approximate temperature range of 900 to 1800 F are subject to a number of precipitation reactions [*1,6*]. In the present study, we shall be concerned with the $M_{23}C_6$ carbides. These carbides precipitate first on grain boundaries (assuming no delta ferrite is present), then, with increasing time, on incoherent twin boundaries, coherent twin boundaries, and finally homogeneously within the matrix. In general, the precipitation reactions in both materials are accelerated significantly by cold work. It has been shown [*7*] that the presence of $M_{23}C_6$ carbides in an 18Cr-12Ni austenitic stainless steel significantly increases fatigue life at 1290 and 1470 F and can affect the mode of fracture.

An examination of the optical microstructure near the fracture surface of test specimens is one approach that is used to understand the effects of prior heat treatment and test conditions on fatigue life. One may consider the specific case of fatigue data obtained for Type 304 stainless steel at 1050 F with $\Delta\epsilon_t = 0.5$ percent (data points plotted in Fig. 1*f*). The specimen initially in the solution-annealed condition failed after 17 273 cycles (12.0 h). The specimen initially in the solution-annealed and aged condition failed after 29 112 cycles (20.2 h), and the specimen in the stress-relieved condition failed after 28 880 cycles (20.0 h). The optical microstructures of the three specimens after testing, sectioned just below the fractured surface, are shown in Fig. 2.

Figure 2*a* shows that the specimen initially in the solution-annealed condition contains both grain-boundary and some incoherent twin-boundary carbide precipitation but only slight coherent twin-boundary precipitation. The specimens initially solution annealed and aged (Fig. 2*b*) or stress relieved (Fig. 2*c*) before testing show a slightly more advanced stage of



(*a*) Specimen in the solution-annealed condition prior to testing (×250).
(*b*) Specimen in the solution-annealed and aged condition prior to testing (×250).
(*c*) Specimen in the stress-relieved condition prior to testing (×250).

FIG. 2—*Optical microstructure near the fracture surface of a Type 304 stainless steel specimen at 1050 F with* $\Delta\epsilon_t = 0.5$ *percent.*

precipitation with carbides clearly visible at the coherent twin boundaries. In general, a correlation was found between longer fatigue life and more advanced carbide precipitation. Precipitation, particularly in the earlier stages, is greatly accelerated by cyclic deformation. Thus, the specimen initially in the solution-annealed condition has reached a stage of precipitation, after a 12-h fatigue test at 1050 F, that is almost as advanced as the specimens that were solution-annealed and aged or stress relieved. For tests at 1202 F, the time required for the precipitation in a specimen initially in the solution-annealed condition to approach that of a specimen initially in the solution-annealed and aged condition is even shorter. Thus, for tests of longer duration or performed at higher temperatures or both, the precipitation effects of the initial heat treatment tend to be obliterated because of the accelerated precipitation that occurs during the time spent at test temperature.

It will be recalled from section (*a*) that stress-relieved Type 304 stainless steel had a shorter fatigue life at 1202 F than at 1050 F, whereas solution-annealed material showed relatively little difference in fatigue life at these temperatures. The reason for this behavior can be qualitatively understood on the basis of the strengthening effect of the early stages of carbide precipitation. The 1050 F fatigue-life curves for the stress-relieved material lie above that for the solution-annealed material (Fig. 1*f*) because of the greater extent of carbide precipitation in the stress-relieved material. At 1202 F, however, sufficient precipitation can occur during the testing of the solution-annealed steel so that its fatigue life is comparable to that of the stress-relieved material (Fig. 1*e*). In fact, at either temperature the solution-annealed material probably experiences sufficient precipitation during testing so that little temperature effect is evident (Fig. 1*c*). The stress-relieved material undergoes much less precipitation during testing, and, therefore, its fatigue life shows a more normal dependence on testing temperature.

Another interesting result of the present work is the effect of tension holdtime on the mode of crack propagation. An examination of fracture surfaces in the scanning electron microscope revealed that the introduction of a relatively short tension holdtime into the fatigue tests of stainless steel at either 1050 or 1202 F caused the crack path to change from transgranular to intergranular. This agrees with the results of Berling and Conway [*8*]. The fracture surfaces of the specimens which failed transgranularly displayed the characteristic fatigue striations, but no striations were seen in specimens which failed intergranularly.

Summary and Conclusions

Fully reversed, axial strain-controlled low-cycle fatigue tests with and without tension holdtime have been conducted in air between 806 and 1202 F and at a strain rate of 4×10^{-3} s^{-1} on Types 304 and 316 stainless steel

after various initial heat treatments. These results can be summarized as follows:

1. For fully reversed tests without tension holdtime, the stress-relieved Type 304 data clearly indicate some temperature effect on fatigue life. However, little temperature effect was observed in the solution-annealed specimens. In the case of Type 316, almost no temperature effect was observed for both the stress-relieved and solution-annealed conditions.

2. Almost no effect of heat treatment on fatigue life was observed at 1202 F for both Types 304 and 316 in fully reversed tests without tension holdtime. Some heat treatment effects are evident at 1050 F as follows: (*a*) Aging at the test temperature of 1050 F appears to prolong the fatigue life of the solution-annealed specimens for both steels. (*b*) There is little difference in fatigue life between Type 304 specimens in the stress-relieved and *solution-annealed and aged* conditions. (*c*) The fatigue life is about the same for Type 316 specimens in the stress-relieved and *solution-annealed* conditions.

3. For both steels, the introduction of tension holdtime clearly decreases fatigue life. The number of cycles to failure decreases continuously with an increase in holdtime, but there appears to be a possible saturation effect at longer holdtimes.

4. The high-temperature fatigue properties of Type 304 stainless steel are superior to Type 316 stainless steel, if the comparison is based on the total strain range. The reverse is true, if they are compared on the basis of the same actual alternating stress level.

5. Much of the macroscopic fatigue behavior of both stainless steels can be understood qualitatively by detailed microstructural examinations of the material prior to and after testing.

Acknowledgment

We wish to thank W. F. Burke, C. Tome, and R. W. Bunce for their substantial help in conducting this test program; and P. G. Shewmon, B. R. T. Frost, and Che-Yu Li for their encouragement.

References

[*1*] Weiss, B. and Stickler, R., *Metallurgical Transactions*, Vol. 3, 1972, pp. 851–866.
[*2*] Conway, J. B., "Evaluation of Plastic Fatigue Properties of Heat-Resistant Alloys," GEMP-740, General Electric Nuclear System Programs, Cincinnati, Ohio, 1969.
[*3*] Berling, J. T. and Slot, T. in *Fatigue at High Temperature, ASTM STP 459*, American Society for Testing and Materials, 1969, p. 3.
[*4*] Slot, T., Stentz, R. H., and Berling, J. T. in *Manual or Low-Cycle Fatigue Testing, ASTM STP 465*, American Society for Testing and Materials, 1969, p. 100.
[*5*] Jaske, C. E., Mindlin, H., and Perrin, J. S., "Low-Cycle Fatigue Evaluation of Reactor Materials," Battelle Memorial Institute, BMI-1903, April 1971, p. A-1 and BMI-1920, Nov. 1971, p. A-1.

[6] Stickler, R. and Vinckier, A., *Transactions*, American Society for Metals, Vol. 54, 1961, pp. 362–380.
[7] Driver, J. H., *Metal Science Journal*, Vol. 5, 1971, pp. 47–50.
[8] Berling, J. T. and Conway, J. B. in *First International Conference on Pressure Vessel Technology, Part II: Materials and Fabrication*, The American Society of Mechanical Engineers, New York, 1969, pp. 1233–1246.

DISCUSSION

L. F. Coffin[1] *(written discussion)*—Have you observed any influence of the carbide precipitation on the fractograph relative to the preferential precipitation on coherent twin boundaries or grain boundaries, and, if so, can you relate these effects to variation in life?

C. F. Cheng, C. Y. Cheng, D. R. Diercks, and R. W. Weeks (authors' closure)—The presence of carbide precipitates along the grain and twin boundaries does not appear to strongly influence the mode of failure, nor does it appear to greatly affect the fracture path on a microscopic scale. We find that specimens with extensive grain boundary carbide precipitation, when tested so as to fail integranularly, exhibit fracture surfaces which clearly reveal the intergranular nature of the fracture, yet have a generally ductile appearance. The surface is not what one would expect if the thin carbide films along the boundaries were fracturing in a brittle manner during the test. Apparently, carbide precipitation causes an increase in fatigue life not because of any great influence which it has on State II cracking, but rather because it delays the initiation and Stage I crack growth processes. We are continuing to look at these effects.

[1] Corporate research and development, General Electric Co., Schenectady, N. Y. 12301

C. E. Jaske,[1] *H. Mindlin,*[1] *and J. S. Perrin*[1]

Combined Low-Cycle Fatigue and Stress Relaxation of Alloy 800 and Type 304 Stainless Steel at Elevated Temperatures

REFERENCE: Jaske, C. E., Mindlin, H., and Perrin, J. S., "**Combined Low-Cycle Fatigue and Stress Relaxation of Alloy 800 and Type 304 Stainless Steel at Elevated Temperatures,** *Fatigue at Elevated Temperature, ASTM STP 520,* American Society for Testing and Materials, 1973, pp. 365–376.

ABSTRACT: A detailed analysis was made of data from low-cycle fatigue tests of solution-annealed, nickel-iron-chromium Alloy 800 at 1000, 1200, and 1400 F and of Type 304 austenitic stainless steel at 1000 and 1200 F with holdtimes at maximum tensile strain. A single equation was found to approximate the cyclically stable stress relaxation curves for both alloys at these temperatures. This equation was then used in making a linear time fraction creep damage analysis of the stable stress relaxation curves, and a linear life fraction rule was used to compute fatigue damage. Creep-fatigue damage interaction was evaluated for both alloys using the results of these damage computations. Strain range was found to affect the damage interaction for Type 304 stainless steel but not for the Alloy 800. With increasing holdtime, both creep and total damage increased for the Alloy 800 and decreased for the Type 304 stainless steel, and fatigue damage decreased for both alloys. A method was developed to relate length of holdtime and fatigue life to total strain range. This method provides a simple and reasonable way of predicting fatigue life when tensile holdtimes are present.

KEY WORDS: fatigue (materials), creep properties, nickel alloys, iron containing alloys, chromium containing alloys, austenitic stainless steels, stress relaxation, tests, evaluation, damage, thermal fatigue

Nomenclature

- A Constant term in relaxation equation
- C Total strain range at one cycle to failure
- D Total creep and fatigue damage
- d Slope of holdtime fatigue curves
- m Exponent term in relaxation equation
- N Number of cycles
- N_f Number of cycles to fracture

[1] Project leader, division chief, and fellow, respectively, Battelle Columbus Laboratories, Columbus, Ohio 43201.

Copyright© 1973 by ASTM International www.astm.org

t Time, min
t_f Time to fracture, h
t_H Length of holdtime, min
t_r Time to stress-rupture, h
Δt Increment of time, h
ϵ Engineering strain
$\dot{\epsilon}$ Engineering strain rate, s^{-1}
$\Delta\epsilon$ Total range of engineering strain
σ Engineering stress, ksi
$\Delta\sigma$ Range of engineering stress, ksi
σ_{max} Maximum algebraic value of engineering stress, ksi
$\Delta\sigma_r$ Range of relaxation of engineering stress, ksi

Equipment that operates at elevated temperature is often subjected to a combination of transient and steady-state loading conditions. For example, material in structural components of a nuclear power plant may undergo a thermally induced strain cycle during start up and shut down or during a variation in operating conditions. Normally, the equipment is operated under steady-state conditions that may produce time-dependent creep or stress relaxation in the material. The possible interaction of cyclic fatigue damage and time-dependent creep damage is an important consideration in the design of elevated-temperature equipment.

For many types of cyclic operation at elevated temperature, the loading history can be approximated by a strain cycle followed by a hold period at constant strain with stress relaxation as illustrated schematically in Fig. 1. A number of experimental studies [*1–7*][2] have shown that such holdtimes can cause a detrimental effect on cyclic fatigue life. Such holdtime effects have been reviewed by Krempl and Wundt [*8*]. In ASME Code Case 1331-5 [*9*], use of a linear life fraction rule is recommended for accounting for creep and fatigue damage interaction in design. Recommendation of this rule was based upon evaluation of tension holdtime, low-cycle fatigue data for Type 304 stainless steel at 1200 F [*10*].

The objective of the present study was to evaluate use of the linear life fraction rule for holdtime, low-cycle fatigue tests of solution-annealed nickel-iron-chromium Alloy 800 at 1000, 1200, and 1400 F [*7*] and of Type 304 austenitic stainless steel at 1000 F. Since previous studies [*6,7*] have shown that holdtimes at peak tensile strain are more detrimental to fatigue life than holdtimes at peak compressive strain, the present work was concentrated only on tensile holdtime data.

Experimental Work

Results of the experimental studies of Alloy 800 have been reported previously [*7*]. Experimental procedures of the present study were the same as

[2] The italic numbers in brackets refer to the list of references appended to this paper.

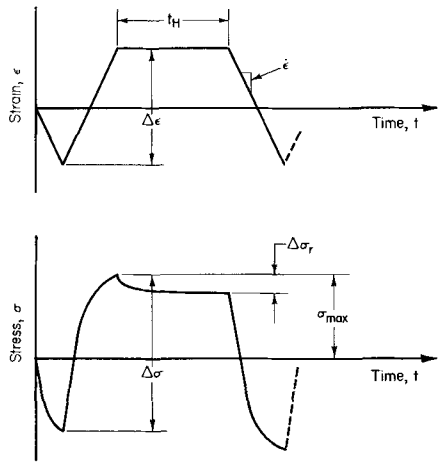


FIG. 1—*Schematic of strain and stress history for a fully reversed strain cycle with holdtime at maximum tensile strain.*

those used for the holdtime tests of Alloy 800 [7]. Tests were performed under fully reversed strain cycling at $\dot{\epsilon} = 4 \times 10^{-3}$ s^{-1}. The annealed Type 304 stainless steel used in this program was from the same heat of material used in a previous hold time study at 1200 F [6] and furnished in the form of $\frac{5}{8}$-in.-diameter bar stock (Heat 55697) by Batelle's Pacific Northwest Laboratories [11].

The influence of tension holdtime on the fatigue life of Type 304 stainless steel at 1000 F is shown in Fig. 2. At $\Delta\epsilon > 0.005$, holdtime tests had significantly shorter cyclic lives than comparable no holdtime tests. At the highest strain range, $\Delta\epsilon = 0.022$, the fatigue life decreased as the length of holdtime increased. However, at $\Delta\epsilon = 0.0044$, a 10-min tension hold period did not significantly affect the cyclic life. This result implies that there may be a

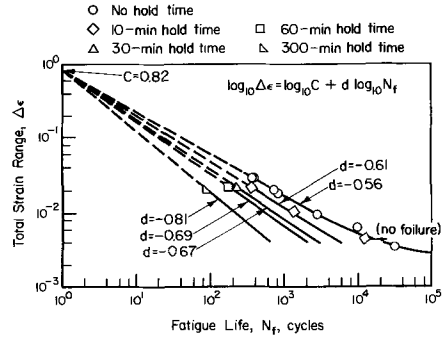


FIG. 2—*Effect of tension holdtime on fatigue life of Type 304 stainless steel at 1000 F and at a strain rate of* 4×10^{-3} s^{-1}.

threshold strain level below which holdtime has little or no detrimental influence on fatigue life.

As shown in Fig. 2, the holdtime data for Type 304 stainless steel at 1000 F can be approximated by a series of straight lines extrapolated to the one-cycle-to-failure intercept of the extrapolated no-holdtime curve. This same method also worked well when data on Type 304 stainless steel at 1200 F [*6*] were analyzed and has been shown to work well with the holdtime data on Alloy 800 [*7*]. This technique provides a method of extrapolating results from relatively short holdtime tests at high strain ranges to much lower strain ranges. Results of tests at $\Delta\epsilon < 0.005$ indicate that this technique may be too conservative at very low strain ranges. However, until more experimental data are developed at these low strain ranges, such conservatism is probably required.

The $\Delta\epsilon$ versus N_f curves for various lengths of holdtime can be described by the equation

$$\log_{10} \Delta\epsilon = \log_{10} C + d \log_{10} N_f \quad \ldots\ldots\ldots\ldots\ldots\ldots (1)$$

Values of the intercepts C and slopes d that characterize the holdtime fatigue behavior of both solution-annealed Alloy 800 and Type 304 stainless steel are presented in Table 1. For each temperature, one intercept value is shown, and the slope increases in magnitude (becomes steeper) as the length of holdtime increases.

Damage Analysis

To evaluate the linear life fraction damage rule recommended by ASME Code Case 1331-5 [*9*], creep and fatigue damage were calculated using the following equation

$$\sum \frac{N}{N_f} + \sum \frac{\Delta t}{t_r} = D \quad \ldots\ldots\ldots\ldots\ldots\ldots\ldots\ldots (2)$$

Actual failure values (N_f and t_r) were used as the damage criteria instead of design values that incorporate safety factors. Use of these actual values permitted a straightforward comparison with simple fatigue and stress-rupture data. If the linear life fraction concept is valid and no creep-fatigue interaction occurs, the value of D should be close to unity. A deviation from unity may indicate that a creep-fatigue interaction takes place. Equation 2 has been also used to evaluate creep-fatigue interaction for holdtime tests of Type 304 stainless steel at 1200 F [*10*].

The fatigue damage term ($\sum N/N_f$) was the ratio of fatigue life in the holdtime test to the mean fatigue life in a comparable no holdtime test. The no holdtime fatigue curve of Fig. 2 was used to obtain mean lives for Type 304 stainless steel at 1000 F, and similar fatigue curves were used to obtain mean lives for Alloy 800 [*12*].

TABLE 1—*Constants for equation relating fatigue life to total strain range as a function of length of tension holdtime.*

Temperature, deg F	C	Slope as Function of Length of Holdtime	
		t_H, min	d
		SOLUTION-ANNEALED ALLOY 800	
1000	0.48	0	−0.47
		10	−0.50
		60	−0.57
		300	−0.71
1200	0.57	0	−0.54
		10	−0.68
		60	−0.79
		300	−0.83
1400	0.84	0	−0.63
		10	−0.74
		60	−0.83
		300	−0.88
		TYPE 304 STAINLESS STEEL	
1000	0.82	0	−0.56
		10	−0.61
		30	−0.67
		60	−0.69
		300	−0.81
1200	0.62	0	−0.54
		1	−0.59
		10	−0.65
		30 to 600	−0.69

The creep damage term ($\sum \Delta t/t_r$) was obtained by numerical integration of the stable stress relaxation curves. To simplify the integration process, relaxation curves were approximated by the function

$$\ln (\sigma_{max}/\sigma) = \frac{A}{1 + m} t^{1+m} \quad \ldots\ldots\ldots\ldots\ldots\ldots (3)$$

This equation was selected because it had been found to work well for similar relaxation curves from holdtime tests of Type 304 stainless steel at 1200 F [*13*] and was used in a creep-fatigue damage evaluation of the same data [*10*]. Best-fit values of A and m were obtained by least squares regression of each stable relaxation curve (see Table 2). Values of t_r were taken from average stress-rupture curves for solution-annealed Alloy 800 [*12*] and Type 304 stainless steel [*14*].

Results of the damage computations are summarized in Table 2. The fraction of creep damage calculated for each relaxation cycle is reported along with values of $\sum N/N_f$, $\sum \Delta t/t_r$, and D.

TABLE 2—*Results of stress-relaxation and creep-fatigue damage analysis for tension holdtime tests.*

Specimen	Length of Holdtime, t_H, min	Total Strain Range, $\Delta\epsilon$	Stable Maximum Stress, σ_{max}, ksi	Best Fit Constants		Creep Damage		Fatigue Damage, $\sum \frac{N}{N_f}$	Total Damage, D
				A	m	$\sum \frac{\Delta t}{t_r}$ per cycle	$\sum \frac{\Delta t}{t_r}$		
SOLUTION-ANNEALED ALLOY 800 AT 1000 F									
11A	10	0.0226	57.2	0.00803	−0.864	6.32×10^{-4}	0.31	0.73	1.04
12A	10	0.0224	54.0	0.0147	−0.724	3.25×10^{-4}	0.16	0.73	0.89
41A	10	0.0053	45.0	...[a]	...[a]	1.09×10^{-4}	0.65	0.27	0.92
29A	60	0.0238	78.6	0.0109	−0.801	7.56×10^{-2}	16.6	0.36	17.0
45A	60	0.0239	71.4	0.0117	−0.617	2.79×10^{-2}	7.06	0.42	7.48
36A	300	0.0238	78.4	0.0110	−0.853	2.26×10^{-1}	16.3	0.12	16.4
SOLUTION-ANNEALED ALLOY 800 AT 1200 F									
9A	10	0.0200	44.7	0.0497	−0.825	1.53×10^{-3}	0.23	0.28	0.51
10A	10	0.0156	41.0	0.0806	−0.665	8.97×10^{-4}	0.17	0.22	0.39
37A	10	0.0054	43.2	0.0488	−0.552	3.60×10^{-3}	3.59	0.093	3.68
40A	10	0.0054	41.8	0.0565	−0.455	2.62×10^{-3}	2.58	0.092	2.67
31A	60	0.0239	67.7	0.0504	−0.721	1.39×10^{-1}	7.77	0.15	7.92
35A	60	0.0243	67.1	0.0601	−0.849	2.62×10^{-2}	1.52	0.16	1.68
43A	60	0.0053	36.3	0.0480	−0.595	2.14×10^{-3}	0.73	0.031	0.76
38A	300	0.0237	69.7	0.0564	−0.832	9.84×10^{-2}	4.63	0.12	4.75

Solution-Annealed Alloy 800 at 1400 F									
13A	10	0.0273	45.7	0.108	−0.879	4.44×10^{-3}	0.54	0.48	1.02
7A	10	0.0228	31.6	0.0999	−0.861	1.70×10^{-3}	0.24	0.43	0.67
8A	10	0.0176	30.5	0.144	−0.802	1.13×10^{-3}	0.25	0.45	0.70
30A	10	0.0055	28.2	0.116	−0.829	1.06×10^{-3}	0.92	0.23	1.15
33A	10	0.0055	26.8	0.135	−0.779	1.04×10^{-3}	0.83	0.21	1.04
47A	60	0.0176	37.4	0.123	−0.827	5.47×10^{-3}	0.72	0.27	0.99
44A	60	0.0056	28.8	0.107	−0.775	5.14×10^{-3}	2.05	0.11	2.16
46A	300	0.0175	39.0	0.0635	−0.915	3.89×10^{-2}	2.06	0.11	2.17
Type 304 Stainless Steel at 1000 F									
SS7	10	0.0222	55.0	0.0200	−0.807	1.99×10^{-3}	0.73	0.53	1.26
SS22	10	0.0104	39.5	0.0146	−0.881	5.73×10^{-5}	0.082	0.49	0.57
SS62[b]	10	0.0044	24.6	...[a]	...[a]	7.45×10^{-6}	0.097	>0.63	>0.73
SS9	30	0.0220	54.6	0.0188	−0.888	2.87×10^{-3}	0.64	0.32	0.96
SS8	60	0.0221	53.2	0.0188	−0.915	2.55×10^{-3}	0.47	0.27	0.74
SS11	300	0.0213	50.2	0.0256	−0.902	2.91×10^{-3}	0.26	0.13	0.39

[a] Amount of stress relaxation was negligible.
[b] Test was stopped without failure.

Discussion

The average trend of the creep-fatigue damage interaction is shown in Fig. 3 where creep damage is plotted against fatigue damage. For Alloy 800 (Fig. 3*a*) most of the results fell close to or above the $D = 1$ curve. There was no significant trend in damage values with total strain range. However, there was a definite trend of decreased fatigue damage and increased creep damage as the length of holdtimes increased. In contrast, damage values for Type 304 stainless steel tended to fall close to or much below the $D = 1$ curve (Fig. 3*b*). The data shown for 1200 F were obtained from Campbell's damage analysis [*10*]. As indicated in Fig. 3*b*, the trend of damage values was different for different strain ranges. The fatigue damage term tended to decrease with increasing length of holdtime and approach a constant saturation level at holdtimes between 10 and 30 min. The creep-damage

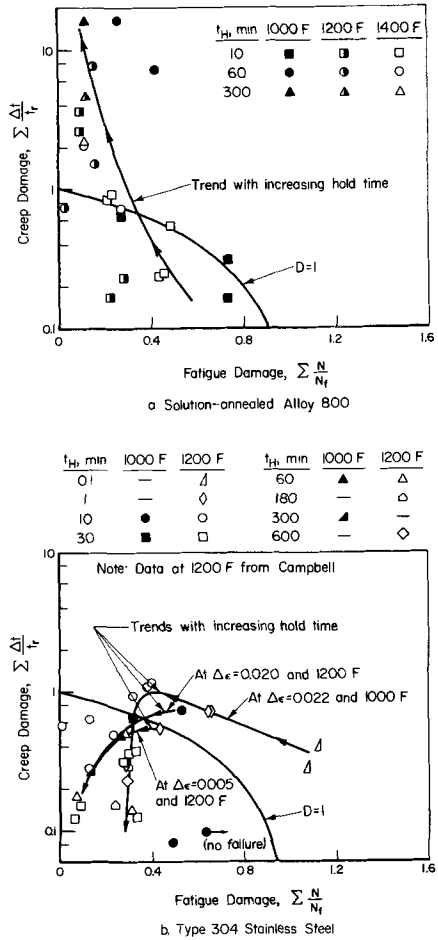


FIG. 3—*Creep fatigue damage interaction for tension holdtime tests.*

term was about constant or increased slightly up to about 10-min holdtimes and decreased very sharply at holdtimes longer than 10 min.

The trend of damage values as a function of holdtime is also illustrated in Fig. 3. For Alloy 800 the total damage values increased with holdtime, and for Type 304 stainless steel they decreased with holdtime. Since holdtimes of practical interest in nuclear equipment design are usually much longer than those shown, it is very important to consider this factor in use of the linear life fraction rule. A value of $D = 1$ appears to be a conservative damage limit for Alloy 800 and may even be too conservative at long holdtimes. However, a damage limit of $D = 1$ for Type 304 stainless steel may be very unconservative and for long holdtimes a limit of $D = 0.1$ may be more appropriate.

Caution must be used in applying this damage rule to actual design situations. In the present analysis and that made by Campbell [*10*], cyclically stable stress-relaxation curves were used to compute creep damage. Since both alloys exhibited a significant amount of cyclic hardening [*15*] at these temperatures, much lower and possibly unconservative creep damage values would have been obtained from monotonic relaxation curves. Thus, it is necessary to base design computations on the stable relaxation curves.

As evidenced by the markedly different trends observed for these two alloys, relating the creep damage for such cyclic relaxation curves to monotonic stress-rupture behavior does not adequately explain the time-dependent damage done during holdtime fatigue tests. Since the relaxation during most of these tests occurred in cyclically hardened materials, it would have been more appropriate to relate creep damage to stress-rupture curves for material that had been cyclically hardened, if such information had been available. Also, the holdtime tests were under constrained conditions as opposed to load-controlled, stress-rupture tests where strain is allowed to increase monotonically up to fracture. It has been shown [*16*] that when cyclic creep tests are conducted under constrained conditions, the cyclic creep-rupture curve usually falls above the monotonic one. Thus, before the time fraction rule can be applied to evaluate creep damage under cyclic loading, a creep-damage criteria other than the monotonic stress-rupture curve must be developed.

Conclusions

As a result of this study, four important conclusions have been reached about the tension holdtime low-cycle fatigue behavior of Alloy 800 at 1000, 1200, and 1400 F and of Type 304 stainless steel at 1000 and 1200 F.

1. It was found that the cyclically stable stress-relaxation behavior could be described by the relationship

$$\ln (\sigma_{max}/\sigma) = \frac{A}{1 + m} t^{1+m}$$

2. Use of the linear lifetime damage rule suggested by ASME Code Case 1331-5 gave opposite trends in calculated damage for the two alloys. For Type 304 stainless steel, creep-fatigue damage interaction was influenced by strain range, and both creep and total damage decreased with increasing holdtime. As a result, use of this damage rule would give unconservative design guidelines for Type 304 stainless steel. For Alloy 800, creep-fatigue damage interaction was not significantly affected by strain range, and both creep and total damage increased with increasing holdtime. For this alloy, the damage rule would give conservative design guidelines.

3. Time-dependent damage during cyclic relaxation was not adequately explained by a simple correlation with monotonic stress-rupture behavior.

4. For a constant length of tension holdtime, total strain range and fatigue life were related by the equation

$$\log_{10} \Delta\epsilon = \log_{10} C + d \log_{10} N_f$$

Acknowledgments

This investigation was sponsored by the U. S. Atomic Energy Commission under Contract W-7405-eng-92. Appreciation is extended to H. J. Malik and J. J. Parks for their assistance in conducting the experimental work, and to K. B. Davies for his help in implementing the stress-relaxation and damage analyses.

References

[*1*] Coles, A., Hill, G. J., Dawson, R. A. T., and Watson, S. J. in *International Conference on Thermal and High-Strain Fatigue*, Metals and Metallurgy Trust, London, 1967, pp. 270–294.

[*2*] Edmunds, H. G. and White, D. J., *Journal of Mechanical Engineering Science*, Vol. 8, No. 3, 1966, pp. 310–321.

[*3*] Coles, A. and Skinner, D., *Journal of the Royal Aeronautical Society*, Vol. 69, Jan. 1965, pp. 53–55.

[*4*] Hill, G. J. in *International Conference on Thermal and High-Strain Fatigue*, Metals and Metallurgy Trust, London, 1967, pp. 312–327.

[*5*] Krempl, E. and Walker, C. D. in *Fatigue at High Temperature, ASTM STP 459*, American Society for Testing and Materials, 1969, pp. 75–99.

[*6*] Berling, J. T. and Conway, J. B. in *Proceedings*, First International Conference on Pressure Vessel Technology, Part II, The American Society of Mechanical Engineers, Sept. 1969, pp. 1233–1246.

[*7*] Jaske, C. E., Mindlin, H., and Perrin, J. S., *Journal of Engineering for Industry, Transactions*, American Society of Mechanical Engineers, Vol. 94, No. 3, Aug. 1972, pp. 930–934.

[*8*] Krempl, E. and Wundt, B. M. in *Hold-Time Effects in High-Temperature Low-Cycle Fatigue, ASTM STP 489*, American Society for Testing and Materials, Sept. 1971.

[*9*] "Nuclear Vessels in High Temperature Service, Section III," *Interpretation of ASME Boiler and Pressure Vessel Code, Case 1331-5*, The American Society of Mechanical Engineers, 1971, pp. 387–427.

[*10*] Campbell, R. D., *Journal of Engineering for Industry, Transactions*, American Society of Mechanical Engineers, Vol. 93, No. 4, Nov. 1971, pp. 887–892.

[*11*] Claudson, T. T., "Fabrication History of Alloys Used in Irradiation Effects on Reactor Structural Materials Program," BNWL-CC-236, Pacific Northwest Laboratories, Richland, Wash., Oct. 1965.

[12] Jaske, C. E., Mindlin, H., and Perrin, J. S., "Low-Cycle Fatigue and Creep Fatigue of Incoloy Alloy 800," BMI-1921, Battelle's Columbus Laboratories, Columbus, Ohio, Feb. 1972.

[13] Conway, J. B., "An Analysis of the Relaxation Behavior of AISI 304 and 316 Stainless Steel at Elevated Temperature," General Electric Report GEMP-730, Cincinnati, Ohio, Dec. 1969.

[14] Smith, G. V. in *An Evaluation of the Yield, Tensile, Creep, and Rupture Strengths of Wrought 304, 316, 321, and 347 Stainless Steels at Elevated Temperatures, ASTM Data Series DS 552*, American Society for Testing and Materials, Feb. 1969.

[15] Jaske, C. E., Mindlin, H., and Perrin, J. S. in *Cyclic Stress-Strain Behavior-Analysis, Experimention, and Failure Prediction, ASTM STP 519*, American Society for Testing and Materials, Bal Harbour, Fla., Dec. 1971.

[16] Halford, G. R., "Cyclic Creep-Rupture Behavior of Three High-Temperature Alloys," NASA TN D-6309, Lewis Research Center-NASA, Cleveland, Ohio, May 1971.

DISCUSSION

I. Le May[1] *(written discussion)*—There has been considerable discussion concerning *in vacuo* tests to eliminate one variable, environment. However, when dealing with stainless steel at high temperature, it is very difficult to achieve a vacuum at the specimen sufficiently good enough to eliminate all oxidation, and what we may see is merely an evaluation of the effect of varying oxidation rates on the creep/fatigue processes. It is important to bear this point in mind in designing and evaluating experiments designed to evaluate the role of environment.

D. R. Diercks[2] *(written discussion)*—(Reply to previous discusser's (I. Le May) statement that austenitic stainless steel would continue to oxidize even in high-vacuum tests.)

Let me comment on the previous statement by pointing up that even though the oxidation of chromium in stainless steel in high-vacuum tests is favored thermodynamically, the kinetics of the process are considerably retarded because of the low O_2 partial pressure. One can perform some simple calculations based on the kinetic theory of gases to show that for vacua of the order of 10^{-6} to 10^{-7} torr or better, the rate at which gas atoms impinge on the specimen surface is quite small.

[1] Department of Mechanical Engineering, University of Saskatchewan, Saskatoon, Sask., Canada.

[2] Materials Science Div., Argonne National Laboratory, Argonne, Ill. 60439.

C. E. Jaske, H. Mindlin, and J. S. Perrin (authors' closure)—As pointed up by the discussers, environment plays an important role in elevated-temperature creep-fatigue and should be considered in future studies of these alloys. In considering what type of environment to use, it is important to keep the objective of these studies in mind. In this instance, we were developing information to use in design of nuclear reactor system components. Thus, studies of environment should simulate those that are to be encountered in service. Results of these studies can be then compared with the baseline of information developed in air.

J. Wareing[3] *(written discussion)*—When considering interaction problems involving creep and fatigue strains, it is important to distinguish between deformation and fracture phenomena associated with the two processes. Damage initiated by creep strain, for example, can propagate under the influence of the strain associated with the fatigue cycle and, thus, increase the growth rate of the fatigue crack.

Messrs. Jaske, Mindlin, and Perrin—We agree with Mr. Wareing's observation that creep and fatigue processes can interact. This observation very likely explains the fact that the linear life fraction damage rule did not adequately account for the results studied in our work. In addition, to his example of creep strain influence subsequent to fatigue damage, it should be pointed up that damage or changes in the structure of the material due to strain cycling also is markedly influenced by subsequent creep damage mechanisms.

[3] United Kingdom Atomic Energy Authority, Lancashire, England.

W. E. White,[1] *R. I. Coote,*[1] *and I. Le May*[1]

Effects of Combined Creep and Fatigue Loading on an Austenitic Stainless Steel at High Temperature

REFERENCE: White, W. E., Coote, R. I., and Le May, I., "**Effects of Combined Creep and Fatigue Loading on an Austenitic Stainless Steel at High Temperature,**" *Fatigue at Elevated Temperatures, ASTM STP 520*, American Society for Testing and Materials, 1973, pp. 377–386.

ABSTRACT: Preliminary data relating to the fatigue life and fracture morphology of an austenitic stainless steel at temperatures of 475 and 745 C are presented. From metallographic examination, fracture at 475 C was seen to be transcrystalline and ductile in nature, while at 745 C it appears that grain boundary cavities formed and subsequently linked up to give a mixed intercrystalline-transcrystalline fracture, the proportion of each depending on the level of the applied stress; fractographic examination supports these observations. Many grain boundary carbides were present on the intercrystalline fracture surfaces formed at 745 C, and the role of these in initiating crack formation is considered worthy of further study.

KEY WORDS: stainless steels, temperature, creep properties, fatigue (materials), fractography, grain boundaries, carbides, fracture, intercrystalline fractures (materials)

Relatively little data are available concerning the fatigue characteristics and resultant fracture morphology of many materials under conditions of elevated temperature where creep deformation may play an important role. This paper describes some preliminary observations made in carrying out elevated temperature fatigue tests on an austenitic stainless steel. In addition to examining the relationship between stress level and cycles to failure, an examination of the fracture surfaces was conducted using conventional fractographic techniques.

A secondary point of interest was the question of a possible increase in the rate of precipitate formation during stressing, as has been noted by Yamazaki[2] in 18Cr-12Ni steels undergoing fatigue at 600 C, while previous

[1] Departmental assistant, assistant professor, and professor, respectively, College of Engineering, University of Saskatchewan, Saskatoon, Sask., Canada.

[2] Yamazaki, M. in *Proceedings*, International Conference on the Science and Technology of Iron and Steel, Part II, Supplement to *Transactions*, Iron and Steel Institute of Japan. Vol. 11, 1971, pp. 1200–1203.

Copyright© 1973 by ASTM International www.astm.org

studies made at the University of Saskatchewan[3] have shown that creep deformation increased the rate of transformation from austenite in a Type 316 stainless steel. In any event, this part of the study has not shown significant effect of stress on precipitation for the particular steel used, but comprehensive studies of precipitation effects under stress are continuing using Type 316, in which precipitation is much more severe.

Experimental

The material used was received in the form of 12.7-mm (0.5-in.) diameter bar stock in the hot-rolled and solution treated condition, its grain size corresponding to ASTM No. 3 minimum. The composition is given in Table 1, and the as-received structure is shown in Fig. 1.

TABLE 1—*Composition of stainless steel in terms of principal alloying elements, weight percent.*

Cr	Ni	C	Mn	Si	Mo	Cb
19.85	11.66	0.08	2.35	1.10	0.285	0.018

Testing was carried out in a Model 810 MTS closed-loop material testing system with the specimen arranged within a wire-wound muffle furnace. Specimens were of 4.5 mm (0.178 in.) diameter with a parallel gage length of 40 mm ($1^{9}/_{16}$ in.): these dimensions correspond to those of specimens of the same material which are being used for standard creep tests without superimposed cyclic load.

All tests were conducted under tensile loading under load control with periodic monitoring of extension based on ram mean position, although in a number of cases this extension was recorded continuously. All tests were conducted using a load signal of triangular wave form and at a frequency of 10 Hz, with a cutoff of approximately 10^6 cycles.

Temperature was monitored by means of three chromel-alumel thermocouples attached to a specimen; the procedure involved bringing the specimen up to temperature and holding for 24 h before applying any load. This procedure corresponds to that used for complementary creep studies, with the hold period necessary for achieving uniform temperature when testing in a controlled gaseous atmosphere as used in part of the creep test program.

After testing, the appearance of the fracture surfaces was examined, and two stage, plastic-carbon replicas were taken from these surfaces for examination in the transmission electron microscope. In order to obtain reasonably clean replicas from the oxidized fracture surfaces, the fractured speci-

[3] Bassett, B. J. and Le May, I. in *Proceedings*, 3rd Annual Technical Meeting, 1970, International Metallographic Society, Los Alamos, N. Mex., 1971, pp. 9–14.

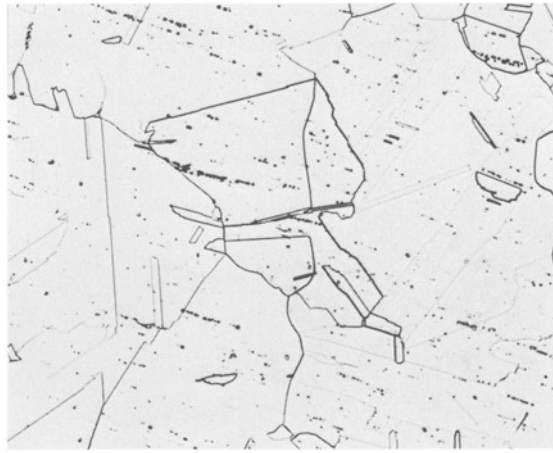


FIG. 1—*As-received material. Etched in diluted aqua regia* (×400).

mens were cleaned by immersing them in acetone in an ultrasonic cleaner. This procedure did not remove adherent scale but was found adequate to remove loose oxide and allow the production of reasonable replicas.

It may be noted here that the absence of a controlled atmosphere chamber in these tests meant that the entire fracture surface was oxidized to some extent. The material fracturing last had a very thin surface oxide layer, while heavier oxidation was present on that part of the fracture formed earlier.

Test Results and Observations

Tests have been conducted at two temperature levels, namely, 475 and 745 C, and the fatigue test results obtained to date are given in Table 2. A measure of their ductility under the test conditions is given in terms of the reduction in area at the fracture for each specimen, and data relating to the room and elevated temperature tensile properties of the material are also tabulated. In addition, the results for the tests at 745 C are plotted in Fig. 2 on the basis of the three mean stress levels used.

475 C Specimens

Sections taken through the 475 C test specimens indicated extensive deformation at all stress levels. Figure 3*a* shows a section through Specimen A6 which failed after 52 000 cycles, while Fig. 3*b* shows a specimen which had not failed at cutoff (Specimen A2): in both cases widespread slip has taken place, while there is little evidence of grain boundary sliding or intercrystalline cavity formation. In both of these photomicrographs, considerable banding can be seen; Marbles reagent and Nomarski interference

TABLE 2—*Data from fatigue and tension tests.*

FATIGUE DATA

Specimen No.	Temperature, deg C	Stress, MN/m^2	N_f Cycles	Reduction in Area at Fracture, %
A1	475	308 ± 185	27	50
A2[a]	475	139 ± 92.4	$>1.53 \times 10^6$	...
A3[a]	475	246 ± 123	$>1.14 \times 10^6$	...
A4	475	246 ± 216	236	64
A5[a]	475	246 ± 185	$>1.44 \times 10^6$	...
A6	475	246 ± 200	5.20×10^4	36
A7[b]	475	246 ± 191	$>6.61 \times 10^5$	...
A8	745	123 ± 92.4	6.80×10^3	64
A10	745	123 ± 61.5	1.30×10^5	...[c]
A11	745	123 ± 76.9	4.25×10^4	67
A12	745	123 ± 46.2	1.35×10^5	53
A13	745	123 ± 36.9	2.84×10^5	46
A14	745	123 ± 111	6.03×10^3	67
A28	745	123 ± 24.6	5.37×10^5	47
A29	745	123 ± 12.3	3.83×10^5	47
A33	745	123 ± 0	...[e]	46
A15	745	92.4 ± 92.4	1.64×10^5	59
A16	745	92.4 ± 61.5	4.01×10^5	50
A17	745	92.4 ± 46.2	5.46×10^5	46
A18	745	92.4 ± 36.9	1.11×10^6	43
A22	745	139 ± 46.2	1.68×10^4	64
A23	745	139 ± 24.6	5.17×10^4	56
A25	745	139 ± 6.15	5.60×10^4	56
A26	745	139 ± 6.15	5.43×10^4	56
A30	745	139 ± 0	...[d]	52
A31	745	139 ± 76.9	1.97×10^4	66
A32	745	139 ± 92.4	4.48×10^3	72

TENSILE DATA

Temperature, deg C	0.2% Yield Stress, MN/m^2	Ultimate Strength, MN/m^2
24	308	569
475	192	446
745	178	363

[a] Did not fail.
[b] Test terminated, machine fault.
[c] Measurement not taken.
[d] Failed in 5.3 h (equivalent to 192 000 cycles at 10 Hz).
[e] Failed in 28.6 h (equivalent to 1 030 000 cycles).

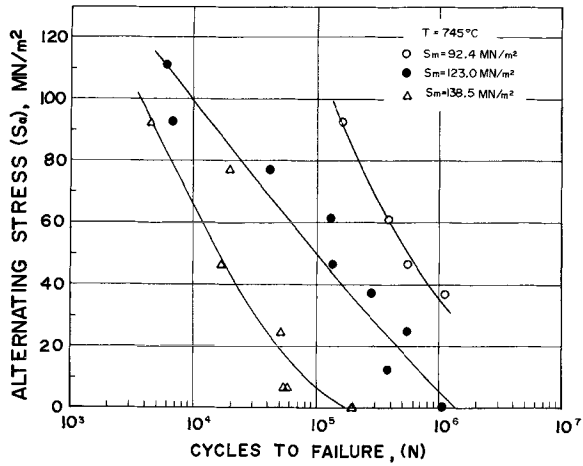


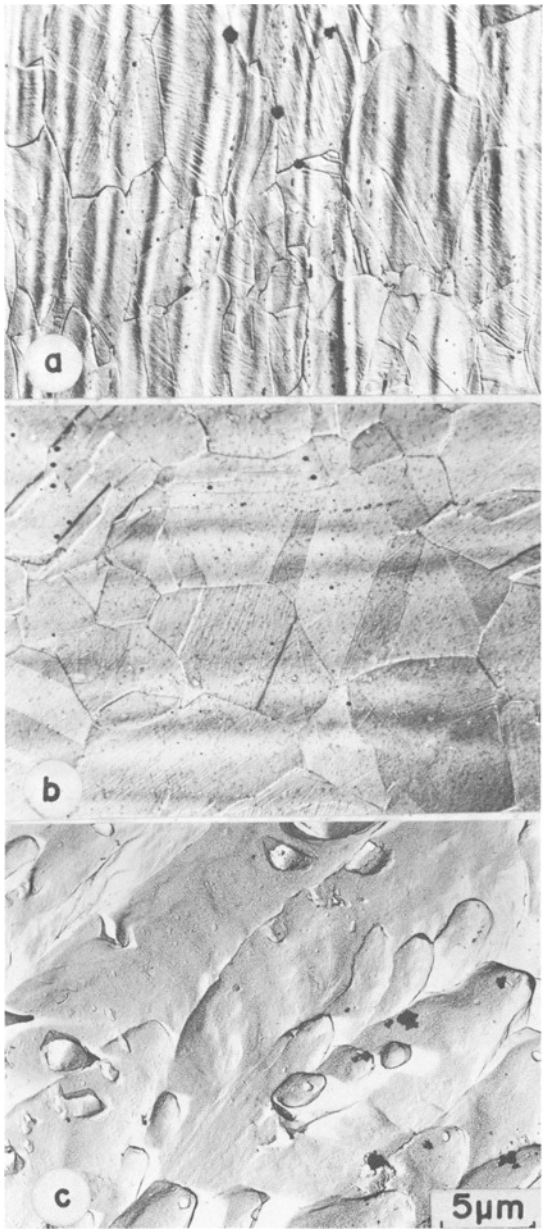
FIG. 2—*Fatigue data at 745 C.*

contrast illumination, which are necessary to produce sufficient contrast to delineate the slip lines clearly, have emphasized this banding. No precipitation was detected at this temperature.

Fracture in all 475 C specimens was clearly transcrystalline and ductile in nature, and the appearance of the facture in specimens failing at short times was similar to that of the hot tension specimens, although the appearance of the fracture of Specimen A6 looked to be more typical of a short time, creep-rupture test: these observations relate to the specimens' appearance to the eye and when viewed under the optical microscope. Figure 3*c* shows the appearance of the fracture surface of Specimen A6 at higher magnification, and this is typical of the specimens examined. The surface is covered with ductile dimples, and the features conventionally looked for in fatigue fractures are not to be found. Fatigue striations were not apparent in these replicas.

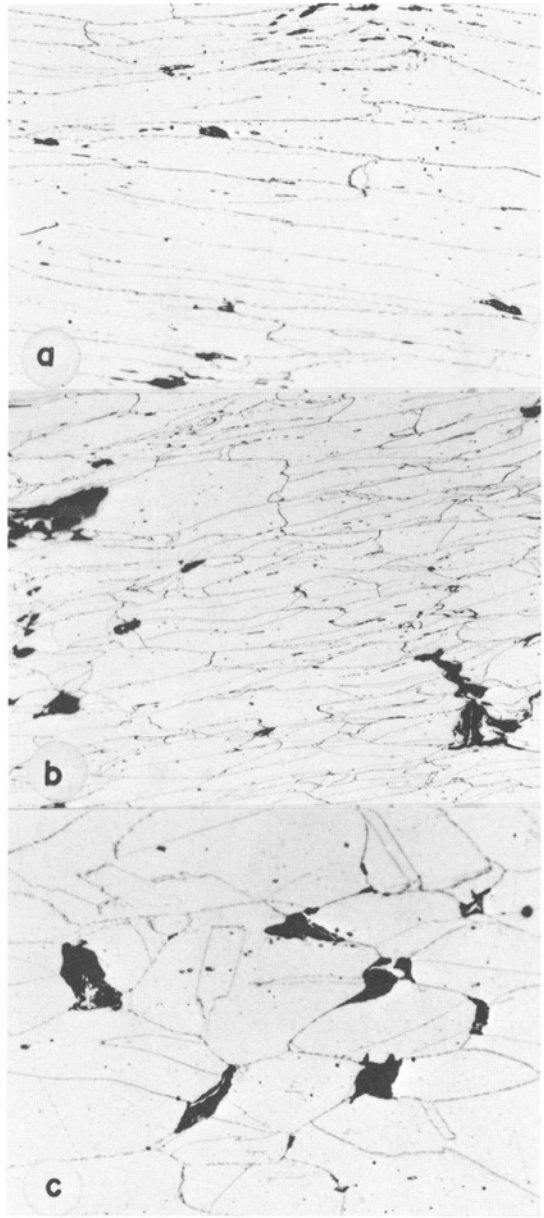
745 C Specimens

Optical metallographic examination of the specimens tested at 745 C indicated that the fracture appearance varied from the typical cup-cone failure in the hot tension test to a morphology typical of creep failure with widespread grain boundary cavitation and many intercrystalline cracks at the lower levels of cyclic stress. Figure 4*a* to *c* shows the variation in grain distortion and grain boundary void formation as a function of stress level, these photomicrographs being taken from regions close to the fracture surface. However it should be pointed out that similar observations held true along the length of the specimens, emphasizing that grain boundary cavitation was an important factor in their failure. On the basis of these observations, it was presumed that fracture initiated from these grain



(*a*) Section through Specimen A6 showing extensive deformation by slip. N_f = 52 000 cycles. Etched in marbles reagent. The banding is accentuated by Nomarski interference contrast (×192).
(*b*) Section through Specimen A2 showing extensive deformation by slip. Tested for 1 534 000 cycles without fracturing. Etched in marbles reagent (×320).
(*c*) Typical electron microfractograph from Specimen A6.

FIG. 3—*Specimens tested at 475 C.*



(*a*) Specimen A8, N_f = 6800 cycles (×320).
(*b*) Specimen A11, N_f = 42 541 cycles (×128).
(*c*) Specimen A18, N_f = 1 112 000 cycles (×320).

FIG. 4—*Sections through 745 C specimens close to fracture surfaces, showing cavities originating at grain boundaries and grain boundary precipitation. Aqua regia etch.*

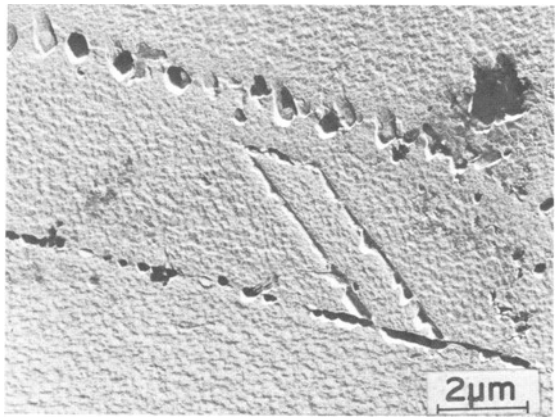


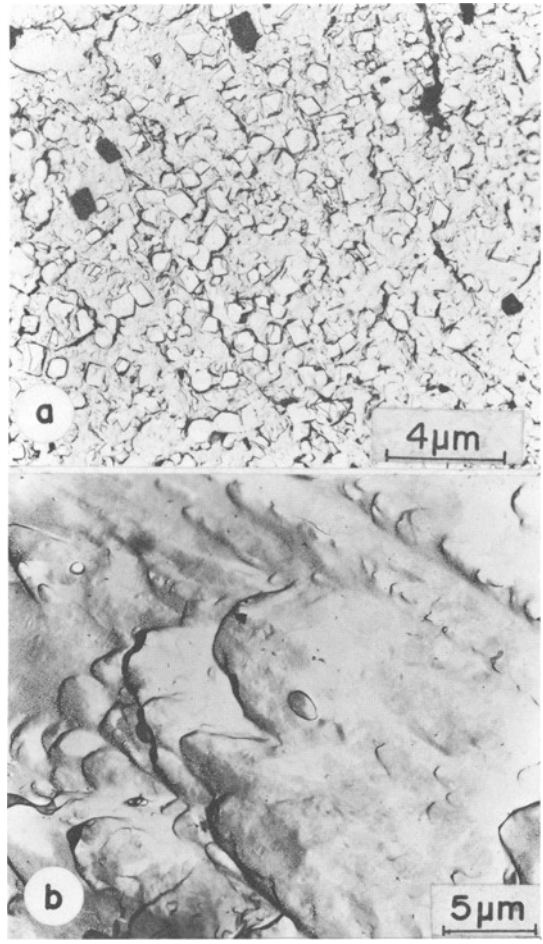
FIG. 5—*Extraction replica showing carbides precipitated along austenite grain and twin boundaries in Specimen A11 tested at 745 C.*

boundary cavities with a mixed intercrystalline and transcrystalline fracture mode.

The carbide precipitation which took place along grain and twin boundaries during testing may be seen in Fig. 4, although it did not appear to have been increased significantly by the stressing, comparison being made with the (virtually) unstressed material at the extreme end of the threaded grip portions of the specimens. Aqua regia has been used to etch these specimens, as Marbles reagent gives a poor result in the presence of so many precipitates. It is considered that the majority of the precipitation took place before loading, during the 24-h temperature stabilization period, as the observations correspond to others reported for Type 310 stainless steel[4,5] which has generally similar precipitation characteristics. The carbides, which were determined by electron diffraction to be of the $M_{23}C_6$ type, formed along grain boundaries, twin boundaries, and, in particular, at triple points on the boundaries. They may be seen more clearly in Fig. 5.

Fractographic examination of several specimens has produced the representative fractographs of Fig. 6. Figure 6*a* shows a region where cracking has taken place on a grain boundary, and there are many carbide particles apparent. The background of such areas was typically pitted, and this is taken to be the effect of the heavier oxidation within the cavity prior to fracture, although it is not clear whether the pitting arises in attempting to remove the scale by ultrasonic cleaning or from the oxidation process itself. Such areas covered only a fraction of the fracture surface and merged into regions of more ductile appearance. Much of the fracture surface appeared as in Fig. 6*b*, which represents transcrystalline fracture in a ductile manner; fracture is presumed to take place in this manner when the grain

[4] White, W. E. and Le May, I., *Metallography*, Vol. 3, 1970, pp. 35–50.
[5] White, W. E. and Le May, I., *Metallography*, Vol. 5, 1972, pp. 333–345.



(*a*) Carbides and surface pitting on a region of intercrystalline fracture in Specimen A15.
(*b*) Region of ductile transcrystalline fracture in Specimen A18.

FIG. 6—*Typical electron fractographs taken from 745 C specimens.*

boundary cavities link up. Of interest are the two rows of precipitates which presumably identify the boundaries of an annealing twin.

Conclusion

Preliminary data have been obtained for fatigue of an austenitic stainless steel at 745 and 475 C where creep effects are of importance. The fractures were seen to be transcrystalline and ductile in nature at the lower test temperature, while at 745 C grain boundary cavities first opened up as in creep deformation. Subsequently, fracture appeared to take place by a linking of these, to give a partly intercrystalline, partly transcrystalline final

fracture surface. The number and size of the intercrystalline voids increased as the stress level was lowered and life increased, and many carbides, which are assumed to have formed largely before loading commenced, were to be seen on these regions. No increase in carbide precipitation was noted which could be attributed to the stressing, but it would seem appropriate that the role of the carbides in the initiation of grain boundary cracking should be examined further.

Acknowledgments

The work described here was supported by funds provided by the American Iron and Steel Institute and the National Research Council of Canada. We wish to acknowledge the assistance of V. H. Meyer in conducting the tests, and thank Atlas Steels Ltd. for supplying the material.

DISCUSSION

G. R. Leverant[1] *(written discussion)*—What is the influence of the superimposed cyclic stress on the creep strain to the onset of intergranular cavitation?

W. E. White, R. I. Coote, and I. Le May (authors' closure)—This is certainly an important question, but we have not yet examined this matter so we are unable to reply directly. It should certainly be looked into further, with test specimens sectioned and examined metallographically at intervals during test.

D. R. Diercks[2] *(written discussion)*—You stated that in the specimens tested at 745 C, essentially all of the carbide precipitation occurred in the first 24 h of testing, and thus carbide reactions played no role in the remainder of the test. Am I to infer from this that no carbide coarsening took place after the initial precipitation?

Messrs. White, Coote, and Le May—The major carbide precipitation on boundaries took place within the 24 h hold period; however, subsequent carbide coarsening and transformation to give a lower energy configuration would undoubtedly take place. The point we wish to make is that any such effect was very minor as compared with the initial grain and twin boundary precipitation.

[1] Pratt & Whitney Aircraft, Division of United Aircraft Corp., Middletown, Conn. 06457.
[2] Materials Science Division, Argonne National Laboratory, Argonne, Ill. 60439.

P. Shahinian,[1] *H. H. Smith,*[1] *and H. E. Watson*[1]

Fatigue Crack Growth Characteristics of Several Austenitic Stainless Steels at High Temperature

REFERENCE: Shahinian, P., Smith, H. H., and Watson, H. E., **"Fatigue Crack Growth Characteristics of Several Austenitic Stainless Steels at High Temperature,"** *Fatigue at Elevated Temperatures, ASTM STP 520*, American Society for Testing and Materials, 1973, pp. 387–400.

ABSTRACT: The resistance to fatigue crack growth of annealed stainless steels, Types 304, 316, 321, and 348, was determined at 77, 800, and 1100 F (25, 427, and 593 C). Crack growth rates were related to the stress intensity factor range (ΔK). With increase in temperature the rate of crack growth for a given ΔK increased. At room temperature the four steels had the same resistance to crack growth. However, at high temperatures crack growth became sensitive to the differences in composition and properties among the steels. At 1100 F (593 C), Type 348 steel had the greatest resistance to crack growth and Type 316 the lowest resistance. As a result, fatigue life was 3.4 times longer for Type 348 steel over Type 316 steel at this temperature. The characteristics of high-temperature fatigue crack growth were examined.

KEY WORDS: fatigue (materials), crack propagation, stainless steels, thermal fatigue, evaluation, nuclear reactors

An important aspect of the design and safety analyses of advanced nuclear reactors is the assessment of the expected performance of cyclically loaded structural components at high temperatures. A realistic approach requires consideration, in particular, of the possibility of fracture originating from existing structural flaws. Information on the rate at which a flaw or small crack may grow to the critical size for failure is of value for predicting safe operation. The success in this respect of the fracture mechanics approach of relating fatigue crack growth rates to crack tip stress intensity factor in metals at or near room temperature has led more recently to application of the approach to high-temperature fatigue data [*1–5*].[2] The initial results have been encouraging, but further investigation is needed to fully validate the approach for high-temperature fatigue and to establish its

[1] Metallurgist, metallurgist, and mechanical engineer, respectively, Metallurgy Division, Naval Research Laboratory, Washington, D. C. 20390.

[2] The italic numbers in brackets refer to the list of references appended to this paper.

Copyright© 1973 by ASTM International www.astm.org

limitations. In addition to providing information useful to design, the approach is convenient for characterizing and evaluating resistance to fatigue crack growth of structural alloys.

In liquid metal fast breeder reactors currently in design or construction, austenitic stainless steels are being considered for extensive use for in-core and out-of-core applications. Available fatigue data on these materials are largely from smooth test specimens and are usually expressed in terms of conventional *S-N* curves. Information on resistance to fatigue crack growth should aid in the selection of alloys for service in reactors and in other high-temperature structures as well. Such data are now being developed [*5–8*] and more are needed to fully evaluate the fatigue characteristics of the alloys.

The main purpose of this investigation was to determine the resistance to fatigue crack growth of austenitic stainless steels, Types 304, 316, 321, and 348, at high temperatures and characterize the crack growth behavior in terms of the fracture mechanics approach to fatigue.

Experimental Procedure

All four of the stainless steels for this study were in the form of hot rolled, annealed plate; the chemical compositions and plastic flow properties are given in Tables 1 and 2, respectively. Fatigue specimens of the single-edge-notch cantilever type (details in Ref *6*) were machined with the orientation (RW) such that the crack growth would be perpendicular to the rolling direction. Side grooves to a depth of 5 percent of the specimen thickness were required to control the direction of crack propagation.

The specimens were cycled at 10 cpm in cantilever bending under zero-to-tension loading (saw-tooth curve) to a constant maximum load. These tests were conducted in laboratory air where the room-temperature relative humidity ranged from 17 to 62 percent during the period of the investigation. Although water vapor does increase fatigue crack growth rate in Type 304 stainless steel [*7*], the variation in humidity experienced during these tests should not have a large effect on growth rate. For the high-temperature tests an induction coil was used to heat a 5-in. section of the specimen, centered at the notch. The temperature gradient, as indicated by spot welded thermocouples, was no greater than 30 F (17 C) in the center 2 in. section and no greater than 10 F (6 C) along the side groove. Tests were interrupted frequently during the night and restarted in the morning after holding at temperature for 10 to 15 min. These interruptions had no noticeable effect on crack growth rate.

Measurements of crack length were made at the root surface of a side groove by means of a measuring microscope. Visibility of the crack was aided by electropolishing of the surface. The tests were terminated when the crack had reached a length of approximately 1 in. (60 percent of specimen width).

TABLE 1—*Chemical compositions of steels.*

Steel Types	Chemical Composition, weight percent										
	C	Mn	P	S	Si	Cr	Ni	Mo	Cu	Co	Other
304.....	0.048	1.48	0.025	0.015	0.52	18.57	9.45	...	...	...	...
316.....	0.060	1.72	0.012	0.007	0.40	17.30	13.30	2.33	0.065	0.030	0.012 Al 0.003 Ti 0.0005 B
321.....	0.031	1.38	0.013	0.010	0.66	17.71	10.00	...	...	...	0.27 Ti
348.....	0.062	1.82	0.008	0.007	0.52	18.64	9.92	0.06	0.2	0.01	0.79 Cb + Ta 0.0005 B

TABLE 2—*Mechanical properties.*

Steel Types[a]	Heat Treatment Anneal	Room Temperature Tensile				1100 F (593 C) Compressive		
		0.2% Yield Strength, ksi	Ultimate, ksi	Elongation, %	Reduction of Area, %	0.2% Yield Strength, ksi	Ultimate, ksi	Strain Hardening Coefficient, *n*
316	2000 F (1090 C)	44.1	82.1	68	63	23.7	61.1	0.323
304	1800 to 1950 F (980 to 1065 C)	37.0	83.0	57	72	23.9	52.8	0.289
321	2000 to 2050 F (1090 to 1120 C)	31.0	79.0	57	71	27.7	50.5	0.272
348	1830 F (1000 C)	35.8	87.5	51	73	32.3	52.6	0.231

[a] Arranged in order of increasing resistance to crack growth.

For analysis of the data the stress intensity factor was calculated from the expression:

$$K = \frac{6P \times L}{(B \times B_N)^{1/2} W^{3/2}} f(a/W)$$

where

P = maximum cyclic load,
L = distance from the plane of the crack to the point of load application,
a = total length of crack and notch,
W = specimen width,
B = specimen thickness, and
B_N = net thickness at the grooves.

This expression is based on that for pure bending given by Gross and Srawley [*9*]. In the calculation corrections were not made for plasticity at the crack tip.

Results

Analysis of the experimental fatigue crack growth data was done on the basis of the power law proposed by Paris and Erdogan [*10*] relating crack growth rate, da/dN, to the range of stress intensity factor, ΔK, which is expressed as:

$$da/dN = C(\Delta K)^m$$

where C and m are constants. The crack growth rate data for the four stainless steels are plotted as a function of the applied stress intensity range on log-log coordinates in Figs. 1 to 4. It is significant that the high-temperature data points from tests at different loads fall on the same curve and can be correlated on the basis of ΔK. In many respects the behavior of the four steels were similar. Crack growth rates for a given ΔK increased significantly with increase in temperature. Also, it appears that the threshold stress intensity below which a crack does not propagate was reduced with increase in temperature.

Certain features of the curves for the higher temperatures differ from those for room temperature; many of these features are common to all of the steels. In comparison to the room-temperature curves which show a single power law relationship over a wide ΔK range in typical behavior, the high temperature curves exhibit shorter straight segments over smaller ΔK ranges. These curves are centered at the crack growth range of 1 to 10×10^{-5} in./cycle and represent test lifetimes ranging from 20 000 to 200 000 cycles. At relatively high values of ΔK for all temperatures there is generally a slope transition in the curves to a higher slope, indicating a more rapid increase in rate of crack growth. However, at relatively low ΔK values

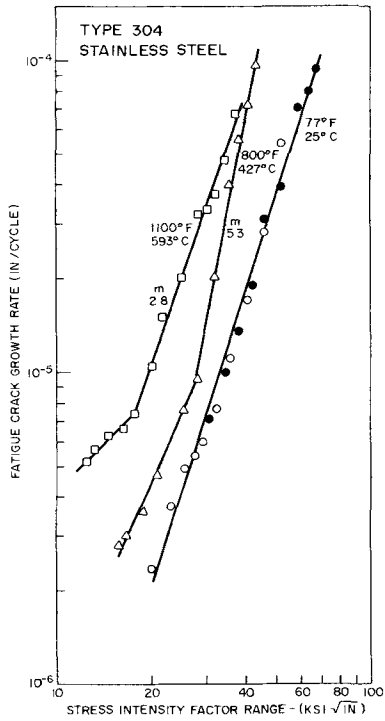


FIG. 1—*The dependence of fatigue crack growth rate in Type 304 stainless steel on stress intensity factor range. Closed symbols represent separate tests.*

the behavior at high temperatures differed from that at room temperature. At the high temperatures there was generally a range of growth rates below the intermediate range (10^{-5} in./cycle) whose curve slope was lower than that for the intermediate range, a characteristic which was not observed at room temperature. It would be expected that at very low ΔK values a threshold ΔK would exist and the curves would have the form of the 1100 F (593 C) curve for Type 348 stainless steel in Fig. 4. The curves at very low crack growth rates are displaced, as temperature is increased, to lower values of ΔK, indicating lower threshold values. While there are usually three distinct ranges of crack growth behavior at room temperature, at high temperatures there appears to be an additional range.

With regard to crack growth in the 10^{-5} in./cycle range the slope of the curve, the exponent m of the power law, is higher at 800 F (427 C) than at room temperature but then decreases at 1100 F (593 C). Consequently, crack growth rates at high ΔK values were about the same at 800 and 1100 F (427 and 593 C), though appreciably higher than at room temperature. In general, growth rates were more sensitive to temperature at low ΔK values.

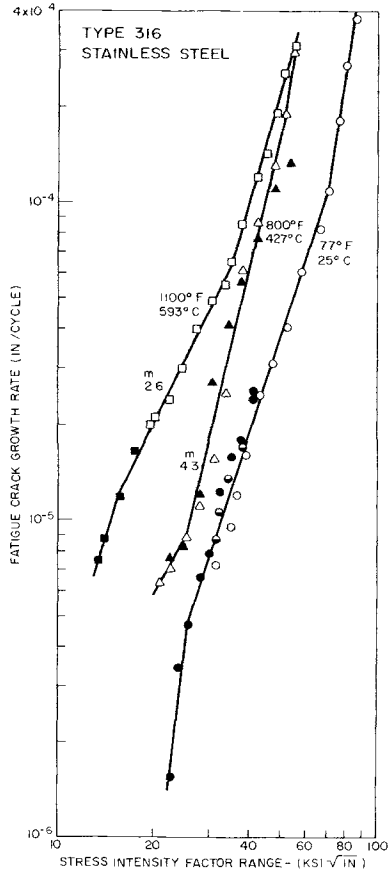


FIG. 2—*The dependence of fatigue crack growth rate in Type 316 stainless steel on stress intensity factor range. Closed symbols represent separate tests.*

Comparisons among the fatigue crack growth rates of the various steels, Fig. 5, showed that the rates at room temperature for a given ΔK were essentially the same in Types 304, 316, 321, and 348 stainless steels. An exception perhaps exists at ΔK values below 30 ksi$\sqrt{\text{in.}}$, but the data are not sufficient to permit meaningful comparisons. The few data points indicate the possibility of slightly different threshold stress intensities for the steels. In contrast to the room-temperature behavior, crack growth rates at 1100 F (593 C) for a given ΔK differed significantly among the four steels; the growth rates were highest for Type 316 steel and lowest for Type 348 steel. Types 304 and 321 steels had essentially equivalent crack growth rates over the range investigated. At 800 F (427 C) differences in growth rates among the steels were noted, but these were smaller than at 1100 F (593 C).

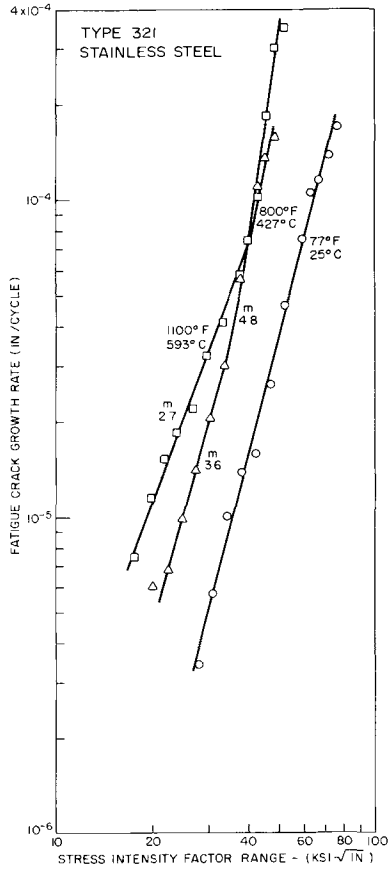


FIG. 3—*The dependence of fatigue crack growth rate in Type 321 stainless steel on stress intensity factor range.*

The extent to which crack growth differences among the steels tested at 1100 F (593 C) and 500-lb load were reflected in fatigue life is shown in Fig. 6. Type 348 steel had a fatigue life 3.4 times longer than Type 316 steel. Other data at a load of 700 lb at 1100 F (593 C) indicate the relative merit of Type 321 steel. At this load the cycles to failure for Types 316, 321, and 348 steels were 23 000, 48 000, and 75 000, respectively.

Discussion

Fatigue crack growth in metals at room temperature has been shown [*11–15*] to be dependent upon certain mechanical properties, such as yield strength and fracture toughness, but the findings have not been consistent. Usually appreciable changes in property were required to influence crack growth rates. In this study the essentially identical crack growth rates at

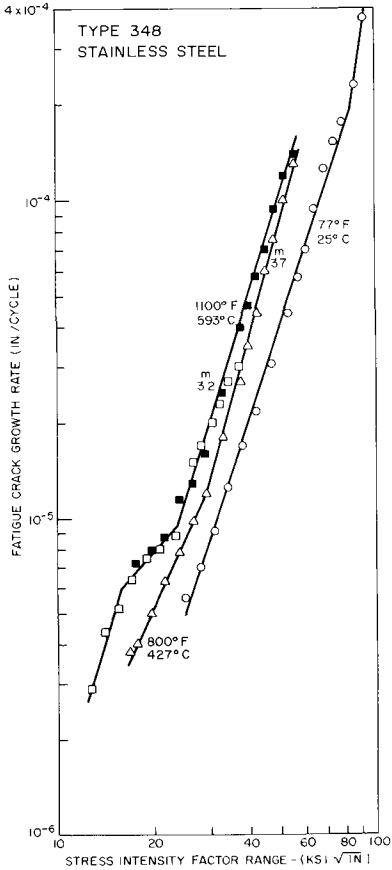


FIG. 4—*The dependence of fatigue crack growth rate in Type 348 stainless steel on stress intensity factor range. Closed symbols represent separate tests.*

room temperature of the 300 series stainless steels indicate an insensitivity to composition and mechanical property variations. However, it should be noted that the property variations were relatively small, being less than 50 percent, Table 2. In constrast, at 1100 F (593 C), crack growth in these steels was significantly influenced by the relatively minor differences in composition and properties. The relative order of the steels in increasing crack growth resistance is Types 316, 304, and 321, and 348. Type 348 steel was also found by Berling and Slot [*16*] to be superior to Types 304 and 316 steels on the basis of fatigue life at 1202 F (650 C). Further, the superiority in crack growth resistance of Type 304 steel over Type 316 steel is in agreement with the high-temperature results of James [*8*].

Examination of the plastic flow data, Table 2, shows that resistance to crack growth generally increases with increasing yield strength and decreasing strain hardening coefficient among the steels. The correspondence

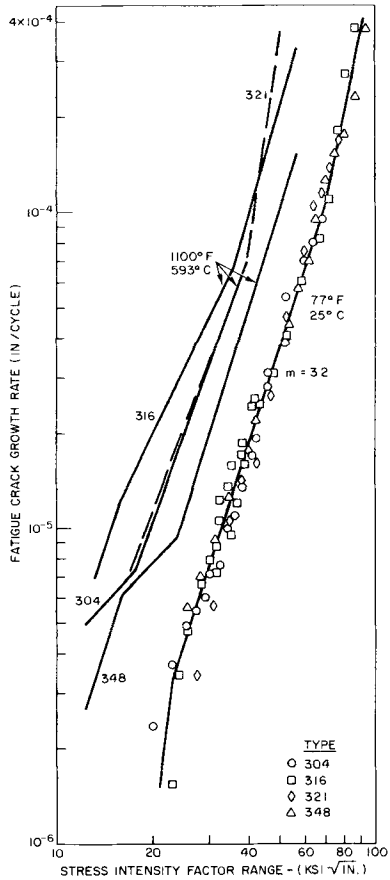


FIG. 5—*Fatigue crack growth rates in series 300 stainless steels at room temperature and 1100 F (593 C).*

of crack growth resistance with strain hardening coefficient was better than with yield strength. Although Types 304 and 321 stainless steels have the same resistance to crack growth, Type 304 steel has a lower yield strength. The power law exponent, m, at 1100 F (593 C) was about the same for each steel, being essentially independent of property variations with the exception that m was highest for the Type 348 steel.

The influence of temperature on the exponent m, which was a maximum at 800 F (427 C), does not correlate with its effect on other properties. Yield and ultimate strengths, of course, are inversely related to temperature and in this temperature range ductility also appears to be. A lack of direct dependence of m on yield strength was also observed by Miller [*12*] and Anctil and Kula [*15*] for tempered 4340 steel at low temperatures, but, in contrast to the stainless steel data, the m exponent for the alloy steel

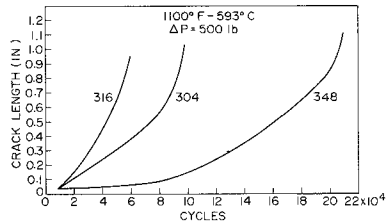


FIG. 6—*Fatigue crack growth curves of Types 304, 316, and 348 stainless steels at 1100 F (593 C).*

reached a minimum value at an intermediate yield strength. It is apparent that the exponent m is not dependent primarily upon yield strength, and its variation with temperature must be related to other properties.

The effect of temperature on crack growth is most likely related to a combination of properties, such as yield strength, strain hardening exponent, and Young's modulus, which control the size and properties of the plastic zone. Increases in growth rate in alloy steel with rising temperature have been correlated by McHenry [*3*] with increases in plastic zone size. In an earlier study [*7*], the variation of fatigue crack growth rates in Type 316 steel with temperature appeared to be related to Young's modulus, but it is evident from this study that other properties are involved. More data are needed for the analysis of behavior to evolve formulas which predict fatigue crack growth at high temperatures.

Summary

It has been shown that the fatigue crack growth rates of Types 304, 316, 321, and 348 stainless steels at high as well as room temperature are governed by the range of stress intensity factor. The characteristics of this dependence are similar for the four steels. An increase in temperature increases crack growth rates for a given ΔK and appears to reduce the threshold ΔK for crack growth. There is a distinct region of crack growth behavior (relatively low slope of da/dN versus ΔK curve) at high temperatures which is not present at room temperature. The power law exponent, m, is higher at 800 F (427 C) than at room temperature and 1100 F (593 C) and thus does not reflect the variation with temperature of a particular mechanical property.

At room temperature the rates of crack growth for a given ΔK were the same for all four steels over the intermediate growth rate region. However, at 1100 F (593 C) the growth rates were markedly different for the steels with Type 348 steel being the most resistant to crack growth and Type 316 steel being the least resistant. The sensitivity of crack growth at high temperature to relatively minor variations in composition and properties is also reflected, as expected, in fatigue life.

Acknowledgments

We appreciate the assistance of J. T. Atwell in the experimental work. The investigation was supported by the Office of Naval Research and the U. S. Atomic Energy Commission.

References

[1] Brothers, A. J., "Fatigue Crack Growth in Nuclear Reactor Piping Steels," GEAP-5607, General Electric Company, San Jose, Calif., March 1968.
[2] Clark, W. G., Jr., *Journal of Materials*, Vol. 6, No. 1, March 1971, pp. 134–149.
[3] McHenry, H. I., "Fatigue Crack Propagation in Steel Alloys at Elevated Temperature," ERR-FW-1029, General Dynamics Corp., Sept. 1970.
[4] Popp, H. G. and Coles, A., "Subscritical Crack Growth Criteria for Inconel 718 at Elevated Temperatures," *Proceedings*, Air Force Conference on Fatigue and Fracture of Aircraft Structures and Materials, AFFDL TR-70-144, 1970.
[5] James, L. A. and Schwenk, E. B., *Metallurgical Transactions*, Vol. 2, 1971, pp. 491–496.
[6] Shahinian, P., Smith H. H., and Watson, H. E., *Journal of Engineering for Industry*, Series B, *Transactions*, American Society of Mechanical Engineers, Vol. 93, No. 4, 1971, pp. 976–980.
[7] Shahinian, P., Watson, H. E., and Smith, H. H., *Journal of Materials*, Vol. 7, No. 4, Dec. 1972, pp. 527–535.
[8] James, L. A., "The Effect of Elevated Temperature upon the Fatigue-Crack Propagation Behavior of Two Austenitic Stainless Steels," presented at International Conference on Mechanical Behavior of Materials, Japan, Aug. 1971.
[9] Gross, B. and Srawley, J. E., "Stress-Intensity Factors for Single-Edge-Notch Specimens in Bending or Combined Bending and Tension by Boundary Collocation of a Stress Function," NASA-TN-D2603, National Aeronautics and Space Administration, Jan. 1965.
[10] Paris, P. C. and Erdogan, F., *Journal of Basic Engineering*, Series D, *Transactions*, American Society of Mechanical Engineers, Vol. 85, No. 4, Dec. 1963, pp. 528–534.
[11] Brothers, A. J. and Yukawa, S., *Journal of Basic Engineering*, Series D, *Transactions*, American Society of Mechanical Engineers, Vol. 89, No. 1, March 1967, pp. 19–27.
[12] Miller, G. A., *Transactions*, American Society for Metals, Vol. 61, 1968, pp. 442–448.
[13] Crooker, T. W. and Lange, E. A. in *Fatigue Crack Propagation*, *ASTM STP 415*, American Society for Testing and Materials, 1967, pp. 94–126.
[14] Throop, J. F. and Miller, G. A. in *Achievement of High Resistance in Metals and Alloys*, *ASTM STP 467*, American Society for Testing and Materials, 1970, pp. 154–168.
[15] Anctil, A. A. and Kula, E. B. in *Effects of Environment and Complex Load History on Fatigue Life*, *ASTM STP 462*, American Society for Testing and Materials, 1970, pp. 297–317.
[16] Berling, J. T. and Slot, T. in *Fatigue at High Temperature*, *ASTM STP 459*, American Society for Testing and Materials, 1969, pp. 3–30.

DISCUSSION

R. Pelloux[1] (*written discussion*)—Do you feel that the different segments of the crack growth rate curves ($da/dN - \Delta K$) represent significantly different phenomena? Or do they represent an expected scatter of the data?

P. Shahinian, H. H. Smith, and H. E. Watson (*authors' closure*)—The general form of the segmented curves of da/dN ΔK for materials at room temperature is well documented in the literature, and there is some understanding of the behavior. The additional segment observed in the elevated temperature curves and discussed specifically in the paper has appeared consistently enough that we do not believe it is due to data scatter. In the Type 348 steel data in Fig. 4, the overlapping data points for the two tests at 1100 F (different loads) would indicate that this characteristic segment represents basic behavior.

K. D. Challenger[2] (*written discussion*)—I agree with your statement that very small changes in chemical composition can significantly alter the mechanical behavior of these alloys. However, it is recognized widely that the elevated temperature properties of the austenitic stainless steels are very sensitive to their pretest condition—primarily heat treatment. For optimum strength it is necessary to solution the carbides completely (Type 347, CbC; Type 321, TiC; Types 304 and 316, $Cr_{23}C_6$) so that strain aging can occur during test. Were your specimens heat treated at temperatures sufficiently high to allow this strain aging to occur during test? If not, I do not believe your results are a fair representation of the individual alloy's relative behavior.

Messrs. Shahinian, Smith, and Watson—The steels were solution annealed at recommended temperatures, but we did not examine the microstructures to determine whether solution was incomplete. Although at this time we do not know the precise required temperatures, they appear to be sufficiently high except, perhaps, that for the Type 348 steel. If this steel, as a result, is below its optimum strength, a higher solution temperature would only increase its superiority over the other steels. We might add that the observed relative order of the steels on the basis of fatigue crack growth

[1] Massachusetts Institute of Technology, Cambridge, Mass. 02139.
[2] Materials development engineer, General Electric Co., San Jose, Calif. 95114.

resistance agrees with that based on fatigue resistances of solution annealed steels reported in the literature (see text), except for Type 321 steel for which no comparative data were found.

M. O. Speidel[3] *(written discussion)*—Your observation that fatigue crack growth at elevated temperatures is sensitive to minor changes in alloy composition (while at room temperature it is not) brings out just one more analogy between corrosion-fatigue crack growth and high-temperature fatigue crack growth. Indeed, these two groups of observations are very analogous because in both cases a time-dependent crack growth component is added to "pure" fatigue crack growth. I would like to suggest that a lot can be learned from a comparison of the phenomena of corrosion-fatigue and high-temperature fatigue. For example, the effect of stress intensity on frequency dependence of fatigue crack growth, which if known in many corrosion-fatigue crack growth situations, may be expected to be qualitatively similar in high-temperature fatigue.

Messrs. Shahinian, Smith, and Watson—Your idea is interesting, and we would like to suggest that consideration be given to the basic mechanisms responsible for the phenomena in making such comparisons.

[3] Brown Boveri Research Center, Baden, Switzerland.

D. H. Boone[1] *and C. P. Sullivan*[1]

Effect of Several Metallurgical Variables on the Thermal Fatigue Behavior of Superalloys

REFERENCE: Boone, D. H. and Sullivan, C. P., **"Effect of Several Metallurgical Variables on the Thermal Fatigue Behavior of Super-Alloys,"** *Fatigue at Elevated Temperatures, ASTM STP 520*, American Society for Testing and Materials, 1973, pp. 401–415.

ABSTRACT: The effect of several metallurgical variables on the thermal fatigue behavior of high-temperature materials systems was studied using a highly characterized high-velocity hot gas stream to produce a well-defined strain/temperature/time cycle. Metallurgical factors considered were: alloy compositions in both cast cobalt- and nickel-base superalloys, degree of microstructural refinement, grain orientation, effect of presence and morphology of carbides, surface/environmental interaction (surface stability), and protective coatings. The nickel-base alloys studied were superior or equivalent to the cobalt-base alloys when compared on uncoated and coated bases. Within a given alloy class the effect of alloy chemistry as it affects oxidation behavior was shown to be significant. On polycrystalline substrates, an inward type of diffusion aluminide coating improved fatigue performance, whereas an outward type was detrimental. "Overlay" coatings show a great deal of potential in providing an optimum in mechanical/protective response. Columnar-grained alloys when strained along the growth direction gave fatigue resistance superior to their polycrystalline counterparts. The importance of recognizing the unique compositional/microstructural/mechanical nature of a coating in achieving optimum thermal fatigue resistance for high-temperature materials systems is emphasized.

KEY WORDS: thermal fatigue, fatigue (materials), heat resistant alloys, cobalt alloys, nickel alloys, solidification, columnar structure, aluminides, coatings, covering, oxidation, carbides, grain size, cracking (fracturing), single crystals

Determination of the thermal fatigue behavior (low-cycle fatigue imposed over a temperature range) of cobalt- and nickel-base superalloys must be an integral portion of any material characterization program directed toward their use as airfoils in gas turbine engines. This understanding is essential from two viewpoints: (1) it enables development of a more effective predictive system for the response of present-day alloys and (2) only by having such knowledge can we hope to make substantial material improvements in a systematic fashion.

[1] Supervisor and assistant manager, respectively, Materials Engineering and Research Laboratory, Pratt & Whitney Aircraft, East Hartford, Conn. 06108.

Copyright© 1973 by ASTM International www.astm.org

It has sometimes been possible to successfully predict isothermal fatigue response by calculations involving so-called first tier properties such as yield strength and ductility [*1*].[2] This type of approach is expecially useful for cases where the maximum temperature is moderate, or the alloy is metallurgically simple or both. However, in the case of a gas turbine airfoil where a relatively complex superalloy is subjected to an involved strain/temperature/time cycle, further refinement in the predictive process is required. The use of testing techniques which permit the incorporation of such factors as the imposition of strain over a temperature range, creep-fatigue interaction, and holdtime effects is certainly critical to our understanding of the thermal fatigue problem. Equally important in this respect, and the concern of the present paper, is consideration of metallurgical factors such as grain size and orientation, alloy composition, presence and morphology of carbides, surface stability (alloy reaction with the atmosphere), and surface protection by coatings.

Uncoated Cast Cobalt-Base Superalloys

Some previous investigations [*2,3*] have suggested that cobalt-base superalloys generally possess thermal fatigue resistance superior to that of nickel-base superalloys. While many factors must be considered in alloy selection, it is our intent in the present discussion to address the question of thermal fatigue behavior, realizing that other criteria are of vital importance as well. In this section the relative ranking of the uncoated cast cobalt-base superalloys WI-52 and Mar-M302 (Table 1) will be examined, reserving any comparison to nickel-base superalloys for the section dealing with that alloy class.

It is important to realize that in addition to the effects of metallurgical variables, some of which will be discussed next, the type of test and thermal cycle employed are extremely critical to the relative rankings of alloys. Since the critical metallurgical variables, which are being examined here for their effects upon thermal fatigue, are temperature related, the exact strain/temperature cycle experienced in the thermal fatigue test is important in determining material behavior. Consequently, different behavior and ranking will be obtained with different test cycles. Unless otherwise specified, thermal cycles were generated by sequentially heating with a well-defined hot, high-velocity gas stream and cooling with a cold air jet. These conditions when coupled with our specimen design produced a controlled strain/temperature profile [*4*]. For the cobalt-base superalloys, Cycle A, having a calculated total strain range of about 0.35 percent with maximum and minimum temperatures of 1800 F (1255 K) and room temperature, respectively, was used. A peak strain in compression of about 0.2 percent at 1400 to 1600 F (1033 to 1144 K) occurred during the heating cycles while a maximum tensile strain of about 0.15 percent at 1200 F (922 K) resulted

[2] The italic numbers in brackets refer to the list of references appended to this paper.

TABLE 1—*Nominal composition of superalloys evaluated in program, weight percent.*

CAST COBALT-BASE ALLOYS

	Co	Cr	C	W	Fe	Cb	Ta	Zr
WI-52	balance	21.0	0.45	11.0	1.75	2.0	...	...
Mar-M302	balance	21.5	0.85	10.0	1.0	...	9.0	0.25

CAST NICKEL-BASE ALLOYS

	Ni	Cr	Co	Ti	Al	Mo	W	C	B	Ta	Zr	Y
Udimet 700	balance	15.0	15.3	3.4	4.3	4.4	...	0.07	0.02	...	...	...
B-1900	balance	8.0	10.0	1.0	6.0	6.0	...	0.11	0.015	4.3	0.07	...
Mar-M200	balance	9.0	10.0	2.0	5.0	...	12.5	0.15	0.015	1.0 Cb	0.05	...
Monaloy 350	balance	16.0	...	2.0	5.7	...	8.0	...	...	...	...	0.1

from the cooling cycle. The period of each cycle was 35 s, which included holdtime of 12 s, at 1800 F (1255 K).

Using WI-52 as a base, the degree of structural coarseness (grain size, dendrite size and spacing, carbide size) was varied by appropriate manipulation of casting conditions to produce three distinct polycrystalline grain structures. "Life" is defined as the approximate number of cycles to initiate a surface crack of about $^1/_{16}$ in. (1.6 mm) length, and generally represents the average of two or more tests. All failures were surface associated, as is the case for actual components. The test results are summarized in Table 2.

Cracking initiated at about 2000, 2500, and 5200 cycles with increasing structural coarseness. In all cases the initiation and propagation of cracking essentially took place in interdendritic regions often between grains, as shown in Fig. 1*a*. It appears that cracking occurred by a complex interplay of chemical and mechanical factors; a similar situation has been described for low-cycle fatigue cracking in cast Udimet 500 [*5*]. Additional details of the relationship between fatigue and environmental reactions have been recently published [*6*]. The improvement in WI-52 life with increasing grain size is not unexpected because there are fewer sites present for cracking as the structure becomes coarser. However, it should be pointed up that under other circumstances increasing grain size may lead to reduced life [*7*].

The use of directional solidification to produce a columnar-grained structure has been shown to markedly improve the thermal fatigue life of nickel-base superalloys [*8*]. Columnar-grained WI-52 remained uncracked after more than 10 000 cycles when strained along the growth direction.[3] This marked improvement can be attributed to: (1) lower modulus associated with the <100> primary dendrite growth direction which gives a reduced thermal stress and plastic strain for a given total strain range and (2) absence of grain boundaries perpendicular to the principal stress axis. Transcrystalline cracks in the material had a relatively blunt profile with attendant slow propagation due to both oxidation and lower stress (Fig. 1*b*). When tested transverse to its grain boundaries, fatigue life was comparable to the intermediate grain size polycrystalline material.

The effect of changing surface stability, and hence the propensity towards intergranular attack, was demonstrated using Mar-M302 which has greater surface stability than WI-52. The better fatigue life shown by Mar-M302 is felt to be related partly to this increased surface stability. Figure 2 illustrates the reason for the improvement; in contrast to WI-52 (Fig. 2*a*), Mar-M302 (Fig. 2*b*) did not show severe intergranular attack but rather a more uniformly broad attack. Metallurgically the improved oxidation resistance is related to differences in: compositions of matrix and carbide together with carbode morphology (discrete carbides in Mar-M302 versus interconnecting ones in WI-52).

[3] The 1800 F (1255 K) tensile and creep properties of polycrystalline and columnar-grained WI-52 are similar.

TABLE 2—*Effect of several metallurgical variables on cycles to initiate thermal fatigue cracking in superalloys.*

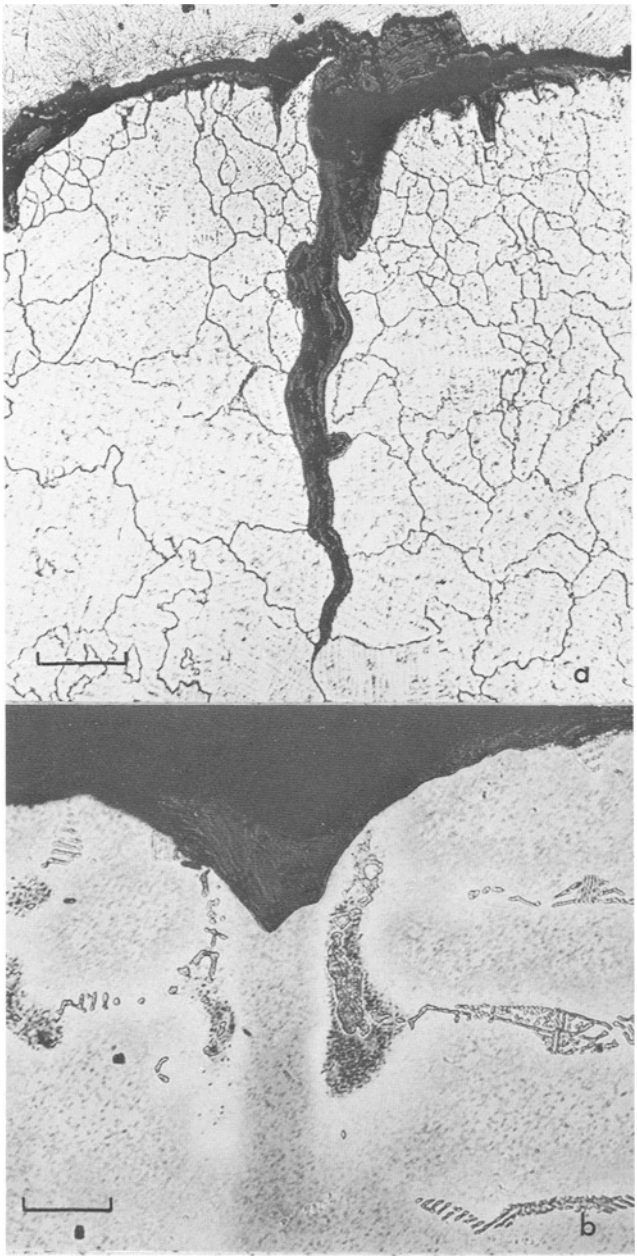
A. Cycle A, 1800 F (1255 K) max temperature, ~ 0.35% calculated total strain range

	WI-52					Mar-M302	U-700
	Polycrystalline			Columnar Grain		Polycrystalline	Polycrystalline
Grain size	fine	medium	coarse	longitudinal	transverse	medium	medium
Uncoated	2000	2 500	5200	14 000	3000	10 000	15 000
Aluminide coated (inward type), 0.002 in. (0.051 mm) thickness		>14 000		17 000		>14 000	>28 000[a]

B. Cycle B, 1900 F (1310 K) max temperature, ~ 0.45% calculated total strain range

	U-700	B-1900	Mar-M200				Monaloy 350
	Polycrystalline	Polycrystalline	Polycrystalline	Columnar Grain		Single Crystal	Single Crystal
Grain size	medium	medium	medium	longitudinal	transverse	...	...
Uncoated	1200	2500	1500	10 000	2000	10 000	13 000
Aluminide coated (inward type), 0.003 in. (0.076 mm) thickness	2000	4500	4500	6 000	4500		6 500
Aluminide coated (outward type), 0.0025 in. (0.064 mm) thickness	800	800		2 500			

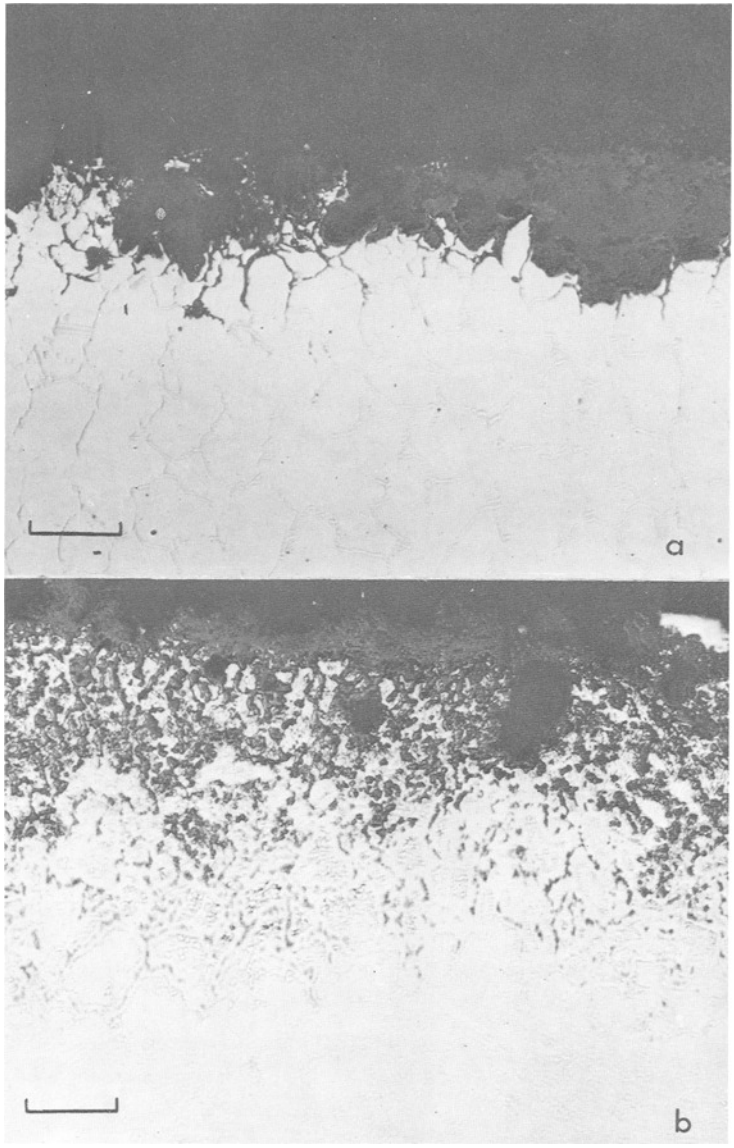
[a] Coating on U-700 0.003 in. (0.076 mm) thickness.



(*a*) Polycrystalline medium grain size WI-52, 3000 cycles.
(*b*) Columnar grain WI-52, 14 200 cycles.

(Scale mark indicates 25 μm).

FIG. 1—*Microstructures of thermal fatigue cracked* (*Cycle A*) *cast cobalt-base superalloys.*



(*a*) Interdendritic oxidation and cracking in WI-52.
(*b*) Uniform surface oxidation and absence of well-defined cracks in Mar-M302.

(Scale mark indicates 25 μm).

Fig. 2—*Microstructures of thermal fatigue cycled cast cobalt-base superalloys showing differences in type of surface attack.*

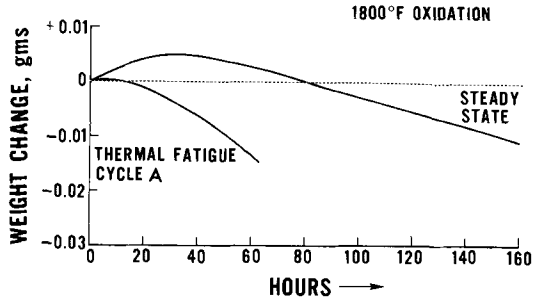


FIG. 3—*Oxidation weight change at 1800 F (1255 K) for WI-52 specimens showing effect of superimposed thermal stresses on oxidation behavior.*

It is pertinent to note how thermal fatigue cycling affects oxidation. Figure 3 compares the weight change for identical WI-52 specimens exposed to 1800 F (1255 K) gas temperatures in one of two ways: (1) steady state with periodic cooling only for weight measurements or (2) thermally fatigued as previously described. For the latter case, exposure time was taken as the cumulative sum of the 1800 F (1255 K) holdtimes of 12 s. Cyclic thermal straining leads to weight losses greater than observed with the more conventional oxidation test as a result of enhanced oxide spallation and increased surface area produced by cracking [*9*]. Generally this behavior would be expected to be observed within any given alloy system; however, the extent would depend on oxide adherence, the inherent thermal fatigue crack resistance of the material, and the specific thermal fatigue cycle employed.

Uncoated Coast Nickel-Base Superalloys

Alloys of higher strength can be utilized to improve response to thermal fatigue conditions provided this increase is not compromised by a marked deterioration in some other critical property such as ductility or oxidation resistance. If a material is cycled to temperatures over 2000 F (1365 K) with included periods of significant holdtime, then emphasis would be placed on a system with possibly lower intermediate temperature strength but a slower decrease in strength at the very high temperature end of the scale. However, if conditions are such that large strains are induced at intermediate temperatures and the maximum temperature is not extremely high [<2000 F (<1365K)], the metallurgical characteristics which are critical to performance at lower temperature are then of prime concern. These two cases identified as Type *II* cycles, are illustrated schematically in Fig. 4*a* and *b*.[4] In Fig. 4*d* alloy X corresponds to a nickel-base superalloy [*10*] and alloy Y to a cobalt-base superalloy [*11*]. Generally it would be

[4] A more detailed discussion of effects of cycle shape is covered in a separate paper presented at this conference by C. A. Rau, Jr., A. Gemma, and G. R. Leverant.

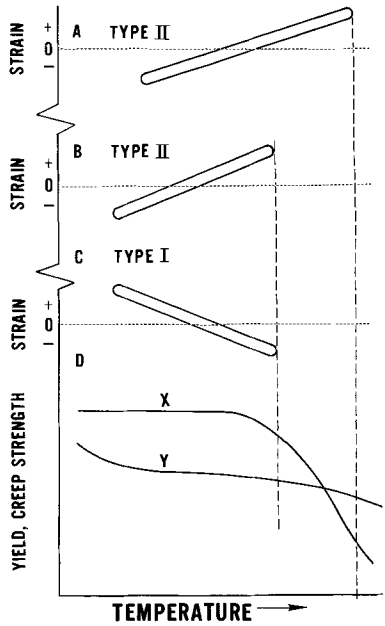


FIG. 4—*Schematic representation of strength versus temperature dependence for a cobalt-* (Y) *and nickel-base* (X) *superalloy in relationship to typical strain/temperature cycles.*

expected that the potent γ' phase strengthening of the former type alloy provides superior thermal fatigue resistance at least throughout the temperature range below the γ' solvus.

The cast nickel-base superalloys studies were Udimet 700, B-1900, Mar-M200, and Monaloy 350 (Table 1). Under Cycle A conditions, Udimet 700 had a life of 15 000 cycles, greater than either of the cobalt-base alloys in any structural condition. Thus, the supposition regarding the superiority of a stronger alloy in the type of test employed in our investigation seems reasonable. Also, to reduce testing time for nickel-base superalloys, a cycle with the same period and holdtime but with more stringent conditions was provided (Cycle B) by an increase in maximum temperature to 1900 F (1310 K), together with a specimen redesign which produced a calculated total strain range of about 0.45 percent; an about 0.25 percent peak compressive strain at 1800 F (1255 K) occurring on heatup, and an about 0.20 percent tensile strain maximum at 1600 F (1144 K) occurring during the cooling cycle.

Using Cycle B it was found that fatigue life in conventionally cast material increased in going from Udimet 700 to B-1900 with Mar-M200 life being similar to Udimet 700. The alloy B-1900 is stronger than Udimet 700 and possesses somewhat better oxidation resistance; hence, its ranking is consistent. Although Mar-M200 is stronger than B-1900, its oxidation re-

sistance and ductility are not as good, thus offsetting the gain is strength. The longitudinal fatigue life of columnar-grained Mar-M200 was superior to all three polycrystalline alloys for the reasons previously given, while transverse life was comparable to polycrystalline Mar-M200.

Use of the single crystalline form of Mar-M200 gave no improvement over the longitudinal properties of columnar-grain material, but the complete absence of grain boundaries will provide a greater isotropy of fatigue resistance. However, by eliminating carbides which can act as crack initiation sites either due to selective oxidation or stress concentration (carbon is no longer required for boundary strengthening), the isothermal low-cycle fatigue life of uniformly loaded single crystals is increased. Some improvement would be expected in thermal fatigue as well.

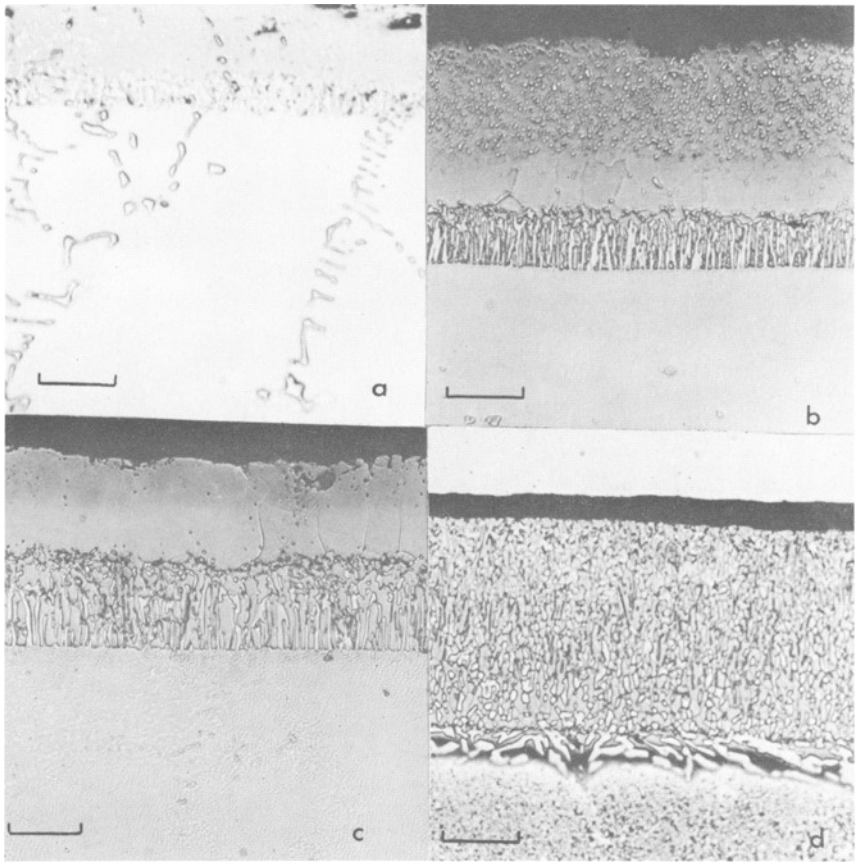
Although not as strong as its Mar-M200 single crystal counterpart, Monaloy 350 [*12*] in single crystal form displayed a superior fatigue life. This carbon-free alloy has been formulated to produce excellent surface stability resulting from the formation of an adherent alumina layer when exposed to elevated temperatures [*13*]; the Mar-M200 chemistry, on the other hand, does not lead to this desirable condition, and furthermore, the presence of carbides provides an additional source of crack initiation sites.

Protective Coatings

The importance of oxidation environmental interaction on the fatigue behavior of cobalt- and nickel-base superalloys has been emphasized in the preceding discussion.[5] The use of diffusion aluminide protective coating systems on superalloys in gas turbines has become quite widespread as a result of increasing cycle temperatures. It is, therefore, essential to examine critically the effect of such coatings on mechanical behavior.

Information has become available in recent years on protective coatings concerning formation mechanisms, microstructure, oxidation behavior, and methods of application [*15*]. However, meager data have been published concerning the effect of potentially critical coating structural and compositional features on mechanical properties. In this investigation the previously studied cobalt-and nickel-base superalloys were coated using an "inward" diffusion aluminide type coating containing 27 weight percent aluminum (Fig. 5*a* and *b*, respectively) with respective thicknesses of 0.002 in. (0.051 mm) and 0.003 in. (0.076 mm). The thermal fatigue behavior was determined using the same procedures outlined previously. Test results are included in Table 2.

[5] In the present paper only oxidation attack has been considered. Greater effects on behavior would result under the more severe conditions produced by the presence of sulfur and seawater, generally referred to as hot corrosion or sulfidation. Furthermore, the emphasis in oxidation has been on processes which produce a visible attack, but it is known that dissolved oxygen in conjunction with stress can produce an almost instantaneous intergranular embrittlement in some nickel-base superalloy [*14*]. Thus, a coating may be also beneficial because it effectively seals off the substrate.



(*a*) Inward type aluminide coating on WI-52.
(*b*) Three-zone inward type aluminide coating on B-1900.
(*c*) Two-zone outward type aluminide coating on B-1900.
(*d*) Vapor deposition overlay type coating on B-1900.

(Scale mark indicates 25 μm).

FIG. 5—*Microstructures of typical protective coatings.*

For polycrystalline WI-52 and Mar-M302 and the longitudinal directionally solidified WI-52, the protective coating increased cycles to cracking, thereby demonstrating its critical effect on performance. Cracks in coated specimens tended to be sharp and straight, rather than broad and rounded in contrast to uncoated material, indicating that oxidative processes played less of a role in cracking the coating than the substrate.

From Table 2 it can be seen that a coating improves the lives of both polycrystalline Udimet 700 and B-1900, and furthermore, that the improvement was greater for the latter alloy. These results are again indicative of

the beneficial effect of a coating. As a first approximation, one may consider the formation of an inward aluminide coating as the making of a high aluminum polycrystalline alloy which inherits some of the chemical and microstructural characteristics of the substrate. As such it possesses a unique set of properties which are influenced to some degree by the mechanical behavior of the underlying substrate. The objective in coating design, therefore, should be to provide the ultimate in atmospheric protection with the best possible mechanical properties.

Both polycrystalline and transverse columnar-grained Mar-M200 (Table 2) were improved to the same level by coating; this behavior would be anticipated from the fact that they are essentially identical. It is further noted that coated polycrystalline B-1900 and Mar-M200 lives were also identical, possibly because the greater substrate strength of the latter was not compromised to as great a degree by its poorer oxidation resistance when coated. Coating of longitudinal columnar-grained Mar-M200 reduced its life, but not to that of the polycrystalline or transverse material. The reduction occurs because the polycrystalline coating mechanical properties become dominant;[6] however, the lower modulus of the substrate still provides some benefit. Single crystals of Monaloy 350 also displayed a reduced life when coated, similar to that for coated longitudinal columnar-grained Mar-M200, possibly due to an offsetting of the superior Monaloy 350 oxidation resistance by the higher Mar-M200 strength, that is, substrate mechanical properties are dominant. On the other hand, coating of longitudinal columnar-grained material can increase life as evidenced by WI-52. Because the columnar-grained cobalt-base superalloy is weaker than its nickel-base counterpart the coating mechanical properties are of less importance.[7] Furthermore, it should be noted that ranking in this study is based on crack initiation, but that propagation is much retarded in a columnar-grained substrate under strain controlled conditions.[8]

Two basic types of aluminide coatings can be formed on nickel-base superalloys: three-zone inward (Fig. 5*b*) and two-zone outward (Fig. 5*c*) [*17*]. A comparison was made between thermal fatigue lifetimes of these two coating structures on polycrystalline Udimet 700 and B-1900 (Table 2). It appears, for these two alloys at least, that the fine grain size alloyed surface layer of the inward coating provides more fatigue resistance than the coarse grained almost pure NiAl (B) surface layer of the outward coating [*18*]. It should be noted that the surface layer of the latter type coating is columnar like, thus presenting relatively long transverse grain boundaries to the stress axis during cycling. The identical lives for outward coated

[6] Coatings are polycrystalline regardless of the grain structure of the substrate.

[7] It is interesting to note that the results of a separate investigation on superalloys using a fluidized bed technique confirm the beneficial effects of both coatings and columnar-grained structures, together with the fact that the combination is not simply additive [*16*].

[8] Rau, C. A., Jr., Pratt & Whitney Aircraft, unpublished research.

Udimet 700 and B-1900 may result from the fact that this type of coating is essentially pure NaAl (B) in both cases and thus largely substrate independent. The life of outward coated longitudinal columnar-grained Mar-M200 is also reduced compared to inward coating but not to the level of the outward coated polycrystalline materials; this effect can be explained by the lower modulus of the substrate in the former case. On other alloy other substrates, the use of the inward type of coating which incorporates substrate phases, such as carbides, may cause a reversal of ranking of these two coating types if such phases are very effective crack initiation sites.

It can be readily appreciated from the previous data that the optimization of coating performance requires as thorough an understanding of a coating as of an alloy. As a further example, it has been shown that aluminide coating exhibit a brittle-ductile transition temperature over the range of 1100 to 1300 F (865 to 975 K) which is dependent upon aluminum content [*15*]. Thus if a thermal cycle, identified as Type I in the schematic of Fig. 4*c*, involves a peaking of tensile strain below the transition, coating cracking can occur on the first cycle. Changes in test conditions, therefore, can result in radical shifts in fatigue behavior demonstrating the critical need for the careful definition and control of testing procedure.

While the use of aluminide coatings can be optimized by thorough characterization, they are limited by the very nature of the processes involved in their formation. Recent work at Pratt & Whitney Aircraft on protective coatings applied by vapor deposition techniques (Fig. 5*d*) has shown great potential for circumventing this situation. The composition and structure of these new "overlay" type coatings can be controlled independently of the substrate and yet be compatible with it. In this way the coating can be tailored both for the required environmental protection and for improved fatigue properties as well. For example, polycrystalline B-1900 has been isothermally cycled at both 600 and 1200 F (590 and 920 K) at a total strain range of about 0.3 percent. The number of cycles to initiate cracking was increased markedly by using an overlay coating rather than an inward aluminide type. The implication of this result with regard to columnar-grained material is clear. Further improvements in thermal fatigue behavior of coated superalloys will involve the consideration of the coating and the substrate as a system with greater attention being paid to the properties of the coating than has been the case previously.

Summary

If materials are to be ranked meaningfully with respect to their thermal fatigue resistance, the cycle(s) chosen must be relevant to the intended application and then carefully controlled. In the case of the thermal fatigue cycle used in this investigation, uncoated cast nickel-base superalloys have been shown to be superior to uncoated cast cobalt-base superalloys. In

addition to the importance of first tier properties such as strength and ductility, characteristics such as structural coarseness, surface stability, grain shape, and phase morphology must be taken into account also. Application of a protective coating can produce marked increases in fatigue life, but careful consideration of the mechanisms of the coating process, interdiffusion with the substrate, and the mechanical characteristics of the coating must be undertaken to realize the fullest potential of the substrate/coating system. The introduction of overlay coatings has now provided the metallurgist with a new degree of freedom in his quest for increased systems performance in high-temperature materials.

References

[1] Manson, S. S., *International Journal of Fracture Mechanics*, Vol. 2, 1966, pp. 327–363.

[2] Fritzlen, G. A. in *High-Temperature Materials*, R. F. Hehemann and G. M. Ault, eds., Wiley, New York, 1959, pp. 56–80.

[3] Sharp, W. H., in *High-Temperature Materials II*, G. M. Ault, W. F. Barclay, and H. P. Munger, eds., Wiley, New York, 1963, pp. 189–213.

[4] Tschinkel, J. G. and Ryan, E. J., "Thermal Fatigue Test Methods Using a Flame Jet (ESOT-METHOD)," MERL Report No. 71-017, Pratt & Whitney Aircraft, Dec. 1971.

[5] McMahon, C. J. and Coffin, L. F., Jr., *Metallurgical Transactions*, Vol. 1, 1970, pp. 3443–3450.

[6] Pettit, F. S. and Tien, J. K., "Hot Gas Environment—Alloy Reactions and Their Relation to Fatigue," *Proceedings*, International Conference on Corrosion Fatigue, Storrs, Conn., June 1971, to be published.

[7] Gell, M., Leverant, G. R., and Wells, C. H. in *Achievement of High Fatigue Resistance in Metals and Alloys, ASTM STP 467*, American Society for Testing and Materials, 1969, pp. 113–153.

[8] VerSnyder, F. L. and Shank, M. E., *Materials Science and Engineering*, Vol. 6, 1970, pp. 213–247.

[9] Deadmore, D. L., "Observations on the Cyclic and Isothermal Oxidation of WI-52 and IN-100," NASA Technical Memorandum X-2195, National Aeronautics and Space Administration, March 1971.

[10] Sims, C. T., *Journal of Metals*, Vol. 18, 1966, pp. 1119–1130.

[11] Sims, C. T., *Journal of Metals*, Vol. 21, 1969, pp. 27–42.

[12] Boone, D. H., Duhl, D. N., and Goward, G. W., German Offen 1,928,509, 1969.

[13] VerSnyder, F. L. in *Proceedings*, Second International Conference on the Strength of Metals, Vol. III, 1970, pp. 1013–1027.

[14] Prager, M. and Sines, G., *Transactions*, Series D, American Society of Mechanical Engineers, *Journal of Basic Engineering*, Vol. 93, 1971, pp. 225–230.

[15] Goward, G. W., *Journal of Metals*, Vol. 22, 1970, pp. 31–39.

[16] Howes, M. A. H., "Thermal Fatigue Data on 15 Nickel- and Cobalt-Base Alloys," NASA Final Report CR-72738, National Aeronautics and Space Administration, IITRI-B6078-38, 1970.

[17] Goward, G. W. and Boone, D. H., *Oxidation of Metals*, Vol. 3, 1971, pp. 475–495.

[18] Anderson, P. J., Boone, D. H., and Paskiet, G. F., "A Comparison of the Effect of Inward and Outward Diffusion Aluminide Coatings on the Fatigue Behavior of Nickel-Base Superalloys," accepted for publication in *Oxidation of Metals*.

DISCUSSION

L. A. Johnson[1] *(written discussion)*—Do you have any results to report on the "overlay" coatings? Under what cycle conditions are they better than the aluminide coatings? What was the composition of the overlay coatings?

D. H. Boone and C. P. Sullivan (authors' closure)—The use of overlay coatings allows the metallurgist to design coating systems that are independent of substrate composition and phases. As noted in the paper and elsewhere [*17*], aluminum coatings have a ductile brittle transition temperature (DBTT). Therefore, under specific thermal fatigue cycles which peak the tensile strain below the DBTT, aluminide coatings would be expected to have reduced lives. Overlay coatings designed for greater low temperature ductility as well as oxidation resistance would be expected to and do have improved fatigue lifetimes. Specific amounts of improvement, of course depend upon specific strain-temperature cycle,[2] substrate, etc. so exact numbers are of little value. Exact overlay compositions are then selected for specific requirements of both fatigue lifetime and oxidation/corrosion resistance.

[1] Schenectady, N. Y. 12301.
[2] Rau et al, pp. 166–178.

D. F. Mowbray,[1] *D. A. Woodford,*[2] *and D. E. Brandt*[1]

Thermal Fatigue Characterization of Cast Cobalt and Nickel-Base Superalloys

REFERENCE: Mowbray, D. F., Woodford, D. A., and Brandt, D. E., "**Thermal Fatigue Characterization of Cast Cobalt and Nickel-Base Superalloys,**" *Fatigue at Elevated Temperatures, ASTM STP 520,* American Society for Testing and Materials, 1973, pp. 416–426.

ABSTRACT: Tapered disk thermal fatigue tests have been conducted on one cobalt- and one nickel-base superalloy for the purpose of characterizing crack growth behavior. It is shown that linear elastic fracture mechanics can be used to represent the crack growth rate data, and that the propagation mode prefers favorably-oriented carbides.

KEY WORD: fatigue (materials), fatigue tests, superalloys, nickel containing alloys, cobalt containing alloys, fracturing, crack propagation, cyclic loads

Competitive pressures are imposed upon bucket and stator vane designers to increase cycle efficiency and time between overhaul. These pressures require a rigorous understanding of the behavior of materials when subjected to the complex cyclic loading conditions found in the modern industrial gas turbine. This paper reports results obtained in a study of one aspect of this problem, namely, thermal fatigue crack propagation. The program has characterized and evaluated the behavior of cast cobalt- and nickel-base superalloys under thermal fatigue conditions similar to those found in the trailing edges of bucket and stator vanes. Testing was conducted on tapered disk specimens using the hot and cold fluidized bath technique originally proposed by Glenny et al [*1*].[3]

Test Program

The test materials were the cobalt-base alloy FSX-414 [*2*] and the nickel-base alloy René 77 [*3*]. These were procured as cast-to-size specimen

[1] Manager, Mechanics of Materials, and manager, Structural Materials Engineering, respectively, Gas Turbine Products Division, General Electric Company, Schenectady, N. Y. 12345.

[2] Senior metallurgical engineer, Materials and Processes Laboratory, General Electric Company, Schenectady, N. Y. 12345.

[3] The italic numbers in brackets refer to the list of references appended to this paper.

Copyright© 1973 by ASTM International www.astm.org

blanks and tested with standard heat treatments for these alloys [*2,3*]. Chemical compositions for the test materials are given next. Some standard mechanical properties are listed in Table 1.

Material	Co	Ni	Fe	Cr	W	Mo	Al
FSX-414	balance	10.4	0.7	29.3	7.2	...	...
René 77	14.5	balance	0.15	14.7	...	4.24	4.20

Material	Mn	Si	Ti	C	B	S
FSX-414	0.77	0.82	...	0.23	0.008	0.009
René 77	<0.1	<0.1	3.48	0.07	0.015	0.003

The test specimen employed was 1.5 times the overall diameter and thickness of the standard tapered disk dimensions given in Ref *1*; diameter = 2.4 in. and center thickness = 0.41 in. A fourfold variation in peripheral radius (R_p = 0.01, 0.02, 0.03, and 0.04 in.) was incorporated as the means of achieving a variation in cyclic strain range for fixed temperature limits. Also, two diametrically opposite, 0.05-in.-deep V-notches were included for the purpose of acting as crack starters.

The disk specimens were subjected to alternate heating and cooling shocks by transferring them between hot and cold fluidized baths of Al_2O_3. The test equipment was similar to that employed by several other investigators [*1,4*]. For the test results reported here, hot and cold bath temperatures were maintained at 1688 and 70 F, respectively. Exposure times in each bath were 4 min.

The procedure for determining crack growth rates involved removing the specimens from the test rig at predetermined intervals of cycles, and using a microscope to measure the length of cracks emanating from the notches. Standard procedure included testing one specimen of each peripheral radius for each material. Values of crack length reported represent the average of four readings, two from each face at each notch.

Test Results and Analysis of Data

Examples of the crack growth data obtained are shown in Fig. 1 for the FSX-414 alloy, on coordinates of crack length (a) and number of cycles (N). The data illustrate that cracks initiate at the notches within the first few shock cycles, propagate with an increasing growth rate to lengths of about 0.10 in., where they begin an essentially constant growth rate to lengths about 0.30 in. Although most tests were stopped at lengths close to 0.25 in., tests carried further show that a decreasing growth rate begins around 0.30 in. Note that the data in Fig. 1 exhibit the expected trend with respect to

TABLE 1—*Mechanical properties.*

Temperature, deg F	FSX-414						René 77					
	Tensile			Rupture			Tensile			Rupture		
	Tensile Strength, ksi	0.2% Yield Strength, ksi	Reduction of Area, %	σ, ksi	t_R h	Reduction of Area, %	Tensile Strength, ksi	0.2% Yield Strength, ksi	Reduction of Area, %	σ, ksi	t_R h	Reduction of Area, %
80	106	60	18	...	...	...	153	122	15	...	...	...
800	86	41	18	...	...	...	148	119	12	...	...	...
1000	79	36	19	...	...	...	145	118	12	...	...	...
1200	74	33	21	...	...	...	143	114	13	...	...	...
1400	65	31	23	...	...	...	127	106	14	...	...	...
1600	45	30	28	...	...	...	96	87	17	...	...	...
1800	...	...	...	4.5	1870	4	...	...	...	22	32	14.5

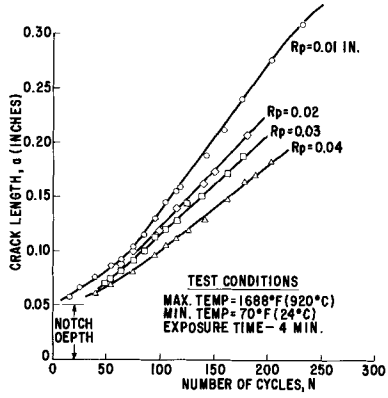


FIG. 1—*Crack growth data for FSX-414.*

peripheral radius, in that the lower the value of R_p, the greater is the crack growth rate.

A method is desired for correlating the crack growth rate data (Fig. 1) such that they can be used to predict growth rates in actual hardware via an appropriate stress analysis. One method presently available which lends itself to such a correlation is that of linear elastic fracture mechanics (LEFM) [5]. The basic premise of this method is that the rate of propagation of fatigue cracks is controlled by the elastically calculated stress intensity factor. Elastic analysis may not at first seem reasonable for this problem because of probable plastic action at the disk periphery [6]. However, as will be shown, there are rapidly decreasing radial stress gradients present which require the cracks to propagate through an essentially elastic stress field.

To our knowledge there is no published information available on the application of LEFM to thermal fatigue crack propagation in disk specimens, and no stress intensity factor solutions available for the present loading and crack geometry. Solutions, therefore, were developed for the stress intensity factors from an existing general method. These are at present approximate solutions, limited to short cracks, less than about 0.30 in. (<25 percent of the overall disk radius). The following assumptions were made in addition to the conventional assumption of LEFM:

1. The temperature field is not disturbed by the presence of the cracks.
2. The hoop stress is uniform through the thickness of the disk in the short crack length range.
3. Cracks of length less than 0.30 in. are equivalent to edge cracks in a semi-infinite body.

The first assumption is necessary for determining stress intensity factors in thermal problems [7] and should be valid. Our stress analysis of the disk

indicated that the second assumption is reasonable. Assumption 3 is not necessary, in general, but made here because it allowed for the construction of approximate stress intensity factor solutions.

A stress analysis of the disk specimen was made using the finite element method [*8*]. Stress field solutions were obtained at the times in the temperature transients when the absolute value of the difference between the peripheral temperature and volume average temperature was a maximum. The respective temperature fields for these times were calculated using a compatible finite element heat transfer program. Both the stress and temperature analyses employed axisymmetric assumptions.

With respect to fatigue crack propagation, the hoop stress provides the driving force. The calculated hoop stress distributions across the specimen midplane are illustrated in Fig. 2 for the times when the difference between peripheral and volume average temperature was a maximum. Peripheral temperatures (T_p) at these times are included in Fig. 2. The hoop stresses possess strong radial gradients, with the peak values occurring at the periphery. The larger the peripheral radius, the lower is the peak value and the milder the gradient.

The solutions for stress intensity factors were constructed by using a weight function method due to Bueckner [*9*]. This method provides the following expression for the opening mode stress intensity factor (K_I):

$$K_I = \sqrt{(2/\pi)} \int_0^a p(x)m(x)dx \quad \ldots\ldots\ldots\ldots\ldots\ldots (1)$$

$p(x)$ is a function representing the stress distribution normal to the crack faces in the *absence of the crack*, and $m(x)$ is a weight function. For an edge crack, the weight function is given by Bueckner as

$$m(x) = (1/\sqrt{x})[1.0 + 0.615\,(x/a) + 0.25\,(x/a)^2] \quad \ldots\ldots\ldots (2)$$

For the present case the stress distributions were represented by second order polynomials,

$$p(x) = C_0 + C_1(x/a) + C_2(x/a)^2 \quad \ldots\ldots\ldots\ldots\ldots (3)$$

$$\left.\begin{aligned} C_0 &= \sigma_0 \\ C_1 &= 4\sigma_1 - \sigma_2 - 3\sigma_0 \\ C_2 &= 2\sigma_2 + 2\sigma_0 - 4\sigma_1 \end{aligned}\right\} \quad \ldots\ldots\ldots\ldots\ldots\ldots (4)$$

σ_0, σ_1, and σ_2 are hoop stress levels corresponding to the tip, midpoint and end positions of the crack. Substitution of Eqs 2 and 3 in Eq 1 yields the following expression for K_I:

$$K_I = \sqrt{a}\,(0.655\,\sigma_0 + 1.126\,\sigma_1 + 0.222\,\sigma_2) \quad \ldots\ldots\ldots (5)$$

Equation 5 was used in conjunction with the stress distributions plotted in Fig. 2 to construct curves of ΔK_I versus a, where ΔK_I is the alternating range

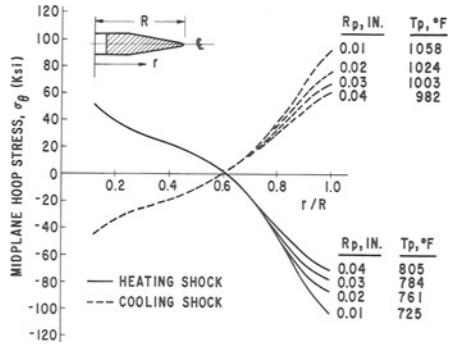


FIG. 2—*Elastically calculated hoop stress distributions in disk specimen at time of maximum thermal stress.*

of K_I. The curves are shown in Fig. 3. Although it is difficult to estimate the accuracy of these results due to the assumptions made, it is noted that the curves are at least qualitatively correct. For example, starting at the shortest crack lengths, ΔK_I increases with increasing crack length, until achieving a relatively constant value, and then decreases at the longer crack lengths. This duplicates the trends exhibited by the crack growth rates (for example, the $R_p = 0.01$ in. curve in Fig. 1). Also, the spacing between the ΔK_I curves is nearly in proportion to the differences in crack growth rates obtained for the different peripheral radii.

Crack growth rates (da/dN) in the 0.10 to 0.30 in. range of crack length were determined for each specimen tested at 1688 F, by first fitting polynomials to the growth curves and then differentiating the resultant polynomials. Results obtained by applying Eq 5 to the data are shown in Fig. 4. A fairly good correlation results for both materials. Although there is scatter present, there does not appear to be any special ordering effect according to peripheral radius. Hence, the scatter present is considered

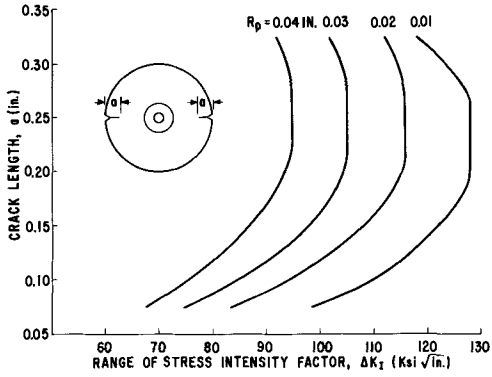


FIG. 3—*Stress intensity factor—crack length relationship for disk specimens.*

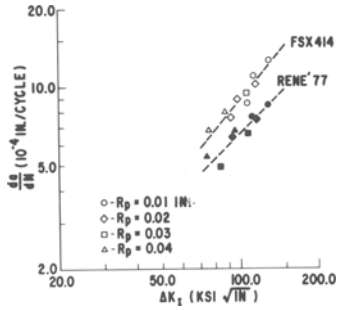


FIG. 4—*Fracture mechanics correlation of crack growth rate data.*

inherent to the test procedure and materials. The curves in Fig. 4 provide a very clear ranking of the materials.

Microstructural Features of Cracking

The objective of the microstructural study was to describe the cracking mode and the detailed characteristics of the morphology of cracking to identify the important structural features. Representative specimens from each alloy were ground to the approximate midplane and examined by optical microscopy.

FSX-414

Considerable crack branching and secondary cracking was apparent as shown in Fig. 5 which also demonstrates that cracking proceeds along networks of $M_{23}C_6$ carbides. The cracks appear to start by interface splitting at the carbide particles. Subsequently, voids form generally on one side of the carbide colony and eventually link up to form a crack. In Fig. 5*b* the main crack has traversed a portion of matrix to join up with a cracked carbide colony. However, an easy path for continued propagation is not available, and secondary cracking on the left of the micrograph has advanced beyond the main crack. It appears that cracking proceeds along favorably oriented carbides. If a grain boundary is aligned parallel to the direction of crack propagation, this may be the preferred path. But a crack encountering a grain boundary which is steeply inclined to the direction of crack propagation will traverse the matrix between the most favorably oriented carbide colonies within the grain. This accounts for the extensive crack branching and secondary cracking.

René 77

In this alloy the grains have good contrast, and Fig. 6 indicates that the crack shows no special preference for grain boundaries. The tip of the

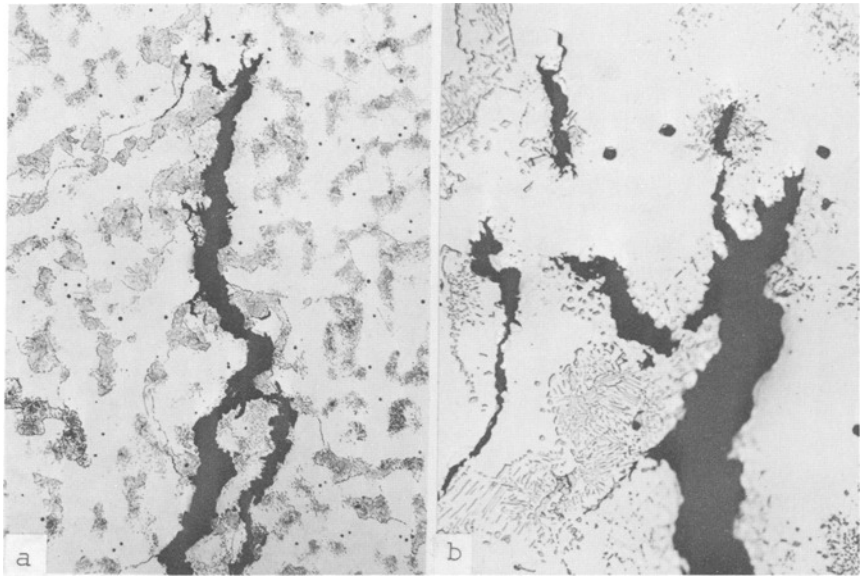


FIG. 5—*Propagation between colonies of* $M_{23}C_6$ *carbide in FSX-414 showing appreciable secondary cracking* (a) $\times 125$ (b) $\times 500$.

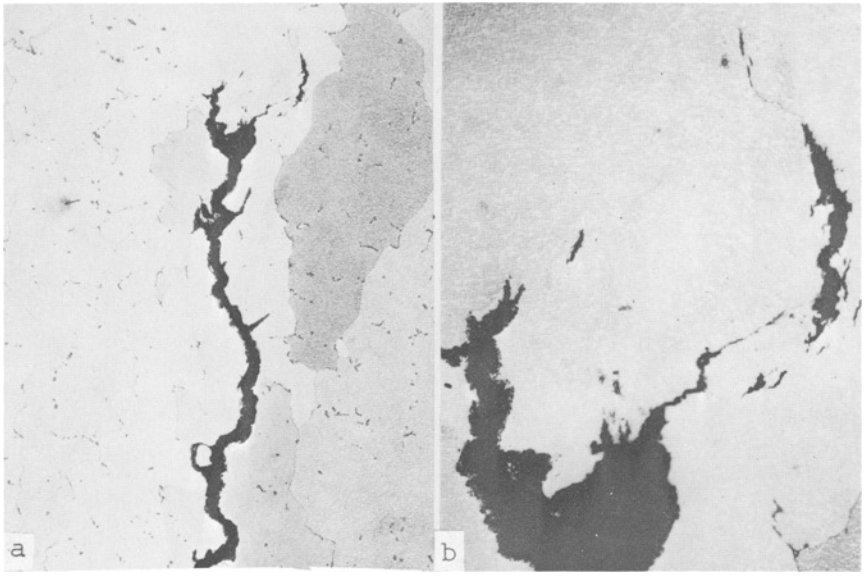


FIG. 6—*Crack-tip details in U-700 showing essentially transgranular mode* (a) $\times 125$ *and* (*b*) $\times 500$.

crack in Fig. 6*b* is branching to find a path between carbides across a large grain. This contrasts with the findings of Wells and Sullivan [*10*] of mainly intergranular cracking in low-cycle fatigue tests at 1700 F on this alloy. No evidence of carbide cracking was reported in their study. The small section size of the specimen is probably responsible for the fairly regular dispersion of what appears to be MC carbide within the material. In larger section sizes the carbides may be concentrated at the grain boundaries.

Effect of Directional Solidification

Observation of small initiating cracks around the specimen pheriphery suggests that grain boundary cracking is preferred for initiation but for propagation the cracks may be either transgranular or intergranular. However, the cracks always appear to grow between favorably oriented carbides to maintain radical crack propagation. This suggests that a directionally solidified structure with both the grains and carbides aligned perpendicular to the crack growth direction should inhibit both initiation and propagation.

The alloy FSX-414 was tested in the conventionally cast (CC) and directionally solidified (DS) condition followed by the regular heat treatment. For this experiment the specimens were in the form of rectangular wedges. Figure 7 compares the cracks after 400 cycles. In the CC condition a number of long cracks regularly spaced along the thin edge of the wedge had initiated at grain boundaries. Figure 7*a* shows one such crack which becomes transgranular after encountering an unfavorably aligned grain boundary. Secondary cracking mainly follows the grain boundaries. In all cases the cracks proceed along carbide networks. Figure 7*b* shows in the

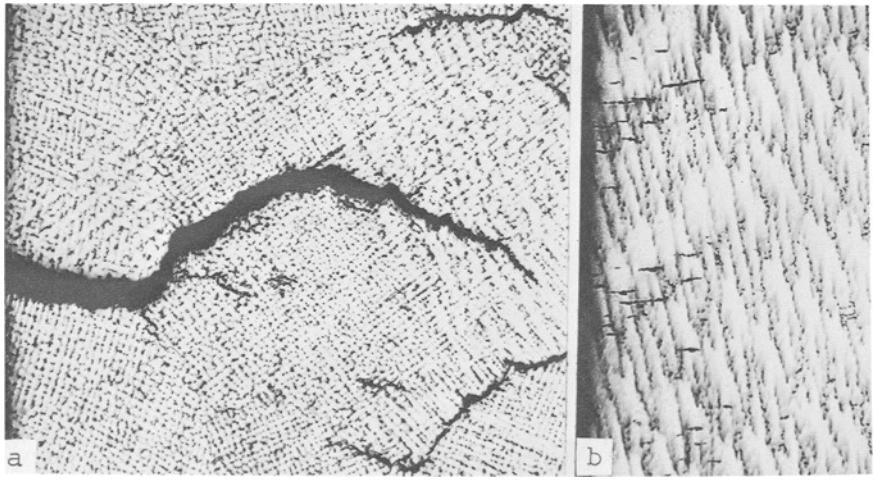


FIG. 7—*Comparison of fatigue crack morphology between* (a) *conventional cast and* (b) *directionally solidified FSX-414 after 400 cycles* (×*12*).

DS condition the many small cracks observed and suggests that the aligned carbides act as crack arresters. At higher magnification the crack segments were seen to have crystallographic facets. It may be that this is influenced by the apparent fine scale precipate on slip planes.

Summary

It has been shown that linear elastic fracture mechanics can be used to characterize thermal fatigue crack propagation and that this propagation prefers favorably oriented carbide networks in the alloys. Directional solidification imparts a considerable improvement in resistance to thermal fatigue.

References

[1] Glenny, E. et al, *Journal*, Institution of Mechanical Engineers, Vol. 85, 1958, p. 294.
[2] Foster, A. D. and Sims, C. T., *Metal Progress*, July 1969.
[3] Murphy, H. J., Sims, C. T., and Heckman, G. R., *Transactions*, American Institute of Mining, Metallurgical, and Petroleum Engineers, Vol. 239, 1957, p. 1961.
[4] Sperra, D. A., Howes, M. A. H., and Bizon, P. T., NASA TMX-5297, National Aeronautics and Space Administration, 1971.
[5] Paris, P. C., *Fatigue—An Interdisciplinary Approach*, Syracuse University Press, Syracuse, N. Y., 1964, p. 107.
[6] Spera, D. A., NASA TMX-52558, National Aeronautics and Space Administration, 1969.
[7] Paris, P. C. and Sih, G. C. in *Fracture Toughness Testing, ASTM STP 381*, American Society for Testing and Materials, 1965, p. 30.
[8] Zienkiewicz, O. C. and Cheung, Y. K., *The Finite Element Method in Structural and Continum Mechanics*, McGraw-Hill, New York, 1967.
[9] Bueckner, H., *Methods of Analysis and Solutions of Crack Problems*, Wolters-Noordhoff, 1972.
[10] Wells, C. H. and Sullivan, C. P., *Transactions*, American Society for Metals, Vol. 61, 1968, p. 149.

DISCUSSION

P. S. Chopra[1] *(written discussion)*—The use of weighting functions or correction factors, as described by the authors, for computing the stress intensity factor, K, is questionable; particularly in view of the fracture morphology shown in which the primary crack is not a smooth linear crack and where multiple cracks also are present. It has been shown by Chopra[2]

[1] Argonne National Laboratory, Argonne, Ill. 60439.
[2] Chopra, P. S., Ph.D. dissertation, University of Washington, Seattle, Wash. 1971.

and Hartz and Chopra[3] that the solutions for K are not generally valid for multiple fracture, and a total strain energy release rate function, G_t, for characterizing multiple fracture and secondary cracking has been proposed. It is felt that use of the correct expression for K or alternately G_t, will help explain the crack growth rate data more realistically.

D. F. Mowbray, D. A. Woodford, and D. E. Brandt (authors' closure)— In reply to the question posed, we should like to point up first, that independent of whether or not multiple cracks are an important consideration in this problem, the use of Bueckner's weight function technique should not be in question. It is a perfectly general method for calculating stress intensity factors, multiple cracks included. We find the method to be especially expedient for problems involving thermal loading, because of the ease with which nonuniform stress distributions can be handled. In regard to the multiple cracking observed, we feel it amounts to at most a secondary effect. The hypothesis that the stress intensity factor controls the fatigue crack growth process is predicated on the assumption that it controls, or has a major influence on, the crack tip plastic zone. For this to be true, the plastic zone must be small compared with the crack length. We believe this is satisfied in our application. For the multiple cracking to be of second order importance, the secondary cracks must be small compared to the plastic zone size. It is our observation that this is satisfied in our application. The final proof of such arguments is, of course, whether or not the analysis works. We believe that our results are sufficiently encouraging at this point to justify the steps taken in the analysis. We further believe that the next step in improving our analysis should be an improved stress intensity factor solution for a single crack.

[3] Hartz, B. J. and Chopra, P. S., International Conference on Mechanical Behavior of Materials, Sendai, Japan, Aug. 1972.

J. H. Weber[1] *and M. J. Bomford*[1]

High-Cycle Fatigue Properties of a Dispersion Strengthened Nickel-Base Superalloy

REFERENCE: Weber, J. H. and Bomford, M. J., "**High-Cycle Fatigue Properties of a Dispersion Strengthened Nickel-Base Superalloy,**" *Fatigue at Elevated Temperatures, ASTM STP 520*, American Society for Testing and Materials, 1973, pp. 427–437.

ABSTRACT: IN-853 is a nickel-base alloy which combines precipitation hardening at low and intermediate temperatures ($\lesssim$1400 F) and dispersion strengthening by Y_2O_3 at elevated temperatures ($\gtrsim$1400 F) with good oxidation resistance.

Rotating beam fatigue tests were conducted in air on IN-853 at room temperature, 1000, 1400, and 1750 F, and on a conventional superalloy with a composition close to that of the IN-853 matrix at room temperature, 1000 and 1400 F. Axial fatigue tests were also conducted on IN-853 at room temperature and 1400 F for minimum stress/ maximum stress ratios of +0.1 and −1.0.

At testing temperatures up to 1400 F the 10^7 cycle fatigue strength of IN-853 was higher than that of the conventional superalloy. At 1750 F the fatigue strength of IN-853 was greater than the ultimate tensile strength measured in a standard (low strain rate) tension test at this temperature.

The modes of crack propagation and fracture have been determined using optical metallography and transmission electron microscopy. The effects of γ' precipitate, Y_2O_3 dispersoid, carbides, and grain boundaries on the fatigue damage and failure are presented.

KEY WORDS: nickel alloys, heat resisting alloys, fatigue (materials), precipitation hardening, dispersion hardening, fatigue tests, cracking (fracturing), grain boundaries

The successful combination of dispersion strengthening and precipitation hardening has recently been obtained in nickel base superalloys using the mechanical alloying process [*1*].[2] One example, designated IN-853, exhibits tensile and rupture strengths typical of thoriated nickel at elevated temperatures (>1500 F), while at lower temperatures the strengths are typical of those of Nimonic[3] alloy 80A, a wrought nickel-base superalloy having a composition similar to that of the IN-853 matrix. The mechanically alloyed

[1] Research metallurgists, The International Nickel Co., Inc., Paul D. Merica Research Laboratory, Sterling Forest, Suffern, N. Y. 10901.

[2] The italic numbers in brackets refer to the list of references appended to this paper.

[3] Trademark of the The International Nickel Co., Inc.

Copyright© 1973 by ASTM International www.astm.org

product also exhibits high resistance to oxidation and sulphidation at elevated temperatures.

In this study, the fatigue properties of the dispersion strengthened nickel-base superalloy IN-853 were determined with the emphasis on the following: (*a*) characterization of the fatigue properties with respect to temperature, (*b*) comparison with a conventional superalloy having a composition close to that of the IN-853 matrix, and (*c*) the role of the dispersoid particles in deformation and failure under fatigue conditions.

Materials and Experimental Procedure

The dispersion strengthened nickel-base superalloy, IN-853, was prepared by mechanical alloying [*1*]. The mechanically alloyed powder was packed into mild steel cans and extruded to bar. Chemical analysis of the extruded bar was 22.3Cr, 1.61Al, 2.65Ti, 0.07Zr, 0.008B, 0.062C, 0.83 O_2(total), 1.3Y_2O_3, balance nickel. Heat treatment was $\frac{1}{2}$ h/2400 F + 7 h/1975 F + 16 h/1300 F. In the heat treated condition, the IN-853 exhibits a microstructure of coarse elongated grains with dimensions typically 1 mm × 0.1 mm.

The conventional superalloy was vacuum induction melted, cast, and hot rolled to barstock. Chemical analysis was 18.7Cr, 1.22Al, 2.36Ti, 0.061Zr, 0.006B, 0.067C, 0.025 O_2, balance nickel. Heat treatment was 8 h/1975 F + 16 h/1300 F. The resultant grain structure was equiaxed with an average diameter of about 0.2 mm.

Rotating bending fatigue testing on IN-853 was conducted at room temperature and 1000 F where γ' precipitation hardening is the dominant strengthening mechanism, at 1750 F in the dispersion strengthening regime, and at 1400 F where both strengthening mechanisms are effective. Tests were conducted on the conventional superalloy at the same four temperatures. All tests were conducted in air at an approximate frequency of 8000 cpm unless otherwise noted.

Axial fatigue testing was conducted on IN-853 at room temperature and 1400 F in air for minimum stress/maximum stress values (R values) of +0.1 and −1.0, at approximately 8000 cpm.

Results and Discussion

Tensile Properties

Tensile properties for the experimental alloys are presented in Table 1. Tests were performed according to ASTM Method of Tension Testing of Metallic Materials (E 8-69) at room temperature and to ASTM Recommended Practice for Short-Time Elevated Temperature Tension Tests of Materials (E 21-70). The tensile strengths of IN-853 are essentially equal to those of the conventional alloy at all temperatures to 1400 F. At 1750 F, IN-853 is about twice as strong due to the influence of the dispersoid. A

TABLE 1—*Tensile properties.*

Material	Test Temperature, deg F	Yield Strength, 0.2% offset, ksi	Ultimate Tensile Strength, ksi	Elongation, %	Reduction of Area, %
IN-853.....	room temperature	139.7	169.6	7	9.5
	1000	116.1	145.3	5	8.5
	1400	87.9	97.4	12	23
	1750	23.1	26.5	15	27
Conventional superalloy..	room temperature	99.6	167.2	27	32.5
	1000	84.7	139.2	32	40
	1400	74.6	96.6	26	19.5
	1750	11.1	14.3	135	96

dispersoid effect is also found at lower temperatures, where the yield strength-to-ultimate tensile strength ratios of IN-853 are much higher than those of the conventional superalloy. High yield-to-ultimate strength ratios are typical of oxide dispersion strengthened alloys, namely, thoriated nickel and thoriated nickel-chrome.

Fatigue Properties

The rotating bending fatigue properties for the IN-853 and the conventional superalloy are presented in Figs. 1 and 2, respectively. The curves were obtained by fitting the experimental data points to an empirical equation of the type:

$$\sigma = A + (B/\ln N)$$

where

σ = applied stress,
N = number of cycles to failure, and
A,B = constants for a particular test condition and material.

Fatigue strengths for failure in 10^7 cycles are shown in Table 2 for both the rotating bending and axial fatigue tests. The figures in parentheses in Table 2 are the 10^7 cycle endurance ratios for each test condition.

At each test temperature, IN-853 is stronger in rotating bending fatigue than the conventional superalloy. Gamma prime precipitation hardening is the dominant strengthening mechanism at room temperature and 1000 F. The higher fatigue strength of the IN-853 at these temperatures can be partially attributed to the higher concentrations of the γ' forming elements, aluminum, and titanium, in IN-853 compared to the wrought superalloy. However, the Y_2O_3 dispersoid does have an effect on the deformation and fracture characteristics in this temperature range (see later discussion).

TABLE 2—*10^7 cycle fatigue strengths, ksi.*

Material	Rotating Bending				Axial (R = 0.1)		Axial (R = −1.0)	
	Room Temperature	1000 F	1400 F	1750 F	Room Temperature	1400 F	Room Temperature	1400 F
IN-853	81.1 (0.48)[a]	69.2 (0.48)	62.0 (0.64)	34.2 (1.29)	107.1 (0.63)	72.9 (0.75)	68.5 (0.40)	56.0 (0.58)
Wrought superalloy	67.2 (0.40)	63.1 (0.45)	55.5 (0.57)	16.9 (1.18)	...	...	...	...

[a] Figures in parentheses are the 10^7 cycle endurance ratios.

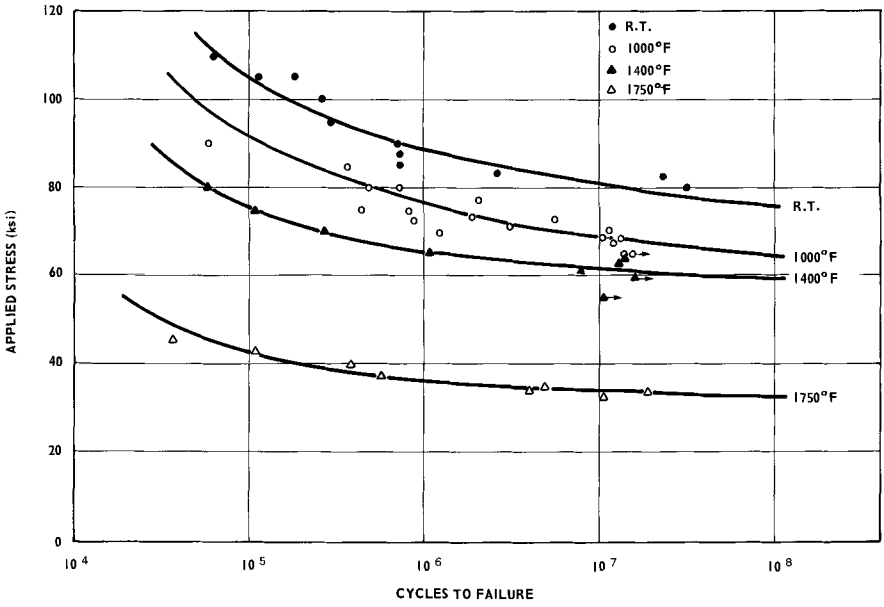


FIG. 1—*Rotating bending fatigue properties of IN-853.*

Both γ' strengthening and Y_2O_3 dispersion strengthening are effective in IN-853 at 1400 F. This is reflected in the fact that short-time mechanical tests do not differentiate between the two materials, while longer time stress rupture tests show a significant difference. The slope of the stress rupture curve for IN-853 [*2*] is less steep than that of Nimonic alloy 80A [*3*] indicating that the Y_2O_3 dispersion is providing a larger portion of the strengthening as the γ' overages during exposure. The fatigue strength of IN-853 at 1400 F is greater than that of the conventional superalloy, but the slope of the *S-N* curve for the conventional alloy is somewhat less than that of the IN-853. One possible explanation for this behavior is that the conventional alloy exhibits greater potential for recovery of the fatigue damage at stresses near the endurance limit, while the recovery in IN-853 is limited by the Y_2O_3 dispersoid particles.

At 1750 F the fatigue strength of IN-853 is much higher than would be expected from the tensile and stress rupture properties. In fact, the rotating bending fatigue strength for 10^7 cycles, 34.2 ksi, is higher than the ultimate tensile strength measured in a standard tension test, 26.5 ksi, performed at a strain rate of 5 percent/min. The reduction in area at tensile fracture was 27 percent. At higher strain rates the ultimate tensile strength and ductility increase so that at about 10 000 percent/min strain rate, the ultimate tensile strength is 54 ksi with a 38 percent reduction in area at fracture.

A few fatigue tests were performed at 1400 and 1750 F at 800 cpm rather than the usual frequency of 8000 cpm. Reductions in life were observed for

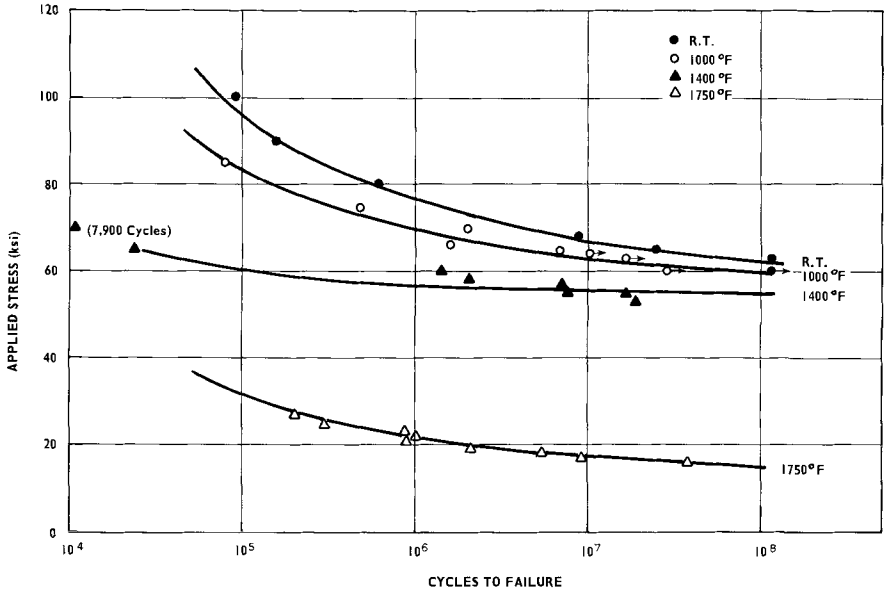


FIG. 2—*Rotating bending fatigue properties of conventional superalloy.*

the lower frequency tests [*4*]. Similar results on the effect of frequency on life for elevated temperature fatigue tests on Udimet[4] alloy 700 have been reported by Organ and Gell [*5*]. They attributed the variation in fatigue life with frequency to the effect of environmental interactions upon the fatigue crack propagation rate. They noted, at higher frequencies, a change in fatigue crack initiation site from surface intergranular to subsurface hard particles located at grain and twin boundaries.

The axial fatigue properties of IN-853 for R values of 0.1 (tension-tension) and -1.0 (fully reversed tension-compression) are compared to the rotating bending fatigue properties at room temperature and 1400 F in Table 1. As expected, the fatigue strength for $R = 0.1$ is greater than that for $R = -1.0$. The rotating bending fatigue strength is intermediate between the two axial values. Although the R value for rotating bending fatigue is -1.0, the maximum stress is only applied at the surface; the rotating bending fatigue strength would thus be expected to be higher than the axial fatigue strength at $R = -1.0$. This effect is observed in a wide variety of metals and alloys [*6*].

Effect of Microstructure Upon Deformation and Failure

The phases present in IN-853 in the fully heat treated condition include Y_2O_3 particles of approximately 100 to 500 Å diameter, γ' particles of 100 to 150 Å diameter, $M(C,N)$ carbonitrides of 0.5 to 2 μm diameter, Al_2O_3

[4] Trademark of Special Metals.

particles, and some chromium-rich grain boundary carbides. Very few dislocation tangles, pileups, or arrays are seen.

Fatigue deformation in IN-853 is heterogeneous at room temperature and 1000 F. Heavy deformation is apparent in some areas with large dislocation tangles caught on the γ', dispersoid, and carbide particles. Individual dislocations may be observed in concentrate in areas rich in carbides and dispersoid (Fig. 3), whereas regions leaner in these phases do not show much evidence of deformation. Therefore, although the γ' can interact with dislocations in the neighborhood of carbides and dispersoid, it does not seem to be the primary obstacle to dislocation movement during fatigue.

The wrought superalloy, fatigued at room temperature shows individual dislocations distributed uniformly throughout the matrix in addition to evidence of dislocation alignment along slip planes. Jogs in the dislocations are apparent where they are pinned to γ' particles (Fig. 4). At 1000 F, similar dislocation arrays are observed with little change in the tendency for alignment along slip planes.

Long life ($>10^6$ cycles) fatigue failure modes for IN-853 up to 1400 F and for the conventional superalloy up to 1000 F are similar to those of nickel-base superalloys at ambient temperatures. Fracture occurs by transgranular initiation and propagation. Coherent twin boundaries, a primary site for crack initiation in conventional superalloys [7], play a very minor

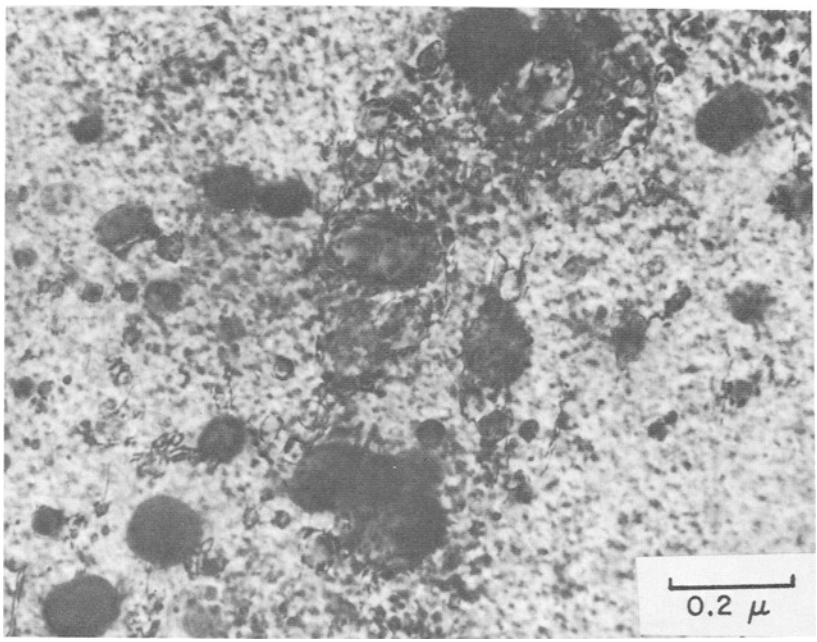


FIG. 3—*Deformation concentrated around carbide and Y_2O_3 particles. IN-853 fatigued at room temperature ±80 ksi, 32.0 × 10^6 cycles.*

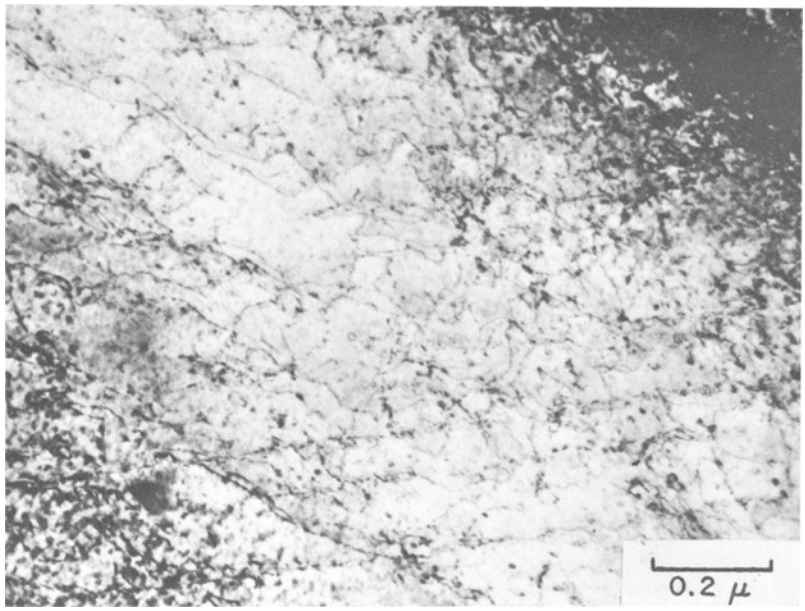


FIG. 4—*Dislocation structure in wrought superalloy. Fatigued at room temperature ±63 ksi 113.3 × 10^6 cycles.*

role in IN-853 as this alloy contains few twins in the heat treated condition used in this study.

IN-853 fatigued at 1400 F exhibits dislocation tangles around carbides and dispersoid particles; dislocations are also pinned on γ' particles in the wrought superalloy.

At 1750 F the γ' is dissolved completely prior to testing. Very heavy dislocation tangles and pileups are apparent in IN-853 (Fig. 5) fatigued at this temperature. Individual dislocations pinned on dispersoid particles are also evident. No well-defined cell structures were observed in IN-853 fatigued at 1750 F or lower temperatures. Dislocation cell structures would be expected to form more readily in high strain fatigue of dispersion strengthened nickel and nickel alloys [7] than in low strain fatigue, as is the present case.

Long life fatigue fractures of IN-853 at 1750 F and the conventional superalloy at 1400 F are initiated by intergranular surface cracking and propagate in a mixed transgranular-intergranular fashion [4]. A primary difference in the failure of the two alloys is the nature of the grain boundary failure in IN-853; intergranular crack propagation is confined usually to the longitudinal grain boundaries. These grain boundary separations connect the transgranular fracture which is essentially perpendicular to the major applied stress axis. IN-853 exhibits a transgranular-to-intergranular fracture transition at about 300 F higher than most conventional nickel-

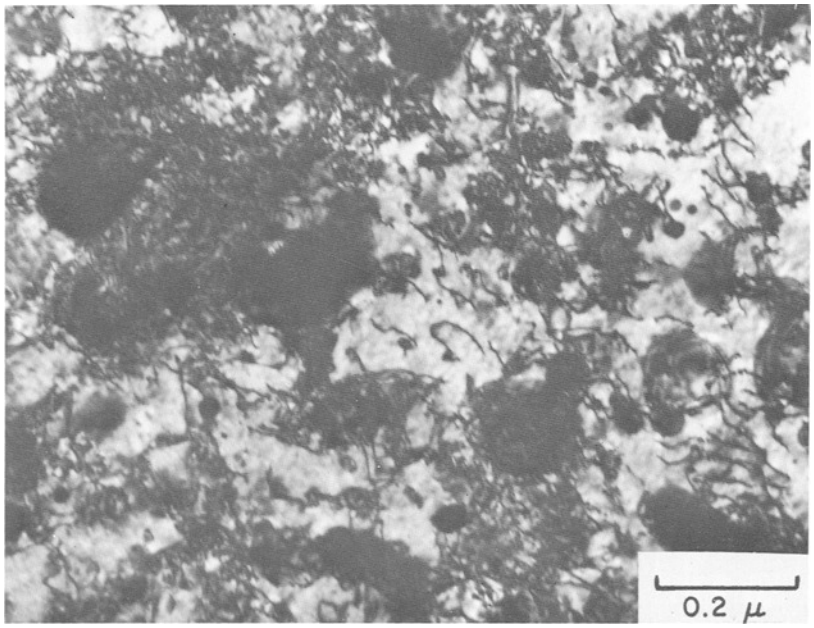


FIG. 5—*Heavy damage and dislocation tangles and pileups on carbides and Y_2O_3 particles. IN-853 fatigued at 1750 F ±33 ksi 19.6 × 10^6 cycles.*

base superalloys [7]. This increase in transition temperature is a result of the combined effect of the elongated grain shape and the restrictive effect of the oxide dispersoid on grain boundary sliding.

Conclusions

1. A nickel-base superalloy dispersion strengthened with Y_2O_3, IN-853, has higher fatigue strengths at room and elevated temperatures than a conventional wrought superalloy with approximately the same composition.

2. The fatigue strength of IN-853 at elevated temperatures increases with increasing frequency within the 800 to 8000 cpm range. At 1750 F, the 10^7 cycle endurance limit is higher than the tensile strength measured in a standard tension test.

3. Although the major strengthening mechanism at low temperatures in IN-853 is γ' precipitation hardening, the Y_2O_3 dispersoid and carbides affect the deformation behavior under fatigue conditions. At 1750 F the fatigue behavior is controlled by the Y_2O_3 and carbides.

References

[1] Benjamin, J. S., *Metallurgical Transactions*, Vol. 1, 1970, p. 2943.
[2] Cairns, R. L., The International Nickel Co., private communication.
[3] Betteridge, W. in *The Nimonic Alloys*, Edward Arnold Ltd., London, 1959, p. 173.

[4] Weber, J. H. and Bomford, M. J., to be published.
[5] Organ, F. E. and Gell, M., *Metallurgical Transactions*, Vol. 2, 1971, p. 943.
[6] Forrest, P. G. in *Fatigue of Metals*, Addison Wesley, Reading, Mass., 1962.
[7] Gell, M., Leverant, G. R., and Wells, C. H. in *Achievement of High Fatigue Resistance in Metals and Alloys, ASTM STP 467*, American Society for Testing and Materials, 1970, p. 113.

DISCUSSION

Lyman Johnson[1] (*written discussion*)—What were the temperature and reduction ratio of the extrusion? In view of the elongated grain structure:

1. What were the transverse properties?
2. At temperatures below those where dispersion strengthening is effective, what is the reason for the improved properties?
3. Was there a preferred orientation or texture of the elongated grains? What was that texture?

J. H. Weber and M. J. Bomford (*authors' closure*)— In view of the dependence of the elevated temperature strength of dispersion strengthened alloys on processing, the information you have requested regarding the temperature and reduction ratio is quite important and is unavailable due to its proprietary nature. The response to your question on the texture of IN-853 is similar, although it can be stated that a well-developed preferred orientation is present.

Transverse properties for IN-853 were not measured in the present study, as the limited size of the transverse dimension precluded the opportunity of producing transverse specimens. The presence of the elongated grain structure and the strong preferred orientation suggests that anisotropy of properties would be present. Recalling the effects of elongated grain structures on other dispersion strengthened alloys, namely, TD nickel and TD nichrome, the transverse strength is expected to be lower than longitudinal.

As noted in the paper, IN-853 has similar tensile strength to Alloy 80A (an alloy having a similar matrix composition) in the low temperature regime where the γ' precipitate is the dominant strengthening mechanism. At elevated temperatures, the tensile strength of IN-853 is greater due to the effect of the dispersion. The fatigue strengths of IN-853 at low temperatures reflect the effect of microstructural features in addition to the dispersoid. The low density and small size of the annealing twins and small size of the

[1] Schenectady, N. Y. 12301.

M(C,N) carbonitrides also contribute to improved fatigue strength. The dispersoid effect at these temperatures is to produce more uniform deformation, thus restricting planar slip. The combined effects of these factors enhance the fatigue strength of IN-853 compared to Alloy 80A through their effect on crack initiation and propagation.

I. P. Bell[2] *(written discussion)*—Both Dr. Weber's and Dr. Merrick's papers embody the theme that minimization of oxidation has a favorable effect of fatigue strength. I have no reason to doubt the truth of this. On the other hand there is a large body of accumulating evidence that in high-temperature creep a low degree of oxidation can be quite detrimental. For instance in low impurity helium where a coherent surface oxide is often absent, creep rates are considerably increased. Two effects at least appear to be important: (1) a coherent layer of oxide inhibits dislocation emergence, enhancing creep strength and (2) the coherent oxide present substantial selective oxidation down grain boundaries, and intergranular oxidation enhances creep at high temperature.

Does the author agree that in developing an alloy for creep and fatigue, one should seek the right sort rather than degree of oxidation?

Messrs. Weber and Bomford—The authors agree with Dr. Bell's conclusion regarding the importance of oxide character in alloy design and application. The degree of oxidation is also important in that without sufficient resistance to degradation during use, the alloy has limited value in high-temperature applications. Although we have noted that good oxidation resistance is a desirable quality for nickel-base superalloys we have not indicated that this property is synonymous with good creep resistance and fatigue strength at elevated temperatures.

Dispersion strengthened alloys are distinct from conventional alloys due to the effect of dispersoid on deformation. As presented in the paper, the dispersoid is shown to produce more uniform deformation during fatigue. Thus, the restriction of surface slip step formation by a coherent oxide may not be as important in dispersion strengthened alloys.

A coherent oxide layer may or may not prevent selective oxidation at grain boundaries. In nickel-base superalloys, the presence of carbides and other minor phases in the grain boundaries provide significantly different oxidation behavior at these portions of the alloy. The effectiveness of a coherent oxide on the grains themselves, thus, may have little effect in preventing selective grain boundary oxidation. In the current work the oxidation behavior of IN-853 is not greatly different from that of the conventional superalloy. As indicated in a previous paper (Ref *1* of the written paper) improved creep and rupture characteristics of IN-853 are related to the elongated grain structure and microstructural features. The deleterious effect of grain boundary oxidation, thus, is compromised.

[2] United Kingdom Atomic Energy Authority, Lancs, England.

D. M. Moon[1] *and G. P. Sabol*[1]

Effect of Mean Stress on the High-Cycle Fatigue Behavior of Udimet 710 at 1000 F

REFERENCE: Moon, D. M. and Sabol, G. P., **"Effect of Mean Stress on the High-Cycle Fatigue Behavior of Udimet 710 at 1000 F,"** *Fatigue at Elevated Temperatures, ASTM STP 520*, American Society for Testing and Materials, 1973, pp. 438–450.

ABSTRACT: The effect of mean stress on the high-cycle fatigue behavior of a wrought nickel-base superalloy, Udimet 710, was studied in air at 1000 F. Under the conditions of testing, which varied from a ratio of the alternating to mean stress, A, of 0.25 to ∞, the endurance limit was almost independent of mean stress. At all values of mean stress, the alloy deformed by superlattice dislocation pairs, shearing both the gamma and gamma-prime phases, resulting in dense planar bands of dislocations. The number of planar bands of dislocations, however, was found to decrease with decreasing mean stress. Independent of the mean stress, fatigue crack initiation took place along the dense bands of dislocations by slip plane decohesion.

Once initiated, the fatigue crack continued to propagate for one or two grain diameters in a Stage I mode before changing to a Stage II mode of propagation. The amount of the remaining fracture surface covered by Stage II crack growth prior to overload decreased with increasing mean stress. However, in the Stage II region of crack growth, the striation spacing, 0.5 μm, was found to be independent of mean stress.

The independence of the fatigue strength on mean stress was concluded to result from the interaction of two competing factors. As the mean stress is increased, the time spent in crack propagation is decreased due to the fact that the Stage I crack growth rate is accelerated, and less Stage II crack growth is required to exceed the fracture strength of the remaining specimen. In addition, at the higher mean stresses, the increased slip dispersal resulted in a greater amount of time being required to build up the dislocation density within a deformation band to the density required for decohesion. The independence of the endurance limit on mean stress, therefore, is related to the shorter time spent in crack propagation at the high mean stress being compensated for by the longer time spent in initiating a crack due to the dispersal of slip onto a greater number of slip planes.

KEY WORDS: fatigue (materials), crack propagation, stresses, fracture strength, metallography, nickel containing alloys, heat resistant alloys, fatigue life, electron microscopy

Nickel-base superalloys have been usually designed to optimize creep strength and corrosion resistance at high temperature. While these normally

[1] Manager, power generation, and engineer, respectively, Research and Development Center, Westinghouse Electric Corp., Pittsburgh, Pa. 15235.

Copyright© 1973 by ASTM International www.astm.org

represent the most important design parameters, there are a number of applications involving rotating equipment where fatigue strength is also an important variable. As with most other alloy systems, in the development of the nickel-base superalloys, very little attention has been given to the factors controlling the fatigue strength. As a result of this situation, the fatigue strength of this class of alloys has not improved in the last 20 years although the creep strength has improved substantially. Recently, however, there has been considerable interest in understanding the fatigue behavior of these materials, and an excellent summary of this work has recently been published [*1*].[2] One of the parameters that has not received much attention from a mechanistic point of view is the effect of mean stress on the high-cycle fatigue strength. This becomes important in a number of applications involving rotating components, such as turbine blades, where a high mean stress due to the centrifugal forces is superimposed on the vibratory stresses. This paper presents the results of a study into the effect of mean stress on the fatigue properties of an advanced nickel-base superalloy, Udimet 710. In order to explain the observed effects, extensive use was made of electron metallography to characterize the effect of mean stress on both the crack initiation and crack propagation stages of fatigue.

Procedure

An advanced, wrought, nickel-base superalloy, Udimet 710, was selected for study. Prior to machining, the material was given a standard four-step heat treatment: 2150 F (1121 C), air cool + 1975 F (1080 C), air cool + 1550 F (843 C) air cool, and 1400 F (760 C) air cool. This heat treatment results in a bimodal size distribution of the precipitation hardening gamma-prime phase, a large blocky size, 0.2 μm on a side and a smaller spherodial size 500 Å in diameter. Specimens having a 0.25 in. gage diameter and 1.00 in. gage length were machined from the heat treated 1.00-in.-diameter bar stock. Load controlled axial fatigue tests were carried out in air at 1000 F in a Sonntag Scientific Corporation Model SF-4 testing machine operated at a frequency of 60 Hz, with an error in the dynamic stress of less than 3 percent.

In order to determine the density of the widely spaced deformation bands use was made of a stain-etching technique developed by Gell and Field [*2*]. Specimens for transmission electron microscopy were prepared by cutting out 0.015-in. slices with a diamond cut-off wheel, followed by mechanical abrasion to approximately 0.005-in. Disks of 0.120 in. diameter were then punched out of these slices and electrolytically thinned to perforation in a twin-jet apparatus utilizing a solution consisting of 32 parts ethanol, 10 parts isobutanol, and 8 parts perchloric acid, operating at room temperature with a current density of approximately 50 mA/mm^2.

[2] The italic numbers in brackets refer to the list of references appended to this paper.

Results

The results of the fatigue testing program are presented in Figs. 1 and 2. Under completely reversed loading, zero mean stress, the 10^8 cycle fatigue strength (defined as the endurance limit) was 37 ksi. With the application of a mean stress of 32 ksi, the alternating stress at the endurance limit decreased to 32 ksi and remained at this value for mean stresses as high as 120 ksi. As indicated in Fig. 2, the peak stress considerably exceeded the 0.2 percent offset yield strength in the 120-ksi mean stress test. At all values of mean stress, the alloy deformed by the movement of pairs of superlattice dislocations shearing both the gamma and ordered gamma-prime phases. Due to the difficulty of the superlattice dislocation pairs to cross slip at 1000 F, dense planar bands of dislocations result, Figs. 3 and 4. As has been noted previously, most of the dislocations do not remain in the larger gamma-prime particles [*4*]. This effect is particularly evident in Fig. 3*a* where the larger gamma-prime particles, approximately 0.2 μm diameter, are clearly outlined by their lack of a high density of dislocations.

The spacing of these planar deformation bands was found to increase with decreasing mean stress or increasing A ratio, defined as the ratio of

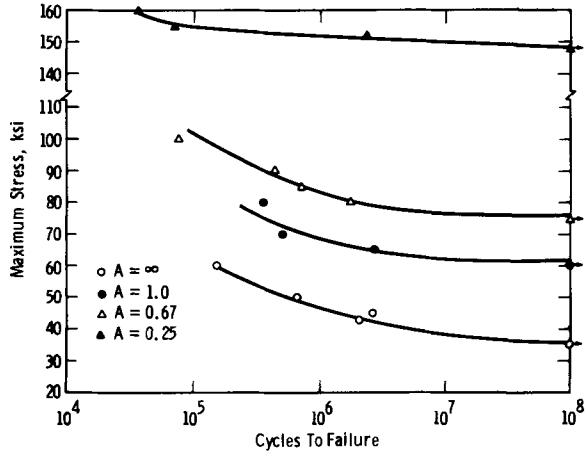


FIG. 1—*Effect of mean stress on the fatigue strength of Udimet 710.*

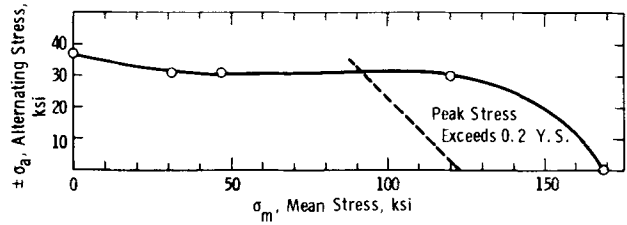


FIG. 2—*Stress-range diagram for Udimet 710 at 1000 F for 464 or 10^8 cycles.*

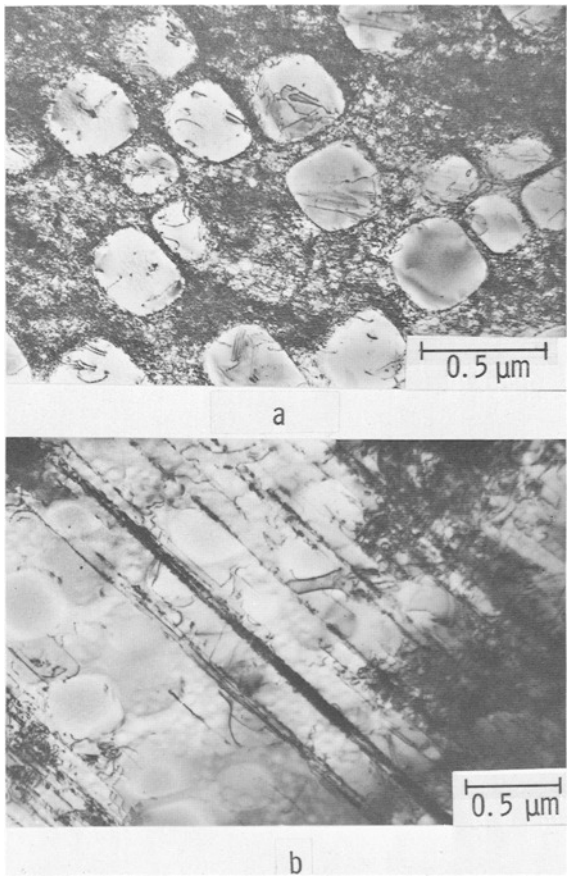


FIG. 3—*Transmission electron micrographs of thin foils taken parallel,* (a), *and perpendicular,* (b) *to the dense bands of dislocations in a specimen tested at* A = *0.25*; σ_{max} = *160 ksi*, N_f = *3.8* × *10⁴ cycles.*

the alternating to the mean stress. At an *A* ratio of 0.25 and a mean stress of 118 ksi, in which case the peak stress exceeded the yield strength, the average spacing between the bands was approximately 0.5 to 2 μm, Figs. 3 and 5. As the mean stress decreased, the spacing of the deformation bands becomes too widely separated to measure reliably using transmission electron microscopy techniques. In order to determine the deformation band spacing in this case, a stain-etching procedure developed by Gell and Field was used [*3*]. Using this technique, the mean spacing of the deformation bands was determined to be approximately 10 μm at a mean stress of 48 ksi and an *A* ratio of 0.667 and approximately 25 μm at a mean stress of 32 ksi and an *A* ratio of 1.0, Fig. 5.

For all specimens tested, independent of *A* ratio, fatigue crack initiation took place along the deformation bands. In several cases, the initiation

event was related to the interaction of a deformation band and a carbide particle, Fig. 6. However, the more typical initiation event took place by simple deformation band cracking without the presence of carbide particles, Fig. 7.

Once initiated, the fatigue crack continued to propagate in a Stage I, transgranular, crystallographic mode along the deformation band for one to three grain diameters before changing to a Stage II mode of propagation,

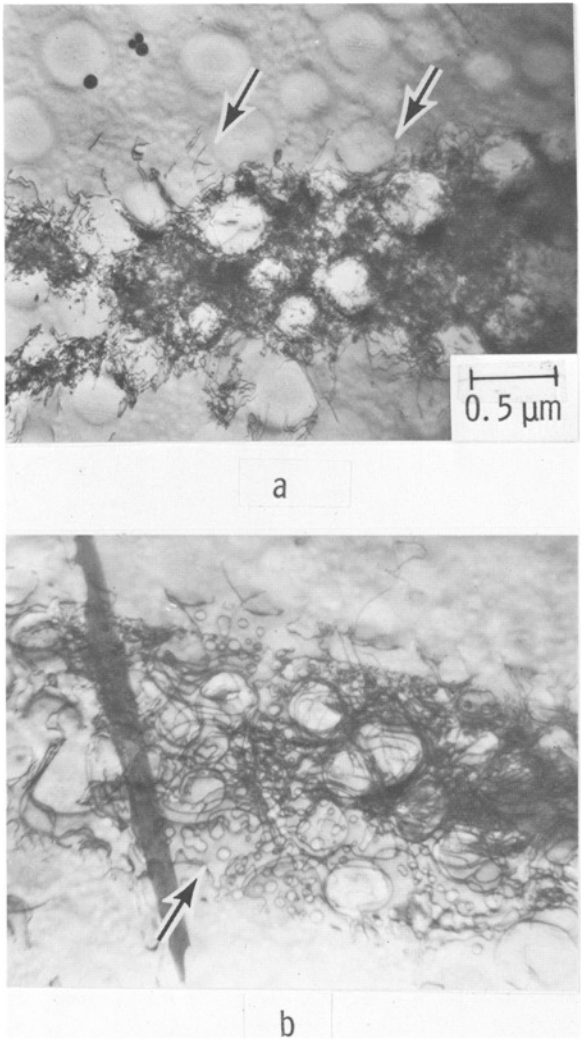


FIG. 4—*Transmission electron micrographs showing bands of dislocations at arrows in* (a), *and dislocation loops around smaller gamma-prime particles at arrow in* (b); σ_{max} = *70 ksi*, N_f = *5.0* × *10*^{5} *cycles.*

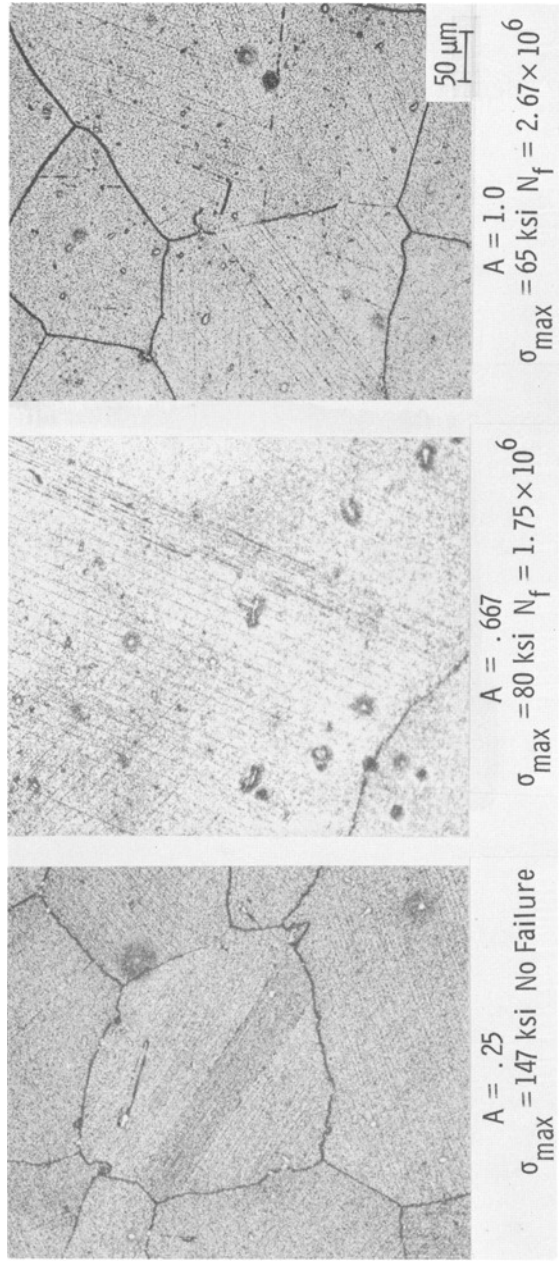


FIG. 5—*Dislocation bands revealed by a stain-etching technique showing a decrease in band density with increasing* A *ratio.*

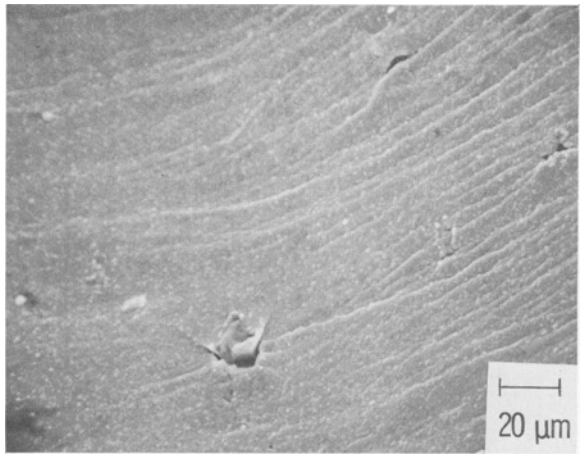


FIG. 6—*Cracking associated with carbide particles on surface,* σ_{max} = *155 ksi,* N_f = *7.0* × 10^4 *cycles.*

Figs. 8 and 9 [5]. The amount of Stage II cracking at a given *A* ratio varied considerably from specimen to specimen as can be seen by comparing Figs. 8 and 9. In Fig. 8, the Stage I mode of propagation persisted for several grain diameters, with the result that the final intergranular overload failure occurred before any Stage II propagation took place due to the high peak stress encountered at this low *A* ratio of 0.25. In Fig. 9, on the other hand, the extent of Stage I propagation was limited to a single grain diameter; therefore, although the peak stress was higher than in Fig. 8, a rather extensive region of Stage II propagation was experienced before final

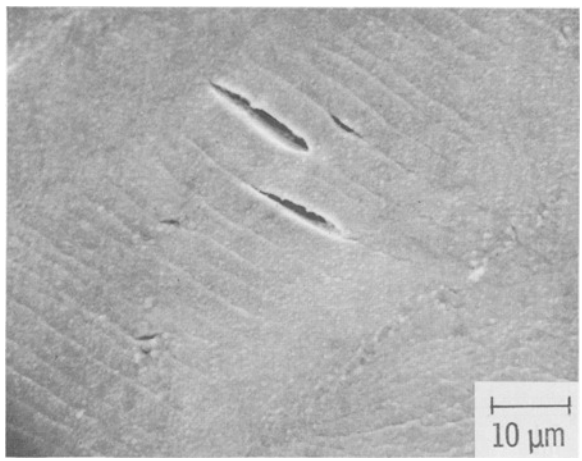


FIG. 7—*Fatigue crack initiation due to decohesion of slip planes on the surface of specimen tested at* A = *0.25;* σ_{max} = *155 ksi,* N_f = *7.0* × 10^4 *cycles.*



FIG. 8—*Fracture surface of specimen tested at* A = *0.25 containing Stage I crack growth for 3-4 grains. Note lack of a Stage II mode propagation at this high level of mean stress;* σ_{max} = *152,* N_f = *2.3* × 10^6 *cycles.*

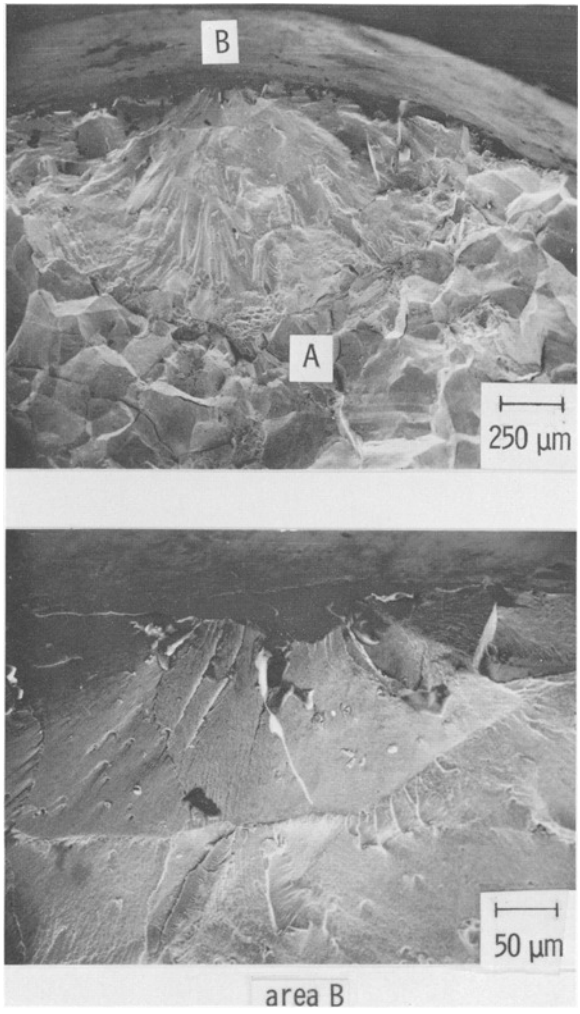


FIG. 9—*Fracture surface of specimen tested at* A = *0.25 containing a short Stage I segment, Area* B, *followed by a more extensive Stage II mode of propagation and final intergranular failure, area* A; σ_{max} = *155 ksi*, N_f = *7.0* × 10^4 *cycles.*

overload failure. Taking into account this wide variation from specimen to specimen at a given *A* ratio, there did not appear to be any dependence of the extent of Stage I propagation on the mean stress.

The extent of Stage II propagation, however, was directly related to the mean stress, increasing as the mean stress was decreased in going from an *A* ratio of 0.25 to ∞.

It was very difficult to determine the spacing of the striations characteristic of the Stage II mode of crack propagation in the scanning electron

microscope. However, at the very end of the Stage II crack region but prior to overload failure, it was possible to resolve in the scanning electron microscope the very coarse striations that contain considerable secondary cracks as previously reported for high-strength steels, Fig. 10 [6]. In replicas of the Stage II region, the smaller ductile striations are clearly resolved, Fig. 11. Taking into account the increase in striation spacing that occurs as a growing crack propagates in a specimen, an average striation spacing of approximately 0.5 μm was found, which was independent of the mean stress.

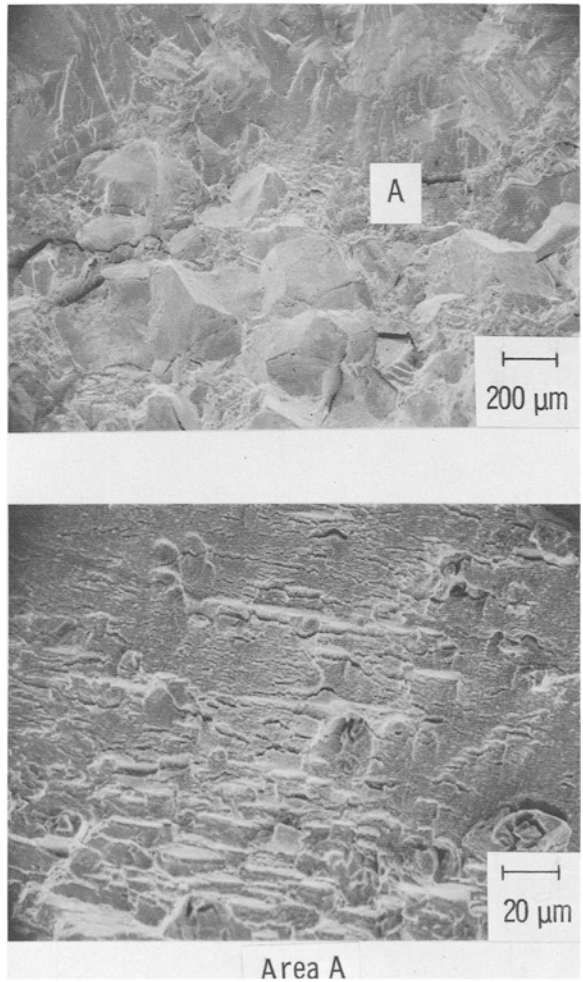


FIG. 10—*End of Stage II fatigue crack propagation in specimen tested at* A = 0.25 *containing cracked striations,* $\sigma_{max} \doteq 140$ *ksi,* $N_f = 5.87 \times 10^5$ *cycles.*

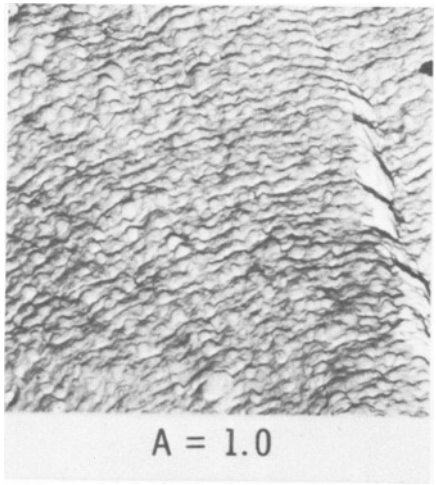


FIG. 11—*Transmission electron micrographs of fatigue striations on the Stage II fracture surface.*

Discussion

Under the conditions of testing, which varied from a ratio of the alternating to mean stress of 0.25 to ∞, the endurance limit was almost independent of mean stress. Since the fatigue life of a specimen is made up of the initiation and subsequent propagation of a fatigue crack, in order to understand the invariance of the fatigue life with mean stress, it is necessary to consider the effect of mean stress on these two processes.

In contrast to the results on cast superalloys where cracked carbides are the primary initiation site, in wrought materials most of the initiation takes place on the surface at deformation bands or twin boundaries, with only limited interaction with second phase particles [*7–10*]. This difference in behavior between cast and wrought materials is no doubt related to the much smaller carbide particles present in the wrought materials.

The transgranular surface initiated cracking at 1000 F in Udimet 710 observed in the present experiment compares more with the surface initiated cracking reported for Udimet 700 at room temperature [*9*] than the internally initiated cracks reported at 1400 F in Udimet 700 [*11*]. Oxidation at 1000 F in Udimet 710 is apparently not sufficient to suppress the surface initiation and transfer the initiation site to the interior, as was found at 1400 F in Udimet 700. The slip band initiation found at 1000 F in Udimet 710, however, does differ somewhat from the high incidence of twin boundary cracking reported for Udimet 700 at room temperature [*9*].

Initiation and subsequent State I crack propagation along deformation bands has been previously observed in a number of nickel-base superalloys [*1,7,9,11,13,14*]. A mechanism involving slip plane decohesion has been

proposed to account for the cleavage type features typical of this mode of crack propagation [*14,15*]. The cohesive energy of the dense dislocation bands is reasoned to be lowered by disordering of the gamma prime particles or the accumulation of a large number of defects.

The effect of mean stress on crack initiation then can be related to the amount of deformation within an individual slipband. As the density of deformation bands is increased by raising the mean stress, the deformation within each slip band is reduced. With the reduced slip activity within a given band, the rate of decrease of the cohesive energy will be slower, resulting in a longer time spent initiating a crack as the mean stress is increased.

The effect of mean stress on the rate of Stage I crack propagation is more difficult to assess. The reduced homogeneity of slip found as the mean stress was reduced was also encountered in high frequency testing where it was reported to result in an increased rate of Stage I crack propagation [*11*]. Mean compressive stresses have been reported to greatly retard the rate of Stage I crack propagation, due to the increased frictional forces that are developed between rubbing crack faces [*9*]. It would appear from the model of slip band decohesion that a mean tensile stress, as was used in the present experiment, would enhance considerably the Stage I crack growth rate, since it would increase the normal stress on a crack and reduce the required lowering of the cohesive energy to allow crack propagation.

Having initiated, the crack propagated for one to three grain diameters in a crystallographic Stage I mode of crack propagation. This limited extent of Stage I cracking has been reported previously and has been related to the difficulty of propagating in a shear mode in adjacent grains of different orientation [*12,13*]. On this basis, the variation in the extent of Stage I cracking can be related to the probability of obtaining a number of adjacent grains suitably oriented. This result does not appear to be applicable in all cases, however, since recent results indicate that at room temperature the entire fracture surface of Udimet 700 is covered by Stage I mode of failure [*9,13*]. In summary, the effect of mean stress on the rate of crack initiation and propagation, therefore, will depend on the relative importance of increased normal stresses and reduced slip activity within a band.

After propagating for one to three grain diameters, in a Stage I mode, the crack is reoriented to approximately 90 deg to the stress axis and continues to propagate in a Stage II mode until overload failure. The amount of Stage II cracking is largely dependent on the mean stress, decreasing in extent with increasing mean stress. Since the striation spacing and hence the microscopic crack growth rate was found to be independent of the mean stress, one can conclude that the time a given specimen spent in Stage II propagation decreased with increased mean stress.

Based on the preceding results, the lack of dependency of the fatigue strength on mean stress in Udimet 710 at 1000 F may be related to the interaction of two competing factors. As the mean stress is increased, the rate of

Stage I propagation is increased, and the duration of Stage II propagation is decreased, due to the fact that less crack growth is required to exceed the fracture strength. In addition, at the higher mean stresses, there is an increased dispersal of slip as evidenced by the higher density of deformation bands. With increased slip dispersal, a greater amount of time is required to build up the dislocation density within a deformation band to the density required for decohesion or crack initiation. The independence of the endurance limit on mean stress, therefore, can be argued to result from the shorter time spent in Stage I and Stage II crack propagation at the high mean stress being compensated for by the longer time spent in initiating a crack due to the dispersal of slip onto a greater number of slip planes.

Acknowledgment

We are indebted to K. K. Kishi for conducting the tests and J. A. Nelson and G. M. Group who assisted in the metallographic characterization. We also wish to acknowledge the support offered by W. J. McCall and D. M. Fantozzi.

References

[1] Gell, M., Leverant, G. R., and Wells, C. H. in *Achievement of High Fatigue Resistance in Metals and Alloys, ASTM STP 467*, American Society for Testing and Materials, 1970, pp. 113–153.
[2] Sabol, G. P. and Stickler, R., *Physica Status Solidi*, Vol. 35, 1969, pp. 11–52.
[3] Gell, M. and Field, T. T., *Transactions*, Metallurgical Society, American Institute of Mining, Metallurgical, and Petroleum Engineers, Vol. 245, 1969, p. 1666.
[4] Leverant, G. R. and Kear, B. H., *Metallurgical Transactions*, Vol. 1, 1970, pp. 491–498.
[5] Forsyth, P. J. E. in *Proceedings of Crack Propagation Symposium*, Cranfield, Beds, College of Aeronautics, 1962, p. 76.
[6] Tomkins, B., *Philosophical Magazine*, Vol. 23, 1971, p. 687.
[7] Gell, M. and Leverant, G. R., *Transactions*, Metallurgical Society, American Institute of Mining, Metallurgical, and Petroleum Engineers, Vol. 242, 1968, pp. 1869–1879.
[8] Sabol, G. P. and Moon, D. M. in *Conference Proceedings*, Second International Conference on the Strength of Metals and Alloys, 1970, p. 1052.
[9] Burck, L. H., Sullivan, C. P., and Wells, C. H., *Metallurgical Transactions*, Vol. 1, 1970, p. 1595.
[10] Wells, C. H. and Sullivan, C. P., *Transaction Quarterly*, American Society for Metals, Vol. 60, 1967, p. 217.
[11] Organ, F. E. and Gell, M., *Metallurgical Transactions*, Vol. 2, 1971, p. 943.
[12] Forest, P. G. and Tate, A. E. L., *Journal*, Institute of Metals, London, Vol. 93, 1964–1965, p. 438.
[13] Paskiet, G. F., Boone, D. H., and Sullivan, C. P., *Journal*, Institute of Metals, Vol. 100, 1972, pp. 58–62.
[14] Gell, M. and Leverant, G. R., *Acta Metallurgical*, Vol. 16, 1968, p. 553.
[15] Duquette, D. J., Gell, M., and Piteo, J. W., *Metallurgical Transactions*, Vol. 1, 1970, pp. 3107–3115.

A. J. Opinsky[1]

Bend Fatigue of Two Iron-Nickel-Base Superalloys at Elevated Temperature

REFERENCE: Opinsky, A. J., "**Bend Fatigue of Two Iron-Nickel-Base Superalloys at Elevated Temperature,**" *Fatigue at Elevated Temperatures, ASTM STP 520,* American Society for Testing and Materials, 1973, pp. 451–461.

ABSTRACT: The iron-nickel-base superalloy A-286 and its improved version, intermediate-aged V-57, were examined in bend fatigue at 950 to 1100 F (510 to 593 C) to determine whether using V-57 would be advantageous in low-frequency applications. The superiority might be expected because the latter is better in stress rupture than A-286. Nonreversed bending was done at frequencies close to 0.1 and 1 cpm, with a few tests at 10 cpm. The transition fatigue life, where the elastic and plastic strain ranges are equal, is below 500 cycles. Since most purely cyclic applications will involve much longer lives, the fatigue component of damage in these applications will be in the high-cycle fatigue regime. The data, which show V-57 to be superior to A-286 at 950 to 1100 F (510 to 593 C), also indicate that test frequencies should be chosen carefully to obtain meaningful data. There are several indications that the specimens can undergo further aging during testing and that their fatigue behavior is affected by the aging.

KEY WORDS: fatigue (materials), creep rupture strength, fatigue tests, bend tests, superalloys, high temperature test, nickel containing alloys, iron containing alloys

Alloy A-286, an iron-nickel-base superalloy, is used widely for turbine applications where the temperature conditions are not too severe. The typical turbine wheel undergoes both thermal and stress cycles of fairly low frequency—certainly less than 1 cpm. On the other hand, the typical fatigue testing program is predicated on finishing the tests as rapidly as possible, at the highest possible frequency. At room temperature, test frequency usually does not significantly affect the cyclic life, unless heating effects are encountered. However, the situation is vastly different at elevated temperature. Beginning with the work of Eckel [*1*],[2] many investigators have shown that decreasing the test frequency at relatively high temperature decreases cyclic life. For a recent review, see Ref *2*.

[1] Metallurgist, Applied Research and Development, General Electric Company, Erie, Pa. 16501.

[2] The italic numbers in brackets refer to the list of references appended to this paper.

Copyright© 1973 by ASTM International www.astm.org

A search of the literature revealed little data on the fatigue of A-286 at high temperature and low frequency. Dawson et al showed that the introduction of a 30-min dwell period reduces the cyclic life of A-286 to about ¼ to ⅓ that obtained at 9 cpm in reversed bending at 600 C (1112 F) [*3*]. Coffin determined the values of the constants in his frequency-modified-life equation for A-286 at 1100 F (593 C) [*2*]. The large frequency sensitivity (Coffin's term is $1 - k$) can be regarded as extreme. In fact, Coffin showed that the frequency dependence is eliminated when fatigue testing is done in high vacuum [*2*].

With so little data available, an investigation was planned into the low-frequency cyclic life characteristics of A-286. Since, as the test frequency is decreased, pure fatigue should shade into a mixed mode and then finally into cyclic rupture, it was decided to study a sister alloy that was developed for better rupture strength. The rationale was that when cyclic rupture occurs, this alloy—V-57—should be superior to A-286. Another point to be investigated was the influence of small changes in chemistry on the extreme frequency sensitivity of A-286 at 1100 F (593 C).

Procedure

There are only slight differences in the chemistry of V-57 and A-286. These are shown in the vendor analyses of the materials investigated (Table 1). The V-57 had an intermediate aging treatment to enhance ductility at the expense of some strength [*4*]. As mentioned previously, V-57 has better rupture strength than A-286. Data from a companion stress rupture investigation are displayed in Fig. 1, which shows the rupture strengths of A-286 and V-57-1 as functions of the Larson-Miller parameter $T[20 +$

TABLE 1—*Analyses of experimental materials.*

	A-286	V-57-1	V-57-2
C	0.05	0.04	0.07
Si	0.89	0.34	0.04
P	0.021	<.001	0.015
Mn	1.50	0.10	0.13
S	0.008	0.004	0.006
Ni	25.78	27.70	27.84
Cr	14.98	15.10	14.15
Mo	1.24	1.23	1.50
V	0.28	0.10	0.03
Al	0.17	0.22	0.11
Ti	2.07	3.14	3.00
B	0.008	0.010	0.008
Heat Treatment	1 h 1800 F 16 h 1325 F	3 h 1850 F, oil 3 h 1500 F, air 16 h 1350 F, air	2 h 1800 F, oil 3 h 1500 F, air 16 h 1350 F, air

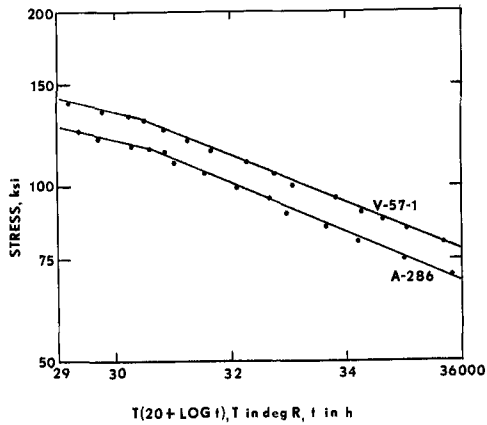


FIG. 1—*Master rupture curves of A-286 and V-57-1.*

log (t)], where T is in degrees Rankine, and t in hours. The difference in parameter to give the same rupture life at a given stress level is equivalent to an increase in temperature of about 50 F for V-57; that is, V-57 is 50 F "better" than A-286.

Tests were performed on a bend fatigue machine of the design described by Forrest and Penfold [5]. Through changes in gearing, frequencies close to 0.1084, 1.044, and 10.1 cpm were available. In most of what follows, these frequencies will be called 0.1, 1, and 10 cpm. Few tests were done at the highest frequency.

Modifications to permit (1) controlled deflection from zero to a maximum value and (2) an autographic record of the hysteresis loop were made, and can be seen in Fig. 2. The former was accomplished by slotting the cross shaft flanges and utilizing split collar keepers to hold the cross shaft in the desired position. The latter was accomplished through three conditioned full bridge strain gage signals. Readings that were linear with applied moment were obtained from moment measuring gages mounted in symmetrical cutouts (one is shown above A in Fig. 2). The two signals (one from each arm) were conditioned and added. The original dial gage spherometer was replaced with one using an Instron G-51-11 extensometer (the third strain gage bridge) to measure the displacement of the central silica rod with respect to the outer rods. The strain in the outer fibers of the specimen is related linearly to the displacement (h) of the center rod as long as h^2 is negligible compared with a^2, where $2a$ is the distance between the outer silica rods.

The test specimen, a rectangular parallelopiped, was cut from pancake forgings. The central 3¾ in. (9.5 cm) was heated by its own resistance. There was about a 10 F (5.5 C) drop across the 1-in. (2.5-cm) span of the spherometer, while the temperature at the point where the specimen entered the clamp was about 200 F (111 C) lower than that of the hot zone.

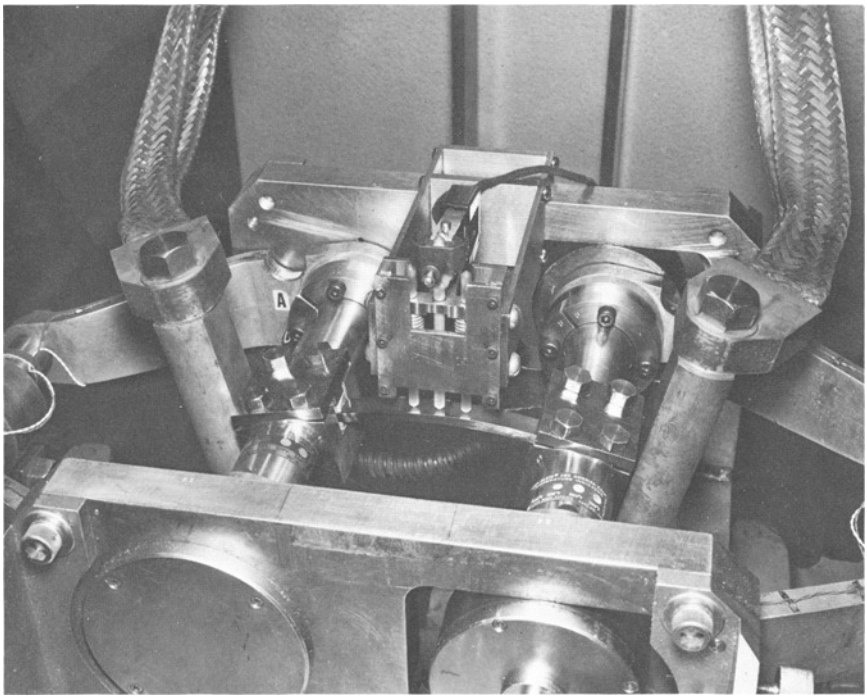


FIG. 2—*Arrangement of Forrest test machine.*

Results

A direct determination of the elastic and plastic strain ranges cannot be obtained from the hysteresis loop in bending (*6,7*]. The Nadai-type construction to obtain true stress from a plastically-bent bar [*8*], while probably not rigorously applicable, was used to determine the stress range from the moment-strain hysteresis loop, and also the plastic strain range. Some of the resulting data are shown in Fig. 3. The equations listed were obtained by analysis of the 1-cpm data. The transition fatigue life (N_t), where the elastic and plastic strain ranges are equal, is commonly accepted to be a boundary between low- and high-cycle fatigue. It is about 470 cycles for V-57-2 at 1 cpm at 950 F (510 C), as can be determined by equating the relationships given in Fig. 3. At 1100 F (593 C), N_t is approximately 230 cycles for this material. Data for A-286 and V-57-1 at 0.1 cpm indicate N_t to be about 250 cycles at 950 F (510 C) and 25 to 50 cycles at 1100 F (593 C). (That there does seem to be a tendency toward lower N_t with lower frequency can be seen in Fig. 3.) Since lives in excess of 1000 cycles are expected in the usual application of these materials, it is anticipated that most purely cyclic applications will be either in the high-cycle fatigue region, or at least in a situation where the elastic strain range is significantly larger than the plastic strain range.

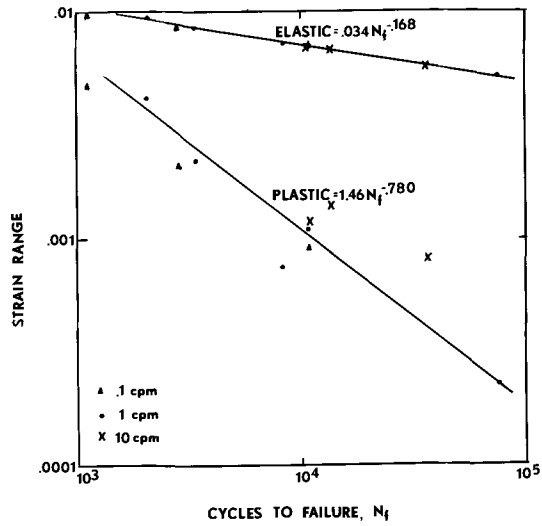


FIG. 3—*Elastic and plastic components of V-57-2 at 950 F.*

On the other hand, the total strain range can be determined more directly; total strain range-life data for the three materials are given in Fig. 4 for 950 F (510 C) tests and in Fig. 5 for 1100 F (593 C) tests. In the illustrations, the strain ranges determined during the fifth cycle at 0.1 cpm and the ninth cycle at 1 cpm were plotted. The curves that are shown in Figs. 4 and 5 represent syntheses based on the least squares analyses of the elastic and plastic components; hence, they do not truly fit the total strain range curve in the least squares sense. Curves were calculated only for the frequency where the most points were available; that is, 0.1 cpm for A-286 and V-57-1, and 1 cpm for V-57-2.

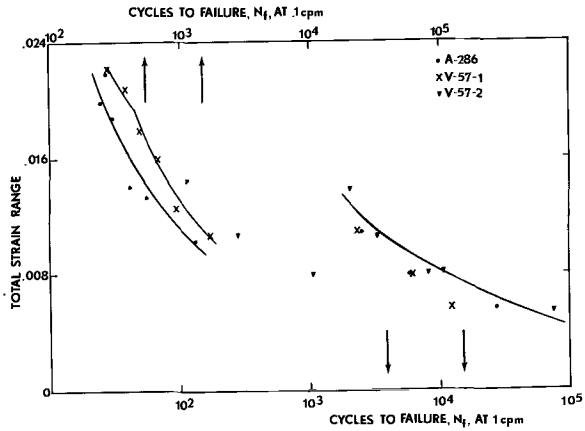


FIG. 4—*Total strain range-life data at 950 F.*

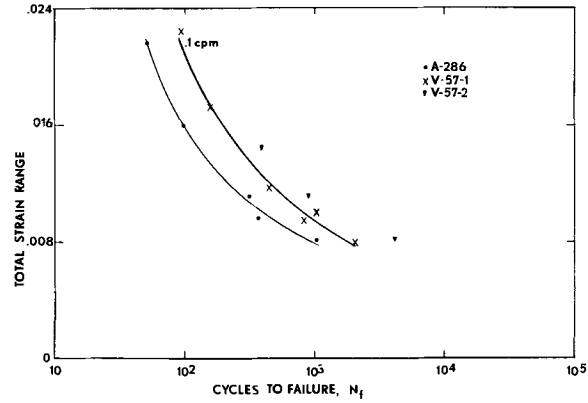


FIG. 5—*Total strain range-life data at 1100 F.*

At 950 F (510 C), Fig. 4, the clear-cut superiority of V-57-1 (symbol *x*, upper curve) over A-286 (symbol ●, lower curve) disappears at 1 cpm, while V-57-2 (symbol ▼, curve at right) retains its superiority over V-57-1 at the higher frequency. Note that the 0.1-cpm data have been offset one decade in life from the 1-cpm data for the sake of clarity. Without this offset, and with fewer points, however, it would be apparent that the V-57-2 curve at 0.1 cpm might intersect the 1-cpm curve at a strain range slightly below 0.008.

The situation is similar at 1100 F (593 C). At 0.1 cpm, the superiority of V-57-1 over A-286 has increased from the about 50 percent at 950 F (510 C) to 100 percent, as measured by the cyclic life at the same strain range. At 1 cpm, which is not shown, A-286 and V-57-1 are indistinguishable, while V-57-2 still retains the superiority shown at 0.1 cpm.

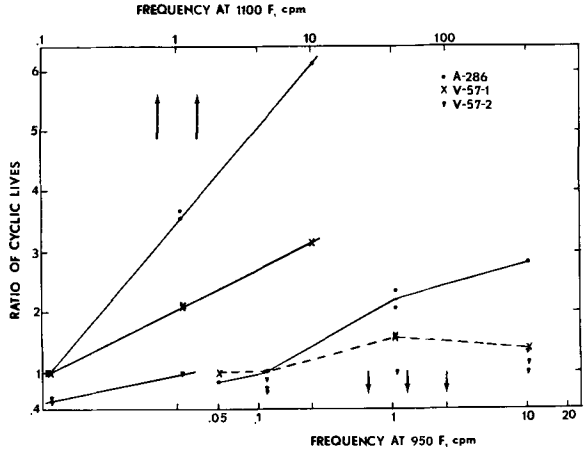


FIG. 6—*Dependence of cyclic life ratio on frequency.*

The frequency dependence is displayed in different fashion in Fig. 6. The values of the ordinates in Fig. 6 represent ratios of actual life to one calculated at the same strain range of 0.1 cpm for A-286 and V-57-1, and 1 cpm for V-57-2. Six sets of equations, similar to the pair shown in Fig. 3, were used to calculate lives. The data are listed in Table 2. (Incidentally, the ratios of observed to calculated lives at the base frequencies were also analyzed. In most instances, the estimated standard deviations of the ratios lay between 0.10 and 0.15.) The calculations were generally limited to strain ranges that fell within those used in fitting the curves. While the data are few, the trend at 1100 F (593 C) is clearly toward straight line dependence of the ratio on log frequency. These data have been displaced in frequency to the left of the 950 F (510 C) data in Fig. 6. Use of a different frequency base for V-57-2 tends to obscure the fact that the two V-57 materials exhibit approximately the same frequency dependence. At 1100 F (593 C), doubling the ordinates of the V-57-2 curve will place it close to the V-57-1 curve, while at 950 F (510 C), the multiplier is close to 1.5. The 950 F (510 C)

TABLE 2—*Fatigue life ratio data.*

Material	Temperature at Failure, deg F	Specimen No.	Total Strain Range	Frequency, cpm	Life, cycles	Calculated Life, This Strain Range at 0.1 cpm	Calculated Life, This Strain Range at 1 cpm	Ratio
A-286...	950	A6	0.0135	0.05[a]	490	601		0.82
	950	A10	0.0114	0.05	778	927		0.84
	950	A24	0.0104	0.05	1057	1197		0.88
	950	A26	0.0110	1	2467	1035		2.38
	950	A14	0.0080	1	5788	2775		2.09
	950	A25	0.0101	10	3662	1307		2.80
	1100	A23	0.0108	1	1152	312		3.69
	1100	A9	0.0080	1	3583	1011		3.54
	1100	A8	0.0108	10	1918	314		6.11
V-57-1...	950	V20	0.0134	0.05	953	943		1.01
	950	V26	0.0111	1	2355	1513		1.56
	950	V23	0.0081	1	6097	3812		1.60
	940	V18	0.0102	10	2636	1858		1.42
	1100	V13	0.0114	1	1165	554		2.10
	1100	V21	0.0082	1	3719	1810		2.05
	1100	V15	0.0109	10	2025	642		3.16
V-57-2...	950	V116	0.0144	0.1	1107		1614	0.69
	950	V119	0.0108	0.1	2803		3809	0.74
	950	V123	0.0080	0.1	10671		11549	0.92
	940	V125	0.0082	10	13651		10243	1.33
	850	V126	0.0081	10	10973		11145	0.98
	930	V118	0.0064	10	36592		31387	1.17
	1100	V115	0.0146	0.1	390		748	0.52
	1100	V120	0.0112	0.1	878		1903	0.46
	1100	V122	0.0082	0.1	4096		7675	0.53

[a] 0.05 cpm obtained by inserting an approximate 11 min hold at maximum deflection.

data exhibit much less frequency dependence. Certain of the V-57-2 ratios at 950 F (510 C) and 0.1 cpm (V116, V119, and V123 in Table 2) indicate alternatively the previous observation that the 0.1 cpm curve might intersect the 1 cpm curve at a total strain range somewhat less than 0.008.

Finally, it should be noted that only 14 test specimens lasted more than 9900 cycles. Of these, ten broke in the gradient portion of the bar, rather than in the central inch. Only two other bars broke outside the central inch. All pertinent data are given in Table 3. Where applicable, the data in Table 3 were plotted in Figs. 3 to 5. It was felt that, if anything, the data in Table 3 understate the actual life, and hence might be shown with the same symbolism as runouts. However, such notation might have been confusing and was not used.

TABLE 3—*Fatigue data where failure occurred either outside the hot zone or beyond 9900 cycles*

Material	Nominal Temperature, deg F	Specimen No.	Approximate Temperature at Failure, deg F	Frequency, cpm	Total Strain Range	Life, cycles
A-286	950	A21	885	1	0.0056	27200
	1100	A22	HZ[a]	1	0.0056	30317
V-57-1	950	V18	940	10	0.0102	2636
	950	V17	925	1	0.0057	12124
	1100	V5	950	1	0.0057	21700
V-57-2	850	V106	HZ	1	0.0080	10689
	900	V107	840	1	0.0081	10047
	950	V112	930	1	0.0138	2075
	950	V123	HZ	0.1	0.0080	10671
	950	V124	915	1	0.0082	10735
	950	V125	940	10	0.0082	13651
	950	V126	850	10	0.0081	10973
	950	V118	930	10	0.0064	36592
	950	V105	750	1	0.0054	74971
	1100	V103	1090	1	0.0079	9908
	1100	V104	HZ	1	0.0057	64391

[a] HZ—occurred within the 1-in. hot zone.

Discussion

The last two observations perhaps can be linked by considering the possibility of strengthening the hot zone by thermo-mechanical treatment during the fatigue test. The indication of a crossover of the 0.1 and 1 cpm total strain range-life curves of V-57-2 at 950 F (510 C) can be interpreted as a manifestation of aging. If the central section is strengthened, especially in those tests where pure high cycle fatigue is approached, the fatigue life there will be increased, and failure may occur in a weaker portion of the

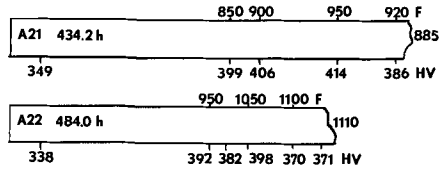


FIG. 7—*Vickers hardness at various points along A-286 specimens tested in fatigue for the hours stated at 1 cpm at* $\Delta\epsilon_T = 0.0056$.

temperature gradient section of the specimen. In Fig. 7, the room-temperature Vickers hardness (average of four 1-kg Vickers indentations performed on a Tukon microhardness tester) is shown in relation to test temperature for two broken A-286 test specimens. Note that the 950 F (510 C) specimen is considerably harder at the center, while maximum hardness does not occur at the center at 1100 F (593 C). The V-57 specimens examined exhibit similar, but less marked, behavior. While it is not known how the room-temperature hardness will correlate with hardness at temperature, it is anticipated that the hardness pattern will persist at test temperature.

In fact, the strange behavior at 950 F (510 C) in Fig. 6 may be caused also by aging during the test. Undoubtedly the positive slopes in Fig. 6 are related to the aggressive (air) environment. The diminution of slope upon going from 1 to 10 cpm may result from a complex interaction between oxidation and hardening, which both have less time to operate as the frequency increases. The one A-286 off-center break (Table 3) was not used in the preparation of Fig. 6, while only one V-57-1 point appears in both Tables 2 and 3, and in Fig. 6. Hence, it cannot be argued that the decrease in slope in Fig. 6 at 950 F (510 C) with increasing frequency is caused by off-center breaks *per se*. The case for V-57-2 is not as good, because all three 10-cpm points (V125, V126, and V118 in Table 2) failed in the gradient region. However, these lives are all over 10 000 cycles and are almost an order of magnitude longer than the 10-cpm lives of A-286 and V-57-1 in Table 2.

While there is no way of knowing with certainty whether the 950 F (510 C) curves in Fig. 6 are levelling off or are going through a maximum, there is some evidence in the literature for the existence of a maximum in the life-frequency curve. Organ and Gell have shown that the high-cycle fatigue life of Udimet 700 at 1400 F (760 C) goes through a maximum [*9*], although the frequency corresponding to maximum life is considerably higher than what is suggested by this investigation.

Fatigue testing at a frequency that lies on the plateau, or even beyond a possible maximum, will yield meaningless data, if the application frequency is on the ascending portion of the life-frequency curve. Therefore, in fatigue testing at high temperature, specimens should be tested either at the application frequency, or at several frequencies on the same side of a possible maximum as the application frequency. The merit of testing at several

frequencies can be seen by referring to Fig. 4. Clearly V-57-1 is superior to A-286 at 0.1 cpm. Suppose that 0.1 cpm is the application frequency. Obviously testing of A-286 and V-57-1 at 1 cpm would not show any difference, and misleading data would be obtained by testing at 1 cpm only.

A replot on log-log paper of Fig. 6 will not yield straight lines. Yet Coffin's treatment [*2,10*] requires one straight line, and Manson's treatment [*11,12*] requires two straight lines, one with a slope of approximately +1 in the region where N_f' should be used, and one with zero slope where N_f should be used, when these theoretical expectations are plotted on log-log paper. The results of Organ and Gell [*9*] and the present investigation indicate that nonlinear behavior will occur. Of the three possibilities, accelerating fatigue tests by increasing frequency is still deemed superior to increasing either the strain range or the temperature of test. However, it would be much more comforting to fall back on a theoretical analysis of the nonlinear behavior that might indicate where one can safely take the second test frequency, after he has obtained data at the first frequency. The only alternative now open is to work at the application frequency: if this happens to be 0.05 cpm, and the desired life is 50 000 cycles, the test could take years —hardly an appetizing thought.

In the introduction, it was stated that V-57 was examined because it could perform better in situations where A-286 approaches cyclic rupture. Under conditions of cyclic rupture, the time to failure is a constant, and hence the cycles to failure (N_f) will equal the failure time multiplied by the frequency (ν). On a log (N_f)-log (ν) plot, the slope will be +1. Consider now the 1100 F (593 C) A-286 data, Table 2 or Fig. 6. If, as an approximation, it is assumed that the frequencies are 0.1, 1, and 10 cpm instead of 0.1084, 1.04, and 10.1 cpm, an approximate relationship between ratio R and frequency is $R = 2.55 \log (\nu) + 3.55$. The slope of the log-log plot becomes $d \log (R)/d \log (\nu) = 0.434/[\log (\nu) + 1.39]$. It will equal 1 at a frequency slightly above 0.1: A-286 at 1100 F (593 C) is possibly on the verge of cyclic rupture at the lowest test frequency investigated. In similar fashion, for V-57-1 at 1100 F (593 C), $d \log (R)/d \log (\nu) = 0.434/[\log (\nu) + 2]$. This equation suggests that the frequency will have to drop to about 0.03 cpm before cyclic rupture can be expected. Thus testing at decreasing frequency below 0.1 cpm might show an increasing superiority af V-57-1 over A-286 at 1100 F until the frequency drops to 0.03 cpm, and then a fixed ratio of the cyclic lives of the two materials as the frequency is decreased still further.

As was stated previously, the frequency dependence of the two V-57 lots is almost identical. However, the level of the curves is different, and this is why A-286, with a larger frequency dependence, can overtake V-57-1 at 1 cpm. Note that the superiority of V-57-2 over V-57-1 is little changed by the shift of a decade in frequency in Fig. 4, because the frequency dependence of the two lots is essentially the same.

Conclusions

1. For meaningful results, candidate materials should be tested either at the application frequency or at several frequencies on the application side of any maximum or plateau that might occur in cyclic life as a function of frequency. At 950 to 1100 F (510 to 593 C) at 0.1 cpm, V-57 is clearly superior to A-286; at 1 cpm, there is already some doubt.

2. In most purely cyclic applications at 950 to 1100 F (510 to 593 C), the fatigue component of damage of A-286 or intermediate-aged V-57 will be in the high-cycle fatigue regime.

3. It is believed that these materials can undergo further aging during fatigue testing, and that this "thermo-mechanical processing" can affect the fatigue behavior.

Acknowledgments

The author wishes to thank K. T. Lindquist for suggesting the investigation. He is indebted to L. F. Coffin, Jr., and A. K. Schmieder for their patience and advice, and to S. J. Duckworth for the split collar arrangement. Many members of the Electromechanical Analysis and Measurements Laboratory are thanked for their contributions toward the automation of the measurement of the hysteresis loop. Finally, S. F. Wurst is thanked for his help in collecting the data.

References

[*1*] Eckel, J. F., *Proceedings*, American Society for Testing and Materials, Vol. 51, 1951, pp. 745–756.

[*2*] Coffin, L. F., Jr., and Goldhoff, R. M., "Predictive Testing in Elevated Temperature Fatigue and Creep: Status and Problems," Technical Report 71-C-114, General Electric Co., Schenectady, N. Y., 1971.

[*3*] Dawson, R. A. T., Elder, W. J., Hill, G. J., and Price, A. T. in *Thermal and High Strain Fatigue*, The Metals and Metallurgy Trust, London, 1967, pp. 239–269.

[*4*] Vinter, Anthony and Wilbers, L. G., *Journal of Metals*, Vol. 22, May 1970, pp. 46–54.

[*5*] Forrest, P. G. and Penfold, A. B., *Engineering*, Vol. 192, 1961, pp. 522–523.

[*6*] Halford, G. R., "Help Keep Mechanics in the Study of the Mechanical Behavior of Materials, or 'Whatever Happened to Stress and Strain,'" Technical Memo PGB No. 21, University of Illinois, Champaign, Ill., 14 May 1964.

[*7*] Gross, M. R. in *Manual on Low Cycle Fatigue Testing, ASTM STP 465*, American Society for Testing and Materials, 1969, pp. 149–162.

[*8*] Oldroyd, P. W. J., *Journal of Strain Analysis*, Vol. 6, Oct. 1971, pp. 286–292.

[*9*] Organ, F. E. and Gell, M., *Metallurgical Transactions*, Vol. 2, 1971, pp. 943–952.

[*10*] Coffin, L. F., Jr., *Metallurgical Transactions*, Vol. 2, 1971, pp. 3105–3113.

[*11*] Manson, S. S. and Halford, Gary in *Thermal and High Strain Fatigue*, The Metals and Metallurgy Trust, London, 1967, pp. 154–170.

[*12*] Manson, S. S., *Experimental Mechanics*, Vol. 8, 1968, pp. 349–355.

P. K. Venkiteswaran,[1] *D. C. Ferguson,*[1] *and D. M. R. Taplin*[1]

Combined Creep-Fatigue Behavior of Inconel Alloy X-750

REFERENCE: Venkiteswaran, P. K., Ferguson, D. C., and Taplin, D. M. R., **"Combined Creep-Fatigue Behavior of Inconel Alloy X-750,"** *Fatigue at Elevated Temperatures, ASTM STP 520*, American Society for Testing and Materials, 1973, pp. 462–472.

ABSTRACT: A study has been made of the effect of superimposing a small lateral vibratory stress on the axial creep behavior of Inconel Alloy X-750 at 700 C. Tests were conducted in a specially designed creep-fatigue testing machine using specimens simulating gas turbine blades. From preliminary data in combined creep-fatigue, it was found that the creep rate was lower and rupture life higher by almost an order of magnitude compared to the creep values. Fracture mode in combined creep-fatigue was a mixture of intergranular, fatigue, and cleavage. It was also observed that the cleavage fracture was "bowed out" or serrated indicating that the intragranular γ' precipitates arrest the propagation of cracks. This and the change in fracture mode could be responsible for the lower creep rates and longer rupture lives. There was no evidence of grain boundary migration, change in grain size, or formation of "diamond" grains.

KEY WORDS: fatigue (materials), fatigue tests, creep rupture strength, stresses, crack propagation, tests

It is well known that intergranular brittle fracture in high temperature ($>0.5\ T_m$ where T_m is the absolute melting temperature) creep is often due to the nucleation, growth, and eventual linking of cavities along grain boundaries. It has been suggested that cavitation in long-life high-temperature fatigue is similar to that in creep. Although a comparatively large amount of work has been done in high-temperature creep and axial fatigue, not much work has been reported on combined creep-fatigue at high temperatures. The work that has been reported to date has been mainly on uniaxial stress systems in which an alternating stress is superimposed on a static stress. However, in such important applications as power plants, supersonic aircraft frames, and gas turbines the stress system is complex in nature. No systematic study has been reported in the literature on materials tested under these conditions. The main objective of the present investigation is to study the effect of superimposing a small lateral vibratory stress

[1] Research assistant and associate professors, respectively, Department of Mechanical Engineering, University of Waterloo, Waterloo, Ont., Canada.

Copyright© 1973 by ASTM International www.astm.org

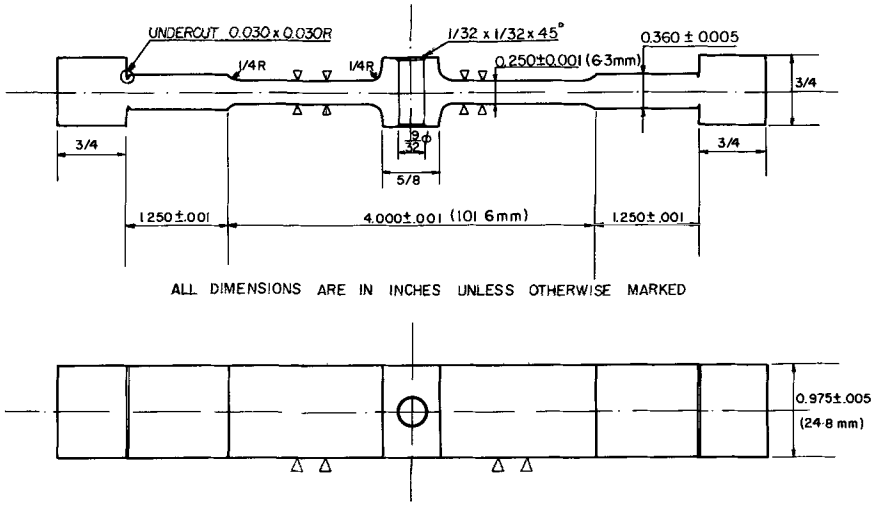


FIG. 1—*Combined creep-fatigue specimen.*

on the axial creep and rupture behavior of a gas turbine blade material, Inconel Alloy X-750. The work is oriented to direct practical applications in the gas turbine industries.

The effect of superimposing a small cyclic stress on the creep behavior has been either an increase [*1–6*][2] or a decrease in creep rate [*2,7,8*]. The increase in creep rate has been attributed to softening due to vacancy condensation on dislocation jogs, the greater mobility of oscillating dislocations in fatigue, vacancy annihilation, and dislocation climb. The hardening has been attributed to vacancies clustering to impede dislocation motion, condensation of vacancies along dislocation lines, and vacancy generation and pinning mechanisms.

The polished specimens were etched electrolytically in 5 percent nital, chemically in $20HNO_3$-3HF solution or 30 lactic acid-$20HCl$-$10HNO_3$ solution to reveal precipitates within the grain and along grain boundaries.

Creep-Fatigue Testing Machine

The specimen used was designed to simulate a gas turbine blade, and the test was carried out in specially designed creep-fatigue testing machine as shown in Figs. 1 and 2. The testing machine consisted of a frame work made of channel sections. At the top of the frame is a fixed cantilever beam and at the bottom is a loading lever with a loading arm ratio of 1 : 1. The fixed cantilever beam has been designed to deflect 25 μm at the maximum load of 10 000 kg. The load is applied to the specimen through knife edges by means of a hydraulic loading jack and regulator which can maintain pres-

[2] The italic numbers in brackets refer to the list of references appended to this paper.

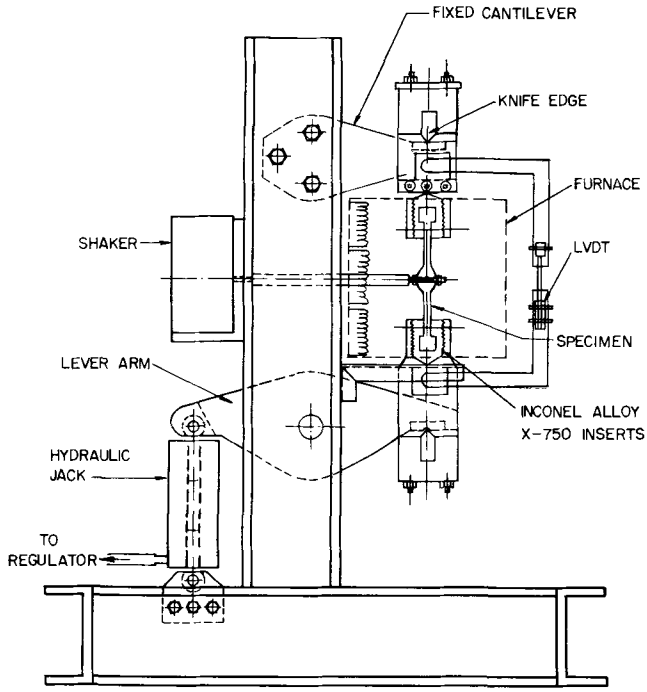


FIG. 2—*Combined creep-fatigue testing machine.*

sures to an accuracy of ±0.25 percent at 41 MN/m² (6000 psi) and ±0.5 percent at 69 MN/m² (10 000 psi). These pressures produce stress levels on the specimen of 445 MN/m² (65 000 psi) and 684 MN/m² (100 000 psi), respectively. The specimen which simulates a two-blade construction is held in stainless steel grips with Inconel Alloy X-750 inserts. This minimizes the deformation of the grips which becomes critical as the load and temperature are increased to the maximum levels. The deformation is measured using a pair of identical linear variable differential transformers (LVDT's), one on either side of the specimen as shown in Fig. 2. The LVDT's are connected in series, and the enhanced output is recorded using a recorder with chart speeds as low as 2½ mm/h. The recorder can measure voltages as low as 10^{-5} V corresponding to 0.025 μm displacement of LVDT.

The lateral vibratory stress is applied by means of an electromagnetic shaker and power amplifier. This unit is capable of applying vibratory load levels of the order of 125 acceleration due to gravity (G) at frequencies of up to 50 KHz with the current test specimen which corresponds to a stress level of ±5.1 MN/m² (7500 psi) in the natural frequency range of 900 to 1000 Hz. The amplitude of vibration (G-level) is maintained by means of a closed loop circuit which includes the electromagnetic shaker, power amplifier tuner filter, servomonitor, and accelerometer.

The axial load is applied after the temperature has reached a steady-state value in a period of 2 h. The amplitude of vibration (G-level) is set at the natural frequency of 555 Hz for the 6.3-mm-thick specimen, and the test is continued. After a period of time, the natural frequency changes due to the formation of cavities, cracks, or changes in internal damping due to hardening or softening processes. When this happens, the power amplifier draws more current in order to maintain the amplitude at the original natural frequency. The vibratory frequency can be retuned to the natural frequency and the test continued. The returning operation can be carried out till the power amplifier is not capable of providing the required power to the shaker. When this condition is reached, the power amplifier switches off which shuts off the furnace and the recorder. Alternatively, the specimen may fail which triggers a microswitch to switch off the power amplifier, furnace, and recorder.

Experimental

Material

The material used in this investigation is Inconel Alloy X-750 which is an age-hardenable nickel-chromium alloy with high corrosion and oxidation resistance up to 810 C. The nominal composition of this material is given in Table 1.

TABLE 1—*Nominal composition of Inconel Alloy X-750.*

Ni	Cr	Fe	Ti	Al	Cb + Ta	Mn	Si	S	Cu	C
7.36	14.9	6.98	2.58	0.61	0.92	0.1	0.18	0.07	0.04	0.03

The following heat treatments were used to give average grain sizes in the range of 9 to 200 μm as measured by the linear intercept method (Table 2).

TABLE 2—*Heat treating sequence to produce variations in grain size.*

200 μm	113 μm
1149 C/4 h air cool	1205 C/1 h air cool
840 C/24 h air cool	840 C/24 h air cool
705 C/20 h air cool	705 C/20 h air cool
61 μm	**9 μm**
1149 C/2 h water quench	None
927 C/24 h water quench	885 C/24 h air cool
705 C/20 h water quench	705 C/20 h air cool

Results

The 200-μm grain size material was stressed to 342 MN/m^2 (50 000 psi) at 700 C and a lateral vibratory stress of $\pm$25 MN/m^2 ($\pm$3600 psi) was applied at the natural frequency of 855 Hz (corresponding to 9$^1/_2$ mm thickness along the gage length). After 410 h, the axial stress was raised to 411 MN/m^2 (60 000), and the test continued for another 500 h. The creep deformation curve is shown in Fig. 3.

The 113-μm grain size material was tested at 411 MN/m^2 (60 000 psi) at 700 C with a lateral vibratory stress of $\pm$25 MN/m^2 ($\pm$3600 psi) at the natural frequency of 555 Hz (corresponding to the new thickness of 6.3 mm along the gage length). The vibratory stress was increased to $\pm$33 MN/m^2 ($\pm$4850 psi) after 392 h, and the test continued till fracture. The creep deformation curve is shown in Fig. 4. Also shown in Fig. 4 is the creep deformation behavior of this material when the vibratory stress level was $\pm$41 MN/m^2 ($\pm$6000 psi).

To analyze the effect of superimposing small lateral vibratory stresses on the axial creep behavior, pure creep tests were also conducted on identical test specimens in this testing machine. The results obtained in the case of 200 and 113-μm grain size materials are shown in Fig. 5.

The fractured surfaces were examined in a scanning electron microscope to study the macroscopic, microscopic, and submicroscopic details of the

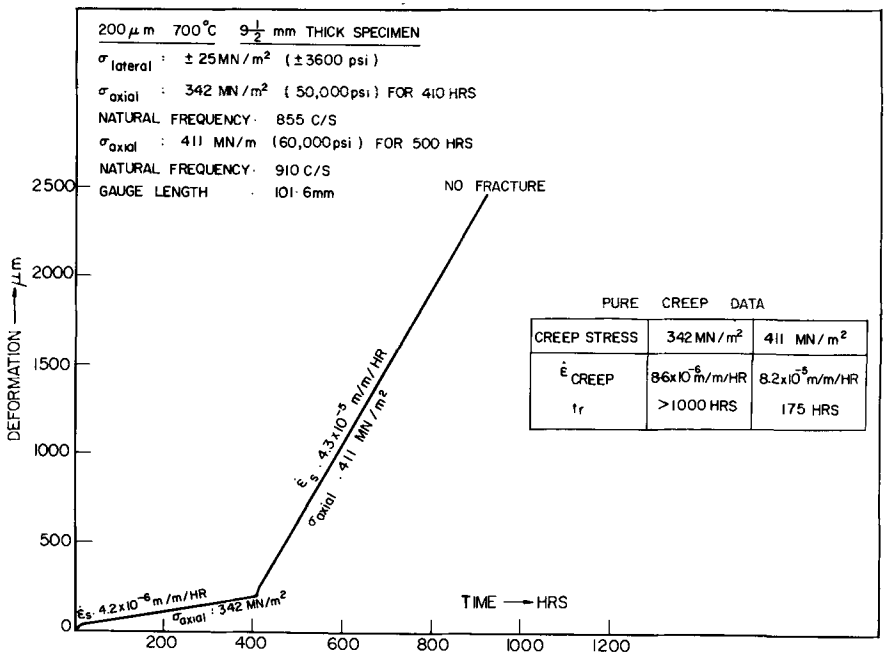


FIG. 3—*Creep deformation behavior under combined creep-fatigue loading: 200-μm grain size.*

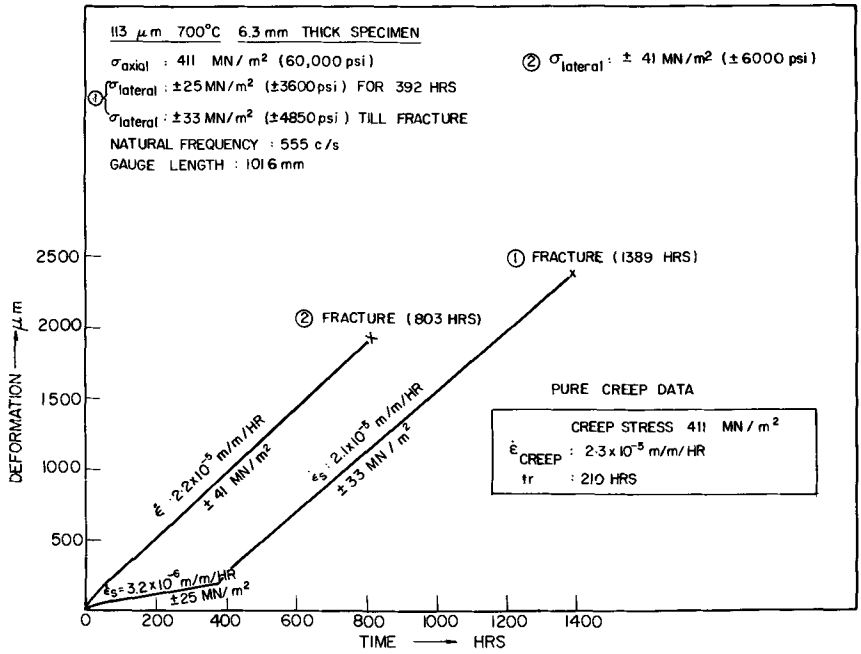


FIG. 4—*Creep deformation behavior under combined creep-fatigue loading: 113-μm grain size.*

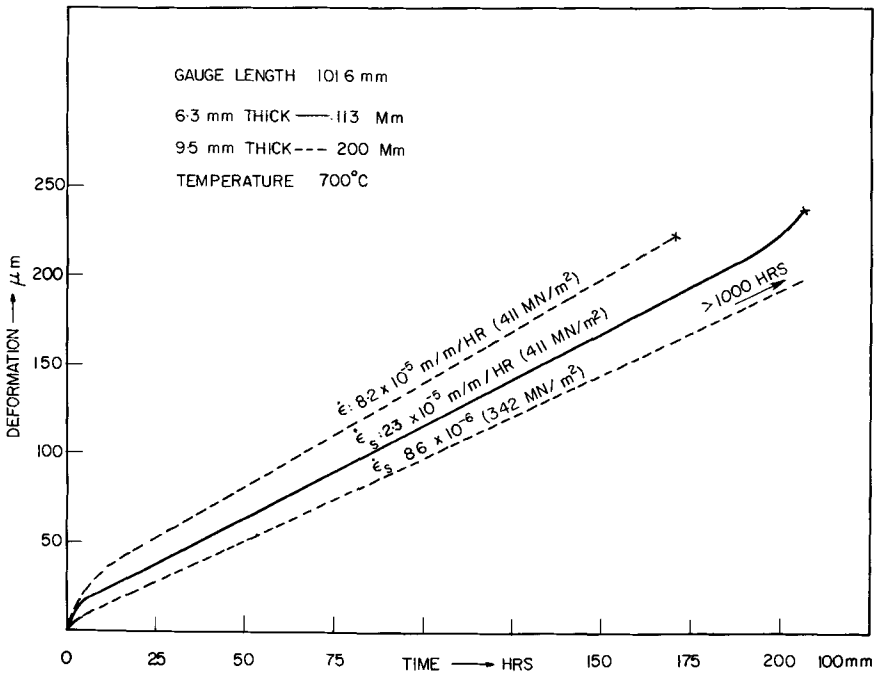


FIG. 5—*Creep deformation curves for specimens of different sizes.*

fracture phases as revealed in the fractured surface. Typical fracture characteristics of Inconel Alloy X-750 in combined creep-fatigue and in creep are shown in Figs. 6 and 7, respectively.

Discussion

It may be seen from Fig. 3 that in the case of 200-μm grain size material, the creep rate increased by an order of magnitude and the natural frequency increased by about 6 percent as the axial stress was increased by 69 MN/m^2

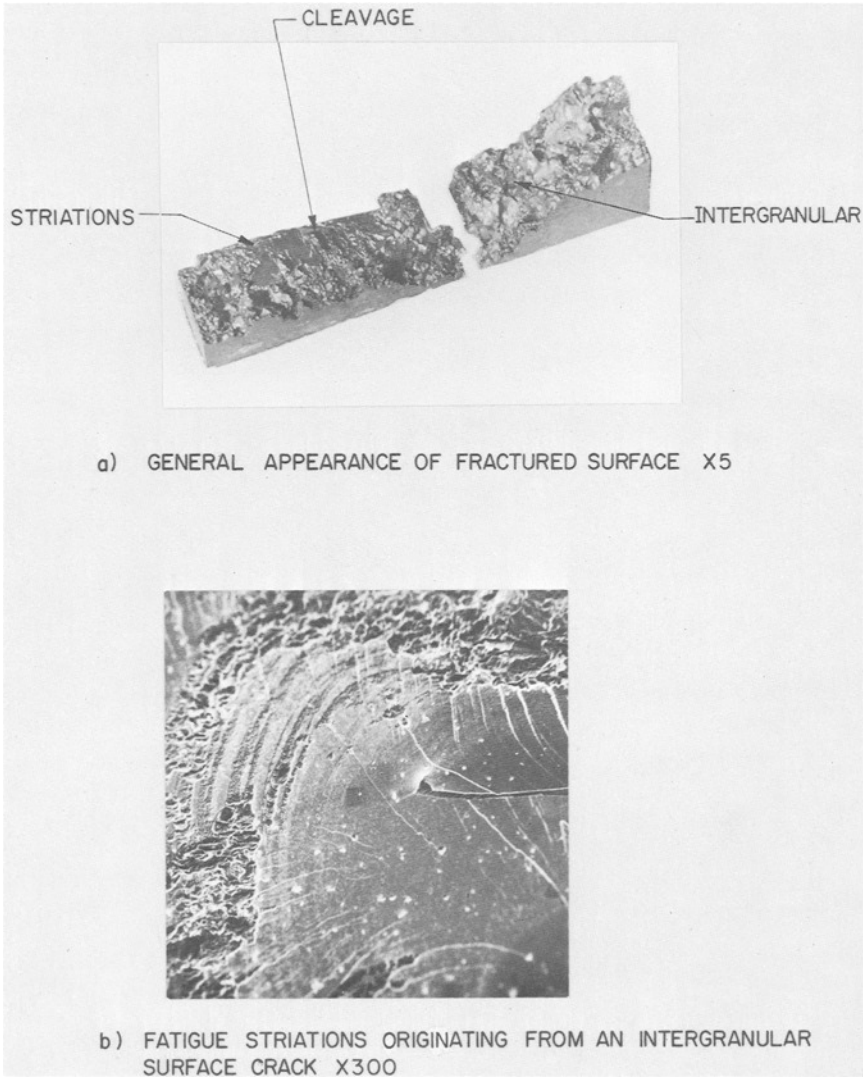


FIG. 6—*Fractographs of fracture surface (in combined creep-fatigue).*

(10 000 psi). From the table in Fig. 3, it is also seen that the minimum creep rate in pure creep was higher than that in combined creep-fatigue at the two stress levels tested. Also, to be noted is that the specimen had not fractured in combined creep fatigue after 910 h, whereas the life of the material in pure creep was 175 h at the stress level of 411 MN/m^2 (60 000

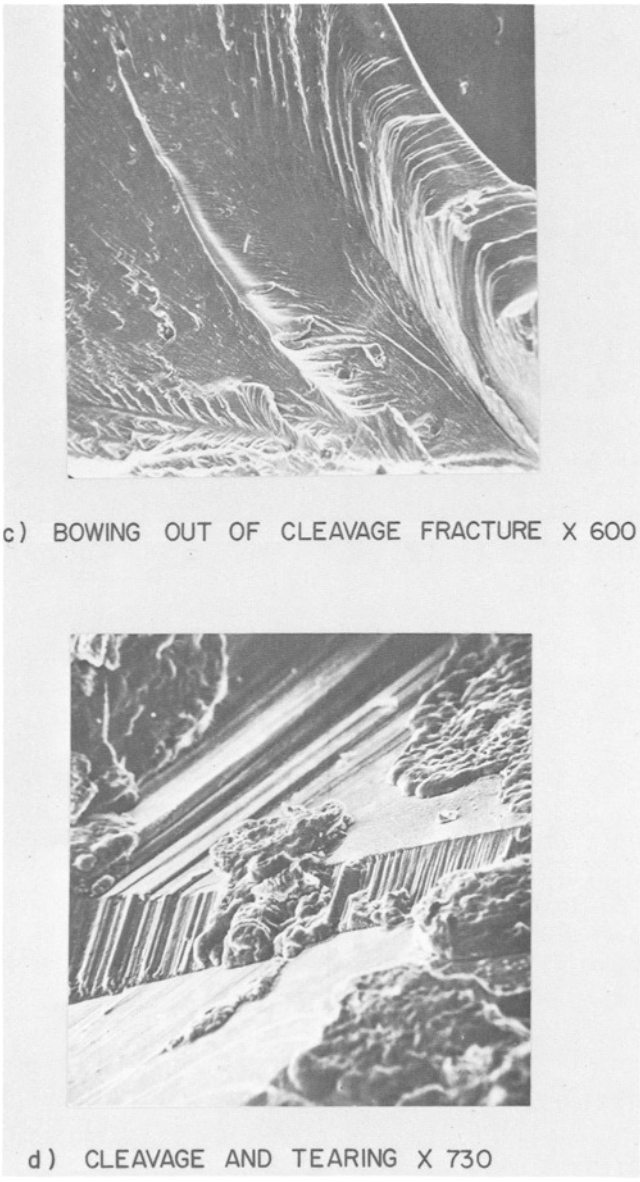


FIG. 6—(*Continued*).

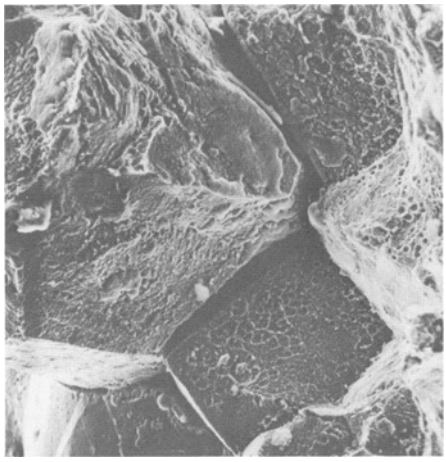


FIG. 7—*Intergranular fracture of Inconel Alloy X-750 during creep at 700 C* σ: *50 000 psi (324 MN/m²) (×200).*

psi). Metallographic examination of the creep-fatigue or creep specimens did not reveal grain boundary migration or change in grain size.

In the case of 113-μm grain size material (Fig. 4), it may be seen that the creep rate increased as the level of vibratory stress was increased. This value closely approached the minimum creep rate value in pure creep when the vibratory stress level was ± 41 MN/m² (± 6000 psi) (Table in Fig. 4). The life of the material in combined creep-fatigue decreased as the level of vibratory stress was increased. However, this was still higher than that in pure creep under similar axial stress.

Examination of the fracture surface in combined creep-fatigue of the 113-μm grain size material (Fig. 6) showed that the fracture mode was a mixture of intergranular, fatigue, cleavage, and plastic tearing. Also, it is to be noted from Fig. 6*a* that the intergranular fracture area oxidized the least, indicating that the final fracture was in intergranular failure. From Fig. 6*b*, it is seen that the fatigue crack originated from an intergranular surface crack. There were no other fatigue cracks on the fracture surface. From Fig. 6*c*, it is seen that the cleavage fracture is serrated or bowed out indicating that the cleavage crack propagation was arrested by, presumably, intragranular γ' (Ni_3Al-Ti) precipitates. Metallographic examination did not indicate any grain boundary migration or change in grain size. However, the number of surface cracks increased compared to that in pure creep.

From the foregoing, it is seen that in the case of 200 and 113-μm grain size materials the creep rate under combined creep-fatigue conditions is lower than that observed in pure creep. Similar observations have been made by various investigators [*3,7,8*]. This behavior is accompanied by an increase in rupture life. This decrease in minimum creep rate could be due

to the formation of complex dislocation tangles, vacancy condensation along dislocation lines and crack tips, and also change of fracture mode, for example, from purely intergranular fracture in creep (Fig. 7) to a mixture of intergranular, fatigue, and cleavage modes of failure in combined creep-fatigue. The fact that the fatigue and cleavage fracture areas were oxidized much more than the intergranular fracture area (Fig. 6*a*) gives support to the supposition that it is difficult for the fatigue and cleavage type of cracks to propagate along the matrix containing γ' precipitates. This, together with the serrated or bowed out appearance of the cleavage fracture, indicates that the crack propagation is being slowed down or arrested presumably by the intragranular γ' precipitates. This could be responsible for the lower minimum creep rates and longer rupture lives in combined creep-fatigue.

Conclusions

This study of Inconel Alloy X-750 suggests that:

1. Effect of superimposing a small lateral vibratory stress is to reduce creep rate and increase rupture life.
2. The fracture mode changes from purely intergranular in creep to a mixture of intergranular, fatigue (striations), and cleavage in combined creep-fatigue.
3. The reduction in creep rate and increase in rupture life in combined creep-fatigue could be due to the change of fracture modes and the effectiveness of the γ' particles in slowing down the intragranular cleavage and fatigue cracks.
4. The intergranular fractures from creep and combined creep-fatigue loading conditions could not be distinguished as creep intergranular fracture or combined creep-fatigue fracture.
5. There is no grain boundary migration or "diamond grain" formation under the present test conditions. The grain size also remained unchanged.
6. Increasing the vibratory stress level decreases its beneficial effects on creep. There appears to be a threshold vibratory stress level corresponding to an axial stress when there will be no beneficial effects from the vibratory stress.

Acknowledgments

The work was supported by the National Research Council and Defense Research Board of Canada. Discussions with Professor D. J. Burns are acknowledged with pleasure.

References

[*1*] Kennedy, A. J. in *Proceedings*, International Conference on Fatigue of Metals, Institute of Engineers, 1956, p. 401.
[*2*] Meleka, A. H. and Evershed, A. V., *Journal*, Institute of Metals, Vol. 88, 1959–1960, p. 411.

[3] Kamel, R. and Bessa, F. A., *Acta Metallurgica*, Vol. 13, 1965, p. 19.
[4] Davies, P. W. and Wilshire, B., *Metallurgia*, Vol. 76, 1967, p. 93.
[5] Sullivan, C. P., Webster, G. A., and Piearcey, B. J., *Journal*, Institute of Metals, Vol. 96, 1968, p. 274.
[6] Ellison, E. G. and Sullivan, C. R., *Transactions*, American Society for Metals, Vol. 60, 1967, pp. 88.
[7] Price, A. T., *Journal*, Institute of Metals, Vol. 95, 1967, p. 87.
[8] Davies, P. W., Sidey, D., and Wilshire, B., *Journal*, Institute of Metals, Vol. 97, 1969, p. 15.

DISCUSSION

M. Manjoine[1] (*written discussion*)—Earlier work by Lazan and myself indicated that at higher creep stress levels, the alternating stress caused an increase in creep rate but at lower stress levels, the alternating stress caused a decrease in creep rate. Question: Was this true in your tests?

P. K. Venkiteswaran, D. C. Ferguson, and D. M. R. Taplin (authors' closure)—Because of the limited number of tests, a positive and conclusive answer cannot be given. However, at the two axial stress levels investigated (50 000 and 60 000 psi), we observed a decrease in the creep rate compared to that in pure creep.

[1] Westinghouse Research Laboratories, Pittsburgh, Pa. 15235.

U. S. Lindholm[1] *and D. L. Davidson*[1]

Low-Cycle Fatigue with Combined Thermal and Strain Cycling

REFERENCE: Lindholm, U. S. and Davidson, D. L., "**Low-Cycle Fatigue with Combined Thermal and Strain Cycling,**" *Fatigue at Elevated Temperatures, ASTM STP 520*, American Society for Testing and Materials, 1973, pp. 473–481.

ABSTRACT: Test data are reported for both isothermal and nonisothermal strain cycling of a nickel-base superalloy in the temperature range from 1100 to 1700 F. The mechanical strain range for all tests was held constant while the mean strain, holdtime, and thermal cycling was varied. The results are discussed in terms of energy criterion for fatigue life.

KEY WORDS: fatigue (materials), isothermal treatment, superalloys, nickel containing alloys, thermal cycling tests, fatigue life, strain tests

High-temperature components, such as turbine blades, experience during actual service a complex, time-varying load and thermal history. Prediction of blade response, or of blade life, based solely on isothermal strength, fatigue or creep tests may not be possible because of complex microstructural dependence on deformation and temperature history. The inelastic response of metals is dependent upon past history of deformation and temperature; therefore, the sequencing of the loading and temperature variations can be important to low-cycle fatigue life. The test program described herein provides some data on the effect of complex strain-temperature cycling on fatigue life of a nickel-base superalloy.

The tests include both isothermal and nonisothermal strain cycling in the temperature range for 1100 to 1700 F. All tests had a mechanical strain range of 0.78 percent and were performed at a constant strain rate of $\pm 2 \times 10^{-4}$ s^{-1}. Therefore, the tests demonstrate the effect on fatigue life of changes in temperature and on the phasing between temperature and strain only. An attempt is made to correlate the cyclic failure life in terms of energy dissipation per cycle and some of the difficulties in this approach are discussed.

[1] Director and senior research engineer, respectively, Department of Materials Sciences, Southwest Research Institute, San Antonio, Tex. 78284.

Copyright© 1973 by ASTM International www.astm.org

Test Procedures

The test specimens were provided by Pratt & Whitney Aircraft Division of United Aircraft Corp. The material was a nickel-based superalloy with nominal composition in weight percent of 8Cr, 10Co, 6Al, 6Mo, 1Ti, 0.1C, and the remainder nickel. Specimens were coated with an aluminum oxide type coating. The gage section was nominally 0.250 in. diameter and 0.250 in. uniform length with threaded end connections.

The tests were conducted in a hydraulic, servo-controlled, cyclic load facility with strain feedback. Strain was measured with an axial, clip-type extensometer referenced to the specimen at the base of the threads. This control extensometer was calibrated to indicate strain at the center of the gage section by comparison with a water-cooled capacitance extensometer attached directly to the gage section center of one fatigue specimen, and then cycling this specimen at temperature. Specimen heating was accomplished by resistance heating, with temperature feedback obtained from a thermocouple attached mechanically (not bonded) to the center of the gage section.

Programmed strain and temperature cycling was accomplished by generating the desired ramping functions to control both strain and temperature. All combined thermal and mechanical testing was done with the machine under strain control. To transform the measured total strain or extensometer signal to mechanical strain (the desired control variable) a linear approximation was made for the thermal coefficient of expansion. However, over the temperature range considered, thermal expansion was a nonlinear function of temperature. Thus, some stress variation did occur during purely thermal cycling because of this incomplete compensation. The maximum strain error from this source was 250 $\mu\epsilon$.

The strain-temperature cycles employed are illustrated schematically in Fig. 1. Cycles numbered 1 through 9 are isothermal with variable mean strain. Cycles, 7, 8, and 9 were also repeated with a 2-min holdtime at maxi-

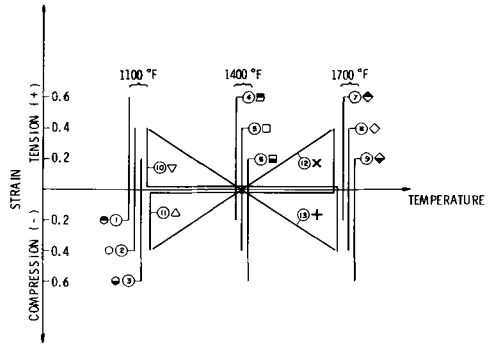


FIG. 1—*Strain-temperature cycles used in fatigue testing. Numbers and symbols are for reference with later figures.*

mum tensile and compressive strain. Cycles 10 through 13 are coupled and uncoupled thermal-strain cycles, including differences in phasing between the temperature and strain. The specimens were cycled to failure (separation) or to at least 50 percent drop in load.

Results

Cyclic life to failure, N_f, for each of the strain-temperature paths of Fig. 1 is shown in Fig. 2. Each data point is the average of two to four specimens per test condition. The following general observations may be made from these results:

1. Cyclic life is reduced with increasing temperature.
2. A tensile mean strain is generally more damaging than a compressive mean strain. The compressive mean strain becomes proportionally more damaging at the higher temperatures, probably because of increasing contribution of creep damage to the total life.
3. The effect of the 2-min holdtime at 1700 F is to reduce the number of cycles to failure and to reduce the effect of mean strain on life. During the holdtime there is a transfer of elastic energy to inelastic deformation accompanied by stress relaxation.
4. For the coupled temperature-strain cycles (12 and 13), the greatest reduction in cyclic life occurs when temperature and strain are in phase; that is, maximum tensile strain occurs at maximum temperature. Life for the coupled cycles is significantly less than for an isothermal cycle at the maximum temperature (1700 F). This suggests that the thermal cycling introduces additional damage associated with thermal inhomogeneities, either microscopic or macroscopic. For the out-of-phase cycle, the life fell between the isothermal lives at the extremes of the temperature range.
5. Cyclic life for both uncoupled temperature-strain cycles (10 and 11) was less than for isothermal cycling at 1700 F. An apparent anomaly exists because the in-phase cycle (11) yields a longer life than the out-of-phase cycle (10). This behavior may be partially explained by examining the cyclic stress-strain curves.

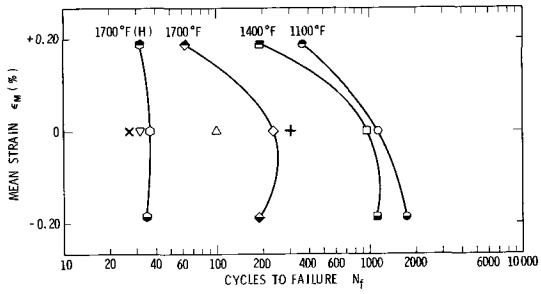


FIG. 2—*Cyclic life for strain-temperature cycles indicated in Fig. 1.*

Some typical cyclic stress-strain curves are shown in Fig. 3 for isothermal and nonisothermal cycles. Curves such as these were integrated to determine the mechanical energy dissipated per cycle. The strains plotted are the total strains measured by the extensometer. The isothermal tests produced hysteresis loops of expected magnitude and shape at both 1100 and 1400 F despite observable crazing of the surface protective coating. At 1700 F the hysteresis loops became nonsymmetric between the tension and compression portions of the cycle, Fig. 3, a condition attributed to the nonsymmetry in measured creep characteristics of the material in tension and compression at this temperature. There was also some evidence of significant porosity

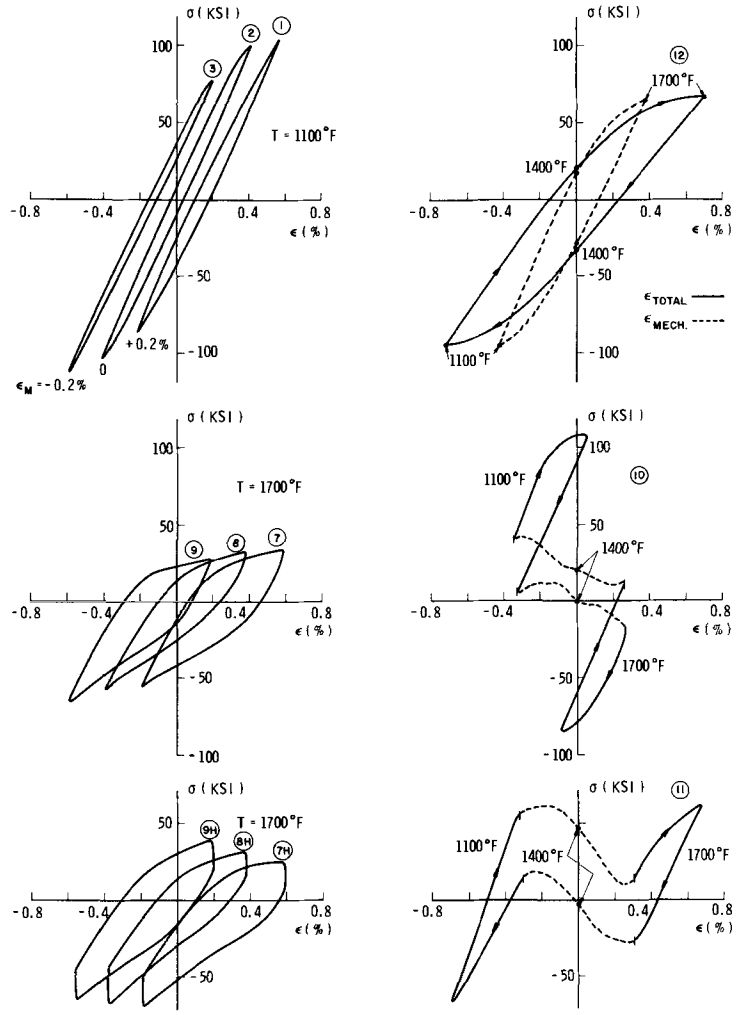


FIG. 3—*Typical cyclic stress-strain curves with mechanical strain range held constant.*

in the castings which could lead to the above observed effects. For the coupled temperature strain cycle (12), the mechanical strain is determined by subtracting an amount equal to the free thermal expansion at each temperature. For the uncoupled tests (10 and 11), the stress variation during the change in temperature (dotted line) arises from the previously mentioned nonlinearity of the expansion coefficient. Thus, a stress offset occurs at the start of each strain half-cycle such that the stress range is greater for the out-of-phase cycle (10) than for the in-phase cycle (11). The higher average stresses in the uncoupled, out-of-phase cycle may explain its lower fatigue life.

It should also be noted that temperature cycling in the uncoupled tests has a marked effect upon the mechanical strain portion of the cycle, as evidenced by comparison of the stress-strain curves for these tests with those obtained under totally isothermal conditions. This is an indication of the importance of temperature and strain history on the instantaneous material response.

One method for correlating data for any arbitrary cyclic-strain-temperature history is by means of the energy dissipated per cycle (the area enclosed within the load-mechanical strain hysteresis loop.) This is the energy expended in altering the internal crystalline structure or dissipated as heat. Thus, it is reasonable to relate this energy to damage accumulation. A plot of energy dissipation per cycle, ΔE_p, versus cycles to failure, N_f for each specimen tested is given in Fig. 4. Since the cycles were fairly stable (negligible cyclic hardening or softening), ΔE_p was nearly constant over the life of the specimen.

In the logarithmic plot of Fig. 4, the isothermal data at the three test temperatures appears to fall along three lines having a constant slope of approximately $-\frac{1}{4}$. The relatively wide variation in cycles to failure at

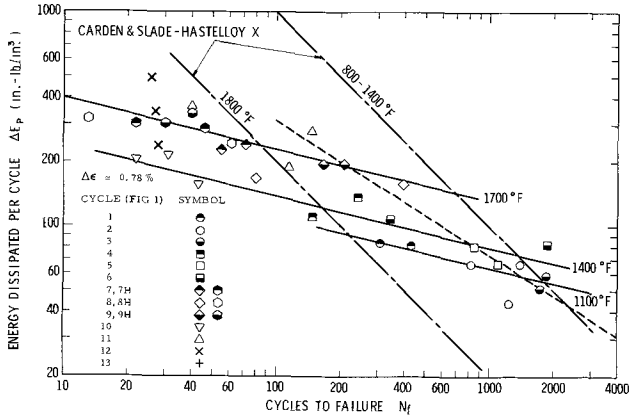


FIG. 4—*Relationship between measured energy dissipated per cycle to number of cycles at failure.*

each temperature is due to a holdtime or change in mean strain, while the temperature and strain range are held constant. The completely reversed cyclic tests (2, 5, and 8) have the longer lives and are connected by a dashed line. Also shown are the slopes obtained by Carden and Slade [*1*][2] at two temperatures for Hastelloy X. These slopes (approximately -1) were defined primarily by tests in which the strain range was varied for completely reversed cycles. The relationship between the various slopes shown in Fig. 4 will be discussed later.

Data points for the nonisothermal cycles 11 and 12, which have maximum tensile strain occurring at the maximum temperature of 1700 F, fall near the isothermal 1700 F data in Fig. 4. For cycle 10, where the tensile half-cycle occurs at 1100 F, the data correlate with the intermediate temperature of 1400 F. The total strains recorded for cycle 13 were so small that it was not possible to accurately determine the energy dissipated, so data for these tests are not shown.

Discussion

For complex or arbitrary cyclic strain and temperature histories, it may be difficult to apply the standard cumulative damage laws based upon isothermal fatigue and creep rupture tests. Therefore, it is tempting to apply an energy criteria based upon the reasonable hypothesis that the cyclic life will be a function of the total energy dissipated. Mathematical representations of this hypothesis have been formulated by Feltner and Morrow [*2*], Stowell [*3,4*], and Lemaitre [*5*]. The formulation of Stowell [*4*] specifically incorporates temperature, but was applied by Stowell only to isothermal test data. There are two critical aspects of the energy approach to fatigue life prediction. First is the establishment of an appropriate constitutive equation which will adequately describe the relationship between the pertinent variables such as stress, strain, temperature, and their time derivatives. This constitutive equation must be integrable over an arbitrary loading cycle to predict energy dissipation. For example, Stowell [*4*] uses the following basic relation which was developed initially for high-temperature creep:

$$\frac{d\epsilon}{dt} = \frac{1}{E}\frac{d\sigma}{dt} + \alpha\frac{dT}{dt} + 2sT\exp\left(-\frac{\Delta H}{RT}\right)\sinh\frac{\sigma}{\sigma_0} \quad \ldots\ldots\ldots (1)$$

Total strain rate in this equation is composed of three parts. The first term on the right-hand side is the elastic contribution, the second term represents the thermal expansion, and the third term is the visco-plastic component.

The second critical aspect of the energy approach is the specification of a failure criteria. The simplest, which is used by Stowell and others, is to assume failure occurs when a certain critical amount of energy is expended.

[2] The italic numbers in brackets refer to the list of references appended to this paper.

This energy is assumed to be constant for all types of loading. For cyclic or fatigue loading, this criteria takes the form

$$N_f \Delta E_p = E_0 \quad \ldots\ldots\ldots\ldots\ldots\ldots\ldots\ldots (2)$$

where E_0 is a constant. The energy dissipated per cycle ΔE_p is determined from the constitutive equation (like Eq 1) and the relation

$$\Delta E_p = \int_0^\tau \sigma(\partial \epsilon / \partial t) dt \quad \ldots\ldots\ldots\ldots\ldots\ldots\ldots\ldots (3)$$

where τ is the period of one cycle. Stowell found reasonable success in predicting life for both isothermal creep rupture (σ = constant) and fatigue [$\sigma = \sigma_0 \sin (2\pi t/\tau)$] using this approach.

The present results indicate that difficulties will arise in using both the constitutive equation, (Eq 1), and the failure criteria, (Eq 2), when applied to more complex temperature and strain cycling. The cyclic stress-strain curves of Fig. 3 indicate that the cyclic history of temperature and strain influence the loop shape and energy loss, a factor not included in Eq 1. Martin et al [*6*] have developed a numerical scheme to account for load history dependence in cyclic straining. Moreover, the data on Fig. 4 indicate that ΔE_p is not a single valued function of N_f with slope $d\Delta E_p/dN_f = -1$ as required by Eq 2. The material tested can accommodate differing amounts of total energy before failure, depending upon its microstructural condition which in turn is dependent upon the cyclic deformation and temperature history.

A qualitative description of the dependence of cycles to failure on cyclic energy dissipation based upon the present data and that of Carden and Slade [*1*] is given in Fig. 5. The solid curves labeled $\bar{T}$ = constant represent completely reversed cycles at constant temperature and strain rate, $\dot{\epsilon} = 4\bar{\epsilon}/\tau$ (see insert). $\bar{T}$ can be considered an "effective" temperature given by $\bar{T} = T\,(A\text{-log }\dot{\epsilon})$. This form assumes an equivalence between temperature

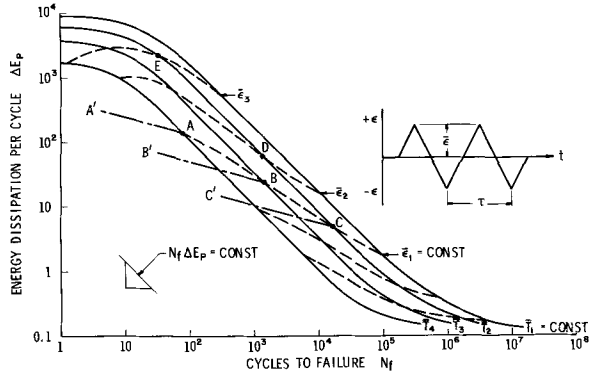


FIG. 5—*Schematic representation of energy dissipation versus fatigue life.*

and strain rate for fatigue as shown by Daniels and Dorn [7], Coffin [8] and is an assumption implicit in Eq 1. The dashed lines (for example, *ABC*) connect values of equal strain amplitude, $\bar{\epsilon}$. The Coffin-Manson relation ($\Delta\epsilon_p N_f^{\alpha} = C$) is represented by intersections such as the points, *C*, *D*, *E* for constant temperature $\bar{T}_2$. An effect of frequency and temperature on the constants in the Coffin-Manson law is implied by Fig. 5. Data from the tests reported herein, fall along the lines *AA'*, *BB'*, *CC'* having a lower slope than the constant $\bar{T}$ or constant $\bar{\epsilon}$ curves. Along these lines, creep or thermal cycling damage or both is added to the basic strain cycling damage, all of which contribute to failure. On an equivalent energy basis, these later damage mechanisms appear more severe in reducing cyclic life than are increases in either strain amplitude or temperature. This agrees with the observation of Kennedy [9] that "for a given life, more plastic strain can be absorbed during isothermal stressing than under thermal cycling condition." It thus appears that for a given cyclic life, there is an appreciable range of energy absorption capacity depending upon the time history of the deformation and the temperature.

Conclusions

The difficulty in predicting fatigue life for complex strain and temperature cycling is apparent. A limited amount of experimental data on a nickel base superalloy has been presented. While some basic difficulties in the energy approach to life prediction have been noted, we feel that this type of formulation should be pursued further because it offers a basic approach of general applicability.

Acknowledgments

The experimental work reported in this paper was performed under contract with the Pratt & Whitney Aircraft Division of United Aircraft Corporation under the supervision of A. E. Gemma. Analysis of the data and preparation of this paper was supported by the Army Research Office, Durham, under Contract DA-31-124-ARO-D-273. We also wish to thank L. M. Yeakley, E. B. Norris, and S. A. Viaclovsky for their contributions to the test program.

References

[1] Carden, A. E. and Slade, T. B., in *Fatigue in High Temperature, ASTM STP 459*, American Society for Testing and Materials, 1969.

[2] Feltner, C. E. and Morrow, J. D., "Micro-plastic Strain Hysteresis Energy as a Criterion for Fatigue Fracture," Paper No. 60-MET-2, American Society of Mechanical Engineers, 1960, pp. 111–129.

[3] Stowell, E. Z., *Nuclear Engineering and Design*, Vol. 3, 1966, p. 32.

[4] Stowell, E. Z., *Nuclear Engineering and Design*, Vol. 9, 1969, p. 239.

[5] Lemaitre, J., "Evaluation of Dissipation and Damage in Metals Submitted to Dynamic Loading," International Conference on Mechanical Behavior of Materials, Kyoto, Japan, Aug. 1971.
[6] Martin, J. F., Topper, T. H., and Sinclair, G. M., *Materials Research and Standards*, Vol. 11, 1971, p. 23.
[7] Daniels, N. H. G. and Dorn, J. E. in *Metals*, *ASTM STP 196*, American Society for Testing and Materials, 1957, pp. 94–110.
[8] Coffin, L. F., Jr., *Transactions*, Metallurgical Society, American Institute of Mining, Metallurgical, and Petroleum Engineers, Vol. 230, 1960 (1964).
[9] Kennedy, A. J., *Processes for Creep and Fatigue in Metals*, Wiley, New York, 1962, p. 446.

R. R. Hosbons[1]

Low-Cycle Fatigue Behavior of Zircaloy at 573 K

REFERENCE: Hosbons, R. R., **"Low-Cycle Fatigue Behavior of Zircaloy at 573 K,"** *Fatigue at Elevated Temperatures, ASTM STP 520*, American Society for Testing and Materials, 1973, pp. 482–490.

ABSTRACT: The 573 K low-cycle fatigue behavior of Zircaloy-2 in various metallurgical states has been studied. Reduction in area as measured in tension tests was found to be a good parameter in determining fatigue life. Holdtimes in tension of 1 h or less did not affect the fatigue life but one of 5 h reduced it. An atmosphere containing iodine reduces the fatigue life under the conditions tested by 40 percent.

KEY WORDS: fatigue (materials), zircaloys, nuclear reactors, fatigue life, fatigue tests, iodine

Many Zircaloy-2 components in nuclear reactors could possibly be subjected to reversed plastic strains during their lifetime. The low-cycle fatigue data published [*1*,*2*][2] have been obtained on annealed material, but much of the Zircaloy-2 used is in the cold-worked and stress-relieved condition. Also many components are joined by brazing. An experimental program was undertaken to determine the low-cycle fatigue characteristics of Zircaloy-2 in the above metallurgical conditions.

In other materials holdtimes in tension reduce the fatigue lives, but holdtimes in compression do not [*3*]. The reduction in life is attributed to creep damage occurring during the holdtimes, and many of the proposed methods to predict fatigue life with holdtimes include some factor to account for creep damage either mathematically or in the test procedures [*4*–*6*].

Corrosive environments can increase the crack propagation rates during fatigue. Iodine can cause stress-corrosion cracking of Zircaloy-2 under certain conditions, and it is therefore possible that the fatigue life of zircaloy will be reduced by an atmosphere containing iodine.

[1] Research engineer, Fuels and Materials Division, Chalk River Nuclear Laboratories, Atomic Energy of Canada, Ltd., Chalk River, Ont., Canada.

[2] The italic numbers in brackets refer to the list of references appended to this paper.

Copyright© 1973 by ASTM International www.astm.org

Experimental

Both uniaxial push-pull and reversed bending tests were used to determine 573 K fatigue life of Zircaloy-2 and Zircaloy-4, the chemical compositions of which are shown in Table 1. In the uniaxial tests strain was measured using a linear variable differential transformer (LVDT) which was attached to the specimen by extension arms with knife edges. The signal from the LVDT was fed into a closed loop system which controlled the test. All these specimens were tested in air at a frequency of 0.01667 Hz. Load-extension loops were recorded during the test, and the size of the hysteresis loop was used to calculate plastic strain.

TABLE 1—*573 K tensile properties of Zircaloy in the conditions tested.*

Material Condition	0.2% Yield Strength, MN/m^{-2}	Ultimate Tensile Strength, MN/m^{-2}	Uniform Elongation, %	Total Elongation, %	Reduction in Area, %
Annealed	150.3	255.9	20.6	49.4	72.2
6% cold work	156.6	243.4	...	...	67.0
12% cold work	232.4	317.2	8.6	41.3	67.0
22% cold work	246.9	321.4	10.0	36.0	59.8
41% cold work	265.5	350.3	...	...	58.3
β-quenched	182.4	324.5	15.1	37.4	62.1

The strain in the reversed bend specimen was controlled by stops which limited the deflection of the end of the specimen. As strain could not be measured directly a strain/deflection curve was used for calibration.

The strain/deflection curve was obtained by fatiguing specimens for 10 cycles for known deflections and measuring the plastic strains from photogrids etched on the gage length; therefore, the figures quoted for reversed bend specimens are for the outside fibers only. The specimens were enclosed in an autoclave so different atmospheres could be used. Most of the specimens were tested in air, but some were tested in air containing 30 g/m^3 iodine. All tests were carried out at a frequency of 0.01667 Hz.

To determine if the creep properties of Zircaloy-2 affects the low-cycle fatigue properties specimens were tested uniaxially with holdtimes of $1/4$, $1/2$, 1, 2, and 5 h at maximum strain.

To determine the effect of metallurgical structure on fatigue life specimens were annealed at 973 K and then coldworked 6, 12, 22, or 41 percent. After cold working they were stress relieved at 823 K. Specimens were tested also after being oil quenched from 1273 K to simulate brazing, which produced a Widmanstätten α structure. The 573 K tensile properties of the specimens in the above metallurgical condition are shown in Table 2.

Uniaxial tests were stopped before final failure so that the specimens could be metallographically examined. However, the cracks in these speci-

TABLE 2—*Chemical composition of alloys tested.*

	%			ppm									
Material	Sn	Cr	Fe	Mn	C	Al	V	Mo	N_2	O_2	H_2	Cu	Ta
Zircaloy-2..	1.49	0.124	0.149	<20	192	29	<20	<20	38	1096	8	<20	...
Zircaloy-4..	1.35	0.08	0.23	<20	89	25	<20	<20	32	1220	...	<20	<100

	ppm												
Material	Ti	U	Hf	B	W	Mg	Co	Si	Ni	Cd	Na	Pb	Cb
Zircaloy-2..	27	<0.2	68	0.33	<20	<10	<5	37	580	<0.25	<10	<20	...
Zircaloy-4..	<20	<1	100	<0.20	<50	<10	<10	32	<30	<0.20	...	<20	<50

mens had nearly propagated across the section, and complete failure would have occurred within 50 cycles.

Results

The results of the uniaxial tests are shown in Table 3. A line representing the least squares fit of the annealed results together with its 95 percent confidence limits are shown in Fig. 1. The cold-worked and stress-relieved results were found to be not significantly different at the 95 percent confidence limit and, therefore, can be represented by the same line. The β quenched results were found to be significantly higher at the 95 percent level but not at the 99 percent level.

The fatigue life of annealed Zircaloy-4 tested in an iodine atmosphere with no holdtime at a total plastic strain of 6 percent decreased by approximately 40 percent, from 212 to 136 cycles, Table 4. (Tests had shown that annealed Zircaloy-4 had the same fatigue properties as annealed Zircaloy-2.)

TABLE 3—*Effect of cold-work and heat-treatment on the fatigue lives of Zircaloy-2 tested in uniaxial tension.*

Treatment % Cold Work + Stress Relieved at 823 K[a] for 1 h	Plastic Strain, %	Cycles to Failure (number of tests)
Annealed	0.55	8470 (2)
	0.87	8353 (1)
	1.4	1686 (5)
	2.1	1595 (1)
	2.5	857 (2)
	2.7	280 (4)
6%	1.65	1290 (2)
	3.3	324 (2)
12%	1.4	2650 (2)
	3.15	440 (2)
22%	1.1	3885 (2)
	1.4	1523 (2)
	2.1	979 (1)
	3.0	214 (2)
41%	1.4	2190 (2)
β-quenched	0.6	9558 (1)
	2.17	2074 (1)
	2.62	842 (1)
	3.7	618 (1)
	5.9	203 (1)

[a] Except annealed material and β-quenched.

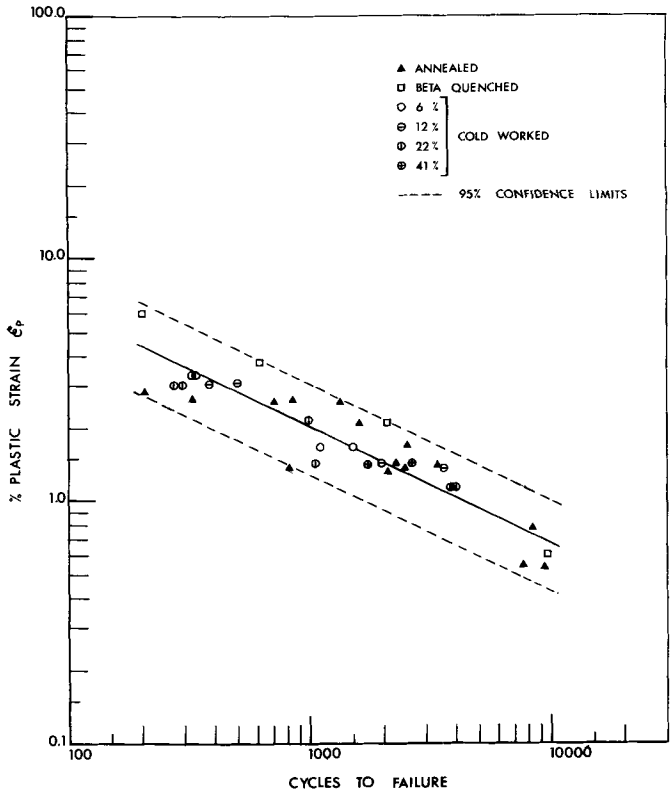


FIG. 1—*Low-cycle fatigue data on Zircaloy-2 at 573 K.*

The specimens oil quenched from 1273 K contained Widmanstätten α in large prior β grains, but this structure did not reduce significantly the fatigue life of Zircaloy-2, Table 3.

Table 5 shows the results of tests with holdtimes of up to 5 h. One specimen was tested at each of the conditions shown. The test with a holdtime of 5 h stopped after 600 cycles before complete failure occurred, but metallographic examination showed that failure would have occurred within 200 cycles: therefore, the life of this specimen has been given as 600 to 800 cycles.

Metallographic examination of the uniaxial tests stopped before complete failure occurred showed that the area through which the primary and secondary cracks had passed had a large amount of twinning but the area in front of the crack tip was not twinned, Fig. 2. In material which had been previously twinned from cold working there were more twins in the area through which the crack had passed than the area in front of it.

TABLE 4—*Effect of strain and atmosphere on the reversed bend fatigue life of Zircaloy-4 at 573 K.*

Atmosphere	Total plastic Strain	Cycles to Failure
Air.....	1.8	856[a]
	3.90	353[a]
	6.0	212[b]
	6.4	208[b]
	10.3	122[b]
Iodine.....	6	136[b]

[a] Average of 20 specimens.
[b] Average of 10 specimens.

TABLE 5—*Effect of holdtime at maximum tension on the fatigue life of cold work + stress relieved Zircaloy-2 and annealed Zircaloy-2 at 573 K* [8,13].

Condition	Holdtime, h	Cycles to Failure
Coldwork..	0	1320
	1/4	1090
	1/2	1425
	1	1500
	5	600 to 800[a]

NOTE—Plastic strain = 0.34%.

[a] Not broken.

Discussion

Manson [7] and Coffin [8] both proposed an equation to relate cycles to failure, N_f, to the total plastic strain, $\Delta\epsilon_p$. It was

$$\Delta\epsilon_p = CN_f^{-B} \quad \ldots\ldots\ldots\ldots\ldots\ldots\ldots\ldots\ldots\ldots (1)$$

where C and B are both constants.

B was originally 1/2, but it has been found to be temperature dependent and varies between 1/2 and 1 [9]. The constant C is such that the formula should predict tensile ductility at $N_f = 1/4$. Equation 1 has been modified to take into account elastic strain [9] (Manson universal slopes) and strain hardening coefficient [10]. However for temperatures where creep is unimportant Eq 1 can still be used.

The equation for the line shown in Fig. 1 which represents the data on annealed Zircaloy-2 was found to be

$$\Delta\epsilon_p = 0.57\ N_f^{-0.48}$$

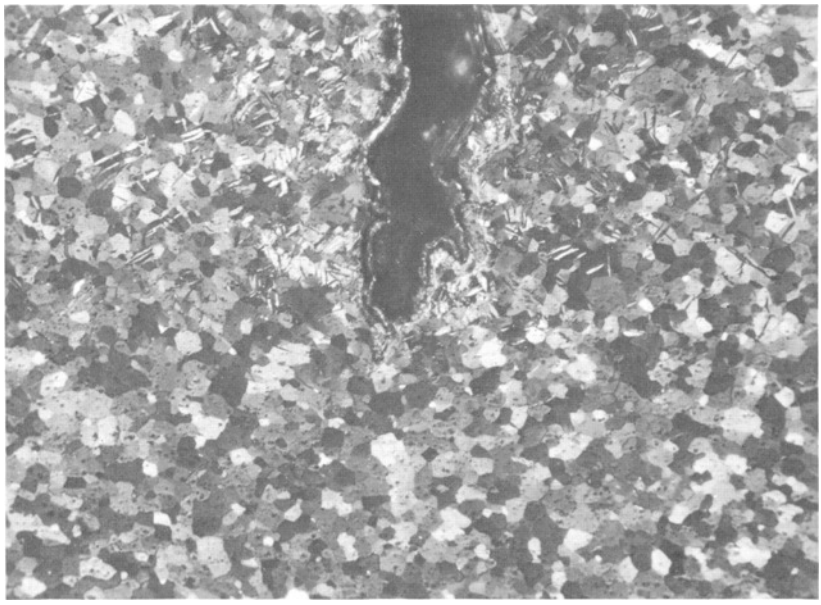


FIG. 2—*Low-cycle fatigue crack in annealed Zircaloy-2* (×250).

which predicts a tensile ductility equivalent to a reduction in area of 69 percent which compares favorably with the 72 percent measured on annealed specimens. As B is close to $1/2$ it would indicate that at 573 K low-cycle fatigue for Zircaloy-2 is not a "high" temperature phenomenon. This is emphasized by the holdtime tests which shows that holdtimes in maximum tension of up to 1 h have no effect on fatigue properties.

The results of the β quenched specimens indicate that the braze heat-treatment may increase fatigue life. This is thought to be due to the Widmanstätten α making the effective grain size smaller than in the annealed α grain. This would increase fatigue life by limiting the initial crack size as in bainitic steels [*11*] when the bainite needle size is the effective "grain size."

Bement [*12*] has shown that the reduction in area of Zircaloy-2 decreases with fast neutron irradiation. As the constant C in Eq 1 is dependent upon tensile ductility the low cycle fatigue life of irradiated Ziracaloy-2 at 573 K may be shorter than for unirradiated Zircaloy-2.

Conclusions

1. The low-cycle fatigue behavior of Zircaloy-2 tested without holdtimes at 573 K can be represented by the equation $\Delta\epsilon_p = 0.57\ N_f^{-0.48}$.

2. Holdtimes in tension of 1 h or less do not affect the 573 K fatigue life of Zircaloy-2.

3. Annealed Zircaloy-2 and cold-worked and stress-relieved Zircaloy-2 have similar low-cycle fatigue properties.

4. An atmosphere containing iodine appears to reduce fatigue life of Zircaloy-4.

Acknowledgments

The author wishes to thank A. R. Daniel of Canadian General Electric Company and G. A. Delvecchio, formerly of Orenda Limited, for permission to publish previously unpublished data. The author also wishes to thank B. L. Wotton for technical assistance in the experimental work.

References

[*1*] Mehan, R. L. and Wiesinger, F. W., KAPL-2110, Knolls Atomic Power Laboratory, Schenectady, N. Y., 1961.
[*2*] O'Donnel, W. J. and Langer B. F., *Nuclear Science and Engineering*, Vol. 20, 1964, p. 1.
[*3*] Conway, J. B. and Berling, J. T., *Metallurgical Transactions*, Vol. 1 1970, p. 324.
[*4*] Conway, J. B., Berling, J. T., and Stenz, R. H., GEMP 702, General Electric Co., Nuclear Systems Programs, Cincinatti, Ohio, 1970.
[*5*] Campbell, R. D., Paper 71-PVP-6, presented at 1st National Congress on Pressure Vessels and Piping, San Francisco, May 1971.
[*6*] Halford, G. R. and Manson, S. S., presented at 1st National Congress on Pressure Vessels and Piping, San Francisco, May 1971.
[*7*] Manson, S. S., NACA Technical Note 2933, National Aeronautics and Space Administration, Lewis Research Center, Cleveland, Ohio, 1954.
[*8*] Coffin, L. F., Jr., *Transactions*, American Society of Mechanical Engineers, Vol. 76, 1954, p. 931.
[*9*] Manson, S. S., *International Journal of Fracture Mechanics*, Vol. 2, 1966, p. 327.
[*10*] Berling, J. T. and Conway, J. B., *Metallurgical Transactions*, Vol. 1, 1970, p. 805.
[*11*] Irving, K. J. and Pickering, F. B., *Journal of the Iron and Steel Institute*, Vol. 201, 1963, p. 518.
[*12*] Bement, A. L., *Radiation Effects*, Gordon and Breach, New York, 1967, p. 671.

DISCUSSION

D. B. Scott[1] (*written discussion*)—The author is to be complimented on his work on the low-cycle fatigue of Zircaloy.

Zircaloy is highly anisotropic and the question then, is: do you intend to do any work to resolve the effects of texture? Also, how do you intend to factor in the effect of irradiation?

[1] Windsor, Conn. 06095.

R. R. Hosbson (author's closure)—We have tested specimens of Zircaloy-2 machined in the short transverse direction, that is, in the thickness direction of a rolled plate. Most of the plastic deformation of these specimens should occur by twinning. These results fall below the scatterband shown in Fig. 1, indicating that twinning reduces fatigue life probably by making crack initiation easier.

We are hoping to perform low-cycle fatigue tests in-reactor, thus determining the effect of fast neutron irradiation on fatigue life.

I. LeMay[2] *(written discussion)*—It was mentioned that deformation should have been completely by slip, but that twinning was observed adjacent to the fatigue cracks. From the micrographs, it appears that there was considerable variation in the orientation of grains, and I should like to know what the texture was, as some grains might be easily oriented for twinning before slip would take place.

This question of texture is an important one, as fatigue cracks do form preferentially at mechanical twins and propagate along their boundaries when Zircaloy is tested in high-cycle fatigue,[3] and, if this effect is also observed at elevated temperature, it has implications on the desirable texture for tubing under such conditions.

Mr. Hosbons—The texture of the alloys tested was such that the [1010] direction was parallel to the tensile axis. The number of grains oriented for twinning was less than random, but almost every grain along the fracture path was twinned; also the number of twins decreased on moving away from the crack. We believe the cracks formed immediately ahead of the crack as it propagates.

T. Udeguchi[4] *(written discussion)*—For pressure piping in advanced thermal reactors, we are planning to use this kind of material in low-cycle conditions at about 300 C, and are making similar low-cycle fatigue tests. I would like to know the temperature effect on low-cycle fatigue behavior of the material you tested. Did you conduct the low-cycle fatigue tests at elevated temperatures, and find out any difference between the behaviors at room temperature and at about 300 C?

Mr. Hosbons—We have not tested Zircaloy-2 at room temperature, but O'Donnell and Langer[5] show that there is no significant difference between the fatigue life of Zircaloy-2 at room temperature and 573 K.

[2] Department of Mechanical Engineering, University of Saskatchewan, Saskatoon, Sask., Canada.

[3] LeMay, I., Glogh, A., and Kaufmann, P., "Fatigue of Zircaloy-4," ASM Westec paper, American Society for Metals, Los Angeles, 1969.

[4] Department of Mechanical Engineering, University of Tokyo, Tokyo, Japan.

[5] O'Donnel, W. J. and Langer, B. F., *Nuclear Science and Engineering*, Vol. 20, 1964, p. 1.

K. D. Sheffler[1] *and G. S. Doble*[1]

Thermal Fatigue Behavior of T-111 and ASTAR 811C in Ultrahigh Vacuum

REFERENCE: Sheffler, K. D. and Doble, G. S., "**Thermal Fatigue Behavior of T-111 and ASTAR 811C in Ultrahigh Vacuum,**" *Fatigue at Elevated Temperatures, ASTM STP 520*, American Society for Testing and Materials, 1973, pp. 491–499.

ABSTRACT: The thermal fatigue behavior of the tantalum alloys T-111 (Ta-8W-2Hf) and ASTAR 811C (Ta-8W-1Re-0.7Hf-0.025C) has been evaluated using completely reversed push-pull fatigue tests conducted in ultrahigh vacuum with independently programmed temperature and strain cycles. Test results showed that cycling of the test temperature simultaneously with the mechanical strain in most cases significantly reduced the cycles to failure of both alloys compared to isothermal testing. Notched specimens had reduced lives under isothermal conditions, but the presence of a notch or use of a 1-h holdtime provided only a small further decrease in life for the temperature cycled tests. Compressive stress at the maximum temperature produced longer lives than tensile stress. ASTAR 811C was more fatigue resistant than T-111 isothermally and did not have as great a decrease in life with thermal cycling. Results are analyzed by partition of plastic strains into creep and creep-independent components and considering where each component was active in the hysteresis cycle.

KEY WORDS: fatigue (materials), tantalum alloys, thermal cycling tests, fatigue tests, isothermal treatment, strains, high temperature materials

The proposed use of the tantalum base alloys T-111 (Ta-8W-2Hf) and ASTAR 811C (Ta-8W-1Re-0.7Hf-0.025C) in space electric power systems has generated a need for thermal fatigue data on these materials in a hard vacuum environment at temperatures to 2100 F. The present study, thus, was undertaken to characterize the vacuum thermal fatigue behavior of T-111 and ASTAR 811C using independently programmed strain and temperature cycles in the range of 400 to 2100 F.

While these two alloys are similar in composition, the high-temperature strengthening mechanisms differ in that T-111 is a single phase solid solution strengthened alloy, while ASTAR 811C is strengthened by a combination of solid solution and precipitation hardening, the latter provided by a tantalum carbide. Both alloys recrystallize at about 2600 F and are used in the recrystallized condition, thereby providing a metallurgically stable structure in the anticipated range of service temperatures. Because of the

[1] Principal engineers, TRW Inc., Cleveland, Ohio 44117.

Copyright© 1973 by ASTM International www.astm.org

relatively low-homologous temperatures involved (~0.44 at 2100 F), creep effects are anticipated only near the upper end of the service temperature cycle. Previous work[2] has shown that both test materials exhibit creep at temperatures as low as 1500 F; however, because of the added carbide strengthening, creep effects at this temperature are much smaller in the ASTAR 811C than in the T-111 alloy.

Experimental Details

Materials Characterization

Thermal expansion, elastic modulus, Poisson's ratio, and tensile properties were measured for both test materials to provide background data for interpretation of the fatigue test results.

Thermal expansion, modulus, and Poisson's ratio measurements were conducted at temperatures between ambient and 2600 F in a 10^{-8} torr vacuum furnace equipped with a tungsten mesh resistance heating element. Thermal expansion measurements were made at 200 F intervals on a specimen having a 2 in. gage length using an optical cathetometer having a precision of ± 50 μ in. Both longitudinal and shear modulus (E and G) were determined by a pulse-echo technique in which the transit time of an extensional or torsional elastic wave was measured in a 1/4 in. diameter rod of known length ℓ and density ρ. A commercial system, the Panatherm Model 5010, manufactured by Parametrics Inc., was used for these measurements. The system consisted of a standard longitudinal and a custom made shear transducer for generating and detecting the elastic wave, together with the electronics required for measurement and display of the transit time t on a digital readout. The elastic modulii were calculated from this information using the formula

$$\text{modulus} = (4\ell^2/t^2)\rho$$

with both length and density being corrected for thermal expansion using the previously measured expansion coefficient. Poisson's ratio ν was calculated from the measured values of E and G using the formula

$$\nu = (E/2G) - 1$$

The ultimate strength, 0.2 percent offset yield strength, elongation, and reduction of area were measured at temperatures between ambient and 2600 F in a Brew vacuum furnace at pressures below 1×10^{-5} torr. Bar-type specimens with a 0.113-in.-diameter by 0.450-in.-long gage section were tested at a constant crosshead speed corresponding to an initial strain rate of 0.0045 in./in./min. Results of these tests (Figs. 1 and 2) show a significant

[2] Sheffler, K. D. and Ebert, E. E., "Generation of Long Time Creep Data on Refractory Alloys at Elevated Temperature," Semi-Annual Report, Contract NAS-3-15554, NASA-CR-120867, TRW-ER-7567, Jan. 1972.

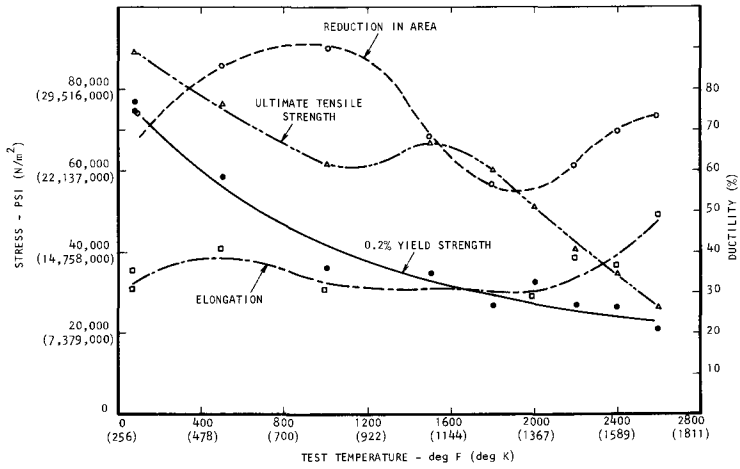


FIG. 1—*Tensile properties of T-111 alloy.*

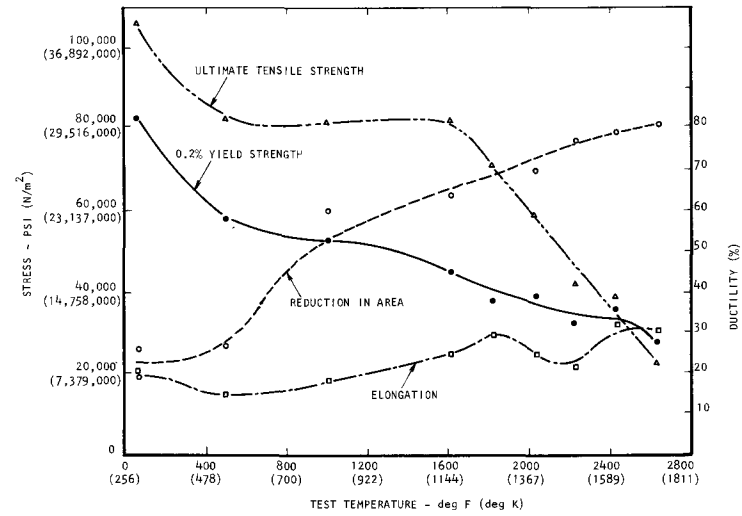


FIG. 2—*Tensile properties as ASTAR 811-C alloy.*

dynamic strain aging effect in the 1200 to 2000 F temperature range for both alloys. This effect is very pronounced in the T-111 alloy and is also noted in the ASTAR 811C alloy.

Apparatus

Completely reversed push-pull fatigue tests were conducted in ultrahigh vacuum on hourglass type specimens using independently programmed temperature and strain cycles. Temperature was programmed using a

thyratron-controlled 50-KV a-c power transformer for direct resistance heating of the specimen, while diametral strain was controlled directly using a linear variable differential transformer (LVDT) type extensometer coupled to a programmable closed loop electrohydraulic servo system.

Specimen blanks were obtained from rolled plate with the tensile axis parallel to the rolling direction. Specimens were machined to a $1\frac{1}{2}$-in.-radius hourglass contour with a $\frac{1}{4}$ in. gage diameter and a surface finish of better than 8 μ in. Two-sided tangential slot notches ($K_t = 3$) were added for notched testing. Testing was performed in a closed-loop servo controlled electro-hydraulic testing machine manufactured by Gilmore Industries and modified by TRW for high-temperature testing in ultrahigh vacuum. The test frame was equipped with a hydraulic actuator fatigue rated at $\pm 50\,000$ lb, and with an interface flat load cell which was mounted in such a way as to provide maximum lateral rigidity. Three-inch-diameter pull bars were attached rigidly to the actuator and to the load cell. The pull bars were designed with a conical recess in the working ends to fit a matching conical taper machined on the ends of the specimen. The specimen was clamped to the pull rods using a threaded collar and collet arrangment which was tightened under a compressive preload to provide a zero backlash joint with good axial alignment. A diametral extensometer constructed at TRW was used for measurement and direct feedback servo control of diametral strain. The extensometer consisted of 2 parallel high-purity alumina tubes joined at their center by a flexible invar ligament which acted as a hinge. A Schaevitz high resolution LVDT was mounted to one end of the extensometer assembly, while the other end was clamped to the test specimen using a tantalum spring clip. Tungsten was plasma sprayed on the alumina rods at the area of specimen contact to avoid possible specimen contamination.

A Duffers Associates Model 510 Gleeble was adapted to provide programmed direct resistance heating of the test specimen. An optical pyrometer precalibrated on a dummy specimen with thermocouples spot welded to the minimum diameter was used to establish the exact temperature at the minimum diameter of the working specimens prior to test initiation, after which tungsten-rhenium thermocouples spot welded to the test specimen a small distance away from the minimum diameter were used for operational measurement and control of specimen temperature during testing. Experience showed that fatigue crack initiation rarely occurred either at the point of thermocouple attachment or at the point of extensometer contact, indicating that neither of these instrumentation attachments significantly influenced the fatigue behavior of the test specimens.

Testing was conducted in an ultrahigh vacuum chamber constructed to TRW specifications by Varian Associates. Using a combination of ion and titanium sublimation pumping, a vacuum of $< 1 \times 10^{-7}$ torr was maintained during testing. The ultrahigh vacuum environment restricted the hardware used inside the chamber to low-volatility and corrosion-resistant

materials. Pull rods were water-cooled stainless steel and the grips were molybdenum TZM alloy. The LVDT was sealed in a stainless steel can and bare wires free of insulation were used for electrical connections and support of the extensometer. Pull rods entered the chamber through flexible stainless steel bellows.

Test Procedures

Tests were performed under diametral strain control at a frequency of 0.0065 Hz using triangular strain and temperature waveforms. The strain and temperature functions were synchronized so that the peak tensile strain coincided with either the maximum or minimum temperature as desired. A free (zero load) thermal cycle was executed prior to the initiation of each test to measure the exact thermal output of the extensometer. This output was used to compensate the strain command signal for direct control of net mechanical strain by subtraction of the thermal output from the strain command program.

Test Program

The test program consisted of seven different types of synchronized triangular loading and heating cycles:

1. Isothermal at 2100 F.
2. Isothermal at 2100 F with notched test specimen $K_t = 3$.
3. Strain and temperature increasing together with maximum tensile strain at maximum temperature and maximum compressive strain at minimum temperature. Temperature cycled from 400 to 2100 F.
4. As in 3, but minimum temperature increased to 900 F.
5. As in 3, with notched test specimen $K_t = 3$.
6. As in 3, but held 1 h at 2100 F at maximum tensile strain each cycle.
7. As in 3, but maximum compressive strain at maximum test temperature and maximum tensile strain at minimum temperature.

A minimum of four tests were conducted on each test material with each type of cycle to define a curve of strain range versus cycles to failure. Both strain and temperature versus time, as well as load versus strain, were measured continuously throughout each test. The vacuum test chamber was equipped with a sight port situated so that the surface of the specimen could be observed during testing with a telemicroscope. While it was possible to observe cracks in the surface of the specimen with this arrangement, it was not always possible to define an end point based on crack formation since only one side of the specimen was visible during testing. Failure, therefore, was defined as complete separation of the specimen into two pieces.

Results

Test results are summarized in Figs. 3 and 4 in which cycles to failure are plotted against total mechanical strain. Plotted for reference are the universal slopes and 10 percent universal slopes predictions[3] which were calculated using the previously discussed tensile and physical property data. For T-111, the isothermal tests at 2100 F followed a straight line with lives between the universal slopes prediction and the 10 percent rule. Use of a notched specimen significantly reduced the life for the isothermal tests but did not change the slope. The in-phase type of temperature cycled testing (cycle type 3) significantly reduced the fatigue life as compared to isothermal tests at 2100 F. The use of a notched specimen, raising the lower cycle temperature, and the use of a 1-h holdtime (cycle types 4, 5, and 6) all provided only a slight additional decrease of life over the basic in-phase thermal cycled life reduction. Tests cycled with compression at the maximum temperature (cycle type 7) had appreciably longer lives than tests cycled with tension at the maximum temperature, with some of the T-111 type 7 results falling above the isothermal line at the lower strain ranges.

Test results for ASTAR 811C generally followed the same order as the T-111 results, although the effects were not as great. For ASTAR 811C, the isothermal tests at 2100 F again had the longest life. The presence of a notch lowered the life in the isothermal tests, and cyclic tests had lower lives than isothermal. The reduction of life due to the notch or the cycling test was not as large as for T-111. Increasing the lower cycling temperature, using a notched specimen, or the use of a 1-h holdtime further lowered the life of cycled specimens. Testing with compressive strain at maximum temperature again provided an increase in thermal cycled life, particularly at smaller strains.

Two significant differences were noted between the behavior of the two alloys tested. First, the basic fatigue resistance of the ASTAR 811C was higher than that of the T-111 alloy, not only on an absolute basis but also with respect to the degree to which the experimental results approached the universal slopes predictions. The second difference was that the ASTAR 811C did not show as great a decrease in life with the use of temperature cycled tests.

Discussion

The thermal fatigue test results showed that synchronized thermal cycling had significant and in some cases even dramatic detrimental effects on the fatigue life of both tantalum alloys. For example, tests conducted on T-111 alloy at a total diametral mechanical strain range of 0.008 in./in. showed a fatigue life of 796 cycles when tested isothermally at 2100 F, as

[3] Manson, S. S. and Halford, G. R. in *Thermal and High-Strain Fatigue*, The Metals and Metallurgy Trust, London, 1967, p. 154.

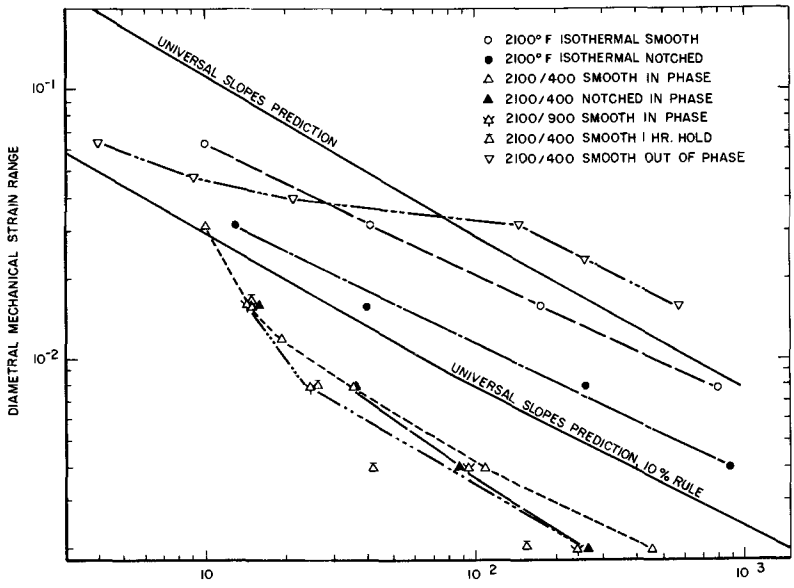


FIG. 3—*Strain controlled low-cycle fatigue results for T-111 alloy.*

compared to a life of only 35 cycles when the temperature was cycled from 2100 to 400 F in phase with the mechanical strain. This result is particularly important because it represents a serious nonconservative strength degradation which could not have been predicted using any of the existing isothermal fatigue or creep-fatigue theories. It is, therefore, highly desirable

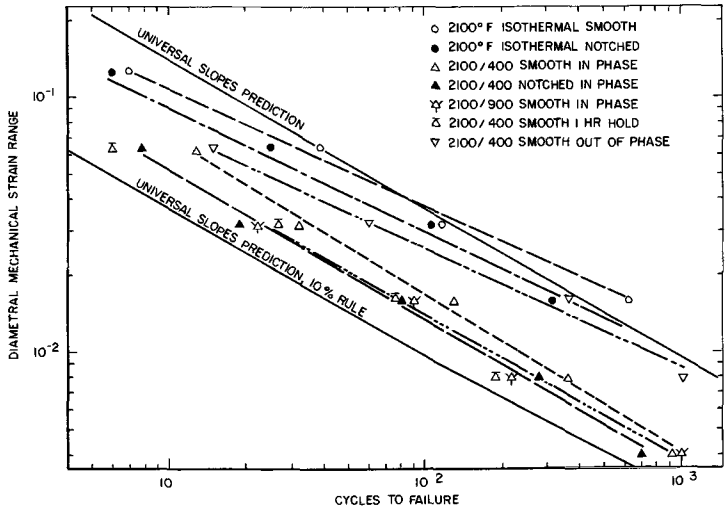


FIG. 4—*Strain controlled low-cycle fatigue results for ASTAR 811-C alloy.*

that the cause of this effect be determined so that the potential existence of similar strength reductions in other metallurgically similar materials may be anticipated.

The fact that the ASTAR 811C alloy appears to be less susceptible to the reduction of fatigue life by thermal cycling may provide a clue to the cause of the degradation. Since it has already been shown by the closer approach of the isothermal ASTAR results to the universal of slopes predictions that creep effects are more significant in the fatigue of T-111 than ASTAR 811C alloy, it is reasonable to assume that the observed reduction in the magnitude of the thermal cycled life degradation in the ASTAR alloy may be also associated with the higher creep strength of this material.

The foregoing supposition implies that creep effects are in some way responsible for the thermal cycled life degradation effect. While no direct proof was available for this hypothesis, examination of results from the various types of thermal-mechanical fatigue cycles applied to these two alloys provided supporting evidence. First, the isothermal notched results clearly demonstrated that the life reduction could not be attributed to a mechanism which shortens the time for crack initiation. Visual observation of the notched specimens revealed that crack initiation occurred during the first two or three cycles in the notched tests, indicating that the notched life represented the crack propagation portion of the smooth fatigue life. While a definite notch effect did exist in the isothermal type of test, the notched life was still well above the smooth thermal cycled in-phase life, indicating that a premature crack initiation effect could not in itself have been responsible for the observed thermal cycled life degradation. It is interesting to note, however, that the thermal cycled in-phase notch effect was much smaller in the T-111 alloy than the isothermal notch effect, indicating for this alloy that the crack initiation phase was significantly shorter in the smooth thermal cycled in-phase tests than in the isothermal tests.

A second observation which supports the hypothesis that the thermal cycled life degradation involves creep effects was the fact that any change in the cycle which increased the potential for creep effects increased the magnitude of the life degradation. Thus, the addition of a 1 h hold at each temperature and tensile strain peak in the 2100/400 F in-phase type of test decreased the fatigue life. Similarly, increasing the minimum temperature from 400 to 900 F, which meant that roughly one half instead of one third of the cycle occurred in the creep temperature range, also decreased the thermal cycled fatigue life. However, it should be noted that the extreme case of this type of change would be to increase the minimum temperature to the level of the maximum temperature, which would represent an isothermal type test where no life degradation would occur. The critical factor thus appears to be the reversal of creep deformation with plastic deformation, which produces a shorter fatigue life than the reversal of creep with creep. Furthermore, the effect appears to be sensitive to sequencing, with

tensile creep reversed by compressive plastic deformation being more severe than the opposite case where tensile plastic deformation is reversed by compressive creep deformation. These observations are consistent with results obtained on two iron alloys by Manson and co-workers, where significant differences in fatigue life were found to result from different sequences of tensile and compressive creep and plastic deformation.[4] However, even assuming that creep effects are responsible for the thermal cycled life degradation, much work remains to be done to define specific mechanisms by which creep deformation accelerates fatigue failure.

To summarize the results observed in this study, cycling of specimen temperature simultaneously with mechanical strain significantly reduced the fatigue life of the tantalum alloys T-111 and ASTAR 811C over comparable isothermally cycled specimens. The reduction in life was more severe for tensile stress at the maximum temperature than for compressive stress at the maximum temperature. The presence of a notch reduced the isothermal test life, but the use of notched specimens or a 1-h holdtime at maximum test temperature produced only minimal lowering of life when the temperature was also cycled. The fatigue resistance of the ASTAR 811C alloy was better than the T-111 alloy with respect to both isothermal fatigue strength and maintenance of fatigue strength with temperature cycling. This improved fatigue resistance of the ASTAR alloy was attributed to the higher creep strength of this material in the range of temperatures studied. It is suggested that lower life with temperature cycling is the result of creep in one portion of the fatigue cycle being reversed by time independent plastic deformation in the other half of the cycle. The condition of tensile creep reversed by compressive time independent plastic deformation is considered more severe than the reverse case.

Acknowledgments

We are grateful to J. W. Sweeney for performance of the experimental work on this program and to the NASA Lewis Research Center for sponsorship under Contract NAS-3-13228. The NASA program manager was P. E. Moorhead.

[4] Manson, S. S., Halford, G. R., and Hirshberg, M. H., "Creep-Fatigue Analysis by Strain Partitioning," NASA TMX-67838, National Aeronautics and Space Administration, May 1971.

J. R. Heath-Smith[1] *and F. E. Kiddle*[1]

Effect of Interrupting Fatigue by Periods of Heat for Aluminum Alloy Structural Elements

REFERENCE: Heath-Smith, J. R. and Kiddle, F. E., "**Effect of Interrupting Fatigue by Periods of Heat for Aluminum Alloy Structural Elements,**" *Fatigue at Elevated Temperatures, ASTM STP 520*, American Society for Testing and Materials, 1973, pp. 500–511.

ABSTRACT: Effects of heat on fatigue have been studied by interrupting fatigue tests at ambient temperature by single periods of heating with and without steady load applied. The tests employed constant amplitude and random loading on various structural elements in a number of aluminium-copper alloy materials. Heating was applied at temperatures in the range 100 to 150 C for times ranging from 1 h to 20 000 h.

The initiation of fatigue cracks was affected by heating, particularly at temperatures above 110 C when the effects occurred comparatively rapidly. The two mechanisms of importance were changes in microstructure at the machined surface which encouraged initiation, and changes in residual stress by creep which encouraged or discouraged initiation according to the creep being compressive or tensile.

It is suggested that similar mechanisms operate also during the crack propagation phase of the fatigue life.

KEY WORDS: fatigue (materials), cracking (fracturing), structural members, aluminium copper alloys, work hardening, heat treatment, creep properties, residual stress, supersonic transports

During the last decade fatigue research aimed at supersonic transport aircraft has been carried out predominantly on titanium alloys in the United States and aluminium alloys in the United Kingdom. The structural fatigue problems introduced by kinetic heating are similar in general terms for both materials, and demand an understanding of cumulative damage under combined mechanical and thermal stresses accompanied by effects of heating, such as microstructural changes in materials and stress relaxation in structural components, which may interact significantly with fatigue.

A particular problem arises from the interspersion of many periods of sustained heating between periods of fatigue activity at near ambient temperatures. The question is whether these periods at elevated temperature, distributed throughout the service life, will modify the accumulation of

[1] Principal scientific officer and scientific officer, respectively, Structures Dept, Royal Aircraft Establishment, Farnborough, Hants, England.

Copyright© 1973 by ASTM International www.astm.org

fatigue damage either by cumulative changes in the material as a whole or by local changes at the site of fatigue damage.

Research into this problem for aluminium alloy structure is being tackled by a series of testing programs ranging from investigations on realistic structure under realistic sequences of load and temperature to basic studies on simple structural specimens using simple load and temperature conditions.

This paper reviews the results of a program of basic fatigue research on four aluminium-copper alloys in the form of notched, lug, and clamped joint specimens. The effects of heat on fatigue were studied by interrupting fatigue tests at ambient temperature by single periods of heating at temperatures in the range 100 to 150 C for times from 1 to 20 000 h. It is shown that there are two mechanisms by which application of heat can significantly modify fatigue crack initiation. One is by causing microstructural changes in machined surfaces and the other is by allowing local redistribution of stress. Brief reference is made to fatigue tests in which many applications of heat were distributed throughout the life; the results suggest that the mechanisms of fatigue-heat interaction, which were observed for crack initiation, have their counterparts during crack propagation.

Experimental Procedure

The equipment used for the experimental work was largely conventional and included a resonant fatigue machine for tests with constant amplitude loading and an electrohydraulic fatigue machine for tests with random loading representing a gust spectrum. Creep loading frames and ovens were used to heat specimens with and without the application of steady load.

Specimens were machined from extruded bar material of four different aluminium-copper compositions, each produced commercially from one melt and fully precipitation hardened: DTD 5014 (RR58), BS L65, 2024-T81, and Al-6 Cu (Hid 54). The types of specimen used, which are illustrated in Fig. 1, consisted of two forms of notched specimen with net stress concentration factors of 2.3 and 3.4, a lug specimen with clearance fit steel pins, and a joint consisting of a lug specimen clamped between steel plates by tensioned bolts. All components were degreased before assembly and were loaded axially during fatigue testing.

The general principle of investigation was to establish a datum fatigue performance by means of continuous fatigue tests to failure at ambient temperature and then to interrupt similar tests at some stage for a single period of heating under steady loading in order to determine the effect on overall fatigue life. The data on endurance were supplemented by fractographic and metallurgical observations on changes in the surface condition of the material and in the mode or crack initiation. One technique employed was the measurement of microhardness across tapered sections to reveal the state of hardness at the machined surface of the specimen. To charac-

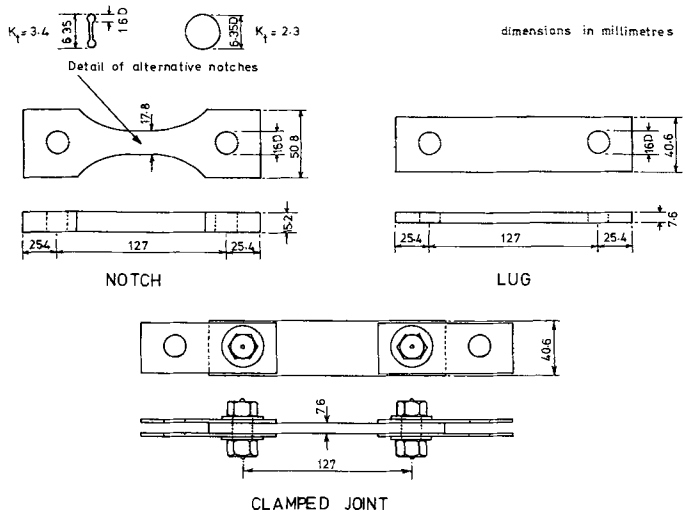


FIG. 1—*Specimens.*

terize crack initiation a count was made of the numbers of independent damage nuclei which were apparent under the microscope on the fracture surfaces, that is, the number of regions from which cracks spread before coalescing to form the main fatigue crack.

Coverage of the test parameters was not comprehensive; emphasis was placed on the DTD 5014 material, on notched specimens, and on heating periods of 1000 h at 150 C.

Discussion of Results

Four different aluminium-copper alloys were included in the program to cover the possibility that fatigue-heat interactions were sensitive to individual composition or microstructure. In fact, the observed effects of heat on endurance and mode of failure were broadly similar in the four materials, only differing to some extent in magnitude, and it is possible therefore to illustrate this review of the results with examples of the trends observed without the frequent need to differentiate between materials. Discussion will center on the results from notched specimens which proved more sensitive to heat than the specimens with fretting, and which therefore illustrate better the mechanisms involved.

Effect of Heat Without Load

Figures 2*a* and *b* show typical results of tests on a notched specimen under constant amplitude loading and random loading, respectively. In both examples the abscissa represents the stage at which the fatigue test was interrupted for a single application of heat, in this case for 1000 h at 150 C,

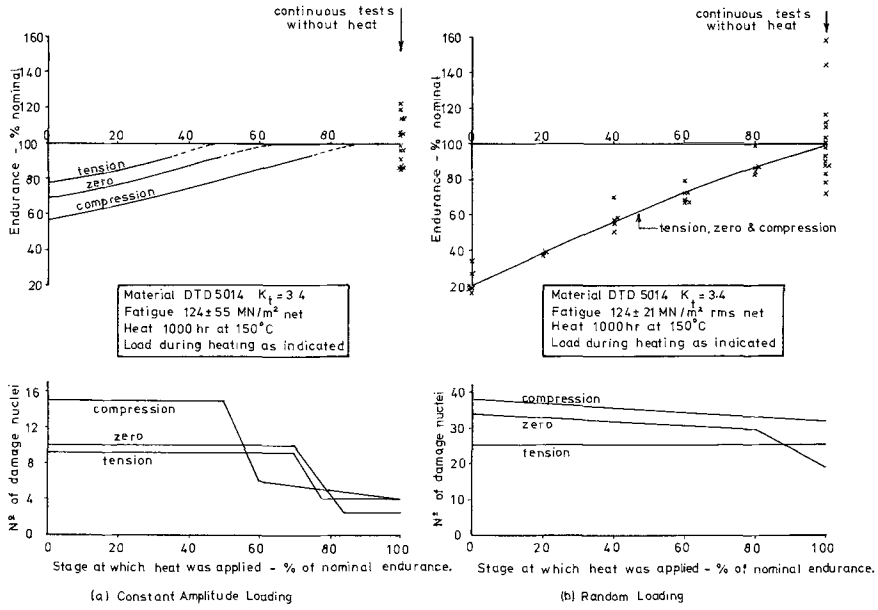


FIG. 2—*Variation in endurance and crack initiation pattern with stage of life at which heat was applied.*

and the ordinates show the effects on endurance and also on the pattern of crack initiation, measured by the number of independent damage nuclei which were observed on the final fracture surface. The figures include information on the effect of heat both with and without load applied. For the present only the effect of heat without load will be discussed; consideration of the effect of load during heating is reserved for the next section.

In Fig. 2*a*, individual test points have been omitted for clarity, although scatter was appreciably less than that for tests without heat which are plotted for convenience at an abscissa of 100 percent. The line labelled "zero" in the upper diagram represents heating without load, and shows that heating reduced endurance if applied before about 60 percent nominal life and had no significant effect when applied later. The reduction in endurance was greatest when the heat was applied before the fatigue test and diminished as it was applied later in the test. The inference is that heat affected the initiation of fatigue cracks, and this is supported by the trend in the lower diagram which shows that the number of damage nuclei was increased markedly when the heat was applied in the earlier part of the life. The corresponding picture for tests [*1*][2] under random loading is presented in Fig. 2*b*. In this case individual test points are shown in order to indicate the reduction in scatter compared with that for tests without heat, which are plotted at an abscissa of 100 percent. As before, the greatest reduction in

[2] The italic numbers in brackets refer to the list of references appended to this paper.

endurance resulted from heating prior to fatigue, but the lower diagram shows no significant increase in the number of damage nuclei, presumably because the large number of nuclei which occur under this loading condition virtually saturate the surface of the notch.

To pursue the apparent connection between the reduction in both endurance and its scatter, and the changes in the pattern of crack initiation, metallurgical and fractographic studies [*2*] were conducted in the region of the specimen surface with the significant result summarized in Fig. 3. It was found that the manufacturing process of drilling and reaming the hole left a work affected zone to a depth of about 40 μm in which the hardness was significantly higher than that of the interior of the material; on unheated specimens, cracks had initiated just below this hard surface film. For specimens which had been heated a number of differences was observed: the work affected surface layer now contained a coarse secondary precipitate, its hardness was reduced to a value comparable with that of the interior, and fatigue cracks had initiated at the surface. It is deduced from this that the effect of heat was to modify the work hardened surface layer such that its resistance to fatigue crack initiation was lowered. As a consequence the

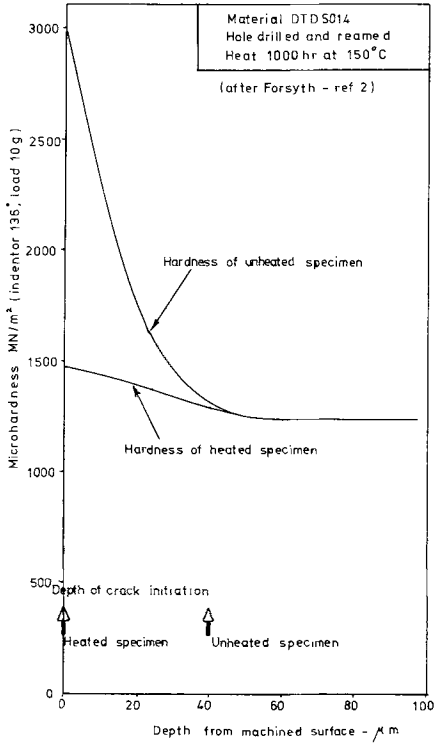


FIG. 3—*Effect of heat on surface hardness and depth of crack initiation.*

development of damage nuclei now took place right at the surface of the material and was more rapid and more uniformly distributed, causing reduction in fatigue endurance and scatter. The effective feature of the change in the surface layer is unlikely to be the relaxation of residual stress for the following reason. In Figs. 2*a* and *b* the trends of endurance with the stage of life at which heat was applied are continuous, including the special case of application at 0 percent, that is, heating prior to fatigue. It follows that the effect of heat is not primarily due to changes in residual stresses as these would be very different before and after the application of fatigue loads. This argument will be reinforced by evidence on the effect of load during heating which is discussed in the following section.

The effects of heat so far discussed resulted from a substantial exposure of 1000 h at 150 C. Tests with other values of temperature and time of exposure showed that the effect of heat on endurance was appreciable after far smaller times and occurred at lower temperatures. Figure 4 shows some of the results obtained. In Fig. 4*a* it is seen that the effect was achieved fully in less than 1 h at 150 C on the Al-6Cu material [*3*]; the other materials

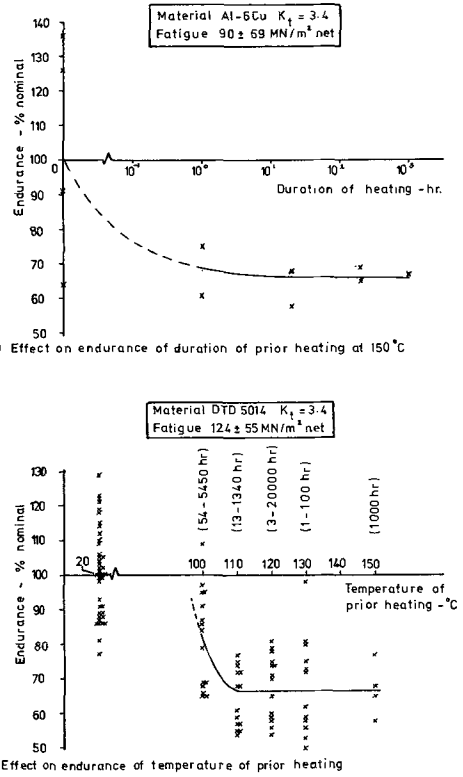


FIG. 4—*Effect of duration and temperature of prior heating on endurance.*

showed similar but less rapid trends. The effect on endurance of varying the temperature of exposure is shown in Fig. 4*b* in which the range of exposure times tested is shown against each temperature. The diagram includes a few test points for which the exposure was comparatively severe, namely, two results for 20 000 h at 120 C and four results for 1000 h at 150 C. The remaining results at temperatures from 100 to 130 C were obtained from several series of tests in each of which the times of exposure were scaled to give equal degrees of exposure at each temperature as measured by the Dorn parameter. It should be remarked that within the band of results at each temperature there is lack of correlation between endurance and time of exposure; the width of each band is due mainly to the scatter arising from small variations in material, specimens, and testing conditions, which is inherent in all such work.

It is seen that for all temperatures from 100 to 150 C, heating reduced mean endurance in relation to the results without heat which are plotted at 20 C. It is particularly noticeable that the reduction in mean endurance is independent of temperature over the range 110 to 150 C, and, in view of the diversity of exposure times used and also the tendency seen in Fig. 4*a* for the effect to reach a limiting value, it seems highly probable that the reduction represents a limit to the effect of heat on this particular specimen, to the extent where the beneficial influence on crack initiation of the work hardened surface has been completely lost.

In the results at 100 C it is noticeable that the mean reduction is considerably less than the limiting value despite the inclusion of results for exposure times in excess of 5000 h. It is suggested that the mechanism by which heat modifies the surface layer weakens considerably as temperature is reduced from 110 C and that the limiting reduction in endurance is unlikely to develop at 100 C even after extremely long times of exposure.

To recapitulate this section, it has been shown that exposure to heat modified the microstructure of the machined surface of a specimen, and thus increased its susceptibility to fatigue crack initiation. At temperatures of 110 C and greater the benefit of the machined surface was progressively lost during heating and the fatigue endurance of notched specimens reduced rapidly with time of exposure to a limiting value which was independent of temperature. Below 110 C the action of heat was considerably weaker.

Effect of Load During Heating

Returning to Fig. 2*a* it is seen that the effect of heat on endurance was modified by the application of steady load such that tensile load during heating gave a relative increase in endurance and compressive load a relative decrease. From studies of cumulative fatigue damage [*4,5*] it is known that residual stress due to local yielding under the applied fatigue loads has a significant influence on fatigue performance by modifying the level of local mean stress, and we suggest that the modification of residual stress

by creep may be responsible for the effects observed previously. Similar effects on endurance have been attributed to creep in earlier work [*6*] on the fatigue of L65 notched specimens at elevated temperature and by other workers, notably Maurin and Barrois [*7*] for elevated temperature fatigue tests of A-U2GN-T6 (RR58), and Hardrath et al [*8–10*] for fatigue tests of Ti-8Al-1Mo-1V at elevated temperature and at room temperature after heating.

A change in residual stress by creep will be effective in modifying fatigue only if the change in local mean stress persists when fatigue loading is resumed, that is, if the fatigue loads are not large enough to cause further yield at the notch. An example of tests in which creep redistribution was nullified by fatigue loading is seen in Fig. 2*b* where the endurance after heating was insensitive to the value of steady load; it can be demonstrated [*1*] by consideration of local stress-strain conditions that the maximum stress cycle of the spectrum used in these tests was more than sufficient to restore the residual stress to the value which was established prior to the occurrence of creep.

Change in endurance due to creep redistribution was found to accumulate rapidly at first with time of exposure in a similar manner to the change due to heating effects on the machined surface which was described in the previous section. Rapid completion of the effect of creep on endurance was reported also by Imig [*9*] for Ti 8-1-1 material. For the aluminium alloys significant changes in endurance were observed after only a few hours at 150 C, as for example in Fig. 5 which shows how the effect varied with applied creep stress over a range of compressive and tensile stresses. It is seen that endurance increased continuously as creep stress was varied through the range from compression to tension. In the compression range the effect tended to be limited by the subsequent readjustment of local stress under fatigue loading in tension. In the upper half of the tension range the increase in endurance which results from compressive residual stress is due partly to creep and partly to static yield under the preloading at elevated temperature.

It is seen from the foregoing discussion that redistribution of stress by creep interacts significantly with fatigue and is a factor of comparable magnitude to the effect of heat on the machined surfaces which was discussed in the previous section.

Lug and Joint Specimens

Specimens in which fretting occurred at the site of crack initiation proved to be less sensitive than notched specimens to the effects of heat without load. This is most probably because the influence of the machined surface is disrupted at an early stage of the life by fretting damage, in both heated and unheated specimens.

The effect of tension and compression during the heating period is however comparable to that observed for notched specimens. Presumably the

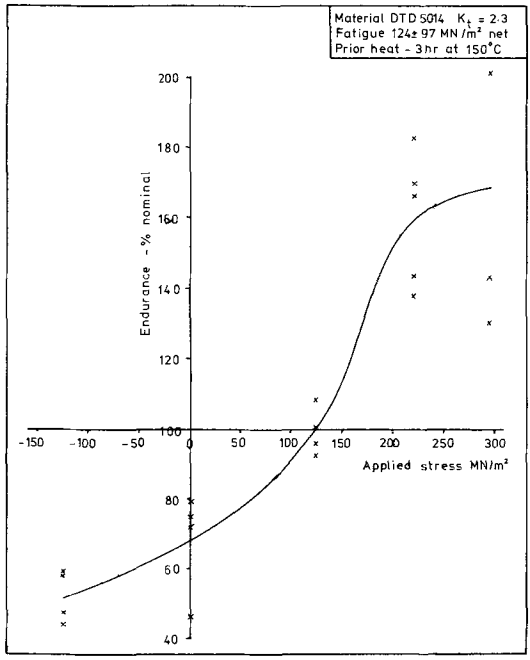


FIG. 5—*Effect on endurance of applied stress during prior heating.*

redistribution of stress by creep modifies the residual stress field and influences the propagation of small cracks, a phase which occupies a considerable proportion of the fatigue life in the types of specimen used.

Cumulative Damage

The use of random loading representing a gust load spectrum in some of the tests provides some information on the influence of heat on cumulative damage under fairly realistic loading conditions. Figure 6 presents information on the S-N performance under constant amplitude loading of unheated and prior heated notched specimens and shows also the shape of the load spectrum applied in the random load tests.

For unheated specimens the life under random loading was assessed by the Palmgren-Miner rule and a value of $\Sigma n/N = 3.3$ was obtained which is characteristic of an aluminium alloy notched specimen under fluctuating tension with a high ratio of peak to rms stress level. This high value of $\Sigma n/N$ depends on the action of the highest loads in the spectrum in causing local yielding and thereby inducing beneficial stresses at the root of the notch and, in the later stages of the life, at the crack tip. It could be expected that, in the absence of residual stress effects, the value of $\Sigma n/N$ would be considerably less than unity, possibly as low as 0.2 or 0.3.

By comparison, tests on specimens which were heated prior to fatigue gave a value of $\Sigma n/N = 0.85$ which suggests that heating drastically cur-

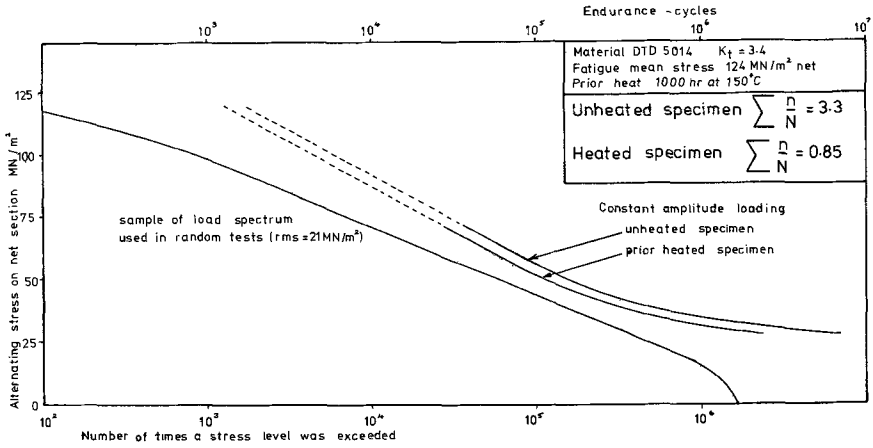


FIG. 6—*Effect of heating on cumulative damage.*

tailed the initiation phase of the life and that in consequence the beneficial effects of local yielding under the random load spectrum were effective only in the crack propagation phase.

Significant reductions in $\Sigma n/N$ are reported also by Imig and Illg [*10*] for Ti 8-1-1 notched specimens $K_t = 4$, when comparing the results of tests under flight-by-flight loading at room temperature and at 288 C.

Crack Propagation

It has been shown that single applications of heat of only a few hours duration can modify significantly fatigue crack initiation in aluminium alloy structure, by modifying the microstructure of the machined surface and by changing the residual stress in the region of the surface. It can be envisaged that these same mechanisms will operate also during the phase of the life when cracks have reached a length at which the crack tip is outside the residual stress field of the stress concentration, by modifying the strain hardened material ahead of the crack and by changing the local residual stress pattern around the crack tip.

The simple form of test used, in which heat was applied only once during the life, was unable to detect any effect when heat was applied at a late stage when a comparatively large crack was propagating. This is understandable, as any effects of heat on conditions at the crack tip would be quickly overtaken by the progress of the crack, and therefore the effect of one application of heat, however significant to the immediate crack propagation rate, could not be expected to affect materially the total endurance.

However, under aircraft service conditions, heating may occur a large number of times during crack propagation, and the cumulative effect on crack propagation rate could be significant. It is relevant to mention here the results of tests outside the scope of the present program, in which many periods of heat were interspersed with fatigue at ambient temperature.

These tests have shown that both the initiation and propagation of cracks are affected in a qualitatively similar manner and that the general trends of behavior with temperature and applied load correspond with those observed in the simple tests described in this paper.

Conclusions

Fatigue tests under constant amplitude and random loading were conducted on simple structural specimens in four aluminium-copper alloy materials, and the effect of applying heat at different stages of the tests was determined:

1. The heating effects observed were qualitatively the same for all four materials.
2. Heating caused microstructural changes in the machined surface of the material which increased its susceptibility to fatigue crack initiation. The result was a significant reduction in the fatigue endurance of notched specimens especially those tested under random loading for which without heating the initiation phase was particularly prolonged. For specimens with fretting the reduction was comparatively small because the influence of the machined surface on crack initiation was short lived under the action of the fretting.
3. By heating at temperatures of 110 C and greater the fatigue endurance was reduced, rapidly with time of exposure, to a limiting value which was independent of temperature. Below 110 C the action of heat was considerably weaker.
4. Steady load during heating caused stress redistribution by creep. The resulting change in local stress in the region of crack initiation was beneficial or detrimental to fatigue performance according to the creep being tensile or compressive. Significant changes in the fatigue endurance of notched specimens were attributed to changes in the initiation phase; for specimens with fretting the effect was attributed to changes in the propagation rate at short crack lengths within the residual stress field of the stress concentration.
5. The concepts which have emerged from this basic research effectively explain behavior observed in tests simulating service conditions in which heat is applied intermittently throughout the life. Results from these tests suggest that the mechanisms of fatigue-heat interaction which have been observed for crack initiation, have their counterparts during crack propagation.

References

[1] Heath-Smith, J. R. and Aplin, J. E., "The Effect of an Application of Heat on the Fatigue Performance Under Random Loading of a Notched Specimen of DTD 5014 (RR58) Material," RAE Technical Report 71209, Royal Aircraft Establishment, Farnborough, England, Oct. 1971.

[2] Forsyth, P. J. E., "The Microstructural Changes that Drilling and Reaming Can Cause in the Bore of Holes in DTD 5014 (RR58 extrusions) and the Effects of Subsequent Heating," RAE Technical Memorandum Mat 110, Royal Aircraft Establishment, Farnborough, England, 1971.
[3] Heath-Smith, J. R. and Kiddle, F. E., "Influence of Aging and Creep on Fatigue of Structural Elements in an Al 6% Cu Alloy," RAE Technical Report 67093, Royal Aircraft Establishment, Farnborough, England, 1967.
[4] Smith, C. R., "Linear Strain Theory and the Smith Method for Predicting the Fatigue Life of Structures for Spectrum Type Loading," Aerospace Research Laboratories Report ARL 64-55, Office of Aerospace Research, USAF, Wright-Patterson Air Force Base, Ohio, April 1964.
[5] Edwards, P. R., "Cumulative Damage in Fatigue with Particular Reference to the Effects of Residual Stresses," RAE Technical Report 69237, Royal Aircraft Establishment, Farnborough, England, 1969.
[6] Heath-Smith, J. R. in *Current Aeronautical Fatigue Problems*, J. Schijve, J. R. Heath-Smith, and E. R. Welbourne, eds., Pergamon Press, London, 1965, pp. 103-130.
[7] Maurin, E. and Barrois, W., "Effect of Frequency and Test Temperature on the Fatigue Life of A-U2GN-T6 Sheet Specimens and Assemblies," (in French) Meeting of International Committee on Aeronautical Fatigue, Stockholm, May 1969.
[8] Hardrath, H. F., "Fatigue of Structural Materials Suitable for the Supersonic Transport," AIME Symposium on Structural Materials in the Environment of the Supersonic Transport, American Institute of Mining, Metallurgical, and Petroleum Engineers, Los Angeles, Feb. 1967.
[9] Imig, L. A., "Effect of Initial Loads and of Moderately Elevated Temperature on the Room-Temperature Fatigue Life of Ti-8Al-1Mo-1V Titanium Alloy Sheet," NASA Technical Note D-4061, National Aeronautics and Space Administration, Washington, D. C., Aug. 1967.
[10] Imig, L. A. and Illg, W., "Fatigue of Notched Ti-8Al-1Mo-1V Titanium Alloy at Room Temperature and 550 F (560 K) with Flight-by-Flight Loading Representative of a Supersonic Transport," NASA Technical Note D-5294, National Aeronautics and Space Administration, Washington, D. C., July 1969.

DISCUSSION

D. Hoeppner[1] *(written discussion)*—Did you notice a change in endurance in the lug-joints as a function of temperature?

Did the fretting damage change character as a function of temperature?

J. R. Heath-Smith and F. E. Kiddle (authors' closure)—Two temperatures only were used in lug specimen tests, 120 and 150 C. Prior heating at either temperature gave a reduction of about 20 percent in the endurance for unheated specimens.

The fretting damage was not quantified. However, the appearance of the fretting damage by direct viewing and by low-power microscope appeared similar for tests at all temperatures.

[1] Lockheed Aircraft Co., Burbank, Calif. 91503.

G. P. Vidal[1] *and P. L. Galmard*[1]

Test Results of Fatigue at Elevated Temperatures on Aeronautical Materials

REFERENCE: Vidal, G. P. and Galmard, P. L., **"Test Results of Fatigue at Elevated Temperatures on Aeronautical Materials,"** *Fatigue at Elevated Temperatures, ASTM STP 520*, American Society for Testing and Materials, 1973, pp. 512–521.

ABSTRACT: This paper shows how fatigue tests at elevated temperature solve many problems pertaining to aeronautical materials. Prolonged periods (5000 or 10 000 h) at 150 C (302 F) did not diminish the fatigue limit at 150 C (302 F) of the aluminum alloy 2618-T6. Consequently, the aerodynamic heating of airframes at Mach 2 does not reduce the fatigue limit of this alloy.

The "bright shot" or shot-peened surface conditions do not increase the hot-fatigue limit of a heat-resistant alloy. The Office National Etudes et Recherches Aérospatiales (ONERA) process for the chromaluminization of the heat- resistant alloy Inconel 713 does not modify the fatigue limit at 700 C (1290 F). Similarly, gases resulting from kerosine (0.5 percent sulfur) combustion do not reduce the hot-fatigue resistance of four heat resistant alloys. The fatigue characteristics of various superalloys— unidirectional or composites made by the ONERA process—at 800 C (1470 F)—are equal to or even superior to those classic heat-resistant alloys, cast or forged. A cermet of 50 percent of chromium and 50 percent of alumina retains, even at 1200 C (2190 F), a resistance to fluctuating flexure stresses of 69 $\pm$ 49 MN/m^2 (10 $\pm$ 7 ksi).

KEY WORDS: test equipment, fatigue tests, high temperature tests, fatigue (materials), aluminum alloys, chemical machining, heat resistant alloys, surface hardening, oriented fiber composites, cermets, aerospace engineering

After a brief description of the apparatus used, this paper deals mainly with the application of hot-fatigue testing to a broad variety of aeronautical materials.

First, as regards supersonic airframes, in particular the Franco-British Concorde airliner, we examine whether long holdings at 150 C (302 F) by kinetic heating modify the fatigue resistance of the 2618-T6 aluminum alloy.

Further, as regards superalloys used for turbojet mobile blades, we try to see if their hot-fatigue limits are influenced, either by surface treatments such as shot peening, bright shot, or chromaluminization, or by holding them in an environment of combusted kerosine fuel-rich gases.

[1] Research leader and research technician, respectively, Office National Etudes et Recherches Aérospatiales (ONERA), 92 Chatillon-sous-Bagneux, France.

Copyright© 1973 by ASTM International www.astm.org

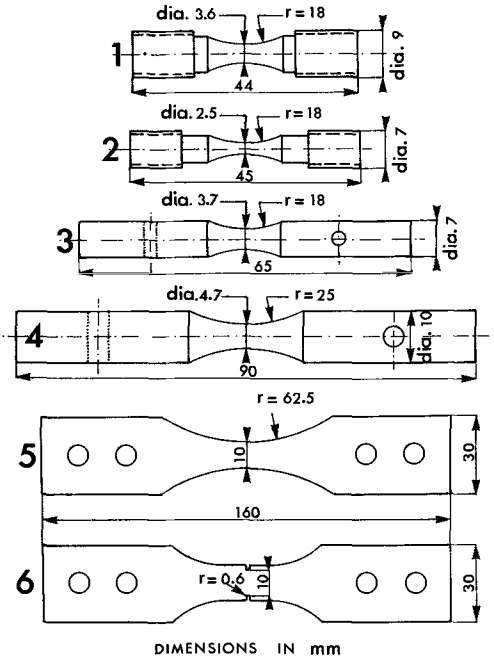


FIG. 1—*Specimens for hot-fatigue tests.*

Lastly, we compare the hot-fatigue limits of classical superalloys with those of new advanced materials such as directionally solidified alloys, composites, and cermets.

Apparatus for Fatigue Tests at High Temperatures

We have set up a large range of fatigue testing machines for elevated temperatures using fluctuating axial tension, rotating flexure, and fluctuating, nonrotating flexure at temperatures varying between 100 C (210 F) and 1300 C (2370 F).

Fatigue tests using fluctuating axial tension on heat-resistant alloys were carried out by means of an Amsler Vibrophore and a device which has been previously described [*1*].[2] On this setup, it is possible to adapt Specimens 1 and 2 whose design is laid out in Fig. 1. The working temperature of this equipment is adjustable, usually between 700 C (1290 F) and 1000 C (1830 F), for aeronautic turbojet alloys.

The installation for hot-fatigue tests with fluctuating tensile stress, under an atmosphere of gases resulting from kerosine combustion was set up so that tests could be carried out on Specimen 1, as shown in Fig. 1 [*2*]. The

[2] The italic numbers in brackets refer to the list of references appended to this paper.

advantage of such an apparatus is that it allows the influence of operational environment on the fatigue of heat-resistant alloys at high temperatures to be studied.

A high-temperature rotating flexure machine was used for temperatures up to 815 C (1500 F) to determine the fatigue limit for this type of stressing at high temperature [*3*]. This machine may use Specimens 3 and 4 in Fig. 1.

For high-refractory materials, a setup for hot-fatigue tests under non-rotating fluctuating flexure, which functions at temperatures up to 1300 C (2370 F), is shown in Fig. 2. Specimen A is a rectangular parallel pipe; its dimensions are: 6, 6, 31 mm (1/4, 1/4, 1 1/4 in.). This specimen is held at its two ends by Support B made from a cermet of 50 percent chromium and 50 percent alumina. Cylinder C, made of the same cermet, acts as a punch. Rods D and E are in alumina and transmit the fluctuating compressive load of an Amsler Vibrophore with a 4-kN (880-lb) dynamometer. The whole assembly is contained in a furnace (inside diameter 41 mm (1 5/8 in.), length 280 mm (11 in.)).

Hot-fatigue tests under fluctuating axial tensile stress were carried out between 100 C (210 F) and 250 C (480 F) on sheets of aluminum alloy using unnotched Specimen 5 and notched Specimen 6, as shown in Fig. 1. The stress concentration factors are, for these two specimens, equal to 1.05 and 3.25, respectively. The assembly is contained in a furnace of large dimensions [inside diameter 60 mm (2 1/3 in.), length 420 mm (16 1/2 in.)] and is mounted on a special Amsler Vibrophore of 100 kN (22 000 lb); the two columns of this Vibrophore are longer than those of the classic Vibrophore.

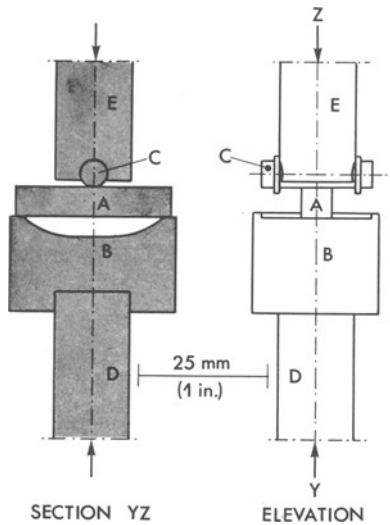


FIG. 2—*Setup for fluctuating flexure fatigue test at very high temperatures.*

Hot-Fatigue Tests on an Aluminum Alloy

The aluminium alloy studied is an English alloy RR 58 which is called AU2GN in France and 2618-T6 in the United States. The thermal treatment of this alloy is a quench from a holding temperature of 530/540 C (986/1004 F) and artificial aging for 25 h at 190 C (374 F). This alloy is used for the construction of supersonic civil aircraft, which may undergo aerodynamic heating up to about 130 C (266 F). It is thus necessary to ensure that long periods in service at this temperature do not diminish the fatigue resistance of this alloy. This is the object of this part of the present study, using a temperature of 150 C (302 F). Temperature is always constant during any test.

The 2618-T6 alloy is studied under hot fatigue in two conditions: an alclad sheet 1.65 mm (0.065 in.) thick and a sheet 1.5 mm (0.059 in.) thick, chemically machined from a sheet 2.5 mm (0.1 in.) thick.

The hot-fatigue tests were carried out under fluctuating tensile stress on unnotched Specimens 5 and on notched Specimens 6. The test frequency was 80 to 86 Hz. The minimum tensile stress was always equal to one tenth of the maximum tensile stress.

Figure 3 shows the results on unnotched and notched specimens for the aluminum alloy with a coating of aluminum. It can be seen that the various points are dispersed about the same curve for the three following conditions:

1. Without previous treatment, fatigue test at room temperature.

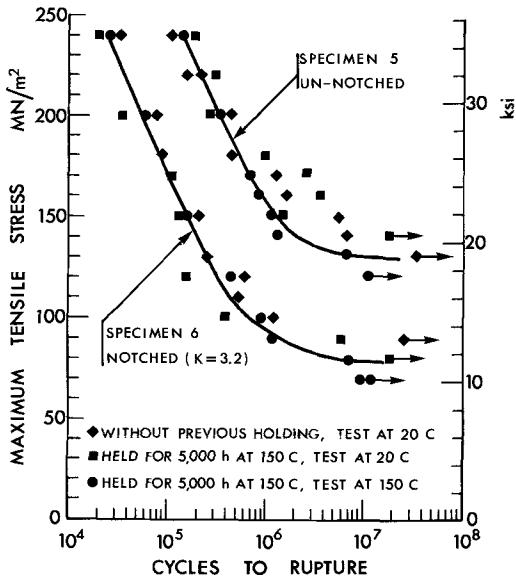


FIG. 3—S/N *fatigue curves for fluctuating axial tension on the alclad 2618-T6 aluminum alloy. (The minimum tensile stress was equal to one tenth of the maximum tensile stress).*

2. Held for 5000 h at 150 C (302 F), fatigue test at room temperature.
3. Held for 5000 h at 150 C (302 F), fatigue test at 150 C (302 F).

These results show not only that a previous holding at 150 C (302 F) for 5000 h did not cause any detectable reduction of fatigue resistance but also that the fatigue resistances were almost identical at room temperature and at 150 C (302 F).

Figure 4 describes the influence of a previous treatment for 10 000 h at 150 C (302 F) on the fatigue resistance at 150 C (302 F) of AU2GN alloy, chemically machined. The different points are dispersed about the same curve, indicating that previous heating had no effect on the fatigue resistance at 150 C (302 F) for the chemically machined AU2GN alloy.

Effect of Various Surface Treatments on the Hot-Fatigue Limit of a Heat-Resistant Alloy

Certain surface treatments, notably shot peening, increase the fatigue resistance of steels at room temperature. Could such an increase be obtained in the particular case of heat-resistant alloys which function at high temperature and which are used in the fabrication of moving blades in turbojets?

To answer this question, Alloy PER2S, which is heat resistant and whose chemical composition is shown in Table 1, was chosen. Fatigue tests were conducted on specimens of this alloy with the following five surface condi-

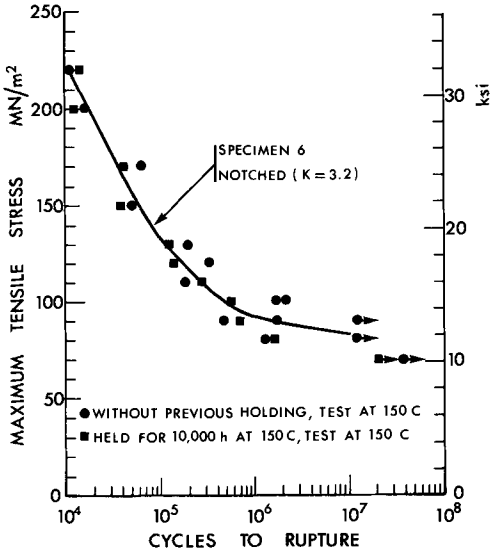


FIG. 4—S/N *fatigue curve for fluctuating axial tension on the chemically machined 2618-T6 aluminum alloy. (The minimum tensile stress was equal to one tenth of the maximum tensile stress).*

TABLE 1—*Influence of various surface treatments on the hot-fatigue limits of a heat-resistant alloy PER2S.*[a]

Temperature, deg C (deg F)	Rotating Flexure Fatigue Limit at 4×10^7 Cycles, MN/m^2 (ksi)				
	After Grinding	After Shot Peening	After Bright Shot	After Electro-polishing	After Electro-polishing + Bright Shot
20 (68)	±324 (±47)	±441 (±64)	±510 (±74)	±331 (±48)	±510 (±74)
650 (1200)	±379 (±55)	±372 (±54)	±379 (±55)	±400 (±58)	±372 (±54)
815 (1500)	±324 (±47)	±345 (±50)	±331 (±48)	±317 (±46)	±317 (±46)

[a] Ni-18Cr-17Co-4Mo-3Ti-2.5Al-0.005B, forged.

tions: after grinding, after classic shot peening, after "bright shot" treatment (peening with glass ball), after electropolishing, and after electropolishing followed by bright shot treatment. The fatigue tests at 650 C (1200 F) and 850 C (1560 F) were carried out in rotating flexure, using Specimen 4 in Fig. 1. The test loading frequency was 48 Hz. Table 1 indicates the results. At room temperature, the shot peened and bright shot surfaces have fatigue limits clearly superior to those surfaces ground and electropolished. However, the fatigue limits for the various treatments become almost identical at temperatures of 650 C (1200 F) and 815 C (1500 F). Consequently, the shot peened and bright shot surfaces lose their advantages at high temperatures. It is probable that the favorable internal stresses induced by these surface hardenings disappear at higher temperatures, either through relaxation or recrystallization.

Effect of an Environment of Combusted Kerosine Gas on the Fatigue Limit of Four Heat-Resistant Alloys

An environment of fuel-rich gases, from the combustion of kerosine (containing sulfur), may cause appreciable intergranular corrosion at high temperatures [*4*]. For this reason, it is necessary to determine if the hot-fatigue resistance is decreased when the tests are carried out in such an environment.

The tests were carried out on four different heat-resistant alloys: ATGS (Ni-19Cr-2.5Ti-1.4Al), Nimonic 90, Nimonic 100, and ATGW2, whose chemical compositions are given in Table 2. The hot-fatigue tests were carried out in fluctuating axial tension at a frequency of 80 Hz using a special instrument already described [*2*]; Specimen 1 was used. Two separate environments were studied: atmospheric air, and the fuel-rich gases from the combustion of kerosine containing 0.5 percent sulfur. The results ob-

TABLE 2—*Comparative results of hot-fatigue tests in air and in fuel-rich gases from combustion of kerosine containing 0.5 percent sulfur.*

Alloy	Temperature, deg C (deg F)	Fatigue Stress,[a] MN/m^2 (ksi)	Environment	Mean Value and Standard Deviation of Cycles to Rupture
Nimonic 90[b]	850	123 ± 103	air	55 000 000 ± 4 000 000
(forged)	(1560)	(18 ± 15)	fuel-rich gases	53 000 000 ± 4 000 000
	950	83 ± 63	air	44 000 000 ± 5 000 000
Nimonic 100[c]	(1740)	(12 ± 9)	fuel-rich gases	40 000 000 ± 2 000 000
(forged)	1000	49 ± 29	air	40 000 000 ± 2 000 000
	(1830)	(7 ± 4)	fuel rich gases	39 000 000 ± 3 000 000
	950	76 ± 56	air	40 000 000 ± 3 000 000
ATGW2[d]	(1740)	(11 ± 8)	fuel-rich gases	34 000 000 ± 8 000 000
(forged)	1000	41 ± 21	air	44 000 000 ± 1 000 000
	(1830)	(6 ± 3)	fuel-rich gases	49 000 000 ± 8 000 000

[a] The first number indicates the mean tensile stress and the second the alternating stress.
[b] Ni-20Cr-18Co-2.5Ti-1.5Al-5Fe-0.1C.
[c] Ni-11Cr-20Co-5Mo-1.5Ti-5Al-2Fe-0.3C.
[d] Ni-19Cr-19Co-4Mo-3Ti-3Al.

tained are shown in Table 2 except for ATGS alloy. In all cases, the fatigue resistance is almost identical. Thus the environment studied had no particularly degenerative effect on hot-fatigue resistance. It is probable that intergranular corrosion does not affect the fatigue crack which is transcrystalline.

Effect of a Chromaluminization Treatment on the Fatigue Resistance of Inconel 713 at 700 C (1290 F)

The Office National Etudes et Recherches Aérospatiales (ONERA) process for the chromaluminization of heat-resistant alloys used for the mobile blades of aeronautic turbojets appreciably increases the oxidation resistance of these alloys [*5–7*]. In a recent article, we have studied the effect of this treatment on the hot-fatigue limit of a cast heat resistant alloy, Inconel 713. The composition of this alloy is Ni-12Cr-4Mo-1Ti-6Al-2Cb-0.1Zr-0.1C-0.01B. A temperature of 700 C (1290 F) was used. This temperature is, for some engines, the base of these blades from which point the fatigue cracks most often start, in service. A summary of these results, already published, is as follows:

1. Without treatment: fatigue limit at 10^8 cycles = 186 ± 166 MN/m^2 (27 ± 24 ksi).
2. With treatment: fatigue limit at 10^8 cycles = 207 ± 186 MN/m^2 (30 ± 27 ksi).

For the tests conditions used, the chromaluminization treatment does not cause any unfavorable effect on the hot-fatigue limit of this alloy.

Comparison of the Hot-Fatigue Limit for Classic Superalloys and Those of Special Fabrication

The trend in the aeronautical turbojet industry is to try to improve the mechanical characteristics at high temperatures for superalloys which are used in the mobile blades of these turbojets. By means of directionally solidified alloys and carbide fiber composites with alloy matrices, progress was made in the technology of advanced materials [*9–14*]. Because of the very special character of the structure of these new alloys, it is essential to compare the hot-fatigue resistance of these alloys with those of classic superalloys. A series of fatigue tests, in fluctuating axial tension at 800 C (1470 F) in air, was carried out with Specimen 2 as shown in Fig. 1; the test frequency was 87 Hz. The advantage of a test under fluctuating stress is that a constant superimposed tensile stress reproduces the service conditions of the mobile blades which are subjected very well by centrifugal force to a constant tension.

Two heat resistant alloys were tested as a basis for comparison. One, a forged alloy PER7; the other a cast alloy IN100. The chemical compositions of these alloys are shown in Table 3. Six special alloys were tested, one of which is the classic alloy MAR M 200, directionally solidified by the ONERA process [*9*]. The five others are fiber composites of tantalum carbides or colombium carbides in various matrices [*10–14*]. Fibers are continuous, and their direction makes an angle of ± 0.1 rad with that of the growth [*10*].

Table 3 shows the fatigue limits at 800 C (1470 F) of these alloys. These limits are superior to those of IN100, sometimes even to those of PER7.

Hot-Fatigue Limit of a Cermet

The cermet studied has 50 percent chromium and 50 percent alumina. Since this cermet is not completely metallic, it was first necessary to discover whether it fatigues like a metal, as a function of the number of cycles, or like a glass, as a function of the time under stress [*15,16*]. In order to answer this question, the fatigue tests were carried out in rotating flexure at room temperature with two different frequencies: the alternating stress was ± 265 MN/m^2 (± 38 ksi): at 48 Hz the number of cycles to rupture was 95 000 $\pm$ 53 000; at 0.4 Hz the number of cycles to rupture was 55 000 $\pm$ 23 000. The fatigue fracture occurs more nearly after the same number of cycles than the same time. Thus this cermet fatigues as a function of the number of cycles.

Using Specimen 4 in Fig. 1, the fatigue limit was determined after 10^7 cycles at room temperature and at 800 C (1470 F), using the rotating flexure machine; the limits found were identical and equal to ± 216 MN/m^2 (± 31 ksi).

TABLE 3—*Fatigue limits in fluctuating tensile stress at 800 C (1470 F) of various classic heat-resistant alloys and heat-resistant alloys of special fabrication.*

Fabrication	Type of Alloy	Fatigue Limit, MN/m^2 (ksi) 10^7 Cycles	Fatigue Limit, MN/m^2 (ksi) 10^8 Cycles
Classic	PER7,[a] forged	276 ± 255 (40 ± 37)	262 ± 241 (38 ± 35)
	IN100,[b] cast	214 ± 193 (31 ± 28)	207 ± 186 (30 ± 27)
Special (all cast)	MAR M 200[c] unidirectionally solidified (ONERA process) [9]	276 ± 255 (40 ± 37)	248 ± 228 (36 ± 33)
	composite (TaC fiber in Co-Cr matrix) [10,11]	228 ± 207 (33 ± 30)	214 ± 193 (31 ± 28)
	composite (TaC fiber in Co-Ni-Cr matrix) [12,13]	255 ± 234 (37 ± 34)	
	composite (TaC fiber in Co-Ni-Cr-Al matrix) [12,13]	255 ± 234 (37 ± 34)	
	composite (CbC fiber in Co-Cr-Ni matrix) [13]	255 ± 234	
	composite (TaC in Ni-Co-Cr matrix reenforced by coherent precipitation of γ' [Ni_3(Ti,Al)]) [14]	37 ± 34	
		302 ± 283 (44 ± 41)	

[a] Ni-15Cr-19Co-5Mo-3Ti-4Al-0.03B.
[b] Ni-10Cr-15Co-3Mo-5Ti-5Al-1V-0.01Zr-0.015B-0.15C.
[c] Ni-9Cr-10Co-2Ti-5Al-12W-1Cb-0.5Zr-0.015B-0.15C.

Using the setup shown in Fig. 2, the hot-fatigue limit was determined at four temperatures under nonrotating fluctuating flexure. The fatigue limits at 4×10^7 cycles are as follows:

1. At room temperature: 157 ± 137 MN/m^2 (22.8 ± 19.9 ksi).
2. At 1000 C (1830 F): 118 ± 98 MN/m^2 (17.1 ± 14.2 ksi).
3. At 1150 C (2100 F): 79 ± 59 MN/m^2 (11.4 ± 8.5 ksi).
4. At 1200 C (2190 F): 69 ± 49 MN/m^2 (10.0 ± 7.1 ksi).

In these tests, the fatigue resistance of this cermet is relatively high, even at a very high temperature of 1200 C (2190 F).

Conclusions

The results of the tests performed during this research work permit several conclusions to be drawn regarding some aeronautical materials.

First, as regards 2618-T6 aluminum alloy, under the form of Alclad sheets or chemically machined sheets, the fatigue resistance remains practically

unaltered in spite of long—5000 to 10 000 h—holdings at 150 C (302 F). Aerodynamic heating at Mach 2 thus should be no worry for this alloy.

Further, as regards some classical superalloys for mobile blades of aeronautical turbojets, we have seen that their hot-fatigue limits are neither influenced by shot peening, bright shot, and chromaluminization surface treatment, nor by holding in an environment of combusted kerosine fuel-rich gases.

Lastly, we found that hot-fatigue limits of advanced superalloys, such as directionally solidified alloys and composites, are equal to and sometimes higher than those of classical superalloys. A 50 percent chromium, 50 percent alumina cermet presents, even at 1200 C (2190 F), a flexure fatigue resistance still appreciable.

References

[1] Vidal, G. P. and Lanusse, P. C., *Recherche Aéronautique*, No. 45, May–June 1955, pp. 45–51.

[2] Vidal, G. P., *Recherche Aéronautique*, No. 46, July–Aug. 1955, pp. 25–29.

[3] Vidal, G. P., *Revue de Métallurgie* (Paris), Vol. 54, No. 12, Dec. 1957, pp. 971–978.

[4] Vidal, G. P., *Revue de Métallurgie*, (Paris), Vol. 50, No. 1, Jan. 1953, pp. 21–34.

[5] Philippe Galmiche, *Metal Forming*, Vol. 35, No. 3, March 1968, pp. 66–73.

[6] Philippe Galmiche, *Metals and Materials*, Vol. 2, No. 8, Aug. 1968, pp. 241–248.

[7] Philippe Galmiche, *Proceedings*, AGARD Conference, Vol. CP 73, Sept. 1970, pp. (20-0)–(20-10).

[8] Vidal, G. P., Galmard, P. L., and Bernard Genty, *Recherche Aérospatiale*, No. 3, May–June 1970, pp. 177–179.

[9] Bibring, H. E., *Proceedings*, AGARD Conference, Vol. 64, April 1970, pp. (6-0)–(6-7).

[10] Bibring, H. E., Rabinovitch, Maurice, and Seibel, Georges, *Comptes Rendus De L'Academie Des Sciences*, Paris, Series C, Vol. 268, May 1969, pp. 1666–1669.

[11] Bibring, H. E. Trottier, J. P., Rabinovitch, Maurice, and Seibel, Georges, *Mémoires Scientifiques De La Revue De Métallurgie*, Vol. 68, No. 1, Jan. 1971, pp. 23–41.

[12] Bibring, H. E., Conference at Journées de Printemps du GAMI, Paris, May 1971, to be published in *Revue de Mécanique, Matériaux et Electricité*.

[13] Bibring, H. E., Seibel, Georges and Rabinovitch, Maurice, *Mémoires Scientifiques De La Revue de Métallurgie*, Vol. 69, No. 5, May 1972, pp. 341–358.

[14] Bibring, H. E., Seibel, Georges, and Rabinovitch, Maurice, *Comptes Rendus De L'Academie Des Sciences*, Paris, Séries C, Vol. 271, Dec. 1970, pp. 1521–1524.

[15] Gurney, C. and Pearson, S., *Proceedings*, Royal Society, Series A, Vol. 192, No. 1031, March 1948, pp. 537–544.

[16] Vidal, G. P., *Revue de Métallurgie*, Paris, Vol. 53, No. 7, July 1956, pp. 485–496.

P. S. Prevey[1] *and W. P. Koster*[1]

Effect of Surface Integrity on Fatigue of Structural Alloys at Elevated Temperatures

REFERENCE: Prevey, P. S. and Koster, W. P., **"Effect of Surface Integrity on Fatigue of Structural Alloys at Elevated Temperatures,"** *Fatigue at Elevated Temperatures, ASTM STP 520*, American Society for Testing and Materials, 1973, pp. 522–531.

ABSTRACT: Surface integrity is a subject covering the description and control of the many possible alterations produced in the surface of a component during manufacturing. Surface integrity is evaluated by measuring the influence of machined surface layers on component reliability. This is accomplished primarily through fatigue testing under both low-cycle and high-cycle conditions. Considerable data have been developed permitting definition of characteristic changes in fatigue strength of a variety of high-strength structural alloys as a function of several different metal removal methods and also variations within these methods.

High-cycle fatigue data have been developed in the cantilever bending mode at temperatures ranging from ambient to 1400 F. Low-cycle fatigue data have been obtained in four-point bending over the same temperature range following the development of a specialized testing technique.

Data are presented showing fatigue behavior of Inconel 718, René 80, and René 95 using specimens finished by variations of grinding, turning, electrochemical machining, and electrical discharge machining.

KEY WORDS: fatigue (materials), fatigue strength, surfaces, machining, fatigue life, stresses, bending, fatigue tests

The fatigue behavior of high-strength materials and structural components has been shown to depend significantly on methods used for machining and finishing the surface [*1*].[2] More specifically, fatigue strength has been shown to vary widely with different metal removal methods such as turning, milling, grinding, hand sanding, electrical discharge machining (EDM), and electrochemical machining (ECM). Variations in cutting parameters within a single metal removal method may also cause large variations in fatigue behavior. The subject covering the quality or condition of a surface, interrelating metal removal, or surface machining and finishing conditions with resulting mechanical properties has come to be known as surface integrity.

[1] Project engineer and director of metallurgical engineering, respectively, Metcut Research Associated, Inc., Cincinnati, Ohio 45209.

[2] The italic numbers in brackets refer to the list of references appended to this paper.

Copyright© 1973 by ASTM International www.astm.org

Design engineers have traditionally related fatigue behavior of metallic materials to surface roughness and orientation of the surface lay due to machining. Recently developed surface integrity information shows clearly that surface finish *per se* exerts a much lower level of influence on fatigue behavior than is commonly believed. More potent factors include residual surface stress profile and also the presence of plastic deformation, microcracking, and metallurgical phase changes produced in the surface as a result of machining operations. Therefore, it has been concluded that any serious use of laboratory fatigue data for component design purposes must give adequate consideration to the method used in manufacturing and finishing the test specimens. Similarly, equal controls must be imposed in the manufacture of critically stressed components since the surface integrity of the component may play a key roll in determining its reliability and performance under design stress conditions.

This paper summarizes the fatigue data developed during surface integrity studies on three nickel-base alloys: Inconel 718, René 80, and AF 95 (René 95). Machining conditions covered include grinding, turning, EDM, and ECM; shot peening is sometimes used as a post treatment. During the original development of this program, the answers to these basic questions were sought:

1. To what extent do machining variables affect the room temperature fatigue behavior of these alloys?
2. Do these effects carry over to an elevated temperature environment typical of the service exposure of each alloy?
3. Do the effects observed in the high-cycle or infinite-life region still exist in the low-cycle or finite-life region?
4. Do the beneficial effects of shot peening on fatigue improvement, well recognized at room temperature, carry over to an elevated temperature environment?

The surface integrity investigation from which these data were taken was sponsored by the Air Force Materials Laboratory in contract to Metcut Research Associates Inc. A majority of the total effort was performed by Metcut. Part of the data reported herein, however, was developed by the General Electric Company, Evendale, Ohio, under subcontract from Metcut on the surface integrity effort. The authors are indebted to W. J. Stross of Metcut and A. Anderson of GE for their contribution to this overall effort.

Surface Conditions

In conducting this investigation, test coupons were machined by a variety of methods using two or three different sets of cutting parameters for each method studied. In general, these parameters were selected to represent

extremes of the possible range of variables that could be used in a manufacturing operation. The terms gentle and abusive describe the extremes of industrial practice in grinding and turning operations. For EDM, the terms finishing and roughing are used. Standard and off-standard are used to describe ECM practice variations. Table 1 outlines the machining parameters which characterize each operation and condition.

TABLE 1—*Machining parameters.*

	Surface Conditions	
Operation	Gentle, Finishing, Standard	Abusive, Roughing, Off-Standard
Ginding	2000 surface ft/min soft wheels chemically active fluids	6000 surface ft/min hard wheels intermittent loss of fluid
Turning	sharp tools wearland: <0.004 in.	relatively dull tools wearland: ≅ 0.030 in.
EDM	low current density low removal rates	high current density high removal rates
ECM	high current density and voltage constant electrode feed electrode gap: 0.010 in.	low current density and voltage stationary electrode electrode gap: 0.040 in.

Gentle conditions are those which are specifically intended to produce a minimum of surface alterations. Abusive conditions, in contrast, are those intended to produce substantial surface damage such as plastic deformation, localized surface heating, etc. Conventional conditions are intermediate conditions generally typical of industrial practice.

Testing Techniques

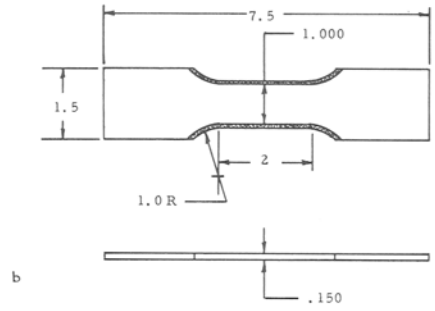
High-Cycle Fatigue

High-cycle fatigue tests were conducted using the flat constant stress specimen shown in Fig. 1*a*. This specimen design provided a large surface area under uniform stress. The specimens were tested in fully reversed cantilever bending, constant force loading, at a frequency of 1800 cpm. A small radiant furnace was used for elevated temperature testing.

Although it is recognized that cantilever bending fatigue testing is not generally suitable for component design purposes, it has been shown that the relative behavior of materials under combined stress tension-tension loading closely approximates that produced by cantilever bending [*2*].

Low-Cycle Fatigue

The specimen shown in Fig. 1*b* was used for low-cycle fatigue testing. The tests were conducted in fully reversed four-point bending to provide (as



All dimensions are shown in inches. Edges of gage sections are rounded and shot peened.

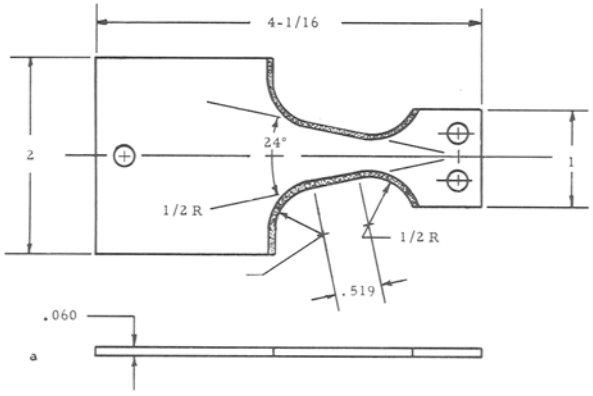


FIG. 1—(a) *High cycle fatigue specimen and* (b) *low cycle fatigue specimen.*

in the case of the high-cycle fatigue specimens) a large surface area of the gage section under uniform stress. Tests were performed on a closed loop hydraulic testing machine with constant fixture amplitude. The loading wave form was triangular at a frequency of 20 cpm.

The fixture displacement, d, as measured with a linear variable differential transformer (LVDT) supplied the feedback signal for the servo system. In the limit of the small fixture displacement required for testing, the fixture displacement is related to the surface strain, ϵ, as

$$d = (aL/h)\epsilon \quad \ldots\ldots\ldots\ldots\ldots\ldots\ldots\ldots (1)$$

where

L = length of the specimen between the fixture grips,
h = specimen thickness, and
a = fixture moment arm.

Equation 1 was used to set the fixture displacement for a desired surface strain. The relationship was verified within the accuracy of available instrumentation by comparing the strain as calculated from Eq 1 with resistive strain gage measurements at room temperature and spherometer measurements at elevated temperatures.

For elevated temperature testing, the specimen was heated radiantly to produce a 1-in. zone in the center of the gage section within ± 10 F of the desired test temperature. The heating apparatus consisted of two sheet heating elements surrounding the specimen and spaced to produce a uniform temperature zone approximately 1 in. long in the gage section.

Low-cycle fatigue tests of René 95 specimens were performed at the General Electric laboratories at Evendale. As with the closed-loop hydraulic system, tests were performed in fully reversed four-point bending with constant cyclic fixture displacement. The testing machine was a crank actuated mechanical system sufficiently rigid to provide approximately constant cyclic displacement despite decrease in specimen compliance during testing.

Specimens were self-resistance heated in the GE system by passing a large current through the specimen. The current was controlled to maintain test temperature. Spherometer measurements were monitored during testing and the machine was adjusted as required to hold the cyclic specimen strain constant.

Consideration had been given to differences in specimen heating between the Metcut (radiation) and the GE (self-resistance systems). It was thought that the possibility of a localized temperature increase at the crack tips in the specimens heated by self-resistance might shorten specimen life. We could not find verification that this phenomenon, in fact, does occur, although there has been much discussion of the possibility. In any event, it was reasoned that the effect, if present, would be small because the majority of test time was consumed in crack initiation rather than crack propagation. As a verification, a group of paired specimens was run under identical strain conditions in both test systems. The results were overlapping, indicating no differences in behavior of the specimens related to these two different heating methods.

Summary of Data

All fatigue data presented in this paper are based on *S-N* curves developed by testing six to ten specimens in fully reversed bending. Typical high-cycle fatigue data for AF 95 are shown in Fig. 2. Similar sets of curves were generated for each material and surface condition investigated. Table 2 summarizes these data in terms of the stress at 10^7 cycles for AF 95, Inconel 718, and René 80 all in the solution treated and aged condition. A typical set of low-cycle fatigue data for Inconel 718 is shown in Fig. 3. Low-cycle fatigue data are summarized in Table 3 in terms of the stress corresponding to a cyclic life of 2×10^4 cycles. In the case of low-cycle fatigue at stress

TABLE 2—*Summary of high-cycle fatigue behavior (endurance limit at 10^7 cycles, ksi).*

Surface Condition, temperature	AF 95, 50 R_c			Inconel 718, 44 R_c			René 80, 40 R_c		
	Gentle	Conventional	Abusive	Gentle	Conventional	Abusive	Gentle	Conventional	Abusive
Surface grind, 75 F	75	24	26	60	24	...	42	18	16
Surface grind, 1000 F	98	...	48						
EDM, 75 F	40	...	35	22	...	22	26	...	26
EDM, 1000 F	50	...	50						
EDM + peen, 75 F	115	...	110	66	...	75			
EDM + peen, 1000 F	95	...	95						
ECM, 75 F	57	...	57	39	...	39	28	...	28
ECM, 1000 F	95	...	95						
ECM + peen, 75 F	105	...	117	78	...	67			
ECM + peen, 1000 F	109	...	109						
Turning, 75 F				60	...	60			
ELP, 75 F				42	...	...			
ELP + peen, 75 F				78	...	...			

TABLE 3—*Summary of low-cycle fatigue behavior (stress at 20 000 cycles, ksi).*

	AF 95, 50 R_c			Inconel 718, 44 R_c			René 80, 40 R_c		
Surface condition, temperature	Gentle	Conventional	Abusive	Gentle	Conventional	Abusive	Gentle	Conventional	Abusive
Surface grind, 75 F				160	...	127	55		45
EDM, 1000 F	90	...	90						
EDM, 1400 F							54	...	54
EDM + peen, 1000 F	137	...	137						
ECM, 1000 F	122	...	122						
ECM + peen, 75 F	195	...	195	158	...	158			
ECM + peen, 1000 F	165	...	165	127	...	125			
ECM + peen, 1400 F							66	...	66
Turning, 75 F	188	...	188	152	...	152			
Turning, 1000 F	162	...	162	118	...	103			

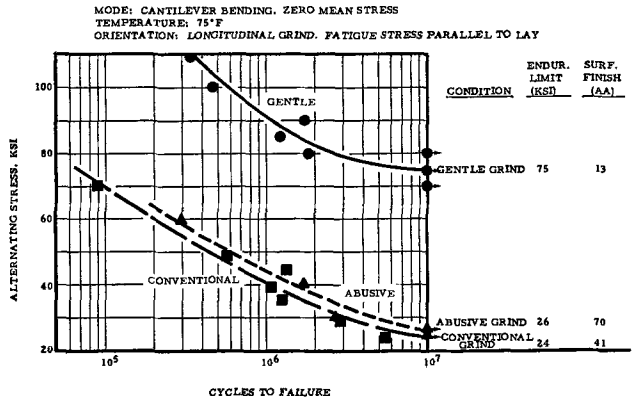


FIG. 2—*High-cycle fatigue characteristics of AF95 (solution treated and aged, 50* R_c*) produced by surface grinding.*

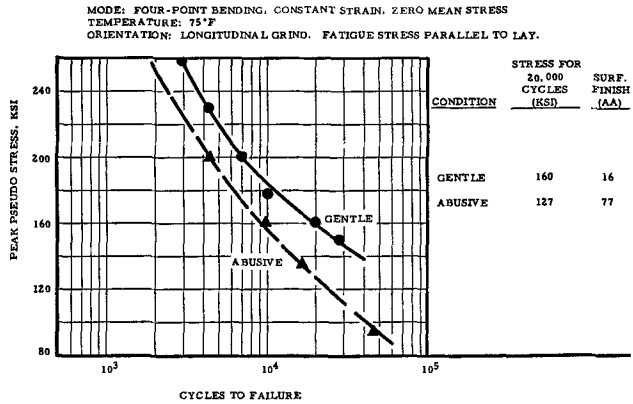


FIG. 3—*Low-cycle fatigue characteristics of Inconel 718 (solution treated and aged, 44* R_c*) produced by surface grinding.*

levels beyond the proportional limit, data are reported in terms of pseudo stress. Pseudo stress is taken to be the product of the elastic modulus and maximum strain amplitude.

While a detailed review of residual stress results is outside the scope of this paper, it is worth noting that this behavior is at least to some degree dependent upon the residual stress profiles of these ground surfaces. Gentle grinding AF 95 usually results in moderately compressive stresses in the ground surface which peak at approximately 60 ksi. In contrast, both conventional and abusive grinding result in peak tensile stresses of approximately 180 ksi. Residual stress data are obtained by a standard dissection technique which is discussed in a variety of sources [*3,4,5*].

In dealing separately with the surface integrity of materials, considerable attention has been paid to the relationship between residual stress and

fatigue. A reasonably good correlation is usually found in ground surfaces. Tensile stress peaks at or near the surface generally promote reduced fatigue life, while compressive stresses on or near the surface are often associated with improvements in the endurance limit level. This trend is not always consistent, however, and may be completely reversed in situations where surface alterations such as cracking, metallurgical phase changes, and plastic deformation are present.

It should be also mentioned that the surface finish does not appear to be related directly to the fatigue life. The surface finish associated with each type of grinding is indicated in Fig. 2. Notice that there is no particular relationship between the fatigue strength and the microinch finish as measured by a stylus instrument. Also, as shown in Table 2, electropolished (ELP) Inconel 718 produced a lower endurance limit than either gently ground or even abusively turned specimens.

The endurance limit of AF 95 was found to increase from room temperature to 1000 F. Normally, reduced fatigue strength is expected with increased temperature. However, for AF 95 and other similar nickel-base alloys, greater high-cycle fatigue strength is sometimes observed in the intermediate or service temperature ranges than at room temperature. The increase in strength has been attributed to a thermal or strain aging reaction. Specific examples of this behavior include unpublished data on René 95 barstock generated by the General Electric Company and Inconel 718 sheet fatigue data published in the *1971 Aerospace Structural Metals Handbook*. In the General Electric data for gentle grinding, the endurance limit in reversed bending at 10^7 cycles was observed to increase continuously from room temperature to 1200 F. Inconel 718, on the other hand, tends to exhibit a peak in fatigue strength as a function of temperatures in the 600 to 800 F range.

Summary

An overall impression can be formed immediately, namely, that the methods used for machining and finishing a structural component can indeed have a significant effect on the resulting fatigue behavior. Abusive and even conventional grinding practices are particularly detrimental to nickel-base alloys. It may be also concluded that EDM produces a low fatigue strength characteristic of the process and without sensitivity to variations in processing parameters. This situation does not condemn EDM as a manufacturing process but implies the need for a post treatment whenever a critically stressed surface is involved. It has been established that the areas of surface integrity sensitivity observed in high-cycle fatigue at room temperature do carry over to elevated temperature exposure of these materials.

In general, differences in fatigue strength associated with surface conditions observed in the high-cycle mode tend to diminish in the low-cycle or finite-life region. Surface grinding is the only process studied which shows

a constant detrimental effect of abusive or conventional processing still present under low-cycle conditions. The data available also indicate that the beneficial effects of shot peening, which generally result in an improvement in fatigue strength, are available at elevated as well as room temperature. However, more specific data would be required before this observation can be accepted as a general conclusion.

From an overview of the effects presented in this paper, it is evident that careful attention must be paid to the finishing of aerospace hardware which must operate under critically loaded conditions. The traditional index of surface quality, namely, surface roughness, is not a good index of fatigue performance. Only through an understanding and a control of metal removal operations will it be possible to achieve a constant high level of component performance and reliability. The need for a similar level of control in the processing of test specimens used for design data purposes as well as basic research studies can be also inferred from this work.

References

[1] "Surface Integrity of Machined Structural Components," AFML-TR-70-11, Air Force Materials Laboratory, March 1970.

[2] Private communication to the authors from P. R. Arzt, McDonnell Douglas Corp., St. Louis, Mo.

[3] Stablein, F., *Kruppsche Monatshefte*, Vol. 12, 1931, pp. 93–99.

[4] Letner, H. R. and Snyder, H. J., *Transactions*, American Society of Mechanical Engineers, Vol. 75, July 1952, pp. 873–882.

[5] Westermann, F. E., "Determining the Distortion and Residual Stresses Produced by Metal Removal Operations," Technical Paper IQ71-224, *Transactions*, Society of Mining Engineers, 1971.

Thermal Ratchetting

David Burgreen[1]

Review of Thermal Ratchetting

REFERENCE: Burgreen, David, **"Review of Thermal Ratchetting,"** *Fatigue at Elevated Temperatures, ASTM STP 520,* American Society for Testing and Materials, 1973, pp. 535–551.

ABSTRACT: The subject of structural ratchetting, or cyclic strain accumulation has been developed primarily during the past 20 years. The major contributions to the literature in this area are reviewed, with particular attention to thermal ratchetting.

An attempt is made to classify the various types of strain accumulations that can be experienced by structures when they are subjected to cyclic loading. Under isothermal cyclic loading, ratchetting mechanisms may be classified as: (*a*) isothermal coaxial cyclic strain accumulation, (*b*) isothermal conjugate cyclic strain accumulation, and (*c*) complex isothermal cyclic strain accumulation. Cumulative stress relaxation growth, sometimes considered to be a form of ratchetting, is time dependent and therefore not properly a form of structural ratchetting.

Most investigations in structural ratchetting have been concerned with simple thermal ratchetting produced by cyclic temperature applications, in the presence of a sustained load or in materials exhibiting different yield points in tension and compression. Studies are reviewed which take into account: (*a*) changes in material properties, (*b*) strain hardening, and (*c*) biaxial stresses. Stress relaxation is studied by some investigators, but this cannot be considered to be *bona fide* thermal ratchetting, as the strain accumulation is time dependent.

Overall progress in thermal ratchetting analysis is reviewed, and areas that require investigation are suggested. A failure criterion is proposed for structures undergoing cyclic strain accumulation.

KEY WORDS: strains, stresses, cyclic loads, stress cycle, creep properties, plastic deformation, yield strength, compressive properties, elastic properties

Thermal ratchetting is a well-defined mechanism of strain accumulation in a structure which is subjected to thermal cycling. It is one of several possible modes of cyclic strain accumulation caused by the periodic application of loads, temperatures, or both of these in some prescribed manner.

It is important that we sort out and define, from a phenomenological point of view, the various types of progressive strain accumulation that can take place, thermal ratchetting being only one of a number of different modes of structural ratchetting. Before proceeding with the discussion of thermal ratchetting I shall examine briefly related phenomena which pro-

[1] Professor, Department of Mechanical Engineering, Polytechnic Institute of Brooklyn, Brooklyn, N.Y., 11201.

Copyright© 1973 by ASTM International www.astm.org

duce cyclic or interrupted growth of structures, in the presence or absence of temperature cycling, but which are distinct from thermal ratchetting. Ratchetting phenomena in complex structures, such as portal frames or nozzles, are not considered here as they do not illustrate the fundamental mechanisms of cyclic strain accumulation.

Isothermal Ratchetting

Isothermal Coaxial Cyclic Strain Accumulation

An example of isothermal ratchetting is the progressive deformation that takes place in a plate which is subjected to a cyclic bending strain in the presence of membrane loads. Figure 1 shows the manner of application of these loads. The progressive axial strain accumulation in the plate, in the σ_1 direction, requires that yielding extend past the midplane during each half-cycle of bending strain application. The plate undergoes a ratchetting growth with the material on each side of the center line (and extending past the center line) alternately becoming elastic and plastic. The orthogonal membrane loads have the effect of producing different bending yield strengths in tension and compression. From the Tresca yield conditions it is clear that when orthogonal membrane stresses are of opposite sign from the bending stresses, the magnitude of bending stress required to produce yielding will be lowered. For ratchetting to take place these differences in stress intensity must be present during a loading cycle. Edmunds and Beer [*1*][2] have derived analytical expressions for the progressive strain accumulation in plates undergoing isothermal ratchetting. They obtain for each half-cycle an irrecoverable plastic strain equal to

$$\epsilon_g = \frac{2e_b(2\sigma_1 - \sigma_2)}{2\sigma_y - \sigma_2} \pm \frac{1}{E}\left(\frac{\sigma_2}{2} - \sigma_y\right) \quad \ldots\ldots\ldots\ldots\ldots\ldots (1)$$

Experimental tests on pipe bends and on plates were performed which demonstrated that ratchetting takes place when the bending strain exceeds a well-defined limit, and that shakedown occurs when the bending strain is below this limit.

Isothermal Conjugate Cyclic Strain Accumulation

When a large uniform cyclic strain is applied in a given axial direction, in a plate or shell, progressive growth can take place along the conjugate axis when a sustained load of sufficient magnitude is present in the conjugate axial direction. Figure 2 shows the orthogonal axes along which the cyclic membrane strain and sustained membrane stresses are applied. It has been demonstrated [*1*] that the application of a cyclic strain e_2 along the 2-axis produces a cyclic growth along the 1-axis, in the direction of the sus-

[2] The italic numbers in brackets refer to the list of references appended to this paper.

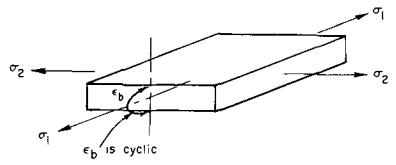


FIG. 1—*Isothermal coaxial cyclic strain accumulation. Plate undergoes cyclic growth in* σ_1 *direction due to cyclic application of bending strain* ϵ_b *which produces plastic yielding.*

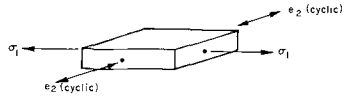


FIG. 2—*Isothermal conjugate cyclic strain accumulation. Application of a cylic strain* e_2 *causes plastic yielding and cyclic growth in* σ_1 *direction.*

tained load. The magnitude of the incremental growth during a single cycle is

$$\epsilon_{1g} = \frac{3\sigma_1}{2\sigma_y - \sigma_1} e_2 \quad \ldots\ldots\ldots\ldots\ldots\ldots\ldots\ldots (2)$$

Complex Isothermal Cyclic Strain Accumulation

A hollow tube that is subjected to a sustained axial load P and concurrently to a large cyclic torsional moment will develop a cyclic accumulation of strain in the axial direction. The loading, shown in Fig. 3, is more complex than that shown in Fig. 2. The cyclic growth mechanism is similar in character to coaxial and to the conjugate strain accumulation, but is analytically more complex since the principal stress directions do not coincide with the principal geometrical axes. Analysis and experimental tests, [*2*], performed on specimens loaded as shown in Fig. 3, show that relatively uniform cumulative axial extensional deformation, up to about 20 percent, can be obtained before local instabilities disrupt the uniform strain accumulation.

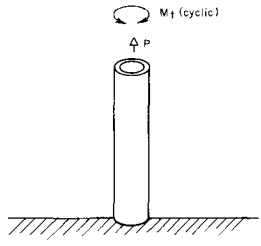


FIG. 3—*Complex isothermal cyclic strain accumulation. A cyclically applied torsional moment* M_t *in presence of a sustained load* P *causes cyclic axial growth.*

Cumulative Stress Relaxation Growth

It is possible to obtain cumulative deformation which is solely due to stress relaxation growth. Materials incur permanent strains due to creep or stress relaxation. In cyclic strain controlled deformations, which characterize isothermal cyclic strain accumulation, we are not concerned with creep or stress relaxation—which are time dependent phenomena.

Stress relaxations (or creep) which produces permanent strain may be present in both thermal and isothermal ratchetting or in other types of cyclic strain accumulation. Progressive deformation due to creep may be present in a part of a cycle, or during a full cycle; or it may be present in one part of a structural element or assembly, and absent in other parts. It cannot be emphasized too strongly that thermal and isothermal ratchetting in which large deformations can be incurred in very short periods of time—sometimes in a few minutes—are completely independent of deformations resulting from creep or stress relaxation, which are incurred over long periods of time. If, in the absence of creep relaxation, there is no cyclic strain accumulation, but in the presence of creep relaxation there is cyclic strain accumulation, then the strain accumulation mechanism is classified properly as cumulative creep or stress-relaxation growth. On the other hand, stress relaxation can be an additional effect which modifies the magnitude of isothermal or thermal ratchetting.

Consider, for example, an analysis performed by Bree [*3*], taking into account stress relaxation, wherein a stepwise cyclic temperature, linear over the thickness of a cylinder wall, is applied in the presence of a constant-internal pressure. In start-up half-cycles, when the temperature is increased, only elastic stresses are developed. As a result of the subsequently prevailing high temperatures, complete stress relaxation is assumed to take place, culminating in a uniform membrane stress in equilibrium with the internal pressure. In the shut-down half-cycle plastic stresses are incurred, but, as the temperature is low, no creep relaxation takes place. The slab thus experiences a net growth during each full cycle. However, it would not experience this growth if it did not undergo stress relaxation while being held at the high-temperature end of a half-cycle. This type of cyclic strain accumulation is not bona fide thermal ratchetting—since there would be no cyclic strain accumulation if the slab were held at the high temperature for only a very short period of time. True thermal ratchetting requires that the plastic strains be incurred during the temperature change. The deformation mechanism just described is, therefore, more properly termed cumulative stress relaxation growth.

In another example of this mode of cyclic strain accumulation, McConnelee [*4*] determined the cumulative stress-relaxation growth in a two-bar assembly consisting of different materials, similar to that shown in Fig. 4. The entire assembly was subjected to a square wave time-temperature history. The stresses remained in the elastic range at all times,

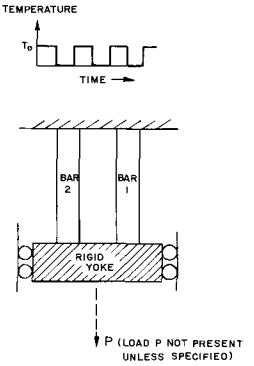


FIG. 4—*Simple thermal ratchetting arrangement of a two-bar assembly.*

but, because of the variation in the creep constants of the two bars and the effect of temperature on the rate of stress relaxation, the assembly extended a greater amount while held at the high-temperature half-cycle, than it shortened during the low-temperature half-cycle. The net effect was a cyclic growth of the assembly.

Strain Accumulation Mechanisms

Cyclic-strain accumulations can be generally placed into three categories: isothermal ratchetting, thermal ratchetting, and cumulative cyclic creep or cyclic stress-relaxation growth. The designation "incremental collapse" has been used often by investigators in Great Britain. It is synonymous with cyclic strain accumulation. The latter designation is preferable since a structure will not necessarily "collapse" as a result of cyclic strain accumulation. Some cyclic growth phenomena are sometimes referred to as "interrupted creep." In order to avoid confusion it would be more desirable to have this terminology applied to structures which undergo creep but have the loading interrupted or the magnitude of the load changed during the loading period.

There is another type of cyclic strain accumulation which deserves mention. Materials such as uranium and graphite are subject to cyclic strain accumulation when thermally cycled [*5–7*]. The cyclic growth is due to the anisotropy that is present in the individual crystals. The behavior of the anisotropic materials is highly complex, and a definitive analytical description of this type of growth mechanism has not yet been developed.

Thermal Ratchetting

Thermal Ratchetting Mechanism

Thermal ratchetting is the progressive deformation of a structural element such as a bar, beam, plate, or shell, or of an assembly of several individual elements, subjected to a cyclic temperature variation. In a

parallel element assembly, or in a bar or plate consisting of parallel fibers or laminae, plastic yielding in the same sense must take place in all the parallel elements or fibers during each cycle. That is, the yielding must extend over all the elements or far enough over the cross section (or thickness) to asure that all elemental fibers or laminae will have yielded during a full-temperature cycle. In thermal ratchetting it may be assumed that the temperature cycles and associated strains take place in times that are of the order of minutes.

A simple example of thermal ratchetting is the progressive lengthening of the two-bar assembly shown in Fig. 4. Assume that both bars consist of the same material and have equal cross section areas, and that the yield points in tension are less than the yield points in compression. Bar 1 is uniformly heated to a temperature T_0 and some time later the temperature is reduced by the same amount. It is assumed that there is no change in the physical properties of the bars with temperature, and that the material becomes perfectly plastic at its yield point. The stepwise change of temperature of Bar 1 with time is shown in Fig. 4. When the temperature T_0 is sufficiently high to cause yielding, namely $E\alpha T_0/2 > \sigma_y$, Bar 2 will yield in tension while Bar 1 will remain elastic, since the tensile yield stress is smaller than the compressive yield stress. Similarly, upon cooling, Bar 1 yields in tension while Bar 2 remains elastic. During the full cycle all of the material in both bars has yielded in tension and there has been incurred a permanent plastic strain, resulting in a net extension of the assembly.

For thermal ratchetting to take place, it is not sufficient that an element or an assembly be subjected to thermal cycling alone. It can be produced, for example, in the assembly of Fig. 4, if the yield strengths of Bar 1 or Bar 2 are different in tension and compression. Or, it can be produced if the thermal cycling is accompanied by a sustained axial load P acting as shown in Fig. 4. Thermal ratchetting may be implemented in other ways. These will be discussed later.

Chronological Development

Thermal ratchetting technology has had its development during the past 20 years. One of the earliest studies of thermal ratchetting was made in 1954 by Parkes [*8*]. He studied the thermal ratchetting of a simplified wing structure, subjected to a cyclic temperature variation, upon which was superimposed a sustained bending moment. He used a four-step temperature cycle as follows: (1) at attaining high speed, an aircraft skin was heated to a temperature T_0 while the web remained at zero temperature; (2) by conduction the web temperature then was elevated to the same temperature T_0; (3) at return to low speed the aircraft skin cooled to zero temperature while the web remained at T_0; and finally 4) by heat dissipation both components returned to zero temperature. Depending upon the magnitude of the applied moment and the magnitude of the cyclic

temperature variation it was found that four possible modes of response could exist. The structure could remain elastic; it could deform plastically during the first cycle and then shake down to elastic cycling; it could exhibit alternate plasticity; or it could undergo cyclic strain accumulation in the form of a continuously increasing wing curvature with each cycle of temperature. In a later paper Parks [*9*] (1960), examined the effect of variation of yield strength with temperature on a two-element assembly consisting of two identical bars, such as that shown in Fig. 4. A four-step temperature cycle was applied whose sequence was as just described. He found that the response of the assembly was dependent upon the relative rates of change of thermal stress with temperature and of the variation of yield stress with temperature.

Gatewood [*10,11*] (1960) performed a number of experiments on a two-element assembly of the type shown in Fig. 4. The assembly was subjected to simple two-step thermal cycling (as shown in Fig. 4) in the presence of an axial sustained load P attached to the yoke. He demonstrated that various types of responses could be elicited, depending upon the magnitude of the cyclic temperature and the magnitude of the sustained load. Cyclic strain accumulation (thermal ratchetting) was shown to be one possible mode of response.

Miller [*12*] (1959) published the results of ratchetting studies on an assembly consisting of two bars of equal cross section area, with one of the bars subjected to a square wave time-temperature variation, and the assembly concurrently subjected to a sustained axial load P, as shown in Fig. 4. He analyzed the effect of linear strain hardening on the cyclic growth of the two-bar assembly, and found that strain-hardening progressively reduced the magnitude of the cyclic growth. He also performed a one-dimensional analysis of the ratcheting of a thin-walled vessel subjected to internal pressure and a concurrent cyclic linear, or parabolic, temperature distribution through the wall.

In 1964 I presented the results of my analysis of the thermal ratchetting of the two-bar model of Feb. 4 [*13,14*], assuming unequal cross section areas, materials having different yield points in tension and compression, and the presence of an axial load P. I also studied the thermal ratchetting of an element subjected to a two-step temperature application in the form of a linear or, alternatively, parabolic temperature distribution, in the presence of an axial load. In the case of the parabolic temperature distribution, modes of cyclic behavior were obtained which had not been considered previously. The detailed analysis of these problems are given in Refs *15* and *16*.

Bree [*17*], (1964) performed an analysis of a circular cylinder subjected concurrently to internal pressure and to a two-step cyclic temperature application of a conduction generated temperature distribution in a cylinder wall. The effect of biaxiality of stress on the yield strength of the material

was taken into account. The biaxiality effect made the problem considerably more complex and required a computer program to carry out the solution. In a later paper [*3*], he made an extensive one-dimensional study of the thermal ratchetting of a cylinder, having a uniform sustained membrane load while subjected to a two-step temperature cycling in the form of a linear temperature distribution through the wall. He pointed up the exact correspondence between a uniaxial stress model and the biaxial stresses in the wall of a thermally cycled spherical shell under internal pressure, and the adequacy of a uniaxial stress model when considering the biaxial (unequal) stresses in a thermally cycled cylindrical vessel with internal pressure. In addition to verifying the results obtained by Miller [12] and me [*14*], he extended his studies to the effect on thermal ratchetting of the variation of yield stress with temperature; he examined the effect of linear strain hardening on ratchetting growth; and he analyzed the effect of stress relaxation on cyclic strain accumulation. It was pointed up earlier that this last analysis could not be classified as true thermal ratchetting, since no ratchetting would have occurred if there were no stress relaxation.

McConnelee [*4*] (*1965*) investigated a two-bar assembly such as the one shown in Fig. 4 in which each of the bars had dissimilar properties which varied with temperature. He assumed an elastic, perfectly plastic material and applied a sawtooth time-temperature variation, with the entire assembly at any instant assumed to be at a uniform temperature. He demonstrated that the changing yield strength of the bars could produce thermal ratchetting. He also analyzed the two-bar assembly for cumulative stress relaxation growth due to a two-step cyclic temperature application. The stress relaxation growth was assumed to take place while the assembly stresses were in the elastic range. Since the structural growth in this case was solely time dependent, this type of deformation is cumulative stress relaxation growth rather than proper thermal ratchetting.

State of the Art

Simple Thermal Ratchetting

As a result of the various complementary studies of the subject, the mechanism of thermal ratchetting is reasonably well understood. The studies by Miller [*12*], Bree [*3,17*], and me [*15,16*], have developed sufficient knowledge of thermal ratchetting to permit its utilization in structural design. Simple thermal ratchetting has been defined as the cyclic strain accumulation in a bar, plate, or shell when subjected to a sustained membrane load (or sustained axial load in the case of a bar) and concurrently to a two-step time temperature cycle. The spatial temperature distribution (through the thickness) is arbitrary. Furthermore, the material is assumed to behave as an elastic, perfectly plastic, material. In lieu of a sustained membrane or axial load it can be specified that the yield strengths of the

material in tension and compression are not the same. In thermal ratchetting analysis this is found to be comparable to the presence of a sustained axial or membrane load, and this is demonstrated in Ref *15*. Temperature distributions of the type shown in Fig. 5*a*,*b*, and *c*, applicable to homogeneous bars or plates have been studied. The analysis of a bar having the rectangular temperature distribution shown in Fig. 5*a*, is identical with that of a two-bar assembly, so that the two-bar analysis [*15*] can be applied directly when such a cyclic temperature variation is present in a homogeneous bar or plate.

The results of ratchetting analyses performed by me are shown graphically in Figs. 6, 7, and 8. In each case the magnitude of ratchetting growth is given as a function of the cyclic temperature and sustained load, and the ratchetting range is delineated. For the rectangular distribution shown in Fig. 5*a*, with $A_1 = 2A_2$, and the linear temperature distribution shown in Fig. 5*b*, the shakedown boundary between alternate plastic yielding and purely elastic behavior are shown in Figs. 6 and 7, respectively. It is observed that the shakedown range is bounded by two lines. One line separates elastic behavior from cyclic ratchetting growth, such that a decrease in the mean or membrane load (moving across this line from right to left) changes the response of the structure from ratchetting behavior to elastic behavior. The second line of separation shows that a decrease in the magnitude of the cyclic temperature (going across the boundary line from top to bottom) changes the behavior of the material from alternate plastic yielding to elastic cyclic. Although the line of separation between alternate plasticity and ratchetting is sometimes referred to as a shakedown boundary, more commonly, the shakedown limit refers to the line of separation between alternate plastic yielding and purely elastic cycling.

The ratchetting analysis of the rectangular temperature distribution shown in Fig. 5(*a*) [*15*] has a considerable degree of versatility, since it can be used to approximate various temperature distributions through bars and plates, and also can be used when the variation of material properties with temperatures must be taken into account. For example, it can be em-

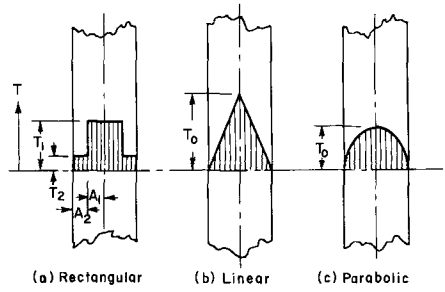


FIG. 5—*Types of cyclically applied temperature distributions in bars, plates, and thin spherical shells for which ratchetting studies have been performed.*

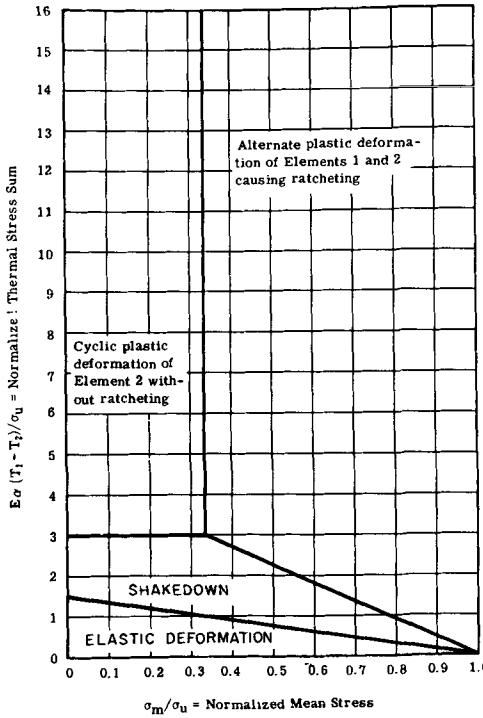


FIG. 6—*Behavior patterns obtainable in a two-bar assembly or in a bar subjected to a cyclic temperature application as shown in Fig.* 5a, *in the presence of a sustained mean stress,* σ_m.

ployed to approximate the linear and parabolic temperature distributions of Figs. 5*b* and *c*.

Changes in Material Properties

The effect of changes in material properties on simple thermal ratchetting was included in Bree's analysis [*3*] of cyclic application of a linear temperature gradient across a cyclinder wall. The difference in the yield strengths at the high-and low-temperature points of the cycle was taken into account.

McConnelee [*4*] included the change in the yield strength, modulus of elasticity, and coefficient of expansion in the ratchetting growth of a two-bar assembly subjected to a sawtooth time-temperature history. Material properties were specified, and numerical analysis was used to obtain results. He demonstrated that ratchetting could be obtained in the absence of an external load. Parkes [*9*] showed that various responses, one of which was thermal ratchetting, could be obtained in a two-bar assembly subjected to a four-step temperature cycle. The results were shown to be dependent strongly upon the rate of variation of yield strength with temperature. Bree's analysis [*3*] demonstrated that the effect of change of yield strength

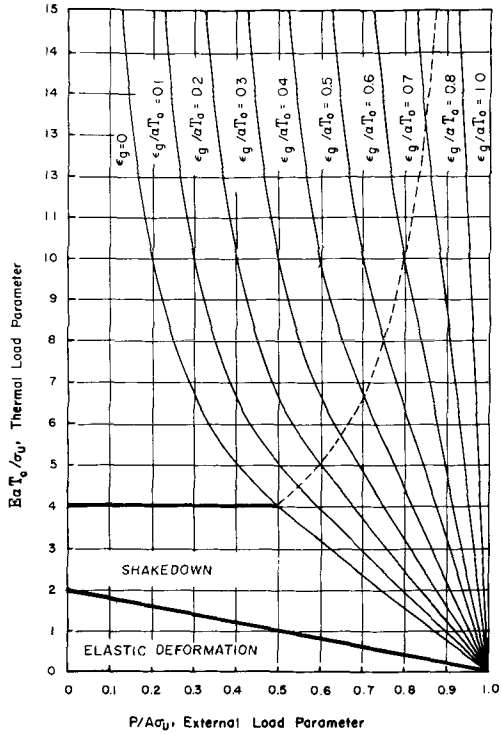


FIG. 7—*Behavior patterns and magnitude of cyclic growth obtainable in a bar subjected to a linear cyclic temperature application as shown as shown in Fig.* 5b, *in the presence of a mean stress,* σ_m.

with temperature could be included in a typical ratchetting analysis without excessive additional labor. Both McConnelee's and Bree's analyses indicated that where significant changes in material properties were caused by temperature variations, they had significant effects on the solutions of the problems.

Strain Hardening

Linear strain hardening is included in Miller's analysis [*12*] of a two-bar assembly of like materials and equal cross section areas (Fig. 4). He found that the effect of strain hardening was to limit the total strain accumulation, or growth in the assembly, and after a larger number of temperature cycles only elastic cyclic deformations were developed. A similar result was obtained by Bree [*3*] in his analysis of the thermal ratchetting of a plate with a linear temperature distribution. After a large number of cycles, growth of the slab stopped and the cyclic stresses became entirely elastic. This is an important result since most structural materials exhibit strain hardening characteristics. The assumption made in simple thermal ratchetting analysis

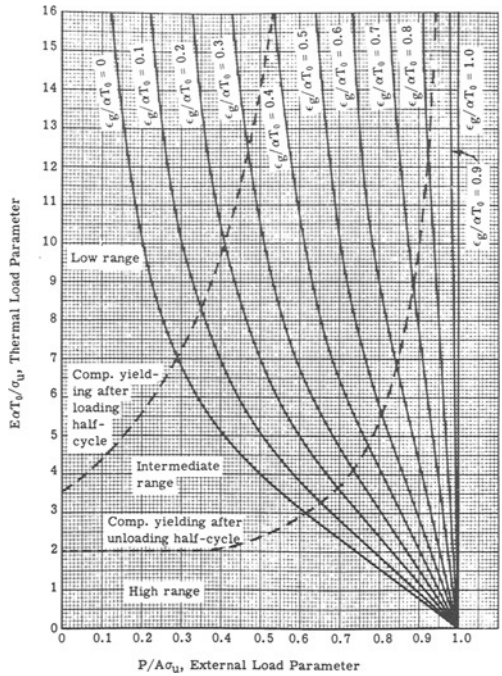


FIG. 8—*Cyclic growth of a bar subjected to a parabolic cyclic temperature application as shown in Fig.* 5c, *in the presence of a mean stress,* σ_m.

that no strain hardening exists is a conservative assumption which leads to a greater computed cyclic growth than will actually take place.

Biaxial Stresses

When the biaxial principal stresses in a plate or shell are uniform and equal, then a simple transformation permits the problem to be treated as a one-dimensional problem. Thus, a thin spherical shell under internal pressure, subjected to simple thermal cycling, can be analyzed in this manner. However, if the biaxial principal stresses are not equal, as in the case of a cyclindrical shell, then the problem becomes complex. The analytical difficulties are, in part, due to the application of the Tresca or Mises yield criteria in a biaxial or triaxial stress problem involving thermal cycling. On the other hand, biaxial ratchetting problems, in which the cyclic strain is specified, do not cause analytical difficulties. The paper by Edmunds and Bree [*1*] is an example of the latter type of analysis. In their analyses these authors prescribe the magnitude of the conjugate cyclic strains. Then a solution is readily obtained. However, as Bree points up (in the Appendix of Ref *3*), in thermal ratchetting problems the strains are not given explicitly, and this necessitates a step by step numerical solution. He sets up a computer program and performs such an analysis

for the case of a cylindrical shell under internal pressure and uniform heat flux [*17*]. Bree indicates [*3*] that the solution for the radial growth of a cylindrical shell may be expected to lie somewhere between the known solution of the spherical shell problem, in which the tangential membrane stresses are uniform, and a uniaxial cylindrical shell problem, in which the axial membrane stresses are disregarded.

Stress Relaxation

The effect of stress relaxation in producing cyclic strain accumulation in a structure subjected to temperature reversals has been studied by both Bree [*3*] and by McConnelee [*4*]. In Bree's study the material remained completely elastic during one step of the thermal cycling, and in McConnelee's study the material was taken to be completely elastic during the full temperature cycle. The cyclic growth in each case was time dependent, and, if the periods during which the stress relaxation took place were very short, there would be no significant structural growth. *Bona fide* thermal ratchetting on the other hand is independent of time. Tsujita [*18*] studied the effect of stress relaxation superimposed on the simple thermal ratchetting of a two-bar assembly. In his study he assumed that stress relaxation took place only in the member which yielded plasticity during the high-temperature part of the cycle. He round that the effect of stress relaxation, superimposed on thermal ratchetting, was to increase the rate of cyclic strain accumulation.

Discussion

Thermal ratchetting is a distinct form of cyclic strain accumulation. Cyclic growth in thermal ratchetting depends upon the number of temperature cycles but is independent of time. Cyclic stress relaxation and interupted creep are, therefore, not forms of thermal ratchetting since these are time dependent.

Structural elements which are most susceptible to thermal ratchetting are those in which more or less equal portions of the cross section are subjected to cyclic heating and cooling. In Fig. 4 for example, ratchetting occurs most readily when $A_1 = A_2$. Plates subjected to a cyclic linear temperature gradient will ratchet more readily than plates subjected to a cyclically applied parabolic temperature distribution. In particular, ratchetting will not take place readily in a plate with a transient temperature distribution wherein only a small part of the plate thickness is one at temperature and the bulk of the plate at a different temperature. Such temperature distributions generally produce alternate plasticity without ratchetting. Furthermore, from Figs. 6, 7, and 8, it is clear that ratchetting requires the most extreme conditions of combined cyclic temperature and membrane load, particularly if there is an unequal distribution of areas undergoing alternate heating and cooling.

Thermal ratchetting requires alternate plasticity in the same sense, which, in a full cycle, must extend over the entire cross section or thickness of the structure. That is, if one portion of a structure yields plastically in tension during a half-cycle the remainder of the structure must also yield plastically in tension during the second half-cycle. In homogeneous structures there generally will be overlapping of the zones of plastic yielding.

The actual cycle of plastic yielding that a particular fiber or lamina will undergo may be of the form shown in Figs. 9 and 10. In Fig. 9 a fiber yields in tension during a half-cycle and remains elastic during the subsequent half-cycle. In Fig. 10 a fiber yields in tension during a half-cycle and yields in compression during the subsequent half-cycle, with the tensile plastic strain of the first half-cycle exceeding the compressive plastic strain of the second half-cycle. There is, therefore, a net tensile strain accumulation.

In interpreting the damaging effect of thermal ratchetting both of these modes of behavior should be taken into account. Figure 10 can be considered to represent the more general type of ratchetting behavior, since in the limit, as the hysteresis loop disappears we obtain the cyclic behavior shown in Fig. 9. In Fig. 10 we have a combination of hysteresis, which produces metal fatigue, and the continuing extension typical of creep and stress rupture. Note that in Fig. 10 the stress is plotted against the thermal strain which is the true strain less αT, and not against the displacement strain, the latter representing the actual cyclic growth. To take into account both of these effects we could define a ratchetting life expenditure, R, as

$$\frac{n}{N} + \frac{\delta}{e} = R \quad \ldots\ldots\ldots\ldots\ldots\ldots\ldots\ldots (3)$$

where

n = number of thermal cycles,
N = number of cycles of plastic strain of magnitude ϵ_p, equal to width of hysteresis loop, that will produce fatigue failure,
δ = cyclic thermal strain accumulation, and
e = total strain in the material at stress rupture.

Failure would then occur when

$$\frac{n}{N} + \frac{\delta}{n} = 1 \quad \ldots\ldots\ldots\ldots\ldots\ldots\ldots\ldots (4)$$

This relationship is similar to proposed expressions for the life of a material subjected to loading which leads to both fatigue and stress rupture.

Conclusions

The development of thermal ratchetting has proceeded in directions which, in general, have complemented each other, so that we have at the present

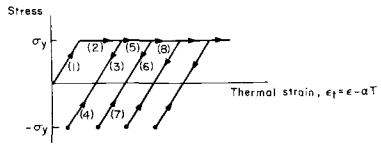


FIG. 9—*Ratchetting growth in which a fiber or lamina undergoes only tensile plastic yielding during a temperature cycle.*

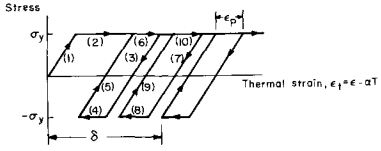


FIG. 10—*Ratchetting growth in which a fiber or lamina undergoes both tensile and compressive plastic yielding during a temperature cycle, with the tensile plastic strain exceeding the compressive plastic strain.*

time a reasonably good understanding of the mechanism of thermal ratchetting. Areas in which additional information is needed are: the effects of strain hardening and the effects of biaxiality of stress.

Most of the studies have been analytical, and those that were experimental have been qualitative rather than quantitative so that accurate experimental information is not available.

It is essential that experimental programs that are undertaken do not simultaneously include several separate effects. One could start, for example, with the controlled experiments on a two-element assembly, such as that shown in Fig. 4, to verify the predicted behavior for simple thermal ratchetting, and then by changing materials include separately the effects of variation of material properties with temperature, the effects of strain hardening, and the effects of stress relaxation. A more advanced test model might utilize a thin spherical shell under internal pressure subject to a two-step temperature cycling of a linear temperature gradient. More advanced tests may utilize cyclindrical shells in which the effects of biaxiality could be explored. Experiments on more complex structures are less valuable since it becomes difficult to interpret the results.

There is need to review and interpret the analytical and experimental results that are already available. The present paper is an initial effort in this direction.

References

[*1*] Edmunds, H. G. and Beer, F. J., *Journal of Mechanical Engineering Science*, Vol. 3, No. 3, 1961.

[*2*] Shimmin, K. D., "Cyclic Strain Accumulation Under Complex Multiaxial Loading," RTD-TDR-63-4120, Dec. 1963.

[*3*] Bree, J., "Ratchet and Fatigue Mechanisms in Sealed Fuel Pins for Nuclear Reactors," TRG Report 1214 (D), 1966.

[4] McConnelee, J. E., "Thermal Stress Ratchet Mechanisms," GE-TM-65-5-31 (NMPO), 1965.
[5] Roberts, A. C., *Acta Metallurgica*, No. 817, 1960.
[6] Chiswick, H. H., *Transactions*, American Society of Metals, Vol. 49, 1957.
[7] Jenkins, G. M. and Williamson, G. K., *Journal of Applied Physics*, Vol. 34, No. 9, Sept. 1963.
[8] Parkes, E. W., *Aircraft Engineering*, Vol. 26, 1954.
[9] Parkes, E. W., *Aircraft Engineering*, Vol. 32, 1960.
[10] Gatewood, B. E., *Journal of the Aerospace Sciences*, June 1960.
[11] Gatewood, B. E., Grothouse, A. P., and Van Housen, W. W., *Journal of the Aerospace Sciences*, June 1961.
[12] Miller, D. R., *Transactions*, American Society of Mechanical Engineers, *Journal of Basic Engineering*, Vol. 8, June 1959.
[13] Burgreen, D., *Transactions*, American Nuclear Society, June 1964.
[14] Burgreen, D., *Transactions*, American Nuclear Society, Nov. 1964.
[15] Burgreen, D., *Journal of Basic Engineering*, American Society of Mechanical Engineers, Sept. 1968.
[16] Burgreen, D., *Journal of Basic Engineering*, American Society of Mechanical Engineers, Dec. 1968.
[17] Bree, J., "Elastic-Plastic Deformation of a Long Hollow Cylinder Under Thermal Cycling and Internal Pressure," TRG Report 790 (D), June 1964.
[18] Tsujita, T., "Limit Analysis of Thermal Relaxation Effect on Thermal Ratcheting," M.S. thesis, Department of Mechanical Engineering, Polytechnic Institute of Brooklyn, Brooklyn, N.Y., Sept. 1968.

DISCUSSION

Alfred Fox[1] *(written discussion)*—You state that cumulative stress-relaxation growth is time dependent and, therefore, not a form of structural ratchetting. The application of force or temperatures is certainly time dependent, no matter how short the time scale. Where do you draw the line?

David Burgreen (author's closure)—In my pages I suggested that the terminology "thermal ratchetting" is inappropriate for ratchetting growth or cyclic strain accumulation that is the result of creep or stress relaxation. The failure to make this distinction would be comparable to the use of "ultimate strength" for both the actual short-time ultimate strength of a material, and the stress-rupture strength of the material. In both cases there is present the steady application of a load associated with a more or less uniform rate of elongation, ultimately causing failure. Whereas the

[1] Bell Telephone Laboratories, Murray Hill, N. J.

ultimate is considered to be essentially independent of the length of time of load application, stress-rupture is time dependent and also dependent on the variation of creep rate with temperature.

Similarly, in the case of ratchetting, I believe that thermal ratchetting should be used to describe the fundamental ratchetting phenomenon, which is time independent, just as ultimate strength is time independent in the engineering sense. Creep ratchetting or stress relaxation ratchetting is, on the other hand time dependent, just as rupture stress is time dependent. I believe it would be confusing and misleading to apply the term thermal ratchetting to both types of ratchetting behavior.

H. Yamanouchi,[1] *Y. Asada,*[2] *Y. Wakamatsu*[1]

Ratchetting Under Cyclic Axial Strain with Torsional Stress

REFERENCE: Yamanouchi, H., Asada, Y., Wakamatsu, Y., "**Ratchetting Under Cyclic Axial Strain with Torsional Stress,**" *Fatigue at Elevated Temperatures, ASTM STP 520*, American Society for Testing and Materials, 1973, pp. 552–562.

ABSTRACT: In order to investigate the fundamental behavior of thermal stress ratchetting, strain controlled push-pull low-cycle fatigue tests with steady torsional stress were conducted on ASTM A302-B steel, AISI 304 steel, and JIS SCM 3 steel under constant elevated and cyclic temperatures. The test results are summarized as follows: (1) Torsional ratchet deformation gradually increased as a permanent deformation fluctuating as axial strain changed. The amplitude of the fluctuation depends on cyclic axial strain, but permanent deformation depends on steady stress as well as cyclic axial strain. (2) Ratchet strain increased at a nearly constant rate for each cycle of axial strain. The rate of increase is proportional to steady torsional stress and exponentially proportional to the axial strain amplitude. (3) The torsional stress and deformation caused by the tests do not influence low-cycle fatigue or thermal-fatigue strength.

KEY WORDS: fatigue (materials), axial strain, shear stress, strain tests, thermal fatigue, low alloy steels, stainless steels, temperature, plastic deformation

Nomenclature

ϵ_t	Axial total strain
γ	Ratchet strain
$\Delta\gamma$	Ratchet strain increment
γ_f	Ratchet strain at fracture
τ	Torsional stress
n	Number of axial strain cycle
N_f	Number of cycles to fracture
T	Temperature
$_a$	Subscript showing amplitude
$_R$	Subscript showing range

[1] Manager, Strength Research Laboratory, and research assistant, First Experimental Laboratory, respectively, Nagasaki Technical Institute, Mitsubishi Heavy Industries, Ltd., Nagaski, Japan.

[2] Assistant professor, Department of Mechanical Engineering, Faculty of Engineering, University of Tokyo, formerly with Nagaski Technical Institute, Mitsubishi Heavy Industries, Ltd.

Copyright© 1973 by ASTM International www.astm.org

Deformation caused by thermal stress ratchet occurs in the equipment of nuclear energy plants and many other mechanical structures, and it is possible that the ratchet deformation accumulates to a large deformation at certain spots, causing an excessive stress and failure at that point. The influence of thermal ratchet effects on low-cycle fatigue and thermal-fatigue strength must be given more attention.

Presented here is the experimental study of dependence of ratchet strain behavior on applied steady stress, plastic deformation and temperature, and the effect of ratchet strain on low-cycle fatigue and thermal-fatigue strength.

Test Materials

Three test materials were used, and their chemical compositions are shown in Table 1. The test results of the tensile properties of the three materials are given in Table 2.

TABLE 1—*Chemical composition of test materials.*

Material		C	Si	Mn	P	S	Ni	Cr	Mo
ASTM A302-B	[a]	0.17	0.29	1.24	0.020	0.011	0.60	...	0.53
	[b]	0.17	0.27	1.31	0.015	0.013	0.54	...	0.52
AISI 304	[a]	0.05	0.54	1.68	0.023	0.010	8.89	18.81	...
	[b]	0.06	0.89	0.97	0.021	0.007	8.34	18.54	...
SCM 3		0.36	0.29	0.78	0.012	0.006	...	1.07	0.20

[a] Material supplied by Committee 7 PCF.
[b] Material supplied by Committee 8 PCF.

Test Method

Torsional stress as a steady stress is applied to a thin cylindrical tube specimen, and cyclic strain and thermal stress are given in the axial direction. In other words, periodically constant torsional stress was superimposed on axial strain controlling low-cycle fatigue or thermal-fatigue tests.

The specimen had the following dimensions: outside diameter 14 mm, thickness 2 mm, and total length 150 mm. For the test, the specimen was heated by passing a large electric current, cooled by feeding compressed air into inner cylinder of the specimen, and the temperature was measured by thermocouple.

The test apparatus used was a thermal stress fatigue tester. This can apply cyclic strain in the axial direction by oil pressure and can change cyclic temperature of the specimen independently. In order to apply torsional stress, a torsional moment loading device employing a weight

TABLE 2—*Static mechanical properties of test materials.*

Materials		Test Temperature, deg C	Yield Point, kg/mm²	Tensile Strength, kg/mm²	Fracture Stress, kg/mm²	Elongation, %	Reduction of Area, %	Young's Modulus, kg/mm²
ASTM A302-B	[a]	R T	53.7	66.0	126.2	27.9	65.6	21.0×10^3
		350	44.4	62.9	106.7	25.8	58.5	18.8×10^3
		500	39.3	47.5	88.0	25.1	68.8	17.0×10^3
	[b]	R T	48.6	63.6	126.4	29.0	68.3	21.3×10^3
		300	44.0	62.3	115.0	25.1	59.6	19.8×10^3
		500	37.2	52.4	102.0	26.4	71.3	17.5×10^3
AISI 304.....	[a]	R T	22.5	60.1	169.8	67.5	75.6	19.8×10^3
		400	13.7	45.2	105.8	49.0	69.9	15.3×10^3
		600	11.6	35.6	75.5	42.8	69.6	13.7×10^3
	[b]	R T	23.3	60.1	170.1	69.0	77.9	18.6×10^3
		400	14.4	43.5	107.5	45.4	71.2	14.5×10^3
		600	12.1	37.3	78.9	42.9	71.6	11.8×10^3
SCM 3.....		R T	78.3	89.9	163.4	23.1	66.3	21.1×10^3
		300	65.5	86.7	158.0	24.4	59.3	20.0×10^3
		500	54.2	67.0	120.2	24.1	74.3	16.6×10^3

[a] Material supplied by committee 7 PCF.
[b] Material supplied by committee 8 PCF.

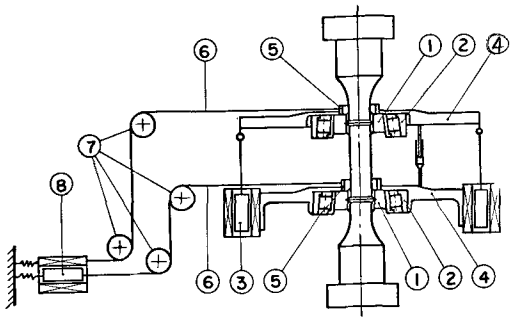


FIG. 1—*Measuring apparatus of axial and torsional strain.*

was fitted at the lower end of the piston rod onto the specimen. Figure 1 diagrams the measuring apparatus for axial strain and ratchet strain. The tests are conducted as follows. Roller bearings *2* are attached on the heat insulation asbestos *1* which are placed on gage marks. Metal fittings *4* to install differential transformers *3* for detecting axial strain are placed on *2*. The upper and lower fittings are restrained by a pin sliding up and down in order not to rotate relatively and can move in the vertical direction only. But, it can turn around freely to the specimen. Asbestos *1* has a cylindrical attachment *5*, on which cotton threads *6* are wound. The threads are connected to the differential transformer *8* through a pulley *7*. When torsional deformation occurs between the gage marks due to ratchetting, the threads are drawn out by unequal length at upper and lower gage marks. By measuring the difference of this length, ratchet strain can be measured and recorded electrically.

Using these apparatus, completely reversed strain-controlled low-cycle fatigue and thermal-fatigue tests were conducted under the conditions listed in Table 3. For test temperature, there were two cases, one is a constant case and the other is a case of thermal fatigue where temperature was changed at the same cycle as axial strain. In the case of thermal-fatigue tests, the temperature condition was shown by upper/lower temperature. The strain history was trapezoidal and adjusted so as to be compressive strain at an upper temperature (high-temperature compression). In the case of low-cycle fatigue tests under a constant temperature, strain was applied sinusoidally with time. Frequency of strain cycle was 0.2 to 0.5 cpm in either case.

Test Results

Figure 2 shows the time history of ratchet strain in one cycle on A302-B steel as an example. Ratchet strain shows sinusoidal variation and when each cycle is completed, increased by $\Delta\gamma$ as is shown in the figure. Then, the accumulation of increment during each cycle grows to a large defor-

TABLE 3—*Test conditions.*

Materials	Test Conditions: Temperature, deg C	Test Conditions: Torsional Stress, kg/mm²	Temperature Conditions
ASTM A302-B.....	500/100	5.02	temperature cycle
	400/100	5.02	temperature cycle
	300	5.02	constant temperature
	500/100	2.51	temperature cycle
	400/100	2.51	temperature cycle
	300	2.51	constant temperature
	500/100	0	temperature cycle
	400/100	0	temperature cycle
	300	0	constant temperature
AISI 304.....	600/100	5.02	temperature cycle
	400/100	5.02	temperature cycle
	350	5.02	constant temperature
	600/100	2.51	temperature cycle
	400/100	2.51	temperature cycle
	350	2.51	constant temperature
	600/100	0	temperature cycle
	400/100	0	temperature cycle
	350	0	constant temperature
SCM 3.....	500/100	10.01	temperature cycle
	500/100	5.02	temperature cycle
	500/100	2.51	temperature cycle
	500/100	0	temperature cycle
	500/100	5.02	temperature cycle
	500/100	2.51	temperature cycle

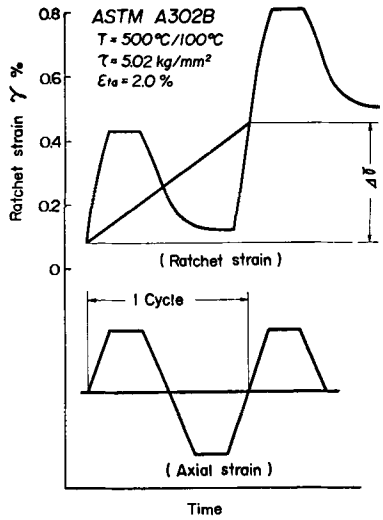


FIG. 2—*Behavior of ratchet strain.*

mation. Ratchet strain per one cycle has a tendency to increase gradually, fluctuating with an increase or decrease of the axial strain. Amounts of fluctuation and increase are dependent on values of steady stress and axial strain.

Using SCM 3 as an example, Fig. 3 shows how the range of ratchet strain γ_R (difference between the maximum and minimum values in one cycle of ratchet strain) changes with the cycle of axial strain. Ratchet strain increment is increased suddenly just before fracture. An almost constant ratchet strain range was maintained during the test period except in some cycles immediately after the test started. This tendency proved to be true regardless of whatever the materials, test temperature, and amplitudes of axial strain may have been.

Relationship between increment of ratchet strain and axial strain amplitude under the same temperature are shown in Fig. 4, taking steady stress as a parameter and assuming γ_f/N_f as an increment $\Delta\gamma$ of ratchet strain for each cycle. In any case, in the range of axial strain amplitude less than 1 percent, ratchet strain increment is exponentially proportional to axial strain amplitude under the same temperatures. The relationship between them is established in the following experimental formula.

$$\Delta\gamma = f(\tau)\epsilon^k{}_{ta}$$

Here, exponent k is a constant independent of steady stress and $f(\tau)$ is an increasing function of τ.

Relationship between increment $\Delta\gamma$ of ratchet strain and axial strain amplitude with temperature as a parameter while steady stress is kept the same is shown in Fig. 5 for A302-B as an example. From this, ratchet strain increment increases when test temperature goes up, but when steady stress remains constant, exponent k is not influenced very much.

Influences on the thermal-fatigue strength or low-cycle fatigue strength by ratchet effect have not been clear until now. The relationship between

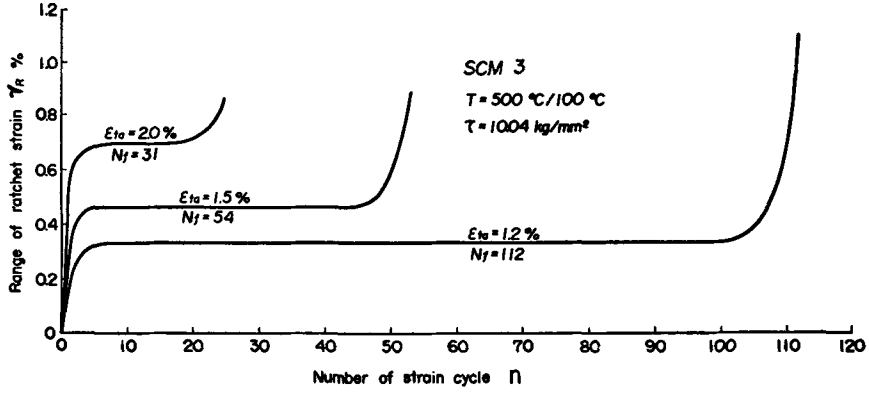


FIG. 3—*Change of ratchet strain range.*

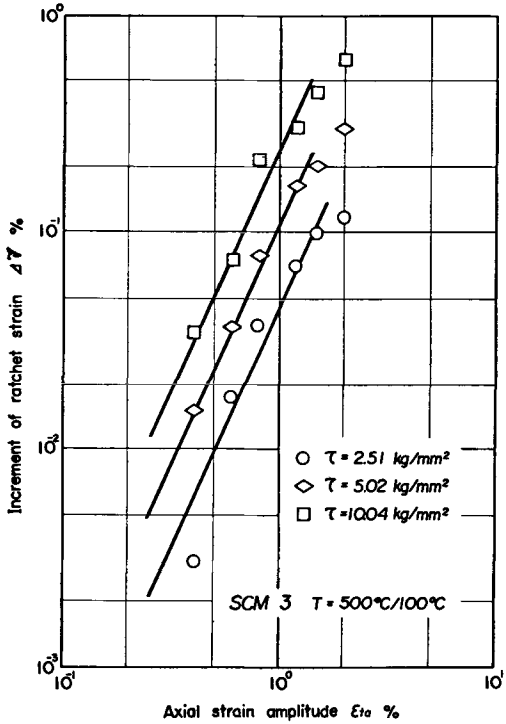


FIG. 4—*Relationship between axial strain amplitude and ratchet strain increment.*

thermal-fatigue strength or low-cycle fatigue strength and test temperature is shown in Fig. 6 for A302-B. It is illustrated by a linear diagram ϵta–N_f with test temperature as a parameter assuming steady stress constant. Figure 7 shows the ϵta–N_f curve obtained for AISI 304 when test temperature is the same and steady stress is different, and it is observed that there is no difference in any of the ϵta–N_f curves even though there is a difference in steady stress. It is still unknown whether this is because the steady stress is too small in this test, the direction of axial strain is different from that of ratchet strain (steady stress), or whether it does not influence fatigue strength substantially. However, cracks developed in all specimens in the vertical direction against axial strain.

Discussion

There are several reports of research which found that members on which steady stress and plastic strain were superimposed deformed permanently and gradually in the direction of steady stress. Feltner and Sinclair [*1*][3] observed the gradual stretching process in the axial direction

[3] The italic numbers in brackets refer to the list of references appended to this paper.

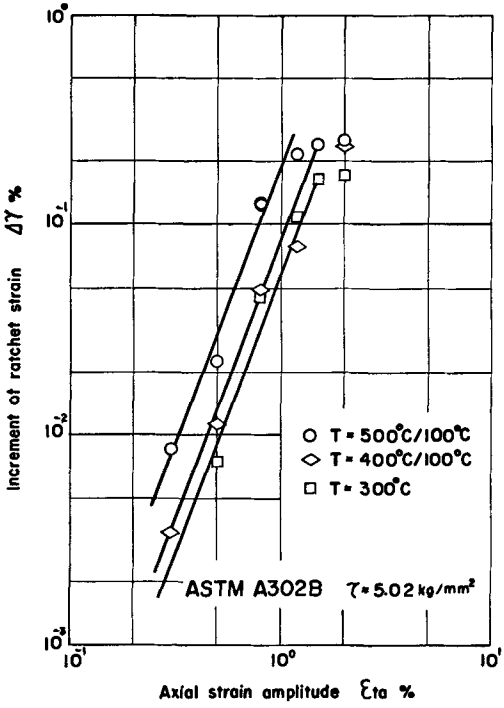


FIG. 5—*Relationship between axial strain amplitude and ratchet strain increment.*

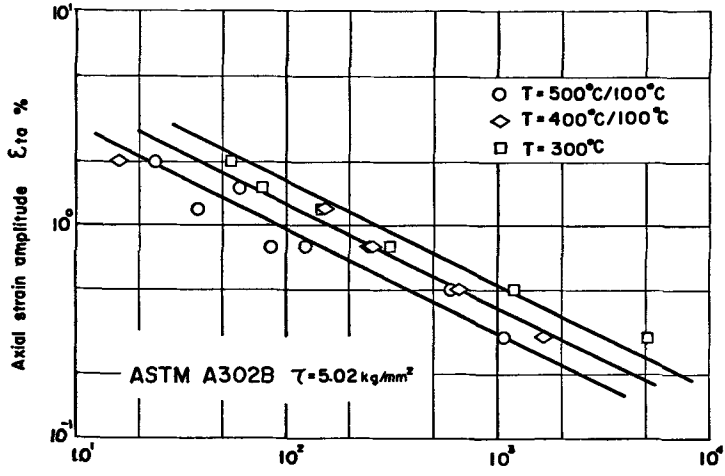


FIG. 6—*Low-cycle fatigue strength of various temperatures under ratchet effect.*

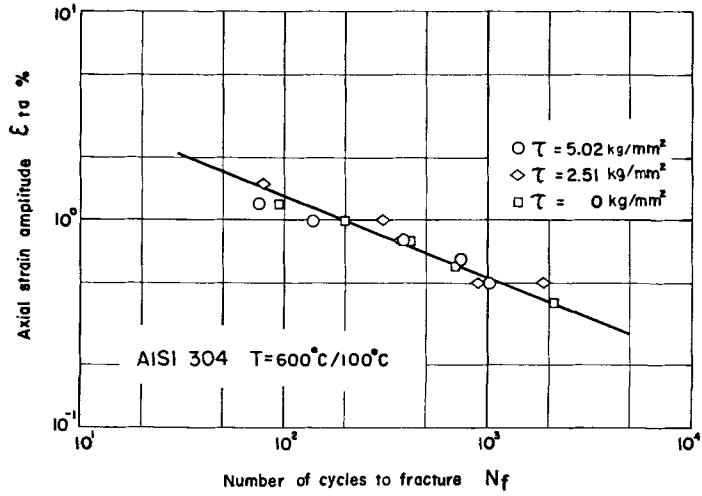


FIG. 7—*Thermal-fatigue strength under ratchet effect.*

giving cyclic plastic deformation to round bars. Coffin, [*2*] conducting an axial strain controlled test under steady torsional moment, found that permanent torsional deformation occurs in a specimen even if torsional moment is very small. Furthermore, he made a cyclic tension test superimposing steady stress in the axial direction and cyclic axial strain. Ronay [*3–5*] and Freudenthal and Ronay [*6*] conducted cyclic torsion tests under steady tensile stress.

Comparing the present experiment with these works, we can discover interesting facts about thermal stress ratchet. From Coffin's experiment, it is understood that elongation is caused by cyclic tension. And according to Miller's [*7*] analysis, decrease of ratchet strain depends only on elastic recovery. But since this experiment and Ronay's experiment show that cyclic strain and steady stress behave similarly even if the directions are not the same, his simple explanation is not considered to be appropriate.

In this experiment, the exponential relationship between axial strain amplitude and increment of ratchet strain is observed not to be applicable if axial strain amplitude exceeds 1 percent. A similar tendency is also observed in Ronay's experiment. It is felt that this is because the slope of the stress-strain curve is reduced under the large axial strain when axial strain amplitude becomes larger. This result, however, is opposite to the results of Miller's analysis, and, according to Miller, the smaller the strain hardening coefficient, the higher the increase of increment of ratchet strain at the same strain amplitude is. This conclusion seems to be reasonable because the direction of steady stress is the same as that of cyclic plastic deformation in Miller's analysis, but it is necessary to continue the study

to see whether that difference is only from the difference in stress-strain conditions.

The directions of cyclic plastic strain and steady stress are different in this experiment, and the results as shown in Fig. 7 do not disclose any influence on fatigue strength. Although the reason is not now known, Manson [*8*] points up that if fracture occurs after deformed elongation reaches static elongation, there are possibilities of fracture life being considerably reduced more than expected from fatigue strength. It also may be true that the unmatching directions of plastic strain and ratchet deformation did not influence fatigue life.

Conclusions

After having studied experimentally various basic properties under stress-strain conditions superimposing steady torsional stress and cyclic axial strain, using ASTM A302-B steel, AISI 304 steel, and JIS SCM 3 steel, the following summarized results are obtained.

1. The torsional ratchet deformation gradually increases permanent deformation fluctuating as the axial strain changes. The amplitude of the fluctuation is controlled by cyclic axial strain, but permanent deformation depends on steady stress as well as cyclic axial strain.

2. Ratchet strain amplitude and ratchet strain increment reach a nearly constant value through the early transient stage, and after that this condition continues until cracking starts.

3. Ratchet strain increases at a nearly constant rate for each cycle of axial strain. The rate of increase is proportional to steady torsional stress and exponentially proportional to the axial strain amplitude in the range of axial strain amplitude is less than 1 percent.

4. The torsional stress and deformation caused by the tests do not influence low-cycle fatigue or thermal-fatigue strength.

References

[*1*] Feltner, C. E. and Sinclair, G. M. in *International Conference on Creep Papers*, 1963, pp. 3–9.

[*2*] Coffin, L. F., *Transactions*, American Society of Mechanical Engineers, Series D, Vol. 82, 1960, pp. 671–682.

[*3*] Ronay, M., *British Journal of Applied Physics*, Vol. 16, 1965, pp. 727–728.

[*4*] Ronay, M., *Journal*, Institute of Metals, Vol. 94, 1966, pp. 392–394.

[*5*] Ronay, M. in *Structural Fatigue in Aircraft, ASTM STP 404*, American Society for Testing and Materials, 1967, pp. 176–189.

[*6*] Freudenthal, A. M. and Ronay, M., *Proceedings*, Royal Society, Series A 294, 1966, pp. 14–50.

[*7*] Miller, D. R., *Transactions*, American Society of Mechanical Engineers, Series D, Vol. 81, 1959, pp. 190–196.

[*8*] Manson, S. S., *Machine Design*, Vol. 21, 1960–1967, pp. 161–167.

DISCUSSION

P. S. Chopra[1] (*written discussion*)—The authors have presented an interesting study of thermal ratchetting. The tests performed on proposed fast breeder reactor fuel element cladding were subjected to internal pressure and axial loads. In the EBR-II experimental mixed-oxide fuel elements, internal pressures are of an order of 500 to 800 psi, and we believe that the major clad load comes from the mechanical action of the expanding fuel. Under such expected loading conditions for fast breeder reactor fuel elements, do you expect thermal ratchetting to be a problem? It so, to what degree does it effect the lifetime of the fuel element cladding?

H. Yamanouchi, Y. Asada, and Y. Wakamatsu (*authors' closure*)—The subject on thermal ratchetting for pressurized cylindrical tube was referred to briefly, and so we would like to present an analysis in detail in the near future.

Specimens were pressurized by N_2 gas at a constant, and cyclic thermal stresses were given to the tube wall (passing an electric current through the specimen and suddenly cooled by compressed air to the outside surface of the specimen), then the thermal ratchet strains (radial deformations) were measured.

The object of these experiments is fast breeder reactor fuel element cladding, and it was to verify a proposed theoretical ratchetting diagram.

We are not the designers, so we can not answer clearly your questions, but, in the case of severe design or operative conditions, it will occur similar to the thermal ratchetting evidenced by our experiments. We think it is important to consider the thermal ratchet effect at the design stage.

[1] Argonne National Laboratory, Argonne, Ill. 60439.

A. V. A. Swaroop[1] *and A. J. McEvily, Jr.*[1]

Analytical and Experimental Study of Thermal Ratchetting

REFERENCE: Swaroop, A. V. A. and McEvily, A. J., **"Analytical and Experimental Study of Thermal Ratchetting,"** *Fatigue at Elevated Temperatures, ASTM STP 525*, American Society for Testing and Materials, 1973, pp. 563–572.

ABSTRACT: The process of thermal ratchetting has been investigated both analytically and experimentally, with a three-bar assembly used as a basis. Steel specimens have been tested under stress during thermal cycling between room temperature and 600 C. Good agreement between experimental results and an improved analytical treatment have been obtained.

KEY WORDS: fatigue (materials), steel structures, thermal stresses, thermal cycling tests, deformation, creep tests, steels, stress strain diagrams, stress relieving, cycle ratio

Nomenclature

Suffix 1 refers to inner bar and suffix 2 refers to the outer bar.

A	Area of cross section
E	Modulus of elasticity
E(eff)	Effective modulus used in computations to account for the elasticity of grips
E_p	Slope of the stress-strain curve (tangent modulus)
k	Spring constant of the grips
ℓ	Gage length
P	External axis load applied on three bar assembly
T_1	Temperature in the gage length of inner bar
T_{max}, T_{min}	Upper and lower limits of temperature T_1 in thermal cycling
α	Coefficient of thermal expansion
ϵ	Longitudinal or axial strain
σ	Stress
σ_y	Flow stress

[1] Graduate assistant and professor and head, respectively, Department of Metallurgy, University of Connecticut, Storrs, Conn. 06268.

Copyright© 1973 by ASTM International www.astm.org

The accumulation of plastic strains under cyclic thermal stresses is known as thermal ratchetting, a process of concern in high-temperature engineering structures. In considering thermal ratchetting in pressure vessels [*1*],[2] nuclear reactor fuel cladding [*2*] and aircraft wings [*3*], it has been recognised that a three-bar assembly (Fig. 1) is the simplest structure that offers a physical insight into the mechanisms involved. For the three-bar assembly, Burgreen [*4*] has developed a criterion for ratchetting and also a method for the computation of the magnitude of the ratchetting strains. In this approach, he assumed the inner and outer bars to have different yield strengths, elastic modulii, etc., while neglecting work hardening (ideal elastic-plastic materials). Miller [*1*] considered work hardening, but, in his analysis, the three bars have the same yield strength, and the dependence of the flow stress on temperature was not considered. Manson [*5*] developed a geometrical solution considering different strain hardening rates of the inner and outer bars.

Despite the importance of thermal ratchetting, there is very little experimental work reported in the literature and little experimental verification of the available analyses. Stentz [*6*] developed a test technique to simulate the ratchetting of three-bar assembly with two specimens in two testing machines, both being controlled by an analog computer. Gatewood et al [*7*] reported experiments on a three-bar assembly under "equivalent" thermal cycling. To avoid the effects of material property changes during thermal cycling, they maintained the test specimens at room temperature, while one of the elements that was in series with the specimens was thermally cycled. The conditions for ratchetting and shakedown were studied, but no attempt was made to compare the experimental results with a theoretical estimate of the magnitude of the ratchetting strains.

The purpose of the present work is to demonstrate a correlation between experimental results and predicted analytical behavior of a three-bar assembly.

Experimental

The experimental setup of the three-bar assembly is shown in Fig. 1. Tubular specimens of 1020 steel were employed in these experiments. Prior to testing, the specimens were annealed to develop a uniform initial condition by heat treating at 1650 F for $\frac{1}{2}$ h followed by furnace cooling. The specimens were machined to have a 2 in. gage length (± 0.001 in.) with the area of cross section of the inner bar (A_1) equal to the sum of the areas of cross sections of the two outer bars (A_2).

In the experiment, the assembly was subjected to a constant axial load, P, with all the bars initially at room temperature. The inner bar was then

[2] The italic numbers in brackets refer to the list of references appended to this paper.

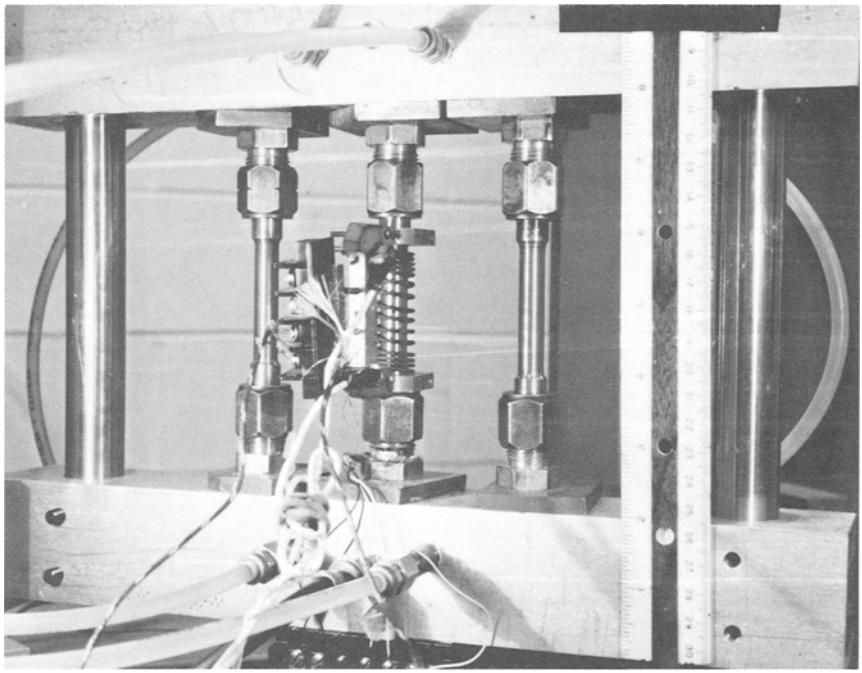


FIG. 1—*Experimental setup of three-bar assembly.*

gradually heated to a temperature T_{max}, while the two outer bars are maintained at room temperature. If the resulting force in the outer bars due to the expansion of the inner bar reached a value corresponding to the yield load ($\sigma_{y2}A_2$) of the outer bars, then the two outer bars would undergo tensile plastic deformation. When the inner bar was cooled to a temperature T_{min}, the tensile stress generated in the inner bar would produce plastic deformation. Thus in a thermal cycle, all the three bars are subjected to tensile plastic deformation, and consequently the length of the assembly increases. At the end of a thermal cycle, residual stresses are left in the assembly, and they affect the further accumulation of axial strain in the succeeding cycle. Each cycle took 2 min: 1 min for heating and 1 min for cooling. At the end of a heating half cycle, the temperature was uniform in the gage length of the inner bar, and the average temperatures (± 3 F) was recorded by means of thermocouples spot welded at several locations on the specimen. The grips were water cooled. During each cycle, the load in the inner bar was monitored by a load cell built into one of the grips (± 5 lb). The strain (ϵ_2) in one of the outer bars was monitored (at room temperature) using an Instron strain gage extensometer. Since $\epsilon_1 + \alpha_1 T_1 = \epsilon_2$, the condition of the inner bar was also known from this measurement. The details of the design and fabrication of the apparatus appear in Ref *8*.

Results

Figure 2 shows the strain accumulation in the assembly as a function of number of thermal cycles. Two of the curves show the unstable condition leading to ductile fracture which is preceded by localized necking. Once necking begins to appear, the rate of accumulation is accelerated. The other two curves in Fig. 2 show the accumulation of strain to a limiting value. Note that either an increase in temperature or an increase in load can lead to change from a stable to an unstable type of ratchetting. The strain-number of cycles curves are linear in the strain range where strain hardening is not appreciable, but they are nonlinear when there is appreciable strain hardening since strain hardening reduces the rate of accumulation.

The load-strain history of the thermally cycled specimen and also that of the outer bars is indicated in Fig. 3. The load in the inner bar ($\sigma_1 A_1$) was measured and recorded on Y-axis. Since

$$\sigma_2 A_2 = P - \sigma_1 A_1 \quad \ldots\ldots\ldots\ldots\ldots\ldots\ldots\ldots\ldots\ldots (1)$$

the load carried by the outer members can be inferred from the measurement of $\sigma_1 A_1$. The inferred values of the load carried by outer bars are shown along with the measured values of $\sigma_1 A_1$. The peaks of all the straight

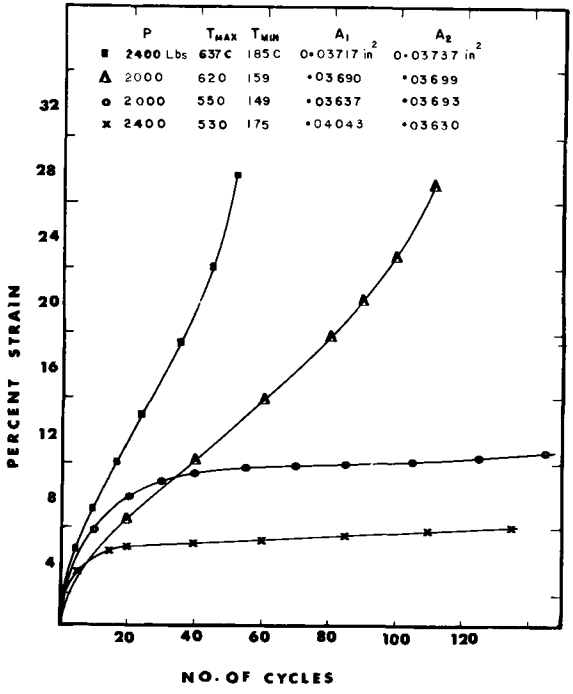


FIG. 2—*Ratchetting strain versus number of cycles.*

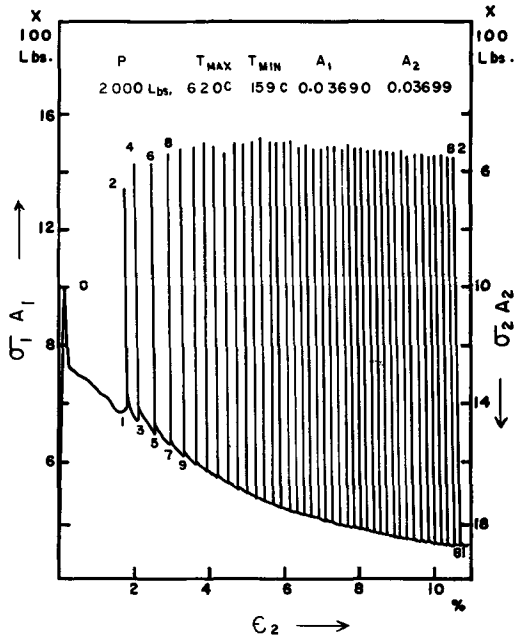


FIG. 3—*Load in the inner bar* ($\sigma_1 A_1$) *versus strain in outer bar* (ϵ_2). *Load in outer bar* ($\sigma_2 A_2$) *was deduced using Eq 1. Number of half cycles are indicated on the figure. Odd numbers indicate the end of a heating half cycle* ($T_1 = T_{max}$). *Even numbers indicate the end of a cooling half cycle* ($T_1 = T_{min}$).

lines indicate the stress-strain condition in the inner bar at the end of the cooling half cycles. The lower envelop of the diagram suggests the stress-strain curve of the outer bars.

Analysis

In Fig. 4, experimental results (Curve *a*) are compared with theoretical computations (Curves *b*, *c*, and *d*) made with three different approaches that are discussed in this section.

In the thermal cycling program employed in this investigation (1 min heating, 1 min cooling), the specimen was at the elevated temperature (T_{max}) for only a few seconds in each thermal cycle. In the following analysis, the creep deformation occuring in such a small interval of time is considered negligible in comparison with the large instantaneous plastic strains produced. From Burgreen's analysis [*5*], the increment of ratchetting strain per cycle is given by

$$\Delta\epsilon = \alpha_1(T_{max} - T_{min}) - \left(\frac{\sigma_{y1}}{E_1} - \frac{P}{E_1 A_1}\right)\left(1 + \frac{E_1 A_1}{E_2 A_2}\right) - \frac{\sigma_{y2}}{E_2}\left(1 + \frac{E_2 A_2}{E_1 A_1}\right) \quad \ldots (2)$$

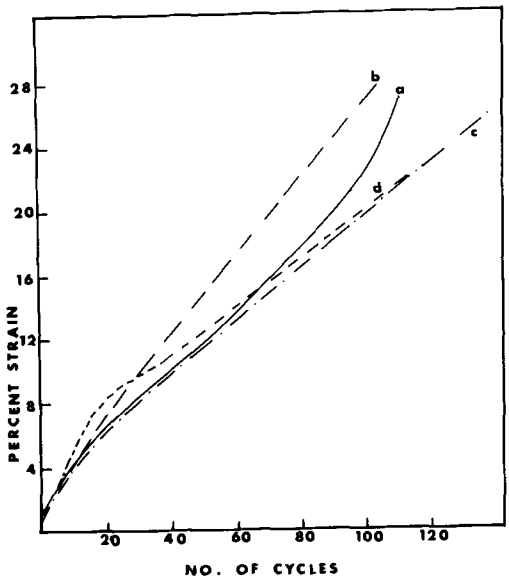


FIG. 4—*Comparison of experimental results* (Curve a) *with theoretical computations.*

and strain in N number of cycles is given by

$$\epsilon(N) = \left[\sum^{N} \Delta\epsilon\right] + \alpha_1 T_{\text{mix}} + \frac{\sigma_{y1}}{E_1} \quad \ldots\ldots\ldots\ldots\ldots\ldots (3)$$

These equations were originally derived from an ideal elastic-plastic material, and, in order to compare with the real situation of the experiment in the present investigation, they are used with a modification. A computer program has been developed to compute $\Delta\epsilon$ in each cycle using values of σ_{y1}, σ_{y2}, A_1 and A_2 appropriate for that cycle. The material is considered elastic-plastic during any particular cycle, but different values of σ_{y1} and σ_{y2} are employed in different cycles, thus accounting for work hardening and the effects of thermal cycling. Stress-strain data obtained during thermal cycling (Fig. 3) were employed in the computations.

The experimental curves show less strain than the strain computed as described previously (Fig. 4*b*), because the small elastic strains in the grips were neglected in the computation just mentioned. When the elastic compliance of the grip arrangement has been accounted for using Eqs. 5 and 6 (discussed next) there is a very good agreement between the experimental results and the analytical computations (Fig. 4*c*).

Since the deformation in the grips is small and elastic, the grips may be treated as elastic springs in series with the specimen. Let d be the total displacement (including the strain in the specimen and in the grips) and ℓ

be the gage length of the specimen. Then deformation in the grips is $(d - \epsilon\ell)$. Let k be the spring constant given by

$$k = \frac{\text{force}}{\text{displacement}} = \frac{\sigma_1 A_1}{(d - \epsilon_1 \ell)} \quad \ldots\ldots\ldots\ldots\ldots\ldots (4)$$

The effective elastic modulus of the inner bar is given by

$$E_1 \text{ (eff)} = \frac{\sigma_1}{(d/\ell)}$$

Substituting for d from Eq 4, we have

$$E_1 \text{ (eff)} = \frac{E_1 k\ell}{E_1 A_1 + k\ell} \quad \ldots\ldots\ldots\ldots\ldots\ldots (5)$$

Since the load $(\sigma_2 A_2)$ is shared by two outer bars, a slightly different expression is obtained for the effective modulus of the outer bars.

$$E_2 \text{ (eff)} = \frac{2\, E_2\, k\ell}{E_2 A_2 + k\ell} \quad \ldots\ldots\ldots\ldots\ldots\ldots (6)$$

The quantity $(k\ell)$ has been experimentally determined by measuring all the terms on the right-hand side of Eq 4. Strains computed on the basis of this analysis are shown in Fig. 4*c*.

In comparing with the experimental results, we used the modified Burgreen approach to predict the amount of ratchetting strain per cycle on the basis of the flow stresses measured at the end of each half cycle in the same test. However, such a procedure extracts much from the experiment, and it would be preferable to be able to make the computations on a purely analytical basis and to use experiments as a check to the theory. In order to do this with Burgreen's results, strain hardening should be neglected. To use Miller's analysis which considers strain hardening, it would be necessary to neglect the fact that the strain hardening rates are different in the inner and outer bars. To overcome these limitations of the earlier analyses, an analytical expression is derived below assuming linear stress-strain relationships with different flow stresses and work-hardening rates for the inner and outer bars. However, a nonlinear stress strain curve can be approximated to a series of linear segments, and isothermal stress-strain curves can be used. The greater the number of linear segments used, the greater will be the accuracy. Such a procedure lends itself nicely to computer programming.

Assuming linear work hardening, we have

$$\sigma_{y1} = \sigma_{o1} + E_{p1}\epsilon \quad \ldots\ldots\ldots\ldots\ldots\ldots (7)$$

$$\sigma_{y2} = \sigma_{o2} + E_{p2}\epsilon \quad \ldots\ldots\ldots\ldots\ldots\ldots (8)$$

where E_{p1} and E_{p2} are slopes of the true stress-strain diagrams. Cross-sectional areas decrease during ratchetting but the area ratio A_1/A_2 remains constant, since all the members are undergoing the same amount of plastic deformation. The term (P/E_1A_1) in Eq 2 has to be replaced by (Pe^{ϵ}/E_1A_1) which can be approximated to $P\ (1 + \epsilon)/E_1A_1$. With this modification and substitution of Eqs 7 and 8, Eq 2 is reduced to the form,

$$\frac{d\epsilon}{dN} = C - D\epsilon \quad \ldots\ldots\ldots\ldots\ldots\ldots\ldots\ldots (9)$$

where

$$C = \alpha_1 (T_{\max} - T_{\min}) - \left(\frac{\sigma_{o1}}{E_1} - \frac{P}{E_1A_1}\right)\left(1 + \frac{E_1A_1}{E_2A_2}\right) - \frac{\sigma_{o2}}{E_2}\left(1 + \frac{E_2A_2}{E_1A_1}\right)$$

and

$$D = \frac{E_{p1}}{E_1}\left(1 + \frac{E_1A_1}{E_2A_2}\right) + \frac{E_{p2}}{E_2}\left(1 + \frac{E_2A_2}{E_1A_1}\right) - \frac{P}{E_1A_1}$$

Integration of Eq 9 gives

$$\frac{C - D\epsilon}{C - D\epsilon_0} = e^{-DN} \quad \ldots\ldots\ldots\ldots\ldots\ldots\ldots\ldots (10)$$

where

$$\epsilon_0 = \alpha_1 T_{\min} + \frac{\sigma_{y1}}{E_1}$$

Suppose the stress-strain diagram consists of two or more linear segments. Let C'' and D'' be the quantities corresponding to the region $\epsilon' \leq \epsilon \leq \epsilon''$ and N' be the number of cycles required to produce a ratchetting strain ϵ'. Then,

$$\frac{C'' - D''\epsilon}{C'' - D''\epsilon'} = e^{-D''(N-N')} \quad \ldots\ldots\ldots\ldots\ldots\ldots\ldots\ldots (11)$$

Then the preceding equations can be used to estimate the number of cycles required to attain a given strain value.

This result is similar to that of Miller [*1*] for the particular case when all the bars have the same properties and $A_1 = A_2$. The preceding results are more general and can be used when the inner and outer bars have different strain hardening rates and different elastic and thermal expansion coefficients.

Using the preceding equations and isothermal stress-strain data, ratchetting strains have been computed and compared with the experimental results, Fig. 4*d*. The stress-strain curves at room temperature and at 200 C

are approximated to linear segments. Even though strain aging and other effects of thermal and mechanical cycling are involved in the deformation process, the predictions based on isothermal data give fairly good, though not exact, estimate of the ratchetting strains.

Conclusions

As a result of this analytical and experimental study we conclude:

1. With suitable modification, the Miller-Burgreen approach to the analysis of thermal ratchetting in tension (with no reversed plastic flow in compression) has been verified experimentally with a three-bar assembly.

2. An improved analytical approach to predicting ratchetting behavior has been developed considering different strain-hardening rates of the inner and outer bars of the three bar assembly. Isothermal stress-strain curves can be used to predict the ratchetting behavior reasonably well, in spite of the complexity of the mechanical behavior under thermal cycling.

Acknowledgment

We would like to acknowledge the support given to this study by the Air Force Office of Scientific Research under Project Themis Contract No. F44620-69-C-0011.

References

[1] Miller, D. R., *Journal of Basic Engineering*, American Society of Mechanical Engineers, Vol. 8, June 1961, pp. 190–196.
[2] Hibeller, R. and Mura, T., *Nuclear Engineering and Design*, Vol. 9, 1969, pp. 131–143.
[3] Parkes, E. W., *Aircraft Engineering*, Vol. 26, No. 12, 1954, p. 402.
[4] Burgreen, D., *Journal of Basic Engineering*, American Society of Mechanical Engineers, Paper No. 68-WA/Met. 13, Sept. 1968.
[5] Manson, S. S., *Machine Design*, 21 July 1960, pp. 161–167.
[6] Stentz, R. H., Meeting of American Society for Testing and Materials, Bal Harbour, Fla., 1971.
[7] Gatewood, B. E., Grothouse, A. P., and Von Hausen, W. W., *Journal of Aeronautical Science*, Vol. 28, 1961, pp. 502–503.
[8] Swaroop, A. V. A., "Thermal Stress Ratchetting of Structures Subjected to Mechanical and Cyclic Thermal Stresses," Ph.D. thesis, University of Connecticut, Storrs, Conn. 1972.

DISCUSSION

David Burgreen[1] (*written discussion*) Although many investigators have made analytical studies of the problem of thermal ratchetting of a two-bar assembly (or the equivalent three-bar assembly, as the present authors have done), there has been essentially no experimental investigation of the predicted ratchetting behavior of such an assembly. The experimental results that the authors have obtained are in remarkably good agreement with predicted behavior, considering the extreme loading conditions required to obtain ratchetting and the associated high magnitudes of the accumulated strains.

More of this type of basic controlled experimental study of ratchetting is needed if we are to develop criteria for failure, based on thermal ratchetting.

The authors are to be complimented for this useful contribution to our understanding of thermal ratchetting.

[1] Department of Mechanical Engineering, Polytechnic Institute of Brooklyn, Brooklyn, N. Y. 11201.

Lifetime Predictions and Design

E. G. Ellison[1] *and E. M. Smith*[2]

Predicting Service Life in a Fatigue-Creep Environment

REFERENCE: Ellison, E. G. and Smith, E. M., **"Predicting Service Life in a Fatigue-Creep Environment,"** *Fatigue at Elevated Temperatures, ASTM STP 520,* American Society for Testing and Materials, 1973, pp. 575–612.

ABSTRACT: Two current approaches to prediction of life to crack initiation are reviewed, the first based on modification of fatigue types of analyses, the second on use of cumulative fatigue and creep damage models. Methods of allowing for stress and strain concentrations are examined, and attention directed to the possibility of environment significantly affecting results. The fracture mechanics approach to estimating rates of crack propagation is discussed.

For computer analyses of highly critical sections of components, formulation of constitutive equations on a continuum-metallurgical basis is considered, some possible directions for future work are indicated. An example of prediction of failure through growth of voids in creep is given.

Finally, present design practice is outlined, and the importance of accurate knowledge of service conditions emphasized.

KEY WORDS: fatigue (materials), thermal fatigue, creep properties, crack initiation, crack propagation, failure, predictions, accelerated tests, damage, stress analysis, constitutive equations, deformation, cavitation corrosion, intergranular corrosion, transgranular corrosion

The number of conferences relating to problems of elevated temperature fatigue and creep in recent years indicates the industrial importance of the topic, various aspects of which have been examined in recent reviews [*1–5*].[3] Power plant components, particularly, are subject to ever increasing stresses and temperatures as designers strive for increased performance and capacity. Reliability is essential, equally for safety and for economic reasons, and since cracking and even failure in some components is encountered, it is clear that sufficiently good methods for predicting life have not yet been achieved.

One major problem of design is that the service cycle involving variable load temperature and hostile environment is usually complex and often

[1] Reader, Department of Mechanical Engineering, University of Bristol, England.

[2] Senior lecturer, Department of Mechanical Engineering, University of Newcastle-Upon-Tyne, England.

[3] The italic numbers in brackets refer to the list of references appended to this paper.

Copyright© 1973 by ASTM International www.astm.org

imprecisely known. The difficulty is further compounded when transient stress and thermal fields exist in the body of a component, resulting in lack of precise information as to local loading conditions at critical points. Thus laboratory simulation of accelerated service cycles for development of life prediction methods must be considered with care. Here the fundamental problem is that selection of the stress and strain cycle to be used in testing must come from analysis of the component, which implies knowledge of the constitutive behavior supposedly under investigation.

Several approaches to prediction of material behavior under cyclic conditions are reviewed in this paper, and correlated with results from different sources where possible. The effect of holdtime is discussed in some detail. An alternative attack based on development of properly formulated constitutive equations for use in computer analyses is also considered.

Review of Predictive Methods

The majority of results have been obtained for the case of hold periods at maximum strain in the cycle, though some data on stress hold are now appearing. When material data are plotted on the basis of amplitude of cyclic total strain versus cycles to failure for tests in air, the curve slopes are steeper for the higher temperatures and longer holdtimes. In general, it appears that slower strain rates or the introduction of hold periods lead not only to a reduction in the cyclic fatigue life but also to an increase in the time to fracture.

There have been suggestions that the effect of holdtime is detrimental at the longer times, and Krempl and Walker [*7*] correlated their axial results together with some reversed bend holdtime data to support this proposition. However, this hypothesis is certainly not general since other results [*8–10*] taken from axial tests can be plotted which show the opposite trend; indeed, in several cases, the cyclic life approaches a lower limit (Fig. 1). It appears that in general the effects of long holdtime are more detrimental for reverse bend than for axial results.

There appears to be some doubt as to the effect of a hold period in the compressive part of the cycle. Berling and Conway [10], for axial tests on Type 304 stainless steel at 1200 F, found that if the cycle contained a 30-min tensile hold and no compressive hold, there was a serious reduction in cyclic life and the mode of crack initiation was intergranular; if even a small 3-min compressive hold was added into the cycle then a healing effect was obtained so that the loss in cyclic life was small and the mode of initiation was transgranular. However, Wells and Sullivan [*11*] for axial tests on a nickel-based alloy at 1400 F concluded that holding compressive strain was more damaging than holding tensile strain. Evidently the mechanism by which voids and cracks are formed under such conditions needs some clarification.

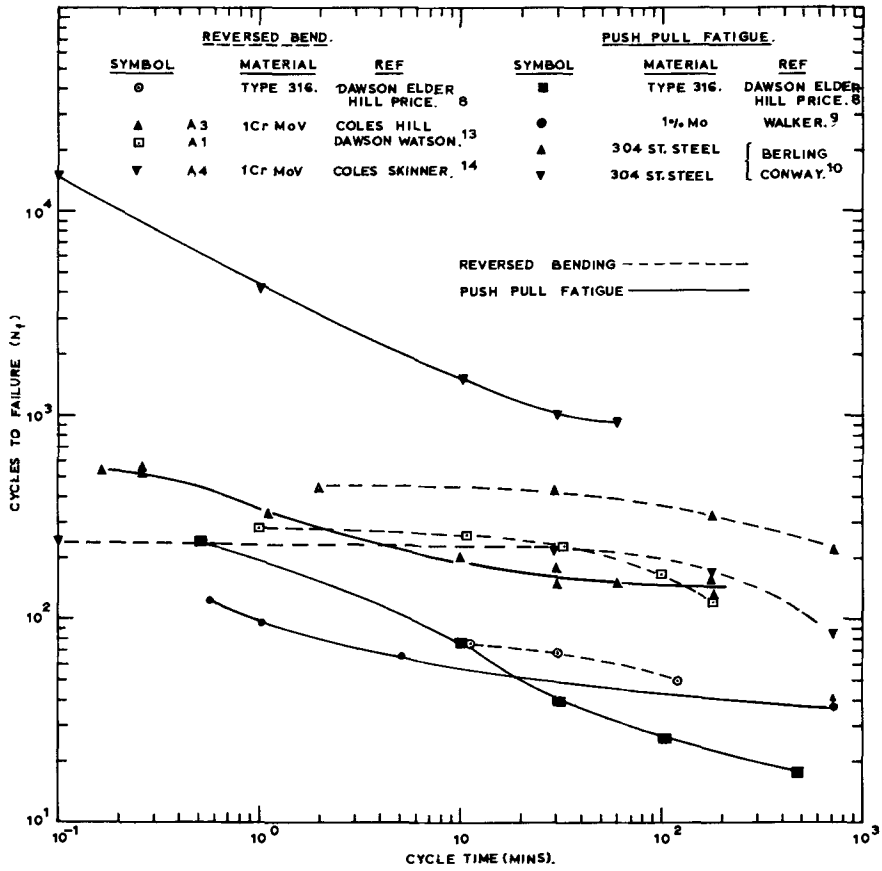


FIG. 1—*Cycles to fracture versus time for axial push-pull and reversed bending tests.*

A linear relationship was obtained by Conway et al [*12*] (Fig. 2) when data for continuous and holdtime tests were plotted on log-log basis for time to fracture versus cycle time. It is seen that there is an increase in time to fracture as the cycle time, and therefore the holdtime was increased. Data from other sources [*6,8,9,13,14*] were replotted and similar correlation obtained.

For most alloys at room temperature good correlation has been obtained under reversed strain cycling by use of the well-known empirical Manson-Coffin relationship, and analyses have been presented [*15*] which support this expression. However, at higher temperatures the effects of strain rate and holdtime is present as might be expected. These effects have been accounted for by development of two different approaches, the first based on modifying the fatigue type of analysis and the second on a cumulative fatigue and creep damage model.

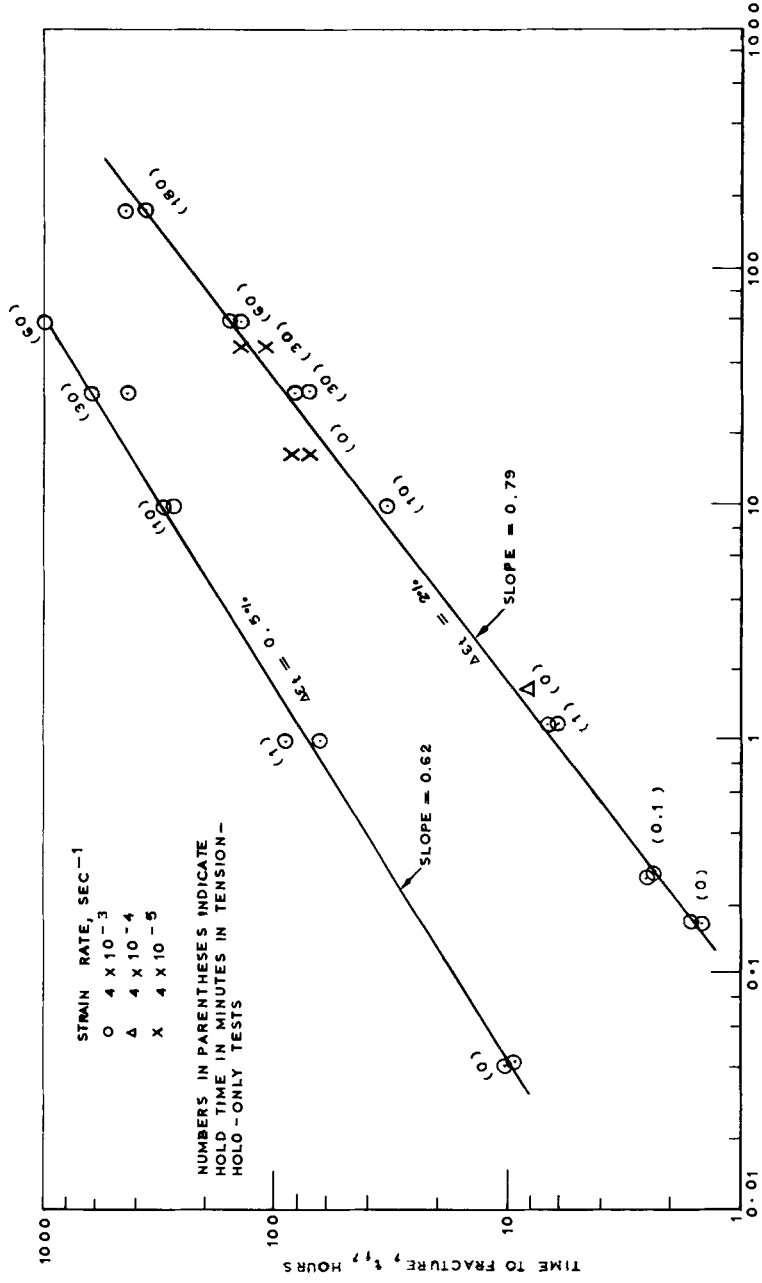


FIG. 2—*Correlation of low-cycle fatigue data for Type 304 stainless steel tested in air at 650 C using no holdtime and holdtimes at peak strain in only the tension portion of the cycle [12].*

Modified Fatigue Approach

1. The method developed by Coffin [*2,16,17*] extended the low-temperature relationship in terms of the concept of frequency modified fatigue life. The effects of frequency had been studied already by Eckel [*18*] and later by Coles et al [*13*] who correlated results by means of the parameter $\nu^k t$ where ν is the frequency and t the total time to failure. This parameter was expressed as $N_f \nu^{k-1}$, the frequency modified life, and it was shown experimentally [*16,17*] that the following relationship held

$$(N_f \times \nu^{k-1})^{\beta} \times \Delta\epsilon_p = C_1 \quad \ldots\ldots\ldots\ldots\ldots\ldots (1)$$

Evidence was produced to show that the curve consisted of two slopes and that the exponent β increased with temperature at the longer lives. This slope change could be due to the crack mode changing from ductile transgranular to brittle intergranular.

The Morrow [*19*] relationship for the cyclic stress-strain curve was also frequency modified, and using this with Eq 1 an expression for the total strain range was derived. For lower temperatures Coffin showed that this expression can be reduced to a form identical with Manson's [*1*] Universal Slopes equation and Langer's [*20*] equation. Correlation was obtained for results from other workers [*13,21,22*] for different strain rates, holdtimes, and materials, the accuracy of life prediction being within 30 percent (Fig. 3). However, the analysis would predict the same cyclic life whether the hold period was in tension or compression which is contrary to the work of Berling and Conway [*10*]. It could be argued that cracks are present for a very large fraction of life and that behavior is governed by stresses at the crack tip which do not necessarily follow the nominal waveform applied to the specimen. In addition, it is possible that other time dependent processes apart from creep are occurring and, as pointed up by Coffin himself, oxidation may be a substantial controlling factor.

2. The Universal Slopes method presented by Manson [*1,23*] may be assumed to describe pure low-cycle fatigue behavior in which the total strain range is related to the tensile strength, elastic modulus, and ductility. An attempt was made [*24*] to predict elevated temperature behavior by inserting the relevant tensile properties, but predicted lives were usually optimistic and the 10 percent rule was introduced; that is, the fatigue lives were taken as 10 percent of these predicted by the method of Universal Slopes. This analysis still did not take account of frequency effects, and the method was further modified [*34*] by means of a linear damage rule to incorporate static creep rupture data. Under combined fatigue and creep the lower life bound is given either by the 10 percent rule or the linear damage life, whichever is lower. This method gave good correlation with data from a wide variety of materials and Berling and Slot [*21*] obtained agreement in later work. The advantage of the method is that only simple

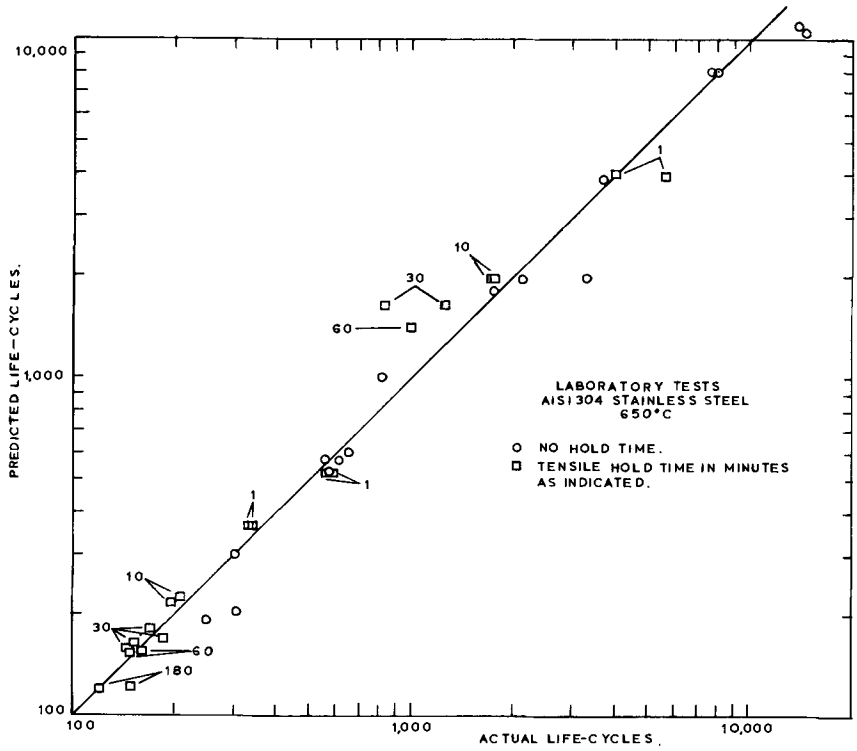


FIG. 3—*Comparison of actual and predicted life with holdtime—AISI 305 stainless steel at 605 C* [2].

monotonic tensile properties and static creep rupture data are required. However, the life ratio between upper and lower bounds is generous.

3. Though holdtime laboratory data are now becoming available the test conditions usually have not been too realistic in terms of service conditions because the accelerated test has been carried out under a high strain range and with a low holdtime. At the more realistic longer times to failure at lower strain ranges, it is postulated [*6,25*] that the holdtime curves be extended to the creep rupture strengths of the material as shown in Fig. 4. The assumption to use the creep rupture strength was justified on the basis that at low strain ranges negligible fatigue damage is produced, so that only creep damage occurs during the holdtime period. For the high strain ranges, it was assumed that the main source of damage was high strain fatigue and that this was relatively insensitive to temperature over a reasonable temperature range. Further information on this method is given in the later section on Industrial Practice.

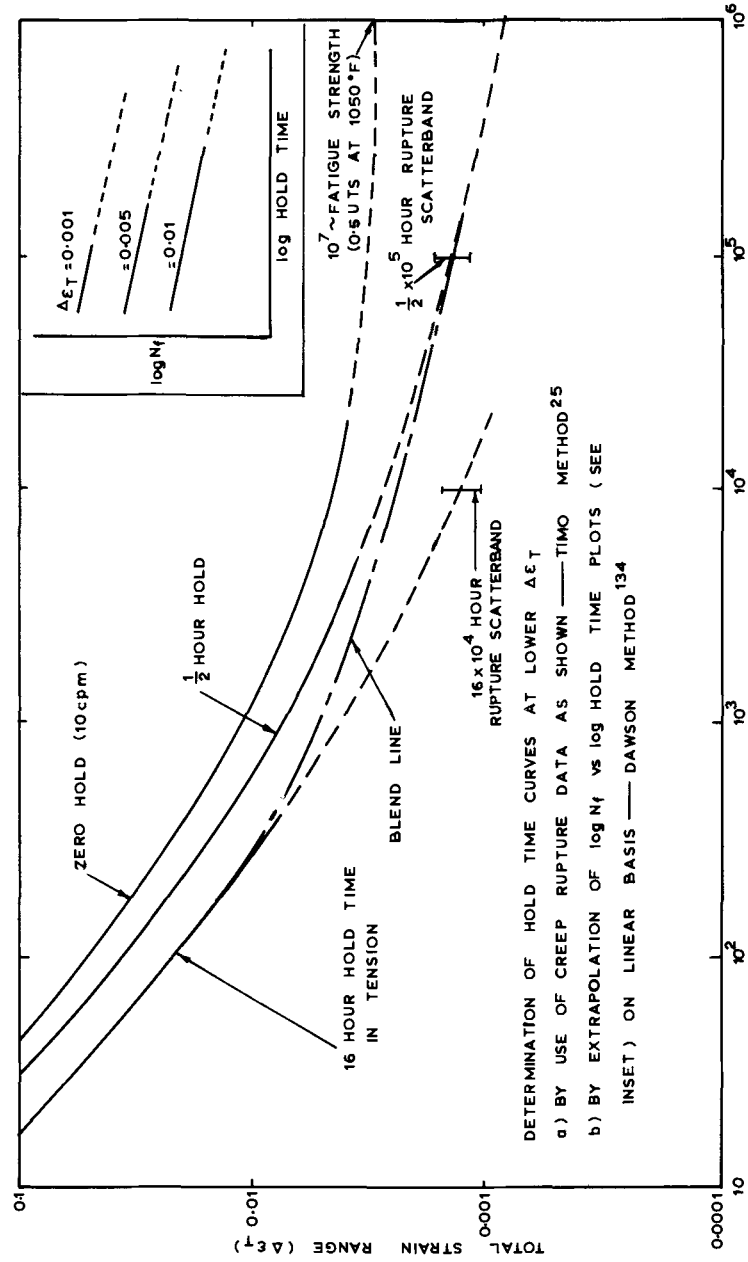


FIG. 4—*Holdtime data extended to lower strain ranges.*

Cumulative Damage Approach

In this method it is necessary to consider the pure fatigue and creep resistances and how the effect of these two processes may be added to predict failure. Pure fatigue damage for a given strain range may be assessed by a cycle fraction. Assessment of the pure creep damage by means of the time fraction rule has been shown [*26,27*] to be good for correlating results when the stress is slowly varying; several other methods have been proposed [*6,28*] but with less success. The cumulative linear damage rule sums the pure fatigue and creep damages to unity.

Much of the early work [*27,29–31*] on combined fatigue creep under sinusoidal stress has been already summarized [*3*], and it may be concluded that for the ratios of alternating to mean stress of less than unity, behavior could be predicted solely from creep data, but that for higher ratios the effects of fatigue had to be introduced into the damage rule.

In other early tests Swindeman [*32*] used a fractional damage rule and also carried out supplementary tests to show how prior fatigue could reduce the subsequent creep ductility. Wood [*33*] later carried out cyclic strain tests, feeding creep into the tensile part of the cycle, and found on a linear damage plot that a harmful interaction existed.

Recently work at National Aeronautics and Space Administration (NASA) [*35*] has taken a closer look at baseline creep data suitable for use in damage calculations. As a first approach the calculation of creep damage was carried out using creep rupture data for smooth and notched specimens to simulate, respectively, unrestricted creep strain at constant stress and restricted creep relaxation at constant strain in a cycle. A rather complicated cyclic creep rupture test has been proposed [*36*] also in which alternate tensile and compressive loads were applied and the specimen allowed to creep between fixed limits. Manson et al [*37*] presented low-cycle fatigue results for two alloys over a wide range of frequencies, strain ranges, and temperature. While the L605 cobalt alloy was frequency dependent, Type 316 stainless steel was not, and by consideration of the cyclic creep or notched-unnotched creep data in the linear damage equation this difference was predicted. In Fig. 5 the effect of temperature on the cyclic behavior was shown for L605; creep is dominant at temperatures greater than 1200 F, fatigue at temperatures less than 1100 F, while fatigue-creep combination only appears in the relatively short range 1100 to 1200 F.

Spera [*35,38,39*] used damage analysis to predict the lives of tapered wedge specimens tested in hot/cold fluidized beds of sand. This cyclic process causes thermal strains in the thin edge of the specimen so that eventually thermal fatigue cracks initiate. Spera analyzed the stresses and strains and compared his predicted lives with experimental results. The correlation is surprisingly good, and for In100 it was seen that creep was dominant for all the results presented; for B1900 alloy evidence of fatigue-creep interaction was obtained. Evidently Spera has made out a

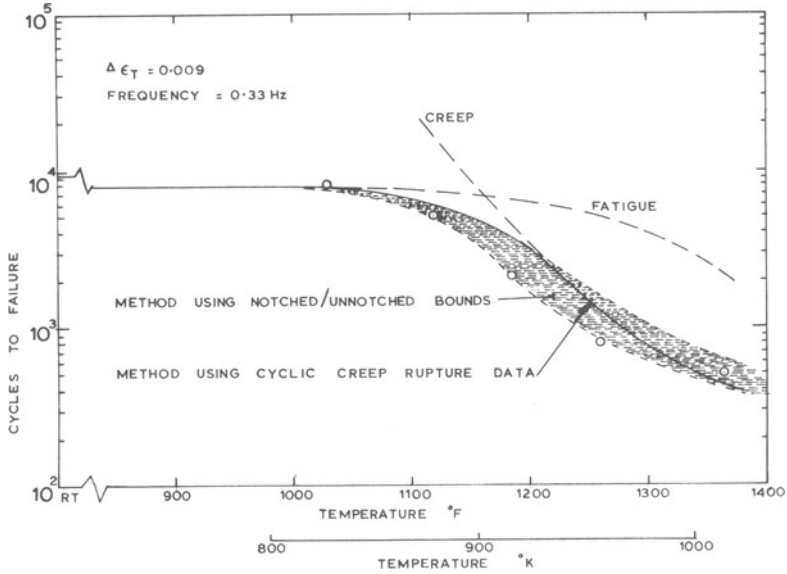


FIG. 5—*Creep fatigue results in low-cycle fatigue of L605 over a range of temperatures* [37].

good case for analyzing some thermal fatigue cases by a creep type of analysis, and with some reservations the authors are in agreement (later section on *Approach Based on Constitutive Equations*). Other results have been presented by Carden and Slade [*40*], and other information can be obtained from recent reviews [*3–5*].

A method of summing damage has been proposed by Marshall and Cook [*41*] who considered a strain controlled holdtime cycle. Their model postulated a transition point on the stress relaxation curve, prior to which cyclic damage occurred, and subsequent to which creep damage at the relaxed stress level occurred. There is evidence [*7,42*] that the loading rate and initial strain level only affects the slope of the initial part of the relaxation curve and that the subsequent stress level is independent of these two factors. Reasonably good correlation with results [*6–8,13,14*] was obtained; it is interesting to note that the transition point usually occurred in the range 15 to 30-min holdtime.

Tilly [*43–46*] has studied the elevated temperature behavior of a 11Cr steel and a nickel alloy, carrying out cyclic stress tests in repeated tension. It appears that the creep damage incurred during the holdtimes in a rectangular cycle is the predominant feature when the ratio of hold-to-loading time was greater than ten, the controlling factor being time at tensile load; also see Swindeman [*32*]. At lower temperatures or higher frequencies or both when failure could occur by a combination of fatigue and creep, a linear damage rule correlation yielded good results. The effect of frequency

at 500 C was studied, and it was found that there was a critical value below which time dependent modes dominated and above which cyclic damage dominated; the transition was sharply defined. See also Miller and Rizk [*47*].

Stress and Strain Concentrations

Every practical structure possesses notches in one form or another, and allowance must be made by multiplying the nominal stress and strain by a factor to obtain the local values at these critical points.

Morrow et al [*48*] summarized work on stress and strain concentrations by Neuber [*49*] and Stowell [*50*]. The rule proposed by Neuber stated the elastic stress concentration factor $K_t = (K_\sigma K_\epsilon)^{1/2}$ where K_σ and K_ϵ are the elastoplastic stress and strain concentration factors, respectively. Stowell [*50*] presented a relationship in the form

$$K_\sigma = 1 + (K_t - 1)\frac{E_s}{E_\infty};\ K_\epsilon = K_\sigma \frac{E_\infty}{E_s} \quad \ldots\ldots\ldots\ldots (2)$$

where E_s and E_∞ are the secant moduli for the material at and remote from the stress raiser.

Data presented by Box [*51*] were correlated, and it was found that both the Neuber and Stowell expressions gave reasonable accuracy though the former rule gave slightly better results especially at higher values of K_ϵ; Neuber's rule is also easier to apply. In fatigue tests the fatigue strength reduction factor K_f was substituted for K_t by Morrow with some success, and support for this development is also given by Baron and Brine [*52*]. Several authors have shown that K_f can exceed K_t. In notched high-strain fatigue tests on three steels Krempl [*53*] measured the cyclic strains at the root of a notch and found that the value of K_f depended on the applied nominal stress and definition of crack initiation.

Timo [*25*] uses a method for determining K_ϵ proposed by Zwicky [*54*] and assumed that $K_f = K_\epsilon$. Tests indicated that this assumption was reasonable; the use of K_ϵ appears to be preferable to K_t especially for larger plastic strains and in any event should be conservative.

Environmental Effects

The majority of work published in the literature has appeared to show that in high-temperature fatigue, especially with holdtimes, the decrease in the number of cycles to failure is due to the time dependent processes of creep. However, recent evidence has been produced which can allow an alternative explanation; that is, the time dependent processes may be partly environmental in effect [*55–57*].

White [*56*] has tested ½Mo steel in reverse bending tests and found that at room temperature for continuously cycled tests the endurance was nearly twice as great in vacuum as in air (Fig. 6). As expected in air the fatigue

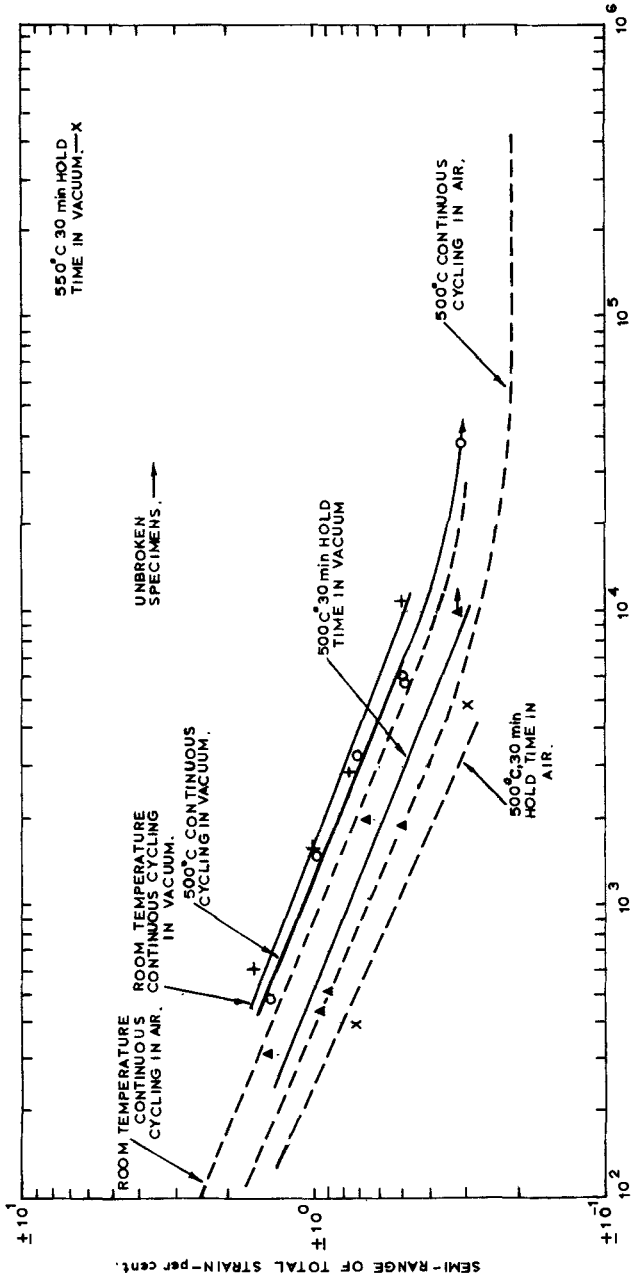


FIG. 6—*Strain cycling tests on ½Mo steel in vacuum and in air* [56].

life at 500 C was considerably less than at room temperature, but in vacuum there was negligible difference between the room temperature and the 500 C results. In addition fatigue lives were shorter when the material was continuously cycled at 500 C in air than when a 30-min hold period was incorporated into the cycle in vacuum at 500 C. White concluded from these results that oxidation had a greater effect than the creep processes for the test conditions used.

Coffin and McMahon [*57,58*] have shown that fatigue crack initiation occurred at points of highly localized surface oxidation, for example, grain boundaries, and in later work Coffin [*59*] attempted to separate the processes of creep and oxidation by comparative high-strain fatigue tests on Udimet 500 and A286 in air and vacuum (10^{-8} torr) at elevated temperature. It was found that in air there is a definite frequency effect and that fatigue lives are shorter than in vacuum. In vacuum, however, there is no frequency effect, and the A286 behaves in a similar manner to ductile metals at room temperature. Propagation generally followed grain boundaries accompanied by oxidation, particularly at the lower frequencies, though in vacuum the mode was transgranular. These results were partially explained by Coffin by the fact that the low-cycle fatigue process is dominantly one of crack propagation and the environmental attack is likely to be more intense in the larger plastic zones at the crack tip. Long hold periods in air at elevated temperature would be obviously detrimental, increasing crack propagation rates.

Spera [*38,39*] has noted the presence of oxidation in thermal fatigue cracks, usually along grain boundaries, and concluded that, in general, alloys with the highest oxidation resistance had the highest thermal fatigue resistance. Other workers [*60–63*] have obtained significant increases in fatigue life in vacuum for several materials at various temperatures, but for more information on the effects of environment on the independent phases of crack initiation and propagation see a recent review [*64*]. Static creep tests carried out by LeMay et al [*65*] on an austenitic stainless steel indicated that the material was weaker in air than in argon or vacuum, significant differences in ductility and creep rates being noted.

Crack Initiation and Propagation

Predictive methods for fatigue to date, have, concentrated mainly on determining life to initiation of a crack. However, at the cyclic strain levels which can occur in some components in power generation equipment, it is possible that engineering size cracks may occur at an early stage so that design rules capable of predicting subsequent crack propagation are also required [*64*].

In the initiation mode cracking (Stage I) is observed along crystallographic slip planes at 45 deg to the stress direction [*66*]. The propagation

mode, Stage II, is however noncrystallographic, cracks tending to grow along a plane perpendicular to the greatest local tensile stress (refer to later discussion on creep damage). Smith and Barnaby [*67*] have discussed crack initiation in crystalline solids, showing that a dislocation model proposed by Cottrell offered particularly easy initiation. Fatigue crack initiation, whether by slip band intensification at low cyclic stresses or by surface rumpling at high cyclic stresses does not seem particularly amenable to analytical investigation. A plastic instability model [*68*] gives some insight into the initiation mechanism at the higher cyclic strains, but in general definitions are arbitrary and estimates empirical.

Failure in high-strain fatigue is predominately by propagation (Stage II), and Laird and Smith [*69*] showed that the percentage of fatigue life spent in propagating a crack increased as the total life reduced. Marsh [*70,71*] and Tompkins [*15*] have emphasized that cracks initiated at a high stress may propagate at a relatively low stress. Thus whether a component fails catastrophically may depend less on cyclic stress to initiate a crack than on stress required to cause a crack to grow.

A wide variety of models has been developed to describe the propagation of fatigue cracks involving many different concepts including dislocation flow, fracture mechanics, and dimensional analysis. One of the more useful correlating parameters has been the stress intensity factor which has been especially successful at lower cyclic stresses [*72*]. Though this parameter has been used also at higher cyclic stresses, results suggest that this approach may be doubtful in this case, largely due to the influence of plasticity and fracture instability. When plasticity is not restricted to a small enclave at the crack tip, a knowledge of the strain field ahead of the crack is required to enable an estimate of the local cyclic damage to be made and so the propagation rate determined. It is also interesting that by considering the dislocation model suggested by Cottrell mentioned earlier, Tompkins [*15*] was able to develop a Stage II crack growth law on a continuum basis which, on integration, led to a modified type of Manson-Coffin relationship; the model has been extended to cope with temperature and cyclic history variations [*73*]. Crooker and Lange [*74*] also recognized the limitations of the stress intensity parameter approach at high cyclic loads and used the total strain range to correlate the propagation results on various materials above and below general yield.

Crack propagation is an important feature in the fatigue failure of welded structures owing to the presence of numerous defects. Indeed conditions are such that it appears the life of a welded component may be predicted from consideration of the propagation phase alone; Jerram [*75*] and Maddox [*76*] integrated the fatigue crack propagation rate in terms of the stress intensity factor to failure to obtain the life. Additional stress concentrations can arise from a change in section often associated with welded joint and the residual stresses of the weld metal, which is often diluted

with the parent material, and the heat affected zone through which the crack propagates. Clearly there is still much to be learned before design rules can be formulated.

Little has been published so far on the rates of creep crack propagation that could possibly occur during dwell periods in a representative service cycle. Some recent results for a typical turbine 1Cr-Mo-V steel presented by Ellison and Walton [*77*] showed that the fatigue crack propagation rates at elevated temperature 565 C are somewhat higher than those at room temperature and that the stress intensity factor appears to be a reasonably good parameter for correlating the results. Creep crack rates for 565 C for the same material were greater especially at the higher values of stress intensity factor though the usefulness of this correlating parameter is doubtful in this particular case since the crack tip plastic zones were large.

Approach Based on Constitutive Equations

The narrowness of the transition zone over which creep fatigue interactions occur eases design for components operating above or below the zone. For conditions straddling the zone low-strain cycling appears to be creep sensitive, while high-strain cycling is fatigue dominated.

Sensible argument can be advanced for full-scale testing of components particularly when temperature transients are involved or when cracking occurs, because of the technical impracticability of maintaining similarity between model and full-scale component; Smith et al [*78*]; Townley and Poyner [*79*]. In appropriate situations, and using creep data, computer prediction of behavior of highly critical sections of complete components can offer economies in testing. For such an approach accurate constitutive equations are required, confirmed by comparing prediction of specimen behavior with results of engineering laboratory tests on specimens or experimental models.

In assessing how this might be done it is useful to consider in turn (1) the basis of continuum theory, (2) metallurgical mechanisms and constitutive equations, and (3) computer prediction of behavior.

Continuum Theory

The equations for a complete simple theory of mechanical and thermal behavior of continua may be divided into three categories.

1. Kinematics—the geometry of deformation, involving only pure mathematics.

2. Basic axioms—physical principles, accepted as true.

3. Constitutive equations—which inject particular material behavior into the general theory.

Fundamental relationships obtained by invoking considerations 1 and 2 are summarized in Appendix A. Assuming body forces b_i and distributed

heat sources $\hat{r}$ to be specified, a count reveals 5 independent equations and 16 unknowns (see Table 1). For coupled theory eleven further (constitutive) equations are thus required, involving response functions such as

stress tensor	$\sigma_{ij}(t)$
heat flux vector	$q_i(t)$
Helmholtz free energy	$F(t)$
entropy	$\hat{S}(t)$

Truesdell [*80*] has listed restrictions and rules which experimentally determined constitutive equations should satisfy, and the work of Coleman [*81,82*] has the intellectual compulsion of satisfying all requirements for a totally consistent theory.

Happily, for most applications an uncoupled approach (Appendix B) is adequate and simpler. By dividing the energy balance equation (Eq 21 of Appendix A) into its mechanical and thermal parts, the stress distribution problem may be handled separately from the temperature distribution problem. The mechanical energy balance is formed by taking the scalar product of $\dot{u}_i$ with the balance of linear momentum and does not add to the number of equations. The thermal balance equation is found by difference from the total balance equation, and constitutive equations for Helmholtz free energy F and entropy $\hat{S}$ are now not required.

In constructing constitutive equations, history functionals describing what has happened to virgin material from time zero are favored by rational mechanists, Onaran and Findley [*84*], for example, giving multiple integral representation for three dimensional small strains as follows:

$$\varepsilon_{ij}(t) = K_0\,\delta_{ij} + \int_0^t K_1(t-\tau_1)\,\dot{\sigma}_{ij}(\tau_1)\,d\tau_1 + \int_0^t\int_0^t K_2(t-\tau_1,\, t-\tau_2)\,\dot{\sigma}_{ik}(\tau_1)\dot{\sigma}_{kj}(\tau_2)\,d\tau_1\,d\tau_2 + \ldots . \quad (3)$$

where K_0, K_1, K_2 are kernel functions containing stress invariants, time and material constants, and τ_1, τ_2 are the arbitrary times of different time intervals. However, nonlinear behavior is not easily represented by such mathematical functionals, Pipkin and Rogers [*83*], and the approach pursued by Findley and others [*85,86*] does not seem to give a good prediction of behavior. In addition, the number of experiments required to determine the kernel functions is large. Lockett [*87*] indicates that the number of tests required to determine one dimensional behavior may be $3 + 3n + \frac{1}{2}n^2$ where n may be of the order of 10. Three dimensional behavior is more complicated.

In 1966 Wang and Bowen [*88*] saw an important simplification to functional constitutive theory for a certain class of deformation temperature

histories (named quasi-elastic response) writing a system of constitutive equations of the form

$$\Phi = G(\Psi,t) \quad \ldots\ldots (4)$$

where

Φ = response function; for example, σ_{ij}, q_i, F, $\hat{S}$

Ψ = present local configuration, $\theta, \frac{\partial\theta}{\partial x_i}, \frac{\partial u_i}{\partial x_f} \ldots$, and

t = time.

Since the parameter t is a real variable, the functional $\mathfrak{F}$ of the earlier integral[4] representation

$$\Phi(t) = \overset{\infty}{\underset{\tau=0}{\mathfrak{F}}} [\Psi(t - \tau)]$$

may be replaced by a function G, and the history of the state variables Ψ is then implicit in the simplified representation Eq 4. The theory was extended to a class of materials with memory (quasi Rivlin-Ericksen material), capable of describing linear viscous behavior and nonlinear generalizations

$$\Phi = G\left(\theta, \frac{\partial\theta}{\partial x_i}, \frac{\partial u_i}{\partial x_j}, \frac{\partial \dot{u}_i}{\partial x_j}, t\right) \quad \ldots\ldots (5)$$

The partial set of constitutive equations necessary for solution of uncoupled problems is then

$$\sigma_{ij} = G_{ij}^{(\sigma)}\left(\theta, \frac{\partial\theta}{\partial x_i}, \frac{\partial u_i}{\partial x_j}, \frac{\partial \dot{u}_i}{\partial x_j}, t\right) \quad \ldots\ldots (6)$$

$$q_i = G_i^{(q)}\left(\theta, \frac{\partial\theta}{\partial x_i}, \frac{\partial u_i}{\partial x_j}, \frac{\partial \dot{u}_i}{\partial x_j}, t\right) \quad \ldots\ldots (7)$$

where parameters listed in G are present to satisfy Truesdell's concept of equipresence. The nature of $G_i^{(q)}$ is reasonably well expressed by Fourier's law for conduction, leaving only the stress-strain relationship to be determined.

This is as far as formal constitutive theory carries us at present. For real applications, phenomenological features have to be introduced, and it is interesting to examine recent proposals in this area to relate them to the quasi-Rivlin-Ericksen material.

Rabotnov [*89,90*] assumed that the creep rate at a given instant is determined by stress, temperature, and present structural state of the

[4] $\Psi\left(t \underset{\tau=0}{\overset{\infty}{-}} \tau\right)$ represents the history of the local configuration.

material, the last being defined by a certain number of structural parameters S_m where m is 1, ... , z.

$$\frac{\partial \dot{u}_i}{\partial x_j} = \Phi\,(\sigma_{ij},\, \theta,\, S_m) \qquad (8)$$

the rate of change of these structural parameters being described by a set of kinetic equations

$$\frac{\partial S_m}{\partial t} = \Psi_m\,(\sigma_{ij},\, \theta,\, S_1,\, \ldots,\, S_z) \qquad (9)$$

Comparison of Rabotnov's Eq 8 with Eq 6 reveals parameters whose presence alone or combined might be expected in any expression for the structure parameter S_m. In a recent United Kingdom study group presentation Grant [*91*] demonstrated that many familiar analytical creep rate expressions for uniaxial loading such as time hardening, strain hardening, work hardening, life fraction, and ductility fraction were included as single structure parameter cases of Rabotnov's set of kinetic equations. The simple expressions obtained involved parameters from Eq 6 in every case. The structure parameter is seen as the criterion which determines what the new creep rate will be when stress and temperature are changed from one condition to another.

The kinetic equation concept embraces Kachanov's ideas discussed by Odqvist [*92*] that creep deformation and deterioration (damage) are independent phenomena. Thus Eq 8 is used to predict creep deformation and Eq 9 (1) to provide S_m parameters for Eq 8 and possibly (2) to predict failure by summation of damage. In published work only single structure parameters appear to have been employed in kinetic equations to date. Prospects of obtaining useful results with the structure parameter approach seem good, as identification with real metallurgical processes appears practicable.

The concepts just mentioned apply when the material is above the region in which yielding can be recognized. For cycling through the creep-fatigue transition zone the concept of a yield surface begins to apply. Green and Naghdi [*93,94*] have presented a general (rate-type) theory[5] of an anisotropic elastic-plastic continua, containing somewhat different parameters to Eq 5, including stress rate and temperature rate. Constitutive assumptions were given for the yield surface and for material behavior including restrictions for (1) elastic state, (2) unloading from an elastic-plastic state, (3) neutral loading, and (4) loading from an elastic-plastic state. However, constitutive equations which will provide the required transition from elastic-plastic to creep behavior seemed yet to appear, before possibly the presentation by Miller[6] at this conference.

[5] Difficulty in formulating the thermodynamics of a functional theory to describe elastic-plastic behavior was mentioned by Green and Naghdi.

[6] See p. 613.

Metallurgical Mechanisms and Constitutive Equations

Deformation—Conrad [*95*] classified time-dependent mechanisms with the aid of absolute melting temperature θ_m roughly as

(*a*) low temperature creep, occurring below 0.3 θ_m,
(*b*) recovery creep, occurring between 0.2 θ_m and 0.6 θ_m, and
(*c*) diffusion creep, occurring above 0.5 θ_m.

Below 0.3 θ_m the process is one of exhaustion of dislocations capable of movement under the stress applied (crystallographic slip within grains). The creep rate reduces with time and deformation finally ceases. Temperatures are too low for dislocation climb to be effective, and behavior is only activated thermally to the slight extent that the initial (Peierls) stress required to move the dislocation is temperature dependent. An equation of the form

$$\frac{d\varepsilon}{dt} = \frac{c}{t} \text{ that is } \varepsilon = A \ln t + B$$

where A, B and C are constants was suggested.

Between 0.2 θ_m and 0.6 θ_m a variety of possible mechanisms may be operating. Webster and Pieacry [*97*] have proposed that apparent activation energy for a nickel-base superalloy may be a consequence of creep being controlled by the product of dislocation velocity and density, which are themselves controlled by an activation energy equal to that for self diffusion in nickel. Their theory suggests that minimum creep rate should be a material property. Representative of steady-state controlling mechanisms are three proposed by Weertman (see Kennedy [*96*]) viscous slip of dislocation lines, motion of dislocation lines through Peierls stress field and the most likely, climb of blocked dislocations to adjoining slip planes as temperatures rise, namely,

$$\frac{d\varepsilon}{dt} = \alpha \left(\frac{\sigma^q}{k\theta}\right)^2 \exp\left(\frac{-Q}{k\theta}\right)$$

Above 0.5 θ_m deformation is mainly by vacancy flow which is stress directed, the ratio of the number of vacancies to the total number of atom sites being

$$\frac{n}{N} = \exp\left(\frac{-(Q - v\sigma)}{k\theta}\right) \quad \ldots\ldots\ldots\ldots\ldots\ldots (10)$$

where

v = volume of a vacancy and
Q = energy of vacancy formation.

Brackets of the type $(Q - v\sigma)$ will predict different behavior in uniaxial tension and compression in accordance with experimental results presented

by Tilly [*98*]. Unfortunately, such discrimination is often obliterated when adapting uniaxial data to prediction of multiaxial behavior. Additional important factors not often modelled explicitly in constitutive equations include phenomena like strain aging and precipitation hardening, and such changes may be reflected by a change of activation energy.

In creep description kinetic equations of the form Eqs 8 and 9 have been in use for some time, although perhaps not formally expressed as functions Φ and Ψ_m. This position is changing as evinced by the recent analysis of Lagneborg [*99*] who made use of a dislocation model to predict primary creep and recovery behavior under cyclic conditions. The representation is expressed as two equations using dislocation density as the structure parameter.

$$\frac{d\varepsilon}{dt} = \dot{\varepsilon}_0 \exp\left(\frac{-\nu\alpha\mu b\,(\rho^{1/2} - \rho_0^{1/2})}{k\theta}\right) \quad \ldots\ldots\ldots\ldots (11)$$

$$\frac{d\rho}{dt} = C\frac{d\varepsilon}{dt} - 2M\tau\rho^2 \quad \ldots\ldots\ldots\ldots\ldots\ldots (12)$$

where

$\dot{\varepsilon}_0$ = creep rate at zero time,
ρ_0 = dislocation density immediately after loading,
ν = activation volume,
μ = shear modulus,
b = Burger's vector,
M = coefficient of mobility of climbing dislocations,
τ = dislocation line tension, and
C, α = constants.

Lagneborg analyzed the case of cycling between upper and lower tensile stress levels for 20Cr-35Ni steel, and showed that when steady cyclic creep is reached, the resulting deformation was always more than that which would have been predicted from steady-state creep rates at the different stress levels. This was attributable to recovery behavior.

The work of Gittus [*100,101*] offers a similar route to predicting variable load behavior. Analytical solutions to a set of four differential equations descriptive of the creep process were derived, and isothermal isostress creep data used to obtain constants for use in prediction of variable stress behavior. Both step changes in stress and cyclic stress behavior have been predicted with some success. The theory has been shown to give reasonably good predictions for load increase, reduction, removal, and reversal experiments on lead, tungsten, stainless steel, nickel, aluminum, and cadmium.

The above microscopic deformation concepts apply to primary and secondary creep alone, but are important for the role that dislocations

play in the initiation of damage. Tertiary creep, discussed next, may be regarded as external manifestation of macroscopic accumulation of damage within a material.

Damage—At temperatures in the creep range intercrystalline failures attributable to formation of either triple point (wedge) cracks or cavitation voids are usually encountered (Beevers [*102*]) although rapid loading can still result in ductile transcrystalline failure. For Nimonic 90, McLean [*103*] has demonstrated that wedge type cracks usually occur at moderate temperatures and high stresses, whereas voids tend to form at high temperatures and low stresses.

Formation of triple point cracks is attributable to grain boundary sliding as, for example, Smith and Barnaby, [*104*] and Gifkins et al [*105*], the identical mechanism (slip bands producing jogs in grain boundaries) also being considered important to nucleation of cavities, but not to their subsequent growth. Toft and Broom [*106*] explored a further important mechanism for nucleation and growth arising during temperature cycling when significant differences exist in coefficients of thermal expansion and in elastic constants between precipitates and matrix of an alloy. Voids occur at right angles to the tensile stress, cavities being strung out along grain boundaries, Ishida and McLean [*107*] suggesting growth being controlled either by diffusion of vacancies or by strain regulated by dislocation movement.

Failures may result when cracks of critical size connect up cavities through essentially undamaged boundaries. Woodford [*108*] found strong evidence that the number of voids is determined by total strain rather than time. Recent work by Dyson and McLean [*109*] on Nimonic 80*A* confirm a strong linear relationship between cavity density and strain. This is in sympathy with the observations of Day and Cummings [*110*] that with uniaxial testing under cyclic temperature, a marked reduction in time to reach specific strain occurs, but no significant effect on rupture ductility is observed. As failure criterion for creep, tensile ductility for principal stress directions in a component appears tenable; however, compressive effects not to be neglected include (1) at low temperatures, resharpening of a crack blunted plastically during tensile straining (Laird and Tompkins), and (2) at creep temperatures, shrinkage of cavities by plastic flow. Gittens [*111*] found for copper that cavities failed to collapse during stress free temperature holds because of internal gas pressure. This, however, is not confirmed by Walker et al [*112*] who found evidence of cavity sintering, and Dyson and McLean in reviewing Gittens work point up that his specimens were crept into the late tertiary stage where cavity linkage is expected to occur, thereby giving large cavities which would only sinter slowly. The work of Davies et al [*113*] on Nimonic 80A confim that annealing in the late secondary stage is more effective in extending life than annealing in the early tertiary stage of creep.

Effort is being directed currently towards incorporation of void damage in expressions for tertiary creep, but modelling of damage recovery during periods of stress free temperature hold seems yet to be developed for design application. The rate of growth of voids has been considered by both Rabotnov [114] and more recently by Leckie [*115*] on phenomenological grounds. The damage function ω initially suggested by Kachanov is the area of cracks in the cross section of the specimen, $(1 - \omega)$ is thus the undamaged effective cross section. Simple expressions for strain rate and rate of void growth are

$$\frac{d\varepsilon}{dt} = K\left(\frac{\sigma}{1-\omega}\right)^n \quad \ldots\ldots\ldots\ldots\ldots\ldots (13)$$

$$\frac{d\omega}{dt} = -A\left(\frac{\sigma}{1-\omega}\right)^m \quad \ldots\ldots\ldots\ldots\ldots\ldots (14)$$

from which time to rupture, strain at rupture, and strain/time curves may be obtained. These equations again follow the kinetic model. At small times $\varepsilon \propto t$ which corresponds with the observations of Bowring et al [*116*]; at large times $\varepsilon \propto t^p$ where p is a constant involving m and n, predicting tertiary creep behavior. Primary creep and recovery is not represented.

On the metallurgical side Speight and Harris [*117*] have proposed a model of void growth in which

$$\frac{dr_0}{dt} = \frac{K(1 - 4r_0^2/a^2)}{\ln\left(\frac{a}{2r_0}\right) - \frac{1}{2}(1 - 4r_0^2/a^2)} \quad \ldots\ldots\ldots\ldots\ldots\ldots (15)$$

where

$$K = \frac{D_g\, \Omega z\, (\sigma - 2\gamma/r_0)}{2k\theta r_0^2}$$

r_0 = radius of void,
a = void pitching,
D_g = grain boundary diffusion coefficient,
Ω = atomic volume,
z = thickness of grain boundary available for diffusion,
σ = applied tensile stress,
γ = surface tension of void,
k = Boltzmann's constant, and
θ = temperature.

It is evident that $(1 - 4r_0^2/a^2)$ of this model corresponds to $(1 - \omega)$ of the Leckie model. These present damage models are not completely satisfactory, and in addition multiple structure parameter models combining both deformation and damage behavior have yet to be developed.

For multiaxial stress conditions, the criterion for failure is not yet clear. Johnson with Frost and others [*118*] showed that for one group of metals

the biaxial rupture criterion agreed most closely with maximum principal tensile stress and noted that cracks were gradually propagating throughout the test (this is not inconsistent with tensile ductility as a criterion). For other materials the Maxwell (equivalent J_2 stress) condition applied, the final crack leading to fracture only appearing in a short period before failure. However, this careful work does not reveal how damage is to be assessed (1) under changing biaxial stress systems, or, more importantly, (2) in components with significantly thick sections where the location of severe damage may change position and direction under variable loading conditions.

Experimental evidence on the failure mode of thick tubes under creep is conflicting. Taira and Ohtani [*119*] noted that cracking may start at the outer surface and progress inwards. Finnie and Abo el Ata [*120*] found that cracking appeared to start at the bore. If cavity nucleation is dependent on slip at grain boundaries (shear stress), but void growth (related to tensile strain) is controlled by maximum tensile stress then clearly rates of loading, rates of initial stress relaxation by creep, as well as material characteristics will determine how and where void damage will accumulate. (Refer to the earlier section on *Crack Initiation and Propagation*). Change of loading system may also modify behavior.

If fracture is the linking up of cavities by cracking through undamaged material, closely pitched cavities may require a lower tensile stress than widely pitched cavities to trigger large scale cracking. On such a basis it might be possible for failure to occur either at the bore or at the outer surface of a thick tube depending on circumstances.

At this point it is perhaps worth noting that void damage may sensitize a material to environmental attack—a topic considered elsewhere in the paper. This could lead to situations more difficult to predict.

Computer Predictions

Forms which correctly formulated constitutive equations might possibly take have been suggested, but for the engineer the problem of how best to employ existing data remains.

A number of research centers are known to be assessing prospects of predicting low-cycle high-temperature fatigue using creep data. One creep model which has been found convenient in computational work is due to Clark [*121*] who represented complete tensile creep curves for Nimonic 90 between 650 and 870 C by a hyperbola

$$3x^2 + 3y^2 - 10xy = 8A^2 \quad \ldots\ldots\ldots\ldots\ldots\ldots (16)$$

where

$x = \ln (t/\tau)$,
$y = \ln (\varepsilon/\lambda)$,

$\tau = \exp [D(\theta) + E(\theta)\sigma]$, and
$\lambda = \exp [B + C\,\sigma)$,

A, B, C, $D(\theta)$, $E(\theta)$ being material constants.

The termination of creep curves may be defined where they are cut by a locus of rupture parameter, one suitable correlation[7] for Nimonic 90 being that proposed by Conrad [*123,124*]

$$t_{\text{rup}} = \exp [A + B/\theta + C(\theta)\,\sigma] \quad \ldots\ldots\ldots\ldots\ldots\ldots (17)$$

based on a dislocation model for creep proposed by Weertman [*123*], Clarke's representation also being related to this model.

The quality of creep data representation obtained with the models just described is illustrated in Fig. 7, together with manufacturers data for short time hot tension tests, the characteristic ductility trough of this material being apparent in both instances.

For multiaxial creep behavior, ductility fraction may be employed as a structure parameter until better formulations are forthcoming, for Goldhoff [127] has shown that it gives reasonable predictions for tensile loading. Accumulation of damage is treated as a separate phenomenon from creep deformation; the concept of tensile ductility fraction

$$f_{td} = \sum \frac{\Delta \varepsilon_{\text{tensile}}}{\varepsilon_{\text{tensile rupture}}}$$

being adopted, this being summed independently in three principal directions, but only when strain increments are tensile. The assumption recognizes damage due to growth of cavities, but may not properly allow for resintering of voids on a stress free temperature hold, or their reduction due to action of compressive stress.

Application of such creep data to prediction of short time hot tension tests is illustrated in Fig. 8. Similar predictions using a Graham-Walles creep equation with a strain hardening structure parameter and supported by experimental results have been recently presented by Tilly [*46*].

Figure 9 illustrates results of predictions on four types of fatigue loading, cycles (*a*) and (*b*) leading to cyclic straining, cycles (*c*) and (*d*) to strain ratchetting. Life predictions are presented on the basis of accumulation of damage only during the tensile part of each cycle. The effect of different holdtimes can be seen, although the small number of cycles may distort values of time to failure somewhat.

Finally, for a multiaxial situation, Fig. 10 shows prediction of behavior of a Nimonic 90 tube subject to internal pressure and end load. In this computation the standard incremental method of Illyushin [*129*] was employed, with automatic time interval control and temperature dependent

[7] Recent papers by Grounes [*125,126*] are useful starting points for a survey of the extensive literature on rupture parameters.

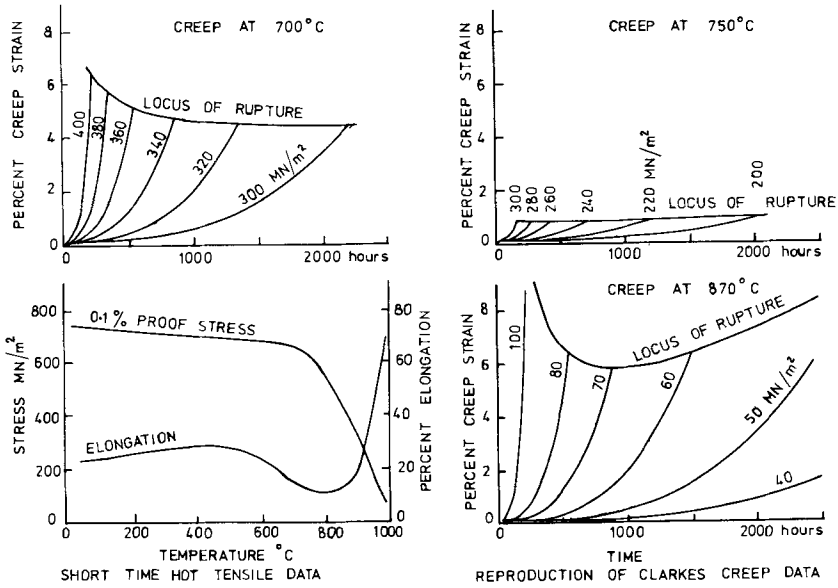


FIG. 7—*Tensile creep curves at 700, 750, and 870 C generated from Clarkes equations together with published data on short-time hot-tension tests.*

material properties. Tensile ductility fractions were summed separately for radial, tangential, and axial directions across the wall. If cracking in multiaxial systems is by tensile rupture of undamaged material between cavities, then continuum stresses σ have to be modified to obtain effective stresses $\hat{\sigma} = \sigma/(1 - f_{td})$. Such computations indicate time, location, and direction of initiation and propagation, and might be regarded as predicting the beginning of the end of in-service life, although remaining material may accept additional load for some time.

For practical applications there is no problem in accommodating time-dependent load and temperature histories with built-in automatic time interval control in the computer program. Work on finite element methods of design in many laboratories is known to be in progress.

Industrial Practice

It is of interest to compare the methods already summarized in previous sections with the type of design procedures used in the turbine industry.

Since the highest thermal stresses in steam power plants occur during start up and shut down, the aim of the analysis must be to match design and operating conditions to ensure maximum flexibility of operating procedures with no cracking. The first consideration in design analysis is that of creep, using static creep rupture strength data for 200 000 h and relevant factors on the allowable stress. If this creep strength is inadequate the designer can

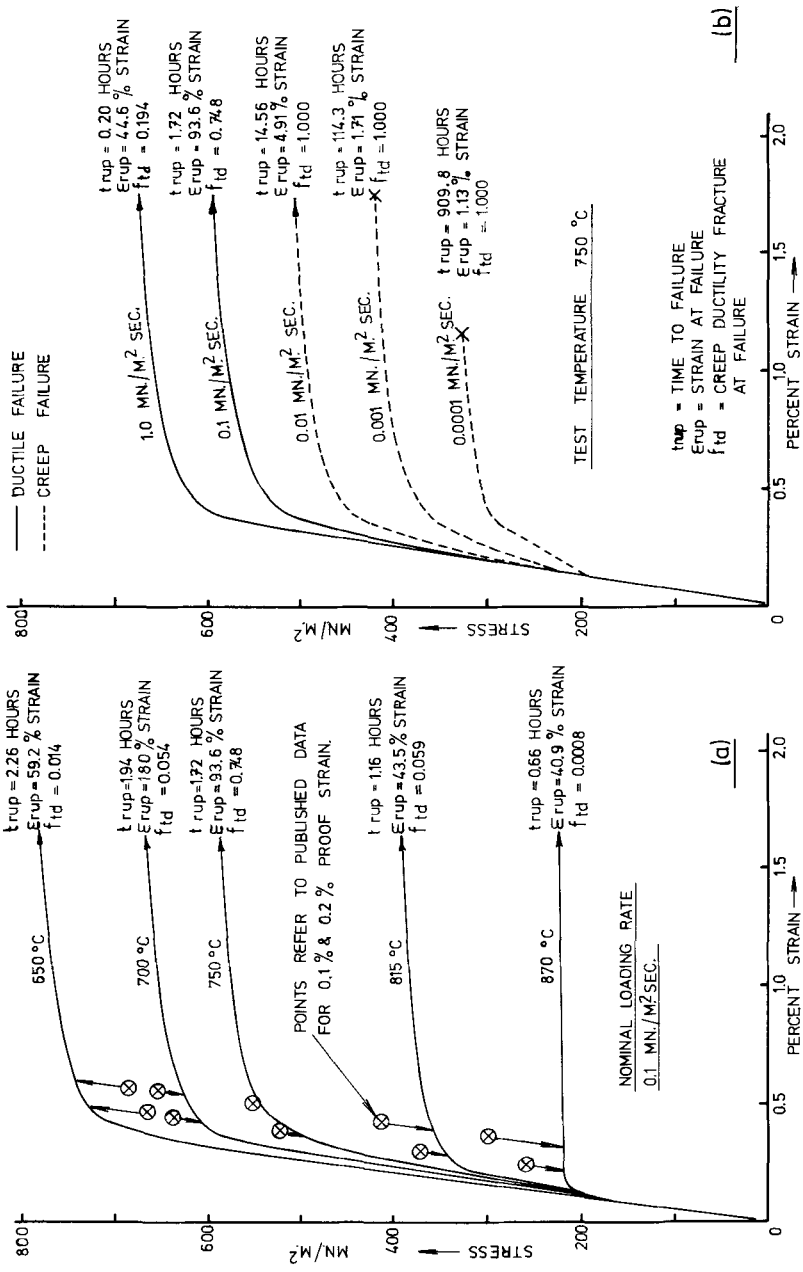


FIG. 8—*Tensile ramp loading behavior of Nimonic 90 prepared from creep data.*

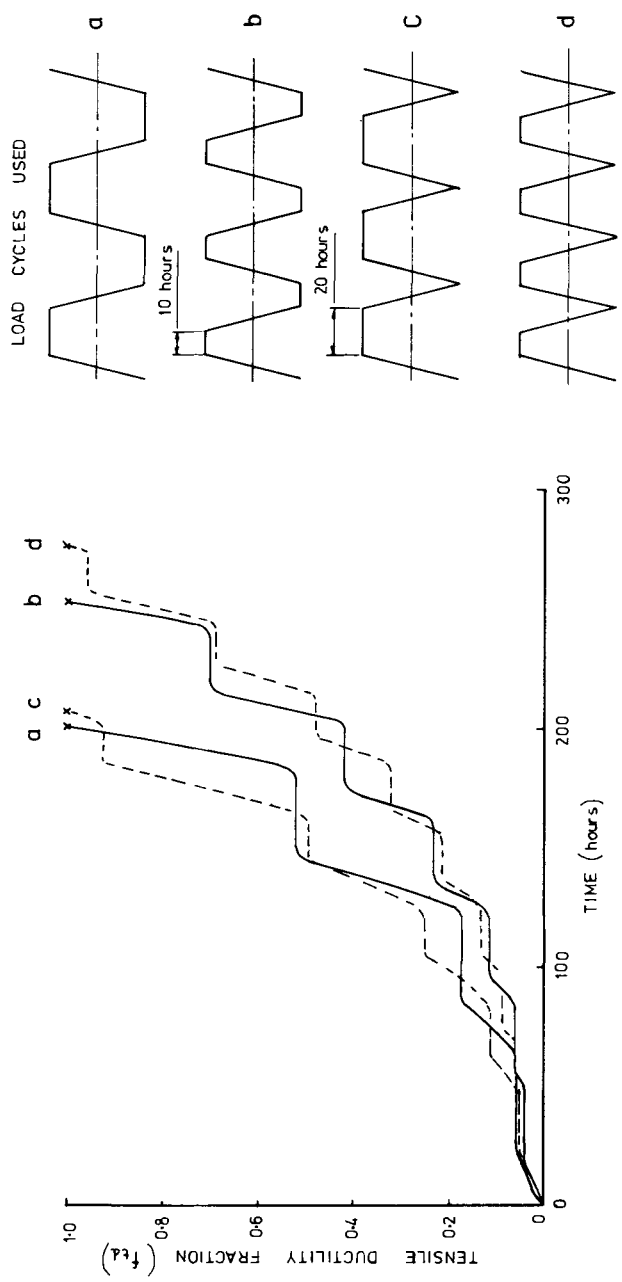


FIG. 9—*Predicted tensile ductility fraction* f_{td} *for Nimonic 90 during uniaxial load cycling at nominal stress range of* ± 200 *MN/m² peak to peak.*

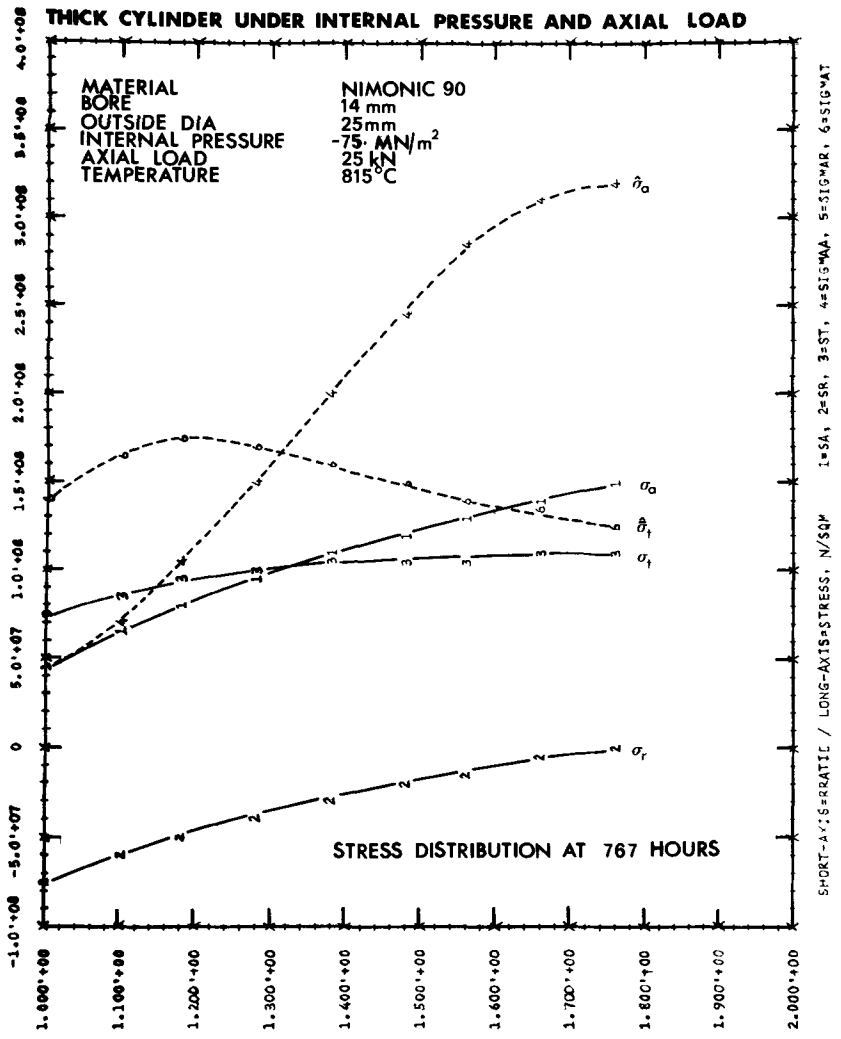


FIG. 10—*Thick cylinder under internal pressure and axial load.*

either thicken the section or, better still, modify the steam flows; usually larger thermal strains are observed in thicker sections.

It is useful to compare laboratory type cycles with actual service conditions in the same manner as Timo [*25*] since the similarity depends on the severity of the load change. For severe start up with fast temperature changes and large thermal gradients, gross compressive yielding of the component surface can occur with the strain range $\Delta\epsilon_T > 0.01$. A tensile residual stress exists when the start up is completed and subsequent creep relaxation occurs during the hold period. On shut down, a fast load de-

crease causes the surface to go further into tension. This severe type of cycle is not easy to simulate accurately and fortunately occurs infrequently so that damage from this source is relatively small; say 10 percent of the total cyclic life damage in the component. Hence, it is reasonable to analyze these cycles accurately though conservatively by assuming that the entire holdtime is spent at maximum tensile strain. In a mild loading cycle the thermal gradients are lower, and strain ranges are below yield so that $\Delta\epsilon_T < 0.001$ and there are no residual stresses. Since there are only negligible tensile stresses during the hot period, the cycle is considered to have no true holdtime but simply has a slow cycling rate. Because in practice this cycle time in service (approximately 1 h) is greater than in a zero hold laboratory test, it is reasonable to consider an effective holdtime of $1/2$ h at maximum strain (Fig. 4) as being representative of service conditions.

Hence to apply laboratory type cyclic hold data to actual service conditions the following procedure was followed. In the high-strain region $\Delta\epsilon_T > 0.01$ the laboratory data for the appropriate holdtime was used; it is assumed usually to be relatively insensitive to temperature. Then the curve (Fig. 4) is extended through the intermediate strain range region and blended into the $1/2$-h holdtime curve at low-strain ranges ($\Delta\epsilon_T < 0.001$).

This approach has been used by both Timo (General Electric Co., U.S.A.) and Dawson (General Electric Co., Ltd., England) though there is a difference in the manner in which the holdtime data for the longer holdtime and lower strain ranges are obtained. Timo extrapolates to lower strain ranges by use of creep rupture data (Fig. 4) as mentioned previously. However, Dawson extrapolates to longer holdtimes at given strain ranges by using the log N_f versus log holdtime plots which he assumes to be linear; the $1/2$-h holdtime data at all strains is obtained by direct testing to typically 5000 cycles, and since there is no need to go beyond 10^4 cycles there is little extrapolation.

To allow for the presence of notches the nominal strain range is multiplied by the elastoplastic strain concentration factor K_ϵ [*50,54*] to obtain the local strain range, and this value then is used to obtain the life from the smooth laboratory $\Delta\epsilon_T$ versus N data (Fig. 4). Design examples using the methods described in this section have been described by Timo [*25,131, 132*] and Dawson [*130,133,134*].

As Timo pointed up, this approach contains many approximations but such is the variability in material properties, the uncertainty in the thermal stress analysis, the variations in the actual service cycles, the effects of biaxiality, and strain concentrations, etc. It is clear that a more exact method is neither possible nor necessary at the present time.

Within the Central Electricity Generating Board (CEGB) United Kingdom, an attempt is being made to determine more accurately the stresses, strains, and temperatures occurring in service. Strain gages and thermocouples have been applied to sets to measure service strains at particular

locations so that extrapolation can be attempted to more difficult points; it has not always been easy to assess the accuracy of such an approach in service. In addition, laboratory thermoplastic model tests to a scale of 6:1 are being carried out with hot air applied to various inlets to simulate the service temperature distribution. Strains are measured by means of strain gages. Finite element programs are also in use, but cyclic plasticity and creep in three dimensions still presents difficulties.

Discussion

A survey of the field shows so many different types of tests that some care must be exercised when comparing results especially when hold periods are present. The difference in trends for the longer holdtimes between results from push-pull axial and reversed bend tests has been noted already in Fig. 1; this may be due to stress redistribution in the bend test which is difficult to interpret. However, the hourglass type of axial specimen has also come in for some comment [*4, 137*], and an axial specimen with a straight cylindrical gage length may offer some advantage. Also when comparing results the definition of failure is clearly important [*53*] since cracks may be present for a substantial fraction of life. There are nearly as many failure definitions as there are tests; rapid load decay, percentage load drop, crack side movement, predetermined crack length, rupture, and leakage.

Often the total damage appears to be due either to cyclic processes or time-dependent processes. [*37,46,138*]. When frequency or temperature is varied in a series of tests there is usually a sharp transition in behavior, the range in which fatigue and creep combine being short (Fig. 5). Indeed, for wedge specimens subject to thermal fatigue a straightforward creep analysis [*38,39*] predicted the number of cycles to failure extremely well. Spera makes the comment that thermal fatigue resistance is improved by increasing the creep rupture strength. In any event the linear damage rule gives a good indication of the life under combined fatigue and creep, and thankfully there appears to be little evidence of a harmful interaction except for a few results presented by Wood [*33*], Ellison [*139*], and Tilly [*45*]. In some circumstances an analysis based solely on creep behavior may thus be appropriate.

An interesting approach by Manson et al [*140*] termed "strain range partitioning" is based on the hypothesis that it is the capacity of the material to absorb inelastic strain, whether it be plastic flow or creep, which governs high-temperature cyclic behavior. In effect, this experimental approach determines which part of the cycle is more damaging for a particular material, and is described by Halford, Hirschberg, and Manson.[8] However, a disadvantage of the method is that certain temperature-load cycles do not lend themselves readily to partitioning. In such

[8] See p. 744.

cases, analysis using properly formulated constitutive equations is the alternative.

The effect of environment is obviously important judging from results already noted in the laboratory [*56,59*]. The part of the cycle which is most damaging has just been described, but we should also consider how damaging are such time-dependent processes as oxidation. Since it is known that environment has a considerable effect on the crack propagation rate, it is probable that damage is directed towards the crack tip; however, there is some evidence that initiation is also very much affected. Clearly present understanding of the relative magnitudes of damage caused by environment and other mechanical processes is not good.

A question may be raised as to what the service cycle describing stress, strain, and temperature in a structure looks like. Many advances have been made with finite element type analyses for calculating thermal strains with time during the cycle, but a few good experimental results would be invaluable as checks on assumptions. Good material behavior data are essential, but predictions of service life can only be carried out accurately if the service conditions are known.

In recent years creep design for high-temperature conditions has seen the introduction of simple analytical techniques [*141*] based on reference stress concepts, in parallel with the fuller continuum approach combining properly formulated constitutive equations with numerical computation. In this paper an attempt has been made to highlight a similar two-level attack currently developing in the prediction of low-cycle fatigue behavior at elevated temperatures. Each approach will find its place in the spectrum of problems to be solved.

APPENDIX A

Fundamental Relationships of Continuum Theory

Kinematics—the Geometry of Deformation

$$\varepsilon_{ij} = \frac{1}{2}\left(\frac{\partial u_i}{\partial x_j} + \frac{\partial u_j}{\partial x_i}\right)$$

Basic Axioms—Physical Principles

Conservation of mass:

$$\frac{D\rho}{Dt} + \rho \frac{\partial \dot{u}_i}{\partial x_i} = 0 \qquad (18)$$

Balance of linear momentum:

$$\rho \frac{D\dot{u}_i}{Dt} = \frac{\partial \sigma_{ij}}{\partial x_j} + \rho b_i \quad \ldots\ldots\ldots\ldots\ldots\ldots\ldots\ldots\ldots\ldots (19)$$

Balance of moment of momentum:

$$\epsilon_{ijk} \times \sigma_{kj} = 0 \qquad \text{(for nonpolar materials only)}^{9} \quad \ldots\ldots\ldots\ldots (20)$$

Balance of total (mechanical + thermal) energy:

$$\rho \frac{D\hat{U}}{Dt} + \rho \dot{u}_i \frac{D\dot{u}_i}{Dt} = \frac{\partial}{\partial x_j} (\sigma_{ij}\, \dot{u}_i) + \rho \dot{u}_i\, b_i + \hat{r} - \frac{\partial q_i}{\partial x_i} \quad \ldots\ldots\ldots\ldots (21)$$

Growth of entropy inequality:

$$-\rho \left(\hat{S} \frac{D\theta}{Dt} + \frac{DF}{Dt} \right) + \sigma_{ij} \frac{\partial \dot{u}_i}{\partial x_j} - \frac{q_i}{\theta} \times \frac{\partial \theta}{\partial x_i} \geq 0 \quad \ldots\ldots\ldots\ldots\ldots (22)$$

where the Helmholtz function $F = u - \theta \hat{S}$ is introduced in place of $\hat{U}$.

[9] Equation 20 implies symmetry of the stress tensor $\sigma_{ij} = \sigma_{ji}$.

TABLE 1—*Coupled theory.*

Equations		Unknowns	
Axiomatic:			
Mass	1	1 Density	ρ
Linear momentum	3	3 Velocity components	$\dot{u}_i$
Moment momentum	[a]	6 Stress components	σ_{ij}
Energy	1	1 Specific internal energy	$\hat{U}$
Constitutive:		3 Heat flux vector components	q_i
Stress/strain	6	1 Temperature	θ
Thermal (Fourier's law)	3	1 Specific entropy	$\hat{S}$
Caloric (energy)	1		
Entropic (entropy)	1		
Equations 16 $\leftrightarrow$ 16 Unknowns			

[a] For nonpolar theory the moment of momentum equation plays the role of reducing the number of unknown stress components to 6 and the number of stress/strain constitutive equations required to 6 also.

Nomenclature not included in Table 1:

ε_{ij} = strain component in ij direction,
t = time,
x_i = distance,
b_i = body forces
ϵ_{ijk} = $\frac{1}{2}(i - j)(j - k)(k - i)$ $\quad (i,j,k = 1, 2, 3,)$ and
$\hat{r}$ = distributed heat sources.

APPENDIX B

Uncoupling of Balance of Energy Equation

Total balance:

$$\rho \frac{D\hat{U}}{Dt} + \rho \dot{u}_i \frac{D\dot{u}_i}{Dt} = \frac{\partial}{\partial x_j}(\sigma_{ij}\,\dot{u}_i) + \rho \dot{u}_i\, b_i + \hat{r} - \frac{\partial q_i}{\partial x_i} \quad \ldots\ldots (23)$$

Mechanical balance:

$$\rho \dot{u}_i \frac{D\dot{u}_i}{Dt} = \frac{\partial}{\partial x_j}(\sigma_{ij}\,\dot{u}_i) + \rho \dot{u}_i\, b_i - \sigma_{ij} \frac{\partial \dot{u}_i}{\partial x_j} \quad \ldots\ldots (24)$$

Thermal balance:

$$\rho \frac{D\hat{U}}{Dt} = -\frac{\partial q_i}{\partial x_i} + \hat{r} + \sigma_{ij} \frac{\partial \dot{u}_i}{\partial x_j} \quad \ldots\ldots (25)$$

This last equation is convertible into the recognizable conduction equation:

$$\rho\, C_\sigma \frac{\partial \theta}{\partial t} = \frac{\partial}{\partial x}\left(k_x \frac{\partial \theta}{\partial x}\right) + \frac{\partial}{\partial y}\left(k_y \frac{\partial \theta}{\partial y}\right) + \frac{\partial}{\partial z}\left(k_z \frac{\partial \theta}{\partial z}\right) + \hat{r} \quad \ldots\ldots (26)$$

TABLE 2—*Uncoupled theory—stress field.*

Equations		Unknowns	
Axiomatic:			
Mass	1	1 Density[b]	ρ
Linear momentum	3	3 Velocity components	$\dot{u}_i$
Moment momentum	[a]	6 Stress components	σ_{ij}
Constitutive:			
Stress/strain	6		
Equations 10 $\leftrightarrow$ 10 Unknowns			

[b] Normally in small deformation theory of solids, density is assumed to be a prescribed constant. Hence, conservation of mass need not be invoked, and ρ may be deleted as an unknown.

TABLE 3—*Uncoupled theory—temperature field.*

Equations		Unknowns	
Axiomatic:			
Thermal energy	1	1 Temperature	θ
Constitutive:		3 Heat flux vector components	q_i
Thermal (Fourier's law)	3		
Equations 4 $\leftrightarrow$ 4 Unknowns			

References

[1] Manson, S. S., *Thermal Stress and Low Cycle Fatigue*, McGraw-Hill, New York, 1966.

[2] Coffin, L. F. and Goldhoff, R. M., Report No. 71-C-114, General Electric Company, April 1971.

[3] Ellison, E. G., *Journal of Mechanical Engineering Science*, Vol. 11, No. 3, 1969, p. 318.

[4] Miller, K. J., CUED/C-Mat/TRI, Cambridge University, Cambridge, England, 1969.

[5] White, D. J. in *Thermal Stresses and Thermal Fatigue*, Central Electricity Generating Board, Berkeley, Butterworth, London, Paper 1, Sept. 1969, p. 3.

[6] Edmunds, H. G. and White, D. J., *Journal of Mechanical Engineering Science*, Vol. 8, No. 3, 1966.

[7] Krempl, E. and Walker, C. D. in *Fatigue at High Temperature, ASTM STP 459*, American Society for Testing and Materials, 1968, p. 75.

[8] Dawson, R. A. T., Elder, W. J., Hill, G. J., and Price, A. T. in *Proceedings*, International Conference on Thermal and High Strain Fatigue, Institute of Metals, London, 1967, p. 239.

[9] Walker, C. D., *International Conference on Creep*, Paper 24, 3.49, Institute of Mechanical Engineers, London, 1963.

[10] Berling, J. T. and Conway, J. B. in *First International Conference on Pressure Vessel Technology*, Part II, Delft, Holland, Sept. 1969, p. 96.

[11] Wells, C. H. and Sullivan, C. P. in *Fatigue at High Temperature, ASTM STP 459*, American Society for Testing and Materials, 1968, p. 59.

[12] Conway, J. B., Berling, J. T., and Stentz, R. H. in *Thermal Stress and Thermal Fatigue*, Central Electricity Generating Board, Berkeley, Butterworth, London, Paper 7, Sept. 1969, p. 89.

[13] Coles, A. D., Hill, G. J., Dawson, R. A. T., and Watson, S. J. in *Proceedings*, International Conference on Thermal and High Strain Fatigue, Institute of Metals, London, 1967, p. 270.

[14] Coles, A. D. and Skinner, D., *Journal of the Royal Aeronautical Society*, Vol. 69, Jan. 1965, p. 53.

[15] Tompkins, B., *Philosophical Magazine*, Vol. 18, 1969, p. 1041.

[16] Coffin, L. F., Jr., in *Proceedings*, Air Force Conference on Fatigue and Fracture of Aircraft Structure and Materials, AFFDL TR 70-144, Air Force Flight Dynamics Laboratory, 1970.

[17] Coffin, L. F., Jr., *Journal of Materials*, Vol. 6, No. 2, 1971, p. 388.

[18] Eckel, J. R., *Proceedings*, American Society for Testing and Materials, Vol. 51, 1951, p. 745.

[19] Morrow, J. in *Internal Friction, Damping, and Plasticity, ASTM STP 378*, American Society for Testing and Materials, 1965, p. 45.

[20] Langer, B. F., *Journal of Basic Engineering*, Series D, *Transactions*, American Society of Mechanical Engineers, Vol. 84, 1962, p. 389

[21] Berling, J. T. and Slot, T. in *Fatigue at High Temperature, ASTM STP 459*, American Society for Testing and Materials, 1969, p. 3.

[22] Cammett, J. T., R69AEG-332, General Electric Co., Cincinnati, Ohio, 1969.

[23] Manson, S. S., *Experimental Mechanics*, Vol. 5, No. 7, 1965, p. 193.

[24] Manson, S. S., *International Journal of Fracture Mechanics*, Vol. 2, No. 1, 1966, p. 327.

[25] Timo, D. P. in *Thermal Stresses and Thermal Fatigue*, Central Electricity Generating Board, Berkeley, Butterworth, London, Paper 28, Sept. 1969, p. 453.

[26] Robinson, E. L., *Transactions*, American Society for Mechanical Engineers, Vol. 74, 1952, p. 777.

[27] Taira, S. in *Creep in Structures*, N. J. Hoff, ed., Academic Press, New York, 1962.

[28] Esztergar, E. P. and Ellis, J. R. in *Thermal Stresses and Thermal Fatigue*, Central Electricity Generating Board, Berkeley, Butterworth, London, Paper 10, Sept 1969, p. 128.

[29] Lazan, B. J., *Proceedings*, American Society for Testing and Materials, Vol. 49, p. 757.

[30] Taira, S. and Koterazawa, R. in *Proceedings*, 4th Japanese Congress on Testing Materials, 1961, p. 50.

[31] Zamrik, S. V. and Shewchuk, J. in *1st International Conference on Pressure Vessel Technology*, Part II, Delft, Holland, Sept. 1969, p. 89.
[32] Swindeman, R. W., International Conference on Creep, Institute of Mechanical Engineering, *Proceedings*, Vol. 178, Part 3A, 1963–1964, pp. 3–71.
[33] Wood, D. S., *Welding Journal Research Supplement*, Feb. 1966.
[34] Manson, S. S. and Halford, G. R. in *International Conference on Thermal Stresses and High Strain Fatigue*, Institute of Metals, London, 1967, p. 154.
[35] Spera, D. A. NASA TMX-52558, National Aeronautics and Space Administration, 1969.
[36] Halford, G. R., NASA-TN-D-6309, National Aeronautics and Space Administration, May 1971.
[37] Manson, S. S., Halford, G. R., and Spera, D. A. in *A. E. Johnson Memorial Volume*, A. I. Smith and A. M. Nicholson, eds., Applied Science Publishers, 1971, Chapter 12, p. 31.
[38] Spera, D. A. Howes, M. A. H., and Bizon, P. T., NASA TMX-52975, National Aeronautics and Space Administration, 1971.
[39] Spera, D. A., NASA SP-227, National Aeronautics and Space Administration, 1969.
[40] Carden, A. E. and Slade, T. B. in *Fatigue at High Temperature*, *ASTM STP 459*, American Society for Testing and Materials, 1968, p. 111.
[41] Marshall, P. and Cook, T. R., *Thermal Stresses and Thermal Fatigue*, Central Electricty Generating Board, Berkeley, Butterworth, London, Paper 6, Sept. 1969, p. 81.
[42] Walter, D. J., Report RD/B/N1214, Central Electricity Generating Board, 1969.
[43] Tilly, G. P., *Proceedings*, Institute of Mechanical Engineering, Vol. 180, Part 31, 1966, p. 403.
[44] Tilly, G. P., *Proceedings*, Institute of Mechanical Engineering, Vol. 180, Part 1, No. 46, 1966, p. 1045.
[45] Tilly, G. P. in *International Conference on Thermal and High Fatigue*, Institute of Metals, London, 1967, p. 198.
[46] Tilly, G. P., *Journal of Strain Analysis*, Vol. 7, No. 1, 1972, p. 61.
[47] Miller, K. J. and Rizk, M. N., *Journal of Strain Analysis*, Vol. 3 No. 4, 1968, p. 273.
[48] Morrow, J. D., Wetzel, R. M., and Topper, T. H. in *Effects of Environment and Complex Load History on Fatigue Life*, *ASTM STP 462*, American Society for Testing and Materials, 1968, p. 74.
[49] Neuber, H., *Journal of Applied Mechanics*, Dec. 1961, p. 544.
[50] Stowell, E. Z., NASA TN 2073, National Aeronautics and Space Administration, 1950.
[51] Box, W. A., *Proceedings*, Society for Experimental Stress Analysis, Vol. 8, No. 2, 1951, p. 99.
[52] Baron, H. G. and Brine, F. E. in *Proceedings*, International Conference on Thermal and High Strain Fatigue, Institute of Metals, London, 1967, p. 113.
[53] Krempl, E. in *1st International Conference on Pressure Vessel Technology*, American Society of Mechanical Engineers, Part II, Delft, Holland, Oct. 1969, p. 1319.
[54] Zwicky, E. E., Paper 67-WA/PVP-6, American Society for Mechanical Engineers, 1967.
[55] Martin, D. E., *Journal of Basic Engineering*, Series D, *Transactions*, American Society for Mechanical Engineers, Vol. 87, 1965, p. 850.
[56] White, D. J., *Proceedings*, Institute of Mechanical Engineers, Vol. 184, Part 1, No. 12, 1969–1970.
[57] Coffin, L. F., Jr., *Transactions*, American Society for Metals, Vol. 56, 1963, p. 339.
[58] McMahon, C. J. and Coffin, L. F., Jr., *Metallurgical Transactions*, Vol. 1, Dec. 1970, p. 3443.
[59] Coffin, L. F., Jr., TIS Report No. 71-C-108, General Electric Company, April 1971.
[60] Achter, M. R. in *Fatigue Crack Propagation*, *ASTM STP 415*, American Society for Testing and Materials, 1967, p. 181.
[61] Stegman, R. L. and Shahinian, P. in *Fatigue at High Temperature*, *ASTM STP 459*, American Society for Testing and Materials, 1968, p. 42.
[62] Nachtigall, A. J., Klima, S. J., Freche, J. C., and Hoffman, C. A., NASA TN-D2898, National Aeronautics and Space Administration, June 1965.

[63] Smith, H. H. and Shahinian, P. in *Effects of Environment and Complex Load History on Fatigue Life, ASTM STP 452*, American Society for Testing and Materials, 1968, p. 217.
[64] Walton, D. and Ellison, E. G., *International Metallurgical Reviews*, June 1972.
[65] LeMay, I., Truss, K. J., and Sethi, P. S., American Society of Mechanical Engineers, 69-Met-3, Metallurgical Engineering and Pressure Vessel and Piping Conference, March 1969, Washington, D. C.
[66] Laird, C. in *Fatigue Crack Propagation, ASTM STP 415*, American Society for Testing and Materials, 1967, p. 131.
[67] Smith, E. and Barnaby, J. T., *Metal Science Journal*, Vol. 1, 1967, p. 56.
[68] Laird, C. and Krause, A. R., *International Journal of Fracture Mechanics*, Vol. 4, 1968, p. 219.
[69] Laird, C. and Smith, G. C., *Philosophical Magazine*, Series 8, Vol. 8, 1964, p. 1945.
[70] Marsh, K. J., Report 373, National Engineering Laboratory, Nov. 1968.
[71] Marsh, K. J., Appendix to NEL Progress Report 1967–1968, "Strength of Components," Report 402, National Engineering Laboratory, March 1969.
[72] Paris, P. and Erdogan, F., *Transactions*, American Society for Mechanical Engineers, Vol. 85, 1963, p. 528.
[73] Tompkins, B., Sumner, G., and Wareing, J., *Proceedings*, 2nd International Conference on Fracture, Paper 62, 1969.
[74] Crooker, T. W. and Lange, E. A. in *Fatigue Crack Propagation, ASTM STP 415*, American Society for Testing and Materials, 1966, p. 94.
[75] Jerram, K. in *Fatigue of Welded Structures*, Conference, The Welding Institute, Paper 2, 1970, p. 18.
[76] Maddox, S. J. in *Fatigue of Welded Structures*, Conference, The Welding Institute, Paper 6, 1970, p. 73.
[77] Ellison, E. G. and Walton, D., Joint International Conference, "Creep and Fatigue in Elevated Temperature Applications," Philadelphia/Sheffield, 1973/74, ASTM/ASME, Institute of Mechanical Engineering.
[78] Smith, E. M., Grant, C., and Booth, J. M., *Journal of Strain Analysis*, Vol. 5, No. 2, 1970, p. 145.
[79] Townley, C. H. A. and Poynor, J. F., *Pressure Vessel Engineering Technology*, Elsevier, Amsterdam, Chapter 3, 1971.
[80] Truesdell, C. in *Non-equilibrium Thermodynamics, Variational Techniques and Stability*, Donnelly, Herman, and Prigogine, eds., University of Chicago Press, Chicago, Ill., 1965, p. 101.
[81] Coleman, B. D., *Archive for Rational Mechanics and Analysis*, Vol. 17, No. 1, 1964, p. 1.
[82] Coleman, B. D., *Archive for Rational Mechanics and Analysis*, Vol. 17, No. 3, 1964, p. 230.
[83] Pipkin, A. C. and Rogers, T. G., *Journal of the Mechanics and Physics of Solids*, Vol. 16, 1968, p. 59.
[84] Onaran, K. and Findley, W. N., *Transactions of the Society of Rheology*, Vol. 9, Part 2, 1965, p. 299.
[85] Onaran, K. and Findley, W. N., *Journal of Applied Mechanics*, Paper 70-WA/APM-21.
[86] Blass, J. J. and Findley, W. N., *Journal of Applied Mechanics*, Paper 70-WA/APM-41.
[87] Lockett, F. J., *International Journal of Engineering Science*, Vol. 3, 1965, p. 59.
[88] Wang, C. C. and Bowen, R. M., *Archive for Rational Mechanics and Analysis*, Vol. 22, 1966, p. 79.
[89] Rabotnov, Y. N., *Creep Problems in Structural Members*, North Holland, Amsterdam, 1969, p. 234.
[90] Rabotnov, Y. N. in *Advances in Creep Design*, A. I. Smith and A. M. Nicholson, eds. Applied Science Publishers, 1971, p. 3.
[91] Grant, C., Course on Continuum Engineering, University of Newcastle upon Tyne, England, March 1971.
[92] Odqvist, F. K. G. in *Advances in Creep Design*, A. I. Smith and A. M. Nicholson, eds., Applied Science Publishers, London, 1971, p. 31.

[93] Green, A. E. and Naghdi, P. M., *Archive for Rational Mechanics and Analysis*, Vol. 18, No. 4, 1965, p. 251.
[94] Green, A. E. and Naghdi, P. M. in *Proceedings IUTAM Symposia*, Vienna, 22–28 June 1966, Springer Verlag, Berlin, p. 117.
[95] Conrad, H. in *Mechanical Behavior of Materials at Elevated Temperature*, J. E. Dorn, ed., McGraw Hill, New York, Chapter 8, 1961, p. 149.
[96] Kennedy, A. J., *Processes of Creep and Fatigue in Metals*, Oliver and Boyd, Edinburgh, 1962.
[97] Webster, G. A. and Piearcey, B. J., *Metal Science Journal*, Vol. 1, 1967, p. 97.
[98] Tilly, G. P., *Journal of Physics E. Scientific Instruments*, Vol. 3, 1970, p. 292.
[99] Lagneborg, R., *Journal of Basic Engineering*, Series D, *Transactions*, American Society of Mechanical Engineers, Paper 71-Met.-F.
[100] Gittus, J. H., *Philosophical Magazine*, Vol. 23, 1971, p. 1281.
[101] Gittus, J. H., *Philosophical Magazine*, Vol. 24, 1971, p. 1423.
[102] Beevers, C. J. in *High Temperature Materials; The Controlling Physical Properties*, A. J. Kennedy, ed., Oliver and Boyd, Edinburgh, 1968, p. 77.
[103] McLean, D., *Journal of the Institute of Metals*, Vol. 85, No. 1, 1956, p. 468.
[104] Smith, E. and Barnaby, J. T., *Metal Science Journal*, Vol. 1, 1967, p. 1,
[105] Gifkins, R. C., Gittens, A., Bell, R. L., and Langdon, T. C., *Journal of Materials Science*, Vol. 3, 1968, p. 306.
[106] Toft, L. H. and Broom, T. International Conference on Creep, New York and London, *Proceedings*, Institute of Mechanical Engineers, Vol. 178, Part 3A, 1963–1964, p. 3.
[107] Ishida, Y. and McLean, D., *Metal Science Journal*, Vol. 1, 1967, p. 171.
[108] Woodford, D. A., *Metal Science Journal*, Vol. 3, 1969, p. 234.
[109] Dyson, B. F. and McLean, D., IMS Internal Report 44, National Physics Laboratory, 1971.
[110] Day, M. F. and Cumming, W. M., *Journal of Mechanical Engineering Science*, Vol. 10, No. 1, 1968, p. 36.
[111] Gittens, A., *Metal Science Journal*, Vol. 1, 1967, p. 214.
[112] Walker, G. K., Evans, H. E., and Waddington, J. S. in *Thermal Stresses and Thermal Fatigue*, Central Engineering Generating Board, Butterworth, London, Paper 19, Sept 1969, p. 157.
[113] Davies, P. W., Dennison, J. P., and Evans, H. E., *Journal of the Institute of Metals*, Vol. 94, 1968, p. 270.
[114] Rabotnov, Y. N., International Conference on Creep, *Proceedings*, Institute of Mechanical Engineering, Vol. 178, Part 3A, 1963–1964, p. 2.
[115] Leckie, F. A., BISRA Symposium on the Presentation of Creep Strain Data, Sheffield, England, Oct. 1971.
[116] Bowring, P., Davies, P. W., and Wiltshire, B., *Metals Science Journal*, Vol. 2, 1968, p. 168.
[117] Speight, M. V. and Harris, J. E., *Metal Science Journal*, Vol. 1, 1967, p. 83.
[118] Smith, A. E. and Henderson, J. in *Advances in Creep Design*, A. I. Smith and A. M. Nicholson, eds., Applied Science Publishers, London, 1971, p. 459.
[119] Taira, S. and Ohtani, R. in *Advances in Creep Design*, A. I. Smith and A. M. Nicholson, eds., Applied Science Publishers, London, p. 289.
[120] Finnie, I. and Abo el Ata, M. M. in *Advances in Creep Design*, A. I. Smith and A. M. Nicholson, eds., Applied Science Publishers, London, 1971, p. 329.
[121] Clarke, J. M., Report 284, National Gas Turbine Establishment, Sept. 1966.
[122] Conrad, H., *Journal of Basic Engineering*, Series D, *Transactions*, American Society of Mechanical Engineers, Vol. 81, Paper 58-A-96, 1959.
[123] Weertman, J., *Journal of Applied Physics*, Vol. 28, 1957, p. 1185.
[124] Conrad, H., *Journal of the Institute of Metals*, Vol. 87, 1958–1959, p. 347.
[125] Grounes, M., *Journal of Basic Engineering*, Series D, *Transactions*, American Society of Mechanical Engineers, Paper 69-Met.-A.
[126] Grounes, M., *Journal of Basic Engineering* Series D, *Transactions*, American Society of Mechanical Engineers, Paper 69-Met.-B.

[*127*] Goldhoff, R. M., *Journal of Basic Engineering*, Series D, *Transactions* American Society of Mechanical Engineers, June 1965, p. 374.
[*128*] Christensen, R. H. and Harman, M. B. in *Fatigue Crack Propagation, ASTM STP 415*, American Society for Testing and Materials, 1967, p. 5.
[*129*] Illyushin, A. A., *Journal of Applied Mathematics and Mechanics*, Vol. 7, 1943.
[*130*] Dawson, R. A. T. in *Proceedings*, International Conference on Thermal and High Strain Fatigue, Institute of Metals, London, 1967, p. 40.
[*131*] Ipsen, P. G. and Timo, D. P., 1969 American Power Conference, General Electric Company.
[*132*] Timo, D. P. and Sarney, G. W., American Society for Mechanical Engineers, Paper No. 67-WA/PWR-4, 1967.
[*133*] Dawson, R. A. T. and Neill, D. A. in *Thermal Stress and Thermal Fatigue*, Central Electricity Generating Board, Berkeley, Butterworth, London, Paper 27, Sept. 1969, p.439.
[*134*] Dawson, R. A. T. et al, General Electric Company Power Engineering, three unpublished reports, Aug. 1968; Feb. 1970; and March 1970.
[*135*] David, T. J. *Proceedings of the Society for Experimental Stress Analysis*, Vol. 8, No. 1, 1971, p. 185.
[*136*] Proctor, E. and Mitchell, D. H. in *Thermal Stress and Thermal Fatigue*, Central Electricity Generating Board, Berkeley, Butterworth, London, Paper 15, Sept. 1969, p. 229.
[*137*] Private communication, J. Miller, unpublished General Electric Report, 1965.
[*138*] Miller, K., *Journal of Strain Analysis*, Vol. 5, No. 3, 1970, p. 185.
[*139*] Ellison, E. G. and Sullivan, C. P., *Transactions*, American Society for Metals, Vol. 60, No. 1, 1967, p. 88.
[*140*] Manson, S. S., Halford, G. R., and Hirschberg, H. M., NASA TM X-67838, National Aeronautics and Space Administration.
[*141*] Townley, C. H. A., Central Electricity Generating Board, Berkeley, RD/B/N2292, April 1972.

DISCUSSION

M. C. Murphy[1] (*written discussion*)—I would like to contest Dr. Ellison's assertion that severe bend test data are inferior to push-pull test data in the high strain high temperature regime. In the particular area of crack initiation studies in heavy section components such as steam turbine casings, it is at least arguable that the reverse bend test more accurately represents the experience of the component. In both test specimen and component there is a rising strain gradient reaching a maximum in the surface region, where the strain in the specimen is measured.

Taking a small reverse bend specimen to failure can be considered in practical terms to represent crack initiation in a large component. However, more detailed interpretations of initiation in terms of visible cracks or strain range history are perfectly possible with normal reverse bend tests.

[1] C. A. Parsons and Co., Heaton Works, Newcastle-upon-Tyne, England.

In contrast, a typical push-pull specimen has a 1/4-in. thickness at a uniform strain, and, although a stress history is measured more readily in a strain controlled test, it is difficult to see how such a specimen can represent more relevantly crack initiation (strain, life) in a component in which there is a strain gradient.

Alan Miller[2] (*written discussion*)—Will your constitutive equations show a Bauschinger effect?

E. G. Ellison and E. M. Smith (*authors' closure*)—Not Eqs 16 and 17; however, Refs *93* and *94* offer guidance on the question. The main point in favor of axial tests is that during holdtime type tests in which creep processes can occur, the relaxation of stress can be measured. This information is just not available from the typical bend type test and the stress redistribution is not easily estimated. The discusser states that the strain gradient present in the bend test might more accurately represent conditions in a heavy turbine section. Surely this will depend on what that gradient looks like.

Of course there are advantages and disadvantages with all types of specimen. For the bending type, cheapness in testing is in its favor. However, the more expensive axial test can give a complete stress-strain-time record which in terms of describing material macro-behavior is invaluable.

[2] Pratt & Whitney Aircraft, Division of United Aircraft Corp., East Hartford, Conn. 06118.

A. K. Miller[1]

A Realistic Model for the Deformation Behavior of High-Temperature Materials

REFERENCE: Miller, A. K., "**A Realistic Model for the Deformation Behavior of High-Temperature Materials,**" *Fatigue at Elevated Temperatures, ASTM STP 520,* American Society for Testing and Materials, 1973, pp. 613–624.

ABSTRACT: A materials model (constitutive equation) is developed for the purpose of obtaining greater realism in high-temperature fatigue analysis. Creep, relaxation, strain hardening, Bauschinger effect, cyclic shakedown, rate effects, and response to more complex loadings are some of the phenomena which this model simulates. Test data from thermal-mechanical fatigue tests verify its predictions quantitatively.

The model's form is an equation for the rate of nonelastic strain as a function of current stress, current temperature, and strain history. Its use in the design of turbine blades and vanes and other high-temperature structures is discussed. A multidimensional form is presented for application to finite element programs.

KEY WORDS: fatigue (materials), thermal fatigue, simulation, deformation, plastic properties, creep properties, Bauschinger effect, dislocations (materials), structures

The determination of the fatigue life of a high-temperature structure usually consists of two major steps: calculation of the stress and strain history in critical regions and estimation of the lives of these regions. This paper concentrates on the first of these tasks.

Depending on the complexity of the structure, this stress-strain phase may be as simple as a uniaxial analysis of a bolt, or as complex as a three-dimensional finite element analysis of a turbine blade or disk. In any event, a good definition of the material's nonelastic behavior is needed. In complex structures, where experimentation is difficult, a good simulation is particularly critical. Yet the weak link in most finite element programs has been this nonelastic deformation behavior. The major purpose of this new materials model is the fulfillment of this need.

One primary consideration in the development of constitutive equations is manageability. Efficiency of computation, and ease of discovering the

[1] Senior analytical engineer, Pratt & Whitney Aircraft, Division of United Aircraft Corp., East Hartford, Conn. 06108, present address: Department of Materials Science, Stanford University, Stanford, Calif., 94305.

Copyright© 1973 by ASTM International www.astm.org

material constants for real metals, both prohibit overly cumbersome equations. Yet most current methods, while fairly manageable, lack sufficient realism, our second consideration. We need a model which truly imitates the material's behavior not only in standard laboratory test situations but also in the complex circumstances seen by engineering structures. The contest between manageability and realism is one dominant theme in this undertaking.

Development of the Model

In general, a model based on true physical mechanisms should yield the greatest accuracy in analysis of high-temperature fatigue problems; purely mathematical extrapolation from laboratory data can often prove erroneous. Thus, a mechanistic approach becomes highly desirable. Because, however, our knowledge of the mechanisms governing nonelastic deformation in engineering materials is incomplete, we must sometimes resort to phenomenology. The result carries the flavor of both approaches.

This materials model is basically an equation for the rate of nonelastic strain as a function of current stress, current temperature, and history. A strain rate equation automatically draws in the time variable so essential to high-temperature fatigue; both Rice [*1*][2] and Hart [*2*], among others, have concluded that it is the most appropriate form. With a properly constructed strain rate equation, we can simulate all of the significant mechanical effects occurring at high temperatures, such as time-dependent plasticity, creep, relaxation, Bauschinger effect, and shakedown.

As a starting point, let us examine the typical creep curve, Fig. 1. The nonelastic strain rate can be obtained by adding two components, one which shows hardening and one which remains constant; these are denoted as $\dot{\epsilon}^1$ and $\dot{\epsilon}^2$, respectively. The hardening in the $\dot{\epsilon}^1$ function should depend on strain, rather than time, to properly include experimental observations [*3*]. So our strain rate calculation will be actually the sum of two separate equations.

Since we wish to simulate a tension test with the same two equations, $\dot{\epsilon}^1$ must be the one which dominates, to produce the characteristic strain hardening. Therefore the equation for $\dot{\epsilon}^1$ should resemble the short-time plasticity equation proposed by Orowan

$$\dot{\epsilon}^p \propto b \bar{V} N_m$$

where

$\dot{\epsilon}^p$ = plastic strain rate,
b = Burger's vector,
N_m = mobile dislocation density, and
$\bar{V}$ = their average velocity.

[2] The italic numbers in brackets refer to the list of references appended to this paper.

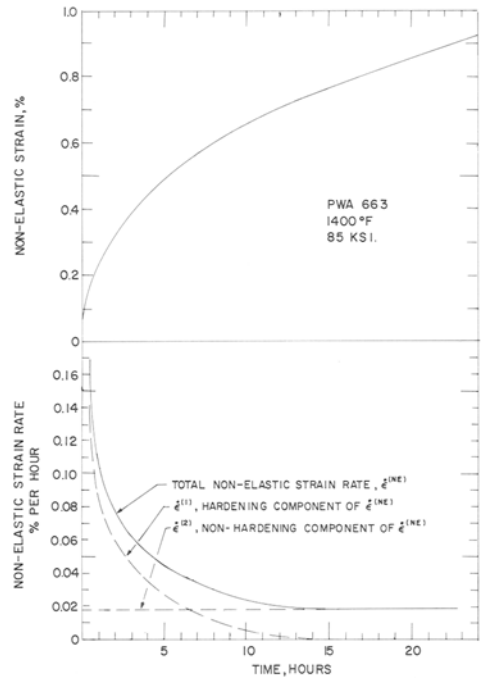


FIG. 1—*Typical creep test behavior*, (upper) *nonelastic strain versus time*, (lower) *nonelastic strain rate versus time.*

However, we must rewrite this equation in a form which includes the two most significant variables: stress dependence and strain hardening.

Gilman [*4*] proposed the following expansion:

$$\dot{\epsilon}^p = gb\,[N_0 + M\epsilon^p]\,[V^* e^{-(D+H\epsilon^p)/\sigma}]$$

where

g = geometric factor,
N_0 = initial dislocation density,
M = dislocation multiplication coefficient,
V^* = shear wave velocity,
D = characteristic drag stress on dislocations,
H = strain hardening coefficient, and
σ = applied stress.

The first bracketed quantity represents the total dislocation density, increasing with plastic strain. The second bracketed quantity is the average dislocation velocity, which depends exponentially on stress and decreases with strain because of dislocation immobilization.

For our present purpose, two modifications of Gilman's equation must be made: (1) to produce a proper Bauschinger effect under multidimensional

stresses, we must be able to subtract the strain hardening tensor ($H\epsilon^p$) from the current stress tensor [*1*], and (2) for the same reason, and also to prevent irreversible cyclic softening without limit, we must relocate the dislocation increase factor ($M\epsilon^p$). The result is the first of our two desired strain rate equations:

$$\dot{\epsilon}^1 = gb\ V^*\ N_0\ e^{-D/|\sigma - H\epsilon^1|}\ sgn\ (\sigma - H\epsilon^1)$$

Here, the combined effect of dislocation immobilization and dislocation multiplication is contained in the term $H\epsilon^1$. This equation's sensitivity to the variables of stress and history equals that of the original Gilman equation. Absolute values and the signum function have been added to allow reversed loading.

The equation for the nonhardening strain rate $\dot{\epsilon}^2$ is simply the secondary creep rate function. For nickel- and cobalt-base superalloys,

$$\dot{\epsilon}^2 = Ae^{-q/kT}\ [\sinh\ |r\sigma|\ ]^n\ sgn\ (\sigma)$$

fits the data quite accurately [*5*] and has been explained by physical mechanisms [*6*].

The separation of nonelastic strain into two components is corroborated experimentally. In a nickel-base superalloy, Leverant et al [*7*] have observed two modes of deformation: heterogeneously distributed planar slip and homogeneous flow. Planar slip and ϵ^1 are favored by low temperature; similarly homogeneous flow and ϵ^2 are favored by high temperature. Thus, the correspondence between this model and the controlling physical mechanisms is striking, though still based on circumstantial evidence.

To summarize, the new materials model is the sum of two nonelastic strain rate equations:

$$\dot{\epsilon}^{ne} = \dot{\epsilon}^1 + \dot{\epsilon}^2$$

These equations can be combined with the standard equations for equilibrium, compatibility, elastic strain, and thermal expansion. Boundary conditions include: (1) loads or displacements and (2) temperature distributions, all as functions of time. These can be applied and the problem solved by numerical integration of small, quasi steady-state increments. When computerized, the result is an efficient, realistic model of the deformation behavior of a high-temperature structure.

Verification of the Model

In using this materials model, we do not specify any particular category of investigation; that is, we do not "tell" the model that it is to do a "creep analysis" or a "short-time yield analysis" or, for that matter, an "elastic analysis." Rather, we just specify the boundary conditions and the model responds appropriately. Since the loadings imposed on real structures are usually a mixture of these categories, this feature is very advantageous.

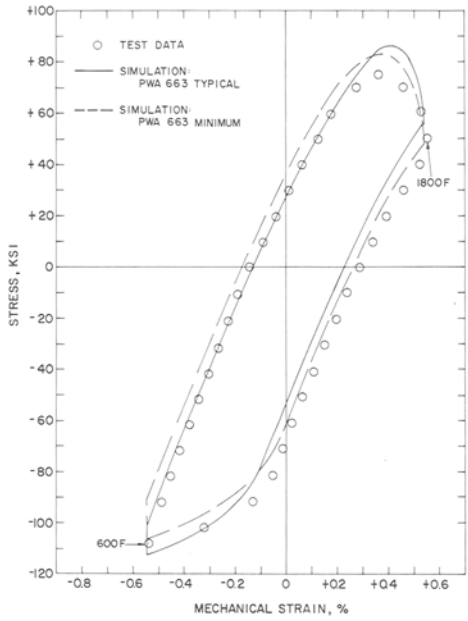


FIG. 2—*Thermal-mechanical fatigue test.*

The simulations presented here were obtained using a digital computer program containing only the equations and logic just described. No special testing was required to obtain the material constants; they were calculated from standard tensile and creep data. Emphasis has been placed on experimental tests which represent gas turbine blade and vane service, but accuracy in simulating these complex tests clearly demonstrates accuracy in much simpler situations, also.

Thermal-mechanical fatigue tests have become a basic tool in turbine airfoil life prediction. Temperature and strain are cycled simultaneously, though not necessarily in phase with each other. Considerable yielding often occurs. Thus successful simulation of such a test is a demonstration of:

1. Elastic behavior under changing temperature.
2. Yielding under changing temperature.
3. Stress relaxation.
4. Bauschinger effect.
5. Shakedown and cyclic stability.

Figure 2 compares experimental data from a high strain range test on PWA 663 [*8*][3] with two simulations, using typical and minimum material properties, respectively. Agreement is good. The most interesting phenomenon, displayed both experimentally and analytically, is the drop-off in

[3] Table 1 gives the compositions of materials mentioned herein.

TABLE 1—*Nominal composition of alloys.*

PWA Specification	Brand Name	Percent by Weight											
		Ni	Cr	Co	Ti	Al	Mo	C	Fe	W	Zr	Cb	B	Other
656	U-700 (cast)	balance	15.0	15.3	3.4	4.3	4.4	0.07	0.5[a]	...	0.06[a]	...	0.016	Cu 0.1[a], Mn 0.15[a], S 0.015[a], Si 0.2[a]
663	B-1900	balance	8.0	10.0	1.0	6.0	6.0	0.11	0.35[a]	0.10[a]	0.07	0.10[a]	0.015	Ta 4.3
664	DS-200	balance	9.0	10.0	2.0	5.0	...	0.13	1.5[a]	12.5	0.06	1.0	0.015	Cu 0.10[a], Mn 0.2[a], S 0.015[a], Si 0.20[a]
1455	...	balance	8.0	10.0	1.0	6.0	6.0	0.11	0.35[a]	0.1[a]	0.08	0.1[b]	0.015	Bi 0.5[b], Hf 1.5, Pb 10.0[b], Ta 4.3
1459	Experimental composition													

[a] Maximum.
[b] Parts per million.

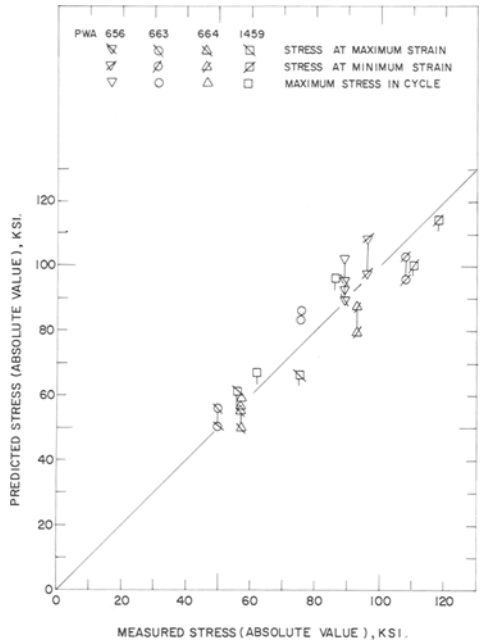


FIG. 3—*Verification of new model using thermal mechanical fatigue tests on various nickel-base superalloys.*

stress at the high-temperature end of the test. The increasing temperature causes the nonelastic strain rate to exceed the applied mechanical strain rate; thus, the stress relaxes. At the low-temperature end, the stress-strain curve has a more ordinary shape.

Simulations of thermal-mechanical fatigue tests on other materials [*8*] produce similar realism; Fig. 3 shows the results. For each measured stress value, the stress predictions from typical property and minimum property simulations form an "error band." The experimental data and the calculations correlate well.

Shifting the strain limits during thermal-mechanical fatigue produces an even more complex test. This represents the superposition of creep (due to centrifugal stresses) and fatigue (due to thermal transients) in a turbine blade. Figure 4 shows the stress history obtained in such a test. With PWA 1455 as the test material, the mean strain was increased by 0.01 percent per cycle (starting at zero), while the strain range was 0.488 percent. Temperature cycled from 600 F (316 C) at the tensile end to 1800 F (982 C) at the compressive end. The agreement between data [*9*] and simulation is good until specimen cracking begins to obscure the material's basic deformation behavior. This simulation definitely utilizes the model's nonelastic capabilities; the stress increase is considerably smaller than the elastic modulus times the strain increase.

Within the scope of the data examined so far, the equations in this model produce the proper strain-rate sensitivity. Figure 5 shows the extent of agreement between experiments on PWA 1418L [7] and simulations of these tension tests. At 1850 F (1010 C) and 1700 F (925 C) the two are quite close; at 1550 F (840 C) agreement is fair. But at 1400 F (778 C) the data are insensitive to strain rate, while the model continues to show a positive sensitivity. Leverant et al [7] explain the experimental behavior at 1400 F in terms of a deformation process (planar slip) which is diffusionless and, therefore, rate insensitive; the present materials model is not sophisticated enough to capture this behavior. Further development is needed.

The new model's capabilities are by no means limited to the above tests. Many other situations have been simulated; although they have not all been compared with test data, the results are qualitatively good and are tabulated next:

Simulation	*Significant Results*
1. Creep test.	Amount of primary creep increases with stress and temperature.
2. Creep of strain hardened material.	Amount of primary creep decreases with increasing prior strain.
3. Hold at constant strain, elevated temperature.	Stress relaxes.
4. Isothermal fatigue test.	Bauschinger effect (reversed "yielding" occurs when the stress reversal equals twice the monotonic "yield strength").
5. Isothermal fatigue test with constant mean strain.	Asymmetric stress cycle decays to a symmetric cycle.
6. Load-yield-unload at elevated temperature.	Anelastic aftereffect (gradual loss of part of the nonelastic strain).
7. Constant stress, increasing temperature.	Heating-rate effect (temperature for 0.2 percent nonelastic strain increases with increasing heating rate).
8. Load-yield-unload. Hold at high temperature. Reload.	Annealing (yield strength of strain hardened material decreases with increasing hold temperature and holdtime).

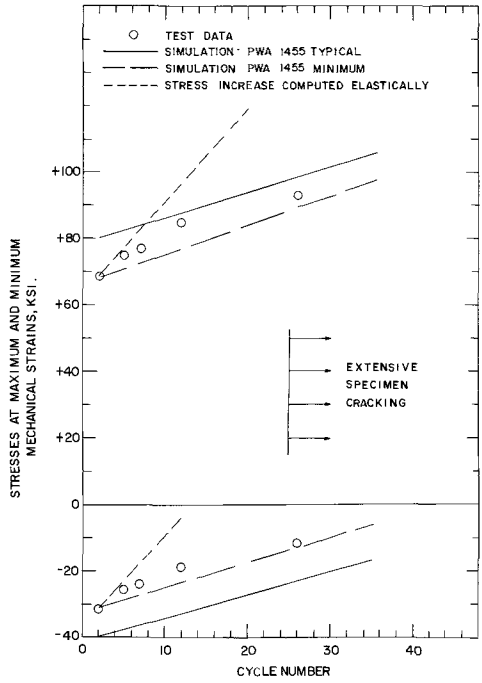


FIG. 4—*Thermal-mechanical fatigue test with mean strain increasing 0.01 percent per cycle. Mechanical strain range = 0.488 percent; temperature at maximum strain = 600 F; temperature at minimum strain = 1800 F.*

Applications

A very useful and fairly expedient analysis of turbine blades and vanes models an airfoil section as a beam under tensile and bending loads. This method permits investigation of some significant three-dimensional effects, while requiring only a one-dimensional description of material behavior. The equations developed above form the nucleus of a new digital computer program for this job. With it, we can "fly a blade" on paper, that is, we can faithfully represent the transient behavior of the engine blade, as well as its steady-state behavior.

One of the model's most promising applications is a two- or three-dimensional finite element program. The constitutive strain rate equations convert directly into tensor form. We assume that the Von Mises, or "effective stress" concept governs the material's nonelastic behavior, and that the components of nonelastic strain are apportioned according to the associated flow rule, drawing on the work of Rice [*1*] to include internal stress effects. The result is

$$\dot{\epsilon}_{ij}{}^{ne} = \dot{\epsilon}_{ij}{}^{1} + \dot{\epsilon}_{ij}{}^{2}$$

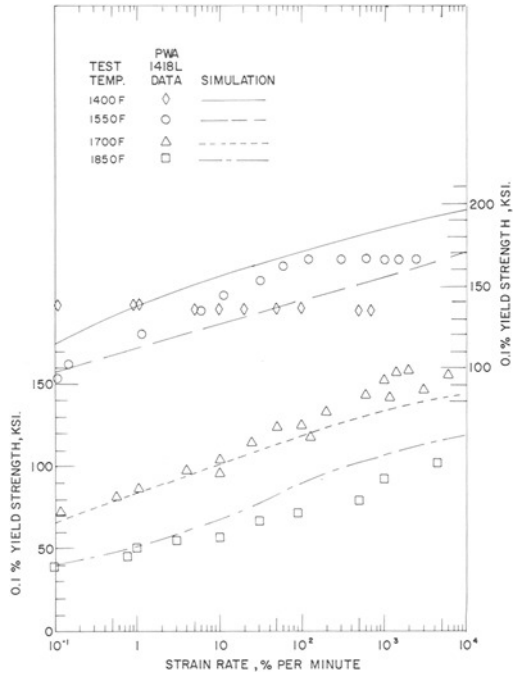


FIG. 5—*Sensitivity of yield strength to applied strain rate.*

where

$$\dot{\epsilon}_{ij}{}^{1} = \frac{3\ gb\ V^{*}\ N_0}{2[3J_2(\sigma_{ij} - R_{ij})]^{1/2}}\ e^{-D/[3J_2(\sigma_{ij}-R_{ij})]^{1/2}}\ (S_{ij} - R_{ij})$$

$$\dot{\epsilon}_{ij}{}^{2} = \frac{3\ Ae^{-q/kT}}{2[3J_2(\sigma_{ij})]^{1/2}}\ \{\sinh\ [r\ [3J_2(\sigma_{ij})]^{1/2}]\}^{n}\ (S_{ij})$$

and

$$\dot{R}_{ij} = H\ \dot{\epsilon}_{ij}{}^{1}$$

$J_2\ (\sigma_{ij})$ denotes the second invariant; S_{ij} denotes the deviatoric part of σ_{ij}; all other quantities have definitions similar to their one-dimensional counterparts. Inspection of these equations shows a mixture of kinematic hardening ($\dot{\epsilon}_{ij}{}^{1}$) and isotropic behavior ($\dot{\epsilon}_{ij}{}^{2}$).

Development and implementation of advanced life prediction methods is another possible application. Methods which require plastic strain range, creep per cycle, stress range, etc. as input are currently receiving the attention of many investigators. See, for example, the paper on strain range partitioning elsewhere in this volume. Obviously, a realistic deformation model is required to supply such input. By simulating completed laboratory tests, one stands a reasonable chance of predicting the experimental fatigue lives by manipulating the quantities ϵ^{1} and ϵ^{2}. Then the same mani-

pulation of variables could be incorporated into hardware analysis. The end product would be a one-step life prediction system.

Further Work

More experimental and analytical work is needed to fully assess the model's behavior and accuracy. Included in this effort should be biaxial situations and a wide variety of materials.

In addition, further development may increase the model's capabilities, drawing in cyclic hardening, cyclic softening, radiation damage, and other metallurgical transformations.

Conclusions

1. A mathematical model has been developed which simulates realistically the types of deformation behavior commonly seen in high-temperature materials.
2. The model is basically an equation which calculates the rate of nonelastic strain as a function of stress, temperature, and history.
3. The new equation, when combined with the equations of equilibrium and compatibility, simulates a wide range of test situations and produces the expected behavior for each.
4. Test data on thermal mechanical fatigue tests and strain rate sensitivity verify the model's quantitative capabilities.
5. The new model has been used successfully in gas turbine airfoil analysis and is directly applicable to two-and three-dimensional finite element programs.

Acknowledgments

Many thanks go to my colleagues at Pratt & Whitney Aircraft for their comments, advice, and encouragement. G. R. Leverant, R. W. Soderquist, C. E. Spaeth, W. H. Vogel, and C. H. Wells have been particularly helpful during the course of this study.

References

[1] Rice, J. R., *Journal of Applied Mechanics*, Vol. 37-E, No. 3, Sept. 1970, pp. 728–737.
[2] Hart, E. W., *Acta Metallurgica*, Vol. 18, June 1970, pp. 599–610.
[3] Hult, J. A. H., *Creep in Engineering Structures*, Blaisdell Publishing Co., Waltham, 1966, pp. 31–32.
[4] Gilman, J. J., *Micromechanics of Flow in Solids*, McGraw-Hill, New York, 1969.
[5] Garofalo, Frank, *Fundamentals of Creep and Creep-Rupture in Metals*, MacMillan, New York, 1965, p. 51.
[6] Reed-Hill, R. E., *Physical Metallurgy Principles*, D. Van Nostrand Co., Princeton, 1964, p. 576.
[7] Leverant, G. R., Gell, M., and Hopkins, S. W., *Materials Science and Engineering*, Vol. 8, 1971, pp. 125–133.
[8] Soderquist, R. W.. Pratt & Whitney Aircraft, unpublished research.
[9] Gemma, A. E., Pratt & Whitney Aircraft, unpublished research.

DISCUSSION

Alfred Fox[1] (*written discussion*)—Would you expect equally good agreement between measured and calculated values of stress-strain relationships for materials exhibiting a significant Bauschinger effect?

A. K. Miller (*author's closure*)—Yes.

K. .C Liu[2] (*written discussion*)—Two temperatures are indicated in the stress-strain diagram in the abstract. What kind of temperature program (or temperature change) is used in your test? Is it a linear change of temperature?

Mr. Miller—Temperature varied sinusoidally with time between the extreme points labelled 600 and 1800 F in the test. In the simulation, several linear steps in temperature were used to closely approximate the sinusoidal variation. The same is true of the strain cycle. Temperature at the maximum stress level was about 1500 to 1600 F in both test and simulation.

E. Krempl[3] (*written discussion*)—(1) Is your model capable of reproducing cycle dependent properties such as we see in cyclic tests? (2) Are you capable of reproducing aftereffect and permanent set as observed after unloading from a stress history to zero stress? Will your permanent strain (if any) depend on prior history and, if yes, in what form?

Mr. Miller—(1) The model will not simulate cyclic hardening or softening. It will, however, show some related effects: (*a*) In a *strain*-controlled situation, the model will show shifts in the peak stress levels due to relaxation of a mean strain. (*b*) In a stress-controlled situation, the model will show shifts (or ratchetting) in the peak strain levels due to imposition of a nonsymmetric stress or temperature cycle or both. (2) The model will exhibit the anelastic aftereffect. After stressing at elevated temperature to build up ϵ^e and the two nonelastic strain components ϵ^1 and ϵ^2, we decrease the stress (analytically) to zero. ϵ_e decreases to zero simultaneously, ϵ_2 remains constant, while ϵ^1 decays gradually to some fraction of its peak value, typically 70 to 80 percent.

[1] Bell Telephone Laboratories, Murray Hill, N. J.
[2] Oak Ridge National Laboratory, Oak Ridge, Tenn. 37830.
[3] Division of Mechanics, Rensselaer Polytechnic Institute, Troy, N. Y. 12181.

J. F. Polhemus,[1] *C. E. Spaeth*,[1] *and W. H. Vogel*[1]

Ductility Exhaustion Model for Prediction of Thermal Fatigue and Creep Interaction

REFERENCE: Polhemus, J. F., Spaeth, C. E., and Vogel, W. H., "**Ductility Exhaustion Model for Prediction of Thermal Fatigue and Creep Interaction,**" *Fatigue at Elevated Temperatures, ASTM STP 520*, American Society for Testing and Materials, 1973, pp. 625–636.

ABSTRACT: Extensive laboratory testing of typical alloys used in gas turbine blading has shown that there is a strong interaction of the thermal fatigue and creep damage modes which is nonlinear in nature. Consequently, a model for cumulative damage analysis was developed using an exhaustion of ductility concept in which the total available ductility is derived from baseline thermal fatigue tests or, alternatively, estimated from stress-rupture tests. A cycle-by-cycle reckoning of ductility used and remaining is made with the use of a digital computer program, and cracking is ultimately predicted at the point where the remaining ductility is insufficient to complete another cycle.

The developed analysis is shown to correlate with laboratory test results. The understanding and design procedure developed make it possible to simulate complex service conditions in digital computer programs and evaluate designs and materials in simulated "fly offs."

KEY WORDS: fatigue (materials), ductility, exhaustion, thermal fatigue, creep properties, damage, creep rupture strength, fatigue tests, failure

Nomenclature

a	Fatigue curve slope
A	Creep coefficient
b	Creep exponent
n	Imposed number of cycles
N	Number of cycles to fail
t	Time
t_{inc}	Increment of creep time
γ	Nickel strengthened by solid solution elements
γ'	Ni_3 (Al-Ti)
Δ	A decrement
ϵ	Strain (imposed or available per subscript)

[1] Assistant project engineer, project engineer, and assistant project engineer, respectively, Pratt & Whitney Aircraft, Division of United Aircraft Corp., East Hartford, Conn. 06108.

Copyright© 1973 by ASTM International www.astm.org

Subscripts

calc Calculated
C Cast
CR Pertains to creep
eq Equivalent
f Value at fracture
F Ductility
FR Remaining ductility
inc Increment
n An arbitrary number
o Virgin material value
TR Total range
W Wrought

Empirical Evidence of Cumulative Damage Phenomenon

Traditionally, high-temperature components were designed to considerations of allowable creep deformation or acceptable stress rupture life or both. However, as temperature levels and excursions increased, it became apparent that other failure mechanisms were involved and needed to be considered. Aside from the important consideration of oxidation-corrosion damage effects, the primary new concern became that of the effect of cycling load and temperature.

Through the research of many contributors in industry and universities, techniques for accounting for low-cycle fatigue and thermal fatigue damage became available, and these modes of damage were widely considered along with the more conventional creep and rupture criteria. Generally, it was assumed that the cyclic and time-dependent modes of damage were independent and could be considered separately (for example, failures were due either to fatigue or stress rupture). Although this approach improved design capabilities and was very often quite successful, it was found to be unconservative in many cases. This experience and deeper probing by researchers in the field led the authors to conclude that the low-cycle fatigue and stress-rupture modes of failure are not independent and that a cumulative damage law is required to account for total damage in cases were both mechanisms are active.

This realization led to a research program conducted jointly by Pratt & Whitney Aircraft and Professor Carden of the University of Alabama, to explore the cumulative damage effects of thermal fatigue and stress rupture. The results of this program [*1*][2] not only showed that these modes of damage interacted, but also that the interaction is nonlinear in nature and that it can be much more severe than would be predicted by application of a

[2] The italic numbers in brackets refer to the list of references appended to this paper.

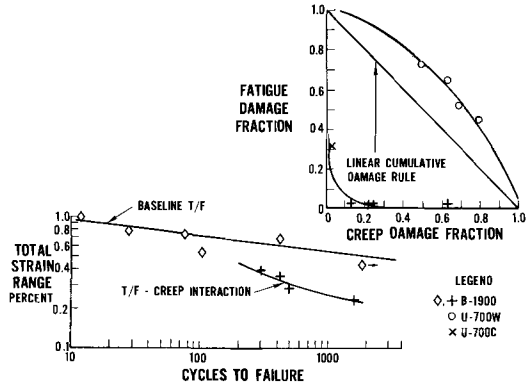


FIG. 1—*Thermal fatigue creep interaction tests, Hollow Laboratory specimens.*

simple linear damage law. The curves of Fig. 1*a* and *b* are reproduced here for the reader's convenience.

Figure 1*a* shows a baseline thermal-mechanical fatigue curve for B-1900 nickel-base superalloy with the results of cumulative damage tests superimposed.

The baseline tests were fully reversed strain cycling tests in which temperature was simultaneously cycled (that is, temperature was varied linearly with strain with maximum temperature at maximum tensile strain and minimum temperature at maximum compressive strain). Cumulative damage tests were conducted with alternating blocks of 100 baseline fatigue cycles and 10 to 12 h of creep at steady load and temperature. These results showed failure occurring before either the baseline fatigue limit or the stress-rupture limit was reached. Consequently, they established a firm case for the existence of thermal fatigue and stress-rupture damage interaction (cumulative damage) for B-1900 in a simulated gas turbine blade environment.

The degree of this interaction was gaged by plotting the foregoing data on a "damage plot" in which the axes are defined by the thermal-fatigue damage ratio and the stress-rupture damage ratio. This plot is shown in Fig. 1*b* along with the hypothetical linear cumulative damage line and data taken from another source on a different alloy. This plot shows that the interaction is nonlinear, in general, and that the linear damage rule will be conservative in some cases and unconservative in others. From this vantage point, it was seen that a general cumulative damage rule was required. To this end, the exhaustion of ductility concept was developed.

Exhaustion of Ductility Analysis

In a limited range of number of cycles to failures, from a few cycles to a few thousand cycles, the low-cycle fatigue results may be well approxi-

mated by a linear relation on the log-log coordinates of the total strain range ϵ_{TR} and number of cycles to failure (N) [2–4]. This power law relation may be given, as in Ref 5, in the form

$$\epsilon_{TR}{}^{a} N = (2\epsilon_{F_0})^{a}/4 \quad \ldots\ldots\ldots\ldots\ldots\ldots (1)$$

where a and ϵ_{F_0} are material constants. Ideally, values of these constants are determined from low-cycle fatigue tests results, but they may also be approximated using static properties of the material [6].

If a specimen is strain cycled through a number of cycles (n) at a strain range ϵ_{TR}, the specimen will then have a residual ductility which can be expressed as in Ref 5 in the form

$$\epsilon_{F}{}' = \epsilon_{F_0}\left(1 - \frac{n}{N}\right)^{1/a} \quad \ldots\ldots\ldots\ldots\ldots\ldots (2)$$

It follows that the original ductility has been reduced by an amount $\Delta\epsilon$ where

$$\Delta\epsilon = \epsilon_{F_0}\left[1 - \left(1 - \frac{n}{N}\right)^{1/a}\right] = \epsilon_{F_0}\left\{1 - \left[1 - 4n\left(\frac{\epsilon_{TR}}{2\epsilon_{F_0}}\right)^{a}\right]^{1/a}\right\} \quad \ldots\ldots (3)$$

The use of sums of these decrements to predict material behavior in mixed cycle situations has been documented [5]. Also, several authors [5–8] have shown how the concept of exhaustion of ductility can be used to model material behavior in the situation involving isothermal strain cycling combined with mean strain. What follows is the application of the same concept to the situation involving thermomechanical strain cycling combined with creep in several nickel-base superalloys.

The scheme for accumulating ductility decrements from such cycling and creeping to the point where the initially available ductility is exhausted can be visualized as a stepwise progression along a graph which represents a constant stress, constant temperature creep curve of the material.[3] The equation of this curve

$$\epsilon_{CR} = At^{b} \quad \ldots\ldots\ldots\ldots\ldots\ldots\ldots\ldots (4)$$

will be used subsequently.

Since both cycling and creep are assumed to contribute to the same failure mechanism, the damage that resulted during the first increment of cycles is equivalent to an increment of creep strain. The magnitude of this increment is further assumed to be numerically equal to the decrement in available ductility given by Eq 3. The graph and Eq 4 yield an equivalent creep time (t_{eq}) corresponding to this damage increment, that is, the time increment of creep exposure at the given stress and temperature which would have been

[3] This is not a limitation in the common situation where a complex creep history can be represented by an equivalent time at a reference stress and a reference temperature.

required to produce a creep strain equal to the decrement in residual ductility caused by the initial period of cycling.

$$t_{eq} = \left(\frac{\Delta\epsilon}{A}\right)^{1/b} \quad \ldots\ldots\ldots\ldots\ldots\ldots\ldots\ldots (5)$$

To this increment of equivalent creep time, an increment (t_{inc}) of actual creep time can be added. A further decrease in available ductility governed by [*4*] results and the residual ductility after one cyclic increment plus one creep increment is given by

$$\epsilon_{FR_1} = \epsilon_{F_0} - A\,(t_{eq} + t_{inc})^b \quad \ldots\ldots\ldots\ldots\ldots\ldots\ldots (6)$$

The solution proceeds with the addition of another increment of cycles, which may have the same strain amplitude or a different one. In either case, an additional decrement in ductility results which is evaluated by replacing n, ϵ_{TR} and ϵ_{F_0} in Eq 3 with n_2, ϵ_{TR_2}, and the value of ϵ_{FR}, as given by Eq 6.

Nonlinearities present in the physical system and the model preclude a general solution in closed form. Consequently, the practical solution of problems usually involves the use of a digital computer. In this connection, the general form of the expression for decrease in ductility resulting from cycling (Eq 3) is

$$\Delta\epsilon_n = \epsilon_{FR_{n-1}} \left\{1 - \left[1 - 4n_n \left(\frac{\epsilon_{TR_n}}{2\epsilon_{FR_{n-1}}}\right)^a\right]^{1/a}\right\}$$

where

$$\epsilon_{FR_{n-1}} = \epsilon_{F_0} - A\,(t_{eq_{n-1}} + t_{inc_{n-1}})^b$$

and

$$t_{eq_{n-1}} = \left(\frac{\Delta\epsilon_{n-1} + \epsilon_{F_0} - \epsilon_{FR_{n-2}}}{A}\right)^{1/b}$$

The stepwise progression is followed until failure occurs. Failure can occur during a strain cycling period in which case the criterion is

$$1 \leq 4_{n_f}\,(\epsilon_{TR_f}/2\,\epsilon_{FR_f})^a$$

Failure may also occur during a creep period in which case the criterion is

$$\epsilon_{F_0} \leq A\,(t_{eq_f} + t_{inc_f})^b$$

Physical Basis for Creep-Thermal Fatigue Interaction

Fundamental to the foregoing derivation was the assumption that a decrement in available ductility resulting from a period of cycling could be represented directly as an increment of creep extension. Consideration will now be given to some qualitative aspects of thermal fatigue failure modes as they relate to this assumption and cumulative damage test results.

Specimens tested in this program exhibited both common and distinguishing features in their mode of cracking. The common feature was secondary cracking not associated with the surface (that is, internal cracking), a phenomenon which was absent in specimens isothermally tested without creep interspersion. The primary significance and nature of the secondary cracking is that the distinguishing features of the failure modes are seen at the earlier stage of their development in the secondary cracks as opposed to that seen in the primary crack. Distinctive features of the cracks were as follows: wrought U-700 cracked exclusively intergranularly, cast U-700 cracked transgranularly (for example, interdendritically), and B-1900 cracked in a mixed mode. It follows that these tests constituted an unusually thorough evaluation of applicability of the exhaustion of ductility concept by virtue of the variety exhibited in the specimen failure modes and that a physical basis for creep-thermal fatigue interaction would necessarily involve creep and fatigue damage both internal to the grain and at the grain boundary.

A physical basis can be identified in studies by Evans and Mushovic of the microstructural changes that occur as a nickel-base alloy is crept or thermally fatigued [*9*]. Figure 2*a*, *b*, and *c* is reproduced for the convenience of the reader with the permission of the authors. Figure 2*a*, (obtained by replication) generally depicts the structure of nickel-base superalloy after elevated temperature exposure. Gamma prime, Ni_3 (Al-Ti), particles are imbedded in a gamma matrix (nickel strengthened by solid solution elements). Note the localized deformation band extending from the lower left to the upper right. Gamma prime particles in this band are extensively deformed, a result shown by Evans and Mushovic to be a product of many repetitions of a thermal fatigue cycle. Figure 2*b* also shows superalloy in which some of the gamma prime is extensively deformed; however, in this case not by fatigue but by creep.

Transmission electron microscopy applied to the specimen depicted in Fig. 2*a* yielded the result depicted in Fig. 2*c*. The dark features of this figure are dislocation buildups which increased in density progressively as the number of thermal fatigue cycles increased. Transmission shots not reproduced here show that increases in dislocation density also accompanied the deformation of gamma prime by creep; hence, within the grain, similar damaging processes occurred as a result of fatigue and creep.

A slip band having the strength of the one exhibited in Fig. 2*a* would produce at the grain boundaries damaging effects similar to those of creep, for example, cracking of brittle carbides in its path [*9*]. Thus, the exhaustion of ductility hypothesis is shown to be consonant with physical reality for the varied failure modes characteristic of cumulative damage testing of nickel-base superalloys. In the next section, supporting evidence of a quantitative nature is considered.

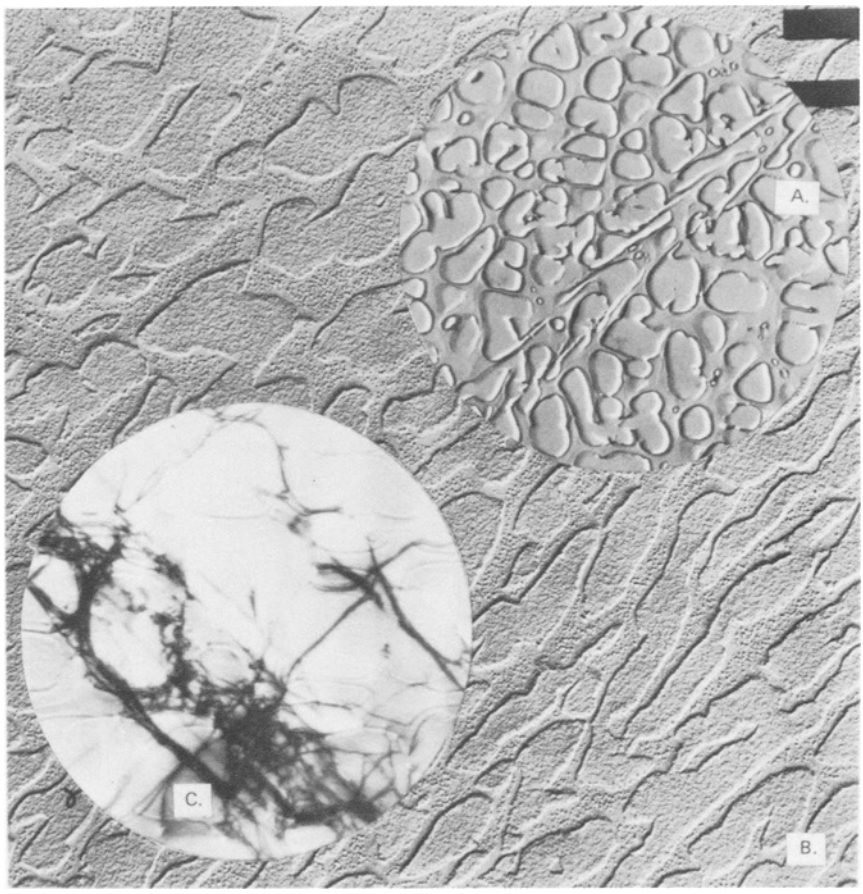


FIG. 2—(a) *Slip band in disk with 0.020 in. radius cycled 150 times between 70 and 1800 F. Note the gamma prime deformation along the slip trace* (×5000). (b) *Specimen which has been stress rupture tested at 1800 F. The gamma prime particles in the lower right hand corner of the photograph are elongated and wavy. The upper left corner represents a structure somewhat more typical of a statically aged material* (×5000). (c) *Appearance of slip bands in 0.020-in.-radius disk after 150 cycles between 70 and 1800 F* (×55 000).

Exhaustion of Ductility Analysis Correlation with Data

Table 1 summarizes the correlation of the analytically predicted life with experimentally determined life under varying combinations of creep-fatigue exposure. Two blocks of data are presented, and they represent results from:

1. Specimen tests conducted at the University of Alabama.
2. Specimen tests conducted at the Advanced Materials Research and Development Laboratory of Pratt & Whitney Aircraft.

TABLE 1—*Exhaustion of ductility analysis correlation with test data*

Type of Test	Material	Total Strain Range, %	Hold Stress, ksi	Holdtime	Hold Temperatures	$N_{f,\text{exp}}$	$N_{f,\text{calc}}$
University of Alabama	B-1900	0.28	20	10 to 12 h/100 cycles	1800	500	800
Thermal fatigue and creep tests	B-1900	0.40	20	10 to 12 h/100 cycles	1800	300	500
	B-1900	0.35	20	10 to 12 h/100 cycles	1800	478	600
	B-1900	0.23	20	10 to 12 h/100 cycles	1800	1600	900
	B-1900	0.30	19.5	10 to 12 h/100 cycles	1800	300	700
	B-1900	0.54	15.7	10 to 12 h/100 cycles	1800	200	300
	B-1900	0.50	15	10 to 12 h/100 cycles	1800	565	500
	U-700C	0.4635	40	10 to 12 h/100 cycles	1600	200	300
	U-700C	0.43	23.25	10 to 12 h/100 cycles	1600	2500	2300
	U-700C	0.5697	30	/100 cycles	1600	700	400
	U-700C	0.5424	35	/100 cycles	1600	400	300
	U-700C	0.5929	30	/100 cycles	1600	500	400
In-house	U-700W	1.6	70	20 min/cycles	1400	171	160
Low-cycle fatigue-creep	U-700W	1.6	70	60 min/cycles	1400	128	130
Interaction tests	U-700W	1.6	80	20 min/cycles	1400	124	100
	Y-700W	1.6	80	60 min/cycles	1400	73	70

The essential description of the test cycles is given by the total strain range per cycle, and the hold stress, time, and temperature for creep. When these parameters are input into the exhaustion of ductility analysis along with the basic description of the thermal fatigue and creep properties of the alloy, the life shown under the column headed $N_{f,\text{calc}}$ is calculated in cycles to observable cracking. As evidenced by comparing the experimentally observed and analytically calculated lives, the correlation is good considering the complexity of the test conditions, varying type of alloys and cycle tested. The analysis when properly used, therefore, is considered to be accurate within an order of closer than 2 to 1 in cycles to failure.

It is of interest to note an important outcome of the analysis that corroborates a conviction born of experience which is that the severity of the creep-fatigue interaction diminishes with increasing alloy ductility. The data from Table 1, when plotted as previously shown in Fig. 1*b*, indicate that the lower ductility alloys (U-700C and B-1900) fall well below the hypothetical linear damage line, whereas the more ductile alloy (U-700W) falls above the linear cumulative damage line. All of the points from Table 1

do not appear in Fig. 1 because Table 1 incorporates data subsequent to publication of Ref *1*.

Exhaustion of ductility analysis likewise shows that the effects of varying available ductility are only partially eliminated in the process of forming the fatigue damage ratio. The permissible sum of the creep and fatigue damage fraction is itself strongly dependent on the available ductility characteristic of the material. Thus, the most gratifying feature of the proposed technique is that, without benefit of specialized empirical constants, it characterizes the interactive behavior of the materials studied in accordance with experience, whereas the linear cumulative damage law, as defined in Fig. 1*b*, appears quite pessimistic for the material which exhibits considerable ductility, appears accurate for materials in a particular intermediate ductility range, and appears to be very optimistic in the case of materials which exhibit very modest ductility.

Use of the Cumulative Damage Analysis for Alloy Evaluation and Selection

The cumulative damage analysis is an extremely useful tool for specifying the optimum combination of material properties desired for a specific application and for ranking the available alloys for service in that application.

Metallurgists, when designing new alloys, are often faced with the problem of having to trade resulting creep strength for ductility. When their design efforts are applied at optimizing or designing an alloy for a specific application, it is essential that they have guidelines for making that trade. Until now, these guidelines have been too vague to permit effective trade studies. This shortcoming can lead to wasted time and money in pursuing the wrong alloy for a specific application. The cumulative damage analysis presented gives the metallurgist the desired guidelines to perform these trade studies and will potentially reduce the cost and lead time in developing or tailoring alloys for a particular application.

Application of Cumulative Damage Analysis in Design

Just as the cumulative damage analysis can be used in alloy evaluation for a specific application, it can also be used in design evaluation studies. When good heat transfer and stress analysis models are formulated for a particular design problem, the anticipated service history of the component can be simulated, and the cumulative damage analysis will provide the criterion for deciding when failure occurs. Although the designer will always want to test his design to prove its acceptability before committing it to service, the ability to simulate service history analytically is valued in that it provides an economical and expedient way of screening alternative designs. Furthermore, it provides the engineer with tools for designing better simulation into the proof test and for evaluating its results.

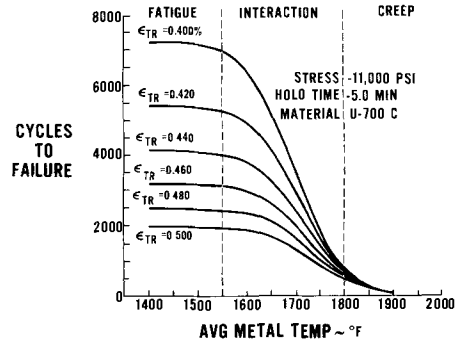


FIG. 3—*Cooling design study.*

The above procedures have been found useful in turbine blade design at Pratt & Whitney Aircraft. A typical problem faced by the designer is that of choosing the optimum air cooling scheme and flow rates for a particular blade. The curves shown in Fig. 3 are a set of parametric curves defining the anticipated cyclic life for a turbine blade subjected to the given conditions of centrifugal stesss and time at the stress per cycle. The parameter is the strain range experienced by the critical element in the blade and is usually a function of the gas temperature and cooling design employed. Study of these curves reveals several important things to the designer:

1. Looking at the higher end of the average blade metal temperature scale, it is seen that life is no longer dependent upon strain range but is primarily creep strength limited.
2. At the lower end of the average metal temperature scale, the curves become asymptotic to the baseline thermal fatigue life at the given strain range. Hence, it is concluded that creep interaction only becomes significant above a certain point in average metal temperature.
3. The middle ground, in which the turbine blade designer often finds himself, is one in which the cumulative damage analysis plus the service simulation analysis is most helpful to the designer.

Conclusions

1. Extensive laboratory testing of typical alloys used in gas turbine blading has shown that there is a strong interaction of the thermal fatigue and creep damage modes that is nonlinear in nature.
2. The exhaustion of ductility model presented, employing a cycle by cycle reckoning of ductility used and remaining, can handle low-cycle thermal fatigue and creep histories characteristic of gas turbine operation.
3. The requisite assumption that thermal fatigue and creep both produce damage which has its equivalent in the other mode is supported by physical evidence.

4. Predicted specimen lives correlate well with those determined experimentally. The analysis apparently applies equally well for the cast and wrought alloys tested and the varied fracture modes experienced.

5. An advantage of the analysis is that knowledge of the creep strain is easily substituted for knowledge of the creep stress in strain controlled applications where it is difficult to determine stress accurately.

6. For the alloys studied, the exhaustion of ductility model shows that the damage fraction summation is considerably less than 1.0 for some alloys exhibiting modest ductility, increases as ductility increases, and is much greater than 1.0 for an alloy exhibiting substantial ductility.

7. Cumulative damage analysis in conjunction with adequate thermal-mechanical structural analysis is a powerful design tool in situations involving combinations of cyclic strain with creep deformation.

References

[1] Vogel, W. H. and Carden, A. E., "Thermal Mechanical Fatigue of Some Super-alloys," paper presented at the National Metal Congress, 1967, Cleveland, Ohio; also available through American Society for Metals report system.

[2] Smith, R. W., Hirschberg, M. H., and Manson, S. S., "Fatigue Behavior of Materials Under Strain Cycling in Low and Intermediate Life Range," NASA TND-1574, National Aeronautics and Space Administration, April 1963.

[3] Manson, S. S. and Hirschberg, M. H., "Fatigue Behavior in Strain Cycling in the Low and Intermediate Cycle Range," paper presented at the 10th Sagamore Army Materials Research Conference, Sagamore, N. Y., Aug. 1963.

[4] Morrow, J. and Tuler, F. R., *Journal of Basic Engineering, Transactions*, Series D, American Society of Mechanical Engineers, Vol. 87, 1965, pp. 275–289.

[5] Ohji, K., Miller, W. R., and Marin, J., "Cumulative Damage and Effect of Mean Strain in Low-Cycle Fatigue of a 2024-T351 Aluminum Alloy," paper presented at the Winter Annual Meeting, Chicago, Ill., 7–11 Nov. 1965.

[6] Manson, S. S., *Thermal Stress and Low Cycle Fatigue*, McGraw-Hill, New York, 1966.

[7] Sachs, G., Gerberich, W. W., Weiss, V., and Latorre, J. V. in *Proceedings*, American Society for Testing and Materials, Vol. 60, 1961, pp. 512–529.

[8] Sachs, G. and Weiss, V., *Zeitschrift für Metallkunde*, Band 53, 1962, pp. 37–47.

[9] Evans, D. J. and Mushovic, N. J., "Behavior of a Nickel Base Superalloy Under the Influence of Thermal Cycling," 1970 Spring Meeting, Metallurgical Society of American Institute of Mining, Metallurgical, and Petroleum Engineers, Las Vegas, Nev., 12 May 1970.

DISCUSSION

M. Manjoine[1] *(written discussion)*—Does this method take account of the change of ductility that can take place with change in creep strain rate? At long rupture times many alloys show a great reduction in total strain.

J. F. Polhemus, C. E. Spaeth, and W. H. Vogel (authors' closure)—Yes, if the time or strain rate dependence of ductility can be defined it can be included in the model.

A. E. Carden[2] *(written discussion)*—The authors have presented a well thought-out analysis of one viewpoint of the creep-fatigue failure mode. There are several factors which may influence a ductility exhaustion concept to creep-fatigue fracture.

1. During creep, especially if held at temperature for a long time, an annealing of the fatigue structure occurs. Thus, for cyclic hardening materials cycled at constant strain range, the ratio of average plastic strain range to total will be larger for the interspersion creep condition.
2. Cracks can propagate during creep holds.
3. There is a significant difference in the thermal coefficient of expansion and modulus of elasticity value for γ-γ' so that thermal cycling produces thermal stresses which can affect the local deformation.
4. If the failure is essentially one of crack propagation, then one would expect large differences between interspersion tests and periodic loading with dwells.

My comment is not meant to detract from the value of this work, only to urge caution in the use of ductility-exhaustion models to situations where the model is not intended to apply.

[1] Westinghouse Research Laboratories, Pittsburgh, Pa. 15235.
[2] University of Alabama, University, Ala. 34586.

J. B. Conway,[1] *J. T. Berling*,[1] *and R. H. Stentz*[1]

Strain Rate and Holdtime Saturation in Low-Cycle Fatigue: Design-Parameter Plots

REFERENCE: Conway, J. B., Berling, J. T., and Stentz, R. H., **"Strain Rate and Holdtime Saturation in Low-Cycle Fatigue: Design-Parameter Plots,"** *Fatigue at Elevated Temperatures, ASTM STP 520*, American Society for Testing and Materials, 1973, pp. 637–647.

ABSTRACT: A detailed study is made of the effect of strain rate and hold periods on the low-cycle fatigue behavior of AISI 304 stainless steel at 650 C (1200 F). Data are presented in terms of a logarithmic plot of N_f versus cycle time to reveal several important regimes. At very small cycle times the fatigue life is independent of strain rate. As the strain rate is decreased the fatigue life is reduced and finally a saturation effect is noted at a strain rate close to 4×10^{-4} s^{-1}. In the region prior to saturation, strain rate and hold periods have the same effect on fatigue life as long as they are compared at the same cycle time. Hold-period effects also exhibit a saturation effect, but this occurs at a fatigue life lower than that corresponding to the strain rate saturation level. For hold periods in tension only the holdtime effect is shown to be dependent upon the strain rate employed in that portion of the cycle exclusive of the hold period. Design-parameter plots are introduced to provide an extensive presentation of fatigue data and a graphical solution for the fatigue life at a given temperature once values for strain range, strain rate, and hold period are selected.

KEY WORDS: fatigue (materials), fatigue tests, strain rate, holdtime, stainless steel, saturation, correlation, design-parameter plots

It is now well established [*1–13*][2] that strain rate (frequency) and hold periods exert a pronounced influence on the low-cycle fatigue behavior of metals at elevated temperatures. The introduction of a hold period at the peak strain point in the fatigue cycle and a decrease in the strain rate both function to reduce the fatigue life, and the extent of the reduction is generally noted to be related to the length of the hold period and to the amount of reduction of strain rate. Essentially all of the reported studies of this subject appear to confirm these effects although the magnitude of the observed change depends on several factors. These include material, temperature, strain range, and strain-wave form. In the latter case the

[1] President, vice-president of engineering, and vice-president of research and development, respectively, Mar-Test Inc., Cincinnati, Ohio 45215.

[2] The italic numbers in brackets refer to the list of references appended to this paper.

Copyright© 1973 by ASTM International www.astm.org

fatigue life depends on whether the hold period is in tension only, compression only, or in both the tension and compression portions of the cycle.

While the study of strain rate and holdtime effects has not been extensive, agreement seems to have been reached on several important conclusions. These include the fact that strain rate and holdtime effects are interrelated and that they both result from an associated creep influence. Also agreed upon is the importance of these two effects and the fact that a detailed evaluation of the low-cycle fatigue characteristics of a material at elevated temperature can not be made without a proper determination of the effect of both these factors.

In the present paper some fairly extensive strain rate data are presented for AISI 304 stainless steel at 650 C (1200 F), and these results are used to amplify a previously reported correlation [*14*] by the authors which dealt with the relationship between strain rate and holdtime effects. Both strain rate and holdtime effects are found to saturate for the material and temperature involved, and these effects have been used to guide the construction of what have been termed, "design-parameter plots." These graphical presentations of fatigue data are equipped with nomographic scales to allow for convenient usage, and the fatigue life for a given strain range and strain rate is obtained in a simple manipulation of the scales furnished. These plots are used to define a "true" holdtime effect which corresponds to the reduction in fatigue life over and above that which is associated with the strain rate effect.

Discussion

Strain Rate and Holdtime Effects

In a recent study [*12*] of the low-cycle fatigue characteristics of annealed AISI 304 stainless steel,[3] axial strain-controlled, push-pull fatigue tests were performed in air at 650 C (1200 F) using hourglass-shaped specimens [*18*]. A portion of these results was utilized [*14*] in the development of a direct relationship between strain rate and holdtime effects (Fig. 1). A linear relationship, on logarithmic coordinates, was noted between the time to fracture (given by the number of cycles to fracture divided by the test frequency employed) and the cycle period (time for one cycle). Data obtained in tests involving low strain rates were found to be colinear with those obtained in tests which employed a hold period (in the tension portion of the cycle only) in conjunction with a high strain rate. In other words, this correlation revealed that, for a given strain range, the same fracture time was obtained at the same value of the cycle time. Some importance was attached to this observation since it indicated that holdtime results could be predicted from a knowledge of completely reversed strain-cycling

[3] See Refs *12* and *19* for material chemistry, heat treatment, heat number, etc.

data obtained at several strain rates. Also, because of the linearity involved some estimate could be made of the results to be expected in very long hold-period tests. This information can lead to a cost saving since one type of test data can provide an indication of the results to be expected for the other.

In a more recent study [*15*] data covering a wider range of strain rates were reported. In addition, a 600-min holdtime test was reported in the same study. These data are presented in Table 1. When these results are introduced into the Fig. 1 correlation three observations emerge. One identifies a transition to a slope of unity in the low cycle-time regime (high strain rates) to define a range wherein N_f, the number of cycles to specimen fracture, is independent of strain rate. This change in slope, of course, limits the extrapolation of the lines in Fig. 1 to obtain fracture times corresponding to smaller cycle times.

A second observation is associated with the fact that the time to fracture for the no-holdtime tests is no longer colinear with the hold-period data in the range of large cycle times. Some hint that a deviation of this sort might be involved was actually suggested by the data at a strain rate of 4×10^{-5} s^{-1} when Fig. 1 was first published, but it was felt at the time that this was merely data scatter. The more recent data (Table 1) have now confirmed that this was indeed the beginning of a deviation from the hold-time results, and hence the same cycle time is now shown to yield larger N_f

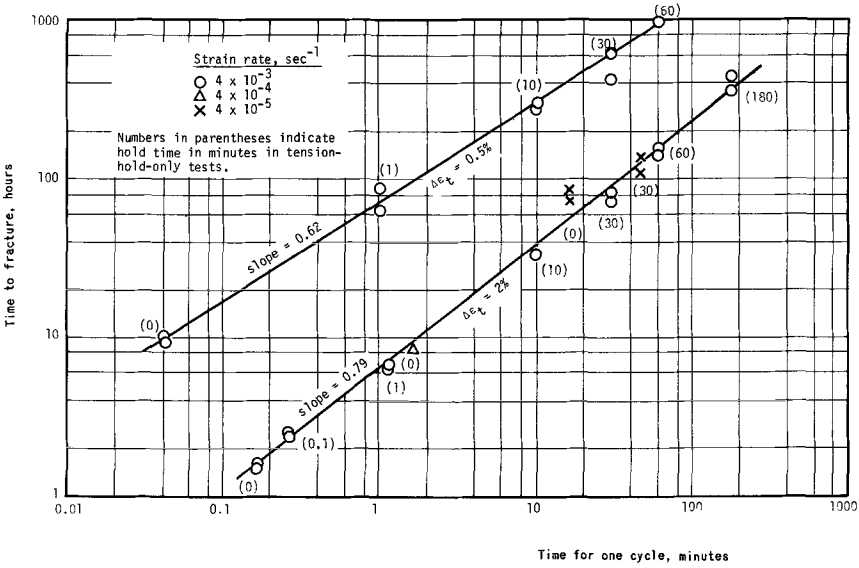


FIG. 1—*Low-cycle fatigue data* [14] *for AISI 304 stainless steel tested in air at 650 C (1200 F) using no holdtimes and holdtimes at peak strain in only the tension portion of the cycle.*

TABLE 1—*Low cycle fatigue data for AISI 304 stainless steel tested in air at 650 C (1200 F) using different strain rates and a 600-min hold period in tension only in one test at a strain rate of* 4×10^{-3} s^{-1}.

Specimen No.	Test Temperature, deg C	Cyclic Frequency, f, cycles/s	Axial Strain Rate, $\dot{\epsilon}_t$, s^{-1}	Axial Strain Range, %, Obtained at $N_f/2$			Stress Range, $\Delta\sigma$, Obtained at $N_f/2$		Fatigue Life [b]			
				$\Delta\epsilon_t$	$\Delta\epsilon_p$	$\Delta\epsilon_e$	psi	kg/mm²	N_0 Cycles	N_5 Cycles	N_f Cycles	N_f Hours
66–3	650	0.8	8.0×10^{-3}	0.49	0.28	0.22	46 700	32.8	9 696	10 170	11 136	3.87
66–2	650	0.8	1.6×10^{-2}	0.99	0.70	0.29	63 100	44.4	2 000	2 280	2 904	1.00
63–8	650	0.0001	4×10^{-6}	1.98	1.76	0.22	47 300	33.3	200	267	307	855.0
63–11	650	0.20	8×10^{-3}	1.98	1.61	0.36	78 200	55.0	536	644	734	1.02
63–7	650	0.40	1.6×10^{-2}	1.98	1.61	0.37	79 600	56.0	465	621	705	0.49
63–12	650	0.80	3.2×10^{-2}	1.98	1.62	0.36	77 800	54.7	481	641	765	0.265
66–8	650	0.05	4×10^{-3}	3.95	3.49	0.46	99 100	69.7	130	170	184	1.01
66–5	650	0.20	1.6×10^{-2}	3.95	3.47	0.48	103 200	72.6	152	208	223	0.31
66–4	650	0.20	1.6×10^{-2}	3.95	3.49	0.46	99 500	70.0	172	277	292	0.40
66–7	650	0.40	3.2×10^{-2}	3.95	3.49	0.47	100 600	70.7	138	280	303	0.21
66–1[a]	650	...	4×10^{-3}	1.98	1.80	0.18	58 100	40.8	80	115	149	1493.0

[a] Tested with a 600-min hold period in the tension portion of the cycle only.

[b] N_0 represents the number of cycles at which the load trace provides the first indication of the presence of a crack. N_5 represents the number of cycles corresponding to a 5 percent reduction of the load range.

values for continuously cycling exposures than for exposures involving hold periods in tension only beyond a certain cycle time.

The third observation is another important one in that it identifies (data available only for a 2 percent strain range) a transition to a slope of unity for both continuous cycling and tension-hold-only data. This observation places another limit on the extrapolation of the line in Fig. 1 to obtain data at longer cycle times. It also defines two other regimes; one within which the fatigue life (N_f) is independent of (or at least essentially so) strain rate, and another wherein N_f is independent of hold-period length. It is worth noting, however, that if an extrapolation is made in Fig. 1 into the long cycle-time range the results obtained for N_f will be conservative.

Employing the observations made above and changing the ordinate in Fig. 1 to read N_f values directly leads to the plot shown in Fig. 2. This graphical presentation reveals the important regimes (at least for the material involved) referred to previously. Focusing on the data for a strain range of 2 percent the following regimes are emphasized:

A. N_f is independent of strain rate above about 8×10^{-3} s^{-1} (cycle time of 0.083 min);

B. N_f is independent of strain rate below about 4×10^{-4} s^{-1} (cycle time of 1.67 min);

C. N_f is independent of hold period duration (for tension hold period only) above about 50 min;

D. N_f decreases with decreasing strain rate in the range from 8×10^{-3} to about 4×10^{-4} s^{-1};

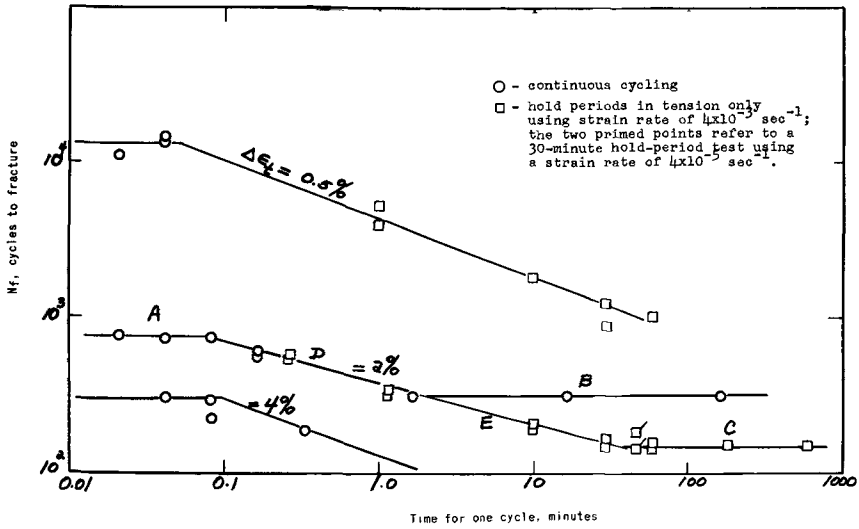


FIG. 2—*Plot of N_f versus cycle time for AISI 304 stainless steel tested in air at 650 C.*

E. N_f decreases with increasing hold period length (tension hold period only) in the range to about 50 min.

Data at other strain ranges are not extensive enough to identify these same regimes accurately, but the available data seem to suggest similar behavior patterns. These data also point to the fact that for the material and temperature involved in Fig. 2 the limit of regime *A* is located between 0.01 and 0.1 min for strain ranges from 4.0 to 0.25 percent, and it appears that as the strain range decreases the limit of regime *A* moves to lower cycle times. This saturation effect was noted by Manson et al [*16*] in introducing the strain-range-partitioning concept, and, for 2¼Cr-1Mo steel at 1100 F, it was stated that fatigue life becomes independent of frequency above approximately 0.1 Hz. This corresponds to a cycle time of 0.16 min which is seen to be in very good agreement with the limit mentioned above.

The saturation effect that is encountered as the strain rate is reduced is an interesting observation. It was suggested, however, that such an effect should exist [*16*], and hence the plateau *B* supplies confirmation for this behavior pattern. It is true that this has been established only at one strain range in Fig. 2, but it appears reasonable to expect that it will be present at other strain values as well. As suggested in the strain-range-partitioning concept this saturation effect on strain rate follows from the fact that a limit is reached on the amount of creep strain that can occur at a given controlled total strain range.

Holdtime saturation effects have not been studied extensively, but for the material and conditions associated with Fig. 2 this behavior pattern is now established. It appears to be related to the relaxed stress levels attained in holdtime tests. Beyond a certain hold period duration (about 50 min in Fig. 2 at 2.0 percent strain range) the relaxed stress level is so low that the additional creep damage resulting from an increased duration is negligible. This is an important consideration and one that can have a substantial effect on experimental investigations insofar as it can reduce the number of test hours required in evaluating detailed hold-period effects. In other words, once the saturation limit is reached for a given material the use of longer hold-period tests would be eliminated or at least drastically reduced. Certainly the importance of this aspect of fatigue testing would justify a more complete evaluation of this saturation effect.

It is evident that the reduction in N_f between plateaus *A* and *C* is a definite function of strain range, and this effect is made very obvious with this method of plotting. This effect, of course, is consistent with previously reported observations that the detrimental effect of hold periods increases with decreasing strain range.

In regime *D*, strain rate and holdtime effects are identical when compared at the same cycle time. The strain-rate effect (at 2.0 percent strain range) saturates at a cycle time of about 2.0 min, but the holdtime effect does not. For this reason the reduction in fatigue life between plateaus *A* and *B*

can be viewed as a strain rate or frequency effect, and any reduction below plateau *B* is a "true" holdtime effect. Admittedly this differentiation between strain rate and holdtime effects is a fine point, but it represents an important consideration in any attempt to interrelate the two effects.

Special attention is called to a particularly valuable piece of information [*15*] which provides convincing evidence as to the validity of the just mentioned differentiation. In duplicate tests involving a strain rate of 4×10^{-5} s^{-1} at a strain range of 2.0 percent, a 30-min hold period was employed in the tension portion of the cycle to yield a fatigue life of 142 and 182 cycles. These results confirm the "true" hold-period effect by revealing a reduction in fatigue life from plateau *B* to *C* (see Fig. 2) through the introduction of a hold period. This reduction in fatigue life from about 320 to about 150 cycles for a 30-min hold period can be compared to the much larger reduction from about 600 to 160 cycles for a 30-min hold period used in conjunction with a strain rate of 4×10^{-3} s^{-1}. One conclusion, here, is that the effect of a given hold-period duration depends on the strain rate employed. Another conclusion, of course, is that part of the 600 to 160 reduction is a frequency effect, while the remainder is a true holdtime effect. In any event, this information suggests that hold-period effects should properly be associated with the strain rate employed in the remainder of the cycle. Further study is needed to define the actual path taken between plateaus *B* and *C* as the hold-period duration is increased.

What has just been said regarding the reduction in fatigue life from plateau *B* and *C* is true only in the case of hold periods in tension only. Had the test at a strain rate of 4×10^{-5} s^{-1} been performed with a hold period of 30 min in the compression portion of the cycle no substantial reduction in fatigue life would be expected as the fatigue life would decrease just slightly below plateau *B*. For a given cycle time, then, hold periods in tension only yield the lowest fatigue life (for the material in Fig. 2), and the fatigue life for compression hold periods or for hold periods in both tension and compression will be located above the lines *D*, *E*, and *C* in Fig. 2.

Another important plateau that can be added to Fig. 2 is that associated with nonisothermal strain cycling. Some limited data of this type have been reported [*17*] based on tests of AISI 304 stainless steel for combined thermal and mechanical strain cycling tests over the temperature range from 800 to 1200 F at a strain range of 2 percent. The most damaging condition was found to correspond to the peak temperature occurring in the tension portion of the cycle with the minimum temperature occurring in the compression portion of the cycle. In continuously cycling exposures cycle times of 16.66 and 166.66 min defined a plateau at about 110 cycles. For the same strain rate, therefore, this cycling exposure yielded a much lower fatigue life than that given by plateau *B*.

A final comment on the value of the type of plot presented in Fig. 2 relates to the creep damage information which is obtainable. If the line representing plateau *A* (at 2.0 percent strain range, for example) is extended to the right, the creep damage associated with decreasing strain rates (this same approach can be applied to holdtime effects) can be calculated as the ratio of N_f obtained from lines *B*, *C*, and *D*, and the N_f value corresponding to plateau *A*. In other words, the vertical distance between lines *B*, *C*, and *D* and the extension of plateau *A* is a measure of the creep damage involved. For a cycle time of 1.0 min, for example, the creep damage is 0.33 (4300/13 000) and 0.51 (380/750) for strain ranges of 0.5 and 2.0 percent, respectively. This type of information should prove useful in developing an expression for creep damage which involves cycle time, strain range, and perhaps stress range. Such an expression would then be useful in assessing creep-fatigue interactions.

Design-Parameter Plots

An interesting extension of the graphical presentation in Fig. 2 leads to what have been termed, "design-parameter plots." Such a plot is presented in Fig. 3 to illustrate a convenient method for summarizing the low-cycle fatigue characteristics at a given temperature. These plots, of course,

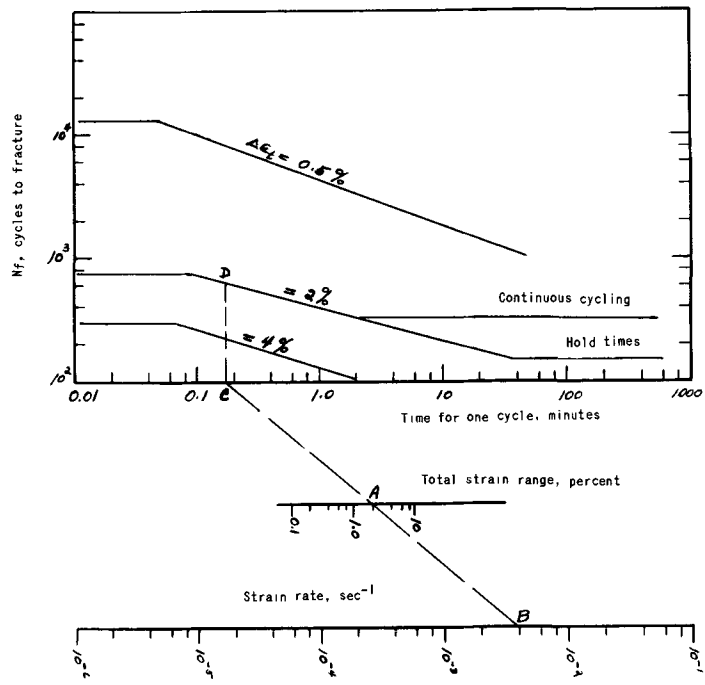


FIG. 3—*Design-parameter plot for AISI 304 stainless steel at 650 C (200 F).*

depend on detailed experimental investigations to provide an exact positioning of the strain range, strain rate, and holdtime patterns. Once established, though, the nomographic scales provide a direct usage for a given combination of these parameters. For a given strain range and strain rate these points are located on the appropriate scales (see points A and B for 2 percent strain range and a strain rate of 4×10^{-3} s^{-1}). A line connecting these points intersects the cycle time scale to yield point C at 0.166 min. A vertical projection to the appropriate strain range line (2 percent in this example) provides point D which, when projected horizontally yields the desired N_f value of 620 cycles. For continuous strain cycling the vertical projection to locate N_f is confined to regimes A, B, and D of Fig. 2.

When a holdtime is involved the cycle time for continuous cycling is located as in the previous example, and then the hold period is added to this to locate the actual cycle time on the abscissa. A vertical projection is then made to the lines in the appropriate regimes, and, as before, the corresponding N_f value is read from the ordinate scale.

An eventual inclusion in the design-parameter plots would be additional strain range lines for intervals of 0.5 percent strain range. This modification need not involve extensive amounts of experimental data for it is felt that once the general behavior patterns for, lets say, 2.0 and 0.5 percent strain range are known the positioning of other lines for other strain ranges can be accomplished with just a few test points. It also seems possible to attain acceptable accuracies by estimating the position of intermediate strain range lines after more experience is obtained with this type of plot. Usually, a fatigue curve at a given strain rate is available, and this can be used to define one point on the line for any strain range desired. This, then, will provide a good guide for interpolation purposes. As a matter of fact, a plot of this type is considered an important adjunct to the design-parameter plot and could be incorporated as a separate curve to be used in conjunction with the N_f scale. Such a plot would, of course, be confined to a specific strain rate and the nomographic scales could be used to locate the N_f point on the design-parameter plot for any desired strain range. This single point, as described previously could then guide the estimates of N_f for any cycle time at the strain range involved.

Another eventual modification of this diagram which has been considered involves the accommodation of cumulative damage. The addition of two other nomographic scales would allow a fatigue life fraction to be read directly. This fraction would be related to a certain exposure, and the remaining life fraction could be easily obtained. This type of approach could handle combined test conditions exposures involving several strain rates, several strain ranges, or several holdtimes. Before this is done, however, more must be understood about the summation of fatigue life fractions. Recent data [*20*] have shown that these provide a summation to unity in certain cases but not in others [*21*].

A great deal remains to be done before the full usefulness of the design-parameter plot is realized completely, but the concept appears to have considerable merit in providing a complete representation of the low-cycle fatigue behavior for each temperature. Also of importance is the fact that a clear indication of the effect of strain rate and holdtime is made available, and the regimes involving saturation of strain-rate and holdtime influences are immediately obvious. And special mention also should be made of the valuable assistance these plots offer in guiding experimental programs designed to yield a detailed characterization of low-cycle fatigue behavior. This guidance will have an effect of minimizing the amount of experimental points required to completely define the fatigue behavior for a given material.

References

[1] Ellison, E. G., *Journal Mechanical Engineering Science*, Vol. 11, 1969, p. 318.

[2] Manson, S. S. and Halford, G. R., International Conference on Thermal and High Strain Fatigue, Monograph and Report Series 32, The Metals and Metallurgy Trust, London, 1967.

[3] Manson, S. S., Halford, G. R., and Spera, D. A. in *A. E. Johnson Memorial Volume*, A. I. Smith, Elsevier, Amsterdam, 1971, p. 229.

[4] Wood, D. S., *Welding Journal Research Supplement*, 1966, p. 92-s.

[5] Eckel, J. F. in *Proceedings*, American Society for Testing and Materials, Vol. 51, 1951, p. 745.

[6] Coles, A. and Skinner, D., *Journal of the Royal Aeronautical Society*, Vol. 69, 1965, p. 53.

[7] Coles, A., Hill, G. J., Dawson, R. A. J., and Watson, S. J., International Conference on Thermal and High Strain Fatigue, Monograph and Report Series 32, The Metals and Metallurgy Trust, London, 1967.

[8] Coffin, L. F., Jr., *Fracture 1969 Proceedings*, 2nd International Conference on Fracture, Chapman and Hall, London, 1969.

[9] Dawson, R. A. T., Elder, W. J., Hill, G. J., and Price, A. T., International Conference on Thermal and High Strain Fatigue, Monograph and Report Series 32, The Metals and Metallurgy Trust, London, 1967.

[10] Edmunds, H. G. and White, D. J., *Journal of Mechanical Engineering Science*, Vol 8, 1966, p. 310.

[11] Walker. C. D. in *Proceedings*, Joint International Conference on Creep, The Institution of Mechanical Engineers, London, 1963, pp. 3-49.

[12] Berling, J. T. and Conway, J. B. in *Proceedings*, First International Conference on Pressure Vessel Technology, Delft, Holland, American Society of Mechanical Engineers, 1970, Part II.

[13] Conway, J. B.. Berling, J. T., and Stentz, R. H., *Nuclear Applications and Technology*, Vol. 9, 1970, p. 31.

[14] Conway, J. B. and Berling, J. T., *Metallurgical Transactions*, Vol. 1, 1970, p. 324.

[15] Conway, J. B., Report No. GEMP-740, 1969, General Electric Company, Nuclear Systems Programs.

[16] Manson, S. S., Halford, G. R., and Hirschberg, M. H. in *Symposium on Design for Elevated Temperature Environment*, American Society of Mechanical Engineers, 1971, p. 12.

[17] Stentz, R. H., Berling, J. T., and Conway, J. B., *Proceedings*, International Conference on Structural Mechanics in Reactor Technology, Berlin, Germany, 1971.

[18] Slot, T., Stentz, R. H., and Berling, J. T. in *Manual on Low-Cycle Fatigue Testing*, *ASTM STP 465*, American Society for Testing and Materials, 1969, p. 100.

[19] Berling, J. T. and Slot, T. in *Fatigue at High Temperature*, *ASTM STP 459*, American Society for Testing and Materials, 1969, p. 3.
[20] Conway, J. B., Berling, J. T., and Stentz, R. H., *Metallurgical Transactions*, Vol. 1, 1970, p. 2034.
[21] Conway, J. B. and Berling, J. T., unpublished notes.

DISCUSSION

J. Wareing[1] (*written discussion*)—I offer one comment. One possible explanation for the difference in fatigue life saturation level for cycles containing tensile hold periods and continuous tests could be related to the fracture pattern associated with the two cycle patterns. The introduction of creep type damage into the bulk of the material, by tensile-stress-relaxation periods, effectively reduces the crack length to failure as tensile failure can intervene at a much shorter time than would be expected in continuous rests where bulk creep damage is not usually observed.

I. LeMay[2] (*written discussion*)—What is the criterion for failure in these tests which, I understand, are conducted in strain control?

J. B. Conway, J. T. Berling, and R. H. Stentz (*authors' closure*)—Two criteria have been used, the cycle number where the tensile load decreases by 5 percent from the maximum, and complete separation of the specimen. There is no significant change to the conclusions related to the criterion of failure.

[1] United Kingdom Atomic Energy Authority, Lancashire, England.
[2] Department of Mechanical Engineering, University of Saskatchewan, Saskatoon, Sask., Canada.

D. A. Spera[1]

Comparison of Experimental and Theoretical Thermal Fatigue Lives for Five Nickel-Base Alloys

REFERENCE: Spera, D. A., "**Comparison of Experimental and Theoretical Thermal Fatigue Lives for Five Nickel-Base Alloys,**" *Fatigue at Elevated Temperatures, ASTM STP 520*, American Society for Testing and Materials, 1972, pp. 648–657.

ABSTRACT: Alloys investigated were Nimonic 90, IN 100, coated IN 100, B 1900, coated B 1900, MAR M200, and MAR M200DS (directionally solidified). Maximum temperatures ranged from 770 to 1120 C (1420 to 2050 F). Specimen geometries included tapered disks, double-edged wedges, and cambered airfoils. The disks and wedges were heated and cooled in fluidized beds. The airfoil specimens were heated by a Mach 1 natural gas burner and rapid-air cooled, with and without spanwise loading. Life calculations included two distinct failure modes: conventional low-cycle fatigue and cyclic creep. Required material properties were limited to conventional thermal, tensile, and creep-rupture data. The complete life calculation system included the calculation of transient temperature distributions, thermal strains, stresses, creep damage, fatigue damage, and finally cycles to first crack. Calculated lives were within a factor of two for 76 of the 86 data points analyzed. Cyclic creep accounted for 80 per cent of all the calculated damage.

KEY WORDS: nickel alloys, thermal fatigue, creep properties, fatigue (materials), stress cycle, grain size, crack initiation, damage, stress analysis

The purpose of this investigation is to evaluate a theory for calculating thermal fatigue life. This theory has evolved from previous work at the Lewis Research Center [*1–3*][2] and from earlier work by Robinson [*4*] and Taira [*5*]. All indications are that this evolutionary process will continue. For example, integration of the new concept of "strain-range partitioning" [*6*] is now being investigated.

The complete life calculation system contains many simplifying assumptions concerning details of heat transfer, thermal stress analysis, plasticity, creep, cumulative damage, crack initiation, etc. Space limitations prohibit examining these assumptions in detail here. However, they will be discussed thoroughly in a forthcoming National Aeronautics and Space Administration (NASA) publication.

[1] Consultant, Fatigue Branch, Lewis Research Center, National Aeronautics and Space Administration, Cleveland, Ohio 44135.

[2] The italic numbers in brackets refer to the list of references appended to this paper.

Copyright© 1973 by ASTM International www.astm.org

Test data were obtained from three sources: the National Gas Turbine Establishment [7] for Nimonic 90 tapered-disk data; the IIT Research Institute [8,9] for IN 100, B 1900, MAR M200 and MAR M200DS double-wedge data; and the Lewis Research Center [10] for IN 100 and B 1900 cambered-airfoil data. Mechanical properties required for analysis were always limited to conventional tensile and creep-rupture data for the alloy in its as-received condition.

Strain-Temperature-Time Calibration

Life analysis starts with the calculation of temperature and mechanical strain cycles at possible points of failure. These calculations are made for representative values of the primary variable which may be maximum temperature, cycle time, or external load. This forms a strain-temperature-time calibration curve from which to extrapolate to other values of the primary variable. Thermocouple data and a thermoelastic strain analysis are the basis of this calibration. For the airfoil specimens, data from infrared photographs, an electrooptical pyrometer, and an electrooptical extensometer were also used.

Figure 1 shows typical strain-temperature-time calibration curves for the three geometries analyzed, for representative alloys. Wide variations among these curves are apparent. Since time, temperature, and strain inter-

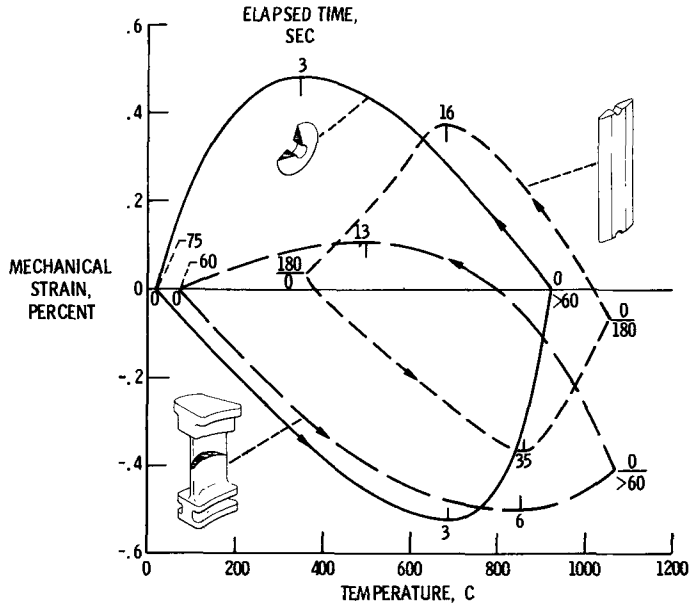


FIG. 1—*Typical strain-temperature-time calibration curves (alloys: Nimonic 90 tapered disk, MAR M 200 double wedge, B 1900 airfoil).*

act to produce failure, an analytical method becomes essential in correlating various laboratory tests and actual service.

Elastic-Plastic-Creep Stress Analysis

The elastically computed mechanical strains were assumed to remain constant in the presence of local plastic flow and creep, as proposed in Ref *11*. The mechanical strain cycle was divided into small increments in order to compute its elastic, plastic, and creep components. Successive iteration was required to produce a stable, repeating hysteresis loop. Details of the cyclic thermal stress analysis will be given in a forthcoming NASA publication. In general, it is a complex but necessary part of the complete life calculation system.

Life Calculation Theory

The life calculation theory used in this study is described in Ref *3*. This theory states that thermal fatigue is a combination of conventional low-cycle fatigue and cyclic creep rupture. Low-cycle fatigue is assumed to be time-independent and usually results in failure by transgranular cracking. On the other hand, cyclic creep rupture is assumed to be time-dependent and usually causes intergranular cracking. Life is calculated separately for each of these two distinct failure modes. A linear interaction between fatigue and cyclic creep lives is assumed. This assumption is made primarily for convenience, since one mode is usually dominant. Then thermal fatigue life can be calculated as follows:

$$\frac{1}{N_t} = \frac{1}{N_c} + \frac{1}{N_f} \quad \ldots\ldots\ldots\ldots\ldots\ldots\ldots\ldots (1a)$$

or

$$N_t = (\varphi_c + \varphi_f)^{-1} \quad \ldots\ldots\ldots\ldots\ldots\ldots\ldots\ldots (1b)$$

where

N = cycles to failure,
φ = damage per cycle, $1/N$, and
t,c,f = thermal fatigue, cyclic creep, and low-cycle fatigue, respectively.

In this investigation, approximately 80 percent of all the calculated damage was by cyclic creep, with 20 percent by fatigue.

Cyclic Creep Damage

Cyclic creep damage, φ_c, is calculated from conventional creep-rupture data. A modification of the life-fraction rules proposed by Robinson and Taira [*4*,*5*] is used, as follows:

$$\varphi_c = \int_0^{\Delta t} \frac{dt}{kt_r\,(|S|,T)} \quad \ldots\ldots\ldots\ldots\ldots\ldots\ldots\ldots (2)$$

where

t = elapsed time, h,
Δt = time per cycle, h,
t_r = conventional creep rupture life, h,
$|S|$ = absolute value of instantaneous stress, N/cm^2,
T = instantaneous temperature, deg C, and
k = 1, for uncoated alloys; or D/D' for coated alloys, assuming cracks initiate in the substrate.

where

D = tensile ductility at temperature T, cm/cm, and
D' = average creep strain during first and second stages at temperature T, cm/cm.

The two values of k are derived from the idealized creep-rupture behavior shown in Fig. 2. First and second stages of creep are linearized, with a constant creep rate $\dot{\epsilon}_c$. Unstable third stage creep occurs at a strain of D' and a time t_r, the conventional creep-rupture life. However, if the creep rate were held constant, it is assumed that rupture would not occur until the creep strain equals the ductility D. Thus the "stable" rupture time would be longer than the "unstable" or conventional rupture life by a factor of D/D'. This is similar to behavior proposed in Ref *12*.

Cyclic creep-rupture is also assumed to occur in either a stable or unstable mode. Isothermal strain cycling, balanced in tension and compression, is usually stable, as discussed in Ref *12*. However, thermal fatigue cycles are potentially unstable. Creep strains in tension and compression are rarely in balance. Usually creep occurs in only one half-cycle and is balanced by time-independent plasticity in the other. Two different flow mechanisms are usually present, with creep occurring at the grain boundaries and plasticity within grains. On an uncoated surface, accumulation of

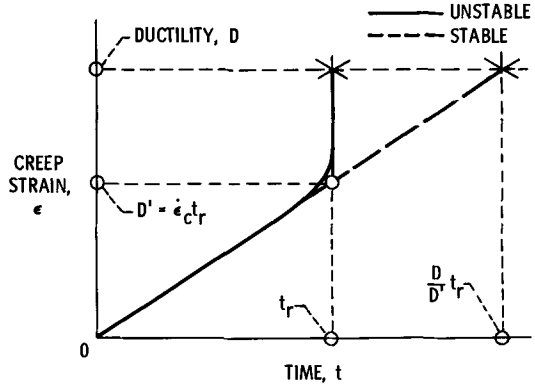


FIG. 2—*Idealized creep-rupture behavior.*

creep at a grain boundary or other discontinuity can cause local bulging or necking. This is assumed to be unstable deformation analogous to conventional creep rupture, and k, therefore, is taken equal to 1.

Grain size can be expected to influence the distribution of inelastic strain along the surface of the material. A fine-grained structure should produce a more uniform distribution of tensile and compressive inelastic strain. Following this hypothesis, it is assumed that a fine-grained, oxidation-resistant coating distributes inelastic strain uniformly along the surface of the substrate, preventing local deformation at grain boundaries. For a coated alloy, then, deformation is assumed to be stable and k is taken equal to D/D'.

The assumption that cracks initiate in the substrate is consistent with the qualities of good high-temperature coatings: oxidation resistance, reasonable ductility, metallurgical bonding, compatible thermal expansion, etc.

Low-Cycle Fatigue Damage

Fatigue damage φ_f was calculated by Manson's method of universal slopes [*11*]. This is an empirical formula relating mechanical strain range, cycles to failure (or fatigue damage), and conventional tensile properties, as follows:

$$\varphi_f = \frac{1}{N_f}, \text{ fatigue damage}$$

$$\Delta\epsilon_m = 3.5 \frac{\text{UTS}}{E} \varphi_f^{0.12} + D^{0.6} \varphi_f^{0.6} \quad \ldots\ldots\ldots\ldots\ldots\ldots (3)$$

where

$\Delta\epsilon_m$ = mechanical strain range, cm/cm,
UTS = ultimate tensile strength, N/cm^2,
E = Young's Modulus, N/cm^2, and
D = tensile ductility, cm/cm.

Equation 3 can be solved either graphically or numerically for φ_f. To be conservative, tensile properties were evaluated at the temperature in the cycle which gives the minimum life (maximum φ_f). This is usually the maximum temperature in the cycle.

The method of universal slopes has been used successfully to correlate data for a wide variety of alloys. However, for a specific alloy, some other empirical formula or fatigue data could be substituted if available.

Results

Figures 3 to 8 present comparisons between observed and calculated thermal fatigue lives for the various alloys and test conditions. Lives are

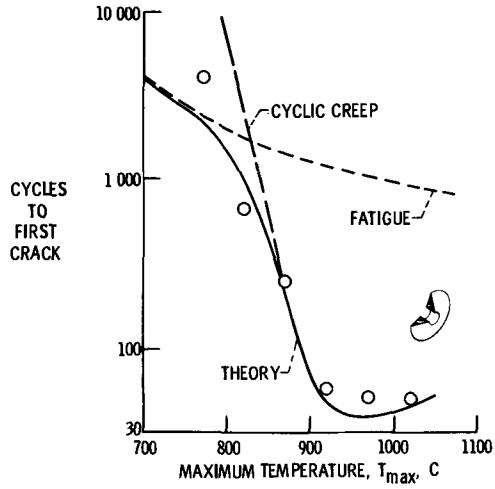


FIG. 3—*Comparison of theoretical and experimental thermal fatigue lives of Nimonic 90 tapered disks (0.25-mm-radius edge, heating and cooling in fluidized beds, 20 C* $\rightleftarrows$ T_{max}, *data from Ref* 7).

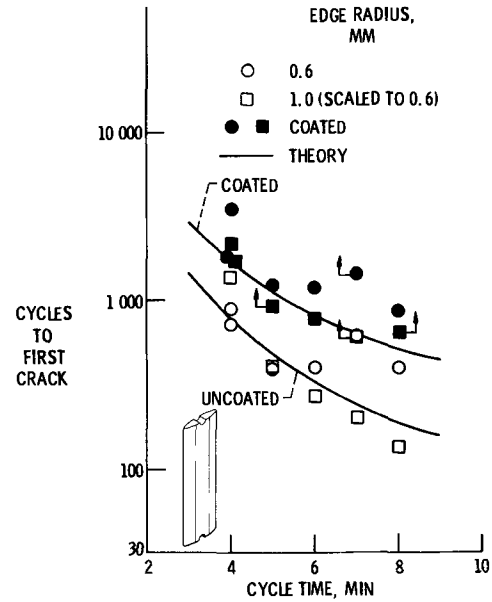


Fig. 4—*Comparison of theoretical and experimental thermal fatigue lives of B 1900 double wedges (0.6 and 1.0-mm-radius edge, heating and cooling in fluidized beds at 320 and 1090 C, data from Refs* 8 *and* 9).

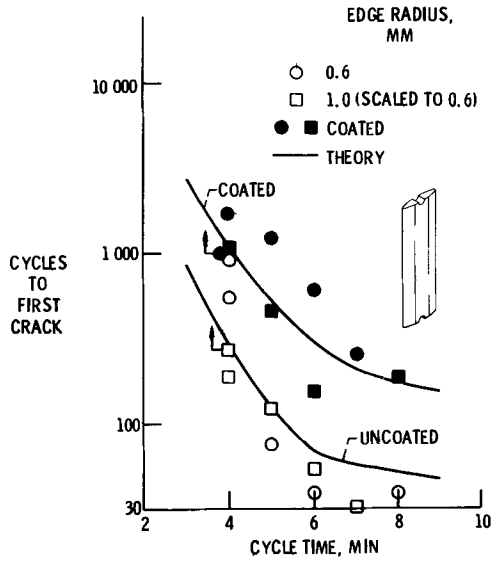


FIG. 5—*Comparison of theoretical and experimental thermal fatigue lives of IN 100 double wedges (0.6 and 1.0-mm-radius edge, heating and cooling in fluidized beds at 320 and 1090 C, data from Refs* 8 *and* 9).

given as "cycles to first crack" which was determined in one of two ways: In the fluidized bed tests, it was the average of the last inspection cycle without cracks and the first inspection cycle with cracks. In the burner-rig tests, sufficient crack propagation data were obtained to extrapolate backwards to "zero" crack length, and that cycle was taken as the life.

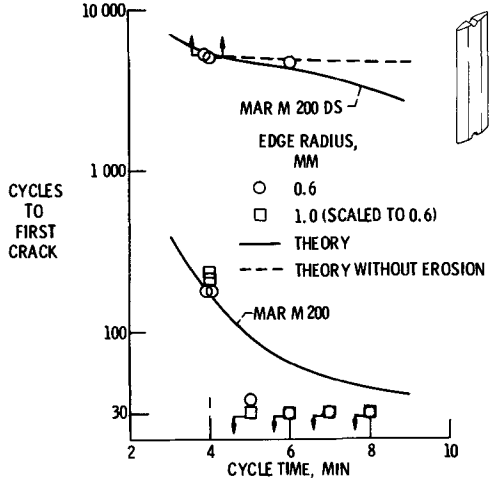


FIG. 6—*Comparison of theoretical and experimental thermal fatigue lives of MAR M200 and MAR M200DS double wedges (0.6 and 1.0-mm-radius edge, heating and cooling in fluidized beds at 320 and 1090 C, data from Refs* 8 *and* 9).

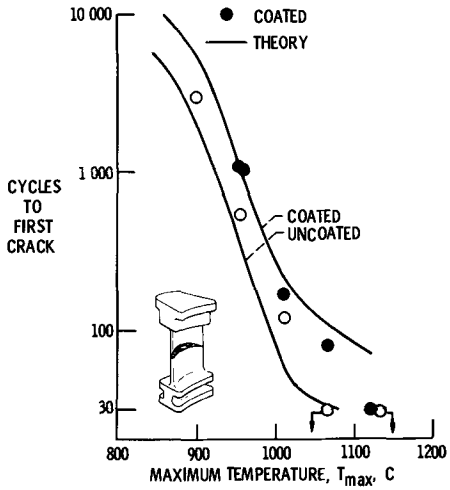


FIG. 7—*Comparison of theoretical and experimental thermal fatigue lives of IN 100 cambered airfoils (1.2-mm radius leading edge, heating in Mach 1 burner, rapid air cooling, 75 C ⇄ T_{max}, data from Ref* (10).

In Fig. 3, representative fatigue and cyclic creep lives are shown for tapered-disk specimens, together with their linear interaction. In Figs. 4, 5, and 6 data for the two different edge radii on double-wedge specimens are compared with the curves for the 0.6-mm-radius edge. For convenience, the data for the 1.0-mm-radius edges have been scaled to 0.6 mm, maintaining the same ratio of calculated to observed life [*9*].

Life calculations for MAR M200DS (Fig. 6) included a first-order correction for sharpening of the edge radius through erosion of the wedge sur-

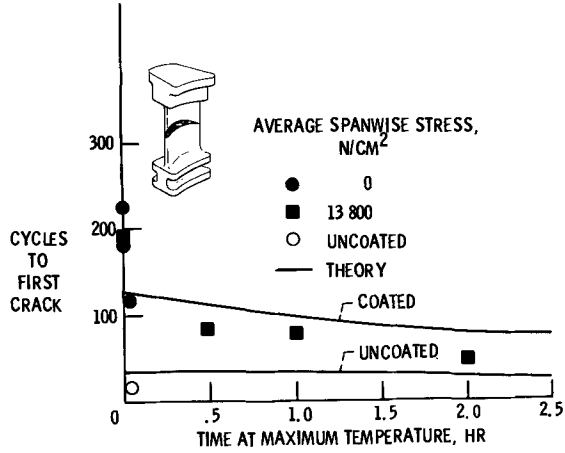


FIG. 8—*Comparison of theoretical and experimental thermal fatigue lives of B 1900 cambered airfoils (1.2-mm radius leading edge, heating in Mach 1 burner, rapid air cooling, 75 C ⇄ 1065 C, data from Ref* 10).

faces. Erosion was found to be relatively high in this directional alloy [9]. This correction produced a 15 percent reduction in calculated life for the 6 min cycle. Erosion corrections for the other alloys were negligible.

For the airfoil tests (Figs. 7 and 8), it was necessary to include the effect of the Mach 1 gas velocity on the static creep-rupture time t_r in Eq 2. As discussed in Ref *10*, this high gas velocity can cause losses in life amounting to more than 90 percent at 1000 C.

Concluding Remarks

Calculated lives were within a factor of two for 76 of the 86 data points analyzed. Log standard deviation was 0.2, or a factor of 1.6. Cyclic creep accounted for 80 per cent of all the calculated damage. Further evaluation is recommended, particularly using data on cobalt and iron-base alloys and specimens with stress concentrations and vibration.

References

[1] Manson, S. S., *International Journal of Fracture Mechanics*, Vol. 2, No. 1, March 1966, pp. 327–363.
[2] Spera, D. A., "A Linear Creep Damage Theory for Thermal Fatigue of Materials," Ph.D. thesis, University of Wisconsin, Madison, 1968.
[3] Spera, D. A., "The Calculation of Elevated Temperature Cyclic Life Considering Low-Cycle Fatigue and Creep," NASA TN D-5317, National Aeronautics and Space Administration, July 1969.
[4] Robinson, E. L., *Transactions*, American Society of Mechanical Engineers, Vol. 74, No. 5, July 1952, pp. 777–781.
[5] Taira, S. in *Creep in Structures*, N. J. Hoff, ed., Springer Verlag, Berlin, 1962, pp. 96–124.
[6] Halford, G. R., Hirschberg, M. H., and Manson, S. S., see p. 658 of this symposium.
[7] Glenny, E. and Taylor, T. A., *Journal of the Institute of Metals*, Vol. 88, 1959–1960, pp. 449–461.
[8] Howes, M. A. H., "Thermal Fatigue Data on 15 Nickel- and Cobalt-Base Alloys," NASA CR-72738, National Aeronautics and Space Administration, May 1970.
[9] Spera, D. A., Howes, M. A. H., and Bizon, P. T., "Thermal-Fatigue Resistance of 15 High-Temperature Alloys Determined by the Fluidized-Bed Technique," NASA TM X-52975, National Aeronautics and Space Administration, March 1971.
[10] Spera, D. A., Calfo, F. D., and Bizon, P. T., "Thermal Fatigue Testing of Simulated Turbine Blades," NASA TM X-67820, National Aeronautics and Space Administration, May 1971.
[11] Manson, S. S., *Experimental Mechanics*, Vol. 5, No. 7, July 1965, pp. 193–226.
[12] Swindeman, R. W. in *Proceedings*, Joint International Conference on Creep, Institution of Mechanical Engineers, London, 1963, pp. 3–71 to 3–76.

DISCUSSION

Lyman Johnson[1] (*written discussion*)—Since this is basically a ductility exhaustion theory, it is critical how you determine what ductility to use. As I understand you, you are using the rupture ductility. Can you comment on how badly this may effect your results obtained under conditions of unstable flow, whereas your model implies a rupture failure under stable flow. It seems highly unlikely that these ductilities are, in fact, equal.

D. A. Spera (*author's closure*)— The model actually uses the tensile ductility, rather than the rupture ductility. Since the tensile ductility is obtained under strain-controlled or "stable" conditions, it is consistent with the stable failure mode.

Lives for uncoated specimens are unaffected by changes in ductility. Lives for coated specimens are changed in proportion to changes in ductility. Therefore, the log of the number of cycles to failure is only moderately sensitive to the ductility assumed for the coated specimens.

[1] Schenectady, N. Y. 12301.

G. R. Halford,[1] *M. H. Hirschberg,*[1] *and S. S. Manson*[1]

Temperature Effects on the Strainrange Partitioning Approach for Creep Fatigue Analysis

REFERENCE: Halford, G. R., Hirschberg, H. M., and Manson, S. S., "**Temperature Effects on the Strainrange Partitioning Approach for Creep Fatigue Analysis,**" *Fatigue at Elevated Temperatures, ASTM STP 520*, American Society for Testing and Materials, 1973, pp. 658–669.

ABSTRACT: Examination is made of the influence of temperature on the strainrange partitioning approach to creep fatigue. Results for 2¼Cr-1Mo steel and Type 316 stainless steel show the four partitioned strainrange-life relationships to be temperature insensitive to within a factor of two on cyclic life. Monotonic creep and tensile ductilities were also found to be temperature insensitive to within a factor of two.

The approach provides bounds of cyclic life that can be readily established for any type of inelastic strain cycle. Continuous strain cycling results obtained over a broad range of high temperatures and frequencies are in excellent agreement with bounds provided by the approach.

KEY WORDS: fatigue (materials), creep-fatigue, strains, strainrange partitioning, creep properties, plastic properties, hysteresis, flow, fatigue failure, life prediction

In a recent paper [*1*][2], the strainrange partitioning approach was proposed for dealing with creep-fatigue interaction in elevated temperature, strain-cycling fatigue. The basic premise is that cyclic lives are governed by the capacity of materials to absorb cyclic inelastic strains. Two types of inelastic strain are considered to be important: time-independent (plastic) and time-dependent (creep) inelastic strain. Four combinations of creep and plasticity have significance since they represent extremes in behavior, and because they may be regarded as building blocks for partitioning more complex cycles. These are shown in Fig. 1 as idealized hysteresis loops whose widths are defined by:

$\Delta\epsilon_{pp}$, tensile plastic strain reversed by compressive plastic strain.

$\Delta\epsilon_{cp}$, tensile creep strain reversed by compressive plastic strain.

[1] Engineer, head, Fatigue Research Section, and chief, Materials and Structures Division respectively, NASA-Lewis Research Center, Cleveland, Ohio 44135.

[2] The italic numbers in brackets refer to the list of references appended to this paper.

Copyright© 1973 by ASTM International www.astm.org

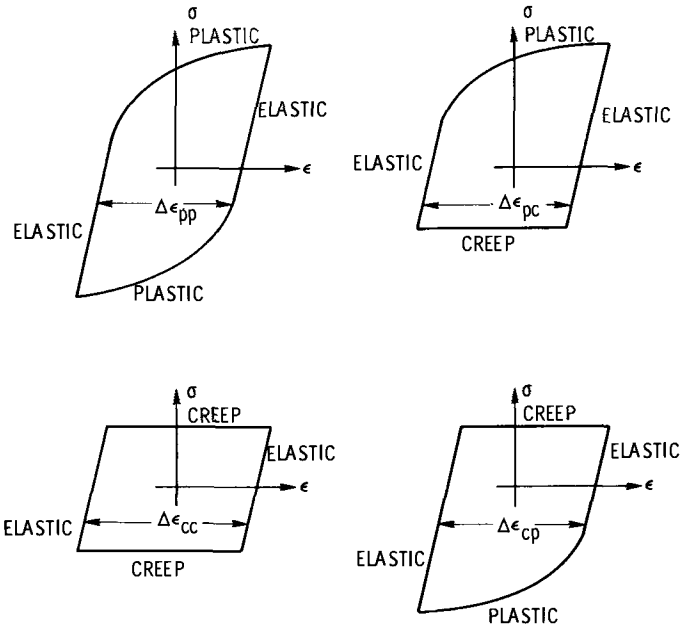


FIG. 1—*Idealized hysteresis loops for the four basic types of inelastic strainrange.*

$\Delta\epsilon_{pc}$, tensile plastic strain reversed by compressive creep strain.
$\Delta\epsilon_{cc}$, tensile creep strain reversed by compressive creep strain.

Procedures for experimentally obtaining the basic partitioned strainrange—cyclic life relationships are presented in Ref *1*.

Preliminary results for 2¼ Cr-1Mo steel presented in Ref *1* and for Type 316 stainless steel presented in Ref *2* suggest that the partitioned strainrange-cyclic life relationships for these two engineering alloys (as well as others in their general class) may be insensitive to test temperature. This would hold special significance for three important reasons: (*a*) the amount of material property data required for analyses could be greatly reduced, (*b*) bounds on cyclic life could be established more readiy, even for complex temperature and loading histories, and (*c*) a better understanding of the physical processes of creep-fatigue interaction could result if the cyclic failure criteria are insensitive to temperature—a variable that is considered normally to be of utmost importance to creep-fatigue analysis.

Although temperature may have a small effect on the failure behavior (the partitioned strainrange-life relationships), temperature does have a generally well known, pronounced effect on the flow behavior (the stress-strain, strain rate-temperature relationships). Flow characteristics govern the amount of creep and plasticity encountered during a cycle of inelastic straining. The amounts of creep and plasticity in tension and compression

combine to form the partitioned strainranges of the cycle. Since the magnitudes of these strainranges dictate the cyclic life, an analyst interested in predicting life must have a knowledge of both the flow and failure behavior. However, as will be discussed, a detailed knowledge of the flow behavior is not always required, particularly if bounds on cyclic life are sufficient.

This paper examines the effects of temperature on the cyclic failure behavior and certain aspects of the cyclic flow behavior of two alloys.

Materials and Experimental Details

The materials studied are 2¼Cr-1Mo steel (ASTM A355, Grade P-22) and Type 316 stainless steel. Both were tested in the fully annealed condition. These alloys are typical representatives of a class of high-temperature engineering materials whose mechanical behavior exhibits stability over extended periods of exposure over a broad range of high temperatures. An example of this stability is indicated by the fact that variations in creep and plastic ductility are generally well within a factor of two [*3*].

Specimens for the cyclic studies were of the tubular, hourglass configuration as described fully in Ref *4*. Heating was either by direct resistance or by an internally positioned silicon carbide heating element. All tests were conducted using closed-loop, servo-controlled, electro-hydraulic equipment. Strains were measured using a diametral extensometer. All strains reported are longitudinal strains calculated from diametral strains. More complete details of the experimental procedures and test equipment can be found in Refs *1*, *4*, and *5*.

Results and Discussion

Partitioned Strainrange-Cyclic Life Relationships

The partitioned strainrange-cyclic life relationships reported in Refs *1* and *2* for the Type 316 stainless steel evaluated at 705 C are shown in Fig. 2. New results generated at 595, 650, and 815 C for this alloy are tabulated in Ref *3* and are plotted here in Fig. 2 along with the 705 C baseline results. Similar results were generated at 510, 565, and 650 C using the 2½Cr-1Mo steel. These latter results are tabulated and plotted in Ref *3*.

A few of the tests were conducted with a different temperature in tension than in compression. The two temperatures are listed with the tensile temperature appearing first. Open data symbols are used for the earlier data and closed for the new results. The symbols were chosen to represent the shapes of the hysteresis loops (see Fig. 1 and Ref *1*) of the tests performed. The procedures of Ref *1* were used to establish the validity of a test result before it was plotted in Fig. 2.

An overall measure of how well the strainrange partitioning approach predicted the creep-fatigue lives for both materials is shown in Fig. 3. All of the data generated at the baseline temperature of 595 C for the 2¼Cr-1Mo steel and 705 C for the Type 316 stainless steel are shown by open

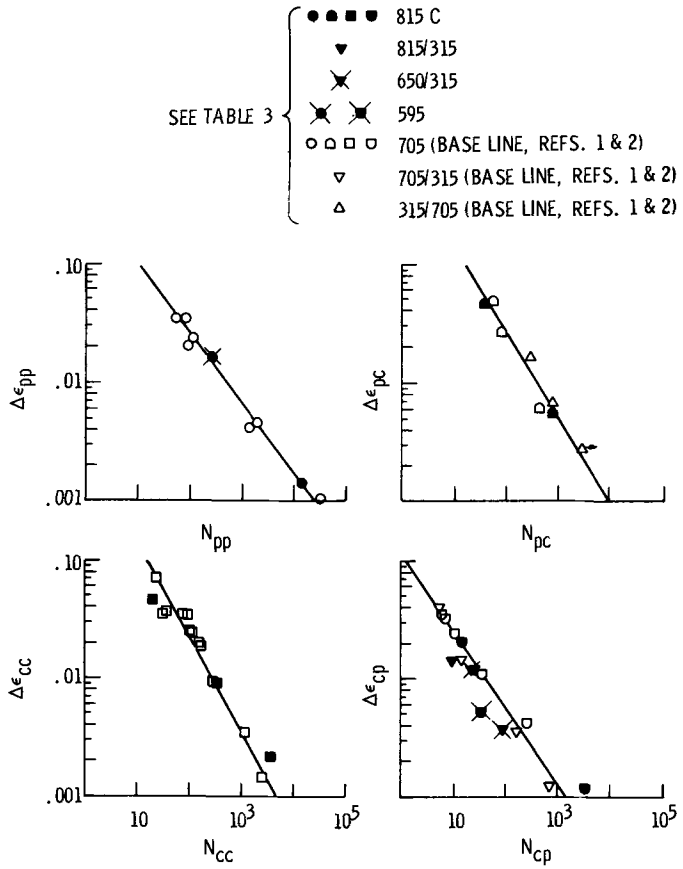


FIG. 2—*Partitioned strainrange-life relationships for Type 316 stainless steel.*

circles. Data for temperatures both higher and lower are indicated by solid circles. Nearly all of the results fall within a factor of two of the cyclic lives predicted from the baseline results. It is clearly demonstrated that the temperature dependence of the cyclic lives corresponding to a particular type of inelastic strain is a small one. Hence, for the materials of this investigation, failure data generated at one temperature are applicable over their entire use range of elevated temperatures.

Ductility Considerations

Each of the four independent strainrange—cyclic life relationships may be written in the form,

$$\Delta\epsilon_{ij} = (D_{ij}/N_{ij})^{s} \qquad , ij = \begin{cases} pp \\ cp \\ pc \\ cc \end{cases}$$

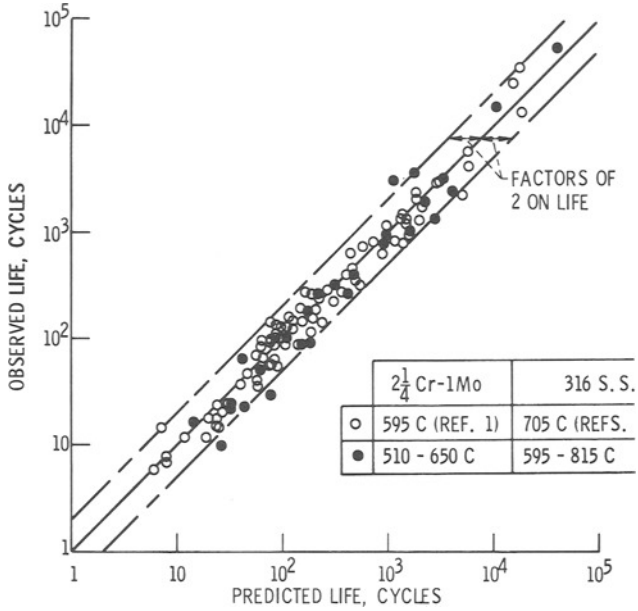


FIG. 3—*Comparison of observed and predicted life at different temperatures using strainrange partitioning approach.*

where N_{ij} is the cyclic life for the partitioned strainrange $\Delta\epsilon_{ij}$ of interest, and s is the slope of the log-log straight-line relationship. The term D_{ij} may be viewed as a measure of the cyclic strain absorption capacity, or simply the cyclic ductility, for the partitioned strainrange of interest. For a given strainrange, a change in the cyclic ductility will produce an equal change in cyclic life.

A possible correlation between monotonic and cyclic ductilities is suggested by the present results on 2¼Cr-1Mo steel and Type 316 stainless steel since both the monotonic and the cyclic ductilities are insensitive to test temperature to within a factor of two.

Application of Strainrange Partitioning Approach

Some examples of the application of the approach will now be presented that illustrate the implications of having a temperature-independent failure criteria together with temperature-dependent flow behavior. The net influences of temperature on isothermal continuous strain cycling lives of tests conducted over a range of temperatures and frequencies is demonstrated using data generated on specimens of Type 316 stainless steel. A brief discussion is also presented regarding the application of the approach to thermal strain cycling problems.

Temperature Effect—Consider a series of constant strainrange inelastic fatigue tests conducted at a constant frequency over a spectrum of isother-

mal elevated temperatures. At the lower temperatures, the flow-behavior is such that the inelastic strain range contains negligible creep. Hence, the inelastic strain range is predominately $\Delta\epsilon_{pp}$, and the resultant cyclic life is N_{pp}. As the test temperature is raised, time-dependent creep deformation is produced along with the plastic strain. For a "balanced" type of strain cycle, wherein the temperature and strain rates in tension are equal to those in compression, one would expect an equal amount of creep strain in tension as compression. Hence, the inelastic strainrange is partitioned by the higher temperature into components of $\Delta\epsilon_{cc}$ and $\Delta\epsilon_{pp}$. The cyclic life will therefore be between the bounding values of N_{cc} and N_{pp}. Finally, at still higher temperatures, the entire inelastic strainrange becomes $\Delta\epsilon_{cc}$ and the ensuing cyclic life is N_{cc}. If the $\Delta\epsilon_{cc}$—N_{cc} relationship is temperature insensitive, any further increases in isothermal test temperature of the strain cycling tests would not cause the cyclic life to drop below the N_{cc} level.

A series of tests as described above were conducted using Type 316 stainless steel. The inelastic strainrange was chosen nominally equal to 0.0045 with a frequency of 0.02 Hz and a triangular strain-time waveform. Test temperatures spanned the range from 540 to 870 C. The results of these tests are plotted in Fig. 4 using circular data symbols. Included in Fig. 4 are the partitioned strainrange—cyclic life relationships for $\Delta\epsilon_{cc}$ and $\Delta\epsilon_{pp}$ taken from Fig. 2. These two life lines bound the experimental results. Furthermore, the lowest temperature results lie near the $\Delta\epsilon_{pp}$—N_{pp} line as expected, and the highest temperature results fall on the $\Delta\epsilon_{cc}$—N_{cc} line, also as expected. The three dashed lines indicate the cyclic lives expected for cycles with known percentages of $\Delta\epsilon_{cc}$ strain present.

Frequency Effect—In a series of constant strainrange tests conducted at a fixed temperature over a range of frequencies, one would expect a variation in cyclic life that is somewhat similar to the variation discussed in the previous section. With a sufficiently high frequency of strain cycling, insufficient time would be available for significant creep to occur. Thus, the inelastic strain in the cycle would be predominantly plastic strain. The corresponding cyclic life, therefore, would be N_{pp}. However, if the temperature is in the creep range, a lower frequency would tend to produce creep rather than plastic strain, and the cyclic life would be lowered, falling between the bounds of N_{pp} and N_{cc}. At extremely low frequencies, one would expect the inelastic strainrange to be composed entirely of completely reversed creep strain $\Delta\epsilon_{cc}$, with an attendant life of N_{cc}. Further decreases in frequency would not be expected to cause further decreases in cyclic life, since all of the inelastic strain has been already totally absorbed as completely reversed creep strain.

Two series of tests such as just described were conducted on the Type 316 stainless steel. Both were conducted with a nominally constant inelastic strainrange of 0.0045. The series of tests conducted at 705 C covered a frequency variation of nearly four orders of magnitude, while the 815 C

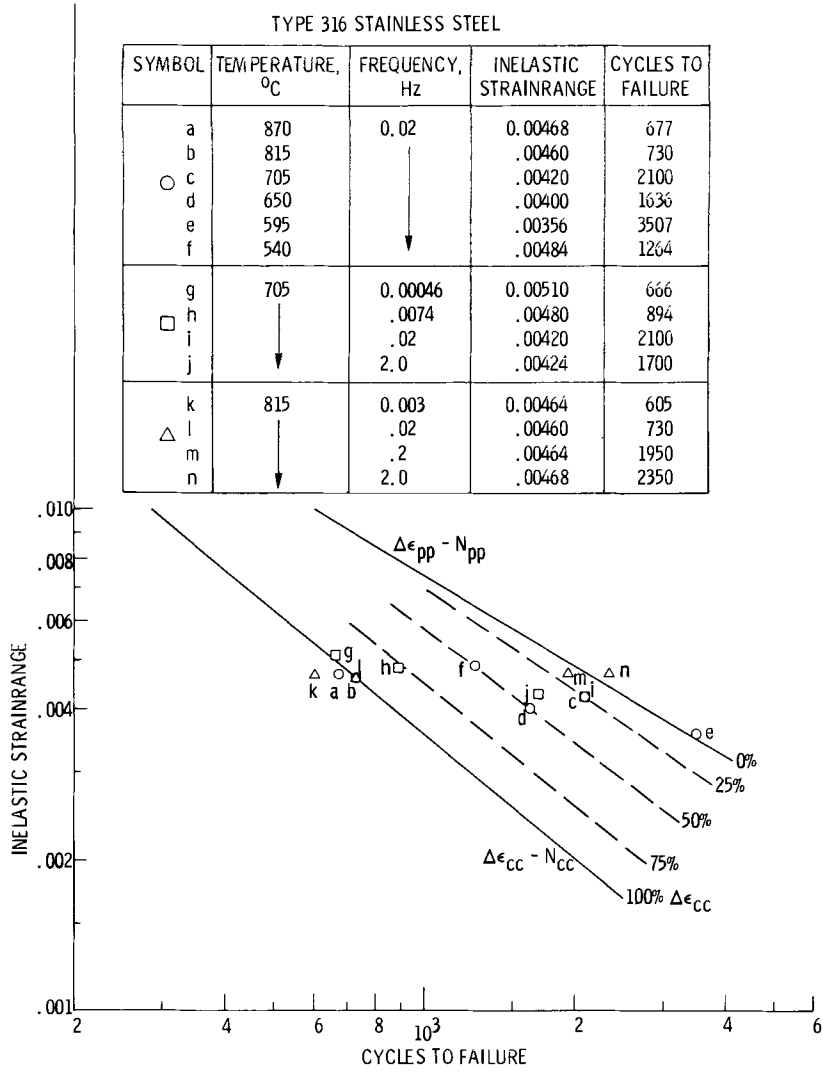


FIG. 4—*Application of strainrange partitioning approach to continuous strain cycling results. Temperature and frequency effects are bounded by* $\Delta\epsilon_{pp}$-N_{pp} *and* $\Delta\epsilon_{cc}$-N_{cc} *relationships.*

tests spanned nearly three orders of magnitude. The results of these tests are also shown in Fig. 4. As expected, the highest frequency tests for both temperatures failed near the upper bound, N_{pp}, and the lowest frequency tests failed near the lower bound N_{cc}.

The results of the strain cycling tests conducted over a range of temperatures and frequencies are in excellent agreement with the strainrange partitioning approach. The $\Delta\epsilon_{pp}$-N_{pp} life relationship provides an upper bound on cyclic life while the $\Delta\epsilon_{cc}$-N_{cc} life relationship provides a lower

bound for cycles wherein the type of strain in tension is the same as that in compression. Furthermore, the transition from one bound to the other is in good qualitative agreement with the approach. The strain cycling lives are functions of temperature and frequency apparently because the flow behavior is highly temperature and rate dependent. The flow behavior governs the amounts of each type of strainrange present, and the temperature and rate insensitive failure criteria in turn govern the cyclic life.

Hence, an important advantage of the approach is that failure data need not be generated over the entire temperature and frequency range. Instead, the life relationships may be determined accurately at a single elevated temperature (with only spot checks conducted at other temperatures) and only the flow behavior determined as a function of temperature and straining rate. Thereby fewer tests are required, and their total duration can be significantly reduced.

If bounds on life are adequate, the details of the flow behavior need not be known. However, if the lives for the respective bounds at a selected strainrange are widely separated and a more accurate estimate of cyclic life is required, the flow behavior must be incorporated into the analysis.

Thermal Strain Cycling—The strainrange partitioning approach is well suited for application to the complex temperature-strain histories associated with typical thermal fatigue problems. Two aspects of the approach are advantageous: (a) the cyclic failure criteria are approximately independent of temperature for certain materials, and (b) bounds on cyclic life can be established directly from the strainrange-life relationships.

Consider, for example, a thermal strain cycle wherein a suddenly applied high-temperature gradient induces compression at the heated surface. Under high stress and temperature, compressive plasticity and creep will be encountered. During the cool down portion of the cycle, the compressive strain is reversed by tensile strain, which, because of the lower temperature, is predominantly plastic strain (assuming the lower temperature is low enough to preclude creep). In this case, neither $\Delta\epsilon_{cp}$ nor $\Delta\epsilon_{cc}$ type strainranges are present, since there is no tensile creep. Therefore, the only possible components of strainrange are $\Delta\epsilon_{pp}$ and $\Delta\epsilon_{pc}$. In the complex thermal cycle, the plastic and creep strains are accumulated at continuously varying temperatures and strain rates. Since the failure criteria of the strainrange partitioning approach may well be insensitive to these variables, the approach is suited ideally for the analysis of thermal cycling problems. To determine the exact proportions of $\Delta\epsilon_{pp}$ and $\Delta\epsilon_{pc}$ within the cycle would require a detailed and complex analysis of the flow behavior. However, a lower bound on cyclic life could be established directly by simply assuming that all of the inelastic strain is of the $\Delta\epsilon_{pc}$ type.

Other types of thermal strain cycles (for example, when the temperature gradient is permitted to disappear at the higher and lower temperatures) may be considered to be composed of $\Delta\epsilon_{cp}$ type strain only. In this case, a

lower bound on life could be determined directly from the $\Delta\epsilon_{cp}$-N_{cp} relationship.

Summary of Results

A study has been made of the effect of temperature on the strainrange partitioning approach for creep-fatigue analysis. Two high-ductility alloys were investigated, 2¼Cr-1Mo steel and Type 316 stainless steel. These alloys were taken to be representative of a class of high-temperature materials whose mechanical and metallurgical behavior exhibits stability over extended periods of time over broad ranges of high temperatures. The following major results obtained on these two materials are expected to be applicable to other materials within this class.

1. The partitioned strainrange-cyclic life relationships are insensitive to test temperature to within a factor of two on cyclic life. These life variations are within the range expected considering that the monotonic tensile (plastic) and rupture (creep) ductilities are also insensitive to test temperature to within a factor of two.
2. The strainrange partitioning approach has provided bounds on cyclic life that are in excellent agreement with isothermal, continuous strain-cycling lives for the Type 316 stainless steel over a wide range of temperatures and frequencies. The observed transition from one bound to the other is in good qualitative agreement with the approach.

Concluding Remarks

For the stable, well-behaved materials studied, we have demonstrated several advantages of the strainrange partitioning approach for creep-fatigue analysis. Since the partitioned strainrange-cyclic life relationships are only a weak function of the elevated test temperature, few data are needed to determine the failure criteria, and bounds on cyclic life can be readily established—even for complex temperature and loading cycles. Since the cyclic lives depend upon the magnitude and types of strains present, rather than on the temperature, stress, or time elapsed to achieve the strains, it appears that strain is the most physically significant of the primary variables in governing the cyclic failure behavior. The flow behavior, which dictates the amount and type of strain encountered, however, is influenced strongly by the imposed temperature, stress, and time.

Despite the numerous advantages of the strainrange partitioning approach presented in this paper and in Refs *1* and *2*, there are a number of aspects of the problem that still require further attention. Some of the desirable features of the approach may be lost when dealing with materials whose mechnical properties are unstable with temperature and exposure time. For example, strain-aging phenomena may cause the partitioned

strainrange-cyclic life relationships to be somewhat temperature and time dependent. This type of material behavior can still be encompassed by the approach. The drawback is the requirement for more data to characterize the failure behavior as a function of temperature and time If lower bounds are of primary concern, it may be possible to determine the life relationships for the material in its fully aged condition, for which the material has the least ductility.

Another problem area that must be dealt with in its relation to the strainrange partitioning approach is that of corrosion and oxidation. Both may seriously reduce ductility.

The approach, as discussed to date, requires the inelastic strainrange to be determined explicitly. When the inelastic strainrange is a small fraction of the total strainrange, an accurate determination becomes extremely difficult. Hence, in applying the approach to a practical problem, it may become necessary to add an elastic strainrange term to the partitioned inelastic strainrange to yield the more easily determinable total strainrange. This could be done in a manner analogous to the addition of the elastic and plastic strainrange terms in the universal slopes equation [*6*]. Alternatively, when the total strains include a very small inelastic component, elastic theory is applicable, and life predictions are better made on the basis of stress. Extensive analysis by Spera[3] have demonstrated that thermal fatigue life can be accurately predicted on the basis of time ratios to represent creep effects and cycle ratios to represent fatigue effects in cases where the stresses are nominally within the elastic range.

References

[*1*] Manson, S. S., Halford, G. R., and Hirschberg, M. H., *Symposium on Design for Elevated Temperature Environment*, American Society for Mechanical Engineers, New York, 1971, pp. 12–24.

[*2*] Manson, S. S. in *Proceedings*, The 1971 International Conference on Mechanical Behavior of Materials, The Society of Materials Science, Japan, 1972, pp. 5–60.

[*3*] Halford, G. R., Hirschberg, M. H., and Manson, S. S., "Temperature Effects on the Strainrange Partitioning Approach for Creep-Fatigue Analysis," NASA TM X-68023, National Aeronautics and Space Administration, Cleveland, Ohio, 1972.

[*4*] Hirschberg, M. H. in *Manual on Low Cycle Fatigue Testing*, *ASTM STP 465*, American Society for Testing and Materials, 1969, pp. 67–86.

[*5*] Halford, G. R., "Cyclic Creep-Rupture Behavior of Three High-Temperature Alloys," NASA TN D-6309, National Aeronautics and Space Administration, Washington, D. C., May 1971.

[*6*] Manson, S. S., *Experimental Mechanics*, Vol. 5, No. 7, July 1965, pp. 193–226.

[3] See p. 648.

DISCUSSION

R. W. Weeks[1] (*written discussion*)—(*a*) How do you decide the strain rate at which you go from "plasticity" to "creep"? (*b*) Have you done any longer-duration tests (for example, greater than 10^4 cycles) to check the divergence between the bounds shown on your last two slides? If the bounds became quite large, the practical value of the bounds may be questionable.

G. R. Halford, M. H. Hirschberg, and S. S. Manson (*authors' closure*)—(*a*) One can judge whether the strain rate is high enough to produce only plasticity by plotting fatigue test results on coordinates of cycles to failure versus strain rate (or frequency). As the strain rate increases, a saturation in cyclic life is indicative of having achieved the desired strain rate. Our experience indicates a test frequency of the order of 0.2 to 2.0 Hz is sufficient to preclude creep effects and ensure reversed plasticity. In terms of strain rate, this corresponds to 0.004 to 0.040 s^{-1} at a total strainrange of 0.01. (*b*) Because of the relatively long times associated with creep-fatigue tests at lives beyond 10^4 cycles to failure, we have been unable to generate such results. However, we have no reason to suspect that the $\Delta\epsilon_{pp}$-N_{pp} and the $\Delta\epsilon_{cc}$-N_{cc} relationships do not continue to diverge as cyclic lives increase. These bounds for balanced cycles, however, still maintain practical importance, since they are indicative of the best and the worst possible situation that can exist. To know that these two conditions are far apart is extremely important in that the actual behavior of an intermediate type cycle may lie over a broad spectrum of lives. This should serve as a warning that an accurate partitioning of the inelastic strain range is required before an accurate life analysis can be made.

A. K. Miller[2] (*written discussion*)—In analyzing a thermal-mechanical fatigue test with a stress-strain curve like the one I showed earlier, how would you decide on the values for the plastic and creep strain ranges?

Messrs. Halford, Hirschberg, and Manson—It requires an accurate knowledge of the material's deformation behavior laws for an accurate partitioning. However, qualitative evaluation of the cycle may reveal that only two of the partitioned strain range components are present (for

[1] Argonne National Laboratory, Argonne, Ill. 60439.
[2] East Hartford, Conn. 06118.

example, $\Delta\epsilon_{pp} + \Delta\epsilon_{pc}$). In this event, it could simply be assumed that all of the inelastic strain is partitioned into the most severe component. Hence, a lower bound on life could be established without having to resort to any quantitative analysis.

E. Krempl[3] (*written discussion*)—Are your strains related to phenomena reported earlier for example, wavy, planar slip? What is the definition of your strains?

Messrs. Halford, Hirschberg, and Manson—For the materials we have studied to date, we have not had to distinguish between wavy and planar slip. However, either would be considered as plastic strain in our framework of thinking. The two inelastic strain components that we consider most important are very simply defined as being time-dependent creep and time-independent plasticity. Creep deformation may take place along grain boundaries or may occur by diffusion controlled mechanisms within the grains. Plasticity occurs by disclocation motion along appropriately oriented crystallographic planes.

Roy Swanson[4] (*written discussion*)—While the *pp* and *cc* loops are symmetrical both in strain and stress, the *cp* and *pc* loops have compressive and tensile mean stresses, respectively. Could the unusually damaging effect of the *cp* loop be due to the residual tensile stress at microcracks which may exist going into the creep phase?

Messrs. Halford, Hirschberg, and Manson—Although this may be a possibility, it must be ruled out for the test data shown because of the generally large inelastic strains employed. With large inelastic strains, residual stresses can not be sustained for any significant period, particularly when temperatures are well within the creep range.

D. A. Woodford[5] (*written discussion*)—Have you applied this analysis to any vacuum data?

Messrs. Halford, Hirschberg, and Manson—Yes, we have applied it to the vacuum (10^{-8} torr) data on two tantalum-base alloys reported by Sheffler and Doble in this conference. Mr. Manson presents some of these results in his summing-up paper.

[3] Division of Mechanics, Rensselaer Polytechnic Institute, Troy, N. Y. 12181.
[4] MTS, Minneapolis, Minn. 55424.
[5] General Electric Co., Schenectady, N. Y. 12345.

S. V. Serensen,[1] *R. M. Schneiderovitch,*[1] *and A. P. Gusenkov*[1]

Kinetic Deformation Criteria of Cyclic Fracture at High Temperature

REFERENCE: Serensen, S. V., Schneiderovitch, R. M., and Gusenkov, A. P., **"Kinetic Deformation Criteria of Cyclic Fracture at High Temperature,"** *Fatigue at Elevated Temperatures, ASTM STP 520,* American Society for Testing and Materials, 1973, pp. 670–677.

ABSTRACT: A strain range partitioning method for the analysis of failure by the interaction of creep and fatigue is proposed. A conception is made of the one-sided deformation (mean strain) to account for part of the creep damage; the time (and temperature) dependent behavior of the strain to failure is used to modify the common low-temperature low-cycle fatigue equations. Data from 18Cr, 8Ni stainless steel are used as a basis for demonstrating the method. A conventional linear damage summation technique is used for comparison with the results of the proposed method.

KEY WORDS: fatigue (materials), cyclic loads, fatigue tests, creep rupture strength, creep tests, failure, damage, stresses, strains

The lifetime of structures under cyclic loading at high temperatures is determined by the accumulation of creep and low-cycle fatigue damage. The analysis of the interaction of creep and fatigue was the subject of several recent investigations. The results and discussions of some of these are found in the proceedings of major conferences on fatigue of the past few years [*1–3*].[2]

The design of elements for low-cycle fatigue at low temperature is based on the ranges of strain and the normal tensile properties of the material [*4*]. In similar fashion, design of members for cyclic loading at elevated temperature should be reduced to simple formulae requiring only a few basic properties.

In this paper a linear summation damage law is used to evaluate the accumulation of damage under each kind of loading; static (creep) or cyclic (fatigue). In earlier methods the sum of the ratios of time (equivalent time to fracture time in the "pure" creep case) and cycles (actual cycles to cycles to failure in the "pure" fatigue case) is set equal to the total damage accumulation. In this paper the effect of dwell time in the fatigue cycle was

[1] Mechanical Engineering Research Institute, Moscow-Centre, USSR.

[2] The italic numbers in brackets refer to the list of references appended to this paper.

Copyright© 1973 by ASTM International www.astm.org

analyzed by treating the plastic strain accumulation resulting from the dwell as wholly creep-type damage. Stress-rupture strain to failure is used to describe the limiting or critical state.

The Method

The limit level of accumulated damages, corresponding to the state where a macrocrack has been initiated, depends on time and deformation conditions. High-temperature failure criteria must take into account the cyclic strain in cycle time and in the unidirectional one-side accumulation of the creep strain in the region of possible fracture, which is generally at a stress concentration. Furthermore, the changes in mechanical properties resulting from the prior history of loading, especially the strain to failure, must be recognized by the failure criteria.

By separating the time-dependent (creep) and time-independent (active) parts of the deformation for each half-cycle of loading a simple set of equations can be used to describe the creep-fatigue limit state.

In the *active* state of loading in the kth half-cycle, after a total time of loading of t hours and at a stress amplitude of σ, the current plastic deformation can be expressed in the form of [5]:

$$\epsilon_p{}^{(k)} = F_1(k) \times F_2(t) \times F_3(\sigma) \quad (1)$$

In the *creep* stage of the kth half cycle after a total deformation of t hours during the dwell time τ at a stress σ, the current creep strain may be written as

$$\epsilon_c{}^{(k)} = \phi_1(k) \times \phi_2(t) \times \phi_3(\tau) \times \phi_4(\sigma) \quad (2)$$

For a given k and t this equation can be transformed to a similar equation from the aging theory of creep. The holdtime τ measures the time from the beginning of the dwell to the reversal of the active part of the load cycle.

The current irreversible strain in the half-cycle is

$$\epsilon_{ir}{}^{(k)} = \epsilon_p{}^{(k)} + \epsilon_c{}^{(k)} \quad (3)$$

The complexity of the equation can be reduced by taking into account the material properties.

The test results for this analysis were obtained from an austenitic 18-8 stainless steel at 650 C. These tests were load controlled, that is, cyclic creep tests. The creep cycle was symmetrical (three different stress amplitude levels) with and without dwell times (1, 5, and 50 min). Dwells were included for tension only (Type I) and for tension and compression (Type II).

Typical results are shown in Fig. 1. the creep (δ_c) and active (δ_p) strains that occur during each half-cycle are shown for two types of dwell cycles; Type I has 5 min hold in tension only, Type II has 5 min hold in both tension and compression. The active (or plastic) and creep strains change

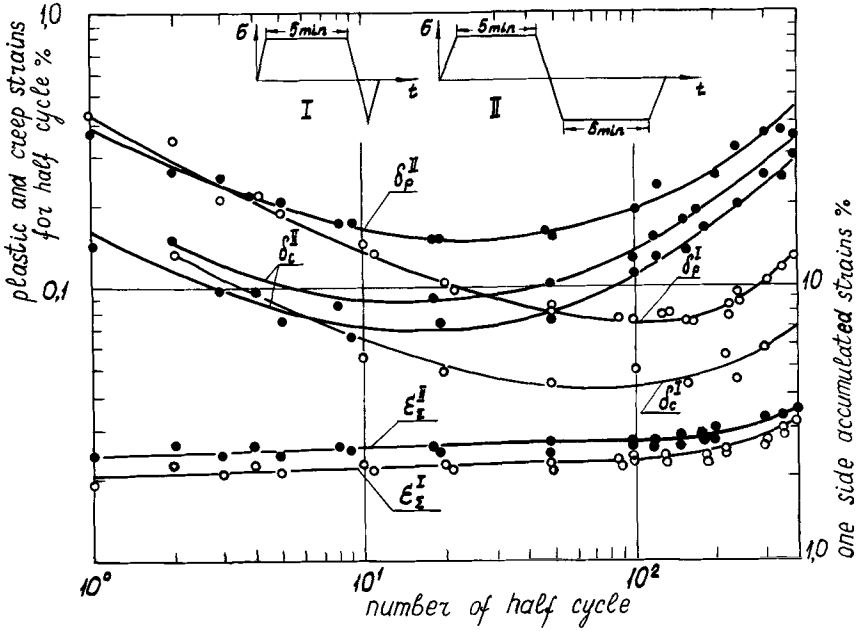


FIG. 1—*Creep and active strains for two types of dwell cycles (Types I and II).*

with cycle number, and the function $\phi_1(k)$ and $F_1(k)$ are near to each other. The difference between the two types of dwell cycles can be seen in the difference of the strains in the even and odd half-cycles. The residual strain during the Nth cycle increases its value by an increment $\Delta^{(N)}$, or

$$\Delta^{(N)} = \delta_{ir}{}^{(k)} - \delta_{ir}{}^{(k-1)} \quad \ldots\ldots\ldots\ldots\ldots\ldots\ldots\ldots (4)$$

and the accumulation of the deformation (mean strain) at any cycle N is

$$\epsilon_\Sigma{}^{(N)} = \sum_{o}^{N} (\Delta^{(N)}) \quad \ldots\ldots\ldots\ldots\ldots\ldots\ldots\ldots (5)$$

Values of accumulated strain are shown at the bottom of Fig. 1. It should be remembered that the accumulation of residual strain can also occur at low temperatures [*1*].

The development of the creep strain during a half-cycle can be aided by the construction of a creep curve in a half-cycle in dimensionless form, putting the current creep strain $\epsilon_c{}^{(k)}$ to the total creep strain during the half-cycle $\delta_c{}^{(k)}$ as the ordinate and the dwell time as the abscissa. Such data are shown in the band of Fig. 2 for many of the half-cycles for tests having 5-min dwell (Type I) at a stress of 25 kg/mm². The circles indicate the initial creep curve for the same material.

When the creep data are plotted in this fashion, the scatter is not very great and is almost centered about the initial curve. Similar results were

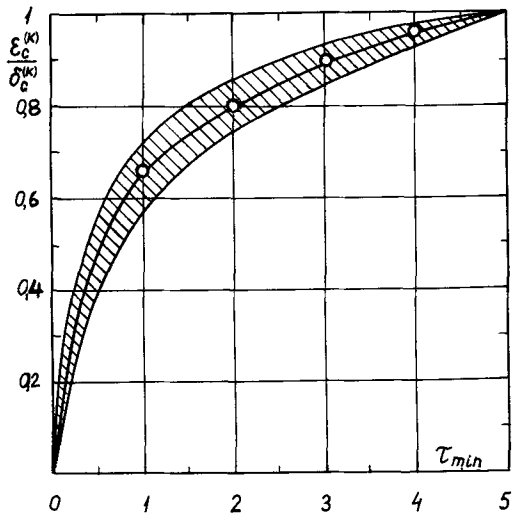


FIG. 2—*Creep strain data for Type I dwell time.*

obtained under alternating tension and compression dwells (Type II), but the scatter was somewhat greater. These results make it possible to determine the function $\phi(\tau)$, in a first approximation, from the initial creep curve.

Cyclic relaxation behavior has been analyzed in similar fashion by plotting the behavior in dimensionless form, and good agreement was obtained in that work [*6*].

The current irreversible strain can be expressed in simplified form as

$$\epsilon_{ir}{}^{(k)} = F_1(k) \times F_2(t)\,[F(\sigma) + \phi(\tau) \times \phi(\sigma)] \quad \ldots\ldots\ldots\ldots (6)$$

The stress function $F(\sigma)$ at $\sigma > \sigma_T$ can be written in the form $F(\bar{\sigma}) = A[f\{(\bar{\sigma}) - 1\}]$,[3]

where

$f(\sigma)$ = initial stress-strain diagram,
σ_T = proportional limit stress, and
A = a constant.

The term $\phi(\sigma)$, is a stress function and can be approximated by the initial creep equation, for instance $\phi(\sigma) = \beta\sigma^n = \dot{\epsilon}_c$. The function $F(k)$ in even and uneven half-cycles can differ by a constant factor, which makes it possible to describe the accumulation of the one-sided deformation.

At a given stress amplitude, Eq 6 describes the hysteresis loop width that is the residual deformation, ϵ_{ir}, during a half-cycle. The total accumulated deformation (mean strain) ϵ_Σ can be obtained from the evaluation of Eq 5.

[3] From the $\bar{\sigma} - \bar{\epsilon}$ curve $\bar{\sigma} = \sigma/\sigma_T$ and $\bar{\epsilon} = \epsilon/\epsilon_T$.

The condition for cyclic (fatigue) and quasi-static (tensile) failure can be expressed from the knowledge of the strain at failure in the tension test [*1*,*6*] and the hypothesis of linear damage accumulation in the low-cycle fatigue test, in the following form[4]

$$\sum \frac{n_i}{N_i} + \frac{\epsilon_\Sigma}{\epsilon_f} = 1 \quad \ldots\ldots\ldots\ldots\ldots\ldots\ldots\ldots (7)$$

where ϵ_f is the plastic deformation at fracture [*8*,*9*]. Equation 7 is a linear damage summation equation for periodic strain cycling at low temperature and can be rewritten as

$$4 \int_0^{N_f} \frac{\delta_p^2 dN}{\epsilon_f^2} + \frac{\epsilon_\Sigma^{(N_f)}}{\epsilon_f} = 1 \quad \ldots\ldots\ldots\ldots\ldots\ldots\ldots\ldots (8)$$

where

δ_p = plastic deformation in the cycle (internal width of the hysteresis loop),
$\epsilon_\Sigma^{(N_f)}$ = one-sided accumulated strain at failure,
N_f = cycle number at failure.

This method can be generalized for high-temperature applications by showing the time and history dependence of the fracture strain. At elevated temperature the loop with δ_{ir} depends on the plastic strain δ_p and the creep strain δ_c. Coffin proposed a parameter method for describing the temperature and strain rate dependence of the strain to failure at elevated temperature [*10*]. These expressions were used to predict frequency or time dependency effects (without dwells) in low-cycle fatigue behavior.

A modification of Eq 8 to account for cyclic and creep damage can be expressed as

$$4 \int_0^{N_f} \left[\frac{\delta_{ir}}{\epsilon_f(t)} \right]^2 dN + \frac{\epsilon_\Sigma^{(N_f)}}{\epsilon_f} = 1 \quad \ldots\ldots\ldots\ldots\ldots\ldots\ldots\ldots (9)$$

Where $\epsilon_f(t)$ is the plastic strain for static fracture in time t. An approximate and conservative method for obtaining the value of $\epsilon_f(t)$ is to set the strain to failure $\epsilon_f(t)$ equal to the strain to rupture in pure creep tests. For long-time tests the difference between the strain to failure for strain rate controlled and load controlled (creep) tests is negligible.

To confirm the validity of the damage accumulation equation, tests of 18-8 stainless steel at 650 C were made In addition to the cyclic creep tests strain controlled, strain range limited, low-cycle fatigue tests with and without dwells at constant strain were also performed. These tests allowed the elimination of the second term of Eq 9 and also to vary the time to fracture over a wide range without drastically changing the number of

[4] This form of damage accumulation was proposed by N. A. Makhutov of the Mechanical Engineering Research Institute in 1967.

cycles to failure. In this manner it was possible to control the estimation of creep damage in the usual time ratio form of $\Sigma(t/t_f)$ where t_f is the time to fracture in the creep-rupture test.

The values for the damage fractions are shown in Fig. 3. The light points were calculated from Eq 9 according to $\epsilon_\Sigma/\epsilon_f(t)$, where $\epsilon_f(t)$ is taken from the static tension test. As is shown in Fig. 3 the calculation by Eq 9 gives results scattered about the linear damage line. The accumulation in the form of

$$4\int_0^{N_f} \frac{\delta_{ir}^2\, dN}{\epsilon_f^2} + \sum \frac{\Delta t}{t_f} = 1 \qquad (10)$$

is plotted by the solid points in the figure. The analysis of the experimental data by Eq 10 are located, in general, much lower than the linear damage accumulation form. For the condition, of strain controlled tests with strain hold periods, the experimental values are much higher; the data could not be plotted on the curve and are designated by the points with arrows.

A comparison of the accumulated damages for different times to fracture calculated by Eq 9 is shown in Fig. 4. The $\epsilon_f(t)$ is taken from static tension (open symbols) and from creep rupture tests (solid symbols). The use of strain to fracture from creep gives conservative results up to about 10 to

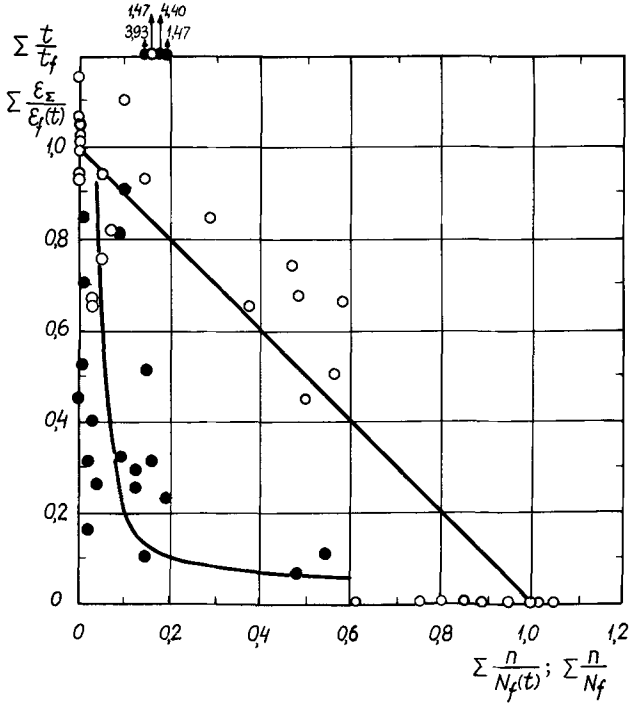


FIG. 3—*Values for the damage fractions in the creep cyclic test.*

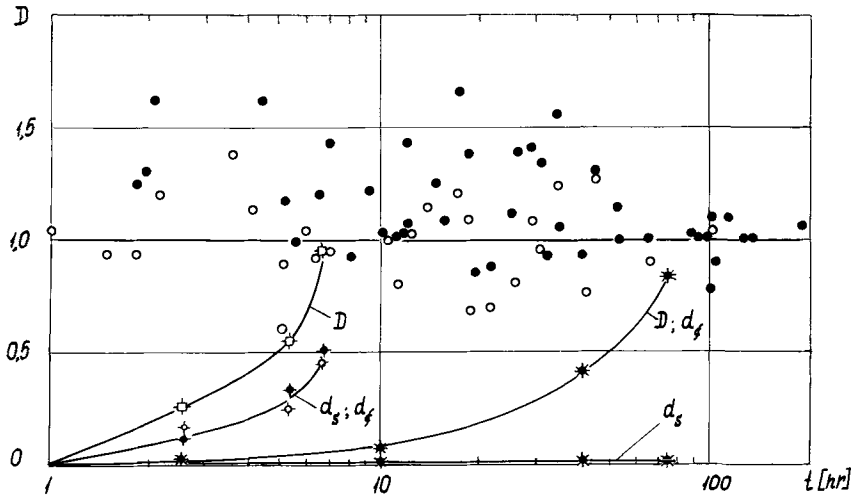


FIG. 4—*Comparison of accumulated damages for different times to fracture.*

20 h. The curves of accumulated cyclic and creep damage are also shown. On the left the creep (d_s) and fatigue (d_f) damages are about equal; on the right the fatigue damage is dominant and about equal to the total damage (D).

Summary

The method set forth in this paper is summarized in Eqs 6 and 9. In the first equation the irreversible strain can be partitioned into time-dependent and time-independent parts and the accumulation of one sided strain (mean strain) evaluated. The irreversible strain is known to affect the fatigue damage; the mean strain, the creep damage. The linear damage summation equation can be used for describing interaction of creep and cyclic damage. The time-dependent value of strain to failure can be used with generally conservative results. The lifetime under low-cycle fatigue with dwell can be calculated with Eq 9.

References

[1] "Deformation and Fracture Resistance at Low-Cycle Loading," *Nauka*, 1967 (Prochnost' Metallov pri Tsiklicheskikh Nagruzkakh, *NAUKA*, 1967).
[2] International Conference on Thermal and High-Strain Fatigue, London, 1967.
[3] Part V (Fatigue) in *Proceedings* International Conference on Fracture, Brighton, Chapman Hall, London, 1969, pp. 552–812.
[4] Schneiderovitch, R. M., "Strength at Statical and Alternating Loading," *Maschinostroenie*, Vol. 48, 1968.
[5] Serensen, S. V. and Schneiderovitch, R. M., "The Effects of Time on Stress Distribution in the Case of Cyclic Deformation," *Proceedings*, 11th International Congress of Applied Mechanics, Munich, 1964.

[6] Krempl, E. and Walker, C. D. in *Fatigue at High Temperature*, *ASTM STP 459*, American Society for Testing and Materials, 1969, p. 75.
[7] Serensen, S. V. and Schneiderovitch, R. M., *Maschinovedenie*, No. 2, 1965, pp. 70–79.
[8] Coffin, L. F., *Transactions*, American Society of Mechanical Engineers, Vol. 76, 1954, p. 3931.
[9] Manson, S. S., NACA Technical Note 2933, National Advisory Committee for Aeronautics, 1954.
[10] Coffin, L. F. in *Proceedings*, First International Conference on Fracture, Sendai, Vol. 3, 1965, p. 1543.

D. C. Gonyea[1]

Method for Low-Cycle Fatigue Design Including Biaxial Stress and Notch Effects

REFERENCE: Gonyea, D. C., "**Method for Low-Cycle Fatigue Design Including Biaxial Stress and Notch Effects,**" *Fatigue at Elevated Temperatures, ASTM STP 520*, American Society for Testing and Materials, 1973, pp. 678–687.

ABSTRACT: A design procedure for predicting low-cycle fatigue cracking is developed that is applicable for most mechanical and thermal cycling problems. Included in the procedure are effects due to stress risers and biaxial stress fields. Use is made of the uniaxial low-cycle fatigue curve and the "cyclic "stress-strain curve, both obtained from standard low-cycle fatigue testing. Major aspects of the analysis include an effective strain parameter which is employed as the cracking criterion and the use of Neuber's equation to estimate stress concentration effects. To illustrate the use and validity of the procedure, data from mechanically and thermally cycled grooved cylinders are presented and compare well with predictions.

KEY WORDS: fatigue (materials), crack propagation, thermal cycling tests, mechanical tests, fatigue tests, cylinders, stress-strain diagrams, low alloy steels

The purpose of this paper is to present a method of estimating the life of service components subjected to low-cycle fatigue (LCF). A number of approximations are made to provide a simple and useful design technique that may be applied to most component LCF problems. The general approach is not new, but the modification of subtle points and introduction of an effective strain to account for stress biaxially provide additional insight into this important area of LCF design. The effect of material properties on plastic strain concentration is discussed, and a design curve is suggested for use with low-alloy steels. The method is applied to grooved cylinders to illustrate the use and validity of the method.

Nearly all component LCF problems occur at areas of stress concentration and involve a biaxial state of stress. Smooth, uniaxial test data cannot be directly applied to estimate service life; many other factors must be considered before an estimate to LCF life can be made. Although investigators have isolated and studied many factors which effect LCF, there always exist questions about the applicability of this information to a

[1] Development engineer, Large Steam Turbine Department, General Electric Co., Schenectady, N. Y. 12345.

Copyright© 1973 by ASTM International www.astm.org

particular design situation. The method presented in this paper deals directly with the following effects:

1. Basic LCF material behavior.
2. Nominal strain (or stress) range.
3. Stress biaxility.
4. Stress concentration.

The inclusion of these effects and the omission or approximation of others, such as those due to environment or frequency, was deemed necessary to establish a simple design method, yet one which incorporates the primary design parameters. In many design situations, an estimate of service life within an order of magnitude is more than sufficient to judge whether a particular design is acceptable or not. Furthermore, many design problems are relative. For example, a designer may wish to estimate the increase in life due to reducing a stress concentration of a component that has failed in 500 service cycles.

Basic LCF Material Behavior

Most LCF tests are performed on smooth, mechanically cycled test specimens. This testing provides the basic information which is required to describe the fatigue and "cyclic" stress-strain behavior of the material in question.

The number of cycles obtained from a standard fatigue test may identify macrocrack initiation (that is, a crack 10 mils in length) or complete separation of the test specimen. The determination of service life should include investigation of crack propagation as well as macrocrack initiation. For design use, the number of cycles to specimen separation may correspond, as Coffin [*1*][2] suggests, to an observable component crack. Judgement, or a consideration of crack propagation by applying fracture mechanics techniques, must be employed to determine the useful service life.

Effective Strain and Stress-Strain Relationships

A biaxial state of stress has been shown to substantially effect LCF life [*2*]. To account for this effect, an elastoplastic effective strain parameter is employed which relates a biaxial stress state to a uniaxial stress state. This effective strain parameter is similar to the Von Mises effective strain but employs a variable Poisson's ratio [*3*] which is determined from the cyclic stress-strain curve.

$$\bar{\epsilon} = \frac{1}{\sqrt{2}\,(1 + \bar{\nu})}\,[(\epsilon_1 - \epsilon_2)^2 + (\epsilon_2 - \epsilon_3)^2 + (\epsilon_3 - \epsilon_1)^2]^{1/2} \quad \ldots\ldots(1)$$

[2] The italic numbers in brackets refer to the list of references appended to this paper.

and

$$\bar{\nu} = 0.5 - (0.5 - \nu_e)\frac{E_s}{E} \quad \ldots\ldots\ldots\ldots\ldots\ldots (2)$$

where

$\bar{\epsilon}$ = effective uniaxial strain,
$\bar{\nu}$ = variable Poisson's ratio,
ϵ_i = principal components of strain,
E = Young's modulus,
E_s = Secant modulus from cyclic curve, and
ν_e = elastic Poisson's ratio.

The secant modulus, E_s, is found from the cyclic stress-strain curve using the effective strain, $\bar{\epsilon}$. Note that the variable Poisson's ratio has initially the elastic value and approaches 0.5 in the plastic range.

For purposes of relating stress to strain and establishing the principal components of strain (as will be later demonstrated), elastoplastic-stress-strain relations from the theory of plasticity [*4*] are used, and, again, the variable Poisson's Ratio and secant modulus are employed.

$$\begin{aligned} \epsilon_1 E_s &= \sigma_1 - \bar{\nu}(\sigma_2 + \sigma_3) \\ \epsilon_2 E_s &= \sigma_2 - \bar{\nu}(\sigma_1 + \sigma_3) \\ \epsilon_3 E_s &= \sigma_3 - \bar{\nu}(\sigma_1 + \sigma_2) \end{aligned} \quad \ldots\ldots\ldots\ldots\ldots\ldots (3)$$

where

σ_1, σ_2, and σ_3 are principal components of stress.

Stress Concentration

Invariably, component LCF problems occur at locations of stress concentration that arise from structural discontinuities, metallurgical defects, or welding imperfections. There presently exist two popular techniques for estimating the concentrated plastic stress and strain that occurs at notches.

One approach is credited to the work of Stowell [*5*] who studied plastic stress and strain concentration at a hole in an infinite plate under uniaxial loading. Hardrath and Ohman [*6*] modified the approach to incorporate a more general stress concentration. Incorporating the concept of the effective strain, the modified Stowell relationship may be extended to include biaxial stress effects.

$$\bar{K}_\epsilon = \frac{\Delta\bar{\epsilon}^*}{\Delta\bar{\epsilon}} = \frac{E_s}{E_s^*} + (\bar{K}_t - 1) \quad \ldots\ldots\ldots\ldots\ldots\ldots (4)$$

where

$\bar{K}_\epsilon$ = elasto-plastic strain concentration factor,
$\Delta\bar{\epsilon}^*$ = concentrated effective strain range,

$\Delta\bar{\epsilon}$ = nominal effective strain range,

E_s^* = secant modulus found using $\Delta\bar{\epsilon}^*$,

E_s = secant modulus found using $\Delta\bar{\epsilon}$, and

$\bar{K}_t = \left[\frac{\Delta\bar{\epsilon}^*}{\Delta\bar{\epsilon}}\right]_e$ elastic strain (stress) concentration factor.

Two subtle points are embodied in Eq 4. The use of effective strain *ranges* implies that symmetric and nonsymmetric cycling are equivalent if the nominal strain ranges are equal. Another point is that the extension of the modified Stowell equation to incorporate general biaxial stresses assumes the *effective* strain is the governing parameter.

The Neuber approach [*7*] is an alternate technique for estimating plastic strain concentration. Again, incorporating the effective strain parameter, Neuber's equation becomes:

$$\bar{K}_\epsilon = \frac{\Delta\bar{\epsilon}^*}{\Delta\bar{\epsilon}} = \bar{K}_t\left[\frac{E_s}{E_s^*}\right]^{1/2} \quad \ldots\ldots\ldots\ldots\ldots\ldots (5)$$

Papirno [*8*] concludes from comparison with measured strains under monotonic, uniaxial loading that both techniques are conservative, predicting higher strains than measured. He further suggests that Neuber's equation has better predictive value for values of $\bar{K}_t$ less than 2, and that Stowell's relationship is preferable for $\bar{K}_t$'s greater than 2.5. Between 2 and 2.5 both techniques yield essentially equivalent results.

Mowbray [*9*] employs a finite element elasto-plastic analysis for the particular geometry and loading in question, together with the cyclic stress-strain curve to predict concentrated stresses and strains. For all cases considered, excellent agreement was found between calculated and measured concentrated strains. While this technique is more accurate than either the Stowell or Neuber approach since it incorporates the particular geometry in question, it obviously lacks the simplicity of these approximate techniques.

Example: Thermal Cycling Tests

The test results of Wozney [*10*] obtained on a thermally cycled, grooved cylinder serve to illustrate the outlined procedure. This test is particularly interesting since many aspects of the procedure are checked. The nominal stress state on the cylinder surface is equibiaxial, and the thermal cycle is nonsymmetric. Thus, both the biaxial stress and strain range concept are included. Furthermore, the stress concentration is included by virtue of the grooves. The fatigue and cyclic curves derived from isothermal mechanical cycling of smooth cylindrical specimens at 950 F serve as a basis for prediction.

The test consists of induction heating and forced air cooling of a solid specimen with two circumferential grooves. The outer surface is controlled between limits of 550 and 950 F with a heating time of 0.5 min and a cooling time of approximately 1.5 min. Periodically, the specimen is inspected for cracks.

The nominal, principal strain range is calculated neglecting the grooves, treating the specimen as a smooth cylinder with radial heat flow only. The measured surface temperature is used as the boundary condition for the analytical model and the temperature response and surface strain range determined. The elastic thermal stress concentration factor (SCF) is estimated by the mechanical bending SCF given by Peterson [*11*].

The nominal effective strain range is determined from the components of principal strain. Because of the thermal nature of the problem, elastic strain invariance is assumed such that the principal strain range is the sum of the elastically calculated strains that develop on heating and cooling. Also, use is made of the fact that an equibiaxial state of stress exists on the surface of the long, unrestrained cylinder.

$$\Delta\sigma_1 = \Delta\sigma_2$$

$$\Delta\sigma_3 = 0$$

and

$$\begin{aligned}\Delta\epsilon_1 = \Delta\epsilon_2 &= \epsilon_h + \epsilon_c \\ &= 1/E_s\,[\Delta\sigma_1 - \bar{\nu}\,(\Delta\sigma_2 + \Delta\sigma_3)] \\ &= \Delta\sigma_1/E_s\,(1 - \bar{\nu}) \\ \Delta\epsilon_3 &= 1/E_s\,[\Delta\sigma_3 - \bar{\nu}\,(\Delta\sigma_1 + \Delta\sigma_2)] \\ &= [-2\bar{\nu}\Delta\sigma_1]/E_s = -2\bar{\nu}\,(\epsilon_h - \epsilon_c)/(1 - \bar{\nu})\end{aligned}$$

where

ϵ_h = principal strain and heating and
ϵ_c = principal strain on cooling.

Substitution of the foregoing into the relationship for effective strain, Eq 1, leads to the following expression for the nominal effective strain range:

$$\Delta\bar{\epsilon} = \frac{\epsilon_h + \epsilon_c}{\sqrt{2}\,(1 + \bar{\nu})}\left[(1 - 1)^2 + \left(1 + \frac{2\bar{\nu}}{1 - \bar{\nu}}\right)^2 + \left(\frac{-2\bar{\nu}}{1 - \bar{\nu}} - 1\right)^2\right]^{1/2}$$

$$= \frac{\epsilon_h + \epsilon_c}{1 - \bar{\nu}} \qquad (6)$$

The effect of the stress concentration is accounted for by use of the extended Neuber relationship, Eq 5, which, combined with the expression for the nominal effective strain, Eq 6, leads to:

$$\Delta\bar{\epsilon}^* = \frac{\epsilon_h + \epsilon_c}{1 - \bar{\nu}}\,\bar{K}_t\left[\frac{E_s}{E_s^*}\right]^{1/2} \qquad (7)$$

A graphical or simple iterative solution technique is necessary since the notch secant modulus depends on the concentrated effective strain range. In practice, solution of Eq 7 presents no problem. The concentrated effective strain range is assumed to be the failure criterion and is used with the smooth, uniaxial fatigue curve to predict failure (cracking).

Table 1 summarizes the results of calculations and gives a comparison of predicted and observed cycles to cracking. The two test points by no means validate the procedure, but the results are very encouraging

TABLE 1—*Thermal cycling tests of Isberg and Wozney* [10].

Groove Number	K_t	ϵ_h	ϵ_e	K_ϵ	$\Delta\bar{\epsilon}^*$	Ncp[a]	Nco[b]
1	2.9	−0.103	0.047	3.08	0.66	2600	2500 to 3070
2	3.4	−0.103	0.047	3.92	0.84	1550	1700 to 2500

[a] Predicted cycles to cracking.
[b] Observed first cracks and complete linkup.

Mechanical Tests of Krempl

Krempl [*12*] presents sufficient data on smooth and grooved cylinder LCF tests to provide an additional comparison to illustrate the validity of the proposed technique. The cylic stress-strain curve and the smooth specimen strain-controlled fatigue curve are available. This information is used to predict cracking in grooved, axially cycled cylinders.

The nominal stress state is assumed to be uniaxial and equal to the load divided by the net sectional area. Notch effects are accounted for by use of the extended Neuber relationship, Eq 5. The numerical values used for the effective SCF are taken from work by Mowbray [*9*]. Figure 1 shows the smooth strain controlled LCF data of Krempl (plotted in terms of stress), the predicted curves for the notched specimens, and the test results of Krempl for the 2¼Cr-1Mo material at room temperature. The largest discrepancy between predicted and observed lives occurs for the 1.37 groove and is believed due to the conservatism of Neuber's equation for low K_t's and the approximation of a uniaxial nominal stress state. Figure 2 illustrates the same comparison for the 550 F tests.

Estimating Strain Concentration

The plastic strain concentration scatterband for a representative number of low-alloy steels is shown on Fig. 3. This plot was generated using the extended Stowell and Neuber relationships with the cyclic stress-strain curve for various low-alloy steels. The plastic strain concentration factor is plotted with respect to a normalized nominal strain range, $\Delta\bar{\epsilon}/2\epsilon_y$. The strain at yield, ϵ_y is taken from the cyclic stress-strain curves at 0.02 per-

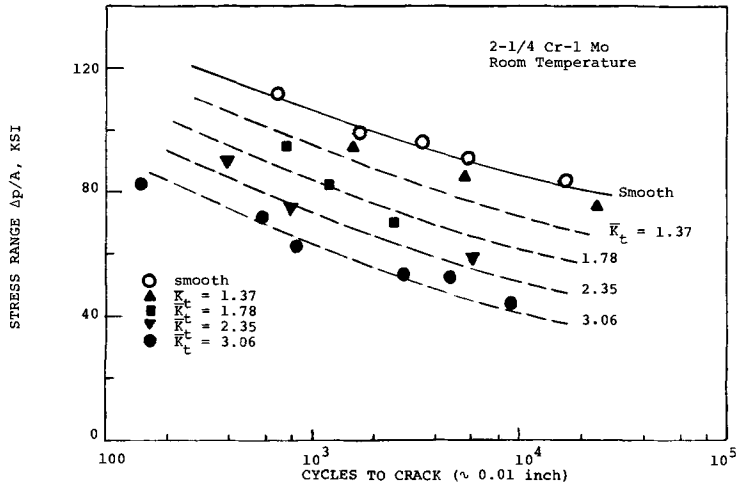


FIG. 1—*Predicted cracking of grooved cylinders using Neuber's equation (data from Kempl* [10]).

cent offset. The range shown on Fig. 3 is more dependent on temperature than material with the upper bound corresponding to 1000 F and the lower bound to room temperature.

For design purposes, it is suggested that a mean value for the range shown be used to estimate the effects of strain concentration. At low values of concentration strain, there exists very little scatter in the plastic strain concentration by virtue of the normalizing parameter. At high

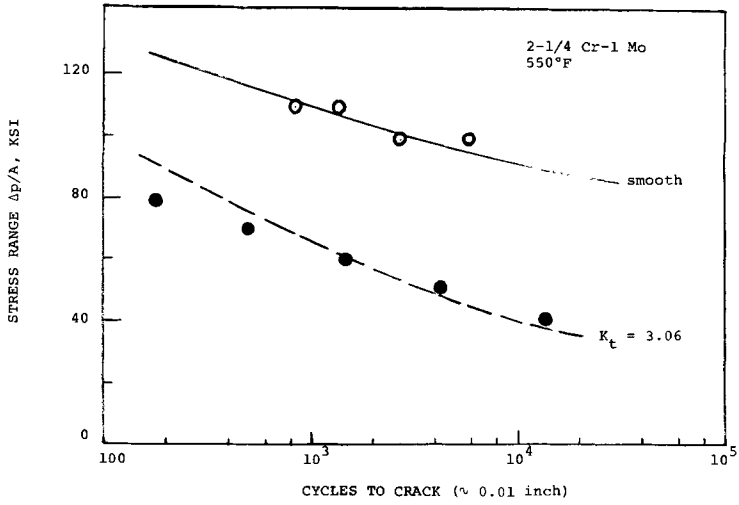


FIG. 2—*Predicted cracking of grooved cylinders using Neuber's equation (data from Krempl* [10]).

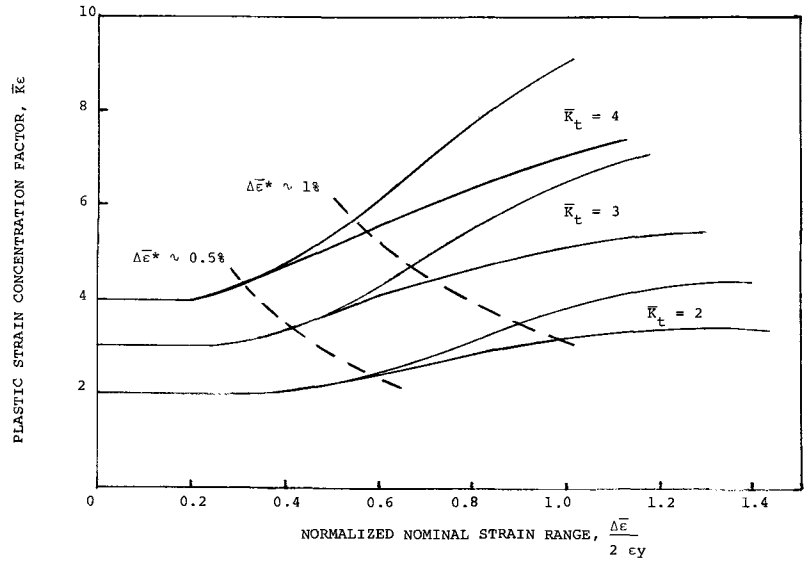


FIG. 3—*Plastic strain concentration factor scatterband including various low-alloy steels.*

values of concentrated strain, there is much more scatter, but the number of cycles in the high strain region of the fatigue curve is less sensitive to strain range. Figure 4 is a normalized strain concentration curve constructed using the mean values, and it is suggested that these curves be used to estimate strain concentration for low-alloy steels.

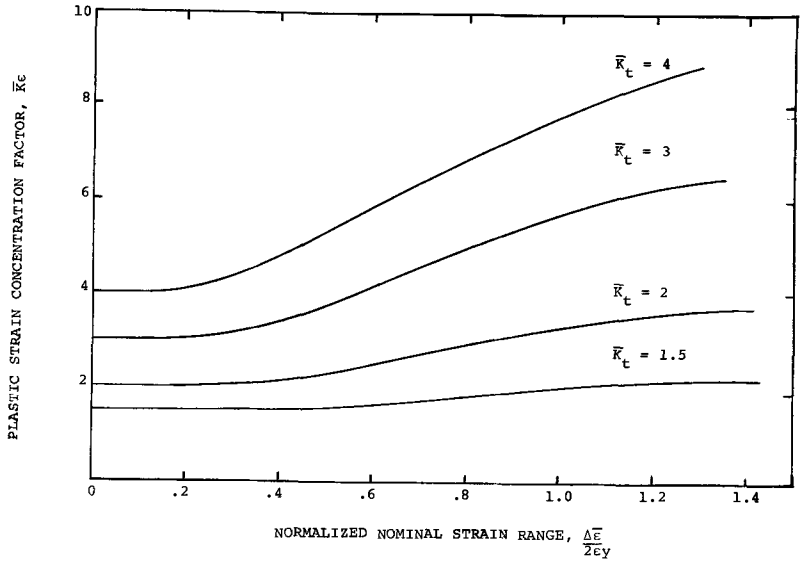


FIG. 4—*Estimate of plastic strain concentration factors for low-alloy steels.*

The strain at yield, ϵ_y, is a normalizing parameter which is required to estimate strain concentration using Fig. 4. As a first approximation, the strain at yield determined from a tension test (0.02 percent offset) may be used if the degree of cyclic hardening or softening is small. Smith et al [*13*] suggest that cyclic hardening or softening can be predicted from a tension test by the ratio of tensile stress to 0.2 percent proof stress. Cyclic hardening will occur if this ratio is less than 1.2. Between 1.2 and 1.4 only a small degree of hardening or softening will occur.

Summary

A technique for incorporating the effects of stress biaxility and stress concentrations into design calculations has been proposed. Use is made of the cyclic stress-strain curve, the low-cycle fatigue curve, and an elasto-plastic effective strain parameter. A number of assumptions and approximations are made to provide a simple yet useful design technique The following steps are followed to determine the number of cycles to component cracking:

1 Develop a relationship similar to Eq 7, relating the known nominal strain (or stress) range and stress state to the nominal effective strain range (defined by Eq 1). The relationships defined by Eqs 1, 2, and 3 are used.

2. Make use of the extended Stowell, Eq 4, or Neuber relationship, Eq 5, to estimate the effect of stress concentration. Alternately, Fig. 4 may be used to estimate plastic strain concentration for low-alloy steels, when the "cyclic" stress-strain curve is not known.

3. Determine cycles to cracking from the smooth uniaxial fatigue curve employing the concentrated effective strain range as the assumed failure criterion.

The technique has been applied to mechanical and thermal LCF tests on grooved cylinders to predict cracking, and the results are very encouraging.

References

[*1*] Coffin, L. F., Jr., "Life Prediction of Metals Subjected To High-Temperature Fatigue," presented at International Conference on Mechanical Behavior of Materials, Kyoto, Japan, Aug. 1971.

[*2*] Ives, K. D. et al, *Journal of Basic Engineering*, Dec. 1966.

[*3*] Stowell, E. Z., "Poisson's Ratio and Volume Changes for Plastically Orthotropic Material," NACA Technical Note 3736, National Advisory Committee for Aeronautics, 1956.

[*4*] Nadai, A., *Theory of Flow and Fracture of Solids*, Vol. I, 2nd edition, McGraw-Hill, New York, 1950.

[*5*] Stowell, E. Z., "Stress and Strain Concentration at a Circular Hole in an Infinite Plate," NACA TN 2073, National Advisory Committee for Aeronautics, 1950.

[*6*] Hardrath, H. F. and Ohman, L., "A Study of Elastic and Plastic Stress Concentration Factors Due to Notches and Fillets in Flat Plates," NACA Report 1117, National Advisory Committee for Aeronautics, 1953.

[7] Neuber, H., "Research on the Distribution of Tension in Notched Construction Parts," WADD TR60-906, Jan. 1961.
[8] Papirno, R., *Experimental Mechanics*, Oct. 1971.
[9] Mowbray, D. F. and McConnelee, J. E., "Application of Finite Element Elastic-Plastic Stress Analysis to Notched Fatigue Specimen Behavior," First International Conference on Reactor Structural Mechanics, West Berlin, Sept. 1971.
[10] Isberg, L. J. and Wozney, G. P., "Mechanical and Thermal LCF Tests on Grooved Cylinders," Internal General Electric Report, General Electric Co., Schenectady.
[11] Peterson, R. E., *Stress Concentration Design Factors*, Wiley, New York, 1953.
[12] Kremple, E., "Low-Cycle Fatigue and Stress Concentrations at Room Temperature and 550°F for Three Low-Strength Structural Steels," GEAP Report No. 10170, March 1970, available from Clearinghouse for Federal, Scientific, and Technical Information Center, Springfield, Va.
[13] Smith, R. W., Hirschberg, M. H., and Manson, S. S., "Fatigue Behavior of Materials Under Strain Cycling in Low and Intermediate Life Range," NASA TN O-1574, National Aeronautics and Space Administration, 1963.

B. J. L. Darlaston[1] *and D. J. Walters*[1]

Some Considerations of the Application of Cyclic Data to the Design of Welded Structures

REFERENCE: Darlaston, B. J. L. and Walters, D. J., **"Some Considerations of the Application of Cyclic Data to the Design of Welded Structures,"** *Fatigue at Elevated Temperatures, ASTM STP 520,* American Society for Testing and Materials, 1973, pp. 688–698.

ABSTRACT: The behavior of a transition joint between 2¼Cr-Mo and Type 316 stainless steel has been analysed. The results are used to define the condition for accelerated laboratory testing under cyclic conditions. The relevance of conventional design methods is discussed, and a design approval route is defined.

KEY WORDS: fatigue (materials), weldments, stress analysis, tests, cyclic loads, creep properties, pipe joints, strains, plastic deformation

The design of high-temperature plant is based normally upon the mechanical properties of the parent material with the weld assumed to have adequate strength. This design method may be questioned on the grounds it is unlikely that material properties can be exactly matched in the creep range; hence, the performance of the component may be significantly influenced. This has given rise to the need for a more detailed method of evaluating weld performance at elevated temperatures, particularly under cyclic conditions. An attempt already has been made to analyze the creep load condition [*1,2*][2] and the high-strain fatigue conditions [*3*].

The behavior of transition welds between austenitic and ferritic materials, specifically the case of the butt welded pipe provides an interesting case and one of considerable importance as well to the power industry. An extensive program of experimental and theoretical work is being undertaken in the United Kingdom by the Central Electricity Generating Board to evaluate the behavior of transition joints and to define the laboratory

[1] Section head, Berkeley Nuclear Laboratories, Central Electricity Generating Board, United Kingdom.

[2] The italic numbers in brackets refer to the list of references appended to this paper.

Copyright© 1973 by ASTM International www.astm.org

test procedures necessary to demonstrate the integrity of such joints under operating conditions. The joints operate typically at 838 K (565 C) with a pressure of approximately 17 atm. One of the necessary requirements of these steam pipe joints is that they shall be capable of withstanding 300 full power cycles which represent a change from the operating conditions to ambient temperature and pressure.

Generally speaking the majority of the mechanical test work on a welded joint will involve uniaxial testing usually on composite specimens. This immediately gives rise to the question of the validity of such tests and the relationship between the simple specimens and the more complex geometry. Such aspects as residual stress, strain distribution, metallurgical effects due to scaling, failure criteria, etc., must be considered also. Assuming that tests on the full size component can be undertaken, there is then the question of the extent to which these tests can be accelerated and the method used for the extrapolation of laboratory results to the operational life.

Finite element stress analysis techniques have been used to examine stress and strain distribution in these multimaterial situations. The results of these analyses are then used to (*a*) attempt to define a Design Approval Route, (*b*) define the conditions for laboratory tests on scale and full size components, and (*c*) assess the relevance of high-strain fatigue data from uniaxial tests on composites. Insufficient material data necessitate the introduction of several assumptions in the theoretical studies. While the initial analysis may be used as a "guideline," a complete solution will be obtained only by an iterative procedure of defining the experimental data required, repeating the theoretical studies and again defining the experimental program.

Analytical Techniques

The stress and strain analysis was conducted using the TESS finite element computer program [*4*]. Previous theoretical studies undertaken with this program have shown reasonable correlation with experimental results for, thermal gradients [*5*], elastic deformation of nozzle-sphere intersections, and creep of nozzle-sphere intersections [*6*]. In all cases material data were obtained from carefully controlled laboratory tests on similar material to that used in the more complex geometry.

Experience has shown that while good correlation can be achieved for carefully controlled laboratory experiments extrapolation to plant operating conditions must be undertaken with caution. The assumptions made in the analysis and the scatterband on material data generally prohibit absolute values of strain being predicted. The calculated stess levels are not particularly sensitive to the scatter in data.

Assumptions Made in the Analysis

1. Four material regions are assumed within the structure: (*a*) $2\frac{1}{4}$Cr, (*b*) 18/8 weld deposit, (*c*) Type 316 stainless steel, (*d*) a weakened transition bond at the ferritic-18/8 interface.

Although the computer program is written to evaluate a maximum of 64 different materials within a structure, the limitation of four zones is imposed by the number of materials whose properties have been identified experimentally.

Theoretical studies have shown only small changes in the general stress distribution occur when an increased number of smaller property changes are introduced. Strain distributions however, may, be significant if localized regions could be identified, and therefore we have reservations upon the strain levels predicted.

2. The boundary between each region is assumed a smooth straight line. This assumption may be modified when a metallurgical examination of the welds is complete and the interface profile is known.

3. Material properties within each region are assumed to be constant. This assumption has caused some concern to the authors since property changes must occur in the ferritic heat affected zone (HAZ). Furthermore the work reported and reviewed by Kent and others at the Newcastle Conference [7] indicate a time dependent decarburization by virtue of carbon migration occurring at the interface. While the computer program has been developed to allow localized and time dependent property changes to occur, an extensive experimental program is necessary to establish these properties for this material combination and welding procedure. The analysis presented in this paper is intended only as a first approximation which will be refined at the time data are available.

4. Bending and self-weight. While the computer program can evaluate these effects, they were not considered to be significant in a laboratory controlled experiment and therefore, were ignored.

5. The creep strain data were normalized to fit the expression

$$\epsilon = K^n \sigma T^m e^{-Q/Rt}$$

where

K, n, m = constants,
σ = stress time,
T = time,
t = absolute temperature,
Q = activation energy, and
R = gas constant.

Previous experience has shown this type of normalization is only applicable to a small temperature and stress range. Where detailed strain-time data are available over the full stress range imposed, good representation

can be achieved by storing the data as a numerical array and using a logarithmic interpolation between stress, time, and temperature. The lack of such data, however, necessitates the use of some form of normalization.

For a homogeneous structure, the stress index n will control the steady-state stress level while K and m control the time to attain this condition. If n can be determined accurately, the parameter K and m may be adjusted to achieve strain correlation with the experimental result. While this method has been satisfactorily applied to homogeneous structures, the current analysis is concerned with dissimilar materials. In such situations, stress is generally off-loaded by the material having the higher creep rate, and the redistributed stresses become a function of both n and K. The predicted values of strain and hence stress, therefore cannot be considered adequate.

6. The stress index n is assumed constant for each material. While n is generally stress dependent, the assumption that n is constant for a small stress range is often valid. Where sufficient data are available we evaluated n by plotting log total creep strain against log stress. If the slope of this graph remains relatively constant over the imposed stress range, n may be assumed constant. In cases where this assumption is not valid, n may be specified as a function of stress.

7. The structure is assumed stress free at its stress relieving temperature. This assumption is necessary as little is known about the residual stress and strain patterns after welding. An extensive research program is being currently conducted to examine this aspect, and the computer program has been modified to impose residual strain patterns when they have been identified.

Results of the Analysis

The stress analysis was conducted in two phases:

1. An elastic calculation which included thermally induced stresses.
2. An elastic-thermal solution modified by an iterative procedure as creep deformation occurred.

From phase one of the analysis the elastic distributions were obtained. Figure 1 was based on a stress free state at room temperature and Fig. 2 on a stress free state at stress relieving temperature.

Phase two of the investigation was conducted to establish the manner in which the stresses would redistribute when a time-dependent deformation occurred. Since the full-scale model tested was not stress relieved and the residual stress pattern was unknown, the vessel was assumed stress free at room temperature, thus imposing a severe thermal stressing condition. The time-dependent redistribution of the maximum stress occurring at the $2\frac{1}{2}$Cr/18/8 interface is shown in Fig. 3 with the elastic distribution superimposed. A general steady-state solution is shown in Fig. 4.

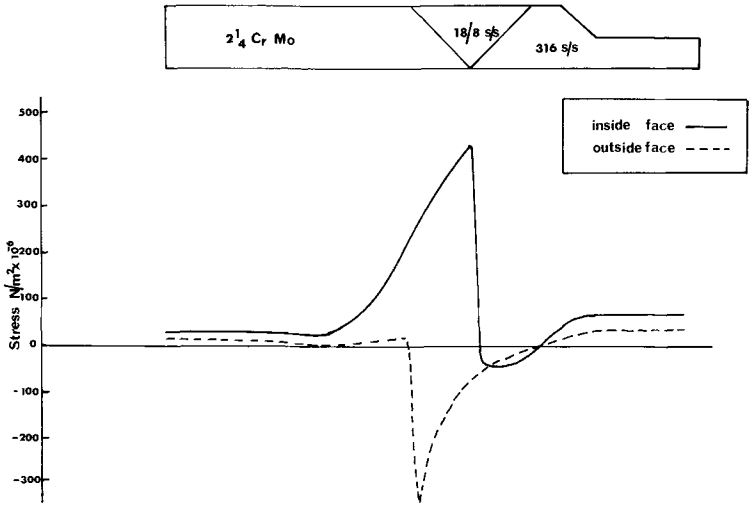


FIG. 1—*The elastic-thermal stress distribution plus pressure.*

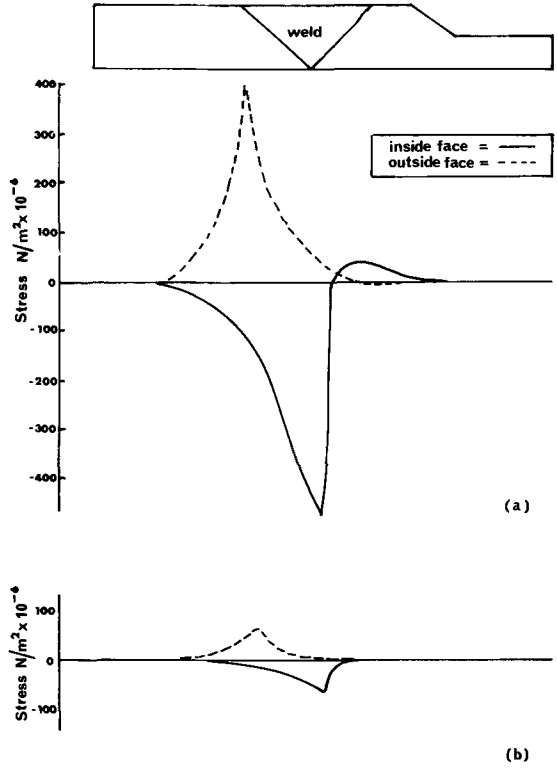


FIG. 2—*The estimated thermal stress distribution,* (a) *at room temperature after stress relieving,* (b) *at operating temperatures after stress relieving.*

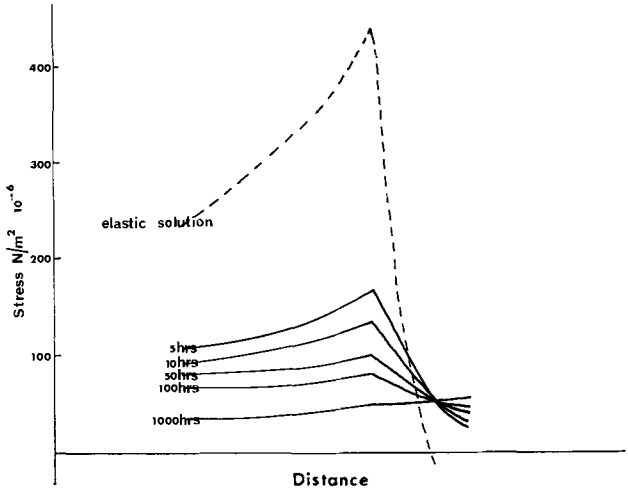


FIG. 3—*The time-dependent redistribution of the peak stress.*

Finally, a theoretical study was undertaken to examine the effects of scaled testing. It was assumed that the vessel dimensions were correctly scaled, while the weld penetration and transition width remained constant. For this simple analysis it was assumed the weld material would creep at a higher rate than the parent pipe. Figure 5 shows the tangential stresses in the weld off-load to the parent material. The relative stress levels obtained were not identical in the two geometries.

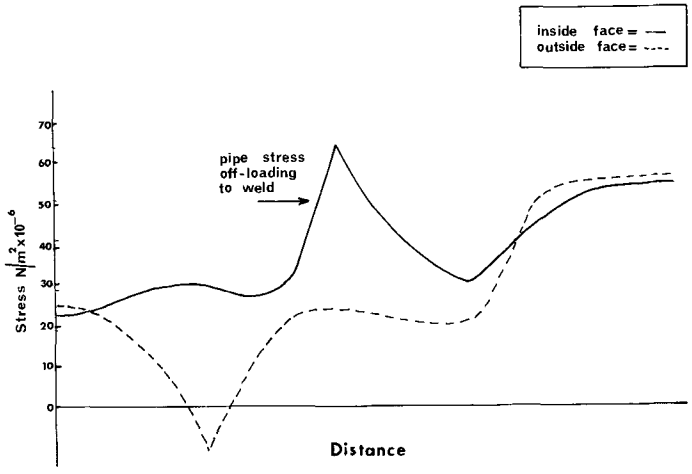


FIG. 4—*The steady-stage tangential stress distribution.*

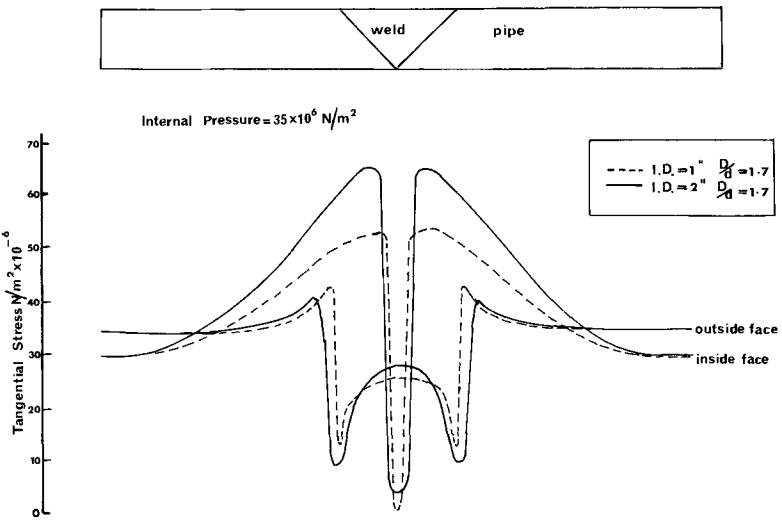


FIG. 5—*A comparison of predicted tangential stress distribution in scaled specimen geometries.*

Failure Predictions

The design approach to transition joints has been to determine the material wall thickness of the joint using the stress rupture properties of the weaker parent material. The joint efficiency, defined as the ratio of the design stress for the joint divided by the design stress for the weaker parent material, then is applied. In the Central Electricity Generating Board a factor of 0.6 is utilized at present and is meant to take into account the cyclic loading effect.

Failure of the joint may occur at shorter times than expected because of cyclic loading. The cyclic loading cannot be readily related to simple fatigue data because of the complexity of the stress cycle at the critical point. This latter aspect is illustrated by the results of the analysis presented earlier in the paper. The conventional laboratory fatigue test usually provides data on either stress or strain controlled cycles including the effect of holdtime. In the case in question the variations of stress and strain with time in the cycle are considerably different from the idealized laboratory cycle. Local strain accumulation and stress redistribution can have a a considerable effect of the life of the component. Uniaxial test data, even imposing a realistic operating cycle, can be often misleading because strain is distributed in a manner which may be very different from that in the more complex geometry.

Failure points can be defined only from tests in which the loading conditions are similar to that of the real component. The failure should then occur in the correct position. Doubt will still arise on the empirical

extrapolation of the results to the longer term operational conditions. This topic has been the subject of many papers some of which appear at this Conference and we do not propose to enlarge on the matter here.

Accelerated Testing

While numerous arguments may be forwarded against accelerating tests, it is essential to evaluate the performance of a weldment in a realistic time scale. A typical cycle is illustrated schematically in Fig. 6. Since the exact state of stress upon application of load cannot be calculated precisely, two conditions can be considered. Firstly, the weld is assumed stress free at its stress relieving temperature. The thermal stress component from the elastic analysis is $\simeq 0.69$ MN/m²/K. Therefore on cooling to room temperature a compressive stress of $\simeq 496$ MN/m² is induced and cold yield will occur at 276 MN/m². Reloading to the test temperature of 838 K will cause a thermal stress of 386 MN/m² plus a pressure stress of 34.5 MN/m² which must reduce significantly as plastic and time-dependent deformation occurs. The rate at which this stress reduces is known approximately from the creep and plasticity calculations. Providing relaxation occurs, cold yield must occur on subsequent unloading; the magnitude

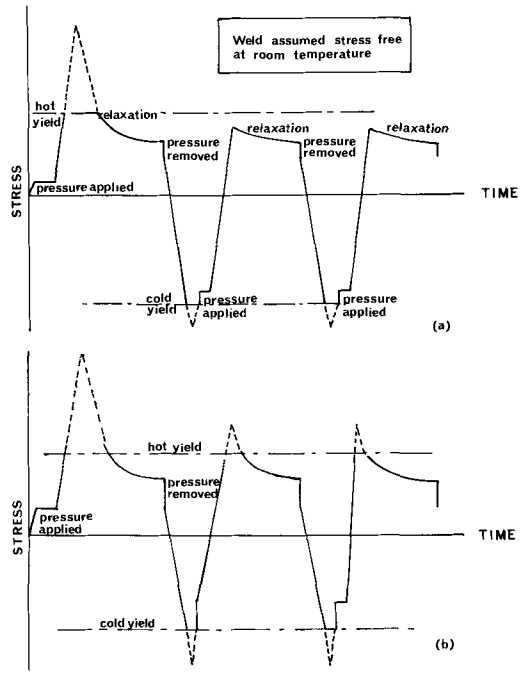


FIG. 6—*Schematic representation of repeated cycles,* (a) *operating temperature and pressure,* (b) *test accelerated by increasing pressure.*

of creep relaxation damage and cold yield will be dependent upon the holdtime.

The second case, assumes the weldment is stress free at room temperature. Initial loading will produce an effective stress of 448 MN/m^2 which must again be modified by plastic and creep deformation. A similar cyclic pattern, therefore, must emerge. Once cold yield occurs, the tensile loading stress becomes the pressure plus thermal component minus compressive yield, that is, approximately 172 MN/m^2. This stress then relaxes as a function of the holdtime and causes subsequent cold yielding.

The effect of increasing the pressure component is illustrated schematically in Fig. 6. Irrespective of the initial state of stress, the subsequent cyclic pattern will approximate to an increased loading stress per cycle, hence an increased creep relaxation component. The magnitude of cold yield will be dependent again on the holdtime.

In this form of acceleration, care is required in establishing the relative changes that may occur in the stress index n. Providing each material experiences a similar change, the subsequent failure should remain representative for long term extrapolation.

Increasing the testing temperature also will induce a higher loading stress and a similar cyclic pattern to the pressure case. This form of acceleration however, may, have two significant effects upon the stress analysis. The stress indices may vary and the relative creep rates may change. Since the creep strain component can influence significantly the redistribution patterns, failure may not be representative for long-term extrapolation.

A third method of acceleration available is an increase in the testing frequency. Since the relaxation rate generally decreases with time, there is an optimum point in the cycle for creep relaxation and cold yield damage. This type of acceleration also requires caution since too great an increase will minimize relaxation and hence cold yielding, thus resembling a reverse elastic stress cycle.

General Comments

Following the simple design approach involving a joint efficiency factor many superheater and a few larger diameter transition joints have given trouble free service. A number of failures have occurred in the United Kingdom, and these are well documented by Wright [*8*] and Rowley [*9*]. There appears to be an increasing number of transition joints being introduced into power plants particularly nuclear plants. This situation coupled with the more severe cycling conditions imposed has led to the need for a better understanding of their behavior.

The analytical method provides stress values. These values cannot be used in conjunction with virgin material data because the welded components often suffer from narrow zones of material with very different

properties in which strain in a macroscopic sense is the controlling feature. The shortcomings of uniaxial tests have been identified elsewhere [*10*].

A "design approval route" [*1*] is a convenient way in which to define experimental and theoretical work necessary to justify a particular design. The extent of each type of test will depend upon its limitations, although it must be remembered that uniaxial tests can be carried out more readily and more cheaply than tests on the full size component. Having defined the "route" for a particular combination of materials, the effect of various operating conditions, various geometries, etc., can be evaluated.

Several methods of life assessment based on local behavior could be submitted as possible replacements for the current designed code methods. The lack of an adequate body of strain-time data prohibits an assessment of local strains and reduces the accuracy of the calculated stress distribution. It is worth noting that the general stress pattern is not particularly sensitive to small regions of slightly differing properties, whereas the strain distribution local and the strain to failure may well be affected markedly. A considerable amount of evidence is still required to support such methods. In the meantime the analytical techniques developed can be used to ensure that the experimental evaluation of scale and full size joints is carried out in a manner which leads to a realistic failure, thus providing information which may be extrapolated empirically to make plant life predictions.

Conclusions

1. Plant experience suggests that no adequate design method at present exists for transition joints and a "design approval route" must be defined for each combination of materials. Experimental work is required as the first stage.

2. Theoretical work carried out in an attempt to define an approval route indicates that:

(*a*) Conditions for laboratory tests on scale and full size components must be such that the stress and strain cycles are similar to those of normal operating cycles.

(*b*) Scale test components must also be scaled in relation to metallurgical structures, for example, width.

(*c*) High-strain fatigue data from uniaxial tests on composites has little relevance to the evaluation of transition joints.

Acknowledgments

This paper is published with the permission of the Central Electricity Generating Board.

References

[*1*] Darlaston, B. J. L. and Featherstone, P. F., "Design Approval Route," Conference on Welding on Creep Resistant Steels, United Kingdom Welding Institute, 1970.

[2] Darlaston, B. J. L. and Walters, D. J., 15th International Welding Congress, Czechoslavakia, Oct. 1971.
[3] Serensen, S. V. and Machutov, N. A., "Low Cycle Fatigue Resistance of Welded Joints of Low Carbon Steel Depending on Properties of Welded Zone," IIW XIII-635-71, International Institute of Welding, 1971.
[4] Ecclestone, M. J. and Leech, A., Report RD/C/N362, Central Electricity Generating Board, 1969.
[5] Chubb, E. J., Report RD/B/N1497, Central Electricity Generating Board, 1970.
[6] Chubb, E. J., Procter, E., and Strong, J. T., Colloquium, International Institute of Welding, Toronto, 1972.
[7] *Proceedings*, Conference on Welding of Creep Resistant Steels, United Kingdom Welding Institute, 1970.
[8] Wright, V. S., Conference on Welding of Creep Resistant Steels, United Kingdom Welding Institute, 1970.
[9] Rowley, T., Rowberry, T. R., and Aldridge, C., Pipe Welding Conference, Paper 15, United Kingdom Welding Institute, 1969.
[10] Kent, R. P., Conference on Welding of Creep Resistant Steels, United Kingdom Welding Institute, 1970, Paper 1.

C. W. Lawton[1] *and J. E. Bynum*[1]

Elevated Temperature Test of Welded Furnace Wall Sections

REFERENCE: Lawton, C. W. and Bynum, J. E., "**Elevated Temperature Test of Welded Furnace Wall Sections,**" *Fatigue at Elevated Temperatures, ASTM STP 520*, American Society for Testing and Materials, 1973, pp. 699–708.

ABSTRACT: Welded furnace walls of a modern utility steam generator are subjected to a cyclic system of complex stresses from thermal gradients and mechanical loads as the generator responds to the power load demand. In the fatigue evaluation of the walls, the designer needs a design curve which relates and incorporates the broad spectrum of production tolerances (geometry and material) to the basic material fatigue properties at the elevated temperatures experienced by the steam generator. A research program has been conducted to evaluate the fatigue behavior of a composite (combined wrought and welded structure) furnace wall section.

The fatigue capabilities of the welded furnace wall construction were established experimentally using production specimens of the wall. The specimens were subjected to deflection-controlled alternating flexure tests. The test series were run at 1050 F and included both continuous cycling and holdtimes applied at both extremes of the deflection cycle and at one extreme of the deflection cycle.

KEY WORDS: weldments, boilers, thermal fatigue, bend tests, creep properties, elastic analysis, stress cycle, loads (forces), fatigue (materials)

The solution of complex structural problems with time-dependent loads and nonlinear material behavior such as creep requires large amounts of computer time even with today's modern machines. Substitution of an elastic analysis with an evaluation of the stresses using a design curve represents an attempt to reduce the cost and time of the analysis for contract design. The program described in this paper was developed to determine the feasibility of this type of analysis for the fatigue evaluation of welded furnace panels in utility steam generators.

The complex loading system imposed on the furnace enclosure of a modern utility steam generator is shown in Fig. 1. These structural systems often reach sizes of 100 ft wide by 200 ft high by 50 ft deep. As can be seen in Fig. 2, the welded furnace wall is, in fact, a large orthotropic plate which is supported by, and thus interacts with, the structural grid system.

[1] Staff engineer and project engineer, respectively, Research and Product Development, C-E Combustion Division, Combustion Engineering, Inc., Windsor, Conn. 06095.

Copyright© 1973 by ASTM International www.astm.org

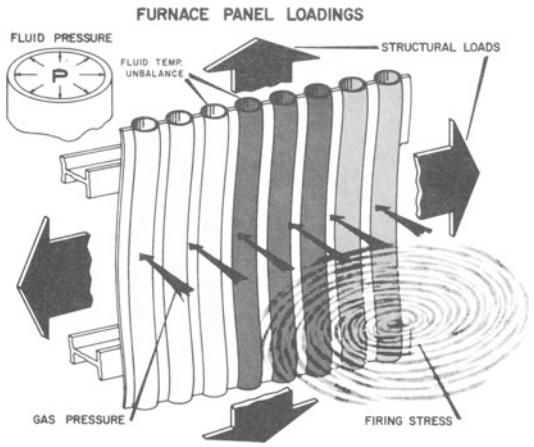


FIG. 1—*Furnace wall panel loadings.*

The design and analysis of such a composite structure requires:

1. Detailed information of the orthotropic constants of the wall.
2. Strain concentration factors of the tube fin geometry.
3. Large digital computing facilities.
4. A relevant fatigue design curve.

The purpose of this investigation was to develop a relevant fatigue design curve. It is worth noting that, because of the economic and time constraints of production designs, an elastic analysis and design basis are also desirable goals.

Evaluation of stresses and strains in the welded wall was limited because data were lacking to evaluate the fatigue behavior of the wall as a composite unit. Low-cycle fatigue data were available for the materials used in the walls, but this had been generated on carefully machined and polished specimens. Experimental work with surface finish and specimen size has shown that these parameters influence fatigue life. Thus, some fatigue reduction factors appear to be needed to account for the geometric and tolerance parameters of production type wall panels.

The ASME Boiler and Pressure Vessel Codes, Section III and Section VIII, Division 2, have some design fatigue curves for low-cycle fatigue. At room temperature, there has been some experimental evaluation of these curves on pressure vessels fabricated to the requirements of Section III of the Code [*1,2*].[2] The data have shown that the design curves are realistic for this quality of construction. The welded furnace wall panels are fabricated to the requirements of Section I of the ASME Power Boiler Code which offers no guidance for fatigue evaluation. To determine if the factors

[2] The italic numbers in brackets refer to the list of references appended to this paper.

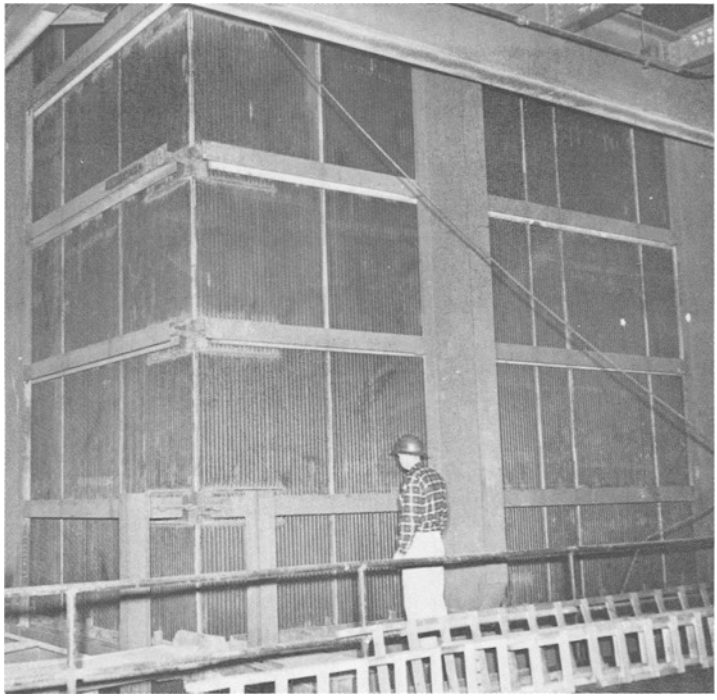


FIG. 2—*View of furnace wall and structural steel.*

used to construct the design curves in the ASME Code were adequate to cover the conditions of high temperature, creep range for the materials, and the geometric and tolerance parameters of a production type panel, a fatigue testing program was developed which used the wall section as a test specimen.

Experimental Program

Specimens which could be analyzed analytically and controlled during the experimental testing consisted of a 4-in.-wide horizontal section of the wall. For a 1¼-in. outside diameter tube wall panel, the specimen had seven tubes with six fins between the tubes. For larger diameter tubes, the number of tubes had to be reduced as shown in Fig. 3. The end tubes were cut in half and the specimen welded to a plate which had the same thickness as the tube outside diameter. Four-point loading was applied through the plate ends to produce bending in the tube section. A wide specimen was chosen to provide lateral restraint as a simulation of the plane-strain loading condition which the panel experiences in the furnace structure. Flexure tests were chosen for the specimens because they would simulate the local stress distribution of the thermal and pressure loads on

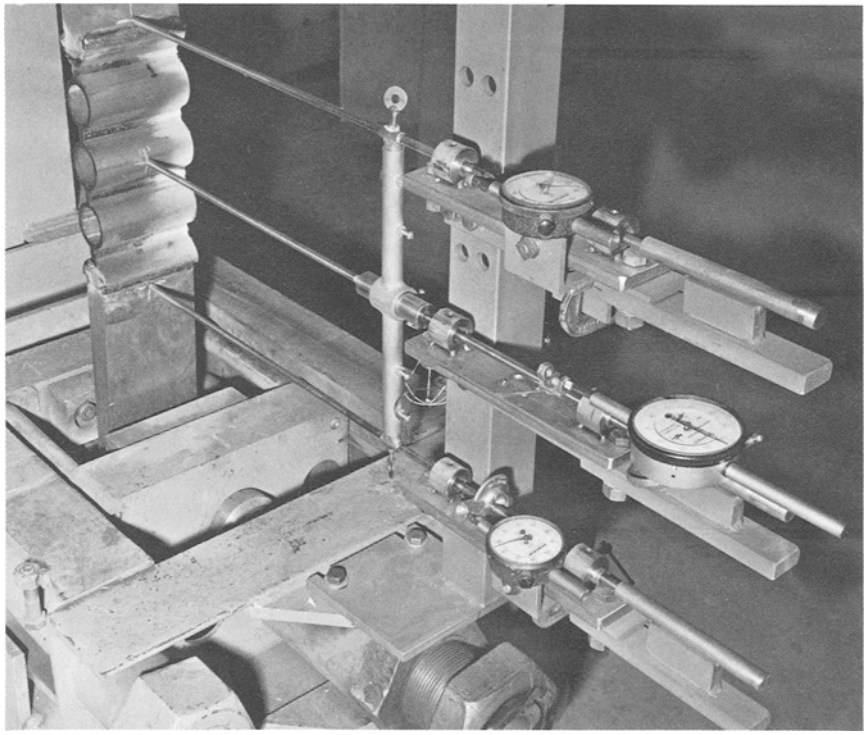


FIG. 3—*View of a welded wall specimen and dial gages for monitoring deflection.*

the furnace wall. An in-line compressive load of sufficient magnitude could not be applied to the specimen because of buckling.

The loading of the specimens was controlled by the displacement of the center of the specimen. Figure 3 shows the dial gage used to adjust the specimen loading and to monitor the displacement during the test. Strain gages were used to establish the relationship between the deflection of the specimen and the strains at critical areas, and to monitor the strains for the room temperature test. However, at elevated temperatures, the tests were run under deflection control because the strain gages would not be suitable. During elevated temperature cycling, the specimen was kept at 1050 F with a furnace built around the specimen. The tube material used for the elevated tests was SA213-T11.

The completely reversed continuous cycling tests were flexed at the rate of 3 cpm. To simulate actual operations in a boiler life cycle, holdtimes were incorporated in the fatigue cycle. Some tests had the holdtime at each extreme of the displacement cycle, while other tests had the holdtime at only one extreme of the displacement cycle.

Results

The configuration of the fin tube intersection is the natural curvature developed by the forces on the weld pool during manufacture. The fins are made by machine welding and have a smooth surface with no weld ripples. Normally, the maximum stress is in the center of the fin when a bending moment is applied to the wall-section specimen as in these tests. The increase in fin thickness at the fin and tube intersection is sufficient to offset the stress concentration effects if the welded fin blends smoothly into the tube. This is shown by the photoelastic fringe pattern in Fig. 4*a* for bending. For tensile loadings, the stress concentration at the tube-fin intersection is shown in Fig. 4*b*. The photoelastic model was made by using a thin slice from one of the test specimens as a template for machining the photoelastic material. The failures were in the centers of the fins for most of the specimens tested. Occasionally, the weld at the fin did not blend in smoothly with the tube, and so a few failures were at the tube-fin intersection because of the notch effect. However, the notch effect was not sufficient to have a noticeable effect on the cyclic life when compared with the other specimens. During manufacture of the walls panels, the lack of blending or the notch effect at the tube fin intersection is controlled within an acceptable tolerance.

Failure of the wall panel specimens at room temperature occurred at a lower number of cycles for a given strain range than would be obtained



FIG. 4—*Photoelastic fringe patterns for two types of loading.*

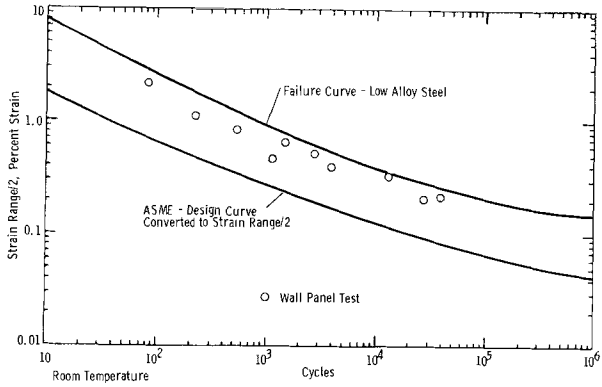


FIG. 5—*Test results for room temperature.*

from material fatigue tests using a machined and polished specimen. In Fig. 5, the failure curve for low-alloy steel shows the results of many fatigue tests made for the Pressure Vessel Research Council on wrought material with both push-pull specimens and the Lehigh bending specimen [*3*]. The design curve shown in Fig. 5 has been constructed from the design curve shown in Section III of the ASME Boiler and Pressure Vessel Code for carbon and low-alloy steel with a change in one of the coordinates to one half the strain range. The room-temperature, continuous-cycling results from this testing program show that a design based on the maximum strains would be conservative if the design curve shown in Fig. 5 was used for fatigue evaluation.

When the results of the continuous cycling tests for the welded wall specimen at 1050 F are compared with data from conventional material fatigue tests at the same temperature, there is a small reduction in cyclic life for a given strain range as shown in Fig. 6. If the results shown in

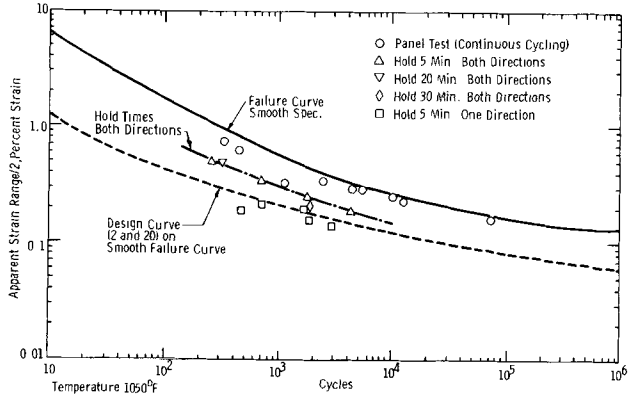


FIG. 6—*Test results at 1050 F.*

Fig. 6 are compared with the results of Fig. 5, there is a noticeable loss of fatigue life because of temperature effects. When holdtime was applied to both extremes of the deflection cycle, there is a definite decrease in cyclic life as shown in Fig. 6. In this test, an extension of holdtime to greater than 5 min did not affect cyclic life to any degree. When holdtime was applied, the load on the specimen dropped rapidly, and after 5 min most of the load change had occurred. At 1050 F, the creep strength of this low-alloy material is low, which accounts for the diminished effect of the holdtime intervals used in this test. If the test had been made at lower temperatures in the creep range of the material, a greater influence of holdtime interval would be expected as has been found by other investigations [*4,5*].

When holdtime was applied to only one extreme of the displacement cycle, another appreciable reduction in cyclic life was noted. Other investigators have recorded greater cyclic damage for holdtimes applied at only one extreme of the strain cycle [*6*]. Berling and Conway have concluded that only a holdtime in tension has a considerable effect in cyclic life reduction [*7*]. In a different evaluation, Manson et al have shown that the inelastic deformation that occurs at high temperature has two distinctly different straining mechanisms—plastic flow and creep—and that the strain range should be partitioned into the several components to evaluate cyclic damage [*8*]. The damage from holdtimes appears to differ in behavior in these tests from that found in some other programs. It also appears that the interactions of creep and fatigue are influenced by the stress field in the test specimen. The interaction behavior will be discussed later in this paper.

Discussion

Fatigue Failures in Fabricated Components

The results of this program showed, as would be expected, a decrease in cyclic fatigue life for the continuous cycling tests as compared with the results from a material fatigue test program which used the conventional machined and polished specimens. The decrease in cyclic life for fabricated components has been recorded in other testing programs by the Pressure Vessel Research Council (PVRC) [*1,2*]. Further study of the fatigue behavior leads one to the conclusion that the failure mechanism in a fabricated component is mostly one of crack propagation of imperfections. Normal practices in nondestructive testing do not detect these imperfections because they are smaller than the sensitivity level used in examinations. However, after a very few cycles of loading, the imperfections start to grow because of the high load levels used in low-cycle fatigue. Thus, the crack initiation period associated with the failure of machined and polished specimen is bypassed in the fatigue process. A similar behavior has been observed

with sharply notched fatigue specimens where up to 90 percent of the fatigue life has been in the propagation of the fatigue crack, whereas in a conventional smooth bar push-pull fatigue specimen, the fraction of life to propagate the crack is about 15 to 20 percent.

Holdtime Behavior

When holdtimes were imposed in the deflection cycle, there was a considerable reduction in cyclic life for all the strain ranges tested. This behavior differs from that found by Edmunds and White, who showed that for beams of uniform cross section the effect of holdtime on cycles to failure was much less pronounced at high-strain ranges than at low-strain ranges [*9*]. Similar results to that of Edmunds and White have been found with push-pull fatigue specimens by Berling and Conway [*7*].

In search for an explanation of the different fatigue behavior to holdtime effects in the test with the welded wall sections, a nonlinear finite element analysis using the MARC II computer program was made [*10*]. Since the bending moment was constant along the specimens, the computer model with only two tubes shown in Fig. 7 was used for the analysis. When a displacement loading was applied to the computer model and held for a period of time to simulate the experimental test, the total strain at the center of the fin increased during the time period. The stress and strain redistributions which occurred in this specimen are very complex, because even the lower stressed areas like the tube had creep taking place which influenced the overall stress and strain distribution. In the tests with the larger strain ranges, the stresses in the tube are greater. With larger stresses in the tube, the creep strain rates increase, which results in larger strains in the centers of the fins and, in turn, results in faster cyclic failure.

In the constant strain holdtime tests discussed previously in the literature, some of the elastic strain was transformed to creep strain with no change in total strain. Thus, the stress decreased as a function of the elastic strain. In the large strain range test, most of the damage was from fatigue. The creep damage was small because of the relatively short time involved. In a welded wall specimen subjected to holdtime, with its complex stress system in creep, the stress and strain redistribution within the specimen

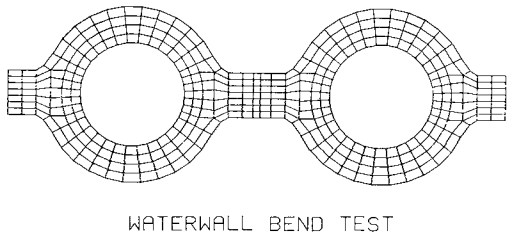


FIG. 7—*Finite element model for inelastic analysis.*

causes further fatigue damage in the high-strain region as compared with a stress system which has only pure relaxation.

Design Curves

The first consideration on which to base design margins is an evaluation of the procedures used to determine the design loads and the applicability of the design analysis to the material behavior. Another consideration is the evaluation of previous operational experience with similar equipment. A design curve for the evaluation of a specific type of equipment made to establish construction standards and establish operating conditions does not require the same design margins as a general purpose design curve. The design margins of the ASME Code, the lesser of 20 on cycles or 4 on strain range, is based on the realistic determination of the strain range for various operational cycles. If the code design margins were used for a design curve, an inelastic analysis of the welded wall for each operating condition would be required to determine the total strain range when creep was a consideration. The design curve would be used to evaluate fatigue damage and another design curve for creep damage. Some further design procedure would be needed to sum the fatigue and creep damage. Although the test results might infer a lesser design margin for strain ranges for welded wall construction, the determination of the strain range and number of cycles from design loads and predicted histogram do not have the necessary precision for a reduction in design margin. In a steam generator, the loading conditions are many, very complex, and difficult to evaluate over the 30 years or longer lifetime of the structure.

The holdtime tests in this program were useful in developing a design curve for the welded walls because they provided a means to evaluate the analytical analysis against controlled and measured parameters which simulate the operational behavior of the welded wall in a furnace structure. The design curve must consider the actual type of design loads on the welded wall in the furnace. The strain ranges may be determined with analytical procedures proven with simulated conditions in an experimental test which was a part of this program. When creep effects are to be factored into design curves for components with complex stress systems, a combined analytical and experimental analysis is needed. Thus, a design curve based on the holdtime test in this program would be for flexure loading.

Conclusion

It was concluded that a fatigue design curve for the welded wall furnace panel can be constructed from the material fatigue curve by using suitable design margins. The design curve would be applicable for the evaluation of fatigue damage, but there should be a realistic determination of strain range. In the creep range, an inelastic analysis would be required to determine strain range.

A design curve for fatigue analysis which includes a margin for creep damage is much more difficult to construct. Holdtime tests, as made in this program, provide a means to evaluate analytical procedures to be used for establishing a design curve. Holdtime tests on simple specimens with pure relaxation, as described in the literature, do not predict the strain behavior and distribution in complex shapes because the creep strain rates are a function of stress magnitude as well as time.

The feasibility of an elastic analysis to evaluate fatigue damage at high temperatures in welded furnace walls is very limited because of the difficulty in determining strain ranges with elastic analysis. Further analytical work is required to develop a special fatigue design curve for welded wall panels for contract work. When inelastic analysis is used to determine strain ranges, the factors of 2 in strain and 20 in cycles are used to develop a fatigue design curve.

References

[1] Murphy, J. J., Soderberg, C. R., and Rossheim, D. B., *Welding Research Council Bulletin No. 27*, May 1956.

[2] Kooistra, L. F. and Lemcoe, M. M., *Welding Journal Research Supplement*, July 1962.

[3] Criteria of the ASME Boiler and Pressure Vessel Code for Design By Analysis in Section III and VIII, Division 2, American Society of Mechanical Engineers, New York, 1969.

[4] Timo, D. P., "Designing Turbine Components for Low Cycle Fatigue," International Conference on Thermal Stress and Thermal Fatigue, Berkeley, England, Sept. 1969; also General Electric Company Report DF 69LS57.

[5] Coles, A., Hill, G. J., Dawson, R. A. T., and Watson, S. J., "The High-Strain Fatigue Properties of Low Alloy Creep-Resisting Steels," The Institute of Metals, M & R Series No. 32, 1967, London, England.

[6] Tuppeny, W. H., Jr., Ed., *High Temperature Low Cycle Fatigue*, Society for Experimental Stress Analysis, Westport, Conn., 1968.

[7] Berling, J. T. and Conway, J. B. in *Proceedings*, 1st International Conference on Pressure Vessels Technology, American Society of Mechanical Engineers, Vol. 2, Sept. 1969.

[8] Manson, S. S., Halford, G. R., and Hirschberg, M. H., "Creep-Fatigue Analysis by Strain Range Partitioning," NASA Technical Memorandum, National Aeronautics and Space Administration, Lewis Research Center, Cleveland, Ohio, 1971.

[9] Edmunds, H. G. and White, D. J., *Journal of Mechanical Engineering Science*, Vol. 8, No. 3, 1966.

[10] Ayres, D. J., "Elastic-Plastic and Creep Analysis Via the MARC Finite Element Computer Program," International Symposium on Numerical and Computer Methods in Structural Mechanics, Urbana, Ill., Sept. 1971.

T. R. Branca[1] *and J. L. McLean*[1]

Parametric Study to Establish Design Curves and to Evaluate Design Rules for Ratchetting

REFERENCE: Branca, T. R. and McLean, J. L., **"Parametric Study to Establish Design Curves and to Evaluate Design Rules for Ratchetting,"** *Fatigue at Elevated Temperatures, ASTM STP 520*, American Society for Testing and Materials, 1973, pp. 709–721.

ABSTRACT: With inelastic analyses requiring a substantially greater expenditure of effort over elastic analyses, there is strong incentive to establish an elastic design criterion for ratchetting that is not excessively conservative and consequently restrictive.

To establish design curves for ratchetting, the Ansys computer program was used to develop elastic-plastic-creep solutions for several cases of a long, sodium-filled pipe. The pipe was subjected to a fluid temperature history which consists of a rapid down-transient followed by an isothermal rise to operating temperature, and a 500 h holdtime at that temperature. The parameters of the analytical solutions covered the range of interest for sodium-cooled nuclear systems. The only material considered was Type 304 stainless steel.

Design curves were developed for ratchet strain as a function of elastic primary and secondary stress intensities and temperature. The diagrams presented here are of similar format to those given by Bree.

The results of this study indicate that the existing design rules of FRA-152 Revision 3 and of the Liquid Metals Engineering Center (LMEC) supplement to the ASME Code Case 1331-5 for loading cycles with long holdtimes are very restrictive, with one exception. That exception is Rule A.2.1.2(4) of the LMEC rules. When compared to the results of the study, the rule is consistently and reasonably conservative for all loadings and temperatures studied.

In this study it was also desired to correlate the ratchetting results of the straight pipe to the analytical ratchetting results for more complex geometries. However, the correlation was not completed in time for this report.

KEY WORDS: fatigue (materials), creep strength, cyclic loads, pipes (tubes), stress-strain diagrams, stainless steels, parametric equations, stresses, computer programs

In previous investigations the complexity of the elastic-plastic-creep ratchetting problem has dictated that numerous assumptions be made to reduce the problem to a manageable form. Bree [*1,2*],[2] who developed a generally applicable closed-form solution for incremental growth, found it

[1] Project engineer and assistant section manager, respectively, Teledyne Materials Research Corp., Waltham, Mass. 02154.

[2] The italic numbers in brackets refer to the list of references appended to this paper.

Copyright© 1973 by ASTM International www.astm.org

necessary to limit his analysis to a uniaxial stress model, linear temperature distributions through the model, and several restrictive approximations concerning the material properties.

The broad capabilities of the finite element method have made it possible to solve the ratchetting problem without many of the restrictions that were necessary in Bree's solution. Minami and Roberts [*3*] demonstrated the use of the finite element method to solve specific ratchetting problems. They considered long circular pipes of $\frac{3}{8}$ and $\frac{5}{8}$ in. wall thickness. The temperature distributions in the cylinder wall of their study resulted from transient temperature solutions. They further consider bilinear, temperature-dependent stress-strain curves, kinematic hardening, and a steady-state creep representation. Since only two cases were studied, the Minami and Roberts work does not have sufficient quantitative results to make it generally applicable to design.

For the present parametric ratchet study, newer, more general finite element programs were available. The Ansys program [*4*] was used to solve all the ratchetting cases of this study. With Ansys we considered a multilinear stress-strain curve, fully temperature-dependent properties, kinematic hardening, and strain-hardening creep.

The 15 Nov. 1971 version of the Ansys program was used on a CDC 6600. The computer is located at the AEC Computer Center of New York University.

We used a "brute force" approach with the finite element method to attempt to obtain generally applicable design curves for ratchetting. We were limited in that we could not cover the full range of ratchetting parameters or materials of interest in a continuous manner, but could only examine selected values of the parameters and only one material. Continuous design curves for the one material were interpolated between the isolated numerical results.

In addition to developing design curves for ratchetting from the straight pipe cases, this study was also intended to address itself to the question of whether or not the straight pipe results can be used to predict the ratchetting strains in more complex sodium-cooled reactor components. To attempt to answer this question, an analytical ratchetting study on a typical nozzle has been proposed. The results of the nozzle study will be then compared to the predictions based on the straight pipe results. At the time of this report, work on this phase of the study is still underway.

Input Parameters for the Different Ratchet Cases

The form of the temperature history considered was similar to that used by Minami and Roberts. In the temperature history used for the present study, the severe down-transient is followed by a short holdtime of approximately $\frac{1}{2}$ h. at the lower temperature. The fluid temperature was then raised slowly to the upper temperature and was held here for 500 h. For

the 26 ratchet cases of this study the pressure was not cycled but was held constant through the entire cycle. Down-transients of 40, 30, 10, and 2 F/s were considered. Temperature drops during the transients of 400 and 300 F were considered. The operating temperatures considered were 1000, 1100, and 1200 F. Pipe wall thicknesses of 0.375 to 1.35 in. were considered. A 15 in. inside pipe radius was considered for all cases. Also only one heat transfer coefficient at the wetted surface was considered, 50 Btu/h-in.^{2}F. The material for all the cases was Type 304 stainless steel. The input parameters of the ratchet cases are summarized in Table 1.

TABLE 1—*Ratchet-run input parameters and incremental hoop strain results.*

Run No.	Operating Temperature, deg F	Thermal Transient, deg F/s	ΔT, deg F	Wall Thickness, in.	Internal Pressure, psi	Incremental Ratchet Strain $\delta_{\theta_{4-5}} \times 10^6$
1	1000	−40	400	0.851	635	105.0
2					423	44.7
3					211	2.3
4		−30	300	1.35	992	91.1
5					496	2.4
6		−10	300	0.531	400	23.1
7					266	0.0
8		−2	300	1.06	787	20.7
9				0.531	400	1.8
10	1100	−40	400	0.851	300	81.5
11		−30	300	1.35	624	113.0
12					208	2.8
13				0.851	300	41.0
14				0.375	134	10.2
15		−10	300	0.700	331	50.8
16					220	5.6
17				0.531	189	5.3
18		−2	300	0.851	400	8.1
19	1200	−40	400	0.851	195	105.0
20		−30	300	1.35	457	179.0
21					229	46.5
22		−10	300	0.700	243	75.0
23					81	0.0
24				0.531	185	45.6
25					123	6.5
26		−2	300	0.851	293	18.4

Analysis

Finite Element Model

With the nodal coupling options available in Ansys, a long axisymmetric cylinder was idealized as shown in Fig. 1. For all ratchet cases considered, there were 16 equal quadrilateral axisymmetric ring elements taken through the wall thickness as shown in Fig. 1. The constraints on the nodes shown

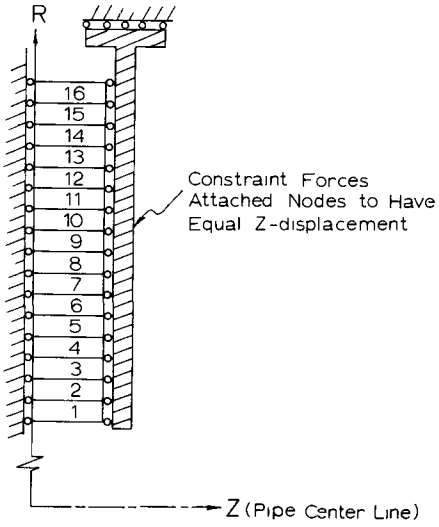


FIG. 1—*Sixteen element model showing boundary conditions used to simulate a long straight pipe.*

in Fig. 1 put the model in a state of generalized plane strain. There are only 18 displacement unknowns in this model. The same model geometry was used for the solution of the associated thermal problem.

Plasticity Solution

The Ansys program uses the initial strain approach for the plastic and creep strains in the formulation of the finite element system of equations. In this technique, for small displacement analysis, only the right-hand side of the equations are modified for each change in the loading or inelastic strains. However, in the ratchet cycle there are large temperature changes; thus, it was necessary to occasionally modify the stiffness matrix during the course of the transient. Approximately 35 temperature distributions were used in the elastic-plastic solution for each ratchet cycle, and at each of these temperature steps, 6 iterations were taken to converge the solution.

The plasticity subroutine of Ansys requires the stress-strain curves to be input in the form of multilinear curves of five segments for each temperature of interest. The stress-strain curves used in this study represent the average properties of Type 304 stainless steel and are given in tabular form in Table 2.

In this study no attempt was made to include the effects of cyclic changes of the stress-strain curves. Thus, the virgin stress-strain curves were used throughout the cyclic loading.

Within the Ansys kinematic hardening option for the monotonic portion of a cyclic loading, the plastic strain increments are calculated by a method of isotropic hardening. The multiaxial plastic stress-strain relationship used

TABLE 2—*Ansys input for average properties of Type 304 stainless steel based on Wadco (Blackburn) expression of 1 Nov. 1971.*

Temperature, deg F	Strain in./in.				
	0.000591	0.001	0.002	0.006	0.03
	Stress, psi				
600	15011	19400	21800	25500	32900
800	14243	17900	20100	23700	31200
1000	13297	16100	18300	21900	29600
1100	12825	15200	17500	21100	28700
1200	12352	14300	16700	20300	27200

is the "modified total strain" version of the Prandtl-Reuss equation as described by Mendelson [5]. If used directly for reversed loading cases, the Mendelson approach is one of isotropic hardening. However, in the Ansys kinematic scheme that was used, when the largest elastic strain component changes sign relative to its corresponding plastic strain component during a load reversal, the required kinematic shift in the origin of the yield surface takes place. During this shift the initial size of the yield surface is resumed.

It should be noted at this point that recent ratchet runs using a newer version of Ansys which contains classical kinematic hardening indicate that, for the two cases studied with both versions, the newer version predicts significantly larger ratchet strains. The reason for the difference is not completely clear. However, it appears that when using kinematic hardening in an elastic-plastic-creep calculation, the shape of the stress-plastic strain curve is extremely important. For the newer version of Ansys, a bilinear curve was used and not the multilinear curve employed in the earlier version used in this study.

Creep Solution

A strain hardening creep form was used throughout this study. The expression selected is given in Eq 1.

$$\frac{d\epsilon_c}{dt} = C_1 e^{-C_2/T}\, \sigma^{C_3}\, \epsilon_c^{C_4} + C_5 e^{-C_6/T}\, \sigma^{C_7} \quad \ldots\ldots\ldots\ldots (1)$$

where

ϵ_c = total time-dependent strain,
C_i = constants,
T = temperature, deg R,
t = time, h, and
σ = stress, psi.

The constants of Eq 1 were determined by a least-squares fit to the average creep properties of Type 304 stainless steel as reported by Blackburn [6]. The values of the constants that result from this least-squares fit are:

$C_1 = 3.9204 \times 10^{-21}$
$C_2 = 8.4281 \times 10^{4}$
$C_3 = 8.4214$
$C_4 = -0.96336$
$C_5 = 6.5232 \times 10^{-14}$
$C_6 = 8.4281 \times 10^{4}$
$C_7 = 7.2089$

Here again there is some question about the material property representations. The creep expression constants as given by Blackburn apparently do not accurately fit the short-time primary creep response. Since the ratchet cycle considered in the present study has a relatively short holdtime (500 h), the influence of a significant change in the short-time creep response would no doubt result in changes in the predictions for ratchet growth.

Evaluation of Thermo-Elastic Solution

To summarize the numerical results, cumulative strain is plotted as a function of the elastic thermal stress and the pressure stress. For the present study the value plotted as the abscissa is the primary stress intensity, P_m. On the ordinate the value plotted is the equivalent linear elastic secondary stress intensity for the thermal loading, Q_{EL}. The following formulas were used to calculate these two quantities:

$$P_m = \frac{1}{a}\int_0^a \sigma_\theta \, dr - \frac{1}{a}\int_0^a \sigma_r \, dr \quad \ldots\ldots\ldots\ldots\ldots\ldots (2)$$

$$Q_{\mathrm{EL}} = \frac{6}{a^2}\int_{a/2}^{a/2} \sigma_\theta r \, dr \quad \ldots\ldots\ldots\ldots\ldots\ldots\ldots\ldots (3)$$

where

a = pipe wall thickness,
σ_θ = hoop stress from elastic calculation,
r = radius, and
σ_r = radial stress from elastic calculation.

Results and Discussion

Computer Results

In addition to the printed output, computer plots were also obtained for each of the ratchet cases. In Fig. 2 the plotted results for hoop stress versus hoop strain for the inside and outside elements for one of the cases (No. 15, Table 1) are presented.

Cumulative Strain Calculation

The values for the incremental strain growth were based on differences between the hoop strain at the inner surface from cycle to cycle, the hoop strain being the maximum positive principal strain. The inelastic ratchet calculations were done for five cycles. The incremental growth did not settle in every case to a steady value by the fifth cycle. Therefore, it was necessary to make some approximation concerning the steady-state growth per cycle. At one point we considered using an extrapolation procedure to determine a steady-state growth value. However, due to uncertainties present in the inelastic and creep analyses, it was decided to adopt a more conservative approach and consider the incremental strain growth between the fourth and fifth cycles as the steady-state incremental strain growth. Approximate calculations based on the ratios of the steady-state creep rates to the total creep rates at the end of five cycles (the creep strains were accumulated from cycle to cycle) indicate that this approximation introduces a factor of conservatism of about 2.0 for the lower temperature and about 1.2 for the higher temperature. No attempt was made to correct for this conservatism. The total strain growth after $n + 5$ ratchet cycles thus was calculated as shown in Eq 4.

$$\epsilon_\theta = \epsilon_{\theta_5} + n\delta_{\theta_{4-5}} \quad (4)$$

where for Eq 4

ϵ_θ = estimated final total hoop strain (minus hoop thermal strain), maximum value of the $n + 5$th cycle for inside surface;
ϵ_{θ_5} = computed total hoop strain (minus hoop thermal strain), maximum value of fifth cycle for inside surface; and
$\delta_{\theta_{4-5}}$ = incremental strain growth from fourth to fifth cycle, $\epsilon_{\theta_5} - \epsilon_{\theta_4}$.

The incremental strain growth from the fourth to fifth cycle, $\delta_{\theta_{4-5}}$, is tabulated along with the ratchet case input parameters in Table 1.

Using Eq 4, 100 cycle cumulative strain results were calculated and are presented in Fig. 3. In this figure contours presented were interpolated between the data points. In Fig. 3 all stresses were normalized to the average yield stress.

Comparison of Results to Existing Design Rules

The results of this study are now compared to the ratchetting rules of FRA-152 Revision 3 [7] and the ASME Code Case 1331-5 [8] with the Liquid Metals Engineering Corporation (LMEC) supplement [9]. Throughout our finite element analysis average properties were used. Therefore, to be consistent with our analysis in our comparison to the ratchetting rules, when the yield stress is given as a limit, we considered it to be the average yield stress.

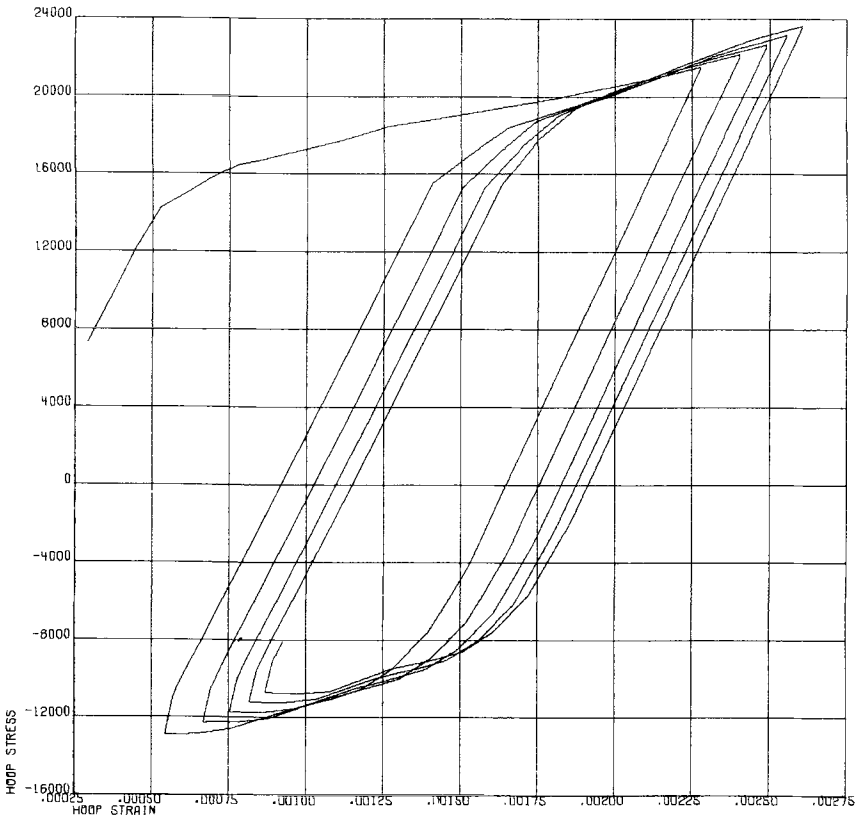
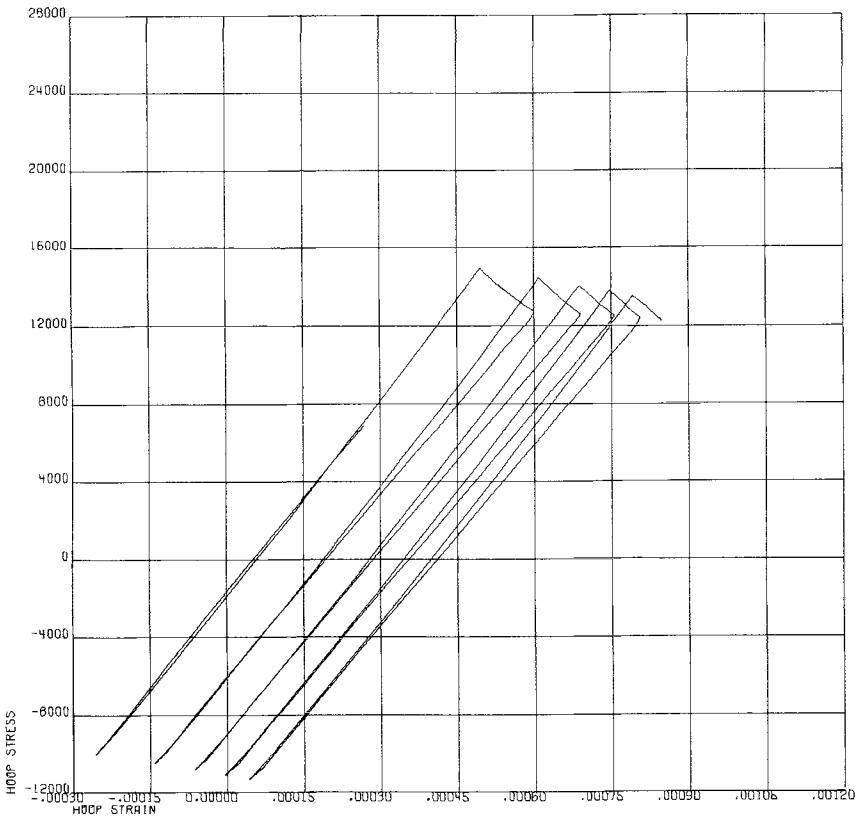


FIG. 2—*Hoop stress versus hoop strain (elastic + plastic + creep).* Thermal transient: *−10 F/s for 30 s. Wall thickness: 0.700 in. Hold temperature: 1100 F. Internal pressure: 331 psi.*

Comparison to FRA-152 Revision 3

In the comparison of the results of this study to the ratchetting rules of FRA-152 Revision 3 further liberty has been taken. First of all, FRA-152 Revision 3 states that the maximum absolute accumulated inelastic strain be used in the deformation limit evaluation. We considered the maximum positive principal strain in the cumulative strain calculations. Secondly, in Paragraph 4.2.4.2(b)2, FRA-152 Revision 3 states that thermal stresses from all sources be less than $2\sigma_y$. We did not consider the peak stress in our evaluation of this paragraph; therefore, for this study the requirements of the paragraph were relaxed to limiting Q_{EL} to be less than or equal to $2\sigma_y$.

In FRA-152 Revision 3 there are essentially three ratchetting rules. The first ratchetting rule, Paragraph 4.2.4.2(a) requires $(P_m + Q_{\mathrm{EL}})_{\mathrm{range}} \leq \sigma_y$.



OUTSIDE ELEMENT

FIG. 2—*Continued.*

Examination of Fig. 3 shows this limit to be very conservative when compared to the 100 cycle cumulative strains of this study. Note, however, that this rule applies for any operational life; therefore, we cannot say that this rule is generally conservative.

The second and third rules of FRA-152 Revision 3 for ratchetting are each made up of three sections. The first and second sections of the two rules are identical and state that the thermal stress from all sources must be less than $2\sigma_y$ and that the primary membrane intensity must be less than $0.5\sigma_y$. The third section of the rules, that is Paragraphs 4.2.4.2(b)3 and 4.2.4.2(c), which limit the total time of the component at a temperature above 900 F, are both equally restrictive for the cycle of this ratchet study. Using the isochronous stress-strain curves given in FRA-152 Revision 3

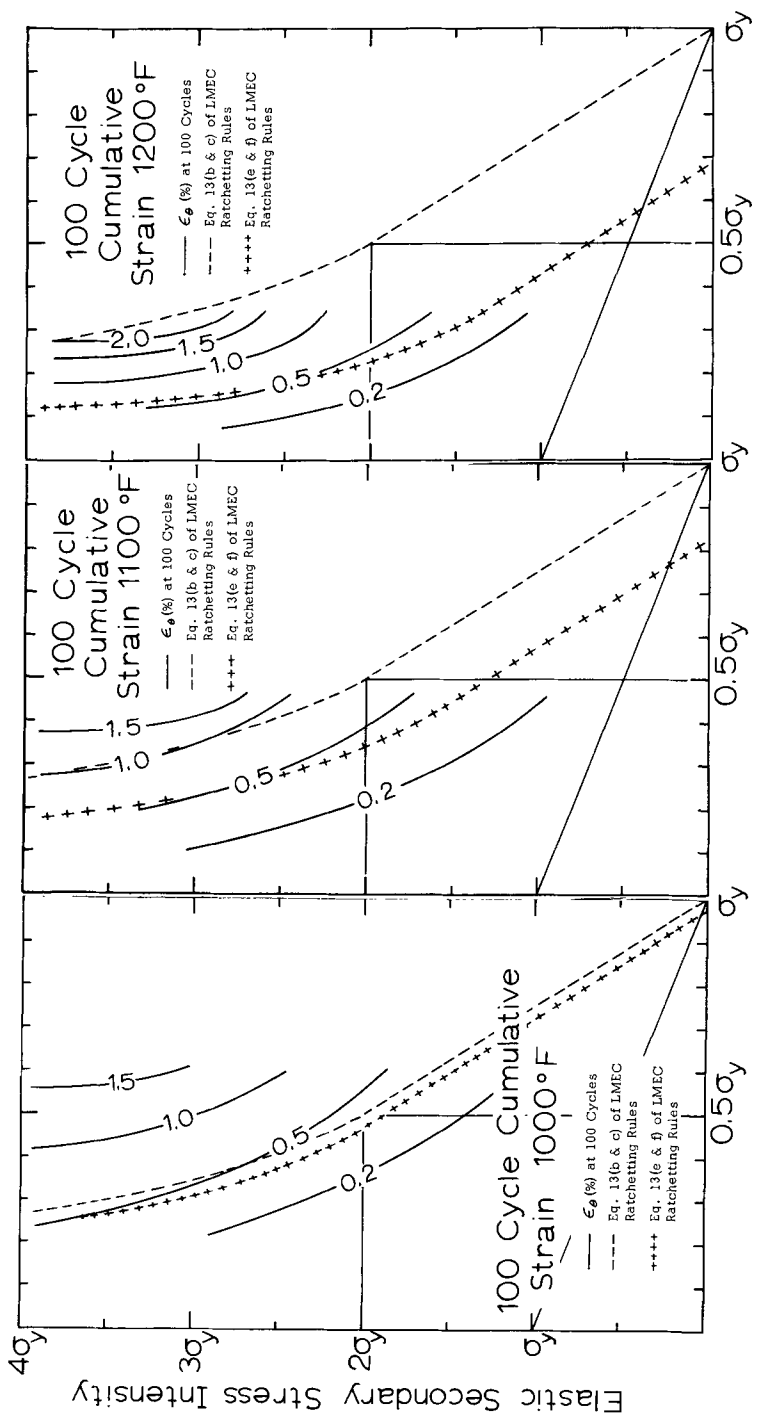


FIG. 3—*Comparison of the calculated cumulative hoop strain after 100 ratchet cycles at operating temperatures of 1000, 1100, and 1200 F to the limit lines of existing ratchet rules.*

to obtain the required parameters, Rules 4.2.4.2(b)3 and 4.2.4.2(c) can only only be invoked if the life in hours is less than the values shown next.

Applicability of Paragraphs 4.2.4.2(b)3 and (c) of FRA-152 Revision 3 for Type 304 Stainless Steel

Temperature, deg F	1000	1100	1200
Life, h	10^4	$<10^3$	0

We see that because of the third sections of the second and third rules, the second and third rules are very restrictive for ratchet cycles with significant holdtimes. We note that the 100 cycle life investigated in Fig. 3 is too long to be considered by the second and third rules of FRA-152 Revision 3. For completeness the limit lines (modified for this study) of Paragraph 4.2.4.2(b) 1 and 2, that is, $Q_{\mathrm{EL}} \leq 2\sigma_y$ and $P_m \leq 0.5\sigma_y$, are shown on Fig. 3.

Comparison of Results to the Ratchetting Rules of the LMEC Supplement for Ratchetting to the ASME Code Case 1331-5

For the simple straight pipe model used for the ratchet cases, the Rule A.2.1.2(1) of the LMEC supplement is approximately the $(P_m + Q_{\mathrm{EL}})_{\mathrm{range}} \leq \sigma_y$ rule discussed for FRA-152 Revision 3 and the same comments apply.

The second and third rules of the LMEC supplement are similar to the second and third rules of FRA-152 Revision 3. However, in the LMEC supplement the $Q_{\mathrm{EL}} \leq 2\sigma_y$ and $P_m \leq 0.5\sigma_y$ limits have been replaced by limit curves based on Bree's analysis.

For the second rule the ratchet limit curve given in the LMEC supplement, A.2.1.2(2a) is shown in Fig. 3. However, this limit curve is not applicable to 100 cycle lives because of the second part of this rule, Paragraph (2b), which limits the operational time above 900 F. From the isochronous stress-strain curves of the Code, Paragraph (2b) limits the design life for Type 304 stainless steel to the following:

Applicability of Rule A.2.1.2(2b) of 1331-5, LMEC Supplement for Type 304 Stainless Steel

Temperature, deg F	1000	1100	1200
Life, h	10^4	<500	<50

Paragraph (2c), which states that one extreme of the temperature cycle which describes the range of secondary stress, Q_{EL}, must be at a temperature below 900 F, is satisfied for all the ratchet cases of this study.

For the cyclic loading used in this study, the limits set by the third rule, A.2.1.2(3), are approximately as restrictive as the limits set by Rule A.2.1.2(2a,b, and c).

The limits set by the fourth rule, A.2.1.2(4a), are specified by two equations, Eq 13(*e*) and 13(*f*) of the LMEC rules. The analytical development of Eqs 13(*e*) and 13(*f*) is given by Anderson [*10*]. Equations 13(*e*) and 13(*f*) were calculated for each of the temperatures considered in this study. The resulting curves are plotted in Fig. 3. The fourth rule of the LMEC supplement has only two sections. The second section is identical to Paragraph (2c) just discussed. Therefore, this rule simply states that freedom from excessive deformation is demonstrated if, at the location being considered, the stress intensities fall to the left of Eqs 13(*e*) and 13(*f*) in Fig. 3, and that part of the cycle is below 900 F.

From Fig. 3 it is seen that the present analysis indicates that Rule A.2.1.2(4) is conservative with respect to the 2 percent surface strain limit of the code. However, because of the uncertainties of the present analysis and the unknowns that may enter due to more complex temperature and pressure cycles and more complex geometries, we do not think that the present analysis indicates that the rule is excessively conservative.

Conclusions

Computer Run Times

Results indicate that the large, general computer programs, Ansys in this case, are capable of producing consistent, reasonable results for ratchetting of a very simple geometry, the straight pipe. However, even for this uncomplicated structure the computer run times were very large, about 600 s per ratchet cycle on a CDC 6600, thus indicating that ratchetting analysis on more complex geometries are going to be very expensive from a computer cost viewpoint. Newer finite element programs by Rashid [*11*] and Saratory [*12*], which were developed specifically for the elastic-plastic creep problem, will no doubt reduce the computer costs. Moreover, available programs [*13*,*14*] written specifically for the ratchetting analysis of simple geometries will allow the development of the Bree-type charts of this report at a fraction of the computer costs.

Design Curves

The results presented in the Bree-type charts of this study, Fig. 3, are useful in that they indicate the analytically predicted ratchet growth as a function of elastic primary and secondary stress intensities. The growth charts were developed for a 500 h hold period, but, based on holdtime considerations, the ratchet charts apply conservatively to loading sequences with shorter holdtimes. However, it should be noted that experimental results and further analytical solutions are necessary to completely evaluate the results of the present study.

Comparison to Existing Design Rules

The present analysis indicates that the ratchetting rules given in both FRA-152 Revision 3 and in the LMEC supplement to the ASME Code Case 1331-5 for loadings with long holdtimes are very restrictive. There is one exception. That exception is Rule A.2.1.2(4) of the LMEC supplement. When compared to the results of this analysis, Rule A.2.1.2(4) of the LMEC supplement is consistently and reasonably conservative for the loadings and temperatures studied.

Acknowledgment

The work of this study was supported by the U. S. Atomic Energy Commission through Oak Ridge National Laboratory, Contract No. W-7405-eng-26, Subcontract No. 3550.

References

[1] Bree, J., *Journal of Strain Analysis*, Vol. 2, No. 3, 1967, pp. 226–238.
[2] Bree, J., *Journal of Strain Analysis*, Vol. 3, No. 2, 1968, pp. 122–127.
[3] Minami, H. M. and Roberts, G. O., *Elastic-Plastic-Creep Ratchetting Study*, Enclosure to 71LMEC-281, Canoga Park, Calif., Feb. 71.
[4] Swanson, J. A., *Ansys User's Manual*, Swanson Analysis System, Inc., Elizabeth, Pa., 1971.
[5] Mendelson, A., *Plasticity: Theory and Application*, Macmillan, New York, 1968.
[6] Blackburn, L. D. in *Liquid Metal Fast Breeder Reactor Materials Handbook*, HEDL-TME 71-32, Handford Engineering Development Laboratory, June 1971, p. 304SS-23.
[7] *Interim Supplementary Structural Design Criteria for Elevated Temperatures*, FRA-152 Revision 3, 6 Nov. 1970.
[8] "Code Case 1331-5:Nuclear Vessels in High Temperature Service," *Section III ASME Boiler and Pressure Vessel Code*, 4 Aug. 1971.
[9] Anderson, W. F., Revision A, Proposed Supplement to Code Case 1331-5, Enclosure to 72LMEC-DRF-0559, Canoga Park, Calif., 21 Jan. 1972.
[10] Anderson, W. F. in *Design for Elevated Temperature Environment*, American Society of Mechanical Engineers, (G34), 1971.
[11] Rashid, Y. R., *Creep-Plast*, Computer Library, Oak Ridge National Laboratory, Oak Ridge, Tenn., 1972.
[12] Sartory, W. K., *Placre*, Computer Library, Oak Ridge National Laboratory, Oak Ridge, Tenn., 1972.
[13] Kopp, Marcel, Program BTI 511, "Transient Heat-Conduction and Inelastic Analysis of a Slab for Evaluation of Creep Fatigue Damage and Strain Ratchetting," Basic Technology Inc., Pittsburgh, Pa., 1972.
[14] Chern, J. M., "Elastic-Plastic-Creep Analysis of a Thick-Walled Cylinder Subjected to Time Dependent Pressure, Temperature and Axial Loads or Displacements," FWR-35, Rev. 0, John Blizard Research Center, Foster Wheeler Corp., Livingston, N. J., 1972.

R. B. Socky[1]

Nondestructive Testing in Fatigue: A 1972 Update

REFERENCE: Socky, R. B., "**Nondestructive Testing in Fatigue: A 1972 Update,**" *Fatigue at Elevated Temperatures, ASTM STP 520*, American Society for Testing and Materials, 1973, pp. 722–732.

ABSTRACT: The application of nondestructive testing (NDT) to the engineering aspects of the fatigue phenomenon offers a classic example of the systems approach that is essential for the successful exploitation of nondestructive testing technology. NDT can make contributions in: the fracture mechanics-nondestructive testing design criteria and related product integrity determination; detection of property-stress gradients; early detection of fatigue damage; and evaluation of stresses.

Earlier work established the ascendancy of ultrasonic testing. Notable advancements in recent work have been in the refinement of data treatment of ultrasonic responses from defects aimed at accomplishing more reliable size assessment and in scanning of large components.

The following NDT methods have demonstrated potential for measurement of fatigue damage: exoelectron emission, acoustic emission, ultrasonic surface wave attenuation and velocity, surface potential difference, ellipsometric parameters, holographic surface correlation index, and positron life times.

Stresses play an important role in failure point detection, location, and growth, and in practical cases, must be measured for each part.

Effective utilization of nondestructive testing at any one portion of the product cycle as related to the fatigue problem requires that it be considered in a system connotation.

KEY WORDS: fatigue (materials), nondestructive tests, fatigue tests, scanners, acoustics, emission, acoustic detection, composite materials

The application of nondestructive testing (NDT) to the engineering aspects of the fatigue phenomenon offers a classic example of the systems approach that is essential for the successful exploitation of nondestructive testing technology. The systems relationships are shown diagramatically in Fig. 1 and form the basis for this 1972 update of NDT in fatigue [*1*].[2] As shown in Fig. 1, NDT can make contributions in: the fracture mechanics-nondestructive testing design criteria and related product integrity determination; detection of property-stress gradients; early detection of fatigue damage; and evaluation of stresses.

[1] Consultant, Quality Measurements, Corporate Consulting Service, General Electric Co., Bridgeport, Conn. 06602.

[2] The italic numbers in brackets refer to the list of references appended to this paper.

Copyright© 1973 by ASTM International www.astm.org

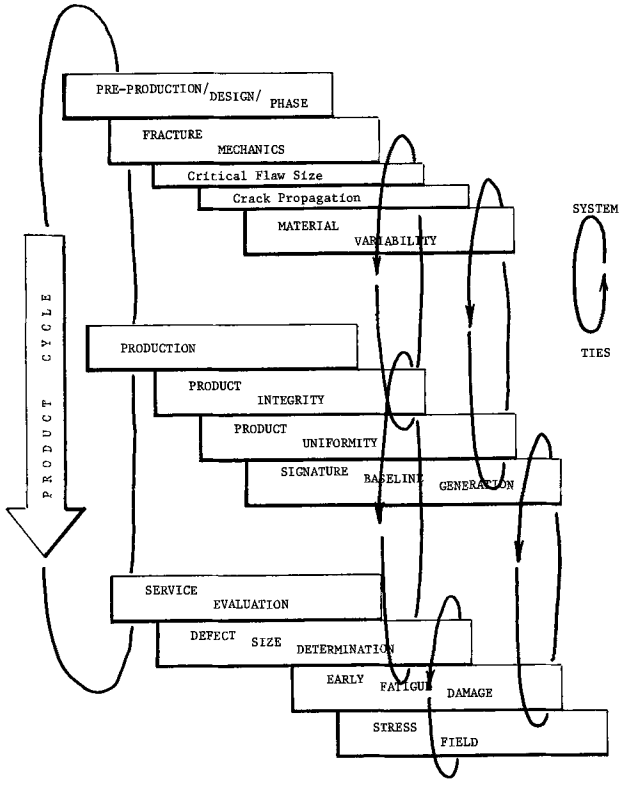


FIG. 1—*System relationships of NDT in fatigue.*

Pre-Production Design

Fracture Mechanics-NDT Design

The potential of a fracture mechanics-nondestructive testing design analysis is shown in Fig. 2 [*2*]. A working stress σ_w has been calculated using a reduced ultimate stress. The mean ultimate strength is divided by a factor K greater than 1.0, which is determined by considering the uncertainties involved in the material, the processing variabilities, and the unknowns involved due to fluctuating loads. The resulting "reduced tensile ultimate" is then assumed to have a distribution function for the strength identical to that for the actual tensile ultimate. The probability of failure at this working stess is 10^{-4}. However, if the distribution function for the actual fracture stresses were used, the probability of failure at the same working stress σ_w would be 10^{-7}. Thus, depending on the reduction of the tensile ultimate, an increase in the reliability of the structure can be obtained using the true fracture stress distribution.

The validity of the fracture mechanics design procedure depends on the

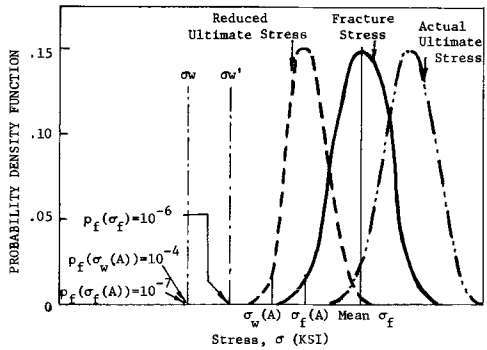


FIG. 2—*Probability of failure at working stress compared using* σ_i *distribution and* σ_{tu} *distribution* [2].

ability to determine the flaw distribution function 2*C*. Since the *a priori* assumption is the material contains flaws, some reliable method must be used to detect these flaws in the component prior to use. The use of nondestructive testing to detect flaws in materials is well known, but a danger exists where some of the flaw sizes may be below the limit of detectability of the NDT procedure. Thus, it is mandatory to know the reliability of the NDT method for each flaw size.

Defect Size Determination

The determination of defect size by means of the ultrasonic echoes returning to the transducer after being reflected from the defect is dependent upon two measurements: (1) transit time between the transducer and defect and (2) amplitude of the echo [*3*]. Transit time measurements are relatively unambiguous and offer no particular difficulties. The echo amplitudes can vary for several reasons. Among them are beam-spreading, near-field diffraction effects, defect contour, and intrinsic attenuation.

In most engineering applications defect sizes are based on comparisons with the amplitudes of echoes from flat bottom holes drilled in blocks of metal called defect standards. To correlate the signals (in a typical water immersion test setup), the return signal for flat holes and spherical defects (related by an echo ratio, *R*) were mathematically modeled. Analytical studies of received echo amplitude as functions of test and defect parameters were performed with the objective of (1) relating the sizes of spherical and flat hole defects yielding the same return signal, and (2) relating the return signals of spherical and flat defects of equivalent size.

Figure 3 depicts the variation of the echo ratio, with changing sphere radius, for four different flat hole sizes, in the vicinity of $R = 1$. The model was used to calculate *R* as a function of other test parameters, such as frequency. The curves oscillate with a general trend of the echo defect to decrease with increasing frequency. Changes in *R* were found to be mono-

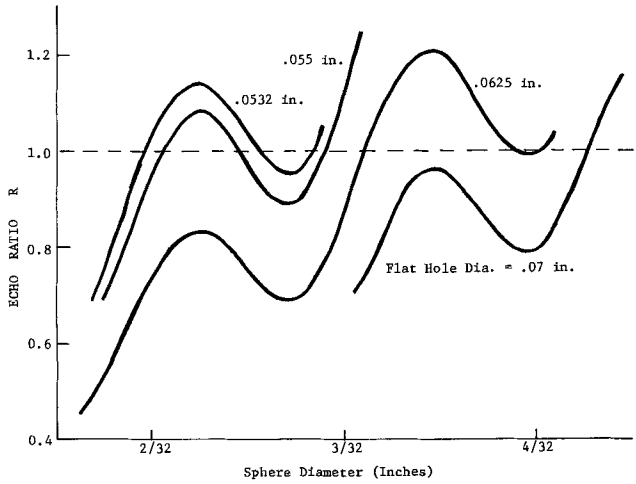


FIG. 3—*Echo ratio versus sphere diameter for four different flat hole sizes* [3].

tonic with changes in transducer diameter, water path length, and defect depth.

Materials Property Variablity

Two points are important from the NDT failure prediction point of view:

1. Individual critical cracks in brittle materials may be too small to be detected by NDT.
2. Critical stress gradients can occur even if there is no preexisting crack, due to structure-property gradients in brittle materials [*4*].

For many materials, properties variability as revealed by sampling destructive tests, for example, tensile, impact, bend, shear, is not at all accurately described. Actual values in local regions of a piece of hardware may differ by 20 to 75 percent from average values. Unless destructive test specimens have been taken by direction from NDT from the extremes of variability, the handbook properties data will not be representative.

Production

Product Integrity

The examination of large manufactured objects for integrity has taken two courses. One is the relatively straightforward application of standard ultrasonic tests through automation of the scan and computer processing of the ultrasonic data. The other is the development of new methods such as ultrasonic synthetic apertures, acoustic holography, and acoustic emission.

One example that is typical of the first course is the automated scanning and data recording and processing technique for testing of welds [5]. In this case, a digital computer is used to analyze the data obtained from an ultrasonic inspection made to determine the integrity of a welded step joint using pulse-echo techniques. A computer is interfaced to a standard ultrasonic flaw detector and to the scanning mechanism. Encoders are used to provide position data, and the amplitudes of the reflected indications are obtained from the ultrasonic flaw detector. At the completion of the test, the computer provides a printout of the test results on a teletypewriter, and the data can be stored on digital tape. In addition, the analog recording normally obtained is still available for cross reference. The basic test equipment is shown diagramatically in Fig. 4.

Another automation application has been the development of remotely controlled devices that precisely position ultrasonic instruments for readings in operating nuclear reactors [6]. Since 1964 nuclear power equipment

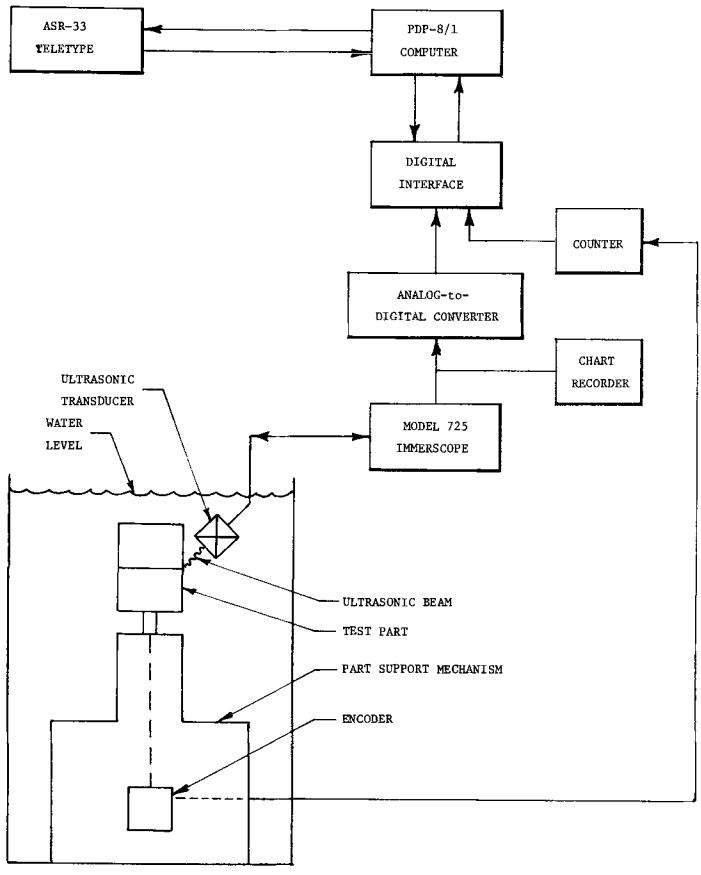


FIG. 4—*Block diagram of data processing for ultrasonic flaw detection* [5].

designers have been designing facilities so they can be inspected while operating. Preservice ultrasonic fingerprints can now be compared to in-service inspection results to maintain a running check on the condition of critical areas. The need for this information has been deemed to be so essential that in 1970 inservice inspection became a Federal requirement.

New developments for the determination of the integrity of large engineered items include the concept of a synthetic aperture [7]. The application of the synthetic aperture concept to ultrasonic examination is illustrated in Fig. 5. An ultrasonic transducer is provided for transmitting ultrasonic energy into the body under examination and for receiving signals in response to echoes from interfaces within the body. The transducer is moved by a scanning mechanism over the surface of the body in a linear path generally parallel to the surface of the body. To provide acoustic coupling, the transducer is operated in a pool of water. As the transducer is moved over the body surface, electrical signals are developed which are converted to light signals and recorded on a film. The film is developed, and the developed film is processed by an optical processing system. Alternately, the electrical signals can be fed into a computer for storage and processing with a suitable printout. In either case, the final product of the

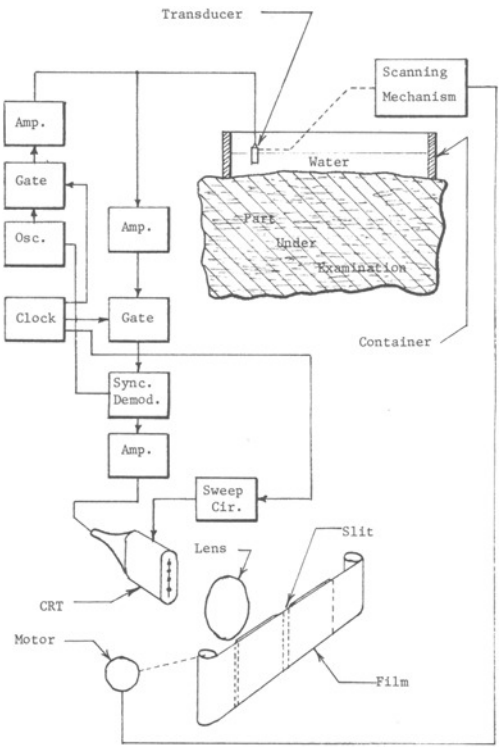


FIG. 5—*Schematic diagram of a simulated array to form a synthetic aperature in ultrasonic testing* [7].

system is a picture showing a cross section of the region of the body examined, and particularly showing the location of any interfaces within the body which will reflect ultrasonic waves.

Acoustic holograph methods are being also used at present to produce images in opaque solids [*8*]. Two methods are of particular interest. In the first, a receiving transducer is scanned over the surface of the specimen containing the flaw in the same manner as in the synthetic aperture method. The received signals are mixed electronically with a reference signal from a continuous wave ultrasonic illuminator. The spot of an oscilloscope is modulated with this signal intensity. Its position is slaved to the position of the transducer. The complete scan develops a hologram on the oscilloscope face, which is photographed and reconstructed by means of a laser light. In the second method the specimen is immersed in a water bath, and it is illuminated by an ultrasonic transducer. The water surface is then also illuminated by a coherent reference signal. The interference between the two signals produces a hologram on the water surface, which can be also photographed and reconstructed. The scanning method can be used on massive parts, and has demonstrated ability to resolve a series of 0.040-in.-diameter holes spaced 0.040 in. apart and varying in depth by 0.040 in.

Acoustic emissions have been used to study the fracture process and to monitor crack growth in precracked specimens so that the fatigue life can be predicted. Measurement of acoustic emissions has the potential of being applied to full-size production items and has been successfully demonstrated on nuclear reactor vessels. Acoustic emission is the propogation of a spontaneously generated elastic wave created by discreet movements within the volume of a material being stressed. The generation of elastic waves is associated with plastic deformation processes, such as twinning, slip, and microcrack formation. This phenomenon also includes the production of released strain energy upon fracturing.

Product Uniformity

Evaluation of products for uniformity of properties has almost been entirely limited to nonmetallic, composite materials used in aerospace applications. For those applications that have been made, modulus determination using either ultrasound velocity changes or ultrasound attenuation changes is predominant. Further, most work has been developmental in nature with little emphasis on actual hardware. This work is still embryonic both from a fracture mechanics and a nondestructive testing standpoint.

Signature-Base-Line Generation

The concept of signature analysis—the identification of a characteristic response of a part or a system and the subsequent monitoring of that characteristic response in time— is initiated in the developmental phases

of a product life-cycle and established on the factory floor where baseline records are made on each unit of production. Applications of signature analysis have been successful in monitoring performance characteristics in aircraft power plants, military land vehicles, and automobile parts and engines. Structural applications have been limited since both the fracture mechanics approach and the related nondestructive testing technology are still developing. The concept is in use on stream turbine rotors, nuclear power reactor vessels and piping, and crane hooks and booms.

Service Evaluation

Early Fatigue Damage

Early fatigue damage appears to consist of the formulation of a thin layer of possible intense dislocation tangling as evidenced on the surface by a dense pattern of slip markings [9]. It is known that most physical properties of metallic materials change with plastic deformation, and it is possible to utilize such changes to indicate fatigue damage. Physical property changes which might be useful are described in the following paragraphs

Exoelectron Emission

The term exoelectron has been used to describe electrons emitted from both metals and nonmetals which have been subjected to various treatments, such as abrasion, mechanical deformation, irradiation with ultraviolet light, X-rays or ultrasonic waves, electron bombardment, electrical gas discharge, chemical interaction between the material surface and the ambient gas, and phase transformation upon heating or cooling.

The emission of electrons from abraded or deformed metal surfaces has been interpreted in several ways: (1) interaction of gas with the freshly worked surface resulting either in the release of energy due to chemisorption of oxygen or the absorption of water vapor or in the formation of a layer of defected structure containing trapping sites which produce a surface of lower work function, (2) release of energy associated with vacancies reaching the surface by diffusion, and (3) transfer of energy associated with the stress field around dislocations to electrons.

Emission from most abraded or otherwise deformation metals is not observed in total darkness. The energy of impinging photons is needed to add to the energy which is released by vacancies at the surface in order to exceed the work function of the surface. Typical equipment is shown in Fig. 6. The exoelectron emission in a fatigue test is characterized by an early rapid rise and fall in emission intensity followed by a final rise near the end of the test (Fig. 7).

Acoustic Emission

Since slip movement in plastically deformed metallic materials can cause acoustic emission, there is a relationship between acoustic emission and

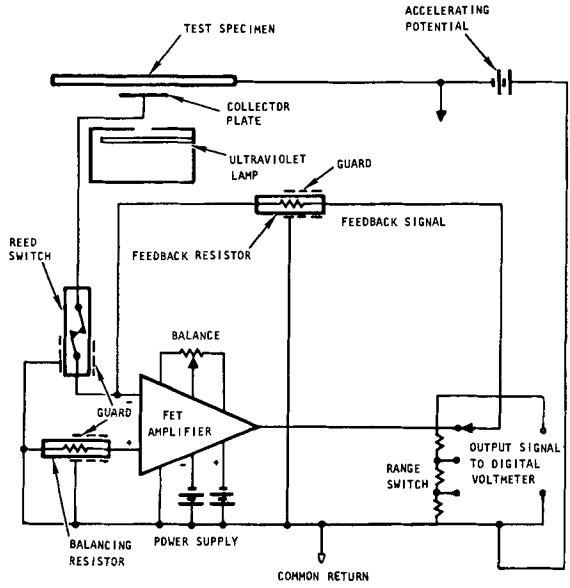


FIG. 6—*Schematic diagram of the system for measuring exoelectron emission in air* [9].

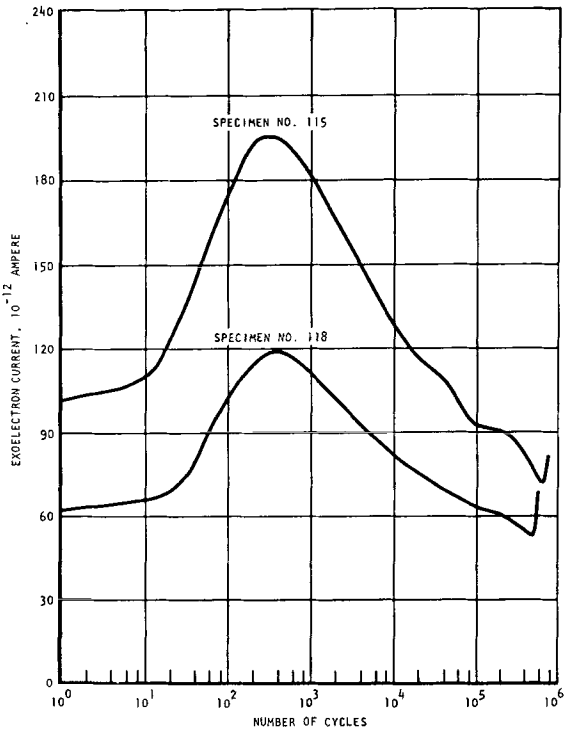


FIG. 7—*Exoelectron emission of 1100-0 aluminum in fatigue test in air at 11 650 lb/in.*^{2} [9].

metallurgical change by fatigue. It is thus possible to detect fatigue damage due to this structural change by determining the acoustic emission characteristics of originally unflawed materials.

Propogation of Ultrasonic Waves

In addition to detecting flaws, propagation of ultrasonic waves in metal parts has been also employed to investigate early fatigue damage by noting the changes in ultrasonic attenuation and velocity. Variation in attenuation with time is attributed to a dislocation effect. Also, under fatigue deformation, the velocity of wave propagation starts to decrease at the beginning with respect to the initial value before deformation. This decrease is characteristic of dislocation damping behavior. The change in velocity becomes smaller as deformation continues until the range of cycling for the attenuation minimum is reached. The change then again begins to increase rather rapidly with an increasing number of cycles.

Since fatigue damage develops mainly at or near the surface of a test specimen, Rayleigh waves or surface waves are most appropriate for studying the change in attenuation and velocity of propagation.

Optical Phenomena

An optical correlation technique has been used to detect changes in surface structure resulting from fatigue deformation. The correlation function for a given surface area is measured before and after cyclic stressing in terms of light intensity output of a coherent optical system. Change in surface structure produces a decrease in correlation intensity. The surface strain that can be detected is of the order of 1 μm.

Positron Lifetime

The half-life of positrons is different in a crystalline material containing dislocations and vacancies [*10*]. When a positron enters the material, it decreases in speed very rapidly and then seeks out an electron in the material with which it combines. With knowledge of the time of entry of the positron into the material, the time duration of existence of the positron in the material before decay thereof may be ascertained to provide data for half-life computations. It has been found that the half-life of positrons is longer in materials containing dislocations and vacancies, and it is believed that this is due to trapping of the positrons within the voids caused by such crystal defects, resulting in a longer time being required for the positron to seek out and combine with an available electron.

Stress Measurement

Fatigue is accelerated at higher stresses, and residual stresses in the material add to the amplitude of applied stresses. The measurement of stresses in the bulk of a body by the birefringence of ultrasonic shear waves has been demonstrated. The ultrasonic measurement of residual stresses in the surfaces of materials has been also accomplished and is more significant

because many of the effects of fabrication, application of loads, and environment occur at the surfaces of materials. Other NDT methods having potential for stress measurement include: Barkhausen effect, magnetoabsorption, ultrasonic reflectivity, holography, and Mossbauer effect.

Total System Summary

In summary, it can be seen that the many aspects of NDT in fatigue require a full systems approach for it to be successfully applied.

The concept of a critical flaw size, for example, is a continuous thread that runs through the product cycle from design to utilization. Allowable defect size is established at design, manufactured product must be scanned for evidence of freedom from such defects, and finally, the product is checked in the field for crack growth.

For the fracture mechanics approach to work other parameters must be assessed for presence and uniformity, such as material properties and stresses (residual and applied).

Finally, since fatigue is a time dependent phenomenon and the product needs to be evaluated initially and periodically in use, a system must be established to allow a signature to be obtained and subsequent service measurements compared against the baseline.

Recognition of the above system precepts will permit immediate application of NDT with today's methods and sound assessment of the fatigue problem. Current NDT developments hold the promise for simpler, easier, less costly, and more accurate methods for controlling fatigue.

References

[1] Socky, R. B., "Fatigue Detection/Measurement/Prediction Using Ultrasound," *Proceedings*, 1967 Technical Conference, Society for Experimental Stress Analysis, Chicago, Ill., 31 Oct.-3 Nov. 1967.

[2] Packman, P. F. et al, "The Applicability of a Fracture Mechanics—Nondestructive Testing Design Criteria," Technical Report AFML-TR-68-32, Air Force Materials Laboratory, Dayton, Ohio, May 1968.

[3] Peterson, R. S. and Bennet, S. in *Proceedings*, Eight Symposium on NDE in Aerospace, Weapon Systems, and Nuclear Applications, San Antonio, Tex., 21-23 April 1971.

[4] Hastings, C. H., *Journal of the Franklin Institute*, Vol. 290, Dec. 1970 (special issue: "Horizons in the Structural Use of Advanced Materials").

[5] Sachs, R. D., Elkins, J. D., and Smith, J. H. "Ultrasonic Data Analysis Using a Computer," Oak Ride National Laboratory Report Y-1808, 22 Feb. 1972.

[6] Wylie, R. D., *Welding Design and Fabrication*, Feb. 1972, p. 53.

[7] Flaherty, J. J., Erikson, K. R., and Lund, V. M., "Synthetic Aperture Ultrasonic Imaging Systems," U.S. Patent No. 3,548,642, 22 Dec. 1970.

[8] Chockie, L. J., "Report of Progress—New Nondestructive Test Methods," Internal Memo, General Electric Atomic Power Equipment Department, San Jose, Calif., 29 Nov. 1971.

[9] Moore, J. F., Tsang, S., and Martin, G., "The Early Detection of Fatigue Damage," Technical Report AFML-TR-71-185, Air Force Material Laboratory, Dayton, Ohio, Sept. 1971.

[10] Grosskreutz, J. C., "Detecting Defects by Distribution of Positron Lifetimes in Crystalline Materials," U.S. Patent No. 3,593,025, 13 July 1971.

W. E. Cooper[1]

Codes: Asset or Liability?

REFERENCE: Cooper, W. E., "**Codes: Asset or Liability?**" *Fatigue at Elevated Temperatures, ASTM STP 520*, American Society for Testing and Materials, 1973, pp. 733–743.

ABSTRACT: Elevated temperature fatigue evaluation rules are now included in the ASME Codes which govern the construction of nuclear power plant components. This paper considers the general question as to whether such Codes consitute an asset or a liability, and the specific question concerning asset versus liability as it relates to elevated temperature fatigue.

It is concluded that the present rules with respect to elevated fatigue represent a liability. The background of this situation is discussed and suggestions are made with respect to the steps required for conversion to an asset.

KEY WORDS: fatigue (materials), heat, breeder reactors, standards, boilers, pressure vessels, creep (materials), stresses, strains, cooperation

As an introduction to the general discussion of the state of the art with respect to fatigue at elevated temperatures, including these activities devoted to transforming the art into a science and the application of such information to design, this paper focusses on the question of whether Codes represent an asset or a liability. By way of definition Codes are a group of administrative and technical rules and standards covering any combination of materials, designs, construction, installation, inspection, and operation of equipment which is prepared for ready adoption into laws of a legal jurisdiction. To be specific, I will limit my remarks to Codes prepared by the American Society of Mechanical Engineers (ASME) which are applicable to the construction of commercial nuclear power plants. It must be emphasized that this paper represents my own opinions, and should not be construed as representing the position of others.

Such a discussion is pertinent to this symposium because of the impact of elevated temperature fatigue considerations on the preparation of ASME Code rules for breeder type nuclear reactors, sodium or gas cooled, which operate at temperatures above 800 F. Such considerations include:

1. Interaction of strain and load cycling with creep and relaxation.
2. Analytical methods for the evaluation of local stress and strain

[1] Vice president and technical director, Teledyne Materials Research, 303 Bear Hill Road, Waltham, Mass. 02154.

Copyright© 1973 by ASTM International www.astm.org

histories under complex loading conditions which include severe thermal transients.

3. Constitutive equations representing the material properties for use in the analytical methods.

4. Environmental effects on the properties.

Where Are We?

Whether or not we consider Codes to be an asset or a liability, they are a reality. If Codes become a liability, it is our responsibility as engineers to convert them into an asset.

In general, I am of the opinion that Codes constitute a significant asset to regulatory agencies, manufacturers, users, the engineering community, and to the public. With respect to the present Code rules for elevated temperature nuclear components, as contained in Code Case 1331-6, the situation is different. While these rules are an asset to regulatory agencies and with respect to public safety, the difficulty of applying the rules related to elevated temperature fatigue is such that the cost of demonstrating structural reliability constitutes a strong deterrent to the development of this needed source of electrical power. This problem results from the failure of the engineers in the field to provide the required technology in a useful form. Although the required technology would be more readily attained if adequate financial support were available, more than money is required.

President Nixon [*1*][2] has established the development of commercial, liquid metal, fast breeder reactors (LMFBR) as a program of national priority. The status of the industry has been reviewed in a recent AEC Report [*2*]. The immediate program includes the construction of the fast flux test facility (FFTF) under the direction of the USAEC Division of Reactor Development and Technology and construction of a demonstration plant under a cooperative industry—USAEC program. The latter program is being jointly managed by Commonwealth Edison and the Tennessee Valley Authority (TVA) and will be a part of the TVA system. Other LMFBR demonstration plants may be authorized. Parallel with this effort, a major gas cooled breeder project is being undertaken by Gulf General Atomic (GGA) for installation in the Philadelphia Electric System. For all these reasons, the need for the technology is urgent.

It is very important to place the shortcomings of our present technology in proper perspective to the all important consideration of public safety. It is my opinion that public safety problems do not result in LMFBR systems as a result of elevated temperature fatigue. In preparing the basic Code Case 1331 rules pertinent to public safety, we have relied upon the many years of successful operating experience with elevated temperature

[2] The italic numbers in brackets refer to the list of references appended to this paper.

pressure components constructed to the ASME Code rules of Section I and of Section VIII, Division 1. In addition we have further restricted the designer in a manner similar to that followed in Section III of the ASME Code for water cooled nuclear power plants.

The major problems which result from our present rules, with respect to elevated temperatures fatigue are:

1. Cost required to demonstrate that structural reliability exists.
2. Restricted number of materials for which adequate material properties are available.
3. Cost and time, including unavailability of essential power supplies, required to perform maintenance if fatigue aspects have not been completely considered.

The current revision of Code Case 1331 contains mandatory rules with respect to primary stresses and requires that cyclic conditions of operation be considered with respect to fatigue; but, it only provides an acceptable set of rules with respect to fatigue evaluation. Alternative rules with respect to fatigue evaluation may be used by agreement between the power plant owner and the component manufacturer. Therefore, there is still plenty of opportunity for contributions to be made to improve the situation. In the last part of this paper I will describe briefly the history of the Code rules with respect to fatigue at elevated temperatures, including our present status. In the future, we must obtain a complete and mandatory set of rules with respect to treatment of elevated temperature fatigue.

Why Are Codes Needed?

The early development of the ASME Code has been described by Greene [*3*]. Boiler explosions in the last half of the 19th century constituted a major public safety problem. During the period of 1898–1903, almost 1200 people were killed in the United States by 1600 boiler explosions. The explosion of a fire-tube boiler at Brockton, Mass., in 1905 killed 58 people and injured 117. In 1907 Massachusetts passed a law to protect against boiler explosions, which was followed by a similar Ohio law in 1911. Other states enacted similar legislation, but the differences between the various laws resulted in restrictions on the free exchange of boilers and pressure vessels between the various states. In response to appeals for the preparation of technically sound rules which would be accepted on a national basis, the ASME Boiler and Pressure Vessel Code was established. Presently, the ASME Code is referenced in the regulations of 70 jurisdictional authorities; including most of the States, the major cities in the remaining states, and all of the Provinces of Canada. In addition a number of Federal Agencies one of which is the USAEC [*4*], have referenced the ASME Code in their respective regulations.

The following statement at a 1970 Hearing before Congresses' Joint Committee on Atomic Energy [5] is pertinent both to the question as to whether or not Codes are required and to the status of our technology:

Codes, Standards, and Quality Assurance

The experience of the past several years has forcefully reconfirmed the fact that the reliability of nuclear power plants can be achieved only through strong and disciplined engineering and quality assurance programs. The need for such emphasis for all types of power generating equipment is being voiced with increasing frequency by industrial and utility leaders. There should no longer be any doubt that careful and systematic planning, and high standards in each phase of development, design, construction, inspection, test and operation of nuclear powerplants are prerequisites to assuring the safety, reliability, and economics needed for utility operation. Adequate, capable, and experienced technical competence and the strongest management support must be available and aligned to focus resources on the planning and production of successful nuclear power plants.

Accordingly, there continues to be increasing recognition throughout the nuclear power industry of the urgent need for development and adoption of engineering standards and other disciplined quality assurance practices.

The AEC has found it necessary to establish, both in its regulatory and development activities, key management positions with appropriate full-time staffs for the development of nuclear standards and quality assurance efforts. We have also found it essential for those with direct-line responsibility to participate and contribute. The time is long overdue where similar recognition and attention on standards should be provided by the various manufacturers and utilities who are involved with nuclear power.

A valuable "outside" appraisal of the need for national Codes and Standards was developed in a British government report of 1969 [6]. Following a discussion of various design approaches, paragraph 10.44 states:

However important these design details may be, a major difficulty is the large number (over twenty) of existing Standards, Codes, and specifications, with overlapping and differing requirements. To these may be added the numerous specifications of customers, of inspection authorities and also public sector organizations. The Committee considers this situation to be inefficient and would welcome a single master standard for pressure-containing parts, covering different types of vessel on the lines recently developed by the BSI/E/-/3 Committee. This would render many specifications in both the public and the private sectors unnecessary . . . .

The ASME Codes establish a necessary point of reference for regulatory bodies, particularly in respect to any legal proceedings, for industrial organizations and individual engineers. The rules are written in such a manner that responsibilities are clear and enforcement is not only possible but is required. The function of the ASME Boiler and Pressure Vessel Code Committee is to establish rules of safety covering materials, design, fabrication, examination, testing, and certification during construction of boilers and pressure vessels and to interpret these rules when questions arise regarding their context. In formulating the rules the Committee considers the needs of users, manufacturers, and regulatory authorities. The objective of the rules is to afford reasonably certain protection of life and property and to provide a margin for deterioration in service so as to give a reason-

ably long safe period of usefulness. Since the rules must be written so as to encompass a broad spectrum of applications, they cannot include all possible considerations for a specific component. Therefore, the Code does not constitute an adequate purchase specification for many applications, and the purchaser must provide additional requirements as needed.

The words "as needed" at the end of the preceding paragraph are important, and care must be taken to completely define any additional requirements. Dogmatic statements are essentially meaningless, but equally bad are requirements which impose uncertainty and confusion with respect to acceptable practice. Many examples could be cited where the cost of developing special practices and obtaining approvals on a case-by-case basis have negated the economic and schedular advantages of codification without increase in safety and reliability.

Since we are considering why Codes are needed, the implications of the preceding paragraph should be restated in a positive manner. The Codes represent the results of a cooperative effort conducted by interested parties and performed in a systematic and orderly manner. When the technology is developed adequately, the Codes reflect this technology in the form of an effective engineering procedure. When the technology is not developed adequately, the Codes reflect a consensus of interested parties as to the best available engineering approach. Whether the resulting rules are simple or are complex, they are of benefit to the user, the manufacturer, the legal jurisdictions, and to the engineering community. When the rules are not thoroughly based on complete technology, an important by-product of the Codes is the encouragement of that research and development which is vital to the solution of specific and important problems.

All of this does not mean that the Codes are perfect and cannot be improved. The next two parts of this paper consider some of these many negative aspects. In order to be effective in assisting in the improvement of the Codes it is important that you understand the system and recognize that the interests of all parties must be considered so that you can make effective suggestions and solutions.

A series of articles is being planned for the magazine *Mechanical Engineering* to provide general information on the Code Committee and its operation. As a general indication approximately 490 people fill about 600 positions in some 60 formally recognized operating entities. Meetings are held during six "Code weeks" each year in addition to occasional meetings of smaller segments of the organization. New editions of the Code are issued at three year intervals, addenda are issued twice a year, and Case interpretations are issued six times a year. All participants, with the exception of the secretarial staff, work on an unpaid basis. Preparation of Codes on other than this professional basis would be extremely expensive, even if competent personnel could be obtained and the interests of all parties considered.

How Do Codes Become Liabilities?

The need to consider the interests of all parties is overlooked by critics [7] of the ASME Code who attempt to interpret the Code to their specific desires. Uniform interpretation of the Code rules is provided by the National Board of Boiler and Pressure Vessel Inspectors in order that enforcement be in the manner intended when the Code is written. The members of this Board are those responsible for enforcement of the Code in the various jurisdictions.

Interpretation of the Code would be simpler if each and every requirement was based upon cold, hard technical fact (or logic) and if each requirement was present only for a single, well-defined purpose. A specific example is the acceptance criteria for nondestructive examinations, such as ultrasonic testing. One might expect there to be some definite relationship between the acceptability of a defect and the significance of that defect to service performance. Unfortunately, there exists no such relationship, and it is only within the last very few years that our technology has developed to such a point that defect significance can be evaluated. The existence of this technology is recognized in the Section XI rules for inservice inspection of nuclear systems. I doubt if the utopia described in the first sentence of this paragraph will ever be obtained, but serious liabilities will exist unless we move in that direction in all possible areas. In the interim, we must work within the established channels to obtain correct and uniform interpretations.

It is unnecessary to go outside of the participants on the Code Committee to find critics of the detailed contents of the Code. Attendance at any of the meetings, which are always open, is the best way to obtain a better understanding of both the administrative and the technical problems which face the committee and which constitute liabilities of various degrees. There are very few technical subjects where additional data and experience are not needed. The problem is mainly one of priorities, and the next section of this paper describes the mechanisms whereby the rules are improved.

Although "outside" experts may not be essential in advising the Code Committee that liabilities exist, it is also important that we be reminded on occasion. Perhaps one of the best appraisals of standards in general was prepared by Francis K. McCune for presentation at the USA Standards Institute (now ANSI, formerly ASA) 50th Anniversary meeting in 1968 upon his retirement as President of the Institute. For example, consider the following excerpts:

—It would be foolish however to say that any of us are completely satisfied. You know and we know that there is still much to be done. In fact there is probably more to be done than will ever be fully accomplished.

—It is industry, trade, commerce, consumers and government that need standards and which are affected by their content, availability, or in some instances, lack of availability.

—Scientific knowledge, technical innovation, communication and human need are moving ahead much faster than the way we develop standards.

—In addition to being often ponderous and pendantic our procedures for developing standards have become a conglomerate of individual views and entirely too defensive to concept.

—Priority must be given to achieving a sense of urgency in standardization.

These are but a few of the points made, and anyone seriously interested in this subject is advised to read the entire talk.

How Are Codes Improved?

There are several choices available: experience, knowledge, hard work, research, etc. Although all of these are important and in part necessitate the large number of participants in Code activities, the present interest is in research activities. I will narrow this aspect down to cooperative research, as opposed to research conducted under the sponsorship of governmental agencies or individual private sources.

The Code Committee maintains formal relations with and requests research assistance from the Pressure Vessel Research Committee (PVRC) of the Welding Research Council and from the Metals Properties Council (MPC), both of which are headquartered in the United Engineering Center in New York City. Both organizations fund research from donations obtained from industrial and governmental sponsors. Although the direct funding is nominal, being of the order of $150 000 per year for each, the value obtained is enhanced by the donation of materials, fabrication, test facilities, and manpower. The latter is most important, since these organizations seek to compile and interpret information from all sources and to, thereby, minimize duplication of effort. Activities include service in an advisory capacity to large programs sponsored by others. However, additional direct financial support is urgently needed by both organizations. It is quite common for available funds to be less than half that required for urgently needed work that would be best sponsored by the organization and which might not be accomplished without such sponsorship.

PVRC was formed in 1946 and has active Divisions in the fields of design, fabrication, and materials. A revival of earlier activities with respect to nondestructive examination is anticipated in the near future. Of particular interest are the efforts of the Subcommittees on Elevated Temperature Design and Plastic Fatigue. Primary activities in the design area include development of improved analytical capabilities with respect to thermal ratchetting and the development of improved constitutive equations. The plastic fatigue effort is currently concentrated on an experimental investigation of thermal ratchetting. Both activities are urgently in need of additional funding in order that they may conduct additional programs.

MPC developed from the activities of the ASME-ASTM High-Temperature Properties Committee. They are continuing the activities of that

group and have expanded to include many other areas of interest, particularly low-cycle fatigue.

Codification of Elevated Temperature Fatigue Rules

In 1952, I first became involved with the development of structural design criteria for sodium-cooled nuclear reactors. At that time, L. F. Coffin, as part of the same effort, was obtaining his first significant results in the field of fatigue at elevated temperatures [*8*]. The need for this effort was described in a subsequent paper [*9*] as follows:

> One of the most important, and heretofore neglected, fields of material behavior important to this program is the fatigue behavior of metals subjected to strain cycling. Although the common stress fatigue test results are usable at low stress levels, power reactor programs required knowledge of the effects of relatively fewer and longer cycles of strain beyond the elastic range.

Later it was noted that:

> In the design of SIR we were concerned with a temperature range where short-term properties are of more significance than long-term properties. Since the natural trend in power plant equipment is to go to higher temperature, we are interested in the performance and interpretation of long-term tests.

Test techniques such as those developed by Coffin and fatigue design techniques which were related thereto, all of which are generally concentrated below the creep range, became the basis for the fatigue evaluation procedures currently contained in Section III of the Code [*10*].

Our first attempt to prepare fatigue evaluation rules at high temperatures was associated with the preparation of the original revision of Code Case 1331 in 1963. At that time very little 1000 F or above data were available, and tests which considered the interaction of creep and fatigue damage were practically nonexistent. Primarily due to the efforts of W. F. Anderson, now of the Liquid Metal Engineering Center (LMEC), fatigue design curves were prepared using the available data and anticipating the seriousness of hold-time effects. Recognizing the need for information in this area and because of some of the results prescribed at the 1963 International Congress on Creep, PVRC prepared a test program and obtained quotations for its performance. Due to the anticipated high cost, the USAEC accepted sponsorship of the program and assigned it to the Aircraft Nuclear Propulsion project at General Electric under the direction of J. E. Conway, now of Mar-Test, Inc.;[3] this project continues at the Argonne National Laboratory.

The most definite warning that something was amiss with the fatigue design procedures contained in Code Case 1331, Revisions 0 through 4, was the interpretation of then recent British data by C. W. Lawton, of

[3] See p. 637.

Combustion Engineering, in 1968 [*11*]. In particular, it appeared from this interpretation that hold-time effects could result in test data below the fatigue design curves if but slightly longer hold times had been considered. This finding provided a strong incentive for the Code's newly formed Subgroup on Elevated Temperature Design to increase their efforts towards a general revision to Case 1331. Among other activities, a Task Group on Creep Fatigue was formed under the chairmanship of G. R. Halford, NASA-Lewis and, more recently, R. D. Campbell, LMEC. This effort results in the preparation of Code Case 1331-5 which was approved in the summer of 1971.

The period 1966–1970 was one of general frustration to those concerned with this problem. Through involvement in the efforts of the Committee, meetings with representatives of the USAEC, and public presentations, those involved with the problem, were advised as to the difficulty and the type of effort required for resolution. Despite this effort, the ten volume 1968 LMFBR Program Plan did not recognize the need for a specific program to resolve this problem. There followed a series of meetings between USAEC, industry and Code representatives in an attempt to formulate the required program and to obtain financial support. The frustration we all felt was typified by a remark I made in June of 1970 while addressing the American Nuclear Society on the subject "Code Considerations for LMFBR"; "Unfortunately, the performance of long-term tests takes a long time. We have lost over 20,000 hours of test time since the need for these developments became apparent. I am afraid we will lose more, since I still do not see such an effort being undertaken."

During 1971 the trend was reversed, although perhaps not all the way, and there are several papers at this Symposium which result directly from LMFBR efforts. Considerable working experience has been gained with an interim set of rules developed for the FFTF Project (WARD-FRA-152-Rev. 3), a complete revision of Code Case 1331, Rev. 5, was prepared covering the design of Class I nuclear components, Code Case 1481 has been approved for Class 2 and 3 components. Of most significance in the long range was the establishment by the USAEC of an LMFBR Structural Design Criteria effort at the Oak Ridge National Laboratory under the direction of our session chairman, W. L. Greenstreet. This program has both short-range and long-range goals and considers all aspects of the elevated temperature design problem.

There have been additional advances made in the first half of 1972. Certainly the contribution of this Symposium will be significant. Case 1331-6 was approved to add Ni-Fe-Cr Alloy 800, Grade 2 to types 304 and 316 austenitic stainless steels considered in Case 1331-5. A further revision of Case 1331 will be approved in 1972. The major purpose of this revision will be to improve the presentation and to make fairly minor revisions based upon experience to date. Fatigue data for Alloy 800, Grade 2 will be also

included. Design data for Alloy 800, Grade 1 and the 2¼Cr-1Mo alloy are being developed for inclusion in further revision.

Based upon our present understanding of the elevated temperature design problem and the programs underway to improve our knowledge of this problem, I would anticipate that it will be at least 3 to 5 years before a mandatory method of fatigue evaluation can be developed for inclusion in the Code. During this period, I would expect that the apparent Code actions will be concentrated on the inclusion of additional materials and upon minor revisions to the rules.

Is There a Lesson Here?

Recognizing that this is not the last time that our profession will face a difficult and urgent problem in codification, what have we learned? The obvious answer is that we should not allow the need for Codes to get ahead of the technology, but this answer is too simple to be useful. Further discussion might provide some understanding of the positive steps required to improve such situations.

I have previously [*12*] discussed that problem which I consider to be the most important one, the inability of the various segments of our profession (for example, metallurgists and stress analysts) to work together. Our training has become so specialized that we do not have time to learn the basics in the other person's field of interest. In our working life there are too few opportunities to share and discuss our mutual problems, meetings such as this one being a notable exception. This separation is encouraged by organizational structures within most companies and governmental organizations and by parochial attitudes within most industries.

These same barriers inhibit the development of required data. The material producers and the material users each think that data should be provided by the other party. Those data that are developed are too often the minimum required to characterize the material, as opposed to those required for selection and evaluation. The same "you first" attitude prevails between industry and government, particularly in fields such as nuclear power. Most of the design procedures and material properties pertinent to the evaluation of operational conditions for water-cooled reactors were developed and applied by government programs with but limited industrial participation. Not having participated extensively in this development, and being fully occupied with today's problems on present systems, I do not believe that most industrial participants recognized that long-range planning was required to develop an equivalent basis for elevated temperature plants. The absence of such a program from the AEC's LMFBR Program Plan, published in 1968, indicates that the AEC was equally delinquent. We, as individuals and as a profession, must accept the blame for this situation. Even if we claim that as individuals or as groups

we recognized that the problem existed, we failed to make the point where it counted.

It seems to me that the only available answer is to improve our efforts in cooperative research. A first step would be to broaden the participation in such organizations as PVRC and MPC. User and government participation in such bodies is very limited, and jurisdictional authorities seldom, if ever, participate. This means that most of our cooperative research is planned by researchers and that details received more attention than do the needs of users and jurisdictions. Increased participation by such interests would result in better planning and better recognition of the need for such planing. Improved acceptance of the cooperative research approach should then follow and result in a significant increase in funding.

Is this answer also too simple to be useful? I don't think so, but it does require that industry, government, and the engineering community be fully willing to cooperate financially and technically. The alternatives are a slowdown in progress or acceptance of the entire task by the government, because no single industrial participant can do the job.

Perhaps it is not too late to try this approach in solving the long-range problem of improving the basic concepts of the elevated temperature design rules. This effort must be completed before 1890 if we are to fulfill our obligations toward the establishment of a viable, commercial, fast-breeder reactor industry. The Code Committee charged with this responsibility needs all possible help.

References

[1] Nixon, R. M., "Energy Resources," The President's Message to Congress, 4 June 1971.
[2] "The Nuclear Industry," U. S. Atomic Energy Commission Report WASH 1174–71, 1971.
[3] Greene, A. M., Jr., "History of the Boiler Code," American Society of Mechanical Engineers, 1955.
[4] Title 10, Chapter I, Codes of Federal Regulations, Part 50, Paragraph 50.55a Codes and Standards, Federal Register, Vol. 36, No. 114—Saturday, 16 June 1971.
[5] AEC Authorizing Legislation Fiscal Year 1971, Hearings before the Joint Committee on Atomic Energy, Second Session on Civilian Power Reactors, 11 March 1970, Part 3, pp. 1191–1193.
[6] Report of the Committee of Enquiry on Pressure Vessels, Ministry of Technology, Her Majesty's Stationery Office, 1969.
[7] Rickover, H. G., "Who Protects the Public," 50th Materials Engineering Congress & Exposition, American Society for Metals, 1968.
[8] Coffin, L. F., Jr., "A Study of the Effects of Cyclic Thermal Stresses on a Ductile Metal," ASME Paper No. 53-A-76, American Society of Mechanical Engineers.
[9] Miller, D. R. and Cooper, W. E., "Structural Problems of a Sodium-Cooled Nuclear Reactor for Submarine Propulsion," ASME Paper No. 54-SA-75, American Society of Mechanical Engineers.
[10] Criteria of the ASME Boiler and Pressure Vessel Code for Design by Analysis in Sections III and VIII, Division, 2 American Society of Mechanical Engineers, 1969.
[11] Lawton, C. W., *Experimental Mechanics*, June 1968, p. 264.
[12] Cooper, W. E., "Interaction of Materials and Design Problems in Critical Vessels," 1st International Conference on Pressure Vessel Technology, 1969, Part III, pp. 29–32.

S. S. Manson[1]

The Challenge to Unify Treatment of High Temperature Fatigue—A Partisan Proposal Based on Strainrange Partitioning

REFERENCE: Manson, S. S., "**The Challenge to Unify Treatment of High Temperature Fatigue—A Partisan Proposal Based on Strainrange Partitioning,**" *Fatigue at Elevated Temperatures, ASTM STP 520*, American Society for Testing and Materials, 1973, pp. 744–782.

ABSTRACT: This paper was presented as an overview lecture summarizing the 1972 International Symposium on Fatigue at Elevated Temperatures held at Storrs, Conn. Starting with the observation of the diversity of subjects covered and lack of unanimity of approaches used, it becomes clear that there exists an urgent need for a unifying framework around which the many facets can be coherently structured. It is proposed that the strainrange partitioning concept has the potential of serving as such a framework. The method divides the imposed strain into four basic ranges involving time-dependent and time-independent components. It is shown that some of the results presented at the symposium can be better correlated on the basis of this concept than by alternative methods. It is also suggested that methods of data generation and analysis can be helpfully guided by this approach. Potential applicability of the concept to the treatment of frequency and holdtime effects, environmental influence, crack initiation and growth, thermal fatigue, and code specifications are then considered briefly. A required experimental program is outlined.

KEY WORDS: fatigue (materials), crack propagation, cyclic loads, deformation, thermal fatigue, fatigue life, ductility, exhaustion, strains, creep rate

My original assignment was to prepare an overview of the symposium that would serve as its summary. In reviewing the papers I was impressed with two major factors: the vastness of subject content and the diversity of treatment. It became clear that what was urgently needed was a unified treatment which would provide direction for the many facets covered by the symposium: how best to generate data, how to analyze and understand the data, and how to use them most effectively for practical purposes. In preparing this presentation I, therefore, have enlarged my scope to include a discussion of the challenge to achieve such unification. Naturally it would be desirable to examine various approaches, and to arrive at an objective

[1] Chief, Materials and Structures Division, Lewis Research Center, National Aeronautics and Space Administration, Cleveland, Ohio 44135.

Copyright© 1973 by ASTM International www.astm.org

conclusion after a careful study of numerous alternatives. However, because of time factors it has been necessary to limit myself to a more modest treatment. Thus, I have included the word "partisan" in my title because I shall limit my attempt at "unification" using only the strainrange partitioning approach on which my colleagues and I are presenting a paper at this symposium [*1*].[2] The use of other methods as frameworks must be reserved for other occasions.

Because the change in format of my presentation—from one wherein I merely reviewed the contents of the symposium, to one structured around a unified approach—developed at a rather late date, it was necessary to put together much of what I shall say rather hurriedly. In this connection, I want to acknowledge the very concentrated and devoted efforts of Gary Halford who not only served as a sounding board for some new concepts that were developed during the preparation but also contributed many ideas, ran tests, made computations, and assisted in the figure preparation. He and Alfred Nachtigall, who also made calculations and prepared figures, were indispensable to me in the preparation of this paper. I should also emphasize that since the paper was prepared rather hastily, many of the conclusions that will be discussed will have to be regarded as provisional, subject to later change as we obtain more extensive information and make further analyses.

Let me start by listing the major areas covered in this symposium. *Life analysis and prediction* is one of the important areas and many different methods have been used at this conference. Many *test methods and materials characterization* approaches appear in the symposium; *mechanisms and environmental effects* have received some attention; *fracture mechanics and crack growth* were given a considerable amount of attention; and *analysis and design codes* have been discussed. That treatment of these subjects needs to be unified, and how the strainrange partitioning concept can contribute toward this goal will be the main theme of my paper.

Review of Life Prediction Methods

Let us first direct our attention to several life prediction methods for high-temperature fatigue analysis. One of these is the *modification of low-temperature relationships*; another is the *summation of creep time and fatigue cycle fractions*; a third is *ductility exhaustion* as covered in the Polhemus et al paper [*2*]; and finally, the *strainrange partitioning* as discussed by Halford et al [*1*].

Looking first at the methods using modified low-temperature relationships, it is noted that one of the early concepts was the 10 percent rule [*3*]. The thought involved here was to account for the accelerated crack initiation and propagation stages brought about by intercrystalline deterioration. The cyclic lives predicted on the basis of the universal slopes equation

[2] The italic numbers in brackets refer to the list of references appended to this paper.

developed [4] for room-temperature behavior were divided by a factor of 10 to account for this acceleration. We have applied this method rather extensively over the past seven years, and, in many cases, it has given excellent results. However, the method has limitations. In some cases, the creep effect reduces life by even more than a factor of ten; therefore, a creep-modified 10 percent rule was proposed [5]. This rule identified conditions under which the ordinary 10 percent rule is to be modified; an improvement was obtained, but even the modified method had limitations. For example, it could not properly account for the complex stress variation that develops when hold periods are introduced in tension and compression; temperature variations during testing could not properly be accounted for in detail; etc.

The frequency-modified life relationship and the characteristic-slope relationship were proposed, respectively, by Coffin [6] and by Berling and Conway [7]. These methods also use the equations which characterize behavior in the room-temperature range but modify the equation to include a frequency term to account for rate effects at high temperature. Both of these methods can give very good results when applied to situations similar to those for which the input information, from which various constants are determined, closely resemble the real application. However, their use can result in considerable error when extensive hold periods are present in tension or compression, either separately or combined. It should also be added that the frequency modification approach requires a considerable amount of imput data, six or more constants for each temperature, and, of course, each temperature of interest requires separate investigation. How to treat cases wherein temperatures vary in a complex manner during the cycles, and how to establish the number representing the frequency in cases of complex loading, are also open questions.

Another approach that has received attention at this symposium is the summation of time and cycle fractions, wherein time fractions are used as a measure of creep damage, and cycle fractions are used as a measure of fatigue damage. The basic approach was initially suggested by Robinson [8] and then modified to apply to thermal fatigue problems by Taira [9], and it has been used for a long time as a basis for the treatment of many problems. Considerable success has been obtained using this method to analyze complex thermal fatigue, for example, the paper by Spera [10] at this symposium. Successful though the method has been, there are situations in which it has limitations—for example, when the static creep-rupture characteristics of materials are altered as a result of cyclic application of loading, and when ambiguity develops as to the treatment of damage due to compressive loading. In order to account for the effect of changes due to creep-rupture during cyclic loading, the use of a cyclic creep-rupture test was introduced [11], wherein the creep-rupture characteristics of the material are obtained under cyclic loading rather than under static stress. This detail improved our ability to explain experimental observations in many cases;

however, it still left open the question of how to treat damage due to compressive stress.

The method of summation of creep-time and fatigue-cycle fractions has also been applied to the study of stress relaxation during strain hold periods. Campbell [*12*] presented such an analysis at the American Society of Mechanical Engineers, Pressure Vessels and Piping Congress; Jaske and his co-workers also used this method in a paper presented in this symposium [*13*]. In many cases, the method can properly predict experimental behavior, but, as shown by Jaske et al, considerable error may result in some applications.

The ductility exhaustion concept is another approach for the treatment of creep-fatigue interaction. One of the early studies utilizing this concept was described in Ref *14* wherein the case of damage due to alternate applications of cyclic loadings and periods of monotonic plastic straining was considered. The resulting equation was

$$D_q = \{ \ldots [\{[(D_0 - \delta_1)^2 - n_1\epsilon_{p_1}{}^2]^{1/2} - \delta_2\}^2 - n_2\epsilon_{p_2}{}^2]^{1/2} - \delta_3 \ldots \} \ldots\ldots (1)$$

We see here that the remaining ductility, D_q, of the material is shown as a rather complex equation involving the number of cycles n for which the completely reversed plastic strain, ϵ_p, is applied, and the monotonic plastic strain, δ, is imposed between periods of cyclic plastic straining. Space does not permit an extensive discussion of this approach, but this formula suggests that a framework does exist for treating fatigue by accounting for the manner in which increments of loading reduce the remaining ductility. This method may also have applicability in the treatment of ratchetting problems. In this symposium, is a paper by Polhemus et al [*2*] in which the interaction of creep and thermal stress is treated by this ductility exhaustion concept. For their treatment, it was necessary to obtain the creep as well as the thermal fatigue characteristics of the material. The combined effect was obtained using a formula resembling Eq (1), although the successive solution of a series of equations was involved, rather than the solution by a single closed-form expression. This concept has considerable merit, but to make it useful in a general way will require much further development.

The last of the methods I shall discuss is strainrange partitioning. Since this method will serve as the main theme of my discussion, I shall now provide some background information, show some new relationships and procedures that have not been previously published, and apply the method to a number of test results present at this symposium. I shall then outline what developments are still required in order to render it suitable for the purpose tht I am proposing, namely, as a framework for unifying the treatment of metal fatigue at elevated temperature.

Background of the Strainrange Partitioning Method

Inherent in the strainrange partitioning method is the concept that several modes of inelastic deformation must be considered. While it is undoubtedly

possible to categorize the deformation modes in fundamental terms—for example, bulk grain deformation and grain boundary deformation, each mode being appropriately subdivided according to other characterizations—the approach used in strainrange partitioning is a compromise with engineering practicality. Only two strain modes are chosen: plastic flow and creep. Of course, there may be important differences between the mechanisms involved in these deformation components. Creep probably involves more grain boundary sliding and atomic diffusion than plasticity, while the latter may involve principally slip-plane sliding. Such distinctions are important from the viewpoint of providing understanding, but, for practical purposes, these considerations are temporarily bypassed by distinguishing between the components only in relation to their time dependency. "Plastic flow" will be regarded as the sum of all inelastic strain components which occur nearly immediately upon application of stress, while "creep" will be regarded as the sum of all time-dependent components. This distinction alone enables us to separate the components by relatively simple experimental procedures.

Strainrange partitioning is based on the concept that the two modes of deformation may exist separately or concurrently, and that their interaction can influence the fracture behavior of the material to a considerable degree. An important feature of the method relates to the manner in which a tensile component of strain is balanced by a compressive component to close the hysteresis loop during completely reversed straining. The method is more fully described in Ref *15*, and will only be described briefly here.

Consider the hysteresis loop shown in Fig. 1*a* .This hysteresis loop was obtained by loading rapidly to a tensile stress, holding that stress for a period of time during which creep occurred, reversing the stress to a compressive value lower than was used for tension, and providing a longer hold period in compression to close the hysteresis loop with creep strain. In the tensile portion of the test, there was more plastic flow than in the compressive portion, while the creep component was lower in tension than in compression. In essence, therefore, while there was a reversed creep component and a reversed plastic flow component, there also appeared a strain component wherein tensile plastic flow was reversed by creep.

Considering other possibilities that could develop, it appeared that a minimum of four basic strain components required attention, as shown in the following table:

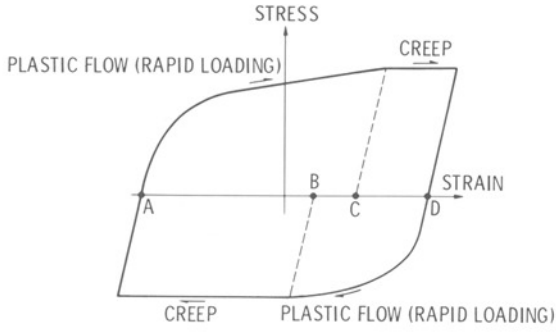
Notation	Tensile Strain	Compressive Strain
$\Delta\epsilon_{pp}$	plastic	plastic
$\Delta\epsilon_{pc}$	plastic	creep
$\Delta\epsilon_{cp}$	creep	plastic
$\Delta\epsilon_{cc}$	creep	creep

Having recognized the four basic components of strain that must be considered, we next set about to devise separate tests in which the major strain component would be one of each of these basic types, and we determined the life relationships associated with each one of them. Typical life relationships are shown in Fig. 1*b*. Lines relating strainrange to cyclic life on logarithmic scales are straight, analogous to room-temperature fatigue behavior. Each strain component, however, has a different life relationship. In Fig. 1*b* the $\Delta\epsilon_{pp}$ component produces the highest life for a given strainrange, while the $\Delta\epsilon_{cp}$ component produces the shortest life for this material by a factor of approximately 20 for the same magnitude of strain.

Figure 1*c* shows that the mechanism of failure is altered considerably by the type of strain range. The top of the figure shows a micrograph of a tested specimen when the $\Delta\epsilon_{pc}$ strainrange was on the order of 1.5 percent. The failure path is transcrystalline; the life was 264 cycles. The bottom of the figure shows a micrograph of another tested specimen, the strainrange was of the $\Delta\epsilon_{cp}$ type, also about 1.5 percent. The life was only 15 cycles; the fracture path is now intercrystalline. Figure 1*d* shows how the results on two materials, 2¼Cr-1Mo, and Type 316 stainless steel, correlated on the basis of strainrange partitioning in tests involving complex cycles. Correlation is within a life factor of approximately two for nearly all cases.

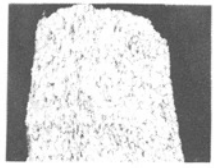
In the Halford et al paper [*1*] the life relationships for each of the four components for the two materials just mentioned were studied over a wide temperature range. These could all be represented by straight lines that are reasonably independent of temperature (see Figs. 2 and 3 of Halford et al paper). What this means is that in these materials the life relationships are governed by the nature of the strainrange and not by the temperature at which the strainrange was imposed. If a particular strainrange is imposed at one temperature, the life will be the same as when the same strainrange of the same type is applied at another temperature. It does not, of course, mean that life is independent of temperature. A given imposed load will produce different strains at different temperatures; a given imposed strain will be partitioned in a different manner depending on the temperature. Therefore, a complete life analysis will involve the determination of how much strain is developed and how this strain is partitioned. Once the partitioned components are known, however, the life is established essentially without regard for temperature. From a practical point of view, this also means that the amount of experimental information to be generated is reduced drastically. Furthermore, convenient temperatures can be used to develop the desired strainranges in relatively short periods of time, thereby avoiding extended testing that might be necessary to obtain the input information required for analysis by alternative methods.

It is important to emphasize that for these two materials just discussed the creep and plastic ductilities were not sensitive functions of temperature or of testing time. As will be indicated later, when materials in which creep

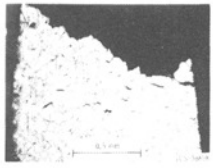


(a) HYSTERESIS LOOP WITH CREEP AND PLASTICITY.

TENSILE PLASTIC FLOW, COMPRESSIVE CREEP, $\Delta\epsilon_{pc} = 0.0162$, N = 264.



TENSILE CREEP, COMPRESSIVE PLASTIC FLOW, $\Delta\epsilon_{cp} = 0.0147$, N = 15.



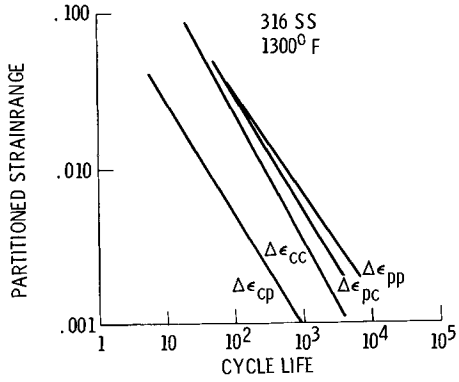
(c) PHOTOMICROGRAPHS OF FRACTURED SPECIMENS OF 316 STAINLESS STEEL TESTED IN CREEP-FATIGUE. CREEP AT 1300° F (705° C), PLASTIC FLOW AT 600° F (315° C). (Ref. 15.)

FIG. 1—*Background of strainrange partitioning concept.*

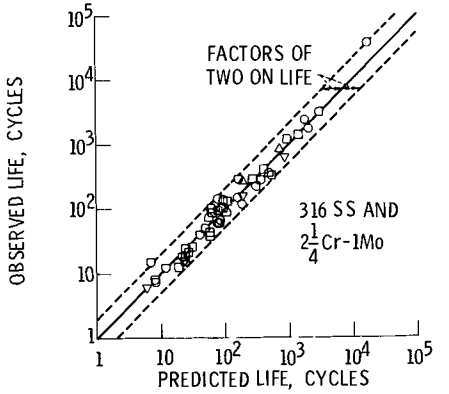
and plastic ductilities sensitive to temperature or time of application are dealt with, temperature or time independence of these life relationships will not be expected. An illustration of this case will be provided later.

Some New Relationships and Procedures Applicable to Strainrange Partitioning

So much, then, for background information on strainrange partitioning and the status of the development of this method up to this point. As already indicated, in order to provide a more substantive presentation, it was necessary to carry the concept a step farther. Several new relationships and procedures that were developed for the purpose of analyzing some of the results presented in this symposium will now be discussed.



(b) SUMMARY OF PARTITIONED STRAINRANGE-LIFE RELATIONS.



(d) LIFE PREDICTABILITY BY STRAINRANGE PARTITIONING.

FIG. 1—(*Continued*).

New Interaction Damage Rule

An important step involved in the application of the strainrange partitioning method is the process of combining the effect of several concurrent strainranges. Figure 2 shows an example wherein a total inelastic strain of 0.01 consists of only two components $\Delta\epsilon_{pp} = 0.009$ and $\Delta\epsilon_{cc} = 0.001$. In the past [*1*] we used a simple linear damage rule, according to which the life N_f would be determined by Eq 3 shown in the figure. A new approach designated in Fig. 2 as an "interaction damage rule," is simpler to apply and has other advantages. Details of the development will be described in a forthcoming publication [*16*]. Basically, the derivation is based on the assumption that in the presence of other strainrange components the life relationship for each strainrange is altered by suitable displacement. The

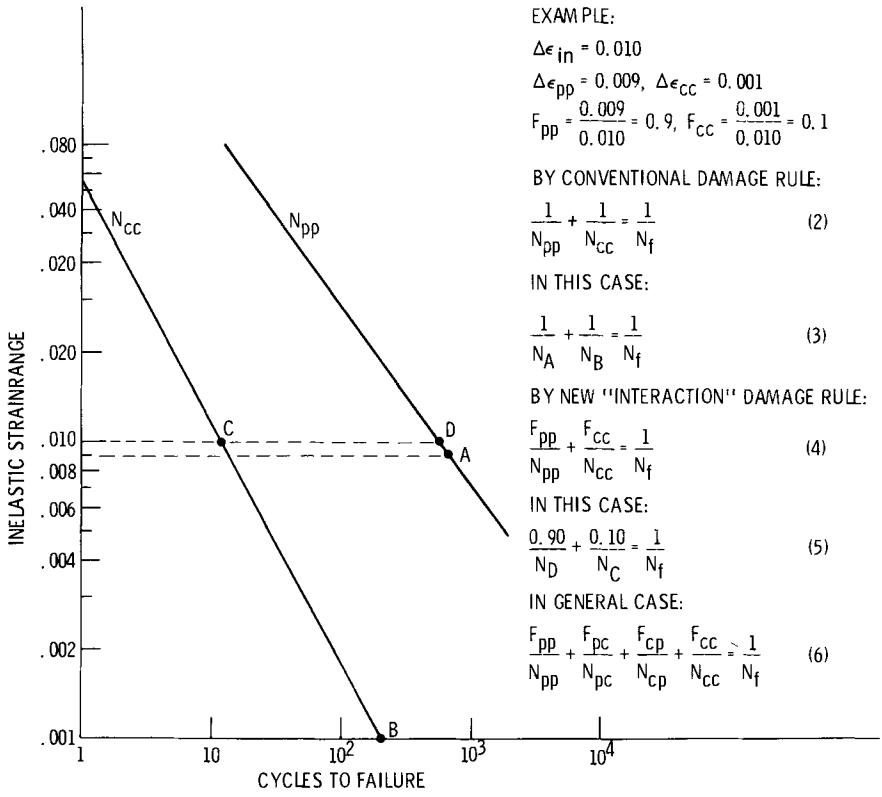


FIG. 2—*Relationships for determining life when two or more strainrange components are present.*

amount of displacement depends on the slope of the line representing the life relationship of that strainrange component, together with the fraction of the total inelastic strainrange associated with the component involved. As shown in Fig. 2 by Eqs 4 to 6 the final result is extremely simple. When several types of strainranges are involved, the first step is to compute a life from the basic life relationship for each strainrange as if that strainrange were the entire sum of the strainranges present. This is done for each of the strainranges involved in the analysis. Once these lives have been calculated, the expected life is obtained by weighting each of the lives calculated according to that fraction of the total inelastic strainrange that is truly associated with that strainrange component. Thus, as shown in the last formula in Fig. 2, the ratio F_{pp}/N_{pp} is obtained by placing in the numerator the fraction of the total inelastic strainrange that is due to $\Delta\epsilon_{pp}$, and using as the denominator the life N_{pp} which is obtained when the entire inelastic strainrange is considered to be $\Delta\epsilon_{pp}$. The other terms are established similarly, and life is computed on the basis of the weighted life relationship shown. We have

termed this procedure the "interaction" rule because it is based on the idea that the strainranges interact to cause displacement of the life relationships.

Life computed by the interaction damage rule and by the ordinary linear damage rule do not differ greatly in most cases, as illustrated in Fig. 3 for Type 316 stainless steel. The lines based on computation by both methods are relatively close to each other both at very high frequencies and at very low frequencies. They differ from each other by only a life factor of two in a relatively small frequency range. The experimental results also agree well with both types of computations, and, at this time, we cannot be certain which damage rule yields more accurate results.

Method of Partitioning Strainranges

Figure 3 also shows an advance that we have made since our last publication regarding the procedure for partitioning a strainrange when only the total value of the inelastic strainrange is known. The concept is applied here to determining the effect of frequency on cyclic life when the total inelastic strainrange is held constant at 0.47 percent. Since we are dealing with continuous cycling, only the balanced components $\Delta\epsilon_{pp}$ and $\Delta\epsilon_{cc}$ should be present, but how much of each component is present at each particular frequency must be determined. An experimental approach is used which is illustrated in the figure. The stabilized hysteresis loop is first established after applying cycles of loading at the frequency involved. This hysteresis loop provides us with information on the maximum stress that develops both in tension and compression for the applied frequency. Since plastic flow depends primarily on the peak stresses, its magnitude can be determined by conducting another test in which the same maximum and minimum stresses are maintained, but in which the frequency is raised to as high a

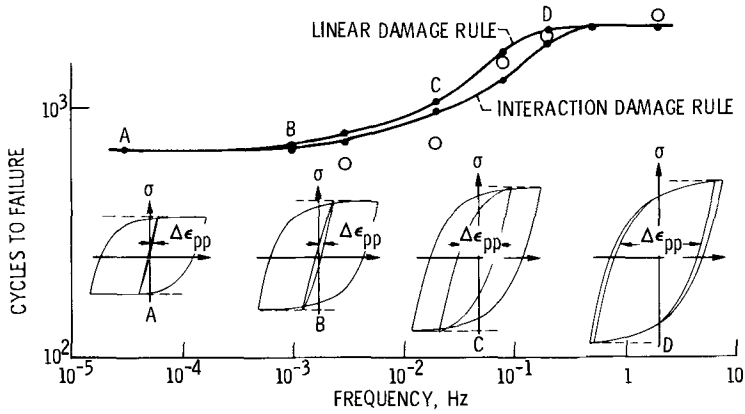


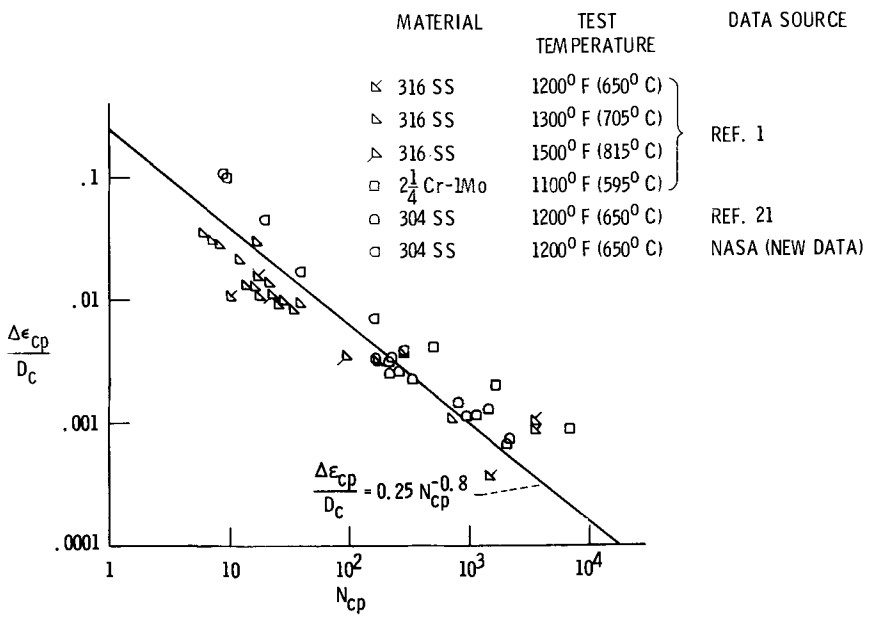
FIG. 3—*Method of partitioning using real-time hysteresis loop and rapid-cycling hysteresis loop between same stress limits. Data for 316 stainless steel tested at 1500 F (815 C),* $\Delta\epsilon_{in}$ = *0.0047, triangular strain waveform (data from Ref* 16).

value as can be achieved. At the high frequency creep will be essentially excluded. The hysteresis loops in the figure were obtained in this way. The inner hysteresis loop in each set shows the amount of inelasticity that develops when the same extreme stresses are applied, but the frequency is sufficiently high to preclude appreciable creep. Note that at point A the hysteresis loop shows that very little $\Delta\epsilon_{pp}$ strain is present. On the other hand, at point D, where the frequency is high, practically all of the inelastic strain is $\Delta\epsilon_{pp}$. At intermediate frequencies, the amount of $\Delta\epsilon_{pp}$ is determined from rapid cycling, and the $\Delta\epsilon_{cc}$ component is determined by the difference from the total inelastic strainrange. Although this method involves some experimentation, it should be emphasized that each hysteresis loop is obtained after only a few cycles of loading and that no test need be carried to fracture. In fact, the same specimen can be used for all the tests, involving a total test time of just several days. For more complex type of loadings, involving other types of strainranges, additional procedures may be required; this subject will be discussed later.

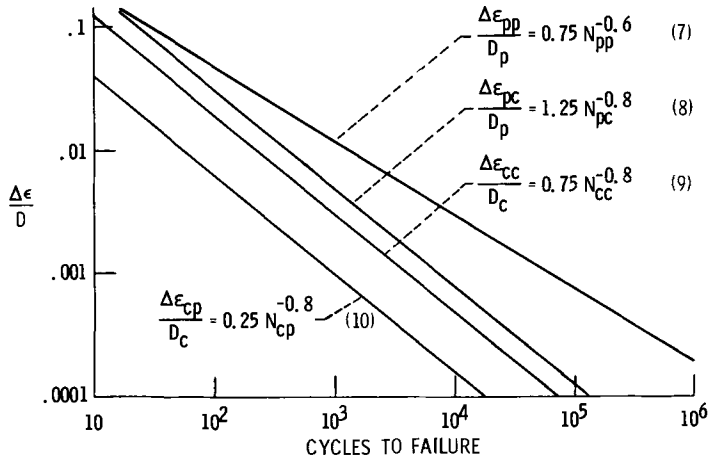
Tentative Universalized Life Relationships

Another new development to be employed in the remaining discussion relates to universalized equations for cyclic life associated with each of the strainrange components, analogous to the universal slopes equation which we have used effectively to treat estimates of fatigue in the subcreep regime. It is recognized that the amount of information available to construct such relationships was limited. However, in order to apply the method to some of the data in this symposium, it was necessary to make estimates of these universalized life relationships. Shown in Fig. 4*a* is an illustration of how we proceeded to obtain this estimate. First, we normalized the strainrange by dividing by ductility (plastic ductility D_p if the tensile half of the strainrange is plasticity, creep ductility D_c if it is creep). The figure shows the results for $\Delta\epsilon_{cp}$, although similar curves were constructed for each of the strainrange components. The ratio $\Delta\epsilon_{cp}/D_c$ is plotted against the life N_{cp} for a number of the materials. It is seen that the points fall near a line having a slope of approximately -0.8. Because of the limited amount of information available to construct such a correlation, no attempt was made at further refinement. After making such plots for each of the four components, using data from our own laboratory as well as those contained in the preprints of the reports presented at this symposium, the lines shown in Fig. 4*b* were obtained. It is apparent that any of the strainranges involving a creep component could be represented in such plots by lines of slope -0.8, whereas the line representing the $\Delta\epsilon_{pp}$ component has a characteristic slope of -0.6, which is equal to that in the universal slopes equations. The coefficients are different for each of the lines.

Figure 5 shows the degree to which these life relationships correlated all the data that were used in their construction. Observed life is plotted



(a) DATA CORRELATION FOR THE $\Delta\epsilon_{cp}$ COMPONENT.



(b) SUMMARY OF RELATIONS FOR ALL STRAINRANGE COMPONENTS.

FIG. 4—*Tentative universalized relationships for the four strainrange components.*

against the predicted value determined from these simplified relationships. The sources for the data are also shown in this figure, and it can be seen that many of the data points were extracted from reports presented in this symposium. While we do not consider the relationships shown here as final ones for estimating life for each strainrange component, the overall correlation is reasonably good. Individual materials, however, may deviate by

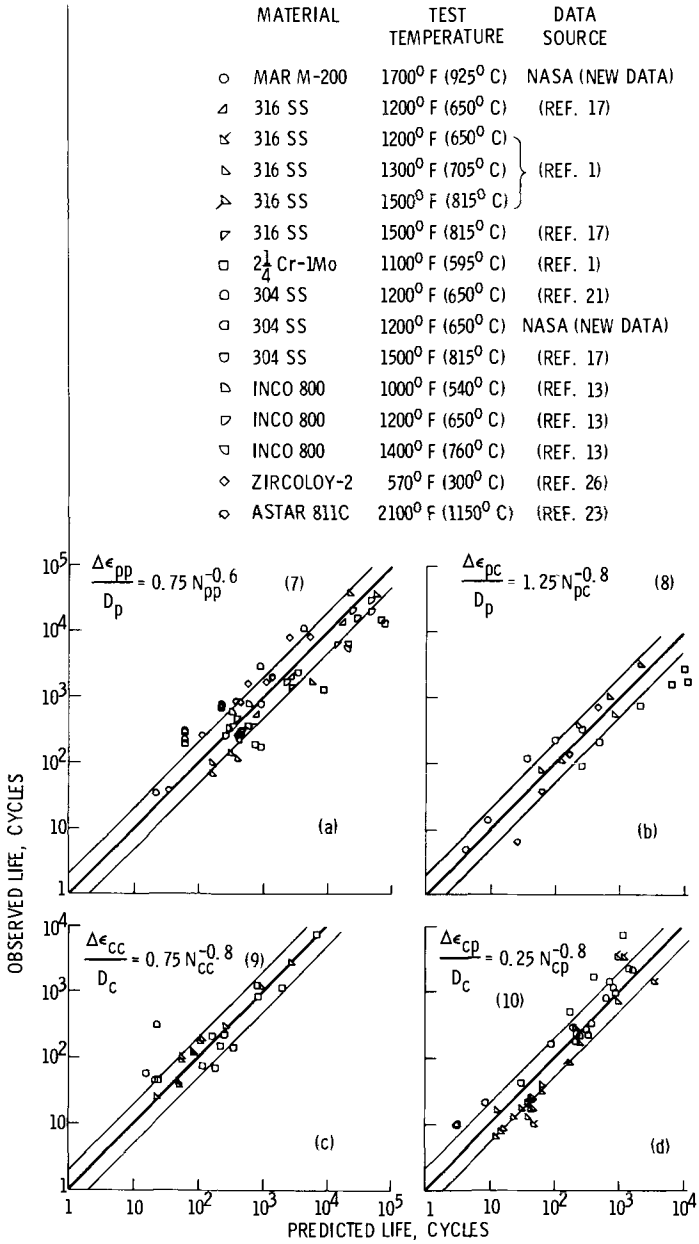


FIG. 5—*Data correlation using tentative strainrange partitioning life relationships.*

more than a factor of two from their predicted behavior. For example, Fig. 5*b* shows that for the 2¼Cr-1Mo alloy (square symbols) the N_{pc} life is overestimated by more than a factor of two, whereas Fig. 5*d* shows that the N_{cp} life is underestimated by more than a factor of two. The net effect is that, for this alloy, a strain absorbed as $\Delta\epsilon_{pc}$ is actually more damaging than if absorbed as $\Delta\epsilon_{cp}$, as was noted in Ref *15*. However, the life relations of Fig. 4 imply $\Delta\epsilon_{cp}$ to be more damaging than $\Delta\epsilon_{pc}$ for the D_p and D_c ductilities associated with this material. Despite occasional recognized inaccuracies, the tentative relationships can be most useful where experimental information is totally lacking for constructing the actual life relationships. Use of the tentative relationships will be illustrated in some later examples.

Application of Strainrange Partitioning to Subjects Covered by Symposium

It shall be now demonstrated that the strainrange partitioning approach addresses itself to many of the subjects covered in this symposium, and that it is useful in overcoming some of the limitations of other methods discussed. As such it has the potential of providing a unifying framework for analyses so urgently needed at this time.

Establishing Bounds on Life

An important use of the concept is the computation of maximum and minimum values that can be expected for a known strainrange. Figure 6 shows two examples. Figure 6*a* presents data on Type 316 stainless steel used by Challenger and Moteff [*17*] taken from the original publication of Berling and Slot [*18*]; Fig 6*b* shows results for A286 referred to by Solomon and Coffin [*19*] and also contains some new data generated in our laboratory. The data show fatigue life at various frequencies and temperature. Since continuous cycling was involved in these tests, only the balanced components $\Delta\epsilon_{pp}$ and $\Delta\epsilon_{cc}$ should be present. The maximum life would occur if all the inelastic strain were absorbed as $\Delta\epsilon_{pp}$; the minimum life would occur if the strainrange were all $\Delta\epsilon_{cc}$.

In Fig. 6*a*, N_{pp} and N_{cc} bound the 1200 to 1500 F (650 to 815 C) data. At 800 F (425 C), the behavior is similar to that at room temperature. From this figure it is observed that there is a difference between the high-temperature line for $\Delta\epsilon_{pp}$ and the universal slopes line at room temperature. The latter line, shown dotted, is higher in life by a factor of about two than the $\Delta\epsilon_{pp}$ line at high temperature. Perhaps this is due to the fact that the oxidizing effect associated with the higher temperatures is absent. Maybe it is just the result of data scatter, or the expected inaccuracies of both the simplified $\Delta\epsilon_{pp}$ relationship and the universal slopes equation. On the other hand, if it is a true behavior pattern, it provides some corroboration to Solomon and Coffin's [*19*] observations regarding vacuum environment

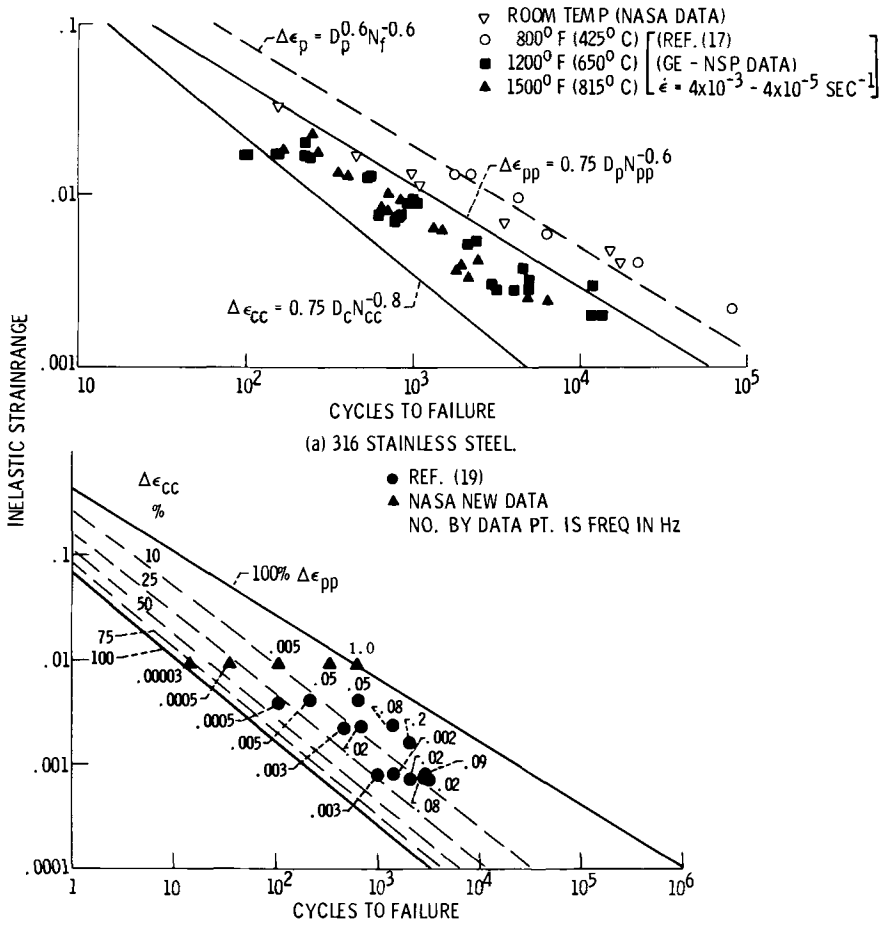


FIG. 6—*Use of strainrange partitioning to establish bounds on life.*

effects which will be discussed later. What the figure shows mostly, however, is that even if there is no quantitative information on the degree of partitioning involved, the life can still be bounded between two lines. In many cases this may be adequate.

Figure 6*b* shows the concept of data bounding applied to A286, the material used by Solomon and Coffin [*19*]. Again, the $\Delta\epsilon_{pp}$ and $\Delta\epsilon_{cc}$ lines bound all the data within the wide frequency range investigated. Also shown in this figure are some dotted lines that indicate what the lives would be if the strains were partitioned according to the amounts designated along each line. To interpret the results more quantitatively within the framework of the strainrange partitioning approach, several tests on A286 were run in which the concept shown in Fig. 3 was used to partition the strain

during continuous cycling. The data points obtained in the program are shown by the triangles. The results will be discussed in the next section. However, it can be noted here that all the data are indeed bounded by the N_{pp} and N_{cc} lines.

Frequency Effects

To obtain more precise information on life, rather than simply determining bounds, it must be determined how the total strainrange involved is partitioned into its components. It has been already shown in Fig. 3 how the frequency effect in Type 316 stainless steel has analyzed by experimental partitioning of the strainranges. Whether the "linear" or the "interaction" damage rule was applied to the data, the predictions never differed from the experimental values by more than a factor of two. Notice, incidentally, the saturation values of life at both low and high frequency. At the low end of the frequency spectrum the applied strain tends to be absorbed as $\Delta\epsilon_{cc}$, and further decreases in frequency do not increase the amount of $\Delta\epsilon_{cc}$, so life levels off at N_{cc} for the applied strainrange. Similarly, at the highest frequencies, life levels off at N_{pp} for the applied strainrange.

Our analysis of the frequency effect for A286 is shown in Fig. 7. This is a material for which the creep ductility varies with rupture time. The information on ductility was obtained by private contact with Dr. Opinsky, who also has presented a paper on A286 at this symposium [*20*]. Thus, the lower curve shown on this figure represents the N_{cc} value as a function of frequency as determined by the simple formula shown. The curve showing the predicted value of life as a function of frequency was determined by partitioning the strain according to the method previously described; good

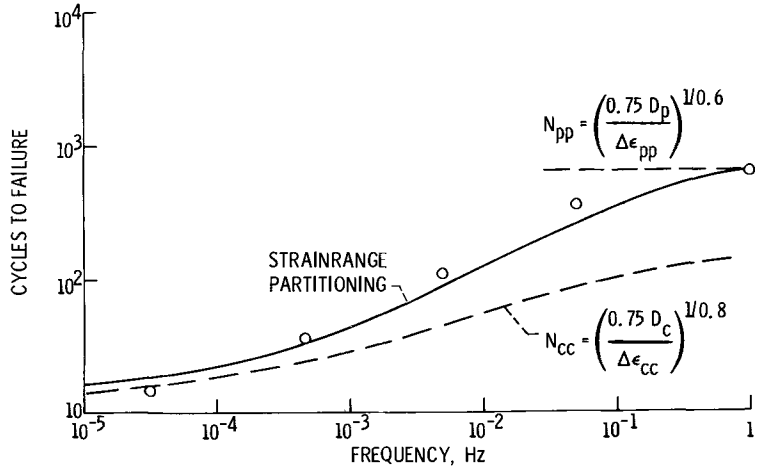


FIG. 7—*Application of strainrange partitioning to frequency effect for a material with time-dependent creep ductility, A286 tested at 1100 F (595 C),* $\Delta\epsilon_{in} = 0.009$.

agreement was obtained with the experimental results (shown as triangle points in Fig. 6*b*).

Holdtime and Relaxation Effects

The strainrange partitioning method lends itself ideally to the treatment of holdtime effects. During a tensile or compression strain hold period, creep occurs and stress relaxes. This creep strain may later be reversed by plastic flow; thus, $\Delta\epsilon_{cp}$ or $\Delta\epsilon_{pc}$ components may develop. Two applications will be used for illustration.

Figure 8 shows results of Conway and co-workers [21] for Type 304 stainless steel involving continuous cycling or tensile hold periods–tests at two strain levels—1/2 and 2 percent. Additional tests, conducted at our laboratory in a short time using a single specimen, permitted partitioning in the manner described earlier. Life computations shown by the lines in this figure agree very well with the experimental results. The curves show, as Conway et al determined experimentally, that there is a saturation life at both very short cycle times as well as at very long cycles times (very high frequency and low frequency, respectively). At the short cycle times, all of the strain is imposed as $\Delta\epsilon_{pp}$, whereas at the higher of the cycle times the strainranges became $\Delta\epsilon_{cc}$ or $\Delta\epsilon_{cp} + \Delta\epsilon_{pp}$, depending on whether the strain cycling is continuous or whether a holdtime in tension is applied. To reach the point shown on the uppermost curve for the 1/2 percent strainrange would require a total test time of approximately 10 000 h. Such infor-

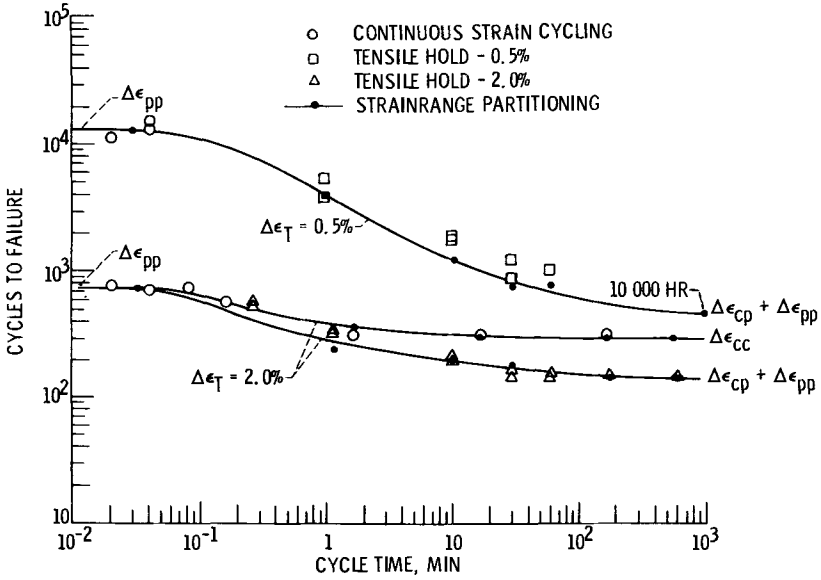


FIG. 8—*Application of strainrange partitioning to data for 304 stainless steel tested at 1200 F (650 C) (taken from Ref* 21).

mation, however, can be obtained in a short time if the strainrange partitioning concept is used.

An analysis using the strainrange partitioning approach was also made of the data presented by Jaske et al [*13*] at this symposium for the alloys Incoloy 800 and Type 304 stainless steel. These authors investigated the validity of the concept of time- and cycle-fraction addition. In these tests, involving holdtimes in tension, they actually measured the stress relaxation during the hold period and made computations based on the static creep-rupture properties. They also computed the cyclic ratios based on pure fatigue. Their results, shown in Fig. 4 of their report, shows large discrepancies between predicted and experimental lives. To analyze the results on the basis of strainrange partitioning, information on measured stress relaxation was used to compute the $\Delta\epsilon_{cp}$ strainrange component. The results are shown in Fig. 9. Here, measured fatigue life is plotted against predicted life. Using the time-and cycle-fraction approach, lives as much as 20 times higher or 5 times lower than predicted were observed, as seen in Fig. 9*a*. Using the strainrange partitioning approach the experiments agreed with the predictions within factors of two, as seen in Fig. 9*b*.

Fatigue Mechanism and Environmental Effects

Both the mechanism of fatigue and environmental effects have received considerable attention at this symposium. These are both broad subjects, and the strainrange partitioning concept can contribute to both in many ways; two facets of the subject will be discussed briefly.

Internal Ratchetting—Because of the dual deformation system hypothesized in the strainrange partitioning concept, it becomes possible for an internal ratchet to develop when a $\Delta\epsilon_{cp}$ or $\Delta\epsilon_{pc}$ component is present:

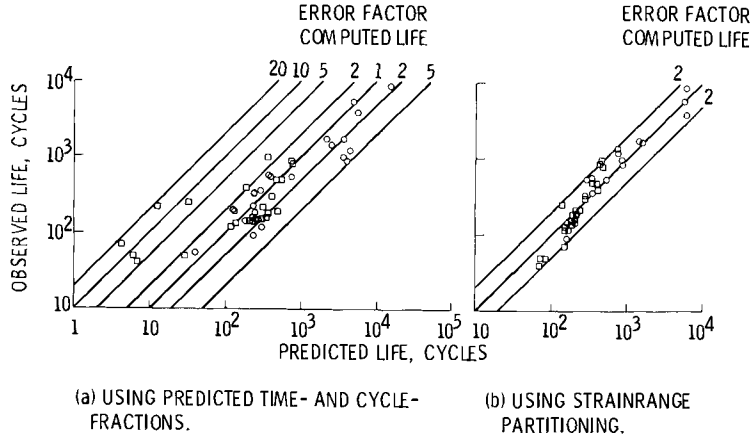


FIG. 9—*Predictability of life relaxation results for tensile strain holdtime cycles. Data on Incoloy 800 and 304 stainless steel (taken from Ref* 13*) for tensile strain holdtime cycles.*

tensile strain accumulates within one deformation system; compressive strain accumulates within the other system. Although externally there may be little net geometrical change after each cycle, the internal effect may be substantial due to cycle-by-cycle strain accumulation. A repetitive $\Delta\epsilon_{cp}$ cycle becomes, for example, more like a continuous monotonic tensile creep-rupture test, since every cycle adds tensile creep. Likewise a repetitive $\Delta\epsilon_{pc}$ cycle simulates a conventional tension test. It is for this reason that the $\Delta\epsilon_{pc}$ component is normalized to the tensile ductility D_p in Eq 8 of Fig. 4*b*, and the $\Delta\epsilon_{cp}$ component is normalized to the creep ductility D_c in Eq 10 of Fig. 4*b*.

To show the detrimental nature of internal ratcheting as compared to balanced strain reversal, consider a simple illustration: a material with a tensile ductility of 0.50 is subjected to a reversed plastic deformation of 0.01 per cycle. Under completely reversed plasticity, using Eq 7 of Fig. 4*b*, the expected life would be 420 cycles. If no plasticity reversal occurred and a series of tensile strains of 0.01 were imposed, obviously only 50 cycles would exhaust the tensile ductility. We see, therefore, that in reversed plasticity there is a certain amount of "healing" that takes place during every cycle, as long as the reversed strain is "undoing" some of the damage due to the strain that had occurred in the forward half of the cycle. On the other hand, if the reversal takes place along a different system, the healing is not possible, and we will get a ratchetting effect in each of the directions. This is a possible cause for reduced life in either the $\Delta\epsilon_{cp}$ or the $\Delta\epsilon_{pc}$ component. For example, if we consider $\Delta\epsilon_{cp}$, tensile creep occurs within one system, but the reversal is along another system and, therefore, does not do any healing. The next cycle of loading simply adds tensile creep during the tensile half of the cycle upon the creep that had already occurred in the previous cycle. Thus, the material ratchets in tensile creep along one system and in compressive plasticity along the other system until the material reaches its creep ductility in tension or its plasticity ductility in compression. Failure then occurs in a manner analagous to that experienced in a monotonic loading test. If this were the exact case, however, the exponent in the $\Delta\epsilon_{cp}$ and $\Delta\epsilon_{pc}$ relationships would be -1 rather than -0.8. Therefore, some "healing" due to the reversal does occur if we assume that the -0.8 exponent is an appropriate one. Nevertheless, the concept of strainrange partitioning gives us better insight into the individual effects of the different strain components. When further information is available to derive a better universalized relationship, we may be able to quantify this effect more accurately.

Inert Environment Effects—Surface interaction with the environment is an additional time-dependent variable in high-temperature fatigue. Thus, when frequency is lowered, not only is there more time for creep but also more time is available for oxidation or other surface interaction. In Fig. 13 of Coffin's paper [*22*] he shows that for A286 in vacuum at high temperature

the effect of frequency becomes very small (except at the very lowest frequencies used); in air the effect is very substantial. In his Fig. 15 he also shows that when plots of inelastic strainrange versus life are made of high-temperature data obtained on many materials in an inert environment the data fall within the same scatterband as room-temperature data on a variety of materials. These and other observations made by Coffin in his paper provide convincing evidence of the importance of oxidation on fatigue life.

The role of creep relative to that of environment needs further clarification. Coffin's plot (Fig. 15 of Ref *22*) does not normalize the strain data relative to ductility, nor are frequencies cited; thus, the wide scatterband (a factor of about 20 in life for a given strainrange) can hide subtleties in behavior that might be more visible on a suitable plot. That a creep effect does occur at high temperature and low frequency is apparent from his Fig. 13 where the tests at 0.0045 and 0.045 Hz do fall below the "least squares" line for the higher frequency. His joint report with Solomon [*19*] also demonstrates higher crack growth rates at reduced frequencies even in an inert environment.

Unbalanced strain of the $\Delta\epsilon_{cp}$ type also tends to emphasize the creep effect. Figure 10 shows an analysis of the data presented by Sheffler and Doble [*23*] on the tantalum alloys T-111 and ASTAR 811C. These tests were conducted in a hard vacuum of 10^{-8} torr, so no environmental interaction is to be expected. The dotted lines in the figure represent Coffin's scatterband. Two types of tests are shown for each alloy, one in which creep and plasticity appear only as balanced strainranges, that is, for the case of continuous cycling wherein only $\Delta\epsilon_{pp}$ and $\Delta\epsilon_{cc}$ occur. These data fall within Coffin's scatterband, although each individual material presents

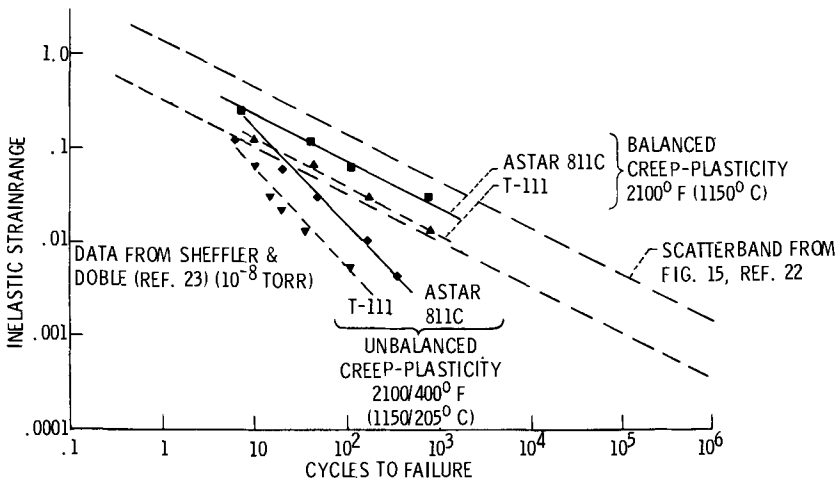


FIG. 10—*Effect of unbalanced creep on life relationships in vacuum.*

its own line of behavior. On the other hand, when unbalanced creep-plasticity occurs, that is, when $\Delta\epsilon_{cp}$ is present (which was introduced by conducting in-phase, thermal-mechanical cycling tests) the lines deviate considerably from the scatterband. Their slope is approximately -0.8, as would be expected according to our simplified relationships for these strain components. These curves demonstrate that even in vacuum environment unbalanced creep-plasticity can cause significant reductions in life.

At this time there is still considerable question regarding the relative roles of creep and environment on high-temperature fatigue life. The strainrange partitioning concept can be helpful in defining the effects by suggesting experiments, such as just cited, where the effects are expected to be greatest, so that the studies can be more definitive. Furthermore, it should be emphasized that even if the environment effect is the dominant one, it would not invalidate the utility of the strainrange partitioning method, since the basic life relationships for its use, in any case, would be obtained under the environment in which it is to be applied. Even if all the life relationships nearly coincide in an inert environment, the approach would still be valid. Finally, it should be emphasized that most practical applications do involve a reactive environment.

Fracture Mechanics and Crack Growth

Next, the application of strainrange partitioning to fracture mechanics and crack growth will be considered. Recent studies of crack growth have made strong use of concepts of elastic fracture mechanics. In many cases, the conditions for crack growth agree reasonably with those hypothesized in the development of the laws of elastic fracture mechanics, and, in such cases, it is appropriate to use the stress intensity in the equations for crack growth. Several applications involving this approach have appeared at this symposium, and some very interesting results have been presented. At the higher temperatures, where large components of inelastic strain are likely to be present, the concepts of elastic fracture mechanics, as derived, must be modified. Several examples have appeared at this symposium wherein plastic strainrange has been used in place of stress when applying fracture mechanics laws to crack growth. These follow the lead of earlier work by Boettner et al [*24*] where the parameter $\Delta\epsilon_p\sqrt{l}$ was used in place of $\Delta\sigma\sqrt{l}$ in the crack growth equations. In Ref *4* the $\Delta\epsilon_p\sqrt{l}$ parameter was also applied to explain the crack growth laws and the life relationships in low-cycle fatigue. Strainrange partitioning concepts now help recognize that in dealing with high-temperature, low-cycle fatigue at least four strainrange components are thought about, not just the plastic flow that was adequate when dealing with low-temperature plasticity.

Before proceeding to crack growth, however, it is desirable to consider the role of strainrange partitioning in explaining the crack initiation equations as well. In Ref *4*, it was demonstrated that the cycles to both

crack initiation and to final fatigue fracture of a laboratory specimen tested in axially reversed loading could be related to plastic strainrange according to a simple power law. When several types of inelastic strainrange components are possible, a different crack initiation law must be stated for each. Thus, it can be written

$$\begin{aligned} N_0]_{pp} &= A_1 (\Delta\epsilon_{pp})^{a_1} \\ N_0]_{cp} &= A_2 (\Delta\epsilon_{cp})^{a_2} \\ N_0]_{pc} &= A_3 (\Delta\epsilon_{pc})^{a_3} \\ N_0]_{cc} &= A_4 (\Delta\epsilon_{cc})^{a_4} \end{aligned} \quad \ldots\ldots\ldots\ldots\ldots\ldots (11)$$

Each of these relationships expresses the number of cycles to crack initiation in terms of the pertinent strainrange component, assuming it to be the only component present. When two or more components are present the relationships must somehow be combined in a manner as yet to be determined, perhaps using the same concepts as those expressed earlier in Eqs 2 to 6 in Fig. 2.

Consider next the equations governing the initial stages of crack growth. First, however, it should be explained that crack initiation is a rather ill-defined term; it is the number of cycles required to develop a crack of arbitrarily specified size. Generally, this size is rather small; in fact, it is too small for the stress field developed in its vicinity to meet the complete requirements of the laws of fracture mechanics in defining this stress field. Therefore, considering the early stages of crack growth, that is, before the crack has grown large enough to develop its own characteristic full stress field, it might be reasonably concluded that the same factors that cause the crack to initiate to its current small size will also govern the growth of the crack during the next few cycles of loading. Thus, an equation expressing the fact that for each strainrange component dl/dN is roughly inversely proportional to the number of cycles to initiate the crack. The resulting equations become

$$\frac{dl}{dN} \propto \frac{1}{N_o^{\,m}}$$

or

$$\begin{aligned} \left.\frac{dl}{dN}\right]_{pp} &= B_1 (\Delta\epsilon_{pp})^{b_1} \\ \left.\frac{dl}{dN}\right]_{cp} &= B_2 (\Delta\epsilon_{cp})^{b_2} \\ \left.\frac{dl}{dN}\right]_{pc} &= B_3 (\Delta\epsilon_{pc})^{b_3} \\ \left.\frac{dl}{dN}\right]_{cc} &= B_4 (\Delta\epsilon_{cc})^{b_4} \end{aligned} \quad \ldots\ldots\ldots\ldots\ldots\ldots (12)$$

Here

$$b_1 \approx -a_1,\ b_2 \approx -a_2,\ b_3 \approx -a_3, \text{ and } b_4 \approx -a_4$$

and

$$\frac{B_1}{A_1} = \frac{B_2}{A_2} = \frac{B_3}{A_3} = \frac{B_4}{A_4}$$

The fact that $m \approx 1$ is verified by thermal fatigue tests reported by Spera et al [*25*].

Consider, finally, the later stages of crack growth, when a fully developed crack has already appeared, and when the $\sqrt{l}$ term can be introduced, analogous to equations derived from elastic fracture mechanics. These equations become

$$\left.\frac{dl}{dN}\right]_{pp} = C_1 (\Delta\epsilon_{pp} \sqrt{l})^{c_1}$$

$$\left.\frac{dl}{dN}\right]_{cp} = C_2 (\Delta\epsilon_{cp} \sqrt{l})^{c_2}$$

$$\left.\frac{dl}{dN}\right]_{pc} = C_3 (\Delta\epsilon_{pc} \sqrt{l})^{c_3}$$

$$\left.\frac{dl}{dN}\right]_{cc} = C_4 (\Delta\epsilon_{cc} \sqrt{l})^{c_4} \quad \ldots\ldots\ldots\ldots\ldots\ldots (13)$$

Both Eqs 12 and 13, of course, must be extended to cases where two or more strainrange components are present and when the hysteresis loop of the bulk material surrounding the crack does not close after each cycle.

Although a number of papers have appeared at this symposium presenting data on crack growth, it has not been possible, because of time limitations, to examine the results in the light of the foregoing equations. Furthermore, no experience is as yet available with their application, and the numerical magnitude of the constants are totally unknown. Finally, it should be recognized that complicated conditions such as residual stresses can develop at the crack tip when a complex history of temperature and load is imposed. Such complications are characteristic of any treatment by fracture mechanics principles, so the validity of the equations should not be judged on the basis of *ad hoc* tests not expressly designed for the purpose. The merit of the strainrange partitioning concept is that it can suggest relationships such as Eqs 2 to 4—relationships that might otherwise elude us—and test programs that might eventually lead to a unified treatment of crack initiation and growth under the complex conditions commonly encountered in practical high-temperature applications. Only after a carefully conceived test program has been conducted can the validity of the approach be evaluated. And even if the results are negative, we will then be in a better position to hypothesize a more proper approach.

Thermal Fatigue

Another subject that has received considerable attention at this symposium is that of thermal fatigue. Spera [*10*] used essentially the time-and-cycle-fraction summation concept to analyze a number of cases of thermal fatigue. In his treatment compressive and tensile stresses were assumed to be equally damaging when determining the creep time ratio. Although excellent results were obtained in all the cases he presented, it has been already indicated that the approach using the time and cycle fraction summation may result in error in some cases (see Fig. 9*a*). Treatment of creep damage due to compressive stress also remains a moot question. The strainrange partitioning approach is helpful in these respects because the stresses enter into the evaluation only to the extent that they influence the strainrange components that develop. Assuming that strainranges can be established either by experimentation or computation, both these complexities vanish. Therefore, how strainrange partitioning can help in unifying the treatment of thermal fatigue will be indicated.

Rather than using a complex structure it is convenient to use a three-bar assembly (Fig. 11*a*) that will incorporate the basic features of performance without the complexity that attends treatment of a real component. The interior bar is massive and usually constrains thermal expansion or contraction of the two outer bars designated as "edges." All three bars are subject to heating and cooling. The assembly is, in a sense, analogous to a turbine blade wherein the outside bars represent the edges of the blade and the inside bar represents the massive center of the blade. When the turbine

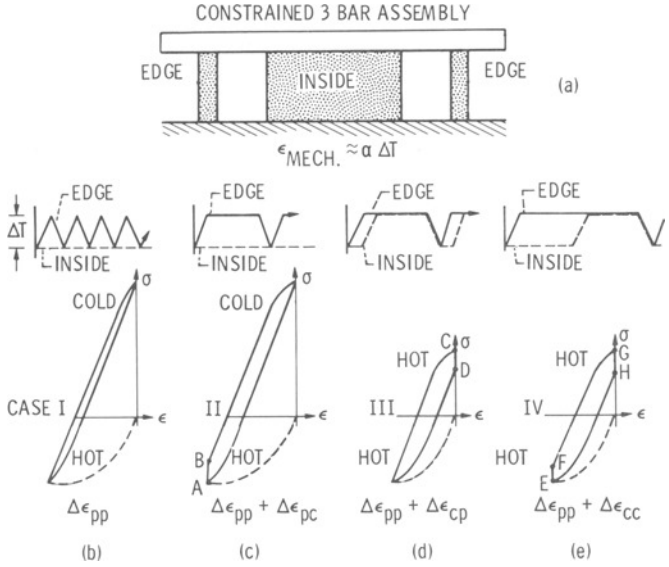


FIG. 11—*Strainrange components produced in edge by several thermal histories.*

blade is subjected to hot gas, the outside edges are first to heat. Their expansion, of course, is constrained by the massive interior bar which is slow to heat, or may never heat up, depending on external conditions imposed. Thus, inelastic flow occurs in compression on the outer edges upon the first loading. What happens to the strains induced in the edges in subsequent time periods will depend on the manner in which the temperature is varied both in the edges and in the inside bar.

Several cases are considered here. In Case I, shown in Fig. 11*b*, it is assumed that the edges are heated and cooled rather rapidly but that the inside massive bar maintains its temperature value throughout the history. This situation is analogous to conventional thermal fatigue type tests wherein the test specimen is constrained between end plates and is repeatedly heated and cooled. If the frequency is reasonably high, the edge bars will simply alternate between tensile and compressive loading, being at all times constrained by the interior bar. The inelastic strainrange developed, which is of the $\Delta\epsilon_{pp}$ form, is shown in Case I of the figure.

In Case II (Fig 11*c*, a hold period is applied to the edge bars after they are heated. Plastic flow occurs immediately upon heating, developing compressive stress and plastic strain. However, as this strain is held at high temperature, relaxation occurs as shown by the line AB, resulting in compressive creep. When the temperature of the edge is later reduced, tensile plastic flow takes place, but no creep can occur because the reduced temperature is low. The inelastic strainranges for this case are, therefore, plastic reversed strain $\Delta\epsilon_{pp}$ and compressive creep balanced by tensile plasticity $\Delta\epsilon_{pc}$.

In Case III (Fig. 11*d*) the edge bars are held at high temperature for an appreciable period just as in Case II. However, the interior bar is now heated to the equilibrium temperature of the edges. This is typical of what might occur in an uncooled turbine blade subjected to extended steady operation at high temperature. A lag occurs, however, between the time when the temperature of the inside bar reaches its maximum value and the time the outside bar reaches its equilibrium value. Thus, compressive plastic flow occurs in the edge bars while their temperature has already achieved maximum value and while the inside bar temperature has not yet begun to rise. No time is allowed, however, for creep. When the inside bar finally reaches the temperature of the edge, it must force the edge bars to flow plastically in tension, since they had already become shortened by plastic compression in their earlier temperature history. A tensile stress develops at C when the inside bar has reached its maximum value. Since, as shown in the figure, both the inside and outside bars are maintained at high temperature for an extended period, creep relaxation of the tensile stress occurs along the line CD producing a $\Delta\epsilon_{cp}$ type of deformation wherein creep occurs in tension but is balanced later in compressive plastic flow.

Finally, we consider Case IV (Fig. 11*e*) wherein, as in Case III, the interior bar reaches an equilibrium temperature equal to that of the edge bars; however, the temperature of the interior is constrained from rising rapidly. A "lag" period is introduced during which the edge temperature is maintained at a high value while the inside bar is still cold. While the inside bar is cold and the edge is hot, compressive plastic flow and stress relaxation occurs along *EF*, as in Case II. Later, when both bars reach the same high temperature, tension occurs in the edge, in the manner already described in connection with Case III. Because of the high-temperature tensile stress, relaxation occurs along *GH*, balancing the creep relaxation *EF*. Thus, the strainrange components present are $\Delta\epsilon_{pp}$ and $\Delta\epsilon_{cc}$, as shown in the figure.

The foregoing discussion demonstrates that, depending on the pattern, any combination of these strain components associated with strainrange partitioning may develop. It is clear, therefore, that because of the diversity of strain types that can be developed, depending on test conditions, a wide variety of results can be expected. Indeed, this has been the experience in thermal fatigue testing, namely, that test results are sensitively related to test conditions and meaningful results can only be obtained by simulating service conditions very closely.

This very point was made during the symposium at a session of the Low-Cycle Fatigue Subcommittee of ASTM Committee E-9. The question related to the possibility of standardizing fluidized bed thermal fatigue tests, and the conclusion drawn was that the diverse results obtainable from such tests make standardization difficult at this time. Perhaps the strainrange partitioning concept can be helpful here. By designing the tests so as to favor each of the basic strainrange components (or perhaps only the most mild and most severe as extremes), the relative behavior of materials can be evaluated under easily analyzable conditions. Behavior under more complex conditions could be possibly synthesized from the basic tests.

Another illustration of the usefulness of the strainrange partitioning concept is shown in Fig. 12. Here the potential beneficial effect of "phasing" the temperature is illustrated. Reference is made to Case IV of the Fig. 11*e* wherein the temperature of the interior of the bar is held back sufficiently long to allow compressive creep to occur. Such compressive creep can then balance the inevitable tensile creep that occurs when the inside bar reaches its maximum temperature coincident with the edge and is held at this value for a long time. Thus, Fig. 12 illustrates the fact that if creep can be forced to occur in compression by proper temperature phasing between the component parts of an assembly, and, if in this way unavoidable tensile creep that occurs later in the cycle can be balanced, it is conceivable that an increase in life could be achieved even though the hysteresis loop is actually widened. A balanced $\Delta\epsilon_{cc}$ strainrange component may be less damaging for some materials than a smaller value of the unbalanced strainrange $\Delta\epsilon_{cp}$. What is plotted on the vertical axis in the lower half of Fig. 12 is the

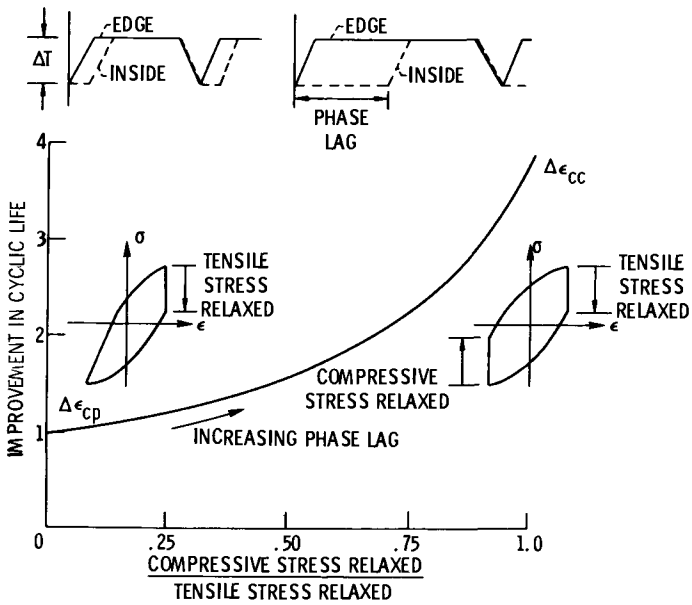


FIG. 12—*Potential benefit of temperature phasing.*

dimensionless improvement in cyclic life as a function of a measure of degree of balance of the compressive and tensile creep strains. These computations use as a parameter the ratio of relaxed compressive stress to the relaxed tensile stress. Of course, the relaxed compressive stress is achieved by the temperature phasing. It is seen that, if the relaxed compressive stress can be made equal to the relaxed tensile stress, life could be increased by as much as a factor of four for a material complying with the basic behavior shown in Fig. 4*b*. The computations are not intended to represent any particular realistic physical situation. However, they do have meaning. For example, the implication is that if tensile creep must occur at the edge of a turbine blade due to hold period at high temperatures of both the interior and exterior parts of the blade, then perhaps by controlling the rate at which the temperature of the interior portion of the blade is increased, a favorable balanced inelastic strain condition can be developed, thus improving the life. Such temperature control might be possible by proper cooling, by surface coatings, or by conductivity control to give the necessary phase relationship between the edge temperature and the inside temperature. Again, the method illustrates a case wherein other approaches such as the time and cycle fraction approach, or the frequency modified life approach, would not suggest that a life improvement is possible in this temperature phasing procedure. It is certainly food for thought and another opportunity to check the validity of the strainrange partitioning concept.

The paper of Lawton and Bynum [27] presented at this symposium lends some support to the concept just discussed. They conducted cyclic deformation tests at 1050 F (565 C) on welded furnace panels. In one series of tests, a 5-min hold period was introduced in one direction of the cycle, and a 5-min hold period was introduced subsequently in both directions in a second series of tests. The latter involved favorably balanced creep strain cycles, and these tests lasted four times longer on the average than the unbalanced series. Only the strainrange partitioning concept would have suggested the possibility of a life improvement under these conditions; other approaches would have predicted a life reduction.

Structural Analysis and Design Codes

Let us consider now the application to design codes. The strainrange partitioning approach has something to say on this subject as well. It will identify what types of tests should be conducted to properly characterize a material. Not only will it directly provide suggestions as to the types of tests to be run, but the amount of data required might be considerably reduced. For example, if the strainrange life relationships are insensitive to temperature, for materials of interest, higher test temperatures can be used to induce the required creep in less time. The method also suggests that information regarding crack initiation and crack propagation under the different types of strain loadings is required in order to treat all situations that can be realistically encountered.

How to gear the complexity of the analysis with the type of information used in design is also suggested by the strainrange partitioning approach. To illustrate, suppose the most simplified type of analysis is made, and all that can be established from the analysis is the total inelastic strainrange. In that case, if the nature of the component strainranges is unknown, the method suggests that, for conservatism, one would have to use the lowest bounds associated with the most damaging type of strainrange that could conceivably occur. On the other hand, suppose only a limited analysis is made, and it is established that certain strain components are present, but that other types of strainranges are excluded. Then it would be appropriate to use the bounds associated only with the strainrange components present. For example, if there is no $\Delta\epsilon_{cp}$ present, then one should not use N_{cp} as a lower bound. In connection with continuous strain cycling, the worst situation develops when only the $\Delta\epsilon_{cc}$ strainrange component is present; then, of course, only the $\Delta\epsilon_{cc}$ component need be used in first approximation calculations. Finally, if a rigorous analysis is made, the pertinent material characteristics that are required for the analysis are used. Knowing the magnitude of each strainrange component present, it is then possible to determine the life accurately. Of course, the magnitude of each strainrange must first be established. This may require a considerable amount of computation, no different from the computations that would be required

for application of other methods of analysis. However, the degree of accuracy required might be considerably reduced when strainrange partitioning is to be applied. Since the total strainrange is often quite accurately known (for example, in thermal stress problems, when the thermal constraint is known), the major purpose of the analysis is to partition the strainrange. But life is not extremely sensitive to small changes in the partitioning; therefore, coarse calculations may suffice. On the other hand, if the summation of the time and cycle fractions are used as a measure of damage, stresses must be determined to a high degree of accuracy because the creep rupture life is very sensitively related to stress.

Required Future Program

In the discussion up to now, a simplified and optimistic approach is presented in hopes of encouraging an acceptance of the concept proposed and a recognization of its potential usefulness. It is realized, of course, that much needs to be done if the method is to be developed to its full potential. Several directions along which further work is required will now be outlined. Obviously, many materials should be examined to determine the utility, strengths, and limitations of this basic method of approach. These should include not only materials of different compositions and different strengthening mechanisms (for example, dispersion strengthened compared to solution strengthened), etc., but materials that have different grain structures (directionally solidified, random polycrystalline), eutectic, and other composite structures. Once a large number of materials have been investigated, it may be possible to refine the universalized relationships (Eqs 7 to 10 shown on Fig. 5).

Separation of the total cyclic life into its crack initiation and crack propagation phases is another important objective. The laws of crack initiation and propagation must be established for situations involving not only single strainrange components, when individually present, but also when several components are collectively present.

We must also learn the most practical methods of partitioning complex strain cycles into their basic components. One method based on an experimental approach has been mentioned already. This method can be extended to consider more complex cases. For example, if other components than $\Delta\epsilon_{pp}$ and $\Delta\epsilon_{cc}$ are present, the same idea can be used, namely, by studying the cycle at two frequencies of loading. First, the stresses would be determined experimentally by traversing the temperature and strain history in real time. Then the plastic strain associated with each half of the cycle could be individually established by traversing both the temperature and stress history rapidly to avoid creep. During rapid loading, only plastic strains would develop; subtraction of the plastic strain from the real-time inelastic strain would lead to the creep component. Once the strain components are known for each half of the cycle, the net strainranges for the

complete cycle can be determined by properly combining the strains according to the basic definition of each strainrange component. An alternate approach is to seek a rheological model, a model consisting of springs, sliders, and dash pots by which the basic behavior of the material can be simulated. The strains associated with each type of cycle can thus be determined directly from the model. Finally, the more conventional approach is to formulate the basic and complete stress-strain analysis using the constitutive relationships and equilibrium and compatibility equations. Analysis is then the same as if other methods of life computation were to be used. Then the strain components would be determined—how much is creep, how much is plastic flow, how much is in tension, how much is in compression—and then they would be combined in a way so as to determine the net values $\Delta\epsilon_{pp}$, $\Delta\epsilon_{pc}$, $\Delta\epsilon_{cp}$, and $\Delta\epsilon_{cc}$ in order to substitute into the life relationships.

A problem not yet discussed is what happens when the elastic component is large relative to the inelastic strain. The cases thus far treated have been those in which most of the strain involved is inelastic. In a sense this problem is analogous to the treatment in the universal slopes equation of the elastic and plastic components. However, in the present case we must consider four inelastic components. When these components are very small, it obviously will not be appropriate to use an experimental approach to measure them, but, instead, they may be computed by analytical procedures. In a sense, when the analysis is made on the basis of time and cycle fractions, the individual creep strains that occur during the various stress loadings are being computed. Then the results of such computations might be applied in connection with strainrange partitioning. The damage rules, the method of combining not only the components that occur within a given cycle of loading but components of strain that vary from cycle to cycle, must also be investigated.

Material behavior which changes as a function of time and temperature, oxidation environments, coatings, and radiation must also be extensively investigated. Whether the strainrange partitioning approach is valid when complex histories of numerous variables are involved is, of course, very important. How to use basic data to make effective computations is equally important.

The mechanistic studies, that is, the studies of the deformation and fracture mechanisms involved, still require considerable investigation. How the dual mode of deformation can explain reduced life in terms of ratchetting is outlined. Obviously, this is a highly simplified picture. What happens during the deformation process and how these deformation components interact with each other must be studied. The environmental effect and how it can introduce behavior patterns that are not anticipated by ordinary analysis is also of interest and should be considered. A host of other variables, a few of which are multiaxial effects, applications to ratchetting, the

effects of mean stress or mean strain, and numerous other parameters, of course, must also be studied. Before this method, or any other, can be accepted as a unified approach much effort will be required; however, a useful start has been made.

Concluding Remarks

An attempt has been made to present a case for the potential applicability of the strainrange partitioning concept to a host of aspects of the treatment of high-temperature fatigue. It has been the contention in this summary talk that this concept provides a framework around which treatment of high-temperature metal fatigue could be perhaps unified. The view presented is admittedly partisan. No attempt has been made to be objective, nor have analogous treatments for alternative points of view been presented. However, it can be said that the viewpoint expressed here was not hurriedly formulated. Over the years, the author has been associated with various attempts to develop suitable methods of analysis. Already cited is the progression of these efforts, starting with the 10 percent rule and its modifications, the introduction of cyclic-creep curves to be used in conjunction with the summation of time and cycle fractions, and various other methods. The view on the potential of strainrange partitioning comes, therefore, after a considerable amount of concentration on the subject. At this point, I am reasonably convinced of its utility, but, of course, it is recognized that further work is required to bring the method to full fruition. We at the NASA-Lewis Research Center intend to pursue the approach vigorously; hopefully others will join with us in completing the program.

References

[1] Halford, G. R., Hirschberg, M. H., and Manson, S. S., see p. 658 of this symposium.
[2] Polhemus, J. F., Spaeth, C. E., and Vogel, W. H., see p. 625 of this symposium.
[3] Manson, S. S., *International Journal of Fracture Mechanics*, Vol. 2, No. 1, 1966, pp. 327–363.
[4] Manson, S. S., *Experimental Mechanics*, Vol. 5, No. 7, July 1965, pp. 193–226.
[5] Manson, S. S. and Halford, G. R. in *Proceedings*, International Conference on Thermal and High-Strain Fatigue, The Metals and Metallurgy Trust, London, 1967, pp. 154–170.
[6] Coffin L. F., Jr., in *Proceedings*, Air Force Conference on Fatigue and Fracture of Aircraft Structures and Materials, AFFDL 70–144, H. A. Wood, R. M. Bader, W. J. Trapp, R. F. Hoener, and R. C. Donat, eds., Air Force Flight Dynamics Laboratory, Sept. 1970, pp. 301–311.
[7] Berling, J. T. and Conway, J. B., *Metallurgical Transactions*, Vol. 1, 1970, pp. 805–809.
[8] Robinson, E. L., *Transactions*, American Society of Mechanical Engineers, Vol. 74, 1952, pp. 777–780, discussion, pp. 780–781.
[9] Taira, S. in *Creep in Structures*, N. J. Hoff, ed., Springer Verlag, Berlin, 1962, pp. 96–119, discussion, pp. 119-124.
[10] Spera, D. A., see p. 648 of this symposium.
[11] Manson, S. S., Halford, G. R., and Spera, D. A. in *Advances in Creep Design*, A. E. Johnson Memorial Volume, A. I. Smith and A. M. Nicholson, eds., Applied Science Publishers Ltd., London, 1971, pp. 229–249.

[12] Campbell, R. D., "Creep/Fatigue Interaction for 304 Stainless Steel Subjected to Strain Controlled Cycling with Hold Times at Peak Strain," presented at First National Congress on Pressure Vessels and Piping, American Society of Mechanical Engineers, Paper No. 71-PVP-6, San Francisco, May 1971.
[13] Jaske, C. E., Mindlin, H., and Perrin, J. S., see p. 365 of this symposium.
[14] Manson, S. S., *Machine Design*, 21 July 1960, pp. 161–167.
[15] Manson, S. S., Halford, G. R., and Hirschberg, H. M., *Design for Elevated Temperature Environment*, American Society of Mechanical Engineers, 1971 pp. 12–24, discussion pp. 25–28.
[16] Manson, S. S. and Halford, G. R., "Some New Relations and Procedures for Applying Strainrange Partitioning to High Temperature Metal Fatigue," proposed NASA Technical Note.
[17] Challenger, K. D. and Moteff, J., see p. 69 of this symposium.
[18] Berling, J. T. and Slot, T. in *Fatigue at High Temperature, ASTM STP 459*, American Society for Testing and Materials, 1970, pp. 3–30.
[19] Solomon, H. D. and Coffin, L. F., Jr., see p. 112 of this symposium.
[20] Opinsky, A. J., see p. 451 of this symposium.
[21] Conway, J. B., Berling, J. T., and Stentz, R. H., see p. 637 of this symposium.
[22] Coffin, L. F., Jr., see p. 5 of this symposium
[23] Sheffler, K D. and Doble, G. S., see p. 491 of this symposium.
[24] Boettner, R. C., Laird, C., and McEvily, A. J., Jr., *Transactions*, American Institute of Mining, Metallurgical, and Petroleum Engineers, Vol. 233, 1965, pp. 379-387.
[25] Spera, D. A., Howes, M. A. H., and Bizon, P. T., "Thermal Fatigue Resistance of 15 High-Temperature Alloys Determined by the Fluidized-Bed Technique," NASA TM X-52975, National Aeronautics and Space Administration, 1971.
[26] Hosbons, R. R., see p. 482 of this symposium.
[27] Lawton, C. W. and Bynum, J. E., see p. 699 of this symposium.

DISCUSSION

H. D. Solomon[1] *and L. F. Coffin, Jr.*[1] *(written discusssion)*—The writers of this discussion have contributed two papers to this symposium wherein it was emphasized that environment plays an important role in high-temperature fatigue.[2,3] It is our feeling that this effect is not accounted for in strainrange partitioning, and, because of this, significant errors can be introduced wherever environment rather than creep is the principal source of life degradation. To bring out this point quantitatively, we have attempted to apply the prediction procedures of strain partitioning outlined in Mr. Manson's paper to fatigue test results obtained in our laboratory

[1] Technical staff, Metallurgy and Ceramics Laboratory, Research and Development Center, General Electric Company, Schenectady, N. Y. 12301.
[2] See p. 5.
[3] See p. 112.

for A286 at 1100 F at several frequencies and strainranges with a triangular waveform. For this waveform at any arbitrary frequency ν,

$$\Delta\epsilon_{cc} = \Delta\epsilon_p - \Delta\epsilon_{pp} \quad \ldots\ldots\ldots\ldots\ldots\ldots (14)$$

where these quantities are defined in Manson's paper. Following the method of partitioning the strainranges described in Manson's paper, $\Delta\epsilon_{pp}$ and $\Delta\epsilon_{cc}$ can be determined at any frequency ν by comparing the plastic strainrange at this frequency with the plastic strainrange observed for the same stress range but with a high frequency $\nu = \nu_{pp}$. These quantities, however, can also be calculated immediately by use of the frequency modified stress range, nonelastic strainrange relationship.[2] This relationship is reproduced here as Eq 15, that is,

$$\Delta\sigma = A\Delta\epsilon_p{}^{n'}\nu^{k_1} = A\Delta\epsilon_{pp}{}^{n'}\nu_{pp}{}^{k_1} \quad \ldots\ldots\ldots\ldots\ldots (15)$$

The coefficients A, n', and k_1 have been previously determined and are given in Table 1 of footnote 2. The right hand term in Eq 15 applies when $\Delta\epsilon_p = \Delta\epsilon_{pp}$. Thus from Eq 15

$$\Delta\epsilon_p = \Delta\epsilon_{pp}\left(\frac{\nu_{pp}}{\nu}\right)^{k_1/n'} \quad \ldots\ldots\ldots\ldots\ldots\ldots (16)$$

and from Eq 14

$$\Delta\epsilon_{cc} = \Delta\epsilon_{pp}\left[\left(\frac{\nu_{pp}}{\nu}\right)^{k_1/n'} - 1\right] \quad \ldots\ldots\ldots\ldots\ldots\ldots (17)$$

Assuming now the situation when $\Delta\epsilon_{pp}$ is 10 percent of $\Delta\epsilon_p$, from Eq 14 $\Delta\epsilon_{cc} = 9\Delta\epsilon_{pp}$. Hence from Eq 17 for this situation

$$\nu = \nu_{pp} \times (10)^{-n'/k_1} \quad \ldots\ldots\ldots\ldots\ldots\ldots (18)$$

Here ν is the frequency required for $\Delta\epsilon_{cc} = 9\Delta\epsilon_{pp}$. From Table 1 of footnote 2, $k_1 = 0.0026$ and $n' = 0.122$ for A286 at 1100 F, and Eq 18 becomes

$$\nu = 1.2 \times 10^{-47}\nu_{pp} \quad \ldots\ldots\ldots\ldots\ldots\ldots (19)$$

Letting $\nu_{pp} = 100$ cpm, from Eq 19, the frequency when $\Delta\epsilon_{pp}$ is only 10 percent of $\Delta\epsilon_p$ is 1.2×10^{-45} cpm or one cycle in 1.53×10^{39} years. One can also calculate the fatigue life for this frequency based on Eq 16 from footnote 2 or

$$\Delta\epsilon_p = C_2(N_f\nu^{k-1})^{-\beta} \quad \ldots\ldots\ldots\ldots\ldots\ldots (20)$$

and

$$N_f = \left(\frac{\Delta\epsilon_p}{C_2}\right)^{-1/\beta}\nu^{1-k} \quad \ldots\ldots\ldots\ldots\ldots\ldots (21)$$

From Table 1, $C_2 = 1.32$, $\beta = 0.97$, and $k = 0.65$ and letting $\Delta\epsilon_p = 0.01$, $N_f = 5.8 \times 10^{-15}$ cycles.

It is quite clear that strain partitioning is predicting meaningless results in this case. If $\Delta\epsilon_{pp} = 0.75\ \Delta\epsilon_p$ is considered, the result is somewhat more credible but still not in agreement with the supplementary data of Manson's Fig. 6. Using the same values for k_1, n', and ν_{pp}, Eqs 14 to 20 predict that the frequency at which $\Delta\epsilon_{pp} = 0.75\ \Delta\epsilon_p$ is 2.5×10^{-6} Hz as compared to Manson's value of greater than 5×10^{-4} Hz.

The reason for these discrepancies is that in our tests we have found that, for A286 at 1100 F, the effect of frequency on the stress range for a given nonlinear strain is very small, at least over the frequency range of 0.01 to 100 cpm; and hence, a change of frequency produces a negligible change in nonlinear strain. Yet a significant decrease in fatigue life does occur in this frequency range as shown in our work, and in Manson's Fig. 6. The effect in this range is due only to the environment as verified by high-vacuum experiments.[2,3]

Many materials may indeed have a reasonable sensitivity to stress range with frequency change to allow a determination of $\Delta\epsilon_{cc}$ from $\Delta\epsilon_p$, but the question still persists as to how much of the degradation in fatigue life is due to creep as Manson assumes, and how much is due to the environment. In other words, both environment and creep are important in the degrading of high-temperature fatigue resistance, and their relative importance is different at various frequency regimes. Strainrange partitioning does not appear to be helpful in cases where environment is the dominant factor.

S. S. Manson (author's closure)—The discussers address themselves to two main criticisms of the strainrange partitioning method:

1. "Strainrange partitioning is predicting meaningless results . . . " for the case they illustrate.
2. " . . . this effect (environment) is not accounted for by strainrange partitioning."

I shall attempt to demonstrate that neither criticism is valid. The "meaningless" results develop because their computations are not made properly according to the requirements of the method. As for the ability to reflect environmental effect, I shall try to show that the strainrange partitioning method is, in fact, better equipped to account for this factor than other life prediction methods proposed to date. These points will become clear in the following discussion.

Since Fig. 7 shows excellent results when A286 data are analyzed by strainrange partitioning, it is surprising that the discussers purport to demonstrate that meaningless results are obtained according to their analysis by this method. Obviously, there is a difference between the manner in which they analyze the data and that used for Fig. 7. It is instructive, therefore, to examine in detail the graphical implications of the two approaches.

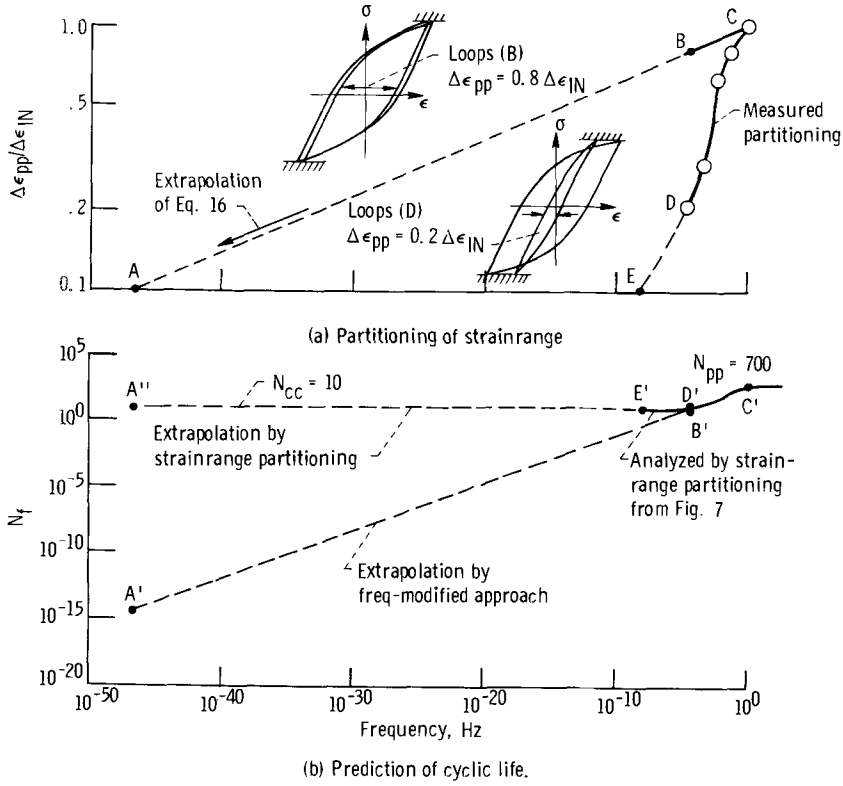


FIG. 13—*Analysis of continuous strain cycling of aged A286 at 1100 F (595 C) with inelastic strainrange of 0.01.*

Figure 13*a* shows the fraction of the total imposed inelastic strain absorbed as plasticity, $\Delta\epsilon_{pp}$, plotted as a function of frequency. For an inelastic strain of 1 percent at 1100 F, the computations made by Solomon and Coffin lie along the line *BC*. Inherent in their computations is an important invalid assumption, which is not really part of the strainrange partitioning method. Their assumption is that the plastic strainrange depends only on stress range, independent of prior history. It is true that we make the assumption that the plastic component depends on the stress range, but we include a *history dependence* by requiring the material to be subjected to the known stress range at high frequency *immediately after* the stable hysteresis loop has developed by realtime application of a number of cycles of the true loading.

Thus, for example, consider how the discussers compute the plastic component, $\Delta\epsilon_{pp}$ at point *B*. They know the stress range through direct measurement; they also know that at their highest frequency of testing where the inelastic strain is nearly all plastic, this stress range produces a certain known amount of plasticity. By equating the two plastic component

values, the point B is computed. If their assumptions were correct, the hysteresis loops obtained by application of the strainrange partitioning procedure would be hysteresis loops (B): the wide loop would refer to the real-time hysteresis at the low frequency, and the narrower loop would refer to the results obtained in fast cycling at the stress range established from the real-time cycling, in accordance with the method described in Fig. 3. Actually, however, the measured hysteresis loops for this condition are shown as loops (D) in Fig. 13*a*. The plasticity that develops in fast cycling *immediately after* a stable real-time hysteresis loop is established is much less than that which develops in a rapidly cycled virgin material. This is so because of structural changes that take place during the real-time, low-frequency cycling. The amount of creep in (D) is thus much higher than computed on the basis of the discusser's equations. The true curve for the plastic flow developed in the range from 1 to 3×10^{-5} Hz is CD, not CB as computed by the discussers. One important difference of their analysis lies, therefore, in their misapplication of the concept involved in rapid cycling as a means of determining the plastic component.

A second significance in their analysis relates to the extrapolation of BC to a frequency where the plastic component would be 10 percent of the total inelastic strain. They accomplish this, in effect, by linear extrapolation of BC to point A. In other words, they take a relationship associated with Coffin's frequency modification concept, established in a range of about 4 orders of magnitude of frequency, and extrapolate another 40 or more orders of magnitude to establish a hypothetical frequency at which the imposed condition might be satisfied. The strainrange partitioning concept does not identify itself with this assumption. Actually, of course, the required condition of 10 percent plastic strain occurs at about 10^{-8} Hz, almost within the experimental range, as seen by the short extrapolation of CD to point E.

A third and the most drastic difference associated with their calculation is the determination of life once frequency is known. Even if it were really necessary to go to a frequency of 10^{-47} Hz in order to reduce the plastic component to only 10 percent of the inelastic strain (as shown by point A), the computation of life would not be as they made it. The difference can be best seen in Fig. 13*b*. Here life is shown as a function of frequency. The region $B'C'$ is roughly the experimental range, and, of course, must be correctly represented by the discussers. They, however, assume that the relationship fits a power law, and therefore their extrapolation, in accordance with one of Coffin's frequency modification equations, is along the dotted line to A'. Again, it is a long extrapolation of a short segment which is only approximately linear, and they should have expected it to break down well before 10^{-47} Hz. Yet they charge the meaningless result obtained in this way to the strainrange partitioning method rather than to the limitations of their own method.

If the strainrange partitioning method were applied properly, the life predictions would be along C' D' E' A'' in Fig. 13*b* (although no one would with reasonable faith extrapolate any method as extensively as required here). This curve is obtained by use of Eq 4 as shown in Fig. 2. Since the plastic flow fraction F_{pp} and the creep fraction F_{cc} are stipulated as 0.1 and 0.9, respectively, they are known automatically. The N_{pp} value is obtained by rapid cycling and is about 700 cycles. The only quantity about which there is any ambiguity is N_{cc}. Normally this value is also determined by experiment, but, if not, then the approximation shown in Fig. 4*b* can be applied. To obtain the value, we would have to know the creep ductility for the time period involved in the test. Since, as discussed in the report, A286 displays a varying ductility depending on test time, a small amount of trial and error calculation is required in order to match the computed rupture time to the creep ductility assumed in the calculation. Actually this is what was done in developing the computed curve in Fig. 7, wherein very good results were obtained for the alloy by strainrange partitioning. But in the absence of detailed computations, we note that if an average creep ductility (from data provided by Opinsky, as noted in the report) were taken at 9 percent, the value of N_{cc} would be approximately 10 cycles (a broad range of assumed ductilities within experimental credibility changes N_{cc} only modestly). Thus, the curve predicted by strainrange partitioning is C' B' E' A''. The expected life at the unrealistic frequency of 10^{-47} Hz is then of the order of 10 cycles, not the meaningless value of 5.8×10^{-15} cycles. The inherent characteristic of the strainrange partitioning method, when properly applied, is that it always bounds the results between credible values; it is the frequency modified relationships that can, when extensively extrapolated, yield meaningless results.

The second major point of the discussion relates to the role of environment. The discussers imply that the meaningless results put forth by their computation suggest that the strainrage partitioning method is inconsistent with the possibility of an important role of environment on high-temperature fatigue. Indirectly, the implication is that the frequency modified method of analysis is consistent with such a role of environment and perhaps even explains it. These implications are not correct. In the report, I discuss in detail the compatibility of the strainrange partitioning method with environmental effects; so repetition is unnecessary. I should just like to make one point in connection with the relative abilities of the strainrange partitioning method and the frequency modification method to define the importance of environment. Suppose, for example, the frequency effect were due only to oxidation, and there were no creep effect. Tests conducted at various frequencies in air would show a time dependency, and analysis by either method would produce relationships suitable for correlation and limited extrapolation. Which would be better for extrapolation is not an issue here. In any case, knowledge of the reason for the frequency

effect will not be known until tests are actually conducted in another environment, say high vacuum. When such tests are conducted with a view toward analysis by the frequency modification method, it would be noted that in vacuum there is no frequency effect, and only through this observation would be the investigator conclude that the effect is entirely environmental. A program conducted with a view toward analysis by the strainrange partitioning method would also include tests at various frequencies, and it also would be noted that the frequency effect has disappeared. The $\Delta\epsilon_{pp}$ and $\Delta\epsilon_{cc}$ lines would now coincide in the vacuum environment, whereas they were different in air. Again the conclusion would be that the effect is entirely environmental and that there is no creep effect in vacuum. In addition, however, we would also establish the $\Delta\epsilon_{cp}$ and $\Delta\epsilon_{pc}$ lines, which are more sensitive to the role of creep than the $\Delta\epsilon_{pp}$ and $\Delta\epsilon_{cc}$ lines, and, if all coincided in the inert environment, we could be even more sure that oxidation was the main factor causing time dependency in air, not creep.

On the other hand, suppose there were a small creep effect and a larger oxidation effect (as very likely is the case of A286). Because the frequency modification method features testing that involves only $\Delta\epsilon_{pp}$ and $\Delta\epsilon_{cc}$, the results would tend to obscure the creep effect, since the life relationships for these two components seldom differ greatly. Strainrange partitioning testing, involving $\Delta\epsilon_{cp}$ or $\Delta\epsilon_{pc}$, would be a better method for revealing creep sensitivity.

For example, for the A286 alloy involved here, the discussers claim that the apparent frequency effect is due entirely to environment. This conclusion is based on results from continuous strain cycling tests over a range of frequencies. We, on the other hand, from our strainrange partitioning tests believe there is a creep effect as well. In order to clarify this point, we arranged for K. D. Sheffler to conduct several tests on A286 for us under contract. The tests were identical to some of those reported by Sheffler and Doble (Ref *23*) at this Conference. These tests were conducted in a 10^{-8} torr vacuum, so oxidation effects should be absent. Some of the results are shown in Fig. 14. Without going into the details of the experiments, the basic ideas of which are described in Ref *23*, the main point of this figure is that, if there were no creep effect, all the lines would coincide. In fact, however, there is a loss in life by a factor of more than 10 at an inelastic strainrange of 0.5 percent between tests conducted at 0.65 Hz and 1100 F (595 C) compared to those wherein the tension was at 0.0065 Hz at 1100 F (595 C), while the compression was imposed at 600 F (315 C) to preclude compression creep (producing a cycle that favors the $\Delta\epsilon_{cp}$ component). Thus, there is a significant creep effect, even in vacuum. Furthermore, the creep effect may depend strongly on the type of cycle imposed. As shown in Fig. 14, at an inelastic strainrange of 0.5 percent, a factor of 6 in cycles to failure is observed between the test cycles favoring

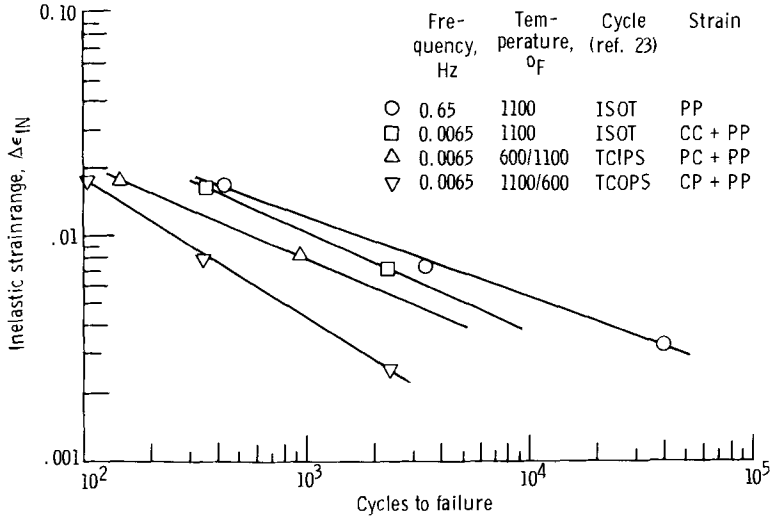


FIG. 14—*Creep effects in high vacuum (10^{-8} torr) during low-cycle fatigue of aged A286. Data by Sheffler of TRW, Inc. under contract to NASA.*

$\Delta\epsilon_{cp}$ and $\Delta\epsilon_{cc}$—in spite of the fact that these tests were conducted at exactly the same frequency. Such observations not only help to elucidate the important mechanisms involved in high-temperature fatigue, but can be important in computations for practical problems for complex loading cycles. They are better brought out by approaches arising out of strainrange partitioning than by other methods.

Closure Statement

Summary

In retrospect, how should we judge the contribution of the Storrs symposium? No unified view emerges: Metallurgists proposed mechanisms, mechanicians correlated data. And yet, there was a curious symbiosis; a sense that the microscopic and macroscopic points of view have begun to converge. Forbearance and mutual respect, if not collaboration, was the tone of the meeting.

Fracture mechanics, almost omitted from the initial program, was rediscovered in the creep range, holding out the promise of extending the advantages of the method to design, testing, and analysis of high-temperature structures. Extensions were demonstrated through modification of the crack growth law by an activation enthalpy term containing, unexpectedly, the stress intensity; also by correlating the crack growth with the range of strain intensity. Underlying this activity, the thought that fracture mechanics, through new concepts such as strain rate intensity and crack closure, may catalyze development of predictive techniques through its unique capability to blend metallurgical and mechanistic constructs.

The promulgators of the Coffin-Manson relationship continued to set the pace for most of us: undisputable evidence that the environment can be the dominant factor at elevated temperature (one is struck here by the similarities between oxidation-controlled fracture and stress-corrosion cracking) and a challenge to view the creep-fatigue interaction as four separate processes depending upon the nature of the strain cycle, that is, whether creep or plastic, or mixed, with one effecting the reversal of the other. Clearly, the limits of validity of these points of view must be probed, especially until they overlap; and the interactions that they illustrate should be interpreted in terms of microstructural mechanisms. The concept of strain range partitioning should be particularly amenable to interpretation by fracture mechanics and appears to offer a useful guide to the development of a model of crack-tip behavior.

Thermal ratchetting, a problem which has long affected designers of high-temperature equipment, has assumed new prominence as a nuclear design code consideration, requiring sophisticated nonlinear, time-dependent computation of strain. Inability to characterize materials under complex loading cycles has, apparently, given ratchetting special status—and

Copyright© 1973 by ASTM International www.astm.org

its own jargon—among problems of constitutive behavior. Nowhere, perhaps, is the importance of microstructural modelling so evident. We were shown, for example, how relatively simple models can provide the theoretical framework (with considerable empirical sheathing) for describing time-dependent cyclic behavior with surprising realism. Such a model can predict the ratchetting of a structure as a matter of course with the aid of a suitable computerized stress analysis program. Strict empirical correlation without the benefit of a microstructural model would be impractical.

It might, in fairness, also be noted what was *not* featured in the Symposium, for example, time-dependent crack displacement observations or analysis. We must learn how creep affects the strain field of a crack in order to represent its effect on the rupture process. Models of cavity growth and coalescense, including sintering are required, especially at grain boundaries.

It is hoped that this symposium will serve as a useful point of departure.

Index

A

Activation
  energy, 592
    fatigue crack growth, 142, 145
  thermal, 592
Aging
  fatigue effects, 236, 250, 356, 363
    in steel, 321, 328, 431
  strain (*see* Strain, aging)
Alloying (*see also* Precipitates)
  aluminum, 429
  boron, 295
  carbon, 332
  and fatigue, 296, 332, 339
  hafnium, 295
  interstitial, 301
  refractories, 296
  and rupture strength, 338
  titanium, 296, 429
  substitutional, 333
  Y_2O_3, 429
  zirconium, 295
Annealing
  polygonization, 75
  recovery, 70, 90, 293, 306, 593, 594
  recrystallization, 491, 517
  temperatures, 288

B

Bauschinger effect
  modelling, 614, 615
Biaxial stress state, 678 (*see also* Combined stress state)

C

Calibration, 211
Carbides (*see* Composites; Precipitates)
Cavitation
  boundary sliding, 46
  crack initiation, 46, 381, 594
  nucleation, 48, 96, 149
Cavity
  linkup and growth, 48, 163, 308, 385, 422, 462, 594, 596
  nucleation, 46, 381, 462, 576, 594
  shape, 64
  stability, 48, 465, 594
  and strain, 594
  and stress, 386
Cermets, 519
Coatings
  cracking, 58, 411, 413, 651
  effects, 51, 58, 168, 174, 235, 277, 279, 287, 410, 412, 651, 652
  formation of, 410
  fracture strain, 58
  lifetime, 58, 235, 401, 409, 411, 651
  morphology, 412, 414, 652
  strain intensity factor, 176
  temperature effects, 176, 235
  testing of, 246
Codes, 733
  applicability, 734
  considerations in coding, 733
  engineering standards, 736
  formulation procedures, 737
  improvement, 739
  influences on, 737

Copyright© 1973 by ASTM International www.astm.org

interpretation, 738
public safety, 734–736
rules for elevated temperature, 735, 771
standardization, 736, 739
and technology, 734, 740
development, 742
Combined stress states, 29, 231, 462 595, 597, 678, 707
in ratchetting, 537
Composites
carbide fiber, 519
Composition (*see* Alloying)
effects (*see* Precipitates; Material types)
Computer use, 211, 258, 588, 596, 714
in ductility exhaustion, 629
Constitutive equations (*see* Equations)
Continuum theory, 588, 604
Corrosion (*see also* Oxidation)
as failure cause, 231
fatigue, 233, 274, 482, 667
hot, 287, 410
intergranular, 517
resistance, 332, 438
stress, 482
testing, 195
Crack
arrest, 425
branching, 422
closure, 181, 252
coalescence, 502
environment, 44, 410
fatigue, 139, 175, 201, 345, 416
activation energy, 142
growth rate, 25, 46, 51, 113, 116, 125, 140, 157, 163, 167–169, 201, 243, 308, 345, 349, 387, 393, 417, 421, 449, 482, 509, 586, 604, 728, 764
frequency effects, 117, 350, 351, 353, 586, 763
oxygen effects, 53, 117, 763
and properties, 395–397
and temperature, 27, 174, 177, 509
and transition with temperature, 391
unstable, 151
and hysteresis loop, 339
initiation (nucleation), 5–9, 17, 21, 39, 46, 50, 90, 113, 128, 146, 149, 243, 246, 292, 296, 320, 404, 410, 412, 413, 417, 424, 439, 449, 500, 502, 503, 509, 526, 576, 586, 604, 652, 671, 679, 705, 745, 764, 772
creep dependency, 43, 498
laws, 765
sites, 43, 96, 250, 251, 279, 292, 296, 404, 410, 411, 422, 433, 441, 448, 470, 494, 504, 507, 518, 558, 586, 652
instability, 151
intergranular, 49, 127, 128, 250, 251, 362, 424, 650
length, 168, 509
critical, 44, 387, 594
initial, 126, 158, 159, 185, 488
measurement, 201, 417
mechanisms, 43, 44, 404, 410, 422
microcracks, 7, 523, 728
mode, 26, 169, 176, 422, 434, 444, 501, 586, 630
prediction, 50
and strain rate, 134
nucleation (*see* initiation)
opening displacement, 9, 158
path, 128, 136, 250, 324, 362, 422, 434
precracking of specimens, 348
propagation, 6, 39, 46, 90, 113, 125, 139, 166, 168, 171, 243, 246, 307, 320, 345, 350, 404, 412, 416, 419, 420, 424, 439, 482, 501, 508, 509, 526, 586, 679, 705, 745, 772

in air, 404
and alloying, 295 (*see also* Alloying)
control in testing, 388
frequency effect, 26, 112, 114, 117, 351, 432
and precipitates, 170 (*see also* Precipitates)
rapid, 46, 170, 172
rate (*see* Crack, growth rate)
and temperature, 26, 419
resharpening, 53, 171, 174, 594
shape, 411, 422
size, 125, 174, 188
slip band, 51 (*see also* Dislocation)
stages
I; 38, 44, 292, 442, 449, 586
II; 38, 44, 53, 442, 449, 587
subsurface, 53
surface, 51, 127, 130, 136, 308, 434, 470, 486
thermal, 242
tip, 44, 46, 146, 171, 180, 308, 420, 471, 486, 509, 586
blunting, 162, 296, 308, 594
heating, 526
radius, 158
stresses, 508, 579, 766
transgranular, 127, 128, 404, 448, 650
holdtime, 49, 362
transition, 46, 58, 127, 362
triple point (wedge), 50, 119, 150, 384, 594
Creep
cavitation, 48
component, 50, 614, 663, 748
compressive, 48, 49, 476, 499, 659, 665
crack initiation, 21, 43, 145, 462
cracking, 46, 462, 588
damage, 176, 321, 366, 369, 482, 580, 745 (*see also* Damage)
deformation (*see* Deformation)
failure, 162, 381, 688
fatigue interaction, 21, 114, 149, 157, 166, 168, 175, 224, 349, 355, 366, 368, 402, 462, 469, 492, 496, 502, 575, 582, 588, 603, 619, 625, 627, 638, 641, 644, 649, 658, 670, 676, 688, 705, 745, 748, 780
fracture, 150, 377
hold, 49
rate, 150, 314, 463, 466, 468, 470, 586, 593, 691, 696
resistance, 287, 295, 476
rupture, 49, 287, 295, 470, 580, 650, 746
strain, 21, 366, 628, 642, 671, 690, 706, 713, 748
and frequency, 153, 642, 663
strength, 498, 626
subgrains, 71, 75
tensile, 48, 49, 476, 499, 659, 665
Crystal
polycrystalline versus columnar, 410
structure, 301
Cyclic
cell formation, 76, 301
control, 225
creep, 149, 158, 650, 671
deformation, 305, 306, 479, 671
energy, 476, 478, 479
growth (*see* Ratchetting)
hardening, 90, 132, 302, 324–327, 373, 463, 465, 623, 686, 712
plasticity, 169, 171, 345, 603
plastic strain, 30
rupture, 452, 460
softening, 90, 132, 463, 465, 616, 623, 686
strain hardening exponent, 11
stress, 293, 463, 553
thermal, 650 (*see also* Cycling, thermal)

stress-strain curve, 126–128, 224, 326, 475, 476, 679, 712
model, 614, 679
serrated, 306
Cycling
A-ratio, 440
bend, 453, 701
compressive, 48
frequency dependence, 112, 351
in fatigue, 114, 555, 576
push/pull (fully reversed), 48, 83, 125, 301, 321, 356, 367, 440, 478, 483, 493, 513, 524, 555, 627, 638, 649
R-ratio, 158, 348, 432
random (temperature), 104
reverse bend, 233, 321, 483, 513, 524
sonic, 256
stability, 651
strain, 167, 195, 334, 366, 473, 482, 491, 553, 577, 582, 627, 638, 651, 771
stress, 248, 265, 451
thermal, 83, 167, 195, 197, 227, 232, 246, 266, 311, 316, 366, 402, 451, 473, 477, 491, 496, 500, 555, 619, 649, 665, 681
torsional, 48, 513
wave form, 637

D

Damage (*see also* Holdtime)
accumulation, 224, 355, 594, 596, 670
and energy, 477
linear, 18, 114, 366, 579, 627, 633, 650, 670, 674
rate, 154
creep, 224, 304, 308, 350, 355, 366, 368, 372, 373, 475, 480, 498, 579, 642, 644, 705, 708, 767
cumulative, 81, 95, 176, 321, 366, 478, 500, 506, 508, 548, 582, 626, 630, 645, 705, 757
fatigue, 91, 134, 224, 321, 368, 372, 431, 475, 480, 498, 633, 652, 705, 707, 708, 729
holdtime, 320, 506 (*see also* Holdtime)
fraction, 675
function, 595
Miner's rule, 91, 508
plot, 627
recovery, 595
rules, 19, 368, 478, 548, 577, 582, 603, 626, 628, 650, 707, 746, 751, 757
surface, 302, 304, 305, 308, 504, 524
Decarburizing
and properties, 335, 690
Defect (*see* Cavity; Crack; Flaws; Voids)
Deformation
behavior, 616
creep, 151, 499, 626, 671, 691
and gamma prime, 295, 429
inelastic (*see* Strain)
mechanical twinning, 128, 486, 490
nonhomogeneous, 305, 433, 508
plastic, 46, 251, 287, 295, 499, 523, 671 (*see also* Strain, plastic)
in crack growth, 151
state, 7
time independent, 151, 671
work hardening, 90, 504 (*see also* Cyclic, hardening)
Dendrite
interdendritic cracking, 404 (*see also* Crack)
spacing, 404
Design, 17, 226 (*see also* Lifetime)
and codes (*see* Codes)
of experiments, 212, 250, 258, 264

Design parameter plots, 638, 644 (*see also* Creep, fatigue interaction; Holdtime)
Diffusion
  of carbon, 333
  coatings, 236, 410
  in LCF, 80, 748
    mechanism, 91
    self, 592
  vacancy, 594, 729
  volume, and crack growth, 139, 145, 147
Dislocation
  arrangements, 69, 70, 305, 433, 449, 587
  bowing mechanisms, 292
  cell formation, 69, 70, 76, 125, 302, 305, 434
    inhomogeneity, 305
    size, 306, 434
  climb, 38, 51, 77, 463, 592
  concentration, 44, 433
  cross slip, 38, 51, 77, 125, 301
  density, 85, 90, 305, 450, 592, 593, 615, 630
  frequency effects, 38
  jogs, 463, 594
  locking, 304
  loops, 70, 71
  mobile, 70
  mobility, 91, 305, 463, 587, 592, 594, 616
  multiplication, 305, 616
  pinning, 61
  strengthening, 306
  subgrain, 70
  substructure, 69, 80, 85, 302, 304
  superlattice, 440
  tangles, 70, 433, 471, 729
  velocity, 592, 614
Driving force
  in crack growth, 144, 147, 420
Ductility, 295, 402
  in creep, 151, 582, 586, 597, 651, 754, 762
  and crack growth, 395
  cyclic, 662
  ductile rupture, 308, 594, 762
  exhaustion, 625–634, 657, 747
  and fatigue, 16, 409, 632, 754
  fraction, 597
  and strain range partitioning, 661
Dwell (*see* Holdtime)

E

Energy equation (constitutive theory), 606
Environment, 195, 243, 482, 584
  air, 51, 112, 233, 296, 321, 329, 348, 356, 401, 404, 410, 459, 584
  argon, 296
  and coatings, 235, 279, 413
  control, 211
  and frequency, 24, 112, 114, 119, 432, 584
  gaseous, 44, 51, 235
  humidity, 140
  iodine, 482
  kerosine, 513, 517
  nitrogen, 140
  oxygen, 21, 51
    and frequency, 117, 432, 777
  protective, 762
  PbO, $PbBr_2$, $PbSO_4$, 235
  salt, 268, 270
  simulation, 256, 274, 773
  sonic, 262
  SO_2, 296
  steam, 273, 324, 329
  vacuum, 21, 51, 296, 324, 329, 452, 491, 584, 777
  V_2O_5-$NaSO_4$, 296
Equations
  basquin, 14
  bowie, 169

Coffin-Manson, 12, 153, 225, 452, 480, 487, 577
constitutive, 588, 621
damage (*see* Damage, rules)
Hall-Petch, 302–305
high temperature fatigue, 11, 17, 25 (*see also* Lifetime, prediction)
Manson universal slopes, 15
Miner's rule (*see* Damage)
Neuber's rule, 30, 584, 681
Paris equation, 141, 180, 351, 391
ratchetting, 570
Stowell, 478, 584, 680
ten percent rule, 496, 579, 745
universalized life, 754
universal slopes, 579, 652, 745
Erosion, 656
Extensometers
analog strain, 197, 356
design, 208, 474
effects, 10, 324, 494

F

Failure (*see also* Creep; Fatigue; Fracture)
criteria, 6, 7, 17, 18, 226, 233, 274, 324, 335, 440, 478, 495, 586, 594, 595, 603, 629, 632, 647, 650, 654, 659, 665, 671, 683
energy, 478
location, 270 (*see also* Crack, initiation, sites)
Failure mechanisms, 761
crack initiation, 44
brittle boundary phases, 119
shear, 50
creep, 119, 470
diffusion control, 91, 93, 144, 147
mode, 502, 629, 749
and models, 614
propagation, 44
slip control, 91, 93
Fatigue (creep interaction), (*see* Creep)
and alloying (*see* Alloying)
coatings (*see* Coatings)
crack, 25, 38, 113, 125, 139, 150, 180, 187, 348, 416, 441, 518, 579, 582, 587
oxidation, 25, 53, 518
endurance, 127, 130, 180, 321, 324, 674
and grain size, 288, 304
high cycle, 9, 274, 524
intergranular, 38, 46, 51
isothermal, 172
life (*see* Lifetime)
limit, 185, 301
low cycle, 68, 172, 287, 332, 339 355, 452, 524, 650, 678
frequency modified equation, 113, 153, 452, 579 (*see also* Frequency)
of oxide coatings, 94, 102
and ratchetting, 553
resistance, 29, 50, 253, 292, 301, 388
striations, 46, 162, 251, 280, 307 308, 362, 446, 449
subgrain size, 75
thermal, 37, 49, 108, 167, 170, 172, 199, 238, 242, 287, 296, 401, 402, 410, 413, 417, 419, 553, 582, 586, 665, 767
transgranular, 38, 50 (*see* Cracks, stage II)
ultrasonic, 280
Finite element analysis, 6, 7, 30, 420, 598, 604, 613, 616, 621, 680, 689, 706, 710
Flaws (*see also* Cavity; Crack)
already existing, 387
distribution, 724
size, 724
critical, 725

shape, 724
echo ratio, 724
Fluidized bed, 242, 416
Forging
effect on fatigue, 237, 329
Fracture
appearance, 162, 170, 251, 307, 308, 425, 449, 471, 501
cleavage, 46, 130, 449, 470
cyclic, 46
dimples, 162, 308, 381
ductile, 377, 381, 470, 566, 594
fatigue, 195, 307, 308, 324, 469, 470, 639
grain boundary (*see* Grain, boundary)
interdendritic, 170
intergranular, 21, 46, 70, 119, 289, 308, 433, 462, 470, 594, 745, 749
oxygen, 51, 56
mechanics, 6, 9, 166, 345, 350, 353, 387, 419, 587, 679, 723, 728, 764
mechanism, 307, 309, 587, 748
mode, 21, 24, 25, 112, 172, 289, 308, 360, 384, 433, 470, 471, 749
shear, 50
strain, 91, 450, 674
stress, 723
surface, 170, 279, 308, 361, 377, 449, 466 (*see also* appearance)
and temperature, 301
transgranular, 44, 119, 170, 289, 308, 381, 749
oxygen, 51
toughness, 182, 394
Frequency, 12 (*see also* Strain rate; Holdtime)
and crack growth, 280, 345, 350, 351, 353 (*see also* Crack)
and creep component, 50, 152, 154, 582
effect, 15, 38, 58, 112, 152, 199, 273, 280, 321, 432, 451, 454, 457, 459, 460, 480, 576, 582, 603, 637, 642, 643, 663, 674, 696, 746, 753, 759, 776
and environment, 112, 280, 586, 757, 761
and oxidation, 53, 108, 117, 273, 280, 459
ranges, 113
ultrasonic, 273
and temperature, 63, 108, 351, 603, 746

G

Grain (*see also* Single crystals)
boundary, 44
cracking, 25, 120, 130, 134, 381, 384, 422
damage, 154, 304, 308, 630, 651, 748
embrittlement, 301
fracture, 119, 134, 295, 434
hardening, 306
ledges, 305
migration, 46, 48, 85, 470
orientation, 404
oxidation at, 53, 296, 586
precipitates, 70, 295, 361 (*see also* Precipitates)
serration, 85, 94
shape, 296
shear, 48
sliding, 46, 96, 119, 150, 296, 379, 435, 594, 596, 748
strength, 128, 295
transverse, 289
orientation, 401, 449
refinement, 287, 288, 292
size, 50, 130, 287, 301, 306, 307, 402, 404, 412, 465, 470, 488, 652
and LCF, 288, 301
structure (duplex), 288

subgrain
boundaries, 85
misorientation, 70
size, 306
substructure, 70, 80, 306
twist boundaries, 70
Gripping, 198
design, 205

H

Hardening (*see* Cyclic; Strain)
Healing, 726 (*see also* Stress, mean)
Heat
affected zone (HAZ), 588, 690
in ferritic welds, 151
methods in testing, 202
treatment effects, 250, 333, 346, 355–357, 485, 488, 506, 515 (*see also* Annealing)
History effects, 591, 613
modeling, 620
Holdtime (*see also* Frequency)
in cyclic creep, 154, 158 (*see also* Creep, fatigue)
creep, 154, 627, 632, 696, 746, 760, 761
component, 19, 50
compressive, 49, 366, 474, 482, 506, 576, 638, 643, 746
tensile, 49, 125, 134, 366, 367, 372, 474, 482, 506, 638, 641, 746
endurance, 136, 576 (*see also* Lifetime)
in fatigue, 17, 19, 27, 321, 326, 356, 357, 362, 366, 372, 402, 408, 452, 474, 475, 478, 482, 486, 488, 496, 516, 586, 597, 637, 639, 670, 702, 705, 706, 746, 760, 761
and particle size, 293
in ratchetting study, 710
saturation, 360, 372, 638, 642, 760
slip dispersal, 38 (*see also* Slip)
and strain rate, 643
threshold, 368
transition, 583, 603
Hysteresis loop, 27, 197, 225, 453, 476, 477, 483, 673
in energy approach, 479
in partitioning approach, 658–660, 753
ratchetting, 548
stability, 477, 650, 748, 753

I

Interaction (*see* Creep, fatigue)
damage rule, 751
Interspersion (*see* Creep, fatigue interaction; Damage, cumulative)

J

Joint efficiency, 694

L

Lifetime
coatings, 410–412
of cermet, 519
crack stages, 25, 38, 404, 410
in creep fatigue, 149, 158–162, 367, 470, 480, 498, 638, 643, 663, 665, 671, 746, 749, 753, 757
design, 5, 15, 49, 633, 670, 678, 694, 697, 704, 707, 771
endurance, 180, 435, 440, 448, 450, 501, 503, 506
fatigue, 44, 61, 83, 112, 126, 166, 268, 273, 301, 304, 307, 368, 429, 448, 451, 456, 475, 482, 496, 501, 530, 558, 561, 586, 597, 663, 670, 694, 699, 703, 706, 728
frequency modified, 12, 16, 25, 339, 357, 404, 409, 410, 452, 745

fatigue transition, 15, 454
frequency effect, 459
initial crack length, 158
notch effect, 498, 502, 678
partitioned strain range, 660, 751–753
porosity, 43, 477 (*see also* Cavity)
prediction, 69, 91, 113, 126–128, 576, 582, 597, 603, 617, 622, 631, 639, 650, 660, 663, 665, 667, 678, 683, 694, 745, 764, 770
in crack growth, 151–153, 186, 295, 394
energy method, 478, 479
with holdtime, 134, 368, 602
service, 57, 679
surface effects (*see* Surface, preparation)
Load ratio (*see* Cycling, R-ratio)

M

Machining
effects, 526–530
parameters, 524
Material types
aluminum, 301
base alloys, 46
1100; 24
2024; 24
2618-T6; 512
5052; 157
5454; 139
7075; 145, 163
Cu; 501
Mg; 139
Brass
alpha, 301
high Zn, 38
Cermet, 519
Cobalt base
MAR-M 302; 402
MAR-M 509; 167
WI-52; 402
FSX-414; 416
Hastelloy-X, 256
Haynes Alloy 25; 256, 295
iron, 301
magnesium
alloys, 50, 124
Nickel A, 24
nickel-base superalloys, 474
ATGW2; 517
B1800; 618
B1900 W/Hf; 167, 409, 627, 649
In 100; 295, 649
In 713; 518
In 718; 24, 523
In 738; 295
In 751; 237
In 853; 292, 427
In X-750; 463
MAR-M200; 26, 38, 167, 291, 409, 649
Monaloy; 350, 409
Nickel A; 24
Nimonic alloys; 296
Nimonic 90; 517, 649
Nimonic 100; 517
713 C; 296
Alloy 800; 366
901; 288
Ni-Cr-Al alloys, 291
René 41; 256
René 77; 416
René 80; 523
René 95; 523
stainless steels
austenitic, 38, 114, 671
low carbon, 46
18Cr-12Ni-Cb; 92, 377
20Cr-25Ni-Cb; 125
A286; 23, 112, 451
304; 11, 49, 69, 276, 355, 366, 387, 403, 553, 637
316; 49, 69, 355, 387, 659, 690
321; 387

347; 24
348; 387
V57; 452
steel
ferritic; 116, 311, 690
low alloy (Ni,Cr,Mo,V), 67
low carbon, 81, 113
C1010; 24
C1018; 24
½Cr, Mo-V; 320
2¼Cr, MoV; 332, 659, 690
A212B; 345
A302B; 553
A517F; 345
9Ni-4Co-0.30C; 345
JIS-SCM-3; 553
21-4N; 238
21-2N; 238
tantalum, 24
ASTAR 811C; 491
T-111; 491
titanium, 264
TDNi; 292
Udimet 500; 21
Udimet 700; 26, 46, 288, 409, 618
Udimet 710; 439
Waspaloy, 292
Zircaloy-2; 482
Zircaloy-4; 483
Microstructure
changes (during fatigue), 83, 361, 479, 630
and coatings, 410
control, 287, 356
and crack growth, 346, 422, 432, 501, 509
and fatigue, 287, 321, 328, 432, 479, 486
refinement, 401, 404
in low-cycle fatigue, 80, 356, 362
stability, 491
twinning, 486, 728
Modulus, 169
effect on life, 404
secant, 584, 680

N

Neutron irradiation, 488, 623
Nondestructive tests, 722
acoustic
emission, 725, 728, 729
holography, 725, 728
applicability, 705, 725
defect standards, 724
exoelectron emission, 729
optical, 731
positron half-life, 731
pulse echo, 726
reliability, 722
in service, 726
signature-baseline generation, 728
slip motion, 729
stress gradients, 722, 731
ultrasonic, 724
in fatigue, 731
synthetic aperatures, 725, 727
Notch, 5, 265, 494, 502, 514, 584, 602, 679
effect at high temperature, 29, 237, 245, 496, 498, 502, 514, 681, 703, 705
root, 6, 508
strains, 7, 507
surface, 504

O

Oxidation
chemistry, 401
and crack measurement, 324
crack tip, 56, 134, 579, 604
fatigue crack initiation, 53, 234, 251, 287, 296, 410, 448, 579, 586, 604
film, 23, 51
frequency effect, 57, 132, 459, 586

growth rate, 109, 132, 296, 604
intergranular attack, 404, 437, 470
layers, 53, 109
preoxidation, 56
rate of formation, 53, 109, 110
resistance, 296, 409, 428, 470, 518, 652
surface, 248, 762
and temperature fluctuations, 102, 108, 234, 251, 401, 408, 626

P

Plastic
blunting, of crack tip, (*see* Crack, tip)
deformation (*see* Deformation, plastic)
instability, 27, 197, 651
strain, (*see* Strain, plastic)
superplastic, 288
zone, 6, 7, 586
and life prediction, 134, 586
measurement, 202
size, 8, 125, 146, 169, 180, 185, 397, 426, 588
Porosity (*see also* Cavitation)
fatigue life, 43, 477
Precipitates (*see also* Alloying)
brittle, 51
carbides, 167, 295, 296, 401, 402, 410, 433, 448, 491
CbC, 49
coherent, 38
and dislocations, 305, 433, 440, 442
dissolution, 292
distribution, 291, 293, 360, 404, 432, 439, 463
fibers, 519
formation, 378
free zone, 50
optimum, 50
heat treatment, 291
gamma prime, 44, 167, 291, 409, 429, 439, 470, 630
growth, 96, 360, 384
incoherent, 38, 49
and life, 25, 361, 404, 410 (*see also* Lifetime)
and matrix, 594
$M_{23}C_6$; 48, 50, 70, 76, 360, 384, 422
MC, 43, 167
oxidation rates, 56, 408
precipitation, 360–362, 523
hardening (*see* Strengthening)
second phases, 48, 504
shape, 43, 404, 439
shear of, 292, 440, 630
size, 43, 293, 404, 410
stability, 355
thoria, 49
volume fraction, 293, 432
Pseudo stress, 360, 529

R

R-ratio (*see* Cycling)
Radiation damage (*see* Neutron irradiation)
Ratchetting, 17, 27, 197, 624, 747
area effect, 547
creep, 538, 567
design, 721
growth, 541, 709, 715, 720, 761
isothermal, 536
combined stress state, 537
material property changes, 544
mechanical, 201
rate, 27
rules, 715–721
shakedown, 541, 543, 564, 615
stability, 566
strain, 29, 548, 555, 560, 565, 567, 713
accumulation, 536, 540, 557, 566, 597, 715, 762

hardening, 545, 566, 568, 714
increment, 567
stress relaxation growth, 538, 542, 547
stress-state, 546
temperature effects, 541, 710
thermal, 201, 539, 540, 564, 568, 710, 711
work hardening effect, 568
Recording, 211

S

Signature-baseline generation (*see* Nondestructive tests)
Single crystals
in fatigue, 410
oxidation, 53
Slip
bands, 280, 301, 379, 439, 449, 587, 630
spacing, 440
character, 38, 69, 291
concentration, 292, 449
dispersal, 38, 61, 450
mechanisms, 80, 91, 94
detection, 728, 729
offsets, 291
planar, 38, 44, 124, 291, 301, 440, 616, 620, 669, 748
homogeneity, 38, 46, 51, 449, 616
planes, 46, 425, 586
decohesion, 448, 450
surface, 51, 729
traces, 304, 379
wavy, 38, 44, 301, 669
$>0.4\ T_m$, 38
Solidification, 250
directional, 404, 424, 519
Sonic response, 256–262
Specimen
applicability, 348, 693
bend test, 453
compliance changes, 526
design, 203
for fluidized bed, 245
hourglass, 196
plastic strip, 348
zero gage length, 196
Stacking fault energy, 69
high, 38, 306
low, 38, 124
Strain
accumulation (*see* Ratchetting)
aging, 12, 61, 120, 187, 530, 571, 593, 666
dynamic, 301, 304, 308, 458, 493
embrittlement, 350
amplitude, 9, 69, 301, 302, 480, 496, 560, 576, 629
in bending, 324
component, 15, 749
concentration, 584, 602, 679, 683, 690
and crack nucleation, 149
creep (*see* Creep, strain)
effective, 678, 679
elastic, 773
energy, 146, 728
gradient, 18
hardening, 73, 76, 154, 459, 542, 545, 614, 710, 712
and crack growth, 395, 509
exponent, 73, 487, 560
inelastic, 659, 747
intensity factor, 169, 172, 584
large, 38, 50, 320, 408
mean, 171, 474, 619, 673
measurement, 208
plane, 185, 701, 712
plastic, 112, 308, 404, 473, 482, 483, 536, 659, 663, 671
concentration, 304, 305, 308, 584
model, 614
prestrain, 154
range, 57, 70, 90, 91, 132, 168, 326, 368, 372, 402, 404, 417, 454,

478, 496, 579, 602, 619, 632, 641–643, 679, 707, 749, 757
damage summation, 751
partitioning, 603, 658, 747
plastic, 12, 454
ratchet, 555 (*see also* Ratchetting)
rate, 12, 38, 70, 120, 124, 134, 166, 197, 199, 304, 306, 316, 356, 366, 577, 614, 637, 658–667 (*see also* Frequency)
at crack tip, 44
intensity factor, 46
saturation, 638, 642
sensitivity, 76, 225, 620
ratio, 29
reversal, 17, 658–659, 747
small, 132
surface, 320
detection, 731
tensile, 366
tensor, 621
yield, 686
Strength
and crack growth, 145, 345
creep, 287, 296, 438, 498, 705, 746
cyclic parameters, 126, 301
and fatigue, 126, 130, 295, 408–410, 435, 436, 439, 530, 561
grain boundary, 128
precipitation, 76
rupture, 452, 746
subgrain size, 74
yield, 345, 394, 402
compressive, 540
and crack growth, 396
and temperature, 541
tensile, 540
Strengthening
dispersion, 293, 427
precipitation, 427, 491, 593
solid solution, 76, 167, 427, 491
by thermal cycling, 318, 362
Stress
amplitude, 7, 180, 266, 465, 502
compressive, 64, 324, 507, 746
mean, 449
concentration, 44, 246, 253, 584, 671, 679, 680, 703
factor, 7, 265, 308
constant, 50, 558
constraint, 163
and creep, 158, 507, 650
critical resolved shear, 44
dwell (*see* Holdtime)
in fatigue, 46, 128, 130, 666
field (distribution), 180, 250, 419, 501, 690, 691, 705, 765
friction, 306
general yield, 180, 188, 348
intensity, 141, 145, 536, 764
factor, 145, 164, 180, 183, 391, 419, 420, 509, 584, 587
minimum, 188
range, 392, 420
threshold, 180, 187, 188, 392
mean, 17, 29, 159, 167, 180, 188, 266, 269, 439, 440, 449, 506
and crack stages, 449
creep component, 50, 506
healing, 49, 64, 506, 576, 762
peak, 324, 327, 530, 753
plane, 174, 185
and precipitation, 377 (*see* Strain, aging)
raiser, 158
effects, 163
range, 90, 515, 519, 679, 690
frequency modified, 12
ratio, 180
and crack growth, 186–188
relaxation, 17, 29, 134, 154, 327, 366, 369, 505, 517, 583, 601, 614, 642, 695, 747, 760
cyclic, 373, 538 (*see* Ratchetting)
residual, 29, 183, 505, 507, 508, 523, 529, 565, 601, 691, 731

response (steady-state), 302, 305, 306, 308
rupture, 332, 335, 368, 373, 431, 694
saturation, 70, 302
grain size, 302
subgrain size, 71
stress-strain curve (*see* Cyclic)
tensile, 324, 507, 515
thermal, 242, 256, 404, 408, 541, 598
vibratory, 464
yield, 304, 345, 394
Striations (*see* Fatigue, striations)
Sulfidation, 287 (footnote), 296, 410, 427
Surface
condition and NDT, 731
energy (fracture), 50, 150
failure, 404
preparation (integrity), 7, 236, 277, 508, 516–517, 518, 522, 530, 700
roughness, 531
stability, 404, 410
yield surface, 713

T

Temperature
brittle-ductile transition, 413
crack growth, 141, 350–353, 391, 395, 498, 510
threshold, 391
cracking mode, 50, 127
creep component, 50, 320, 508
and dislocation cell size, 302
equivalent, 93–96, 480
fatigue effects, 9, 12, 16, 21, 61, 68, 91, 127, 130, 141, 166, 357, 417, 451, 475, 480, 498, 579, 603, 659, 660, 746
fluctuations, 312, 478, 498, 501, 503, 510, 712, 746, 769
amplitude, 103, 108, 166, 417
and oxides, 102
and fracture, 21, 479, 498, 510 (*see* Fracture, mode)
frequency effects, 63 (*see* Frequency)
and grain boundary, 292, 295, 462 (*see also* Grain, boundary)
high temperature alloys, 285, 320, 410
life prediction, 94, 127, 478, 498, 579, 652, 659, 662–663, 666, 684, 746, 749 (*see also* Lifetime)
oxidation effects, 51, 53
ranges, 102, 225, 690
recovery, 70, 75, 90 (*see also* Annealing)
strain rate effects (*see also* Strain, rate), 124, 305, 314, 616, 659
and testing, 196
Test methods, 10, 11, 17, 194, 198, 225, 228, 460, 695, 749
data comparisons, 603
simulation, 232, 459, 601, 633, 689, 707, 769
Thermal
cycling (*see* Cycling, thermal)
fatigue (*see* Fatigue, thermal)
ratchetting (*see* Ratchetting, thermal)
strain (in creep), 601
stress, 5, 151, 500 (*see also* Stress, thermal)
Thermal protection system, 255
Time (*see* Creep; Cycling, ratio; Frequency; Holdtime)
dependent mechanisms, 592 (*see* Creep)
independent mechanisms (*see* Fatigue)
fraction rule, 584, 674 (*see also* Damage, rules)

in strain range partitioning, 666
testing cycle, 195
Twinning (*see* Deformation; Microstructure)

U

Ultrasonic measurement (*see also* Nondestructive tests)
crack growth, 139

V

Vacancies
annihilation, 463
condensation, 46, 463, 471
flow, 592 (*see also* Cavitation)
pinning, 463
production, 48
supersaturation, 48
Vacuum (*see also* Environment)
life effects, 51, 757 (*see also* Lifetime)
and frequency, 112, 114, 757 (*see also* Frequency)
Vapor deposition
of coatings, 413
Variables in testing, 214, 224
Voids (*see* Cavitation; Cavity)
formation, 576
growth, 595

W

Weld and design, 688, 699
fatigue in, 587

X

X-ray
analysis for subgrains, 85–87
integral breadth ratio, 87